REPORT SERIES IN AEROSOL SCIENCE
N:o 180 (2016)

Proceedings of the 2nd Pan-Eurasian Experiment (PEEX) Conference and the 6th PEEX Meeting

Editors: Hanna K. Lappalainen, Alla Borisova, Dong Liang, Joonas Enroth and Markku Kulmala

Helsinki 2016

ISSN 0784-3496
ISBN 978-952-7091-46-3 (electronic publication)
Aerosolitutkimusseura ry – Finnish Association for Aerosol Research FAAR
http://www.atm.helsinki.fi/FAAR/

PREFACE

Kulmala, M., Lappalainen, H.K., Petäjä, T., Bondur, V., Baklanov, A., Wang, C., Xue, Y., Zhang, J., Zilitinkevich, S., and Guo, H.

These are Conference Proceedings of the 2nd Pan-Eurasian Experiment (PEEX) Conference and the 6th PEEX Meeting held in Beijing, China from May 18-20. The Eurasian Pan-Eurasian Experiment (PEEX) is a multidisciplinary, multi-scale program focused on solving Grand Challenges in northern Eurasia and China. The program has a main focus in arctic and boreal regions but is also interested in solving and providing solutions for air quality questions especially in China. PEEX is a bottom-up initiative by several European, Russian and Chinese research organizations and is currently representing research communities from 20 different countries. The PEEX emphasizes that solving challenges related to climate change, air quality and cryosphere change requires large-scale coordinated co-operation of the international research communities and development of advanced research infrastructures observing land – atmosphere interaction across Northern Eurasian and in China.

The 2nd PEEX conference themes include global scale feedbacks and interactions, air quality issues, anthropogenic emissions, big data, development of coherent, coordinated, comprehensive research infrastructures, knowledge transfer and international collaboration. A wide variety of disciplines is covered within the PEEX conference. It is illustrated by the large number (174 altogether) multidisciplinary conference abstracts. We thank all the researchers and the research teams, who contributed to the proceedings and participate the conference.

In order to expand the impact of the scientific results introduced during the PEEX conference we recommend the participants to submit full papers in the PEEX Special Issue in Atmospheric Chemistry and Physics (ACP) journal. The PEEX Special has been opened in ACP with the themes of climate change, air quality, biodiversity loss, chemicalization, food supply, fresh water and the use of natural resources through mining, industry, energy production and transport. The Editors in the special issue consists of an international, multidisciplinary team of V.-M. Kerminen, M. Heimann, D. Spracklen, T. Laurila, A. Ding, and I. Salma. By publishing your scientific results in the PEEX Special issue your work will be part of the periodic PEEX Scientific Assessment and contributing the implementation of the PEEX Science Plan.

Finally, we would like to extend our gratitude towards a large group of people and sponsors (Sponsors; Chinese Academy of Sciences Institute of Remote Sensing and Digital Earth (RADI), AEROCOSMOS and University of Helsinki. Co-sponsors; International Society for Digital Earth (ISDE), Group on Earth Observations (GEO), International Centre on Space Technologies for Natural and Cultural Heritage (HIST) under the Auspices of UNESCO, Integrated Research on Disaster Risk (IRDR), CAS-TWAS Centre of Excellence on Space Technology for Disaster Mitigation (SDIM), CRAICC, NordForsk, Lomonosov Moscow State University, Integrated Land Ecosystem-Atmosphere Processes Study (iLEAPS), International Eurasian Academy of Sciences (IEAS)) that enable the organization of the 2nd PEEX in Beijing, China at the facilities of Beijing International Convention Center (BICC).

More information about PEEX is available: ***https://www.atm.helsinki.fi/peex/***

May 2016

Conference Chairs
Chair of Organization Committee Academician H. Guo (RADI)
Chairs of Science Committee Academician V. Bondur (AEROCOSMOS) and Prof. M. Kulmala (Univ.Helsinki)

Science Committee: Prof. A. Baklanov (WMO), Prof. T. Petäjä (Univ. Helsinki), Prof. C. Wang (RADI), Prof. Y. Xue (RADI), Prof. J. Zhang (RADI) and Prof. S. Zilitinkevich (Finnish Met. Inst.)

TABLE OF CONTENTS

P. Alekseychik, H. Lappalainen, T. Petãjã, N. Zaitseva, M. Heimann, T. Laurila, H. Lihavainen, E. Asmi, M. Arshinov, V. Shevchenko, A. Makshtas, S. Dubtsov, E. Mikhailov, E. Lapshina, S. Kirpotin, Yu. Kurbatova, A. Ding, H. Guo, S. Park, J. V. Lavric, F. Reum, A. Panov, A. Prokushkin and M. Kulmala
OVERVIEW OF THE GROUND-BASED STATION NETWORK IN THE PEEX REGION
……...20

X. An, J. Zhang, X. Liu, F. Yao
AEROSOL DETECTION ANALYSIS FROM SATELLITE DURING THE HARVEST SEASON OVER NORTH CHINA PLAIN
……...26

X.Y. Ao, C.S.B. Grimmond, J.G. Tan, Y.Y. Chang, D.W. Liu and Y.Q. Tang
PRELIMINARY EVALUATION OF AN URBAN LAND SURFACE MODEL IN SHANGHAI
……...28

S.R. Arnold, K.S. Law and S.A. Monks
RADIATIVE FORCING SENSITIVITY TO MODEL BIAS IN HIGH LATITUDE OZONE PROFILES
……...33

A. Asmi, L. Järvi, F. Bonet-García
COOP+: PROMOTING THE COOPERATION AMONG INTERNATIONAL RESEARCH INFRASTRUCTURES TO ADDRESS GLOBAL ENVIRONMENTAL CHALLENGES
……...35

K. Atlaskina, V.-M. Kerminen, P. Aalto, J. Kontkanen, M. Kulmala and T. Petäjä
ANALYSIS OF AEROSOL PROPERTIES DYNAMICS IN RELATION TO THE AIR MASS TRANSPORT DURING BAECC CAMPAIGN
……...37

A. Baklanov and WMO GAW and WWRP teams
WMO GLOBAL ATMOSPHERE WATCH (GAW) AND WORLD WEATHER RESEARCH PROGRAMME (WWRP) RESEARCH FOR THE NORTHERN EURASIA
……...41

P.Ya. Baklanov
GEOGRAPHIC AND GEO-ECONOMIC FACTORS OF LONG-TERM DEVELOPMENT OF PACIFIC RUSSIA,
……...42

I. Bashmakova
EUROPEAN CENTRE OF INTERNATIONAL EURASIAN ACADEMY OF SCIENCES (EC-IEAS) – PRIORITIES AND COLLABORATION WITH PEEX
……...44

F. Berninger, K. Köster, X. Zhou, H. Aaltonen, M. Palviainen and J. Pumpanen
LONG TERM EFFECTS OF FIRE ON NORTHERN GREENHOUSE GAS EXCHANGES IN NORTHERN FORESTS
……...45

L. Bobylev, O.M. Johannessen, S. Kuzmina and E. Shalina
SUMMER ICE TRANSFORMATION IN THE EURASIAN ARCTIC SEAS IN THE 20TH AND 21ST CENTURIES
……...48

V. Bondur et al.
SATELLITE MONITORING OF TRACE GAS AND AEROSOL EMISSIONS INTO THE ATMOSPHERE OF NORTHERN EURASIA
……...53

R. Bornstein, J. Dou, S. Miao and X. Liang
GUIDELINES FOR ANALYSIS OF URBAN WEATHER AND CLIMATE DATA
……...55

R. Bossi and H. Skov
VOC MEASUREMENTS AT VILLUM RESEARCH STATION, NORTH GREENLAND, WITH PTR-TOF-MS
……...60

D. Brus, K. Doulgeris, K. Neitola, J. Backman, E. J. O' Connor, M. Komppula, M. Filioglou, K. A. Nicoll, R. G. Harrison, P. Tisler, J. Schwarz, P. Vodicka, V. Vakkari, M. Aurela, E. Asmi and H. Lihavainen
OVERVIEW OF PALLAS CLOUD EXPERIMENT, PACE 2015
……...63

M. Brus, A. Asmi, W. Kutsch, P. Laj and S. Sorvari
ENVRIPLUS – ENVIRONMENTAL RESEARCH INFRASTRUCTURES PROVIDING SHARED SOLUTIONS FOR SCIENCE AND SOCIETY
……...67

J.K. Bäck, R. Makkonen, D. Taipale, A. Mãkelã, A. Lohila, T. Vesala, E. Nikinmaa, F. Berninger, T. Kalliokoski, T. Petãjã, P. Paasonen, and M. Kulmala
TERRESTRIAL ECOSYSTEM–CLIMATE FEEDBACKS IN BOREAL AND TROPICAL FORESTS
……...70

C. Cavazos-Guerra, A. Lauer, A. Herber and T. Butler
CONTRIBUTION OF LOCAL EMISSIONS AND THE LONG RANGE TRANSPORT TO THE BLACK CARBON CONCENTRATIONS IN THE EURASIAN ARCTIC IN WRF-CHEM MODEL SIMULATIONS
……...73

F. Chen and B. Yu
ASSESSING NITROGEN DIOXIDE FROM BIOMASS BURNING IN SOUTH AND SOUTHEAST ASIA
……...79

L. Chen and O.M. Johannessen
REVISITING THE DRIVES OF NORTHERN HEMISPHERE WINTER SURFACE AIR TEMPERATURE VARIABILITY DURING 1901-2010
……...82

P. Chen, Y. Xue and J. Guang
HIGH PERFORMANCE RETRIEVAL OF FY3 GLOBAL SURFACE ALBEDO
……...85

X. Chen, V.-M. Kerminen, P. Paasonen, J. Paatero, H. E. Manninen, T. Petäjä and M. Kulmala
ON THE IONISING CAPACITY IN THE LOWER ATMOSPHERE AND ITS CONNECTION TO AIR ION OBSERVATION
……...88

X. Chen, S. Dubtsov, T. Ovchinnikova, S. Valiulin, H.E. Manninen, P.P. Aalto and T. Petäjä
APPLICATION OF THE AEROSOL DIFFUSION SPECTROMETER TO MEASURE ATMOSPHERIC NEW PARTICLE FORMATION
……...92

B. Cheng, Z. Tian, J. Zhao, T. Vihma and Z. Li
OBSERVED AND MODELED SNOW AND ICE THICKNESS IN CHUCKCHI SEA WITH CHINARE 2014 DATA
……...96

M.V. Cherepova and S.P. Smyshlyaev
METHANE COLUMN ABUNDANCE AND SURFACE CONCENTRATION VARIATIONS OVER EUROASIA
…….103

T. Chimitdorzhiev, P. Dagurov, M. Bykov, A. Dmitriev and I. Kirbizhekova
A COMPARISON OF ALOS PALSAR INTERFEROMETRY AND FIELD GEODETIC LEVELING FOR MARSHY SOIL THAW/FREEZE MONITORING, CASE STUDY FROM THE BAIKAL LAKE REGION, RUSSIA.
…….105

O.G. Chkhetiani, M.S. Artamonova, M.A. Iordanskii, M.V. Kurgansky, V.A. Lebedev, L.O.Maximenkov, Y.I. Obvintsev and N.V. Vazaeva
AEROSOL EMISSION IN THE ARID AND SEMI-ARID REGIONS OF SOUTHERN RUSSIA
…….111

N. Chubarova, Ye. Zhdanova and Ye. Nezvalâ
A NEW PARAMETERIZATION OF THE UV IRRADIANCE ALTITUDE DEPENDENCE FOR CLEAR-SKY CONDITIONS AND ITS APPLICATION FOR THE UV INTERACTIVE TOOL
…….114

T. Cömert, N. T. D. van de Koppel and H. H. G. Savenije
THE IMPORTANCE OF MOISTURE RECYCLING IN CHINA
…….116

R. Davy and I. Esau
SURFACE AIR TEMPERATURE CHANGES IN THE HIGH-LATITUDE BOUNDARY LAYER
…….123

G. de Leeuw, L. Sogacheva, P. Kolmonen, G. Saponaro, T.H. Virtanen and E. Rodriguez
SATELLITE REMOTE SENSING OF AEROSOL AND CLOUD PROPERTIES OVER THE PEEX AREA
…….128

A.J. Ding, W. Nie, X. Huang, X.G. Chi, Z. Xu, V. Thouret, P. Nedelec, L.F. Zheng, Z.N. Xu, Y.N. Xie, Y.C. Shen, X.M. Qi, J.P. Wang, K. Ding, J.N. Sun, T. Petaja, V.-M. Kerminen, M. Kulmala and C.B. Fu
OZONE IN THE WESTERN YANGTZE RIVER DELTA OF CHINA: A SYNTHESIS STUDY BASED ON GROUND, AIRCRAFT AND SOUNDING MEASUREMENT, 2011-2015
…….134

C. Donmez and S. Berberoglu
MODELLING OF HYDROLOGICAL RESPONSES TO CLIMATE-INDUCED CHANGES IN A SEMI-ARID WATERSHED
…….137

J. Duplissy, Q. Nguyen, E.S. Thomson, L. Ahonen, M. Kulmala, T. Petäjä, M. Sipilä, M. Bilde and E. Swietlicki
DEVELOPMENT OF AN ICE NUCLEATION CHAMBER TO STUDY ICE ABILITIES OF PARTICLES FROM NOTHERN EURASIA
…….141

E.A. Dyukarev, M.N. Alekseeva and E.A. Golovatskaya
EVALUATION OF THE VEGETATION STRUCTURE AND ABOVEGROUND NET PRODUCTION OF WETLAND ECOSYSTEMS USING SATELLITE DATA
…….143

I. Esau, V. Miles and A. Kurchatova
SURFACE URBAN HEAT ISLANDS IN NORTHERN CITIES
…….147

N. Filatov, N. Diansky, R. Ibraev and T. Viriuchalkina
EURASIAN GREAT LAKES: DIAGNOSIS AND PREDICTION OF THE WATER LEVEL FLUCTIUATIONS UNDER CLIMATE CHANGES AND ANTROPOGENIC IMPACTS
…….148

T.A. Fisher, S.A. Petrov, O.V. Frolova and M.V. Narushko
ADAPTIBILITY INDIGENOUS ARCTIC POPULATION BY "URBAN HEAT ISLAND"
…….149

C. Fu, Z. Xu, R. Mahmood, Z. L. Yang, H. Su, W. Guo, and S. Wang
TOWARDS FURTHER UNDERSANDING THE IMPACTS OF LAND USE AND COVER CHANGE ON REGIONAL CLIMATE OF MONSOON ASIA
…….153

J. Gao, Y. Zhang, Hao. Wang, Han. Wang, H. Li and F. Chai
THE CHARACTERISTICS AND SOURCES OF PARTICLE MATTERS IN HEAVY POLLUTION EPISODES IN NORTH CHINA
…….158

Z.H. Gao, B. Sun and Z.Y. Li
LAND DEGRADATION ASSESSMENT BY COUPLING NPP AND CLIMATE IN XILIN GOL LEGUE, INNER MONGLIA, CHINA
…….159

L.L. Golubyatnikov, V.S. Kazantsev and M.Yu. Cherbunina
PRELIMINARY ESTIMATE OF METHANE EMISSION DURING ICE THAW FROM SOUTHERN TUNDRA LAKES IN WESTERN SIBERIA
…….163

C. Gong and M. Wang
UNCERTAINTIES IN SATELLITE-DERIVED RAIN SUSCEPTIBILITY TO AEROSOLS
…….165

I.M. Gubenko and K.G. Rubinstein
MATHEMATICAL SIMULATION OF THE PARAMETERS OF THE ATMOSPHERIC ELECTRIC FIELD DURING THUNDERSTORMS BASED ON THE CUMULONIMBUS ELECTRIZATION MODEL
…….166

H. D. Guo
SPACEBORNE EARTH OBSERVING TECHNOLOGIES FOR ENVIRONMENTAL MONITORING IN THE BELT AND ROAD REGION
…….168

W. Guo, Y. Liu and Y. Xue
IMPACT OF ACCURATE DESCRIPTION OF LAND USE TYPE AND VEGETATION ON SIMULATION OF THE EAST ASIAN MONSOON PRECIPITATION
…….170

H. Hakola, V. Tarvainen, M. Hemmilä, A. P. Praplan and H. Hellèn
HIGH SESQUITERPENE EMISSIONS FROM NORWAY SPRUCE IN SUMMER
…….174

X. Han, F. Yao, J. Zhang and M. M. Waqar
HAZE DETECTION BY USING MODIFIED NORMALIZED DIFFERENCE HAZE INDEX IN BEIJING, TIANJIN AND HEBEI PROVINCE
…….178

Z. Han, J. Tan and Y. Chang
WARNING METHOD OF URBAN RAIL TRANSIT OPERATION SAFETY UNDER STRONG WIND
…….184

J. Heiskanen, I. Mammarella, A. Ojala and T. Vesala
ATMOSPHERE-LAND-LAKE CARBON CYCLE PROVIDES POSSIBILITIES FOR ECONOMIC STUDIES
…….187

A.A.M. Holtslag
CHALLENGES FOR STABLE ATMOSPHERIC BOUNDARY LAYERS
…….189

J. Hong, M. Äijälä, S. Häme, L. Hao, J. Duplissy, L. Heikkinen, J. Mikkilä, M. Ehn, W. Nie, P. J. Passonen, M. Kulmala, D. R. Worsnop, T. Petäjä, I. Riipinen and V.-M. Kerminen
RETRIEVE THE ORGANIC VOLATILITY DISTRIBUTION OF SUBMICRON AEROSOLS IN A BOREAL FOREST ENVIRONMENT USING A KINETIC EVAPORATION MODEL
…….190

X. Huang, L. X. Zhou, A. J. Ding, X. M. Qi, W. Nie, M. H. Wang, X. G. Chi, T. Petaja, V.-M. Kerminen, P. Roldin, A. Rusanen, M. Kulmala, and M. Boy
COMPREHENSIVE MODELLING STUDY ON NEW PARTICLE FORMATION AT THE SORPES STATION IN NANJING
…….193

A. Jain, B. El-Masri and S. Shu
IMPLEMENTATION OF DYNAMIC VEGETATION STRUCTURE PROPERTIES INTO A LAND SURFACE MODEL: EVALUATION OF CARBON, WATER, AND ENERGY FLUXES IN NORTHERN HIGH LATITUDE ECOSYSTEMS
…….202

L. Johansson, A. Karppinen and L. Dong
DEVELOPMENT OF AIR QUALITY MODELLING SYSTEM IN LANGFANG BASED ON SENSOR MEASUREMENTS AND DATA FUSION
…….205

L. Järvi, C.S.B. Grimmond, A. Christen, J.P. McFadden and I.B. Strachan
THE EFFECT OF SURFACE COVER AND CLIMATE CONDITIONS ON THE SURFACE ENERGY AND WATER BALANCE IN COLD CLIMATE CITIES
…….211

D.V. Karelin, E.P. Zazovskaya, V.A. Shishkov, A.V. Dolgikh, I.G. Sharkunov, A.V. Pochikalov, A.A. Karpov, E.V. Antonov and S.V. Goryachkin
THE EMISSIONS OF BIOGENIC GREENHOUSE GASES FROM ARCTIC AND NORTH BOREAL SOILS DUE TO THE DIFFERENT TYPES OF ANTHROPOGENIC LAND USE AT LOCAL AND REGIONAL SCALES: PROSPECTS AND DYNAMICS
…….215

N.S. Kasimov, S.R. Chalov and M.Y. Lychagin
HYDROCLIMATIC IMPACTS ON CATCHMENT-SCALE WATER CYCLE AND METAL AND CARBON FLUXES IN SELENGA-BAIKAL RIVER SYSTEM
…….221

M.T. Kaukolehto, J. Bãck, P. Hari, V.-M. Kerminen, J. Kujansuu, H.K. Lappalainen, J. Levula, T. Petãjä, T. Vesala and M. Kulmala
TOWARDS GLOBAL SMEAR NETWORK TO PROVIDE COMPREHENSIVE DATA FOR KNOWLEDGE BASED DECISIONS
…….225

V.-M. Kerminen, T. Nieminen, T. Petäjä, A.J.Ding, M. Hu, L. Wang and M. Kulmala
TOWARD GLOBAL PICTURE OF ATMOSPHERIC NEW PARTICLE FORMATION BASED ON OBSERVATIONS
…….229

N.F. Kharlamova and I.N. Rotanova
CLIMATE AS A FACTOR OF SUSTAINABLE DEVELOPMENT OF ALTAI-SAYAN MOUNTAIN COUNTRY
…….232

E. Kharyutkina, S.V. Loginov and I.I. Ippolitov
CLIMATE VARIABILITY OVER THE TERRITORY OF WEST SIBERIA
…….235

M.V. Kiselev, N.N Voropay and E.A. Dykarev
TEMPERATURE REGIME OF OLIGOTROPHIC AND EUTROPHIC MIRES AT SOUTH OF WEST SIBERIA
…….241

A. Kislov, P. Konstantinov, M. Varentsov, T. Samsonov, I. Gorlach, L. Alekseeva and E. Vasilenko
URBAN AMPLIFICATION OF THE GLOBAL WARMING: DIGNOSTIC, MODELLING, FORECASTING
…….244

X. Kong, A. Waldner, F. Orlando, L. Artiglia, M. Ammann, and T. Bartels-Rausch
A PRELIMINARY VIEW ON ADSORPTION OF ORGANICS ON ICE AT TEMPERATURES CLOSE TO MELTING POINT
…….246

P.I. Konstantinov, M.I. Varentsov, A.B. Akhmetova, E.A. Kukanova and A.A.Baklanov
URBAN HEAT ISLAND'S RESEARCH IN EX-USSR REGION. METHODOLOGY AND FIRST RESULTS
…….247

J. Kontkanen, . Paasonen, J. Bäck, T. Petäjä and M. Kulmala
A SIMPLE PROXY FOR THE CONCENTRATIONS OF MONOTERPENES AND THEIR OXIDATION PRODUCTS IN BOREAL FOREST
…….249

O. Krüger, Y. Liu, H. Guo, J. Zhang, A. Ding, M. Kulmala1 and T. Petäjä
POTENTIAL IMPACT OF POLLUTION ON CLOUDS AND PRECIPITATION OVER CHINA
…….253

J. Kujansuu, M. Kulmala and T. Petäjä
BEAUTIFUL CHINA – HOW TO TACKLE AIR POLLUTION
…….258

M. Kulmala, H. K. Lappalainen, T. Petäjä, V.-M. Kerminen, R. Makkonen, P.Alekseychik, N. Zaitseva, J. Kujansuu, A. Scherbinin, P. Konstantinov, M. Kaukolehto, N. Chubarova, M. Arshinov, A. Mahura, S. Arnold, D. Spracklen, S. Juhola, J. Bäck, T. Vesala, P. Hari, A. Ding, C. Fu1, H.-C. Hansson, V. Melnikov, Y. Viisanen, G. Matvienko, A. Baklanov, N. Kasimov, H. Guo, V. Bondur and S. Zilitinkevich
PAN-EURASIAN EXPERIMENT (PEEX) – AS A TOOL TO UNDERSTAND AIR QUALITY – CLIMATE INTERACTIONS AND FEEDBACKS
…….259

A. Kumar
GEOSPATIAL STRATEGY FOR ADVERSE IMPACT OF URBAN HEAT ISLAND VIA SURFACE TOPOGRAPHY USING LANDSAT ETM+ SENSORS
…….264

W-L Kutsch, E. Juurola, J. Lavric, J. Lätti and ICOS Central Facilities team
ICOS RESEARCH INFRASTRUCTURE —INTEGRATING EUROPE'S GREENHOUSE GAS OBSERVATIONS FOR BETTER FUTURE
…….265

T. Kühn, H. Kokkola, K. Kupiainen, K. Kulovesi, and K. Lehtinen
MODELLING BLACK CARBON: FROM INTERNATIONAL CLIMATE LAW TO IMPACT ON ARCTIC CLIMATE (WHITE)
…….267

H.K. Lappalainen, T.Petäjä, V-M. Kerminen, R.Makkonen, A.Malkamäki, P. Alekseychik, N. Zaitseva, J. Kujansuu, T. Ruuskanen, A. Lauri, E. Kyrö, S. Mazon, A. Scherbinin, P. Konstantinov, M. Kaukolehto, N. Chubarova, T. Laurila, E. Asmi, S. Juhola, J. Bäck, T. Vesala, P. Hari, M. Arshinov, A. Mahura , S. Arnold, D. Spracklen, A. Ding, C. Fu, H-C. Hansson, V. Melnikov, G. Matvienko, A. Baklanov, Y. Viisanen, N. Kasimov, H. Guo, V. Bondur, S. Zilitinkevich and M. Kulmala
PAN-EURASIAN EXPERIMENT (PEEX) PROGRAM OVERWIEV - ACTIVITIES IN 2012-2015 AND FUTURE PROSPECTS
…….270

A. Lauri, L. Riuttanen, P. Sihvonen, S. Westerberg, P. Hari, T.M. Ruuskanen and M. Kulmala
THE ATMOSPHERIC SCIENCE PARADIGM AND HORIZONTAL LEARNING: EXPERIENCES FROM SHORT RESEARCH-INTENSIVE COURSES
…….275

T. Laurila, E. Asmi, J. Hatakka, J. Rainne, T. Mäkelä, H. Lihavainen, Y. Viisanen, P. Taalas, V. Movchan, V. Kustov and A. Makshtas
NEW CONTINUOUS AEROSOL AND GREENHOUSE GAS MEASUREMENTS IN RUSSIAN ARCTIC ICE BASE CAPE BARANOVA -STATION
…….277

F. Li, H. Wang and Y. Gao
EXTRA-TROPICAL OCEAN WARMING AND WINTER ARCTIC SEA ICE COVER SINCE THE 1990S
…….281

H. Li, L. Yang and J. Lei
SOIL EROSION ANALYSIS IN RED SOIL HILLY REGION BY USING HJ-CCD：A CASE IN GANZHOU
…….283

T. Li, B. Xie, G. Wang, W. Zhang, Q. Zhang, T. Vesala and M. Raivonen
FIELD-SCALE SIMULATION OF METHANE EMISSIONS FROM COASTAL WETLANDS IN CHINA USING AN IMPROVED VERSION OF CH4MODWETLAND
…….284

Z. Li, Y. Bai, H. Li, R. Li, L. Arvola and M. Leppäranta
SPATIAL AND TEMPORAL DISTRIBUTIONS OF DISSOLVED OXYGEN UNDER ICE IN LAKE VALKEA-KOTINEN, FINLAND
…….285

Z.Q. Li, Y.S. Xie and L. Li
REMOTE SENSING OF AEROSOL OPTICAL, MICROPHYSICAL AND CHEMICAL PROPERTIES BASED ON SUN-SKY RADIOMETER MEASUREMENTS OVER POLLUTED CITIES
…….290

K. Liang, L.C. Sui and Y.Q. Guo
SPATIAL AND TEMPORAL VARIABILITY IN THE NET PRIMARY PRODUCTION OF SHAANXI PROVINCE FROM 2000 TO 2014
…….295

X. Lin and C. Tao
QUANTIFYING SNOW ALBEDO RADIATIVE FORCING AND ITS FEEDBACK USING SATELLITE OBSERVATIONS
…….300

X. Ling, C. Fu, Z. Yang and W. Guo
A PRELIMINARY STUDY OF IMPROVING GLOBAL LEAF AREA INDEX (LAI) ESTIMATION BASED ON DATA ASSIMILATION RESEARCH TESTBED AND THE COMMUNITY LAND MODEL VERSION 4
…….304

A. Lintunen, T. Paljakka, L. Lindfors and T. Hölttä
TREE WATER RELATIONS DURING WINTER
…….309

J. Liu, Y. Xue and J. Garcke
EFFICIENT REMOTE SENSING DATA STORAGE AND MANAGEMENT BASED ON PARALLEL FILE SYSTEM AND NOSQL DATABASE
…….313

Y. Liu, O. Krüger, H. Guo, J. Zhang, M. Kulmala and T. Petäjä
A STUDY OF CHARACTERISTICS OF WATER CLOUDS OVER HYYTIÄLÄ BASED ON CLOUDSAT/CALIPSO DATA
…….317

S. Luo, B. Chen, S. Lü, Y. Zhang and D. Ma
EFFECTS OF THE SOIL FREEZE−THAW PROCESS ON THE REGIONAL CLIMATE OF THE TIBET PLATEAU
…….321

H. E. Manninen, J. Lampilahti, S. Mirme, T. Nieminen, M. Ehn, I. Pullinen, K. Leino, S. Schobesberger, J. Kangasluoma, T. Yli-Juuti, R. Krecji, R. Väänänen, R. Tillmann, A. Wahner, D.R. Worsnop, F. Rohrer, T. Petäjä, Th. F. Mentel, and M. Kulmala
ONSET OF NEW PARTICLE FORMATION WITHIN A RISING MIXED BOUNDARY LAYER: ZEPPELIN FLIGHTS OVER HYYTIÄLÄ
…….322

G.G. Matishov
ENVIRONMENTAL AND CLIMATIC CHANGES IN THE NORTHERN HEMISPHERE AND INTERNATIONAL ECOLOGICAL CO-OPERATION
…….325

T.C. Maximov, A.V. Kononov, A.P. Maksimov, R.E. Petrov and M.P. Teretentyeva
ANALYSIS OF LONG-TERM CARBON STOCKS IN PERMAFROST-DOMINATED FOREST ECOSYSTEMS OF NORTH-EAST RUSSIA
…….327

S. B. Mazon, J. Kontkanen, H. E. Manninen, T. Nieminen, V.-M. Kerminen and M. Kulmala
CLUSTER EVENTS IN A BOREAL FOREST: COMPARING NIGHT-TIME WITH DAY-TIME ION CLUSTERS FROM 2003–2013
…….328

O. Meinander, A. Virkkula, A. Kontu, J. Svensson, H.-R. Hannula, P. Dagsson-Waldhauserova, A. Arola, L. Backman, T. Manninen, G. De Leeuw and M. Leppãranta
LIGHT ABSORBING PARTICLES AND DENSITY OF MELTING SURFACE SNOW
…….330

T. Mielonen, A. Hienola, H. Kokkola, T. Kühn, J. Merikanto, H. Korhonen, A. Arola, P. Kolmonen, L. Sogacheva, S. Romakkaniemi, and G.F.R De Leeuw
DOES INCREASING TEMPERATURE INCREASE CARBONACEOUS AEROSOL DIRECT RADIATIVE EFFECT?
…….334

V. Miles and I. Ezau
REMOTE-SENSING INDICATORS OF URBAN EFFECTS IN THE ARCTIC: FOCUS ON NORTHERN WEST SIBERIA
…….338

N.S. Molokitina, A.O. Drachuk and L.S. Podenko
ICE FOR NATURAL GAS STORAGE
…….339

M. Mäki, J. Heinonsalo, H. Hellén and J. Bäck
DECOMPOSING PROCESSES REGULATE BVOC EMISSIONS FROM BOREAL SOIL DURING FALL
…….342

A. Nikandrova, R. Väänänen, K. Atlaskina, V.-M. Kerminen, M. Kulmala, T. Petäjä, M. Komppula and E. O'Connor
COMBINING AIRBORNE AND LIDAR MEASUREMENTS FOR ATTRIBUTION OF AEROSOL LAYERS
…….347

W. Nie, A.J. Ding, Z. Xu, X. Huang, X.G. Chi, Y.N. Xie, V.-M. Kerminen, T. Petaja, A. Virkkula, M. Kulmala, X. Q. Yang, J. N. Sun and C. B. Fu
FEEDBACK OF AEROSOL POLLUTION TO ATMOSPHERIC CHEMISTRY IN EASTERN CHINA
…….351

S.M. Noe, A. Krasnova, D. Krasnov, Ü. Niinemets, K. Jõgiste, U. Hõrrak, M. Vana, S. Mirme, K. Komsaare and A. Kangur
DYNAMICS OF CARBON, NITROGEN AND OTHER CLIMATE RELEVANT TRACE GASES MEASURED AT SMEAR ESTONIA
…….354

A. Ojala, I. Mammarella, J. Bäck, J. Pumpanen, M. Rantakari, H. Miettinen, J. Heiskanen, E. Peltomaa, K.-M. Erkkilä, M. Provenzale, P. Hari, T. Vesala and M. Kulmala
INTEGRATED AQUATIC STUDIES BASED A CONTINUOUSLY OPERATED MEASURING PLATFORM: POSSIBILITIES AND CHALLENGES
…….359

P. Paasonen, K. Kupiainen, Z. Klimont, A. Visschedijk, H. Denier Van Der Gon and M. Amann
ANTHROPOGENIC PARTICLE NUMBER EMISSIONS AND THEIR SIZE DISTRIBUTIONS IN NORTHERN AND EASTERN EURASIA
…….363

A. Panov, G.K. Zrazhevskaya, M.A. Korets, A.V. Bryukhanov, N.V. Sidenko, A.V. Timokhina and M. Heimann
SOIL CO2 EFFLUX RATES AFTER WILDFIRES IN CENTRAL SIBERIAN ECOSYSTEMS
…….368

V.V. Penenko, A.V. Penenko and E.A. Tsvetova
VARIATIONAL MODELING TECHNOLOGY WITH DATA ASSIMILATION FOR ENVIRONMENTAL PREDICTION AND RISK ASSESSMENT
…….371

S.A. Petrov, N.L. Mamaeva, D.A. Khrupa and V.A. Malchevskiy
ASSESSMENT OF ANTHROPOGENIC CONTAMINATION IN GEOCRYOLOGICAL AREAS OF THE ARCTIC ZONE OF WESTERN SIBERIA
…….377

T. Petäjä, D. Moisseev, E. O'Connor, V. Sinclair, A. Manninen, H. K. Lappalainen, V.-M. Kerminen and M. Kulmala
BIOGENIC AEROSOLS – EFFECTS ON CLOUDS AND CLIMATE (BAECC) STUDY AS AN EXAMPLE FOR SCIENTIFIC INTEGRATION
…….381

D. Pozdnyakov and L. Pettersson
CONTEMPORARY TENDENCIES IN PRIMARY PRODUCTION DYNAMICS IN THE ARCTIC OCEAN UNDER CONDITIONS OF GLOBAL WARMING
…….384

A.S. Prokushkin, I.V. Tokareva, M.A. Korets, R. Amon and O.S. Pokrovsky
DRIVERS OF TERRESTRIAL CARBON RELEASE TO RIVERS: CENTRAL SIBERIAN PLATEAU CASE STUDY
…….390

Y. Qiu and H. Guo
SATELLITE-BASED SNOW WATER EQUIVALENT ESTIMATION AND CLIMATOLOGY ANALYSIS OVER CENTER ASIA AND XINJIANG PROVINCE, CHINA
…….396

S. Raasch
EFFECTS OF LAND SURFACE HETEROGENEITIES ON CONVECTIVE BOUNDARY LAYERS. WHAT DID WE LEARN FROM LARGE-EDDY SIMULATION SO FAR?
…….398

V.S. Rakitin, G. Wang, P. Wang, A.V. Dzhola, A.N. Safronov, E.I. Grechko and A.V. Shilkin
TOTAL COLUMN OF CARBON MONOXIDE AND METHANE OVER EURASIA: LONG-TERM TRENDS, SEASONAL AND WEEKLY VARIATIONS ANALYSIS BASED ON GROUND-BASED AND SATELLITE SPECTROSCOPIC OBSERVATIONS
…….404

I.A. Repina, M.I. Varentsov, Aniferov, A.A. Artamonov and Mazilkina
INTERCOMPARISON OF SURFACE HEAT TRANSFER IN THE ARCTIC FOR MULTIPLE REANALYSES, SATELLITE DATA AND FIELD OBSERVATIONS
……409

Y. Ruan, Y. Qiu and X. Yu
PASSIVE MICROWAVE REMOTE SENSING OF LAKE FREEZE-THAW OVER EURASIA
……415

T.M. Ruuskanen, P. Sihvonen, L. Riuttanen, A. Lauri and M. Kulmala
MULTIDISCLIPINARY AIR QUALITY CAPACITY BUILDING
……419

N. Sarnela, H. Junninen, L. Ahonen, T. Jokinen, J. Mikkilä, O. Peräkylä, D. Wimmer, T. Petäjä, H. Skov, M. Kulmala and M. Sipilä
ARCTIC AEROSOLS AND PARTICLE FORMATION IN NORTHERN GREENLAND
……421

E.V. Shalina and S. Sandven
NEW SNOW DEPTH DISTRIBUTION OVER ARCTIC SEA ICE FROM HISTORICAL DATA
……425

A. Shcherbinin, R. Makkonen, P. Paasonen and S. Juhola
ATTRIBUTION OF CLIMATE IMPACTS TO ORGANIZATIONS: GAS AND OIL OPERATION IN THE ARCTIC
……429

X.J. Shen, J.Y. Sun, X.Y. Zhang, N. Kivekäs, Y.M. Zhang, T.T. Wang, X.C. Zhang, Y. Yang, D.Z. Wang, Y. Zhao and D.H. Qin
PARTICLE CLIMATOLOGY IN CENTRAL EAST CHINA RETRIEVED FROM MEASUREMENTS IN PLANETARY BOUNDARY LAYER AND IN FREE TROPOSPHERE AT A 1500-M-HIGH MOUNTAINTOP SITE
……433

X. Shi, L. Yu, S. Nie, Y. Zhang and W. Zhou
SIMULATED IMPACTS OF DIFFERENT VEGETATION LANDCOVER DATASETS ON THE HIGH-LATITUDE LAND SURFACE CLIMATE
……437

Z. Shirazi and F. Chen
RELATIONSHIP BETWEEN INTER-ANNUAL WILDFIRE DENSITY AND ET/PET RATIO IN SOUTH CHINA
……439

A.I. Skorokhod, I.B. Belikov, K.B. Moiseenko, N.V. Pankratova, Y.A. Shtabkin and M. Heimann
REACTIVE GASES OVER CENTRAL SIBERIA: OBSERVATIONS AND BALANCE
……443

H. Skov, R. Bossi, A. Massling, J.K. Nojgaard, I.E. Nielsen, K. Vorkamp, U. B. Gosewinkel, R. Lange, M.B. Poulsen, J.H. Christensen, K.M. Hansen, M. Bilde, M. Glasius, T.Šantl-Temkiv, K. Finster, S. Pilgaard and L.L. Sørensen
FIRST YEAR OF RESEARCH ACTIVITIES AT VILLUM RESEARCH STATION, STATION NORD, NORTH GREENLAND
……448

Y. Skryzhevska, V.-P. Tynkkynen and S. Leppänen
RUSSIAN CLIMATE POLICIES AND LOCAL REALITY
……452

V.M. Stepanenko, A.V. Glazunov, I.A. Repina and V.N. Lykosov
NUMERICAL MODELLING OF LAKE-ATMOSPHERE CONTINUUM IN FORESTED LANDSCAPES
……453

D.A. Subetto, N.A. Belkina, N.M. Kalinkina, G.S. Borodulina, A.I. Sidorova, A.U. Tarasov, M.S. Potakhin, M.B. Zobkov, N.N. Filatov, M.S. Bogdanova, V.N. Baklagin, A.V. Litvinenko, T.S Shelekhova, U.U. Fomina and N.B. Lavrova
THE PROJECT ”LAKE ONEGO AND ITS WATERSHED: GEOLOGICAL HISTORY, ANTHROPOGENIC TRANSFORMATION AND CURRENT STATE”, PRELIMINARY RESULTS
……458

A.M. Subbotin, M.V. Naruschko, A.S. Bazhin, S.A. Petrov and L.F. Kalenova
ADAPTOGENESIS OF OAT (AVENA SATIVA L.) TO OIL POLLUTION OF SOIL
……461

T. Suni and I. Koskinen
FUTURE EARTH: CO-DESIGNING GLOBAL CHANGE RESEARCH TO RESPOND TO GRAND SOCIETAL CHALLENGES
……464

J. Svensson, O. Meinander, A. Kontu, H.-R. Hannula, A. Virkkula, E. Asmi and H. Lihavainen
LIGHT-ABSORBING IMPURITIES IN SURFACE SNOW FROM SODANKYLÃ, SUBARCTIC FINLAND 2009-2015
……469

Y.Q. Tang, J.G. Tan, C.S.B. Grimmond, Y.Y. Chang and X.Y. Ao
AERODYNAMIC PARAMETERS ESTIMATION FOR A HIGH-RISE REGION OF SHANGHAI
……471

X. Tian, Z.Y. Li, E.X. Chen, Q.W. Liu and M. Yan
THE COMPLICATE OBSERVATIONS AND MULTI-PARAMETER LAND INFORMATION CONSTRUCTIONS ON ALLIED TELEMETRY EXPERIMEN (COMPLICATE)
……476

A. Timokhina, A. Prokushkin, Y.V. Lavric and M. Heimann
THE ISOTOPIC COMPOSITION OF ATMOSPHERIC CO2 AND CH4 OVER CENTRAL SIBERIA
……482

J.-P. Tuovinen, M. Aurela, T. Virtanen, J. Hatakka, M. Linkosalmi, V. Ivakhov, A. Makshtas and T. Laurila
METHANE FLUXES ON SIBERIAN PERMAFROST TUNDRA: UNRAVELLING INDIVIDUAL LAND COVER TYPES FROM EDDY COVARIANCE DATA
……487

R. van der A, G. de Leeuw, B. Mijling, J. Ding, D. Balis, J. Stavrakou, A. Mahura, K.Kourtidis, J. Bai, B. Martínez, V. Amiridis, P. Xie, R. Timmermans, L. Zeng, Q. Zhang, N. Veldeman and Y. Xue
MONITORING AND ASSESSMENT OF REGIONAL AIR QUALITY IN CHINA USING SPACE OBSERVATIONS (MARCO POLO)
…….491

A. Virkkula, X. Chi, A. Ding, Y. Shen, W. Nie, X. Qi, L. Zheng, T. Petäjä and M. Kulmala
VARIATIONS OF AEROSOL OPTICAL PROPERTIES DURING A POLLUTED WINTER PERIOD IN NANJING, CHINA
…….493

A. Virkkula, X. Chi, A.Ding, Y. Shen, W. Nie, X. Qi, L. Zheng, X. Huang, Y. Xie, J. Wang, T. Petäjä and M. Kulmala
ON THE INTERPRETATION OF THE LOADING CORRECTION OF THE AETHALOMETER
…….498

I.S. Vitkovskaya, M.Zh. Batyrbayeva and L.F. Spivak
SOME RESULTS OF SPACE MONITORING OF VEGETATION COVER OF KAZAKHSTAN ARID AND SEMI-ARID ZONES BY LONG TERM SERIES OF VEGETATION INDEXES
…….502

V.A. Volkov, A.V. Mushta and A.Yu. Yurova
REALTIVE VORTICITY AS A DYNAMIC FACTOR OF THE ARCTIC SEA ICE
…….505

N.N. Voropay and E.V. Maksyutova
DYNAMICS OF ARIDITY IN PREDBAIKALIE AT PRESENT CLIMATE CHANGES
…….507

D. Wang, Q. Fu, A. Ding, G. Xiu, Z. Ning, J. Huo, Y. Duan, X. Yang, X. Wang, Y. Yang and K. Zhang
THE CHARACTERISTICS OF VERTICAL DISTRIBUTION AND REGIONAL TRANSPORT OF PM2.5 WITHIN THE LOWER TROPOSPHERE DURING HIGH POLLUTION EPISODE WINTER OF 2015 IN SHANGHAI, CHINA BASED ON TETHERED BALLOON
…….510

D. Wang, Z. Wang, Z.-R. Peng
PERFORMANCE EVALUATION OF LINE SOURCE DISPERSION MODELS FOR SHORT-TERM ESTIMATION AT ROAD INTERSECTION
…….511

K. Wang, X.H. Zheng, Z.S. Yao, H. Zhang, L. Ma and L. Li
TWO-YEAR COMPARISON OF METHANE FLUX MEASUREMENTS USING STATIC CHAMBER AND EDDY COVARIANCE TECHNIQUES ON AN ALPINE WETLAND ON THE QINGHAI-TIBETAN PLATEAU
…….517

M. Wang, X. Niu, S. Chen, F. Wang, G. Yang
INVERSION OF VEGETATION COMPONENTS BASED ON THE SPECTRAL MIXTURE ANALYSIS USING HYPERION DATA
…….521

X. Wang, R. Gu, L. Wang, L. Xue, W. Xu, Y. Zhang, B. Chen, W. Li and W. Wang
EMISSIONS OF NITRATED PHENOLS IN FINE PARTICLES FROM BIOMASS BURNING
…….528

X. D. Wang, C. Wang and X.H. Xi
SPATIO-TEMPORAL ANALYSIS OF GREENLAND SNOWMELT USING MICROWAVE RADIOMETIER DATA (1988-2014)
…….529

Y. Wang and R.M. Castelao
VARIABILITY IN ESTUARINE SALINITY AND INUNDATION WITH CHANGING CLIMATE
…….533

Z. Wang, Y. Tham, T. Wang, W. Wang, X. Wang, N. Ma, K. Lu, Y. Zhang, A. Wiedensohler and W. Wang
DIRECT MEASUREMENT OF REACTIVE UPTAKE OF N2O5 AND YIELD OF CLNO2 ON AMBIENT AEROSOLS IN NORTH CHINA PLAIN
…….534

Z. Wang, X. Yu, S. Kecorius, Z. Xie, G. McMeeking, C. Pöhlker, M. Zhang, A. Wiedensohler, U. Kuhn, Y. Cheng, U. Pöschl and H. Su
ONLINE MEASUREMENTS OF FLUORESCENT AEROSOL PARTICLES AT A POLLUTED REGIONAL SITE IN THE NORTH CHINA PLAIN: INSIGHTS INTO THE POTENTIAL IMPACT OF BURNING ACTIVITIES
…….535

T. Wolf, I. Esau and J. Reuder
THE BREEZE INDUCED MODIFICATION OF THE LOCAL CIRCULAION IN A COASTAL MOUNTAINOUS VALLEY – A CASE STUDY FOR BERGEN, NORWAY.
…….537

T. Wu, L. Han and Q. Liu
CLOUD DETECTION BASED ON TEXTURE FEATURE AND SUPPORT VECTOR MACHINE
…….542

T. Wu, R. Li, T. Wang and L. Zhao
OBSERVED NON-UNIFORM WARMING ON THE QINGHAI-TIBETAN AND MONGOLIAN PLATEAU FROM 1961 TO 2013
…….544

F. Xausa, P. Paasonen, R. Makkonen and V.-M. Kerminen
IMPLEMENTATION OF A NEW SIZE-SEGREGATED AEROSOL NUMBER EMISSIONS MODULE IN GLOBAL CLIMATE MODELING
…….551

Y. Xie, Y. Xue, C. Fan, Y. Che and J. Guang
IMAGE FUSION OF AATSR AOD PRODUCTS BASED ON THE MAXIMUM LIKELIHOOD ESTIMATE METHOD
…….555

G. Xiu, M. Zhao, T. Qiao ja J. Yu
ATMOSPHERIC HULIS-CARBON IN PM2.5 AND PM1 IN SHANGHAI: IMPLICATION FOR HAZE POLLUTION
…….558

W. Xu, D. Yang, Y. Li and R. Xiao
INVESTIGATION OF MACKENZIE RIVER DISCHARGE AND NDVI RELATIONSHIP
…….561

Z. Xu, T. Wang, J. Wu, L. Xue, P.K.K. Louie, C.W.Y. Luk, W. Nie and A. Ding
NITROUS ACID IN A POLLUTED SUBTROPICAL ATMOSPHERE: SEASONAL VARIABILITY, DIRECT VEHICLE EMISSIONS AND HETEROGENEOUS PRODUCTION
…….562

L. Xue, L. Wen, L. Yang, X. Wang, Y. Zhang, T. Wang and W. Wang
PARTICULATE NITRATE AND SULFATE AT URBAN AND MOUNTAIN SITES IN THE NORTH CHINA PLAIN: DECADAL CHANGE FROM 2005-2015 AND FORMATION MECHANISMS
…….565

C. Yan, W. Nie, M. Äijälä, S. Häme, M. P. Rissanen, T. Jokinen, H. Junninen, M. Sipilä, M. Kulmala, D. Worsnop and M. Ehn
POSITIVE MATRIX FACTORIZATION ON CI-API-TOF SPECTRA – TOWARD THE UNDERSTANDING OF FORMATION MECHANISMS OF HIGHLY OXIDIZED MULTIFUNCTIONAL COMPOUNDS IN A BOREAL FOREST ENVIRONMENT
…….566

M. Yan, Z.Y. Li, L. Zhang, X. Tian and E.X. Chen
SIMULATION OF FOREST CARBON FLUX BY MODEL INCORPORATION AND ASSIMILATION
…….570

L. Yang and H. Li
ANALYSIS AND EVALUATION OF SOIL EROSION IN SOUTHERN RED SOIL EROSION AREA: A CASE IN GANZHOU
…….575

Q. Ye, J. Zong, L. Tian, J.G. Cogley, C. Song and W. Guo
THREE EPOCHS OF DATA ON GLACIER CHANGES ON THE TIBETAN PLATEAU DERIVED FROM LANDSAT IMAGERY, FROM THE 1970S TO 2013
…….578

L. Yu, Y. Huang, W. Zhang, W. Sun and T. Li
ESTIMATING METHANE UPTAKE FROM GLOBAL FOREST AND GRASSLAND BY A STATISTICAL MODEL
…….579

X. Yu, Y. Qiu, H. Guo and L. Chen
CLOUD REMOVING METHOD FOR DAILY SNOW MAPPING OVER CENTRAL ASIA AND XINJIANG,CHINA
…….580

H. Yuan and R. Sun
ASSESSMENT AND HYDROLOGIC APPLICATIONS OF THE LATEST SATELLITE-GAUGE PRECIPITATION ESTIMATES OVER THE HUAIHE RIVER BASIN
…….583

Bai Yun and Zhang Jiahua
ACCURACY OF RIVER NETWORK EXTRACTED FROM DIFFERENT DEM DATASET AND THE RELATIONSHIP WITH TERRAIN UNDULATION
…….585

A.Yu. Yurova, J. Tang and B. Tupek
BOREAL ECOSYSTEM BIOGECHEMISTRY SIFTED THROUGH THE CATCHMENT-RESOLVING ANALYSIS
…….588

E. A. Zarov, L.L. Golubyatnikov and E.D. Lapshina
MICROLANDSCAPE STRUCTURE OF SOUTH TUNDRA LANDSCAPES BASED ON A FIELD SURVEY
…….590

N.A. Zaytseva, Yu.A. Kurbatova and I.M. Kurganova
ABOUT POSSIBILITY TO STUDY MESO - AND MICROSCALE INTERACTIONS WITHIN THE SYSTEM “CLIMATE-TERRESTRIAL ECOSYSTEMS” IN THE FRAMEWORK OF THE PAN-EURASIAN EXPERIMENT PEEX
…….594

A. Zhang and G. Jia
SATELLITE BASED DROUGHT AND VEGETATION CHANGES OVER SEMI-ARID AREAS
…….595

L. Zhang, J. Xiao, Y. Zheng and Y. Zhou
ASSESSING THE CARBON AND WATER FLUXES IN GLOBAL RANGELANDS
…….596

S. Zhang, J. Yuan and J. Zhang
ANALYSIS ON CORRELATION BETWEEN NPP OF DIFFERENT VEGETATION TYPE AND AIR TEMPERATURE, PRECIPIATION LAI AND NDVI IN EAST ASIAN MONSOON REGION—A CASE IN HEBEI PROVINCE
…….599

X. Zheng, W. Zhang, Y. Li, B. Zhu and C. Liu
A CATCHMENT MODEL COUPLING THE CYCLING PROCESSES OF WATER, CARBON AND NITROGEN: ATTEMPTS OF ESTABLISHMENT AND VALIDATION
…….603

X. Zhong, T. Zhang, K. Wang, L. Zheng and H. Wang
SPATIONTEMPORAL VARIABILITY IN SNOW PHENOLIGY OVER EURASIAN CONTINENT DURING 1966-2012
…….605

P. Zhou, L. Ganzeveld, Ü. Rannik, L. Zhou, R. Gierens, D. Taipale, I. Mammarella and M. Boy
SIMULATING OZONE DRY DEPOSITION AT A BOREAL FOREST WITH A MULTI-LAYER CANOPY DEPOSITION MODEL
…….610

S. Zilitinkevich
COGNITIVE CHAOS: TURBULENCE AND PLANETARY BOUNDARY LAYERS IN EARTH SYSTEMS
…….614

OVERVIEW OF THE GROUND-BASED STATION NETWORK IN THE PEEX REGION

P. ALEKSEYCHIK[1], H. LAPPALAINEN[1], T. PETÄJÄ[1], N. ZAITSEVA[2], M. HEIMANN[3,1], T. LAURILA[4], H. LIHAVAINEN[4], E. ASMI[4], M. ARSHINOV[5], V. SHEVCHENKO[6], A. MAKSHTAS[7], S. DUBTSOV[8], E. MIKHAILOV[9,10], E. LAPSHINA[11], S. KIRPOTIN[12], YU. KURBATOVA[13], A. DING[14], H. GUO[15], S. PARK[3], J. V. LAVRIC[3], F. REUM[3],A. PANOV[16], A. PROKUSHKIN[16] AND M. KULMALA[1]

[1]Department of Physics, University of Helsinki, PO Box 48, FI-00014 Helsinki, Finland

[2] Department of Earth Sciences, Russian Academy of Sciences, Leninsky pr., 32F, 119991, Moscow, Russia

[3]Max Planck Institute for Biogeochemistry, Hans-Knöll-Straße 10, 07745 Jena, Germany

[4]Finnish Meteorological Institute, Atmospheric Composition Research, PO Box 503, 00101 Helsinki, Finland

[5]V.E. Zuev Institute of Atmospheric Optics SB RAS, 1, Academician Zuev square, 634055 Tomsk, Russia

[6]P. P. Shirshov Institute of Oceanology, Russian Academy of Sciences, 36 Nakhimovsky prospect, 117997 Moscow, Russia

[7]Arctic and Antarctic Research Institute, Roshydromet, Sankt-Petersburg, Russia

[8]V. V. Voevodsky Institute of Chemical Kinetics and Combustion, SB RAS, Institutskaya str., 3, Novosibirsk, Russia

[9]Atmospheric Physics Department, St. Petersburg State University, St. Petersburg, Russia
[10] Biogeochemistry and Multiphase Chemistry Departments, Max Planck Institute for Chemistry, Mainz, Germany

[11]Yugra State University, 16 Chekhova str., 628012 Khanty-Mansiysk, Russia

[12]Bio-Clim-Land Center of Excellence, Tomsk State University, Tomsk, Russia

[13]A.N. Severtsov Institute of Ecology and Evolution, RAS, 33 Leninsky pr., 119071 Moscow,

[14]Institute for Climate and Global Change Research & School of Atmospheric Sciences, Nanjing University, 210023 Nanjing, China

[15]Institute of Remote Sensing and Digital Earth, Chinese Academy of Sciences, Beijing, 100094, China

[16] I.V. Sukachev Institute of Forest, SB RAS, Krasnoyarsk, Russia

Keywords: PEEX REGION, GROUND-BASED STATIONS, STATION NETWORKS, RESEARCH INFRASTRUCTURE

INTRODUCTION

The PEEX project (Kulmala et al. 2011b, Kulmala et al. 2015, Lappalainen et al. 2014) aspires to elucidate the climate change processes across Eurasia at a high spatiotemporal resolution. This target can only be achieved by integrating ground observations and remote sensing data, and the use of advanced modeling approaches (Kulmala et al. 2015). It is clear that in such a large region as Eurasia, only a very extensive ground-based observation network would yield satisfactory results. PEEX proposes such a network as a part of its 2nd focus area, PEEX Infrastructure (Hari et al. 2015, Kulmala et al. 2015, Kulmala et al. 2016). The Siberian region is currently lacking a coordinated coherent ground based atmosphere-ecosystem measurement network crucial for observing and predicting the effects of climate change in the

Northern Pan-Eurasian region. This study makes the first attempt to overview the existing ground station network and its development needs in the Arctic-Boreal region with the focus on Russia. The topics discussed here will be presented in more detail in the manuscript Alekseychik et al. (2016, in preparation).

METHODS

This study is based on the ground-based observational infrastructure inventory conducted by the Russian Academy of Sciences and Moscow State University together with the University of Helsinki. We begin with an overview of the existing facilities within Russia, and then discuss their geographical distribution, representativeness of ecosystems and climates. Particular attention was paid to the presence of modern instrumentation, such as aerosol measurement instruments and eddy-covariance setups.

With the use of mapping tools, spatial distribution of the research facilities was investigated in relation to the geographical areas, climates, and vegetation zones. The Natural Earth (http://www.naturalearthdata.com/) satellite-derived spatial data were used to build the underlying land cover map. For the climate analysis, the Köppen-Geiger classification scheme was employed. The Köppen-Geiger scheme classifies climates according to the seasonality and mean levels of precipitation and air temperature (Peel et al. 2007). A raster map of Köppen-Geiger climates by NASA Earth Data was used (http://webmap.ornl.gov/ogcdown/wcsdown.jsp?dg_id=10012_1). The heights of the sites above sea level, where the data were was missing, were estimated from a world digital elevation map (https://asterweb.jpl.nasa.gov/gdem.asp).

RESULTS

Fig. 1 shows the locations of the land observational facilities in the PEEX domain in comparison with the stations belonging to the major European environmental research infrastructures, such as ICOS (Integrated Carbon Observation System), Aerosols, Gases and Trace Gases Research Infrastructure network (ACTRIS), and the International Network for Terrestrial Research and Monitoring in the Arctic (INTERACT). It is easy to see the contrast between the well-covered (Western Europe, European Russia, West Siberia and East China) and the poorly covered regions (Northern Urals, Central and East Siberia, West China).

The sites in Russia equipped with aerosol or EC instrumentation are shown in Fig. 2. The emerging spatial distribution of the sites, while covering the main geographical units of Russia, still leaves extensive areas empty. The existing EC flux and aerosol measurements are concentrated in the Western part of European Russia, around the populated areas of West and central Siberia, around the Baikal Lake and along the Arctic Ocean coast. Some areas, including the North-East of European Russia, the Urals, and large areas of Siberia and the Russian Far East are not covered by the measurements at all. A number of stations contribute to the Global Atmospheric Watch network (WMO-GAW), providing data on precipitation chemical composition, total ozone and greenhouse gas concentrations from different parts of Russia.

For a more in-depth view, one may assess the number or observational stations for the climate/ecosystem pairs (see Table 1). This analysis reveals the apparent lack of any measurements or monitoring in many ecosystem/climate pairs. While the major temperate, Boreal, and arctic climates (*Dwc*, *Dfb*, *Dfc*, tundra) can be described as well as represented in terms of ecosystem coverage, the rest climates are poorly covered by measurements.

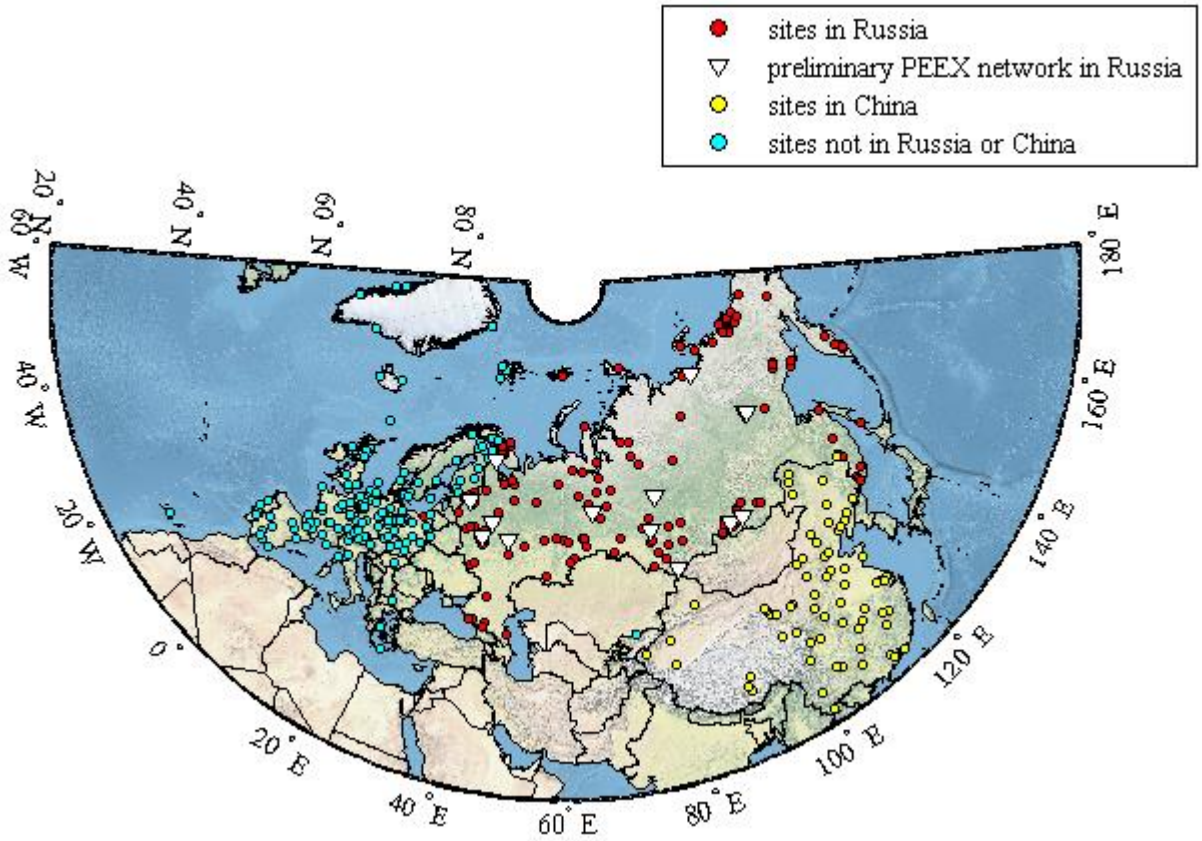

Fig.1. Locations of permanent ground-based observational stations in the PEEX domain (Lappalainen et al. 2016, manuscript in preparation).

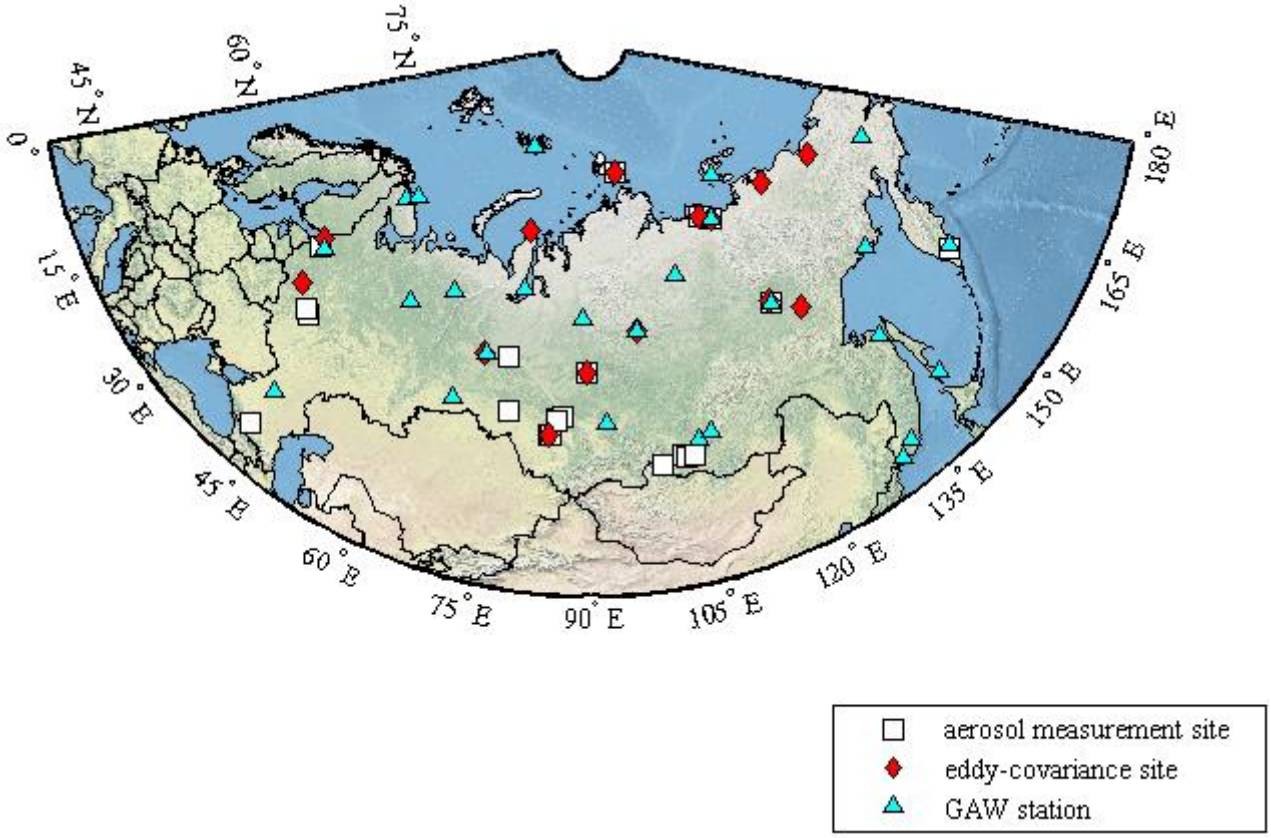

Fig.2. Eddy-covariance, aerosol measurement sites and GAW stations in Russia.

Mountainous areas in many climatic zones are represented as scantly. A few climates represented by small fractions of land do not host any measurement stations at all. It is particularly striking that the number of permanent wetland sites is incomparably smaller then the number of forest sites, in all climates. The steppe climate *Bsk* and one of the boreal types *Dfd* are also represented by a disproportionately small number of stations. Although the population is sparse in large parts of Siberia and the Russian Far East, sizeable urban areas do occur everywhere, and they, too, frequently lack continuous observations.

Table 1. Russian land-based station numbers for the climate/ecosystem pairs. "Cover fraction" is the fraction of the land area a given climate makes up of the total land area within 45˚-90˚ N, 15˚-180˚ E. Green shading indicates the presence of at least one station in a given combination of climate and ecosystem, while brown shading highlights the absence of stations. "Freshwater" unifies rivers, lakes and reservoirs. "Wetland" unifies peatlands of all types. The station counts of 10 or more are entered in bold numbers.

Köppen-Geiger climate type description	**Cover fraction (%)**	**K-G index**	**Ecosystem types**							
			freshwater	wetland	forest	steppe	high-elev.	tundra	marine	urban
mild desert	1.5	Bwk	0	-	-	-	-	-	-	0
mild steppe	5.9	Bsk	0	-	-	1	1	-	0	0
humid subtropical	<<1	Cfa	1	0	0	-	2	-	1	0
humid continental	<<1	Dsb	0	0	0	-	0	-	0	0
boreal, cold/dry summer/cold summer	0.5	Dsc	0	0	0	-	0	-	0	0
boreal, cold/dry summer/very cold winter	0.1	Dsd	0	0	0	-	0	-	-	0
humid continental, cold/dry winter/hot summer	0.7	Dwa	0	0	0	-	0	-	0	0
humid contin., cold/dry winter/warm summer	0.2	Dwb	1	0	2	-	2	-	0	2
boreal, cold/dry winter/cold summer	7.5	Dwc	2	0	**14**	1	1	1	0	2
boreal, cold/dry winter/very cold winter	1.6	Dwd	0	0	0	-	0	-	0	0
humid contin., cold/no dry season/hot summer	2.4	Dfa	0	0	0	-	1	-	-	1
humid contin., cold/no dry season/warm summer	19.5	Dfb	**16**	3	**27**	4	0	-	1	**15**
boreal, cold/no dry season/cold summer	44.3	Dfc	6	3	**42**	-	2	**13**	0	**12**
boreal, cold/no dry season/very cold winter	6.9	Dfd	0	2	4	-	0	0	-	1
polar/tundra	8.6	ET	0	0	-	-	0	**25**	1	0
polar/frost/ice	0.3	EF	0	-	-	-	0	-	1	-

CONCLUSIONS

The success of the PEEX mission to provide the next generation solutions to the climate change problems directly depends on the quality and coverage of the ground station data. The ground measurement network in its current shape needs being upgraded and extended to the previously under-represented ecosystems and climatic zones. To address these needs, we motivate the foundation of a network of Flagship, Flux and Standard stations that would cover the PEEX domain. The region under consideration features some of the most remote areas of the world, with harsh climate, low infrastructure development and sparse population. While the existing Eurasian research infrastructure provides a

valuable basis, building a network complying with the criteria proposed by Hari et al. 2015 will require extensive efforts.

ACKNOWLEDGEMENTS

We acknowledge the support from “International Working Groups, Markku Kulmala” Grant by Finnish Cultural Foundation; Academy of Finland projects ICOS 271878; ICOS-Finland project No. 281255; ICOS-ERIC projects No. 281250, No. 259537, 218094, 255576, 286685, 280700 and 259537; Tekes project Beautiful Beijing; Nordforsk NCoE-CRAICC project № 26060; the Academy of Finland Centre of Excellence (project No. 272041 and 118780); Finnish Academy of Sciences Academy Professor projects (No. 1284701 and 1282842); ICOS (project No.271878); ICOS-Finland (project No.281255); Nordic Centre of Excellence DEFROST; Faculty of Science and Forestry, University of Eastern Finland; Norwegian University of Technology (NTNU); the Centre for Studies of Carbon Cycle and Climate Interactions (LUCCI) financed by a Linnaeus grant (Swedish research council); CRAICC-PEEX-Amendment to contact 26060; Russian Science Foundation grant №14-27-00065; Russian Foundation for Basic Research grants №14-05-00526, №14-05-00590, №14-05-93089, №15-05-07622 and №15-44-00091. We acknowledge the financial support from the grant in accordance with the Resolution of the Government of the Russian Federation No. 220 dated April 09, 2010, under Agreement No. 14.B25.31.0001 with the Ministry of Education and Science of the Russian Federation dated June 24, 2013 (BIO-GEO-CLIM). We gratefully acknowledge the assistance of the staff of N. Pertsov White Sea Biological Station (Moscow State University). Finally, we acknowledge the support of the International Network for Terrestrial Research and Monitoring in the Arctic INTERACT for funding the project “Greenhouse gas exchange in boreal wetland and freshwater ecosystems: a multi-scale approach” (GHG-FLUX).

REFERENCES

Hari, P., Petäjä, T., Bäck, J., Kerminen, V-M., Lappalainen, H. K., Vihma, T., Laurila, T., Viisanen, Y., Vesala, T. and Kulmala, M. (2015).Conceptual design of a measurement network of the global change, Atmos. Chem. Phys. Discuss., 15, 21063−21093.

Kulmala, M., Alekseychik, P., Paramonov, M., Laurila, T., Asmi, E., Arneth, A., Zilitinkevich, S. and Kerminen, V.-M. (2011). On measurements of aerosol particles and greenhouse gases in Siberia and future research needs. Boreal Env. Res. 16, 337-362.

Kulmala, M., Lappalainen, H.K., Petäjä, T., Kurten, T., Kerminen V.-M., Viisanen, Y., Hari, P., Sorvari, S., Bäck, J., Bondur, V., Kasimov, N., Kotlyakov, V., Matvienko, G., Baklanov, A. Guo, H.D., Ding A., Hansson H.-C. and Zilitinkevich, S. (2015). *Introduction*: The Pan-Eurasian Experiment (PEEX) – multi-disciplinary, multi- scale and multi-component research and capacity building initiative, Atmos. Chem. Phys., 15, 13085-13096.

Kulmala, M., Lappalainen, H.K., Petäjä, T., Kerminen, V.-M., Viisanen, Y., Matvienko, G.,Melnikov, V., Baklanov, A., Bondur, V., Kasimov, N. and Zilitinkevich, S. (2016). Pan-Eurasian Experiment (PEEX) Program: Grant Challenges in the Arctic-boreal context.to be submitted to J. Geography, Environment, Sustainability.

Lappalainen, H.K., Petäjä, T., Kujansuu, J., and Kerminen, V-M., Shvidenko, A., Bäck, J., Vesala, T., Vihma, T., de Leeuw, G., Lauri, A., Ruuskanen, T., Flint, M., Zaitseva, N., Arshinov, M., Spracklen, D., Arnold, S., Juhola, S., Lihavainen, H., Viisanen, Y., Chubarova, N., Filatov, N., Skorokhod, A., Elansky, N., Dyukarev, E., Hari, P., Kotlyakov, V., Kasimov, N., Bondur, V., Matvienko, G., Baklanov, A., Guo H., Zilitinkevich, S. and Kulmala, M. (2014). Pan-Eurasian Experiment (PEEX) – a research initiative meeting the grand challenges of the changing environment of the northern Pan-Eurasian arctic-boreal areas, J. Geography, Environment, Sustainability, 2, 13-48.

H. K.Lappalainen, V. M Kerminen, T. Petäjä, T. Kurten, A. Baklanov, A. Shvidenko, J. Bäck, T. Vihma, P. Alekseychik, S. Arnold, M. Arshinov, E. Asmi, B. Belan, L. Bobylev, S. Chalov, Y. Cheng, N. Chubarova, G.de Leeuw, A. Ding, S. Dobrolyubov, S. Dubtsov, E. Dyukarev, N. Elansky, K. Eleftheriadis, I. Esau, N. Filatov, M. Flint , C. Fu, O. Glezer, A. Gliko, M. Heimann, B. Holtslag, J.

Janhunen, S. Juhola, L. Järvi, H. Järvinen, A. Kanukhina, P. Konstantinov, V. Kotlyakov, A-J. Kieloaho, A. Komarov, J. Kujansuu, I. Kukkonen, A. Laaksonen, T. Laurila, H. Lihavainen, A. Lisitzin, A. Mahura, A. Makshtas, E.Mareev, D. Matishov, S. Mazon, V. Melnikov, E. Mikhailov, D. Moisseev, R. Nigmatulin, S.M. Noe, A. Ojala, M. Pihlatie1, O. Popovicheva, J. Pumpanen, T. Regerand, I. Repina, A. Shcherbinin, V. Shevchenko, M. Sipilä, A. Skorokhod, D.V. Spracklen, H. Su, D. Subetto, J. Sun, A. Terzhevik, Y. Timofeyev, Y. Troitskaya, V-P. Tynkkynen, V.I. Kharuk, N. Zaytseva, J. Zhang, Y. Viisanen, T. Vesala, P. Hari, H-C Hansson, G.Matvienko, N. Kasimov, H.Guo, V. Bondur, S. Zilitinkevich and M. Kulmala (2016). Pan-Eurasian Experiment (PEEX): Towards holistic understanding of the feedbacks and interactions in the land - atmosphere - ocean- society continuum in the Northern Eurasian region, to be submitted to Atmos. Chem. Phys.

Peel, M., Finlayson, B. and McMahon, T. (2007). Updated world map of the Köppen-Geiger climate classification, Hydrol. Earth Syst. Sci., 11, 1633–1644.

AEROSOL DETECTION ANALYSIS FROM SATELLITE DURING THE HARVEST SEASON OVER NORTH CHINA PLAIN

X.AN[1], J.ZHANG[2] ,X.LIU[1] AND F.YAO[3]

[1] School of geoscience, Yangtze University,
Wuhan, Caidian District, NO.1 Daxue Road, China.

[2] Lab of Digital Earth Science, Institute of Remote Sensing and Digital Earth Chinese Academy of Sciences,
Beijing, Haidian District, NO.9 Dengzhuang South Road, China.

[3]College of Earth Science, Graduate University of Chinese Academy of Science,
Beijing, Shijiangshan District, NO.19 Yuquan Road, China.

Keywords: AEROSOL OPTICAL DEPTH, BIOMASS BURNING, FINE MODE FRACTION, FIRE HOTSPOTS.

INTRODUCTION

Aerosol produced by biomass burning affects the global atmospheric environment, and is an important factor in global climate system and ecological system (Andreae ,1991;Penner et al.,1992;Mandalakis et al.,2005). To investigate the aerosol pollution distribution pattern over the North China Plain during the harvest season of 2014 and the cause behind this, MODIS aerosol optical depth (AOD),aerosol fine mode fraction（FMF）,fire hotspots, and a backward trajectory in June of 2014 were analyzed.

METHODS

In this paper, we used daily satellite MODIS aerosol optical depth (AOD), aerosol fine mode fraction (FMF) and fire hotspots data to analysis the distribution of aerosol optical thickness and the fire distribution in the North China Plain in June 2014, and two interest areas (the southern part of North China and Yangtze River Delta) were chose and the month of June was divided into three periods. Through the contrast analysis of aerosol temporal and spatial distribution characteristics in different periods and two typical backward trajectory characteristics in the interest area, we determined the pollution sources and transmission paths during the summer harvest.

CONCLUSIONS

Results showed that the average AOD ranged from 1.2 to 2.0 in June and was much higher than the annual average AOD of 1.0-1.2 in 2014.The fire hotspots distribution primarily concentrated during the period of June 6-14, leading to AOD values higher than those prior to (after) this period investigated here. Over two regions of interest such as southern part of North China Plain and Yangtze River Delta, the fine particle increased during the period with intensive fire hotspots detected by MODIS, which could be likely due to straw burning. Backward trajectory simulation analyses further confirmed that air pollution basically originated from regions characterized by heavy fire spots. Both MODIS AOD and backward trajectory analyses showed that the biomass burning during harvest season resulted in such heavy aerosol pollution episode.

ACKNOWLEDGEMENTS

This work was supported by the 1-3-5 Innovation Project of the Chinese Academy of Sciences (NO. Y3ZZ15101) and the Hundred Talents Program of the Chinese Academy of Sciences (NO.Y1ZZ12101A).

REFERENCES

Andreae M.0.(1991). Biomass burning: Its history use, and distribution and its impact on environmental quality and global climate,A.Global biomass burning: atmospheric climatic , and biospheric implications[C].Cambridge, Mass: MIT Press,3-21

Mandalakis M., Gustafsson O., Alsberg T., et al(2005).Contribution of Biomass Burning to Atmospheric Polyeyclie Aromatic Hydrocarbons at Three European Background Sites, J. Environ .Sci. Technol.,39(9):2976-2982.

Penner J.E., Diekinson R.E., O'Neill R.E(1992).Effects of aerosol from biomass burning on the global radiation budget ,J.Science ,256,1432-1434.

PRELIMINARY EVALUATION OF AN URBAN LAND SURFACE MODEL IN SHANGHAI

X.Y. AO[1], C.S.B. GRIMMOND[2], J.G. TAN[1], Y.Y. CHANG[1], D.W. LIU[1], Y.Q. TANG[1]

[1.] Shanghai Institute of Meteorological Science, Shanghai 200030, China.

[2.] Department of Meteorology, University of Reading, Earley Gate, PO Box 243, Reading, RG6 6BB, UK.

Keywords: SUEWS, SHANGHAI, RADIATION FLUX, TURBULENT HEAT FLUX.

INTRODUCTION

Two thirds of the world's population will live in cities by 2050, with the most rapid rates of urbanization in Asia and Africa. Urban growth has been particularly rapid in eastern China following the reform policies and opening-up in the late 1970s. Urbanization alters both the surface and the atmosphere. These alterations result in modifications to the urban surface energy, mass and momentum exchanges (Loridan and Grimmond 2012) creating distinct urban climate features such as the urban heat island, enhanced heat waves and flooding. In the numerical models, the surface energy balance (SEB) is the key factor that determines the dynamic thermal distribution near the surface. Therefore, an accurate description of the urban SEB is important for improving the capacity to simulate the urban area in numerical weather forecast models. Over the last decade there have been significant advances in Urban Land Surface Models (ULSM) (Grimmond et al. 2010). These ULSM has been used in many mesoscale numerical models. However, the capability of these ULSM is not well tested because of the lack of observations in urban area. As the structure of the urban area in China has many more tall buildings and therefore potentially more complicated than that of many European or American cities, it is necessary to investigate the applicability of these ULSM for the different urban areas. In this study, the surface urban energy and water balance scheme (SUEWS, Järvi et al. 2011) and the local-scale urban meteorological scheme (LUMPS, Grimmond and Oke 2002, Loridan et al. 2011) is evaluated based on a full year (December 2012 – November 2013) SEB observations at a Shanghai urban site, China. SUEWS and LUMPS use the surface energy balance (SEB) as one of their basic frameworks:

$$Q^*+Q_F=Q_H+Q_E+\Delta Q_S$$

where the flux densities (W m^{-2}) are: Q* the net all-wave radiation, Q_H the turbulent sensible heat flux, Q_E the latent heat flux and ΔQ_S the net storage heat flux. The methods used to determine each flux can be seen in previous papers (Offerle et al. 2003, Järvi et al. 2011, Loridan et al. 2011, Ward et al. 2016).

METHODS

SUEWS and LUMPS (V2015a) was run for an area of 500 m radius around a measurement site in Shnaghai. The measurements were undertaken in a dense neighbourhood with tall buildings (XJH site, 31.19 °N, 121.43 °E) at the headquarters of the Shanghai Meteorological Service. The micrometeorological instrumentation was mounted on the top of a 25 m triangular tower (side = 0.45 m) installed on the roof of the 55 m high building. Thus, the main sensors are 80 m above ground level (agl). The turbulent fluxes (Q_H, Q_E) are measured with an open-path infrared absorption gas analyzer integrated with a three-dimensional sonic anemometer (IRGASON, Campbell Scientific). A net radiometer (CNR4, Kipp & Zonen) measures the four components of net all-wave radiation, A Vaisala HMP155A probe measures air temperature and relative humidity. Precipitation is measured with a Vaisala MILOS500 automated meteorological station (AWS) at the Xujiahui Observatory (60 m from the tower). The storage heat flux (ΔQ_S) is determined as the residual in the SEB. Details of instrumentation and data processing can be seen in Ao et al. (2016).

The model was run for December 2012 through November 2013. The downward longwave radiation L↓ is simulated using air temperature and relative humidity. Local field surveys were conducted to aid determination of the required model input parameters. To evaluate the performance the root mean square error (RMSE), mean bias error (MBE) and mean absolute error (MAE) are used with locally observed fluxes.

CONCLUSIONS

Evaluation of the components of the radiation balance shows that the model can reproduce the diurnal patterns (Figure 1). The daily peak of net all-wave radiation flux (Q*) was underestimated by about 25 W m^{-2}. The amplitude of the diurnal variation of the downward long-wave radiation flux (L↓) was underestimated for all seasons, the performance for upward long-wave radiation flux (L↑) was much better than L↓.

The time of the daily peak of sensible heat flux (Q_H) for each season (except spring) was simulated well by SUEWS, while the magnitude of Q_H for each season was underestimated. The performance of SUEWS model for latent heat flux (Q_E) in winter, spring and autumn was good, while the simulated Q_E in summer was much lower than the observed Q_E. SUEWS model successfully reproduced the transition time of the sign of the storage heat flux (ΔQ_S) in winter, spring and autumn, while has a lag about 2 h in summer. The seasonal variation of the model performance for ΔQ_S was relatively large (Fig. 2).

Analysis of the model error (not shown) dependency on a set of meteorological variables indicates that there was an increased underestimation of Q_H and Q_E and increased overestimation of ΔQ_S under higher air temperature or stronger wind speed conditions. The Q_H has an obvious underestimation by about -50 W m^{-2} for easterly wind while overestimation by about 15 W m^{-2} for the westerly wind mainly due to the model parameters currently being for an areal average rather than varying by turbulent flux footprint. So there is no consideration of the dense buildings to the east and the green park to the west in the model runs.

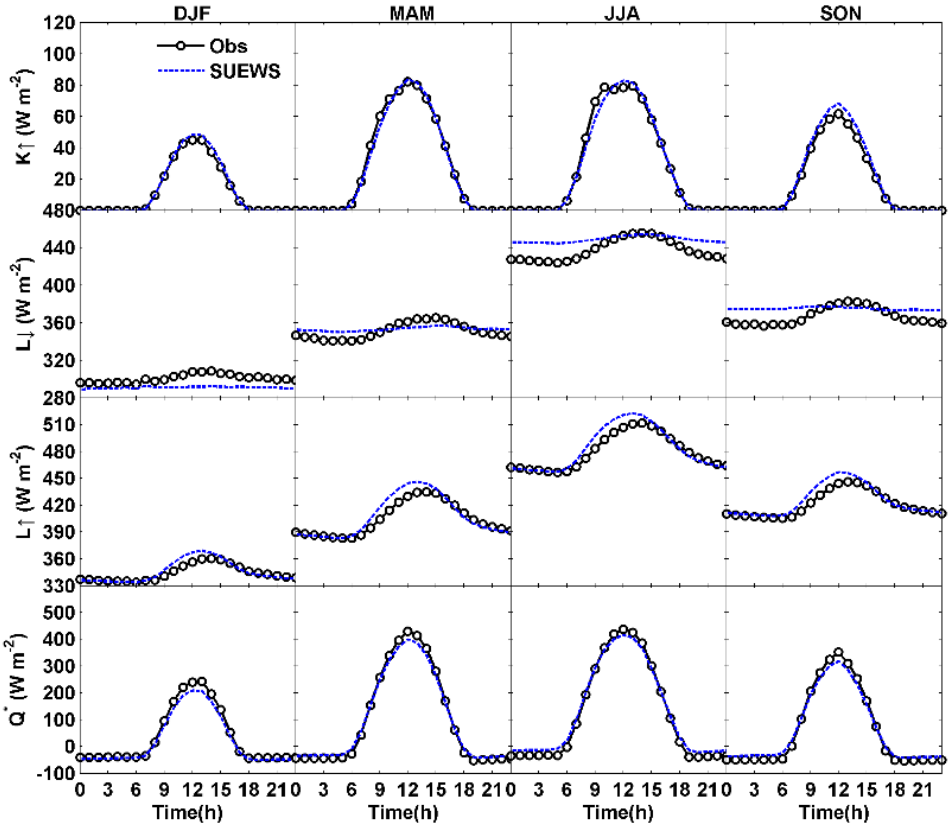

Figure 1 Comparison of modelled and observed seasonal (DJF: winter; MAM: spring; JJA: summer; SON: autumn) mean diurnal variation of radiative fluxes: K↑, upward shortwave radiation flux; L↓, downward longwave radiation flux; L↑, upward longwave radiation flux; Q^*; net all-wave radiation flux.

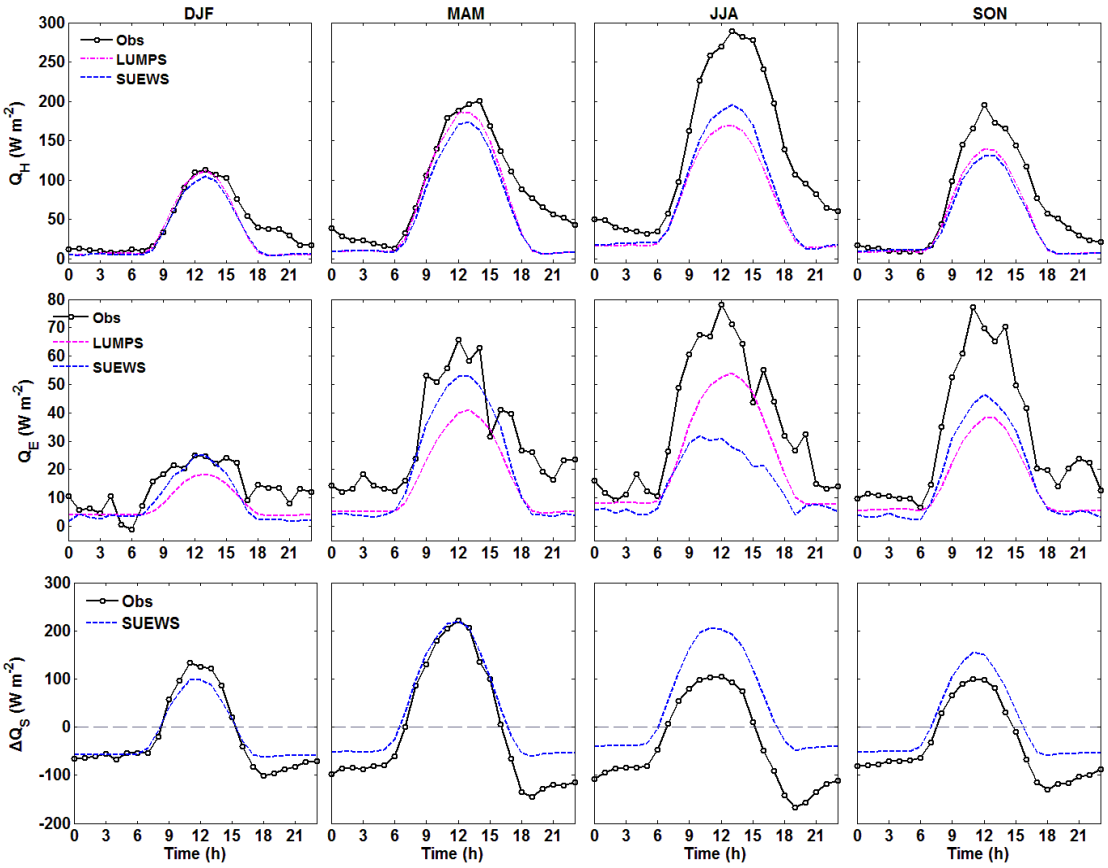

Figure 2 Comparison of modelled (SUEWS/LUMPS) and observed seasonal mean diurnal variation of sensible heat flux (Q_H); latent heat flux (Q_E) and storage heat flux (ΔQ_S).

ACKNOWLEDGEMENTS

This work was supported by The Natural Science Foundation of China (No. 41275021), China Special Fund for Meteorological Research in the Public Interest (No.GYHY201306055; GYHY201306010), the Research Programme of the Shanghai Meteorological Service (YJ201404) and the UK-China Research & Innovation Partnership Fund through the Met Office Climate Science for Service Partnership (CSSP) China as part of the Newton Fund (Grimmond). All those who support the operations of the instrumentation are gratefully thanked for their contributions.

REFERENCES

Ao XY, Grimmond CSB, Chang YY, Liu DW, Tang YQ, Hu P, Wang YD, Zou J, Tan JG (2016) Heat, water and carbon exchanges in the tall megacity of Shanghai: Challenges and results, International Journal of Climatology (In press).

Grimmond CSB, M Blackett, M Best, J Barlow, JJ Baik, S Belcher, SI Bohnenstengel, I Calmet, F Chen, A Dandou, K Fortuniak, ML Gouvea, R Hamdi, M Hendry, T Kawai, Y Kawamoto, H Kondo, ES Krayenhoff, SH Lee, T Loridan, A Martilli, V Masson, S Miao, K Oleson, G Pigeon, A Porson, YH Ryu, F Salamanca, GJ Steeneveld, M Tombrou, J Voogt, D Young, N Zhang 2010: The International Urban Energy Balance Models Comparison Project: First results from Phase 1 J. of Applied Meteorology & Climatology, 49**,** 1268-92,

Järvi L, Grimmond CSB and Christen A (2011) The Surface Urban Energy and Water Balance Scheme (SUEWS): Evaluation in Los Angeles and Vancouver. J Hydrol 411: 219-237.

Loridan T, Grimmond CSB, Offerle BD, Young DT, Smith TEL, Järvi L and Lindberg F (2011) Local-Scale Urban Meteorological Parameterization Scheme (LUMPS): Longwave Radiation Parameterization and Seasonality-Related Developments. J Appl Meteorol Climatol 50: 185-202.

Loridan T, Grimmond CSB (2012) Characterization of Energy Flux Partitioning in Urban Environments: Links with Surface Seasonal Properties. J Appl Meteor Climatol, 51: 219–241.

Offerle B, Grimmond CSB and Oke TR (2003) Parameterization of Net All-Wave Radiation for Urban Areas. J Appl Meteorol 42: 1157-1173.

Ward HC, Kotthaus S, Järvi L, Grimmond CSB (2016) Surface Urban Energy and Water Balance Scheme (SUEWS): development and evaluation at two UK sites (under review).

RADIATIVE FORCING SENSITIVITY TO MODEL BIAS IN HIGH LATITUDE OZONE PROFILES

S.R. ARNOLD[1], K.S. LAW[2] and S.A. MONKS[3,4]

[1]Institute for Climate and Atmospheric Science, School of Earth & Environment, University of Leeds, Leeds, LS2 9JT, United Kingdom.

[2]Sorbonne Universités, UPMC Univ. Paris 06; Université Versailles St-Quentin; CNRS/INSU; LATMOS-IPSL, UMR 8190, Paris, France.

[3]Earth System Research Laboratory, National Oceanic and Atmospheric Administration, Boulder, Colorado, United States.

[4]Cooperative Institute for Research in Environmental Sciences, University of Colorado, Boulder, Colorado, United States.

Keywords: ARCTIC, OZONE, CLIMATE, ATMOSPHERIC CHEMISTRY

INTRODUCTION

Model calculations suggest that changes in short-lived climate pollutants (SLCPs) such as ozone and aerosol may have contributed significantly to rapid Arctic warming over the past century (Shindell and Faluvegi, 2009). Arctic tropospheric budgets of SLCPs are impacted by long-range transport of trace gases and aerosols from Europe, Asia and N. America, but also by local sources such as gas flaring, shipping and boreal fires. Recently, model comparison exercises, such as the POLARCAT Model Intercomparison Project (POLMIP) (Emmons *et al*., 2015) and the Arctic Monitoring and Assessment Programme report on Black Carbon and Ozone in the Arctic (AMAP, 2015), have shown that significant model biases persist through the depth of the European and North American high latitude troposphere in simulated trace-gas and aerosol abundances compared with aircraft observations. These biases in the mid an upper troposphere, suggest that models do not adequately simulate the influence of remote emission sources at mid-latitudes on high latitude SLCP budgets. This has implications for our confidence in model predictions of high latitude SLCP response to future mid-latitude emission changes, and the ability of models to correctly simulate climate response to SLCPs at high latitudes. In particular, the radiative forcing efficiencies of both ozone and black carbon aerosol are highly sensitive to their vertical concentration profiles in the troposphere.

METHODS AND RESULTS

In this study we investigate the sensitivity of modelled ozone production in plumes imported into the Eurasian Arctic to the simulated background tropospheric ozone profile. We use a tropospheric chemical box model CiTTyCAT (Pugh *et al*., 2012), to simulate the ozone evolution in upper tropospheric air masses initialised with a pollutant signature of reactive nitrogen (NO_Y) and volatile organic compounds (VOCs), under different conditions of background ozone. Our box model experiments indicate that in models in which background ozone is biased high in the Arctic upper troposphere (UT), the ozone response to a given import of NO_Y into the UT is lower than in models where the UT ozone profile is close to that observed or biased low. This difference in ozone response is related to the difference in plume NO/NO_2 ratio produced by different background ozone concentrations. We also find strong sensitivity of this effect to VOCs in the imported plume, due to the role of PAN in changing the availability of NO_2 for ozone production. Our results imply that ozone radiative forcing estimates derived

from simulation of ozone response to regional emission perturbations may be biased low in models that have a high bias in UT ozone, which is commonly the case at high latitudes.

ACKNOWLEDGEMENTS

This work was supported by the UK Natural Environment Research Council under the BORNET-Eurasia grant (NE/L013347/1).

REFERENCES

AMAP, (2015), Black carbon and ozone as Arctic climate forcers, Arctic Monitoring and Assessment Programme (AMAP), Oslo, Norway. vii + 116 pp.

Emmons, L. K., Arnold, S. R., Monks, S. A., Huijnen, et al., (2015), The POLARCAT Model Intercomparison Project (POLMIP): overview and evaluation with observations, *Atmos. Chem. Phys.*, **15**, 6721-6744, doi:10.5194/acp-15-6721-2015.

Pugh, T. A. M., Cain, M., Methven, J., Wild, O., Arnold, S. R., et al., (2012), A Lagrangian model of air-mass photochemistry and mixing using a trajectory ensemble: the Cambridge Tropospheric Trajectory model of Chemistry And Transport (CiTTyCAT) version 4.2, *Geosci. Model Dev.* , **5**, 193-221, doi:10.5194/gmd-5-193-2012.

Shindell, D. and G. Faluvegi (2009), Climate response to regional radiative forcing during the twentieth century, *Nature Geosci.* **4**, 294-300. doi:10.1038/ngeo473.

COOP+: PROMOTING THE COOPERATION AMONG INTERNATIONAL RESEARCH INFRASTRUCTURES TO ADDRESS GLOBAL ENVIRONMENTAL CHALLENGES

A. ASMI[1], L. JÄRVI[1] and F.J. BONET-GARCÍA[2]

[1]Department of Physics, University of Helsinki, Finland.

[2]Departamento de Ecología, Instituto Interuniversitario Sistema Tierra en Andalucía, Universidad de Granada, Spain

Keywords: RESEARCH INFRASTRUCTURES, INTERNATIONAL COLLABORATION, ENVIRONMENTAL CHALLENGES.

INTRODUCTION

During the Anthropocene, mankind will face several global environmental challenges. One of the first and more successful responses provided by Science to these challenges is the collecting of long-term series of biophysical variables in order to improve our knowledge of natural systems. The huge amount of information gathered during the last decades by Research Infrastructures (RIs) has helped to understand the structure and functioning of natural systems at local and regional scales. But how can we address the global cross-scale and cross-disciplinary challenges posed by the global environment change? We believe that it will be necessary to observe, model better and understand the whole biosphere using long term data generated by international RIs. RIs play a key role on many of the last advances and discoveries in science, from the observation of the Higgs Boson at CERN to the exploration of the Universe by the telescopes of the European Southern Observatory in Chile. The scale of complexity, instrumentation, computing resources, technological advances, and also of the investments, and the size of research collaborations, do not have precedents in Science. RIs in environmental field are developing fast, but the corresponding communities need yet to further reflect the need for a wider global collaboration because the challenges to tackle are in essence of global nature.

METHODS

This contribution describes how COOP+ project (EU Horizon 2020 Coordination and Support Action) will promote the cooperation among RIs at a global scale to address global environmental challenges. Our project evolves from the experience of the successful FP7 COOPEUS project (see http://www.coopeus.eu), which explored the use and access to data from RIs in environmental research in Europe and USA.

The general goal of COOP+ is to strengthen the links and coordination of the ESFRI RIs related to Marine Science (EMSO), Arctic and Atmospheric Research (EISCAT), Carbon Observation (ICOS) and Biodiversity (LifeWatch) with international counterparts (NEON, TERN, AMISR/SRI, CGSM, OOI, INPA/LBA, IMOS, OCN, AMERIFLUX, etc.) and to leverage international scientific cooperation and data exchange with non-EU countries.

During the time span of COOP+ (March 2016 to July 2018), we will address several important questions regarding RIs:

- What could be the contribution of international RIs to address cross-disciplinary global challenges like modelling and understanding the carbon cycle?
- Is it feasible to join the knowledge gathered in Arctic research with marine science outputs into comprehensive global models?

- What collaboration approaches could be implemented to foster the cooperation among RIs?
- What is the role of local observatories (bottom-up) in this cooperation framework?

CONCLUSIONS

This contribution will describe COOP+ project using the concept of global challenge. We will describe several possible case study that could be addressed by a network of international RIs.

ACKNOWLEDGEMENTS

This work is supported by the European Commission H2020 project COOP+ (654131).

ANALYSIS OF AEROSOL PROPERTIES DYNAMICS IN RELATION TO THE AIR MASS TRANSPORT DURING BAECC CAMPAIGN

K. ATLASKINA[1], V.-M. KERMINEN[1], P. AALTO[1], J. KONTKANEN[1], M. KULMALA[1] and T. PETÄJÄ[1]

[1]Department of Physics, University of Helsinki, Helsinki, Finland.

Keywords: AEROSOL-CLOUD INTERACTIONS, BIOGENIC AEROSOLS, BOREAL FOREST

INTRODUCTION

Boreal forest is a zone of active biogenic secondary organic aerosol (BSOA) formation. Tunved *et al*. (2006) showed that volatile organic compounds (VOC) originating from the forest contribute to the aerosol number concentration and mass growth during transport of clean marine air masses over the forested territories of Fenno-Scandinavian domain. BSOAs grow to the sizes sufficient to act as cloud condensation nuclei (CCN) (Kerminen *et al*, 2005), and can influence cloud properties, such as cloud lifetime, albedo or precipitation offset. Uncertainties related to the BSOA-cloud interaction remain high and need to be studied experimentally. Biogenic Aerosols – Effects on Clouds and Climate (BAECC) campaign (Petäjä *et al*, 2016) aimed to link biogenic aerosols and clouds took at place at the SMEAR II station in Hyytiälä, Finland, from February to September 2014. In this study we investigate properties of aerosols measured at the surface level during BAECC campaign. We concentrate on the properties dynamics in relation to the air mass history, namely the time that air mass spent over land (TOL). The goal of this work is to 1) describe aerosol properties observed during campaign; 2) study effect of air mass transport history; 3) evaluate representativeness of the campaign period.

METHODS

Data collected from April to September 2014 were analyzed. For the air mass history analysis we used the HYSPLIT (Hybrid Single Particle Lagrangian Integrated Trajectory) model four-day (96 h) 27-member ensemble mean backtrajectories arriving every hour at the 100-m height to the SMEAR II. The area of research is limited to a sector shown on the Figure 1, and trajectories that spent minimum 95% of travel time in the sector are selected. If for a given TOL number of trajectories was less than 5, corresponding data was discarded from the analysis. Total number of accepted trajectories is 1342. Measurements within the interval of ±1h from arrival time are averaged and attributed to a given trajectory for the further analysis.

Following data is considered in this study:

a) The number size distribution data collected with differential mobility particle sizer (DMPS)
b) New particle formation (NPF) event day classification
c) Mass of aerosols of sizes smaller than 450 nm from the number size distribution data
d) CCN concentrations at five supersaturation levels (S_C) from CCN counter. S_C of 0.1, 0.3 and 1.03% are discussed here
e) Critical diameter D_{cr} inferred from number size distribution

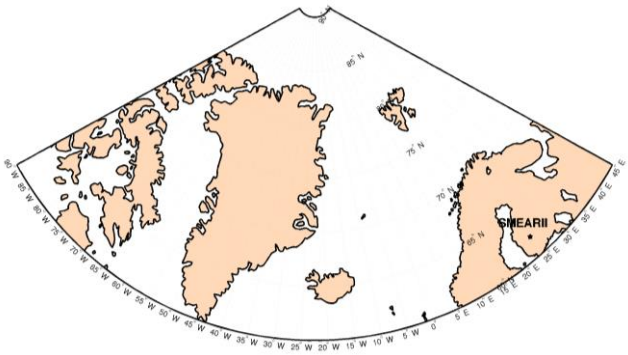

Figure 1. Map of the area used in the air mass history analysis. All territories west from Scandinavia are excluded from the time-over-land counting. Trajectory is accepted if it spent at least 95% of time within the sector. Total number of trajectories is 1342.

RESULTS

Observed aerosol number size distributions (Fig. 2) show that on average during campaign period shorter TOL is characterized by high number concentration in the nucleation mode with concentration as high as 4000 cm^{-3} peaking at the 20 nm. As time of travel increases, distribution mode shifts toward larger particles – Aitken mode for TOL of 30-60 h and accumulation mode for 80-90 h travel time. This finding agrees with long-term observations of size distribution at the SMEAR II station, confirming that longer travel time of air masses results in the prevalence of larger aerosols.

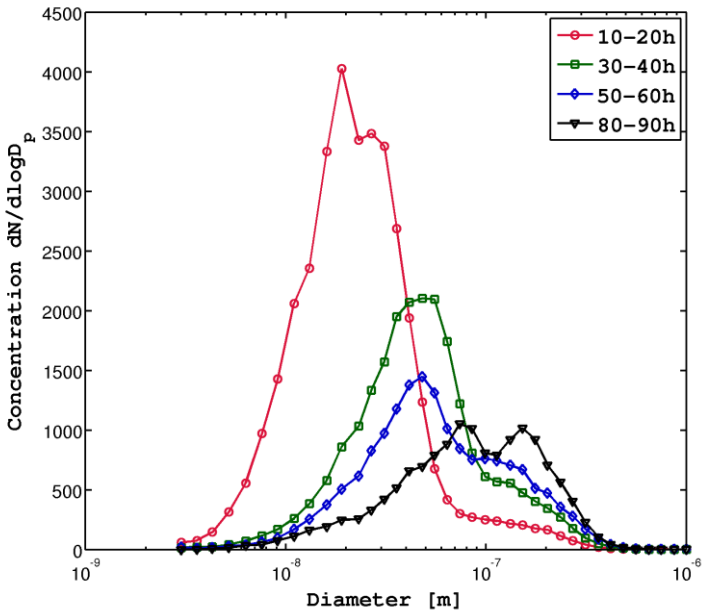

Figure 2. Median number size distribution for different times air mass spent over land.

Event days classification (Fig. 3) showed that arriving to the station clean air masses favor NPF events. Low aerosol loading in marine air masses that were moved over boreal forest results in a smaller condensation sink (CS) – a parameter that describes loss of condensable vapor molecules onto existing particles. In a favorable conditions, available VOCs have higher chances to participate in the nucleation process and form new aerosol particles. Similar results were also found previously for other sites situated in the boreal Finnish forest (see e.g. Väänänen *et al*, 2013).

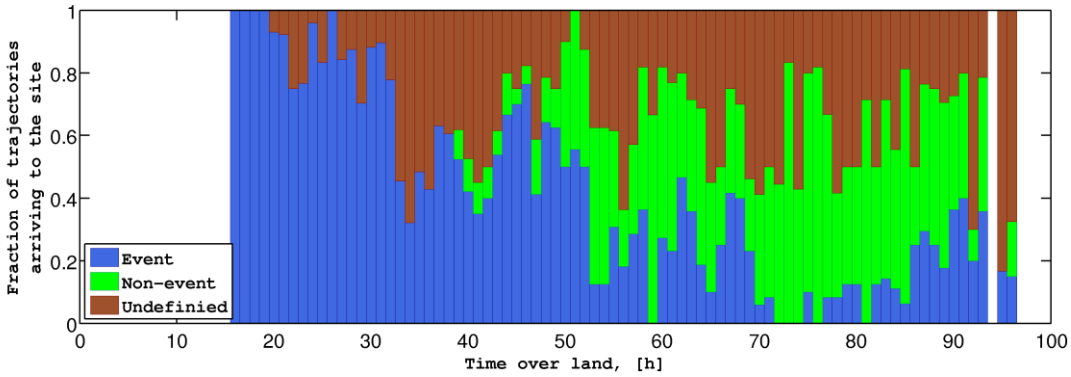

Figure 3. Fraction of trajectories arriving to the station during event, non-event and undefined days as a function of time air mass spent over land.

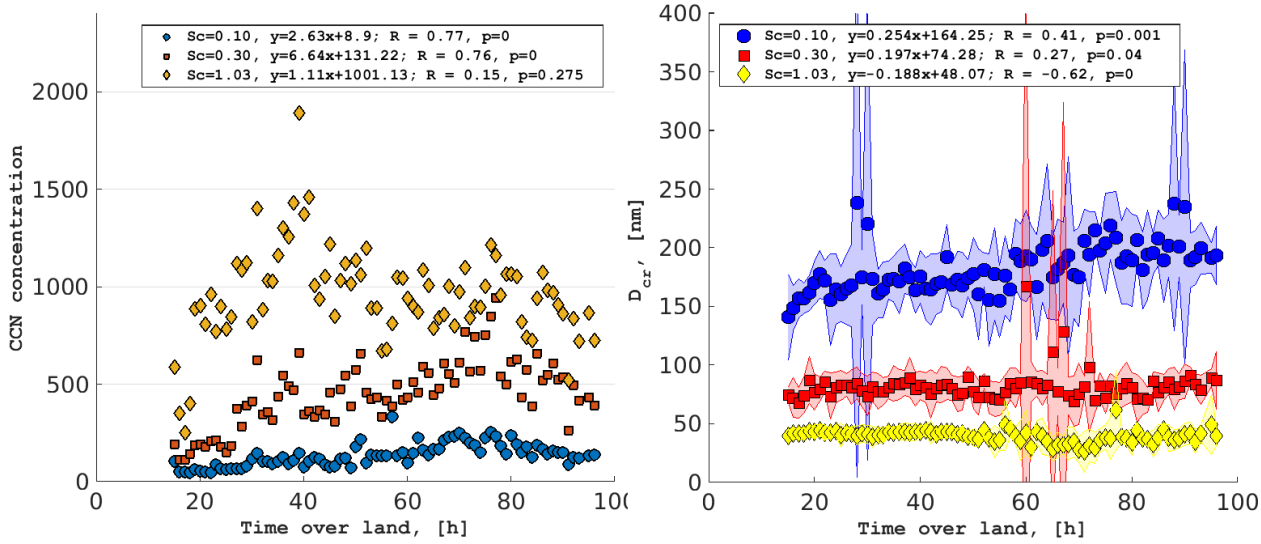

Figure 4. Left: Cloud condensation nuclei concertation [cm^{-3}] as a function of time air mass spent over land. Shown for supersaturation levels of 0.1, 0.3 and 1.03%. Linear weighted fit coefficients, correlation coefficients and corresponding p-values are shown in the legend. Right: Critical diameter inferred from DMPS size distribution data. Shaded area depicts ±STD. Linear weighted fit coefficients, correlation coefficient and corresponding p-values are shown in the legend.

As an air mass travels over the boreal forest, and aerosols grow in size, more aerosols particles can be activated as CCN and participate in the aerosol-cloud interaction. Measurements show that CCN concentrations increase by the number of 2.6 h^{-1} and 6.6 h^{-1} for S_C of 0.1% and 0.3% correspondingly. CCN concentrations at these two S_C increase for about 72 hours of travel time, and after that numbers start to drop. At the S_C of 0.1% and 0.3% aerosols with diameter from 150 nm to 70 nm are activated (Fig.4, right). At the shorter TOL, fewer large aerosol particles are present (Fig. 2), while nucleation processes produce particles of much smaller sizes. It takes tens of hours for a small particle to grow to the CCN sizes, and it is reflected at the CCN concentrations measurements.

At the largest measured supersaturation level of 1.03% much smaller particles (about 40 nm in diameter) can be activated as CCN. CCN concentration increase very fast at short TOLs, from 200 cm^{-3} after 16 h of travel time till 1500 cm^{-3} at about 40 h TOL. After that CCN concentration gradually decreases, that can be explained by the decrease of the total number concentration of aerosols larger than D_{cr} caused by coagulation losses. Critical diameter decreases by 0.2 nm h^{-1}, which means that aerosols become more hygroscopic with time as oxidized organic vapors condense on the growing particles. Sihto *et al.* (2011) observed similar behavior of D_{cr} at the S_C of 1.0% at the SMEAR II during an NPF event.

CONCLUSIONS

Our analysis shows that air mass history had strong influence on the observed aerosol properties during BAECC campaign period. We found that clean air arriving from the marine environment favors NPF and it goes in line with previous studies on this matter. If air mass continues traveling over boreal forest, VOCs are oxidized and condensed onto freshly formed aerosol particles. As a result, aerosol size grows, and size distribution shifts from nucleation to the Aitken and accumulation modes. More and more aerosols can be activated to CCN and influence formation and life of clouds.
We also conclude that campaign period represents well average conditions at SMEAR II station and can be used for the further studies of aerosol-cloud interaction in the boreal forest environment.

ACKNOWLEDGEMENTS

This work was supported by the Office of Science (BER), U.S. Department of Energy via Biogenic Aerosols - Effecs on Clouds and Climate (BAECC) and European Commission via projects ACTRIS and ACTRIS2, Academy of Finland Centre of Excellence in Atmospheric Sciences (grants no. 1118615 and 272041) and Nordforsk via Cryosphere-Atmosphere Interactions in a Changing Arctic Climate, CRAICC.

REFERENCES

Kerminen, V.-M., H. Lihavainen, M. Komppula, Y. Viisanen, and M. Kulmala (2005). Direct observational evidence linking atmospheric aerosol formation and cloud droplet activation, *Geophysical Research Letters*, **32** (14)

Petäjä, T., E.J. O'Connor, D. Moisseev, V.A. Sinclair, A.J. Manninen, R. Väänänen, A. von Lerber, J.A. Thornton, K. Nicoll, W. Petersen, V. Chandrasekar, J.N. Smith, P.M. Winkler, O. Krüger, H. Hakola, H. Timonen, D. Brus, T. Laurila, E. Asmi, M.-L. Riekkola, L. Mona, P. Massoli, R. Engelmann, M. Komppula, J. Wang, C. Kuang, J. Bäck, A. Virtanen, J. Levula, M. Ritsche, and N. Hickmon, (2016) BAECC, A field campaign to elucidate the impact of Biogenic Aerosols on Clouds and Climate, *Bull. Am. Met. Soc.* (accepted).

Tunved, P., H.-C. Hansson, V.-M. Kerminen, J. Ström, M. Dal Maso, H. Lihavainen, Y. Viisanen, P. P. Aalto, M. Komppula, and M. Kulmala (2006) High Natural Aerosol Loading over Boreal Forests, *Science*, **312,** 261-263.

Väänänen, R., E. M. Kyrö, T. Nieminen, N. Kivekäs, H. Junninen, A. Virkkula, M. Dal Maso, H. Lihavainen, Y. Viisanen, B. Svenningsson, T. Holst, A. Arneth, P. P. Aalto, M. Kulmala, and V. M. Kerminen (2013). Analysis of particle size distribution changes between three measurement sites in northern Scandinavia, *Atmos. Chem. Phys.* **13** (23), 11887-11903

WMO GLOBAL ATMOSPHERE WATCH (GAW) AND WORLD WEATHER RESEARCH PROGRAMME (WWRP) RESEARCH FOR THE NORTHERN EURASIA

A. BAKLANOV[1]

[1]World Meteorological Organization (WMO), Geneva, Switzerland.

Keywords: ATMOSPHERIC COMPOSITION, POLAR METEOROLOGY, SEAMLESS COUPLED MODELLING.

The World Meteorological Organization (WMO) is the UN system's authoritative voice on the state and behavior of the Earth's atmosphere, its interaction with the oceans, the climate it produces and the resulting distribution of water resources.

The Global Atmosphere Watch (GAW) programme of WMO (SSC chair G. Carmichael, AER chief O. Tarasova) is a partnership involving the Members of WMO, contributing networks and collaborating organizations and bodies which provides reliable scientific data and information on the chemical composition of the atmosphere, its natural and anthropogenic change, and helps to improve the understanding of interactions between the atmosphere, the oceans and the biosphere. GAW focal areas are aerosols, greenhouse gases, selected reactive gases, ozone, UV radiation and atmospheric deposition. More than 100 countries have registered more than 800 stations with the GAW Station Information System (GAWSIS). Various GAW expert groups and central facilities exist including:
- 7 Scientific Advisory Groups (SAGs) to organize and co-ordinate GAW activities by parameter, and the Expert Teams on World Data Centres (ET-WDC) and Near-Real-Time Chemical Data Transfer (ET-NRT CDT).
- 4 Quality Assurance/Science Activity Centres (QA/SACs) perform network-wide data quality and science-related functions.
- 35 Central Calibration Laboratories (CCLs) and World and Regional Calibration Centres (WCCs, RCCs) maintain calibration standards and provide instrument calibrations and training to the stations.
- 6 World Data Centres archive the observational data and metadata, which are integrated by GAWSIS.

The World Weather Research Programme (WWRP, SSC chair S. Jones, WWRD chief P. Ruti) advances society's resilience to high impact-weather through research focused on improving the accuracy, lead time and utilization of weather prediction. It engages with users and stakeholders to define research priorities and facilitate transition to applications. WWRP aims at Seamless Prediction of the Earth System from minutes to months using coupled systems – thus applying expertise in weather science to promote convergence between weather, climate and environmental communities.

The WWRP Polar Prediction Project (PPP, chair T. Jung) will promote cooperative international research in order to enable the development of improved weather and environmental prediction services for the Polar Regions on timescales from hours to seasonal. The PPP (http://polarprediction.net) is organizing the Year of Polar Prediction (YOPP), which will cover an extended period of coordinated intensive observational and modeling activities in order to improve polar prediction capabilities on a wide range of time scales in both Polar Regions.

The presentation includes suggestions for collaboration of the GAW and WWRP programmes with the PEEX program specifically for the YOPP campaigns and joint strategy for integrated environmental modelling relate to interactions of the atmosphere – aquatic - anthropogenic activities in the Northern Eurasia.

GEOGRAPHICAL AND GEO-ECONOMIC FACTORS AND DIRECTIONS OF THE LONG-TERM DEVELOPMENT OF PACIFIC RUSSIA

P.Ya. BAKLANOV

Pacific Geographical Institute, FEB RAS, Bldg. 7, Radio St., 690041, Russia

Keywords: FACTORS, REGIONAL DEVELOPMENT, PACIFIC RUSSIA.

In recent times, economic-geographical attraction of the eastern regions of Russia to the Pacific Ocean strengthens. By attraction level and the prerequisites of the developing marine-economical structures, three groups of the areas are well-pronounced: 1 – the maritime subjects of RF (the Chukot National Okrug, the Kamchatka, Primorskii and Khabarovskii Krais, the Sakhalin and Magadan Oblasts). 2 – the Republic of Sakha (Yakutia) enters the seas of the Arctic Ocean. 3- Amurskaya Oblast and Jewish Autonomous Oblast have no direct access to the Pacific Ocean but gravitate economically toward its resources, transport potential, the development of foreign economic relations through the Amur River and the Pacific Ocean. The TransSib-Baikal-Amur railways and the main oil pipeline “East Siberia” run toward the Pacific Ocean through this region. The largest gas-oil pipeline “Siberia’s Force” is being constructed. The 1st and 2nd groups experience the greatest gravitation toward the Pacific Ocean.

Within the maritime 200-mile economic zone contiguous to the dry land, the Russian sovereignty extends to all sea resources. But the coastal bases, ports and also close cooperation with them are necessary for their effective development.

Thus, the Far Eastern region within the Far Eastern Federal Okrug as well as contiguous to it the maritime 200-mile economic zone (about 5 million km2) and the Russian eastern part of the Arctic shelf (about 1.5 million km2) form the largest Russian aqua-territorial macro-region which can be called Pacific Russia (PR) [8]. The geographical factors of its long-run development include: a geographical and geoeconomic (economic-geographical) position; the natural-resource potential of the land and the sea, its distribution and dynamics; environmental conditions and their spatial differentiation, extreme natural phenomena as well as established territorial social-economic systems, their response and dynamics.

To the geoeconomic and geopolitical factors of the long-term development of the PR, the geopolitical position of the macro-region, its free access to the Far Eastern seas, the Arctic and Pacific Oceans, to the largest countries of the world – PRC, USA, Japan – as well as its multilevel trans-boundary nature – from the North-Pacific trans-boundary basin to trans-boundary basins of the North Pacific seas (Bering, Okhotsk, Japan-Eastern, Yellow) and trans-boundary basins of rivers (for example, the Amur, the Tumen River) should be referred.

The feature of action of the geographic factors is their spatial differentiation and dispersion. Their effect on the regional development is exercised through the geographical space. So, the natural-resource potential of the territory, as the geographical factor of the regional development acts through its natural-resource space. In the latter, the whole combination of natural resources of the territory (an area) with their spatial-temporal attributes as well as with the inter-resource relations and conjunctions is presented. The same specially-distributed effect is taken by the primary geographical factor – environmental conditions – through its geographical space.

The spatially-distributed effect on the regional development is exercised by the geographical and geoeconomic, economic-geographical positions, territorial social organization.

The most important characteristic of the geoeconomic position of the region (area) is its location with regard to the markets and market zones. Here, the external in relation to the area, the markets related to resources and markets for realization of finished goods and services are kept in mind. Such markets can be either primary or additional for the domestic markets of the region which will develop, diversify and extend in proportion to its economic development.

Within the bounds of the PR, there are various natural resources of the land and the sea, including ones with substantial stocks (reserves). By now, their estimates are available; however, they should be brought to the integrated assessments of the territorial and aqua-territorial combinations of natural resources. Just on the basis of such combinations, the different regional systems of nature management develop.

The most important feature of the environmental conditions having a very significant effect on the regional development is the extreme natural processes and their territorial combinations. In estimating the latter, it is expedient to use, to a greater degree, the cartographic methods.

In the Pacific Geographical Institute, FEB RAS the approaches to the functional zoning of territories and offshore strips (near-shore zones) were developed. On the ground of estimating the territorial and aqua-territorial combinations of natural resources and environmental constraints for certain parts of the territories and water areas, the priority-oriented and admissible types of nature management are identified. After that, the matrix models of the regional nature management for such territories can be developed which discover the whole circle of interrelations between the population and the kinds of activities, the combinations of natural resources and the components of the environment.

Taking into account the prognosis estimates stated in the Program of the regional development and generalizations of researches, the priority directions of the long-term development of the Pacific Russia are:
1. The development of different marine-economy structure, including harvesting and advanced processing of fish and sea foods, mariculture, shipbuilding and ship repairing, production of various equipment and devices for development of ocean resources, including autonomous underwater vehicles. The development of the sea transport, including the Northern Sea Route.
2. Extraction and treatment of ores of metals, including ones of ferrous, nonferrous, base metals, rare earth metals.
3. Oil and gas production, their transportation and processing with production of liquefied natural gas, different oil products, petrochemical products and products extracted from the natural gas which are used for domestic needs and export.
4. The development of the forest-industry structures, including the advanced processing of the low-grade wood and other forest resources, artificial regeneration of forests.
5. The development of tourism, including ecological, marine, northern ones.
6. The development of the research-education cluster, innovative technologies.
7. The development and modernization of the transportation infrastructure, including the trans-boundary one: railroad and highway, pipeline and electric-power.

The international ties, first of all, with the countries of the North-East Asia, will strengthen greatly.

EUROPEAN CENTRE OF INTERNATIONAL EURASIAN ACADEMY OF SCIENCES (EC-IEAS) – PRIORITIES AND COLLABORATION WITH PEEX

I. BASHMAKOVA[1]

[1]Division of Atmospheric Sciences, University of Helsinki, Finland

European Centre of IEAS (EC-IEAS) provides a bridge between the IEAS national science programs and international science communities in Eurasia. EC-IEAS aims to lead international and national activities, to play a proactive role in developing new research initiatives and research programs, to influence the research funding programs, etc.

General implementation: EC-IEAS coordinates the ongoing research and educational activities, guides the decisions on priorities and strategies for maintenance and enhancement of scientific research in Eurasia, and facilitates successful implementation of scientific initiatives in a way that is beneficial to the northern Eurasia region and the Global Change science.

Collaboration with Pan-Eurasian Experiment (PEEX): EC-IEAS represents an interdisciplinary research platform involving leading scholars from European countries. Current EC-IEAS activities focus on research and education in environmental sciences, but prospectively the focus area will be extended to a wide range of the exact sciences and the humanities. EC-IEAS maintains close collaboration with the recently launched international interdisciplinary program “Pan-Eurasian Experiment” (PEEX), which involves more than a hundred universities, research centers and enterprises in the European Union, Russia and China, and aims at resolving the major uncertainties in the Earth-system science and global sustainability questions in the Arctic and boreal Pan-Eurasian regions.

LONG TERM EFFECTS OF FIRE ON NORTHERN GREENHOUSE GAS EXCHANGES IN NORTHERN FORESTS

F, BERNINGER[1], K. KÖSTER[1], X. ZHOU[1], H. AALTONEN[1], M. PALVIAINEN[1] and J. PUMPANEN[2]

[1]Department of Forest Sciences, University of Helsinki, POBox 27, 00014 University of Helsinki, Finland

[2]Department of Environmental Science, University of Eastern Finland, P.O. Box 1627,70211 Kuopio, FINLAND

Keywords: FIRE, SOIL ORGANIC MATTER DECOMPOSITION, CARBON BALANCE

INTRODUCTION

About 1% of the boreal land area is burning each year and boreal forest fires are major problems for air quality and a large source of CO2 and black carbon. Also it is likely that boreal forest fires will increase in the future due to climate change. While the direct emissions of carbon from forest fires have received quite a lot of attention there is less research on how forest fires will affect the carbon turnover in the years and decades after the burn.

METHODS

We established three chronosequences consisting of forests of different ages after fires in Northern Finland (69 ºN 27 ºE), Yukon Canada (63 ºN 136ºW) and at the border of Yukon and the North West Territories (67 ºN 137 ºW). The species of the sites were Scots pine (Finland) and white and black spruce (Canada). The series were spanning ages after fire of 2-3 year to over 100 years.

On each site we measured the ecosystem carbon stocks, productivity of the tree layer as well as the fluxes of CO_2. CH_4 and N_2O using chambers. Carbon turnover was furthermore measured in the laborartory from incubated soil samples. Also microbial biomasses and fungal biomass (using ergosterol as an indicator) were measured.

RESULTS

On the permafrost site the fire lead a clear increase in the depth of the active layer. (Figure 1) The results indicate that fires slow down the turnover of soil organic matter for at period of at least 40 years. This decrease in the carbon turnover was related to a reduction of the fungal biomass.(Köster et al. 2014).

The slow recovery of fungal biomass after fires seems to be the cause of the decrease since sites with a higher concentration of fungal biomass in the soils had shorter soil organic matter turnover rates. Increases in stand foliar biomass were less important for the turnover of soil organic matter.

We tried to explore the potential importance of our finding using a simple data driven simulation model that estimates soil carbon dynamic from litter input and the measured soil carbon turnover times. The results indicate the initial post-fire slowdown of soil carbon turnover is an important component of the boreal carbon cycle. Using our fire intervals the simulated soil carbon stocks with a lower post-fire soil organic matter turnover were up to 15 % larger than simulations assuming a constant carbon turnover rate. Our sensitivity analysis indicates that the effects will be larger in areas with frequent fires. We do not know which environmental factors cause the delay in the turnover time and the effects of fires on post fire soil organic matter turnover could be considerably smaller or larger. Altogether our results fit well to published results from laboratory studies and show that post-fire depression of microbial activities are important on the ecosystem and landscape level.

CONCLUSIONS

The results show that fires have long term cosequences for the carbon turnover in forest ecosystems. A better description of the long term efffects of fires on boreal carbon and greenhouse gas balances is, therefore, imperative for a better understanding of the role of boreal forests in the climate system.

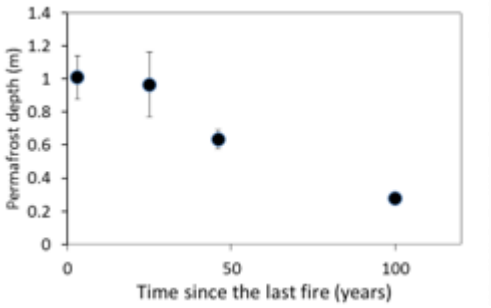

Figure 1 Depths of the Active layer vs time since last fire for the chronosequence in Yukon North West terriotires.

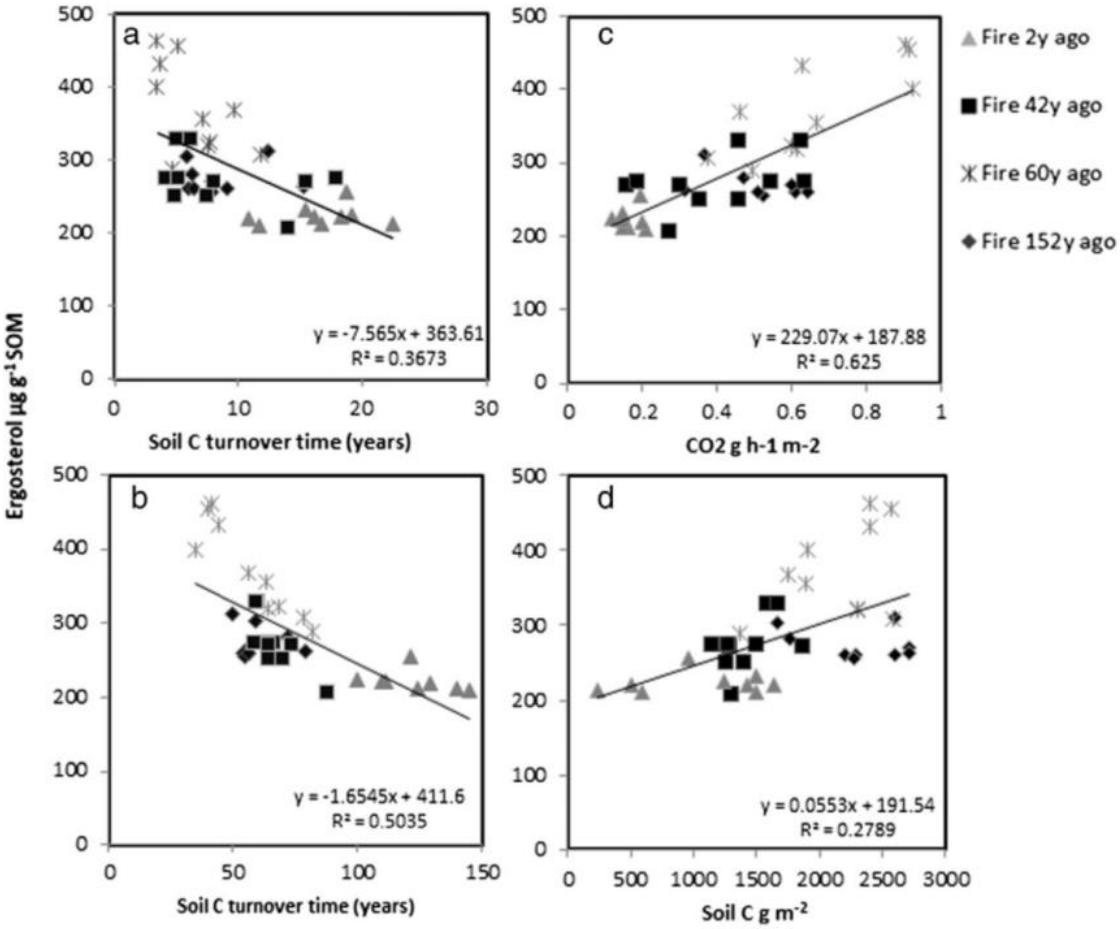

Figure 2) Relationships of ergosterol content of areas with different times since fire occurrence to: a) soil C turnover times (in years) calculated from direct soil CO 2 efflux values (root respiration included) from the field measurements, b) soil C turnover times (T, years) calculated from lab incubation study values (root respiration excluded), c) soil CO 2 efflux (g CO 2 h −1 m −2), d) soil C stock (g m −2). Reprinted from Köster et al. 2014.

ACKNOWLEDGEMENTS

We thank Saara Berninger for her help in the field work an her great persistance for a 14 year old girl in the North. The work was made possible through funding by the Finnish Academy to the Arcticfire project and the NcoE “The Centre of Excellence in Atmospheric Science - From Molecular and Biological processes to The Global Climate”.

REFERENCES

Köster, K.; Berninger, F.; Linden, A.; Köster, E. & Pumpanen, J. (2014) Recovery in fungal biomass is related to decrease in soil organic matter turnover time in a boreal fire chronosequence Geoderma, 235-236, 74-82

SUMMER ICE TRANSFORMATION IN THE EURASIAN ARCTIC SEAS IN THE 20th and 21st CENTURIES

L.P. BOBYLEV[1,2], O.M. JOHANNESSEN[2,3], S.I. KUZMINA[1], E.V. SHALINA[1]

[1]Nansen International Environmental and Remote Sensing Centre, St. Petersburg, 199034, Russian Federation.

[2]Nansen Environmental and Remote Sensing Centre, Bergen, N-5006, Norway.

[3]Nansen Scientific Society, Bergen, N-5006, Norway.

Keywords: EURASIAN ARCTIC SEAS, SEA ICE, CLIMATE CHANGE, GLOBAL WARMING, CLIMATE MODELS, SATELLITE OBSERVATIONS, SEA ICE PROJECTIONS, MARINE SHIPPING, NORTHERN SEA ROUTE.

INTRODUCTION

Present global warming is enhanced in the Arctic. One of the most striking manifestations of this enhancement is significant shrinking of sea ice cover in the Arctic since the beginning of 1980s (ACIA 2005, IPCC 2013). The most dramatic decline is observed for the summer sea ice (Kauker et al., 2009). Moreover, retreat of summer ice accelerated in the beginning of the current century (Comiso et al., 2008). Thus, the six lowest September minimum ice extents over the whole period of satellite observations have occurred between 2007 and 2012 (NSIDC, 2012) The most low sea ice extent occurred in September 2012 when it fell down up to 3.41 mln km^2, about half (51 %) of the 1979-2000 average September minimum extent (NSIDC, 2012; 2013). It was 760,000 km^2 below the previous record minimum extent, which occurred in September 2007. Sea ice decrease is observed in nearly all sectors of the Arctic Ocean. Thus, for the Eurasian Arctic seas 2012 was the year of absolute September minimum sea ice extent in the satellite record when it accounted for only 2.0%, 5.4%, 5.7%, 0.8% and 1.7% of average values for the Barents, Kara, Laptev, East-Siberian and Chukchi seas correspondingly (our estimations).

Projected by climate models further global warming, amplified in the Arctic, will lead to unprecedented changes in the Arctic environment including further decline of sea ice with likely sea ice-free Arctic Ocean in summer (Wang and Overland, 2009). These changes may have both positive and negative critical socioeconomic consequences. Yet, anyway they open new significant perspectives in the growing activities in the Arctic including shipping, resource extraction, fishery and tourism. This circumstance originated manifold discussions in the scientific community and among stakeholders about the future of the Arctic. Especially abundant discussions have been originated by possible opening of new international shipping routes between Atlantic and Pacific oceans through the Northern Sea Route (NSR) and/or Northwest Passage (NWP), which are geographically shorter than that through the Suez Canal (Cressey, 2011; Lasserre and Pelletier, 2011; Schoyen and Brathen, 2011; Astill, 2012; Blunden, 2012). However, such discussions remain highly speculative, because only few studies have attempted to merge climate model results with numerical transportation analysis (Smith and Stephenson, 2013). Therefore, further analysis and a quantitative assessment of impact of anticipated climate changes on the trans-Arctic navigation is necessary. For the practical applications of future Arctic sea ice projections for this task it is important to assess regional features of the ice cover transformation first of all in the Eurasian Arctic seas along the Northern Sea Route.

DATA AND METHODS

The objective of presented study is twofold: 1) to analyse past and present summer sea ice conditions in the Eurasian Arctic seas; and 2) to estimate future changes in September sea ice in these seas in the 21st century.

Analysis of past and present sea ice extent (SIE) in five Eurasian Arctic seas (Barents, Kara, Laptev, East-Siberian, and Chukchi) in summer is based on the new regional SIE dataset compiled by merging Zakharov unique historical SIE dataset and satellite passive microwave records. Zakharov (2003) SIE dataset has been created for the Barents, Kara, Laptev, East-Siberian seas, and western part of the Chukchi Sea for the period 1928-2014 from the collection of sea ice charts stored at the Arctic and Antarctic Research Institute (AARI) and based on shipboard, airplane and other observations. Ice extent data for the Barents Sea was based on the sea ice charts collected at the Danish Meteorological Institute for 1900-1956 and at AARI for 1946-2005. Satellite SIE record has been calculated for the Eurasian Arctic seas for the period 1979-2014 from sea ice concentrations obtained from passive microwave measurements using NORSEX algorithm (Svendsen et al. 1983). For the calculation of sea ice extent for the Eurasian Arctic seas, land-sea masks were applied based on the AARI's definition of seas boundaries. Merging these two SIE datasets applying special adjustment procedure using the overlap period 1979–2014 resulted in a creating new consistent regional SIE dataset for the Eurasian Arctic seas over the long 86-year period 1928-2014. This combined dataset shows more realistic behavior of sea ice across the transition between the historical and satellite records and thus provides higher confidence in trend estimates from 1928 through 2014.

Estimation of the future regional summer sea ice conditions in the Eurasian Arctic seas has been performed by model simulations using ensemble of climate models CMIP5 (Taylor et al., 2012). However, even if CMIP5 multi-model mean September sea ice trend is more consistent with satellite observations than CMIP3 model-mean, it still underestimates the observed trend. And, as in the case of CMIP3, the inter-model spread is considerable. Therefore, for getting more reliable projections of SIE in the Eurasian Arctic seas in the 21st century the selection of models from CMIP5 ensemble which best match SIE observations was performed. Before selecting model sub-ensembles, evaluation of CMIP5 model performance in reproducing summer sea ice extent and its trends really observed in the past decades in the Eurasian Arctic seas has been carried out by means of comparing model simulations with observational data from the new regional SIE dataset. Then, models from CMIP5 ensemble best matching past and present observed summer sea ice extent and trends were selected applying special criteria. For each sea the specific climate CMIP5 model sub-ensemble has been selected.

Using selected CMIP5 model sub-ensembles future projections of sea ice extent in the Eurasian Arctic seas in the 21st century have been calculated for the moderate anthropogenic scenario RCP 4.5. Using these projections, changes in the length of the navigation season on the NSR have been estimated.

RESULTS AND CONCLUSIONS

Summer sea ice conditions in the Eurasian Arctic seas in the past and present have been analysed on the base of new regional SIE dataset. Fig. 1 shows time-series of September sea ice extent and its 30-year running linear trends for five Eurasian Arctic seas over the period 1928-2014. In all seas sea ice extent is characterised by large interannual variability. Yet, there are some periods characterised by average sea ice increase or decrease. Thus, during 1928-1935/40 average SIE was decreasing in all seas. Then, during 1940-1960/70 SIE was increasing on average in Barents and Kara seas, whereas in Laptev, East-Siberian and Chukchi seas average SIE did not show any tendencies from 1940 to late 1990s. Since 1970 to present SIE was decreasing in Barents and Kara seas. On-going decrease in average SIE in Laptev, East-Siberian and Chukchi seas started in late 1990s. Anyway, current period of on-going global warming is characterised by decline of summer sea ice in all considered Eurasian Arctic seas. All of them are now nearly ice-free in September depending on the year.

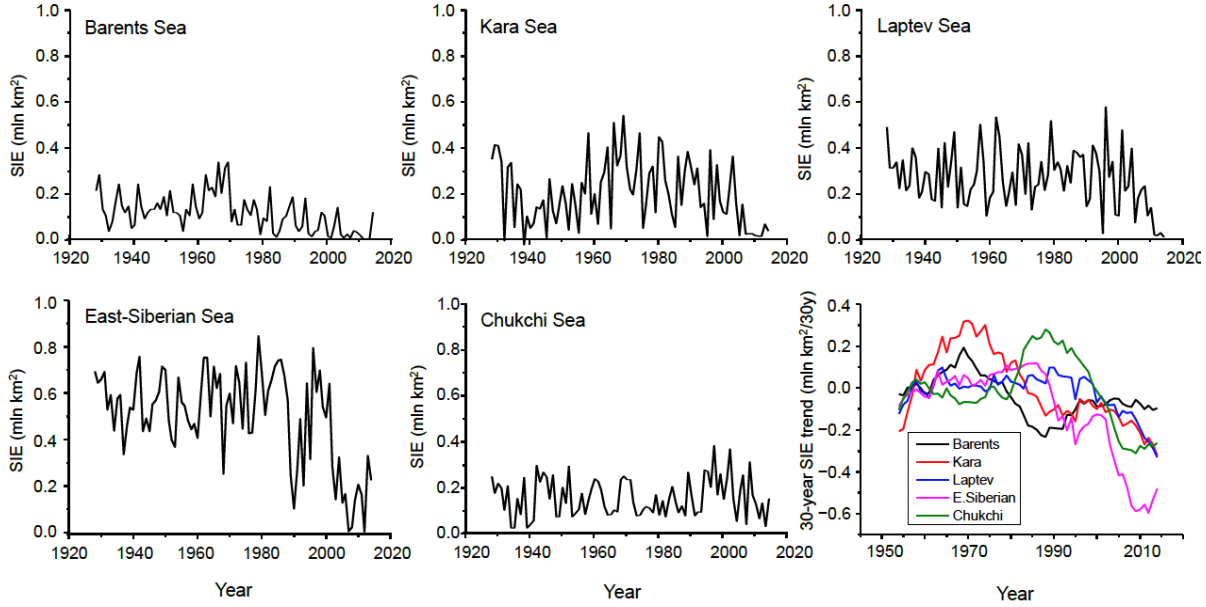

Figure 1. September sea ice extent (SIE) and 30-year linear SIE trends (right bottom) for five Eurasian Arctic seas. 30-year running trends are computed at one-year increments: X-axis indicates last year of 30-year period, e.g. 1983 indicates 1954-1983, and so on.

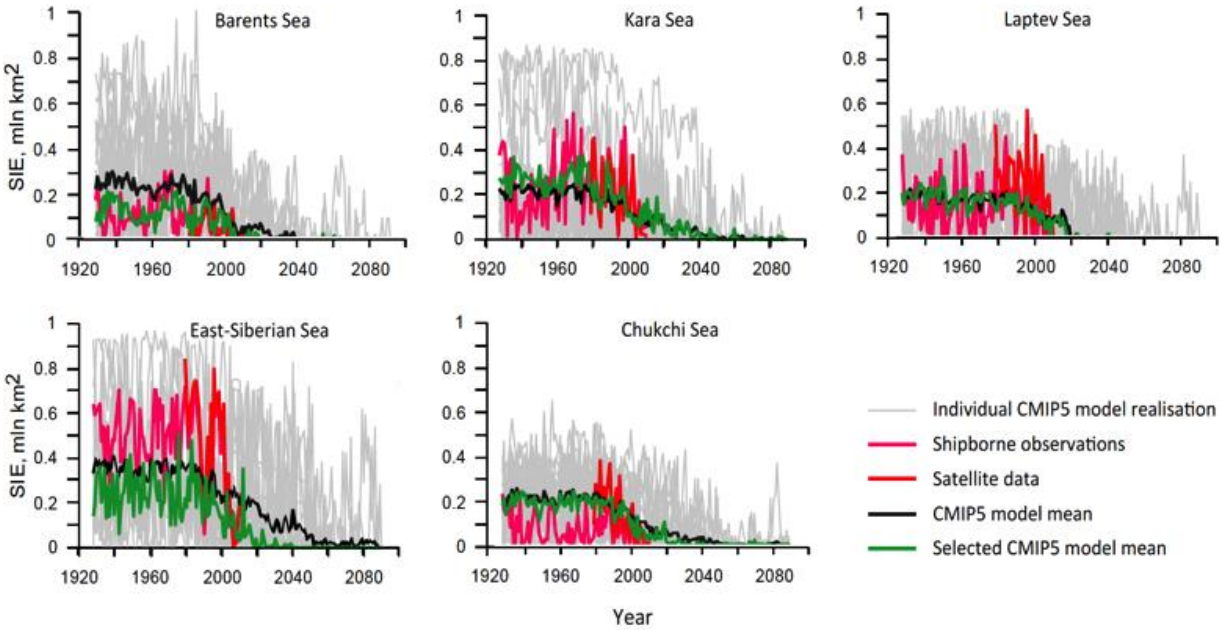

Figure 2. September sea ice extent in five Eurasian Arctic seas reproduced for 1928-2014 and projected for 2015-2100 by 20 CMIP5 model-mean and selected CMIP5 model-means under emission scenario RCP4.5.

Evaluation of CMIP5 models showed that the difference between model mean and observed SIE in the whole Arctic Ocean is significantly smaller than for CMIP3 models and do not exceed 30%. For CMIP5 ensemble spread between models is smaller than for CMIP3 for entire Arctic basin and especially for Eurasian seas. However, this evaluation showed that CMIP5 ensemble model-mean SIE is not fully reliable for the future projections of sea ice in the Eurasian Arctic seas (Fig.2). Therefore, the selection of model sub-ensembles from the whole CMIP5 ensemble has been performed for calculation of more

reliable projections of summer sea ice in the considered seas. Selected models showed trends for September SIE in the 20th century larger by 21% than the CMIP5 ensemble mean and more close to observed trend. Fig. 2 indicates that in general CMIP5 model sub-ensembles better match observed SIE than the entire CMIP5 model-mean.

Fig. 2 also shows projections of sea ice extent over the 21st century for five Eurasian Arctic seas performed by entire CMIP5 ensemble and its selected sub-ensembles using moderate anthropogenic scenario RCP 4.5. Based on the selected model sub-ensembles, future projections indicate further dramatic decrease of sea ice in all Eurasia Arctic seas with the sea ice-free conditions in summer in 2030-2050.

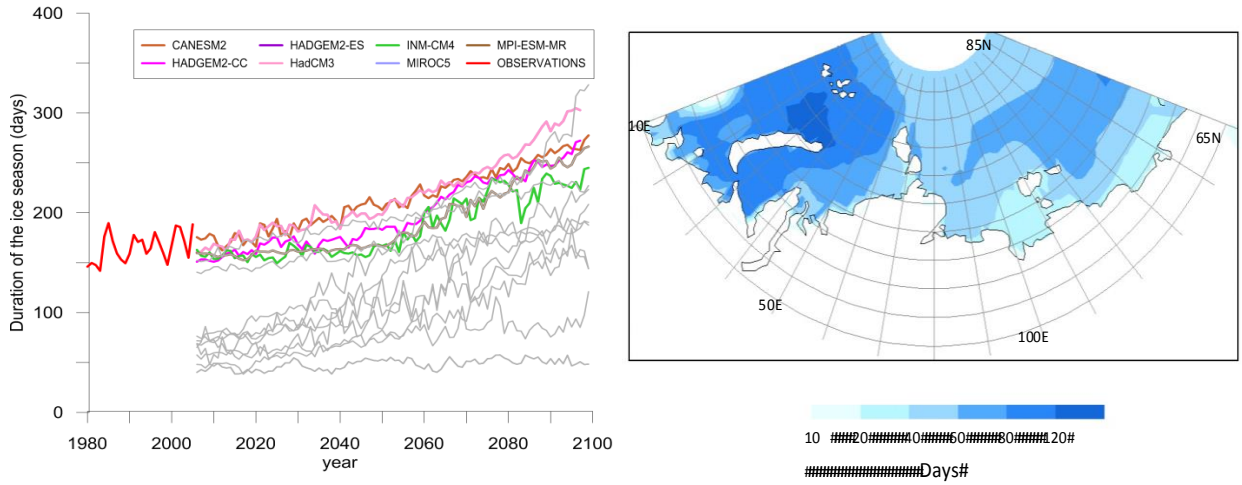

Figure 3. Observed and CMIP5-modelled (colour curves – selected models) average duration of the navigation season at the Northern Sea Route. (left). Changes in duration of navigation season at the Northern Sea Route for the period 2050-2070 relative to 2010-2020 estimated by selected CMIP5 models (right).

Calculated projections of SIE in the Eurasian Arctic seas provided the estimation of future duration of the navigation season at the Northern Sea Route (Fig. 3). This estimation showed that the length of the navigation season at NSR might increase about twice to the end of the 21st century.

ACKNOWLEDGEMENTS

This study was supported by the subsidy from the Ministry of Education and Science of the Russian Federation for the project RFMEFI61815X0005 “Ships and Waves in the Polar Regions” (Agreement No. 14.618.21.0005).

REFERENCES

ACIA (2005). *Arctic Climate Impact Assessment*, (Cambridge University Press, Cambridge, U.K.), 1042 pp.

Astill, J. (June 16, 2012). The melting north (special report: The Arctic), *The Economist*. Available at www.economist.com/node/21556798.

Blunden, M. (2012). Geopolitics and the Northern Sea Route, *Int. Aff.*, **88**(1), 115-129, 10.1111/j.1468-2346.2012.01060.x.

Comiso, J.C., C.L. Parkinson, R. Gersten, and L. Stock (2008). Accelerated decline in the Arctic sea ice cover, *Geophys. Res. Lett.*, **35**, L01703, doi:10.1029/2007GL031972.

Cressey, D. (2011). Scientific challenges in the Arctic: Open water, *Nature*, **478**(7368), 174-177, 10.1038/478174a.

IPCC (2013). *Climate Change 2013: The Physical Science Basis. Contribution of Working Group I to the Fifth Assessment Report of the Intergovernmental Panel on Climate Change* [Stocker, T.F., D. Qin, G.-K. Plattner, M. Tignor, S.K. Allen, J. Boschung, A. Nauels, Y. Xia, V. Bex and P.M. Midgley (eds.)]. (Cambridge University Press, Cambridge, U.K., and New York, NY, USA), 1535 pp.

Kauker, F., T. Kaminski, M. Karcher, R. Giering, R. Gerdes, and M. Voßbeck (2009). Adjoint analysis of the 2007 all time Arctic sea-ice minimum, *Geophys. Res. Lett*., **36**, L03707, doi:10.1029/2008GL036323.

Lasserre, F., and Pelletier, S. (2011). Polar super seaways? Maritime transport in the Arctic: An analysis of shipowners' intentions, *J. Transp. Geogr*., **19**(6), 1465-1473, 10.1016/j.jtrangeo.2011.08.006.

NSIDC (2012). Arctic Sea Ice News and Analysis, http://nsidc.org.

NSIDC (2013). A real hole near the pole.

Schoyen, H., and Brathen, S. (2011). The Northern Sea Route versus the Suez Canal: Cases from bulk shipping, *J. Transp. Geogr*., **19**(4), 977-983, 10.1016/j.jtrangeo.2011.03.003.

Smith, L.C., and S.R. Stephenson (2013). New Trans-Arctic shipping routes navigable by mid-century, *PNAS*, **110** (13), E1191-E1195; doi:10.1073/pnas.1214212110.

Svendsen, E., K. Kloster, B. Farrelly, O.M. Johannessen, J.A. Johannessen, W.J. Campbell, P. Gloersen, D. Cavalieri, C. Matzler (1983). Norwegian Remote Sensing Experiment' Evaluation of the Nimbus 7 Scanning Multichannel Microwave Radiometer for Sea Ice Research, *Journal of Geophysical Research*, **88**(C5), 2781-2791.

Taylor, K.E., R.J. Stouffer, and G.A. Meehl (2012). An Overview of CMIP5 and the Experiment Design, *Bull. Amer. Meteor. Soc.*, **93**, 485-498.

Wang, M., and J.E. Overland (2009). A sea ice free summer Arctic within 30 years? *Geophys. Res. Lett*., **36**, L07502, doi:10.1029/2009GL037820.

Zakharov, V.F. 2003. Changes of the Arctic sea ice extent in XX century. *Meteorologiya I Gidrologiya*, **5**, 75-86 (*in Russian*).

SATELLITE MONITORING OF TRACE GAS AND AEROSOL EMISSIONS INTO THE ATMOSPHERE OF NORTHERN EURASIA

V.G. BONDUR

AEROCOSMOS Research Institute for Aerospace Monitoring, Moscow, Russia

Main sources of hazardous gases and aerosols in Northern Eurasia has been analyzed. It has been shown that wildfires are one of the most dangerous natural disasters menacing the lives of people and objects of infrastructure and destroying forest resources. They are the intense sources of emissions of chemically active gases and fine particulate matter into the air environment, which is the most important factor determining the balance of trace gas components and aerosols in the Earth's atmosphere (Bondur, 2011, 2015; Bondur, Ginzburg, 2016).
The main components of the initial products of emission during burning are the following: carbon dioxide CO_2; carbon monoxide CO; nitrogen oxide NO; volatile organic compounds; fine-particulate matter of dispersed aerosol (PM); sulfur dioxide SO_2; and methane CH_4, etc. Entering the atmosphere, primary combustion products are drawn into the system of air movements. Then they are subjected to further transformation, which leads to high concentrations of toxic compounds causing adverse health effects. The combustion products are transported by convective currents via the free troposphere to the stratosphere, which leads to their rapid spreading over long distances in the largescale circulation systems. Emission plumes of CO and CO_2 and families of odd nitrogen and aerosols from large natural fires are traced in the lee direction over distances of a few thousand kilometers, which determines the nonlocal character of their influence. This has an impact on the ecological state of the air environment and also on the Earth's climate (Shvidenko et. al, 2011). Such peculiarities and characteristic scales of natural fires require application of space methods of monitoring to solve the problem of their detection and estimation of consequences (Bondur, 2011, 2015).

The aspects of generation of carbon-bearing gas and fine aerosol emissions into the atmosphere during wildfires are analyzed here. On-line space-borne monitoring system and methods used for assessment of burned areas and volumes of CO_2, CO и $PM_{2.5}$ emissions during wildfires are described. The results of satellite monitoring of wildfires are given; burned areas and volumes of carbon-bearing gas and aerosol emissions over the entire territory of the Northern Eurasia and its regions for different months over a period covering 2005-2015 have been assessed. The aspects of seasonal frequencies of wildfires and volumes of harmful gas and fine aerosol emissions across studied areas have been identified.

Based on the results from processing of satellite monitoring data, monthly distributions of the areas covered by fire and also the emissions of CO_2, CO, and $PM_{2.5}$ for the entire territory of the Russian Federation and its individual regions (European part of Russia and the Siberian and Far Eastern Federal Districts), as well as for the Eastern Europe and the Northern part of China have been analyzed. An analysis of the results obtained has shown that the monthly distributions of areas covered by fire in the European part of Russia have two characteristic maxima in April and in the hottest summer months (July–August). The year of 2012 is an exception because the maximum is displaced to September. The maximum areas of the natural fires in this region were recorded in August 2002 and 2010. For the territory of the Siberian Federal District, the monthly distributions of the areas covered by fire also have two characteristic maxima: in the spring months (April–May) and in the summer months (generally in June–July). For the territory of the Far Eastern Federal District of Russia, the distribution of the areas of natural fires from April to August is more uniform. The maximum areas covered by fires in this region were recorded in the summer months of 2012 and also in May and July 2011.

The maximum areas of fires in Northern Eurasia were detected in April - May in 2006 and 2008, as well as in July in 2006 and 2012.

For the territory of the European part of Russia and the Far Eastern Federal District, the distribution of the volumes of emissions of CO_2, CO, and $PM_{2.5}$ practically repeat the evolution of the graphs of fire area distributions. At the same time, emission volumes are not always proportional to the areas covered by fires. For example, in July 2010, the area of fires in the European part of Russia was significantly smaller than that in July 2011, but the emission volumes of CO_2 and CO were much greater. The emissions of $PM_{2.5}$ were approximately proportional to the areas of the fires.

In the Siberian Federal District of Russia, where the areas covered by fires were relatively large in April–May of 2005–2015, the volumes of the gas and aerosol emissions in these months were insignificant. At the same time in summer (July–August), the volumes of emissions of CO_2, CO, and $PM_{2.5}$ were approximately proportional to the areas of the fires. This may be related to the fact that in spring the major part of the fires appears in the southern part of this region, where open woodlands dominate with unblown leaves, which are characterized by low values of emission coefficients. The characters of monthly distributions of fire areas and carbon-bearing gas and aerosol emission volumes over the whole territory of the Russian Federation are most similar to the characters of comparable distributions for Siberian Federal District where boreal forests prevail. This is the evidence of the greatest contribution of such kind of vegetation into CO_2, CO, and $PM_{2.5}$ emissions due to wildfires.

The results obtained testify to high efficiency of satellite monitoring methods, technologies, and assets for urgent detection of wildfires and assessment of carbon-bearing gas and aerosol emissions into the air due to them.

REFERENCES

1. Bondur V.G. Satellite Monitoring of Wildfires during the Anomalous Heat Wave of 2010 in Russia // Izvestiya, Atmospheric and Oceanic Physics. 2011. Vol. 47. No. 9, P. 1039-1048.

2. Bondur V.G. Space-borne Monitoring of Trace Gas and Aerosol Emissions During Wildfires in Russia // Issledovanie Zemli iz Kosmosa. 2015. No. 6. P.21-35.

3. Bondur V.G., Ginzburg A.S. Emission of Carbon-Bearing Gases and Aerosols from Natural Fires on the Territory of Russia Based on Space Monitoring // Doklady Earth Sciences. 2016. Vol. 466. No. 2. P. 148-152. DOI 10.1134/S1028334X16020045.

4. Shvidenko A.Z., Shchepashchenko D.G., McCallum I., Lakyda I.P., Vaganov E.A., Sukhinin A.I., Maksyutov Sh.Sh. Impact of wildfire in Russia between 1998-2010 on ecosystems and the global carbon budget // Doklady Earth Sciences. 2011. T. 441. № 2. C. 1678-1682.

GUIDELINES FOR ANALYSIS OF URBAN WEATHER AND CLIMATE DATA

R. BORNSTEIN[1], J. DOU[2], S. MIAO[2] and X. LIANG[2]

[1]Denpartment of Meteorology and Climate Science, San Jose State University, San Jose, CA, USA.

[2]Institute of Urban Meteorology, China Meteorological Administration, Beijing, China.

Keywords: URBAN, WEATHER, CLIMATE, ANALYSIS.

INTRODUCTION

Urban areas modify regional weather and climate patterns in complex nonlinear ways, so mesoscale (i.e., local scale) meteorological parameters are increased or decreased within urban planetary boundary layers (PBLs), dependent on which conflicting impact wins "the battle" at a given moment. Some parameters over cities are impacted in only one way, e.g., visibility always decreased, (mechanical and thermal) turbulence is always increased, and (synoptic and sea breeze) fronts always slowed. Other parameters are either increased or decreased (e.g., precipitation, wind speed), while wind direction either converges into the city or diverges around it, and thunderstorms can be triggered over the city or split (and go around it).

Finally, cities are either warmer or cooler than surrounding areas, thus having either an urban heat island (UHI) or urban cool island (UCI), respectively. UHIs form because grass and soil surfaces are replaced by concrete and buildings, which alters surface sensible and latent heat fluxes into the atmosphere. In addition, fossil fuel use in high latitude cities creates fluxes of pollutants, heat, and water vapour into the atmosphere. Finally, pollutant layers and building-structures decrease incoming solar and outgoing long wave IR terrestrial radiations. A net effect of many of these processes is that cities lose stored solar energy more slowly at night and thus remain warmer, i.e., nocturnal UHIs form; this process is a localized global warming analogy. The above processes can be observed during long-term climatological studies or short term field campaigns, and can be simulated by use of highly nonlinear computer codes (Bornstein, 1968).

Urban weather and climate impacts produce important societal impacts, e.g., UHIs produce thermal stress and global-warming enhancements, while precipitation enhancement can produce flooding. In addition, altered urban dispersion (i.e., transport & diffusion) patterns can result in pollution episodes and impact emergency response decisions when reacting to toxic releases in urban atmospheres.

This paper thus presents guidelines for successful analyses of urban PBL weather and climate data, both under current climate forcings and under IPCC future climate scenarios. It then discusses data from two Beijing studies to illustrate the successful application of these guidelines.

METHODOLOGY: GOOD-ANALYSES GUIDELINES

Estimation of true-magnitudes of urban-induced weather and/or climate changes for a given area in a changing climate requires "segmented" data-analyses (e.g., by wind direction, UHI-magnitude, time of day, season, and/or historical period). If this guideline is not followed (and if all data are "lumped together"), only small-differences between the compensating urban-impacts listed above are obtained. A productive analysis requires "good intuition" to pose questions (i.e., how to segment data, based on researcher meteorological/climatological knowledge) that will produce new understandings of the physical processes altering the weather and/or climate in urban PBLs.

Certain planning efforts, e.g., watershed management, may not require such an approach, as planners may only be interested in the total urban climatological enhancement or suppression of precipitation. Urban

flood forecasters, however, want to understand where (and under what circumstances) urban areas will enhance precipitation, information useful for planning future urban developments.

Application of the "segmentation" methodology to understanding urban thermodynamic impacts on summer convective thunderstorms follows, based on: climatological analysis for New York City (NYC) by Bornstein and LeRoy (1990) and case study analysis in Atlanta by Bornstein and Lin (2000. These analyses indicate that two ideal extreme-cases (i.e., initiation vs. bifurcation) depend on UHI magnitude. The current study (Dou et al., 2015) is the first to use UHI magnitude to segment urban precipitation impacts, rather than to segment storms by impact (and then assume a relationship with UHI magnitude). Note that aerosols have a secondary effect (after initiation vs. bifurcation) on precipitation timing, location, and magnitude via radiative-effects on the surface and atmospheric energy balances and on atmospheric stability, and via a vast array of cloud microphysical-effects (Rosenfeld, 2000).

Synoptic conditions	UHI mag-nitude	Urban winds	Urban impacts on storm movement	Urban precipitation pattern
Total regional cloud–cover, storms, and fast winds	Small	Diverge around city	Storm diverges/ bifurcates around city	➢ Lateral-max along diverging streamlines ➢ Min over city and down-wind in urban rain-shadow
No regional clouds or storms, and slow winds	Large	Converge into low - pressure over city	Storm forms over city	➢ Max over city

Table 1. Summary of urban thermodynamic-effects on summer convective thunderstorms.

Table 1 states that large UHIs results with clear-sky background synoptic-conditions (i.e., neither clouds nor storms, and slow regional wind speeds). Near surface winds thus converge into the thermal low pressure (that forms in the large UHI) area over the city, resulting in upward motion and thunderstorm initiation over the city, and thus a precipitation maximum over the city. With regional cloud cover and storms, UHIs are weak (as heat is advected from the city). Near surface winds thus diverge around the city (due to its building barrier effect), resulting in downward motion over the city. Moving storms thus also bifurcate around the city, producing a precipitation minimum over and downwind of the city (i.e., a rain shadow effect), but also producing precipitation maxima along the diverging streamlines around the city.

This summary thus depends on the segmentation of urban precipitation data according to storm type (as these results have not been tested on winter synoptic storms), wind direction (or downwind cannot be defined), and UHI magnitude (as controlled by synoptic wind speed). The next section will illustrate this analysis method with data from a climatological study over Beijing

A limitation of such climatological studies is that a “bifurcation area” of precipitation, can in fact be a collection of urban deflections (some rightward and some leftward). To investigate this possibility over Beijing, the Institute of Urban Meteorology (IUM) is undertaking a series of case studies of urban thunderstorm impacts as part of the Field Study of Urban Rainfall and Fog/Haze (SURF) project (Li et al., 2015). This inter-national study involves deployment of a wide variety of PBL sensors from Chinese meteorological and air quality institutes in and around Beijing. Preliminary analyses of a case study will be shown below.

RESULTS

Analyses were carried out into the detailed characteristics of meteorological elements in the Beijing urban area for the summers (June-August) of 2008-12 by Dou et al. (2015). Data from 83 Air Weather Service (AWS) sites in and around Beijing were used to obtain average daytime (08-19) and nighttime (20-07 LST) temperatures. The 850 hPa rawinsonde wind velocity prior to initiation of a rainfall-event was defined as the low-level “PBL wind”. Southwesterly flows accounted for 134 cases (or 40% of all events), with southerly flow as second most common (51 cases). To evaluate up- and down-wind urban- impacts on each storm, precipitation data were segmented by PBL wind direction, and only southwesterly flow cases were studied.

Cases were further segmented by “event” UHI value, with those above and below 1.25°C (average Beijing UHI value) categorized as “strong- or weak-UHI events,” respectively. Most (35 of 61) strong events occurred at night (20-07 LST), while most (53 of 73) weak events occurred during daytime (08-19 LST). Regional-normalized total rainfall-amount NR eliminates large-scale effects, thus highlighting local impacts (Yu. 2007); it was thus used in the Beijing study.

Results showed that when NR values are segmented by event-UHI magnitude (regardless of time of day), weak-UHI cases (Fig. 1a) show large urban-barrier-induced bifurcation-impacts, i.e., two terrain-enhanced western maxima (> 15%) that are greater than the urban-only enhancements on the eastern urban edge (> 5%). Urban precipitation suppression is seen over the city (> -15%) and in a downwind urban rain shadow (> -35%). These results are consistent with the urban-barrier part of the urban-precipitation-synthesis hypothesis (Table 1) of Bornstein (2015).

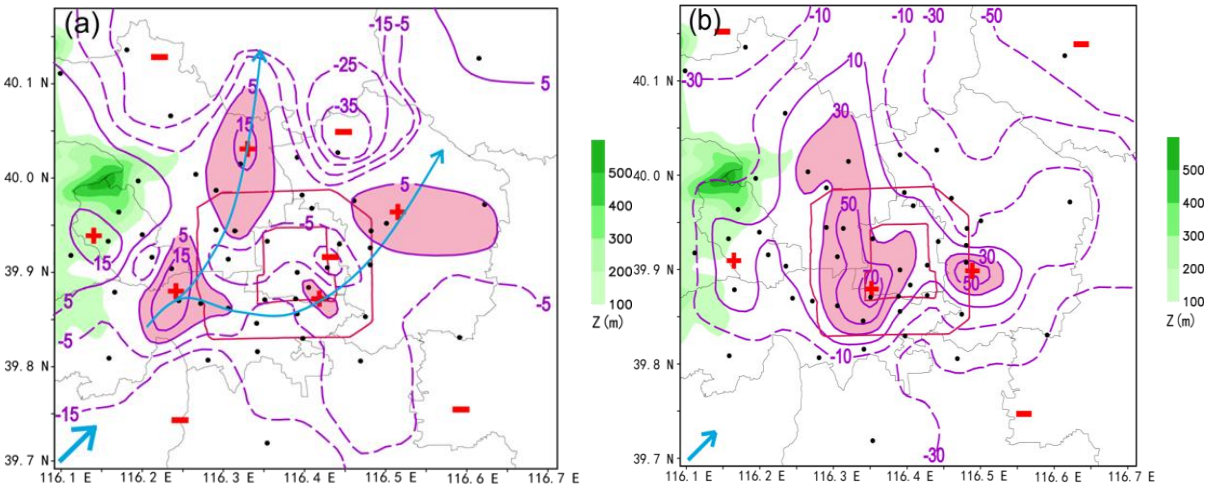

Figure 1. Average 2008-12 summer Beijing urban area NR (%) amounts for (a) weak- and (b) strong-UHI (°C) cases (with 850 hPa winds from SW, blue arrow). Also shown are Second and Fourth Ring Roads (red circles, which define area of maximum urbanization), terrain heights (m, green shading), idealized bifurcating stream flow lines (in blue), and high precipitation areas (in red); from Dou et al. (2015).

The corresponding strong-UHI cases (Fig. 1b) do not show barrier-induced bifurcation, but instead show two UHI-induced urban-max (> 60 and > 75%) generally in the most urbanized areas (between two Ring Roads, i.e., around Old Town low building urban-core). This UHI-induced convection is also consistent with the second part of the Bornstein (2015) hypothesis.

Preliminary results from the 2015-6 SURF observational case studies are becoming available. One case from 22 July 2015 (Fig. 2) clearly shows a storm bifurcating, while others (not shown) show right or left deflection. Further statistical analyses are underway to determine the frequency of each type of event over Beijing.

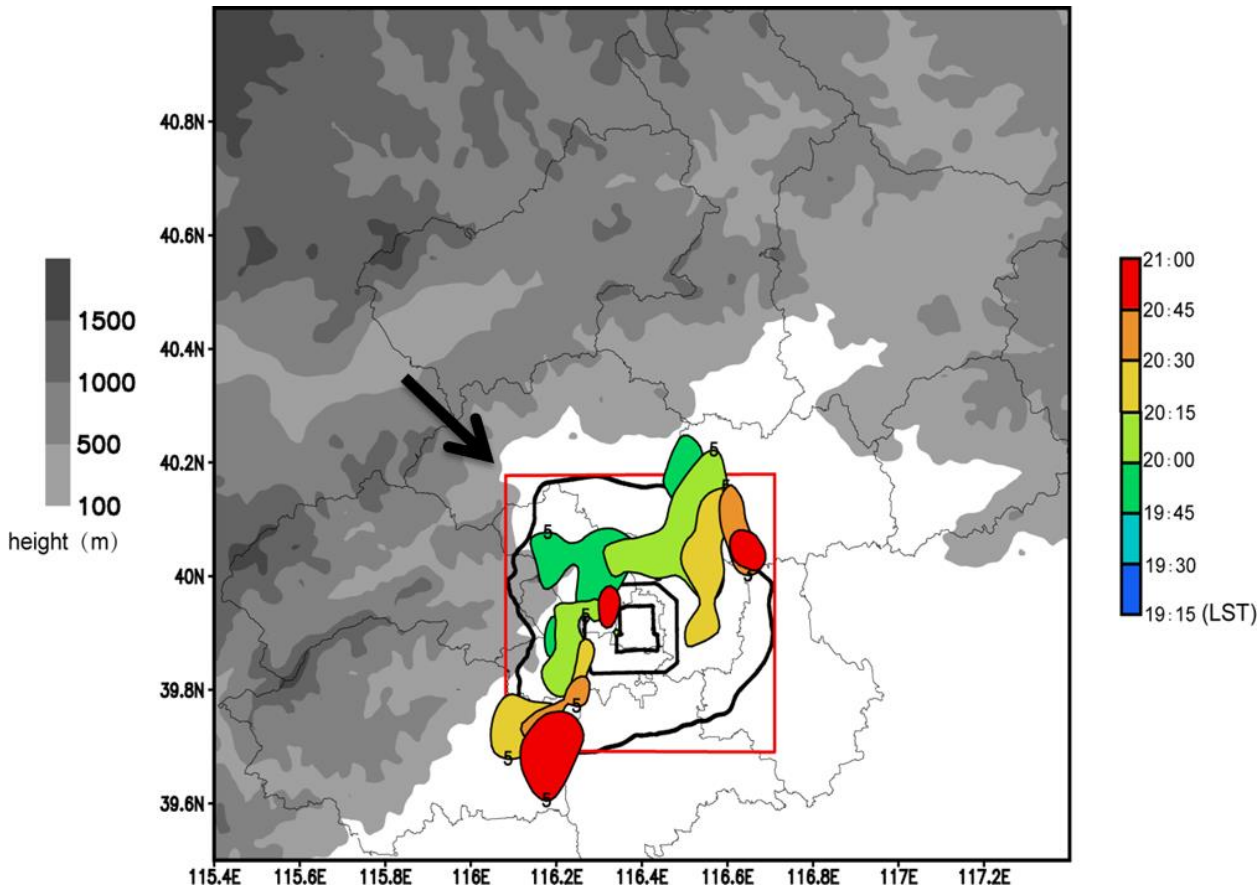

Figure 2. Observed thunderstorm precipitation-footprints on 22 July 2015, where black circles are the Second and Forrh Ring Roads, colors are areas with precipitation > 5-mm per15-min interval from 1915-2100 LST, grays are topographic heights (m), and arrow is surface storm movement direction.

CONCLUSION

The current climatological and case-study results are consistent with the synthesis-hypothesis of Bornstein (2015) concerning urban impacts on summertime convective-thunderstorm- dynamics. The current study, however, goes beyond this synthesis, as while the older studies of Bornstein and LeRoy (1990) and Bornstein and Lin (2000) segmented initiated vs. bifurcated thunder-storm cases *a priori*, they only were thus able to hypothesize that UHI-magnitude was the controlling parameter. The current study, however, started with a critical-UHI magnitude (1.25^{0}C, the average Beijing value) and then proceeded to show that it resulted in initiated-cases with stronger values and in bifurcated cases with weaker values.

In contrast to other prior reviews (e.g., Shepherd, 2005), the current study does not show (regardless of UHI magnitude) increased precipitation directly downwind of the city, although in weak-UHI cases, areas

with max precipitation exist, but only on its downwind lateral corners. This apparent inconsistency may result, as this study examined downwind areas in a more detailed manner.

The results are scientifically important, as they provide the first detailed and comprehensive study of the spatial distributions of daytime and nighttime summer Beijing impacts on precipitation. Summertime urban thunderstorm-induced flooding in Beijing and other cities produces large losses in human life and infrastructure. These results will thus be useful in planning for disaster prevention and mitigation.

As only summer-thunderstorms were considered herein, additional seasons and precipitation mechanisms (e.g., synoptic fronts) need analysis. Physical mechanisms by which cities alter precipitation patterns have not been completely examined, and future efforts should thus include both climatological and short-term intensive field-studies with PBL observations, as in the current Beijing SURF study.

Numerical simulations are being carried out at IUM with the NCAR highly-urbanized version of WRF (Chen et al. 2011), and with foci on urban-aerosol impacts and on urban mechanisms that bifurcate moving thunderstorms. Such storms (less frequently) bifurcate over the US Great Plains in the presence of anti-cyclonic vertical wind-shears, and perhaps the more frequent urban bifurcation is related to anti-cyclonic turning (towards low pressure) of urban PBL flows due to wind speed reductions, as flows enter urban areas (with their higher surface-roughness values). Another explanation could be formation of an upwind urban high pressure (and downward motion) area, associated with urban-induced upwind downward-motions that form to compensate for mass re-distributions associated with urban-induced upward motions over city centers

ACKNOWLEDGEMENTS

The authors would like to thank Lin Li and Jiqin Zhong for providing the data used in the study. This work was supported by National Natural Science Foundation of China (Grant No. 41175015) and Beijing Municipal Science & Technology Commission (Grant No. Z111100074211010).

REFERENCES

Bornstein, R. (1968). Observations of the urban heat island effect in NYC. *J. Appl. Meteor.* **7,** 575-82.

Bornstein, R. (2015). Influence of cities on clouds, precipitation, and thunderstorms. Presented at 9th International Conference on urban Climate (ICUC9), Toulouse, France, 22 July.

Bornstein, R. and G. LeRoy (1990). Urban barrier effects on convective and frontal thunder- storms. *Preprint Vol.,4th AMS Conf. on Mesoscale Processes,* Boulder, CO, 25-29 June, 2 pp.

Bornstein, R.D. and Q. Lin (2000). Urban heat islands and summertime convective thunder- storms in Atlanta: three case studies. *Atmos. Environ.* **34,** 507-16.

Chen, F., R. Bornstein, S. Grimmond, J. Li, X. Liang, Alberto Martilli, S. Miao, James Voogt, and Y. Wang (2011). Research priorities in observing & modeling urban weather. *BAMS.* **93**, 1725-8.

Dou, J., Y. Wang, R. Bornstein, and S. Miao (2015). Observed spatial characteristics of summertime Beijing urban-climate impacts, with a thunderstorm focus. *J. Appl. Meteor. Climatol.* **54,** 94-105.

Li, J., X. Liang, S. Miao, J. Dou and R. Bornstein (2015). Field study of urban rainfall and fog/haze (SURF). *IUM-CMA Report,* Beijing, China, 21 pp.

Rosenfeld, D. (2000). Suppression of rain by urban and industrial air pollution. *Science.* **287,** 1793-6.

Shepherd, J.M. (2005). A review of current investigations of urban-induced rainfall and recommendations for the future. *Earth Interaction,* **9,** 1-27.

Yu Q. (20070. Inter-annual variability of precipitation urbanization effects in Beijing. *Progress in Natural Sci.* **17,** 632-38.

VOC MEASUREMENTS AT VILLUM RESEARCH STATION, NORTH GREENLAND WITH PTR-TOF-MS

R. BOSSI[1] and H. SKOV[1]

[1]Department of Environmental Science and Arctic Research Center, Aarhus University, Roskilde, Denmark.

Keywords: VOLATILE ORGANIC COMPOUNDS, BIOMASS BURNING TRACERS, ARCTIC, PTR-TOF-MS.

INTRODUCTION

Biomass burning has been identified as a significant source for aerosol and trace gases in the Arctic. The importance of biomass burning is more important to the Arctic than previously believed and thus more accurate measurements of tracers for biomass burning are necessary to model parameterization and to understand the chemical processes leading to SOA and particle formation in the Arctic atmosphere.
Volatile Organic Compounds (VOCs) are emitted in large quantities to the Earth's atmosphere, most of which originate from biogenic emissions (Guenther et al., 1995). VOCs play a critical role in tropospheric chemistry and are associated with ozone production and secondary organic aerosol (SOA) formation, which affect human health, regional air quality, and the global climate. VOCs undergo photochemical oxidation in the troposphere to form a variety of products. Once oxidized, VOCs become more polar, less volatile and more hygroscopic, which leads to formation of SOA (Kroll and Seinfeld, 2008). Despite much recent progress in understanding SOA formation chemistry, current models based on parameterizations of laboratory experiments cannot fully explain the evolution of atmospheric SOA and tend to underestimate the total mass of particles in the atmosphere, and this is particular true for the Arctic (Zare et al., 2014). Atmospheric particles can be understood as so-called short-lived climate forcers (SLCFs) and are expected to significantly influence the Arctic climate.
Biomass burning is a major source of gases and particles to the atmosphere at concentrations that have a significant influence on tropospheric chemistry on local, regional and global scale (Levine, 2000). Biomass burning is responsible for a large fraction of black carbon (BC) in Arctic atmosphere and snow samples (Massling et al. 2015). This finding is significant to climate forcing because light-adsorbing BC in the atmosphere and deposited on snow surfaces accelerate temperature increase and snowmelt (Flanner et al., 2007)).
Several non-methane organic compounds (NMOCs) have been identified as specific molecular markers for biomass burning (Hornbrook et al., 2011). The most important volatile tracer for biomass burning is acetonitrile, which has an atmospheric lifetime of many months.
VOCs are typically measured with off-line methods, where air samples are first collected on desorption tubes and analyzed in the laboratory by gas chromatography-mass spectrometry (GC-MS). These methods are quite time-consuming, expensive and do not allow to follow the complex dynamics of VOCs chemistry in real-time.
Proton Transfer Reaction-Time-of- Flight Mass Spectrometry (PTR-TOF-MS) is a recently introduced technique, which allows for on-line monitoring of VOCs at low detection limits and fast response time. The principal of PTR-MS is the utilization of proton transfer reaction from H_3O^+ to VOCs with a proton affinity larger than that of water (166.55 kcal mol^{-1}). The charged VOC molecules are then detected by a TOF mass spectrometer (Graus et al., 2010). PTR-TOF-MS provides on-line quantification and, at the same time, formula confirmation of VOCs. PTR-TOF-MS has been recently used for identification of biomass burning plumes and observing their transport and chemical processing.

METHODS

A PTR-TOF MS 1000 (Ionicon, Innsbruck, Austria) has been installed in December 2015 at Villum Research Station (VRS), Station Nord in Greenland (81° 36' N, 16° 40' W at 24 m ASL). The instrument is set up for continuous monitoring of VOC concentrations by scanning the mass range 0-200 amu. The data acquired by the PTR-TOF-MS will be processed and the concentrations of detected VOCs will be integrated over time. VOC concentrations will be correlated to other compounds or parameters originating from biomass burning. Year round measurements at VRS are carried out within the framework of the international program AMAP (Arctic Monitoring and Assessment Program) financed by DANCEA (Danish Cooperation for Environment in the Arctic) administered by the Danish Environmental Protection Agency. The measurements comprise gas phase constituents (NO_2, CO, gaseous elemental mercury, O_3) measured by monitors and SO_2 as well as particle phase constituents by filter pack samplers and high volume samplers, in addition to particle physical and optical properties. Meteorological data are also available and will be used for data interpretation.
By using state of the art emissions inventories of biomass burning based on satellite observations in the Danish Eulerian Hemispheric Model (DEHM), time series of concentrations fields of VOC, SOA and BC will be made and compared with the measurements at VRS.

CONCLUSIONS

The combination of the use of measurements, satellite based estimated of biomass burning and model calculations could reduce the current high uncertainties in the knowledge about the contribution of biomass burning to the SLCF (short lived climate forcers) and other contaminants. This could result in a more accurate understanding of importance of biomass burning for the chemical processes influencing the Arctic climate.

ACKNOWLEDGEMENTS

This work is supported by the Villum Foundation and the Danish Environmental Protection Agency (DANCEA funds for environmental support to the Arctic Region).

REFERENCES

Flanner, M.G., Zender, C.S., Randerson, J.T., P.J. Rasch (2007). Present-day climate forcing and response from black carbon in snow. *J. Geophys. Res.* 112, D11202.

Graus, M., Müller, M., Hansel, A. (2010). High resolution PTR-TOF: quantification and formula confirmation of VOC in real time. *J. Am. Soc. Mass Spectrom*. 21, 1037-1044.

Guenther, A.C., Hewitt, N., Erickson, D., Fall, R., Geron, C., Graedel, T., Harley, P., Klinger, L., Lerdau, M., Mckay, W. A., Pierce, P., Scholes, B., Steinbrecher, R., Tallamraju, R., Taylor, J., and P. Zimmerman (1995). A global model of natural volatile organic compounds emissions. *J. Geo. Res. Atm*., 100, 8873-8892.

Hornbrook R.S., Blake D.R., Diskin G.S., Fried A., Fuelberg H.E., Meinardi S., Mikoviny T., Richter D., Sachse G.W., Vay S.A., Walega J., Weibring P., Weinheimer A.J., Wiedinmyer C., Wisthaler A., Hills A., Riemer D.D., and E.C. Apel E.C. (2011) Observation of nonmethane organic compounds during ARCTAS- Part 1: Biomass burning emissions and plume enhancements. *Atmos. Chem. Phys.* 11, 11130.

Kroll, J.H. and J.H. Seinfeld (2008). Chemistry of secondary aerosol: formation and evolution of low-volatility organics in the atmosphere. *Atmos. Environ*., 42, 3593-3624.

Levine, J.S. (2000). Global biomass burning: A case study of the gaseous and particulate emissions released to the atmosphere during the 1997 fires in Kalimantan and Sumatra, Indonesia. In: Biomass Burning and Its Inter-Relationship with the Climate System. Kluwar Academic Publisher, Boston, 15-31.

Massling, A., Nielsen, I. E., Kristensen, D., Christensen, J. H., Sørensen, L. L., Jensen, B., Nguyen, Q. T., Nøjgaard, J. K., Glasius, M., and H. Skov (2015). Atmospheric black carbon and sulfate concentrations in Northeast Greenland, Atmospheric Chemistry and Physics, Vol. 15, pp. 9681-9692, doi:10.5194/acp-15-9681-2015, available at: www.atmos-chem-phys.net/15/9681/2015/.

Zare, A., Christensen, J. H., Gross, A., Irannejad, P., Glasius, M., and J. Brandt (2014). Quantifying the contributions of natural emissions to ozone and total fine PM concentrations in the Northern Hemisphere, *Atmos. Chem. Phys*., 14, 2735-2756.

OVERVIEW OF PALLAS CLOUD EXPERIMENT, PACE 2015

D. BRUS[1], K. DOULGERIS[1], K. NEITOLA[1], J. BACKMAN[1], E. J. O'CONNOR[1], M. KOMPPULA[2], M. FILIOGLOU[2], K. A. NICOLL[3], R. G. HARRISON[3], P. TISLER[1], J. SCHWARZ[4], P. VODICKA[4], V. VAKKARI[1], M. AURELA[1], E. ASMI[1] AND H. LIHAVAINEN[1]

[1]Finnish Meteorological Institute, Erik Palménin aukio 1, P.O.Box 503, FI-00101, Helsinki, Finland

[2]Finnish Meteorological Institute, Yliopistonranta 1F, P.O. Box 1627, FI-70211 Kuopio, Finland

[3]University of Reading, Earley Gate, Whiteknights, Reading, RG6 6BB, Berkshire, UK

[4]Institute of Chemical Process Fundamentals CAS, Rozvojova 135, 16502 Praha 6, Czech Republic

Keywords: AEROSOL, CLOUDS, CCN, IN-SITU, REMOTE SENSING, ARCTIC.

INTRODUCTION

Anthropogenic emissions affect Earth climate in many ways. Very important but a less recognized climate forcing is that caused by aerosols. The aerosols do reflect sunlight and they have a potential to activate into cloud droplets i.e. act as cloud condensation nuclei (CCN). Currently, clouds and their interaction with aerosol particles provide some of the greatest uncertainties in predictions of climate change, this is due to: (1) environment-dependent sources of primary and secondary particles, (2) varying spatial and temporal distribution and composition of aerosol particles, (3) cloud and below-cloud dynamics, microphysics and precipitation (e.g. Makkonen et al., 2012). Clouds are a major component in the global hydrological cycle, since they store, transport and redistribute water. They also contribute to global energy balance through reflecting, transmitting and re-radiating solar energy. Vulnerable Arctic region is slowly heading towards a new climatic state with substantially decreased permanent ice cover. However, due to poorly understood feedback mechanisms, the rate of Arctic climate response to changes is very hard to predict with current global models. Arctic clouds are supposed to have central role in these feedback processes (Vavrus, 2004). Many of the climatically important cloud properties (e.g. albedo, precipitation rate and lifetime) depend, amongst other factors, on the number concentration of aerosol particles and on their chemical composition (Komppula *et al*., 2005; Lohmann and Feichter, 2005; Lihavainen *et al*., 2008). Clouds, and their interaction with the environment, are in general investigated through two types of measurements: (1) In-situ, airborne or ground-based campaigns and (2) Ground-based remote-sensing techniques (i.e. lidar, ceilometer and radar) and satellite.

METHODS

The 6th Pallas cloud experiment was carried out ten weeks, between September 25th and December 5th 2015, at Finnish Meteorological Institute's Pallas-Sodankylä Global Atmosphere Watch (GAW) station in Finnish sub-Arctic region (Hatakka *et al.*, 2003). During the campaign we utilized both in-situ and remote-sensing techniques to investigate aerosol-cloud interactions. Ground based measurements were conducted at Sammaltunturi station (67°58′N, 24°07′E, 565 m. a. s. l., Fig.1, place A) which resides on a top of the second southernmost fjeld, a round topped treeless hill, in a 50-km-long north and south chain of fjelds at an elevation of 565 m a. s. l. Sammaltunturi station is, due to topography of the surrounding terrain, a great place for ground-based observations of low level and also orographic clouds (Kivekäs *et al.*, 2009; Anttila *et al.*, 2012). The measurements at Sammaltunturi station included wide range of instrumentation: aerosol number size distribution with differential mobility particle sizers (DMPS), total number particle counters (CPC, TSI 3010, Airmodus A20), particle absorption with Aethalometer (model AE 31, Magee Scientific), Multi-Angle Absorption Photometer (MAAP, Thermo Scientific), the Single

Particle Soot Photometer (SP2, DMT), field EC/OC Analyzers (Sunset, USA) and particle scattering with the integrating Nephelometer (model 3563, TSI). The ambient RH was measured with Vaisala HUMICAP sensor, and visibility and temperature were measured with Vaisala FD12P weather sensor. In addition to the above mentioned equipment, the aerosol CCN and hygroscopic properties were measured with the HTDMA (Hygroscopicity Tandem Differential Mobilitity Analyzer) and the Cloud Condensation Nuclei Counter (CCNc, DMT model CCN-100). In situ cloud properties were measured on the roof of the station with a Forward Scattering Spectrometer Probe (FSSP, 3-47 µm, model SPP-100, DMT) and the Cloud, Aerosol and Precipitation Spectrometer (CAPS, DMT), which includes three instruments: the Cloud Imaging Probe (CIP, 12.5 µm-1.55 mm), the Cloud and Aerosol Spectrometer (CAS-DPOL, 0.51-50 µm) with depolarization feature, and the Hotwire Liquid Water Content Sensor (Hotwire LWC, 0 - 3 g/m3), see Fig 2A. Mass and chemical composition of non-refractory submicron particulate matter was characterized with an Aerosol Chemical Speciation Monitor (ACSM, Aerodyne).

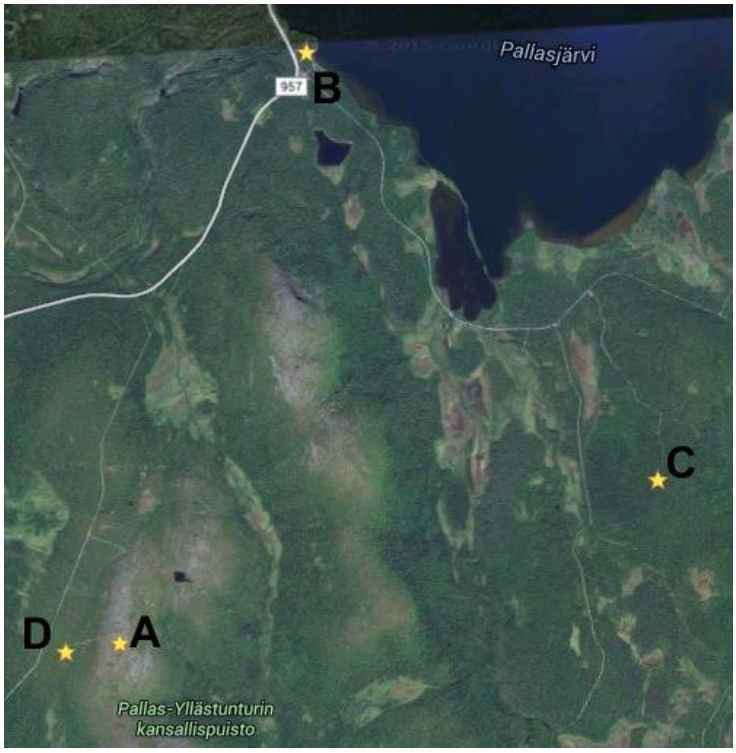

Figure 1. Locations of measurement sites: A) Sammaltunturi station, B) sounding launching site at Pallasjärvi, C) and D) remote sensing sites, the air distance between A-B-C sites is about 6 km.

In situ airborne measurements were conducted at Pallasjärvi lake site (300 m a. s. l., see Fig. 1, place B). A disposable backscatter instrument for optical detection of clouds in the atmosphere designed for use on routine radiosonde balloon flights (Harrison and Nicoll, 2014) was used to measure cloud droplet microphysical properties. The sensor employs the backscatter principle, using an ultra-bright LED as the illumination source, with a photodiode detector. The meteorological balloons were launched twice a day during site overpass of Terra or Aqua NASA satellites, see Fig 2B. Also FMI-owned RPAS (Remotely Piloted Aircraft System) quadcopter platform was used in order to carry on instruments (Jonassen *et al.*, 2015) and to perform airborne measurements from the lowest 150 m - aviation authorities restricted above ground height - layer of the atmosphere. The instrumentation carried on-board of RPAS was a CPC model 3007 (TSI Inc., USA), an OPS model 3330 (TSI Inc., USA), a micro-Aethalometer model AE51 (AethLabs, USA), see Fig. 2C. Columnar profiles were measured at sites B, C and D, we omitted measurements at site A, on top of the hill, due to high winds, ~10 m/s.
Ground based remote sensing site (Kenttärova station, 345 m a. s. l., see Fig. 1, place C) utilized three instruments, Lidar – Polly^{XT} (Althausen et al., 2009), HALO Photonics Streamline scanning Doppler Lidar

(Pearson *et al.*, 2009) and cloud radar (O'Connor *et al.*, 2015), see Fig. 2D. Using such instrumentation setup we were able to obtain columnar information of wind profiles, updraft velocity, aerosol-particle properties, boundary layer height, cloud base height, water vapour, mixed phase or ice clouds and precipitation with high resolution in real-time. Another Doppler lidar was placed down, about 500 m, at the foothill of Sammaltunturi station (440 m a. s. l.) upwind the main wind direction (W – NW, see Fig. 1, place D).

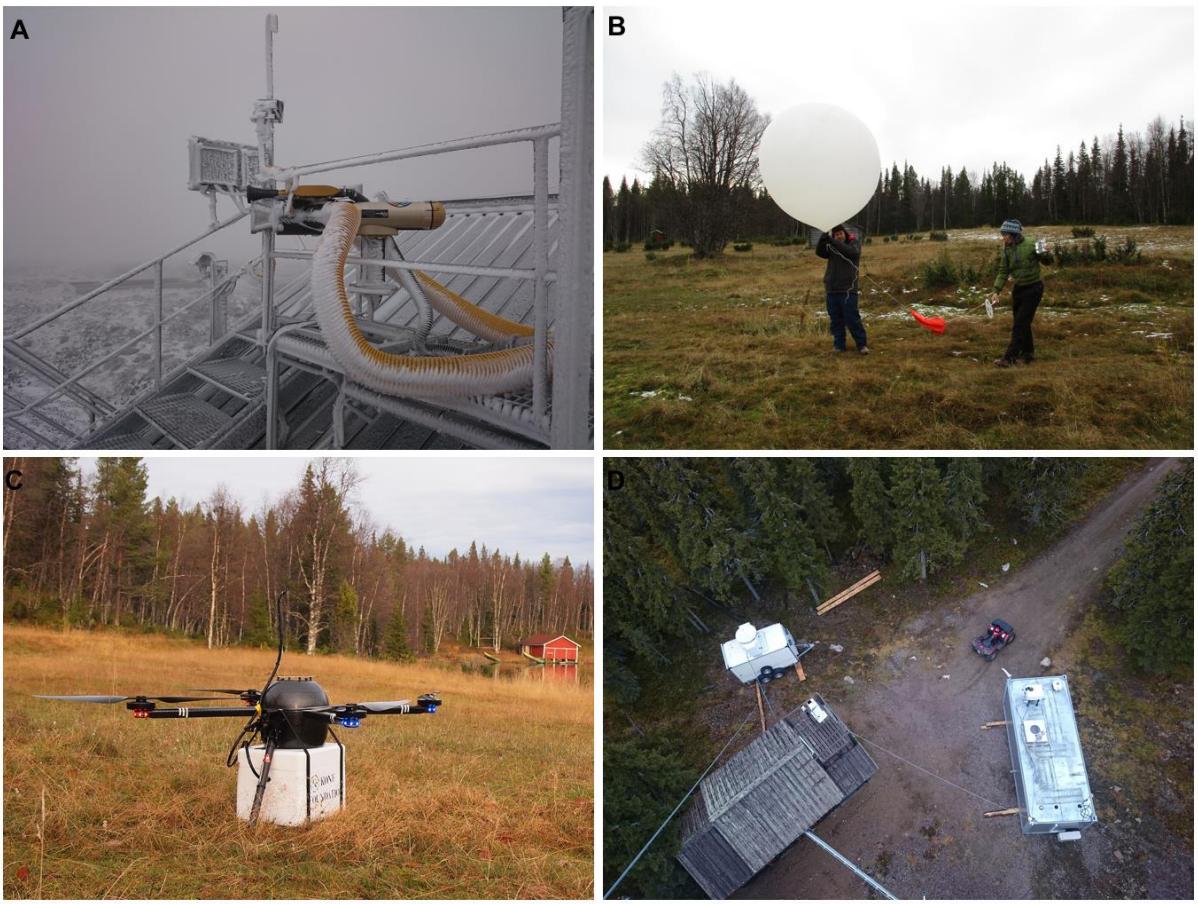

Figure 2. A) In-situ cloud droplets measurements with CAPS probe on the roof of Sammaltunturi station, B) meteorological balloons launching site at Pallasjärvi, C) FMI-RPAS platform carrying aerosol instrumentation in Styrofoam box and D) remote sensing site at Kenttärova station – Cloud radar in left-up corner, Lidar Polly^{XT} inside the cargo container in right down corner, Doppler lidar on top of the cargo container.

ACKNOWLEDGEMENTS

This work was supported by KONE foundation, Nordforsk Contract number 26060, CRAICC Amendment on CRAICC-PEEX Collaboration, Academy of Finland project: Greenhouse gas, aerosol and albedo variations in the changing Arctic (project number 269095), Academy of Finland Center of Excellence program (project number 272041), BACCHUS (EU 7th Framework program), Natural Environment Research Council (NERC), grant number NE-L011514-1 and ACTRIS-2, the European Research Infrastructure for the observation of Aerosol, Clouds, and Trace gases. This project has received funding from the European Union's Horizon 2020 research and innovation programme under grant agreement No 654109

REFERENCES

Makkonen, R., *et al.* (2012): Air pollution control and decreasing new particle formation lead to strong climate warming, *Atmos. Chem. Phys.*, **12**, 1515–1524.

Vavrus, S. (2004). The impact of cloud feedbacks on Arctic climate under greenhouse forcing, *J. Climate*, **17**, 603.

Lohmann, U. and Feichter, J. (2005): Global indirect aerosol effects: a review, *Atmos. Chem. Phys.*, **5**, 715–737.

Komppula, M. *et al.*, (2005). Measurements of cloud droplet activation of aerosol particles at a clean subarctic background site, *J. Geophys. Res.*, **110**, D06204.

Lihavainen, H. *et al.*, (2008). Measurements of the relation between aerosol properties and microphysics and chemistry of low level liquid water clouds in Northern Finland, *Atmos. Chem. Phys.*, **8**, 6925

Hatakka, J. *et al.*, (2003). Overview of the atmospheric research activities and results at Pallas GAW station, *Boreal Environ. Res.*, **8**, 365.

Kivekäs, N. *et al.*, (2009). Physical and chemical characteristics of aerosol particles and cloud-droplet activation during the Second Pallas Cloud Experiment (Second PaCE), *Boreal. Environ. Res.*, **14**, 515.

Anttila, T. *et al.*, (2012). Relationships between particles, cloud condensation nuclei and cloud droplet activation during the third Pallas Cloud Experiment, *Atmos. Chem. Phys.*, **12**, 11435.

Harrison, R.G. and Nicoll K. A. (2014): Active optical detection of cloud from a balloon platform, *Rev. Sci. Instrum.*, **85**, 066104.

Jonassen, M. O. , et al. (2015): Application of remotely piloted aircraft systems in observing the atmospheric boundary layer over Antarctic sea ice in winter, *Polar Research*, **34** (25651).

Althausen, D., et al. (2009): Portable Raman lidar Polly^{XT} for automated profiling of aerosol backscatter, extinction, and depolarization, *J. Atmos. Ocean. Tech.*, **26**, 2366–2378,

Pearson, G., et al. (2009): An Analysis of the Performance of the UFAM Pulsed Doppler Lidar for Observing the Boundary Layer, *J. Atmos. Ocean. Tech..*, **26**(2), 240–250.

O'Connor, E. J., et al. (2005): Retrieving Stratocumulus Drizzle Parameters Using Doppler Radar and Lidar, *J. Appl. Meteorol*., **44**, 14–27.

ENVRIplus – ENVIRONMENTAL RESEARCH INFRASTRUCTURES PROVIDING SHARED SOLUTIONS FOR SCIENCE AND SOCIETY

M. BRUS[1], A. ASMI[1], W. KUTSCH[2], P. LAJ[3], S. SORVARI[4]

[1]Division of Atmospheric Sciences, Department of Physics, University of Helsinki, Helsinki, Finland

[2]Integrated Carbon Observation System, Head office, Helsinki, Finland

[3]Laboratoire de Glaciologie et Géophysique de l'Environnement, Grenoble, France
[4]Finnish Meteorological Institute, Helsinki, Finland

Keywords: ENVIRONMENTAL SCIENCE, RESEARCH INFRASTRUCTURES, EARTH SYSTEM, MULTIDISCIPLINARITY, INTEROPERABILITY

INTRODUCTION

European long-term environmental research infrastructures (often referred as ESFRI RIs) provide key tools and instruments for the researchers to address specific challenges within their own scientific fields. However, to tackle the grand challenges facing human society, scientific collaboration across the traditional fields is necessary. The Earth system is highly interlinked and the area of focus for environmental research is therefore our whole planet. It is clear that strong collaboration among research infrastructures is needed to serve the trans-boundary research that requires exploring scientific questions at the intersection of different scientific fields, conducting joint research projects and developing concepts, devices, and methods that can be used to integrate the knowledge.

OBJECTIVES

ENVRIplus is a European Union (Horizon 2020) funded project bringing together Environmental and Earth System Research Infrastructures, projects and networks together with technical specialist partners to create a more coherent, interdisciplinary and interoperable cluster of Environmental Research Infrastructures across Europe. The objective of ENVRIplus is to provide common solutions to shared challenges for European Environmental and Earth System Research Infrastructures in their efforts to deliver new services for science and society. To reach this overall goal, ENVRIplus creates a cluster that builds common synergic solutions for pressing issues in Research Infrastructure construction and implementation.
ENVRIplus is driven by 3 overarching goals: 1) favouring cross-fertilization between Research Infrastructures, 2) implementing innovative concepts and devices across Infrastructures, and 3) facilitating research and innovation in the field of environment to an increasing number of users outside the Research Infrastructures.

Figure 1. This figure illustrates the research infrastructures and projects directly participating in ENVRIplus. They represent different domains of the Earth System, with some of them having multi-domain approach. The inner grey circle shows Reearch Infrastructures in the ESFRI 2010 Roadmap.

Collaboration within the ENVRIplus will enable the multidisciplinary Earth system science across the traditional scientific fields, which is so important in order to address today's global challenges. The cooperation will avoid the fragmentation and duplication of efforts, making the Research Infrastructures' products and solutions easier to use with each other, improving their innovation potential and cost/benefit ratio of the Research Infrastructure operations.

CONCEPT

To achieve its goals, ENVRIplus consists of one Management and 18 Research and Innovation Work Packages that are further organized under 6 conceptual Themes.
The goal of Theme 1 "**Technical Innovation**" is to improve the Research Infrastructures' abilities to observe the Earth System, particularly in developing and testing new sensor technologies, harmonizing observation methodologies and developing methods to overcome common problems associated with distributed remote observation networks.
Theme 2 "**Data for Science**" aims at generating common solutions for shared information technology and data related challenges of the environmental Research Infrastructures in data and service discovery and use, workflow documentation, data citations methodologies, service virtualization, and user characterization and interaction.
Develop harmonized policies for access (physical and virtual) for the environmental Research Infrastructures, including access services for the multidisciplinary users is the ultimate goal of Theme 3 "**Access to Research Infrastructures**".
Theme 4 focusing on "**Societal Relevance and Understanding**" investigates the interactions between Research Infrastructures and society. The team will find common approaches and methodologies how to assess the Research Infrastructures' ability to answer the economical and societal challenges, develop ethics guidelines for Research Infrastructures and investigate the possibility to enhance the use Citizen Science approaches in Research Infrastructure products and services.

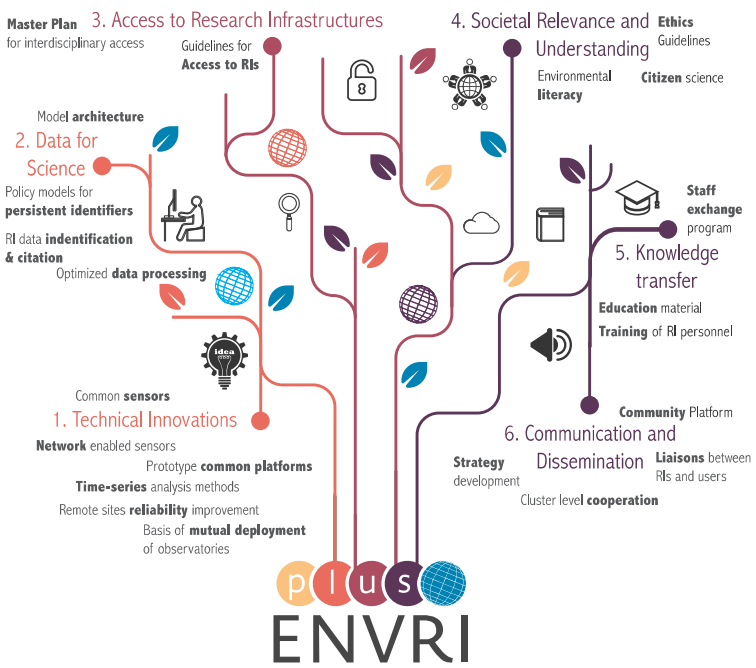

Figure 2. This figure illustrates the six central "themes" of ENVRIplus as well as products and solutions to be delivered by them.

Theme 5 "**Knowledge Transfer**" ensures the cross-fertilisation and knowledge transfer of new technologies, best practices, approaches and policies of the Research Infrastructures by generating training material for Research Infrastructure personnel to use the new observational, technological and

computational tools and facilitate inter-Research Infrastructure knowledge transfer via a staff exchange program.
Finally, Theme 6 "**Communication and Dissemination**" works towards creating a Research Infrastructure communication and cooperation framework to coordinate activities of the environmental Research Infrastructures towards common strategic development, improved user interaction and interdisciplinary cross- Research Infrastructure products and services.

CONCLUSIONS

ENVRIplus is a four-year, EU Horizon 2020 funded project, clustering 20 Research Infrastructures. Each of them offers high quality, open services for the scientific users in all regions of Europe regardless whether their research organisations or countries are members of the Research Infrastructures. By this, environmental Research Infrastructures are maximising use and impact of information and knowledge provided. ENVRIplus has the needed critical mass of Research Infrastructure operators to help European environmental and Earth system research communities to evolve towards open, interconnected, multidisciplinary, data-driven and computer-intensive science. All the ENVRIplus actions are aiming for providing user-friendly means to perform modern science. Its products, services and solutions will be accessible at ENVRIplus project website available at www.envriplus.eu.

ACKNOWLEDGEMENTS

This project has received funding from the European Union's Horizon 2020 research and innovation programme under grant agreement No 654182.

TERRESTRIAL ECOSYSTEM – CLIMATE FEEDBACKS IN BOREAL AND TROPICAL FORESTS

J.K. BÄCK[1], R. MAKKONEN[2], D. TAIPALE[1, 3], A. MÄKELÄ[1], A. LOHILA[4], T. VESALA[1, 2], E. NIKINMAA[1], F. BERNINGER[1], T. KALLIOKOSKI[1], T. PETÄJÄ[2], P. PAASONEN[2], AND M. KULMALA[2]

[1]Department of Forest Sciences, University of Helsinki, Finland.

[2]Department of Physics, University of Helsinki, Finland

[3] Department of Plant Physiology, Estonian University of Life Sciences, Tartu, Estonia

[4]Finnish Meteorological Institute, Finland

Keywords: ECOSYSTEM-CLIMATE FEEDBACKS, BOREAL FOREST, TROPICAL FOREST

INTRODUCTION

It has been recognized for centuries that the Earth's biosphere plays an important role in climate. Climatic feedbacks between terrestrial ecosystems and the atmosphere are related to both biogeochemical and biophysical interactions and processes on the Earth. These processes have great importance in determining the radiative balance of vegetated surfaces, but their relative importance and even the direction of impact depends on the ecosystem type and present climatic conditions.

Ecosystem activity affects the greenhouse gas concentrations in the boundary layer and during the growing season decreases the atmospheric CO_2 concentration due to photosynthesis. Respiration releases part of the fixed carbon and the net accumulation to ecosystems is a result of release in respiration and uptake in photosynthesis. An important climatic feedback is caused by the decomposing micro-organisms, which release stored carbon from the dead plant material and organic soils in a strongly temperature-dependent manner. These biogeochemical feedbacks and their effects on the atmospheric greenhouse gas (GHG) concentrations are rather well understood in the current climate. Tropical moist forests hold globally the largest carbon storages (ca. 50% of all carbon stored in terrestrial ecosystems), and are active carbon sinks with fast growing plants, however the carbon is mostly stored in aboveground biomass and rather little carbon is accumulating in tropical forest soils. Boreal forests, on the contrary, grow slowly and store only less than 10% of terrestrial carbon, but most of it is in the soil pool. The turnover rate of the boreal soil pool is very slow, can be several hundreds of years. Over recent years, the seasonal amplitude in the boreal regions' carbon exchange has grown significantly larger, whereas the amplitude in tropics has not significantly changed (Graven *et al.* 2013).

On the other hand, ecosystems reflect or absorb incoming radiation which contributes to carbon uptake (light use for photosynthesis) or surface heating. Vegetation also affects atmospheric aerosol formation by producing copious amounts of reactive vapours, which are able to both form new aerosol particles and to condense onto pre-existing particles and enable them to grow into cloud condensation nuclei (e.g. Kulmala *et al.* 2013, Paasonen *et al.* 2013). In addition to the direct warming due to the greenhouse effect, an increase in atmospheric CO_2 may also indirectly lead to a positive feedback via photosynthesis due to an increased scattering efficiency of atmospheric particles and thus greater diffuse/global solar radiation ratio (Kulmala *et al.* 2014). These biophysical feedbacks have received much less attention than the biogeochemical feedbacks, but their importance has recently been recognized also by IPCC (IPCC AR5). This study aims at clarifying and quantifying these feedbacks and analysing their relative importance in tropical and boreal forested areas.

METHODS

With the long-term field measurements at the SMEAR II station in southern Finland, located in the boreal zone, we have quantified two important loops in the biophysical feedback, presented in Kulmala *et al.* (2004, 2014). These feedbacks are illustrated in figure 1.

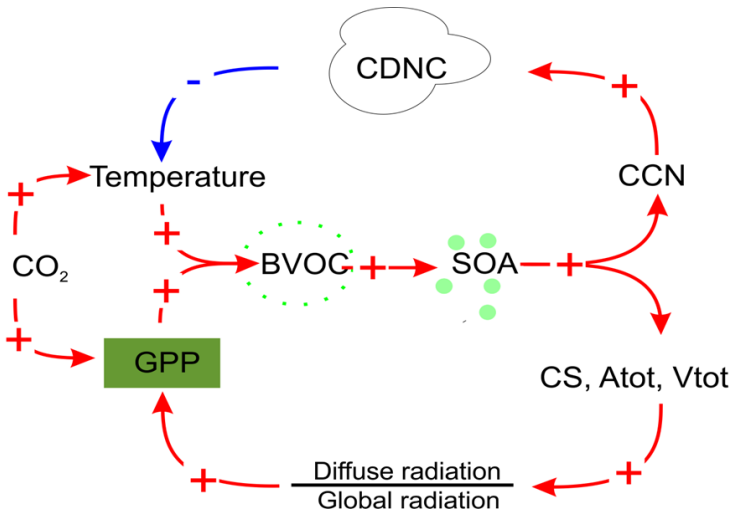

Figure 1. Two biophysical feedback loops (Kulmala *et al.* 2014, Paasonen *et al.* 2013) connecting the increase in atmospheric CO_2 and aerosol production. The lower loop forms a positive feedback via the terrestrial carbon sink (GPP feedback), whereas the upper loop forms a negative feedback via the ambient temperature change (temperature feedback). GPP = gross primary production, BVOC = biogenic volatile organic compounds, SOA = secondary organic aerosol, CS = condensation sink, Atot = total aerosol surface area, Vtot = total aerosol volume, CCN = cloud condensation nuclei, and CDNC = cloud droplet number concentration.

We have tested the effect of increasing CO_2 concentration on the predicted aerosol number concentration using the Norwegian ESM (Makkonen et al 2014), where these feedbacks have been implemented. We have also performed simulations where we sum up the impact of different biogeochemical (carbon exchange) and biophysical (albedo, aerosols) feedbacks on radiative forcing in several boreal forest stands utilising rotation periods of various lengths (Nikinmaa *et al.* in prep.).

In simulations with NorESM, global average atmospheric 2m-temperatures increase by ~3.5 K due to doubling of CO_2. The temperature change is pronounced in the Northern Hemisphere and the Arctic. The increase in temperature and CO_2 concentration lead to increased biogenic VOC emissions: monoterpene emissions are increased globally by ~20%. The increase in VOC emission results in increased SOA formation, which both increases aerosol mass and growth of nucleated particles. Increase in aerosol formation, aerosol optical depth and cloud droplet number concentrations in the $2xCO_2$ climate lead to increased aerosol forcing. According to the NorESM simulations, BVOC-aerosol-climate feedback can act to reduce the climate warming.

CONCLUSIONS

The presentation will illustrate the reasons and consequences of these feedbacks and compare their importance in different forested regions (tropical *vs* boreal). Potential ways for mitigating climate change via these feedbacks will be discussed.

ACKNOWLEDGEMENTS

This work was supported by the Academy of Finland Center of Excellence (Grants no. 1118615 and 272041), the Nordic Centers of Excellence CRAICC and DEFROST, and Helsinki University Centre for Environment (HENVI) programme 'Forest and Climate Change'.

REFERENCES

Graven, H. D. , R. F. Keeling, S. C. Piper, P. K. Patra, B. B. Stephens, S. C. Wofsy, L. R. Welp, C. Sweeney, P. P. Tans, J. J. Kelley, B. C. Daube, E. A. Kort, G. W. Santoni, and J. D. Bent (2013) Enhanced Seasonal Exchange of CO_2 by Northern Ecosystems Since 1960. Science 341, 1085-1089. DOI: 10.1126/science.1239207

Kulmala M., Suni T., Lehtinen K.E.J., Dal Maso M., Boy M., Reissell A., Rannik Ü., Aalto P., Keronen P., Hakola H., Bäck J., Hoffmann T., Vesala T. & Hari P. (2004). A new feedback mechanism linking forests, aerosols, and climate. Atmospheric Chemistry and Physics 4: 557-562.

Kulmala M., Kontkanen J., Junninen H., Lehtipalo K., Manninen H.E., Nieminen T., Petäjä T., Sipilä M., Schobesberger S., Rantala P., Franchin A., Jokinen T., Järvinen E., Äijälä M., Kangasluoma J., Hakala J., Aalto P.P., Paasonen P., Mikkilä J., Vanhanen J., Aalto J., Hakola H., Makkonen U., Ruuskanen T., Mauldin R.L. III, Duplissy J., Vehkamäki H., Bäck J., Kortelainen A., Riipinen I., Kurten T., Johnston M.V., Smith J.N., Ehn M., Mentel T.F., Lehtinen K.E.J., Laaksonen A., Kerminen V.-M., & Worsnop D.R. (2013) Direct observations of atmospheric nucleation. Science 339, 943-946, DOI: 10.1126/science.1227385

Kulmala, M., Nieminen T., Nikandrova A., Lehtipalo K., Manninen H., Kajos M., Kolari P., Lauri A., Petäjä T., Krejci R., Hansson H.-C., Swietlicki E., Lindroth A., Christensen T.R., Arneth A., Hari P., Bäck J., Vesala T., & Kerminen V.-M. (2014) CO_2 induced terrestrial climate feedback mechanism: From carbon sink to aerosol source and back. Boreal Env. Res. 19 (suppl. B): 122–131.

Makkonen, R., Seland, Ø., Kirkevåg, A., Iversen, T., and Kristjánsson, J. E.: Evaluation of aerosol number concentrations in NorESM with improved nucleation parameterization, Atmos. Chem. Phys., 14, 5127-5152, doi:10.5194/acp-14-5127-2014, 2014.

Paasonen, P., A. Asmi, T. Petäjä, M. K. Kajos, M. Äijälä, H. Junninen, T. Holst, J.P.D. Abbatt, A. Arneth, W. Birmili, H. D. van der Gon, A. Hamed, A. Hoffer, L. Laakso, A. Laaksonen, W.R. Leaitch, C. Plass-Dülmer, S. C. Pryor, P. Räisänen, E. Swietlicki, A. Wiedensohler, D.R.Worsnop, V.-M. Kerminen and M. Kulmala (2013) Warming-induced increase in aerosol number concentration likely to moderate climate change. Nature Geosciences DOI: 10.1038/NGEO1800

CONTRIBUTION OF LOCAL EMISSIONS AND THE LONG RANGE TRANSPORT TO THE BLACK CARBON CONCENTRATIONS IN THE EURASIAN ARCTIC IN WRF-CHEM MODEL SIMULATIONS

C. CAVAZOS-GUERRA[1], A. LAUER[2], A. HERBER[3], T., BUTLER, .[1]

[1.] Institute for Advanced Sustainability Studies (IASS), Potsdam, Germany.

[2.] Institute of Atmospheric Physics, Deutsches Zentrum für Luft- und Raumfahrt (DLR), Oberpfaffenhofen, Germany.

[3.] Alfred Wegener Institute, Helmholtz Centre for Polar and Marine Research, Research Unit Bremerhaven, Germany

Keywords: REGIONAL CLIMATE MODELLING, BLACK CARBON, EURASIAN ARCTIC.

INTRODUCTION

The atmospheric conditions in the Arctic are very unique as a result of the high sea ice concentration and the relatively flat and homogeneous terrain in the inner part of the Arctic Ocean (Bradley et al., 1992). The pronounced seasonal cycle in the Arctic atmosphere is characterised by strong near-surface temperature inversions that limit turbulent mixing and vertical transport thus isolating the Arctic lower troposphere and acting as a barrier also called the Arctic front (Stohl, 2006). The position of the Arctic front throughout the year is important for the transport of pollutants such as black carbon (BC). Black carbon (BC), a main compound of soot, is a short-lived climate-forcing pollutant (SLCP) formed by incomplete combustion of fossil fuels (primarily coal and diesel) and from the burning of biomass or biofuel. It is the most strongly light-absorbing component in the atmosphere acting as warming agent affecting the climate through absorption of solar radiation while in the atmosphere and when deposited on snow and ice (Myhre et al., 2013). The high level of Arctic pollution including BC particles or Arctic haze is presently mainly caused by long-range transport of pollutants from source regions outside the Arctic (Stock et al., 2012) with a maximum in winter/early spring when northern Eurasia is the major source region for the Arctic pollution and a minimum in summer when the Arctic aerosol seasonal cycle is mostly dominated by clouds and precipitation. In summer, also local emission by gas and oil extraction and ship activity in the summer months is a second source for Arctic pollution (Stohl et al., 2013). Polluted air masses from densely populated areas over East-Asia and North America are too warm and moist to directly penetrate the polar dome, but they can lifted by strong convection and transported into the upper Arctic atmosphere before descending into the Arctic middle or upper troposphere creating the Arctic haze (Stohl, 2006). Some model studies suggest that the BC column burden within the Arctic region north of 60°N is 180 μg m^{-2} which is smaller than the 360 μg m^{-2} typically found in mid-latitude regions (e.g. Europe). Nevertheless, model studies suggest that local BC emissions have a much larger radiative forcing (RF) per mass than emissions originating elsewhere (Sand et al., 2013). At this time, large uncertainties exist on how emissions and long range transport will change with increased resource exploitation and shipping emissions predicted for the Arctic (Corbertt et al., 2010). On regards to resource extraction, recent studies suggest that gas flaring and residential combustion in the Arctic are already responsible for about 40% of the BC in the Arctic and projections indicate an increase in such activities due to the imminent Arctic sea-ice free environment in the upcoming decades. Furthermore, at the present, gas flaring has been largely underestimated in most global estimates (Stohl et al., 2013). This is because most of the global inventories of BC do not account for gas flaring emissions due to the scarcity of data. This is of critical importance, especially when existing inventories are used to re-create emissions datasets and chemical boundary conditions for models, which may lead to systematic errors in the simulations when estimating the BC budget in the Arctic.

In this work, we aim at to quantify the efficiency and accuracy of regional atmospheric model simulations on emissions of BC over the Eurasian Arctic. It this way we can also identify and evaluate local emissions related to resource exploration and extraction within our area of study compared to those resulting from long-range transport. It will allow us to eventually separate and quantify the contribution of long-range transport to background aerosol levels and deposition of BC over the Eurasian Arctic in order to assess the maximum effect on Arctic BC concentrations that can be expected from restricting (future) local emissions as well as reductions in non-Arctic emissions.

Results of model simulations conducted in this study over the Eurasian Arctic is an ongoing work, part of the activities within the IASS project: SMART (Sustainable Modes of Arctic Resource-driven Transformations and global interconnections). SMART is an inter- and trans-disciplinary project aiming at understanding the interdependence and feedback processes within and among Arctic regions and with non-Arctic regions due to the projected transformations taking place particularly in the Eurasian region driven by extraction of resources such as oil and gas, predominantly by Norway and Russia. This includes the effects of climate change and air pollution on the Arctic environment as well as societal and legal implications within the framework of sustainable governance.

METHODS

We conduct a suit of several high-resolution regional model simulations using the Weather Research and Forecasting model coupled with chemistry and aerosol (WRF-Chem) over the Eurasian Arctic where important contributions to local emissions of BC are related to offshore oil and gas (gas flaring), infrastructure and transport (including shipping) activities. WRF-Chem is a state-of-art model designed to calculate chemical processes online including emissions, transport of chemical species and aerosols, chemical transformation of species, aerosol processes and other important processes interacting with the atmosphere (Grell et al., 2005). It is able to run at much higher horizontal and vertical resolution than global models allowing to better resolve fine-scale features, interactions and feedbacks of the Arctic climate with air pollutants. Model configuration and description of case studies are described in Table 1. Diverse case studies are performed for which data from different sources are available. As noted, observational data are scarce for the Russian Arctic, nevertheless the availability of data in selected sites dispersed around the area is helpful to validate and quantify distribution of BC emissions and total concentrations over our study domain during our simulation period. As a first step, sun photometer observations from AERosol NETwork (AERONET) stations are used to validate Aerosol Optical Depth (AOD) in order to evaluate how the model represents atmospheric loading characteristic for the analysed periods. Additionally, available observations of total BC concentrations from the EBAS database operated by the Norwegian Institute for Air Research (NILU) are used to validate trends and veracity of our model simulations in terms of total BC concentrations. Figure 1 shows the model domain together with the location of the stations used to evaluate our model results. Correlations of our simulations for each station and period are calculated and shown in Table 2.

Table 1. Model configuration used in this study.

Model	**WRF-Chem version 3.7**
Simulation period	April 2008, July 2008, April 2009, July 2010
Domain Size	270 X 252 (175°W-175°E and 45°N-90°N)
Center	70°N and 40°E
Resolution	15x15 km horizontally and 30 vertical σ-levels
Chemistry	RADM2 (gas phase) + CMAQ (aqueous phase)
Aerosols	MADE/SORGAM
Boundary conditions and emissions	
Meteorology	Arctic System Reanalyses (ASR)
Anthropogenic emissions	EDGAR HTAP v2.2 (resolution 0.1°)
Fire emissions	NCAR FINN v1.0
Biogenic emissions	MEGAN (online)

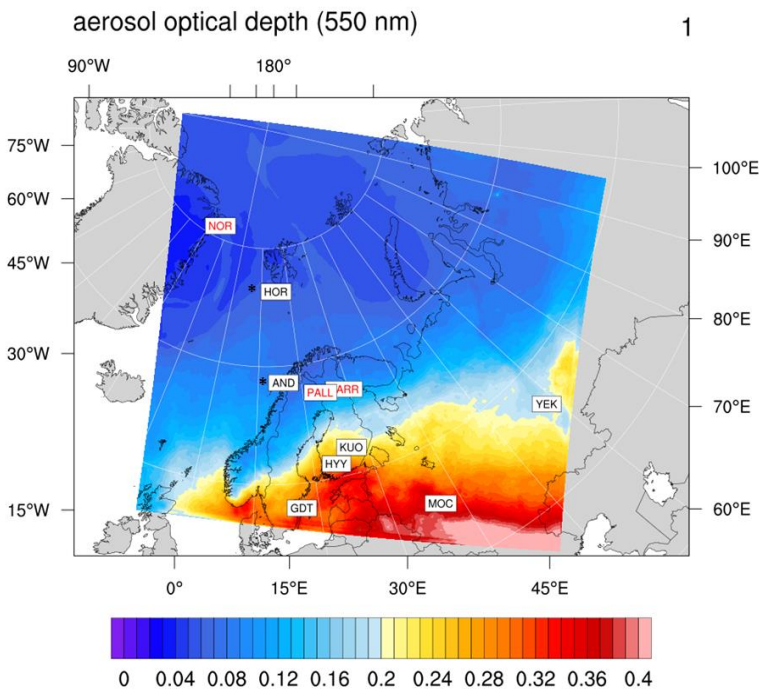

Figure 1. Simulated monthly mean AOD (500 nm) for April 2008. Labels are stations used for validation: AERONET (black font) and EBAS (red font), (*) measurements from both datasets.

RESULTS AND CONCLUSIONS

In this work, we assess the capability of the WRF-Chem model simulate BC emissions over the Eurasian Arctic and evaluate model total BC concentrations over selected stations around the region. Several case studies coinciding with maxima and minima of BC over this region and availability of data for validation were selected. We first assess the model AOD at 550nm against observations from AERONET sun-photometers for April and July 2008, specifically for spring, high aerosol loading is expected which include a significant contribution of BC. As seen in Figure 1, the spatial distribution of AOD in our model, as expected, is mostly concentrated over North Europe and in the surrounded areas to Moscow (MOC) with maxima values of AOD (0.4-0.5). Our results in general coincide with AOD observations at most of the selected stations; the WRF-Chem is able to represent AOD magnitude well in all case studies (between

0.3–1.5). As an example, Figure 2 shows AOD timeseries from Hornsund (HOR) station, which is the closest station to the Arctic at 77°N, 15°E and Gustav Dalen Tower (GDT) which is the closest station to the European region. Some missing data indicate the occurrence of clouds which makes limits data measurements. However, several authors have reported that contributions of the aerosol loading to the Arctic AOD are mostly dominated from sulphate in spring and OC (fires) in summer (Breider et al 2014).

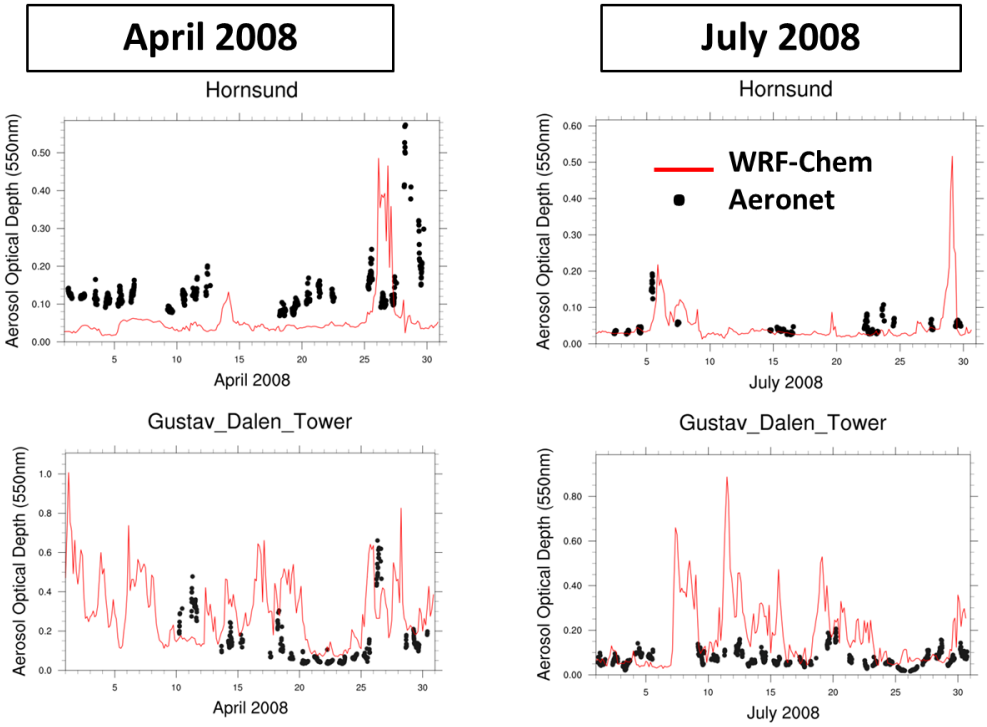

Figure 2. Time-series of AOD (500 nm) observed and simulated for April 2008 and July 2008 at the two stations Hornsund (Svalbard archipelago) and Gustav Dalen (Sweden).

Observed high concentrations of BC during April are characteristic to high aerosol loadings in late winter and early spring. During this period conditions are generally favourable for the transport of air pollutants forming the Arctic haze, for example, during April 2009 the atmosphere over the European and North American Arctic was variably hazy, with transport mainly from Eurasia (Stone et al., 2010). In Figure 3 we show how concentrations for BC vary for both periods. The spatial distribution of emissions averaged for both periods along North Europe are well represented, including Moskow and any other cities with large industrial and urban activities leading to high aerosol loadings. Unfortunately, emissions expected in the higher Eurasian Arctic where emissions in this area would be expected from diverse projects including the Yamal LNG project, the Kharyaga oil project, and Achimgaz located in the Nenets, the Yamalo-Nenets Autonomous Okrugs and the Novy Urengoy in Siberia (black circule in Figure 3). This is consistent with the reported by previous authors (e.g. Eckardt et al., 2015), where the high BC concentrations observed in Russia are currently not captured by models suggesting an underestimation of BC sources in Russia in current emission inventories.for the Ålesund observations (measurements are done at the Zeppelin station – 475 m a.s.l.) (Figure 3 and marked as "HOR" in Figure 1)higher concentrations of BC extended along the vertical column are mostly characteristic in April compared to July. This is denoted in the model where concentrations are presented above the 200hPa, compared with a rather clean higher atmosphere for July. Simulations of BC in spring indicate a mean concentration of 0.1 ± 0.1 μg m3 north of 60°N, which is consistent with other model simulations reported by other authors (i.e. Breider et al 2014 with 0.12 ± 0.05 μg m3)

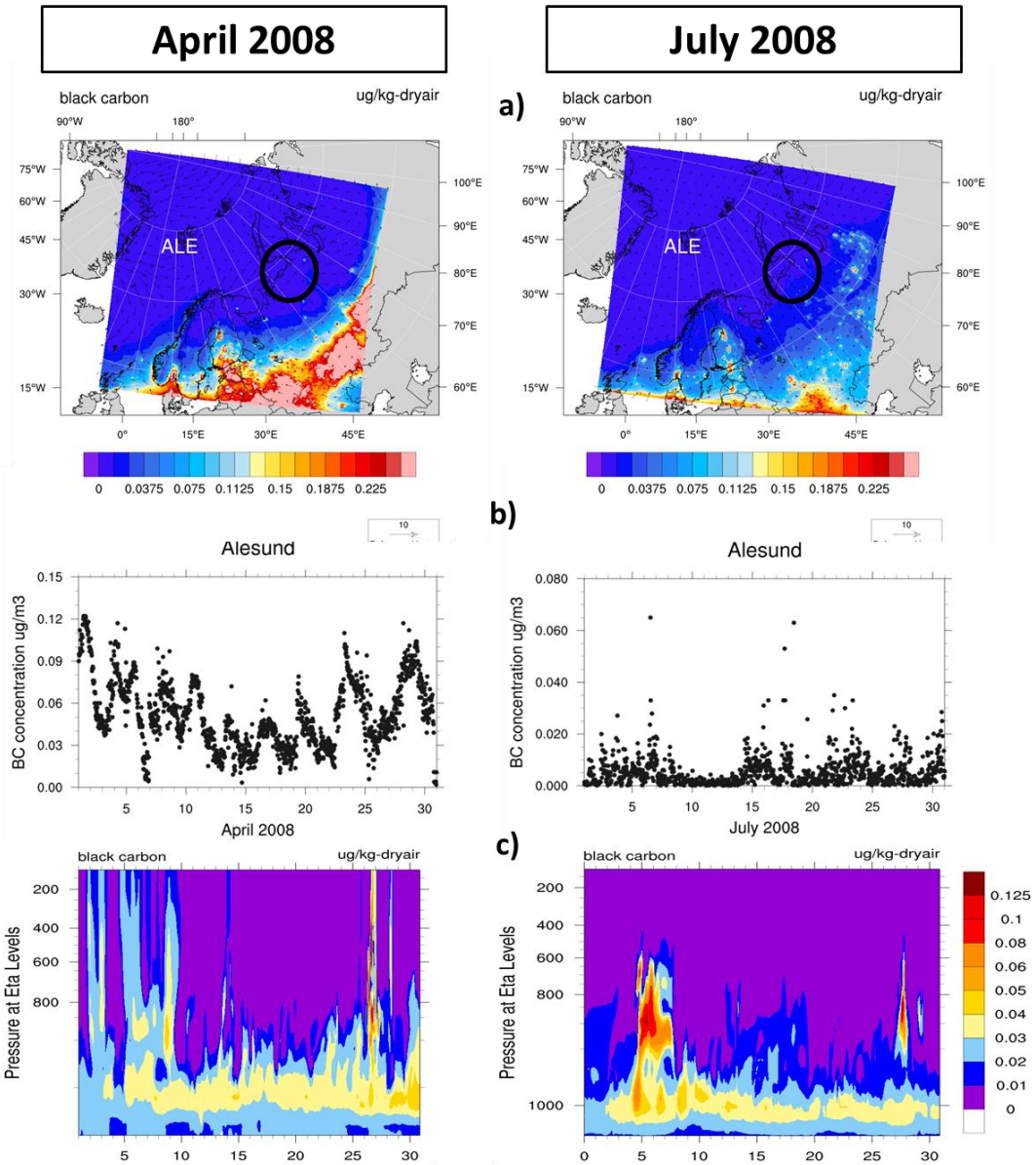

Figure 3. a) Simulated monthly mean of BC concentrations at the surface and wind speed at 10 m for both studied periods, ALE represents the location for the station Alesund in the Svalbard archipelago. b) timeseries of BC concentrations observed at Alesund and c) vertical distribution of modelled BC.

The results shown here is part of the ongoing work aiming to evaluate the capability of WRF-Chem to represent emissions of BC around the Eurasian Arctic. While the trends in emissions from our model are consistent with observations in terms of spatial distribution and timeseries, concentrations of BC are still underestimated or hardly visible, as mentioned previously especially in Russia. Next steps will consists of a more detailed model evaluation using observations collected from aircraft transections that within the PARACIMP campaign (Stone, et al 2010). In the meantime, our plan is to implement ECLIPSE dataset (including gas flaring) for future model experiments. Also, in order to evaluate and separate properly local emissions from long range transport, future analyses will include back-trajectories analysis to estimate the the path of the BC transported towards the Arctic and to evaluate the role played by atmospheric circulation as simulated by our model.

REFERENCES

Bradley, R.S., Keimig, F.T. and Diaz, H.F. (1992) Climatology of Surface-based Inversions in the North American Arctic. Journal of Geophysical Research, 97(D14), 15699-15712.

Breider, T. J., L. J. Mickley, D. J. Jacob, Q. Wang, J. A. Fisher, R. Y.-W. Chang, and B. Alexander (2014), Annual distributions and sources of Arctic aerosol components, aerosol optical depth, and aerosol absorption, J. Geophys. Res. Atmos., 119, 4107–4124, doi:10.1002/2013JD020996

Corbett, J., Lack, D., and Winebrake, J. (2010). Arctic shipping emissions inventories and future scenarios. Atmospheric Chemistry and Physics, (10), 9689–9704.

Grell, G. A., S. E. Peckham, R. Schmitz, S. A. McKeen, G. Frost, W. C. Skamarock, B. Eder (2005): Fully coupled "online" chemistry within the WRF model, Atmos. Environ., 39, 6957-6975.

Myhre, G., et al. (2013). Anthropogenic and Natural Radiative Forcing. In T.F. Stocker et al. (Eds.), Climate Change 2013: The Physical Science Basis. Contribution of Working Group I to the Fifth Assessment Report of the Intergovernmental Panel on Climate Change (pp. 659-740). Cambridge and New York: Cambridge University Press.

Samset, B. , Myhre, G. , Herber, A. , Kondo, Y. , Li, S. M. , Moteki, N. , Koike, M. , Oshima, N. , Schwarz, J. , Balkanski, Y. , Bauers, S. , Bellouin, N. , Berntsen, T. , Bian, H. , Chin, M. , Diehl, T. , Easter , R. , Ghan, S. , Iversen, T. , Kirkevåg, A. , Lamarque, J. F. , Lin, G. , Liu, X. , Penners, J. , Schulz, M. , Seland, Ø. , Skeie, R. , Stier, P. , Tamemura, T. , Tsigaridis, K. and Zhang, K. (2014) Modeled black carbon radiative forcing and atmospheric lifetime in AeroCom Phase II constrained by aircraft observations.

Sand, M., et al. (2013). Arctic Surface Temperature Change to Emissions of Black Carbon within Arctic or Midlatitudes. Journal of Geophysical Research, 118(14), 7788-7798.

Stohl, A. (2006). Characteristics of Atmospheric Transport into the Arctic Troposphere. Journal of Geophysical Research, 111(D11), 1-17.

Stohl, A., et al. (2013). Black carbon in the Arctic: the underestimated role of gas flaring and residential combustion emissions, Atmos. Chem. Phys., 13, 8833-8855.

Stone, R., et al. (2010). A Three-dimensional Characterization of Arctic Aerosols from Airborne Sun Photometer Observations: PAM-ARCMIP. Journal of Geophysical Research, 115(D13), 1-18.

ASSESSING NITROGEN DIOXIDE FROM BIOMASS BURNING IN SOUTH AND SOUTHEAST ASIA

F. CHEN[1], B. YU[1]

[1]Key Laboratory of Digital Earth Science, Institute of Remote Sensing and Digital Earth, Chinese Academy of Sciences, Beijing 100101, China

Keywords: REMOTE SENSING, NITROGEN DIOXIDE, ANTHROPOGENIC ACTIVITIES

INTRODUCTION

Nitrogen dioxide (NO_2) is one of the most prominent pollutant gases in troposphere, synthesizing industrial nitrous acid and nitric acid, which affects public health. In developing areas, such as most countries in South Asia, the concentration of nitrogen dioxide is strongly influenced by both biomass burning and anthropogenic activities. The launch of Ozone Monitoring Instrument (OMI) on NASA'S Aura satellite (Levelt et al., 2006) and Global Ozone Monitoring Experiment (GOME) on European Space Agency (ESA)'s European Remote Sensing (ERS)-2 satellites (Burrows et al., 1999) has made it easier for researchers to retrieve NO_2's total columns and tropospheric vertical columns. In addition, Fire radiative power (FRP) data, which are provided from the MODerate resolution Imaging Spectroradiometers (MODIS) on NASA's Terra and Aura satellites, have been widely used to represent fire for the analysis of its relationship with emission gases (Boschetti & Roy, 2009; Freeborn, Wooster, & Roberts, 2011; Vermote et al., 2009; Wooster, 2002). Many studies have focused on assessing NO_2 from biomass burning, however, such studies are conducted in relatively sparsely populated areas to avoid anthropogenic impact, but more complicated circumstances should be included. In this study, we proposed a method that considers population density when calculating correlation coefficients and this method would be applied in larger scales with more diverse lands and climate conditions conducting more reliable studies on fire emission gases. We also analysed the general correlation of our study area with monsoon impact and land use product. The impact of monsoon on the concentration of NO_2 is described in terms of monsoon wind blowing and NO_2 deposition by monsoon rains. Land cover products were used to further analyze the impact that different kind of land cover or land uses have on the fire emissions.

METHODS AND RESULTS

The monthly mean MODIS FRP products and monthly mean tropospheric NO_2 Level 2 (L2) (0-30% Cloud) products from Ozone Monitoring Instrument (OMI) from 2005 to 2014 are used in this study. Population density product is obtained from the Gridded Population of the World Version 3 (GPWv3) product, which is primarily supported by the National Aeronautics and Space Administration (NASA).

To analyse the impact of biomass burning on tropospheric NO_2, the column of background NO_2 over the study area is subtracted using the 'background' value, which is the column of NO_2 in years with least FRP. After subtracting background tropospheric NO_2 from that in the other 9 years, the general mean correlation coefficients between FRP and NO_2 of the whole study area in each month were calculated based on the proposed method, which subtracts the influence of anthropogenic activities by dividing the column of NO_2 in each location using population density. As shown in Figure 1, we compared the correlation performance between two methods, one is calculating correlation coefficient between FRP and NO_2 directly, the other is our proposed method, dividing the column of NO_2 in each location by population density. FRP is further adopted as a reference for the two correlation coefficients. The concentration of FRP decreases to a large extent during monsoon transition period (from April to June) and moves smoothly from June to September, because of monsoon rains and decrease in fire events and consequent emissions. The correlation between concentrations of NO_2 and FRP is therefore weak during summer

monsoon period. Winter monsoon enhances the correlation with increasing the fire emissions to the troposphere. It can be noted in Figure 1 that the proposed method reveals more reliable relationship between biomass fires and tropospheric NO_2, in terms of monsoon impact.

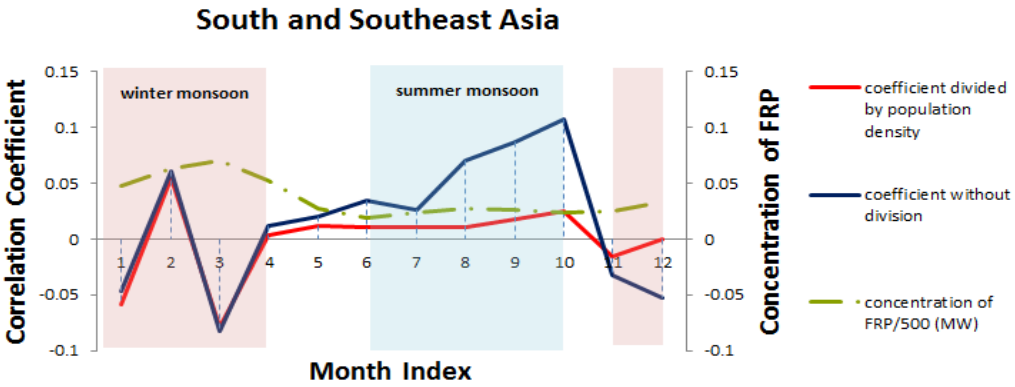

Figure 1 Mean correlation coefficient and FRP concentration of study area for each month during 10 years

In order to analyse the influence of monsoon on the correlation between NO_2 and FRP, we generated a 10-year correlation of determination map for the whole study area for each of the five time periods (January to March, April to May, June to September, October, and November to December). The correlation of determination maps are calculated from the 10-year mean of NO_2 and mean FRP for each period. 'Mean' represents averages of all the months belonging to each year's corresponding period. The experiment generally shows strong correlation between FRP and NO_2 from January to March and reduces with the arrival of summer monsoon. In countries like Laos, Vietnam and Thailand, that represent high FRP and NO_2 values from January to March, also show a high correlation. North India is a place with low FRP but high NO_2 and population density. The correlation in North India is comparatively strong and validates the efficiency of our approach as human impact is reduced by dividing the column of NO_2 using population density.

Land cover classification is another factor considered in our work as impacting the correlation coefficient between FRP and NO_2. We used the most recent available Global Mosaics of land cover product (MCD12Q1) (Channan, Collins, & Emanuel, 2014; Friedl et al., 2010) as land cover reference. We calculated annual mean concentrations of NO_2 and FRP for the pixels belonging to Forest, Grasslands, Croplands and Urban areas respectively. The correlation of determination over the nine years, the corresponding significance value and a simple linear relationship between NO_2 and FRP, for each land type was calculated (Table 1). Most land types are significantly correlated. It can be noted that forest areas have the strongest correlation, while urban areas have the weakest correlation in terms of coefficient determination and statistically significance value.

Table 1 Summary of coefficient of determination (CD), significant value (SV) and relationship between annual NO_2 (N) and FRP (F) in four land use types in South and Southeast Asia

Land use type	CD	SV	Relationship
Forest	0.160	0.704	N=0.0044F+0.0168
Grasslands	0.0276	0.971	N=-0.0004F+0.0039
Croplands	0.0722	0.845	N=0.00009F-0.0008
Urban	0.0298	0.643	N=-0.5991F-5.1381

CONCLUSIONS

Many studies are focusing on analysing fire emissions, such as NO_2, which are heavily influenced by anthropogenic activities. Usually, such studies are conducted in relatively sparsely populated areas to

avoid anthropogenic impact, but more complicated circumstances should be included. In this study, we proposed a method that considers population density when calculating correlation coefficients. This method was applied on larger scales with more diverse land types and climate conditions to get a more reliable study on fire emission gases. We also analysed seasonal impact of biomass fires on tropospheric nitrogen dioxide in South and Southeast Asia for a period of ten years from 2005 to 2014. Experiments show a general statistically strong significant correlation between FRP and NO_2, especially in the flammable areas like Forest. The results of this study also demonstrated that the climatic characteristics in summer monsoon and winter monsoon heavily influence the concentration of FRP and NO_2 in the atmosphere, and the correlation in most locations corresponds reasonably well. We concluded that population density can be used to effectively decrease human impact, but it cannot be used to fully represent anthropogenic impacts. More social related parameters also need to be considered (e.g., industrialization level, local economic structure and the type of industrialization) in further research.

ACKNOWLEDGEMENTS

This work was supported by the Hundred Talents Program of Chinese Academy of Sciences (Y34004101A), and the Comparative Study on Global Environmental Change Using Remote Sensing Technology (41120114001), the National Natural Science Foundation of Major International (regional) Collaborative Research Project. We thank Center for International Earth Science Information Network (CIESIN), Columbia University; and Centro International de Agricultural Tropical (CIAT) for providing population density data. The global land cover product from University of Maryland, Department of Geography and NASA is much appreciated. We wish to thank NASA's Goddard Earth Sciences Data and Information Services Center (GES DISC) for providing OMI and FRP data. The Giovanni system, supported by GES DISC, is of great help in accessing OMI and FRP data.

REFERENCES

Boschetti, L., & Roy, D. P. (2009). Strategies for the fusion of satellite fire radiative power with burned area data for fire radiative energy derivation. *Journal of Geophysical Research: Atmospheres (1984–2012), 114*(D20). doi: 10.1029/2008JD011645

Burrows, J. P., Weber, M., Buchwitz, M., Rozanov, V., Ladstätter-Weißenmayer, A., Richter, A., . . . Eichmann, K.-U. (1999). The global ozone monitoring experiment (GOME): Mission concept and first scientific results. *Journal of the Atmospheric Sciences, 56*(2), 151-175. doi: http://dx.doi.org/10.1175/1520-0469(1999)056<0151:TGOMEG>2.0.CO;2

Channan, S., Collins, K., & Emanuel, W. (2014). Global mosaics of the standard MODIS land cover type data. http://www.landcover.org/data/lc/

Freeborn, P. H., Wooster, M. J., & Roberts, G. (2011). Addressing the spatiotemporal sampling design of MODIS to provide estimates of the fire radiative energy emitted from Africa. *Remote Sensing of Environment, 115*(2), 475-489.

Friedl, M. A., Sulla-Menashe, D., Tan, B., Schneider, A., Ramankutty, N., Sibley, A., & Huang, X. (2010). MODIS Collection 5 global land cover: Algorithm refinements and characterization of new datasets. *Remote Sensing of Environment, 114*(1), 168-182. doi: 10.1016/j.rse.2009.08.016

Levelt, P. F., Van den Oord, G. H., Dobber, M. R., Mälkki, A., Visser, H., De Vries, J., . . . Saari, H. (2006). The ozone monitoring instrument. *Geoscience and Remote Sensing, IEEE Transactions on, 44*(5), 1093-1101. doi: r 10.1109/TGRS.2006.872333

Vermote, E., Ellicott, E., Dubovik, O., Lapyonok, T., Chin, M., Giglio, L., & Roberts, G. J. (2009). An approach to estimate global biomass burning emissions of organic and black carbon from MODIS fire radiative power. *Journal of Geophysical Research: Atmospheres (1984–2012), 114*(D18), 205-227. doi: doi:10.1029/2008JD011188

Wooster, M. J. (2002). Small - scale experimental testing of fire radiative energy for quantifying mass combusted in natural vegetation fires. *Geophysical Research Letters, 29*(21), 23-21-23-24. doi: 10.1029/2002GL015487

REVISITING THE DRIVES OF NORTHERN HEMISPHERE WINTER SURFACE AIR TEMPERATURE VARIABILITY DURING 1901-2010

L. CHEN[1], O.M. JOHANNESSEN[2]

[1]Nansen Environmental and Remote Sensing Centre, and Bjerknes Centre for Climate Research, Bergen, Norway

[2]Nansen Scientific Society, and Nansen Environmental and Remote Sensing Centre, Bergen, Norway

Keywords: NORTHERN HEMISPHERE, WINTER, SURFACE AIR TEMPERATURE, VARIABILITY

ABSTRACT

Despite amplified warming in the Arctic (Bengtsson et al., 2004; Johannessen et al., 2004; Serreze and Francis, 2006; Serreze and Barry, 2011), we have experienced several severe winters with cold spell in the Northern Hemisphere (NH) mid-latitudes (Overland et al., 2011; Cohen et al., 2012; Greene, 2012). Similarly, there were some extremely cold winters being documented during the early 20th century warming period (Brönnimann et al., 2004). Fig.1 demonstrated: 1) the NH annual mean Arctic Surface Air Temperature (SAT) anomalies (°C) relative to base period 1951-1980 from Goddard Institute for Space Studies (GISS) SAT analysis data (Hansen et al., 1999; Hansen et al., 2010). The early 20th century warming (1910-1950) and recent warming (since 1990s) periods could be recognized (Fig.1 (a), black curve); 2) Apparently negative linear trends of the winter SAT in Eurasian region could be found during both warming periods (Fig.1 (b) and (c)); 3) Arctic sea ice extent (10^6 km^2) during these two periods decreased (Fig.1 (a), blue curve).

The question is to what extent we can explain the severe weather conditions in these periods. Cohen et al. (2012) suggested that winter mid-latitude cooling trends shown in Fig.1 could not be explained entirely by internal variability of the climate system (e.g. North Atlantic Oscillation or the Arctic Oscillation). Both observational and modeling work suggested that the Arctic sea ice loss might have played an important role during current warming period (Francis et al., 2009; Honda et al., 2009; Simmonds and Keay, 2009; Deser et al., 2010; Overland and Wang, 2010; Cohen et al., 2012; Francis and Vavrus, 2012; Greene and Monger, 2012; Jaiser et al., 2012; Liu et al., 2012; Tang et al., 2013; Mori et al., 2014; Francis and Skific, 2015; Handorf et al., 2015; Overland et al., 2015; Screen et al., 2015). However, the robust dynamical link between proceeding summer sea-ice loss and winter weather in Europe is still under debate (Hopsch et al., 2012; Barnes, 2013; Screen and Simmonds, 2013; Barnes et al., 2014; Cohen et al., 2014; Wallace et al., 2014; Barnes and Screen, 2015). In this study, we analysed the dynamical features of those severe winters during both warming periods. The purpose is to provide better understanding and long-term perspective of the drivers of SAT variability in the mid-latitude.

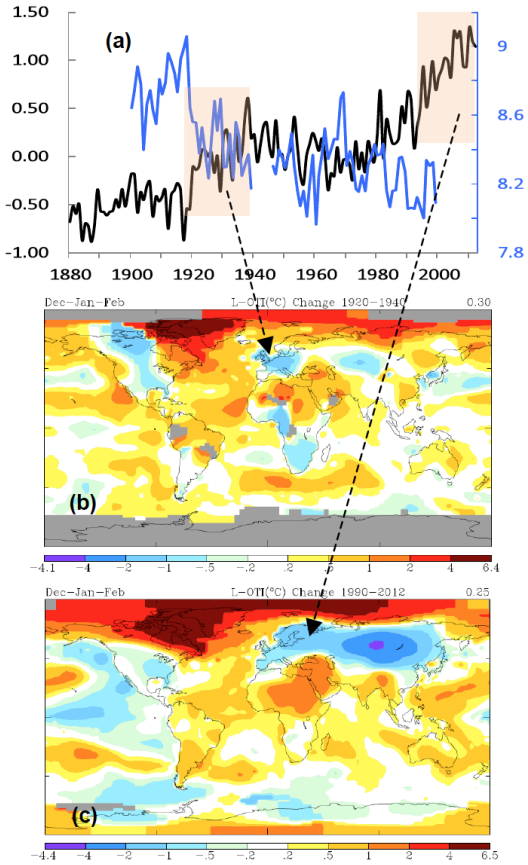

Fig.1 (a) NH annual mean Arctic SAT anomalies (°C) relative to the base period of 1951-1980 from GISS SAT data and mean annual ice extent (10^6 km^2) from Johannessen et al., (2004), with data coverage of 77% of the Arctic ocean; (b) Linear trends of the winter (Dec-Jan-Feb) SAT anomaly (°C) during the period of 1920-1940; (c) same as (b), but for the period of 1990-2012. Areas with missing data are shadowed in gray. SAT fields are plotted through http://data.giss.nasa.gov/gistemp/.

ACKNOWLEDGEMENTS

This work was supported by the Research Council of Norway under grant EuropeWeather (231322 / F20).

REFERENCES

Barnes EA. 2013. Revisiting the evidence linking Arctic amplification to extreme weather in midlatitudes. *Geophysical Research Letters* **40**(17): 4734-4739.

Barnes EA, Dunn- Sigouin E, Masato G, Woollings T. 2014. Exploring recent trends in Northern Hemisphere blocking. *Geophysical Research Letters* **41**(2): 638-644.

Barnes EA, Screen JA. 2015. The impact of Arctic warming on the midlatitude jet- stream: Can it? Has it? Will it? *Wiley Interdisciplinary Reviews: Climate Change* **6**(3): 277-286.

Bengtsson L, Semenov VA, Johannessen OM. 2004. The early twentieth-century warming in the Arctic-A possible mechanism. *J. Climate* **17**(20): 4045-4057.

Brönnimann S, Luterbacher J, Staehelin J, Svendby T, Hansen G, Svenøe T. 2004. Extreme climate of the global troposphere and stratosphere in 1940–42 related to El Nino. *Nature* **431**(7011): 971-974.

Cohen J, Furtado JC, Barlow MA, Alexeev VA, Cherry JE. 2012. Arctic warming, increasing snow cover and widespread boreal winter cooling. *Environ. Res. Lett.* **7**(1): 014007.

Cohen J, Screen JA, Furtado JC, Barlow M, Whittleston D, Coumou D, Francis J, Dethloff K, Entekhabi D, Overland J. 2014. Recent Arctic amplification and extreme mid-latitude weather. *Nature Geoscience* **7**(9): 627-637.

Deser C, Tomas R, Alexander M, Lawrence D. 2010. The seasonal atmospheric response to projected Arctic sea ice loss in the late twenty-first century. *J. Climate* **23**(2): 333-351.

Francis J, Chan W, Leathers DJ, Miller JR, Veron DE. 2009. Winter Northern Hemisphere weather patterns remember summer Arctic sea- ice extent. *Geophys. Res. Lett.* **36**(7): L07503.
Francis J, Vavrus S. 2012. Evidence linking Arctic amplification to extreme weather in mid- latitudes. *Geophys. Res. Lett.* **39**(6).
Francis J, Skific N. 2015. Evidence linking rapid Arctic warming to mid-latitude weather patterns. *Philosophical Transactions of the Royal Society of London A: Mathematical, Physical and Engineering Sciences* **373**(2045): 20140170.
Greene CH. 2012. The winters of our discontent. *Scientific American* **307**(6): 50-55.
Greene CH, Monger BC. 2012. An Arctic wild card in the weather. *Oceanography* **25**.
Handorf D, Jaiser R, Dethloff K, Rinke A, Cohen J. 2015. Impacts of Arctic sea ice and continental snow cover changes on atmospheric winter teleconnections. *Geophysical Research Letters* **42**(7): 2367-2377.
Hansen J, Ruedy R, Glascoe J, Sato M. 1999. GISS analysis of surface temperature change. *J. Geophys. Res.* **104**(D24): 30997-31022.
Hansen J, Ruedy R, Sato M, Lo K. 2010. Global surface temperature change. *Reviews of Geophysics* **48**(4): RG4004.
Honda M, Inoue J, Yamane S. 2009. Influence of low Arctic sea- ice minima on anomalously cold Eurasian winters. *Geophys. Res. Lett.* **36**(8).
Hopsch S, Cohen J, Dethloff K. 2012. Analysis of a link between fall Arctic sea ice concentration and atmospheric patterns in the following winter. *Tellus A* **64**.
Jaiser R, Dethloff K, Handorf D, Rinke A, Cohen J. 2012. Impact of sea ice cover changes on the Northern Hemisphere atmospheric winter circulation. *Tellus A* **64**.
Johannessen OM, Bengtsson L, Miles MW, Kuzmina SI, Semenov VA, Alekseev GV, Nagurnyi AP, Zakharov VF, Bobylev LP, Pettersson LH. 2004. Arctic climate change: Observed and modelled temperature and sea- ice variability. *Tellus A* **56**(4): 328-341.
Liu J, Curry JA, Wang H, Song M, Horton RM. 2012. Impact of declining Arctic sea ice on winter snowfall. *Proceedings of the National Academy of Sciences* **109**(11): 4074-4079.
Mori M, Watanabe M, Shiogama H, Inoue J, Kimoto M. 2014. Robust Arctic sea-ice influence on the frequent Eurasian cold winters in past decades. *Nature Geoscience* **7**(12): 869-873.
Overland J, Wang M. 2010. Large- scale atmospheric circulation changes are associated with the recent loss of Arctic sea ice. *Tellus A* **62**(1): 1-9.
Overland J, Wood KR, Wang M. 2011. Warm Arctic-cold continents: climate impacts of the newly open Arctic Sea. *Polar* Research **30**: 15787.
Overland J, Francis JA, Hall R, Hanna E, Kim S-J, Vihma T. 2015. The Melting Arctic and Midlatitude Weather Patterns: Are They Connected?*. *Journal of Climate* **28**(20): 7917-7932.
Screen JA, Simmonds I. 2013. Exploring links between Arctic amplification and mid- latitude weather. *Geophys. Res. Lett.* **40**: 1-6.
Screen JA, Deser C, Sun L. 2015. Projected changes in regional climate extremes arising from Arctic sea ice loss. *Environmental Research Letters* **10**(8): 084006.
Serreze MC, Francis JA. 2006. The Arctic amplification debate. *Climatic Change* **76**(3-4): 241-264.
Serreze MC, Barry RG. 2011. Processes and impacts of Arctic amplification: A research synthesis. *Global and Planetary Change* **77**(1): 85-96.
Simmonds I, Keay K. 2009. Extraordinary September Arctic sea ice reductions and their relationships with storm behavior over 1979–2008. *Geophys. Res. Lett.* **36**(19).
Tang Q, Zhang X, Yang X, Francis JA. 2013. Cold winter extremes in northern continents linked to Arctic sea ice loss. *Environ. Res. Lett.* **8**(1): 014036.
Wallace JM, Held IM, Thompson DW, Trenberth KE, Walsh JE. 2014. Global warming and winter weather. *Science* **343**: 729-730.

HIGH PERFORMANCE RETRIEVAL OF FY3 GLOBAL SURFACE ALBEDO

PAN CHEN[A], YONG XUE[B,C], JIE GUANG[B]

[a] Beijing Capital Normal University, Beijing 100048, China

[b] Key Laboratory of Digital Earth Science, Institute of Remote Sensing and Digital Earth, Chinese Academy of Sciences, Beijing 100094, China

[c] Faculty of Life Sciences and Computing, London Metropolitan University, 166-220 Holloway Road, London N7 8DB, UK

{Email: 1393239821@qq.com; yx9@hotmail.com}

ABSTRACT

Surface albedo is the diffuse reflectivity or reflecting power of a surface. It is the ratio of reflected radiation from the surface to incident radiation upon it (Guang et al. 2013, Xue et al. 2014). Its dimensionless nature lets it be expressed as a percentage and is measured on a scale from zero for no reflection of a perfectly black surface to 1 for perfect reflection of a white surface. It is an important concept in climatology, astronomy, and calculating reflectivity of surfaces in LEED sustainable-rating systems for buildings. Since different object on earth have different albedo in certain conditions, it will help us recognize and analysis different ground objects.

Guang et al. (2012) has developed the FY3 aerosol and surface reflectance determination program V1.0. According to her work, we are going to realize global surface albedo calculation with FY-3A and FY-3B data. The data we have got are FY3A_MERSI L1, FY3B_MERSI L1, FY3A_MERSI cloud data, FY3B_VIRR cloud data, FY3B_VIRR L1. We have also got some auxiliary data, such as NCEP water vapor data and ozone data, MOD04 data, MCD43 data, *MOD09GA and MYD09GA data. The calculation flowchart is shown in FIG 1. The surface albedo and AOD can be calculated simultaneously.

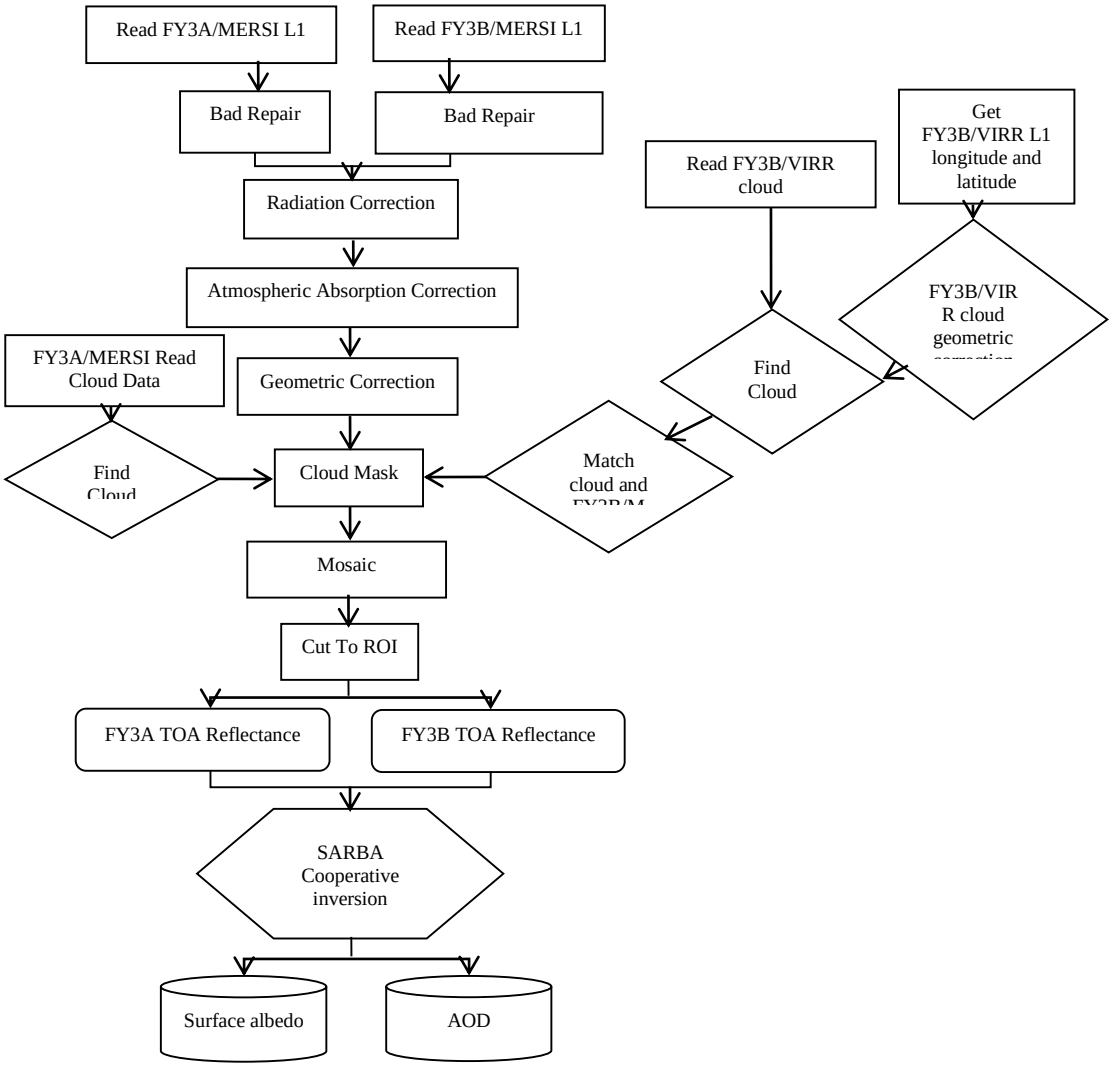

FIG. 1 the process of global surface albedo determination

To produce long-term time series global surface albedo dataset, huge amount of data need to be processed through the determination workflow shown in Fig. 1 and is quite time-consuming task. To improve efficiency, two levels of parallel computing are applied to the albedo determination procedures.

a) Data-level parallelism is applied to the pre-processing and calculation procedures, such as the absorption correction, geometric correction etc. through the multi-core parallel on a single computing node computing based on OpenMP.
b) Function-level parallelism were applied to the whole workflow, thus the processing which are independent with each other can be executed simultaneously on different computing nodes in a cluster environment.

REFERENCES

[1] Michael J. Quinn. Parallel programming in C with MPI and openMP[M]. New York: The McGraw-Hill Companies, Inc, 2004: 8-10.

[2] Yong Xue, Xingwei He, Hui Xu, Jie Guang, Jianping Guo, and Linlu Mei, 2014, CHINA COLLECTION 2.0: The Aerosol Optical Depth Dataset from the Synergetic Retrieval of Aerosol Properties Algorithm. *Atmospheric Environment*, Volume 95, October 2014, Pages 45–58.

[3] Yun Fen, Shuqiu Zhou. Research on the application of MPI+OpenMP hybrid parallel programming model[J]. Computer system application, 2006, 02:86-89.
[4] Jie Guang, Yong Xue, Leiku Yang, Linlu Mei, and Xingwei He, 2013, A Method for Retrieving Land Surface Reflectance Using MODIS Data. *IEEE Journal of Selected Topics in Applied Earth Observations and Remote Sensing*, **6(3)**, 1564 - 1570.
[5] J. Guang, Y. Xue, Y. J. Li, S. L. Liang, L.L. Mei and H. Xu, 2012, Retrieval of Aerosol Optical Depth over Bright Land Surfaces by Coupling Bidirectional Reflectance Distribution Function Model and Aerosol Retrieval Model. *Remote Sensing Letter*, **3 (7)**, 577-584.

ON THE IONISING CAPACITY IN THE LOWER ATMOSPHERE AND ITS CONNECTION TO AIR ION OBSERVATION

X. CHEN[1], V.-M. KERMINEN[1], P. PAASONEN[1], J. PAATERO[2], H. E. MANNINEN[1], T. PETÄJÄ[1] and M. KULMALA[1]

[1]Department of Physics, University of Helsinki, Finland

[2] Finnish Meteorological Institute, Helsinki, Finland

Keywords: IONISING CAPACITY, IONISATION, AIR IONS, NUCLEATION

INTRODUCTION

Ionising radiation in the lower atmosphere produces electric charges via the ionisation of air molecules. The potential production rate of electric charges by the ionising radiation is termed as the ionising capacity. Radioactivity released during radon decay as well as gamma radiation of terrestrial and cosmic origins are the main contributors to the ionising capacity in the lower atmosphere. The initially formed electric charges are known as primary ions, which may either end up in the recombination process or undergo a series of other processes, including clustering, coagulation and condensational growth, and eventually become detectable air ions. Although the connection of air ion formation to ionising radiation is self-evident, except for a few attempts (Laakso et al., 2004; Hirsikko et al., 2007), minor efforts have been paid in understanding this causality in the lower atmosphere and there is a lack of quantification on the underlying processes. In this study, we aim to examine the relation of observed air ions to ionising radiation, based on ambient measurements deployed at Hyytiälä SMEAR II station (Hari and Kulmala, 2005), to assist a better understanding on air ion formation and atmospheric nucleation processes.

METHODS

The SMEAR II station ((61º50´40´´N, 24º17´13´´E) locates in a boreal forest in Southern Finland. A radon monitor and a total gamma detector serve the measurement of ionising radiation on this site. These devices are maintained by the Finnish Meteorological Institute. The total ionising energy carried by the radiation was first determined based on the measured quantities. For the ionising energy involved in radon decay processes, energy from the alpha and beta decays of radon-222 and its short-lived daughter nuclides, as shown in Table 1, were accounted. Then, by assuming an expense of 34 eV per production of an ion pair in the lower atmosphere, the ionising energy was converted to the ionising capacity in produced ion pairs per cubic centimetre per second.

Various instrumentations are applicable to characterise air ions. There are two main categories: ion spectrometers for providing number concentration and size information as well as mass spectrometers for determining chemical compositions. Since this study aims to explore the linkage of air ion formation to ionising radiation (quantified as the ionising capacity), the number size information is of more relevance. Therefore, ion data obtained from a balanced scanning mobility analyser (BSMA (Tammet, 2006)) was used in the analysis. The BSMA measures air ion concentration in segregated mobility channels. These concentrations measured in mobility domain were then converted into number size distribution with particle size expressed in mobility diameter following the Stokes-Cunningham-Knudsen-Weber-Millikan model standardised by the International Organization for Standardization in ISO 15900:2009. The equivalent mobility diameter range of the BSMA is from 0.8 to 8 nm.

To assist the investigation, also recorded meteorological data from the mast measurement, particle data, snow depth data and soil data collected at the station were used in this work. In addition, mixing layer height

(MLH) estimates retrieved from the Meteorological Archival and Retrieval System (MARS), the main repository of meteorological data at the European Centre for Medium-Range Weather Forecasts (ECMWF), and trajectory data calculated from the FLEXible TRAjectories (FLEXTRA) model (Stohl et al., 1995) were analysed in this work together with the measured data.

Table 1. Decay mode and energy of radon-222 and its short-lived progeny taken into account in ionising capacity determination. Decay partitioning is accounted in the weighted average decay energy. The data are extracted from the National Nuclear Data Centre of Brookhaven National Laboratory (http://www.nndc.bnl.gov/chart/).

Nuclide	Decay mode	Weighted average decay energy [keV]
^{222}Rn	α □□□□□□	5589
^{218}Po	α (99.98%)	6001
^{214}Pb	β^- (100%)	225
^{214}Bi	β^- (100%)	642
^{214}Po	α (100%)	7687

RESULTS AND DISCUSSIONS

The ionising capacity followed the variation in the ionising radiation. In general, the ionising capacity was high in summer and autumn and low in spring and winter, with the median values being 8.9 $cm^{-3}s^{-1}$, 11.2 $cm^{-3}s^{-1}$, 11.3 $cm^{-3}s^{-1}$ and 8.7 $cm^{-3}s^{-1}$ in spring (March-May), summer (June-August), autumn (September-November) and winter (December-February), respectively. Both radon and gamma components contributed to the seasonality of the ionising capacity, whereas the diurnal feature was primarily related to the dynamical response of radon to the mixing layer evolution. The variability of the radon ionising capacity was influenced by mixing layer dynamics, soil type, soil and meteorological conditions, long-distance transportation, etc. Compared with the radon ionising capacity, the pattern in the gamma ionising capacity was simpler and exhibited little diurnal cycles. The seasonal variation in the gamma ionising capacity was primarily contributed by the snow attenuation effect on terrestrial gamma in winter. The share of the radon ionising capacity in the total accounted only for 10-20%, with the contribution of the radon component found to be typically below 10% on new particle formation (NPF) event days. The classification of NPF event and non-event days followed the criteria explained by Dal Maso et al. (2005). The low radon share on NPF event days was likely related to the fact that air masses originated from Arctic and north Atlantic oceanic regions tend to induce NPF events (Nilsson et al., 2001) and they usually have low radon content (Wilkening and Clements, 1975; Chen et al., 2016).

The transformation from primary ions to cluster (0.8-1.7 nm) ions involves complicated physical and chemical processes. As a consequence, the observed variations in cluster ions hardly follow the features of the ionising capacity, but blurred by ion-ion recombination, photochemical processes, vapour uptake, attachment to pre-existing particles, etc. Nevertheless, when the cluster size range was chopped to narrower bins, clearer linkage to the ionising capacity was discernible in the 0.8-1 nm ion concentration. Yet, influences from atmospheric conditions on this connection were seen.

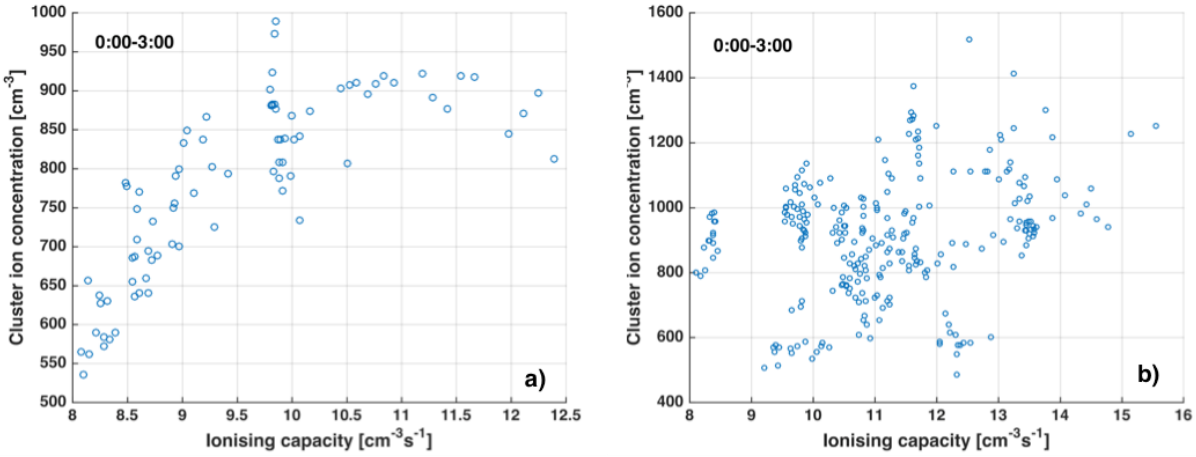

Figure 1. Cluster ion (0.8-1.7 nm) concentration as a function of ionising capacity on a) event days and b) non-event days, for selected data between morning hours of 0:00 and 3:00 during snow-free period in September-December of 2003-2006, when the condensation sink (CS (Kulmala et al., 2012)) derived from the particle number size distribution was in between 10^{-5} and $2*10^{-3}$ s^{-1} and wind direction was between 280° and 30°.

Although various processes contribute to the transition of primary ions to observable cluster ions, the relation of cluster ion formation to the ionising capacity was pinpointed, when the key parameters involved in these processes were carefully constrained. Figure 1 shows the correlation between the ionising capacity and the cluster ion concentration on both NPF event and non-event days. A clear relationship between the ionising capacity and cluster ion concentration was observed on NPF event days, with a correlation coefficient (R) of 0.77. Such correlation, however, was less evident on non-event days (R = 0.27) and associated with higher degree of dispersion. For larger ionising capacity than 10.5 $cm^{-3}s^{-1}$on event days, the observed cluster ion concentration levelled up, which may be related to the winning of the recombination between primary ions over the processes leading to cluster ion formation. The higher degree of dispersion on non-event days may be attributed to the higher variability in atmospheric conditions on non-event days than on event days.

CONCLUSIONS

A deeper understanding on the relationship between the ionising radiation and air ion formation is essential to puzzle out atmospheric aerosol formation processes, which further would assist in solving air-quality- and climate-related problems. Assessment on the closure of air ion formation from radiation is in progress to explore the transformation from primary ions to cluster and lager ions.

ACKNOWLEDGEMENTS

This study was supported by the Academy of Finland Centre of Excellence (project no. 272041 and 1118615), CRAICC (Cryosphere-atmosphere interactions in a changing Arctic climate) project within the Nordforsk Top-level Research Initiative Programme Interaction between climate change and the cryosphere as well as European Union Seventh Framework Programme (FP7/2007-2013) under grant agreement n° 262254. Measurements at Hyytiälä have been performed by the University of Helsinki.

REFERENCES

Chen X., Paatero J., Kerminen V.-M., Riuttanen L., Hatakka J., Hiltunen V., Paasonen P., Hirsikko A., Franchin A., Manninen H.E., Petäjä T., Viisanen Y. & Kulmala M. (2016) Responses of the atmospheric concentration of radon-222 to the vertical mixing and spatial transportation. *Boreal Env. Res.* **21**:In press.

Dal Maso M., Markku Kulmala, Ilona Riipinen, Robert Wagner, Tareq Hussein, Pasi P. Aalto & Lehtinen K.E.J. (2005) Formation and growth of fresh atmospheric aerosols: eight years of aerosol size distribution data from SMEAR II, Hyytiälä, Finland. *Boreal Env. Res.* **10**:323 - 336.

Hari P. & Kulmala M. (2005) Station for measuring ecosystem-atmosphere relations (SMEAR II). *Boreal Environ. Res.* **10**:315-322.

Hirsikko A., Paatero J., Hatakka J. & Kulmala M. (2007) The ^{222}Rn activity concentration, external radiation dose and air ion production rates in a boreal forest in Finalnd between March 2000 and June 2006. *Boreal Env. Res.* **12**:265 - 278.

Kulmala M., Petaja T., Nieminen T., Sipila M., Manninen H.E., Lehtipalo K., Maso M.D., Aalto P.P., Junninen H., Paasonen P., Riipinen I., Lehtinen K.E., Laaksonen A. & Kerminen V.M. (2012) Measurement of the nucleation of atmospheric aerosol particles. *Nat. Protoc.* **7**:1651-1667.

Laakso L., Petäjä T., Lehtinen K.E.J., Kulmala M., Paatero J., Hõrrak U., Tammet H. & Joutsensaari J. (2004) Ion production rate in a boreal forest based on ion, particle and radiation measurements. *Atmos. Chem. Phys.* **4**:1933–1943.

Nilsson E., Paatero J. & Boy M. (2001) Effects of air masses and synoptic weather on aerosol formation in the continental boundary layer. *Tellus* **52B**:462–478.

Stohl A., Wotawa G., Seibert P. & Kromp-Kolb H. (1995) Interpolation errors in wind fields as a function of spatial and temporal resolution and their impact on different types of kinematic trajectories. *J. Appl. Meteorol.* **34**:2149-2165.

Tammet H. (2006) Continuous scanning of the mobility and size distribution of charged clusters and nanometer particles in atmospheric air and the Balanced Scanning Mobility Analyzer BSMA. *Atmos. Res.* **82**:523-535.

Wilkening M.H. & Clements W.E. (1975) Radon 222 from the ocean surface. *J. Geophys. Res.* **80**:3828-3830.

APPLICATION OF THE AEROSOL DIFFUSION SPECTROMETER TO MEASURE ATMOSPHERIC NEW PARTICLE FORMATION

X. CHEN[1], S. DUBTSOV[2], T. OVCHINNIKOVA[3], S. VALIULIN[2,4], H.E. MANNINEN[1], P.P. AALTO[1] and T. PETÄJÄ[1]

[1]Department of Physics, University of Helsinki, P.O.BOX 64 FI-00014, Finland

[2]Institute of Chemical Kinetics and Combustion SB RAS, 630090, Institutskaya str., 3, Novosibirsk, Russia

[3]Institute for Water and Environmental Problems SB RAS, 630090, Morskoi avenue., 2, Novosibirsk, Russia

[4]Novosibirsk State Pedagogical University, 630126, Viluiskaya str., 28, Novosibirsk, Russia

Keywords: AEROSOL DIFFUSION SPECTROMETER, DIFFERENTIAL MOBILITY PARTICLE SIZER, NEUTRAL CLUSTER AND AIR ION SPECTROMETER, NEW PARTICLE FORMATION

INTRODUCTION

Atmospheric aerosol particles affect climate, cloud formation, air quality, visibility and human health (Poschl, 2005; von Klot et al., 2005). The number size distribution of ambient aerosol particles covers wide size and concentration ranges (Poschl, 2005). Yet, no a single instrument can measure the full observed size or concentration range in the atmosphere (McMurry, 2000). Therefore, in order to characterise atmospheric aerosol particles, a combination of various instruments and techniques is necessary. However, since instrumentations are developed from different physical bases, the performance of measurement devices requires intercompared to ensure the reliability of the data and the corresponding interpretation. The ambient performance of the ADS is assessed based on data collected at Hyytiälä SMEAR II in southern Finland (Hari and Kulmala, 2005), by comparison with aerosol and ion instruments.

METHODS

ADS measures concentration and size distribution of nanoparticles. It is composed primarily of a diffusion battery (DB), a condensation particle magnifier (CPM), an optical particle counter (OPC), and an interface controller (IC) (Figure 1). The DB has several stages, where the diffusional losses of particles passing through this section are controlled by the number of meshes. The volumetric flow rate through DB is kept at1 l/min. Particles that survive the DB section, enter in a mixing type condensation particle magnifier, similar to that described by Fuchs and Sutugin (1965), where they are grown by the condensation of dibuthylphthalate (DBP). Subsequently, the particle concentration is determined with an optical particle counter. Without dilution, the ADS is able to classify aerosol particles with a total number concentration between 10 and $2\times10^5 cm^{-3}$. The minimal time for one measurement cycle of the size distribution is about 4 min. Eventually, the particle size distribution is reconstructed in the range of 3-200 nm, based on the model of diffusional particles deposition on wire meshes proposed by Mavliev and Ankilov (1985).

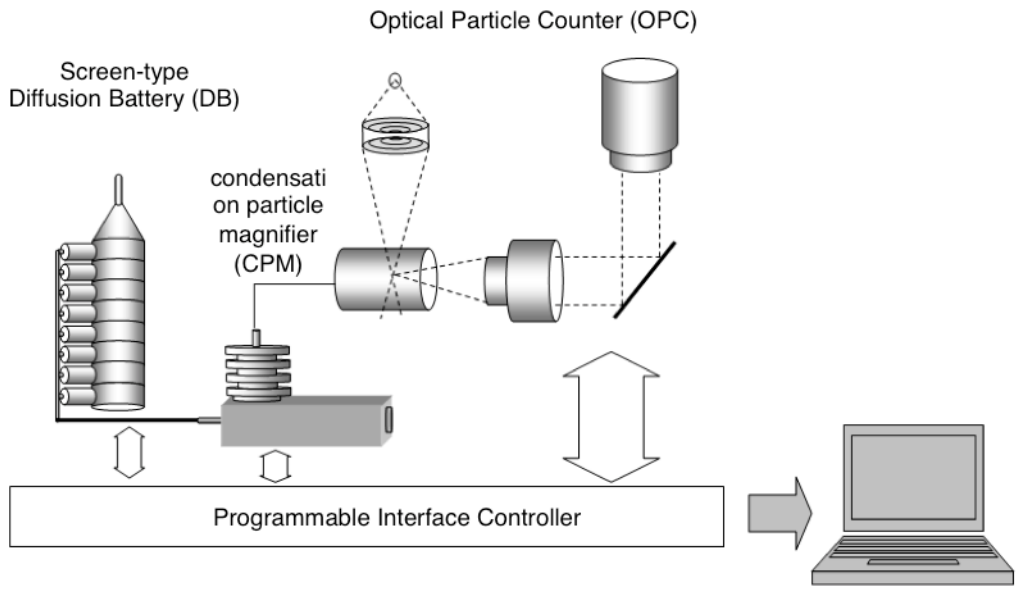

Figure 1. Major components in an Aerosol Diffusion Spectrometer (ADS).

The ADS was compared with a Differential Mobility Particle Sizer (DMPS) for the measurement of atmospheric aerosol particles, during a field campaign (April 29 - May 15, 2013) at Hyytiälä SMEAR II station. A Neutral cluster and Air Ion Spectrometer (NAIS) was additionally used to assess the ADS performance in measuring atmospheric new particle formation (NPF). Since the DMPS system involves a diffusion drier on the sheath flow line, the distribution of aerosol particles measured by the DMPS resembles the dry size distribution (Yli-Juuti et al., 2011). Thus, a hygroscopic correction, according to Laakso et al. (2004), was introduced in processing the DMPS data.

RESULTS AND DISCUSSIONS

During the field comparison in general, a good correlation was found between the total concentrations measured by the ADS and DMPS in the size range of 3-200 nm (Figure 2), apart from on the days with ADS malfunction. The size distributions above 6 nm measured by the ADS and DMPS were identified with similar features on a NPF day (March 3, 2013). However, the ADS detected more aerosol particles than the DMPS on the NPF day between size range of 20-50 nm, but less above 50 nm. On a non-event day (March 5, 2015), the particle size distribution of the ADS peaked at smaller size and did not capture a shoulder appearing at around 100 nm shown by the DMPS. In the size range of 2.9 – 6 nm, the ADS detected higher concentration of aerosol particles than the DMPS, which however, was similar to that given by the NAIS, suggesting that the ADS has better ability than the DMPS in counting small particles.

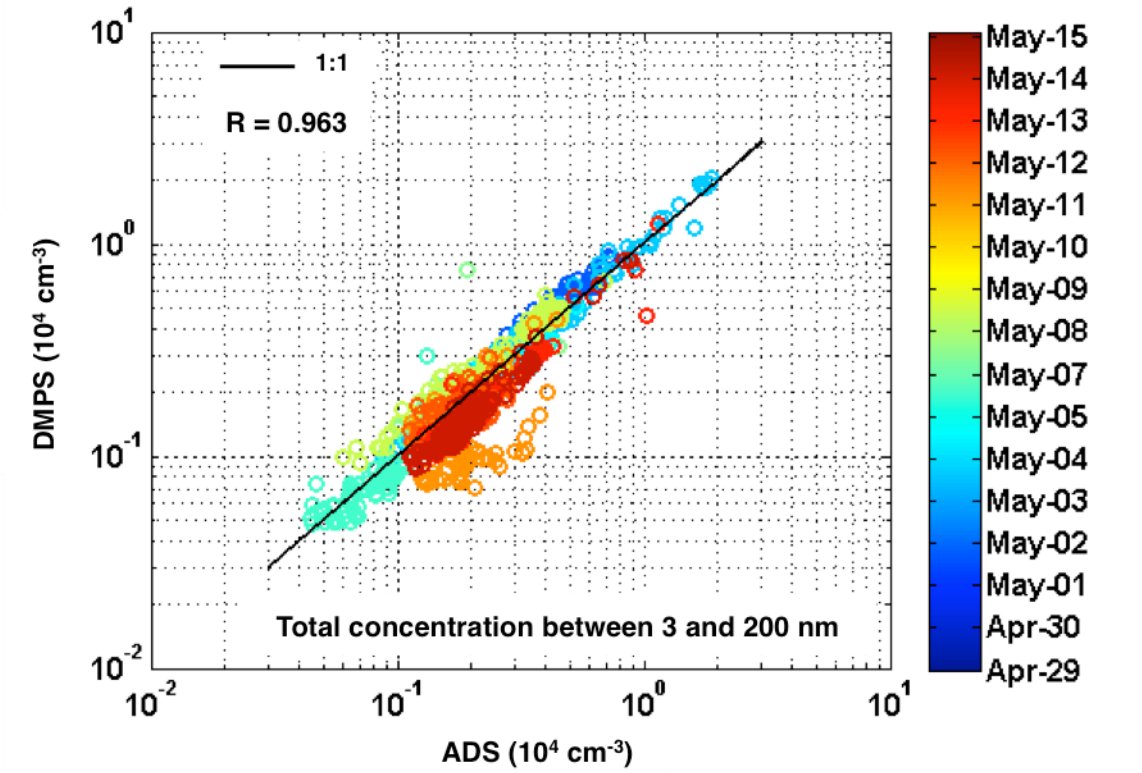

Figure 2. Correlation between the total particle number concentrations measured by the DMPS and ADS in the size range of 3-200 nm. Dates are indicated by colour. The ADS was off on May 6 and functioned improperly during May 9-12. The DMPS data was presented with hygroscopic correction.

As for mean diameters, the difference between the sizes derived from the DMPS and ADS was smaller on the event day whereas more notable on the non-event day. On NPF event days, better agreement in arithmetic and geometric diameters was observed between the ADS and DMPS measurements, but poorer in the case of the volumetric diameter. The ADS tended to slightly underestimate the size of aerosol particles compared with the DMPS, especially on the non-NPF day.

Table 1. NPF event parameters determined from the ADS, NAIS and DMPS data: growth rate (GR), condensation sink (CS), formation rate (J) and vapor source rate (*Q*).

Date	May 1, 2013			May 3, 2013		
Instruments	ADS	NAIS	DMPS	ADS	NAIS	DMPS
GR (nm/h)	4.1	4.4	4.2	6.4	6.2	5.3
CS (10^{-3} s^{-1})	0.2	-	0.5	0.6	-	1.1
J ($cm^{-3}s^{-1}$)	0.6	-	0.8	2.1	-	2.4
Q (10^4 $cm^{-3}s^{-1}$)	2.6	-	6.0	6.2	-	10.2
Date	May 8, 2013			May 14, 2013		
Instruments	ADS	NAIS	DMPS	ADS	NAIS	DMPS
GR (nm/h)	6.0	6.4	5.6	21.6	19.3	19.3
CS (10^{-3} s^{-1})	0.4	-	1.1	0.9	-	2.1
J ($cm^{-3}s^{-1}$)	0.08	-	0.1	1.1	-	1.3
Q (10^4 $cm^{-3}s^{-1}$)	6.9	-	20.2	4.3	-	9.7

The concentration difference between the NAIS and DMPS or ADS diminished upon the occurrence of the NPF and tended to retain at its minimum during the event. However, outside the event period, the disagreement was seen. Smallest differences between condensation sinks derived from the ADS and DMPS were observed on NPF days, yet lower sinks from the ADS than those from the DMPS measurement. Similar GR were acquired from DMPS, NAIS and ADS measurements (Table 1). The obtained *J* from the DMPS and ADS for 3-25 nm particles were also comparable, showing the capability of the ADS in measuring atmospheric new particle formation. More detailed analyses can be found in Dubtsov et al. (2015).

CONCLUSIONS

The ADS was intercompared with aerosol and ion instruments at Hyytiälä SMEAR II station in southern Finland, for the evaluation of the ADS ability in the classification of ambient aerosol particles. In general, the performance of the ADS during the field campaign was comparable with the DMPS and NAIS for ambient aerosol measurement in the size range of 3-200 nm. The number concentration measured by ADS and DMPS showed typically a good agreement. Differences between condensation sinks derived from the ADS and DMPS were smaller on NPF event days than those on non-NPF days. The DMPS, NAIS and ADS measurements gave similar formation rates and growth rates, proving the capability of the ADS in depicting atmospheric new particle formation.

ACKNOWLEDGEMENTS

The Academy of Finland via Finnish Center of Excellence (no. 272041) and European Commission via ACTRIS and PEGASOS projects are acknowledged for funding support. This project has received funding from the European Union’s Horizon 2020 research and innovation programme under grant agreement No 654109 and the European Union Seventh Framework Programme (FP7/2007-2013) under grant agreement n° 262254.

REFERENCES

Dubtsov S., T. O., Valiulin S., Chen X., Manninen H.E., Aalto P.P. & Petäjä T. (2015) Laboratory verification of Aerosol Diffusion Spectrometer and the application to ambient measurements of new particle formation, submitted to J. Aero. Sci.

Fuchs N.A. & Sutugin A.G. (1965) Coagulation Rate of Highly Dispersed Aerosols. *Journal of Colloid Science* **20**:492–500.

Hari P. & Kulmala M. (2005) Station for measuring ecosystem-atmosphere relations (SMEAR II). *Boreal Environ. Res.* **10**:315-322.

Mavliev R.A. & Ankilov A.N. (1985) Methods for the treatment of data for a netlike diffusion battery *Kolloidn. Zhurn. (in Russian)* **47**:523 – 530.

McMurry P.H. (2000) A review of atmospheric aerosol measurements. *Atmospheric Environment* **34**:1959-1999.

Poschl U. (2005) Atmospheric aerosols: composition, transformation, climate and health effects. *Angewandte Chemie* **44**:7520-7540.

von Klot S., Peters A., Aalto P., Bellander T., Berglind N., D'Ippoliti D., Elosua R., Hormann A., Kulmala M., Lanki T., Lowel H., Pekkanen J., Picciotto S., Sunyer J., Forastiere F. & Health Effects of Particles on Susceptible Subpopulations Study G. (2005) Ambient air pollution is associated with increased risk of hospital cardiac readmissions of myocardial infarction survivors in five European cities. *Circulation* **112**:3073-3079.

OBSERVED AND MODELED SNOW AND ICE THICKNESS IN CHUCKCHI SEA WITH CHINARE 2014 DATA

B. CHENG[1], Z. TIAN[2], J. ZHAO[2] ,T. VIHMA[1] and Z. LI[3]

[1]Finnish Meteorological Institute (FMI), 00101, Helsinki Finland.

[2]National Marine Environmental Forecasting Centre (NMEFC), 100081, Beijing, China.

[3]Dalian University of Technology (DUT), Dalian, China

Keywords: SEA ICE, THICKNESS, CHINARE, ARCTIC

INTRODUCTION

The sea ice is a critical component of the Arctic system playing an important role in the earth climate system. Sea ice is sensitive to atmospheric and oceanic variability because many climate feedbacks were linked with or enhanced by sea ice. The long term sea ice gauge measurements have been carried out during annual field expeditions in the Arctic Ocean, such as SHEBA ice camp ((Uttal et al., 2002). DAMOCLES Tara ice camp (Gascard et al, 2008). There are a number of short term ice expeditions, such as CHINARE program (e.g. Zhang, 2004), where sparse borehole ice thickness was measured in a time scale of 2 - 4 months covering domain of CHINARE. In order to obtain long term sea ice thickness, ice mass balance buoys (IMB) were also deployed (Lei et al., 2014). In recent CHINARE expeditions (e.g. CHINARE2014), two high-resolution Snow and Ice Mass Balance Array known as SIMBA units (Jackson et al., 2013) were deployed in the north Beaufort Gyre region. Snow and sea ice thickness can be derived from SIMBA data (Cheng et al, 2015). The cost cutting design of SIMBA makes it applicable for snow and ice monitoring in seasonal ice covered seas and lakes (Cheng et al, 2014). The performance of SIMBA in the Arctic Ocean, however, needs to be investigated more in detail. In this study we compared SIMBA snow and ice thickness with results from a numerical sea ice model. We want to assess how similarity snow and ice thickness yielded from two independent data sets. The results analysis from Argos buoys deployed during CHINARE 2003 was also presented in this paper for comparison.

DATA AND MODEL

The 6th Chinese National Arctic Research Expedition (CHINARE 2014) was carried out from July 11 to September 22, 2014. A long-term ice camp was constructed at initial location of 157.59°W and 80.86°N. The R/V Xuelong was anchored in the ice floe for 10 days (17 –26 August 2014). The first SIMBA (labelled as NMEFC02) was deployed on 20 August 2014 at 157.41°W, 81.1°N (Fig. 1). The in-situ snow and ice thickness are 7.5 cm and 194 m, respectively. The second SIMBA (NMEFC03) was deployed on 28 August 2014 at 152.63°W, 79.98°N, on a 118 cm thick ice floe with 7 cm snow on top. The NMEFC02 worked more than 15 months. The last iridium data transmission took place 2 December 2015. The NMEFC03 worked also long about 12 months however the GPS stopped working after 3 months. In this study we focus on NMEFC02 data analyses.

In order to carry out snow and ice modelling experiments, the short-term analyses and forecasts from numerical weather prediction (NWP) models are applied. For CHINARE2014, we applied ECMWF

(European Centre for Medium-Range Weather Forecasts) reanalyzes and forecasts. The analyses were available with 6 h intervals. The 2-m air temperature (T_a) and dew point temperature (T_d) as well as the 10-m wind speed (V_a) and total cloud cover (CN) were extracted from ECMWF server. The downward solar shortwave (Q_s) and thermal long-wave (Q_l) radiative fluxes were 12-h operational forecasts. The snow precipitation ($PrecS$) was 24-h forecasts. In order to access the quality of weather forcing data, the air temperatures measured by buoys are compared with NWP model results (Fig. 2).

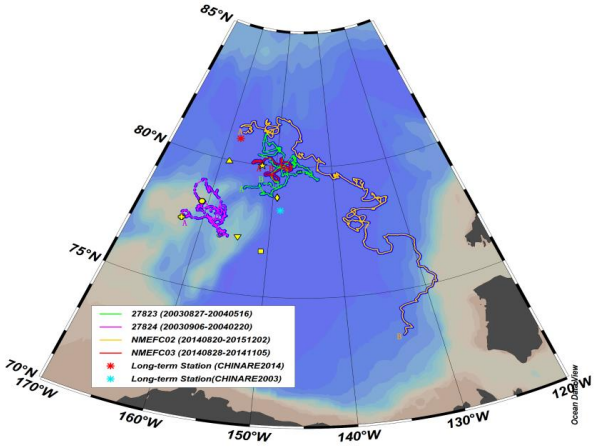

Figure 1. The survey domain of CHINARE Arctic expeditions. The drift trajectories of several buoys deployed during CHINARE program. The NMEFC02 and NMEFC03 are SIMBA units deployed during CHINARE 2014. The Argos buoys (27823, 27824) were deployed during CHINARE 2003. "A" and "B" present the buoy initial and last recorded positions. The short and long term ice camps were marked with various symbols

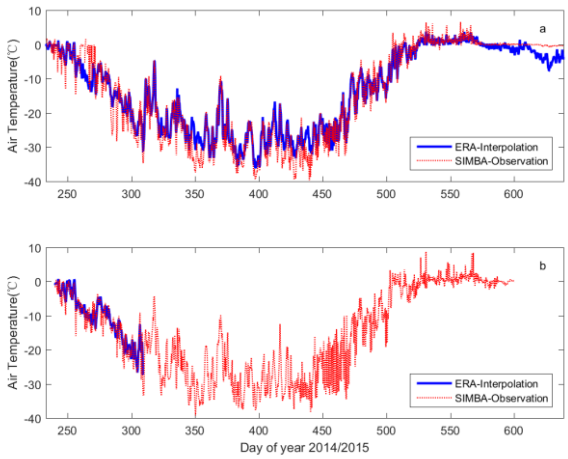

Figure 2. The comparison of ECMWF 2m modeled (blue) and SIMBA buoy (red) observed near surface air temperature along buoy drifts trajectories of a) NMEFC02; b) NMEFC03. After 5 November

The ECMWF 2m air temperature reanalyzes agreed quite well with SIMBA measured air temperature. The SIMBA air temperature was the average reading of upmost 10 temperature sensors in the air. The correlation coefficient between ECMWF and SIMBA temperature was 0.98 for NMEFC02 and 0.95 for NMEFC03. The mean biases between two temperature time series were 0.33ºC and 0.61ºC for NMEFC02 and NMEFC03. The root mean square errors (RMSE) for NMEFC02 and NMEFC03 were 3.1ºC and 2.2ºC, respectively. The visual inspection concluded that the NMEFC02 and NMEFC03 have similar air temperature patterns indicating buoys may locate under a similar synoptic weather system.

A numerical model HIGHTSI (High resolution Thermodynamic Snow and Ice) is applied to simulate snow and ice thickness along the buoy drift trajectories. HIGHTSI is a snow/ice 1-D physical model targeted to solve the snow/ice surface temperature, in-snow/ice temperature and snow/ice thickness (Launiainen and Cheng, 1998). The model includes surface heat/mass balance (with air-ice interactions);

parameterization of snow properties, surface albedo; penetrating solar radiation in snow/ice; heat conduction equations in snow/ice; sub-surface melting. The upper boundary conditions are given as the surface heat and mass balance equation, which yields the surface temperature and melting. A constant ocean freezing temperature is assumed, and the bottom freezing or melting is calculated from the difference between the conductive heat flux and the oceanic heat flux at the ice-ocean interface. The in-snow and in-ice temperature is solved by partial differential heat conduction equation. The model has a numerous applications for sea ice (Vihma et al., 2002, Cheng et al., 2008) and lakes (Semmler et al., 2012, Yang et al., 2012; 2013, Cheng, et al, 2014).

RESULTS AND DISCUSSION

The SIMBA buoy measures temperature profile in vertical direction (Fig. 3). In cold condition, temperature reveal mostly a pricewise linear distribution within air-snow-ice-water system (Leppäranta, 1993). The inflection points may well represent closely to the air-snow, snow-ice and ice-water interfaces. Because heat conductivities of air, snow, ice and water are considerably differing from each other, so the temperature gradient in those materials are different in response to different heat conduction. It also results different temperature increasing in response to the short heating cycle of sensors (1-2 minutes per day). On the basis of a simple procedure (Cheng et al, 2015), snow and ice thickness along NMEFC02 buoy trajectory is retrieved. One important assumption is that the initial ice surface is defined at snow/ice interface when SIMBA was deployed and this position remains unchanged as ice surface until the surface melting occurred in the next early summer season, in another word, ice growth at ice bottom and snow thickness accounts upward from this level.

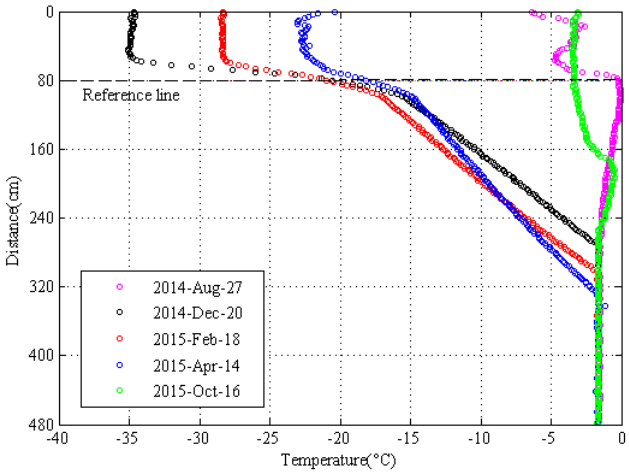

Figure 3. Temperature profiles of NMEFC02 measured at diffierent time. One can see clearly the downward moving of ice bottom indicating the ice growth at ice bottom. There is also a significant surface moving downward between April and October, 2015

The comparison between SIMBA observed and HIGHTSI modeled snow and ice thickness are given in Figure 4.

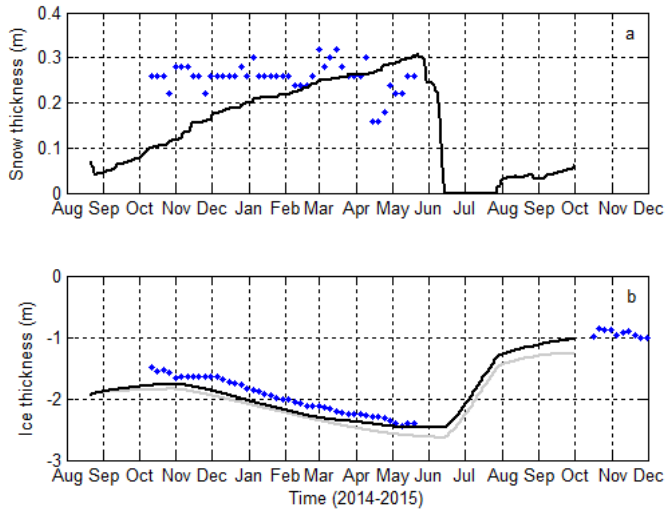

Figure 4. HIGHTSI modeled (black line) snow and ice thickness along NMEFC02 buoy drift trajectory. The blue dots are snow (a) and ice thickness (b) analyses based on NMEFC02 temperature measurements. The gray line was model run using constant ocean heat flux while the black line is model result using SHEBA observed oceanic heat flux

The NMEFC02 observed and HIGHTSI modeled snow thickness differs from each other. The NMEFC02 data indicated a rather constant snow thickness in winter season. A large temporal variation was detected in mid-April. The modeled snow thickness however showed a steady snow accumulation from late August until snow melt occurred in late May. The snow free season was from mid-June until late July. During this time period ice was in a melting phase. This was consistent with the NMEFC02 near surface zero temperature measurement (Fig. 2a).

The modeled ice thickness was thicker than the NMEFC02 ice thickness in general. Both ice thicknesses tend to be close to each other before the onset of ice melting. The in situ measurements suggested that ice bottom was still in a melting phase between September and October 2014. In summer season, the solar radiation could penetrate snow, ice and melt ponds giving significant contribution to increase the oceanic heat flux. During SHEBA ice camp, the observed ocean heat flux was as large as 13W/m^2 in mid-August and it was reduced to about 2W/m^2 in December and gradually increased to its maximum value of 16W/m^2 in July. Applying such prescribed oceanic heat flux, the modeled ice thickness (black line in Figure 4) has better agreement compared with NMEFC02 ice thickness, particularly from late fall to early spring season.

The modeled snow and ice temperature regimes are given in Figure 5. We can conclude that ice bottom was in a freezing phase from November until May. The surface melting seems dominate the total ice mass balance of along NMEFC02 drift trajectory. NMEFC02 drifted quit far south during the while period (Fig.1). The solar radiation at lower latitude contributed significantly to melt the ice surface. The large displacement of ice surface in summer is coherent with vertical temperature profile illustrated in Fig. 3. Modelling indicated that the ice floe initially placed in far north of ChuckChi Sea has drifted southeast for more than 500 km distance into the Beaufort Sea in one and half year and thickness reduced from original 1.97 m to about 1 meter.

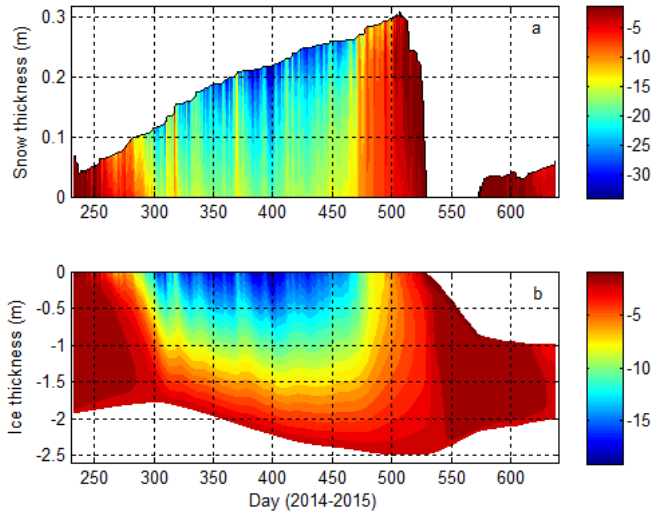

Figure 5. Modeled snow and ice temperature regimes. The moving boundaries at snow and ice surface, and ice bottom were response to the snowfall, melting and freezing, respectively.

Figure 6 illustrated the HIGHTSI parameterized and EMCWF forecasted daily mean longwave radiative flux. The correlation coefficient between HIGHTSI and ECMWF result is 0.97. The mean bias was 7W/m^2. The agreement is reasonable well.

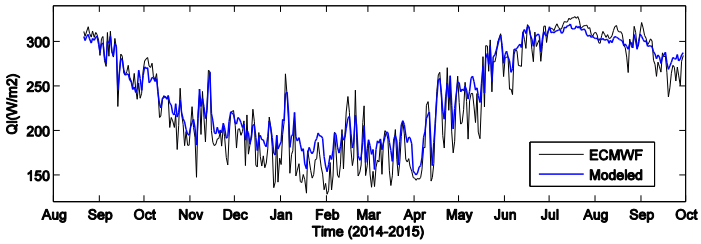

Figure 6. ECMWF forecasted and HIGHTSI model parameterized daily mean downward long wave radiative flux along NMEFC02 drift trajectory.

For comparison, the Argos buoys deployed during CHINARE 2003 was used to analyses snow thickness. Two Argos buoys labelled as B27823 and B27824 were deployed. The initial snow and ice thickness at deployment sites were 0.1m and 4.4m for B27813 and 0.15 and 3.6m for B27824, respectively.

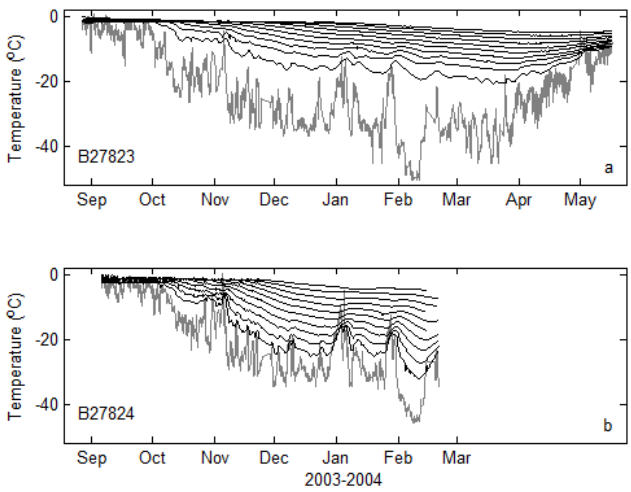

Figure 7. The air and in-ice temperature time series of Argos buoys B207823 in a) and B27824 in b). Argos buoys equipped with 10 thermistor sensors. Those sensors were placed at ice surface and every 0.32 cm even spacing below ice surface. The air temperature was measured at 2.5m

In cold winter during a snow free condition, thicker ice tends to have a lower surface temperature under the same atmospheric forcing condition (Leppäranta and Lewis, 2007). The buoy measurement indicated that the air temperature at B27823 site is slightly colder than air temperature at B27824 site. The in-ice temperature of B27823 should, accordingly, be colder than that of B27824. However the measurement suggested that ice temperature of B27824 is colder than that of B27823 (Fig.7). This may be explained by the difference of snow thickness at both sites. During deployment, the first thermistor sensor was placed at ice surface at both buoy sites and the rest sensors were evenly lied below with a 0.32m interval. The initial ice was thick making ocean flooding unlikely occur during the measurement. Assuming snow thickness is h_s, the continuity of heat flux at snow/ice interface should valid, i.e. $-k_s \partial T/\partial z|_{snow} = -k_i \partial T/\partial z|_{ice}$. If we look an average condition from beginning of November to end of December, the average air temperature of B27823 and B27824 are -28.1ºC and -25.6ºC. Assuming those are the snow surface temperatures at both sites. The heat conductivity of snow and sea ice are set to be k_s = 0.35 $Wm^{-1}K^{-1}$ *and* k_i =2.1$Wm^{-1}K^{-1}$. The calculated average snow thickness at both B27823 and B27824 are therefore 0.21m and 0.10 m, respectively. Modelling experiments reveal that snow thickness at B27823 was indeed thicker than those at B27824, partly due to the different precipitation pattern.

CONCLUSIONS

Snow and ice thickness in the Arctic Ocean was derived from SIMBA (NMEFC02) ice mass balance buoy deployed during CHINARE 2014 expedition. HIGHTSI model is applied to simulate snow and ice thickness along NMEFC02 drift trajectory. The ice thickness retrieved from NMEFC02 data and calculated by HIGHTSI agrees reasonable well, especially when oceanic heat flux is prescribed based on local measurements. Both NMEFC02 and HIGHTSI reveal a large surface ablation. The snow thickness derived buoy data and ice model differs from each other. This problem remains to be solved. The ECMWF reanalyses of 2m air temperature as well as forecasted long wave radiative flux are in good agreement with buoy measurement and HIGHTSI parameterized results. The SIMBA snow and ice thickness should also be compared with other advanced ice mass balance buoy measurements (e.g. Perovich, et al, 2003) in order to increase the reliability of SIMBA data interpretation.

ACKNOWLEDGEMENTS

This work was also supported by the Academy of Finland (contract 259537) and National Natural Science Foundation of China (Grant nos. 41476170). The ECMWF is acknowledged for data supply.

REFERENCES

Cheng, B., Zhang, Z., Vihma, T., Johansson, M., Bian, L., Li, Z. and Wu, H (2008). Model experiments on snow and ice thermodynamics in the Arctic Ocean with CHINARE 2003 data, J. Geophys. Res., 113, C09020, doi:10.1029/2007JC004654.

Cheng, B., T. Vihma, L. Rontu, A. Kontu, Pour H. Kheyrollah, C. Duguay and J. Pulliainen (2014). Evolution of snow and ice temperature, thickness and energy balance in Lake Orajärvi, northern Finland, Tellus A 2014, 66, 21564, http://dx.doi.org/10.3402/tellusa.v66.21564

Cheng, B., Vihma, T. and Zhao, J (2015). Analyses snow and ice thickness from high resolution thermistor temperature profiles, Proceedings of the 1st Pan- Eurasian Experiment (PEEX) Conference and the 5th PEEX Meeting. Report series in Aerosol science N:o 163, P 99 -104

Gascard, J.-C., Festy, J., le Goff, H., Weber, M., Bruemmer, B., Offermann, M., Doble, M., Wadhams, P., Forsberg, R., Hanson, S., Skourup, H., Gerland, S., Nicolaus, M., Metaxian, J.-P., Grangeon, J., Haapala, J., Rinne, E., Haas, C., Heygster, G., Jakobson, E., Palo, T.,

Wilkinson, J., Kaleschke, L., Claffey, K., Elder, B., and Bottenheim, J (2008). Exploring Arctic transpolar drift during dramatic sea ice retreat, Eos, Trans. Amer. Geophys. Union, 89, 21–22, 2008

Jackson, K., J.Wilkinson, T. Maksym, D. Meldrum, J. Beckers, C. Haas, and D. MacKenzie (2013). A novel and low cost sea ice mass balance buoy. J. Atmos. Ocean. Tech. 30(11), 2676 - 2688. DOI: 10.1175/JTECH-D-13-00058.1.

Launiainen, J. and Cheng, B (1998). Modelling of ice thermodynamics in natural water bodies. Cold Reg. Sci. Technol., 27(3), 153-178.

Lei, R., Li, N., Heil, P., Cheng, B., Zhang, Z., and Sun, B (2014). Multiyear sea-ice thermal regimes and oceanic heat flux derived from an ice mass balance buoy in the Arctic Ocean, J. Geophys. Res. Oceans, 119, doi:10.1002/2012JC008731.

Leppäranta M (1993) A review of analytical sea ice growth models. Atmosphere–Ocean. 31(1): 123-138.

Leppäranta, M. and Lewis, J. E (2007). Observations of ice surface temperature and thickness in the Baltic Sea. Int. J. Remote Sens. 28, 39633977.

Perovich, D. K., T. C. Grenfell, J. A. Richter-Menge, B. Light, W. B. Tucker III, and H. Eicken (2003). Thin and thinner: Sea ice mass balance measurements during SHEBA, J. Geophys. Res., 108 (C3), 8050, doi:10.1029/2001JC001079, 2003

Semmler, T., Cheng, B., Yang, Y., and Rontu, L (2012). Snow and ice on Bear Lake (Alaska) – sensitivity experiments with two lake ice models. Tellus A, 64, 17339, doi: 10.3402/tellusa. v64i0.17339.

Uttal, T., Curry, J. A., Mcphee, M. G., Perovich, D. K., Moritz, R. E., Maslanik, J. A., Guest, P. S., Stern, H. L., Moore, J. A., Turenne, R., Heiberg, A., Serreze, M. C., Wylie, D. P., Persson, O. G., Paulson, C. A., Halle, C., Morison, J. H., Wheeler, P. A., Makshtas, A., Welch, H., Shupe, M. D., Intrieri, J. M., Stamnes, K., Lindsey, R. W., Pinkel, R., Pegau, W. S., Stan- ton, T. P., and Grenfeld, T. C (2002). Surface heat budget of the Arctic ocean, B. Am. Meteorol. Soc., 83, 255–275, doi:10.1175/1520-0477(2002)083<0255:shbota>2.3.co;2, 2002. 10314

Vihma, T., Uotila, J., Cheng, B., and Launiainen, J (2002). Surface heat budget over the Weddell Sea: Buoy results and model comparisons. J. Geophys. Res. 107(C2) 3013, doi:10.1029/ 2000JC000372.

Yang, Y., Leppäranta, M., Cheng, B., and Li. Z (2012). Numerical modelling of snow and ice thickness in Lake Vanajavesi, Finland. Tellus A 2012, 64, 17202, DOI: 10.3402/tellusa.v64i0.17202.

Yang, Y., Cheng, B., Kourzeneva, E., Semmler, T., Rontu, L., Leppäranta, M., Shirasawa, K. and Li, Z (2013). Modelling experiments on air–snow–ice interactions over Kilpisjärvi, a lake in northern Finland. Boreal Env. Res. 18: 341–358.

Zhang, Z. (Ed.) (2004). The Report of 2003 Chinese Arctic Research Expedition, 229 pp., China Ocean Press, Beijing.

METHANE COLUMN ABUNDANCE AND SURFACE CONCENTRATION VARIATIONS OVER EUROASIA

M.V. CHEREPOVA[1], S.P. SMYSHLYAEV[1]

[1]Department of Weather Forecasting, Russian State Hydrometeorological University , Saint-Petersburg, Malookhtinsky prospect 98, Russian Federation

Keywords: METHANE, POLAR AND SUB-POLAR REGION, SURFACE CONCENTRATION, COLUMN ABUNDANCE, TEMPORAL VARIABILITY, CONTINENTAL AIR QUALITY MODEL.

INTRODUCTION

Methane is one of the most abundant tropospheric greenhouse gases following H_2O and CO_2. In addition its reactivity is important for both tropospheric and stratospheric chemistry.

The oxidation of CH_4 by hydroxyl (OH) in the troposphere leads to the formation of formaldehyde (CH_2O), carbon monoxide (CO), and ozone (O_3), in the presence of sufficiently high levels of nitrogen oxides (NOx). Along with CO, methane helps control the amount of OH in the troposphere. It also affects the concentrations of water vapor and ozone in the stratosphere, and plays a key role in the conversion of reactive chlorine to less reactive HCl in the stratosphere (Wuebbles, Hayhoe, 2002).

Radiative effect of methane includes two factors: the first is absorb long-wave radiation, the second is to form radiative gases owing to methane oxidation reactions. Consequently methane concentration variability influences radiative trace gases abundance such as ozone and carbon oxides.

The purpose of this paper is to examine the past trends in the concentration of methane, the sources affecting its growth rate and to define distribution features.

Methane has some distribution feauters in Arctic and Subarctic area which depends to local factors (atmospheric circulations, methane hydrate sours, solar insolation amount and its duration). Polar and sub-polar atmosphere in Euroasia is contained methane concentration higher for 10-15% than global average according NOAA database. Because of long atmospheric lifetime growing concentration of methane in Arctic and Subarctic can change its global abundant in the atmosphere and influence radiative and chemical balance in polar and sub-polar region.

It is important to note that observation data and its analysis can be the key for understanding methane variability and its precursors.

Research of column abundance and surface concentrations radiative gases variabilities has been done for 2009-2015. The analysis to obtain results has been made analytically. Namelly observation and model simulation data were studied. To estimate character of temporal variability and concentrations radiative gases global air quality model of low and middle atmosphere, coupled to continental model are used.

METHODS

Two methods are used in our research. The first method is radiative gases numerical simulation. We used global chemistry-transport model of the low and middle atmosphere, coupled to continental air quality model.

The continental air quality model coupled to global model are assimilated observations data. Global model has horizontal resolution 4x5 degree and 31 vertical levels, which includes troposphere and stratosphere while continental model covers troposphere and low stratosphere and has resolution 0.5x0.5 degree and 22 vertical levels. Area for simulation is defined between 28^0 and 80^0 northern latitudes. The grid size of model provides more detailed gases distribution.

The model describe mesoscale feauters of 74 tracers distribution such as ozone, methane, nitrogen compounds, hydrogen compounds, carbon oxides, some hydrocarbons, oxidized organic compounds and others. Both the global model and the continental model describes surface emissions, chemical transformations, dry and wet depositions, advections, eddy transfer.

Meteorological database is Global Forecast System (GFS) (Saha, 2006), it could be launched for two case such as analysis and forecast. The GFS data has 0.5^0 regular latitude-longitude grid the same like the continental model. The database renews 4 times for 24 hours (00,06,12,18ч. UTC). Time step is 3 hours. Forecast data is given for 180 hours. Vertical structure of GFS describes 64 σ-levels which located between surface and 10 hPa. The data describes temperature, zonal and meridional wind, humidity.

Biogenic and atropogenic sources are defined as surface flux. Database MEGAN-MACC have been used. It describes biogenic emissions of methane and carbon monooxide. Also we used some database such as EDGAR, GISS NASA, GEIA, GEIA.

We used MEGAN-MACC biogenic flux data for CO and CH4. The data is globally and its grid size is 0.5 latitude-longitude grid.

CONCLUSIONS

Our research is discussed methane variabilyties namely surface concentrations and column abundance. The results for some polar and subpolar stations were obtaibed. Petergof station (59.88^0 N 29.83^0 E, H=20m) and Harestua station (60.22^0 N 10.75^0 E, H=569m) have been measured column abundance of methane. Besides Teriberka (69.20^0 N 35.10^0 W, H=40m) and Tiksi (71.59^0 N 128.92^0 E, H=8m) stations have been measured surface concentrations of methane.

Seasonal variability surface emissions of CH4 are different for measuring stations as shown fig.1 but one has distinct character. Higher surface emissions are obtained in summer (average is July), smaller surface emissions are obtained in winter. Arctic hydrates melting is reason of summer maximum biogenic methane flux. Stations which situated in higher latitudes such as Teriberka and Tiksi have smaller suface flax than Harestua and Petergof stations.

Obtained maximum of biogenic methane flux between 2001-2011were different for measuring stations. Summer maximum of emissions were 6,5 kg/m2/c in Ptergof and 5,4 kg/m2/c in Harestua, 2,5 kg/m2/c in Teriberka, 1,7 kg/m2/c in Tiksi. Consequently biogenic emissions is less into area which situated more nothern and they have minor variability.

ACKNOWLEDGEMENTS

This work was supported by the Russian Scientific Foundation (project 14-17-00096).

REFERENCES

Donald J. Wuebbles, Katharine Hayhoe. Atmospheric methane and global change, *Earth-Science Reviews* **57** (2002), 177–210.

Saha S.. The NCEP Climate Forecast System, *J. Climate* ***19***, 2006, 3483-3517

A COMPARISON OF ALOS PALSAR INTERFEROMETRY AND FIELD GEODETIC LEVELING FOR MARSHY SOIL THAW/FREEZE MONITORING, CASE STUDY FROM THE BAIKAL LAKE REGION, RUSSIA.

T. CHIMITDORZHIEV, P. DAGUROV, M. BYKOV, A. DMITRIEV and I. KIRBIZHEKOVA

Institute of Physical Materials Science, SB RAS, Sakhyanovoy str., 6, Ulan-Ude, Russia, 670047

Keywords: DInSAR OF LAYERED SURFACE, GEODETIC LEVELING, SEASONAL THAWING/FREEZING, SOIL MOISTURE.

ABSTRACT

Estimation of vertical ground displacements due to seasonal periods of freezing and thawing was carried out on the Selenga River mouth using differential radar interferometry. The results of seasonal radar interferometry measurements for 2008-2010 have been compared with the survey data for 2011, under the assumption that the seasonal deformation is comparable for different years and lie within the limits of geodetic leveling error. The difference between the interferometric and geodetic measurements is below 1 cm in winter months, whereas in summer, as the upper soils moisture content varies, the difference reaches 2-2.7 cm. It has been concluded that the moisture content and its profile should be taken into consideration in summer or when choosing the radar interferometry in winter

1. INTRODUCTION

The problem of climate change involves the development of new methods and technologies for large-scale studies of arctic and subarctic regions, including a remote quantitative evaluation of the frost heave or subsidence, which is due to permafrost layer thawing.

Observation of surface changes is especially relevant in permafrost regions. This includes geometrical horizontal variations as well as seasonal and long-term vertical variations of the ground surface. Apart from its scientific importance, this problem is of relevance [1]: detection of frost heave areas to evaluate potential risk and damage during designing, construction and subsequent operation of buildings, main pipelines, roads and other linear constructions.

In this paper, the method of spaceborne differential radar interferometry and field measurements with geodetic leveling is applied to analyze the seasonal deformations of marshy soils from the Baikal Lake region.

Today, the radar interferometry is widely used in glaciology [2], to monitor ground surface deformations after earthquakes [3], landslides and destruction of coastline, in order to evaluate regional subsidence in oil fields [4], as a useful tool for estimating aboveground boreal biomass [5].

Against the background of significant growth of the number of studies on the deformation of permafrost [6,7], the information currently available about the accuracy of satellite radar interferometry techniques is still insufficient. In the arid regions, satellite and ground-based methods are consistent with sub-centimeter accuracy. However, in wetland arctic tundra, during the process of freezing and thawing, the error according to satellite measurements can reach 1.5 cm in the L-band (ALOS PALSAR), and 5 cm in C-band (RADARSAT-2) [8-10]. Therefore, an attempt was made to describe the mechanism of such discrepancies between the satellite and field measurements.

2. TEST AREA DESCRIPTION

The test area was chosen in the Baikal Rift Zone in the Selenga River mouth, which is characterized by high seismic activity. The areas of surface deformations observed through the satellite data, are of local character and are associated solely with river's flood plain and marshy soils, whereas seismogenic

deformations are related with epicenters of earthquakes and geological lineaments. Moreover, the geodynamic activity of the Selenga River mouth was low within the observation period of 2008-2011. When inflowing into Baikal Lake, the Selenga river forms a large mouth, with an area of 1,120 km^2 and consisting of many creeks and islands. Terrace aggradations of low and medium-altitude levels, oxbow lakes, levees and lagoons all prevail in the delta. The upper part of the geological profile consisting of mellow Quaternary sediments. It is characterized by significant variability of the thickness, lithological structure and ground water. This structure certainly affects the seasonal heaving and subsidence of soils.

3. EXPERIMENTAL TECHNIQUE

To detect the deformations in the underlying surface of the Selenga River mouth, the PALSAR data (λ = 23.8 cm) from the ALOS satellite was used. Forty-six days was the minimum possible time interval between two consequent acquisitions of the same ground section. The relevant scanning mode for this study permitted to obtain the images with the spatial resolution from 10 m to 100 m with the swath from 40-70 km to 250-350 km. A distinguishing feature of ALOS PALSAR compared to other up-to-date satellite radars is its performance in a longer- wave range (L-band). In most cases, it solves the problem of time decorrelation of reflected signals caused by varying vegetation and snow covers, as well as by signal fluctuations resulting from tropospheric irregularities. In this study, we used the radar images obtained in the FBS mode (transmitted and received signals are horizontally polarized), with the ground spatial resolution of approximately 7 m.

The imaging of the Selenga river mouth with ALOS PALSAR allowed us to create a set of 14 radar images, which form interferometric pairs for various time intervals during 2008-2010. The data with high coherence values (greater than 0.2) were chosen for the interferometric measurements. The values of vertical deformations of the surface were calculated from these interferometric pairs for various time gaps as in Ref. 30.

Theodolitic field measurements were carried out in the test area for evaluation of the satellite derived results. The vertical deformations were measured at three reference sites with three leveling points in each. The distance between the leveling points was 3 m - 5 m, and the sites were located 150 m - 250 m apart from each other. The reference point was identified apart from the leveling points in the stable section of the terrace above the floodplain, which according to the differential interferometry results, did not undergo seasonal vertical deformations.

From October 2010 to October 2011, geodetic leveling of the test section was done every month. The high-precision leveler was used for the field measurements along with a 3 m checkered rod. The leveler maximum mean-square error was 3 mm per 1 km. The mean-square error of the geodetic measurements was 0.5 cm. Altitude marks of the leveling points were calculated relatively the reference point. The resulting value for the heave or subsidence was calculated as an average value of the heaves or subsidences of all nine leveling points in the three test sites.

The same algorithm of the measurement of the relative deformations (from this reference point above) was used to find out the values of the ground heave or subsidence by means of DInSAR. A total of 12 interferograms was selected and processed using Sarmap SARscape™ software. We used 90 m resolution digital elevation model (DEM), which was generated by the NASA Shuttle Radar Topography Mission (SRTM) to remove the topography and flat-earth phase contributions from the interferograms. The differential interferograms were filtered using a Goldstein's technique, unwrapped and mapped from the original SAR slant range coordinates onto a geographic grid.

4. RESULTS AND DISCUSSION

Fig. 1a shows the radar backscattering amplitude projected into the geographic system of coordinates (latitude and longitude). In this figure, the gray scale represents the sections with various values of radar backscatter: bright tones correlate with volumetric nonuniformities (e.g. a forest, tussock bog, etc.), while dark tones indicate flat areas. The spatial resolution of the radar image is 25 meters. Fig. 1b and 1c represent the unwrapped phase and coherence map between 1/13/2009 and 2/28/2009 respectively. The plot in Fig. 1d shows the unwrapped phase variations, which took place along the white line on the Fig.

1b. One sees that jump of the unwrapped phase within the test area (which is highlighted by dashed lines in the Fig. 1d) can run up to 5.8 - 6 radian. Thus, the deformation of soil due to heaving is equal to approximately 11 cm.

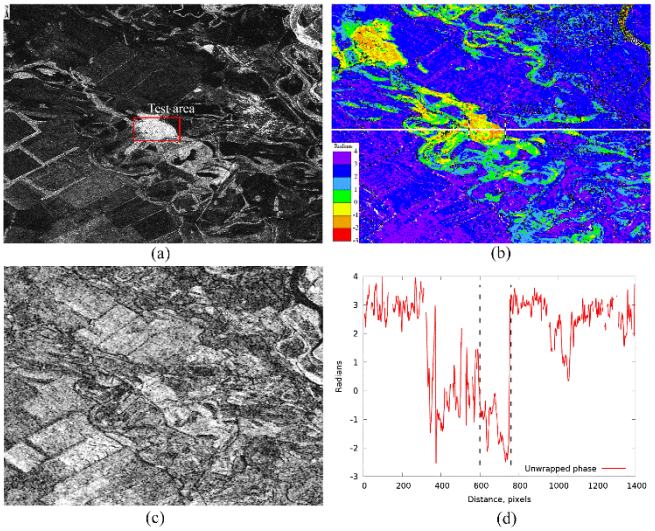

Fig. 1 (a) radar backscattering amplitude, (b) unwrapped phase map, (c) coherence map, and (d) unwrapped phase profile in the winter (Jan. 13 – Feb. 28, 2009).

Fig. 2 shows the seasonal dependencies of the vertical deformations in the test section obtained by the DInSAR method and by the field geodetic leveling. One sees from Fig. 2 that the maximum values of the seasonal ground deformations reached 11 cm, relative to the specified zero level that occurred in early March of 2011. The maximum subsidence, which is equal to 5 cm, took place in summer. The results obtained from the DInSAR processing and from field measurements are in quite good agreement. The maximum difference in vertical deformation values is 2.3 cm, i.e. 14% from the deformation variation range, which confirms the high accuracy of the DInSAR method.

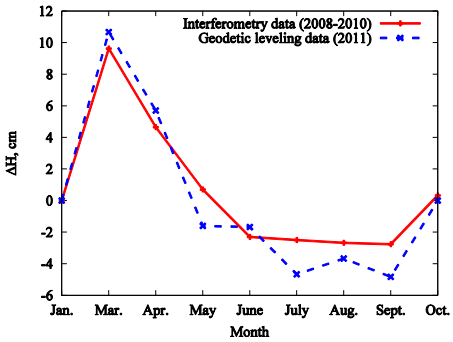

Fig. 2 Seasonal vertical deformation (ΔH) of ground relative to the reference point in January 2011.

Fig. 3 shows the difference between geodetic leveling measurements and radar interferometry results when we estimate the seasonal vertical deformations according to the data presented in Fig 2. Fig. 3 also shows variations in the soil moisture content (0 cm - 10 cm) which was obtained simultaneously with the geodetic leveling. Fig. 3 demonstrates that the moisture content successfully correlates with the values of this difference, i.e. the moisture content peaks correspond to the maximum differences. It may indicate a possible influence of the soil moisture content on the accuracy of DInSAR. Though the discrepancy between the radar and geodetic methods was relatively small, let us evaluate the possible impact of the soil moisture content on the measurement results. We will further assume that effects due to asynchronous measurements are negligible.

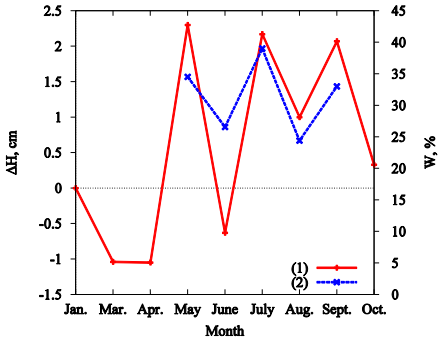

Fig. 3 Monthly differences between the results of both DInSAR processing and geodetic leveling (1) and soil moisture content *W* (2).

The possible difference between the arguments of the reflection coefficient from the same ground section are transformed into the variation of the real difference between wave propagation paths if the radar images are obtained at different times (from different orbit passes). This may cause the incorrect definition of the geometric altitude of the section. However, the potential impact of this phenomenon is usually neglected in the radar interferometry.

Electrical properties of the ground described by the complex dielectric permittivity (CDP), which is expressed by

$$\varepsilon = \varepsilon_1 + \varepsilon_2 \qquad (1)$$

where ε_1 is the real part of ε, ε_2 is its imaginary part.

The CDP of a soil is a complex function of the following parameters: soil moisture content, electromagnetic radiation frequency, soil temperature and soil composition. Normally, empirical and semiempirical models are used for the analytical description of the CDP. The moisture content applies the strongest effect on the CDP (much stronger than the other parameters) due to the great difference between the dielectric permittivity of dry soil (ε_1 = 2 - 3) and that of water (ε_1 = 80). Let us use the empirical model to evaluate numerically effect of the moisture content on the argument of the reflection coefficient [11]. On the basis of experimental investigations which were carried out in [11], the quadratic dependence of ε_1 and ε_2 from the soil moisture content *W* was obtained. It depends also on the clay and sand content.

It is a common case when the moisture content varies in depth, so the soil is realized as layered medium. In regards to soil properties, the layer structure may be continuous or discrete. In order to evaluate the effect of the layer structure on the argument of the reflection coefficients, let us consider the simplest case of a two-layer soil. Let the soil layer with a thickness d and a fixed moisture content lies on a second soil, which occupies the half-space and has a different moisture content. The interface between these media is assumed to be flat.

The reflection coefficient of a two-layer medium is found from the formula [12]

$$R = \frac{(Z_3+Z_2)(Z_2-Z_1)e^{ik_{2z}d}+(Z_3-Z_1)(Z_2+Z_1)e^{-ik_{2z}d}}{(Z_3+Z_2)(Z_2+Z_1)e^{ik_{2z}d}+(Z_3-Z_1)(Z_2-Z_1)e^{-ik_{2z}d}}, \qquad (2)$$

where Z_1 is the wave impedance of the media from which the wave is incident (in the case under consideration, it is air), Z_2 is the wave impedance of the layer, Z_3 is the underlying semi-space wave impedance, k_{2z} is the wave number in the layer.

Fig. 4 shows the results of the numerical calculations of the argument ϕ of the reflection coefficient for the normally incident wave. For calculations, we used equation (2) and the following parameters: wavelength λ = 23 cm, the layer thickness d = 2 cm. The results prove that the layer structure of the soil causes visible changes in the argument of the reflection coefficient up to 54° (curve 3) within the range of moisture content variations from 0 to 40%. Note that the dependencies are quite intricate: the argument of the reflection coefficient can either increase as the moisture content grows, decrease, or be of nonmonotonic character.

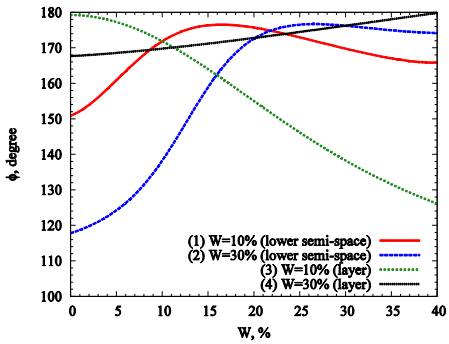

Fig. 4 Dependencies of the argument ϕ of the reflection coefficient from the moisture content W for layered soil with d = 2 cm and λ = 23 cm.

Thus, taking into account that the surface movement by $\lambda/2$ corresponds to the phase difference being equal to 2π, the errors in the displacement value definition may reach 1.7 cm when the moisture content varies from 0% to 40%. In the case under consideration (Fig. 3), the moisture content varies from 25% to 40%. This might cause an error approximately equal to 0.6 cm when we try to determinate the magnitude of displacement.

5. CONCLUSIONS

Comparison of the satellite interferometric measurements of different years with the geodetic leveling data for 2011 revealed that, regarding the seasonal freeze-thaw cycles, the two datasets are in good agreement. The interferometric errors compared with the field geodetic measurements is less than 0.5 cm. The discrepancy of 2 cm in July is caused by differences in soil moisture content in different years. This fact may be used as a certain indirect indicator for soil moisture content monitoring in conditions of climate change and thawing of permafrost.

Thus, the combination of particular water and thermal regimes along with the clay and loamy soils create the most favorable conditions for the evolution of the frost heave process in the upper part of floodplain sediments. The formation of frosty deformations must be considered as an effect of significant swelling of these floodplain sediments

This work is supported by the Russian Foundation for Basic Research (grant no. 16-08-00646 A).

6. REFERENCES

[1] A. Dmitriev, T. Chimitdorzhiev, M. Gusev, P. Dagurov, K. Emelyanov, A. Zakharov, and I. Kirbizhekova, “Basic products of earth remote sensing by means of spaceborne synthetic aperture radars [in russian],” *Issledovanie Zemli iz Kosmosa*, no. 5, pp. 83–98, 2014.

[2] H. Liu, Z. Zhao, and K. Jezek, “Synergistic fusion of interferometric and speckle-tracking methods for deriving surface velocity from inter ferometric SAR data,” *IEEE Geosci. Remote Sens Letters*, vol. 4, no. 1, pp. 102–106, 2007.

[3] Y. Xia, “Bam earthquake: Surface deformation measurement using radar interferometry,” *Acta Seismologica Sinica*, vol. 18, no. 4, pp. 451–459, 2005.

[4] E. Fielding, R. Blom, and R. Goldstein, “Rapid subsidence over oil fields measured by SAR interferometry,” *Geophys. Res. Lett*, vol. 25, no. 17, pp. 3215–3218, 1998.

[5] D. Atwood, H.-E. Andersen, B. Matthiss, and F. Holecz, “Impact of topographic correction on estimation of aboveground boreal biomass using multi-temporal, L-band backscatter,” *IEEE J. Sel. Topics Appl. Earth Observ*, vol. 7, no. 8, pp. 3262–3273, 2014.

[6] F. Chen, H. Lin, W. Zhou, T. Hong, and G. Wang, “Surface deformation detected by ALOS PALSAR small baseline SAR interferometry over permafrost environment of Beiluhe section, Tibet plateau, China,” *Remote Sens. Environ*, vol. 138, pp. 10–18, 2013.

[7] T. Jagdhuber, J. Stockamp, I. Hajnsek, and R. Ludwig, “Identification of soil freezing and thawing states using SAR polarimetry at C-band,” *Remote Sens,* vol. 6, no. 3, pp. 2008–2023, 2014.
[8] V. L. Mironov, K. V. Muzalevskii, “Impact of a Freezing Topsoil on Determining the Arctic Tundra Surface Deformation Using InSAR,” *International Siberian Conference on control and communications (SIBCON),* 2013 [doi:10.1109/SIBCON.2013.6693624].
[9] N. Short, B. Brisco, K. Murnaghan, “Monitoring permafrost environments with INSAR and polarimetry, case studies from Canada,” *Proc. IGARSS,* pp. 4034-4037, 2012.
[10] T. Chimitdorzhiev, I. Kirbizhekova, and M. Bykov, “Study of landslide processes and deformations of the landscape of the yamal peninsula by radar interferometry and texture analysis [in russian],” *Atmospheric and Oceanic Optics Journal,* vol. 27, no. 7, pp. 610–614, 2014.
[11] M. Hallikainen, F. Ulaby, M. Dobson, M. El-Rayes, and L.-K. Wu, “Microwave dielectric behavior of wet soil part I: Empirical models and experimental observations,” *IEEE Trans. Geosci. Remote Sens,* vol. 23, pp. 25–34, 1985.
[12] L. Brekhovskikh, *Waves in Layered Media*. Academic Press, 1960.

AEROSOL EMISSION IN THE ARID AND SEMI-ARID REGIONS OF SOUTHERN RUSSIA

O.G. CHKHETIANI[1,2], M.S. ARTAMONOVA[1], M.A. IORDANSKII[3], M.V. KURGANSKY[1], V.A. LEBEDEV[3], L.O.MAXIMENKOV[1], Y.I. OBVINTSEV[3] and N.V. VAZAEVA[1]

[1]Obukhov Institute of Atmospheric Physics, Russian Academy of Sciences, Moscow, Russia.

[2]Space Research Institute, Russian Academy of Sciences, Moscow, Russia.

[3]Karpov Physics and Chemistry Institute, State Corporation «Rosatom», Moscow, Russia.

Keywords: AEROSOL EMISSION, ARID LANDS, SOUTHERN RUSSIA.

We present the systematized data results from field measurements of submicron aerosol. These measurements were carried out in the steppe regions (Rostov region) and in semi-desert areas of Kalmykia Republic (the Caspian lowland) during the summer period of years 2007-2015 (Fig.1).

Figure 1. Location of measurements sites in Rostov region and Kalmykia (also in zoomed window).

These data include the diurnal variation of the counting and mass dust aerosol concentration in the range of 0.1-15 microns at two levels: 0.5 m and 2.0 m, the elemental composition of aerosol and soil samples, meteorological parameters. Methods of measurement are discussed in detail in (Chkhetiani *et al.* 2012, Artamonova *et al.* 2016).

Obtained data show the presence of convective lifting and outflow of fine aerosol in the low wind conditions during the daytime over dry sandy areas and dry loamy soils. The removal of the fine aerosol

increases proportionally to the temperature lapse rate in the surface air layer and decreases with increased wind speed. Physical mechanisms of the such dependence have been considered in (Gledzer *et al.* 2010; Chkhetiani *et al*. 2012). The coarser fraction of aerosol prevails in the airflow for wind speed of 5 m/s and more (see Fig.2 in Chkhetiani *et al.* 2012).

There is a noticeable relationship between the aerosol emission and the stability of the atmospheric boundary layer (Monin-Obukhov length-scale).

Aerosol mass concentration at different periods of observations was from a few dozen to several hundred $\mu g/m^3$.

Submicron aerosol flux depending on the conditions varies from a few tenths to units of $\mu g/m^2s$ (Fig 2).

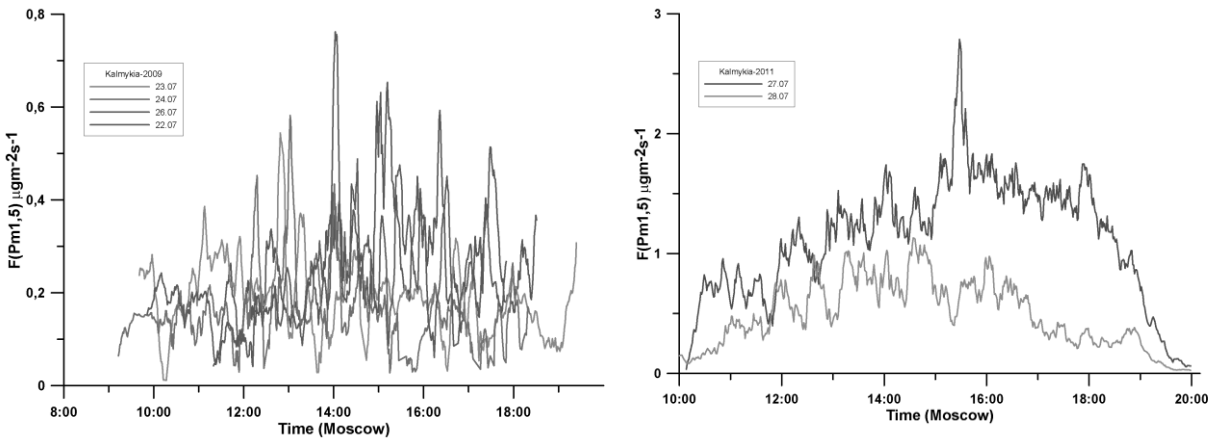

a) b)

Figure 2. Aerosol PM1.5 flux (Kalmykia; a) 2009; b) 2011). Method of flux calculation is described in (Gillette *et al.* 1997)

A noticeable component of submicron aerosol transferred from the arid lands of Kalmykia to the steppe of Rostov region. The comparison of the elemental composition of air samples collected on the spot and in Kalmykia and trajectory analysis indicates this fact in particular.

Though the intensity of the observed aerosol emission is weaker than saltation, nevertheless, it may occur almost every day during the hot season in arid lands. Together with stochastic convective dust emission occurring also permanently but on a more large scale (Klose *et al.* 2014) this process can make a noticeable contribution make a noticeable contribution to regional and global dust aerosol recirculation.

REFERENCES

Gledzer, E.B., I.G. Granberg, and O.G. Chkhetiani (2010). Air dynamics near the soil surface and convective emission of aerosol. *Izvestiya, Atmospheric and Oceanic Physics*, **46**, 29.

Chkhetiani, O.G., E.B. Gledzer, M.S. Artamonova and M.A. Iordanskii, (2012). Dust resuspension under weak wind conditions: direct observations and model. *Atmospheric Chemistry and Physics*, **12**, 5147.

Artamonova, M.S., D.P. Gubanova, M.A. Iordanskii , V.A. Lebedev, L.O. Maksimenkov, V.M. Minashkin, Y.I. Obvintsev and O.G. Chketiani (2016*)*. Variations of the aerosol concentration and chemical composition over the arid steppe zone of Southern Russia in summer, *Geofizicheskie Protsessy i Biosfera* **15**, 1.

Gillette, D. A., D.W. Fryrear, T.E. Gill, T. Ley, , T.A. Cahill and E.A. Gearhart, (1997). Relation of vertical flux of particles smaller than 10 μm to total aeolian horizontal mass flux at Owens Lake. *Journal of Geophysical Research: Atmospheres*, **102**(D22), 26009.

Klose, M., Y. Shao, X. Li, H. Zhang, M. Ishizuka, M. Mikami and J.F. Leys (2014). Further development of a parameterization for convective turbulent dust emission and evaluation based on field observations. *Journal of Geophysical Research: Atmospheres*, **119**, 10441.

A NEW PARAMETERIZATION OF THE UV IRRADIANCE ALTITUDE DEPENDENCE FOR CLEAR-SKY CONDITIONS AND ITS APPLICATION FOR THE UV INTERACTIVE TOOL

N. CHUBAROVA, YE. ZHDANOVA, YE. NEZVAL'

Moscow State University, Faculty of Geography, GSP-1, 119991, Moscow, Russia

Keywords: UV RADIATION, ALTITUDE, AEROSOL, ALBEDO, OZONE, PEEX DOMAIN

INTRODUCTION

Biologically active UV radiation (BAUVR) is an important environmental factor, which significantly affect human health and nature. The altitude above sea level is a very important factor, which has a significant influence on UV irradiance (Bais et al., 2007). In this presentation we propose a new method for calculating the altitude UV dependence for different types of biologically active UV radiation (erythemally-weighted, vitamin-D and cataract-weighted types) and present the results of its application over the PEEX domain using the on-line tool.

METHODS

We show that for the specified groups of parameters the altitude UV amplification (A_{UV}) can be used as a composite of independent contributions of UV amplification from different factors within a wide range of their changes with mean uncertainty of 1% and standard deviation of 3%. The proposed parameterization considers the altitude dependence of molecular number density, ozone content, aerosol and spatial surface albedo. We also provide generalized altitude dependencies of the parameters for evaluating the $A_{UV.}$ The resulting comparison between the altitude UV effects from the proposed method with generalized altitude parameters dependencies and the accurate 8 stream DISORT model simulations is shown in Fig.1. One can see a good agreement with correlation coefficient $r>0.996$. A satisfactory agreement was also obtained with the experimental UV data in mountain regions.

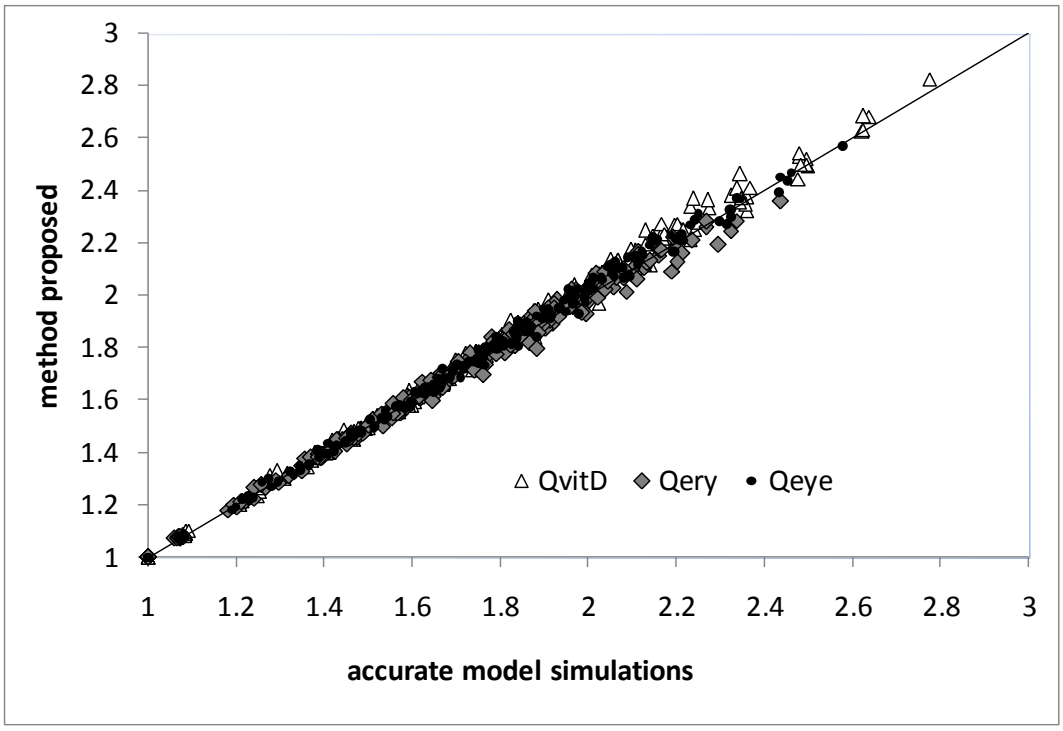

Figure 1. The comparison between the total altitude UV amplification (A_{UV}) according to the proposed method and the A_{UV} values evaluated using the accurate RT model

CONCLUSIONS

We have developed the analytical flexible approach based on rigorous model simulations with account for generalized correlation of parameter altitude dependencies. The parameterization takes into account for the altitude dependence of molecular number density, ozone content, aerosol loading, and spatial surface albedo. We show that for the specified groups of parameters we can present the altitude UV amplification (A_{UV}) for different types of biologically active UV radiation as a composite of independent contributions of UV amplification from different factors with the mean uncertainty of 1% and standard deviation of 3%. Using this parameterization we analyzed the role of different geophysical parameters in UV variations with altitude. The decrease in molecular number density, especially at high altitudes, and the increase in surface albedo play the most significant role in the UV growth. Typical aerosol and ozone altitude UV effects do not exceed 10-20%. Using the proposed parameterization implemented in the on-line UV tool (http://momsu.ru/uv/) we analyzed the altitude UV increase over the PEEX domain with different atmospheric conditions for the different skin types. Using this tool we evaluated the UV conditions (UV deficiency, UV optimum or UV excess) at different altitudes for a given skin type and open body fraction over the PEEX domain.

ACKNOWLEDGEMENTS

The work was partially supported by the RFBR grant № 15-05-03612.

REFERENCES

Bais, A.F., Lubin, D., Arola, A., Bernhard, G., Blumthaler, M., Chubarova, N., Erlick, C., Gies, H.P., Krotkov, N., Mayer, B., McKenzie, R.L., Piacentini, R., Seckmeyer, G., Slusser, J.R., 2007. Surface Ultraviolet Radiation: Past, Present, and Future, in: Scientific Assessment of Ozone Depletion: 2006, Global Ozone Research and Monitoring Project—Report No. 50. World Meteorological Organization, Geneva, Switzerland. Chapter 7.

THE IMPORTANCE OF MOISTURE RECYCLING IN CHINA

T. CÖMERT, N.T.D. VAN DE KOPPEL and H.H.G. SAVENIJE

Water Resources Section, Faculty of Civil Engineering and Geosciences, Delft University of Technology, P.O. Box 5, 2600 AA Delft, The Netherlands.

Keywords: MOISTURE RECYCLING, FORECASTING

INTRODUCTION

Water scarcity has already been a problem for the last two centuries, with the first occurrence around the year 1800 (Kummu *et al*., 2010). It was after the year 1900 that the world population really began to experience water scarcity. In 1960, 9% of the world population was under water shortage. This number has only been increasing, with 50% of the world population under water shortage in the year 2005 (Kummu *et al*., 2010). Of this 50% an astounding 25% is under high water shortage, and as high as 10% of the population is dealing with extreme water shortage (Kummu *et al*., 2010). Although the problem is known, the urgency for solutions is lacking (Falkenmark, 1989; Falkenmark, 1998).

Water scarcity in China is not only a problem for the country itself, but for the whole world. The main question in particular is how China is going to feed its rapidly growing population while water resources are depleting. Import of large tons of grains could be of massive impact on the world economy, raising the prices of cereal (Seckler *et al*., 1999).

Throughout time there have been many studies addressing water scarcity (e.g. Pereira *et al*., 2009). In China, three factors contribute to water scarcity. Although two of them cannot be adjusted, the poor water resource management can be improved a lot (Jiang *et al*., 2009). Efficient use of irrigation water and improvement of irrigation schedules have been proposed (Pereira *et al*., 2002). Although these propositions will definitely decrease water scarcity on the short term, on the long term the water scarcity will again rise because of the growing population and thus the demand for water. (Pereira *et al*., 2009).

In this study, we want to zoom in on new ways to solve water scarcity. Moisture recycling is an important hydrologic aspect which could contribute to reducing water scarcity. To preserve rainfall, evaporation is required. This is called moisture feedback. Transpiration from plants make up a big part of the total evaporation that sustains rainfall (Wang-Erlandsson *et al*. 2014). Therefore transpiration could be influenced to increase total evaporation, but this is not the topic of this study.

This study is based on the following research question:

How strong is the relation between evaporation in Eurasia and precipitation in China?

The aim of this study is to quantify the relation between evaporation and precipitation and look at how strong this relation is. This will be done for Eurasia and China, because earlier studies have shown that there is a connection between moisture evaporating from the Eurasian continent and precipitation in China (van der Ent *et al*., 2010). This means China and its surrounding areas are sink regions whereas the countries in Eurasia are their source regions. The size of these regions are however unknown, therefore this research shall try to find the areas that have a high correlation. The hypothesis of the research is that the precipitation in China is greatly dependent on the evaporation in Eurasia. Therefore a high correlation is expected to be found.

THEORETICAL FRAMEWORK

Moisture fluxes and recycling ratio's (van der Ent *et al*., 2010) show that mainly the part from Eastern-Europe till Siberia (from here on in this study referred to as the Eurasian continent) is responsible for the moisture recycling and thus precipitation in China.

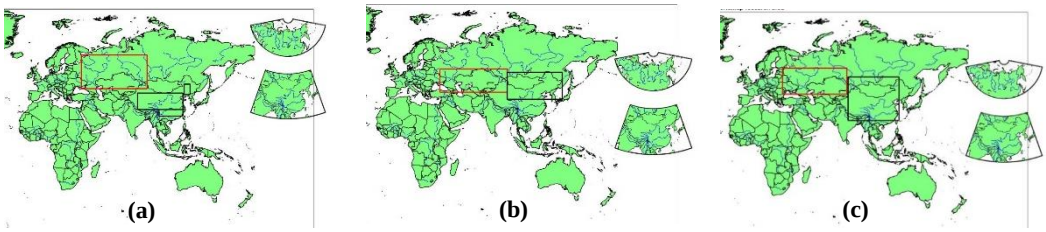

Figure1. World map MATLAB models with research areas.

(a) Research area 1 (E 45-66°N, 35-90°E, P 30-42°N, 82-120°E; 40-48°N, 120-126°E; 25-30°N, 100-120°E),
(b) Research area 2 (E 45-58°N, 35-90°E, P 39-53°N, 90-135°E),
(c) Research area 3 (E 44-60°N, 27-80°E, P 25-55°N, 81-123°E).

Moisture fluxes from India to China are also present and account for about 10% of the total rainfall in China, however these are only present in wet years. These Southerly water vapour flows move over the Tibetan Plateau and therefore only reach China when the precipitation is very heavy (Yatagai *et al*., 1998).

The areas being researched are shown in figure 1. The red box outlines the area of evaporation, also known as the source region. The blue box refers to the area in which the precipitation falls, known as the sink region. These areas are chosen by using wind directions, a matching area size and known sink and source region from other researches (van der Ent *et al*. 2010). It can be seen that several research areas have been chosen. This is done to gain the best results in terms of correlation. The highest correlated areas will be most suited for further research purposes.

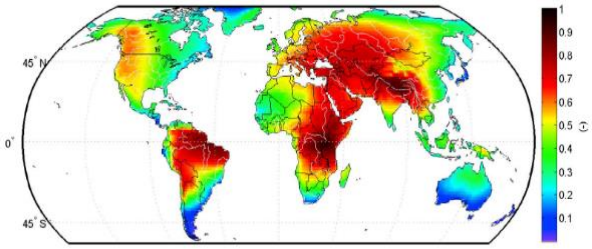

Figure 2. Continental evaporation recycling ratio ε_c (van der Ent, 2010)

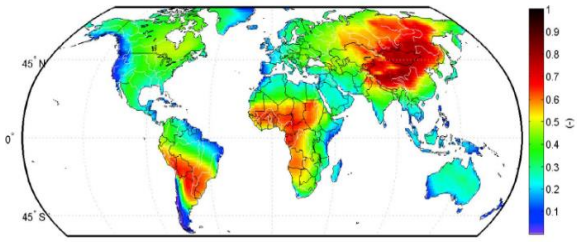

Figure 3. Continental precipitation recycling ratio ρ_c (van der Ent, 2010)

METHODS

DEFINITIONS

One way to prove a relation between two variables, is making use of the Pearson correlation coefficient (TUDelft, Kansrekening & Statistiek):

$$\rho(\mathrm{P}(t,x,y),\mathrm{E}(t,x,y)) = \frac{\mathrm{cov}(\mathrm{P}(t,x,y),\mathrm{E}(t,x,y))}{\sigma(\mathrm{P}(t,x,y))\sigma(\mathrm{E}(t,x,y))} \qquad (1)$$

in which P is the daily precipitation in the sink region and E the daily evaporation in the source region. Both parameters are longitude, latitude and time dependent.

The Pearson correlation coefficient tells how strong the linear relation is between two variables. The rating is between -1 and 1, with 1 being a perfect positive relation and -1 a perfect negative relation. What this means, is the higher the Pearson correlation coefficient, the stronger the relation between the variables. The assumption is however, that the variables have a linear relation, so non-linear behaviour is excluded.

The correlation coefficient is an excellent way to tell how variables interact with each other, but this is not sufficient. A high correlation coefficient doesn't necessarily mean a causal relation between two variables (Wright, 1921). For this causality, the continental precipitation multiplier will be used (Savenije, 1995a):

$$m_c(t,x,y) = \frac{P}{P_o} = 1 + \frac{P_c}{P_o} = \frac{1}{1-\rho_c} \qquad (2)$$

The continental precipitation multiplier describes the needed causal relation between precipitation and evaporation in the two regions. This is because of the amplification of precipitation due to continental evaporation, described in equation [4] (van der Ent *et al*., 2010].

When a correlation is proved it is possible to calculate the continental precipitation multiplier, since the slope of the evaporation vs. precipitation data figure should be the same as the multiplier. For this purpose the least-squares method is used. This method estimated the unknown parameters by minimizing the sum of the squared deviations between the data and the model (NIST, 2012). In our case the formula is of the form P = a*E + b, in which parameters a and b are unknown and are therefore solved using the least-squares method.

DATA

The data used is taken from ERA-Interim reanalysis. For this study, the two most important parameters are the precipitation in the sink area and the evaporation in the source area. However other parameters which should be included are the wind direction, length scales and time scales to be able to define the different areas in an appropriate way. In the paragraphs below this is explained further.

Due to the fact that it is simply not possible that water evaporates at one place and precipitates at another location at exactly the same moment, time and length scales are included. The used time scales are defined in previous research [van der Ent et al. 2011]. It is given that length and time scales are linked to one another. For this research, the assumption is that a year consists of two periods, namely summer and winter. At the middle of the summer period, the time moisture needs to reach China is 10 days whereas in the winter, this process takes 20 days. Throughout the year a linear relation between these values is assumed as shown in the figure below. To choose a suitable research area the maximum depletion time of 20 days is assumed meaning a length scale of about 5000-6000 kilometres [van der Ent et al. 2011]. The defined regions in figure 1 are chosen according to these conditions.

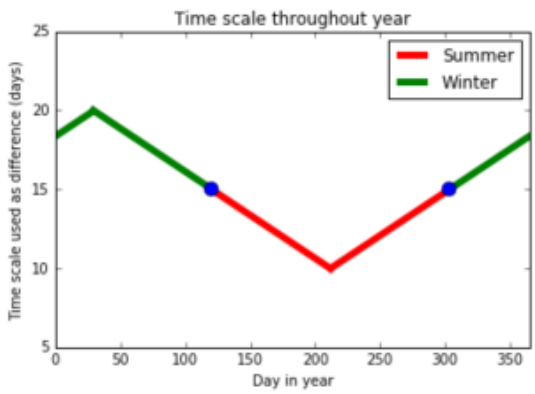

Figure 4. Linear relation for time scale throughout year; summer starts at 1 May (120th day), winter starts at 31 October (303th day)

ANALYSIS MODEL

In wet years the precipitation in China is also dependent on Asian monsoons, as described earlier in section 2. Therefore it is important to account for this part in the analysis model. To find the wet years in the ERA reanalysis data the formula in equation [1] has been used. The formula describes the total average precipitation in China which is dependent of the time, latitude and longitude. By summing up all the 12 hourly data for every grid point and dividing by the total area this gives the average rainfall in the whole researched sink

region for a year. The assumption for the analysis model is that all data above the 90 percentile range can be classified as a wet year, whereas the remaining years are 'normal' years. As can be seen from the figure below the years 1998, 1999, 2002 and 2003 are wet years.

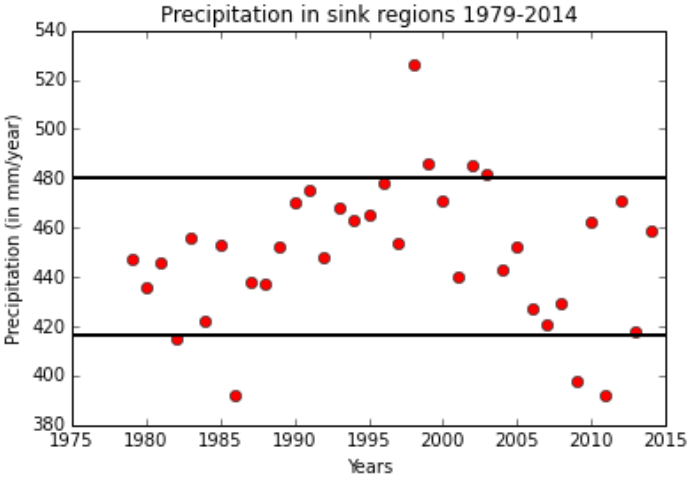

Figure 5. Average precipitation in China

ASSUMPTIONS

In the analysis model, there are some assumptions that need to be clarified for validity. The first assumption is that the atmosphere is well-mixed, the same as in the WAM model (van der Ent *et al*., 2010). This assumption follows from figure 2 and 3.

The length and time scales for the analysis model are based on the assumption that there is a linear relation between the maximum and minimum day in each period. A year is divided in two periods, which is of course not true, but well enough to make an assumption from.

Thirdly, an assumption is done in defining the different areas. It is assumed that a sink region receives all its precipitation from the defined source area. For wet years, it is assumed that this is 90 percent, whereas about 10 percent is received from the region behind the Tibetan plateau. In this research internal vapour recycling is therefore not included, meaning we assume that all precipitation originates outside the sink area and is not recycled within the area itself.

The last assumption, as already explained in section 3.1, is a linear relation between the two region and thus between the evaporation originating in the source area and the precipitation in the sink area.

RESULTS AND DISCUSSION

RESEARCH AREAS

As stated in section 2, three areas have been researched in the analysis model. The correlation coefficients are the following:

Table 2. Correlation coefficients research areas

Research area 1		Research area 2		Research area 3	
Year	ϱ	Year	ϱ	Year	ϱ
2005	0.78	2005	0.79	2005	0.87
2006	0.74	2006	0.79	2006	0.85
2007	0.77	2007	0.62	2007	0.86
2008	0.77	2008	0.76	2008	0.87
2009	0.74	2009	0.73	2009	0.86
2010	0.73	2010	0.69	2010	0.84
2011	0.80	2011	0.81	2011	0.89
all	0.76	all	0.74	all	0.86

As can be seen from the results, all three research areas have quite a high correlation coefficient regarding the theory behind the correlation coefficient, explained in section 3.1. These results show that it can be

stated that the assumption of the areas having a high relation with each other is correct, although the correlation coefficients differ from each other. The reason for this can be found in figure 4. The blue boxes of research area 1 are quite concentrated in China, whereas in figure 4, the precipitation tends to fall in and around China, especially in the north where Mongolia and other countries lay. Also, the moisture fluxes do not correspond with the choice of the red and blue boxes, which results in a lower correlation.

In research area 2, the blue box is much better placed. However, South-China is neglected completely where big rivers like the Yangtze flow and collect a lot of precipitation.

Research area 3 has without a doubt the highest correlation and best choices for its red and blue box.

CORRELATION COEFFICIENT

Since research area 3 has the highest correlation coefficient from all studied areas, this area has been chosen to be researched further. For more results of the other research areas, appendix A contains them all. The correlation coefficients from years 1991 till 2011 are given:

Table 3. Correlation coefficients research area 3

Year	ρ	Year	ρ	Year	ρ	Year	ρ
1991	0.86	1997	0.85	2002	0.87	2007	0.87
1992	0.82	1998	0.86	2003	0.87	2008	0.87
1993	0.86	1999	0.91	2004	0.85	2009	0.86
1994	0.86	2000	0.86	2005	0.87	2010	0.84
1995	0.87	2001	0.86	2006	0.85	2011	0.89
1996	0.86					all	0.84

When the daily evaporation and precipitation are plotted against each other, the next figure appears:

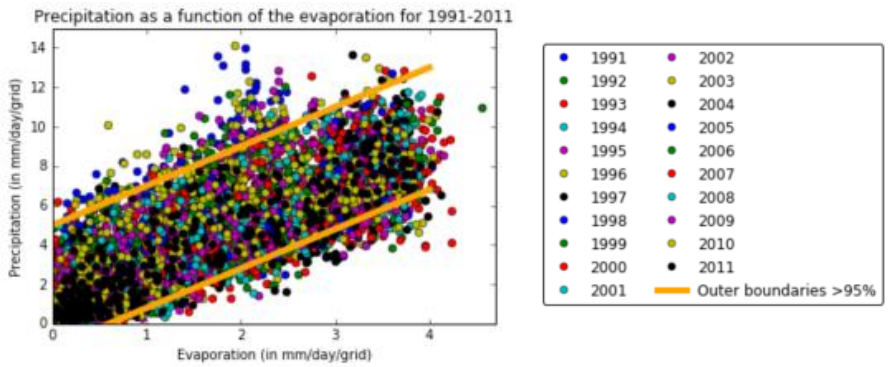

Figure 6. Precipitation plotted against evaporation for research area 3, 1991-2011

It is clear from the graph that there is a linear relation between evaporation and precipitation, as presumed, which is further clarified with the outer boundaries. It appears that when evaporation increases, precipitation also increases. But as mentioned before, correlation coefficients do not account for causality, so the continental precipitation multiplier from section 3.1 will be needed to prove the causality. The continental precipitation multiplier is calculated when the precipitation data is known, since ρ_c is the inverse of the slope of figure 7, however the slope is not immediately clear from the graph. Therefore a fitted line is needed which will tell the slope thus making it possible to calculate the multiplier.

From the analysis model, it follows that the slope of the fitted lines is 2.03 [-], which leads to ρ_c of 51%. This means 51% of the precipitation in the blue box from research area 3 depends on continental evaporation and the multiplier is 2.03 as well.

The wet years analysis show that this recycling ratio decreases, which seems logic as a large part of the precipitation originates from the region up and over the Tibetan plateau. Although the increase in correlation coefficient due to including the different areas in wet years was not significant (lower than 2%), the importance from the wet year analysis can be found back in the multiplier. The fitted lines were

also made for the wet years and their slope has also been calculated, meaning the multiplier and thus each ρ_c for the different wet years are known:

Table 3. Slope and multiplier for wet years

Year	Slope (-)	ρ_c(%)	M_c[-]
1998	3.95	25	1.34
1999	3.63	27.5	1.38
2002	3.35	30	1.43
2003	3.46	29	1.41

4.3 Forecasting model

The results found with the fitted lines are really interesting for the meteorological and hydrological departments in especially China and its surroundings. Insights in the precipitation in this area and its pattern could provide a long term solution for water scarcity. Therefore this study will try to make a simple forecasting model, based on the results in section 4.1 and 4.2 in the hope that further researches will take this model as base and try to make it robust and much more accurate.

The fitted line from the analysis model is the base for the forecasting model. Since precipitation measures need to be known with low failure ratings, the fitted line can be improved by adding the standard deviation times two. This improves the model to an accountability of the prediction within a confidence interval of 95%. In formula form the forecasting model is:

$$P(E) = 2.03 * E + 1.15 \quad \text{(average)}$$
$$P(E) = 2.03 * E + 4.47 \quad \text{(maximum)} \qquad (3)$$
$$P(E) = 2.03 * E - 2.17 \quad \text{(minimum)}$$

The evaporation input data is the average evaporation per day per grid from the red box in figure 1C.

CONCLUSION

The main question in this research is - how strong is the relation between evaporation in Eurasia and precipitation in China? The relation was first proposed by van der Ent et al. [2010] and this study has quantified this relation in mathematical manner. The hypothesis has been proved true, because the correlation coefficient between evaporation in Eurasia and precipitation in China is very high. The question needs to be rephrased though because the area chosen for the precipitation isn't only China but also China's surrounding areas.

However, a high correlation coefficient doesn't necessarily mean there is indeed a causal relation between evaporation and precipitation. This facet of the study has been done with the continental precipitation multiplier and its value for the researched area. The multiplier shows values close to that of van der Ent et al. [2010]. The closer ρ_c is to 100%, the more we know about the origin of the precipitation.

During the research large uncertainty still remained considering the different areas. A correlation is clearly recognised in the data but specific areas cannot be distinguished. Results of research area 3 are promising. Therefore it is indeed true that there is a high correlation, however this is only true for large regions. It can't be said which areas are connected specifically. Nonetheless, this research has shown the correlation is present and by expanding this field of search one should be able to find the specific regions.

REFERENCES

Ent, R.J. van der., Savenije, H.H.G., Schaefli, B. and S.C. Steele-Dunne (2010). *Origin and fate of atmospheric moisture over continents*, http://onlinelibrary.wiley.com/doi/10.1029/2010WR009127/full, 2010.

Ent, R.J. van der. and H.H.G. Savenije (2011). *Length and time scales of atmospheric moisture recycling*, http://www.atmos-chem-phys-discuss.net/10/21867/2010/acpd-10-21867-2010-print.pdf

Falkenmark, M. (1989). *The massive water scarcity now threatening Africa: Why isn't it being addressed?*, http://www.jstor.org/stable/4313541?seq=1#page_scan_tab_contents

Falkenmark, M. (1998). *Dilemma when entering 21st century – rapid change but lack of sense of urgency*, http://www.sciencedirect.com/science/article/pii/S1366701798000324

Jiang, Y. (2009). *China's water scarcity,* http://www.sciencedirect.com/science/article/pii/S0378377402000756

Kummu, M., Ward, P. J., de Moel, H. and O. Varis (2010). *Is physical water scarcity a new phenomenon? Global assessment of water shortage over the last two millennia*, http://iopscience.iop.org/article/10.1088/1748-9326/5/3/034006/meta;jsessionid=42C0CB995F07F658DD909411EABD95C0.c3.iopscience.cld.iop.org

Pereira, L.S., Oweis, T. and A. Zairi (2002). *Irrigation management under water scarcity,* http://www.sciencedirect.com/science/article/pii/S0378377402000756

Savenije, H.H.G. (1995). *Does moisture feedback affect rainfall significantly?,* http://www.sciencedirect.com/science/article/pii/S0079194696000146

Seckler, D., Barker, R. and U. Amarasinghe (2010). *Water scarcity in the twenty-first century*, http://www.tandfonline.com/doi/pdf/10.1080/07900629948916

Technische Universiteit Delft, course Kansrekening & Statistiek, https://blackboard.tudelft.nl/bbcswebdav/pid-2407001-dt-content-rid-8105015_2/courses/32024-141502/week_4.1.pdf

Wang-Erlandsson, L., Ent, R.J. van der., Gordon, L.J. and H.H.G. Savenije (2014). *Contrasting roles of interception and transpiration in the hydrological cycle – Part 1: Temporal characteristics over land*, https://tinyurl.com/gwuamov

Wright, S (1921). *Correlation and causation,* http://www.ssc.wisc.edu/soc/class/soc952/Wright/Wright_Correlation%20and%20Causation.pdf

Yatagai, A. and T. Yasunari (1998). *Variation of summer water vapour transport related to precipitation over and around the arid region in the interior of the Eurasian continent*, http://www.chikyu.ac.jp/yasunari/yasunari.bak/list/pdf/yatagai.yasunariJMSJ.1998.pdf

BOOKS

Deng, X. (2011). *Modeling the dynamics and consequences of land system change.*

Pereira, L.S., Codery, I. and I. Iacovides (2009). *Coping with water scarcity.*

SURFACE AIR TEMPERATURE CHANGES IN THE HIGH-LATITUDE BOUNDARY LAYER

R. DAVY[1] and I. ESAU[1]

[1]Nansen Environmental and Remote Sensing Centre, and Bjerknes Centre, Bergen, Norway.

Keywords: BOUNDARY-LAYER, DIURNAL, WARMING, EXTREMES.

INTRODUCTION

The second half of the twentieth century saw a pronounced warming over continental Eurasia. However, the rate of warming was strongly varied inter-seasonally and within the diurnal cycle e.g. winter-time temperatures increased more rapidly than summer temperatures (Cohen et al., 2012) and night-time temperatures increased faster than day-time temperatures (Vose et al., 2005; Davy et al., 2016). Understanding the causes of these asymmetries has been identified as crucial in giving us insights into the nature of the climate system's response to forcing (Braganza et al., 2004; Cohen et al., 2012). Numerous processes have been proposed to be the cause of these asymmetries; principally through introducing asymmetries in the surface energy budget e.g. increases in cloud cover during the day can reduce incoming shortwave radiation, and so dampen the rate of warming, leading to a reduction in the diurnal temperature range (Dai et al., 1999; Zhou et al., 2009). In some cases there has been strong links demonstrated between a given process and one of these asymmetries e.g. Tang and Leng (2012) showed that the relatively slow warming in the Eurasian summer-time was strongly correlated to an increase in cloud cover in this region at this time. Global climate models (GCMs) are one of the common tools used to explore the causes of these changes. While these models do a good job of reproducing the observed changes in the mean surface air temperature (SAT) during the 20th century, they do not have the same skill when it comes to climate extremes, including changes to the diurnal temperature minimum, T_n, maximum, T_x and range, *DTR* (Dai and Trenberth, 2003; Lewis and Karoly, 2013).

The warming in the 20th century also brought large changes to the temperature extremes in the Eurasian continent. As would be expected, the number of hot (cold) extremes has increased (decreased) under the general warming trend. However, there has been a much more pronounced increase in hot extremes than there has been a decrease in cold extremes (Rahmstorf and Coumou, 2011). There has also been a decrease in the SAT variability during the second half of the 20th century as the mean temperature increased (Michaels et al., 1998), with a bigger decrease in the variability of night-time temperatures than day-time temperatures (Davy et al., 2016).

These, perhaps counter-intuitive, results can be understood through consideration of an energy-budget model of the climate system. One aspect which has often been overlooked when seeking to understand these patterns of climate change is how the climatology of the atmospheric boundary layer (ABL) affects the response of surface temperatures to external forcing. Since the climatology of the ABL defines the effective heat capacity of the atmosphere (Esau and Zilitinkevich, 2010), it can strongly determine how much the SAT will change in response to a change in the forcing (Esau et al., 2012). Here we will review the changes in the SAT over Eurasia in the second half of the 20th century, and discuss how the climatology of the ABL can help us understand this pattern of climate change.

DATA AND METHODS

We use high-resolution, gridded observations, the latest dataset from the Climate Research Unit (CRU), CRU v3.2 (Harris et al., 2014), to assess changes in the temperature extremes. The monthly-mean values of T_n and T_x were obtained from this dataset, which is publicly available at crudata.uea.ac.uk/cru/data/hrg/. The suite of contemporary climate model results that comprised the IPCC AR5 Atlas subset of the Climate Model Intercomparison Project phase 5 (CMIP5) were used to assess model representation of changes in

climate extremes in the 20th century. These are also publicly available through the CMIP5 data portal: http://cmip-pcmdi.llnl.gov/cmip5/data_portal.html.
Monthly anomalies were calculated by removing the climatological mean (average of the full-period of the time series) of each month from the time-series of each variable. The trend in each variable was calculated from the time series of monthly anomalies using a least-squares linear regression, with the trends filtered for significance using a requirement that $p<0.05$. The variability of a given variable was defined as the standard deviation of the monthly-anomaly time series, and extremes were defined as the anomalies which exceed two standard deviations. The significance of the difference between two distributions was tested using a two-sample F-test and the null hypothesis that they were drawn from the same distribution rejected with $p<0.05$.

HYPOTHESIS

If we consider the response of the SAT to a perturbation in the external forcing, this can be described through an energy-budget model of the form:

$$\frac{dT}{dt} = C^{-1} dQ \qquad \text{Eqn. 1}$$

where T is the SAT; C is the effective heat capacity, which can be linearly related to the PBL depth; and dQ is the perturbation in the forcing. From this formulation we can expect that, under an evenly-distributed positive perturbation in the forcing, such as you get from an increase in greenhouse gases, that the places and times with the shallowest boundary layers will warm the fastest. So if we apply this model to consideration of the diurnal temperature extremes T_n and T_x, we can expect there to be a stronger trend in T_n than T_x, leading to a reduction in the *DTR*. This will be most pronounced when there is the biggest difference in the reciprocal boundary layer depth within the diurnal cycle. Similarly we can apply this formulation to the diurnal mean temperature – in which case it is the locations with the shallowest boundary layer that we can expect to have warmed the fastest in recent decades. Furthermore, inter-seasonally we can expect the winters to have warmed faster than the summers, due to the shallower boundary layers found in the winter.
This formulation also applies to the surface temperature variability – so we can expect an inverse relationship between boundary layer depth and SAT variability. Given the expectation that in a warming world the mean boundary-layer depth will tend to increase, especially in the shallow boundary layers which warm the fastest, the SAT variability may be expected to decrease. The most rapid decrease may be expected to be seen in those locations and times with the highest variability – so we anticipate a greater decrease in the variability of T_n than T_x.

RESULTS

There has been a general reduction in the diurnal temperature range in the second half of the twentieth century, especially over continental Eurasia (Braganza et al., 2004). This negative trend is also present in the CMIP5 results, as can be seen in Figure 1 which shows the DTR trend for the annual average, and for the winter and summer months. There is a strong seasonal component to this trend: in the summer months there is even a strong positive trend in the *DTR* in some locations, whereas in winter there is a strong negative trend almost everywhere in Eurasia.

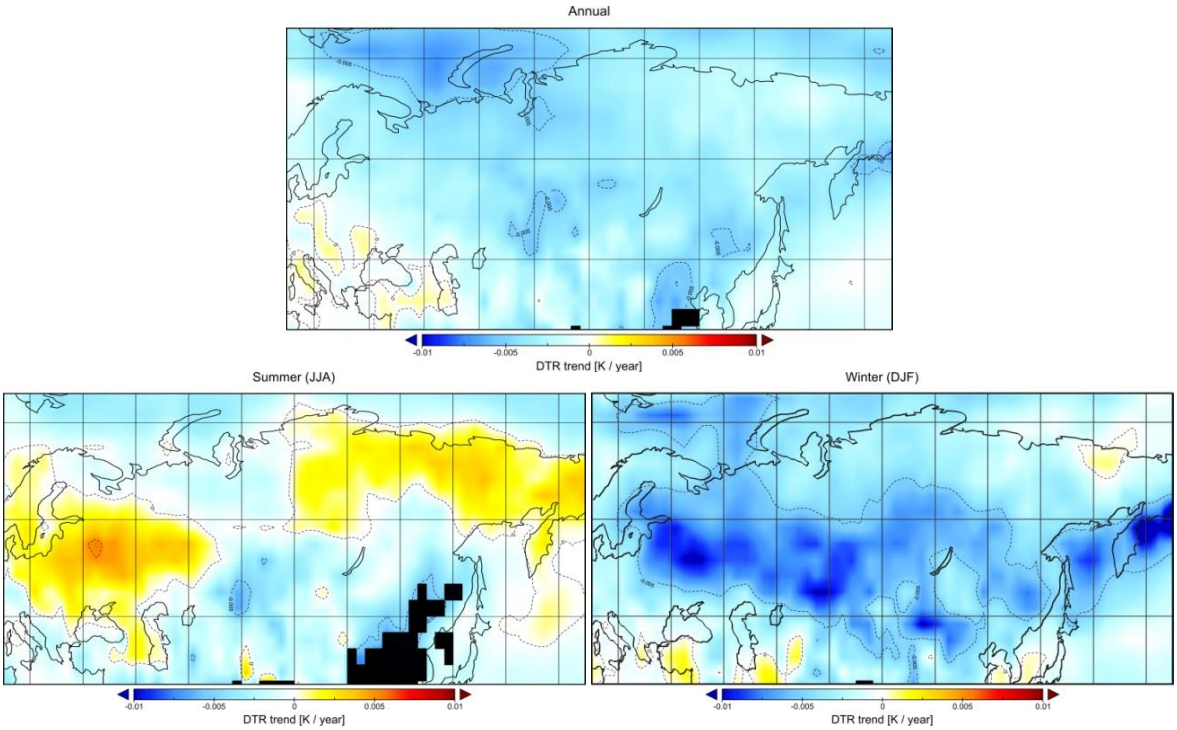

Figure 1. The best-fit linear trends in the Diurnal Temperature Range from 1950 to 2000 for the annual average, Winter (DJF) and Summer (JJA) months. Data are the average of the IPCC AR5 Atlas subset of CMIP5 model results. The trends have been filtered using a two-tailed Student-t distribution test, with the requirement $p<0.05$. Areas which didn't pass this test have been masked-out in black.

There is also a strong seasonal asymmetry to the overall warming trend: the winters have warmed at a faster rate than the summers (Figure 2). In the winter the most pronounced warming is seen over sea-ice and the high-latitude continental regions; whereas in the summer there is a much more uniform pattern of warming.

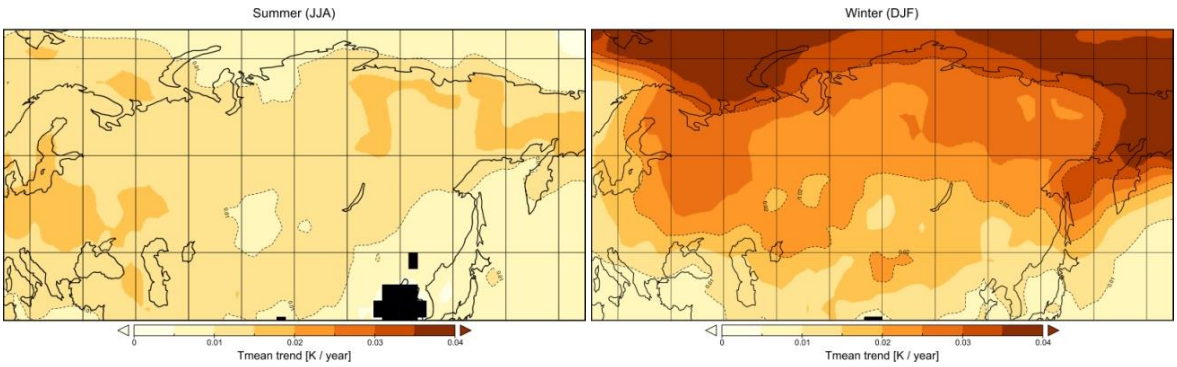

Figure 2. The best-fit linear trends in the diurnal mean temperature from 1950 to 2000 for the Winter (DJF) and Summer (JJA) months. Data are the average of the IPCC AR5 Atlas subset of CMIP5 model results. The trends have been filtered using a two-tailed Student-t distribution test, with the requirement $p<0.05$. Areas which didn't pass this test have been masked-out in black.

We can see a clear pattern in the changes of the SAT variability and extremes between the current period, 1980-2009, and a reference period, 1950-1979 (Table 1). There has been a reduction in the SAT variability overall, with a greater reduction in the variability of T_n than T_x, as anticipated. Similarly, while there has been a reduction in the cold extremes in both metrics, the reduction in cold extremes of T_n is more pronounced. Accordingly, there has been a greater increase in the hot extremes of T_n than T_x.

Table 1. Three measures of the change in the properties of the diurnal minimum and maximum temperatures from the current period, 1980-2009, and the reference period, 1950-1979. $\Delta\sigma$ is the area-weighted percentage-change in the standard deviation and ΔT_{Cold} and ΔT_{Hot} are the change in the area-weighted average number of cold and hot extremes respectively. Temperature extremes are defined as being anomalies in excess of 2σ of the relevant temperature in the reference period. Data are taken over the northern hemisphere land from the gridded observations, CRU v3.2.

	$\Delta\sigma$ (%)	**ΔT_{Cold} (%)**	**ΔT_{Hot} (%)**
T_{min}	**-1.47** +/- .02	**-47.7** +/- 0.6	**+247** +/- 3
T_{max}	**-1.18** +/- .02	**-27.0** +/- 0.3	**+175** +/- 2

DISCUSSION

The PBL-control mechanism we discuss here is not introducing some climate-forcing perturbation, but rather controls the degree to which a given process affects the surface air temperature. For example, there are many factors which may affect the radiative forcing on the diurnal extreme temperatures differently, and so lead to an increase or decrease in the diurnal temperature range. However, the shallow boundary layers associated with night-time temperatures mean that these are inherently more sensitive to perturbations to the radiation balance than daytime temperatures. Consequently, in the absence of other strong processes, the night-time temperatures will warm more rapidly on a uniform forcing (such as that from the build-up of greenhouse-gases). Similarly with the diurnal mean temperature – in the deep boundary layers found during the summer the inverse relationship of SAT trends with PBL depth becomes less important, and so other factors may control the different rates of warming over land. But in the winter time, when you get very shallow boundary layers, this inverse relationship can dominate, and be the principal determinant of the pattern of warming. Overall we see a clear pattern of changes to the surface air temperature consistent with this hypothesis: that it is the coldest locations and times that have warmed the most rapidly, and have seen the greatest reduction in variability during the latter half of the 20th century.

ACKNOWLEDGEMENTS

This work was supported by the Bjerknes Centre for Climate Research project, BASIC.

REFERENCES

Braganza, K., D.J. Karoly and J.M. Arblaster (2004). Diurnal temperature range as an index of global climate change during the twentieth century. *Geophys. Res. Lett.* **31**, L13217.

Cohen, J.L., J.C. Furtado, M. Barlow, V.A. Alexeev and J.E. Cherry (2012). Asymmetric seasonal temperature trends. *Geophys. Res. Lett.* **39**, L04705.

Dai, A., K.E. Trenberth and T.R. Karl (1999). Effects of Clouds, Soil Moisture, Precipitation and Water Vapor on Diurnal Temperature Range. *J. Climate***12**, 2450-2473

Dai, A., and K.E. Trenberth (2003). The diurnal cycle and its depiction in the community climate system model. *J. Climate* **17**, 930-951.

Davy, R., I. Esau, A. Chernokulsky, S. Outten and S. Zilitinkevich (2016). Diurnal asymmetry to the observed global warming. *Int. J. Climatol.*, in press.

Esau, I., R. Davy and S. Outten (2012). Complementary explanation of temperature response in the lower atmosphere. *Environ. Res. Lett.* **7**, 044026.

Esau, I. and S. Zilitinkevich (2010). On the role of the planetary boundary layer depth in the climate system. *Adv. Sci. Res.*, **4**, 63-69.

Harris, I., Jones, P.D., Osborn, T.J. and D.H. Lister (2014). Updated high-resolution grids of monthly climatic observations – the CRU TS3.10 Dataset. *Int. J. Climatol.* **34**, 623-642.

Lewis, S., and D. Karoly (2013). Evaluation of historical diurnal temperature range trends in CMIP5 Models. *J. Climate* **26**, 9077-9089.

Michaels, P.J., R.C. Balling Jr, R.S. Vose and P.C. Knappenberger (1998). Analysis of trends in the variability of daily and monthly historical temperature measurements. *Clim. Res.* **10**, 27-33.

Rahmstorf, S. and D. Coumou (2011). Increase of extreme events in a warming world. *PNAS*, **108** (44), 17905-17909.

Tang, Q. and G. Leng (2012). Damped summer warming accompanied with cloud cover increase over Eurasia from 1982 to 2009. *Environ. Res. Lett.* **7**, 014004.

Vose, R.S.., D.R. Easterling and B. Gleason (2005). Maximum and minimum temperature trends for the globe: An update through 2004. *Geophys. Res. Lett.* **32**, L23822.

Zhou, L., A. Dai, Y. Dai, R.S. Vose, C.-Z. Zou, Y. Tian and H. Chen (2009). Spatial dependence of diurnal temperature range trends on precipitation from 1950 to 2004. *Clim. Dyn.*, **32**, 429-440.

SATELLITE REMOTE SENSING OF AEROSOL AND CLOUD PROPERTIES OVER THE PEEX AREA

G. DE LEEUW[1,2], L. SOGACHEVA[1], P. KOLMONEN[1], G. SAPONARO[1], T.H. VIRTANEN[1] AND E. RODRIGUEZ[1]

[1]Finnish Meteorological Institute, Helsinki, Finland

[2]Department of Physics, University of Helsinki, Finland.

Keywords: SATELLITE REMOTE SENSING, AEROSOL, CLOUDS, AOD.

INTRODUCTION

Satellite remote sensing provides the spatial distribution of aerosol and cloud properties over a wide area. As such, information from satellite remote sensing is complementary to in situ measurements from surface stations or aircraft, as well as from ground-based remote sensing. Satellites provide less detail due to limited information content, have limited temporal coverage, but provide a wide view over a very large area showing the spatial distribution of a variety of retrieval parameters. This is especially important over areas for which no in situ information is available. Polar orbiting satellites provide on the order of 14 orbits per day and the swath width of instruments used for observations of atmospheric properties such as aerosol or cloud parameters, atmospheric trace gases or surface properties may vary from a few hundred kilometres to ca. 2300 km (MODIS) or more. Their importance is, among others, that they use optical techniques to obtain information on aerosol properties and hence the results are of direct relevance to climate because particles are observed in the optically active size range. These particles are also important for air quality, since they contribute to particulate matter concentrations included in PM1 or PM2.5 (Van Donkelaar et al. (2010). The column- integrated aerosol extinction, aerosol optical depth (AOD), which is primarily reported from satellite observations, is used as a proxy for cloud condensation nuclei (CCN), i.e. for the ability of aerosol particles to form clouds (Andreae, 2009). Hence, connecting this and other information with satellite observations of cloud properties makes it possible to study aerosol-cloud interaction.

On the other hand, particles smaller than about 100 nm are important for many processes but cannot be observed from satellites. In that case, atmospheric trace gases which can serve as aerosol precursors (e.g., NO_2, SO_2, VOCs), as well as other proxies such as UV radiation and AOD, which serves as a proxy for condensation sink, can be observed from satellites and are these observations are used to provide information on new particles formed through nucleation (Kulmala et al., 2011; Sundström et al., 2015).

Whereas all these processes can be studied in great detail from ground-based measurements involving a comprehensive instrument suite to provide information on a wide variety of parameters, satellites are very limited as regards the number of parameters they can provide and the detail of their properties. Satellites measure only a few signals, in particular the intensity of the upwelling solar radiation reflected by atmospheric constituents (clouds, aerosols, trace gases) and the Earth surface, in several wavebands (radiometers) or as a wide spectrum (spectrometers) over a certain wavelength range, sometimes at more than one viewing angle and sometimes with polarization information. The more of such parameters are measured, the more information is available, but still only few degrees of freedom, i.e. only few parameters can be retrieved. With this difference in mind, the complementarity of satellite and in situ ground-based observations needs to be explored, where satellites are very important to provide information over the vast areas where no ground-based information is available. This applies, for instance, over the larger part of the Eurasia, the study domain of PEEX.

SATELLITE DATA

Retrieval algorithms for aerosol and clouds have been developed for the (Advanced) Along Track Scanning Radiometer (A)ATSR, consisting of a series of instruments of which we use the second and third one: ATSR-2 which flew on the ERS-2 satellite (1995-2003) and AATSR which flew on the ENVISAT satellite (2002-2012) (both from the European Space Agency, ESA). The ATSR instruments provide two views: one near-nadir and the other at 55 degrees forward. In each view, the radiances at the top of the atmosphere (TOA) are measured in 7 wavebands from the visible (VIS) to the thermal infrared (TIR). The TIR wavebands are mainly used for cloud detection, in combination with a number of other tests including shorter wavelengths. The VIS and NIR (near-infrared) wavebands are used for aerosol retrieval. Over land the ATSR dual view algorithm (ADV; Kolmonen et al., 2015) is used, in which the effect of the land surface reflectance is accounted for by using the ratio of both views in the 1.6 µm band, assuming that the effect of aerosols on the TOA reflectance is small (Veefkind et al., 1998). Together with some other assumptions, the dual view algorithm provides information on the aerosol properties over land with a quality which is similar to that of other satellites which are commonly used as a reference for aerosol retrieval (in particular MODIS, MISR) (de Leeuw et al., 2015). However, ATSR has a smaller swath and thus less coverage than MODIS, and a bit better than MISR. Over ocean only a single view (ASV, Veefkind and de Leeuw, 1998) is used (forward) and also here the quality of the data is competitive with that of other instruments (de Leeuw et al., 2015; Kolmonen et al, 2015). The validation of ADV and ASV versus independent ground-based measurements using AERONET sun photometer AOD data (Holben et al., 1998) has been illustrated in Kolmonen et al. (2015). The ATSR-2/AATSR combination provides a time series of 17-years, longer than any other of the currently available quality products (MODIS, MISR, SeaWiFS). This time series will be further expanded with those from the Sea and Land Surface Temperature Radiometer (SLSTR) on the ESA/EU GMES Sentinel-3 mission planned to be launched in February 2016.

The Dual View algorithm (ADV) provides aerosol data on a global scale with a default resolution of 10x10km^2 (L2) and an aggregate product on 1° x1^o (L3). Optional, a 1x1 km^2 retrieval product is available over smaller areas for specific studies. As an example, the aggregated AOD (i.e. the average of the AOD values when retrieval was successful) over the PEEX area, for the years 2003-2011, is presented in Figure 1. Figure 1a shows the AOD with the standard cloud post-processing (Kolmonen et al., 2015), in Figure 1b extended cloud post-processing has been applied (Sogacheva et al., 2016) as will be explained below.

For the retrieval of cloud properties, the SACURA algorithm (Kokhanovsky et al., 2003) has been implemented in the ADV/ASV aerosol retrieval suite. Cloud properties retrieved from AATSR data are cloud optical thickness, cloud droplet effective radius, liquid water path. In addition to AATSR data we also use publicly available MODIS cloud properties.

Land surface reflectance can also be provided from ATSR (Sogacheva et al., 2015). The retrieval of the AOD using the ADV algorithm does not require any prior information on land surface properties as described above. In fact, the effect of land surface reflectance on the TOA radiation is essentially eliminated to retain the path radiance from which the AOD is retrieved. Hence, the AOD can be used as an independent (from the surface) parameter to provide the atmospheric correction needed to retrieve the surface reflectance.

In this contribution we focus on the direct retrieval of aerosol information using ADV.

APPLICATIONS TO THE PEEX STUDY AREA

Aerosol and cloud properties are applied for different studies over the PEEX area. As reported in 2015, the transition from the aerosol regime to the cloud regime is studied using the simultaneous retrieval of aerosol and cloud properties retrieved for single AATSR pixels (nominal 1x1 km^2 sub-nadir). Aerosol cloud interaction is also studied using large data sets over Fennoscandia, the Baltic Sea and adjacent

regions over the European mainland, with the aim to study the effect of different types of air masses (polluted to clean) on aerosol-cloud interaction using a large aerosol and cloud data set provided by MODIS.

Aerosol studies focus on the effects of forest fires and pollution for a wide range of conditions from rather clean over Finland with AOD usually on the order of about 0.05 (Aaltonen et al., 2011) , to more polluted areas over Central Europe or Russia and the effect of different sources of aerosols (desert dust, photochemistry and direct emissions) over China. In the retrieval process, mixtures of four different aerosol components are used, two fine mode with different absorption coefficients, plus coarse mode sea spray and desert dust aerosol. These components are mixed into aerosol types with mixing fractions which are semi-continuously varied until the best fit is obtained for the TOA radiances at all four wavelengths. (cf. Kolmonen et al., 2015, for more detail). Using these mixing rations, in principle also information is available on aerosol properties such as fine mode fraction or single scattering albedo (ssa) (cf. Rodríguez et al., 2015 for a study on how well this works for ssa). Also the spectral dependence of the AOD, expressed in the Ångström exponent (AE), provides particle size information.

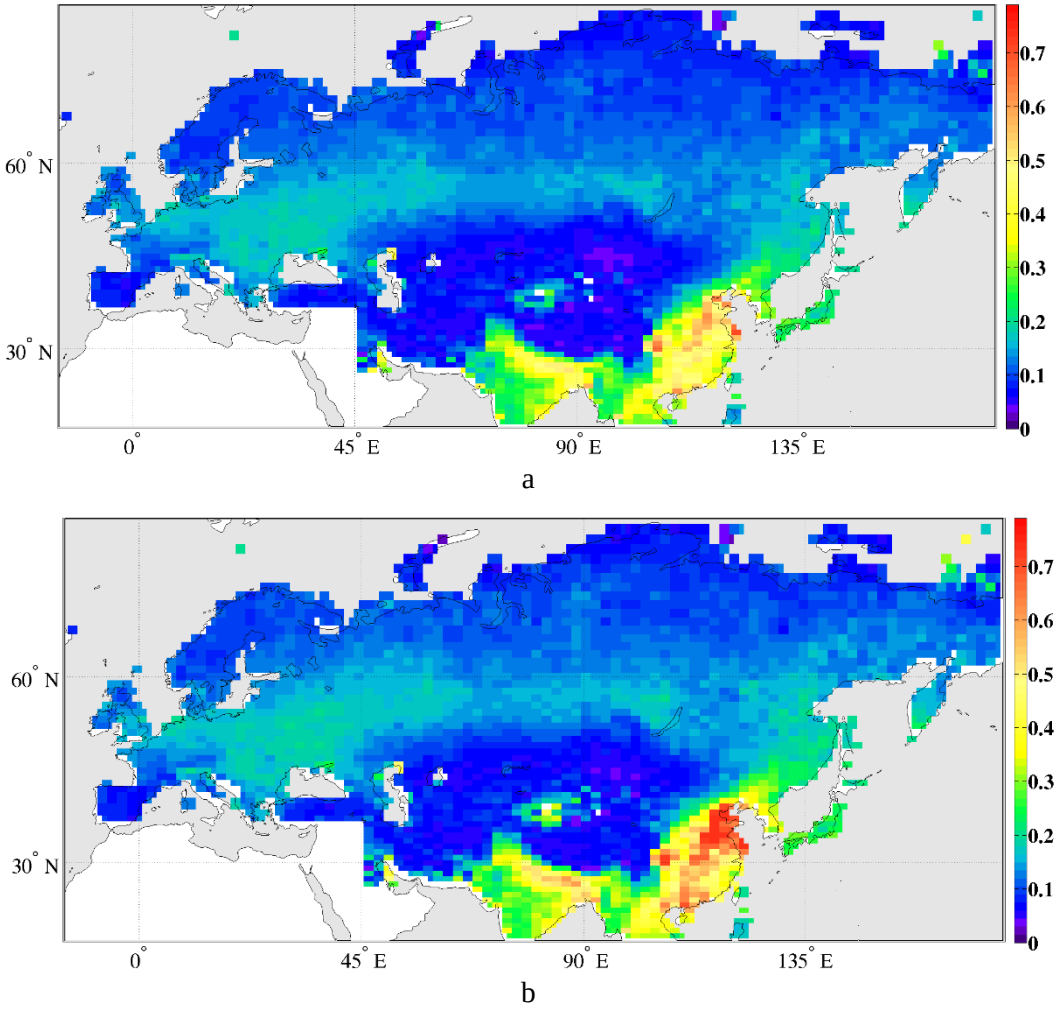

Figure 1. Aggregated AOD distribution over land for the PEEX area for the years 2003-2011: a) application of standard cloud post-processing (Kolmonen et al., 2015), average AOD over the area shown is 0.141; b) after extended cloud post-processing (Sogacheva et al., in preparation) , average AOD over the area shown is 0.156. See text for further explanation. Note that the AOD scale, shown on the right hand side of the maps, ranges from 0 to 0.8, all higher values are plotted at this maximum value. White areas mean no retrieval was achieved (see text).

An important application of satellite observations of aerosol properties is the estimation of direct radiative effects (Sundström et al, 2015) or the application with chemical transport models to estimate emissions from forest fires (e.g., Sofiev et al., 2013) or other sources, as well as for application of surface level PM2.5 concentrations (van Donkelaar, 2010; Xu et al., 2015). For such applications it is important to have the most accurate information on the aerosol properties, in particular AOD since this is the parameter that is most often used in such studies. This means that AOD should not be contaminated by residual clouds, i.e. which slipped through the cloud detection process (e.g. Robles-Gonzalez, 2013, which is applied with ADV). To this end cloud processing has been developed for application to the ADV retrieval results. As described in Kolmonen et al. (2015), the cloud post-processing compares the values of the AOD in neighbouring pixels and when large jumps occur the pixel is declared cloud contaminated and discarded as a valid AOD pixel. The AOD map shown in Figure 1a has been subjected to this process which has been adopted in the ESA Aerosol_cci project (Hollmann et al., 2013; Holzer-Popp et al., 2013) for the current AATSR algorithms including ADV. Figure 1a shows the spatial distribution across the PEEX area, with elevated AOD values (ca. 0.2) over a large part of western and central Europe, extending eastward over Asia, and higher (ca. 0.4) over parts of India and China, up to locally ca. 0.6. It is noted that these are multi-year averages, but still the values seem to be on the low side. Further inspection of short term averages (daily overpasses) shows the occurrence of large areas with much higher AOD (1.0 or more), before cloud post-processing, which are clearly not cloud-contaminated but yet screened out. Apparently these high AOD pixels are discarded due to the occurrence of rather sharp edges. In response to this finding, an extended cloud post-processing has been worked out with criteria to switch off the standard cloud post-processing and thus retain pixels with high AOD, while also the rejection criteria have been re-investigated (Sogacheva et al., 2016). The effect of this extended cloud post-processing is most visible in individual overpasses, but also in the multi-year average shown in Figure 1b the AOD is clearly higher. In particular this is evident over parts of China and India, with values up to 0.8 (and possibly higher). In these maps the maximum value of 0.8 was selected to visualize the increased AOD also over areas with low AOD. Indeed, Figure 1 b clearly shows that the extended post-processing influences the AOD over most of the PEEX area. The integrated AOD over the whole area (not including the deserts in Saudi Arabia and North Africa because ADV is known to perform less reliably due to the very high surface reflectance sometimes leading to saturation of the detectors) is 0.141 when standard cloud-processing is applied and 0.156 with the extended cloud post-processing.

Comparison of the validation results, i.e. comparison of the ADV retrieved AOD with standard and extended cloud post-processing with the reference AOD values from AERONET shows that with the extension higher AODs are retained while the cloud-contaminated pixels are still effectively removed. Also the validation metrics are somewhat better with the extended cloud post-processing than with the standard method (Sogacheva et al., 2016).

CONCLUSIONS

The rationale for the application of satellite observation over the vast PEEX study area has been outlined above. Satellites can provide information on a variety of phenomena over both the boreal forest and over industrialized and urban areas in EURASIA, including the local generation of aerosols by nucleation using proxies (Kulmala et al., 2011; Sundström et al., 2015), the transport of aerosols from elsewhere and their effects on air quality and climate, both direct and indirect through aerosol cloud interaction. Aerosols and cloud also affect the surface radiation level and thus the biosphere by limiting radiation. To fully explore the use of satellite-retrieved AOD, the most accurate information must be available and the study presented above contributes to further improvement. Comparison with ground-based reference data shows a slight improvement of the validation metrics but the main value is in retaining the retrieval areas with high AOD.

Together with satellite observations by other PEEX participants on land and water surfaces, forests, vegetation, snow and ice, satellites are crucial in the PEEX project. They provide the spatial extent which cannot possibly be covered by ground-based or airborne observations. In this way they fill the gaps

between the planned supersites and other stations. Furthermore, since the same instruments are used over a long period of time and over the same area, a consistent source of information on phenomena over the boreal forest is provided. The long time series show the temporal variation (e.g. de Leeuw et al., MarcoPolo progress reports for AOD). Another example is the analysis of trends in the albedo of snow-covered surfaces in the Northern hemisphere (Atlaskina et al, 2015). Other work includes studies on the effect of soot on snow properties, snow melt and snow albedo.

ACKNOWLEDGEMENTS

This work was supported by This work was supported by the Centre on Excellence in Atmospheric Science funded by the Finnish Academy of Sciences Excellence (project no. 272041), the CRAICC (Cryosphere-atmosphere interactions in a changing Arctic climate), which is part of the Top-level Research Initiative (TRI) of the joint Nordic research and innovation initiative, the ESA-ESRIN projects Aerosol-cci (project AO/1-6207/09/I-LG), STSE-ALANIS Atmosphere-Land-Interaction Study, Theme 3 Aerosols (Contract No 4200023053/10/I-LG), and Globemission (ESA-ESRIN Data Users Element (DUE), project AO/1-6721/11/I-NB), the EU FP7 projects MarcoPolo (Grant agreement no 606953) and BACCHUS (Grant agreement no 603445), and the Nessling Foundation.

REFERENCES

Aaltonen, V., E. Rodriguez, S. Kazadzis, A. Arola, V. Amiridis, H. Lihavainen, and G. de Leeuw (2011). On the variation of aerosol properties over Finland based on the optical columnar measurements (2012). *Atm. Res.*, 116, 46-55 (http://dx.doi.org/10.1016/j.atmosres.2011.07.014).

Andreae, M. O. (2009b), Correlation between cloud condensation nuclei concentration and aerosol optical thickness in remote and polluted regions, Atmos. Chem. Phys., 9, 543–556.

Atlaskina, K., Berninger, F., and de Leeuw, G.: Satellite observations of changes in snow-covered land surface albedo during spring in the Northern Hemisphere, The Cryosphere, 9, 1879-1893, doi:10.5194/tc-9-1879-2015, 2015

de Leeuw, G., T. Holzer-Popp, S. Bevan, W. Davies, J. Descloitres, R.G. Grainger, J. Griesfeller, A. Heckel, S. Kinne, L. Klüser, P. Kolmonen, P. Litvinov, D. Martynenko, P.J.R. North, B. Ovigneur, N. Pascal, C. Poulsen, D. Ramon, M. Schulz, R.Siddans, L. Sogacheva, D. Tanré, G.E. Thomas, T.H. Virtanen, W. von Hoyningen Huene, M.Vountas, S. Pinnock (2015). Evaluation of seven European aerosol optical depth retrieval algorithms for climate analysis, Remote Sensing of Environment 162 (2015) 295–315. DOI information: 10.1016/j.rse.2013.04.023.

Holben, B., Eck, T., Slutsker, I., Tanre, D., Buis, J., Setzer, A., Vermote, E., Reagan, J., and Kaufman, Y.: AERONET a federated instrument network and data archive for aerosol characterization, Remote Sens. Environ., 66, 1–16, 1998.

Hollmann, R., C. Merchant, R. Saunders, C. Downy, M. Buchwitz, A. Cazenave, E. Chuvieco, P. Defourny, G. de Leeuw, R. Forsberg, T. Holzer-Popp, F. Paul, S. Sandven, S., Sathyendranath, M. van Roozendael, W. Wagner (2013).The ESA climate change initiative: satellite data records for essential climate variables. Bulletin of the American Meteorological Society Oct. 2013, 1541-1552. ; e-View: doi: http://dx.doi.org/10.1175/BAMS-D-11-00254.1.

Holzer-Popp, T., de Leeuw, G., Griesfeller, J., Martynenko, D., Klüser, L., Bevan, S., Davies, W., Ducos, F., Deuzé, J. L., Graigner, R. G., Heckel, A., von Hoyningen-Hüne, W., Kolmonen, P., Litvinov, P., North, P., Poulsen, C. A., Ramon, D., Siddans, R., Sogacheva, L., Tanre, D., Thomas, G. E., Vountas, M., Descloitres, J., Griesfeller, J., Kinne, S., Schulz, M., and Pinnock, S.: Aerosol retrieval experiments in the ESA Aerosol_cci project, Atmos. Meas. Tech., 6, 1919-1957, doi:10.5194/amt-6-1919-2013, 2013.

Kokhanovsky, A. A., Rozanov, V. V., Zege, E. P., Bovensmann, H., and Burrows, J. P.: A semianalytical cloud retrieval algorithm using backscattered radiation in 0.4–2.4 μm spectral region, J. Geophys. Res., 108, 4008, doi:10.1029/2001JD001543, 2003.

Kolmonen, P., L. Sogacheva, T.H. Virtanen, G. de Leeuw and M. Kulmala (2015). The ADV/ASV AATSR aerosol retrieval algorithm: current status and presentation of a full-mission AOD data set. International Journal of Digital Earth. pp. 1-17 | DOI: 10.1080/17538947.2015.1111450 , published on-line 18 Nov 2015.

Kulmala, M., Arola, A., Nieminen, T., Riuttanen, L., Sogacheva, L., de Leeuw, G., Kerminen, V.-M., and Lehtinen, K. E. J.: The first estimates of global nucleation mode aerosol concentrations based on satellite measurements, *Atmos. Chem. Phys.*, 11, 10791-10801, doi:10.5194/acp-11-10791-2011, 2011.

Rodríguez, E., Kolmonen, P., Virtanen, T. H., Sogacheva, L., Sundström, A.-M., and de Leeuw, G.: Indirect estimation of absorption properties for fine aerosol particles using AATSR observations: a case study of wildfires in Russia in 2010, Atmos. Meas. Tech., 8, 3075-3085, doi:10.5194/amt-8-3075-2015, 2015.

Sofiev, M., Vankevich, R., Ermakova, T., and Hakkarainen, J.: Global mapping of maximum emission heights and resulting vertical profiles of wildfire emissions, Atmos. Chem. Phys., 13, 7039-7052, doi:10.5194/acp-13-7039-2013, 2013.

Sogacheva, L., Kolmonen, P., Virtanen, T. H., Rodriguez, E., Sundström, A.-M., and de Leeuw, G.: Determination of land surface reflectance using the AATSR dual-view capability, Atmos. Meas. Tech., 8, 891-906, doi:10.5194/amt-8-891-2015, 2015.

Sogacheva et al. (2016). In preparation for submission

Sundström, A.-M., Arola, A., Kolmonen, P., Xue, Y., de Leeuw, G., and Kulmala, M.: On the use of a satellite remote-sensing-based approach for determining aerosol direct radiative effect over land: a case study over China, Atmos. Chem. Phys., 15, 505-518, doi:10.5194/acp-15-505-2015, 2015.

Sundström, A.-M., Nikandrova, A., Atlaskina, K., Nieminen, T., Vakkari, V., Laakso, L., Beukes, J. P., Arola, A., van Zyl, P. G., Josipovic, M., Venter, A. D., Jaars, K., Pienaar, J. J., Piketh, S., Wiedensohler, A., Chiloane, E. K., de Leeuw, G., and Kulmala, M.: Characterization of satellite-based proxies for estimating nucleation mode particles over South Africa, Atmos. Chem. Phys., 15, 4983-4996, doi:10.5194/acp-15-4983-2015, 2015.

van Donkelaar, A., R.V. Martin, M. Brauer, R. Kahn, R. Levy, C. Verduzco, and P.J. Villeneuve (2010)**.** Global Estimates of Ambient Fine Particulate Matter Concentrations from Satellite-Based Aerosol Optical Depth: Development and Application. *Environ Health Perspect* 118:847–855. doi:10.1289/ehp.0901623.

Veefkind, J.P., G. de Leeuw and P.A. Durkee (1998). Retrieval of aerosol optical depth over land using two-angle view satellite radiometry during TARFOX. Geophys. Res. Letters. 25(16), 3135-3138.

Veefkind, J.P. and de Leeuw, G. (1998). A new algorithm to determine the spectral aerosol optical depth from satellite radiometer measurements. *Journal of Aerosol Sciences,* **29**, 1237-1248.

Xu, J.-W., Martin, R. V., van Donkelaar, A., Kim, J., Choi, M., Zhang, Q., Geng, G., Liu, Y., Ma, Z., Huang, L., Wang, Y., Chen, H., Che, H., Lin, P., and Lin, N.: Estimating ground-level $PM_{2.5}$ in eastern China using aerosol optical depth determined from the GOCI satellite instrument, Atmos. Chem. Phys., 15, 13133-13144, doi:10.5194/acp-15-13133-2015, 2015

OZONE IN THE WESTERN YANGTZE RIVER DELTA OF CHINA: A SYNTHESIS STUDY BASED ON GROUND, AIRCRAFT AND SOUNDING MEASUREMENT, 2011-2015

A.J. DING[1], W. NIE[1], X. HUANG[1], X.G. CHI[1], Z. XU[1], V. THOURET[2], P. NEDELEC[2], L.F. ZHENG[1], Z.N. XU[1], Y.N. XIE[1], Y.C. SHEN[1], X.M. QI[1], J.P. WANG[1], K. DING[1], J.N. SUN[1], T. PETAJA[3], V.-M. KERMINEN[3], M. KULMALA[3], C.B. FU[1]

[1]International Joint Research Laboratory of Atmospheric and Earth System Science & School of Atmospheric Sciences, Nanjing University, Nanjing 210023, China

[2]Laboratoire d'Aerologie, UMR 5560, Université Paul Sabatier, Toulouse, France

[3]Department of Physics, University of Helsinki, 00014 Helsinki, Finland

Keywords: TROPOSPHERIC OZONE, PHOTOCHEMISTRY, REGIONAL TRANSPORT

INTRODUCTION

Ozone (O_3) is one of the most important secondary pollutants and greenhouse gases. Increasing trend of surface or tropospheric O_3 has been reported in development regions in eastern China (Ding et al., 2008; Xu et al., 2008; Wang et al., 2009), together with a fast increase of O_3 precursors like NO_x (Richter et al., 2005; Itahashi et al., 2014). However, there is limit knowledge of temporal variations and their courses in the downwind region of fast-developed urban city clusters, such as the Yangtze River Delta (YRD). In this study, we present a synthesis analysis of ozone in the western YRD region of China based on ground-based and tagged balloon sounding measurements at the SORPES station (Ding et al., 2013a) and IAGOS aircraft measurement (Petzold et al., 2015) during 2011-2015.

METHODS

The ground and tagged balloon sounding measurements of O_3 was conducted at the Station for Observing Regional Processes of the Earth System (SORPES), in Nanjing in the western YRD of eastern China. The station is located on the Xianlin Campus of Nanjing University in the suburban area northeast of Nanjing (118°57'10'' E, 32°07'14'' N), about 20 km from the downtown area. Under the condition of prevailing winds from northeast and southeast, the site is generally downwind of the most developed mid-YRD regions including the megacity Shanghai and the Suzhou–Wuxi–Changzhou city cluster. Therefore, the measurements at the station can help address impacts from these areas of highly intensive human activity in a regional air quality perspective.

Ground based measurements of ozone and its precursors at the SORPES station began in the summer of 2011. Most of the instruments are housed on the top floor of a laboratory building, which sits on the top of a hill about 40m above the ground level. Ozone was measured using online analyzer TEI 49i (Thermo Instruments) at a resolution of 1 min. The instrument precision was ±2 ppbv for O_3.Tagged balloon observations were mainly conducted at the SORPES station in spring of 2014 and 2015. The 2B POM instrument was used for ozone sounding. The balloon measurements were conducted every 3-hour for selected days to characterize the diurnal variations of ozone and relevant parameters. The sounding altitudes mainly from ground surface to about 1200 m. Aircraft measurements of O_3 and carbon monoxide (CO) were made by IAGOS in-service airline (Frankfut-Nanjing) on-board instruments (Ding et al., 2008; Petzold, et al. 2015). Since 2011-2014, over 200 vertical profiles of O_3 and CO were measured above Nanjing international airport, which is about 50 km south to the SORPES station.

To understand the general transport characteristics of air masses, we conducted backward particle simulations using a Lagrangian dispersion model Hybrid Single-Particle Lagrangian Integrated Trajectory (HYSPLIT) (Draxler and Hess, 1998) based a method developed by Ding et al. (2013b). For each study point, the model was run 7-day backwardly with 3000 particles released. The spatiotemporal distributions of these particles were used to further calculate the source–receptor relationship.

CONCLUSIONS

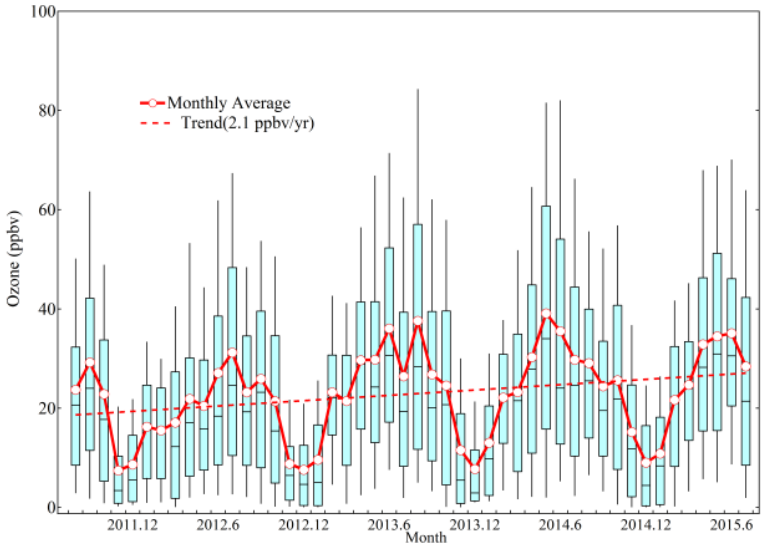

Figure 1. Time series of ozone observed at the SORPES station in Nanjing, 2011-2015.

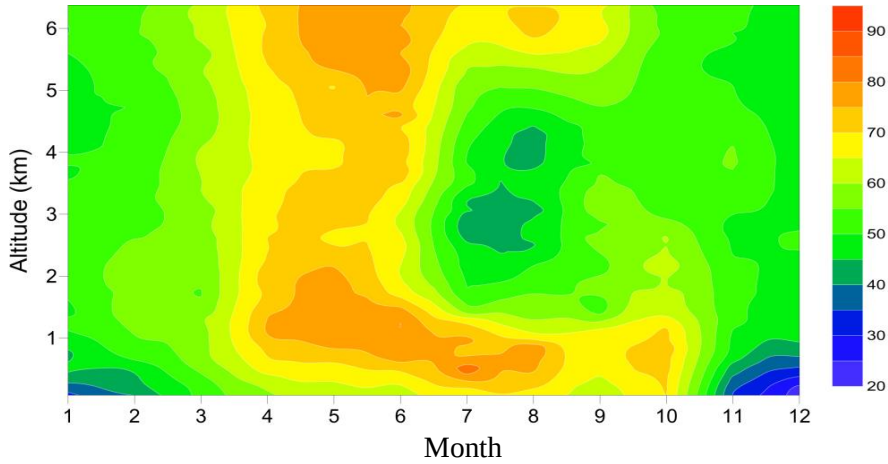

Figure 2. Averaged vertical profiles of O_3 as a function of month of a year.

Ground based measurements at the SORPES station show a positive trend of ozone (about 2.1 ppbv per year) and an increased frequency of ozone episodes in Nanjing during 2011-2015 (Figure 1). A springtime ozone maximum was observed in free troposphere and a summer maximum in boundary layer (Figure 2). High concentration of O_3 was observed in upper boundary layer, which was mainly due to sub-regional transport from the city cluster in the YRD region and also influenced by the regional transport from the biogenic emission from the South China.

ACKNOWLEDGEMENTS

The work was supported by NSFC (D0512/41422504; D0512/91544231) and Jiangsu Provincial Science Fund (No. BK20140021). The IAGOS aircraft data, which was supported by the European Commission, Airbus, and the Airlines (Lufthansa etc.), were provided by IAGOS central database hosted by ETHER (CNES-CNRS/INSU).

REFERENCES

Ding, A.J., T. Wang, V. Thouret, J.-P. Cammas, and P. Nédélec (2008). Tropospheric ozone climatology over Beijing: analysis of aircraft data from the MOZAIC program, *Atmos. Chem. Phys.* **8**, 1-13.

Ding, A.J. *et al.*(2013a), Ozone and fine particle in the western Yangtze River Delta: an overview of 1 yr data at the SORPES station, *Atmos. Chem. Phys.* **13**,11, 5813-5830.

Ding, A.J., T. Wang, C.B. Fu (2013b). Transport characteristics and origins of carbon monoxide and ozone in Hong Kong, South China. *J. Geophys. Res.* **118,** DOI: 10.1002/jgrd.50714.

Itahashi, S., I. Uno, H. Irie, J.-I. Kurokawa, and T. Ohara (2014). Regional modeling of tropospheric NO2 vertical column density over East Asia during the period 2000–2010: comparison with multisatellite observations. *Atmos. Chem. Phys.* **14**, 3623-3635, doi:10.5194/acp-14-3623-2014.

Petzold, A. et al. (2005). Global-scale atmosphere monitoring by in-service aircraft – current achivements and future prospects of the European Research Infrastructure IAGOS. *Tellus B* **67**, 28452, doi:10.3402/tellusb.v67.28452.

Richter, A., J.P. Burrows, H. Nüß, C. Granier, U. Niemeier (2005). Increase in tropospheric nitrogen dioxide over China observed from space. *Nature* **437**, 129-132, doi:10.1038/nature04092.

Xu, X., W. Lin, T. Wang, P. Yan, J. Tang, Z. Meng, and Y. Wang (2008). Long-term trend of surface ozone at a regional background station in eastern China 1991–2006: enhanced variability. *Atmos. Chem. Phys.* **8**, 2595-2607, doi:10.5194/acp-8-2595-2008.

Wang, T., X.L. Wei, A.J. Ding, C.N. Poon, K.S. Lam, Y.S. Li, L.Y. Chan, and M. Anson (2009).Increasing surface ozone concentrations in the background atmosphere of Southern China, 1994-2009. *Atmos. Chem. Phys.* **9**, 6217-6227, 2009.

MODELLING OF HYDROLOGICAL RESPONSES TO CLIMATE-INDUCED CHANGES IN A SEMI-ARID WATERSHED

C.DONMEZ, S.BERBEROGLU

Department of Landscape Architecture, Faculty of Agriculture, University of Cukurova, Adana, 01330, Turkey.

Keywords: PROCESS-BASED MODELLING, REMOTE SENSING, HYDROLOGY, WATERSHED, MEDITERRANEAN.

INTRODUCTION

The impact of climate change on water resources is a global concern and likely to have serious impacts on water cycle in arid and semi-arid basins. Projected climate change may affect future freshwater availability, supply and demand through changes in the timing of snowmelt, reduced river flows and irregular precipitation trends (Barnett et al., 2008; Gober and Kirkwood, 2010). Particularly Changes in precipitation directly affect snow accumulation and runoff volume. Temperature changes mostly affect runoff timing since it may include a reduction in snowpack volume and an earlier onset of melt (Barnett et al., 2005). These alterations of the hydrological cycle in Mediterranean regions could have major implications, such as regional water shortages and irregular water supplies where built storage capacity is inadequate to cope with seasonal shifts in streamflow.

Due to the importance of water cycle for the eco-system and human welfare, the impacts of global climate changes on hydrological processes on various scales have been investigated by many research studies. Different hydrological models are commonly used in these studies to estimate past and current hydrological dynamics such as runoff, ground water and snow dynamics. Projections of climatic variables globally can be performed with General Circulations Models (GCMs), which, are currently the most effective tools for simulating the response of the global climate system to the greenhouse gases and to provide estimates of climate variables (e.g. air temperature, precipitation, wind speed, etc.). However, modelling the future predictions of hydrological dynamics using hydrological models is still a research question. In this regard, in cooperation of the hydrological models and future climate variables deriving from the GCMs may provide a remarkable approach to estimate possible changes of regional hydrological cycles in refer to the expected climate changes.

The overall objective of the study is to present application of a process-based hydrological model to simulate the effects of climate changes on the hydrologic response of Seyhan Watershed in Turkey. The research focuses on the simulation of climate-induced hydrologic changes particularly in runoff generation between a baseline (2000-2010) and a future (2070–2080) period, building on the analysis of GCM outputs. The future climate projections are based on the following four Representative Concentration Pathways (RCPs -2.6) scenarios defined in 5th Assessment Report of The Intergovernmental Panel on Climate Change (IPCC). The present and future hydrological dynamics of the study area will be estimated using hydrological model J2000 in cooperation with GCMs data.

Study Area

The Upper- Seyhan Basin (Figure 1) in the Eastern Mediterranean Region of Turkey selected for this project has a very high local environmental quality and sensitivity in respect to water resources. The basin covers an area of approximately 19 000 km2. The elevation ranges from 200 m to 3700 m. This area is known as one of the most important agricultural areas in Turkey (about 10% of the total irrigated agricultural production). Therefore, possible water scarcity and its management are very important problem for the future of agricultural production, food security of Turkey and biodiversity for the basin.

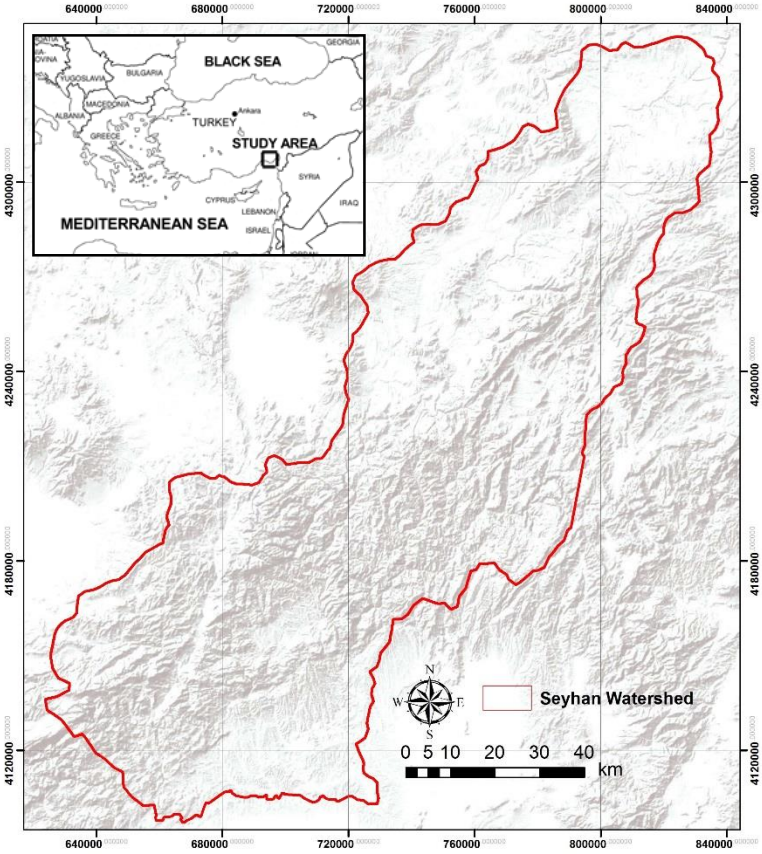

Figure 1. Location of the Seyhan Watershed, Turkey.

At present, the area is undergoing a rapid development with consequent impacts including seepage of waste water and irrigation return flow, land reclamation, degradation and loss of forest by accelerated erosion and fire, salinization of freshwater resources and soil, pesticides, and related industrial activities, exploitation for tourism and recreation. As a result of these impacts, the water quality of the Seyhan River is reducing, but has not yet reached a level at which mitigating actions would be effective. The water potential in USB depends on the hydrological cycle is which considered to be a continuous circulation of water from water vapour to precipitation, stream flow, lakes, reservoirs, snow melt runoff, soil moisture, groundwater, and out of basin transfer, to the return to water vapour through evaporation and transportation.

METHODS

The methodology of the study combines process-oriented hydrological modelling approach with information obtained by remote sensing, GCMs and in-situ data. It comprises six main steps: i) Data Acquisition and Pre-Processing, ii) Remote Sensing and GIS Analysis, iii) Deriving future climate data, iv) Watershed System Analysis and Regionalization, v) Modelling and mapping present and future hydrological dynamics, vi) Evaluation of the modelling results.

The quantification process of the hydrological dynamics will be based on time series of temperature, precipitation, wind speed and humidity along with spatial data including topography, land cover/use, soils and geology. The hydrological quantities will be estimated for recent and future conditions to provide a basis for the analysis of the potential long-term impact resulting from projected climate changes.

The J2000 will be used in this study to model the hydrological dynamics. It is a spatially distributed conceptual hydrological model (Krause, 2001, 2002). The concept of the J2000 model is given in Figure 2.

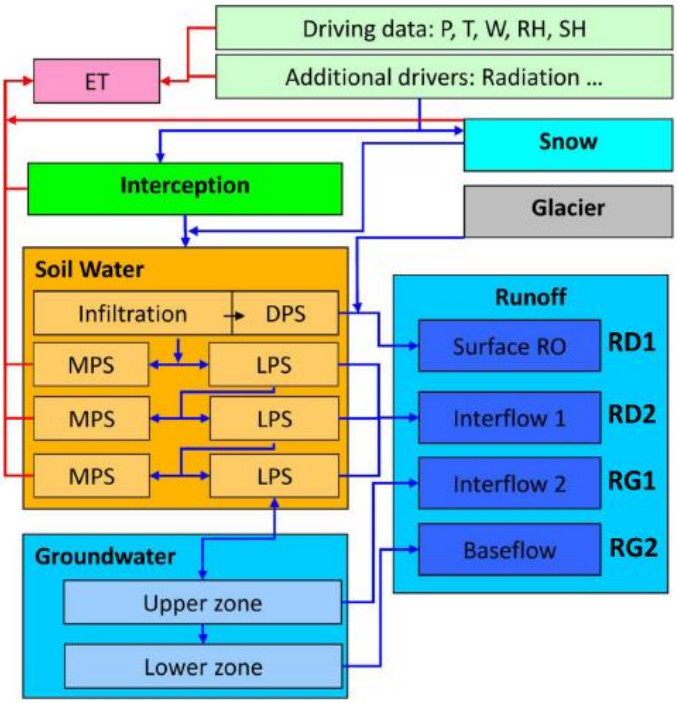

Figure 2. Principal layout of the J2000 model concept (Krause et al., 2009)

The J2000 is a modular process-oriented hydrological system, which implements single hydrological processes as encapsulated process modules. Different modules including interception, soil-water, snow, groundwater can be used depending upon the availability of the data for the simulation of runoff generations (Nepal, 2012).

The model will be run for the baseline and future periods using time series data spatial information within the study. For these periods, spatially distributed long-term estimates of the seasonal distribution of the hydrological quantities such as actual evapotranspiration, runoff generation, and groundwater recharge will be provided.

REFERENCES

Barnett, T.P., J.C., Adam, D.P. Lettenmaier (2005). Potential impacts of a warming climate on water availability in snow-dominated regions. *Nature* 438 (7066), 303–309.

Barnett T.P., D.W. Pierce, H.G. Hidalgo, C. Bonfils, B.D. Santer, T. Das, G. Bala, A.W. Wood, T. Nozawa A.A. Mirin, D.R. Cayan, M.D. Dettinger (2008). Human-induced changes in the hydrology of the Western United States. *Science* 319:1080–1083.

Gober P, C.W. Kirkwood (2010). Vulnerability assessment of climate-induced water shortage in Phoenix. *PNAS*. 107:21295–21299.

Krause, P., (2001). Das hydrologische Modellsystem J2000: Beschreibung und Anwendung in groen Flueinzugsgebieten, Schriften des Forschungszentrum Jülich. Reihe Umwelt/Environment; Band 29.

Krause, P., (2002). Quantifying the Impact of Land Use Changes on the Water Balance of Large Catchments using the J2000 Model. *Physics and Chemistry of the Earth* 27, 663–673.

Krause, P., U. Bende-Michl., M. Fink, J. Helmschrot, S. Kralisch, A. Kuenne, (2009). Parameter sensitivity analysis of the JAMS/J2000-S model to improve water and nutrient transport process simulation - a case study for the Duck catchment in Tasmania, 18th World IMACS / MODSIM Congress, Cairns, Australia 13-17 July 2009. pp. 1727–1732.

Nepal S., (2012). Evaluating Upstream-Downstream Linkages of Hydrological Dynamics in the Himalayan Region. PhD Dissertation submitted to Faculty of Chemical and Earth Sciences of the Friedrich-Schiller-University Jena, p.262.

DEVELOPMENT OF AN ICE NUCLEATION CHAMBER TO STUDY ICE ABILITIES OF PARTICLES FROM NOTHERN EURASIA

J. DUPLISSY[1], Q. NGUYEN[2], E.S. THOMSON[3], L. AHONEN[4], M. KULMALA[4], T. PETÄJÄ[4], M. SIPILÄ[4], M. BILDE[2] AND E. SWIETLICKI[5]

[1]Helsinki Institute of Physics, University of Helsinki, 00014, Helsinki, Finland
[2]Department of Chemistry and iNANO, Aarhus University, 8000 Aarhus, Denmark
[3]Department of Chemistry and Molecular Biology, Atmospheric Science, University of Gothenburg, 41296, Gothenburg, Sweden
[4]Department of Physics, University of Helsinki, 00014 Helsinki, Finland
[5]Department of Physics, Lund University, Box 118, 222 11 Lund, Sweden

Keywords: ICE NUCLEI CHAMBER, PINC, ZINC, ICE NUCLEI, CRAICC

INTRODUCTION

The importance of ice crystals in clouds for our climate is manifold: Their presence, number and shape influences the optical properties of clouds, the formation of precipitation and their lifetime. All of these aspects have an impact on the radiation balance and therefore on climate. Within the CRAICC project (Cryosphere-atmosphere interactions in a changing Arctic climate) we aim to investigate the ice nuclei properties of aerosols present in the artic region by continuous measurements at different Nordic field stations.

METHODS

Two new ice nucleation chambers have been built based on the concept of the laboratory instrument ZINC (Zurich Ice Nucleation Chamber) and PINC (Portable Ice Nucleation Chamber), both being developed at ETHZ, Switzerland. The field instrument PINC has already successfully participated in a couple of laboratory campaigns (Chou et al, 2013; Kanji et al, 2013; Wex et al, 2014; Hiranuma et al, 2014) as well in field campaign (Chou et al, 2011). Our improved PINC has two portable refrigerant compressors to directly cool the walls of the chamber without the use of an intermediate cooling liquid. In this configuration, the instrument is able to measure ambient ice nuclei (IN) concentrations at conditions as cold as -40°C and relative humidities exceeding water saturation. Our improved PINC has a longer ice nucleation chamber (1 meter) similar to the ZINC.

CONCLUSIONS

A successful collaboration between ETHZ and the CRAICC partners has led to technology transfer for the manufacture of the two Ice Nucleation Chambers. An inter-comparison prior to their first campaign is scheduled in autumn 2016. The status of the ice chambers, their operational field modes as well as their improvement will be presented during this meeting.

Figure 1. The 1 m long ice nucleation chamber close to the refrigeration unit is installed in a transportable rack for field measurement.

ACKNOWLEDGEMENTS

This work was supported by CRAICC, the Finnish Center of Excellence and the Swedish Research Councils

REFERENCES

Chou et al. (2011), Atmos. Chem. Phys., 11, 725-4738
Chou et al. (2013), Atmos. Chem. Phys., 13,761-772
Kanji et al. (2013), Atmos. Chem. Phys., 13, 9097-9118
Wex et al. (2014), Atmos. Chem. Phys. Disc., 14, 22321–22384
Hiranuma et al. (2014), Atmos. Chem. Phys. Disc., 14, 22045–22116

EVALUATION OF THE VEGETATION STRUCTURE AND ABOVEGROUND NET PRODUCTION OF WETLAND ECOSYSTEMS USING SATELLITE DATA

E.A. DYUKAREV[1], M.N. ALEKSEEVA[2] and E.A. GOLOVATSKAYA[1]

[1]Institute of Monitoring of Climatic and Ecological Systems SB RAS, Tomsk, Russia

[2]Institute of Petroleum Chemistry SB RAS, Tomsk, Russia.

Keywords: PEATLANDS, VEGETATION PRODUCTION, SPACE IMAGES.

INTRODUCTION

The use of satellite images for a comprehensive study of natural objects, including the assessment of the wetlands conditions and rate of peat accumulation is relevant in the study of remote areas of wetlands in Western Siberia. Structure of bog complexes well reflected at satellite images due to its indicator specific texture and color of bog landscapes. Satellite images allow to evaluate current state and disturbances in wetland ecosystems. Satellite observations in combination with ground vegetation surveys can be used for estimation of vegetation production and study of climate-vegetation-carbon cycle feedbacks at high latitudes.

STUDY AREA

The study area is located in the south-west part of Western Siberia in two different bioclimatic zones including South Taiga and Sub-Taiga zones. This territory is drained Chaya River and its feeders: Iksa, Bakchar, Teterenka, Andarma and Parbig rivers. Elevation varies from 110 to 130 m a.s.l. Watersheds are occupied by bogs. Bog massifs formation started 4.5–5 thousand years ago and since that time the peat deposits cover the initial relief roughness. Watershed bogs have peat depth about 3-4 m. The continuous cover of both coniferous and broad-leaved species are dominated at the well and low drained territories

VEGETATION COVER MAPPING

The Landsat 7 (ETM+) and Landsat 5 (TM) data obtained via the Global Visualization Viewer (GloVis) web interface (http://glovis.usgs.gov/) were used for analysis of vegetation structure. Each image consisted of six spectral reflective bands, thermal band and a panchromatic band. Six spectral bands were used in processing. The study area is covered by satellite images obtained for path 150 row 20 in Worldwide Reference System-2 (WRS-2) of path and row coordinates at 13 July2007.
A number of datasets, including aerial photos from GoogleEarth™, expert information on the landscape types, fieldwork data (stationary and track observations, botanical descriptions, landscape-typological maps) were used as reference materials to select training points. The legend for vegetation mapping was developed for the study area (Alekseeva *et al* 2015). The legend describes vegetated land as being occupied by forests (dark coniferous, deciduous and mixed), watershed wooded bogs (tall/low/drained ryams and hollow-ryam complexes), watershed open bogs (ridge-hollow complexes and various fens), mesotrophic and eutrophic wetlands at river terraces (swamp, birch-herb-hypnum peatland etc.) and other lands (fields, meadows, croplands, settlements, water objects).

NORMALIZED DIFFERENCE VEGETATION INDEX

Normalized Difference Vegetation Index (NDVI) was used for comparison of ground observations of bog vegetation production and satellite data. NDVI is one of the most successful of many attempts to simply and quickly identify vegetated areas and their condition, and it remains the most well-known and used

index to detect live green plant canopies in multispectral remote sensing data. NDVI maps were obtained from MODIS product MOD13Q1 for each month of vegetation period (May-September) for 2000-2011. We calculate average NDVI values for each wetland vegetation class from the study area. Maximal NDVI observes in June-July depending on the vegetation type. Minimal NDVI finds in September at eutrophic open wetlands. Oligotrophic bogs have moderate NDVI values in mid-summer and autumn.

GROUND SURVEYS OF VEGETATION PRODUCTION

Ground studies of net primary production (NPP) of oligotrophic and eutrophic peatlands have been conducted at field station "Vasjuganie" at the Bakcharskoe bog in 2000-2011. The studied ecosystems includes: pine– shrub–sphagnum community (tall ryam), a similar community with low pine trees (low ryam), sedge–sphagnum fen, ridge-hollow complex and two observation point at eutrophic wetland. A detailed description of the vegetation at the studied plant communities is presented in (Golovatskaya, 2009).

The aboveground biomass was measured by clipping 0.25 m^2 quadrates (three to five per site). Clipped plants were divided into living and dead biomass. The total dead biomass consists of litter and dead parts of mosses. Live biomass consists of annual, and perennial photosynthetic biomass (shrub leaves, green parts of herbs and mosses), and nonphotosynthetic biomass (steam shrubs, roots of herbs and shrubs). Below the surface (below moss capitulums) some amount of green parts of mosses exists. We consider these parts belonging to living biomass. Depending on the ecosystem the "green moss layer" varies from 2-3 cm to 15 cm. A layer with 20-cm thickness, located deeper the green mosses, was considered to be related to dead part of mosses. Samples were oven-dried at 80 ^{o}C till the constant weight. Seasonal dynamics growth was established by weighing the green parts of plants and mosses of the current year. The amount of total biomass was determined at the period of maximum vegetation development (in the end of July – the beginning of August). Litter, above and belowground biomass was determined each month from May till October at each mire site.

Aboveground production (ANP) of herbs was taken as equal to maximal storage of green phytomass of herbs. The production of deciduous shrubs was calculated as a sum of the seasonal maximum of green leaves and young shoots of the current year, production of evergreen shrubs - sum of the maximal phytomass of the current shoots and their leaves. We estimate the production of sphagnum mosses as a difference between seasonal maximum and minimum of green phytomass. ANP was calculated as a sum of production of herbs, shrubs and mosses. Ground observations at six "base" wetland ecosystems were interpolated to other ecosystems using botanical surveys, micro relief structure and data on projective cover of herbs, shrubs and mosses.

Average ANP value varies from 198 to 369 $gC/m^2/yr$ for oligotrophic and from 266 to 511 $gC/m^2/yr$ for eutrophic wetlands depending on the vegetation structure. Oligotrophic bogs have similar values of ANP, because high part in production contributes sphagnum mosses (45-60%). Eutrophic wetlands with sporadic moss cover have low contribution of mosses (20-25%), but part of herbs and shrubs in ANP rises to 20-60%.

CORRELATION NDVI AND VEGETATION PRODUCTION

Correlation analysis of annual NDVI and ANP shows existence of two types of relations (See table 1). Aboveground net production increases with NDVI rise for wooded bogs (classes 4-8). Pearson correlation coefficient is significant and varies from 0.45 to 0.83. Rate of ANP rise is 28-50 $gC/m^2/yr$ for each 0.01 NDVI. Relation between ANP and NDVI is negative for complex (classes 10-12) and open oligotrophic wetlands. Reduce of ANP with increasing NDVI can be explained by a large contribution of herbs in the total production Aboveground parts of herbs have high NDVI only in mid-summer. In autumn they become brown and NDVI significantly decreases and therefore annual NDVI with high herb ANP would be low.Correlation coefficient for these ecosystem varies from – 0.41 to – 0.61. Reducing of ANP at NDVI increase at ridge-hollow complexes is higher (17-33 $gC/m^2/yr$ per 0.01 NDVI), than at open fens (6-8 $gC/m^2/yr$ per 0.01 NDVI). Similar relation observes at eutrophic and mesotrophic wetlands at river terraces (classes 17-21), but correlation and regression coefficients variability is higher. The last column in

Table 1 shows average module of difference between ground measurements of ANP and modeled ANP using NDVI data.

n	Vegetation class	R	mANP	erANP
4	Tall ryam	0.63	343.7	45.6
5	Medium ryam drained	0.83	338.7	49.7
6	Low ryam drained	0.59	231.9	73.9
7	Low ryam	0.45	317.7	55.5
8	Small-hollow-ryam complex	0.61	284.8	68.5
9	Medium-hollow-ryam complex	0.46	239.7	49.4
10	Ridge-small-hollow complex	-0.48	368.9	79.0
11	Ridge-medium-hollow complex	-0.53	301.2	62.1
12	Ridge-large-hollow complex	-0.48	262.2	39.5
13	Scheuchzeria-Sphagnum fen	-0.61	236.0	24.9
14	Sedge-Sphagnum fen	-0.51	265.3	19.3
15	Sphagnum floating fen	-0.41	197.6	22.7
17	Bog pine forest	-0.50	266.4	41.6
18	Swamp forest	-0.43	289.0	46.2
19	Pine-herb-moss wetland	-0.34	315.3	46.5
20	Birch-herb-hypnum wetland	-0.65	371.9	59.4
21	Dwarf birch-sedge-hypnum wetland	-0.42	511.1	76.2

Table 1. Aboveground vegetation production for wetland ecosystems calculated using NDVI (mANP, $gC/m^2/yr$), R – correlation coefficient for ground data on ANP and NDVI, erANP – average module of estimation error ($gC/m^2/yr$).

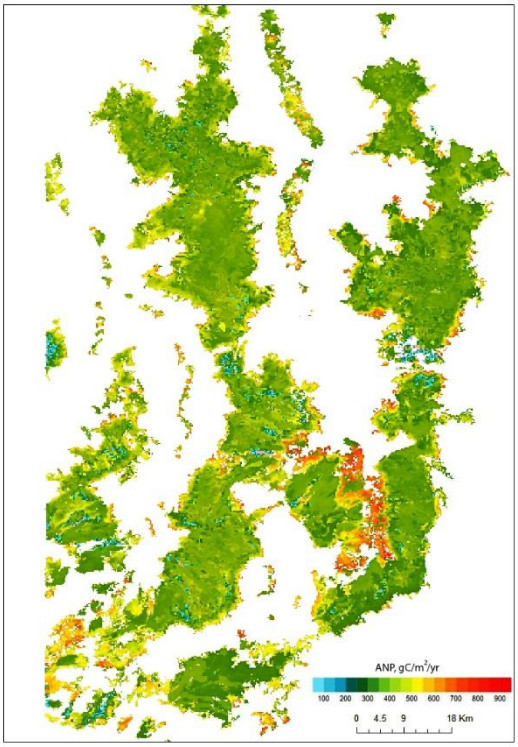

Figure 1. Map of average (2000-2011) aboveground vegetation production for wetland ecosystems.

Using obtained relations between NDVI and ANP for each wetland ecosystem we reconstruct spatial distribution of ANP for wetlands of the study area (Fig. 1). Minimal values ANP observed in the central parts of watershed bogs at floated fens surrounding bog lakes. Most of the oligotrophic bogs have similar values of ANP about 200-400 $gC/m^2/yr$. Aboveground net primary production raises at moving to the edge of bog massif up to 700 $gC/m^2/yr$. Maximal ANP is typical for eutrophic wetlands, periphery of oligotrophic bogs an drained areas.

CONCLUSIONS

The total area of wetlands at the study site is 545 200 ha. The average wetlands fraction is about 37%. Average aboveground net primary production for all wetland ecosystems estimated using satellite derived NDVI and ground ANP measurements is 302 $gC/m^2/yr$. It results in accumulation of 1.64 MT of carbon in aboveground vegetation of wetlands at the study area.

ACKNOWLEDGEMENTS

This work was supported by the Russian Foundation for Basic Research under grant 13-05-98048_r_sib_a.

REFERENCES

Alekseeva M.N., Preis Yu.I., Dyukarev E.A. (2015) Spatial structure of vegetation cover and top layer of peat of northeastern spurs of the Great Vasyugan mire by remote and ground data, *Bull. of the Tomsk Politech. Univ.*, **4**, 81-90.

Golovatskaya, E.A. (2009) Biological productivity of oligotrophic and eutrophic wetlands at South Taiga zone of West Siberia, *J. of Siberian Federal Univ. Biology* **3,** 38–53.

SURFACE URBAN HEAT ISLANDS IN NORTHERN CITIES

I. ESAU, V. MILES, A. KURCHATOVA

Surface air temperatures in the Northern Hemisphere and specifically in Northern Eurasia are rapidly raising during the last three decades. This study reveals that the urban temperatures in the Northern Siberia are raising even faster. The urban climates, as measured by the surface temperature difference between the city core and the surrounding natural environment, correspond to the climate zone, which could be found 4 to 6 degrees south. These temperature differences are known as surface urban heat islands (SUHIs). We calculated SUHIs for 28 northern cities in Siberia with population ranging from a few thousands to as much as 300.000 inhabitants. The temperatures were obtained from the MODIS LST 1 km resolution product covering 2000-2014. We found that the regional SUHIs nearly linear scale with the city population size, which suggest that the anthropogenic impact on the surface heat balance is the strongest control factor. However, local spatial heterogeneities and seasonal spatial shifts of the heat islands indicate that the SUHIs are rather controlled by the differences in the surface albedo and the thermos(cryo)dynamic soil properties than by the direct anthropogenic heat emission.

EURASIAN GREAT LAKES: DIAGNOSIS AND PREDICTION OF WATER LEVEL FLUCTIUATIONS UNDER CLIMATE CHANGES AND ANTROPOGENIC IMPACTS

NIKOLAI FILATOV[1], N.DIANSKY[3], R. IBRAEV[3], T.VIRIUCHALKINA[2]

[1] Northern water problems institute Karelian Research center RAS, Petrozavodsk,

[2] Water Problems Institute RAS, Moscow,

[3] Institute of Numerical mathematic RAS, Moscow
nfilatov@rambler.ru

Russia has more than 2.7 million lakes, among them such as Lakes Baikal, Ladoga, Onego and Caspian Sea-Lake (situated partly on the Russian territory). The features of the intrasecular changes in the water level of the largest lakes of Eurasia Russia are jointly considered for the first time on the basis of the long-term (more them 100 years) data of observations.

Data analysis long term observations of water level fluctuations showed that response of the hydrological regime and water level on climate warming differs significantly. It depended from regional features, type of the watershed and anthropogenic factors. Forecast of water level fluctuations of Great lakes of Eurasia is important for planning the economic activity in the regions of Lake Baikal, Caspian Sea-Lake and Ladoga and Onego.

ACKNOWLEDGEMENTS

This work is based on support of Russian Science Foundation № № 14-17-00740 and PEEX project.

ADAPTIBILITY INDIGENOUS ARCTIC POPULATION BY "URBAN HEAT ISLAND"

T.A. FISHER[1], S.A. PETROV[1], O.V. FROLOVA[2], M.V, NARUSHKO[1]

[1] Tyumen Scientific Center of the Siberian Branch of the Russian Academy of Sciences, Tyumen, Russia
[2]Department of anatomy and physiology of humans and animals, Tyumen State University, Tyumen, Russia

Keywords: ethnic group "Forest Nenets', adaptability, the psyche, the immune system.

INTRODUCTION

Ethnic groups Northern indigenous peoples (NIP) is a unique social phenomenon. In spite of the extreme climate conditions, the interference of industrial civilization, the environmental consequences of scientific and technological progress, they continue to maintain a traditional lifestyle. NIP shows to modern society a high level of adaptability to rapidly changing conditions. Adaptivity is the level of congenital and acquired psychophysiological human capabilities provide the ability to adapt (Garbuzov, 1999). A special role in maintaining the life support system in all conditions of existence performs the psyche and the immune system (Sukhovey, Dotsenko, 2012; Daruna, 2012). Adaptivity is most often seen in extreme conditions, in all kinds of trials in a competitive relationship in resistance to stress. The ability to maximally realize its claims, it is important for the ethnic communities in the contemporary world. That ethnic group in the current global climate change process (Petrov, Mamaeva 2014; Vikulin, 2015; Charles, 2012) and environmental degradation (Korchina et al., 2012), are at risk until the threat of extinction. The Arctic is being actively developed. Construction of new industrial complexes in the oil, chemical and other industries, expand towns and villages, which leads to the development of social infrastructure. All this affects the change of anthropogenic transformations of the earth's surface, resulting in higher temperatures in urban centers, compared with the surrounding natural landscape (Myaghkov, 2007; Hebbert et al., 2010; Rizka, Henze, 2010). In this phenomenon, attention was drawn even 1810's. He was named *urban heat island* (UHI) (Howard, 1818). It was found that in the cities of Barrow and Fairbanks (Alaska) with a population of 35 thousands man with traditional low-rise buildings in the winter months, temperatures average more than 1 ° C higher than outside the city. It has been suggested that the duration of heat pollution leads to local ecosystems to adapt to warmer environmental conditions (Magee et al., 1999). Thus, the study of the phenomenon of adaptation to climate warming in urban areas is becoming increasingly important. NIP enjoys the benefits of civilization, to radically change their way of life. Therefore, evaluation of the quality of their lives, their psychophysiological state is a priority area. The ethnic populations of the tundra are educated at first in system of boarding schools, then in the large cities and almost don’t back to the tundra. They remain in the city or township urban centers UHI.
This imposes extremely high demands on the adaptive capabilities of the organism, where the main burden presented to the psyche and the immune system. They provide adequate adaptive response of the body to maintain life-support systems in conditions of macro and microcosm.

The purpose of research - to evaluate the adaptability (conjugated psychological and immune regulation) Northern indigenous peoples to UHI.

METHODS

The study was conducted in the village Kharampur and nomad camp "Chebache" of Purovsky district YaNAO. In to the landscape relation they are in the subzone of the forest-tundra on the surface of the right bank of floodplain terraces of the river Kharampur. Kharampur village is divided into the inner territorial units: residential and administrative buildings, a boarding school (one- and two-storey buildings), industrial area and so on. There is a network of water communications, sewerage and heating networks,

asphalt and concrete coatings. The nomad camp "Chebache" has a chooms and small houses of inhabitants in the tundra are 2-3 km from each other in a radius of 10 km. The temperature in the village Kharampur and nomad camp "Chebache" was measured in six months (from June to December), two autonomous temperature digital stations located in specially equipped shaded, louvered booths with accuracy 0,05ºC. One station has been installed in an open area in the nomad camp "Chebache." The distance from the buildings - 250 m, height from the ground - 2 m. The second platform is equipped in the center of the village Kharampur. The distance from the building - 500 m, height from the ground - 2 m.
The first group of NIP is totaled 36 people of forest Nenets, living in the tundra. They are engaged in fishing and housekeeping (natural existence). The age of this group was 41,48 ± 1,85 years. The second group is made up NIP of 39 forest Nenets, long-living and working in the village (urban conditions of existence). The age of this group - 36,25 ± 1,98. To study the psychological characteristics was used the method of "Study of anxiety" in Ch.D. Spielberg. Estimated the self-rating level of situational and personal anxiety. Questionnaire Bass-Darky examined expression of the essential forms of aggression (the index of aggression and hostility index). To study the immune status of blood sampling was carried out. All subjects signed a consent form. Consent forms and the research plan were approved by the Ethics Commission on the basis of federal law under Articles 18,20,21,22, 28 and 41 of the RF Constitution and Articles 18-22 of 21.11.2003 of №323 «On the basis of the health of citizens of the Russian Federation". The functional activity of T-cellular link of immunity was assessed by the level of serum repertory cytokines IL-4 and IFN-γ by the method of enzyme immunoassay (EIA). Statistical analysis of the material held on the IBM / PC using standard statistical packages «SPSS 11,5 for Windows» (parametric comparison of the t-test, Pearson correlation analysis).

CONCLUSIONS

It was found that in December, when the measurements were carried out of the psychological and immune parameters, the temperature in the village Kharampur was 27,89 ± 1,29 ° C, in the nomad camp "Chebache» - 29,08 ± 1,35 ° C. The difference in air temperature in the settlements was 1,2 ° C. Consequently, this gives grounds Kharampur village considered "heat island". It was found that the level of situational (46,9 ± 0,9) and trait anxiety (48,4 ± 0,62) among residents of the tundra (Group 1) - high. At Forest Nenets (group 2) the level of anxiety - medium. So, situational anxiety in them was 43,55 ± 0,88 ($p < 0.05$), and personal -43,88 ± 1,78 ($p < 0.01$). The index of aggressiveness (17,2 ± 2,25) in the first group does not exceed the the norm (21,0 ± 4,0), and the second group there was a slight decrease (16,77 ± 1,69). The index of hostility towards the established norm is significantly reduced ($p < 0.01$) in the first group was 8,6 ± 1,33, in the second - 10,68 ± 1,67.

Thus, the high level of anxiety among people living in the tundra, may be associated with the expectation of "unfavorable development of events" in the future (Petrovsky, Yaroshevskii, 2003). Whereas, NIP people, living in the village corresponds to the average level of anxiety. Perhaps this is due to the fact that in the urban centers of social wellbeing level is high enough in relation to the conditions of tundra and stable. This is reflected in the quality of life and creates a certain sense of security. Reduced index of aggression and hostility of the index may be a sign of obvious accentuation of character. Perhaps, this feature of Forest Nenets personality is a form of generalized (congenital) psychological protection. At Forest Nenets viewed evolutionary mechanisms of adaptation. Availability of external and individual factors, especially hereditarily determined, influences on the implementation of strategies of behavior and personality characteristics. This is the problem of the psyche - to regulate vital functions in the outside world (the macrocosm).

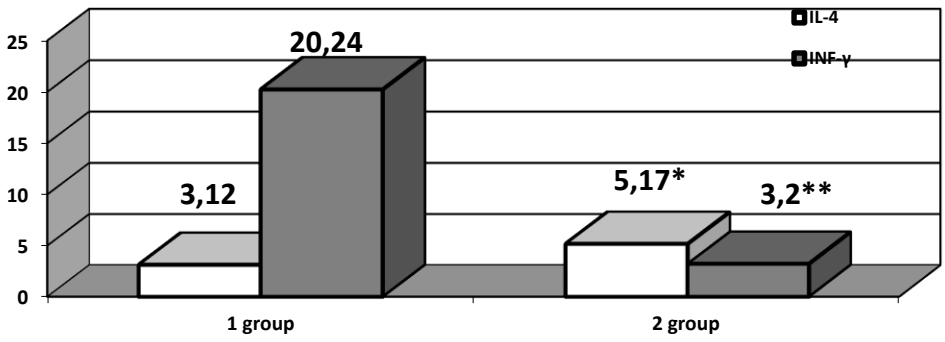

Figure 1. Comparative characteristics of immune parameters. Note: * - significant differences in group 1 (* - p <0,05; ** - p <0,01). Reference values: IL-4 - 0-4 pg / ml; IFN-γ - 0-15 pg / ml

The task of the immune system - to regulate vital functions in the microcosm (the protection of the body). It is found that the repertoire marker humoral immune system (IL-4) does not exceed the reference values. At the same time the people living in the tundra (group 1), IL-4 was 3,12 ± 0,53, which was significantly lower relative (5,17 ± 0,59; p <0.05) to people living in the village Kharampur (group 2). Established correlation connections of IL-4 with the air temperature in group 1 (r = -0,421; p <0,05) and group 2 (r = 0,434; p <0,05). Repertory marker cell immunity IFN-γ tundra residents (group 1) was 20,24 ± 2,11, which is higher than the reference value, and 6.3 times higher in relation to the villagers (group 2). In group 2, this figure amounted to 3,22 ± 0,31 (p <0.01). It can be assumed that in respect of the activity of specific immunity (do not go beyond the norm) at the Forest Nenets temperature promotes the development of a particular form of a specific immune response. High activity of cellular immunity can talk about the individual characteristics of this population group. It can be assumed that the antigenic activity under conditions of the tundra is extremely enhanced.

Adaptability to the new conditions of existence (from the wild to the urban) in the UHI is obvious. NIP, despite their individual characteristics, quite successfully adapted to the new conditions of existence, and learn new social norms. It is possible to suggest that the psyche and the immune system interact in a positive feedback mechanism: the mobilization of psychological defenses appears alarm for the immune defense, and vice versa, "start" signal the immune defense appears to mobilize psychological defenses. At the same time social (living conditions), psychological and physiological (in particular, immune) adaptation mechanisms life support systems are one mechanism to respond to changes in both endo- and exo-factors.

ACKNOWLEDGEMENTS

This work was supported by the grant of the RAS Presidium "Search basic research in support of development the Arctic zone of the Russian Federation" and the international grant RFFR and HIARC «Anthropogenic heat island in the Arctic - a window into the future regional climate conditions, ecosystems and society» (№ 15-55 -71004).

REFERENCES

Vikulin A.V., Wolfson I.F., Grachev L.A., Dolgaya A.A. (2015) Geology, medicine and Socium. Bulletin Kraunts. *Of Earth Sciences*, **1(25)**, 41-52.

Garbuzov V.I. (1999) *Conception of instincts and psychosomatic pathology*. 312.

Korchina T.J., Korchin V.I., Kushnikova G.I. et al. (2012) The main directions of reducing the anthropogenic burden on the environment of the northern oil-producing region. *Human Ecology*. **9**, 15-22.

Myaghkov M.S., Gubernskiy Y.D., Konova L.I., Litskevich V.K. (2007) *City, architecture, people and climate* (Moscow, "Architecture-C.").

Petrov S.A., Mamaeva N.L. (2014) Immune tundra Nenets characteristics depending on the climatic and geographical conditions of residing. *Bulletin of the Tyumen State University*, **6**, 187-193

Petrovsky A.V., Yaroshevskii M.G. (2003) *Theoretical psychology: Textbook for students of psychological faculty of higher educational institutions* (Moscow, publishing center "Academy").

Charles S. (2012) Zender Cryoscience: Snowfall brightens Antarctic future. *Nature Climate Change*. **2**, 770-771

Grimmond C. S. B. (2006) Progress in measuring and observing the urban atmosphere. *Theoretical and Applied Climatology*. **1-3(84)**, 3-22.

Howard L. The climate of London, deduced from Meteorological observations, made at different places in the neighbourhood of the metropolis, *London*, **2**, 1818-20.

Hebbert M., Janković, V., Webb B. (2010) *City Weathers: meteorology and urban design 1950- 2010.* (University of Manchester, Manchester Architecture Research Centre [Network resource]. – URL).

Magee N., Curtis J., Wendler G. (1999) The Urban Heat Island Effect at Fairbanks, Alaska. *Theor. Appl. Climatol.* **64**, 39-47.

Rizka A. A., Henze G. P. (2010) Improved airflow around multiple rows of buildings in hot arid climates. *Energy and Buildings*, **42(10)**, 1711-1718.

Daruna J. H. (2012) *Introduction to Psychoneuroimmunology* (Academic Press – Elsevier. Second Edition).

Sukhovey Y.G., Dotsenko E.L. (2012) Immanence and is isomorphic to the psyche and the immune system. *Bulletin of the Ural Medical Academia*. **4**, 62-63.

TOWARDS FURTHER UNDERSANDING THE IMPACTS OF LAND USE AND COVER CHANGE ON REGIONAL CLIMATE OF MONSOON ASIA

C. FU[1,2,3], Z. XU[2,3], R. MAHMOOD[4], Z. L. YANG[5], H. SU[5], W. GUO[1,3], and S. WANG[1,3]

[1] Institute for Climate and Global Change Research and School of Atmospheric Sciences, Nanjing University, Nanjing, China.

[2] RCE-TEA, Institute of Atmospheric Physics, Chinese Academy of Sciences, Beijing, China.

[3] Jiangsu Collaborative Innovation Center for Climate Change, Nanjing University, Nanjing, China.

4 Department of Geography and Geology, Western Kentucky University, Bowling Green, Kentucky, USA.

[5] Department of Geological Sciences, Jackson School of Geosciences, University of Texas at Austin, Austin, Texas, USA

Keywords: LAND COVER CHANGE, ASIAN MONSOON, DIURNAL TEMPERATURE RANGE, ANNUAL CYCLE, INTERANNUAL VARIABILITY.

INTRODUCTION

Land use and land cover change (LULCC) is primarily characterized as forest conversion to cropland for the development of agriculture. Approximately half of the world's population lives in monsoon Asia, where the land cover has been dramatically changed by human activities over the past centuries. Many of previous modeling studies on the climatic effects of land cover change did not consider ocean-atmosphere interactions (e.g., Fu, 2003), but recent works suggest that the ocean-atmosphere coupling effect may modulate the magnitude of the climate response to LULCC (Delire et al., 2001). In this study, we investigate the LULCC impacts on the monsoon Asian climate by generally following the experimental design of Lawrence and Chase (2010) using the Community Earth System Model (CESM).

METHODS

This study uses CESM version 1 (Gent et al., 2011). CESM is a fully coupled Earth system model comprising four separate models that simultaneously simulate the Earth's atmosphere, ocean, land surface, and sea ice. The atmospheric model is the Community Atmosphere Model (CAM) (Lin, 2004). The ocean component is the Parallel Ocean Program version 2 (Smith et al., 2010). The land surface model is the Community Land Model version 4 (CLM4), with 15 vertical levels for vegetated, wetland, and glacier land units and 10 vertical levels for lakes (Dai et al., 2003). The sea ice component is the Community Ice Code (Bitz et al., 2001; Lipscomb, 2001). CESM and its predecessors, the Community Climate System Model (CCSM), have been widely used to study the paleoclimate and climate of the recent past and to project future climate change. In comparison with CCSM3, the improvements in the simulated precipitation, soil water, and monsoon variabilities provide more confidence for investigating the impacts of LULCC on Asian climate using CESM.

To examine the effect of large-scale LULCC on monsoon Asia climate, two experiments were conducted using the fully coupled CESM. The first experiment (PotVeg) was driven by potential vegetation cover data, and the second (CurVeg) was driven by current vegetation cover data. The potential vegetation distribution data were provided by Lawrence and Chase (2010) and were derived from the global land

cover change data created by Ramankutty and Foley (1999). In the CurVeg experiment, a remote sensing vegetation map valid in 2000 from Moderate Resolution Imaging Spectroradiometer data was used. Both simulations were integrated for 100 years, and the first 40 years of the simulations were discarded for spin-up purposes.

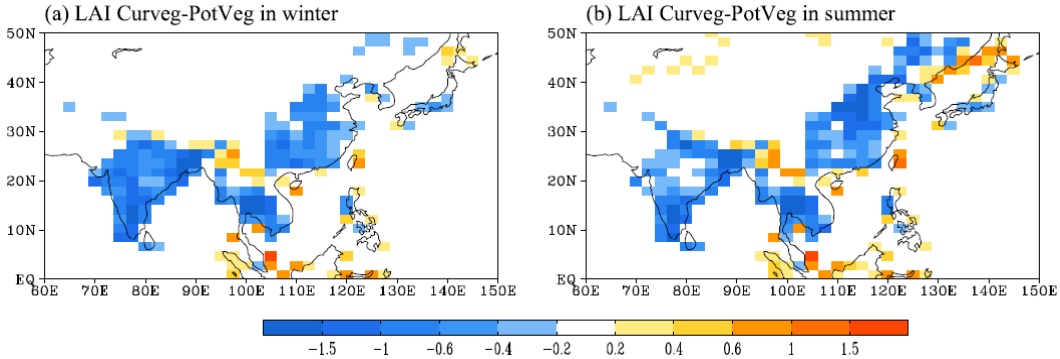

Figure 1. LULCC-induced changes (CurVeg-PotVeg) in leaf area index (LAI) in (a) winter (December-January-February) and (b) summer (June-July-August).

LAI shows a remarkable decrease over eastern China, the Indo-China peninsula, and India (Figure 1). The decrease in LAI is greater in India than in eastern China throughout the year because a higher percentage of forest is converted into cropland in India than in China.

The statistical significance of the difference in the time series between the CurVeg and PotVeg experiments was evaluated using the Student's t test, which takes the serial correlation into account (Zwiers and von Storch, 1995). A field significance test (Livezey and Chen, 1983; Elmore et al., 2006) was employed to evaluate the collective significance of the differences between two spatial distributions. The F test was employed to examine the significance of differences in the standard deviations between the CurVeg and PotVeg experiments.

CONCLUSIONS

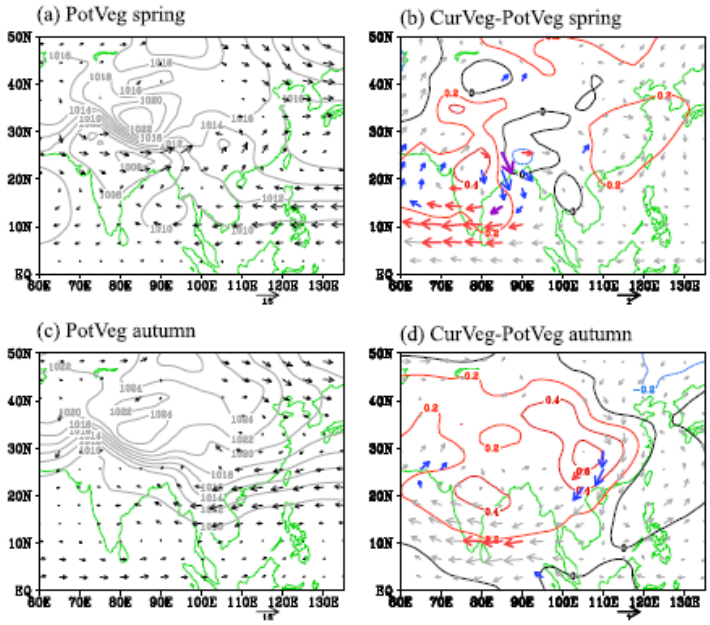

Figure 2. Climatological 850 hPa wind vectors (m s^{-1}) and sea level pressure (hPa) for the PotVeg experiment in (a) spring and (c) autumn. The difference in the 850 hPa wind vectors and sea level pressure between the CurVeg and the PotVeg experiments in (b) spring and (d) autumn. The red, blue, and purple arrows denote the changes in the zonal wind, meridional wind, and both of them that reach the significance level of 0.05.

The difference between the CurVeg and PotVeg experiments shows a clear anticyclonic circulation anomaly at 850 hPa over India in spring (Figure 2b); the circulation anomaly is associated with a tropospheric anomalous subsidence, which suppresses precipitation (Figure 3a). The enhanced surface albedo helps reduce the tropospheric air temperature by reducing both the longwave radiation emitted from the land surface and the sensible heat flux due to the lower land surface temperature. The decrease in the surface roughness length reduces convergence and causes anomalous subsidence. Meanwhile, the decrease in the moisture content helps further cool the atmosphere. In turn, the temperature decrease enhances the anomalous subsidence and leads to a decrease in the moisture content and precipitation (Figure 3). This positive feedback of temperature-subsidence-moisture likely plays an important role in enhancing the anomalous subsidence over India. Meanwhile, the decrease in the precipitation leads to a drier soil, which increases the land surface albedo and reduces evapotranspiration. The positive feedback of precipitation-soil moisture-evaporation also enhances the impact of LULCC on the regional climate. These atmospheric responses to LULCC are more obvious in spring and autumn when advection is weaker than in the summer and winter monsoon seasons.

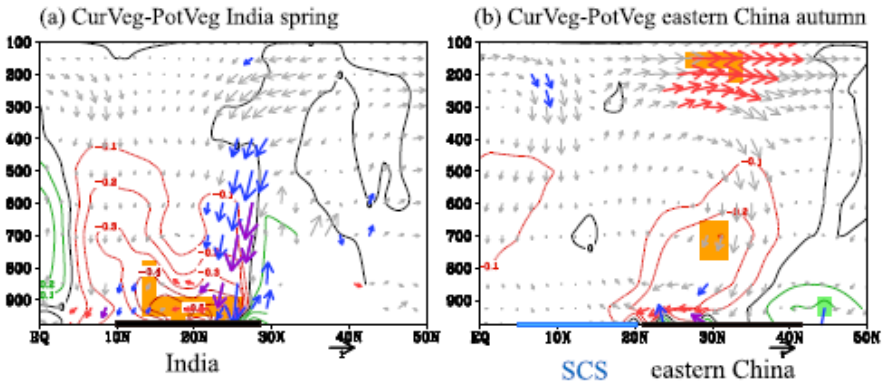

Figure 3. Difference in the meridional-vertical circulation and specific humidity (in g kg^{-1}) between the CurVeg and PotVeg experiments. The shaded area denotes that the difference in the specific humidity reached the significance level of 0.05. The blue, red, and purple arrows indicate the differences in vertical velocity, meridional wind, and both of them that reached the significance level of 0.05.

LULCC also results in detectable changes in the T2m variability over India and over the north China–east Mongolia (NCEM) region. In autumn, the LULCC causes an eastward extension of the dry-to-wet transition zone in northern India, where the variability in T2m is enhanced due to the strengthening land-atmosphere coupling. In winter, LULCC leads to enhanced T2m variability in India and reduces T2m variability in the NCEM region. Both changes are likely related to changes in the variability of the vertically integrated precipitable water (VIPW). A decrease in the VIPW results in reduced downward longwave radiation, which decreases the land surface temperature, and vice versa. In autumn, in addition to the change in the VIPW variability, LULCC leads to a decrease in the climatological mean meridional temperature gradient between 30°N and 50°N, where T2m also exhibits a significantly reduced variability in the NCEM region (Figures 5 and 4c). In association with the decrease in the meridional temperature gradient, cold advections associated with northerly anomalies and warm advections associated with southerly anomalies are reduced; in turn, the variability in 850 hPa air temperature decreases.

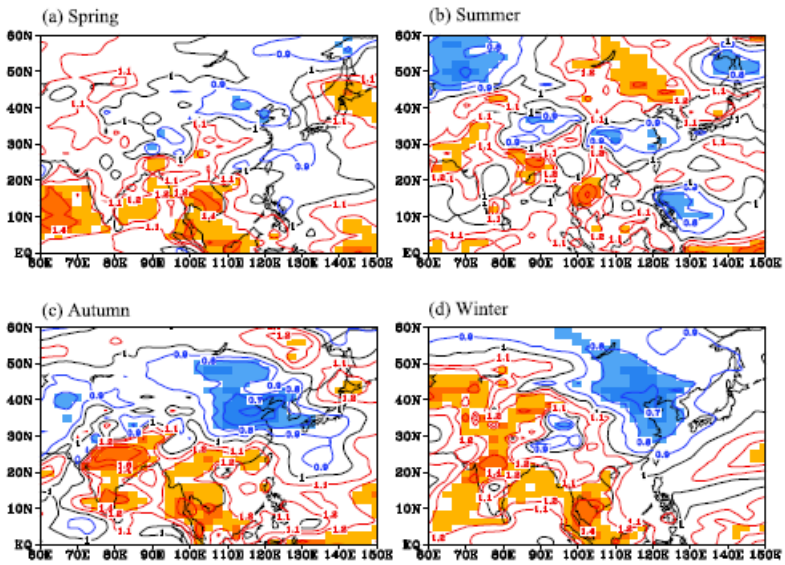

Figure 4. LULCC-induced changes in the standard deviation of the seasonal surface air temperature measured by the ratio of the standard deviation simulated by the CurVeg to the PotVeg experiment. The standard deviations were computed from seasonal anomalies of T2m. The dark (shallow) shaded area denotes that the difference reaches the significance level of 0.01 (0.05).

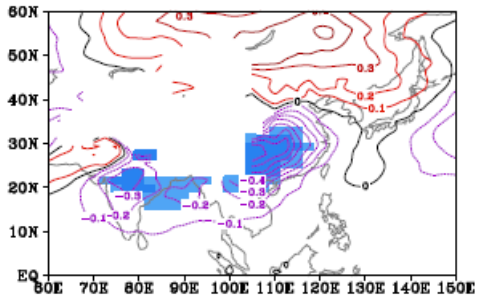

Figure 5. LULCC-induced changes (CurVeg-PotVeg) in the climatological mean 850 hPa air temperature in autumn. The shallow (dark) shaded area denotes differences that reach the significance level of 0.05(0.01).

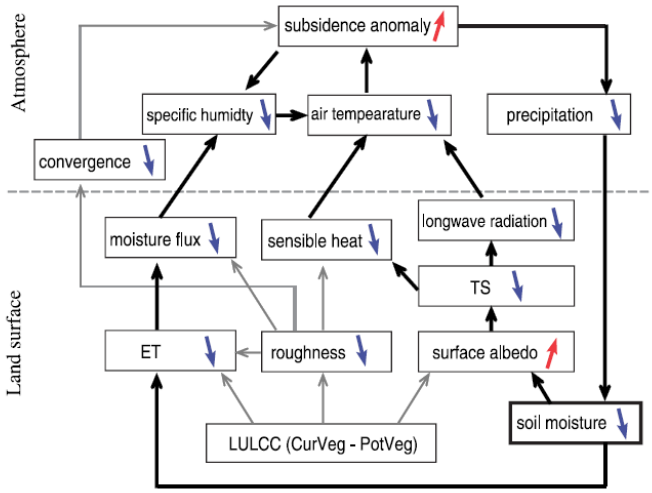

Figure 6. Schematic chart of the influence of LULCC on land surface fluxes and atmospheric circulation in Asia. The positive feedback loops are shown using thicker and darker arrows.

As summarized in Figure 6, the impact of the LULCC on the regional circulation could be enhanced by two positive feedbacks when the background circulation is weak during the monsoon transition seasons: (1) the temperature-subsidence-moisture feedback in the atmosphere and (2) the precipitation-soil moisture-evapotranspiration/albedo feedback between the land and atmosphere.

ACKNOWLEDGEMENTS

This research is supported jointly by the "National Basic Research Program of China" project 2011CB952004 and 2012CB956203, National Natural Science Foundation of China General Program (grants 40905042 and 41105039), and Carbon Budget and Relevant Issues of the Chinese Academy of Sciences (grant XDA05090207). NCEP-NCAR reanalysis 2 data and CMAP precipitation data are provided by the NOAA/OAR/ESRL PSD, Boulder, Colorado, USA, from their website at http://www.esrl.noaa.gov/psd/. We thank Michael Notaro and two anonymous reviewers for their insightful and helpful comments.

REFERENCES

Bitz, C. M., M. Holland, M. Eby, and A. J. Weaver (2001), Simulating the ice-thickness distribution in a coupled climate model, *J. Geophys. Res.*, **106**, 2441–2463.

Dai, Y., et al. (2003), The common land model, Bull. *Am. Meteorol. Soc.*, **84**, 1013–1023.

Delire, C., P. Behling, M. Coe, J. Foley, R. Jacob, J. Kutzbach, Z. Liu, and S. Vavrus (2001), Simulated response of the atmosphere-ocean system to deforestation in the Indonesian Archipelago, *Geophys. Res. Lett.*, **28**, 2081–2084.

Elmore, K. L., M. E. Baldwin, and D. M. Schultz (2006), Field significance revisited: Spatial bias errors in forecasts as applied to the Eta model, *Mon. Weather Rev.*, **134(2)**, 519–531.

Fu, C. (2003), Potential impacts of human-induced land cover change on East Asia monsoon, *Global Planet. Change*, **37**, 219–229.

Gent, P. R., et al. (2011), The Community Climate System Model version 4 (CCSM4), *J. Clim.*, **24**, 4973–4991.

Lawrence, P. J., and T. N. Chase (2010), Investigating the climate impacts of global land cover change in the community climate system model, *Int. J. Climatol.*.

Lin, S. J. (2004), A"vertically Lagrangian" finite-volume dynamical core for global models, *Mon. Weather Rev.*, **132**, 2293–2307.

Lipscomb, W. H. (2001), Remapping the thickness distribution in sea ice models, *J. Geophys. Res.*, **106**, 13,989–14,000.

Livezey, R. E., and W. Y. Chen (1983), Statistical field significance and its determination by Monte Carlo Techniques, *Mon. Weather Rev.*, **111**, 46–59.

Ramankutty, N., and J. A. Foley (1999), Estimating historical changes in global land cover: Croplands from 1700 to 1992, *Global Biogeochem. Cycles*, **13(4)**, 997–1027.

Smith, R. D., et al. (2010), The Parallel Ocean Program (POP) reference manual, Los Alamos National Laboratory, Tech. Rep. LAUR-10-01853, 140 pp.

Zwiers, F., and H. von Storch (1995), Taking serial correlation into account in tests of the mean, *J. Clim.*, **8**, 336–351.

THE CHARACTERISTICS AND SOURCES OF PARTICLE MATTERS IN HEAVY POLLUTION EPISODES IN NORTH CHINA

GAO JIAN*, ZHANG YUECHONG, WANG HAO, WANG HAN, LI HUI, CHAI FAHE

Chinese Research Academy of Environmental Sciences

Key words: BEIJING; PARTICULATE MATTER; HEAVY POLLUTION EPISODES; SOURCE APPORTIONMENT

As a mega city in north China, Beijing experienced extreme pollution episodes in autumn-winter in 2015. In this study we analyzed the physical, chemical and optical properties of PMs and the impact of major sources on PMs' concentration, based on the intensive measurement conducted in Chinese Research Academy of Environmental Sciences. Multi-time-resolution source apportionment method was used to identify the sources of PMs during the episodes. Biomass burning contributed a lot for the episodes in October and early November. When north China enters into the heating period, coal burning turned to be another important contributor for the formation of the pollution processes. The contribution of traffic can be partly controlled by the "special control measures" when Beijing announced the "air quality red alarm" for the first time. However, the source apportionment of PM2.5 proved that coal burning still played the most important role in this episode. The government should pay more attention on the emission control in the rural or surrounding area of Beijing to prevent the formation of the pollution episodes, especially during the heating period.

LAND DEGRADATION ASSESSMENT BY COUPLING NPP AND CLIMATE IN XILIN GOL LEGUE, INNER MONGLIA, CHINA

Z.H. GAO, B. SUN and Z.Y.LI

Institute of Forest Resource Information Techniques, Chinese Academy of Forestry, No.1 Dongxiaofu, HaidianDistrict, Beijing, China.

Keywords: LAND DEGRADATION, NET PRIMARY PRODUCTIVITY (NPP), MOISTURE-RESPONDED NPP (MNPP).

INTRODUCTION

Land degradation is a process that land productive capacity continues to decline or even lose completely under the influence of natural forces and human activities. The scope of land degradation may be extended during this century, which threatens the safety of grain production in China (Wang *et al*.,2008).

With the development of remote sensing technology, long time series remote sensing data have been available for land degradation assessment and monitoring (Bai *et al*.,2008a;del Barrio *et al*.,2010), and the vegetation indicators, such as the normalized difference vegetation index (NDVI) and the net primary productivity (NPP), were commonly used(Bai *et al*.,2008a;Wu *et al*.,2014). In recently years, many scientists focused on improving the method for land degradation assessment and its applicability in different areas (Zhang *et al*., 2014;Xu *et al*.,2014). Wessels et al (2006)proposed the residual trends (RESTREND) method to assess the land degradation and distinguish the drivers from human activity or climate change by statistical model. Under the project of Global Assessment of Land Degradation and Improvement(GLADA) organized by GEF/UNEP/FAO, a method of land degradation based on trend analysis of vegetation change was developed to evaluate the land degradation all over the world by using the GIMMS NDVI data(Bai *et al*.,2008a; Bai *et al*.,2008b). del Barrio et al (2010) proposed the relative RUE (rRUE) and considered it could be a better indicator than RUE indicating land degradation, and found that it may resolve the problem that the RUE can't be compared among different climatic zones.

However, for the RESTREND method, the information of vegetation degradation is sheltered to a certain extent by vegetation variation caused by climatic fluctuation, thus, the statistical models of vegetation change are unable to truly reflect the trend of land degradation and the potential land productivity. For the GLADA method, even the significant level of determination was not considered in trend analysis for defining the areas of land degradation, thus it is possible that many areas were incorrectly identified as degraded lands (Bai *et al*.,2008a).

In this study, a new approach for land degradation by defining a new indictor of vegetation, the Moisture-responded Net Primary Productivity (MNPP)and integrated analysis of NPP and MNPP over time and relationship between MNPP and Moisture Index(MI). The study was conducted in Xilin Gol league, Inner Mongolia Autonomous Region, China, where the land degradation is prevailing. It was expected that provide an example for land degradation assessment, and promote the basis scope for land degradation degree division and cause analysis.

METHODS

The Xilin Gol league is situated in the middle eastern part of Inner Mongolia Autonomous Region, China, and a key part of the Beijing-Tianjin Sand Source Region. Climate zones ranges from semi-arid, semi-humid and humid from west to east. The main land cover type is rangeland and was occupied by almost 95%. Because of the significance in ecological status in the Beijing-Tianjin Sand Source Region, more

and more studies focused on the ecological change in this area (Li *et al*., 2015;Wu *et al*.,2012). Study showed that land degradation has been mainly attributed to overgrazing and climate change in this area (Wu *et al*.,2013).

MOD13A1 monthly NDVI data at 1km resolution during 2001 to 2012 were used in this study. The Savitzky-Golay(S-G) filter (Chen *et al*.,2004) were applied for building the NDVI time-series datasets to remove the interrupt of cloud, ice/snows cover and other residual noise. Besides, the land cover data downloaded from the website of the Environmental & Ecological Science Data Center for West China (http://westdc.westgis.ac.cn) was used for the study as well. Annual NPP was estimated by applying the improved Carnegie-Ames-Stanford Approach model (CASA) (Zhu *et al*.,2007) based on the reconstructed MODIS NDVI and the same period meteorological raster dataset with 0.1°resolution (Yang *et al*.,2011). The precipitation and temperature data were also used to estimate the MI using Thornthwaite method (Thornthwaite,1948;Sun *et al*.,2015).

A new vegetation indictor MNPP was defined, which is the NPP divided by MI:

$$MNPP = \frac{NPP}{MI * 100}$$

A large number of random samples in study area were selected for analysis of the NPP and MNPP trends. A new approach for land degradation assessment was promoted based on NPP and MNPP changes. The areas with significant decrease of NPP over time were directly identified as degraded lands. Some areas, where the MNPP change over time is significant decrease and insignificantly correlated with MI, although the NPP change is not significant, also were identified as degraded lands with integrated analysis between NPP, MNPP and MI, thus the slight degraded areas can be extracted from NPP fluctuation. So the degraded areas caused by both climatic change and human activities could be defined more accurately.

RESULTS AND ANALYSIS

The spatial distribution of land degradation and restoration in Xilin Gol league during 2001-2012 were shown in Fig.1. The results indicated that land degradation was much serious in this area, especially in northeastern parts. Most of the west Ujimqin Banner experienced severe land degradation during 2001 to 2012, and it was important ranch in study area. The restored lands were mainly distributed in northern and middle western parts of Xilin Gol league, especially in Otindag sandylands, which indicated that the ecological engineering projects have achieved significantly.

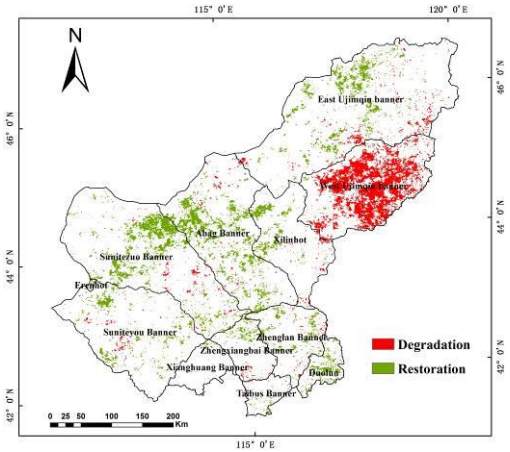

Fig.1 Distribution of land degradation and restoration in Xilin Gol league during 2001-2012

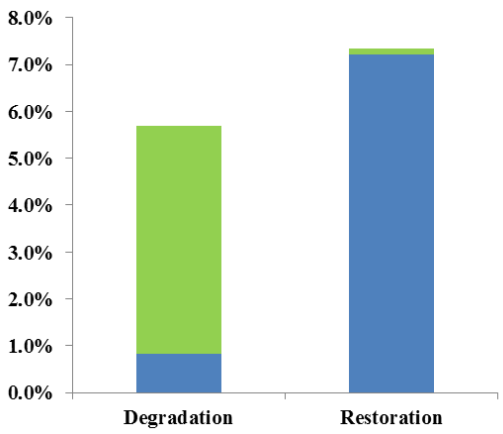

Fig.2 Histogram of land degradation and restoration

Statistical data of degradation and restoration were shown in Fig.2. The farmlands and artificial ecosystems such as cities and roads were excluded in assessment. Results showed that degraded lands and restored lands account for 5.7% and 7.3% respectively. 4.9% degraded lands and 0.1% restored lands were distinguished from lands where NPP has normal fluctuation trend.

CONCLUSIONS

In this study, a new approach for land degradation assessment was preliminary promoted based on NPP and MNPP changes. The applicability of the method should be further studied in the future.
Results of land degradation and restoration assessment showed that5.7% and 7.3% lands suffered from land degradation and restoration respectively in Xilin Gol legue during 2001 to 2012. The ecological engineering projects were implemented in the study area have achieved significantly, especially in Otindag sandylands.

ACKNOWLEDGEMENTS

The study was funded by National Major Program of China (No. 21-Y30B05-9001-13/15) and National Natural Science Foundation of China (No. 41501467, No. 41571421).

REFERENCES

Bai,Z.G. Dent,D.L. Olsson, L.et al.(2008a). Proxy global assessment of land degradation, *Soil Use and Management*,24, 223-234.

Bai,Z.G. Dent,D.L. Olsson,L. et al. (2008b). Global Assessment of Land Degradation and Improvement 1. Identification by remote sensing. LADA / ISRIC / FAO. LADA technical report N.

Chen,J. Jonsson,P. Tamura,M. et al.(2004). A simple method for reconstructing a high quality NDVI time-series data set based on the Savitzky–Golay filter, *Remote Sensing of Environment*,91, 332-344.

del Barrio,G. Puigdefabregas, J. Sanjuan,M.E. et al. (2010). Assessment and monitoring of land condition in the Iberian Peninsula,1989-2000, *Remote sensing of environment*,114, 1817-1832.

He,J. Yang, K. (2011). China Meteorological Forcing Dataset,*Geographical Review*,doi:10.3972/westdc.002.2014.db.

Li,X.S. Wang,H.Y. Wang,J.Y. et al. (2015). Land degradation dynamic in the first decade of twenty-first century in the Beijing–Tianjin dust and sandstorm source region, *Environmental Earth Sciences*,74, 4317-4325.

Sun,B. Gao,Z.H. Li,Z.Y. et al .(2015). Dynamic and dry/wet variation of climate in the potential extent of desertification in china during 1981-2010, *Environmental Earth Sciences*,73,3717-3729.

Thornthwaite,C.W. (1948). An approach toward a rational classification of climate,, *Geographical Review*,38, 55-94.

Wang,X.M. Wu,F.H. Hasi,E.et al.(2008).Desertification in China: An assessment, *Soil Earth-Science Reviews*,88, 188-206.

Wessels,K.J. Prince,S.D. Malherbe,J. et al. (2007). Can human-induced land degradation be distinguished from the effects of rainfall variability? A case study in South Africa, *Journal of Arid Environments*,68, 271 – 297.

Wu,J.J. Zhao,L. Zheng,Y.T. et al.(2012). Regional differences in the relationship between climatic factors, vegetation, land surface conditions, and dust weather in China's Beijing-Tianjin Sand Source Region, *Natural Hazards*,62, 31-44.

Wu,Z.T. Wu,J.J. Liu, J.H. et al. (2013). Increasing terrestrial vegetation activity of ecological restoration program in the Beijing-Tianjin Sand Source Region of China, *Ecological Engineering*,52, 37-50.

Xu,D.Y. Li,C.L.Song,X.et al. (2014). The dynamics of desertification in the farming-pastoral region of North China over the past 10 years and their relationship to climate change and human activity, 123, 11-22.

Zhang,J. Niu,J.M. and Bao.T.L. (2014). Human induced dryland degradation in Ordos Plateau, China, revealed by multilevel statistical modeling of normalized difference vegetation index and rainfall time-series, *Journal of Arid Land* ,6, 219-229.

Zhu, W.Q. Zhang,J.S. Pan,Y.Z. et al. (2007). Measurement and dynamic analysis of ecological capital of terrestrial ecosystem in China, *Chinese Journal of Applied Ecology*,18, 586-594.

PRELIMINARY ESTIMATE OF METHANE EMISSION DURING ICE THAW FROM SOUTHERN TUNDRA LAKES IN WESTERN SIBERIA

L.L. GOLUBYATNIKOV[1], V.S. KAZANTSEV[1] and M.Yu. CHERBUNINA[2]

[1]Laboratory of Mathematical Ecology, A.M.Obukhov Institute of Atmospheric Physics, Moscow, Russia.

[2]Department of Geology, Lomonosov Moscow State University, Russia

Keywords: METHANE EMISSION, LAKES, ICE THAW, TUNDRA, WESTERN SIBERIA.

INTRODUCTION

Among natural sources of methane, lakes are second in its emission intensity into the atmosphere (Anderson *et al.*, 2010; Golubyatnikov and Kazantsev, 2013). Global methane emissions from lakes is estimated at 71.6 MtCH4/year (Bastviken *et al*., 2011), which is about 35% of global methane emissions from natural sources. During the open water season, a part of methane produced in lake sediments is released into the atmosphere by diffusion and ebullition. The production of methane in the lake sediments still continues during the winter season till the lake is completely frozen. The bottom sediments of many tundra lakes do not freeze in winter and methane is produced in these lakes all the year. The methane produced under the ice cover is accumulated in the water column and partially freezes into ice. Methane produced during the winter subsequently releases to the atmosphere during ice break-up at spring. This early spring release of methane should be accounted for more realistic annual methane emission, especially in northern regions with a great number of lakes.

METHODS

We have estimated the methane emission from tundra lakes in Western Siberia after early spring breakup of ice cover. Field experiments were carried out in June-July 2015 at two lakes located in the southern tundra zone of the Yamal-Nenets Autonomous District. In this region lakes are ice covered for about nine months (September-June). The presented lakes are typical thermokarst lakes for the northern part of Western Siberia: the small one (№1) with the area $6*10^3$ m^2 up to 2.0 m depth, sapropel sediments (67,3839N, 78,6091E), the biggest one (№2) is $97*10^3$ m^2 up to 1.8 m depth, silty sediments (67,3697N, 78,6108E) (Fig.1). The lake water and ice were sampled for the measurement of methane content right before the ice thawing started.

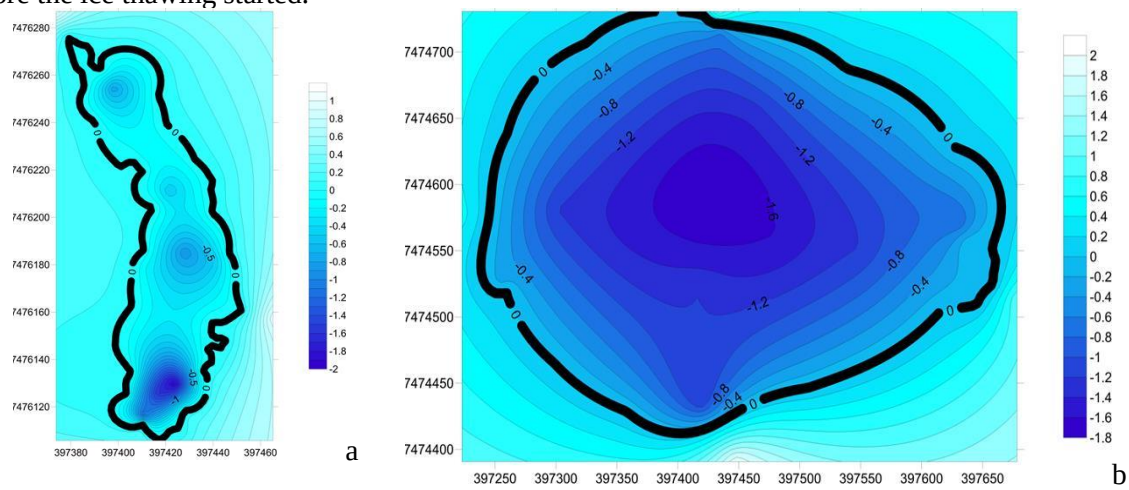

Figure 1. Lakes under study: (a) №1, (b) №2 and depths these lakes.

The lake ice and water were sampled through a hole drilled in the ice of the lake. Sampling was made in the ice at depths with different intervals (0.15-0.4 m for the ice cover; for the water layer under the ice cover at the upper level right under the ice, and at the lower one, near the bottom). After ice thaws the lake water was sampled for the measurement of dissolved methane. Sampling was made at the water surface, in the middle of the water column for different depths. Calculation of methane emission during spring ice thawing was carried out as the difference in the mass of methane before and after ice melt, assuming that a slight part of the methane storage under ice was oxidized in the water column (Michmerhuizen *et al*., 1996).

CONCLUSIONS

According to our field data and calculations, methane store in the ice is about 0.0 µmol/l (median average) for the lakes under study. The single data about concentration in air bubbles and soil bottom layer are obtained (up to 96 µmol/l). The water under the ice is saturated with methane - methane concentration reaches 395 µmol/l. After ice melts the concentration of methane in water is sufficiently small, and varies from 0.11 to 4.71 µmol/l for the lake №1 and from 0.34 to 3.02 µmol/l for the lake №2. On the basis of experimental data we produced the calculations of methane emissions by diffusion during spring ice thawing for lakes under study. The calculated spring methane emissions for the lakes is ranged from 200 to 400 $mgCH_4/m^2$, which is 20-45% of the methane emissions from southern tundra lakes in Western during the warm period.

ACKNOWLEDGEMENTS

This work was supported by the Russian Foundation of Basic Research (projects 14-05-00193, 16-35-00097), the Basic Research Program (Department of Earth Sciences, Russian Academy of Sciences) “Integrated studies on actual problems of Earth Sciences” and in the framework of the FP7 Marie Curie Actions IRSES (grant 612642).

REFERENCES

Anderson, B., K. Bartlett, S. Frolking, et al. (2010). *Methane and Nitrous Oxide Emissions from Natural Sources*, (EPA, Washington, DC).

Bastviken, D., L.J. Tranvik, J.A. Downing, P.M. Crill and A. Enrich-Prast (2011). Freshwater methane emissions offset the continental carbon sink, *Science* **331**(6013), 50-50.

Golubyatnikov, L.L. and V.S. Kazantsev (2013). Contribution of tundra lakes in western Siberia to the atmospheric methane budget, *Izvestiya, Atmospheric and Oceanic Physics* **49,** 395-403.

Michmerhuizen, C.M., R.G. Striegl and M.E. McDonald (1996). Potential methane emission from north-temperate lakes following ice melt, *Limnol. Oceanogr.* **41**, 985-991.

UNCERTAINTIES IN SATELLITE-DERIVED RAIN SUSCEPTIBILITY TO AEROSOLS

C. GONG[1,2,3], AND M. WANG[1,2,3]

[1]Institute for Climate and Global Change Research & School of Atmospheric Sciences, Nanjing University, Nanjing, 210023, China

[2]Joint International Research Laboratory of Atmospheric and Earth System Sciences of Ministry of Education, Nanjing, China

[3]Collaborative Innovation Center of Climate Change, Jiangsu Province, China

Keywords: AEROSOL-CLOUD INTERACTIONS, SATELLITE OBSERVATIONS, UNCERTAINTY

ABSTRACT

Quantifying rain susceptibility to aerosols is important for understanding aerosol-cloud interactions and for further constraining aerosol indirect effects. However, it has been challenging to derive rain susceptibility to aerosols from satellite observations and different studies have shown large discrepancy in their derived rain susceptibility. These discrepancies may depend on the collocation of aerosol and cloud fields, and different aerosol and cloud retrieval products used. These discrepancies may also depend on different definitions of rain susceptibility, such as whether cloud droplet number concentration or aerosol optical depth is used to derive rain susceptibility. In this study, we quantify the uncertainty in satellite-derived rain susceptibility by using different products of aerosol and cloud retrievals and by using different definitions of rain susceptibility with the goal of reconciling the discrepancy in previous studies. Regional differences between high latitudes and mid- and low latitudes are also further highlighted and their relationships with aerosol loading and cloud regimes are further discussed.

ACKNOWLEDGEMENTS

The work was supported by the National Natural Science Foundation of China (D0512/41575073).

MATHEMATICAL SIMULATION OF THE PARAMETERS OF THE ATMOSPHERIC ELECTRIC FIELD DURING THUNDERSTORMS BASED ON THE CUMULONIMBUS ELECTRIZATION MODEL

I.M. GUBENKO[1] and K.G. RUBINSTEIN[1]

[1] Hydrometeorological Research Center of the Russian Federation, 11-13, B. Predtechensky per., Moscow, Russia

Keywords: THUNDERSTORMS, ATMOSPHERIC ELECTRICITY, CUMULONIMBUS, NUMERICAL SIMULATION.

INTRODUCTION

Thunderstorm study is one of the main research fields of atmospheric electricity. Prediction of "cloud-to-ground" lightning discharges is the most important aspect since they are the greatest threat to human, technical devices and engineering structures. For this moment the electric field of the atmosphere is insufficiently studied. That is why thunderstorm forecast methods mainly are based on atmospheric instability analysis. However, such techniques do not explicitly consider electrical processes occurring in convective clouds.

The objectives of this study are:

1. Physical and mathematical description of the cumulonimbus (Cb) model electrization. The model uses the forecasts of numerical predictive mesoscale model WRF-ARW and allows to predict the parameters of the atmospheric electric field, including specific to thunderstorm activity.
2. Comparison of the prognostic values of electrical breakdown with observed of thunderstorm activity.

METHODS

Cumulonimbus electrization model is a set of equations describing the processes of the generation and separation of electric charges in convective clouds, constants and profiles of meteorological data. The process of charge generation is described by equations taking into account the diameters of interacting hydrometeors (snow, ice particles, graupels, cloud droplets), their concentration, the fraction of particles between which there was a collision /merger, the resulting charge from a collision/merger, gravitational speed of particles' sedimentation and air temperature (Gardiner, 1985; MacGorman *et al.*, 2001; Mansel and MacGorman, 2005; Ziegler *et al.*, 1991). The model includes the equations describing non-inductive, inductive mechanisms and its combination - the integrated schemes of charge generation.

The non-inductive mechanism of the charge generation implies the interaction of solid hydrometeors (ice crystals+graupels, particles of snow+graupels). The equation of the inductive charging implies the interaction of graupels and cloud droplets (Zeigler *et. al.*,1991). Pairwise interaction between other hydrometeors is neglected because of the small charge generated as a result of the collision/merger between particles (Latham and Mason, 1962; Gaskel, 1989; Mansell, 2005).

Charge separation unit of the elecrization model includes equations of the total volume charge, potential and electric field intensity.

The breakdown electric field intensity sufficient for the development of lightning is set in 220 kV/m.

The input data for the electrization model (meteorological data profiles) are calculated by the hydrodynamic mesoscale model WRF-ARW. Its entire configuration is presented in (Gubenko and Rubinstein, 2015). Here the input data for electrization model are profiles of hydrometeors' fractions (snow, ice particles and graupels), cloud water content, air temperature and vertical wind component in the layer 1020-300 hPa.

The possibility of using the electrization model for the thunderstorm forecast is studied in this paper. For the quality assessment of the thunderstorm forecast calculated from the electrization model was chosen Russian Central Federal District (CFD) for May 13 - August 31, 2013. Statistical estimations are made using synoptic station network and Worldwide Lightning Location Network (WWLLN) data (Lay, 2008). The total number of observed thunderstorms by the network of synoptic stations and WWLLN is 1105. The total number of forecasts is 8809. The number of thunderstorms predicted by the electrization model based on non-inductive, inductive and integrated mechanisms of charge generation and matched with the observed data equal to 781, 528 and 682 respectively. Validation of the electrization model includes calculation of the common accuracy, accuracy of thunderstorm availability, accuracy of the absent thunderstorms and Piercy- Obukhov's criterion (Table 1).

Accuracy of electrization model, units	Non-inductive scheme	Inductive scheme	Integrated scheme
Common accuracy	0,79	0,74	0,70
Accuracy of thunderstorm availability	0,33	0,44	0,24
Accuracy of absent thunderstorm	0,95	0,91	0,91
Piercy- Obukhov's criterion	0,50	0,39	0,39

Table 1. Accuracy of Cb electrization model based on three charge generation schemes.

CONCLUSIONS

The accuracy of the thunderstorm forecast given by the electrization model based on the non-inductive charge generation scheme showed the best results: accuracy of the absence of the thunderstorm is 0,95, common accuracy is 0,79, Piercy- Obukhov's criterion is 0,50.

ACKNOWLEDGEMENTS

This work was supported by the RFBR (Russian Foundation for Basic Research) under grants A 14-08-01105, A 15-05-02395 and A 16-05-00822.

REFERENCES

1. Gardiner B., D. Lamb and R. Pitter (1986). Measurements of initial potential gradient and particle charges in a Montana summer thunderstorm, *J. Geophys. Res.*, **90**, N D4, pp. 6079-6086.
2. Gaskell W. (1981). A laboratory study of the inductive theory of thunderstorm electrification, *Quarterly Journal of Royal Meteorological Society*, **107**, N 454, pp.955-966.
3. Gubenko I. M. and K.G. Rubinstein (2015). Analysis of the resultsof thunderstorm forecasting based on atmospheric instability indices using WRF-ARW numerical model data, *Russian Meteorology and Hydrology*, **40,** №1, pp.16-24.
4. Latham J. and B.J. Mason (1962). Electrical charging of hail pellets in a polarizing electric field, *Proc. R. Soc. London*, Ser. A., **266**, pp. 387-401.
5. Lay E.H. (2008). *Investigating lightning-to-ionosphere energy coupling based on VLF lightning propagation characterization*, (University of Washington, Seattle, Washingtom State, USA).
6. MacGorman D. R., J. M. Straka and C.L. Ziegler (2001). A lightning parameterization for numerical cloud models, *J. Appl. Meteor*., **40**, pp. 459–478.
7. Mansel E. R., D.R. MacGorman, C.L. Ziegler, and J. Straka (2005). Charge structure and lightning sensitivity in a simulated multicell thunderstorm, *J. Geophys. Res*., **110**, pp.12-20.
8. Sartor J.D. (1981). Induction charging of clouds, J. *Atmos. Sci.*, **38**, pp. 218-220.
9. Ziegler C., J. D. MacGorman and P. Ray (1991). A model evaluation of noninductive graupel-ice charging in the early electrization of a mountain thunderstorm, *J. Geophys. Res.*, **96**, N D7, pp. 12833-12855.

SPACEBORNE EARTH OBSERVING TECHNOLOGIES FOR ENVIRONMENTAL MONITORING IN THE BELT AND ROAD REGION

H. D. GUO

Institute of Remote Sensing and Digital Earth (RADI), Chinese Academy of Sciences (CAS), Beijing 100094, China; E-mail: hdguo@radi.ac.cn

Keywords: SPACEBORNE EARTH OBSERVATION, THE BELT AND ROAD REGION, ENVIRONMENTAL MONITORING, RECOGNITION AND ASSESSMENT

INTRODUCTION

In 2013, Chinese President Xi Jinping initiated the Silk Road Economic Belt and the 21st-Century Maritime Silk Road (abbreviated as "the Belt and Road" or "B&R") initiative. The construction of the Belt and Road is an important initiative for China's government facing 21st Century economic development. The former links the Asia-Pacific economic circle in the east and the well-developed European economic circle in the west, and the latter links the major port cities in China and Southeast Asian countries. It is the longest economic corridor in the world with the most potential. The Belt and Road is composed of 65 countries with a population of 4.4 billion, which is 63% of the world's population. Overall, the Belt and Road is a breakthrough initiative with a wide range, long-term outlook, and applicability in multiple fields. It is vital for macro-dynamic analysis of resource and environmental patterns and potential development for the countries along the Belt and Road. Basic macro-environmental data are significant for the construction of the Belt and Road. Spaceborne Earth observation is an effective tool for environmental change monitoring with its capacity for macro-level, rapid, accurate and objective data acquisition. It will provide spaceborne research and information support. This paper introduces the progress of eco-environmental monitoring along the Belt and Road countries using spaceborne Earth observation technologies.

ECO-ENVIRONMENTAL MONITORING ALONG THE BELT AND ROAD REGION USING SPACEBORNE EARTH OBSERVATION

The Belt and Road faces many problems and risks that cannot be ignored, such as increasing extreme climate events, frequent occurrence of major natural disasters, sea level rise, eco-environmental degradation and water resource shortages. To effectively cope with these challenges, it is necessary to conduct science in overall recognition and assessment of macro patterns and development potential of the eco-environment along the Belt and Road region using spaceborne Earth observation technologies.

Based on multi-source, multi-platform and long-term time series remote sensing datasets, eco-environmental monitoring research based on spaceborne Earth observation can be summarized as follows:

(1) Ecological and environmental patterns and potential impact of global change in the Belt and Road region

The land use/land cover change, vegetation degradation, lake area and level change, snow area and SWE change, soil moisture change and global environmental change in Central Asia were investigated from 1982 to 2011. The vegetation in most areas in Central Asia was degraded from April to September, especially from June to September, where the degraded areas were more than 70% of the area of vegetation. From 1988 to 2010, the soil moisture of Central Asia showed a decreasing tendency, which is highly correlated to the increasing temperature of Central Asia.

In this study, the ecological environment's basic status, forest biomass and carbon sequestration, crop condition monitoring and status of water resources in the valley of Lantsang-Mekong were investigated in the China-ASEAN region. Contrastive analysis on per capita ecological resources was also conducted. Brunei and Malaysia have high ecological resources per capita and high economic development. China

and Indonesia have high ecological resources, but less per capita. Laos, Cambodia and Burma have low economic development, but high ecological resources per capita.

(2) Monitoring marine environments and natural disasters from space in the regional seas of the maritime silk road

Regional spatial and temporal variations of sea surface dynamic and bio-optical parameters were investigated. Based on ENVISAT/ASAR wave mode data from its entire mission (2002 – 2012), global ocean swell propagation was revealed, which is a new insight from space in this field. In addition, the countries along the maritime silk road often suffer severe natural hazards, such as earthquakes, flooding, drought, and tsunamis. The CBERS-04 satellite on Oct. 10th, 2015, monitored flooding in Thailand, fire spots in Indonesia, and typhoons over the Philippines.

(3) Monitoring and developmental protection of world heritage and culture adoption along the Belt and Road region

Based on Landsat MSS, Landsat TM (1985-2014), HJ-1A and Landsat LOI datasets, the land cover change over Angkor, Cambodia, was studied. The preliminary results show that urban area is gradually increasing, forest area is unstable and decreasing and water area has seasonal fluctuations. In addition, the first inversion of surface deformation was conducted using 42 scenes of TerraSAR-X images (3m) in the observation period from 2011-2013. Although it is significant, the motion of relics and their surroundings is hampered by other movements triggered by urbanization, farming as well as surface erosion after wild-fires.

(4) Monitoring city expansion and urbanization of the Belt and Road region

Based on Landsat TM, SPOT and CEBERS-2 datasets, the change in urban impervious surface of more than 30 megacities along the Belt and Road region from 1973 to 2015 was observed, the city expansion and urbanization spatial patterns were investigated along with the main factors restricting urbanization.

CONCLUSIONS

This paper introduces research progress and preliminary results on a variety of fields and applications related to the Belt and Road, such as ecological environmental patterns and potential impact of global change, monitoring marine environments and natural disasters, monitoring and developmental protection of world heritage and culture, and monitoring city expansion and urbanization along the Belt and Road region. It demonstrates the important role and significance of spaceborne Earth observation for environmental monitoring and assessment along the Belt and Road region.

ACKNOWLEDGEMENTS

This work was supported by Major Program of National Natural Science Foundation of China: “Moon-based Earth Observation Research of Large-scale geoscientific phenomena” (Grant No. 41590850), Academician Consulting Project of the Chinese Academy of Sciences: “Spatial cognition study of resource and environment macro-pattern and development potential of the Silk Road Economic Belt based on Earth Observation”, and the Key Projects in the National Science & Technology Pillar Program (Grant No. 2012BAH27B05).

REFERENCES

K. Unger-Shayesteh et al., “Introduction to ‘Water in Central Asia—perspectives under global change’,” Global Planet. Change 110,1 –3 (2013).

R. Ragab an C. Prudhomme, “Climate change and water resources management in arid and semi-arid regions: prospective and challenges for the 21st century,” *Biosystems Eng*. 81(1), 3–34 (2002).

Foley J A, DeFries R, Asener G P, et al. 2005. Global consequences of land use. Science, 306: 570–574

IMPACT OF ACCURATE DESCRIPTION OF LAND USE TYPE AND VEGETATION ON SIMULATION OF THE EAST ASIAN MONSOON PRECIPITATION

W. GUO[1], Y LIU[1] AND Y XUE[2]

[1]Institute for Climate and Global Change Research, School of Atmospheric Sciences, Nanjing University, China

[2]Department of Geography, University of California, Los Angeles, California, USA

Keywords: LAND SURFACE PARAMETERS. REGIONAL MODEL, LEAF AREA INDEX. MONSOON PRECIPITATION.

INTRODUCTION

The summer monsoon is one of the most unique components in East Asian climate system. Currently most regional climate models can realistically simulate the longitudal movement of monsoon rainbelt in East Asia, whereas precipitation is often overestimated in high-latitudes (Fu et al., 2005). Various factors are involved in the ocean-land-atmosphere interaction and affect the intensity and evolution of East Asian summer monsoon. Surface characteristics directly determine the energy budget within a specific region and the surface-atmosphere moisture exchange and transport, and subsequently affect the model capability in regional climate simulation (Xue et al., 2004).

In fact, the description of surface characteristics is largely focused on accurate representation of land use type and reasonable settings of parameters in surface physics. Among various parameters involved in the surface physics, the leaf area index (LAI, Tang et al., 2009) affects surface radiation balance, evapotranspiration, and biochemical process of vegetation, etc., and thus is a key parameter that affects surface-atmosphere water and energy exchange and transport (Liu et al., Chen; 2013). However, continuous field measurements of LAI are relatively rare. The high inhomogeneity of land surface characteristics makes it hard to determine regional-scale LAI based on station observations. Satellite remote sensing can provide spatially and temporally continuous measurements of surface parameters at high-resolution. In recent years, many studies have been conducted to improve simulations of surface temperature and precipitation using satellite remote sensing data. Unfortunately, not many studies have been performed over East Asian monsoon region.

METHODS

In order to explore the application of satellite remote LAI products in regional climate models to improve simulation of the East Asian summer monsoon precipitation, we replace the default LAI in WRF_NMM/SSiB2 by the GLOBMAP LAI. The model domain is shown in Fig. 1. During the growing process of vegetation, there exist large differences in the biophysical and biochemical characteristics for both green and yellow leaves. However, satellite remote sensing can only provide the LAI information for green leaves. Thereby, the LAI information for yellow leaves are produced based on the vegetation growth characteristics. Furthermore, some parameters used for retrieval need to be determined based on information of land use type. For this reason, the land use type is also changed in this study, corresponding to the replacement of LAI by GLOBMAP LAI to ensure the consistency between surface parameters and vegetation type (Fig. 2). Two experiments have been conducted, i.e. the control experiment in which nothing is changed in the WRF_NMM/SSiB2, and a sensitivity experiment (hereafter GLOBMAP) in which LAI, green-leaf vegetation fraction, and land use type are changed. The simulation period is from January to December of 2008. Results of the two experiments are compared with GPCP.

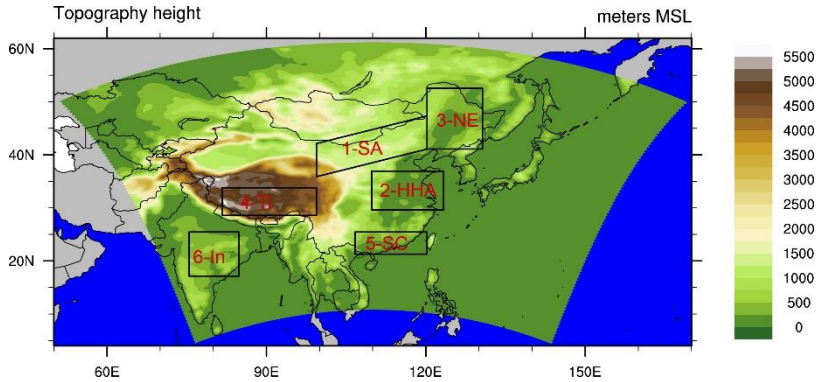

Fig 1. Model domain, topography, and sub-regions for analysis

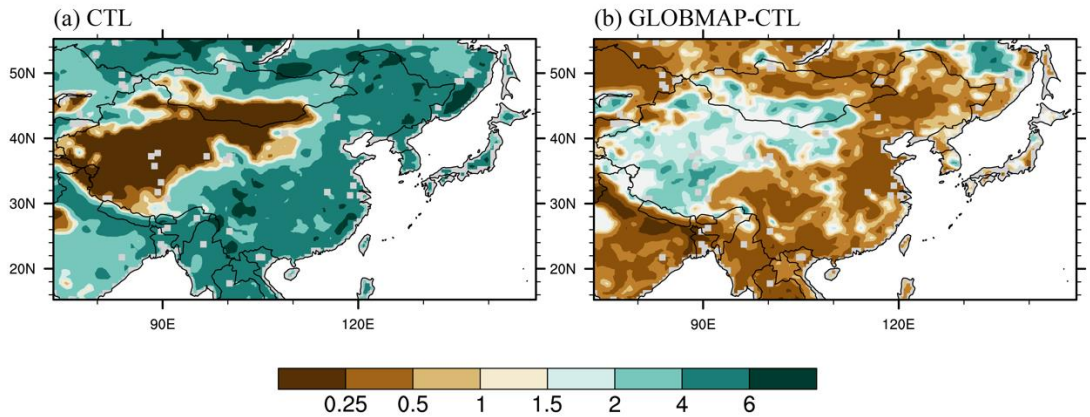

Fig 2. (a) Summertime average LAI in CTL；(b) difference in LAI between CLOBMAP and CTL

CONCLUSIONS

Results indicate that the CTL experiment overestimates precipitation in the semi-arid region of China, southern China, southwestern China, and northern India, while it underestimates precipitation in Huang-Huai River Valley, middle- and lower Yangzi-River valley, the Tibetan Plateau, and northern India Peninsula (Fig. 3). The above precipitation biases are significantly improved in the GLOBMAP experiment. The forecast Skill-Score defined in the "Remarks on Statistical Parameters for Model Evaluation" by Dr. Petra Seibert is used to evaluate the difference in simulations between the two experiments over several key regions, where large biases are found in the CTL experiments. The results indicate that the simulation of GLOBMAP experiment has been significantly improved over these key regions.

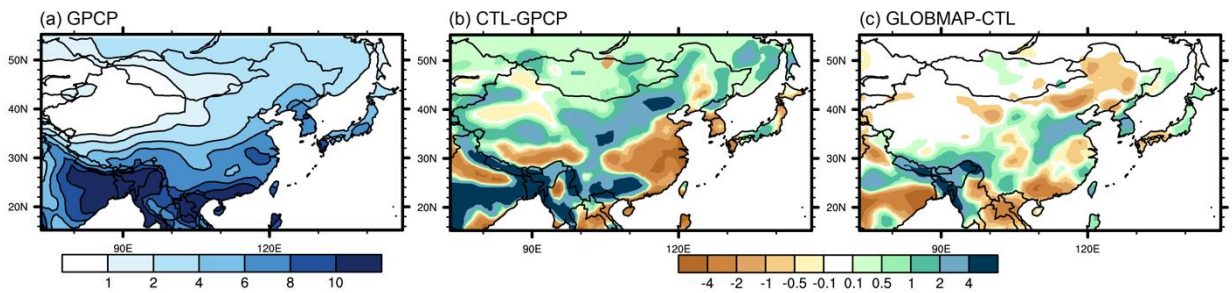

Fig 3. Summertime precipitation distribution. (a) GPCP；(b) difference between CTL and GPCP；(c) difference between GLOBMAP and CTL simulations.

After the onset of the East Asian monsoon, atmospheric moisture is transported northwards along the periphery of the subtropical high, and form precipitation under favorable condition of subtropical high and westerly trough. Accompanied with the northward advancement and southward withdrawal of the subtropical high, strong precipitation occurs alternatively in South China, the Yangzi-River Valley, and North China. When the monsoon weakens, the northward movement of rainbelt reverses to southward withdrawal and the rainbelt finally moves out of mainland China. Therefore, realistic simulation of the northward movement and southward withdrawal of the monsoon rainbelt is a critical criterion to evaluate the model capability. Fig. 4 depicts the zonal mean rainbelt evolution between 105°N ~120°N, which jumps from 22°N to 34°N in middle July, and retreats to 24°N in early August before it jumps northward again to 30°N and 40°N successively. The first northward jump of the rainbelt simulated by the CTL is abnormally northerly (over 40°N), and remains in high-latitudes for quite a while, leading to overestimation of precipitation in North China and underestimation of precipitation in Huan-Huai River Valley. In contrast, the northward jump of rainbelt simulated by the GLOBMAP experiment is more realistic than that simulated by the CTL, with the simulated precipitation center located at around 35oN. The second northward jump of the rainbelt simulated by GLOBMAP and CTL is consistent with that in the GPCP, but the simulated precipitation intensity is weaker than in the GPCP. In late June, a fictitious precipitation center at high latitudes is found in both simulations of the CTL and GLOBMAP experiments, probably due to the possible systematic errors in the model system.

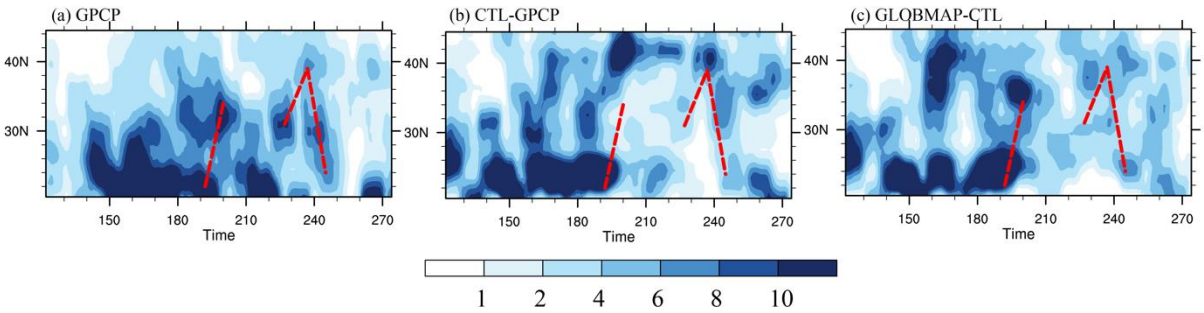

Fig 4. The evolution of monsoon rainbelt. (a) GPCP；(b) CTL；(c) GLOBMAP

Li et al. (2004) once pointed out that the East Asian monsoon activities are closely related to the location of monsoon jet stream in the upper level. Meanwhile, longitudal temperature gradient plays an important role in the movement of upper level jet streams. For this reason, in this study we compare the longitudal temperature gradient simulated by the CTL and GLOBMAP experiments (Fig. 5). It is found that from the surface to 500 hPa, longitudal temperature gradient simulated by the GLOBMAP is larger than that simulated by the CTL. According to the thermal wind equation, upper level westerly winds intensify correspondingly in the GLOBMAP simulation.

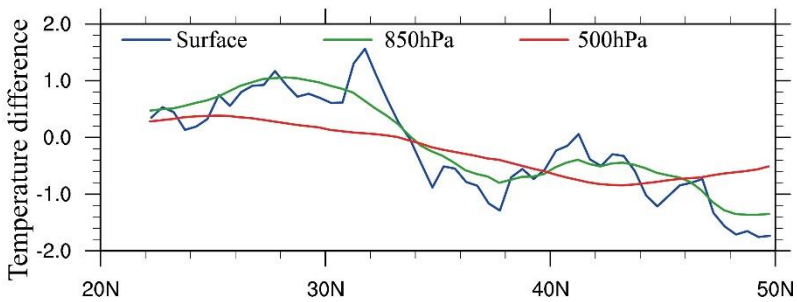

Fig 5. Difference in zonally mean temperature over 105°E~120°E between GLOBMAP and CTL simulations

ACKNOWLEDGEMENTS

This study is jointly supported by the Jiangsu Collaborative Innovation Center for Climate Change and the Joint International Research Laboratory of Atmospheric and Earth System Sciences (JirLATEST).

REFERENCES

Fu, C., et al., Regional Climate Model Intercomparison Project for Asia. Bulletin of the American Meteorological Society, 2005. 86(2): p. 257-266.

Kusunoki, S. and O. Arakawa, Are CMIP5 Models Better than CMIP3 Models in Simulating Precipitation over East Asia? Journal of Climate, 2015. 28(14): p. 5601-5621.

Rummukainen, M., State-of-the-art with regional climate models. Wiley Interdisciplinary Reviews-Climate Change, 2010. 1(1): p. 82-96.

Xue, Y., et al., Role of land surface processes in monsoon development: East Asia and West Africa. Journal of Geophysical Research: Atmospheres (1984–2012), 2004. 109(D3).

Tang, J. and Q. Zhuang, A global sensitivity analysis and Bayesian inference framework for improving the parameter estimation and prediction of a process-based Terrestrial Ecosystem Model. Journal of Geophysical Research: Atmospheres (1984–2012), 2009. 114(D15).

Liu, Y., W. Guo, and Y. Song, Estimation of key surface parameters in semi-arid region and their impacts on improvement of surface fluxes simulation. Science China Earth Sciences: p. 1-13.

Chen, J.M., Remote Sensing of Leaf Area Index of Vegetation Covers. Remote Sensing of Natural Resources, 2013: p. 375.

Baret, F., et al., LAI, fAPAR and fCover CYCLOPES global products derived from VEGETATION: Part 1: Principles of the algorithm. Remote sensing of environment, 2007. 110(3): p. 275-286.

Masson, V., et al., A global database of land surface parameters at 1-km resolution in meteorological and climate models. Journal of climate, 2003. 16(9): p. 1261-1282.

Deng, F., et al., Algorithm for global leaf area index retrieval using satellite imagery. Geoscience and Remote Sensing, IEEE Transactions on, 2006. 44(8): p. 2219-2229.

Yang, W., et al., MODIS leaf area index products: From validation to algorithm improvement. Geoscience and Remote Sensing, IEEE Transactions on, 2006. 44(7): p. 1885-1898.

Liu, Y., R. Liu, and J.M. Chen, Retrospective retrieval of long-term consistent global leaf area index (1981–2011) from combined AVHRR and MODIS data. Journal of Geophysical Research: Biogeosciences (2005–2012), 2012. 117(G4).

HIGH SESQUITERPENE EMISSIONS FROM NORWAY SPRUCE IN SUMMER

H. HAKOLA, V. TARVAINEN, M. HEMMILÄ, A. P. PRAPLAN, H. HELLÈN

Finnish Meterological Institute, Air Quality, P.O. Box 503, 00101 Helsinki, Finland

Keywords: PICEA ABIES, NORWAY SPRUCE, BVOC EMISSIONS, MONOTERPENE, SESQUITERPENE, ON-LINE GC

INTRODUCTION

A large amount of biogenic volatile organic compounds (VOCs), mainly monoterpenes and sesquiterpenes, is emitted to the atmosphere by vegetation, especially in the densely forested boreal regions (Hakola et al., 2001, 2006; Tarvainen et al., 2005). In the atmosphere these compounds are oxidized, which affects the tropospheric ozone formation (Chameides et al., 1992). In addition reaction products of VOCs also take participate in the formation and growth of new particles (Tunved et al., 2006). In smog camber studies secondary organic aerosol (SOA) yields for different hydrocarbons and even for different monoterpenes have been found to vary considerably (Griffin et al., 1999). Therefore detailed knowledge of the composition of the atmospheric mixture of mono- and sesquiterpenes is crucial for fine particle studies as well as for the development of ozone reduction and climate change abatement strategies.

The emissions of mono- and sesquiterpenes have not been measured individually and continuously in Northern Europe. In the present study we conducted on-line gas-chromatographic measurements of mono- and sesquiterpene emissions of Norway spruce. This tree species was chosen, because there is only a limited amount of data published on its emissions (Bourtsoukidis et al., 2014; Hakola et al., 2003; Grabmer et al., 2006) although it is one of the most common species in the Northern boreal zone. The on-line measurements were considered essential for evaluating the factors affecting emission rates, for example their temperature and light dependence. The emissions have also been shown to vary considerably throughout the year (Hakola et al., 2006). Therefore we conducted on-line measurement campaigns at the SMEAR II station (Station for Measuring Forest Ecosystem-Atmosphere Relations, $61^0$51'N, $24^0$18'E, 181 a.s.l) at Hyytiälä, in southern Finland (Hari and Kulmala 2005) for three years: 2011, 2014, and 2015. The measurements covered spring/early summer 2011 (2 weeks in April, 5 days in May and 3 days in June), 1 week in May, 2 weeks in June and one week in July in 2014, and one week in June and two weeks in August in 2015.

METHODS

The emissions measured in 2011 were from a different tree than in 2014 and 2015. The selected trees were growing in a natural forest environment, about 5 meters from the measurement container. The height of the tree in 2011 was about 10 meters. The samples were collected at a height of about 2 meters from a fully sunlit branch. In 2014 and 2015 the tree was the same, about 1 m tall and the distance from the tree measured in 2011 was about 5 meters. The branches were placed in a Teflon enclosure and the emission rates were measured using a dynamic flow through technique. The volume of the cylinder shape Teflon enclosure was approximately 8 litres and it was equipped with inlet and outlet ports and a thermometer inside the enclosure. The cover of the enclosure was made of transparent Teflon film. The photosynthetically active photon flux density (PPFD) was measured just above the enclosure. The flow through the enclosure was kept at about 3-5 litres per minute. Ozone was removed from the ingoing air using MnO_2 coated copper nets. The emission rates were measured using an on-line gas-chromatograph-mass-spectrometer. VOCs in a 40-60 ml/min subsample were collected in the cold trap of a thermal desorption unit (Perkin Elmer ATD-400) packed with Tenax TA in 2011 and Tenax TA/Carbopack-B in 2014 and 2015. The trap material was changed since isoprene was found not to be retained fully in the

cold trap in 2011. The trap was kept at 20^0C during sampling to prevent water vapour present in the air from accumulating into the trap. This allowed the analysis of mono- and sesquiterpenes. The thermal desorption instrument was connected to a gas chromatograph (HP 5890) with DB-1 column (60 m, i.d. 0.25 mm, f.t. 0.25 µm) and a mass selective detector (HP 5972). One 20-minute sample was collected every other hour. The system was calibrated using liquid standards injected on Tenax TA-Carbopack B adsorbent tubes and analyzed using the offline mode of the instrument. We had no standard for sabinene and therefore sabinene was quantified using the calibration curve of β-pinene. The detection limit was below 1 ppt for all mono- and sesquiterpenes, much lower than in the corresponding off-line analysis. The following compounds were included in the calibration solutions: isoprene, 2-methyl-3-buten-ol (MBO), camphene, 3-carene, p-cymene, 1,8-cineol, limonene, linalool, myrcene, α-pinene, β-pinene, terpinolene, bornylacetate, longicyclene, isolongifolene, β-caryophyllene, aromadendrene, α-humulene.
The emission rate is determined as the mass of compound per needle dry weight and time according to

$$E = \frac{(C_2 - C_1)F}{m} \qquad (1)$$

Here C_2 is the concentration in the outgoing air, C_1 is the concentration in the inlet air, and F is the flow rate into the enclosure. The dry weight of the biomass (m) was determined by drying the needles at 75 ºC for 24 hours.

RESULTS AND DISCUSSION

In April, May and still in the beginning of June the total monoterpene emission rates were quite low for every measurement year (below 50 ng g(dry weight)$^{-1}$ h^{-1} most of the time). At the end of June the emission rates started to increase to the level where they remained until the end of August, daily maxima remaining below 300 ng g(dry weight)$^{-1}$ h^{-1}. Mean monthly emission rates of isoprene, 2-methylbutenol (MBO), monoterpenes and sesquiterpenes are presented in Table 1.

Monoterpene emissions pattern was somewhat different between the two trees measured. The tree measured in 2011 emitted mainly α-pinene in May, whereas the tree measured in 2014 and 2015 emitted mainly limonene in May. During summer these differences got smaller. The relative abundance of measured compounds in the spruce emission is presented in Table 2 for all measurement months. The Norway spruce emissions have been measured earlier for instance by Hakola et al. (2003) and Bourtsoukidis et al. (2014). The measurements by Hakola et al. covered all seasons, but only a few days for each season, whereas the measurements by Bourtsoukidis et al. covered three weeks in September-October in an Estonian forest. The main monoterpenes detected in the Estonian forest were α-pinene (58.7 %) and 3-carene (25.8 %), but also camphene, limonene, β-pinene and β-phellandrene were measured. In the study by Hakola et al. (2003) the monoterpene emission composed mainly of α-pinene, β-pinene, camphene and limonene, but only very small amounts of 3-carene were observed, similarly to the present study. This raises a question whether genetic origin would affect the emission pattern in a similar way as in Scots pine emissions (Bäck et al., 2012).

A substantial change in the emissions took place at the end of July, when sesquiterpene emission rates increased to 3-5 times higher than monoterpene emission rates (Fig. 1, Table 1). In the study by Bourtsoukidis et al. (2014) sesquiterpene emissions (112.8 ng g(dry weight)$^{-1}$ h^{-1} at 30°C) were about 20 % of the monoterpene emissions (539.5 ng g(dry weight)$^{-1}$ h^{-1} at 30°C), but these emissions were measured during fall.
In the current study the emission increase was measured in 2015 only. In July 2014, the measurements were ended 14.7 2014, earlier than they started to increase in 2015. The sesquiterpenes measured were not the ones we had in our standard and hence they are only tentatively identified and quantified. Based on the NIST mass spectra library (NIST/EPA/NIH Mass Spectral Library, version 2.0) the two most abundant sesquiterpenes were β-farnesene and zingiberene. The maximum β-farnesene emission rate (750 ng g(dry weight)$^{-1}$ h^{-1}) was measured on 31 July 2015 in the afternoon. Linalool emissions increased simultaneously

with sesquiterpene emissions, in the same way as was observed in the measurements of Scots pine emissions in Hyytiälä (Hakola et al., 2006). Then also the sesquiterpene emissions were found to increase late summer.

Table 1: Mean monthly emission rates of isoprene, 2-methylbutenol (MBO), monoterpenes and sesquiterpenes ng g(dry weight)$^{-1}$ h^{-1}.

	isoprene	MBO	monoterpenes	sesquiterpenes
April 2011			7.6	0.0
May 2011	17.5	1.7	6.1	0.1
May 2014	0.5	1.0	11.1	0.1
June 2011	0.3		29.4	2.1
June 2014	0.5	0.8	10.9	0.7
June 2015	3.1	5.7	25.8	26.1
July 2014	0.9	2.3	39.6	2.9
July 2015	1.5	2.5	52.4	170.9
August 2015	10.2	2.3	31.2	246.9

Table 2: Average monthly abundances of emitted monoterpenes

	a-Pinene	Camphene	Sabinene	b-Pinene	Myrcene	3-Carene	p-cymene	Limonene	1,8-Cineol
April 2011	29%	16%	0%	16%	1%	4%	5%	16%	13%
May 2011	53%	8%	1%	6%	1%	1%	8%	9%	10%
May 2014	16%	10%	0%	9%	5%	5%	2%	50%	3%
June 2011	5%	18%	11%	0%	24%	2%	7%	3%	30%
June 2014	24%	13%	0%	13%	5%	4%	3%	26%	12%
June 2015	26%	19%	7%	5%	6%	5%	3%	13%	15%
July 2014	29%	11%	1%	5%	5%	6%	6%	32%	5%
July 2015	30%	17%	3%	4%	8%	4%	1%	23%	10%
August 2015	32%	11%	3%	3%	14%	3%	2%	26%	5%

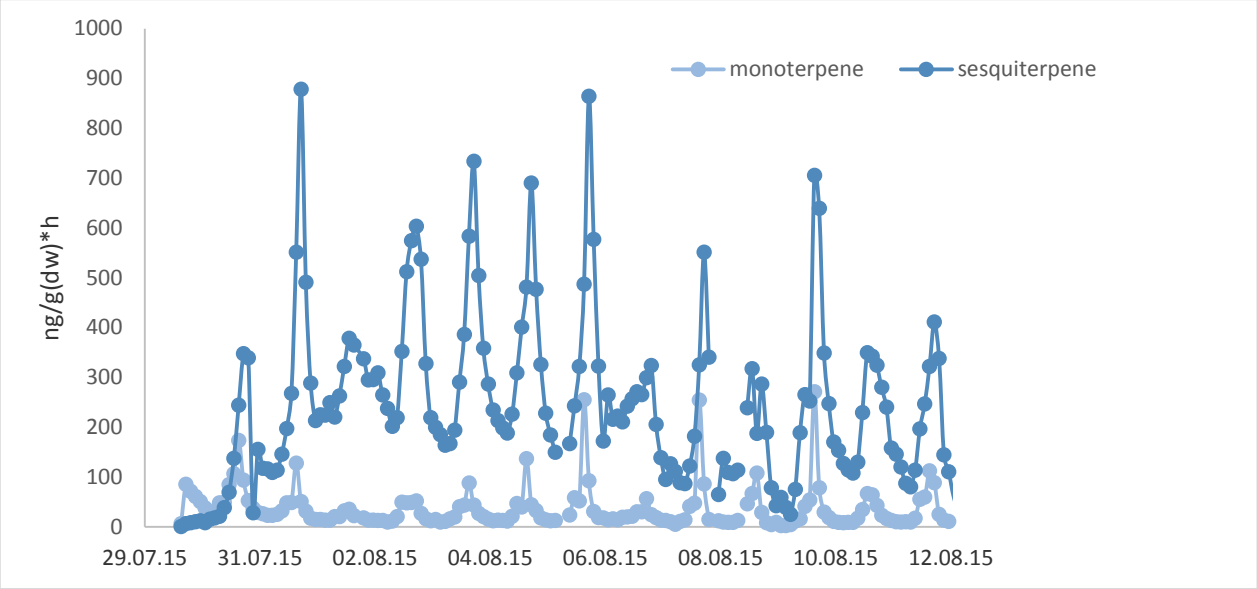

Fig. 1: Mono- and sesquiterpene emission rates in July-August in Hyytiälä

ACKNOWLEDGEMENTS

The financial support by the Academy of Finland Centre of Excellence program (project no 272041) is gratefully acknowledged.

REFERENCES

Bourtsoukidis E., Bonn B., Noe S., 2014. On-line field measurements of BVOC emissions from Norway spruce (Picea abies) at the hemiboreal SMEAR-Estonia site under autumn conditions. Boreal Environment Research 19: 153–167

Chameides, W. L., Fehsenfeld, F., Rodgers, M. O., Cardelino, C., Martinez, J., Parrish, D., Lonneman, W., Lawson, D. R., Rasmussen, R. A., Zimmerman, P., Greenberg, J., Middleton, P., and Wang, T., 1992. Ozone precursor relationships in the ambient atmosphere, Journal of Geophysical Research 97(D5), 6037-6055.

Griffin, R. J., Cocker III, D. R., Flagan, R. C., and Seinfeld, J. H., 1999a. Organic aerosol formation from the oxidation of biogenic hydrocarbons, Journal of Geophysical Research 104(D3), 3555-3567.

Griffin, R. J., Cocker III, D. R., Seinfeld, J. H., and Dabdub, D., 1999b. Estimate of global atmospheric organic aerosol from oxidation of biogenic hydrocarbons, Geophysical Research Letters 26(17), 2721-2724.

Grabmer, W., Kreuzwieser, J.Wisthaler, A., Cojocariu, C., Graus, M., Rennenberg, H., Steigner, D. Steinbrecher, R., Hansel, A.: VOC emissions from Norway spruce (Picea abies L. [Karst]) twigs in the field - Results of a dynamic enclosure study. Atmospheric Environment 40 S1, 128-S137.

Hakola H., Laurila T., Lindfors V., Hellén H. Gaman A. and Rinne J.; Variation of the VOC emission rates of birch species during the growing season. Boreal Environment Research, 6, 237-249, 2001.

Hakola, H., Tarvainen, V., Laurila, T., Hiltunen, V., Hellén, H. and Keronen, P.; Seasonal variation of VOC concentrations above a boreal coniferous forest. Atmos. Environ., 37, 1623-1634, 2003.

Hakola, H., Tarvainen, V., Bäck, J., Rinne, J., Ranta, H., Bonn, B., and Kulmala, M.: Seasonal variation of mono- and sesquiterpene emission rates of Scots pine. Biogeosciences, SRef-ID: 1726-4189/bg/2006-3-93, 93-101, 2006.

Hari, P. and Kulmala, M.: Station for measuring ecosystem-atmosphere relations (SMEAR II). Boreal Env. Res., *10*, 315-322, 2005.

Tarvainen V., Hakola H., Hellén H., Bäck J., Hari P., Kulmala M.:Temperature and light dependence of the VOC emissions of Scots pine. Atmos. Chem. Phys., 5, 6691-6718, 2005.

Tunved P., Hansson H.-C., Kerminen V.-M., Ström J., Dal Maso M., Lihavainen H., Viisanen Y., Aalto P.P., Komppula M., and Kulmala M.. High natural aerosol loading over boreal forests. Science 312, 261-263, 2006.

HAZE DETECTION BY USING MODIFIED NORMALIZED DIFFERENCE HAZE INDEX IN BEIJING, TIANJIN AND HEBEI PROVINCE

HAN XINLEI[1], YAO FENGMEI[1], ZHANG JIAHUA[2] and MIRZA MUHAMMAD WAQAR

[1] Key Laboratory of Computational Geodynamics, Chinese Academy of Sciences, Beijing 100049, China.

[2] Institute of Remote Sensing and Digital Earth, Chinese Academy of Sciences, Beijing 100094, China.

Keywords: MODIFIED NORMALIZED DIFFERENCE HAZE INDEX, MODIS REFLECTANCE, $PM_{2.5}$, HAZE INDEX.

1. INTRODUCTION

Haze is a serious deterioration in air quality that is composed of dust, fog and other solid suspend particles, which can scatter and absorb the incident light and lead to atmosphere opacity and horizontal visibility degradation (Shang Liu *et al*., 2008). According to the criteria from China Meteorological Administration, if the visibility is less than 10 km, with the relative humidity range from 80 percent to 95 percent then it is defined as Haze weather (China Meteorological Administration, 2010). Considering in January 2013, only five days were non-hazy days in Beijing. The hazy weather seriously influenced the atmospheric visibility, causing traffic congestion, harming normal life and economic activities (Yong Zha *et al*., 2012). In the year of 2013, China has experienced several large-scale haze processes, which are the combination of stable weather conditions and increasing emission of pollutants from human activities (Meina Li *et al*., 2014).

The $PM_{2.5}$ (refers to the fine particulate matter of less than 2.5-micron aerodynamic diameter) is a good index to characterize the air pollutants emitted by human activities (Y. Sun *et al*., 2006). Most importantly, part of $PM_{2.5}$ which enters the human body may deposit in bronchial and alveolar, cause respiratory system diseases and do direct or indirect damage to human health (NA Janssen *et al*., 2011). In urban areas, the concentration of haze is an index of air quality (Kang Sun *et al*., 2015). Due to its short duration and greater extent, the choice of using remote sensing technology to study the hazy weather is realistic (Ying Zhang *et al*., 2015), especially using high temporal resolution of meteorological satellite, such as Modified High Resolution Radiometer (AVHRR) or Moderate Resolution Spectroradiometer (MODIS).

This study focuses on development of new index named modified Normalized Difference Haze Index (m-NDHI) to study haze over all land covers. A comparative analysis was also performed between modified Normalized Difference Haze Index (m-NDHI) and Normalized Difference Haze Index (NDHI) over the water in the BTH region (that includes: Beijing, Tianjin and Hebei Provinces). The results of correlation between m-NDHI and $PM_{2.5}$ over different land covers is quite significant however the correlation results over the water is most sensitive to haze detection (m-NDHI). However, regression results between m-NDHI with $PM_{2.5}$ over the build-up is more significant than over the water in hazy days. By correlating the m-NDHI value with in situ $PM_{2.5}$ data for the three cities of Beijing, Tianjin, and Shijiazhuang revealed that this developed index is better than NDHI index, which can be used to evaluate the atmospheric pollutant concentration.

2. METHODS

2.1 Dataset Used and Processing

The MODIS-Terra level 1B MOD02 HKM data was used in this study for winters of 2013 and 2014. During this period, 46 sunny days were chosen over the study area. This data set includes MODIS bands 1−7 at a spatial resolution of 500 m (the raw bands 1 and 2, at a spatial resolution of 250m, were resampled to 500 m). The reflectance of the data set was used directly to construct the m-NDHI and NDHI in this study. The reflectance data with a geographic coordinate system were re-projected to the Universal Transverse Mercator (UTM) coordinate system (zone 50 north, datum: WGS-84). The $PM_{2.5}$ data used in this study were collected from the Chinese Ministry of Environmental Protection.

2.2 Derivation of m-NDHI

When establishing an index to characterize the terrain features, the value of the element to be extracted from the spectral band is higher than other features in resulted image. For example, in the Normalized Difference Vegetation Index (NDVI), the value for vegetation is higher than water, buildings and bare land. Similarly, in m-NDHI index, the value for haze compared to the other elements is higher. However, it should be noted that the m-NDHI index is different from the other indices like NDVI, the Normalized Difference Water Index (NDWI), and the Normalized Difference Built-up Index (NDBI) because haze is a substance formed above the surface, and the spectral values on the satellite images included the haze plus the ground elements. So, in order to effectively monitor haze, the underlying surface factors should be suppressed.

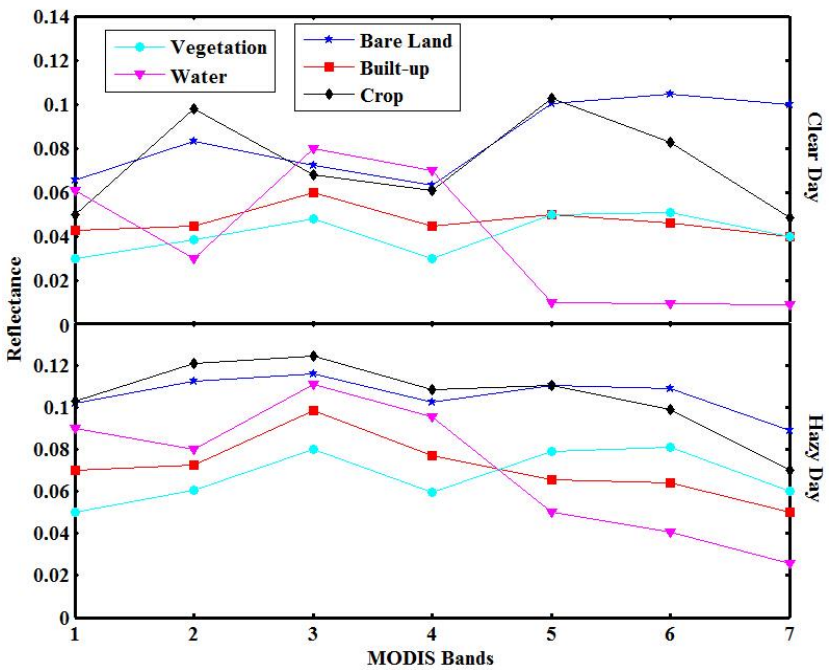

Figure 1. Variation of reflectance with MODIS 7 bands (wavelength) over different land covers of (a) bare land, (b) build-up, (c) crop, (d) vegetation, (e) water

From the (Figure 1), reflectance of different land covers varies with the MODIS 7 bands. By comparing the results of clear day and hazy day, it is identified that band 3 (blue band; 459-479nm) is the most sensitive to the haze and the spectral variation between band 1 (red band; 620-670nm) and band3 is the largest (Table 1) while other bands have fluctuations in different land covers. Hence, band3 and band1 were chosen to construct modified Normalized Difference Haze index, which is (band1-band3) /

(band1+band3). The developed index is capable of detecting haze over different land covers in the absence of clouds, snow and bare soil. The developed m-NDHI is written as followed (Equation 1):

$$m - NDHI = (Band1 - Band3) / (Band1 + Band3) \quad (1)$$

Table 1. Variation of different bands and m-NDHI values for different surface features (In the table B1, B2, B3, B4 are respective MODIS Bands)

Land Covers	Weather	B1	B2	B3	B4	B1-B3	B1+B3	m-NDHI
Bare Land	Clear	0.0655	0.0832	0.0725	0.0632	-0.0070	0.1380	-0.0507
	Haze	0.1021	0.1122	0.1158	0.1025	-0.0137	0.2179	-0.0629
	Variation	0.0366	0.0290	**0.0433**	**0.0393**			
Build-up	Clear	0.0428	0.0448	0.0602	0.0448	-0.0174	0.1030	-0.1689
	Haze	0.0702	0.0726	0.0986	0.0768	-0.0284	0.1688	-0.1683
	Variation	0.0274	0.0278	**0.0384**	**0.0320**			
Crop	Clear	0.0501	0.0982	0.0682	0.0608	-0.0181	0.1183	-0.1530
	Haze	0.1028	0.1208	0.1245	0.1082	-0.0217	0.2273	-0.0955
	Variation	**0.0527**	0.0226	**0.0563**	0.0474			
Vegetation	Clear	0.0302	0.0388	0.0482	0.0302	-0.0180	0.0784	-0.2296
	Haze	0.0502	0.0604	0.0801	0.0596	-0.0299	0.1303	-0.2295
	Variation	0.0200	0.0216	**0.0319**	**0.0294**			
Water	Clear	0.0608	0.0302	0.0802	0.0701	-0.0194	0.1410	-0.1376
	Haze	0.0898	0.0801	0.1108	0.0955	-0.0210	0.2006	-0.1047
	Variation	0.0290	**0.0499**	**0.0306**	0.0254			

Among 46 effective scenes, two images were chosen, i.e. December 12 and 25 corresponding to clear day and hazy day respectively. The image of December 12 is clear with high visibility however December 25 image was covered by a layer of haze where visibility was as low as 2 km. Comparing MODIS bands of 1,4,3 true colour composite with m-NDHI distribution in clear day and hazy day, it can be seen that new developed index can detect distribution of haze effectively. However, this algorithm is not feasible in the area of high reflectance pixels, such as clouds, snow, frozen ice and bare soil.

During clear days, the reflectance from atmosphere is little, so the differences of spectrum mainly come from the lands covers, which are the bright surface features. It can be seen that m-NDHI is giving good results for haze detection except over bright areas like cloud, snow, frozen ice and bare soil. In the presence of cloud, snow and ice m-NDHI assign highest value to these land covers and intermediate values are assigned to haze. From result images, it can be seen that Tianjin and Shijiazhuang cities are affected by haze heavily (Dated: December 25, 2013). The corresponding value of m-NDHI is also high for haze day. On the north of Tianjin, there are low convective clouds on that day; hence, m-NDHI is not affective over that area.

3. RESULTS

3.1 m-NDHI above the water as an indicator of urban air pollution

In order to validate the m-NDHI index properly, its value must relate positively to the phenomenon it represents. As confirmed by Cao et al. (2003), the $PM_{2.5}$ is a good index to characterize the pollutants caused by human emission. Hence, by correlating m-NDHI with $PM_{2.5}$, urban air pollution can be detected. Among the correlation of m-NDHI above all land covers with $PM_{2.5}$, m-NDHI above the water is the most sensitive to haze detection, R square in Beijing is up to 0.7096 as compared to vegetation, build-up, cropland. Therefore, the developed m-NDHI can be an effective method to characterize atmospheric pollution based on remote sensing instead of $PM_{2.5}$.

3.2 Comparing the m-NDHI with NDHI in three cities

In order to verify the validity of m-NDHI and NDHI, the ROI was extracted over the water in BTH regions during 46 days and the average value of m-NDHI and NDHI was calculated for three cities respectively. Correlation analysis between m-NDHI and NDHI with $PM_{2.5}$ was investigated and the results showed coefficient of correlation in BTH to be 0.7096, 0.5864 and 0.4857 for m-NDHI and 0.5625, 0.5321 and 0.4618 for NDHI respectively. This comparative analysis revealed that m-NDHI is better predictor of atmospheric conditions as compared to NDHI. Correlation analysis between $PM_{2.5}$ and m-NDHI in Beijing was performed, t test shows the significance level, up to 0.7096 (Equation 2), at 0.01 level.

$$PM_{2.5} = 389.1(m\text{-}NDHI) + 191 \qquad (R2 = 0.7096) \qquad (2)$$

The result of the correlation for m-NDHI and $PM_{2.5}$ in the BTH regions shows that m-NDHI over water is positive correlation with $PM_{2.5}$, which is consistent with the requirement of any index, therefore can be used to be as surrogate for air quality.

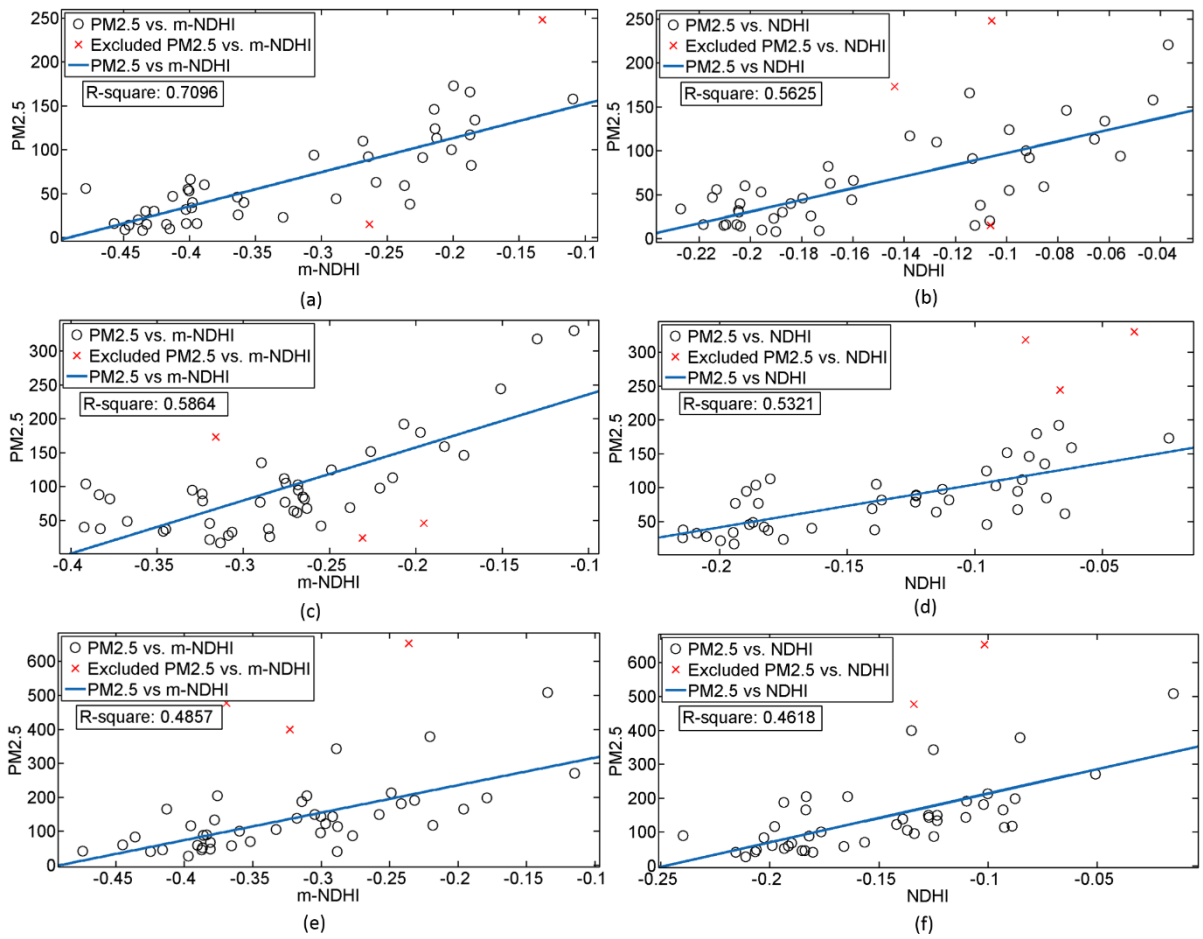

Figure2. The comparison of Correlation between m-NDHI and NDHI with $PM_{2.5}$ for Beijing (a, b), Tianjin (c, d) and Shijiazhuang (e, f).

4. DISCUSSION AND CONCLUSIONS

This work analysed the spectral responses of various land cover types in the BTH regions, China, during clear and hazy days and a new haze index named modified Normalized Difference Haze Index (m-NDHI) was developed. It revealed that the m-NDHI is not only sensitive to water but also to other land covers; however, NDHI is only sensitive to water and vegetation. Similarly, m-NDHI have more significant correlation coefficient with $PM_{2.5}$ as compared to $PM_{2.5}$ with NDHI. The correlation coefficient of m-NDHI and $PM_{2.5}$ is 0.7096, 0.5864 and 0.4857 in Beijing, Tianjin and Shijiazhuang, respectively. Moreover, this method can only be employed in detecting the light haze since it is hard to accurately discriminate between heavy haze and clouds.

Although the proposed index of NDHI can indicate the level of air pollution to some extent, the application is limited to the water areas. Therefore, comparing the spectral variation of different land covers between haze day and clear day, a new index of modified NDHI is developed in the form of m-NDHI=(MODIS1-MODIS3)/(MODIS1+MODIS3). This new index can detect the haze distribution and intension in large scales. Moreover, the value of m-NDHI can also detect the clouds, snow, bare soil and frozen ice with high atmosphere apparent reflectance. The future work will analysis the values of this index, and define specific threshold to separate the haze from surface features with high reflectance.

The application for m-NDHI index in the BTH region is quite viable. In addition, the modified NDHI can be used as a simple and effective means for monitoring the distribution and intension of air pollution from satellite imagery.

5. ACKNOWLEDGEMENTS

This study was supported by the Hundred Talents Program of CAS (No. Y24002101A), the National Natural Science Foundation of China (No. 31571565), the CAS-RADI 1-3-5Innovation Project (No. Y3ZZ15101A), the CASTWAS Project of Drought Monitoring in Asia (No. YEYI2701KB), and Universities Affiliated with the Hebei Province (No. Z2014090).

6. REFERENCES

Shang Liu, Min Hu, Zhijun Wu, Birgit Wehner, Alfred Wiedensohler, and Yafang Cheng (2008), "Aerosol number size distribution and new particle formation at a rural/coastal site in pearl river delta (prd) of china," Atmospheric Environment, vol. 42, no. 25, pp. 6275–6283.

China Meteorological Administration (2010), "Observation and forecasting levels of haze," in Meteorological Publishers 2010. Meteorological Publishers, Beijing, 2010, pp. 1–1.

Yong Zha, Jay Gao, Jianjun Jiang, Heng Lu, and Jiazhu Huang (2012), "Normalized difference haze index: a new spectral index for monitoring urban air pollution," International journal of remote sensing, vol. 33, no. 1, pp. 309–321.

Meina Li and Lulu Zhang (2014), "Haze in china: Current and future challenges," Environmental Pollution, vol. 189, pp. 85–86.

Y. Sun, G. Zhuang, A. Tang, Y. Wang, and Z. An (2006), "Chemical characteristics of pm2. 5 and pm10 in haze-fog episodes in beijing," *Environmental science & technology* **40**(10), 3148–3155.

NA Janssen, Gerard Hoek, Milena Simic-Lawson, Paul Fischer, Leendert Van Bree, Harry Ten Brink, Menno Keuken, Richard W Atkinson, H Ross Anderson, Bert Brunekreef, et al. (2011), "Black carbon as an additional indicator of the adverse health effects of airborne particles compared with pm10 and pm2. 5.," Environ Health Perspect, vol. 119, no. 12, pp. 1691–1699.

Kang Sun, Xingang Liu, Jianwei Gu, Yunpeng Li, Yu Qu, Junling An, Jingli Wang, Yuanhang Zhang, Min Hu, and Fang Zhang (2015), "Chemical characterization of size-resolved aerosols in four seasons and hazy days in the megacity beijing of china," Journal of Environmental Sciences, vol.32, pp. 155–167.

Ying Zhang and Zhengqiang Li (2015), “Remote sensing of atmospheric fine particulate matter (pm 2.5) mass concentration near the ground from satellite observation,” Remote Sensing of Environment, vol. 160, pp. 252–262.

JJ Cao, SC Lee, KF Ho, XY Zhang, SC Zou, Kochy Fung, Judith C Chow, and John G Watson (2003), “Characteristics of carbonaceous aerosol in pearl river delta region, china during 2001 winter period,” Atmospheric Environment, vol. 37, no. 11, pp. 1451–1460.

WARNING METHOD OF URBAN RAIL TRANSIT OPERATION SAFETY UNDER STRONG WIND

HAN. ZHIHUI, TAN JIANGUO and CHANG YUANYONG

Shanghai Institute of Meteorological Science, Shanghai, 200030, China.

Keywords: URBAN RAIL TRANSIT; WARNING METHOD; STRONG WIND; AERODYNAMIC CHARACTERISTICS

INTRODUCTION

Urban rail transit is one of the important traffic facilities for urban economic development and social service, is an important approach to alleviate the urban traffic congestion problem. However, with the increasing mileage and driving speed, urban rail transit safety problem is also growing, especially under the influence of bad weather. Urban rail transit has the characteristics of great quality, high speed and so on. The aerodynamic forces of rail transit vehicle under strong wind can influence its stability, even can lead to derailment accident, producing huge economic loss and casualty. Many developed countries have established different forms of road weather information systems (Wu Jianxia, 2011). The United States, Japan, France and other countries even integrate RWIS with existing intelligent transportation system, making use of accurate weather information to improve their traffic management(Lin Yu *et al.*, 2007). The Chinese meteorological department also has carried out monitoring of visibility, pavement temperature, wind, and forecasting methods research and related application systems development for highway, high-speed railway. But these research results are mainly based on meteorological observation data and conventional weather forecast products and services. There is also lack of refinement, pertinent service application technology. Referring to the above research results, it can be seen that development of warning method of rail transit operation safety is one of the effective methods to solve the problem. In this paper, taking Shanghai rail line 16 vehicle as a research object, the numerical wind tunnel method (Carrarini, 2007; Xi Yanhong, 2012) is used to analyze its aerodynamic characteristics, and a warning method of urban rail transit operation safety is explored by combining with AWS wind data.

METHODS

The vehicle of Shanghai rail transit line 16 is 71.6m long, 3 m wide and 3.055m high. CFD method is used to simulate aerodynamic force. In order to control the quality of grid, subdomain method and Size function is adopted to divide the computational domain. The grids is mainly hexahedral and cylinder. And grid refinement technique is used to simulate the violent flow change near the model (Fang Pingzhi, 2010). The total grid number is 2 million.

The aerodynamic force of rail transit vehicle is taken as a quantitative indicator of risk. Risk factor R, which is defined as the ratio of a kind of aerodynamic force to corresponding threshold, is used to measure risk under extreme windy weather. When rail transit vehicle runs under a limited speed, the aerodynamic force is the threshold. The expression of risk factor is as follows:

$$R = MAX[(\frac{F_S}{\Delta_S})_{side}, (\frac{F_L}{\Delta_L})_{lift}, (\frac{M}{\Delta_M})_{moment}] \quad (1)$$

Where F_S, F_L, M are lateral aerodynamic force, aerodynamic lift force and overturning moment, respectively. Δ_S, Δ_L, Δ_M are threshold, respectively.

CONCLUSIONS

The main conclusions are: the head vehicle close to the windward side is affected seriously by the wind loading; the wind direction has a great influence on aerodynamic force of rail transit vehicle. Under the condition of the same wind speed and vehicle speed, dose the rail delivery vehicle need speed limit or not depend on the judgment of the main wind direction; aerodynamic force of rail transit vehicle is more sensitive to wind speed. When the wind speed is doubled, the vehicle speed need to reduce more multiples in order to achieve security purposes; the proposed warning technology of rail transit vehicle operation safety can quickly give real-time safety risk level during a typhoon, provide sophisticated warning information of rail transit vehicle operation safety, greatly improve the decision accuracy of rail transit management department for the strong wind weather.

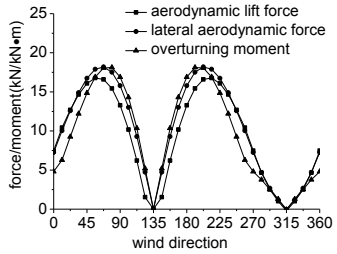

Fig.1 Aerodynamic force vs. wind direction

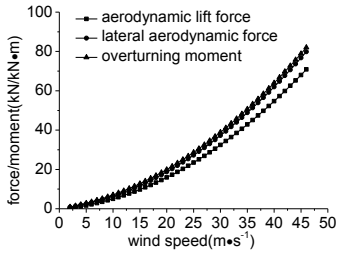

Fig.2 Aerodynamic force vs. wind speed

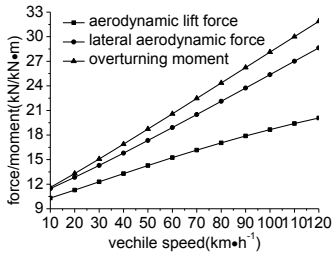

Fig.3 Aerodynamic force vs. vehicle speed

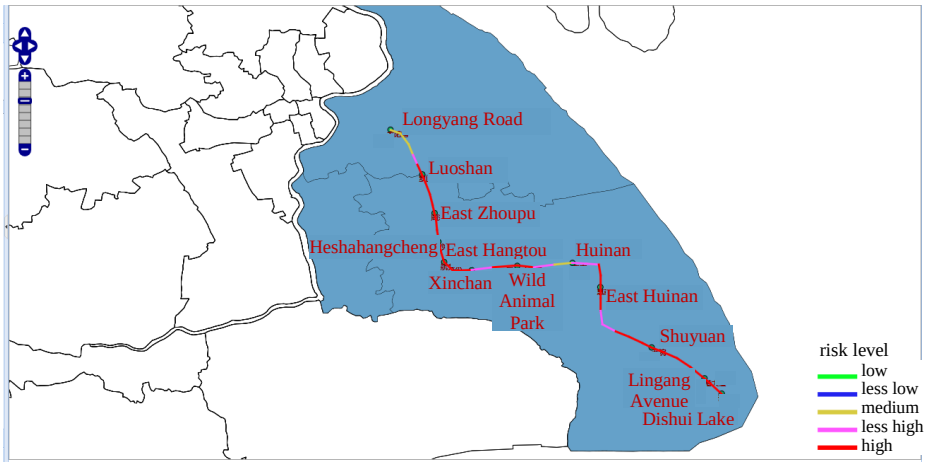

Fig.4 Risk level of rail transit operation safety during Chan-hom

ACKNOWLEDGEMENTS

This work was supported by China Special Fund for Meteorological Research in the Public Interest (Grant No. GYHY201306055), and the Research program of China Meteorological Administration (Grant No.CAMGJ2014M18).

REFERENCES

Wu Jianxia. The study of safety fore-warning system of freeway based on the typhoon weather. Fujian: Fujian Agriculture and Forestry University,2011.

Lin Yu, Fang Shouen. Driving speed management of high-grade highway under disastrous weather condition. Journal of Natural Disaster, 2007,16（5）:96-99

A Carrarini. Reliability based analysis of the crosswind stability of railway vehicles. Journal of Wind Engineering and Industrial Aerodynamics, 2007,95:493-509

Xi Yanhong. Research on Aerodynamic Characteristics and Operation Safety of High-speed Trains under cross winds. Beijing: Beijing Jiaotong Univerdity,2012

Fang Pingzhi, Gu ming, Tan Jianguo. Numerical wind fields based on the $k-\varepsilon$ turbulent models in computational wind engineering. Chinese Journal of Hydrodynamics, 2010, 25(4): 475-483.

ATMOSPHERE-LAND-LAKE CARBON CYCLE PROVIDES POSSIBILITIES FOR ECONOMIC STUDIES

J. HEISKANEN[1], I. MAMMARELLA[1], A. OJALA[2,3], T. VESALA[1]

[1]Department of Physics, University of Helsinki, P.O. Box 48, FI-00014 University of Helsinki, Finland

[2]Department of Forest Sciences, University of Helsinki, P.O. Box 27, FI-00014 University of Helsinki, Finland

[3]Department of Environmental Sciences, University of Helsinki, Niemenkatu 73, FI-15140 Lahti, Finland

Keywords: LAKES, GREENHOUSE GASES, BOREAL ZONE, ENVIRONMENTAL ECONOMICS, CARBON CYCLE

INTRODUCTION

Carbon cycle tightly links land ecosystems to aquatic environments. Significant part of the carbon fixed from the atmosphere to plant matter is leached to aquatic systems via rivers as organic carbon. Most of this carbon is processed in lakes resulting in high aquatic greenhouse gas emissions. Recent findings indicate that about 10 % of the terrestrial net ecosystem exchange is released back to the atmosphere from lakes (see Heiskanen 2015). However, considering land use and land-use change, carbon cycle is only limited to changes in carbon pools within the land ecosystem and to fluxes between the ecosystem and the atmosphere (IPCC 2006). This approach omits the loss of carbon from the ecosystem via streams and rivers to lakes.

In addition to greenhouse gas (GHG) fluxes, carbon is elemental component in creating the living conditions of aquatic ecosystems. Dissolved organic matter fundamentally affects the thermal structure via the absorption of solar radiation. Thermal structure plays a key role how atmospheric forcing, such as wind, influence the lake, as well as how gases and nutrients cycle within the lake. Some visible outcomes of these factors are magnitude of algal blooms and the quality of fish stocks.

Even though being fundamental, there is currently no economic value for carbon cycle in aquatic environments. This development has been hindered by our lack of understanding how elementary the aquatic carbon cycle is and especially how in various ways it is governed by aquatic physics, and due to difficulties in providing appropriate economic valuation to non-market resources, such as water quality or eutrophication.

APPROACH

Full understanding of the driving forces of climate change requires precise quantification of the greenhouse gas sources and sinks in and between different ecosystems. Carbon cycle in land-lake-atmosphere continuum is multifaceted problem and needs the expertise of many different scientific fields, which explains the lack of direct studies of carbon cycle in a scale this vast. However, research infrastructures such as PEEX or ICOS (Integrated Carbon Observation System) provide the needed framework for these studies, both the technical aspect (vast array of instruments and needed technicians) and the scientific aspect with experts from different fields. This solid science basis can then be utilized in detailed studies of environmental economics.

Hyytiälä is a unique multisite where extensive lake-atmosphere measurements on Lake Kuivajärvi are run simultaneously with different ecosystem-atmosphere measurements (Siikaneva station, SMEAR II station) in the lake's catchment. This allows to combine studies of carbon and nutrient dynamics in the catchment primary vegetation types to C and nutrient loading to the lake and to the processing and exporting of these substances within and from the lake. The results and insights of the related processes can be used to improve both lake and catchment modeling. This provides powerful tool to estimate the effect of different climate change scenarios and changes in land use, such as forest cuts, to the whole C cycle from sinks to sources.

There are many opportunities to link environmental economics to these studies. For example, carbon cycle could be valued as ecosystem service similarly as in a recent study concerning nitrogen loading (Andersen et al., 2015). On the other hand, changes in aquatic GHG emissions can be related to land-use change and climate-change-induced alterations in the catchment, and carbon emission trading schemes could then be utilized using market value for carbon fluxes.

CONCLUSIONS

Recent studies have shown the importance of inland waters for the carbon cycle even in global scale. Aquatic carbon cycle and physics are inseparably linked, and via aquatic physics, land-water-atmosphere carbon cycle can be valued economically. The physical aspects of the carbon cycle can be parameterized into modelling which allows generalizations made both in space (other regions) and in time (future and climate change). Economic approaches, such as impact pathway approach and carbon emission trading, can then used to estimate the value of the whole carbon cycle. This same approach can later on be expanded to include e.g. lake ecosystem services related to C cycle, such as fish stocks, water quality, biomass production and wildlife habitat.

Similar method could be applied to other sites thus widening the range of ecosystems, e.g. agricultural land, this approach covers. Since water flows, and related carbon and nutrient transport, connects different ecosystems together, related processes should be understood. This needs comprehensive direct measurements along the whole water and carbon cycle. Research infrastructures such as ICOS and PEEX are crucial platforms in solving these interdisciplinary questions.

REFERENCES

Andersen, M. S., Kronvang, B. et al. Conference paper in EAERE21, 2015.
Heiskanen, J. J. 2015. PhD thesis. University of Helsinki, department of physics.
IPCC, 2006. Guidelines for national greenhouse gas inventories. http://www.ipcc-nggip.iges.or.jp/public/2006gl/.

CHALLENGES FOR STABLE ATMOSPHERIC BOUNDARY LAYERS

PROF. DR AAM (BERT) HOLTSLAG

Meteorology and Air Quality, Wageningen University, the Netherlands (www.wageningenur.nl/maq)
Bert.Holtslag@wur.nl

ABSTRACT

In this talk an overview is given of the current understanding and model performance for stable atmospheric boundary layers. Many challenges still occur, in particular for clear skies and low wind speed conditions at night as well as during winter in stably stratified conditions over land and ice. Results from weather forecast and climate models are used to illustrate the state of the art as well as findings and recommendations from the Global Energy and Water Exchanges (GEWEX) Atmospheric Boundary Layer Study (GABLS).

RESUME

Prof. Bert Holtslag, is a Senior Professor of Meteorology and Chair of the Meteorology and Air Quality Section at Wageningen University, the Netherlands. His research focusses on modeling and conceptual analysis of observations dealing with atmosphere-land interactions, surface fluxes, boundary layer processes, wind energy and urban meteorology. He is a fellow of the American Meteorological Society and (co-) author of more than 400 scientific publications, including about 140 well-cited peer reviewed articles in the international atmospheric scientific literature.

RETRIEVE THE ORGANIC VOLATILITY DISTRIBUTION OF SUBMICRON AEROSOLS IN A BOREAL FOREST ENVIRONMENT USING A KINETIC EVAPORATION MODEL

J. HONG[1], M. ÄIJÄLÄ[1], S. HÄME[1], L. HAO[2], J. DUPLISSY[1,3], L. HEIKKINEN[1], J. MIKKILÄ[1], M. EHN[1], W. NIE[4], P. J. PASSONEN[1], M. KULMALA[1], D. R. WORSNOP[5], T. PETÄJÄ[1], I. RIIPINEN[6], V.-M. KERMINEN[1]

[1]Department of Physics, University of Helsinki, P.O. Box 64, 00014 Helsinki, Finland.

[2]Department of Physics and Mathematics, University of Eastern Finland, Kuopio, Finland.

[3]Helsinki Institute of Physics, University of Helsinki, P.O. Box 64, 00014 Helsinki, Finland.

[4]Institute for Climate and Global Change Research & School of Atmospheric Sciences, Nanjing University, Nanjing, 210093, China

[5]Aerodyne Research, Inc., Billerica, Massachusetts, USA

[6]Department of Applied Environmental Science, Stockholm University, 10961 Stockholm, Sweden

Keywords: VOLATILITY, SOA, KINETIC EVAPORATION MODEL.

INTRODUCTION

Atmospheric aerosols influence Earth's climate both directly and indirectly through affecting the radiation balance, altering the albedo, lifetime and precipitation patterns of clouds (IPCC 2013). However, inadequate determination of the spatial and temporal variability of the aerosol size distribution, chemical composition and physical-chemical properties make it very difficult to quantify the aerosol climatic effects. The physical-chemical properties of the aerosol size distribution vary largely in the atmosphere (e.g. Jimenez et al., 2009). In terms of aerosol chemical composition measurement, the biggest challenges are due to the presence in the aerosol particles of a vast number of different organic components. One of key physical-chemical properties of organics is volatility, which describes the affinities of different species partitioning between the gas and particle phase. Atmospheric aerosol particles are mixtures of organic and inorganic compounds having different volatilities. Volatilities of inorganic species are relatively well known, while information on volatility of organic species still remains poor.

Different species evaporate at different temperatures regarding to their saturation concentration and enthalpies of vaporization at that temperature (Kreidenweis et al., 1998). Therefore, measuring the evaporation of the particles at different temperatures, helps on getting information on the chemical composition of particles. Quantitative information on the volatility distribution can further be derived by coupling the volatility measurement data, with a kinetic evaporation model of Riipinen et al. (2010), which described the evaporation rate of aerosols inside a heated flow tube. In this presentation, we report, for the first time, quantitative information on volatility distribution of organic species of ambient aerosol formed in boreal environment.

METHODS

The measurements were carried out during 14 April to 31 May 2014 at SMEAR II (Station for Measuring Ecosystem-Atmosphere Relations II), located in Hyytiälä, Southern Finland, and surrounded by pine forest (Hari and Kulmala, 2005). Volatility measurements were conducted for particles of 30 nm, 60 nm 100 nm and 145 nm using a Volatility Tandem Differential Mobility Analyzer (VTDMA), which is part of

a Volatility-Hygroscopicity Tandem Differential Mobility Analyzer (VH-TDMA) system (Hong et al., 2014). The heating temperature of the setup ramped from 25 °C to 280 °C with a time resolution of around one hour. The VTDMA measures for each temperature and particle size the Mass Fraction Remaining (MFR). MFR describes the percentage of remaining mass of the particle after traveling through the thermodenuder. MFR equals 1 if the particle is non-volatile, and MFRs is equal to 0 if the particle fully evaporates. In addition, a High-Resolution Aerosol Mass Spectrometer (HR-AMS) was used to determine the chemical composition of aerosol particles during the experimental period.

We use a kinetic evaporation model (Riipinen et al., 2010), based on the mass transfer theory, to simulate the evaporation of the aerosols inside the thermodenuder. According to Donahue et al. (2013), components with different effective saturation vapour concentration ($1e^{-5}$, 0.1, 5 $\mu g/m^3$) are referred to be extremely low volatile (ELVOC), low volatile (LVOC) and semi-volatile (SVOC) compounds respectively. In the model, we use as an input a mixture of three compounds having the characteristic effective saturation vapour concentration of ELVOC, LVOC and SVOC and an effective vaporization enthalpy of 65 KJ/mol. As a result, the corresponding average volatility distribution of the ambient aerosol is obtained by letting the difference between the measured and modelled evaporation of the ambient aerosol to reach a minimum with a certain pair of mass fraction of all these three components.

PRELIMILARY RESULTS

Figure 1 shows the optimum solution of the volatility distribution by minimizing the difference between the measured (blue solid line) and modeled evaporation (black solid line) for a certain day among the campaign. In this example, there is a substantial amount of extremely low volatile compounds in 100 nm particles. These compounds could be inorganic salts, extremely low volatile organics or organic salts with low volatility.

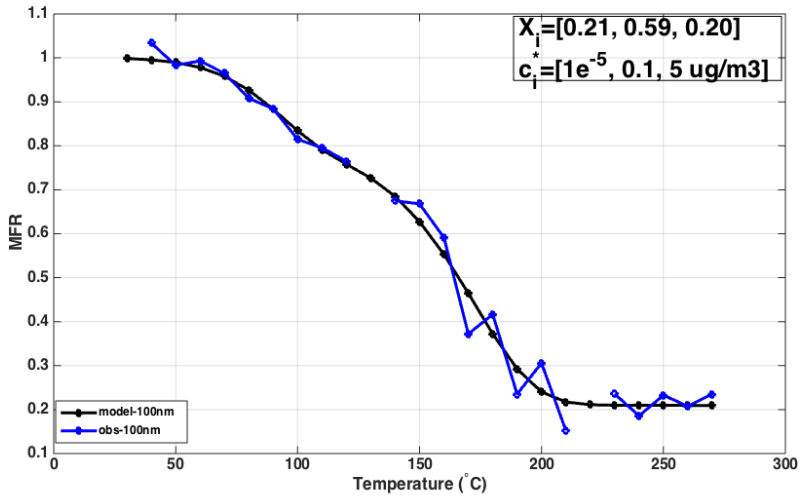

Figure 1: Example of measured and modelled evaporation of ambient aerosols upon to different heating temperatures for a certain day during the campaign. As a result of the agreement between the model and the data, the different mass fraction of extremely low volatile, low volatile and semi volatile compounds were obtained.

ACKNOWLEDGEMENTS

This work was supported by the Academy of Finland Center of Excellence (grant no. 272041), European Research Council (ATM-NUCLE), University of Helsinki funds, and European Commission (ACTRIS, N° 262254).

REFERENCES

Donahue, N. M.; et al (2013). How do organic vapors contribute to new-particle formation? Faraday Discuss. 165 (0) 91, DOI: 10.1039/c3fd00046j.

Hari, P. and Kulmala, M (2005). Station for measuring ecosystem- atmosphere relations (SMEAR II), Boreal Env. Res., 10, 315–322.

Hong, J., et al (2014). Hygroscopicity, CCN and volatility properties of submicron atmospheric aerosol in a boreal forest environment during the summer of 2010, Atmos. Chem. Phys., 14, 4733-4748, doi:10.5194/acp-14-4733-2014.

IPCC 2013. Climate change 2013: the physical science basis. Working Group I Contribution to the Fifth Assessment Report of the Intergovernmental Panel on Climate Change, Cambridge University Press, Cambridge, United Kingdom and New York, NY, USA.

Jimenez, J. L., et al (2009). Evolution of organic aerosols in the atmosphere, Science., 326, 1525–1529, doi:10.1126/science.1180353.

Kreidenweis, S. M., et al (1988). Observations of Aerosol Volatility and Elemental Composition at Macquarie Island during the First Aerosol Characterization Experiment (ACE1), J. Geophys. Res., 103:16, 511.

Riipinen I., et al (2010). Equilibration time scales of organic aerosol inside thermodenuders: Kinetics versus equilibrium thermodynamics, Atmos. Environ., 44, 597–607.

COMPREHENSIVE MODELLING STUDY ON NEW PARTICLE FORMATION AT THE SORPES STATION IN NANJING

X. HUANG[1,2], L. X. ZHOU[3,4], A. J. DING[1,2,*], X. M. QI[1,2], W. NIE[1,2], M. H. WANG[1,2], X. G. CHI[1,2], T. PETAJA[3], V.-M. KERMINEN[3], P. ROLDIN[3], A. RUSANEN[3], M. KULMALA[3], M. BOY[3]

[1]Institute for Climate and Global Change Research & School of Atmospheric Sciences, Nanjing University, Nanjing, 210023, China

[2]Collaborative Innovation Center of Climate Change, Nanjing, Jiangsu Province, China

[3]Department of Physics, University of Helsinki, P. O. Box 64, 00014 University of Helsinki, Finland

[4]Helsinki University Centre for Environment, P. O. Box 65, 00014 University of Helsinki, Finland

Keywords: NEW PARTICLE FORMATION, SORPES, WRF-CHEM, MALTE-BOX MODEL.

INTRODUCTION

Atmospheric new particle formation (NPF), characterized by a sharp increase in number concentration of nucleation-mode aerosol, has been observed under a wide variety of circumstances and has been shown as a significant source of atmospheric fine particles. As the newly formed particles and their following growth may lead several-fold increases in aerosol number concentrations, atmospheric NPF could substantially contribute to the global CCN (Cloud condensation nuclei) budget and its subsequent cooling effect. It is well known that particle formation in the atmosphere is strongly dependent on the abundance of sulphuric acid (Weber et al., 1999; Kulmala et al., 2004). Meanwhile, other compounds in the atmosphere may be responsible for NPF occurrence in different environments. Iodine-containing vapours were identified as the precursors for marine new particle formation (O'Dowd et al., 2002). Observations in Pittsburgh imply that ammonia could considerably enhance the atmospheric particle formation (Zhang et al., 2004). In the boreal forest, oxidation products of monoterpenes together with sulphuric acid were very likely to lead to NPF (Schobesberger et al., 2013) and new findings indicate that organic amines (e.g. dimethylamine) can enhance water-sulphuric acid particle formation rates more than 1000-fold compared to ammonia (Almeida et al., 2013). In addition to direct in-situ observations of NPF events, model simulation has been serving as a useful tool for analysing NPF dynamics since 1990s. In recent years, MALTE model has been successfully utilized in NPF analysis, for instance, reproducing OH radical and gaseous sulphuric acid levels (Petaja et al., 2009), validating various plausible nucleation mechanisms and particle growth (Boy et al., 2007), and identifying important factors influencing NPF occurrence (Boy et al., 2006).

As one of the most economically invigorating and densely populated countries, China features simultaneous high aerosol loadings and NPF rates (Guo et al., 2012). Moreover, the condensational growth of nucleation-mode particles has been indicated as a plausible cause of regional haze events (Guo et al., 2014). Since 2000s, several field campaigns as well as long-term measurements have been conducted in several regions such as Beijing, the Pearl River Delta as well as the Yangtze River Delta, showing high occurrence frequencies and formation rates across China (Gao et al., 2009; Yue et al., 2010; Herrmann et al., 2014; Qi et al., 2015). However, modelling studies that provide a further insight into the processes of atmospheric aerosol formation, are still very limited in China. Numerical simulations of formation and growth processes usually require detailed and high time-resolving measurements of the relevant compounds, however, hardly can any field campaign or in-situ measurement station in China meet this requirement. The novel combination of a regional chemical transport model and a zero-dimensional box model with detailed aerosol dynamics makes it possible to accomplish NPF studies without direct measurements of all specific chemical species. Here, we present a comprehensive

modelling study targeting at reproducing observed NPF events under distinct conditions at the Station for Observing Regional Processes of the Earth System (SORPES) at Nanjing University in Nanjing, China (Ding et al., 2013a). This is the first attempt to integrate the regional model, box model and in-situ measurements to investigate NPF events in China, enabling us to gain more insights into NPF mechanism in the YRD region.

METHODS

On-line and high time-resolving measurements of trace gases, aerosol characteristics, and relevant meteorological parameters have been conducted since the summer of 2011. Ozone (O3), sulphur dioxide (SO2), nitrogen monoxide (NO), nitrogen dioxide (NO2), total reactive nitrogen (NOy), carbon monoxide (CO) and PM2.5 (fine particulates less than 2.5 microns in aerodynamic diameter) are routinely measured by Thermo Instruments (TEI 49i, 43i, 42i, 42iY and 48i) and MARGA (Monitor for Aerosols & Gases in Ambient Air) (Ding et al., 2013a,b). The Differential Mobility Particle Sizer (DMPS) coupling a differential mobility analyzer with two different flow rates and a condensation particle counter are used to measure number distributions of atmospheric particles from 6 to 800 nm.

MALTE is a one-dimension model comprising of boundary layer meteorology, biogenic emission of volatile organic compounds, gas-phase chemistry and aerosol dynamics in order to predict particle formation and growth processes under atmospheric conditions (Boy et al., 2006). Here, we apply the zero-dimensional version, namely, MALTE-BOX model, to simulate NPF events at the SORPES station. In the MALTE-BOX model, boundary layer meteorology and biogenic emission modules are switched off; instead, the biogenic and anthropogenic VOC emissions and their following transport and dispersion are calculated by the regional chemical transport model WRF-Chem. Concentration of various organic compounds at the SORPES station predicted by WRF-Chem model are inputted into MALTE-BOX model every 10 minutes. Likewise, measured concentrations of trace gases including CO, SO_2, NO, NO_2 and O_3, with the same temporal resolution, are also included as input fields. In addition to gas phase precursors, the inputs also include an initial particle number size distribution at 0:00 LT on each day, ambient temperature, relative humidity and the condensation sink of sulphuric acid. In the MALTE-BOX model, particles are assumed to be spherical. Fixed sectional approach with 40 size bins ranging from 1.4 to 2000 nm in diameter is used in the present study. The aerosol dynamics has all basic aerosol processes, including nucleation, condensation, coagulation, and deposition. The new particle formation rates of newly formed clusters are estimated by the kinetic nucleation theory of sulphuric acid. Apart from sulphuric acid, about twenty low-volatility organic compounds (ELVOCs) and seven selected semi-volatile organic compounds (SVOCs) are regarded as condensing vapours, following the simplified chemical mechanism presented by Ehn et al. (2014).

The WRF-Chem version 3.6 was used here to estimate concentrations of various organic vapours from anthropogenic and biogenic emissions as there was no VOCs measurement at the SORPES site during the study period. WRF-Chem is an online three-dimensional, Eulerian chemical transport model that considers the complex physical and chemical processes, such as emission and deposition of pollutants, advection and diffusion, gaseous and aqueous chemical transformation, aerosol chemistry and dynamics (Grell et al., 2005). In this study, the model domain covered East China and its surrounding area, centring at 32.0°N, 119.0°E with a 20×20 km grid resolution. There are 24 vertical layers from the ground level to the top pressure of 50 hPa, in which 10 layers are placed under 1 km to better resolve the boundary layer process. The 6 hourly Final operational global analysis (FNL) data with a 1°× 1° spatial resolution produced by the National Centres for Environmental Prediction (NCEP) was used as initial and boundary conditions of meteorological fields. The simulations were conducted for June to August 2013 when NPF events were frequently detected (Qi et al., 2015). During the simulation period, each run covered 60 hours, in which the first 12 hours were just for model spin-up and the last 48-hour results were adopted for following analysis and box modelling. Anthropogenic emissions from power plants, residential combustion, industrial processes, on-road mobile sources and agricultural activities were derived from the MEIC database (Multi-resolution Emission Inventory for China, see www.meicmodel.org). Emissions of major

pollutants, such as carbon monoxide, sulphur dioxide, nitrogen oxides, ammonia and speciated VOCs are all included in this emission inventory database. MEGAN (Model of Emissions of Gases and Aerosols from Nature, version 2) module embedded in WRF-Chem is used to calculate biogenic emissions online (Guenther et al., 2006). It estimates the net emission rates of isoprene, monoterpene and other biogenic VOCs from terrestrial ecosystems into the above-canopy atmosphere. Gas-phase chemistry is explicitly represented by the model through the SAPRC photochemistry scheme (Carter, 1999), which includes 225 gas-phase reactions among 81 chemical species in the model.

RESULTS

Summer marks the season with frequent NPF events at the SORPES site, especially in the year of 2013. From June to August 2013, 50 NPF events were detected during the 76-day measurement period when DMPS functioned normally, resulting in the particle formation probability of 66%. Among the observed NPF events, three representative cases were identified according to the retroplumes calculated based on Lagrangian dispersion model HYSPLIT (Hybrid Single Particle Lagrangian Integrated Trajectory Model) following the method developed by Ding et al., (2013c). These selected NPF days are 22 June, 10 July and 22 August 2013, when the site was dominantly influenced by air masses from the YRD region, South China, and mixed ocean and continental areas, respectively (Fig. 1).

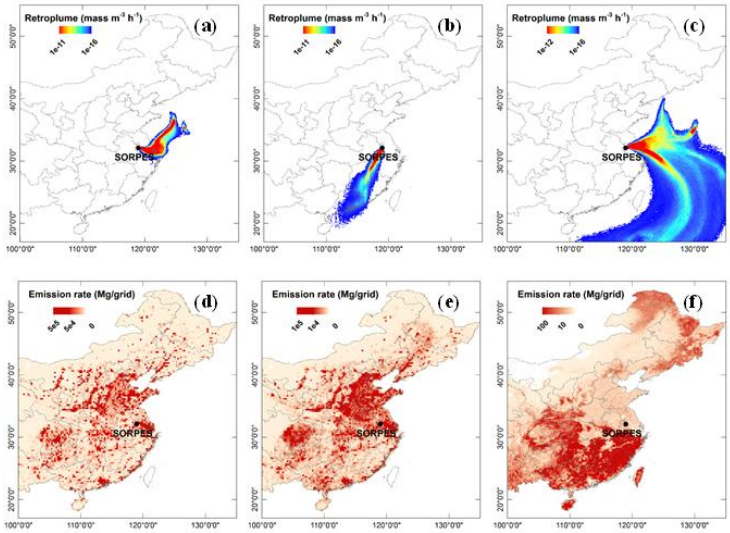

Figure 1. Retroplume (footprint residence time) showing transport pathways of air masses measured at the SORPES site for 22 June (a), 10 July (b) and 22 August(c). Spatial distributions of anthropogenic SO_2 (d), primary $PM_{2.5}$ (e) and biogenic monoterpene (f) emission rates.

Modelled VOC concentrations, which are vital for NPF simulation, are included as an input field in the MALTE-BOX model. Although there was no VOC measurement during the summer of 2013, the SORPES site and the Environmental Monitoring Centre of Jiangsu Province (118°47'E, 32°4'N) were equipped with GC/MS (gas chromatography/mass spectrometry) in the summer of 2014. In order to evaluate model's performance in simulating VOC concentrations, we conducted another WRF-Chem run for the August of 2014 and then compared the model results with corresponding observations. The comparison of alkene, aromatic and isoprene concentrations in Fig. 2(a-c) illustrates that WRF-Chem is capable of reproducing the magnitude and temporal variations of VOC concentration originating from both anthropogenic and biogenic sources. Specifically, modelled results tend to underestimate alkene concentration but over predict aromatic level with normalized mean bias of -11% and 20%, similar to previous simulations for Shanghai (Tie et al., 2013). There still exist substantial uncertainties in China's

anthropogenic VOC emission inventory, particularly speciated estimations, which was ascribed to uncertainties in the activity data, limited direct experiments on emission factors and source profiles. Large biases in model-predicted aromatic level are expectable since it mainly emitted from petrochemical plants, gasoline vehicle and biomass burning with greater uncertainties in activity level estimation. In term of biogenic VOC, simplification in vegetation classification and numerical descriptions, limited understanding of controlling factors could introduce biases in modelled levels of BVOCs.

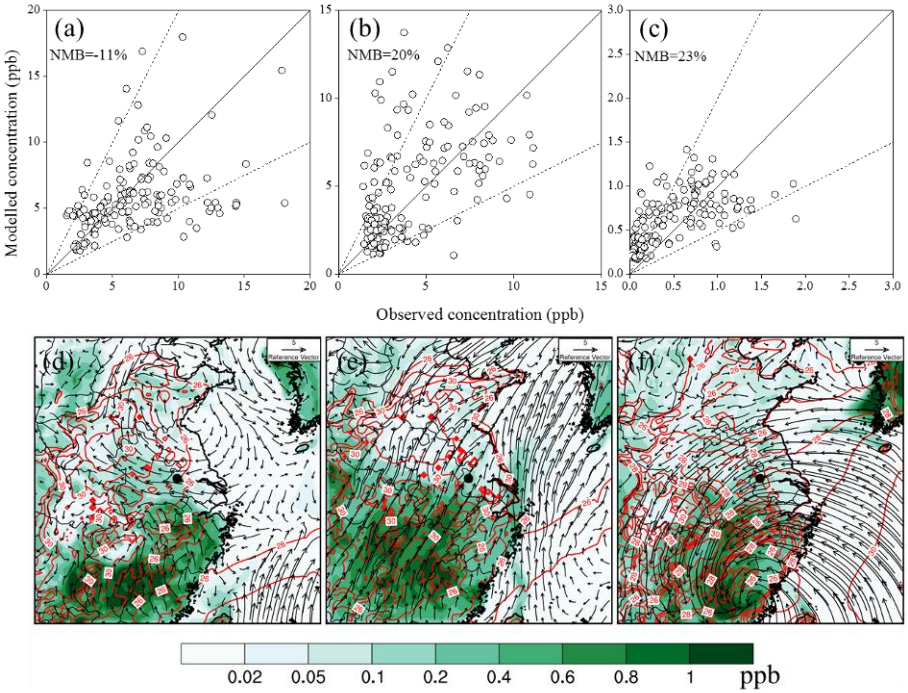

Figure 2. Scatter plots of observed and simulated alkene (a) aromatic (b) and isoprene (c) concentrations (NMB represents the normalized mean bias) in August 2014. The solid 1:1 lines and dashed 1:2 and 2:1 lines are shown for reference. Spatial distributions of terpene concentrations at 9:00 LT on 22 June (d), 10 July (e), and 22 August (f), 2013. 2-meter temperature are marked in red lines.The black dot marks the location of the SORPES station.

On 22 June 2013, a clear banana-shaped particle size distribution was captured by the DMPS in the morning (9:00-11:00 LT, Fig. 3). According to the DMPS observations, the number concentration of particles with diameter ranging from 6 to 30 nm reached up to 10,000 # cm-3 around 10:00 LT. The formation rate of 6 nm particles, namely J_6, was 7.6 cm^{-3} s^{-1}. This NPF event featured a large background particle loading with $PM_{2.5}$ mass concentration exceeding 50 μg m^{-3} because the air mass was lingering over city clusters in the YRD region before approaching the SORPES station, as shown in Fig. 1(a). Dense particle emissions from the rapidly urbanized and industrialized YRD region (Fig. 1(e)) corresponded to a high condensation sink of 4.2×10^{-2} s^{-1} (Table 1). The model system does reproduce the occurrence of these three NPF events although they were under distinct meteorological conditions and affected by entirely different potential source regions. On 22 June when measured air masses originated from the urbanized YRD region, the calculated onset of activation of freshly formed cluster to grow above the 6 nm line appeared around 08:30 LT. According to the diurnal pattern of simulated concentrations of gaseous compounds illustrated in Fig. 4, the OH radical level increased rapidly from 1×10^5 to 3×10^6 # cm^{-3} just after sunrise, promoting the gaseous oxidation of SO_2 in the atmosphere and subsequent accumulation of sulphuric acid from nealy zero to around 5×10^6 # cm^{-3}. Simultaneously, the pre-existing particle concentration dropped down due to the boundary layer evolution. The continuously growing sulphuric acid concentration and decreasing condensation sink jointly led to this fast NPF event. Simulated J_6 was

9.3 cm^{-3} s^{-1}, slightly higher than the observed value of 7.6 cm^{-3} s^{-1}. Among different kinds of condensing vapours, sulphuric acid contributed most to the growth of newly formed particles. While considering the growth of particles less than 10 nm in diameter, sulphuric acid's contribution accounted for more than 50%. The reason is that, influenced by air mass from the emission-intensive YRD region, SO_2 was reaching up to 20 ppb and the contribution of sulphuric acid on this day was much higher compared with the other two days. $GR_{6\text{-}30}$ was simulated to be 6.9 nm h^{-1}, about half of that derived from measurements. Overestimated newly formed clusters might be one reason for smaller simulated $GR_{6\text{-}30}$. Another, as described before, condensing vapours in the box model only included biogenic low volatile compounds. However, aromatic-related oxidation products have been suspected to be contributing to particle growth, especially in polluted area like China (Yue et al., 2010). Failing to characterize condensing vapour originating from anthropogenic organic compounds might be another cause for under predicted growth rate.

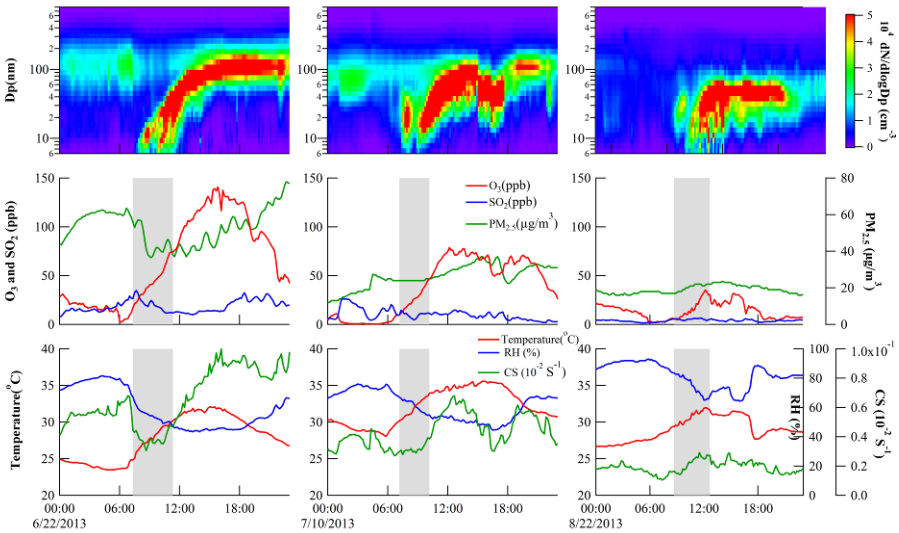

Figure 3. Measured diurnal variations of particle size distributions (upper panel), concentrations of SO_2, O_3 and $PM_{2.5}$ (middle panel), meteorological conditions and condensational sinks (bottom panel) during the three NPF days. Grey boxes show the time span of NPF events.

Table 1. Formation rate of 6-nm particles (J_6), and particle growth rates from 6 to 30 nm ($GR_{6\text{-}30}$) of 3 NPF events based on DMPS measurements and numeric modelling[a].

	Date	J_6 (cm^{-3} s^{-1})	$GR_{6\text{-}30}$ (nm h^{-1})	CS (10^{-2} s^{-1})
Case1	20130622	7.6(9.3)	12.6(6.9)	4.2
Case2	20130710	1.2(1.6)	13.5(10.7)	3.2
Case3	20130822	3.4(10.0)	15.7(2.3)	1.9

[a]values out of the parentheses are observations and those in the parentheses represent the corresponding model results.

On 10 July when the air masses mostly came from the densely wooded area in South China, NPF showed much lower new particle formation rates than on 22 June, yet a slightly faster particle growth rate (Table 1). Fig. 1(f) presents the spatial distribution of monoterpene emission rates during summertime across China calculated by the MEGAN model. It is obvious that monoterpene emission is overwhelmingly intensive in South China, which is covered by large areas of broadleaf forests and shrubs. It is plausible

that air masses passed over biogenic VOC-rich regions were saturated with sufficiently low volatile oxidation products, which enhanced the observed particle growth. The simulation results from the WRF-Chem model supported this view. Modelled isoprene and terpenes concentrations were 1.2 and 0.15 ppb at the SORPES site during NPF on 10 July, 150% and 50% higher than the corresponding values on 22 June. The OH radical concentration was mostly less than 1×10^{6} # cm^{-3}. The production of sulphuric acid was expected to be relatively slow due to the simultaneous lower concentrations of both SO_2 and OH radical. As demonstrated in Fig. 4, the concentration of sulphuric acid was approximately 3×10^{5} # cm^{-3} just when the NPF started, about one-tenth and one-seventh of the corresponding values on 22 June and 22 August, respectively. Nonetheless, prevailing south-westerly winds brought along terpenes-rich air masses. Some of the terpenes, such as alpha-pinene and limonene, feature significantly high yields of ELVOCs as well as SVOCs while reacting with ozone or OH radicals (Ehn et al., 2014). Such dense low volatile oxidation products substantially enhanced condensational growth of newly formed particles. The individual contributions from sulphuric acid, SVOCs, ELVOCs to growth of newly formed particles indicated that biogenic low volatile compounds overwhelmingly dominated in the very initial stage of cluster growth with contribution as high as 95%, demonstrating a vital role of ELVOCs and SVOCs in this NPF event.

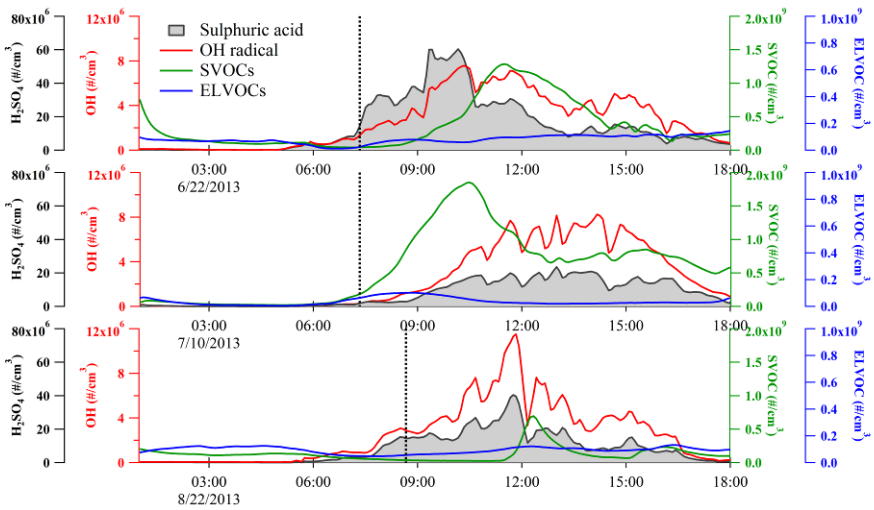

Figure 4. Time series of several gas concentrations (# cm^{-3}) during the three selected NPF days. Sulphuric acid, OH radical, SVOCs and ELVOCs are marked in grey area, red, green and blue lines, respectively. Dashed lines show the onset time of NPF according to DMPS measurements for reference.

Another NPF event, characterized by mixed marine and continental source regions, occurred on 22 August. Because of relatively clean air from the ocean and high wind speed of around 8 m s^{-1}, $PM_{2.5}$ and SO_2 concentrations were unusually low, only 11.0 μg m^{-3} and 2.8 ppb when NPF event took place. Accordingly, the condensation sink fell down to 1.9×10^{-2} s^{-1}. Existing measurements and analysis concluded that the main obstacle for the initial onset of new particle formation at the SORPES site is condensation sink, since SO_2 concentration is always high and there tends to be enough solar radiation as well (Herrmann et al., 2014). So, even though the SO_2 concentration was pretty low during that day, a fairly small condensation sink could trigger the onset of this NPF event. The nuclei growth rate, $GR_{6\text{-}30}$, was estimated to be 15.7 nm h^{-1}. Unlike during the first two NPF cases, the level of pre-existing particles was unusually low during the third event because a strong wind from the ocean swept over East China. The clean air mass reduced the condensation sink (see Table 1 and Fig. 3), much lower than the values typically observed at the SORPES site before. Even though SO_2 concentrations were pretty low, sulphuric acid accumulated remarkably and probably initiated this NPF event. As listed in Table 1, during Case 3 when the air mass originated partly over the Shanghai and surrounding city clusters, the model underpredicted the growth rate nearly by a factor of 7 and overestimates the particle formation rate by 3 times. This means that most probably anthropogenic low volatile compounds not included in the model were contributing to the growth and decreased the surviving probability of the newly formed clusters in

the model. It is completely opposite for Case 2 when the air mass originated not from strong anthropogenic influenced areas and the model outcome was in good agreement with the measurements.

CONCLUSIONS

This study combines the regional chemical transport model and box model to investigate atmospheric new particle formation and its subsequent nuclei condensational growth at the SORPES site in Nanjing, China. This combination makes it possible to simulate chemical and aerosol dynamical processes. Three NPF cases, during which entirely different potential source regions influenced the experimental site, were successfully reproduced by the modelling system. When the site was predominately influenced by air masses from city clusters in the YRD region on 22 June, 2013, despite a high condensation sink, the NPF event featured fast new particle formation rate due to the continuously accumulating sulphuric acid. Under the circumstance that biogenic VOC-rich air masses dominated, rapid growth of freshly formed particle was detected on 10 July, 2013, which was predominately attributed to the low-volatility oxidation products of terpenes. Air masses from marine origin could lead to the relatively low condensation sink on 22 August, 2013, thereby facilitating the occurrence of NPF event. On the basis of measurements and the corresponding modelling, we infer the controlling factors of the selected three NPF events, and these were mostly associated with sulphuric acid accumulation and low condensation sink. The comparison with the observations suggested that low-volatility organic compounds, including both SVOCs and ELVOCs, played a substantial role in the initial condensational growth of newly formed particles, particularly when the station was influenced by air masses originated from the South China. In addition, anthropogenic VOCs and the following photochemical oxidation produce a considerable amount of condensable compounds, exerting a significant impact on particle growth in the emission-intensive YRD region. Although some inadequacies still remain, such as the inclusion of anthropogenic non-volatile organic compounds as condensable vapours, the comprehensive modelling work provides a better insight of NPF processes.

ACKNOWLEDGEMENTS

This work was supported by the National Natural Science Foundation of China (D0512/41422504, D0510/41505109, D0512/91544231 and D512/41305123), the National Key Technology Research and Development Program (2014BAC22B02) and the Science and Technology Support Program of Jiangsu Province (SBE2014070928). Part of this work was supported by the Jiangsu Provincial Science Fund for Distinguished Young Scholars awarded to A. J. Ding (No. BK20140021) and by the Academy of Finland projects (1118615, 139656) and the European Commission via ERC Advanced Grant ATM-NUCLE. We also thank the financial support from Helsinki University Centre of Environment (HENVI).

REFERENCES

Almeida, J., Schobesberger, S., Kurten, A., Ortega, I. K., Kupiainen-Maatta, and coauthors: Molecular understanding of sulphuric acid-amine particle nucleation in the atmosphere, Nature, 502, 359-363, doi:10.1038/Nature12663, 2013.

Boy, M., Bonn, B., Kazil, J., Lovejoy, N., Turnipseed, A., Greenberg, J., Karl, T., Mauldin, L., Kusciuch, E., and Smith, J.: Relevance of several nucleation theories in different environments, in: Nucleation and Atmospheric Aerosols, Springer, 87-91, 2007.

Boy, M., Hellmuth, O., Korhonen, H., Nilsson, E. D., ReVelle, D., Turnipseed, A., Arnold, F., and Kulmala, M.: MALTE - model to predict new aerosol formation in the lower troposphere, Atmos. Chem. Phys., 6, 4499-4517, 2006.

Carter W. P. L. Documentation of the SAPRC-99 chemical mechanism for VOC reactivity assessment, University of California, Riverside, CA, 446 pp.,1999.

Ding, A. J., Fu, C. B., Yang, X. Q., Sun, J. N., Petaja, T., Kerminen, V. M., Wang, T., Xie, Y., Herrmann, E., Zheng, L. F., Nie, W., Liu, Q., Wei, X. L., and Kulmala, M.: Intense atmospheric pollution modifies weather: a case of mixed biomass burning with fossil fuel combustion pollution in eastern China, Atmos. Chem. Phys., 13, 10545-10554, doi:10.5194/acp-13-10545-2013, 2013b.

Ding, A. J., Fu, C. B., Yang, X. Q., Sun, J. N., Zheng, L. F., Xie, Y. N., Herrmann, E., Nie, W., Petaja, T., Kerminen, V. M., and Kulmala, M.: Ozone and fine particle in the western Yangtze River Delta: an overview of 1 yr data at the SORPES station, Atmos. Chem. Phys., 13, 5813-5830, doi:10.5194/acp-13-5813-2013, 2013a.

Ding, A. J., Wang, T., and Fu, C. B.: Transport characteristics and origins of carbon monoxide and ozone in Hong Kong, South China, J Geophys Res-Atmos, 118, 9475-9488, 10.1002/jgrd.50714, 2013c.

Ehn, M., Thornton, J. A., Kleist, E., Sipila, M., Junninen, H., Pullinen, I., Springer, M., Rubach, F., Tillmann, R., Lee, B., Lopez-Hilfiker, F., Andres, S., Acir, I. H., Rissanen, M., Jokinen, T., Schobesberger, S., Kangasluoma, J., Kontkanen, J., Nieminen, T., Kurten, T., Nielsen, L. B., Jorgensen, S., Kjaergaard, H. G., Canagaratna, M., Dal Maso, M., Berndt, T., Petaja, T., Wahner, A., Kerminen, V. M., Kulmala, M., Worsnop, D. R., Wildt, J., and Mentel, T. F.: A large source of low-volatility secondary organic aerosol, Nature, 506, 476-479, doi:10.1038/Nature13032, 2014.

Gao, J., Wang, T., Zhou, X. H., Wu, W. S., and Wang, W. X.: Measurement of aerosol number size distributions in the Yangtze River delta in China: Formation and growth of particles under polluted conditions, Atmos. Environ., 43, 829-836, doi:10.1016/j.atmosenv.2008.10.046, 2009.

Grell, G. A., Peckham, S. E., Schmitz, R., McKeen, S. A., Frost, G., Skamarock, W. C., and Eder, B.: Fully coupled “online” chemistry within the WRF model, Atmos. Environ., 39, 6957-6975, 2005.

Guo, H., Wang, D. W., Cheung, K., Ling, Z. H., Chan, C. K., and Yao, X. H.: Observation of aerosol size distribution and new particle formation at a mountain site in subtropical Hong Kong, Atmos. Chem. Phys., 12, 9923-9939, doi:10.5194/acp-12-9923-2012, 2012.

Herrmann, E., Ding, A. J., Kerminen, V. M., Petaja, T., Yang, X. Q., Sun, J. N., Qi, X. M., Manninen, H., Hakala, J., Nieminen, T., Aalto, P. P., Kulmala, M., and Fu, C. B.: Aerosols and nucleation in eastern China: first insights from the new SORPES-NJU station, Atmos. Chem. Phys., 14, 2169-2183, doi:10.5194/acp-14-2169-2014, 2014.

Kulmala, M., Vehkamaki, H., Petaja, T., Dal Maso, M., Lauri, A., Kerminen, V. M., Birmili, W., and McMurry, P. H.: Formation and growth rates of ultrafine atmospheric particles: a review of observations, J. Aerosol. Sci., 35, 143-176, doi:10.1016/j.jaerosci.2003.10.003, 2004b.

O'Dowd, C. D., Jimenez, J. L., Bahreini, R., Flagan, R. C., Seinfeld, J. H., Hameri, K., Pirjola, L., Kulmala, M., Jennings, S. G., and Hoffmann, T.: Marine aerosol formation from biogenic iodine emissions, Nature, 417, 632-636, doi:10.1038/Nature00775, 2002.

Petaja, T., Mauldin, R. L., Kosciuch, E., McGrath, J., Nieminen, T., Paasonen, P., Boy, M., Adamov, A., Kotiaho, T., and Kulmala, M.: Sulfuric acid and OH concentrations in a boreal forest site, Atmos. Chem. Phys., 9, 7435-7448, 2009.

Qi, X. M., Ding, A. J., Nie, W., Petaja, T., Kerminen, V.-M., Herrmann, E., Xie, Y. N., Zheng, L. F., Manninen, H., Aalto, P., Sun, J. N., Xu, Z. N., Chi, X. G., Huang, X., Boy, M., Virkkula, A., Yang, X.-Q., Fu, C. B., and Kulmala, M.: Aerosol size distribution and new particle formation in the western Yangtze River Delta of China: 2 years of measurements at the SORPES station, Atmos. Chem. Phys., 15, 12445-12464, doi:10.5194/acp-15-12445-2015, 2015.

Schobesberger, S., Junninen, H., Bianchi, F., Lonn, G., Ehn, M., and coauthors: Molecular understanding of atmospheric particle formation from sulfuric acid and large oxidized organic molecules, Proc. Natl. Acad. Sci. U. S. A., 110, 17223-17228, doi:10.1073/pnas.1306973110, 2013.

Tie, X., Geng, F., Guenther, A., Cao, J., Greenberg, J., Zhang, R., Apel, E., Li, G., Weinheimer, A., Chen, J., and Cai, C.: Megacity impacts on regional ozone formation: observations and WRF-Chem modeling for the MIRAGE-Shanghai field campaign, Atmos Chem Phys, 13, 5655-5669, doi:10.5194/acp-13-5655-2013, 2013.

Weber, R. J., McMurry, P. H., Mauldin, R. L., Tanner, D. J., Eisele, F. L., Clarke, A. D., and Kapustin, V. N.: New particle formation in the remote troposphere: A comparison of observations at various sites, Geophys. Res. Lett., 26, 307-310, doi:10.1029/1998gl900308, 1999.

Yue, D. L., Hu, M., Zhang, R. Y., Wang, Z. B., Zheng, J., Wu, Z. J., Wiedensohler, A., He, L. Y., Huang, X. F., and Zhu, T.: The roles of sulfuric acid in new particle formation and growth in the mega-city of Beijing, Atmos. Chem. Phys., 10, 4953-4960, doi:10.5194/acp-10-4953-2010, 2010.

Zhang, Q., Stanier, C. O., Canagaratna, M. R., Jayne, J. T., Worsnop, D. R., Pandis, S. N., and Jimenez, J. L.: Insights into the chemistry of new particle formation and growth events in Pittsburgh based on aerosol mass spectrometry, Environ. Sci. Technol., 38, 4797-4809, doi:10.1021/Es035417u, 2004.

IMPLEMENTATION OF DYNAMIC VEGETATION STRUCTURE PROPERTIES INTO A LAND SURFACE MODEL: EVALUATION OF CARBON, WATER, AND ENERGY FLUXES IN NORTHERN HIGH LATITUDE ECOSYSTEMS

A. K. JAIN[1], B. EL-MASRI[2], AND S. SHU[1]

[1]Department of Atmospheric Science, University of Illinois, Urbana, IL 61874, USA.

[2]Department of Geosciences, Murray State University, Murray, Kentucky, USA.

Keywords: PHENOLOGY, LAND SURFACE MODEL, ROOTING DEPTH, CARBON, WATER.

INTRODUCTION

The northern high latitude ecosystems (NHLEs) have experienced rapid warming over the recent decades, in response to increased air temperature, and the same trend is expected throughout this century. Some of the major responses of the NHLE to warming include the changes in carbon (C) storage in vegetation and soil, mainly as a result of advancement in the onset of the NHLE growing season (Myneni *et al*., 1997), shifts in ecosystem composition and abundance, such as higher shrub density (Rogers *et al*., 2013), and latitudinal advances in the tree line. Given these changes, it is important to understand and quantify the response of the NHLE to changes in C, water, and energy fluxes under climate change.

While continued research on the development of more detailed Earth system models (ESMs) is essential to understand the interactions and feedbacks among vegetation, soil, and climate change in the NHLE, one of the challenges for the Land Surface Models (LSMs), a land component of the ESMs, is the treatment of the exchanges of C, water, and energy between the terrestrial ecosystems and the atmosphere and the impact of these exchanges on climate through a variety of biophysical and biogeochemical pathways over a range of spatial and temporal scales. Several inter-comparison projects have highlighted the differences between LSM simulations and observational data for the C fluxes. The differences are projected larger for the NHLE, because they are complicated to model due to the presence of snow, permafrost, peat lands, N limitation, complex topography, etc.

The structural properties of vegetation, particularly the phenology and rooting depth, are important to study the exchanges of C, water, and energy between the terrestrial biosphere environment of the NHLE and the atmosphere. Additionally, changes in structural properties can also impact the global and regional climate due to their feedbacks with environmental factors, such as atmospheric CO_2 concentration. Modelling the vegetation structural properties is more challenging in the NHLs, because of the scarcity of observational data to evaluate the model performance. The objective of this study is to implement the dynamic vegetation structure properties (dynamic phenology and dynamic rooting depth and distribution) in a LSM, the Integrated Science Assessment model (ISAM), to understand how these properties are changing due to changes in environmental factors that impact the C, water, and energy fluxes.

METHODS

ISAM is a LSM that simulates the terrestrial C, N, water, and energy cycles at $0.5^o \times 0.5^o$ spatial resolution and at multiple temporal resolutions ranging from half hourly to yearly time scales. ISAM soil column consists of ten hydrologically and thermally active layers, five hydrologically inactive layers, and one thermally active bedrock layer that are used to calculate soil temperature and moisture. ISAM biogeochemistry is composed of eight vegetation pools, four litter pools, and four soil organic C pools. ISAM contains comprehensive biogeophysics (Barman *et al.*, 2014 a and b; Song et al., 2013) and biogeochemical (El-Masri *et al.*, 2013; Yang *et al.*, 2009) components. The model includes the following

snow dynamic processes that are important to the NHLEs (Barman and Jain, 2016): 1) energy exchange between shallow and deep soils, by representing soils up to ~50 meters, (2) effect of SOC on thermal/hydrological properties, (3) wind compaction of snow depth (and density), and (4) depth hoar formation in snow. The biogeochemistry component of ISAM accounts for major N processes, such as nitrification, denitrification, immobilization, leaching, and volatilization (Jain *et al*., 2009). The stem C allocation is parameterized based on the pipe model (Shinozaki *et al.*, 1964), which assumes light limitation under high LAI conditions and wood C allocation increases to compete for light (akin to structural support). The extended version of ISAM ($ISAM_{DYN}$) accounts for a C-gain-based dynamic phenology and corresponding LAI. For instance, when C assimilation is less than the leaf respiration, LAI will decrease and it can trigger a change in the phenological stage if a decrease in LAI continuous for a period of time. Similarly, when C assimilation is greater than the leaf respiration, LAI will increase and such an increase will trigger a change in the phenological stages. The dynamic LAI approach assumes that LAI is a function of photosynthesis that is dependent on soil moisture, solar radiaion, maximum leaf photosynthetic capacity, and fraction of allocated C to the leaves. Dynamic LAI was estimated using stem leaf area (SLA) and leaf biomass. The dynamic rooting depth distribution process assumes that the vegetation structure is driven by plant phenology, C allocation, and root distribution (El-Masri *et al*., 2015)

The model parameters related to these processes were calibrated and evaluated using measured data from 16 sites (12 flux net sites and 4 non-flux net sites) representative of the dominant NHLEs.

CONCLUSIONS

By including these dynamic processes, ISAM was able to capture the measured seasonal variability in leaf area index (LAI) and root distribution in the soil layers. The evaluation of the model results suggested that without including the dynamic processes, the modeled growing season length (GSL) in the NHLE was almost two times higher, as compared to measurements. To quantify the implication of these processes on the C, water, and energy fluxes, we compared the results of two different versions of ISAM, a dynamic version that include dynamic processes ($ISAM_{DYN}$) and a static version that does not include dynamic processes ($ISAM_{BC}$), with measurements from 12 eddy covariance flux sites. The results showed that $ISAM_{DYN}$, unlike $ISAM_{BC}$, was more capable to capture the flux site-based seasonal variability in GPP, water, and energy fluxes. Regional analysis revealed that the growing season length increased on average by about 5 days in the NHLs in the 2000s compared to 1990s.

ACKNOWLEDGEMENTS

This work was partly supported by the U.S. Department of Energy (DOE) Office of Science (DOE-DE-SC0006706).

REFERENCES

Barman, R., A.K. Jain (2015). Comparison of effects of cold-region soil/snow processes and the uncertainties from model forcing data on permafrost physical characteristics, *Journal of Advances in Modeling Earth Systems*, Accepted Article, doi: 10.1002/2015MS000504.

Barman, R., A. K. Jain, M. Liang (2014a). Climate-driven uncertainties in modeling terrestrial energy and water fluxes: a site-level to global scale analysis. *Global Change Biology*, 20, 1885.

Barman, R., A. K. Jain, M. Liang (2014b). Climate-driven uncertainties in modeling terrestrial gross primary production: a site-level to global scale analysis. *Global Change Biology*, 20, 1394-1411, DOI:10.1111/gcb.12474.

El-Masri, B., R. Barman, P. Meiyappan, Y. Song, Y, M. Liang, and A. K. Jain, A. K. (2013). Carbon dynamics in the amazonian basin: Integration of eddy covariance and ecophysiological data with a land surface model. Agricultural and Forest Meteorology, 182-183, 156.

El-Masri, B., S. Shu, A. K. Jain (2015). Implementation of a dynamic rooting depth and phenology into a land surface model: Evaluation of carbon, water, and energy fluxes in high latitude ecosystems. *Agricultural and Forest Meteorology*, 211, 85.

Jain, A., X. Yang, H. S. Kheshgi, A. D. McGuire, W. Post, D. Kicklighter (2009). Nitrogen attenuation of terrestrial carbon cycle response to global environmental factors. Global *Biogeochemical Cycles*, 23, GB4029, doi:10.1029/2009GB003474.

Myneni, R.B., C.D. Keeling, C. J. Tucker, G. Asrar, and R. R.Newmani (1997). Increased plant growth in the northern high latitudes from 1981 to 1991. *Nature*, 386.

Rogers, B.M., J. T. Randerson, and G Bonan,(2013). High Latitude cooling associated with landscape changes from North American boreal forest fires. *Biogeosciences*, 10, 699.

Song, Y., A. K. Jain, A, and G. F. McIsaac (2013). Implementation of dynamic crop growth processes into a land surface model: evaluation of energy, water and carbon fluxes under corn and soybean rotation. *Biogeosciences*, 10, 8039.

Yang, X., V. Wittig, A. K. Jain, W. M. Post (2009). Integration of nitrogen cycle dynamics into the Integrated Science Assessment Model for the study of terrestrial ecosystem responses to global change. *Global Biogeochemical Cycles*. 23, GB4029, doi:10.1029/2009GB003474.

DEVELOPMENT OF AIR QUALITY MODELLING SYSTEM IN LANGFANG BASED ON SENSOR MEASUREMENTS AND DATA FUSION

L. JOHANSSON[1], A. KARPPINEN[1] and L. DONG[2]

[1]The Finnish Meteorological Institute (FMI), Erik Palmenin aukio 1, 00101 Helsinki, Finland

[2]Pegasor, Hatanpään valtatie 34 c, 33100 Tampere, Finland

Keywords: AIR QUALITY, DATA FUSION, LAND USE REGRESSION, DISPERSION MODELLING.

INTRODUCTION

The amount of environmental information that can be used for the assessment of air quality in urban areas has increased substantially during the recent years. Sensor network are becoming denser and regional air quality forecasts are freely available online. However, for a citizen that is interested in the urban air quality the measurements of a single sensor, even the closest one, may require interpretation and expertise. Indeed, the pollutant concentrations in urban areas show great geographical variability to the extent that even the close by buildings, roads and measurement height can significantly affect the pollutant concentrations measured by the sensors. It therefore makes sense to fuse all the available information with methods that can take the above mentioned aspects into account and assess the air quality in the whole city. Given that weather forecasts are available, it is also possible to forecast the air quality in the near future based on the current state, future meteorology and modelled long range transportation of pollutants.

The fusion of measured air quality data is especially demanding, since each data point is also subject to meteorological conditions, human activities and background concentrations. Furthermore, the individual sensor quality must be considered and if modelled air quality data is also included the fusion the limitations and imprecision of the included modelled data must be taken into account.

In this paper we present the FMI-ENFUSER model that fuses environmental information for the assessment of urban air quality in a high resolution based on local sensor network, meteorological data and a collection of Geographic Information System (GIS) datasets (Johansson, et al. 2015a). The model has been developed and used in Finland, where its performance has been evaluated in the Helsinki Metropolitan Area for NO_2, $PM_{2.5}$ and PM_{10} pollutants (Johansson et al 2015b). The presented methodology can be applied in other regions as well given that sufficient amount of GIS-data is available. The paper focuses on a practical demonstration of the modelling system, in which the model was setup in Langfang, China, where several $PM_{2.5}$ sensors were installed around the city and used as input data for the model.

METHODS

Land Use Regression (LUR) approaches in air quality modelling are widely used since they are simple and there is a well-established way to build and train LUR-models (Briggs et al., 1997, de Hoogh et al., 2014). LUR-models can be used to estimate annual averages, e.g. for epidemiological studies, but cannot be used in more dynamic situations where meteorological conditions and long range transport of pollutants cause significant variability to the observed pollutant concentrations. In general, the average concentrations given by LUR-models tend to correlate well with observed averages, but the behaviour of the models are usually physically unrealistic and have a large number of explaining variables. One of the most appealing properties of LUR-models is that they don’t require a-priori information about emission sources. Rather, the model is calibrated (trained) based on observed pollutant concentrations with statistical regression.

In contrast to statistical LUR-models, the more dynamic dispersion models are rooted in the laws of physics, taking into account meteorological conditions in the environment. The price of added realism is of course, that the computational burden is much greater than with LUR-models. Consequently, the resolution of dispersion models is usually coarse for the needs of urban air quality assessment. Crucially, dispersion models always require very detailed information about emission sources and hence local dispersion models are usually difficult to be set up in a completely different environment.

The FMI-ENFUSER (The Finnish Meteorological Institute's Environmental information FUsion SERvice) is a hybrid model that combines statistical air quality modelling (Land Use Regression), dispersion modelling techniques (Gaussian plume) and information fusion algorithms. A more complete description of the methodology that can be described as 'dynamic land use regression' is given in (Johansson et al, 2015b) and the main components of the modelling system has been illustrated in Figure 1. Shortly put, the model is a 'tabula rasa' dispersion model without knowledge of local emission sources and their temporal/seasonal variation. With sufficient amount of calibration material that includes GIS-datasets, sensor measurement time series and weather data, the model detects the most notable local emission sources based on the GIS-data (including temporal variation) through multivariable regression. Then, given any meteorological condition time and location, the model can assess the expected pollutant concentration in those conditions. Finally, given a set of recent sensor observations the model is able to adjust to the perceived conditions (ambient concentrations, urban atmospheric inversion layers, special traffic peaks, etc.).

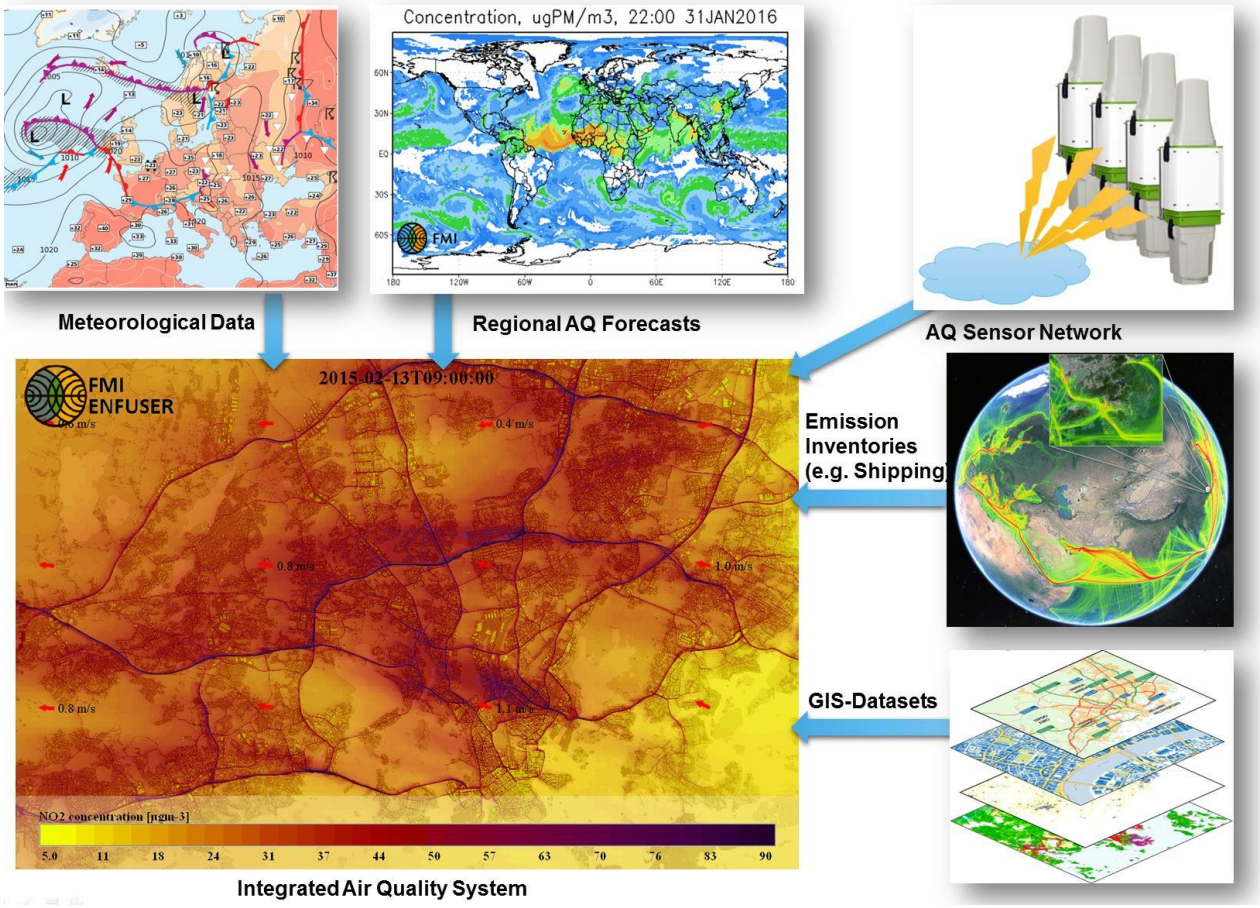

Figure 1: The core components of FMI-ENFUSER modelling system, which utilizes latest sensor observations, meteorological data and regional air quality forecast in the production of high resolution AQ heatmaps for the current and future situation in urban locations. GIS-datasets and emission inventories together with archived concentration time series are used for the calibration of the model.

The main advantages of the combination of techniques are as follows:

- **Dispersion modelling** facilitates the inclusion of meteorological variables including wind direction, wind speed, boundary layer height and atmospheric stability parameters. Height differences and topography can be taken into account.
- **Statistical LUR methodology** allows the model to be calibrated without a priori knowledge of local emission sources, using a large set of historical pollutant concentration time series. However, known emission inventories can be included in the modelling if available[1] (such as the modelled shipping emissions of Fig 1 which are provided by FMI-STEAM model (Jalkanen et al, 2012)). Furthermore, the model can automatically recalibrate it's parameters since it continuously extracts and archives sensor measurements.
- **Data fusion algorithms** makes it possible to fuse the information from multiple sensors and supporting air quality models of variable quality, also taking into account the temporal and spatial separation of datapoints. In theory, the more data is available (regardless of quality) the better the model output should become (Potemski and Galmarini, 2009).
- Computationally light-weight and exportable to other regions.

The drawbacks of the approach are as follows:

- Chemical interaction of pollutants can only be dealt with statistical post-processing (not included currently).
- The calibration of the model is difficult when only low quality (low resolution, insufficient amount environmental drivers) GIS-datasets are available.
- Physical limitations of Gaussian plume –based dispersion modelling (Stockie, 2009). However, models that provide input for FMI-ENFUSER may exhibit more sophisticated approaches.

Before using the model in Langfang a collection of GIS-datasets to describe the environment and population was collected. The usage of several GIS-datasets simultaneously in the model requires additional data fusion techniques, which are not discussed in this paper. Nevertheless, it can be said that there can be significant differences in resolution, information content and reliability within the obtained GIS-datasets.

Even though most of the previously utilized datasets in Finland were open-source and globally available, the information content in China proved to be lower than in Europe. In particular, GIS-data from openstreetmap.org as limited to a mapping of the road network in Langfang and only crude mappings of population density for China were available. Also, CORINE land cover[2], which FMI-ENFUSER utilizes, was naturally not available in China. Due to these difficulties in gaining access to relevant GIS-datasets new capabilities were implemented in the model, including the capability to assess rudimentary land use types (distinction between vegetation, urban areas and suburban areas) directly from satellite images based on the soil colour properties. The satellite images were also utilized to enhance the resolution of the obtained crude population mapping in China.

A high resolution GIS-dataset (5 x 5m) describing Langfang was obtained by the courtesy of local authorities that included the mapping of buildings in Langfang. The mapping of buildings is especially important for the FMI-ENFUSER model since the vicinity of buildings can affect local air quality significantly depending on wind conditions (e.g. urban street canyons). Moreover, individual households can be associated as a significant source for $PM_{2.5}$ through heating. Fortunately, these numerous small sources for $PM_{2.5}$ can be individually detected from the GIS-data by evaluating the physical area of the building and local environment properties. In Helsinki Metropolitan Area the model distinguishes close to

[1] The inclusion of known emission inventories requires that during calibration of the model the contribution from known sources is subtracted from the multivariate regression (Johansson et al, 2015b). Otherwise the contribution of known emission sources are associated to other GIS-factors and are double counted when the model is being used.
[2] CORINE data describes the European soil in 20 x 20m resolution, http://land.copernicus.eu/pan-european/corine-land-cover

100 000 households that contributes to $PM_{2.5}$ and the geographical distribution of them is in agreement with respective studies conducted by local authorities in Helsinki. It is also worth noting that the model calibration in Finland detected a stronger statistical link between local small houses and $PM_{2.5}$ concentrations than the statistical link between local vehicular traffic and $PM_{2.5}$ concentrations[3].

The key source of information for the whole modelling system was the $PM_{2.5}$ sensor network established by the Finnish sensor manufacturer Pegasor. 5 sensors were originally installed in selected locations around Langfang and 10 more will be installed in the near future. The installation sites were specifically selected to cover a wide range of different environments. While most sensors were placed near ground level, some of the sensors were placed on roof tops. The FMI-ENFUSER model can take into account the individual measurement heights of sensors and variable measurement heights can enrich the information content available for the system, which in turn makes it easier to establish a comprehensive picture of the air quality in the city. The sensor measurements were connected to the Pegasor's cloud service and a real time connection between this cloud service and the FMI-ENFUSER model was implemented. In order to address the long range transportation of pollutants and enhance the forecasting capabilities of the model, the globally operational FMI-SILAM regional air quality model was included in the pool of information (Sofiev et al, 2014).

CONCLUSIONS

As a demonstration for the modelling system, In Figure 2 the modelled hourly average pollutant concentration based on measurements from 5 sensors in a selected hour in Langfang is presented.

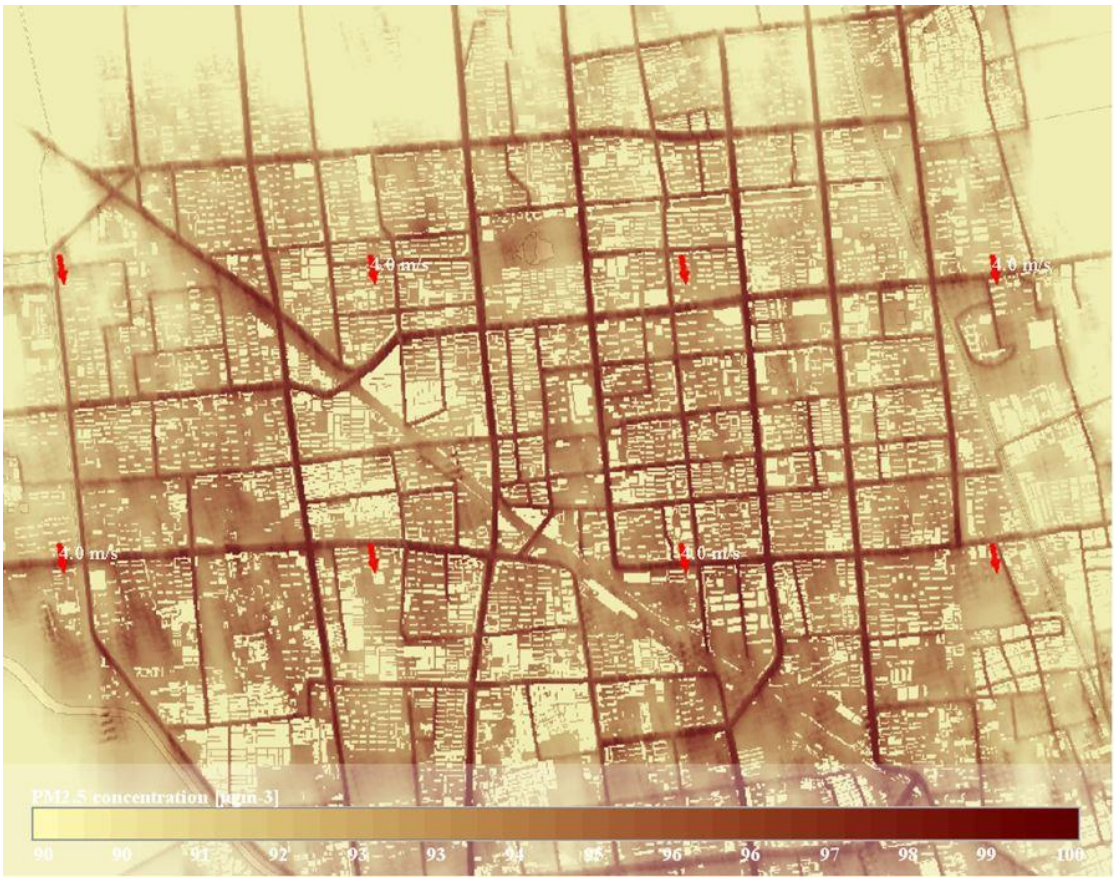

Figure 2: Modelled hourly $PM_{2.5}$ concentration in Langfang based on Pegasor sensor measurements during 2015-06-20T19:00. Wind conditions (direction, speed) have been illustrated with red arrows.

[3] More information on the calibration routines of LUR-models can be found in (Hoogh et al, 2014).

FMI-ENFUSER was demonstrated in Langfang together with Pegasor's newly established sensor network. A complete calibration of the model at the time of writing was not possible since lengthy measurement time series was not yet available for the test site. However, the amount of archived data is accumulating steadily and in the near future full annual time series will be available and the FMI-ENFUSER model can properly be calibrated in Langfang.

The integrated modelling system was originally developed for the cities in Finland and because of this several adjustments and improvements for the model were needed to be made during the Langfang pilot study. For instance, there are national 'specialities' that will require attention in future model development. As an example, one of the installed sensors was placed in a busy commercial street with several street kitchens. Consequently, the measured $PM_{2.5}$ concentrations of this particular sensor were usually very high. Since such a source of emissions is not taken into account in the model (nor present in GIS-data) the higher concentration levels will be associated as higher ambient $PM_{2.5}$ concentrations and this can bias the predictions of the model in other nearby locations.

Setting up the model to operate in China was a challenging task especially due to the lack of high quality GIS-datasets. Cooperation with local authorities is in key role when GIS-data is being gathered and while open source information is available it can only serve as supporting information for the evaluation of environmental characteristics in China.

While the pollutant concentrations are generally much larger in China, the same calibration routines can be applied and the model is able to distinguish the relationships between observed pollutant concentrations, meteorological conditions and GIS-properties. Similarly as in Finland, the availability of forecasted weather- and regional air quality data facilitates the possibility to produce short forecasts for urban air quality by the FMI-ENFUSER model. Later on, the model can be extended to cover multiple cities in China given that the coverage if GIS-datasets are extended. By covering several cities in China will also improve the calibration quality as the amount of data and environmental diversity increases.

ACKNOWLEDGEMENTS

This work was supported and funded by TEKES SHOK/CLEEN MMEA project.

REFERENCES

Johansson, L., Epitropou, V., Karatzas, K., Karppinen, K., Wanner, L., Vrochidis, S., Bassoukos, A., Kukkonen, J. and Kompatsiaris I. (2015a). Fusion of meteorological and air quality data extracted from the web for personalized environmental information services. Environmental Modelling & Software, Elsevier, 64 (2015) 143-155.

Johansson, L., Karppinen, A. and Loven ,K. (2015b). Evaluation of Air Quality Using Dynamic Land-use Regression and Fusion of Environmental Information, Proceedings of the 2nd International Workshop on Environmental Multimedia Retrieval, Pages 33-38, ACM New York, NY, USA, ISBN: 978-1-4503-3558-4.

Jalkanen, J.-P., Johansson, L., Kukkonen, J., Brink, A., Kalli, J. and Stipa, T. (2012). Extension of an assessment model of ship traffic exhaust emissions for particulate matter and carbon monoxide. Atmos. Chem. Phys., 12, 2641–2659.

Sofiev, M., Vira, J., Kouznetsov, R, Prank, M., Soares, J., Alves Antunes, J., and Genikhovich, E. (2015). Construction of the SILAM Eulerian atmospheric dispersion model based on the advection algorithm of Michael Galperin, Geosci.Model Developm. 8, 3497-3522, doi:10.5194/gmd-8-3497-2015.

Stockie, J.M. (2011). The Mathematics of Atmospheric Dispersion Modeling, SIAM Rev., 53(2), 349–372. (24 pages), DOI:10.1137/10080991X.

de Hoogh, K. et al. (2014). Comparing land use regression and dispersion modelling to assess residential exposure to ambient air pollution for epidemiological studies, Environment International 73 (2014) 382–392, Elsevier.

Briggs, D. et al. (1997). Mapping urban air pollution using GIS: a regression-based approach, International Journal of Geographical Information Science, Volume 11, Issue 7, 1997, DOI:10.1080/136588197242158.

Potempski, S. and Galmarini, S. (2009). Est modus in rebus: analytical properties of multi-model ensembles. Atmos. Chem. Phys. 9, 9471e9489. http://dx.doi.org/10.5194/acp-9-9471-2009.

THE EFFECT OF SURFACE COVER AND CLIMATE CONDITION ON THE SURFACE ENERGY AND WATER BALANCE IN COLD CLIMATE CITIES

L. JÄRVI[1], C.S.B.GRIMMOND[2], A. CHRISTEN[3], J.P. MCFADDEN[4] and I.B. STRACHAN[5]

[1]Division on Atmospheric Sciences, Department of Physics, University of Helsinki, Helsinki, P.O. Box 48, Finland.

[2]Department of Meteorology, University of Reading, Reading, UK.

[3]Department of Geography and Atmospheric Science Program, University of British Columbia, Vancouver, BC, Canada

[4]Department of Geography and Earth Research Institute, University of California, Santa Barbara, CA, USA

[5]Department of Natural Resource Sciences, McGill University, Montreal, QC, Canada

Keywords: HIGH-LATITUDES, SURFACE ENERGY BALANCE, URBAN, WATER BALANCE.

INTRODUCTION

Currently over half of world's population lives in urban areas and the fraction is further expected to increase in the future. With this, a growing number of people are affected by urban climate and hydrology phenomena such as increased air temperature and increased risk for flooding. Thus, it is important to understand and forecast the impact on atmospheric conditions and the water cycle processes in urban areas. The most dramatic climate change is expected at high-latitudes (IPCC, 2013) and therefore it is particularly important to understand how climate variations will potentially affect the surface energy and water balances in urban areas in high latitudes. High-latitude regions are characterized by strong intra-annual variability in solar radiation and air temperature, further affecting vegetation phenology. In addition, snow on the ground is common in the winter and spring modifying the surface albedo and surface water availability (Semádeni-Davies and Bengtsson, 1998). Furthermore, the urban effects on local climate are often pronounced in winter due to large anthropogenic heat releases and different snow coverage in urban areas and surrounding rural areas.

The purpose of this study is to examine the surface energy and water balances year-round in continental and cold climate cities. We are interested in how these balances vary in different climatic conditions, their inter-annual variability and their dependency on different land cover. Particularly, interest lies in the behavior of surface runoff and the partitioning of the available energy into sensible and latent heat fluxes.

METHODS

The model used in the study, the Surface Urban Energy and Water balance Scheme (SUEWS, Järvi *et al.*, 2011; Ward *et al.*, 2016), has been designed to use a minimum amount of input variables and model parameters. In addition to the commonly measured meteorological forcing data (air temperature, relative humidity, solar radiation, precipitation, wind speed and air pressure), the model needs surface cover information including surface cover fractions, building and tree heights, and population densities of the studied areas. The model contains several submodels (e.g. for net all-wave radiation, anthropogenic and storage heat fluxes and irrigation). In a recent study, the model was further developed to simulate the surface energy and water balances in cold climate cities, and a good model performance was found when comparing the model output against observed surface runoff, snow properties and turbulent fluxes on

sensible and latent heat in Helsinki, Finland, and Montreal, Canada (Järvi *et al.*, 2014, Karsisto *et al.*, 2015).

The model is run for four mid- to high-latitude cities characterized by cold winter climates with snow (Table 1): Helsinki (Finland), Montreal (Canada), Minneapolis (USA) and Basel (Switzerland). The 11 analysed sites vary with respect to land cover fractions, irrigation habits and population densities. For example, the plan area fraction of impervious surfaces varies from 5% in Minneapolis to 84% in Basel. As the modelled time periods are for one (Basel) to 7.5 years (Helsinki), a wide range of meteorological conditions occur. For each site, the model is run in an offline mode using measured hourly meteorological data with a time step of 5-min.

	Helsinki					*Montreal*		*Minneapolis*		*Basel*	
Site	Ku1	Ku2	Ku3	Pa	Pi	Rl	Pr	Mi1	Mi2	BSPA	BSPR
Lat	60.20°N	60.20°N	60.20°N	60.20°N	60.24°N	45.46°N	45.50°N	45.00°N	45.00°N	47.55°N	47.55°N
Lon	24.96°E	24.96°E	24.96°E	24.94°E	25.01°E	73.592°W	73.81°W	93.19°W	93.19°W	7.57°E	7.58°E
LCZ	3	6	9	2	9	3	6	9	B	2	2
f_{pav}	0.42	0.39	0.30	0.42	0.22	0.44	0.37	0.08	0.04	0.32	0.30
f_{bldg}	0.20	0.15	0.11	0.20	0.12	0.27	0.12	0.12	0.01	0.37	0.54
f_{veg}	0.38	0.45	0.59	0.38	0.66	0.29	0.50	0.76	0.93	0.31	0.16
f_{water}	0	0.01	0	0	0	0	0.01	0.04	0.02	0	0
z (m)	31	31	31	31	31	25	25	40	40	29.9	31.7
z_h (m)	10.4	11.5	12.6	15.2	10.8	7.9	6.4	6	6	12.5	14.6
z_t (m)	10	8.8	8.5	8	8	13.0	13.8	12	12	12.5	14.6
p (# ha^{-1})	31	37	44	42	55	84	24	10	0	103	158
A (ha)	44.7	78.2	78.2	23.8	44.8	314.2	314.2	174.5	78.5	19.6	
Reference	Karsisto et al. (2015)			Järvi et al. (2014)		Bergeron and Strachan (2012)		Peters et al. (2011)		Christen and Vogt (2004)	
Modelled period	7/2005-12/2012			7/2005-12/2012		12/2007-9/2009		7/2006-4/2009		09/2001-08/2002	1/2001-7/2002

Table 1. Modelled sites and the site-specific parameters used in the model runs. Lat and Lon are the latitude and longitude of the modelled sites, LCZ is the Local Climate Zone (Stewart and Oke, 2012), f_{pav}, f_{bldg}, f_{veg} and f_{water} are the surface plan area fractions of paved surfaces, buildings, vegetation and water, respectively, z is the modelled height, z_h and z_t are the height of buildings and trees, p is the population density and A is the area of the simulated site.

CONCLUSIONS

Our results show how evapotranspiration and surface runoff are more dependent on the climatological factors than the fraction of impervious surfaces in the study area. For example, in the summer period in Montreal and Helsinki, the mean air temperature between different years causes more variability in both normalised evapotranspiration and surface runoff than the fraction of impervious surfaces (Figure 1, Table 1). Thus, using simply the fraction of impervious or pervious surfaces when estimating the surface runoff at different sites is not sufficient, but rather inter-annual variability in climatology also needs to be considered.

In winter and spring periods, the amount of snow and length of snow cover become important factors especially in determining the amount of surface runoff. The shorter the snow cover period is, the larger the cumulative runoff tends to be. Thus, the results suggest that warmer winters with shorter snow covered periods will increase the water stress in urban ecosystems and drainage systems.

ACKNOWLEDGEMENTS

The work was supported by Academy of Finland (Project numbers 138328, 1127756, ICOS 271878, ICOS-Finland 263149 and ICOS-ERIC 281250), Academy of Finland Centre of Excellence (project no 1118615), NERC TRUC (NE/L008971/1) and Met Office /Newton CSSP.

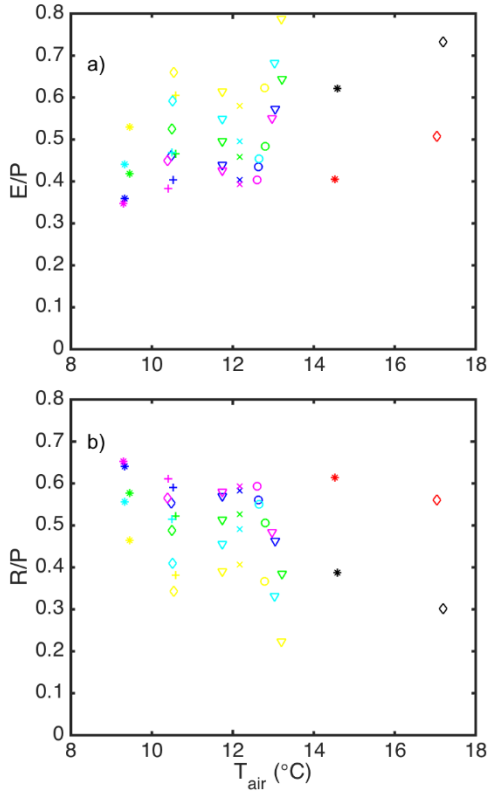

Figure 1. Normalized a) evapotranspiration and b) surface runoff sums as a function of mean air temperature for summer period (June-August) in Montreal and Helsinki for the simulated years (Table 1). *E* = evapotranspiration, *R* = runoff and *P* = precipitation. The different colours show the different sites: blue = Ku1, green = Ku2, yellow = Ku3, pink = Pi, light blue = Pa, black = Pr and red = Rl.

REFERENCES

Bergeron, O. and I.B. Strachan (2012). Wintertime radiation and energy budget along an urbanization gradient in Montreal, Canada, *Int. J. Clim.* **32**, 137.

Christen A. and R. Vogt (2004). Energy and radiation balance of a central European city, *Int. J. Climatol.* **24**, 1495.

IPCC. 2013. Climate Change 2013: The Physical Science Basis. Contribution of Working Group I to the Fifth Assessment Report of the Intergovernmental Panel on Climate Change. Cambridge University Press: Cambridge, UK and New York, NY.

Järvi, L., C.S.B. Grimmond and A. Christen (2011). The surface urban energy and water balance scheme (SUEWS): Evaluation in Los Angeles and Vancouver, *J. Hydrol.* **411**, 219.

Järvi, L., C.S.B. Grimmond, M. Taka, A. Nordbo, H. Setälä and I. Strachan (2014). Developments of the Surface Urban Energy and Water balance Scheme (SUEWS) for cold climate cities, *Geosci. Mod. Dev.* **7**, 1691.

Karsisto, P., C. Fortelius, M. Demuzere, C.S.B. Grimmond, K. Oleson, R. Kouznetsov, V. Masson and L. Järvi (2015). Seasonal surface urban energy balance and wintertime stability simulated using three land-surface models in the high-latitude city Helsinki, *Q. J. Roy. Met. Soc.* **142**, 401.

Peters, E.B., R.V. Hiller and J.P. McFadden (2011). Seasonal contributions of vegetation types to suburban evapotranspiration, *J. Geophys. Res.-Biogeo.* **116**, doi:10.1029/2010JG001463.

Semádeni-Davies, A. F. and L. Bengtsson (1999). The water balance of sub-arctic town, *Hydrol. Process.* **13**, 1871.

Stewart I. D. and T.R. Oke (2012). Local climate zones for urban temperature studies, *Bull. Am. Meteorol. Soc.* **93**, 1879.

Ward, H.C., S. Kotthaus, L. Järvi and C.S.B. Grimmond (2016). Surface urban energy and water balance scheme (SUEWS): development and evaluation at two UK sites. In review in *Urban Climate*.

THE EMISSIONS OF BIOGENIC GREENHOUSE GASES FROM ARCTIC AND NORTH BOREAL SOILS DUE TO THE DIFFERENT TYPES OF ANTHROPOGENIC LAND USE AT LOCAL AND REGIONAL SCALES: PROSPECTS AND DYNAMICS

D.V. KARELIN[1,2,3], E.P. ZAZOVSKAYA[1], V.A. SHISHKOV[1], A.V. DOLGIKH[1], I.G. SHARKUNOV[1], A.V. POCHIKALOV[2,3], A.A. KARPOV[2], E.V. ANTONOV[1] and S.V. GORYACHKIN[1]

[1] Institute of Geography, Russian Academy of Sciences, Staromonetny 29, 119017 Moscow, Russia.

[2] Lomonosov Moscow State University, Faculty of Biology, 1-12 Leninskie Gory, 119991 Moscow, Russia.

[3] Center for Problems of Ecology and Productivity of Forests RAS, Profsouznaya ul. 84/32, str.14, 117997 Moscow, Russia.

Keywords: ARCTIC, GREENHOUSE GASES, SOIL EMISSION, ANTHROPOGENIC FACTORS

INTRODUCTION

Scientific interest to the Arctic, while the least affected by human activity and at the same time the most vulnerable region, was always high. This interest is especially intensified in the current period of pronounced human-affected climate change, as a result of increased industrial and agricultural emissions of greenhouse gases. The Arctic is critical to earth's climate not only through the balance of greenhouse gases between ecosystems and atmosphere, and changes of surface albedo, but also due to vast reserves of greenhouse gases stored in the permafrost. In recent years, the scientific focus turned not only on the global impacts of human activity, but also to figure out how different forms of local anthropogenic impacts could affect greenhouse gas emissions, and how this influence is comparable to the influence of global climate changes. In addition, it is important to establish a net of circumpolar monitoring stations of soil emissions of biogenic greenhouse gases in the Arctic. With this purpose in 2014-2015 we organized the field measurements of emissions of soil biogenic greenhouse gases and related parameters in the key Arctic locations under the influence of the main local anthropogenic factors. In addition we analysed official data on the emissions of these gases in the Arctic zone of the Russian Federation from stationary sources and the statistics of land use for the last years. Our first results were already published (Goryachkin *et al*., 2015, Karelin *et al*., 2016).

RESULTS

1. For the Arctic and North-boreal zone of the Russian Federation it was shown that under anthropogenic impact the deviations of soil emission rates of biogenic greenhouse gases from background values occur in all cases. Thus, depending on the nature and duration of anthropogenic influence and depending on a particular ecosystems, it can be observed both increase or decrease of soil emissions of biogenic greenhouse gases (CO_2, methane, nitrous oxide) compared to their background levels in local ecosystems not affected by anthropogenic activity. Thus, the anthropogenic factors (AF) lead to increase in the spatial variance of soil fluxes of these gases. Acting in complex, AF with high probability lead to the resulting source of CO_2 at the local and regional scales for the period of equilibrium of C-balance, that is due to disbalance between Gross Primary Production and Gross Respiration rates, in favor of respiration. In all cases, constant and powerful sources of CO_2, targeted only amenable to reclamation, are the territories of settlements. It was also shown that the most serious destructive factors among studied ones should be

considered those associated with the destruction of the soil layer. The role of the entire AF complex, affecting C-balance and CO_2 emissions, increasing with the onset of winter season in Arctic communities, which may input to the observed CO_2 emission. As an example, Fig.1 shows the local effects and the rate of the CO_2 emissions in the area of inactive since year 2000 coal mine in the subarctic zone (Vorkuta region). This example (see also Fig. 3 for the same data points) illustrates a general decrease of soil emissions of self-restoration site for 15 years after its abandonment. Despite the overall decline in soil respiration at this period the territory remains a net source of CO_2 due to the lower rate of primary production.

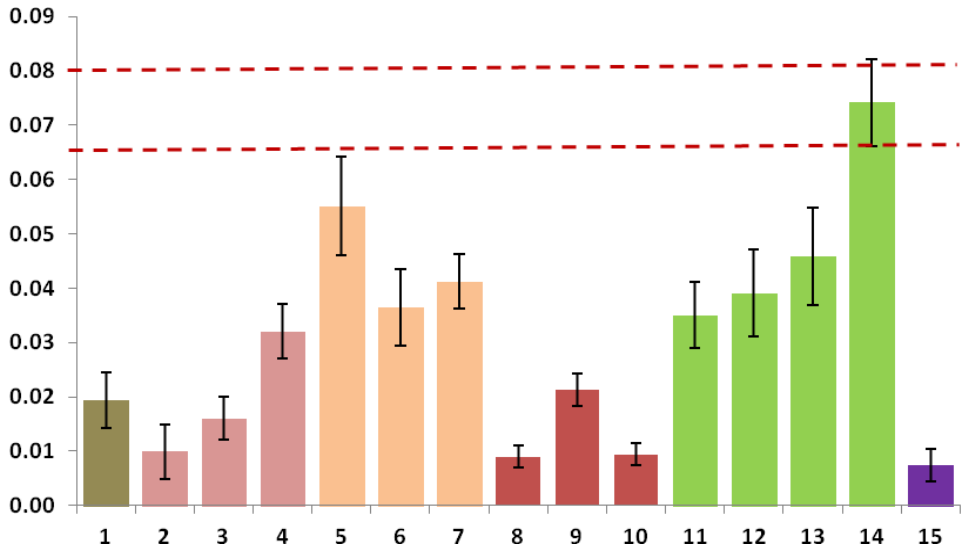

Figure 1. Anthropogenic soil emissions of CO_2 (gC m^{-2} h^{-1}) in the territory of the coal mine complex in southern shrub tundra (Vorkuta region, 18 - 21 September 2015, the total area is 0.447 km^2). Types of anthropogenic impacts: 1 – the unused railway embankment, 2-4 – plots with concrete and brick buildings without roofs, 5-7 – industrial waterlogged zones, 8 – gravel roads, 9 – ground roads, 10 – central square, 11-14 – tracks of all-terrain machinery, 15 – landfills. The dashed lines are emissions from natural meso-depressions (top line) and meso-elevations (bottom line) in the natural shrub tundra. Presented mean values and their standard errors. The colors on the figure are used for grouping purposes of AF.

Fig.2 shows an opposite example – at the site of arctic tundra the local variants of AF lead mainly to excess of the background natural rates of the soil emission, which is mostly associated with the actively used territory of settlements and mining areas.

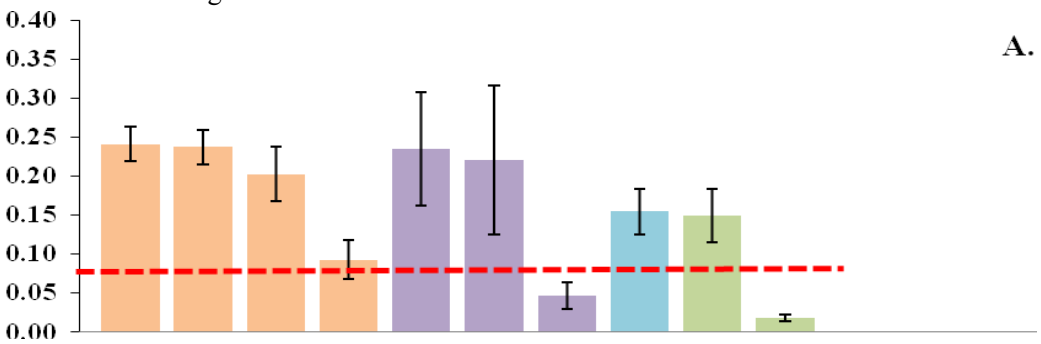

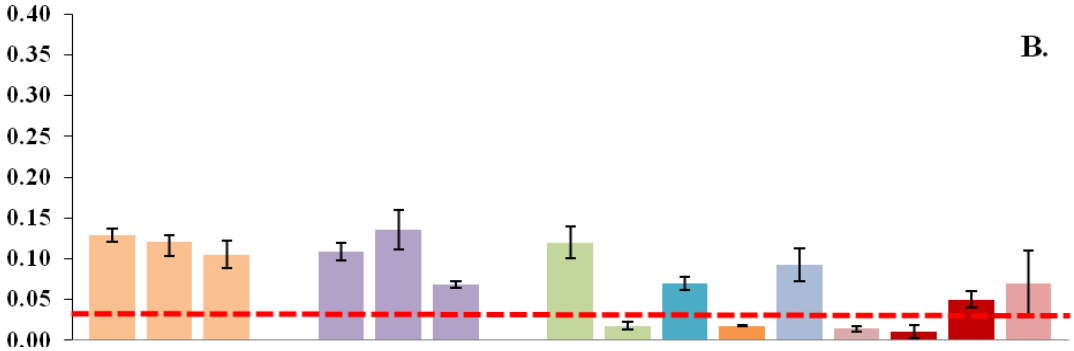

Figure 2. Measurement of soil CO_2 emissions (gC m^{-2} h^{-1}) in Arctic tundra in the area "Svalbard" in A. July 21-24, 2014. B. August 5-8, 2015. The dashed line is the mean background natural rate of emission in arctic tundra. Bar colors denote different groups of anthropogenic impacts (included are different variants of settlements, roads and ATV-tracks and coal piles).

The area is also mostly a net source of carbon to the atmosphere, although some abandoned sites, with an active growth of vegetation, could provide a carbon net sink. Note that this figure shows, first, the steady relative rates of different types of anthropogenic emissions from year to year, which is characteristic for all anthropogenic sites, and in addition, it shows how the influence of the weather conditions of a given year can proportionally shift the whole picture of the spatial emission. New data revealed that during self-restoration through the mechanism of autotrophic succession, the abandoned industrial buildings and communications in tundra are functioning as a reduced source of carbon emissions to the atmosphere from soil, with high probability of being a weak net sink of carbon. In opposite the actively used territories in the Arctic are mostly functioning as well-expressed soil and net carbon sources, as well. For expert estimation of the sign of net carbon balance of arctic territories under influence of AF, we applied a simple field method illustrated in Fig. 3. All human-affected ecosystems, as well as natural control ecosystems, have to be plotted using two variables – the storage of the aboveground plant biomass, which could be estimated using regression equations between projective cover and maximum aboveground phytomass storage, and specific rates of soil respiration. Variance of natural (not affected by AF) ecosystems provide (Fig. 3) a line, which considered to mark a carbon balance zone, whereas the affected ecosystems which appear in the lower section of the graph, are supposed to be a net carbon sinks, and in its upper part – net carbon sources. As one can see, in this example the most of the self-restoring after AF sites in the abandoned coal mining area are now weak carbon sinks.

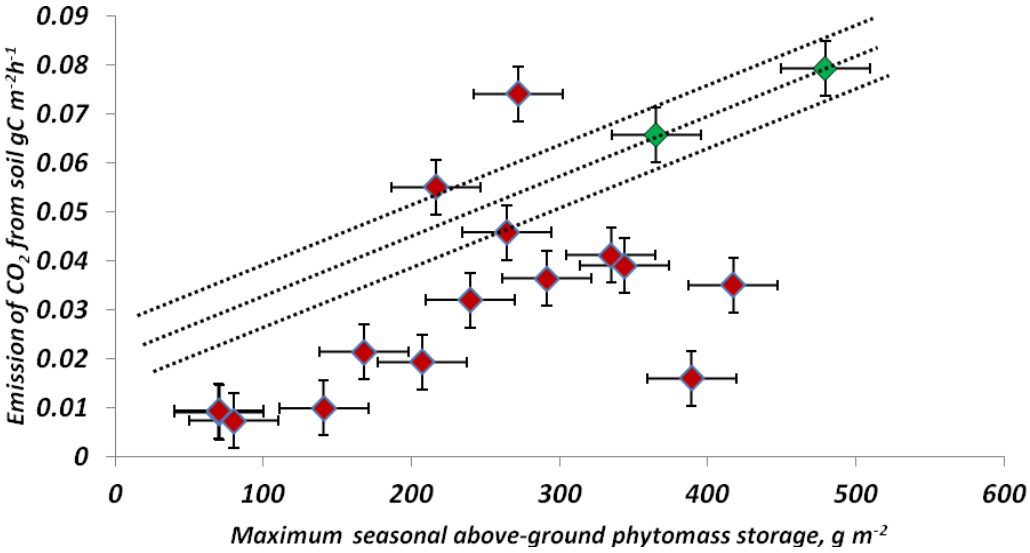

Figure 3. The dependence of CO_2 emission from the soils in anthropogenically-affected (red markers) and natural (green upper marker – tundra meso-depressions, green lower marker – meso-elevations) sites in the area of abandoned in 2000 coal mining complex (18-21 September 2015, Vorkuta region). Data are means and their standard errors. Dotted line – linear extrapolation of the "standard error corridor" for the equilibrium ratio of soil emission to maximum seasonal storage of aboveground biomass in natural ecosystems.

2. It is evident, that the balance of carbon in ecosystems (net ecosystem flux) cannot be accurately evaluated as a difference between soil respiration (in units of gC m^{-2} hr^{-1}) and aboveground phytomass storage (in units of g dry mass), first, because of different units, and second, because the first value is less than the Gross Ecosystem Respiration on respiration of aboveground ecosystem components, and the second is less than Gross Primary Production by the amount of respiration of autotrophs and by amount of belowground primary production. Besides, the aboveground phytomass storage is less than aboveground NPP by the amount of aboveground phytomass being decomposed during the same vegetative season, and by phytomass which is not yet produced. Nevertheless, the relationship may be useful as a simple index for evaluating the ratio of respiration and production in ecosystem, which correlates with the general direction (the sign) of its carbon balance, in particular for monitoring of anthropogenic impact, if there exist a simple way to estimate the stocks of the aboveground plant biomass. This is especially true for such a low stature ecosystem, as tundra. The method is convenient for expert estimates of growing anthropogenic impact to the natural complexes in the Arctic, reinforced by Global climate changes, which are also mainly due to global human activity. This could be also of help, when estimating the relative impact of different forms of local human activities, as compared to the impact of climate change. Our field observations of emission of greenhouse gases, related parameters, and data on productivity of a major types of cryogenic ecosystems, provides an opportunity to establish a monitoring network sites for measurement of soil emissions and productivity of anthropogenically affected ecosystems in Arctic region. The rates of greenhouse gases soil emissions can serve as a key indicators of the environment in the Arctic and adjacent regions.
3. Our results of field observations obtained in 2014-2015, suggest that deviations of soil emission from the background zonal rates under any local AF, occur in all cases. The natural arctic ecosystems being modified by local AF, could demonstrate for a long time a rates different from the background soil emission of biogenic greenhouse gases. The relative differences of CO_2 soil emissions between the sites with different type of anthropogenic impact are constantly persisted. North-boreal ecosystems (soil complexes) are more stable in this respect, as compared to tundra ecosystems. Anthropogenic CO_2 soil emission may exceed or be below the natural background level, depending on the form or varying degree of human impact, or weather conditions. But in all cases, when the vegetation cover is absent, they result in a net source of carbon dioxide to the atmosphere. This is especially true for active sites of human settlements and all kinds

of roads. At the same time, the creation of any artificial embankments or hollows in the Arctic regions (in particular, road construction) creates plots of prolonged net sink of carbon dioxide, as cryogenic landscapes are extremely sensitive to the slightest change in micro- and mesorelief, which could enhance hydro-thermal conditions for wintering plants.

4. Simultaneously with the study of the influence of local anthropogenic effects on soil greenhouse gas emissions, we studied the contribution of stationary anthropogenic sources, including residential and infrastructure industry, to the emission of greenhouse gases into the atmosphere in Arctic zone of Russian Federation, using official sources of information. The variable dynamics of emissions of carbon dioxide and methane with a local maximum in 2007-2009 yrs and with significant decrease in the period 2009-2013 were found. This is due to the adoption of the new legislation restricting gas flaring during oil and gas production. Technological modernization of equipment and crafts together with the development of infrastructure for the transportation of associated gas to processing facilities significantly reduced the impact of anthropogenic sources to the emissions of greenhouse gases in this region. This in general acts to decrease the total amount of greenhouse gases produced in the Arctic.

5. To evaluate the contribution of greenhouse gases from the surface of the anthropogenically-disturbed lands we conducted studies of the dynamics of different types of land use in the Arctic regions of Russian Federation. It was found that the total area of land occupied by buildings, infrastructure, roads, cropland, and human-disturbed lands has increased in all administrative regions of the Arctic zone (excluding the Krasnoyarsk region) by 6% for the period 2000-2013. The biggest increase of the disturbed area is observed in the regions of active exploitation of oil and gas resources in the Yamal–Nenets Autonomous district (31%), Nenets district (91%), and the Magadan region (14%). In contrast to (4), if take into consideration our findings (1-3), this in general should act to increase the total amount of greenhouse gases produced in the Arctic.

CONCLUSIONS

Our data allow to predict future changes in emissions of greenhouse gases from anthropogenic territories, on the basis of the revealed features of influence of different AF on soil emission and primary production in Arctic ecosystems, as well as to evaluate and compare the greenhouse gas emissions resulting from economic activities, with emission of those gases as a result of changes in the local and regional land use. Nevertheless the obtained in this study decrease of emissions from stationary sources and simultaneous increase of human-modified areas in the Arctic regions require accurate calculations in the forecasts taking into account specific types of land use, which could specifically change soil emission and primary production. The results also have prospects (*a)* to monitore of CO_2 emissions and primary production at selected observation sites in the key geographical subzones and regions and for the main types of anthropogenic impacts in the Arctic, (*b*) to obtain data on other major biogenic greenhouse gases (nitrous oxide and methane) at all selected key sites, (*c*) to expand the spatial coverage of soil emission estimates; include into analysis of new geographic sub-zones and soil types in the Arctic, (*d*) to calculate for each monitoring site (currently this is done only for Vorkuta site) a spatial assessments of soil emissions including all local AF with use of remote sensing data, (*e*) to apply a new distant methods for estimation of net primary production rates (based on LAI and NDVI), and chamber estimates of net ecosystem fluxes of CO_2, methane and N_2O using closed-path technique.

ACKNOWLEDGEMENTS

The research was supported by the Program "Searching basic studies for the development of the Arctic zone" of the Presidium of the Russian Academy of Sciences.

REFERENCES

Goryachkin S.V., Karelin D.V., Dolgikh A.V., Lyuri D.I., Shishkov V.A., Zazovskaya E.P. The Role of Anthropogenic Activities in CO_2 and CH_4 Emission from Soil to Atmosphere in Polar Regions of East Europe. "Report Series in Aerosol Science" Finnish Association for Aerosol Research FAAR. 2015. P. 167-171.

Karelin, D.V., Goryachkin S.V., Zamolodchikov D.G., Dolgikh A.V., Zazovskaya E.P., Shishkov V.A., Pochikalov V.A., Sirin A.A., Suvorov G.G. THE INFLUENCE OF THE LOCAL ANTHROPOGENIC FACTORS ON SOIL EMISSIONS OF BIOGENIC GREENHOUSE GASES IN CRYOGENIC ECOSYSTEMS. Zh. OBSCH. BIOLOGII. 2016. 2. (IN RUSSIAN, ACCEPTED).

HYDROCLIMATIC IMPACTS ON CATCHMENT-SCALE WATER CYCLE AND METAL AND CARBON FLUXES IN SELENGA-BAIKAL RIVER SYSTEM

N.S. KASIMOV[1], S.R. CHALOV[1] and M.Y.LYCHAGIN[1]

[1]Lomonosov Moscow State University, Moscow, Leninskie gory, GSP-1, 119991.

Keywords: CLIMATE CHANGE, CATCHMENTS, WATER, METAL FLUXES, CARBON.

INTRODUCTION

Rivers are major conduits of metal and carbon from land to coastal seas. Recent studies explain the significant role of the Northern high-latitude rivers system in the Arctic freshwater and chemical budget. Fewer studies considered the hydroclimatic impacts on water and geochemical fluxes in the Southern edge of the permafrost zone in the headwaters of the largest Arctic rivers.

The present study considers the Selenga River which originates in Mongolia and contributes about 50 % of the total inflow into Lake Baikal and together with the Angara and Yenisey rivers forms the longest river network in Eurasia. Mining, industrial and agricultural activities within the Selenga drainage basin affect metal delivery into rivers (Chalov et al., 2015). At the same time, the region is reported to experience the warming trends with acceleration since the 1970s (Unger-Shayesteh et al., 2013), what has a profound impact on the components of hydrological system and permafrost degradation in the area. Permafrost degradation, as a result of climate change, accelerates both river discharge and may cause shifts in riverine biogeochemistry as this old source of organic matter is exposed. In most cases the permafrost temperature in the Selenga River basin is close to 0^0 C. Hence, the permafrost is thermally unstable and vulnerable to changing climate conditions and adverse human activities (Törnqvist et al., 2015).

This study considers the Selenga River and its major tributaries (fig. 1) and aims at revealing water, metals and carbon fluxes and their spatio-temporal distribution. Recognizing the knowledge gaps on water-borne pollution spreading to Lake Baikal, a particular aim of the paper is to link geochemical data with pollution sources and estimate seasonal geochemical flows over scales that are larger than the ones previously considered. It also focuses on organic carbon fluxes that link runoff from the catchment into Baikal Lake in regards to the catchment or in-channel sediment origin.

DATASETS AND METHODS

For the hydroclimatic assessment we use area-averaged monthly data of air temperature T and P precipitation for the period 1938–2009 from the CRU TS3.10/CRU TS3.10.01 datasets. Daily discharge data gathered from 60 hydrological gauges (Figure 1) was used for analysis. Stream flow data for each gauging station was available for the entire study period 1978-2014.

Discharge measurement and sampling of water and suspended particulate matter (SPM) were collected during fieldwork periods of 2011-2015 over 50 sites each field campaign. Sampling field campaigns were done in summer-autumn periods during various hydrological conditions. In particular we obtained data for contrasting hydrological conditions, ranging from flood to low water. The campaigns were carried out from 15 July to 20 August 2011 (Summer flood), from 08 June to 15 July 2012 (low water), from 05 September to 30 September 2013 (flood recession); from 06 August to 25August 2014 (summer flood) and from 03 March to 23 March 2015 (winter low water) (fig. 1). Field were analyzed with mass spectroscopy and atomic emission methods (ICP-AES and ICP-MS) using Elan 6100 and Optima 4300 equipment (Perkin Elmer, USA). The content of 71 elements was determined in samples of water, suspended matter and bottom sediments. Thirteen main contaminants (Fe, Al, Mn, Zn, Cu, Mo, V, Cr, As, Co, Ni, Pb, Cd) were selected and further used in the analyses. Organic carbon (C_{org}) in SPM (particulate

organic carbon, POC) has been determined using CHNS Elementar analyzer based on the Whatman GF/F glass fiber filter analyses. Summary of SPM parameters is presented in table 1.

Figure 1. Selenga River Basin showing location of field sites

Table 1. SPM structure within Selenga river system in 2011-2015

Field campaign		Area	Q, m^3/s		S, mg/l			Clay (<0.001 mm), %			SPM average diameter, мм			POC (Corg,%)		
year	Dates		max	min	max	min	aver	max	min	aver	max	min	avg	max	min	avg
2011	15.07–25.08	1	465	0,1	2850	6,4	229	31	1,08	7	0,12	0,01	0,04	16,3	0,92	6,75
		2	902	-	47	1,4	18	-	-	-	-	-	-	-	-	-
2012	08.06–15.07	1	107	0,1	1249	1,7	82	4,62	1,16	2,49	0,48	0,01	0,08	12,8	2,25	5,62
		2	1439	-	150	1,7	50	3,6	0,24	2,08	0,02	0,54	0,09	13,3	2,75	6,09
2013	05.09–30.09	1	105	0,3	225	6,7	73	54,4	0,1	8	0,79	0,01	0,11	12,6	0,42	3,75
		2	-	-	43	2	25	4,9	0,1	2,8	0,92	0,02	0,21	23,6	6,21	2,26
2014	06.08-25.08	1	-	-	147	0,5	43	9,2	1,6	4,57	0,58	0,02	0,22	-	-	-
		2	-	-	31	2,9	15,3	12,6	1,4	6,02	0,88	0,01	0,09	-	-	-
2015	03.03.–25.03	1	64,8	0	312	0,7	18 (5)	41,2	0,6	4,97	0,32	0,03	0,08	3,99	0,23	0,71
		2	-	-	9,12	0,9	2,2	-	-	-	0,21	0,02	0,07	-	-	-

Area: catchment part within 1 – Mongolia, 2 - Russia

RESULTS AND CONSLUSION

The detailed results of the study could be found in (Chalov et al., 2012; 2013; 2015, Pietroń et al., 2015). Below we summarize the main conclusions on the hydroclimatic change in water, metal and carbon fluxes

1. Long-lasting low water period (since around 1995) is observed for the Selenga River. The runoff records for downstream Selenga (Mostovoy) shows statistically significant downward trend from 903 m^3/s (for the period since 1941 to 1982) to 888 m^3/s (for the period since 1983 to 2011), or even more drastic for the recent decades – from 940 m^3/s (for the period since 1975 to 1995) to 689 m^3/s (for the period since 1995 to 2011). The mean annual discharge at some gauging stations within the Mongolian part of the basin) demonstrated even more significant decrease during the

last decades, from an average of 53,3 m^3/s during the period 1975-1995 to only 18,1 for the years 1996-2011 at the upper Orkhon river (Orkhon-Orkhon) and from 35,3 m^3/s to 14,9 m^3/s for the Tuul river at UlaanBaatar respectively. The changes were caused mostly by intensive rainfall floods which determined high water period in the early 1990 and late 1970-1980. Present and expected hydrological changes in the Selenga River Basin are caused by three processes: land use changes, the impacts of global climate change on precipitation and evaporation and permafrost, and increasing water withdrawals. This lead to decline in sediment delivery to Lake Baikal: the annual total sediment load (suspended and bed load) delivered to the Selenga River Delta at Lake Baikal is about 2.5 Mt/year. Reported multi-decadal declines in sediment loads (up to 20%) in the downstream part of Selenga River can be attributed to the abandonment of cultivated lands and changing hydroclimatic factors, such as in particular climate-driven decrease of water flows and intensified water use for irrigation purposes.

2. Results indicate that high sediment and metal fluxes were reported both for altered and natural rivers. Mining impacts on sediment loads were seen mostly during relatively short hydrological events, during which an intensified slope wash near floodplain mining activities could flush large amounts of turbid water into the river. Whereas sediment flows were connected with the hydroclimatic conditions in the catchment, elemental composition of the mass flows mostly relate to the soil/petrologic conditions. With the exception of small impacted rivers where water quality impacts associated with mining were found, the formation of elemental compositions and sediment-associated chemical constituents generally reflects catchment characteristics.
3. Silt (< 0.05 mm) and sand (> 0.05 mm) are primary constituents of the observed sediment load in the Selenga River Basin. Fine sediments that range in grain size from 0.01 to 0.05 mm represent more than 50 % of the total suspended sediment load. The volume of particles that have a grain size of <0.05 mm constitutes over 60 % of the total particle volume. Since significant correlations were found for concentrations of Fe, Co, As, Cu and Zn with grain size fractions we conclude that particle size is one of the main factors that govern HMM contamination levels. This provide an important conclusion that long-lasted low water period associated mostly with changes in precipitation patters have a significant impact on geochemical fluxes due to changes in sediment delivery and sources related to the shifts in catchment erosion processes.
4. Significant inter-annual variability in mean values of particulate organic carbon POC has been found. POC content in total SPM reached 23,6 % during flood in 2013 and was negligibly small during winter low water season. The annual Selenga River discharge of particulate organic carbon (POC) can be as high as 0,0005 Tg (1Tg = 10^{12} g) which is 3-4 orders of magnitude less then POC flux in the Enisey River outlet (Holmes et al, 2015). As far as catchment area of Enisey and Selenga are differed in just 1 order of magnitude (2540000 km^2 against 477000 km^2), this emphasize significant differences in fluvial carbon input between headwaters and downstream of large Arctic catchment (Enisey river).
5. Important role of the fluxes delivery to Lake Baikal is played by delta. The delta network has a large influence on the mass of metals reaching Lake Baikal at the delta outlet. Up to 50 % of suspended and up to 70 % of the total sediment loads are stored in certain parts (sectors) of the delta. Although the differences in average conditions between the channels are not large, there are generally larger differences within each channel reach.

ACKNOWLEDGEMENTS

The work at Selenga River is implemented under support of Russian Scientific Foundation project (№ 14-27-00083).

REFERENCES

Chalov Sergey R., Jarsjö Jerker, Kasimov N., Romanchenko A., Pietron Jan, Thorslund J., Belozerova E.. (2015) Spatio-temporal vari-ation of sediment transport in the Selenga River Basin, Mongolia and Russia // Environmental Earth Sciences. Vol. 73, Iss. 2 pp 663-680

Chalov S, Lychagin M, Kasimov N, Belozerova K, Shinkareva G, Romanchenko A, Khristoforov A (2013) Water Resources assessment of the Selenga-Baikal river system. Geo-Öko (Journal of Geoecology) 34 (70): 77-102. Special Issue "Central Asian Ecosystems under Water Scarcity"

Chalov SR, Zavadsky AS, Belozerova EV, Bulacheva MP, Jarsjö J, Thorslund J, Yamkhin J (2012) Suspended and dissolved matter fluxes in the upper Selenga River Basin. Geography, Environment, Sustainability 02(05) 2012: 78-94

Holmes, R.M., J.W. McClelland, B.J. Peterson, S.E. Tank, E. Bulygina, T.I. Eglinton, V.V. Gordeev, T.Y. Gurtovaya, P.A. Raymond, D.J. Repeta, R. Staples, R.G. Striegl, A.V. Zhulidov, and S.A. Zimov. 2012. Seasonal and annual fluxes of nutrients and organic matter from large rivers to the Arctic Ocean and surrounding seas. Estuaries and Coasts 35:369-382, doi: 10.1007/s12237-011-9386-6

Pietroń J, Jarsjö J, Romanchenko AO, Chalov S R (2015) Model analyses of the contribution of in-channel processes to sediment concentration hysteresis loops. Journal of Hydrology 527: 576-589

Törnqvist R, Jarsjö J, Pietron J, Bring A, Rogberg P, Asokan SM, Destouni G (2014) Evolution of the hydro-climate system in the Lake Baikal basin. J Hydrol 519:1953-1962

Unger-Shayesteh K, Vorogushyn S, Farinotti D, Gafurov A, Duethmann D, Mandychev A, Merz B (2013) What do we know about past changes in the water cycle of Central Asian headwaters? A review. Global Planet Change 110(Part A):4–25. doi:10.1016/j.gloplacha.2013.02.004

TOWARDS GLOBAL SMEAR NETWORK TO PROVIDE COMPREHENSIVE DATA FOR KNOWLEDGE BASED DECISIONS

M.T. KAUKOLEHTO[1,2], J. BÄCK[2], P. HARI[2], V.-M. KERMINEN[1], J. KUJANSUU[1], H.K. LAPPALAINEN[1,3], J. LEVULA[4], T. PETÄJÄ[1], T. VESALA[1] AND M. KULMALA[1]

[1]Department of Physics, University of Helsinki, Helsinki, Finland

[2]Department of Forest Sciences, University of Helsinki, Helsinki, Finland

[3]Finnish Meteorological Institute, Helsinki, Finland

[4]SMEARII, Hyytiälä Forestry Field Station, University of Helsinki, Korkeakoski, Finland

Keywords: SMEAR, RESEARCH INFRASTRUCTURE, IN-SITU EARTH OBSERVATION, DATA

INTRODUCTION

Humanity faces several grand challenges that are of global nature, and associated with e.g. climate change, clean air, fresh water and food security. It is recognized that climate change represents an urgent and potentially irreversible threat to human societies and the planet requiring the widest possible cooperation by all countries. COP21 agreement in December 2015 called Parties to “strengthen scientific knowledge on climate, including research, systematic observation of the climate system and early warning systems, in a manner that informs climate services and supports decision-making”. It is evident that the grand challenges cannot be solved using only traditional sources of information that are currently generated by, for example, fragmented environmental monitoring. There is urgent need for an integrated approach to observe in a coherent way all the components affecting the air quality and climate change to fill the in-situ observational gaps in the world (see Kulmala *et al*. 2015). This needs to be done with a station network to provide comprehensive policy relevant data.

The Finnish Stations to Measure Ecosystem – Atmosphere Relations, SMEAR, have globally renowned reputation and knowledge base in continuous, comprehensive measurements of fluxes, storages and concentrations of energy and matter in the ecosystem atmosphere continuum (Figure 1). SMEAR is particularly designed for multidisciplinary research on ecosystem-atmosphere interactions including not only the measurement system but also data issues. SMEAR concept is unique in the world. A network of SMEAR type stations would be invaluable source of comprehensive data for knowledge based decision making. We describe the basic elements of SMEAR and invite all interested to participate in the Global SMEAR network. Our solution provides means not only to solve Grand Challenges, but also to train world class researchers and to be in the forefront of the technological development. The solution is to establish SMEAR type measurement stations over the globe during 2018-2030.

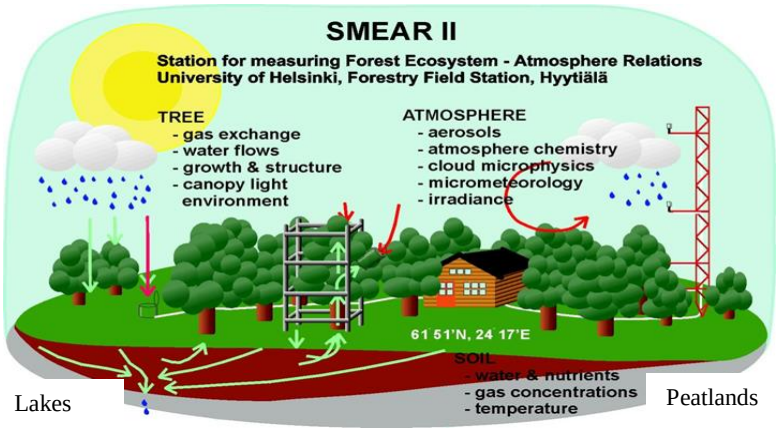

Figure 1. Picture showing the scientific concept of the SMEAR II station measurements in Hyytiälä, boreal Finland.

STATIONS TO MEASURE ECOSYSTEM – ATMOSPHERE RELATIONS, SMEAR

International scientific interest towards SMEAR stations is increasing. SMEAR station is a comprehensive and integrated set of sophisticated measurement and observation equipment, their installations, data infrastructure, configurations and processing. Science methodological idea of a SMEAR station is to combine the following aspects:

i) continuous and comprehensive in situ observations in different types of environments or ecosystems and platforms,
ii) ground- and satellite-based remote sensing,
iii) targeted laboratory experiments and
iv) multi-scale modeling efforts, in order to provide improved conceptual understanding over the relevant spatial and temporal scales.

To be fully functional and able to exploit its full capacity the SMEAR station needs to include the following components:

A) Scientific measurement equipment. Atmospheric composition: high precision mass spectrometers and analyzers for trace gases and aerosols, boundary layer properties (lidar, cloud radar etc), and all the other sensitive equipment located in the measurement building(s); flux measurements: eddy covariance for GHGs, aerosols and trace gases, and small scale gas exchange measurement systems (enclosures); meteorological/environmental variables: temperature, moisture etc. from atmosphere, soil and aquatic phase.
B) Data infrastructure, software and quality assurance and control tools. SmartSMEAR tool is part of the scheme. It enables the process-level understanding that can be expanded to continental and global scales together with advanced data analysis, earth system modelling and satellite remote sensing.
C) Standardised working methods and interoperability; trained and skilful station staff.
D) Civil construction and basic infrastructure to support the SMEAR activities: internet connection, roads to access, buildings, station staff.

BENEFITS OF GLOBAL SMEAR

Scientifically the benefits of having a Global SMEAR network are fundamental. Global SMEAR encourages to open cooperation over the domain boundaries and exchange of ideas between the researchers from different disciplines in solving the Grand Challenges. Researchers are be able to employ an integrated systems approach to solve complex environmental problems, such as quantifying consequences, impacts, and effects, recognizing the signal within the natural variability, identifying feedback mechanisms and effectively communicating uncertainty and relative risks, and eventually enable

evidence based policy making. Global SMEAR provides an efficient tool for Measurement, Reporting and Verification (MRV) for the COP process.

Global SMEAR decreases fragmentation and joins forces for global scale environmental observations. Work done in the framework of Global SMEAR would enhance the sharing of technical knowhow and knowledge transfer. Especially, with the tailor-made help, training and consultation from the groups at the University of Helsinki, adoption of the concept would save time and effort from participating institutes to become part of a world class research facility.

High quality observational data, data management and interoperability are in the heart of the SMEAR concept. The visibility and usage of data from the Global SMEAR stations would increase internationally. SMEAR stations are able to feed data to many international Earth Observation systems and networks, such as to ICOS, ACTRIS, ANAEE, LiFeWatch, EMEP, WMO GAW, FluxNet, AERONET, SOL-RAD-NET and EARLINET. University of Helsinki SMEAR teams are to help the participating institutes in data related issues.

Being part of Global SMEAR network would bring solutions not only for global questions but also for regional level questions, such as air quality issues. Global SMEAR network generates innovation (markets, products), growth and employment opportunities on national and international levels.

IMPLEMENTATION

The University of Helsinki, Finnish Meteorological Institute and University of Eastern Finland have a long experience on integrative atmospheric and biosphere-atmosphere observations. Therefore we have good experience for MRV, to measure all radiative components, to report results using open science, open data and also to validate the impact of those measurements as well as policy actions. Lappeenranta University of Technology has long experience on data assimilation and inversion. All partners are highly integrated in European and global projects and networks. We have demonstrated how the SMEAR concept is successfully implemented in Finland especially at the SMEAR II station. The SMEAR II station has produced >2000 scientific publications over 20 years (Figure 2), and the data has been used e.g. in Inter-governmental Panel for Climate Change (IPCC). SMEAR II has become a globally attractive and acknowledged research facility and we have a vision how this could be up scaled to global level.

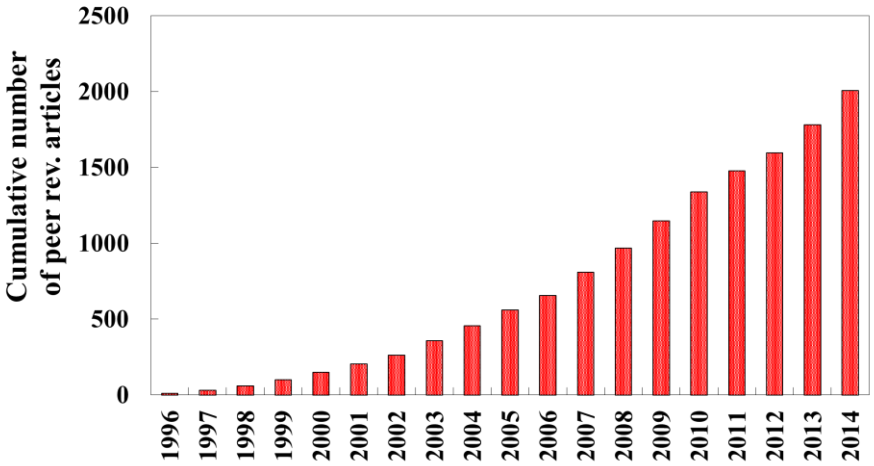

Figure 2. From 1996 to now, more than 2000 peer-reviewed articles have been published using SMEAR II data, 34 of them in Nature and Science.

We can enable participation in the Global SMEAR network by providing ready concept how to build up a SMEAR station. The station network can be implemented using the existing station infrastructure and by

constructing new ones (Hari *et al.* 2016). University of Helsinki would closely collaborate and consult the participating institutes in developing the stations. Training, knowledge transfer and technical guidance are important parts of the process. We offer a service package that can be discussed and further elaborated to best fit the services into the needs of participating institutes.

The construction of the Global SMEAR network takes years, but we need to start now to be able to tackle Grand Challenges early enough. There is need for coordinated investments from the governments, research institutes, and industry and commerce. By 2020 we aim to have a preliminary network in place producing open data. Policy relevant results and outcomes will follow and within seven-ten years to be used for decision making affecting the future of humanity.

REFERENCES

Hari, P., Petäjä, T., Bäck, J., Kerminen, V.-M., Lappalainen, H. K., Vihma, T., Laurila, T., Viisanen, Y., Vesala, T., and Kulmala, M. (2016). Conceptual design of a measurement network of the global change, *Atmos. Chem. Phys.*, 16, 1017-1028, doi:10.5194/acp-16-1017-2016.

Kulmala, M., Lappalainen, H. K., Petäjä, T., Kurten, T., Kerminen, V.-M., Viisanen, Y., Hari, P., Sorvari, S., Bäck, J., Bondur, V., Kasimov, N., Kotlyakov, V., Matvienko, G., Baklanov, A., Guo, H. D., Ding, A., Hansson, H.-C., and Zilitinkevich, S. (2015). Introduction: The Pan-Eurasian Experiment (PEEX) – multidisciplinary, multiscale and multicomponent research and capacity-building initiative, *Atmos. Chem. Phys.*, 15, 13085-13096, doi:10.5194/acp-15-13085-2015, 2015.

TOWARD GLOBAL PICTURE OF ATMOSPHERIC NEW PARTICLE FORMATION BASED ON OBSERVATIONS

V.-M. KERMINEN[1], T. NIEMINEN[1,2], T. PETÄJÄ[1], A.J..DING[3,4], M. HU[5], L. WANG[6], and M. KULMALA[1],

[1]Department of Physics, University of Helsinki, Helsinki, Finland.

[2]University of Eastern Finland, Kuopio, Finland.

[3]Joint International Research Laboratory of Atmospheric and Earth System Sciences (JirLATEST) between Nanjing University and University of Helsinki

[4]School of Atmospheric Sciences, Nanjing University

[5]State Key Joint Laboratory of Environmental Simulation and Pollution Control, College of Environmental Sciences and Engineering, Peking University, Beijing 100871, China

[6]Department of Environmental Science and Engineering, Fudan University, Shanghai, China

Keywords: NUCLEATION, PARTICLE FORMATION AND GROWTH RATE, CLOUD CONDENSATION NUCLEI

INTRODUCTION

Atmospheric aerosols have a large impact on air quality, human health and even the global climate. One of the largest uncertainties related to climate change is the magnitude of the cooling effect of aerosols that counteracts the warming caused by greenhouse gases (IPCC, 2013). Formation of secondary aerosol particles is a major source of atmospheric aerosol particles, and eventually cloud condensation nuclei (Kerminen et al., 2012). Regional events of new particle formation (NPF) have been observed worldwide (Kulmala et al., 2004), yet there is little information about the seasonality of the NPF and related parameters in different environments.

The aim of this study was provide a global view on atmospheric new particle formation based solely on measurements. In order to do this, we gathered observations of the annual cycle of new particle formation (NPF) events from as many measurement sites as possible, but with the condition that at least one year of particle size distribution measurements were available. As the number of such sites is rather limited, we included sites with a shorter data coverage but what could be parsed into a full seasonal cycle.

DATA AND METHODS

Aerosol number concentration size distribution data were obtained from the EBAS database (http://ebas.nilu.no/) and from several research groups running long-term aerosol measurements. The Differential Mobility Particle Sizer (DMPS) or Scanning Mobility Particle Sizer (SMPS) instruments typically had lower detection limits varying between 3 and 10 nm. In order to have comparable results between different sites, a common size range of 10–25 nm was used for nucleation mode particles in this study. Altogether, we identified 32 measurement sites worldwide where aerosol size distributions have been measured for at least one year (either continuously or in separate campaign covering a full annual cycle). The majority of the sites is located in the Northern Hemisphere in Europe.

The size distribution data was classified into NPF event, non-event and undefined days according to the guidelines presented by Kulmala et al. (2012). We included so-called class I events, in which the formation and subsequent particle growth is distinguishable for at least several hours.

To quantify the NPF events, the formation rate J_{nuc} of nucleation mode particles (10–25 nm in diameter) was calculated as

$$J_{nuc} = \frac{dN_{10-25}}{dt} + CoagSN_{10-25} + \frac{GR}{15nm} N_{10-25}$$

where CoagS is the coagulation sink of the nucleation mode particles into the pre-existing larger particles and GR is the condensational growth rate out from the nucleation mode. The growth rate was calculated by fitting log-normal modes to the measured size-distribution data and following the time evolution of the geometric mean of the nucleation mode.

RESULTS

Regional NPF events were observed at all the sites throughout the year. Averaged over all the sties, the frequency of NPF events ranged from 12% in December–February to 31% in March–May. The event frequencies did not show a clear environmental pattern, except that higher frequencies in many "rural" environments and lower ones at high-latitude areas. The NPF frequency was the highest in the savannah area in Southern Africa. A surprising finding was the common occurrence of NPF under extremely polluted conditions, such as those encountered in Chinese megacities.

The formation rates of 10-nm particles, averaged over the sites, varied from 0.6 cm^{-3} s^{-1} in winter to 0.9 cm^{-3} s^{-1} in spring. Although the particle formation rates did not show large a seasonal variation, there were large differences between the different environments. The highest formation rates were >1 cm^{-3} s^{-1} and took place in cities and other heavily-polluted areas, while substantially lower rates were observed in remote sites. In many polluted areas, SO_2 concentrations are high, leading to high concentrations of sulfuric acid which is a key precursor species in atmospheric NPF.

The average growth rate of 10 –25 nm particles varied from about 2.7 nm/hour in winter to 4.4 nm/hour in summer. The growth rated did not show any environmental dependences, but hints of a clear biogenic and/or photochemical influence was observed (the summer peak in growth rate). The observed growth rates mean that, in most sites, it takes between 1 and 3 days for newly-formed particles to reach sizes at which they can act as cloud condensation nuclei.

CONCLUSIONS

We have made a global analyses of atmospheric new particle formation events based on a very large data set of aerosol number size distribution measurement. We found that NPF occurs relatively frequently (typically 10-30% of days) throughout the continental boundary layer. Considering the typical particle formation and growth rates at different sites, we may conclude that NPF gives a significant contribution not only to the particle number concentration budget, but also to cloud condensation nuclei concentrations in continental boundary layers. Our analysis reveals several interesting, yet not well understood features, such as the relatively frequent occurrence of NPF in highly-polluted environments.

ACKNOWLEDGEMENTS

This work was supported by the Academy of Finland Centre of Excellence (grants no. 1118615 and 272041).

REFERENCES

IPCC: The Physical Science Basis, Contribution of Working group I to the Fifth Assessment Report of the Intergovernmental Panel on Climate Change (2013), edited by: Stocker, T.F., Qin, D., Plattner, G.-K. and others, Cambridge University Press, Cambridge, United Kingdom and New York, NY, USA.

Kerminen, V.-M., Paramonov, M., Anttila, T., Riipinen, I., Fountoukis, C., Korhonen, H., Asmi, E., Laakso, L., Lihavainen, H., Swietlicki, E., Svenningsson, B., Asmi, A., Pandis, S. N., Kulmala, M. and Petäjä T. (2012) Cloud condensation nuclei production associated with atmospheric nucleation: a synthesis based on existing literature and new results. *Atmos. Chem. Phys.*, **12**, 12037−12059.

Kulmala, M., Vehkamäki, H., Petäjä, T., Dal Maso, M., Lauri, A., Kerminen, V.-M., Birmili, W. and McMurry, P. H (2004). Formation and growth rates of ultrafine atmospheric particles: a review of observations. *J. Aerosol Sci.* **35**, 143–176.

Kulmala, M., Petäjä, T., Nieminen, T., Sipilä, M., Manninen, H.E., Lehtipalo, K., Dal Maso, M., Aalto, P.P., Junninen, H., Paasonen, P., Riipinen, I., Lehtinen, K.E.J., Laaksonen, A. and Kerminen, V.-M. (2012) Measurement of the nucleation of atmospheric aerosol particles. *Nature Protocols*, **7**, 1651-1667.

CLIMATE AS A FACTOR OF SUSTAINABLE DEVELOPMENT OF ALTAI-SAYAN MOUNTAIN COUNTRY

N.F. KHARLAMOVA, I.N. ROTANOVA

Altai State University, Barnaul, Russia

In the last decade, the increased interest to the problems of global climate change is primarily related to climate impact on human life and functioning of various sectors of the economy. Global climate change is the scope of regional changes at different temporal and spatial scales. Often, regional changes are of extreme nature (droughts, floods, severe and mild winters).They had and still have the most significant effect on economic and social life. The events associated with the latest global warming have urged scientists, practitioners and policy makers to consider the climate as a major natural resource, which redistribution among countries may have serious socio-economic and political consequences.

Particular emphasis has been made on climate change impact on the standard of living and life quality in the mountain areas, i.e. Inner Asia. Chapter 27 of the UN Resolution "Millennium Ecosystem Assessment" (2005) says that mountain dwellers face such challenges as severe weather conditions, the vulnerability of mountain ecosystems to natural and anthropogenic impacts and low agricultural productivity. Interestingly, the mentioned changes are all climate-induced themselves (Aidaraliev, 2009). Along with other objective factors, climatic conditions seem to be more important than, for example, inaccessibility and isolation of territories.

The Agenda of XXI Century adopted by the UN conference in Rio- de- Janeiro (1992) clearly shows that "the mountains are very susceptible to disturbance of ecological balance caused by human activity or natural processes." The increase in the surface temperature leads to reduction in the mountain glacier area. In addition to risks associated with the decrease in strategic reserves of fresh water, the glacier melting results in seasonal increase of flow, which, in turn, causes a dramatic increase in the frequency of landslides, avalanches and landslides, flooding, soil salinization and soil erosion. Soil erosion and decline in pasture productivity because of intensive use and climate change in the mountains of Central Asia have become critical. Many areas of the intermountain basins have a strong tendency to climatic desertification, particularly in Mongolia, China and Kazakhstan that substantially aggravates the ecological and economic situation. Natural conditions, hard for living in the inland mountain areas, lag living standards, intensify migration and the development of other negative social and economic processes.

Currently, the mountain ecosystems have become a haven for nearly half of the world's biodiversity. The presence of many species of plants and especially animals determines and forms the basis for the traditional way of life, including cultural and spiritual development of the local population. Among the main threats to the biodiversity of mountain ecosystems, climate change also plays a significant role.

Thus, we can identify the direct and indirect impacts of climate change on natural systems, living conditions and socio-economic development of the plains and mountain areas of continental Asia.

A brief overview of potential effects and risks of climate change is evidence of urgent study of this topical problem. According to the Fourth Assessment Report of the IPCC, rise in the air temperature in Russia for the past 100 years (1907-2006) made up 1,29°C (Evaluation Report ..., 2008) at an average global warming of 0,74°C (2007). Meanwhile, it is known that often a global averaging eliminates various trends in regional and local change. Hence, "despite the fact that the global average temperature, rainfall, etc. are suitable for tracking changes in the global climate, many sectors of the society need for more practical information applicable to small scales" (Bassalachi, Asrar, 2009). The demand for climate change data on regional and local scales are one of the main issues of global change to be discussed.

Note that according to the data from Barnaul weather station, the annual temperature increased by 1,8°C for 100 years (1901-2000). Warming is most typical for winter and spring seasons. Long-term trends are accompanied by a small-scale positive and negative deviations of cyclic (rhythmic) character. Still, late spring and early autumn frosts with increased extreme variability are probable. In recent years, a growing frequency of a very low absolute minimum of air temperature indicative of strengthening winter severity has been observed. Inter-annual variability (contrast) of seasons intensifies (Kharlamova, 2013).

In order to identify climate change trends, the series of meteorological data from weather stations in the Russian part of the Altai-Sayan mountain country (ASMC) are compared to those (most complete) from Barnaul station (BWS) situated in the south-east of West Siberia. Good correlation of changes in the air temperature and annual precipitation from ASMC stations and BWS makes it possible to use long-term trends identified by BWS as background ones for the study area.

Linear trends of annual air temperature for all weather stations are positive, except for some deceleration in the last decade due to strengthening of winter severity. Meanwhile, the cold snap is still observed on the ascending branch of

the long-term trend of global warming.

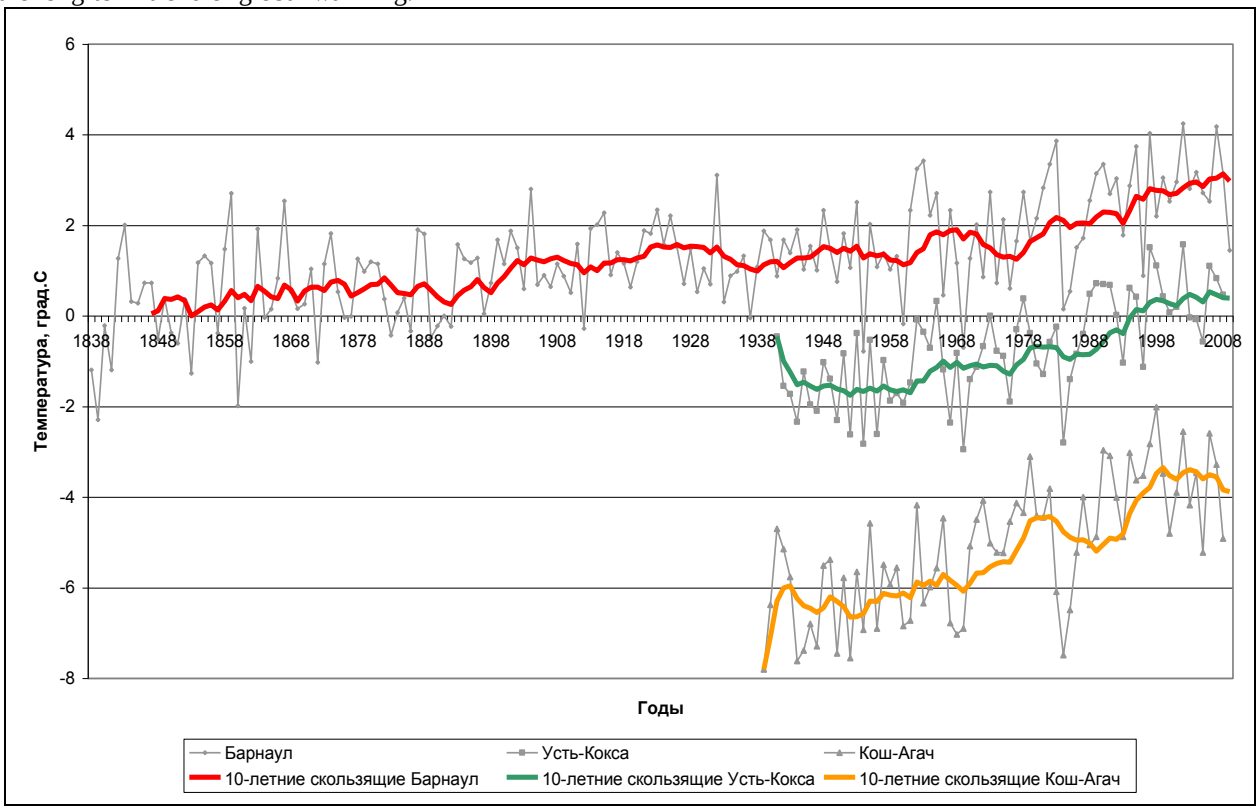

Fig 1. Annual air temperature: values and 10-year moving average for Barnaul (1838-2010), Ust-Koksa, Kosh-Agach (1944-2010)

Linear trends demonstrate maximum increase in the annual air temperature for the 50 years for the intermountain basins (Kyzyl +3,5 ° C; Erzin +3,4 ° C; Kosh-Agach +2,7 ° C, Ust- Koksa +2,1 ° C) and minimum - for highlands (Kara-Turek +1,2 ° C; Akkem +1,5 ° C). In all high-altitude zones, the change in the average annual temperature is synchronous and cyclic.

The data on atmospheric precipitation is distinguished by considerable heterogeneity. The correlation analysis of the series on annual precipitation shows their asynchronous character (especially noticeable when comparing the stations in the intermountain basins and on the slopes of the mountain ranges). This is due to transformation of precipitation fields and different structure of annual precipitation. In the intermountain basins, most precipitation falls on the warm season: here, the sources are front cloud fields and local convective processes influenced by the topography and depression position relative to air masses transport. However, it is possible to establish good correlation in the change of precipitation recorded by BWS and many other weather stations located on the mountain slopes. For distribution of precipitation, we used the secular cycle of 1850-1976 with its maximum in 1907-1912. From 1977-1978 a new secular cycle with its probable maximum in 2038 has started. The increase in annual precipitation may reach 15-20% as compared to the year 2000. At present, after a humid period of 1986-2002, the growing inter-secular cycle of decreased humidity is observed. Important initial phases of vegetation period are accompanied with scarce moisture supply in spring and the first half of summer.

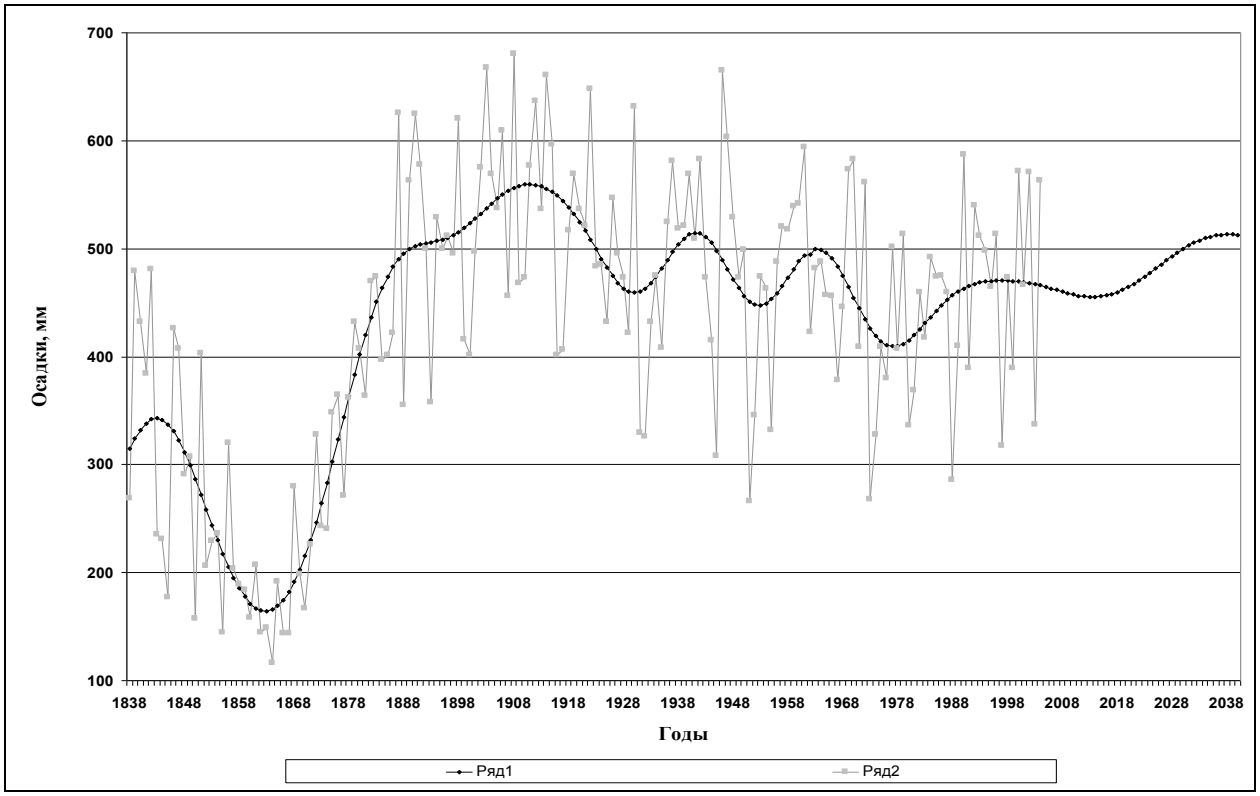

Fig 2. Annual precipitation: values and smooth low-frequency filter for Barnaul (1838-2038)

The ratio of heat and moisture is indicative of probable occurrence of further aridization (progressively developing xerothermic trend). This is supported by the increase in number of days with dry winds, dry weather and dust storms. Another characteristic of warming is increased inter-annual variability (contrast) of seasons and probability of adverse, severe weather events (hail, squalls, floods, etc.). These processes are cyclic, characterized by own territorial and regional specific manifestation.

Therefore, the implementation of the concept of sustainable development requires the consideration of climatic factors for functioning of the natural and socio-economic communities. The analysis of current climate in continental Asia, the identification of regional characteristics of potential climate change and the development of strategies for economy adaptation to the changing climate are urgent and of great importance for ensuring sustainable communities.

The solution of these extremely challenging problems related with defining trends of climate change to provide biodiversity conservation should be based on research coordination, joint efforts of scientists from different organizations and the use of different methods.

The report was supported by the Department of Earth Sciences № 13.3 «Bioclimatic potential as a factor of sustainable development of the Russian Altai under economy reformation and regions diversification."

REFERENCES

1. Assessment Report on climate change and its consequences the RF territory / Federal Service for Hydrometeorology and Environmental Monitoring. Moscow, 2008. 28 .
2. The Fourth Assessment Report of the IPCC, 2007. IPCC Fourth Assessment Report: Climate Change 2007 (AR4). IPCC, Geneva, Switzerland:104. http / / www.ipcc.ch/ipccreports/ar-4-wg1.htm
3. Bassalachi A.Dzh, Asrar G.R. World Climate Research Programme: Achievements, activities, and tasks / / WMO Bulletin. T. 58 (3), July 2009: 51-161.
4. Kharlamova N.F. Assessment and forecast of current climate changes in Altai Region: monograph. - Barnaul: ASU Publ. 2013:172.

CLIMATE VARIABILITY OVER THE TERRITORY OF WEST SIBERIA

E.V. KHARYUTKINA, S.V. LOGINOV, I.I. IPPOLITOV

Institute of Monitoring of Climatic and Ecological Systems SB RAS,
634055, 10/3 Academichesky ave., Tomsk, Russia

Keywords: CLIMATE VARIABILITY, SURFACE AIR TEMPERATURE, ATMOSPHERIC PRESSURE, RADIATIVE AND CIRCULATION FACTORS, WEST SIBERIA

INTRODUCTION

According to climatic observations, global surface air temperature and sea surface temperature rise has decelerated from the beginning of XXI century (Trenberth and Fasullo, 2013; Chen and Tung, 2014). The anomaly is in the fact that it has appeared against the background of ongoing increase in the greenhouse gases concentration in the atmosphere, providing the positive (0.5-1.0 W/m^2) radiative balance at the top of atmosphere (Trenberth *et al.*, 2014). It means that the Earth's climatic system receives an additional heat, which doesn't change surface air and sea surface temperature, because the most part of the «missing heat» is accumulated in deep layers of the ocean (Katsman, van Oldenborgh, 2011; Loeb *et al.*, 2012; UK Met Office, 2013; Chen and Tung, 2014). The understanding of the reasons demands the integrated investigation of regional climates and different factors, which influence on climate (by International Geosphere-Biosphere Programme IGBP). Temperature field investigation over the north part of Eurasia, carried out by Outten and Esau (2012), has shown that during last decade in winter months in middle latitudes regions with negative temperature trend appeared. The similar tendencies were also obtained by Overland *et al.* (2008). According to the authors, the reason of such tendency deals with ice melting in the coastal Arctic seas; it leads to decrease of meridional temperature gradient and weakening of west transfer, which brings heat to this region from the North Atlantic.

Climate changes have significant seasonal differences, which are result from the complex of physical processes in climatic system. Seasonal variability of meteorological parameters and its features in different latitudinal zones of the Earth are first of all determined by the amount of solar radiation, which earth's surface and ocean receive during a day. Thus, the main factor which play an important role in the weather and climate formation is solar radiation. Significant contribution to the study of radiative fluxes, which are the part of the earth's surface heat balance, was made by Budyko (1958). Current constructions of radiative balance are based on the analysis of assimilated data, satellite estimates of global radiant and/or the hybrid approach of in-situ and satellite measurements (Da Silva *et al.*, 1994; Rossow and Zhang, 1995; Trenberth and Stepaniak, 2004). Global warming is accompanied with the changes of atmospheric circulation and it leads to spatial distribution of heat and moisture and, as a result, spatio-temporal climate peculiarities. The relationship between atmospheric circulation in the North Eurasia and surface air temperature changes is investigated in many studies. Byshev et al. (2004) have found a good agreement between atmospheric circulation patterns and the sign of surface air temperature anomaly. The research for winter months over the period of 1951–2004 was carried out by (Popova, 2006). It was revealed that the processes of west transfer blocking by mesoscale baric systems (vortices and ridges in the North Atlantic) play a significant role in atmospheric circulation changes.

According to the Report on climate features over the territory of Russian Federation for 2011, global warming rates in West Siberia over the period of 1976-2013 are less than that in other regions of Russia. Thus, the main goal of this study is to determine the contribution of radiative fluxes and large-scale atmospheric circulation to the temperature and pressure variability over West Siberia against the background of surface temperature rise deceleration over last decades.

METHODS

The characteristics of the spatial and temporal variability of meteorological parameters were calculated using daily observational data at 169 stations in West Siberia (50-70ºN, 60-90ºE) over the period of 1976−2014 (ftp://ftp.cdc.noaa.gov/pub/data/gsod/). To reveal the long-term variability of radiative fluxes at the surface JRA-55 reanalysis data (http://jra.kishou.go.jp/JRA-55/index_en.html) with spatial resolution 1.25º × 1.25º.

The large-scale atmospheric circulation indices, selected from the set of Northern Hemisphere circulation indices (Barnston and Livezey, 1987), describe the main atmospheric circulation modes over West Siberia: Arctic Oscillation (AO) and Scandinavian Index (SCAND) (http://www.cpc.ncep.noaa.gov/data/indices).

To estimate the significance of correlation coefficient, the Fisher transformation was used with further two-sided *t*-test of the null hypothesis at significance level α=0.05 (von Storch *et al.*, 2003).

The climatic tendencies in the end of XX and in the beginning of XXI centuries were assessed through the comparison of temperature and pressure variability estimates for two time intervals: 1976–2005 and 1985–2014. It was established that climatic changes during the second period as before have the tendency to annual average temperature increase, but the warming process was less intensive during the first period. Annual average trend estimates of temperature are the following: T_{tr1}=0.36°C/decade with σ_1=±0.27°C/decade over the first period and T_{tr2}=0.24°C/decade with σ_2=±0.11°C/decade over the second one.

A large role in the decrease of the temperature rise rates belongs to the winter months when the warming process is replaced by the cooling process (Fig.1a). Furthermore, there is a tendency to pressure rise for the second time interval (Fig.1b).

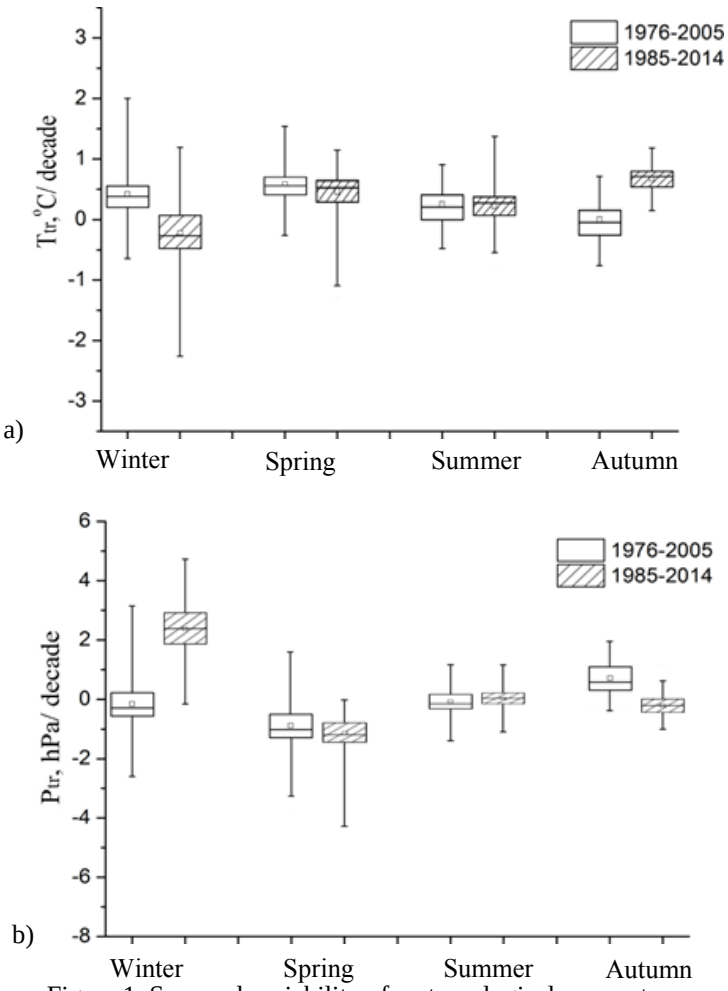

Figure 1. Seasonal variability of meteorological parameters

To reveal the reason of such changes it is important to take into account, first of all, the variability of radiative balance elements and sensible and latent heat fluxes between atmosphere and surface. Any identified patterns of radiation can be subsequently used to explore potential relationships between surface energy budget and atmospheric circulation or other atmospheric parameters. In addition, identification of regions with common variability in radiative fluxes and their trends may be valuable in the understanding of driving physical processes.

Heat balance equation at the surface is (Budyko, 1958):

$$B_s = Q_n + L_n - LE - P, \qquad (1)$$

where B_S – net radiation at the surface, $Q_n = Q_{\downarrow S} - Q_{\uparrow S}$ – net shortwave radiation at the surface, $L_n = L_{\downarrow S} - L_{\uparrow S}$ – net longwave radiation at the surface, and $L_{nS} = - E_{eff}$, where E_{eff} – effective radiation. LE and P – latent and sensible fluxes, respectively. Q_S and L_S – shortwave and long wave radiation, coming to the surface (↓) or outgoing from the surface (↑).

According to the interannual variability of heat balance elements in winter months, there is a statistical significant increase of both net shortwave radiation Q_n and effective radiation E_{eff} at the beginning of XXI century. Such behavior is probably connected with the variability of cloudiness characteristics, which is included in the equation (1) in implicitly form. And *Eg* parameter statistically significantly decrease due to snow cover characteristics variability.

As for circulation indices variability it was revealed that global circulation indices with the highest correlation with temperature for the territory of West Siberia have changed their phase during the first

decade of XXI century: AO index – from positive to negative and SCAND – conversely, from negative to positive. Their interannual variability and eigen vectors (EOFs) can indicate that meridional temperature gradient decrease and weakening of midlatitude west transport probably cause the development of blocking processes.

Thus, we chose two groups of climate formation factors: radiative and circulation factors. To estimate the contribution of each group to temperature variability the heat balance equation (1) could be rewritten in the following way:

$$\delta T = \beta_1 \delta Q_n + \beta_2 \delta E_{eff} + \beta_3 \delta E_g + \beta_4 \delta SCAND + \beta_5\ \delta AO, \qquad (2)$$

To solve multi-linear regression equations, a stepwise regression algorithm was applied.

It is supposed that temperature and pressure fields are interrelated, so to describe pressure variability (δP) we can use the same form of equation (2).

Derived monthly average estimates of determination coefficients (R^2) are statistically significant for both time intervals 1976-2005 and 1985-2014. According to constructed regression models, dominating role in the variability of understudy parameters belongs to radiative factors (i.e. components of heat balance). However, in winter season during 1985-2014 the part of these factors decreased from 81% to 69%, whereas the influence of circulation factors has enhanced: the part of AO index statistically significantly increased in 10% in temperature variability (Fig.2a) and the part of SCAND index increased in 15% in pressure variability (Fig.2b). In contrast to winter season, in autumn months when consistent temperature and pressure changes are observed (Fig.1), the influence of circulation factors has not been revealed.

Thus, according to enhanced role of circulation indices in temperature and pressure variability, there is an opportunity for blocking process development, weakening west transfer and changing climatic characteristics in West Siberia (Petoukhov and Semenov, 2010; Semenov and Mokhov, 2012).

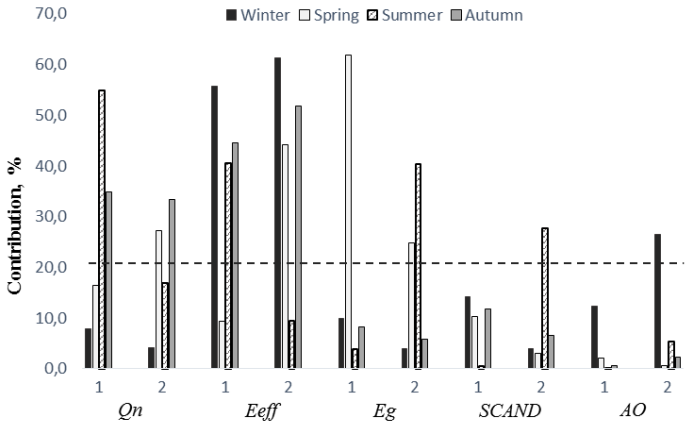

a)

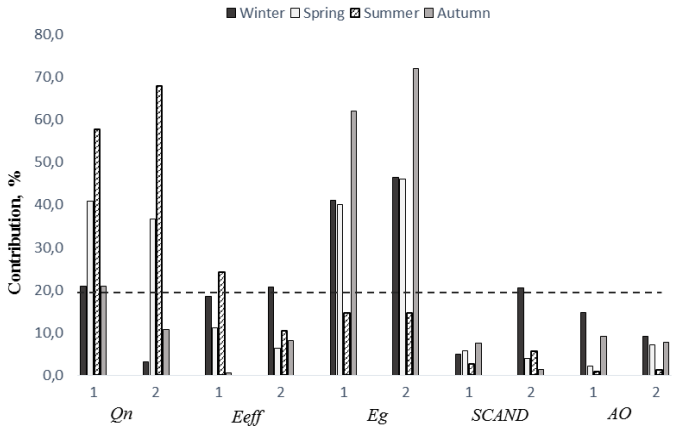

b)

Figure 2. Contribution of each predictor in regression analysis to temperature variability (a) and atmospheric pressure (b) over the territory of West Siberia, where 1 - 1976-2005; 2 - 1985-2014; dash line – level of significance.

CONCLUSIONS

It was revealed that climatic changes during the period of 1985-2014 as before there is a tendency to annual average temperature increase, but the warming process was less intensive than during the first period. A large role in the decrease of the temperature rise rates belongs to the winter months when the warming process is replaced by the cooling process. Furthermore, there is a tendency to pressure rise over the time interval of 1985-2014. The influence of radiative factors decreases in winter months during last decade, whereas the influence of circulation factors has enhanced: the part of AO index statistically significantly increased in 10% in temperature variability and the part of SCAND index increased in 15% in pressure variability. In addition, global circulation indices have changed their phase during the first decade of XXI century: AO index – from positive to negative and SCAND – conversely, from negative to positive. According to enhanced role of circulation indices in temperature and pressure variability, there is an opportunity for blocking process development, weakening west transfer and changing climatic characteristics in West Siberia. However, it should be noted that radiative factors were estimated using only one reanalysis database, but it is necessary to compare derived results with that from other databases.

Thus, this research shows the example of winter local cooling over the territory of West Siberia. Nevertheless, there is a positive annual averaged temperature trend but it have been significantly decreased during last decade.

ACKNOWLEDGEMENTS

The work is supported by the grant of the RF President MK-5969.2015.5.

REFERENCES

Barnston A. G., R. E. Livezey (1987). Classification, Seasonality, and Persistence of Low-Frequency Atmospheric Circulation Patterns. *Monthly Weather Review*. 6. P. 1083-1126.

Budyko, M.I. (1958). *The heat balance of the earth's surface* / transl. from the Russ. N.A. Stepanova. (Washington, U.S.: Dept. of Commerce, Weather Bureau). 259 pp.

Byshev, V.I., V.G. Neiman, Yu.A. Romanov, N.K. Kononova (2004). Quantitative assessment of the parameters of sea-air system climatic variability. *Oceanology*. **44**. 315-326.

Chen, X. and Ka-Kit, Tung (2014). Varying planetary heat sink led to global-warming slowdown and acceleration. *Science*. **345**. 6199. P. 897-903.

Da Silva, A. M., C.C. Young and S. Levitus (1994). *Atlas of Surface Marine Data, Algorithms and Procedures*, NOAA Atlas NESDIS 6, U.S. Dep. of Commer., Natl. Oceanic and Atmos. Admin./ (Natl. Environ. Satellite Data Inf. Serv., Silver Spring, Md., v.1.)

Katsman, C.A., G.J. van Oldenborgh (2011). Tracing the upper ocean's "missing heat". *Geophys. Res.Lett.* **38**. L14610, doi:10.1029/2011GL048417.

Loeb, N.G., J.M. Lyman, G.C. Johnson, R.P. Allan, D.R. Doelling, T. Wong, B.J. Soden, G.L. Stephens (2012). Observed changes in top-of the atmosphere radiation and upper-ocean heating consistent within uncertainty. *Nature Geoscience*. DOI: 10.1038/NGEO1375. PP.1-4.

Outten, S.D., I. Esau (2012). A link between Arctic sea ice and recent cooling trends over Eurasia. *Climatic Change*. **110**. N 3-4. P. 1069-1075. doi:10.1007/s10584-011-0334-z.

Overland, J., M. Wang, S. Salo. (2008). The recent Arctic warm period. *Tellus* A, **60**. 589-597.

Petoukhov V., V. Semenov (2010). A link between reduced Barents-Kara sea ice and could winter extremes over northern continents. *J. Geoph. Res.* **115.** D21111DOI: 10.1029/2009JD013568.

Popova V.V. (2006). Dynamics of climate extremes in northern Eurasia in the late 20th century. *Izvestiya, Atmospheric and Oceanic Physics*, **42.** 138-147.

Report on climate features over the territory of Russian Federation for 2011 (2012). Federal Service for Hydrometeorology and Environmental Monitoring (ROSHYDROMET). 83pp.

Rossow, W. B., E. Duenas (2004). The International Satellite Cloud Climatology Project (ISCCP) web site: An online resource for research. *Bulletin of the American Meteorological Society*. **85.** 167-172. doi: 10.1175/BAMS-85-2-167.

Semenov V.A., I.I. Mokhov, M. Latif. (2012). Influence of the ocean surface temperature and sea ice concentration on regional climate changes in Eurasia in recent decades. *Izvestiya, Atmospheric and Ocean Physics*. **48**. 4. P. 355.

Trenberth, K.E. and D.P. Stepaniak (2004). The flow of energy through the Earth's climate system. *Quarterly Journal of the Royal Meteorological Society*. **130**. 2677– 2701.

Trenberth, K.E. and J.T. Fasullo (2013). An apparent hiatus in global warming? *Earth's Future*. 1. P. 19-32. DOI: 10.1002/2013EF000165.

Trenberth, K.E., J.T. Fasullo, M.A. Balmaseda (2014). Earth's Energy Imbalance. *J.Clim.* **27**. 9. P. 3129-3144. DOI: 10.1175/JCLI-D-13-00294.1.

UK Met Office (2013). The recent pause in global warming (2): what are the potential causes? Accessed July 2013. P.1-22.

von Storch H., F.W. Zwiers (2003). *Statistical Analysis in Climate Research* (Cambridge: Cambridge University Press. ISBN 0-521-45071-3. 484pp.

TEMPERATURE REGIME OF OLIGOTROPHIC AND EUTROPHIC MIRES AT SOUTH OF WEST SIBERIA

M.V. KISELEV[1,2], N.N. VOROPAY[1,3] and E.A. DYKAREV[1]

[1]Institute of Monitoring of Climatic and Ecological Systems SB RAS, Russia, Tomsk.

[2]Tomsk State University, Russia, Tomsk.

[2]V.B.Sochava Institute of Geography SB RAS 664033, Russia, Irkutsk.

Keywords: WEST SIBERIA, GREAT VASJUGAN MIRES, PEAT SOILS, SOIL TEMPERATURE, WETLANDS.

Bogs are unique natural landscape, involved in the regulation of the gaseous composition of the atmosphere, the water balance of the biosphere, biodiversity on the Earth.

Soil temperature is a key factor in controlling many biotic and abiotic processes in soils: decomposition and mineralization of soil organic matter, emission of greenhouse gases (CO_2, CH_4, N_2O), allocation of dissolved organic carbon, affects the growth of terrestrial vegetation(mosses, shrubs, etc.) and the formation of a microclimate (Golovatskayaet al., 2008). Thermal regimes of organic and mineral soils vary considerably. The peat deposit is a complex organic-system with specific properties: high water content and porosity containing large amounts of weak decomposed organic matter (Romanov, 1961). Soils are one of the main sources of CO_2, CH_4 and N_2O, the increasing atmospheric concentrations of which are among the most widely discussed, but there is not enough study of the causes of climate change (Semenov, 2004). Greenhouse gases are products of the metabolism of bacteria, which is regulated by the temperature. Climate warming leads to an increase in temperature of the soil, which provides an increase in greenhouse gas emissions. Production of CO_2 and CH_4 and emissions through seasonally frozen layer and snow cover occurs even in winter (Golovatskaya et al., 2008).

The study of the temperature regime of peat soils is an important task as the current global warming is based on data for the period from 1976 to 2012 was observed for the whole territory of Russia, but air temperature of the winter season in the south of West Siberia for the past few years has some cooling trend (Second assessment report Hydromet..., 2014). The main world reserves of peat and carbon are located in West Siberia. According to various estimates wetland ecosystems in Western Siberia contain up to 70 billion tons of carbon (IPCC, 2014). Such a considerable reservoir of carbon can be partially moved into the atmosphere as CO_2 and CH_4 due to climate change or anthropogenic impact and make a significant contribution to the carbon balance of the atmosphere.

West Siberia is located in the area of the three types of climate: the climate of the Arctic tundra and deserts, tundra and forest tundra climate, continental climate. In the summer over the territory of the West Siberian Plain is dominated cyclonic activity, the intensity of which decreases from north to south. The average July temperature ranges from 5°C in the north to 20,4°C in the south. In winter, the climate is influenced by cyclonic activity in the north-western regions, and spurs of Siberin High in the south. The average January temperature ranges from -15,50°C in the south to -28°C in the northeast. Annual precipitation ranges from 300 to 700 mm. Snow cover varies from 20-30 cm up to 80-90 cm.

A huge area of wetlands has an impact on the humidity and temperature of the air, especially in the summer. High humidity tends to promote some reduction in temperature especially in a day time. It leads to a decrease in the amplitude of the daily temperature and, consequently, to a certain reduction of continentality (Rusanov, 2004).

Our research focuses on the study of temperature of the Great Vasjugan Mires the largest wetland system in the world. They are located in West Siberia, between the Ob and Irtysh rivers on the territory Vasjugan plain, located mostly within the Tomsk region and partially in the Novosibirsk and Omsk regions, and Khanty-Mansi Autonomous District. The area of the Mires is53 thousand sq. km, length from west to east is 573 km, from north to south is– 320 km. Explored reserves of peat account for more than 1 billion tons, the average depth – 2.4 m, maximum depth is 10 meters (Kabanov, 2002).

A very significant role of bog vegetation in the production and supply of oxygen to the atmosphere when you consider it sin significant consumption for decomposition of organic matter under anaerobic conditions for the activity of the horizon of the peat deposits. It can be assumed that large-scale Vasjugan Mires in West Siberia, and possibly all of North Asia is a huge natural filter-absorber dust and various chemical air pollutants, including toxic.

An unique combination of different stages in the development of raised bog sexists at the Great Vasjugan mires (Zemtsov, 2010). Studies of temperature condition of bogs of West Siberia have been conducted since the

beginning of the XX century (Gordyagin, 1901; Bronzova, 1930; Kuzmina, 1949; Linevich, 1980; Dykarev et al., 2009; Ineshevaet al., 2014).

In recent decades, the number of Russian bogs observation stations and posts was significantly reduced from 8 to 3 stations and from 28 to 1 post, respectively (Bhutaev et al, 2011). This reduction has resulted in widespread areas is constantly updated to the absence of solid data, including peat soils temperature. In this regard the resumption of such observations by installing automatic monitoring equipment allows us to track changes in bog soil temperature, either alone or in combination with other hydro-meteorological characteristics. On top of that presence is constantly updated data sets will allow to use them for the calibration and verification of models of heat-mass transfer in the soil and short-term weather prediction models as components of regional climate models.

Since2011at the territory of West Siberia bogs we condicting monitoring of soil temperature at typical wetland landscapes and surrounding upland areas using automatic monitoring devices. Soil temperature recorded at some depths from the underlying surface to 320 cm, and the air temperature at a height of2 meters. Devices are located in 5 observation areas from oligotrophic not drained in the southern taiga to eutrophic in the middle taiga. Each observation area have several (3-10) observation plots. Observations are made with time step from 15 minutes to1 hour.

Atmospheric-soil measuring system (ASMS) was used for automatic monitoring of soil temperature. It was designed to record the temperature of the soil at a set time, accumulate data over a long period of time. ASMS has the ability to connect additional modules aimed at measuring of other meteorological characteristics such as the air temperature, the height of the snow cover, incoming solar radiation, water level depth, wind speed and direction, etc (Automatic measuring..., 2008).

Monthly and annual average soil temperatures were calculated throughout the profile and the air temperature. Dates of start and end of the cold period, the depth of soil freezing, the rate of freezing and thawing of the soil were estimated

The automatic monitoring of soil temperature in South Taiga of West Siberia show that the warm period lasted from April to November. Negative soil temperatures were registered at depths of up to 60 cm. The duration of the frozen layer decreases with depth. At depths below 60 cm for the year soil temperatures do not fall below 0°C. Minimum freezing depth of peat soil is observed in drained oligotrophic bog ecosystems The snow cover is observed from October-November to April-May. In the cold period the minimum negative temperature sometimes can be below that -10°C in a 5 cm layer, because the snow cover slowing penetration of negative temperature in peat soils. The dates of transition of peat soils temperature below 0°C from warm to cold period and back are differ on various depths. Transition dates through 0°C shifts to late dates with moving downward the soil profile.

Peat soil temperature have big annual amplitude in layers above 120 cm, but deeper 120 cm annual fluctuations is only 2-4°C. We do not observed daily peat soils temperature amplitude fluctuation below 30 cm.

Fig 1 shows an example of peat soil temperature variations on surface and at 80 cm depth in the oligotrophic bog system.

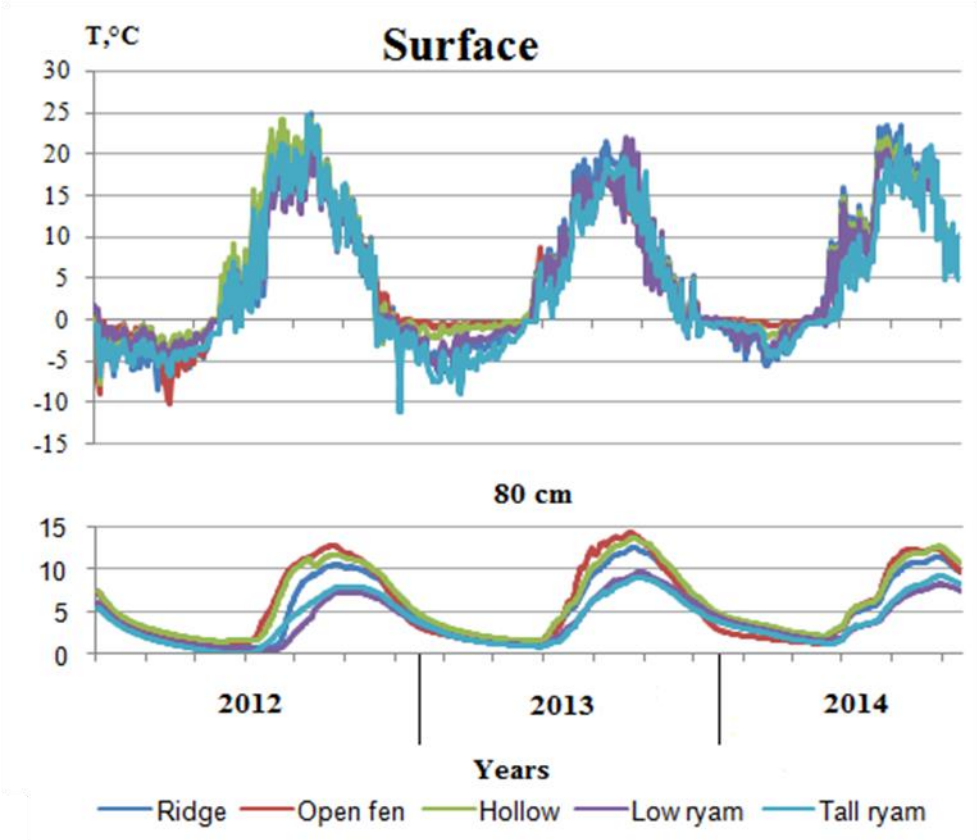

Figure 1. Soil temperature oscillations on surface and at depth of 80 cm at five observation sites.

The results of long-term monitoring of peat soil temperature can be used for cooperative complex studies to assess the impact of global warming on changes in wetland ecosystems and the impact of these changes on the emission of greenhouse gases (CO_2, CH_4, N_20); estimates of changes in vegetation structure, etc.

REFERENCES

Autonomous measuring the temperature profile AIPT: Instruction (IMCES, Tomsk, 2008).

Kabanov M.V. (2002) The Great Vasjugan Mires: Current state and development processes (Institute of Atmospheric Optics SB RAS press, Tomsk).

Golovatskaya E.A.et al. (2008) Influence of landscape and meteorological conditions on emissions of CO2 in the peat bog ecosystems, *Reports RAS* 4 (418), 1.

Zemtsov A.A. (2010) Modern geoecological condition of Vasjugan bog complex, *Biodiversity, environmental problems of Altai Mountains and adjacent regions: past, present, future* 4, 7.

Romanov V.V. (1961) Hydrophysics of bogs (Hydrometeoizdat, Leningrad).

Rusanov V.I. (2004) Bio Climate of West Siberian Plain (Institute of Atmospheric Optics SB RAS press, Tomsk).

IPCC (2014) *Climate Change 2014: Synthesis Report Contribution of Working Groups I, II and III to the Fifth Assessment Report of the Intergovernmental Panel on Climate Change* (IPCC, Geneva, Switzerland), 151.

Second Assessment Report of Roshydromet on climate change and their impact on the territory of the Russian Federation (Federal Service for Hydrometeorology and Environmental Monitoring, 2014), 61.

URBAN AMPLIFICATION OF THE GLOBAL WARMING: DIGNOSTIC, MODELLING, FORECASTING

A. KISLOV[1], P. KONSTANTINOV[1], M. VARENTSOV[1], T. SAMSONOV[2], I. GORLACH[1,3], L. ALEKSEEVA[1] and E. VASILENKO[1]

[1] Lomonosov Moscow State University, Faculty of Geography, Dpt. of Meteorology and Climatology, Moscow, Russian Federation.

[2] Lomonosov Moscow State University, Faculty of Geography, Dpt. of Cartography and Geoinformatics, Moscow, Russian Federation.

[3] Hydrometeorological Centre of Russia, Moscow, Russian Federation

Keywords: URBAN CLIMATE, GLOBAL WARMING, COSMO MODEL

INTRODUCTION

Climate change has been governing by global changes of the greenhouse gases, aerosols, and regional variations of atmospheric circulation. Within large urban area, microclimate change (especially the warming) is amplified due to influence of sharply modified land properties. It can be characterized as the urban amplification of the global warming. The focus of this paper is the climate change of the Moscow megacity, including changes of the structure of the atmospheric boundary layer, changes of the urban heat island (UHI), and determination of the microclimatic features of the local environment.

METHODS

Available meteorological observations within the Moscow urban area and surrounding territory allow us to assess the human-induced climate warming component separately from climate variations inherent to the whole the central part of the East European Plain. To obtain more precisely viewing on the UHI structure we have included into the analysis together with the ground observation the satellite data (METOP-A and METOP-B), providing temperature and humidity profiles with spatial resolution 25x25 km^2. Data volume presented in “Bufr” format includes combined information from NOAA sensors (ATOVS and AVHRR) and data of numerical model ECMWF.

CONCLUSIONS

Today, integrated climate management is an important approach for sustainable management and protection of large city areas. One of the core challenges for such successful program is the assessment of climate change impacts on the local microclimate changes as well as related socioeconomic sectors. In this context, the results of the regional climate model COSMO-CLM+TEB were used to investigate the mechanism of the urban amplification. Climate change differences between urban and rural areas are determined by changes of the shape of the UHI and their relationships with changes of building height and density. Therefore, the urban module of COSMO-CLM+TEB model is fed by information from special GIS database contenting both geometric characteristics of the urban canyons and other characteristics of the urban surface. The sources of information were maps belonging to the Open Street Map, and digital elevation models SRTM90 and ASTERGDEM v.2 as well. The multiscale GIS database allows us to generate such kind of information with different spatial resolution (200, 500 and 1000 meters).

ACKNOWLEDGEMENTS

This work was supported by the Russian Geographical Society under grant № 12/2014.

REFERENCES

Konstantinov P.I., M.I. Varentsov, E.P. Malinina (2014). Modeling of thermal comfort conditions inside the urban boundary layer during Moscow's 2010 summer heat wave (case-study), *Urban Climate*, **10**, 563-572.

Kislov A.V., M.I. Varentsov, L.L.Tarasova (2015**).** Role of Spring Soil Moisture in the Formation of Large-Scale Droughts in the East European Plain in 2002 and 2010 *Izvestiya - Atmospheric and Oceanic Physics, Maik Nauka/Interperiodica Publishing (Russian Federation)*, **51**, 405-411.

A PRELIMINARY VIEW ON ADSORPTION OF ORGANICS ON ICE AT TEMPERATURES CLOSE TO MELTING POINT

X. KONG, A. WALDNER, F. ORLANDO, L. ARTIGLIA, M. AMMANN, AND T. BARTELS-RAUSCH

Ice and snow play active roles in the water cycle, the energy budget of the Earth, and environmental chemistry in the atmosphere and cryosphere. The uptake of trace gases from the atmosphere may induce changes in the structure of the surface layer of ice crystals and has important consequences for atmospheric chemistry and the climate system. However, a molecular-level understanding of trace gas adsorption on ice is still missing, and also little is known about the impurity-induced ice-surface disorder in the context of environmental relevance.

It is a general challenge to apply highly sensitive experimental approaches to ambient air conditions, e.g. studies of volatile surfaces, because of the strict requirements of vacuum experimental conditions. In this study, we employed synchrotron-based X-ray Photoelectron Spectroscopy (XPS) and partial electron yield Near Edge X-ray Absorption Fine Structure (NEXAFS) in a state-of-the-art Near-Ambient Pressure Photoelectron (NAPP) spectroscopy end station. The NAPP enables to utilize the surface sensitive experimental methods, XPS and NEXAFS with electron detection, on volatile surfaces, i.e. ice at temperatures approaching zero degrees Celsius. XPS and NEXAFS provide unique information of hydrogen bonding network, surface concentration of organic adsorbates, depth profile of dopants in the ice, and acid-base dissociation on the surfaces. For instance, a few carboxylic acids, e.g. acetic acid and formic acid, have been recently studied by XPS and NEXAFS in NAPP.

Amines are a group of nitrogen-containing basic organics with atmospheric relevance. Only few studies have been focused on amines, and atmospheric models rarely take account of them due to the limitation of knowledge. Several amines have been found to play active roles in the processes of aerosol formation, e.g. dimethylamine (DMA), trimethylamine (TMA) and 1-propanamine. In this study, we will focus on one of these three amines after pre-tests, and perform core-level spectroscopies to reveal the behaviour of adsorption and dissociation on ice. Additionally, pure ice and amine doped ice will be compared for their surface structure change at different temperatures, which will indicate the differences of surface disordering caused by different factors. For instance, we will have a chance to know better if impurities will cause local disordering, i.e. forming hydration shell, which challenges the traditional picture of a homogenous disordered doped ice surface. The findings of this study could not only improve our understanding of how acidic organics adsorb to ice, and of their chemical properties on ice, but also have potentials to know better the behaviour of pure ice at temperatures approaching to the melting point.

URBAN HEAT ISLAND'S RESEARCH IN EX-USSR REGION. METHODOLOGY AND FIRST RESULTS

P.I.KONSTANTINOV[1], M.I.VARENTSOV[1,2], A.B.AKHMETOVA[1], E.A.KUKANOVA, A.A.BAKLANOV[3]

[1] Lomonosov Moscow State University, Faculty of Geography, 119991, Leninskie Gory, 1, Moscow, Russia

[2]A.M. Obukhov Institute of Atmosphere Physics RAS, Pyzhevsky per.3, Moscow, Russia
[3]World Meteorological Organization (WMO)

Keywords: URBAN HEAT ISLAND, URBAN CLIMATE, ARCTIC ZONE.

INTRODUCTION

Urban Heat Island (UHI) phenomenon is well known in scientific literature since first half of the 19th century [1]. By now the climatology of world capitals is described in detail, especially in mid-latitudes. In beginning of XXI century new studies focus on heat island of tropical cities due to lack of info about its climatology.
However dynamics UHI in Arctic zone and in extreme continental climates is insufficiently investigated, due to the fact that there isn't large cities in Europe and Northern America within that climate type.

In this paper we investigate seasonal and diurnal dynamics UHI intensity for l2 largest cities of Russia, Kazakhstan (including Astana, capital city of Kazakhstan - the second coldest capital city in the world after Ulaanbaatar, Mongolia) and several Arctic cities.

METHODS

For large cities of Russian Federation and Kazakhstan we used meteorological data created by regular state meteorological observations network. For every city we selected couple of stations [3]:

1. One located into city in high and midrise buildings area (extensive lowrise and high-energy industrial - LCZ classification) and second one located in rural site (sparsely built or open-set and lightweight lowrise according LCZ classification).
2. These couples of stations must be close by distance (less than 100 km) and altitude.

For selection operation was constructed spatial database in ESRI ArcGIS Desktop environmental.
In Arctic zone due to severe climatic conditions, we ought to use three types of different measurements techniques for experimental research (there was no any possibility to get long data series for these cities) :

- Mounting of two automatic weather stations (AWS) in rural zone and city center
- Development of small temperature sensors (iButton) network in the city and suburbs
- Regular car-based temperature sounding of the city with AWS.

CONCLUSIONS

For 12 Russian cities were obtained numerical evaluations for UHI climate dynamics, UHI dependence of synoptic situations and total UHI climatology on monthly and daily averages. Long-data climatic trends of UHI in Moscow, Saint-Petersburg, Kursk and Ekaterinburg were investigated.
Analysis of the collected data in Arctic zone showed the existence of UHI with the difference between city center and surrounding landscape up to 5-7 degrees Celcius. UHI characteristics in view of synoptic conditions was analyzed for several typical situations.

In Astana (Kazakhstan)[2] average value of the UHI intensity (approximately 1,26°C) is the indicator of high-intensity urban heat island for the steppe zone, and detected the positive trend of UHI

intensity. The population growth of the Astana (mainly due to labor migration) raises the question of the expansion of the area of the city and the construction of new housing.

ACKNOWLEDGEMENTS

This study was financially supported by the RSCF (Russian Science Foundation) project № 15-17-30009, Russian Foundation for Basic Research within the framework of the scientific project № 15-55-77004 (Research grant of Belmont Forum: HIARC: Anthropogenic Heat Islands in the Arctic: Windows to the Future of the Regional Climates, Ecosystems, and Societies), RFBR 15-35-21129-mol_a_ved and project № 15-35-70006. The work of Dr. Konstantinov is partially supported by President of Russia grant for young PhD scientists MK-6037.2015.5.

REFERENCES

1. Howard, L. (1833) The Climate of London, Deduced from Meteorological Observations. Volume 2, London.
2. Konstantinov Pavel and Akhmetova Alina. Urban Heat island phenomenon in extreme continental climate (Astana, Kazakhstan). In European Geosciences Union General Assembly 2015, volume 17 of Geophysical Research Abstracts, pages 8105–8105. EGU General Assembly 2015
3. Kukanova E.A., Konstantinov P.I. An urban heat islands climatology in Russia and linkages to the climate change In Geophysical Research Abstracts, volume 16 of EGU General Assembly, pages EGU2014–10833 Germany, 2014. Germany.

A SIMPLE PROXY FOR THE CONCENTRATIONS OF MONOTERPENES AND THEIR OXIDATION PRODUCTS IN BOREAL FOREST

J. KONTKANEN[1], P. PAASONEN[1], J. BÄCK[2], T. PETÄJÄ[1] AND M. KULMALA[1]

[1]Department of Physics, University of Helsinki, Helsinki, Finland

[2]Department of Forest Sciences, University of Helsinki, Helsinki, Finland

Keywords: VOCS, MONOTERPENES, OXIDATION PRODUCTS, BOREAL FOREST

INTRODUCTION

Terrestrial ecosystems emit large amounts of volatile organic compounds (VOCs) into the atmosphere (Günther *et al*., 2012). In boreal forests these emissions are dominated by monoterpenes. Recent studies have shown that the low volatile oxidation products of monoterpenes may participate in new particle formation and growth, and thus affect the concentrations of CCN (cloud condensation nuclei) (Ehn *et al*., 2014; Jokinen *et al.*, 2015). Therefore, the knowledge of the concentrations of monoterpenes and their oxidation products is crucial when estimating the climate effects of biogenic VOCs and aerosol particles.

The measuring of monoterpenes, and especially their oxidation products, is challenging. Thus, their concentrations have been estimated by parametrizing the measured concentrations of monoterpenes as a function of temperature, and then calculating the concentration of the oxidation products of monoterpenes by OH and O_3 (Nieminen *et al.*, 2014). However, this approach has several limitation: 1) the mixing of the boundary layer diluting the monoterpenes concentration is not taken into account 2) the oxidation of monoterpenes by NO_3 is not included 3) only daytime values of the measured monoterpenes concentration are used for the parametrization. Therefore, these proxies do not capture the diurnal variation of the concentrations of monoterpenes and their oxidation products.

In this work we construct improved proxies for the concentrations of monoterpenes and their oxidation products. Our proxy for the monoterpenes concentration includes the effect of boundary layer mixing, and the oxidation of monoterpenes by O_3, OH and NO_3. For deriving the monoterpenes proxy we use data measured at a boreal forest site in Hyytiälä, southern Finland. We also test how well our proxy is able to describe the variation of monoterpenes concentration at another boreal forest site, located in Yakutsk, eastern Siberia.

MEASUREMENTS

The measurements were performed during the years 2006–2013 at the SMEAR II station in Hyytiälä, Finland, in the southern boreal vegetation zone. The concentration of monoterpenes was measured with a proton transfer reaction mass spectrometer (PTR-MS) (Taipale *et al.*, 2008). In addition, other data measured continuously at the station (O_3 concentration, UV-B radiation, temperature, wind speed) were used in the analysis. The aerosol particle size distribution used for calculating the condensation sink (CS) was measured with a Differential Mobility Particle Sizer (DMPS). Furthermore, ECMWF (European Centre for Medium-Range Weather Forecasts) reanalysis data were used for determining the boundary layer height (BLH).

PROXY CALCULATIONS

For monoterpenes emission we use a temperature (T) -dependent exponent function (Tarvainen *et al.*, 2005; Lappalainen *et al.*, 2009):

$$E = \alpha \times \exp(\beta(T - T_s)) \quad (1)$$

Here α and β are empirical fitting parameters and T_s is 303.15 K.
The sink of monoterpenes due to oxidation by O_3, OH and NO_3 can be calculated from

$$S_{oxidation} = k_{OH+MT}\,[OH] + k_{O3+MT}\,[O_3] + k_{NO3+MT}\,[NO_3] \quad (2)$$

Here k_{OH+MT}, k_{O3+MT} and k_{NO3+MT} are temperature-dependent reaction rate coefficients between monoterpenes and different oxidants. O_3 is the only oxidant in Eq. (2) having its concentration directly measured in Hyytiälä. The concentration of OH was calculated by scaling the measured UV-B radiation with the empirically derived factors from Petäjä *et al.* (2009). The steady-state concentration of NO_3 can also be estimated if the monoterpenes concentration is known (see Peräkylä et al., 2014).

To investigate how well the proxy performs without including the oxidation by NO_3, we first constructed a proxy for monoterpenes by neglecting the last term in Eq. (2). When including the emissions presented by Eq. (1) and the effect of boundary layer mixing described by the mixing layer height (BLH) and wind speed (*ws*), the first version of the proxy for monoterpenes concentration becomes:

$$[MT]_{proxy,1} = \frac{a_1 \exp(b_1 T)}{k_{OH+MT}\,[OH] + k_{O3+MT}\,[O_3]} \times BLH^{c_1} \times ws^{d1} \quad (3)$$

Here a_1, b_1, c_1, and d_1 are empirical fitting parameters, which were obtained by searching the minimum of the ratio between the 90th and 10th percentiles of the ratio of the measured and proxy concentrations (Paasonen *et al.*, 2010).

In the second version of the proxy, we included the oxidation by NO_3, in which case the proxy becomes:

$$[MT]_{proxy,2} = \frac{a_2 \exp(b_2 T)}{k_{OH+MT}\,[OH] + k_{O3+MT}\,[O_3] + k_{NO3+MT}\,[NO_3]} \times BLH^{c_2} \times ws^{d2} \quad (4)$$

The concentration of NO_3 concentration in Eq. (4) was calculated by using a constant value for the monoterpenes concentration.

We also tested a simplified version of the proxy by including only the monoterpenes emissions and the mixing of the boundary layer:

$$[MT]_{proxy,simple} = a_3 \exp(b_3 T) \times BLH^{c_3} \times ws^3\,. \quad (5)$$

Finally, we utilized our monoterpenes proxies to calculate the concentration of oxidation products of monoterpenes by taking into account their production in the reactions between monoterpenes and different oxidants, and their removal due to condensation sink. Thus, the concentration of monoterpenes oxidation products was calculated from:

$$[OxOrg] = \frac{(k_{OH+MT}\,[OH] + k_{O3+MT}\,[O_3] + k_{NO3+MT}\,[NO_3]) \times MT_{proxy}}{CS} \quad (6)$$

Here MT_{proxy} is the concentration of monoterpenes based on the selected monoterpenes proxy and CS is the condensation sink.

RESULTS

The time series of the measured monoterpenes concentration and three monoterpenes proxies during year 2013 in Hyytiälä are shown in Fig. 1. All three proxies follow the measured monoterpenes concentration well in an annual scale. The proxies are able to capture the build-up of the concentration during spring and the variation in the concentration during summer and autumn months. When looking at the performance of the proxies during one week in September 2013, it can be seen that the proxies are able to describe the daily variation in monoterpenes concentration fairly well. Although measurements and proxies behave

differently on some days, most of the time the proxies follow the measurements peaking the same time at night.

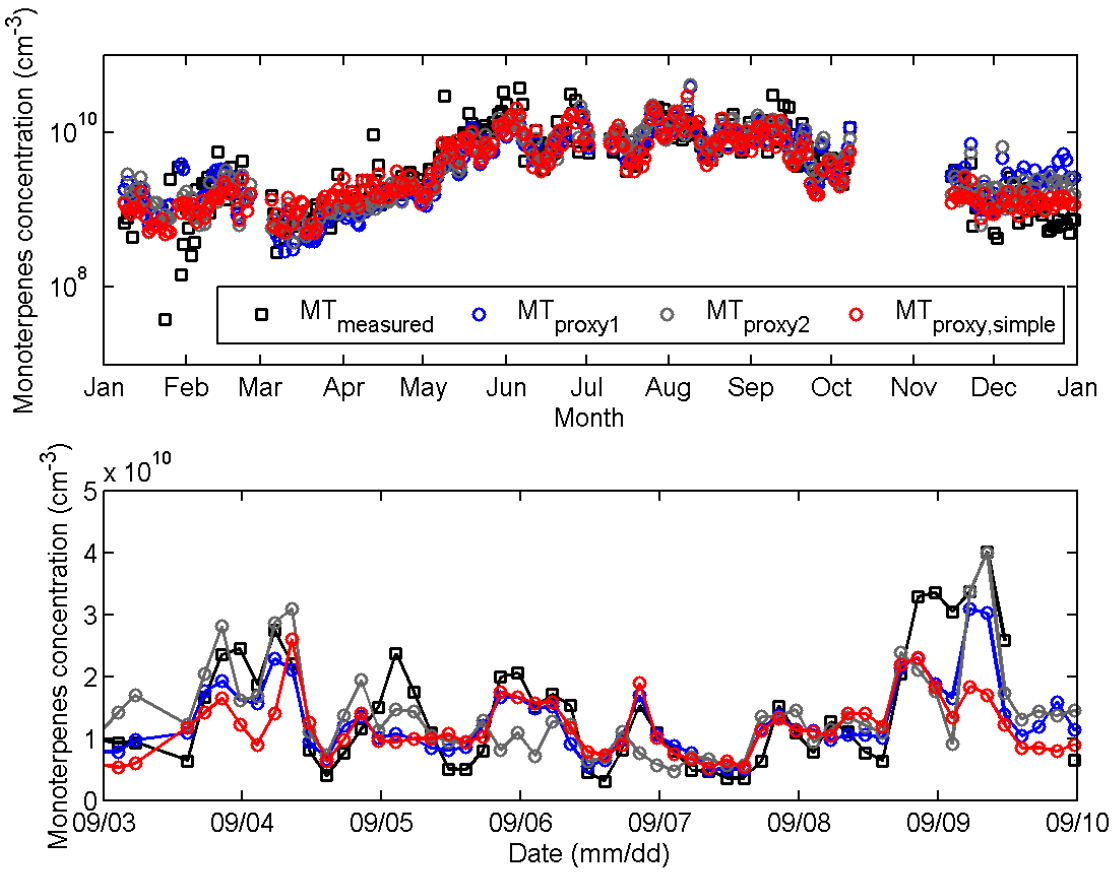

Figure 1. The concentrations of measured monoterpenes and different proxies during the whole year 2013 (top), and 3– 9 September 2013 (bottom).

To further analyze the performance of the proxies in Hyytiälä, we studied their correlation with the measured monoterpenes concentration using data from the years 2006–2014. The best correlation with measurements was obtained with $MT_{proxy,simple}$, for which the correlation coefficient was 0.73. For $MT_{proxy1,}$ not including the oxidation by NO_3, the correlation coefficient was 0.70 and for $MT_{proxy,2}$ the correlation coefficient was 0.68. Thus, it seems that the simple version of the proxy is able to describe the seasonal variation of the monoterpenes concentration best.

Finally, we also tested how well $MT_{proxy,simple}$, derived for Hyytiälä, is able to describe the variation of monoterpenes concentration in Yakutsk, eastern Siberia, during a measurement campaign conducted in summer 2009. It seems that the proxy can predict the behavior of monoterpenes concentration rather well also in Yakutsk (Fig. 2). This indicates that our proxies could be utilized for estimating the concentration of monoterpenes concentration and their oxidation products also at other sites in the boreal forest region.

CONCLUSIONS

In this work we derived proxies for the concentrations of monoterpenes and their oxidation products at a boreal forest site in Hyytiälä, southern Finland. The proxy for the monoterpenes concentration was observed to correlate well with measurements capturing the seasonal and diurnal variation. Furthermore, the results suggest that our proxies could also be applied at other boreal forest sites.

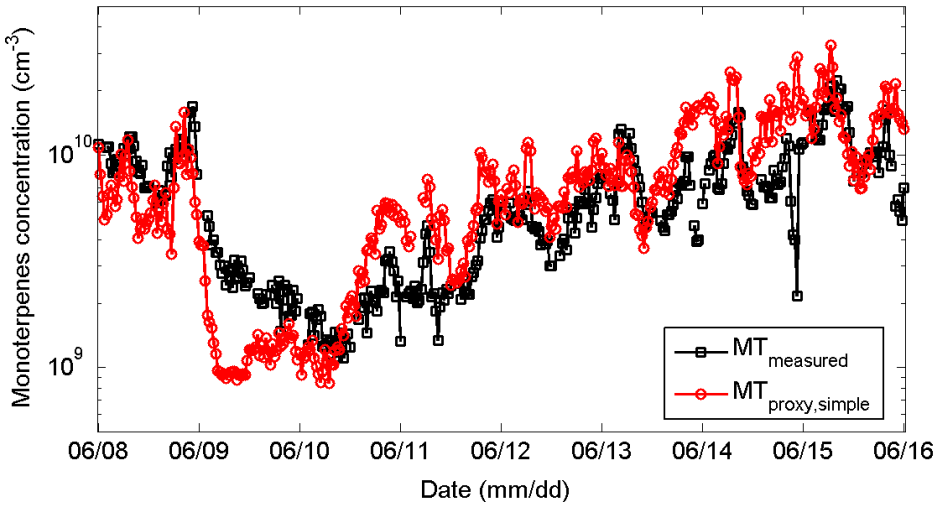

Figure 2. The concentrations of measured monoterpenes and proxy during 8–15 June 2009 in Yakutsk, eastern Siberia.

ACKNOWLEDGEMENTS

This work was funded by Academy of Finland Centre of Excellence program (grant no. 272041).

REFERENCES

Ehn, M. *et al.* (2014). A large source of low-volatility secondary organic aerosol. *Nature*, **506**, 7489, 476-479.

Günther, A. B. *et al.* (2012). The Model of Emissions of Gases and Aerosols from Nature Version 2.1 (Megan2.1): An Extended and Updated Framework for Modeling Biogenic Emissions. *Geosci. Model Dev.*, **5**, 1471−1492.

Jokinen, T. *et al.* (2015). Production of extremely low volatile organic compounds from biogenic emissions: Measured yields and atmospheric implications. *Proceedings of the National Academy of Sciences*, 201423977.

Lappalainen, H. K. *et al.* (2009). Day-time concentrations of biogenic volatile organic compounds in a boreal forest canopy and their relation to environmental and biological factors. *Atmospheric Chemistry and Physics*, **9**, 15, 5447-5459.

Nieminen, T. *et al.* (2014). Trends in atmospheric new-particle formation: 16 years of observations in a boreal-forest environment. *Boreal Environment Research*, **19.**

Paasonen, P. *et al.* (2010). On the roles of sulphuric acid and low-volatility organic vapours in the initial steps of atmospheric new particle formation. Atmospheric Chemistry and Physics, **10**, 22, 11223-11242.

Petäjä, T. *et al.* (2009). Sulfuric acid and OH concentrations in a boreal forest site. *Atmospheric Chemistry and Physics*, **9**, 19, 7435-7448.

Peräkylä, O. *et al.* (2014). Monoterpenes' oxidation capacity and rate over a boreal forest: temporal variation and connection to growth of newly formed particles. *Boreal Environment Research*, **19**.

Taipale, R. *et al.* (2008). Technical Note: Quantitative long-term measurements of VOC concentrations by PTR-MS–measurement, calibration, and volume mixing ratio calculation methods. *Atmospheric Chemistry and Physics*, **8**, 22, 6681-6698.

Tarvainen, V. *et al.* (2005). Temperature and light dependence of the VOC emissions of Scots pine. *Atmospheric Chemistry and Physics*, **5**, 4, 989-998.

POTENTIAL IMPACT OF POLLUTION ON CLOUDS AND PRECIPITATION OVER CHINA

O. KRÜGER[1], YUQIN LIU[2,3], HUADONG GUO[4], JIAHUA ZHANG[4], AIJUN DING[5,6], M. KULMALA[1] and T. PETÄJÄ[1,6]

[1]Department of Physics, University of Helsinki,
P.O.Box 64, FI-00014 University of Helsinki, Finland,

[2]Institute of Remote Sensing and Digital Earth, Chinese Academy of Sciences, Beijing, China

[3]University of Chinese Academy of Sciences, Beijing, China

[4]Institute of Remote Sensing and Digital Earth, Chinese Academy of Sciences, Beijing, China

[5]Nanjing University, Nanjing, China

[6]Joint International Research Laboratory of Atmospheric and Earth System Sciences & School of Atmospheric Sciences, Nanjing University, China

Keywords: POLLUTION, CLOUDS, PRECIPITATION, HAZE LAYERS.

INTRODUCTION

The enormous source strength of pollution ingredient originating from megacities and industrial areas in China (Kulmala, 2015) can potentially have high impact on horizontal and vertical gradients of atmospheric temperature – resulting in a change of atmospheric circulation. The effect on stability and vertical motion may occasionally change cloud properties and consequently could increase or decrease precipitation dependent on the state of the boundary layer. Furthermore, aerosol forcing is an important driver of atmospheric circulation change inducing precipitation response (Xie et al., 2015).

In order to explain changes of precipitation at the synoptic scale in China, including heavy rain events, flooding and droughts in recent decades, distinct hypotheses considering the potential influence of aerosols have been suggested. The one by Xu (2001) discusses a reduced move of the summer monsoon rain belt northward connected to a slight southward shift of the mid-summer west Pacific high. The investigation was performed using radiation and precipitation measurements. Based on these observations it was suggested to explain the abnormal climate pattern of “north drought and south flooding” by an enhanced negative radiative forcing of sulphate aerosols in central east China, which by far exceeds the radiative forcing by greenhouse gases in summer. The consequence is a cooling over land and a less strong northward shift of the summer monsoon rain belt. However, in Eastern China also global warming may induce changes in rainfall due to recuced thermal contrast between East Asia and the adjacent oceans (Zhao et al., 2010).

Another early hypothesis by Menon et al. (2002), regarding the climate effects of air pollution in China, gives the preference to black carbon. They stated that absorbing aerosols have a strong influence on radiative transfer in clouds. Menon et al. argue that absorbing aerosols heat the air, alter regional atmospheric stability and thus vertical motion, which affect the hydrological cycle. This explanation, which includes the surface cooling caused by aerosol extinction has been derived from climate model experiments.

There is also the Elevated Heat Pump Hypothesis formulated by Lau (e.g. see Lau and Kim, 2006, Wonsick et al., 2014) proposing that the load of absorbing aerosols over the Indo-Gangetic Plain could

even shift the Mei-yu rain belt northward with effects on precipitation over Central China. This also points to changes in circulation on larger scale.

The influence of pollution on cloud processes can be attributed to the layering of aerosols and depends on stability. Based on large eddy simulations Feingold et al. (2005) found that aerosols originating from biomass burning could reduce or increase cloudiness in the concetive boundary layer whereas increased stability due to aerosols clearly reduces cloudiness.

The study of Ding et al. (2013) provides evidence for such modification of boundary layer temperature by comparing comprehensive measurements in Nanjing, China, and atmospheric modelling. In detail mixed agricultural burning plumes together with fossil fuel combustion pollution induced a decrease in short wave radiation by more than 70 %, a decrease in the sensible heat by more than 85 % and a cooling by almost 10 K. These changes were accompanied by a reduction of precipitation during both daytime and nighttime.

Lately Fan et al. (2015) showed that suppression of convection caused by increasing aerosol indiced atmospheric stability could even lead to redistribution of moisture. The authors suggest that if the moisture is advected to mountainous areas and orographically lifted, strong convection and extreme precipitation events could be generated, which means that pollution could effectively mitigate floods in China.

The work presented here bases on different satellite data and discusses its significance in view of the earlier findings and hypotheses related to the potential influence of pollution on clouds and precipitation over China. Based upon this analysis the future direction for synergistic analysis of satellite observations and in-situ measurements is delineated.

METHODS

In our study we use data from the Atmospheric Infrared Sounder (AIRS), AIRS AIRX3STM v0006, the Moderate Resolution Imaging Spectroradiometer (MODIS), TERRA_MODIS_M3_V6, and the CloudSat 2B-TAU profiles within the region 27^0-34^0E longitude and 115^0-122^0N latitude.
In addition we use the reprocessed global NOAA/NASA Pathfinder data set from the Advanced Very High Resolution Radiometers (AVHRR) on board the afternoon-viewing NOAA series satellites (NOAA-7, 9, 11, and 14) within the region 20^0-45^0E longitude, 100^0-122^0N latitude.
With our region of interest we embed the Station for Observing Regional Processes of the Earth system (SORPES) on a regional scale. The platform designed for high quality in-situ measurements was developed by the Institute for Climate and Global Change Research (ICGCR) at Nanjing University (NJU) in collaboration with the University of Helsinki and is under continuous further development.

The station is of high importance for future synergistic analysis of satellite data and in-situ data directed to understand the nature of regional processes of the Earth system in eastern China, a region strongly influenced by monsoon weather and by intensive human activities. With a joint effort between NJU and the University of Helsinki, SORPES is in the process of being developed into a SMEAR (Station for Measuring Ecosystem–Atmosphere Relations) type measurement station (Hari et al., 2009), but focuses more on the impact of human activities on the climate and on the environment system in the rapidly urbanized and industrialized Jangtze River Delta region.

We analysed the aerosol optical thickness (12 years, from 2003 to 2015), the cloud top temperature (12 years, from 2003 to 2015), the cloud optical thickness (from 2007 to 2010) and the channel 2 reflectance from AVHRR at 0.7-1.1μm (episodes from 1985-1989 and 1996-1999).

CONCLUSIONS

The local planetary (LPA) over China decreased during winter north of 28^0N from the late 1980s to the late 1990s by more than 5% (Krüger and Graßl, 2004). Amazingly, the picture during the summer monsoon reverses: South of 28^0N there is a conspicuous increase of LPA by more than 5%. Satellite data indicate high convective clouds over China close to polluted regions. In the southern part of the highly polluted regions cloud top temperatures were falling, i.e. cloud top height is rising, from the late 1980s to the late 1990s. Cloud brightness temperature from the late 1980s to the late 1990s decreased by values sometimes higher than 5K. The maximum decrease in cloud brightness temperature corresponds to the areas with maximum LPA increase. South of 28^0N the coverage of convective clouds clearly enhances. However, despite the frequent lifting of cloud tops in the South, i.e. in the polluted regions of Nanning, Hong Kong and the Pearl River Delta, there is an increase of 2K over the cities in the Red Basin.

For the region of the Jangtze River Delta NASA's A-Train satellites observe a conspicuous relation of aerosol optical depth and cloud top temperature indicating heigher clouds occur under strongly polluted conditions (figure 1). This conspicuous relation needs further detailed investigation accompanied by a synergistic analysis of in-situ maesurements from SORPES station and satellite observations. The cloud optical thickness (figure 2) from satellite shows a high potential for modification of the cloud albedo and therefore would change the radiation balance if pollution approaches the cloud level over the Nanjing region. On the other hand CloudSat data likely indicate the existence of haze layers. This is another interesting result which also needs further attention. Haze layers are without doubt a major precondition for the impact of pollution on clouds and precipition.

Overall, these observed characteristics imply that future studies should show emphasis on highly polluted regions in China, i.e. close to emission sources of aerosol particles and their precursor gases, thus focussing on the role of enhanced cloud condensation nuclei numbers. The processes need to include feedback of accumulation of aerosols and CCN in the boundary layer through stabilization caused by pollution (Petäjä et al., 2015). Especially haze layers over large polluted cities or within basins and numerous valleys in China, e.g. the Red Basin, the Jangtze River Basin or the Pearl River Delta Region, must be further investigated with regard to their influence on the cloud formation process. In these studies emphasis should be given to the constraints, which favour the occurrence of extreme precipitation events. This research is of special importance with respect to the projected increase of future extreme precipitation in China (Bao et al., 2015).

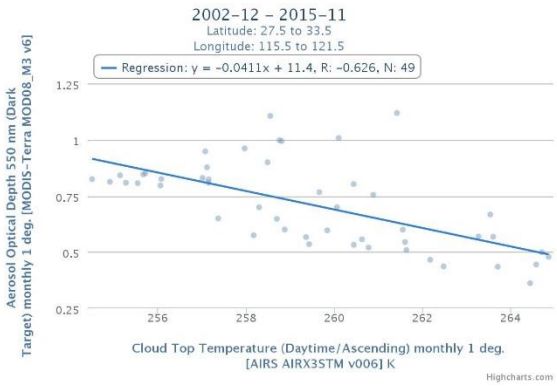

Figure 1. The relation of aerosol optical depth (AOD) and cloud top temperature (CTT) for the region 27^0-34^0E longitude, 115^0-122^0N latitude.

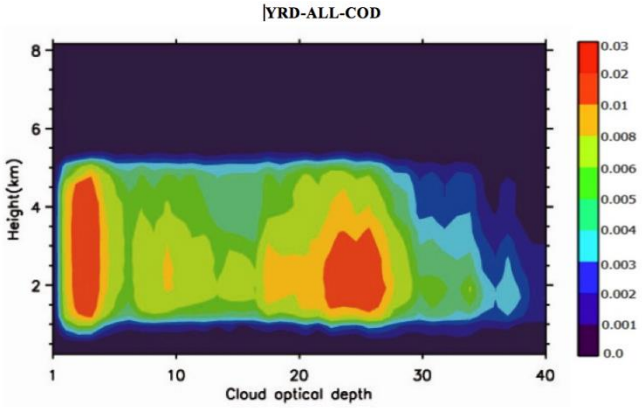

Figure 2. Contoured frequency by altitude diagram (CFAD) of the cloud optical thickness (COT) from 2007-2010 for the region 27^0-34^0E longitude, 115^0-122^0N latitude.

ACKNOWLEDGEMENTS

We would like to acknowledge the Academy of Finland Center of Excellence on Atmospheric Sciences and Nordic Center of Excellence in e-Science (E-STICC). We also acknowledge the AIRS and MODIS mission scientists and associated NASA personnel for the production of the data used in this research effort. Further the CloudSat Data Processing Center at CIRA/Colorado State University was providing the CloudSat data products used in our work.

REFERENCES

Bao, J., J. Feng, and Y. Wang (2015). Dynamical downscaling simulation and future projection of precipitation over China, *Geophys. Res. Atmos.*, 120, 8227–8243, doi:10.1002/2015JD023275.

Ding, A. J., C. B. Fu, X. Q. Yang, J. N. Sun, T. Petäjä, V.-M. Kerminen, T. Wang, Y. Xie, E. Herrmann, L. F. Zheng, W. Nie, Q. Liu, X. L. Wei and M. Kulmala (2013). Intense atmospheric pollution modi es weather: a case of mixed biomass burning with fossil fuel combustion pollution in the eastern China. *Atmos. Chem. Phys.* 13, 10545–10554.

Fan, J., D. Rosenfeld, Y. Yang, C. Zhao, L. R. Leung, and Z. Li (2015). Substantial contribution of anthropogenic air pollution to catastrophic floods in Southwest China, *Geophys. Res. Lett.*, 42, 6066–6075, doi:10.1002/2015GL064479.

Feingold, G., H. Jiang, and J. Y. Harrington (2005). On smoke suppression of clouds in Amazonia, *Geophys. Res. Lett.*, 32, L02804, doi:10.1029/2004GL021369.

Hari P., Andreae M.O., Kabat P. & Kulmala, M. (2009). A comprehensive network of measuring stations to monitor climate change. *Boreal Env. Res.* 14: 442–446.

Kulmala, M. (2015). China's choking cocktail, *Nature*, 526, 497-499.

Krüger, O. and Graßl, H. (2004) Albedo reduction by absorbing aerosols over China. *Geophys. Res. Lett.*, 31, doi:10.1029/2003GL019111.

Lau, K.-M., and K.-M. Kim (2006). Observational relationships between aerosol and Asian monsoon rainfall, and circulation, *Geophys. Res. Lett.*, 33, L21810, doi:10.1029/2006GL027546.

Menon, S., Hansen, J., Nazarenko, L., Luo, Y. (2002). Climate Effects of Black Carbon Aerosols in China and India. *Science* 297, 2250-2253.

Petäjä, T., L. Järvi, V.-M. Kerminen, A.J. Ding, J.N. Sun, W. Nie, J. Kujansuu, A. Virkkula, X.-Q. Yang, C.B. Fu, S. Zilitinkevich & M. Kulmala (2016). Enhanced air pollution via aerosol-boundary layer feedback in China. *Sci. Rep.* 6, 18998; doi: 10.1038/srep18998.

Xie, S.-P., C. Deser, G. A. Vecchi, M. Collins, T. L. Delworth, A. Hall, E. Hawkins, N. C. Johnson, C. Cassou, A. Giannini and M. Watanabe (2015). Towards predictive understanding of regional climate change, *Nature Clim. Change*, 5, 921−930.

Xu, Q. (2001) Abrupt change of the mid-summer climate in central east China by the influence of atmospheric pollution. *Atmospheric Environment* 35, 5029-5040.

Wonsick, M.M., R. T. Pinker, and Y. Ma (2014) Investigation of the “elevated heat pump” hypothesis of the Asian monsoon using satellite observations, *Atmos. Chem. Phys.*, 14, 8749–8761.
Zhao, P., S. Yang, and T. Yu (2010). Long-Term Changes in Rainfall over Eastern China and Large-Scale Atmospheric Circulation Associated with Recent Global Warming. *J. Climate*, 23, 1544–1562.

BEAUTIFUL CHINA – HOW TO TACKLE AIR POLLUTION

J. KUJANSUU, M. KULMALA and T. PETÄJÄ

Sino-Finnish project Beautiful Beijing has proposed a roadmap to solve air pollution problem in capital region. Chemical cocktail of air pollutants in China has significant local characteristics and is very complicated. Thus, it is important to extent the project to include whole China - Beautiful China. The roadmap is summarised in Nature Comment, 2015, by prof. Kulmala. Understanding the composition of chemical cocktail is scientifically challenging and societally very important. New phenomena will be seen and actions needs to be formed. The co-operation is crucial between all parties. It is important to enhance collaboration between parties inside China and also to implement open data policies. Without open data it is very difficult to know which actions are most effective, and without smooth communication and trust between parties the proposed actions for decision makers are not best possible and hinder necessary actions. It is not useful to compare historical air pollution conditions with what we have now because the chemical cocktail is different. We need urgently most suitable infrastructure to first measure and understand what is happening in detail in China's atmosphere because there are no short cuts for most practical solutions. The most effective solutions needs to form inside, in China. Only solutions formed in China can solve China's problems. For concrete actions, first there is a need to upgrade present measurement station infrastructure up to the standard to measure all the needed components. China has lots of measurement stations, but most of them are not comprehensive enough. We can use the existing one's as a base for this development. Task ahead is enormous, but on the other hand have also huge potential. If we can solve China's air there is a huge market potential for these solutions globally, such as in India, Bangladesh and Indonesia. Rushed actions are only going to waste time, money and effort. It is vital to keep up the steady economic growth so the pace for clearing the air is hard to estimate. Only through understanding comes the most practical solutions. Chinese people deserve Beautiful China, China deserves to be beautiful.

PAN-EURASIAN EXPERIMENT (PEEX) – AS A TOOL TO UNDERSTAND AIR QUALITY – CLIMATE INTERACTIONS AND FEEDBACKS

M. KULMALA, H. K. LAPPALAINEN[1,2], T. PETÄJÄ[1], V-M. KERMINEN[1], R. MAKKONEN[1], P. ALEKSEYCHIK[1], N. ZAITSEVA[3], J. KUJANSUU[1], A. SCHERBININ[4], P. KONSTANTINOV[5], M. KAUKOLEHTO[1,9], N. CHUBAROVA[5], M. ARSHINOV[6], A. MAHURA[7], S. ARNOLD[8], D. SPRACKLEN[8], S. JUHOLA[4], J. BÄCK[9], T. VESALA[1], P. HARI[9], A. DING[10], C. FU[10], H-C. HANSSON[11], V. MELNIKOV[12,13], Y. VIISANEN[2], G. MATVIENKO[6], A. BAKLANOV[14], N. KASIMOV[5], H. GUO[15], V. BONDUR[16], S. ZILITINKEVICH[1,2,5,17,18]

[1)]Dept. of Physics, University of Helsinki, Finland.

[2)]Finnish Meteorological Institute, Helsinki, Finland

[3)] Dept. of Earth Sciences, Russian Academy of Sciences, Russia

[4)] Dept. of Environmental Sciences, University of Helsinki, Finland.

[5)] Moscow State University, Russia

[6)] Institute of Atmospheric Optics, Tomsk 634021, Russia

[7)]Danish Meteorological Institute, Research and Development Department, 2100, Copenhagen, Denmark

[8)] Institute for Climate and Atmospheric Science, School of Earth and Environment, University of Leeds, Leeds, LS2 9JT, UK

[9] Dept. of Forest Ecology, University of Helsinki, Finland

[10)] Institute for Climate and Global Change Research & School of Atmospheric Sciences, Nanjing University, 210023 Nanjing, China

[11)] Dept. of Environmental Science and Analytical Chemistry, Stockholm University, Sweden

[12)] Tyumen State University, Russia
[13)] Tyumen Scientific Center SB RAS, Russia

[14)]World Meteorological Organization, 1211 Genève, Switzerland

[15)] Institute of Remote Sensing and Digital Earth, Chinese Academy of Sciences, Beijing 100101, China

[16)] AEROCOSMOS Research Institute for Aerospace Monitoring, Moscow, Russia

[17)] Dept. of Radiophysics, Nizhny Novgorod State University, Russia

[18)] Institute of Geography, Russian Academy of Sciences, Moscow, Russia

Keywords: GRAND CHALLENGES, CLIMATE CHANGE, AIR QUALITY, SUPRADISCIPLINARY APPROACH, MULTISCALE RESEARCH, ARCTIC-BOREAL, URBAN, OBSERVATION NETWORKS

BACKGROUND

The Grand Challenges (GC) such as climate change are the main factors controlling human well-being and security and the stability of future societies. The GCs are highly connected and interlinked. The potential solutions are typically tightly coupled with each other (e.g. Kulmala *et al*., 2015). In order to meet these tasks, we need a multidisciplinary scientific approach with the required critical mass and an approach being strongly connected to fast-tracked policy making.

The atmosphere forms a major part of the environment to which life on Earth is sensitively responsive. The atmosphere closely interacts with the biosphere, hydrosphere, cryosphere and lithosphere as well as with the urban surfaces on time scales from seconds to millennia (Wanner *et al.*, 2008). Changes in one of these components are directly or indirectly communicated to the others via intricately-linked processes and feedbacks. In recent years, a lot of research has been motivated by the importance of atmospheric aerosols on the global radiation budget, cloud formation and human health. Concentrations of reactive gases, greenhouse gases and atmospheric aerosol particles are tightly connected with each other via physical, chemical and biological processes occurring in the atmosphere, biosphere and at their interface (Arneth *et al*. 2010, Stocker *et al*., 2013; Kulmala *et al.*, 2014a; Unger, 2014). Human and societal actions, such as emission control policies, urbanization, forest management and land use change, as well as various natural feedback mechanisms involving the biosphere and atmosphere, have substantial impacts on the complicated couplings between atmospheric aerosols, trace gases, GHG, air quality and climate (Raes *et al*. 2010; Shindell *et al.* 2012; Stocker *et al.* 2013, Kulmala *et al*. 2015, Kulmala 2015).

Here we summarize the present knowledge on air quality – climate interactions and feedbacks and also give future perspectives particularly in Pan-Eurasian Experiment (PEEX) approach point of view.

DISCUSSION

The Northern Eurasian continent and particularly boreal and arctic areas are crucial for understanding future climate and air-quality climate interactions. Only via further development of continuous comprehensive observations in these areas and the associated data flows we are able to determine and quantity these interactions. The existing Pan-Eurasian Experiment (PEEX) a program focused on arctic-boreal regions, consists of more than 80 institutes (Kulmala *et al*. 2015). Within the PEEX collaboration, we will focus on quantification of the COBACC (COntinental Biosphere-Aerosol-Cloud-Climate) feedback loop and its different steps, such as the effectiveness of changing ecosystems to act as carbon sink, present and future BVOC emissions and concentrations, new particle formation and gas-to-particle transformation in the boreal area, and the effect of changing aerosol load on carbon sink via increased levels of diffuse solar radiation.

The first estimates of the feedback loop based on comprehensive SMEAR II (Station for Measuring Forest Ecosystem-Atmosphere Relations) measurements and data analysis demonstrate how important biosphere processes affect not only to the carbon and aerosol budgets, but also to the whole climate system. The COBACC feedback mitigates global warming, thereby giving the mankind a window of opportunity to reduce global carbon emissions (Kulmala *et al*. 2014). The strength of the COBACC feedback is connected tightly with the functioning of the biosphere, including the observed yet poorly-understood greening and other vegetation changes currently taking place in boreal and Arctic environments (Buermann *et al*., 2013; Reich *et al*., 2015). Thus next step is to find out how important this feedback loop is globally and particularly in the boreal and arctic environments, and how the feedback loop will develop in the future.

The rapid, large-scale urbanization and industrialization of China are unique in history (http://gains.iiasa.ac.at/gains3/). Atmospheric concentrations of primary and secondary pollutants in China are 10 to 100 times (sometimes even 1000 times) higher than currently in Europe or Northern America. The fact that new particle formation does occur in polluted Chinese megacities like Beijing and Shanghai

(Xiao *et al*. 2015), or even during dust-storms (Nie *et al*. 2014), suggests that there are several major physical and chemical mechanisms in a heavily-polluted atmosphere that have not been recognized before and may not even be operating in clean or moderately-polluted environments.

A holistic scientific understanding on the atmospheric phenomena associated with air quality as a whole, as well as on the connection between air quality and climate, is lacking at the moment (Fiore *et al*., 2012; Fuzzi *et al*., 2015; Kulmala 2015). Together with emission reductions, the key way to get forward is to make long-term, continuous and comprehensive observations on aerosol, trace gases and atmospheric oxidants as well as greenhouse gases (Kulmala *et al.*, 2015). With a network of such observation stations (Hari *et al*. 2016), we will be able to understand the interactions and feedbacks associated with the urban pollution mixture and, ultimately, be ready to make targeted strategies for the pollution control. Recent advances in our theoretical understanding has made it possible to explain how enhanced pollution decreases atmospheric turbulence and mixing, reducing the boundary layer height and causing further enhancement of pollution levels (Petäjä *et al.*, 2016).

SUMMARY AND FUTURE PROSPECTS

Megacities and industrial areas in China and Russia contribute significantly to the pollution load of the global atmosphere. These pollutants have the potential to impact atmospheric circulation and weather close to their sources areas (Ding *et al*., 2013; Xie *et al*., 2015). Further away, and especially in boreal and Arctic regions, pollutants originating from China, Europe and Russia may significantly affect the chemical composition of the atmosphere (Monks *et al*., 2015; Acosta et al.), thereby affecting e.g. the biosphere by altering the VOC emissions, their atmospheric chemistry and resulting secondary aerosol formation. As described above, the air quality in polluted areas and climate change are tightly interlinked and therefore they cannot be solved separately.

The long data series and versatile measurement equipment like those that we have in SMEAR II (Station for Measuring Ecosystem-Atmosphere Relations) in Finland provide continuous information on the long-term trends in the aerosol, trace gas and greenhouse gas loadings over boreal forests, and make it possible to test novel theories and instrumental techniques under boreal forest conditions. The first international SMEAR station has been established in Nanjing, China, by the Institute for Climate and Global Change Research, Nanjing University. The Station for Observing Regional Processes in the Earth System of Nanjing University (SORPES-NJU) is a national key research infrastructure (Ding *et al*., 2013). The station is operated in collaboration with Nanjing University and University of Helsinki under joint international research laboratory of Atmospheric and Earth System Sciences (JirLATEST). Besides SORPES in Nanjing, observations in Beijing and Shanghai are also foreseen in China in collaboration with Peking University and Fudan University, respectively. In Russia already work is on-going (Tiksi, Cape Baranova, Bolsevik Island) and several activities are envisioned (Tomsk, Yamal) (Zhang *et al.*, 2012; Schutgens and Stier, 2014). To cover the whole globe, new proxies based on satellite data are required to be developed as well (e.g. Kulmala *et al*. 2011).

There are three items, which we will focus in future:

- Establishment of a continuous, comprehensive measurements network (Global SMEAR network) for global observations, including ACTRIS, Beautiful Beijing/China (BB/C) and PEEX (Pan Eurasian Experiment) supersites and the connections with satellite remote sensing. Upgrading existent stations and updating software and instrumentation.
- Classifying and quantifying the most important interactions and feedbacks affecting pollutant concentrations and climate in heavily-polluted environments, particularly in megacities in China using connections within Beautiful Beijing/China initiative; finding out the interactions and feedbacks in the past, present and future, taking into account the interactions between urban planetary boundary layer and primary vs secondary pollution; using ground based observations, together with multiscale modelling from process models (GTP/NPF) to regional modelling of air quality, and remote sensing.

- Determining and quantifying biosphere - trace gas - aerosol - cloud interactions and feedbacks in the PEEX area (boreal and Arctic) in the past, present and future conditions; finding out on a continental scale, how arctic greening and changes in boreal and arctic environments will affect the interactions and feedbacks; finding out anthropogenic and biogenic contribution to arctic pollution and climate change.

ACKNOWLEDGEMENTS

We would like to acknowledge the following support or funding from the following bodies: Academy of Finland via Finnish Center of Excellence in Atmospheric Sciences (grant no. 272041), Finnish Cultural Foundation, Grant: Prof. Markku Kulmala "International Working Groups"; Russian Mega-Grant No. 11.G34.31.0048; Russian Science Foundation projects No. 15-17-20009 (2015-2018) and No. 15-17-30009 (2015-2018); Academy of Finland contracts 259537 and 280700, Beautiful Beijing (Finland- China collaboration project) funded by TEKES, EU projects InGOS and Erasmus+ CBHE ECOIMPACT 561975-EPP-1-2015-1-FI-EPPKA2-CBHE-JP; NordForsk Nordic Centre of Excellence ~~of~~ CRAICC (no 26060) and NordForsk CRAICC-PEEX (amendment to contact 26060).

REFERENCES

Acosta Navarro, J.C., V. Varma, V., Riipinen, I., Seland, Ø., Kirkevåg, A., Struthers, H., Iversen, T. Hansson H.-C & Ekman, A. M. L. 2016. Amplification of Arctic warming by past air pollution reductions in Europe, Nature Geoscience, 9, 277–281.

Arneth, A., Harrison, S.P., Tsigaridis, K., Menon, S., Bartlein, P.J., Feichter, H., Korhola, A., Kulmala, M., O'Donell, D., Schurgers, G., Sorvari, S., Vesala, T., and Zaehle, S. 2010. Terrestrial biogeochemical feedbacks in the climate system: from past to future, Nature Geoscience, 3, 525-532.

Buermann W., Buermann W., Bikash P.R., Martin Jung M., Burn D.H. and Reichstein M. 2013. Earlier springs decrease peak summer productivity I,n North American boreal forests, Geop. Res. Lett., 41, 1995.

Ding, A., Fu, C.B., Yang, X.Q., Sun, J.N., Peteja, T., Kerminen, V.-M., Wang, T., Xie., Y.N., Herrmann, E., Zheng, L.F., W. Nie, W., Liu, Q., Wei, X.L., and Kulmala, M. 2013. Intense atmospheric pollution modifies weather: a case of mixed biomass burning wither fossil fuel combustion pollution in the eastern China, Atmospheric Chemistry and Physics, 13,10545-10554.

Fiore, A.M., V. Naik, D.V. Spracklen, A. Steiner, N. Unger, M. Prather, D. Bergmann, P.J. Cameron-Smith, I. Cionni, W.J. Collins, S. Dalsoren, V. Eyring, G.A. Folberth, P. Ginoux, L.W. Horowitz, B. Josse, J.F. Lamarque, I.A. MacKenzie, T. Nagashima, F.M. O'Connor, M. Righi, S.T., Rumbold, D.T. Shindell, R.B. Skeie, K. Sudo, S. Szopa, T. Takemura, and G. Zeng, 2012: Global air quality and climate. *Chem. Soc. Rev., 41,* 6663-6683, doi:10.1039/c2cs35095e.

Fuzzi, S., Baltensperger, U., Carslaw, K., Decesari, S., Denier van der Gon, H., Facchini, M. C., Fowler, D., Koren, I., Langford, B., Lohmann, U., Nemitz, E., Pandis, S., Riipinen, I., Rudich, Y., Schaap, M., Slowik, J. G., Spracklen, D. V., Vignati, E., Wild, M., Williams, M., and Gilardoni, S. 2015. Particulate matter, air quality and climate: lessons learned and future needs, Atmos. Chem. Phys., 15, 8217-8299, doi:10.5194/acp-15-8217-2015.

Hari, P., Petäjä, T., Bäck, J., Kerminen, V.-M., Lappalainen, H.K., Vihma, T., Laurila, T., Viisanen, Y., Vesala, T. and Kulmala, M. 2016. Conceptual design of a measurement network of the global change. Atmospheric Chemistry and Physics 16: 21063–21093.

Kulmala, M., Arola, A., Nieminen, T., Riuttanen, L., Sogacheva, L., de Leeuw, G., Kerminen, V.-M., and Lehtinen, K. E. J.: The first estimates of global nucleation mode aerosol concentrations based on satellite measurements, Atmos. Chem. Phys., 11, 10791-10801, doi:10.5194/acp-11-10791-2011, 2011.

Kulmala, M., Nieminen, T., Nikandrova, A., Lehtipalo, K., Manninen, H., Kajos, M., Kolari, P., Lauri, A., Petäjä, T., Krejci, R., Hansson, H.-C., Swietlicki, E., Lindroth, A., Christensen, T.R., Arneth, A., Hari, P., Bäck, J., Vesala, T. and Kerminen, V.-M. 2014a. CO_2 induced terrestrial climate feedback mechanism: From carbon sink to aerosol source and back, Boreal Environment Research 19B:122-131.

Kulmala, T. Petäjä, M. Ehn, J. Thornton, M. Sipilä, D.R. Worsnop, and V.-M. Kerminen 2014b. Chemistry of Atmospheric Nucleation: On the Recent Advances on Precursor Characterization and Atmospheric Cluster Composition in Connection with Atmospheric New Particle Formation, Annu. Rev. Phys. Chem., 65: 21–37.

Kulmala, M. 2015. China's choking cocktail, Nature, 526, 497.

Kulmala, M., Lappalainen, H.K., Petäjä, T., Kurtén, T., Kerminen, V.-M., Viisanen, Y., Hari, P., Sorvari, S., Bäck, J., Bondur, V., Kasimov, N., Kotlyakov, V., Matvienko, G., Baklanov, A., Guo, H.D., Ding, A.,

Hansson, H.-C. and Zilitinkevich, S. 2015. Introduction: The Pan-Eurasian Experiment (PEEX) – multidisciplinary, multiscale and multicomponent research and capacity-building initiative, Atmospheric Chemistry and Physics, 15: 13085-13096.

Monks, S. A., Arnold, S. R., Emmons, L. K., Law, K. S., Turquety, S., Duncan, B. N., Flemming, J., Huijnen, V., Tilmes, S., Langner, J., Mao, J., Long, Y., Thomas, J. L., Steenrod, S. D., Raut, J. C., Wilson, C., Chipperfield, M. P., Diskin, G. S., Weinheimer, A., Schlager, H., and Ancellet, G., 2015. Multi-model study of chemical and physical controls on transport of anthropogenic and biomass burning pollution to the Arctic, Atmos. Chem. Phys., 15, 3575-3603.

Nie, W., Ding, A., Wang, T., Kerminen, V-M., George, C., Xue, L., Wang, W., Zhang, Q., Petäjä, T., Qi, X., Gao, X., Wang, X., Yang, X., Fu, C., and Kulmala, M., 2014. Polluted dust promotes new particle formation and growth, Scientific Reports, 4 (6), doi:10.1038/srep06634.

Petäjä, T., Järvi, L., Kerminen, V.-M., Ding, A., Sun, J., Nie, W., Kujansuu, J., Virkkula, A., Yang, X., Fu, C., Zilitinkevich, S. and Kulmala, M. 2016. Enhanced air pollution via aerosol-boundary layer feedback in China, Sci. Rep. 6, 18998, doi: 10.1038/srep18998.

Qi, X.M., Ding, A.J., Nie, W., Petäjä, T., Kerminen, V.-M., Herrmann, E., Xie, Y.N., Zheng, L.F., Manninen, H., Aalto, P., Sun, J.N., Xu, Z.N., Chi, X.G., Huang, X., Boy, M., Virkkula, A., Yang, X.-Q., Fu, C.B. and Kulmala, M. 2015. Aerosol size distribution and new particle formation in western Yangtze River Delta of China: two-year measurement at the SORPES station. Atmospheric Chemistry and Physics, 15: 12445-12464

Raes, F., H. Liao, W.-T. Chen, and J. H. Seinfeld, 2010. Atmospheric chemistry-climate feedbacks. J. Geophys. Res., 115, D12121.

Reich, P.B., K.M. Sendall, K. Rice, R. L. Rich, A. Stefanski, S.E. Hobbie, R.A. Montgomery. 2015. Geographic range predicts photosynthetic and growth response to warming in co-occurring tree species , Nature Climate Change 5(2):148-152.

Shindell, D.Kuylenstierna, J.C.I., Vignati, E., van Dingenen R., Amann, M., Klimont, Z., Anenberg, S.C., Muller, N., Janssens-Mae, nhout G., Raes, F., Schwartz, J., Faluvegi, G., Pozzoli, L., Kupiainen, K., Höglund-Isaksson, L., Emberson, L., Streets, D., Ramanathan, V., Hicks, K., Oanh, N.T.K., Milly, G., Williams, M., Demkine V., and Fowler D., 2012. Simultaneously Mitigating Near-Term Climate Change and Improving Human Health and Food Security, Science, 335, 183-189.

Schutgens J. and Stier P. 2014. A pathway analysis of global aerosol processes, Atmos. Chem. Phys., 14, 11657-11686.

Stocker, B. D., Roth, R., Joos, F., Spahni, R., Steinacher, M., Zaehle, S., Bouwman, L., Xu-Ri and Prentice, I.C. 2013. Multiple greenhouse-gas feedbacks from the land biosphere under future climate change scenarios Nat. Clim. Change, ***3,*** *666–72.*

Unger, *N. 2014. Human land-use-driven reduction of forest volatiles cools global climate,* Nature Climate Change, 4, *10, 907.*

Wannera, H., Beerb, J., Bütikofera, J., Crowleyc, T.J., Cubaschd, U., Flückigere, J., Goossef, H., Grosjeana, M., Joosg, F., Kaplanh, J.O, Küttela, M., Müllerg, S.A., Prenticei, I.C., Solominaj, O., Stockerg, T.F., Tarasovk, P., Magner M., and Widmannm, M. 2008. Mid- to Late Holocene climate change: an overview, Quaternary Science Reviews, 27 (19–20), 1791–1828

Xiao, S., Wang, M. Y., Yao, L., Kulmala, M., Zhou, B., Yang, X., Chen, J. M., Wang, D. F., Fu, Q. Y., Worsnop, D. R., and Wang, L. 2015. Strong atmospheric new particle formation in winter in urban Shanghai, China, Atmos. Chem. Phys., 15, 1769-1781, doi:10.5194/acp-15-1769-2015.

Xie, S-P., Deser, C., Vecchi, G.A., Collins, M., Delworth, T.L., Hall, A., Hawkins, E., Johnson, N.C., Cassou, C., Giannini, A. and Watanabe, M. 2015. Towards predictive understanding of regional climate change, Nature Climate Change 5, 921–930 doi:10.1038/nclimate2689

Zhang, Y., C. Seigneur, M. Bocquet, V. Mallet, and A. Baklanov, 2012.Real-Time Air Quality Forecasting, Part II: State of the Science, Current Research Needs, and Future Prospects, Atmos. Environ., 60, 656-676. Atmos. Environ., 60, 656.

GEOSPATIAL STRATEGY FOR ADVERSE IMPACT OF URBAN HEAT ISLAND VIA SURFACE TOPOGRAPHY USING LANDSAT ETM+ SENSORS

A. KUMAR[1]

Haryana Institute of Public Administration, Gurgaon, India

We are living in the age of rapidly growing population and changing environmental conditions with advance technical capacity. This has been resulting in wide spread land cover change. Among several human induced environmental and urban thermal problems are reported to be negatively affecting urban residents in many ways. Urban Heat Islands exist in many large cities especially metropolitan cities and can significantly affect the quality of life in affected areas. The adverse effect of urban heat island has become the subject of numerous studies in recent decades and is reflected in many major cities around the world. The built-up structures in urbanized areas considerably alter land cover thereby affecting thermal energy flow which leads to development of elevated surface and air temperature. The Urban Heat Island (UHI) for the temporal period is estimated using geospatial techniques which are then utilized for the impact assessment on climate of the surrounding regions and how it reduce the sustainability of the natural resources like air, vegetation (Wang, 1990). Rapid growth of industries in peri-urban areas results in excessive warming and variations in weather conditions. Remotely sensed data of thermal infrared band in the region of 10.4-12.5 μm of EMR spectrum, available from LANDSAT-7 Thematic Mapper and Enhanced Thematic Mapper (TM and ETM+) with 60 m resolution is proved to be very helpful to identify urban heat islands using surface topography. Thermal infrared data acquired during the daytime and night time can be used to monitor the heat island associated with urban areas as well as atmospheric pollution. To ascertain the influence of land use and land cover categories and vegetation density on surface temperature LANDSAT 7 ETM+ and ASTER Advanced Space-borne Thermal Emission and Reflection Radiometer with 90 meters resolution data sets can be used (Kim, 1992; Weng, 2001).The present paper describes the methodology and resolution dynamic urban heat island change on climate using geospatial approach for Haridwar district of Uttrakhand. NDVI were generated using day time LANDSAT ETM+ image of 1990, 2000 and 2005. Temperature of various land use and land cover categories was estimated. In Haridwar district the temperature is inversely related and negatively correlated with NDVI value. The present study has showed that heat island effect need not be limited to a particular temperature epoch which signals towards the increasing dominance of anthropogenic heat emissions in rapidly developing cities such as Haridwar District in Uttrakhand, India. For compensation of the adverse effect of UHI, the urban built up cover should be reduced to an extent but in real, it is not possible due to proclivity of the human towards urbanization.

REFERENCES

Wang, W. C., Zeng, Z. and Karl, T. R.,1990. Urban heat islands in China. Geophysical Research Letters 17, 2377-2380.

Weng, Q., 2001. A remote sensing-GIS evaluation of urban expansion and its impact on surface temperature in the Zhujiang Delta, China. International Journal of Remote Sensing, 22, 1999-2014.

Kim, H.H., 1992. Urban heat island. International Journal of Remote Sensing, 13, 2319-2336.

ICOS RESEARCH INFRASTRUCTURE —INTEGRATING EUROPE'S GREENHOUSE GAS OBSERVATIONS FOR BETTER FUTURE

W.L. KUTSCH, E. JUUROLA, J. LAVRIC, J. LÄTTI, ICOS CENTRAL FACILITIES TEAMS

ICOS ERIC Head Office, Erik Palménin aukio 1, 00560 Helsinki, Finland

Keywords: GREENHOUSE GASES, LONG TERM OBSERVATIONS, CLIMATE CHANGE, DISTRIBUTED RESEARCH INFRASTRUCTURE

Climate change is one the most challenging problems that mankind will have to cope with in the coming decades. The driving force of current and future climate change is the increasing concentration of greenhouse gases (GHG) in the atmosphere, driven by man-made emissions that overtake the natural cycles of carbon dioxide (CO_2), methane (CH_4) and nitrous oxide (N_2O). The concentrations of CO_2 and CH_4 in the atmosphere are at their highest in the past 25 million years. Current levels of CO_2 have increased by 30% from pre-industrial times and they continue to rise, as fossil fuel emissions are climbing up. Current levels of CH_4 are nearly triple the pre-industrial value.

Profound understanding of the driving forces of climate change requires full quantification of the greenhouse gas emissions and sinks and their dynamics. These can be assessed by long term, high precision observations in the atmosphere and at the ocean and land surface. The Integrated Carbon Observation System, ICOS, is a distributed European Research Infrastructure to provide the long-term observations required to understand the present state and predict future behavior of the global carbon cycle and greenhouse gas emissions. ICOS provides data and knowledge on greenhouse gas (GHG) budgets and their perturbations. The backbone of ICOS are atmosphere, ecosystem and ocean station networks with long-term observations required to understand the present state and predict future behavior of the global carbon cycle and GHG fluxes.

Environmental Research Infrastructures like ICOS generate important knowledge on our ecological life support systems that provide priceless services to mankind. This is particularly evident in the field of climate change and GHG budgets, as not reaching our safe climate change mitigation goals will lead to extremely large societal costs for adaptation. The investments and running costs needed for a global GHG observations are marginal compared to these costs.

Through its Carbon Portal ICOS provides effective access to a single and coherent European data set on GHG concentrations, related emissions and natural sinks. Detecting changes in regional GHG fluxes enables early warning of negative trends or extreme events. It will also support countries in decision making about their Intended Nationally Determined Contributions (INDCs). ICOS also aims to establish a template for the future development of similar observation networks beyond Europe. The data policy of ICOS RI endorses full and open exchange of data, metadata and data products that will be made available with minimum time delay. It follows general data sharing principles as outlined by Group on Earth Observation (GEO).

In order to provide this information ICOS builds National Networks of atmospheric, ecosystem and ocean stations. European level ICOS Centres called Central Facilities, have specific tasks in collecting and processing the data received from the national station networks, and providing calibration gases and specific analyses.
The information provided by ICOS will reduce uncertainties in Earth System models and their predictions as used in the Assessment Reports of the Intergovernmental Panel on Climate Change (IPCC). ICOS data and ICOS community will play a key role in development of new decisive tools for climate policy in the coming years. Additional benefit will come from detecting surprise changes in the Earth System that

would require changes in a mitigation strategies as well as from detecting non-compliance of regions, sectors or countries.

ICOS contributes to several international research projects, such as ENVRI PLUS, EUDAT 2020 and INGOS by providing high quality greenhouse gas data, enabling modeling and participating methodological research to improve the capabilities to solve the grand challenge of climate change. Technological developments and implementations, related to GHGs, will be promoted by the linking of research, education and innovation.

ICOS is currently supporting a GEO Flagship initiative on GHG and the global carbon cycle. In this context we are inviting other countries in Europe as well as globally to cooperate or even join us. ICOS aims to expand its station network in Europe and in adjacent regions to reach scientifically sound geographical coverage and to establish a stable and trustful position in its scientific and societal environment. The latter has become even more important after the encouraging results of the COP21 at Paris in December 2015. One result of the so called 'Paris Agreement' is the necessity of a science-based in-situ observation system that enables in cooperation with space-based observations and model-data-fusion a detailed knowledge base to support and verify future mitigation and adaptation processes.

The ambition is to further develop ICOS as the European pillar of global in-situ observations of GHG and provide in addition a repository service for higher integrated knowledge e.g. for modelling results and comparisons.

MODELLING BLACK CARBON: FROM INTERNATIONAL CLIMATE LAW TO IMPACT ON ARCTIC CLIMATE (WHITE)

T. KÜHN[1,2], H. KOKKOLA[2], K. KUPIANEN[3], K. KULOVESI[4], AND K.E.J. LEHTINEN[1,2]

[1]Department of Applied Physics, University of Eastern Finland (UEF), Kuopio, Finland.

[2]Finnish Meteorological Institute (FMI), Kuopio, Finland.

[3]Finnish Environment Institute (SYKE), Helsinki, Finland.

[4]Department of Law, University of Eastern Finland (UEF), Joensuu, Finland.

Keywords: GLOBAL MODELLING, ARCTIC, FLARING, BLACK CARBON.

INTRODUCTION

The WHITE project is a novel multi-disciplinary collaboration between the UEF Law School, the Finnish Environmental Institute (SYKE) and the UEF Aerosol Research Group. Its ultimate goal is to identify national and international regulatory options that have the highest potential in mitigating arctic warming. To this end, different regulatory frameworks are analysed and used to construct emission scenarios, whose long-term impact on the Arctic climate is then assessed using global climate modelling. Here we present first results showing the importance of the correct spatial and temporal distribution of emissions on pollutant concentrations in the arctic.

METHODS

For our simulations we used the global aerosol-climate model ECHAM-HAMMOZ (ECHAM6.3-HAM2.2) with the sectional aerosol module SALSA. We compare two different aerosol emission inventories. The ACCMIP emission inventory (Riahi 2007), which is the standard ECHAM, is by default restricted to yearly average emissions. In contrast, the ECLIPSE emission inventory (Klimont 2016a, 2016b) contains detailed monthly variations for the relevant emission sectors and regions. Additionally, the ECLIPSE emission inventory includes flaring emissions from oil production, which make a large contribution to Arctic pollutant concentrations. As an example, we show the monthly emission strengths for black carbon (BC) for the two emission inventories in Figure 1.

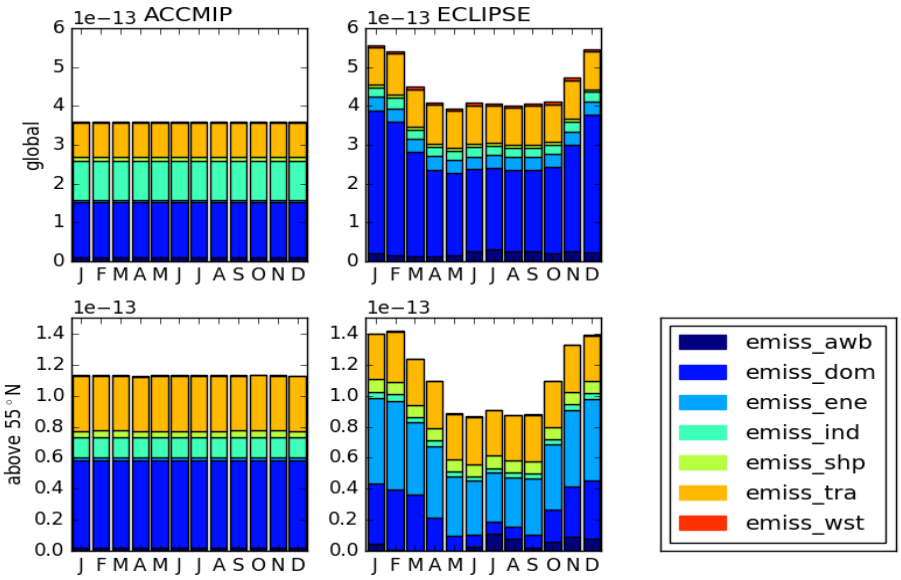

Figure 1. Black carbon (BC) emission inventories by sector and month for ACCMIP (left) and ECLIPSE (right) data sets. Emission strengths are given in kg/m^2/s

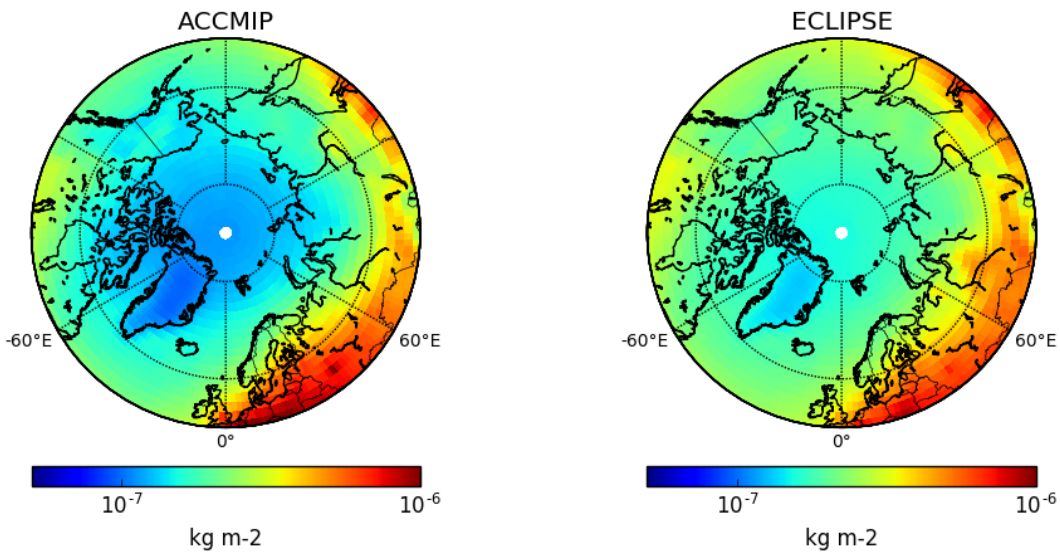

Figure 2: Yearly averages of the BC burdens in the Arctic region for the ACCMIP (left) and ECLIPSE (right) emission inventories.

CONCLUSIONS

Even though the yearly average BC emission strengths do not differ much between the two emission inventories, the BC burdens seen in the Arctic region are clearly higher for the ECLIPSE emission inventory. This higher BC burden is thus caused by both the higher temporal resolution of the emissions and the inclusion of the flaring emissions caused by oil production.

ACKNOWLEDGEMENTS

This work was supported by the Academy of Finland, grant no. 286613 and the Centre of Excellence (grant no. 272041).

REFERENCES

Klimont, Z., Kupiainen, K., Heyes, C., Purohit, P., Cofala, J., Rafaj, P., Borken-Kleefeld, J., Schoepp, W. (2016a). *Global anthropogenic emissions of particulate matter*. In preparation.

Klimont, Z., Höglund-Isaksson, L., Heyes, C., Rafaj, P., Schöpp, W., Cofala, J., Borken-Kleefeld, J., Purohit, P., Kupiainen, K., Winiwarter, W., Amann, M, Zhao, B., Wang, S.X., Bertok, I., Sander, R. (2016b). *Global scenarios of air pollutants and methane: 1990-2050*. In preparation.

Riahi, K., Grübler, A. and Nakicenovic, N., (2007). *Scenarios of long-term socio-economic and environmental development under climate stabilization*. Technological Forecasting and Social Change, *74*(7), pp.887-935.

PAN-EURASIAN EXPERIMENT (PEEX) PROGRAM OVERWIEV - ACTIVITIES IN 2012-2015 AND FUTURE PROSPECTS

H.K. LAPPALAINEN[1,2], T.PETÄJÄ[1], V-M. KERMINEN[1], R.MAKKONEN[1], A.MALKAMÄKI[1], P. ALEKSEYCHIK[1], N. ZAITSEVA[3], J. KUJANSUU[1], T. RUUSKANEN[1], A. LAURI[1], E. KYRÖ[1], S. MAZON[1], A. SCHERBININ[4], P. KONSTANTINOV[5], M. KAUKOLEHTO[1], N. CHUBAROVA[5], T. LAURILA[2], E. ASMI[2], S. JUHOLA[4], J. BÄCK[6], T. VESALA[1], P. HARI[6], M.ARSHINOV[7], A. MAHURA[8], S. ARNOLD[9], D. SPRACKLEN[9], A. DING[10], C. FU[10], H-C. HANSSON[11], V. MELNIKOV[12,13], G. MATVIENKO[7], A. BAKLANOV[14], Y.VIISANEN[2], N. KASIMOV[5], H. GUO[15], V. BONDUR[16], S. ZILITINKEVICH[1,2,17] AND M. KULMALA[1]

[1)] Dept. of Physics, University of Helsinki, Finland.

[2)] Finnish Meteorological Institute, Helsinki, Finland

[3)] Dept. of Earth Sciences, Russian Academy of Sciences, Russia

[4)] Dept. of Environmental Sciences, University of Helsinki, Finland.

[5)] Moscow State University, Russia

[6)] Dept. of Forest Ecology, University of Helsinki, Finland

[7)] Institute of Atmospheric Optics, Tomsk 634055, Russia

[8)] Danish Meteorological Institute, Research and Development Department, 2100, Copenhagen

[9)] Institute for Climate and Atmospheric Science, School of Earth and Environment, University of Leeds, Leeds, LS2 9JT, UK

[10)] Institute for Climate and Global Change Research & School of Atmospheric Sciences, Nanjing University, 210023 Nanjing, China'

[11)] Dept. of Environmental Science and Analytical Chemistry, Stockholm University, Sweden

[12)] Tyumen State University, Russia

[13)] Tyumen Scientific Center, Siberian Branch, Russian Academy of Science, Russia

[14)] World Meteorological Organization, 1211 Genève, Switzerland

[15)] Institute of Remote Sensing and Digital Earth, Chinese Academy of Sciences, Beijing 100101, China

[16)] AEROCOSMOS Research Institute for Aerospace Monitoring, Moscow, Russia 167 Dept. of Radiophysics, Nizhny Novgorod State University , Russia

Keywords: MULTIDISCIPLINARY APPROACH, MULTISCALE RESEARCH, GRAND CHALLENGES, ARCTIC-BOREAL, OBSERVATION NETWORKS, LAND-ATMOSPHERE INTERACTIONS

INTRODUCTION

Pan-Eurasian Experiment (PEEX) initiative (https://www.atm.helsinki.fi/peex/) is an international, multi disciplinary, multiscale bottom up initiative established in 2012. The main focus of the initiative is to solve interlinked global environmental challenges influencing societies in the Northern Eurasian region. The goal is to solve with comprehensive, continuous observations the scientific questions that are specifically important for the Arctic-boreal region in the coming years, in particular the global climate change and its consequences to nature and the Northern societies. PEEX aims to deliver novel ground

based land-atmosphere data for constructing reliable early warning systems (floods, forest fires, droughts), for predicting extreme weather events and estimating the environmental contamination of industrial accidents

The initiative has grown fast and at the moment it is involving research communities from 20 different countries from Europe, Russian and China. Altogether 80 institutes have contributed to the PEEX Science Plan, which identifies the program at large, introduces the research agenda, the components of the future PEEX research infrastructure, the topics relevant for impact making and outreach activities. The program is coordinated by the University of Helsinki and the Finnish Meteorological Institute together with the Moscow State University (MSU) and AEROCOSMOS from Russia and Institute of Remote Sensing and Digital Earth (RADI) and University of Nanjing from China.

PROGRAM APPROACH IN 2012-1015

In 2012-2015 PEEX has established a program organization, determined the program structure and aims and taken the first steps towards implementation. The Program headquarters is situated at the Kumpula Campus in Helsinki, Finland and is coordinated by the University of Helsinki, Div. Atmospheric Sciences of the Physics Department and the Finnish Meteorological Institute. The main offices in Russia are hosted by AEROCOSMOS and Moscow State University and in China by Institute of Remote Sensing and Digital Earth (RADI, CAS) and University of Nanjing. In addition to the above listed institutes The Program Scientific Steering Committee consists representatives of Institute of Atmospheric Optics, Tomsk (RAS, RU), Inst. of Geography (RU), Institute of Atmospheric Physics (CAS, CN), World Meteorological Organization and the iLEAPS program within Future Earth.

The program structure, concept and the research agenda including the key topics for the first five years are described in the PEEX Science Plan (http://www.atm.helsinki.fi/peex/images/PEEX_SP__27052015.pdf; see also Lappalainen et al. 2016) . In implementing the PEEX research agenda we have opened the PEEX Special issue in the Journal of Atmospheric Chemistry and Physics (http://www.atmos-chem-physdiscuss.net/special_issue265.html). The special issue serves as a primary platform collecting PEEX relevant scientific results for the periodic PEEX science assessment. The Assessment(s) will be distributed to different stakeholders and policy making processes such as the Arctic Council, IPCC, Future Earth and the European, Russian and Chinese ministries. In 2015-2016 we have published the first PEEX papers determining the mission goals and concepts (Kulmala et al. 2015, Hari et al. 2016, Lappalainen et al. 2016) and presented first assessment of the competing effects of CO2 and secondary organic aerosols in Eastern Siberia (Arneth et al. 2015) Furthermore, PEEX has been actively promoted to the Russian science community and aspects of the PEEX research infrastructure development in Russia have been introduced by Lappalainen et al. (2014), Kulmala et al. (2016) and Alekseychik et al. (2016). PEEX has also been proposed to the central government of China as one of the key projects in the Silk Road Economic Zone initiative (Kujansuu et al. 2015).

For establishing a multidisciplinary research community PEEX has organized series of joint workshops together with the Nordic Center of Excellence (NCoE) called “Cryosphere-atmosphere interactions in a changing Arctic climate” (CRAICC) . The aim of the workshops has been deepen the research collaboration between PEEX and CRAICC and to identify the most relevant research questions for a more specific topics compared to Science Plan such as “Arctic shipping and climate change”. The first bilateral research approach in the frame of PEEX collaboration has been initiated between University of Helsinki and AEROCOSMOS. The Finnish Center of Excellence on in Atmospheric Science – “From Molecular and Biological processes to The Global Climate” funded by the Academy of Finland for the years 2014-2017 and “Development of methods for monitoring of the dynamics of natural and anthropogenic emissions of trace gases and aerosols in the atmosphere based on satellite data and modeling” funded by the Russian Ministry of Education for the years 2014-2016 provides the backbone to the joint research activities.

Education of the next generation of scientists as well as capacity building of the experts takes place at the workshops and international courses. PEEX benchmarked courses are especially suitable for networking and collaboration and are typically intensive field or laboratory courses. Topics range from hands on data-analysis field courses on atmospheric processes and feedbacks and atmosphere-biosphere interactions in Hyytiälä, Finland; Integrated Carbon Observation System (ICOS); permafrost-biogeochemistry-climatology-ecology in Spasskaya, Russia; laboratory course on stable isotopes in Sapporo, Japan. The courses bring together experts of the PEEX topics and facilitate horizontal learning among the participants and teachers. Courses organized by PEEX contributing institutes are opened, when possible, to other the community. Some of the examples are air pollution – from local to global in Nanjing, China; atmospheric optics, Moscow, Russia, paleolimnology of Northern Eurasia, Petrozavodsk, Russia; application of weather and cloud radars in Hyytiälä, Finland.

PEEX has also been introduced in several conferences or executive forums such as Valdai Club in Russia or "Beautiful China - Steps Towards 21st Century" symposium in China. Furthermore, PEEX Special Sessions has been organized, for example, in the International Geographical Union (IGU) Conference – Moscow in August and European Aerosols Conference (EAC) - Milan in September. The 1 st PEEX Science Conference was held on 10-12.February.2015 in Helsinki, Finland. The conference gathered ca 150 participants from Europe, Russia and China including plenary speakers such as Director General Pavel Kabat, IIASA. PEEX has also established a collaboration between the European, Russian, Chinese and global partners to maximize the impact of the becoming research highlights, scientific assessment and research infrastructure development in the climate policy relevant processes. The key partners and stakeholders here are IIASA, International Eurasian Academy of Sciences (IEAS); Digital Earth, Future Earth, Arctic Council (SAON), WMO and GEO - GEOSS.

The strategically important task of PEEX is to filling the observational gap in atmospheric in-situ data in the Northern Eurasian region regions. In 2012-2015 PEEX has made preparatory work with the Russian station networks so that the metadata approach is ready to be launched and would be the first step connecting the Russian RI to international research infrastructure frameworks. As a part of this task we have also published the "PEEX view tool" (http://www.atm.helsinki.fi/aapon_demo_php/test15_demo.html), which enables the comparison between the in situ data and the modelled data. The PEEX-View is an online tool for visualizing and analyzing of simulation and observational data and a demo version has recently been released in the PEEX website In the future, the PEEX-View is envisioned to combine multidisciplinary datasets of varying temporal and spatial scales.

One of the concrete tasks of the PEEX is to establish a coordinated, coherent land based PEEX observation network over the Northern Pan-Eurasian region. The concept of the hierarchical PEEX in situ station network is based on the know-how from 20 year development of the SMEAR-II flagship station measurement theory and techniques (Hari et al. 2016). The backbone of the station network is built on the existing biosphere (ecological) and atmospheric observation networks in collaboration with European, Russian, Chinese and global partners. In practice this would mean the upgrading and expanding the current measurement capacity of the stations step by step with the new blocks of instruments (Kaukolehto et al. of this issue). The station upgrading and /or establishing news stations would need national investments of Russia and China.

FUTURE PROSPECTS

PEEX continues expanding the stakeholder and contact networks in 2016. Having new contacts with the Northern American teams are one of the priority areas. For example joint workshops on Arctic measurements are to be organized in Helsinki. Furthermore, the PEEX aims to strengthen the collaboration with the China Silk Road Economic Belt Initiative. PEEX recognizes the unique opportunity to explore cooperation in the sustainable development of environments along the Silk Road Economic Belt and Road. PEEX has the potential to establish a framework for solving environmental problems in the Belt

and Road countries, and become a community of shared interests. PEEX research outcome and observation activities and the new methodological concepts are providing new information not only for the climate policy making in the global scale but also for the regional scale; including mitigation and adaption planning.

The PEEX contribution to the Paris COP process is strongly linked with the establishment of the GlobalSMEAR station network and the SMEAR-concept. The first ideas of Global SMEAR network has been introduced just recently at a Paris COP side-meeting in December 2015. The PEEX in situ station network over Northern Eurasian is based on the SMEAR-II flagship station measurement theory and techniques (Hari et al. 2016, Kulmala et al. 2016). We are currently working on documenting the SMEAR-Concept, which includes hierarchical blocks of instruments setups for different surfaces (boreal forest, peatland, urban, Arctic marine etc.) and technical descriptions of the data processing and storage system. Furthermore, we underline that the satellite observations are to be connected to the ground based observations of the PEEX network.

In the first phase PEEX is expanding gradually the existing SMEAR station network in Finland, Estonia and China and will be establishing the first stations based on SMEAR concept in Russia during 2016-2018. With the PEEX network based on SMEAR concept we are able to make reliable estimation and identification of the real carbon (CO2) sources leading to enhanced atmospheric CO2 emissions. We are also able to estimate the carbon sink, especially the role of boreal forest being able store the atmospheric CO2. For example, via the flux towers with a height larger than 100m high we are able to calculate the carbon sink-source balance over 1000 km2 footprint area. After having a reliable quantitative estimations of the current sink-source dynamics over wide boreal forest regions the next step would be to make practical actions to determine that the CO2 sink (storage) would be stronger than the CO2 source (emissions) in the future.

Besides CO2 dynamics also the dynamics related to the Short-Lived Climate Forces (SLCF), e.g. air pollutants like black carbon, ozone and aerosol particles are crucial for global climate. Using extensive, comprehensive, continuous observations we are able to understand how SLCF contributes over arctic-boreal regions and in China to regional and global climate. PEEX research approach aims to spann over scientific boundaries and start a more intensive interaction between natural sciences and socio-economics. Novel socio-economic pathways and recommendations for policy making are crucial to meet regional and global challenges. On the other hand if socio-economic investigations are interacting with exiting and improving natural scientific knowledge we can together find sustainable solutions to meet the requirements given by the COP21 agreement in Paris.

ACKNOWLEDGEMENTS

A major part of the PEEX Preparatory Phase work in years 2010–2015 has been based on the in-kind contribution of several European, Russian and Chinese research institutes via supporting active participation to the PEEX meetings, conference organized in Helsinki, Moscow, Hyytiälä and Saint Petersburg. In addition we would like acknowledge the following support or funding from the following bodies: Finnish Cultural Foundation, Grant: Prof. Markku Kulmala “International Working Groups”; Russian Mega-Grant No. 11.G34.31.0048 (University of Nizhny Novgorod), Academy of Finland contract 259537, Beautiful Beijing (Finland- China collaboration project) funded by TEKES, EU project InGOS and the NordForsk Nordic Centre of Excellence of CRAICC (no 26060) and Nordforsk CRAICC-PEEX (amendment to contact 26060).

REFERENCES

Alekseychik, P., Lappalainen, H.K., Petäjä, T., Zaitseva, N., Heimann, H., Laurila, T., Lihavainen, H., Asmi, E., Arshinov, M., Shevchenko, V., Makshtas, A., Dubtsov, S., Mikhailov, E., Lapshina, E., Kirpotin, S., Kurbatova, Yu., Ding, A., Guo, H., Park, S., Lavric, J.V, Reum, F., Panov,A.,

Prokushkin, A., and Kulmala M.,2016: Ground-based station network in Arctic and Subarctic Eurasia: an overview, J. Geography Environment Sustainability, in press.

Arneth, A., Makkonen, R., Olin, S., Paasonen, P., Holst, T., Kajos, M. K., Kulmala, M., Maximov, T., Miller, P. A., and Schurgers, G.: Future vegetation–climate interactions in Eastern Siberia: an assessment of the competing effects of CO2 and secondary organic aerosols, Atmos. Chem. Phys. Discuss., 15, 27137- 27175, doi:10.5194/acpd-15-27137-2015, 2015.

Hari, P., Petäjä, T., Bäck, J., Kerminen, V-M., Lappalainen, H.K. Vihma, T., Laurila, T., Viisanen, Y., Vesala, T., and Kulmala M., 2016. Conceptual design of a measurement network of the global change, Atmos. Chem. Phys., 16, 1017-1028, http://www.atmos-chem-phys.net/16/1017/2016/ , doi:10.5194/acp-16- 1017-2016

Kaukolehto, M. Bäck, J., Hari, P., Kerminen, V-M., Kujansuu, J., Lappalainen, H.K., Levula, J., Petäjä T., Vesala, T., and Kulmala, M 2016. Towards global SMEAR network to provide comprehensive data for knowledge based decisions, of this issue.

Kujansuu, J.,, c.b. Fu, h.d. guo, Lappalainen, H.K., Ding, A.J., Petäjä, T., Hu, M., Järvi, L., Zheng, X.H., Vesala, T., Wang and Kulmala, M.:Scientific collaboration with china: holistic approach. Proceedings of 'the Center of Excellence in Atmospheric Sciences (CoE ATM) -From Molecular and Biological Processes to the Global Climate' Annual Meeting 2014, Editors: Markku Kulmala, Anna Lintunen and Jenni Kontkanen (2014), 369-373.

Kulmala, M., Lappalainen, H.K., Petäjä, T., Kerminen, V-M., Viisanen, Y., Matvienko, G., Melnikov, V., Baklanov, A., Bondur, V., Kasimov, N., and Zilitinkevich, S. 2016: Pan-Eurasian Experiment (PEEX) Program: Grant Challenges in the Arctic-boreal context, J. Geography Environment Sustainability, in press.

Kulmala, M., Lappalainen, H.K., Petäjä, T., Kurten, T., Kerminen, V-M., Viisanen, Y., Hari, P., Bondur, V., Kasimov, N., Kotlyakov, V., Matvienko, G., Baklanov, A:, Guo, H., Ding, A., Hansson, H-C., and Zilitinkevich, S., 2015. Introduction: The Pan-Eurasian Experiment (PEEX) – multi-disciplinary, multi-scale and multi-component research and capacity building initiative, Atmos. Chem. Phys., 15, 13085-13096, 2015 doi:10.5194/acp-15-13085-2015

Kulmala, M., Lappalainen, H.K., Bäck, J., Laaksonen, A., Nikinmaa, A., Riekkola, M-L., Vesala, T., Viisanen, Y., Aalto, T., Boy, M., Dal Maso, M., Ehn, M., Hakola, H., Hari, P., Hartonen, K., Hämeri, K., Hölttä, T., Junninen, H., Järvi, L., Kurten, T., Lauri, A., Laurila, T., Lehtipalo, K., Lihavainen, H., Lintunen, A., Mammarella, I., Manninen H., Petäjä, T., Pihlatie, M., Pumpanen, J., Rinne, J., Romakkaniemi, S., Ruuskanen, T., Sipilä, M., Sorvari, S., Vehkamäki, H., Virtanen, A., Worsnop, D., Kerminen, V-M.: Finnish Centre of Excellence in Physics, Chemistry, Biology and Meteorology of Atmospheric Composition and Climate Change: Preface, summary and outlook. Boreal Env. Res. 19 (suppl. B): 1.2014.

Kulmala, K., Asmi, A., Lappalainen, H.K. & EUCAARI teams: General overview: European Integrated project on Aerosol Cloud Climate and Air Quality interactions (EUCAARI) – integrating aerosol research from nano to global scales. Atmos. Chem. Phys., 11, 13061-13143, 2011.

Kulmala, M., Asmi, A., Lappalainen, H.K., Carslaw, K.S., Pöschl, U., Baltensperger, U., Hov, Ø., Brenquier, J.-L., Pandis, S.N., Facchini, M.C., Hansson, H.-C., Wiedensohler, A., and O'Dowd, C.D., 1 Introduction: European Integrated project on Aerosol Cloud Climate and Air Quality interactions (EUCAARI) - integrating aerosol research from nano to global scales. Atmos. Chem. Phys., 9, 2825-2841, 2009 .

Lappalainen, H.K., Petäjä, T., Kujansuu, J., and Kerminen, V.-M. et al. : Pan-Eurasian Experiment (PEEX) – a research initiative meeting the grand challenges of the changing environment of the northern Pan-Eurasian arctic-boreal areas, J. Geography Environment Sustainability, 2(7), 13-48, 2014.

Lappalainen, H.K., Kerminen, V.-M., Petäjä, T. et al.: Pan-Eurasian Experiment (PEEX):Towards holistic understanding of the feedbacks and interactions in the land - atmosphere - ocean- society continuum in the Northern Eurasian region. To be submitted to J. Atmos. Chem. Phys., 2016.

Pan Eurasian Experiment (PEEX) Science Plan (2016). Editors Lappalainen H.K., Kulmala M. & Zilitinkevich S. http://www.atm.helsinki.fi/peex/images/PEEX_SP__27052015.pdf

THE ATMOSPHERIC SCIENCE PARADIGM AND HORIZONTAL LEARNING: EXPERIENCES FROM SHORT RESEARCH-INTENSIVE COURSES

A. LAURI[1], L. RIUTTANEN[1], P. SIHVONEN[1,2], S. WESTERBERG[1], P. HARI[3], T.M. RUUSKANEN[1,4] and M. KULMALA[1]

[1]Division of Atmospheric Sciences, Department of Physics, University of Helsinki, P.O.Box 64, FI-00014, Helsinki, Finland.

[2]Heinola upper secondary school, Rajakatu 29, 18100 Heinola, Finland.

[3]Department of Forest Sciences, University of Helsinki, P.O.Box 27, FI-00014, Helsinki, Finland.

[4]University of Helsinki Centre for Continuing Education, P.O.Box 53, FI-00014, Helsinki, Finland.

Keywords: HIGHER EDUCATION, MULTI-DISCIPLINARY, PEDAGOGY, PARADIGM.

INTRODUCTION

Atmospheric research involves several fields of science such as chemistry, physics, meteorology, mathematics, biology, agricultural and forest sciences, technology, and geosciences, combining observations, experimentation and modelling. We have realized that the shift from discipline-tied fundamental education towards multidisciplinarity is imperative for a successful career in climate and global change science (Nordic Climate Change Research, 2009). Therefore we suggest here a model to improve the learning outcomes in multidisciplinary atmospheric science. It is based on our experiences organizing more than 50 research-intensive short courses over the past 20 years. The typical length of such a course is 5 to 12 working days.

THE ATMOSPHERIC SCIENCE PARADIGM

Here we do not assess the building of individual paradigms of different disciplines. For simplicity, we consider four disciplines – physics, chemistry, meteorology and biology. On an average atmospheric science short course, we have participants (students, postdoctoral researchers, professors and other senior researchers) from each of these disciplines. In Figure 1, each triangle represents one discipline. Each one of the triangles can be seen as a pyramid representing the learning of the methodologies and concepts of that particular discipline – the paradigm.

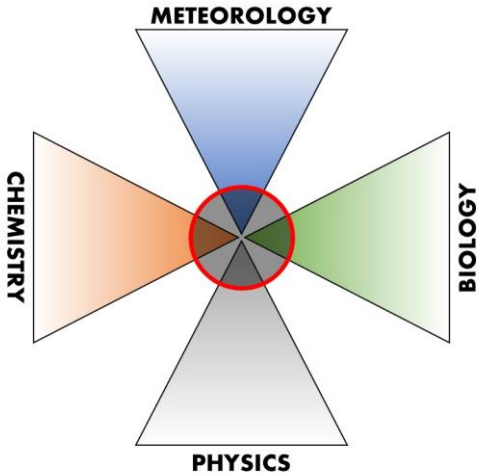

Figure 1.Where the tops of the pyramids meet – an example from a research-intensive short course.

During a research-intensive short course the learning happens and new ideas arise in the shaded centre of Fig. 1, where the tops of the pyramids meet.

HORIZONTAL LEARNING

A pedagogically very interesting fact has been the horizontal learning process during these short courses. Because the participants of the events come from very different backgrounds, a traditional training course approach involving a set of lectures and perhaps some exercises does not work. Instead, we have adopted horizontal learning as a broader approach, addressing a cross-section of knowledge from different fields and blending the information to reach new levels of understanding (see Fig. 2). Students from different fields of study give small lectures to each other in the groups, and several times it has occurred that students wanted to present their ideas to the whole audience for a common discussion. This horizontal learning principle has been shown to be a good example of participatory action research (Hennessy and Murphy, 1999).

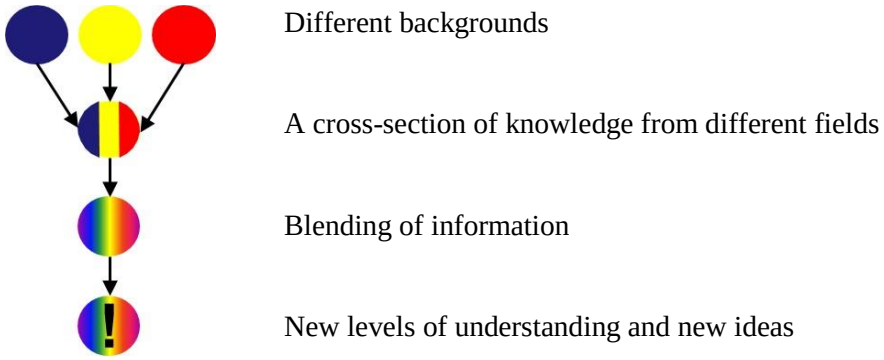

Figure 2.The principle of horizontal learning.

CONCLUSIONS

Special forms of teaching, namely research-intensive courses, can improve the learning compared to a traditional classroom course. Transferable skills can, and have also been successfully taught using these teaching forms.

The development of research-oriented joint programmes has not been without its challenges, and the improvement of these programmes is an utmost priority. In the past several years, the rapid internationalization of the research community has resulted in a few challenges both for students and the staff, bringing notably in not only the differences between disciplines and paradigms, but also the cultural differences of the participating students and researchers.

Despite of the challenges, the experiences have been very encouraging, and the horizontal learning principle has proved to be a fruitful approach to address problems of a multidisciplinary nature.

REFERENCES

Hennessy, S. and Murphy, P. (1999). The Potential for Collaborative Problem Solving in Design and Technology. *International Journal of Technology and Design Education* **9**(1), 1–36.

Nordic Climate Change Research (2009). *NordForsk Policy Briefs 2009-8*, (Mandag Morgen, Oslo, Norway).

NEW CONTINUOUS AEROSOL AND GREENHOUSE GAS MEASUREMENTS IN RUSSIAN ARCTIC ICE BASE CAPE BARANOVA -STATION

T. LAURILA[1], E. ASMI[1], J. HATAKKA[1], J. RAINNE[1], T. MÄKELÄ[1], H. LIHAVAINEN[1], Y. VIISANEN[1], P. TAALAS[1], V. MOVCHAN[2], V. KUSTOV[2] and A. MAKSHTAS[2]

[1]Finnish Meteorological Institute, Atmospheric Composition Research, Helsinki, Finland.

.

[2] Arctic and Antarctic Research Institute, St. Petersburg, Russia.

Keywords: GREENHOUSE GASES, AEROSOL PARTICLES, MEASUREMENTS, ARCTIC.

INTRODUCTION

Our planet is currently under high pressures as a consequence of the increased anthropogenic activities during the past decades (IPCC, 2013). The impact of these activities is in particular realized in fragile Arctic ecosystems which are changing in fast speed. To understand the impact of humans to the Arctic as well as to predict the future of this region and its habitants, direct observations of different climate variables are urged. Greenhouse gases and aerosol particles are among those variables, both affecting the radiation balance of the planet and thereby largely controlling the ongoing change in this balance. For both of these variables much deeper scientific understanding is needed to resolve their sources, and processes especially in the Arctic atmosphere, as well as to predict their future trends. Unfortunately, the geographical coverage of high-quality aerosol and greenhouse gas concentration measurements is still poor in the Arctic. World Meteorological Organization (WMO) and the Arctic Monitoring and Assessment Programme (AMAP) have stressed very much the need to intensify Arctic observation network (e.g. AMAP 2015 assessments on black carbon, ozone and methane). To answer the needs of global scientific community, Finnish Meteorological Institute (FMI) in collaboration with Roshydromet unit of Arctic and Antarctic Research Institute (AARI), started a new long-term program to measure greenhouse gas concentrations and aerosol particle number and optical properties, along with many meteorological and albedo data in the high Arctic research station “Ice base Cape Baranova”. This program is continuation for the successful climate research and monitoring initiated by Roshydromet, FMI and NOAA (National Oceanic and Atmospheric Administration, Boulder, CO) in Tiksi, Russia since year 2010 (Uttal *et al.*, 2013; Asmi *et al.*, 2015). For these new measurements in Russian Arctic, research and atmospheric monitoring is formally approved within the framework of the bilateral agreement of scientific cooperation between Roshydromet and FMI. Precision data of continuous measurements meet international standards of WMO Global Atmosphere Watch (GAW) programme, and will serve as a basis for attaining in the future the status of GAW station by WMO for the research station "Ice base Cape Baranova". Here we describe in detail the status and scientific motivations for these new measurements as well as present the first data from the station.

METHODS

Research station "Ice base Cape Baranova" (79°16.82'N, 101°37.05'E) is in the very northern part of the Bolshevik island, which is part of the Northern Land. The station was reopened in August 2013 by AARI to serve as a year-round scientific base for various oceanic, cryospheric and atmospheric studies. Since 2013, observations of sea ice, snow, glacier, lakes and ocean parameters, ecological studies and measurements of meteorological parameters have been performed at Cape Baranova. To further complete this measurement program, during years 2013-2014 FMI and AARI agreed on and planned the atmospheric composition measurements to be added. This included greenhouse gas and aerosol instrumentation with a complete measurement unit built in Finland that was designed and tested in 2014-2015 and shipped to Russia in summer 2015. Further transportation to Cape Baranova was in October

2015 via ship Akademik Troshnikov leaving from Arkhangelsk. Along with this cruise were researchers from FMI and AARI who installed the new unit and started the measurements in October 16, 2015.

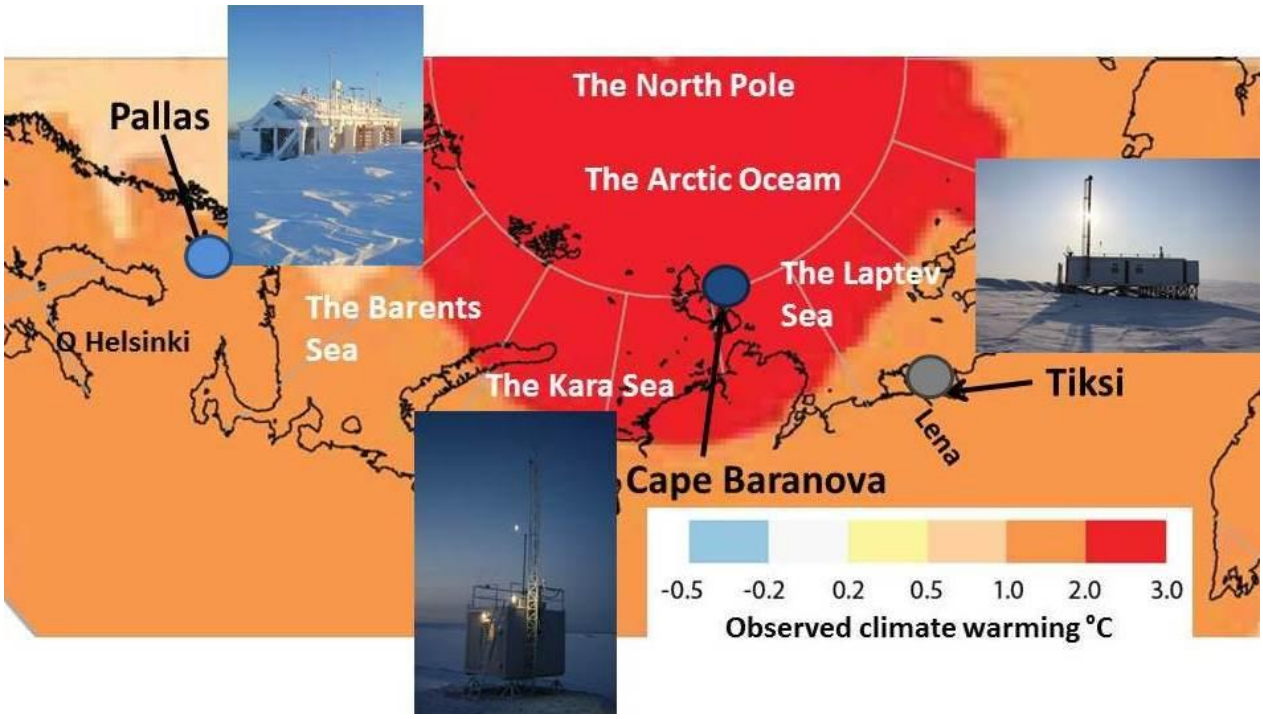

Figure 1. FMI atmospheric aerosol and GHG measurements in the Arctic. The new unit (in photo) was installed at Cape Baranova station.

The new measurement unit (Fig. 1) is about 80 m from the seashore about 20 m a.s.l. (79° 16.824'N, 101° 37.053'E). It is well exposed to winds from the most common wind directions southwest and northeast. Local pollution, generator building in particular, is in the southeast direction.

Details of instrumentation installed within this new unit are presented in Table 1. Most of the sensors operate continuously inside the new measurement cabin or in the near proximity of the cabin (roof and soil installations). In addition, one instrument to study the ice development was brought to Cape Baranova (SIMBA thermistor chain, SAMS Research Services Ltd).

Instrument name	Measured parameter
DMPS (TSI Inc. 3010 CPC)	Aerosol number size distribution
MAAP, Thermo Sci. 5012	Absorbing aerosol concentration
Nephelometer, Ecotech 3000	Aerosol scattering and back-scattering at 3 wl
Picarro G2401 spectrometer	CO_2, CH_4, CO, H_2O concentration
Thermo Sci. 43iTLE	SO_2 concentration
uSonic-3 anemometer, Metek	Wind speed, direction, turbulence

HMP155, BARO1QMLSP, Vaisala	T, RH, pressure
CMP11, CGR4, NR-LITE2, Kipp & Zonen	Global, longwave and net radiation
5x PT100, Nokeval ; 2x ML-3, DeltaT Devices ; HFP-3, Hukseflux	Soil temperature, humidity and flux measuremements
CMP11, Kipp & Zonen	Surface albedo

Table 1. Instrumentation installed to Cape Baranova on October 16, 2015.

CONCLUSIONS

New measurements started successfully. Data from Cape Baranova are regularly transferred via satellite link to AARI and FMI servers. An example of development of high temporal resolution GHG data at Cape Baranova are presented in Figure 2 during a two months period of sea ice freezing in winter 2015. Temperature over the island drops permanently below zero in mid-November. The general trend is increasing CO_2 and CO concentrations towards the winter season but also several short episodes with increasing CO_2 and methane concentrations are observed in data. Air masses to Cape Baranova frequently pass over continental Siberia where extensive wetlands and hydrocarbon production networks are located. Highest episodic methane concentrations (Figure 2) were observed during advection from western Siberia lowland area. Concomitant increase of CO_2 concentration is by seasonal net respiration of terrestrial ecosystems. Regional fluctuations in oceanic and sea-ice sources and sinks are studied as possible reasons for these fluctuations and data are modelled within the framework of global GHG observations for better understanding the Arctic GHG sources and sinks. Terrestrial uptake and respiration of CO_2 and emissions of methane will be studied together with the other Arctic stations.

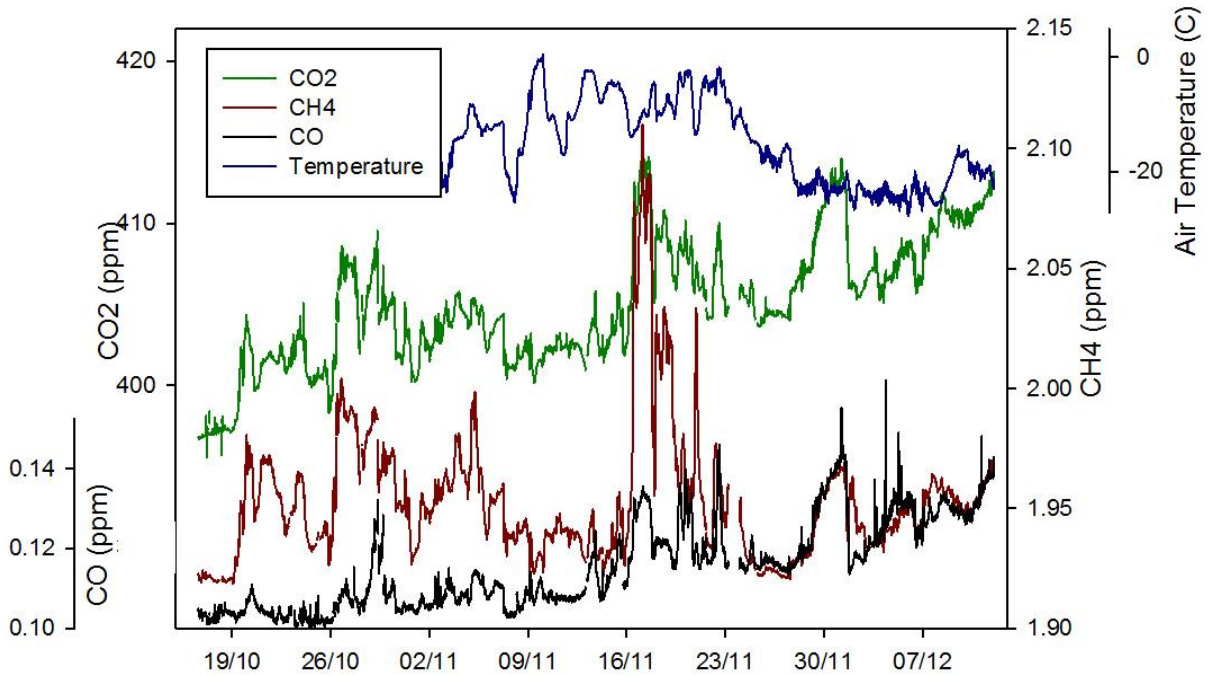

Figure 2. Time series of concentrations of gases CO_2, CH_4 and CO and of air temperature between October 16 and December 31, 2015 measured in Cape Baranova.

Aerosol particle concentration in Cape Baranova in winter 2015 were low (typically some tens of particles per cc). However, a few episodes of increased number concentrations and/or increased aerosol scattering and absorption were already observed. The annual cycles and sources of particles as well as their aging over the passage via the Arctic are topics that are further studied based on the data.

ACKNOWLEDGEMENTS

This work was supported by the Academy of Finland projects Greenhouse gas, aerosol and albedo variations in the changing Arctic (project number 269095), Carbon balance under changing processes of Arctic and Subarctic cryosphere (project number 285630), the Academy of Finland Center of Excellence program (project number 272041) and the Arctic and Antarctic Research Institute of Roshydromet (CNTP 1.5.3.4).

REFERENCES

AMAP, 2015. AMAP Assessment 2015: Black carbon and ozone as Arctic climate forcers. Arctic Monitoring and Assessment Programme (AMAP), Oslo, Norway. vii + 116 pp.

AMAP, 2015. AMAP Assessment 2015: Methane as an Arctic climate forcer. Arctic Monitoring and Assessment Programme (AMAP), Oslo, Norway. vii + 139 pp.

Asmi, E., V. Kondratyev, D. Brus, T. Laurila, H. Lihavainen, J. Backman, V. Vakkari, M. Aurela, J. Hatakka, Y. Viisanen, T. Uttal, V. Ivakhov and A. Makshtas (2015) Aerosol size distribution seasonal characteristics measured in Tiksi, Russian Arctic, Atmos. Chem. Phys. Discuss., 15, 18109-18149, doi:10.5194/acpd-15-18109-2015.

IPCC, 2013: Climate Change 2013: The Physical Science Basis. Contribution of Working Group I to the Fifth Assessment Report of the Intergovernmental Panel on Climate Change [Stocker, T.F., D. Qin, G.-K. Plattner, M. Tignor, S.K. Allen, J. Boschung, A. Nauels, Y. Xia, V. Bex and P.M. Midgley (eds.)]. Cambridge University Press, Cambridge, United Kingdom and New York, NY, USA, 1535 pp, doi:10.1017/CBO9781107415324.

Uttal, T., A. Makshtas and T. Laurila (2013) The Tiksi International Hydrometeorological Observatory – 5 An Arctic Members Partnership, WMO Bulletin 62(1), p.22–26.

EXTRA-TROPICAL OCEAN WARMING AND WINTER ARCTIC SEA ICE COVER SINCE THE 1990S

FEI LI[1], HUIJUN WANG[1], YONGQI GAO[1,2]

[1] Nansen-Zhu International Research Center, Institute of Atmospheric Physics, Chinese Academy of Sciences, Beijing, China

[2] Nansen Environmental and Remote Sensing Center/Bjerknes Centre for Climate Research, Bergen, Norway

Keywords: ARCTIC SEA ICE, EXTRA-TROPICAL OCEAN WARMING, TELECONNECTION

INTRODUCTION

Sea ice covers most of the Arctic Ocean in winter and is a sensitive indicator of climate change. Observations have indicated that the Arctic ice cover has declined over the satellite era. Early studies have suggested that changes in atmospheric circulation, oceanic heat transport from the Atlantic or Pacific Oceans, local radiative processes, and ice transport through the Fram Strait can lead to inter-annual changes in ASIC. As ASIC can be partly driven by poleward heat and moisture transport from lower latitudes, we speculate that the enhanced warming in extra-tropical oceans may also contribute to the Arctic warming and sea ice reduction.

METHODS

We have used the ERA-Interim data from 1979 to 2014; the National Centers for Environmental Prediction reanalysis, version 1 (NCEP1) from 1948 to 2014; the National Oceanic and Atmospheric Administration (NOAA) SST data from 1854 to 2014; and the Met Office Hadley Centre Sea Ice and SST dataset, version 1 (HadISST1) from 1870 to 2014. We have also used the National Center for Atmospheric Research Community Atmospheric Model, version 3 (CAM3) with dedicated sensitivity experiments to verify our observation-based analysis.

CONCLUSIONS

This study reveals a close connection (R=0.5) between the extra-tropical sea surface temperature (ET-SST) and winter ASIC from 1994 to 2013. This relationship might be maintained because of the impact of warming extra-tropical oceans on the polar vortex. Positive SST anomalies in the mid-latitudes of the North Pacific and Atlantic (around 40ºN) strengthen the equatorward planetary wave propagation, whereas negative SST anomalies in the high latitudes weaken the upward planetary wave propagation from the lower troposphere to the stratosphere. The former indicates a strengthening of the poleward meridional eddy momentum flux, and the latter implies a weakening of the poleward eddy heat flux, which favors an intensified upper-level polar night jet and a colder polar vortex, implying a stronger-than-normal polar vortex. Consequently, an anomalous cyclone emerges over the eastern Arctic, limiting or encouraging the ASIC by modulating the mean meridional heat flux. A possible reason for the long-term changes in the relationship between the ET-SST and ASIC is also discussed.

ACKNOWLEDGEMENTS

This research was supported by the National Natural Science Foundation of China (Grants 41210007 and 41130103) and the Special Fund for Public Welfare Industry (meteorology) (GYHY201306026). The third

author is also supported by the European Union 7th Framework Programme (FP7 2007–2013) through the NACLIM project (308299).

REFERENCES

Li, F., Wang, H.J., Gao, Y.Q. (2015): Extra-tropcial Ocean Warming and Winter Arctic Sea Ice Cover since the 1990s. Journal of Climate, 28, 5510-5522, doi: 10.1175/JCLI-D-14-00629.1

SOIL EROSION ANALYSIS IN RED SOIL HILLY REGION BY USING HJ-CCD：A CASE IN GANZHOU

LI HENGKAI, YANG LIU, LEI JUN

Faculty of Architectural and Surveying Engineering, Jiangxi University of Science and Technology, Ganzhou 341000, China

Keywords: SOIL EROSION; RUSLE EQUATION;HJ-CCD; RED SOIL ;HILLY REGION

The southern red soil hilly region is one of the most serious soil erosion areas in our country, the special technical standards (SL657-2014) for comprehensive control of soil and water loss has been implemented in 2014 by ministry of water resources. For accurate evaluating soil erosion status and analyzing space-time evolution law in red soil hilly region, the paper quantitatively analyzed soil erosion condition and spatial distribution of Ganzhou in 2008 and 2013 under the guidance of new technical standards by using RUSLE model. Compared with 2008, the area of soil erosion condition improved a certain extent, the total erosion reduced to 5867.589t from 5225.733t. Slope in 15-30 ° is a major area of moderate or more of erosion, the maximum of soil erosion was appeared in 250-350 m elevation, 150-550 m is main elevation area of soil erosion occurred. The ecological environment is still fragile from southwest to the northeast of Ganzhou,Xingguo is a improve intensified trend of soil erosion, 3 county including Shangyou, Chongyi and Huichang is an intensified trend of soil erosion.

FIELD-SCALE SIMULATION OF METHANE EMISSIONS FROM COASTAL WETLANDS IN CHINA USING AN IMPROVED VERSION OF CH4MOD$_{WETLAND}$

TINGTING LI[A*], BAOHUA XIE[B*], GUOCHENG WANG[A], WEN ZHANG[A], QING ZHANG[A], TIMO VESALA[C,D]

[a] LAPC, Institute of Atmospheric Physics, Chinese Academy of Sciences, Beijing, 100029, China

[b]Key Laboratory of Coastal Environmental Processes and Ecological Remediation, Yantai Institute of Coastal Zone Research (YIC), Chinese Academy of Sciences (CAS); Shandong Provincial Key Laboratory of Coastal Environmental Processes, YICCAS, Yantai Shandong 264003, P. R. China

[c] Department of Physics, P.O. Box 48, FI-00014 University of Helsinki, Finland

[d] Department of Forest Sciences, P.O. Box 27, FI-00014 University of Helsinki, Finland

Keywords: CH_4 EMISSIONS, SALINITY, COASTAL WETLANDS, CH4MOD$_{WETLAND}$ MODEL, CHINA

Coastal wetlands are important CH_4 sources to the atmosphere. Coastal wetlands account for ~10% of the total area of natural wetlands in China, but the size of this potential CH_4 source remains highly uncertain. We introduced the influence of salinity on CH_4 production and CH_4 diffusion into a biogeophysical model named CH4MOD$_{wetland}$ so that it can be used in coastal wetlands. The improved model can generally simulate seasonal CH_4 variations from tidal marshes dominated by *Phragmites* and *Scirpus*. However, the model underestimated winter CH_4 fluxes from tidal marshes in the Yellow River Delta and YanCheng Estuary. It also failed to capture the accurate timing of the CH_4 peaks in YanCheng Estuary and ChongMing Island in 2012. The improved model could generally simulate the difference between the annual mean CH_4 fluxes from mangrove sites in GuangZhou and HaiKou city under different salinity and water table depth conditions, although fluxes were systematically underestimated in the mangrove site of HaiKou city. Using the improved model, the seasonal CH_4 emissions simulated across all of the coastal wetlands ranged from 0.1 to 44.90 g m^{-2}, with an average value of 7.89 g m^{-2}, which is in good agreement with the observed values. The improved model significantly decreased the *RMSE* and *RMD* from 424% to 14% and 314% to -2%, respectively, and improved the *EF* from -18.30 to 0.99. Model sensitivity analysis showed that CH_4 emissions were most sensitive to P_{ox} in the tidal marshes and salinity in the mangroves. The results show that previous studies may have overestimated CH_4 emissions on a regional or global scale by neglecting the influence of salinity. In general, the CH4MOD$_{wetland}$ model can simulate seasonal CH_4 emissions from different types of coastal wetlands under various conditions. Further improvements of CH4MOD$_{wetland}$ should include the specific characteristics of CH_4 processes in mangroves to decrease the uncertainty in estimating regional or global CH_4 emissions from natural wetlands.

SPATIAL AND TEMPORAL DISTRIBUTION OF DISSOLVED OXYGEN UNDER ICE IN LAKE VALKEA-KOTINEN, FINLAND

Z. LI[1], Y. BAI[2], H. LI[2], R. LI[1], L. ARVOLA[3] and M. LEPPÄRANTA[4]

[1] State Key Laboratory of Coastal and Offshore Engineering, Dalian University of Technology, China.

[2] College of Mathematics and Physics, Bohai University, Jinzhou, China.

[3] Lammi Biological Station, University of Helsinki, Lammi, Finland.

[4] Department of Physics, University of Helsinki, Finland.

Keywords: DISSOLVED OXYGEN, ICE-COVERED LAKE, DATA ANALYSIS.

INTRODUCTION

Based on the dissolved oxygen (DO) measurements under ice in a small Finnish lake (Valkea-Kotinen) during the winter 2010-2011, the vertical distribution patterns of DO were examined and a mathematical function was fitted to describe the DO profiles. The function parameter may depend of time in ice period. The smooth curved shape of the DO concentration with depth and time was obtained. In comparison with the result of the wavelet analysis, this surface describes the evaluation of the DO concentrations more consistently with the measured DO results. This work will be extended in future to numerical simulations and applications for under ice conditions in Chinese water bodies.

MEASUREMENT SITE AND DATA

Lake Valkea-Kotinen is located in southern Finland at 61°14´N, 25°03´E, with a mean depth of about 300 cm (Fig.1). It is a seasonally freezing boreal lake. During 1990–2011, the average freezing date was November 15. The average length of the ice season was 5.5 months and the ice broke up around April 30 (Jylhä *et al*., 2014). The measurement data consist of approximately 10,500 sets, which were acquired at 17-min time intervals from 12:00 on January 13, 2011 until May 17, 2011. In this winter, the lake froze over on November 8, 2010, and the ice broke up on April 26, 2011. There were three chains of sensors measuring automatically water temperature and DO concentration. The data for this presentation were taken from the middle of the lake where the depth was about 600 cm. The sensors were deployed at seven depths: 20 cm, 45 cm, 70 cm, 95 cm, 195 cm, 295 cm, and 395 cm. The zero reference level for the depth was the ice-water interface (Bai *et al*., 2016). The oxygen concentration and temperature curves from January 13, 2011 to April 25, 2011 are shown in Fig.2.

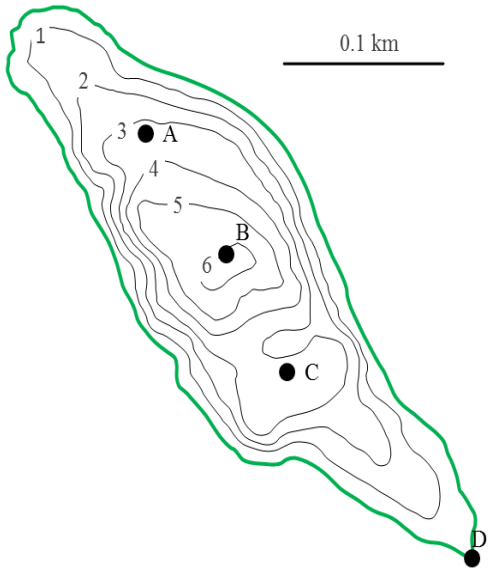

Figure 1. Shape of Lake Valkea-kotinen (A, B, C are measurement sites, and the data from Site B is used in this abstract. D is the position of outflow).

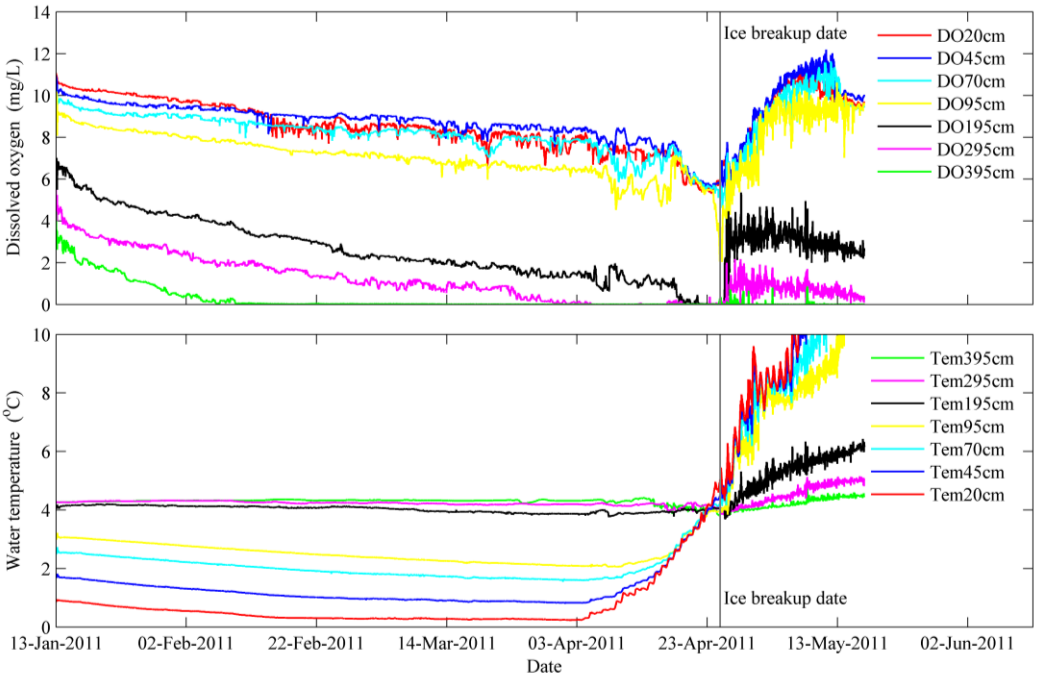

Figure 2. Water temperature and DO concentration curves at different depths (Bai *et al*., 2016).

SPATIAL AND TEMPORAL DISTRIBUTIONS OF DISSOLVED OXYGEN UNDER ICE

The DO concentration was decreasing with depth and time. In January DO concentration decreased beneath the ice almost steadily down to 300 cm depth, while in March the DO concentration was lower just below the ice cover than at 50 cm deeper. Deeper, i.e. below 100 cm, the DO concentrations declined more rapidly than near the surface. As a result the vertical patterns of DO changed and eventually the water layers below 300 cm became anoxic (Fig. 3). Similar phenomena occurred in a marine-culture pond, Liaoning, China and were explained by Li *et al*. (2014). With time increasing, the DO concentration decreased. Its peak value became lower and lower, the depth of the peak depth was more far from ice bottom, and the depth of oxygen-poor water became more and more shallow (see Fig. 3).

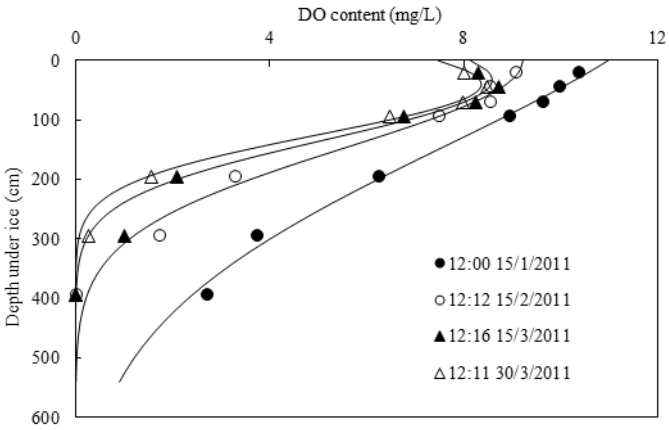

Figure 3. The vertical distributions of DO at different dates.

Based on the characteristics of the vertical DO distribution, an equation similar to Gaussian type function is used to describe the curve and MATLAB is used to fit the curve from measurement data:

$$DO(h) = a(t) \cdot \exp\left(-\left(h - b(t)\right)^2 / 2c(t)^2\right) \tag{1}$$

where $DO(h)$ is DO concentration at a depth h (cm) under ice (mg/L); and $a(t)$, $b(t)$, $c(t)$ are the fit parameters. In this expression, $a(t)$ denotes the maximum DO concentration at the peak point in the curve, and it decreases with increasing time in ice period; $b(t)$ is the depth of the DO peak point, and it increases along with the time in ice period, and this means that this depth moves down along with the time in ice period, $c(t)$ is the half-width at the maximum DO concentration, which decreases along with increasing time in ice period.

Using Eq (1), the vertical distribution of DO as a function of time can be obtained. Concerning the characteristics of the vertical distribution, the three parameters (a, b, c) can be utilized. The function tells that 1) the ice season is much shorter than the open water season, 2) the DO concentration is highest at the ice-on date and lowest at the ice-out date, and 3) the DO concentration is similar at ice-on date in each winter. To be a proper fit, an equation must be selected with two inflection points, the peak value and the lowest value. Between the peak value and lowest value is the parameter value. For any a (t), $b(t)$ and $c(t)$, the equation form is the same (see Eq.2):

$$Y(t) = a + b\ln(t)^2 + ct^{0.5} \tag{2}$$

where $Y(t)$ denotes the $a(t)$, $b(t)$, $c(t)$; t is a date from lake frozen over day (November 8, 2010) (d); a, b, c are the fit parameters.

Using the fitted parameters at noon from January 14, 2011 to April 3, 2011, an example of $a(t)$ is shown in Fig. 4. The whole data were not used because the daily variation is not considered in this plot. The parameters are summarized in Table 1.

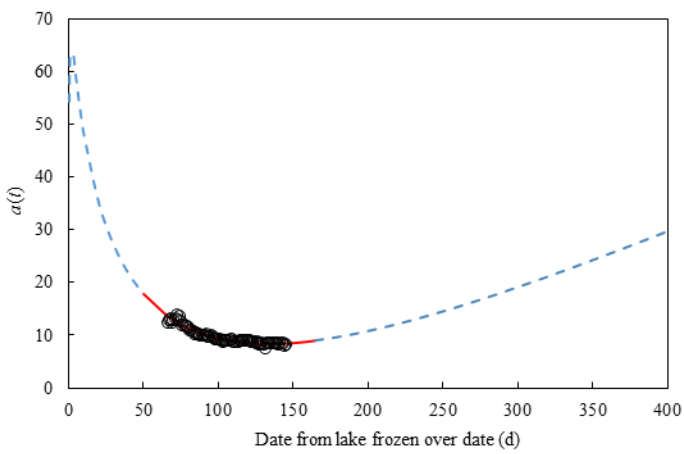

Figure 4. The $a(t)$ curve from Eq (2).

Table 1. The fitted parameters of *a*, *b*, *c* at noon from January 14, 2011 to April 3, 2011.

	a	*b*	*C*
a(*t*)	47.8428	-9.0412	15.3242
b(*t*)	-1873.9032	469.6498	-808.0878
c(*t*)	1665.5196	-345.4060	579.6184

Using Eqs (1) and (2), the vertical and temporal distributions of DO under ice can be obtained. As an example, the DO distribution at noon from January 14, 2011 to April 3, 2011 was analyzed using Eqs (1) and (2), and the result is shown in Fig. 5. In the future research, also the daily water temperature and DO variations should be considered especially shortly before the ice-out. Due to the northern location, solar radiation is rapidly increasing in the lake during the spring months, in particular in April due to snow melt. As Kirillin *et al*. (2012) have suggested also numerical simulations are needed for more complete understanding of the physical and chemical processes under ice, and thus we hope that our new equations (Eqs 1 and 2) can be applied in modelling. Mostly it is useful for determine the coefficients in the mathematical equations. In comparison with the wavelet method (Li *et al*., 2015), 24-hour moving average and Gaussian fitting time series (Bai *et al*., 2016), Eqs (1 and 2) gave a rather similar DO evaluation (Fig.6). However, the DO concentration was decreasing faster according to the wavelet analysis, 24-hour moving average and Gaussian fitting time series, and the DO jump occurred slightly deeper as well.

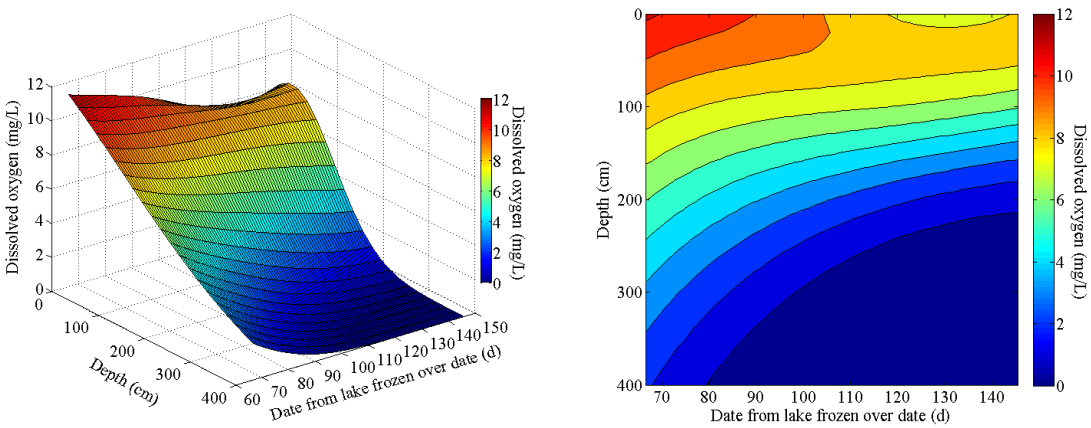

(a) curved surface (b) evaluation isolines

Figure 5. Curved surface (a) and evaluation isolines (b) of DO concentration from Eqs (1) and (2).

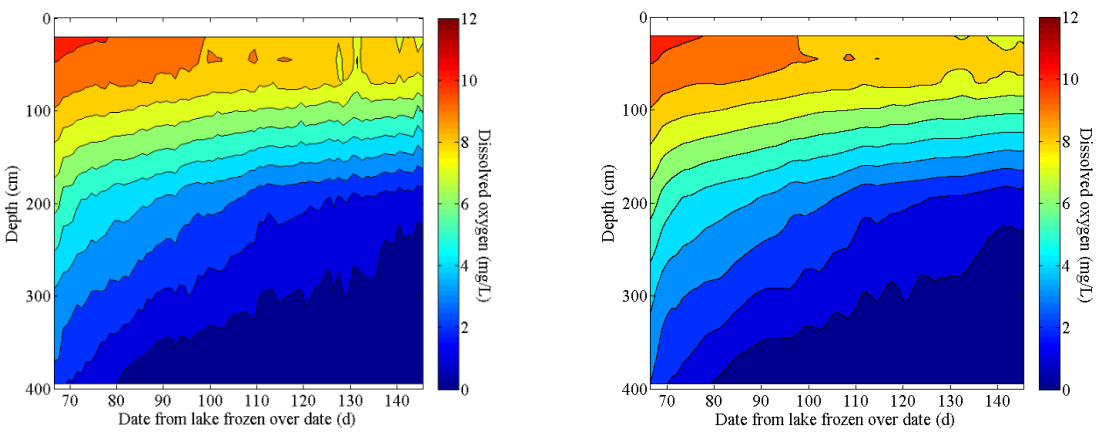

(a) result from measurement data (b) result from wavelet (Li *et al*., 2015)

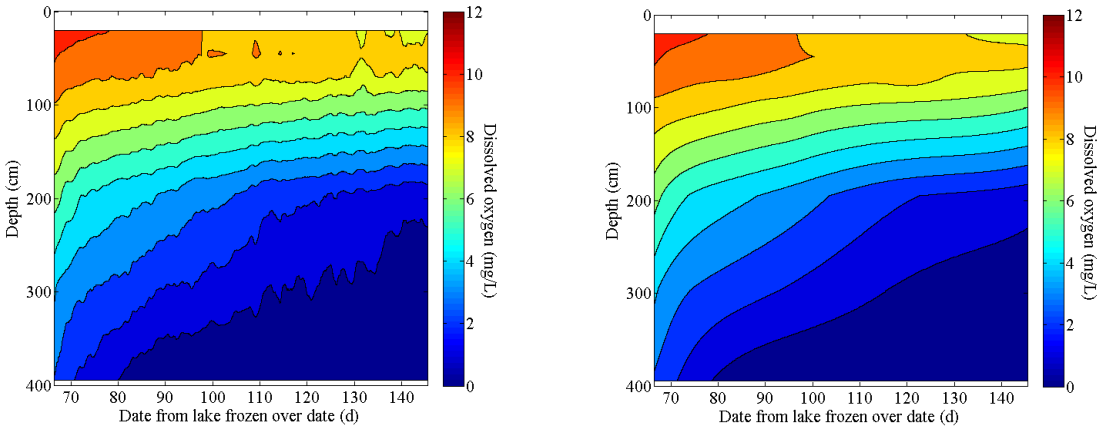

(c) result from 24-hour moving average (data from Bai *et al*., 2016)

(d) result from Gaussian fitting time series (data from Bai *et al*., 2016)

Figure 6. Measurement and evaluation of DO concentration isolines.

CONCLUSIONS AND DISCUSSIONS

The results based on Eqs (1) and (2) fit much better with the measured DO concentrations than those based on the wavelet analysis. However, still there are some gaps, which future research has to consider. These include 1) the daily variation of DO at the time of snow and ice-melt, 2) numerical simulations to perform process based understanding on the evaluation of water temperature and dissolved oxygen concentration under ice, 3) the accuracy analysis of our method based on data sets of several lakes, and 4) the application of the present method for the DO evaluation in several Chinese water bodies, e.g., Ulansuhai Lake, Inner Mongolia, and marine-culture ponds, Liaoning, 5) the ice thickness is suggested to instead of time from lake frozen over date after the ice thickness is also measured in future.

ACKNOWLEDGEMENTS

This work was supported continuously by the exchange projects between National Natural Science Foundation of China (NSFC) and Academy of Finland (AF) under the NSFC projects (Nos. 51579028, 41376186, 51221961), and the foundation of State Key Laboratory of Coastal and Offshore Engineering, Dalian University of Technology, China (No. SL14-5-3).

REFERENCES

Bai, Q., R. Li, Z. Li, M. Leppäranta, L. Arvola, and M. Li (2016). Time-series analyses of water temperature and dissolved oxygen concentration in Lake Valkea-Kotinen (Finland) during ice season, *Ecologic Informatics*, doi: 10.1016/j.ecoinf.2015.06.009.

Jylhä, K., P. Pirinen, M. Laapas, K. Ruosteenoja, L. Arvola, A. Drebs, K. Juha, S. Saku, H. Gregow and H. Hannula (2014). Climate variability and trends in the Valkea-Kotinen region, southern Finland: comparisons between the past, current and projected climates, *Boreal Environment Research*, **19** (suppl. A), 4-30.

Kirillin, G., M. Leppäranta, A. Terzhevik, N. Granin, J. Bernhardt, C. Engelhardt, T. Efremova, S. Golosov, N. Palshin, P. Sherstyankin, G. Zdorovennova and R. Zdorovennov (2012). Physics of seasonally ice-covered lakes: a review, *Aquatic Sciences*, **74** (4), 659-682.

Li, M., R. Li, Q. Bai and Z. Li (2015). Discrete wavelet analysis of dissolved oxygen concentration variation under ice in a Finnish freshwater lake, *Mathematics in Practice and Theory*, **45** (7): 149-155.

Li, R., P. Lu, J. Ding and Y. Chang (2014). Observations of ice and water under ice in aquaculture zone in the Liaodong Gulf of the Bohai Sea, China, in Proceedings of the 22nd IAHR International Symposium on Ice, Singapore, 916-923, doi:10.3850/978-981-09-0750-1-1216.

REMOTE SENSING OF AEROSOL OPTICAL, MICROPHYSICAL AND CHEMICAL PROPERTIES BASED ON SUN-SKY RADIOMETER MEASUREMENTS OVER POLLUTED CITIES

Z.Q. LI[1], Y.S. XIE[1] and L. LI[1,2]

[1]State Key Laboratory of Remote Sensing Science and State Environmental Protection Key Laboratory of Satellite Remote Sensing, Beijing, China

[2]University of Chinese Academy of Sciences, Beijing, China

Keywords: AEROSOL OPTICAL AND MICROPHYSICAL PROPERTIES, AEROSOL COMPOSITION, BEIJING, KANPUR.

INTRODUCTION

Aerosol optical and physical properties have significant variations globally due to their short residence times, complexity in composition, and particulate size resulting from different sources and different atmospheric physical and chemical processes. There is a great need of better assessments of the aerosol impacts caused by megacities where anthropogenic activities of large population could probably create a complex mixture of primary and secondary particles. The issue is even more important in rapidly developing countries like China and India where particle emissions likely affect the regional climate and environment. Beijing, China, and Kanpur, India, are located in Asian monsoon regions with aerosol mixtures composed of coarse and fine particles, both of which have complex aerosol composition and thus the properties difficult to describe. In order to understand the seasonal variations of aerosol optical and physical properties affecting the assessment of the radiative impact of aerosol and to identify the major sources influencing Beijing and Kanpur, information on the composition is highly essential. Hence, this paper focuses on AERONET measurements collected at these two locations from 2002 to 2013 which allow for a statistically meaningful analysis of aerosol optical and physical properties together with aerosol columnar composition information.

METHODS

Dubovik and King (2000) and Dubovik et al. (2006) proposed an inversion strategy of aerosol optical and microphysical properties. A homogeneous mixture of aerosol and gas particles is assumed for the retrieval, and the aerosol properties are adjusted until a forward radiation model matches the measurements (both AOD and sky radiances) in a “best fit” sense (Dubovik et al., 2000). The volume particle size distribution dV/dlnr ($\mu m^3/\mu m^2$) is retrieved in the range of particle sizes (0.05 μm≤ radius ≤ 15 μm). Bimodal distributions tend to suggest more than one type of aerosol, and the total volume of the coarse and fine modes can indicate the dominant aerosol in the region (Dubovik et al., 2002). However, the aerosol size distribution could hardly give certain information on aerosol composition since pollution and biomass particles can yield similar size distributions due to their close particulate size. The single-scattering albedo (SSA) describes the scattering percentage of total extinction, which is useful to identify particle absorption and thus composition, especially for carbonaceous particles (Corrigan et al., 2006). The real part of refractive index represents refraction of particle matter, and the imaginary part of refractive index represents particle absorption, as a higher imaginary part indicates stronger absorption. The real and imaginary parts of the complex refractive index retrieved for the wavelengths corresponding to sky radiance measurements are assumed in the ranges of 1.33–1.6 and 0.0005–0.5, respectively. An accuracy assessment of the aerosol properties (including size distribution, refractive index and SSA) can be found in the work of Dubovik et al. (2000, 2006). The quality assured AERONET Level 2.0 data is employed in this study.

We utilize a five-component aerosol mixture model proposed by Li et al. (2013), including Black Carbon (BC), Brown Carbon (BrC), Mineral Dust (DU), Ammonium Sulfate (AS), and Aerosol Water (AW)), to describe the aerosol composition of Beijing and Kanpur. This model was developed on the basis of the three-component model of Schuster et al. (2005) and four-component model of Arola et al. (2011). We assume that sea salt can be generally neglected in Beijing and Kanpur due to far distance to the ocean, and the AS can be used as a proxy for non-absorbing dry components (Schuster et al., 2005; Dey et al., 2006; Arola et al., 2011). Moreover, compared to other previous studies, this model has advantages on identifying and separating the three absorbing components (BC, BrC and DU) by employing a useful information on SSA (Wang et al., 2013). This is important for the composition retrieval in regions with abundant carbonaceous particle emission, especially during spring, pre-monsoon, and monsoon seasons in the study areas.

The five-component model utilizes real refractive index, spectral imaginary refractive index as well as the spectral SSA. In the retrieval, refractive indices of five components, mass absorption efficiency (MAE) of the three absorbing components, and density of each component are set according to related literatures as listed in Table 1. We assume an internal mixture of all components and employ the volume average mixing rule to calculate aerosol refractive index and SSA for each volume fraction combination through the parameters. Then we calculate the residuals between the aerosol physical and optical properties (aerosol refractive index and SSA) generated by parameters of each combination and those retrieved from AERONET Sun-sky radiometer data. Finally, we choose the best component combination fitting the parameters and output the fractions of BC, BrC, DU, AS, and AW components correspondingly. The algorithm on the aerosol composition retrieval are presented in detail in the work of Wang et al. (2013) and Li et al. (2013).

	n	k			MAE		Density
Components	440–1020 nm	440 nm	670 nm	870-1020 nm	670 nm	870 nm	g/cm^3
BC	1.95	0.66	0.66	0.66	8.14	6.32	2.0
BrC	1.57	0.01	0.004	0.001	0.045	0.035	2.6
DU	1.53	0.063	0.005	0.001	0.067	0.05	1.8
AS	1.53	10^{-7}	10^{-7}	10^{-7}	0	0	1.76
AW	1.53	0	0	0	0	0	1.0

Table 1. Aerosol components and parameters used in this study (Li et al., 2013).

RESULTS

The seasonal average of aerosol volume size distributions over Beijing and Kanpur exhibit a typical bimodal lognormal structure with a fine mode (peak at 0.17 μm in Beijing and 0.18 μm in Kanpur) and coarse mode (peak at 2.75 μm in Beijing and 2.64 μm in Kanpur), as shown in Figure 1. The variations of size distribution among seasons are significant in Beijing. Coarse particles originated from the Kumutage and Taklamakan deserts in western China and Mongolian deserts in north of Beijing (Sun et al., 2001), are dominant during spring months. Fine particles that come from combustion of fossil fuel and vehicle exhaust emissions are prevalent in summer. The volume concentration of fine mode (0.13 $\mu m^3/\mu m^2$) is larger than that of coarse mode (0.11 $\mu m^3/\mu m^2$) in Beijing. Meanwhile, the median radius of fine mode and coarse mode are 0.16 μm and 2.59 μm during spring, and 0.21 μm and 2.87 μm during summer in Beijing, respectively. It can also be seen in Figure 1 that the coarse modes in Beijing are comparable with fine modes even during the heating period (winter and late autumn). In Kanpur, the median radius of fine mode has a significant increase resulting from the growth of hygroscopic particles from pre-monsoon to monsoon, while the median radius of coarse mode has a slight decrease (r_f = 0.14 μm, r_c = 2.58 μm during pre-monsoon months and r_f = 0.19 μm, r_c = 2.47 μm during monsoon). Note that the total particle size distributions have no significant discrepancy between Beijing and Kanpur from September to February as the fine mode volume is slightly lower than the coarse mode for both sites.

Refractive indices are important parameters of aerosol particles and key indicators of aerosol component composition. The real refractive index is found to be wavelength dependent over Beijing and Kanpur, which was also validated by other studies (Wang et al., 2013; Xie et al., 2015). As shown in Figure 2, for Beijing, the multiyear average real refractive index value has a slight increase from 440 nm to 1020 nm. During the year, the real refractive index value is the highest in spring, lower in winter and autumn, and the lowest in summer because of the abundant precipitation during summer months. The values have slight increases at 440–1020 nm in spring, autumn, and winter; however, the values remain stable at 440–1020 nm (about 1.46) in summer. While for Kanpur, the multiyear average of real refractive index increases gradually from 1.48 at 440 nm to 1.51 at 670 nm and then remains approximately constant at 670–1020 nm (about 1.51), similar to Beijing. During the year, the real refractive index value is the highest in pre-monsoon season as well and apparently higher than the values in the other three seasons. The imaginary part of the refractive index is found to be wavelength dependent over Beijing and Kanpur, as shown in Figure 2. For Beijing, the multiyear average of imaginary refractive index decreases from 0.014 at 440 nm to 0.009 at 670 nm and remains stable (about 0.009) at 670–1020 nm. The imaginary refractive index decreases significantly at 440–670 nm during spring, autumn, and winter; however, the value remains almost constant at 440–1020 nm during summer. For Kanpur, the multiyear average imaginary refractive index value decreases gradually from 0.012 at 440 nm to 0.008 at 1020 nm. The values have spectral decrease at 440–1020 nm during pre-monsoon, post-monsoon, and winter; however, it remains nearly stable during-monsoon, which is similar to Beijing.

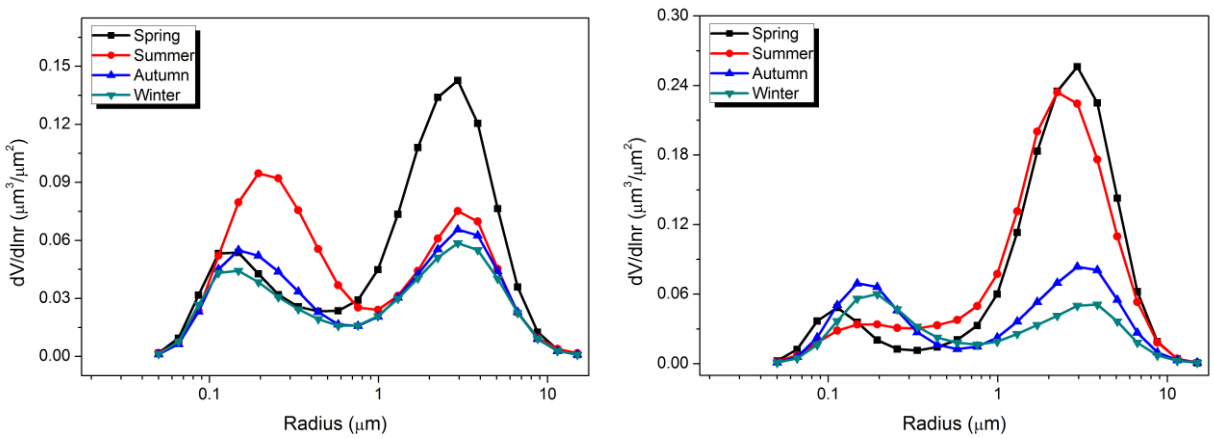

Figure 1. Seasonal average of aerosol volume size distribution of Beijing (left) and Kanpur (right) from 2002 to 2013.

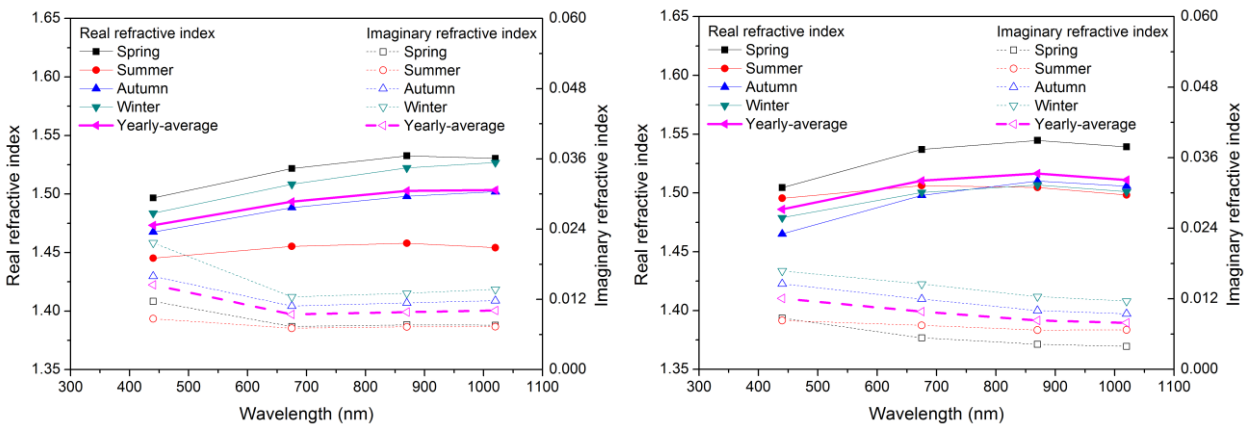

Figure 2. Seasonal and yearly average of aerosol refractive index (real part and imaginary part) of Beijing (left) and Kanpur (right) from 2002 to 2013.

The mass concentrations of aerosol components over Beijing and Kanpur show some seasonal variations, as shown in Figure 3. The multiyear average mass concentration of BC is higher in Beijing than that in Kanpur for all seasons. The BC concentration during winter and post-monsoon are larger than those during other seasons at both sites, which can be probably attributed to the combustion emission of fossil fuels and biomass burning. The multiyear average mass concentration of BrC in Beijing has a larger seasonal variance than that in Kanpur. In particular, BrC in Beijing in winter is about 4 times the BrC concentration in Kanpur, possibly due to abundant coal consumption for heating during late autumn to winter period in Beijing. BrC during pre-monsoon and post-monsoon seasons are higher than monsoon and winter months in Kanpur. The mass concentration of DU is obviously higher in spring than in other seasons at the two sites, and it is noted that the mass concentration of DU has a distinct discrepancy between Beijing and Kanpur during summer/monsoon. The mass concentration of AS during monsoon (967.11mg/m^2) and pre-monsoon (868.05 mg/m^2) in Kanpur is significantly higher than those in other seasons (256.55 mg/m^2 during winter and 342.71 mg/m^2 during post-monsoon). We also note that AS can be about 3 times higher in Kanpur during monsoon than Beijing during summer, which may be related to gas-to-particle conversion depending on temperature and humidity. The aerosol water content at both sites during summer months is clearly higher, because AW concentration is affected by wet monsoon. These seasonal variations of BC and BrC are comparable with that of BC and particulate organic matter (POM) in situ measurements in Beijing (Zhang et al., 2013). The trends of retrieved DU and AS are also consistent with in situ measurements (Zhang et al., 2013) during different seasons. For example, DU is highest in spring and lowest in summer, and AS is highest in summer and lowest in winter.

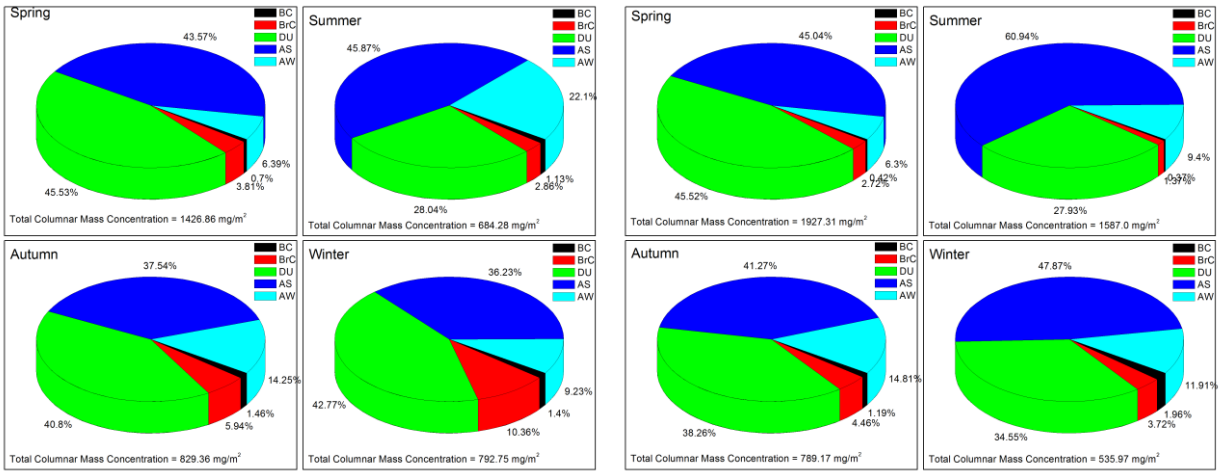

Figure 3. Seasonal average of aerosol mass concentration of components over Beijing (left) and Kanpur (right) from 2002 to 2013.

CONCLUSIONS

This paper presents seasonal variations of the aerosol optical and physical properties over Beijing, China and Kanpur, India, and focuses on jointly retrieved aerosol compositions for these two typical sites. The main conclusions drawn from this study are summarized as follows:

1. The aerosol size distribution exhibits distinct seasonal characteristics at both sites. Coarse particles are prevalent in aerosol from March to May at both sites. However, the fraction of coarse mode in Kanpur is higher than that in Beijing. Fine particles are prevalent from June to August, and particle radius in Beijing during this period has an obvious increase compared with other seasons. In contrast, coarse particles are still prevalent from June to August for Kanpur.

2. The seasonal trends of refractive indices are similar between Beijing and Kanpur. For example, the real part values are the highest during spring/pre-monsoon. However, the variability of real part values during

different seasons is more significant in Beijing than that in Kanpur. The imaginary part values are higher in Beijing than those in Kanpur due to the absorbing aerosol components.

3. The BC concentration during winter and post-monsoon months are larger than that during other seasons at both sites. BrC during winter and late autumn are much higher than other months, which is attributed to abundant coal consumption for heating. The mass concentration of DU is higher in spring than other seasons at Beijing and Kanpur, with large difference between the two sites. The AS content during monsoon and pre-monsoon in Kanpur is higher than those in other seasons, with AS in Kanpur during monsoon about 3 times higher than Beijing during summer. The aerosol water content at both sites during summer is higher than other seasons because AW concentration is affected by wet monsoon.

ACKNOWLEDGEMENTS

This work was supported by the National Natural Science Foundation of China (41222007, 41501395).

REFERENCES

Arola, A., G. Schuster, G. Myhre, S. Kazadzis, S. Dey, and S. N. Tripathi (2011). Inferring absorbing organic carbon content from AERONET data, *Atmos. Chem. Phys.* **11**, 215–225.

Corrigan, C. E., V. Ramanathan, and J. J. Schauer (2006). Impact pact of monsoon transitions on the physical and optical properties of aerosols, *J. Geophys. Res.* **111**, D18208.

Dey, S., S. N. Tripathi, R. P. Singh, and B. N. Holben (2006). Retrieval of black carbon and specific absorption over Kanpur city, northern India during 2001–2003 using AERONET data, *Atmos. Environ.* **40**, 445–456.

Dubovik, O., and M. D. King (2000). A flexible inversion algorithm for retrieval of aerosol optical properties from Sun and sky radiance measurements, *J. Geophys. Res.* **105(D16)**, 20,673–20,696.

Dubovik, O., A. Smirnov, B. Holben, M. D. King, Y. J. Kaufman, T. F. Eck, and I. Slutsker (2000). Accuracy assessments of aerosol optical properties retrieved from Aerosol Robotic Network (AERONET) Sun and sky radiance measurements, *J. Geophys. Res.* **105(D8)**, 9791–9806.

Dubovik, O., B. Holben, T. F. Eck, A. Smirnov, Y. J. Kaufman, M. D. King, D. Tanré, and I. Slutsker (2002). Variability of absorption and optical properties of key aerosol types observed in worldwide location, *J. Atmos. Sci.* **59**, 590–608.

Dubovik, O., A. Sinyuk, and T. Lapyonok (2006). Application of spheroid models to account for aerosol particle nonsphericity in remote sensing of desert dust, *J. Geophys. Res.* **111**, D11208.

Li, Z., Gu, X., Wang, L., Li, D., Xie, Y., Li, K., Dubovik, O., Schuster, G., Goloub, P., Zhang, Y., Li, L., Ma, Y., and Xu, H. (2013). Aerosol physical and chemical properties retrieved from ground-based remote sensing measurements during heavy haze days in Beijing winter, *Atmos. Chem. Phys.* **13**, 10,171–10,183.

Schuster, G. L., O. Dubovik, B. N. Holben, and E. E. Clothiaux (2005). Inferring black carbon content and specific absorption from Aerosol Robotic Network (AERONET) aerosol retrievals, *J. Geophys. Res.* **110**, D10S17.

Sun, J., M. Zhang, and T. Liu (2001). Spatial and temporal characteristics of dust storms in China, *J. Geophys. Res.* **106(D10)**, 10,325–10,333.

Wang, L., Z. Q. Li, Q. J. Tian, Y. Ma, F. X. Zhang, Y. Zhang, D. H. Li, K. T. Li, and L. Li (2013). Estimate of aerosol absorbing components of black carbon, brown carbon, and dust from ground-based remote sensing data of sun-sky radiometers, *J. Geophys. Res. Atmos.* **118**, 6534–6543.

Xie, Y., Li, Z., Li, D., Xu, H., Li, K. Aerosol optical and microphysical properties of four typical sites of SONET in China based on remote sensing measurements, *Remote Sensing* **2015(7)**, 9928-9953

Zhang R., Jing J., Tao J., Hsu S.-C., Wang G., Cao J., Lee C. S. L., Zhu L., Chen Z., and Zhao Y. (2013). Chemical characterization and source apportionment of PM2.5 in Beijing: Seasonal perspective, *Atmos. Chem. Phys.* **13**, 7050–7074.

SPATIAL AND TEMPORAL VARIABILITY IN THE NET PRIMARY PRODUCTION OF SHAANXI PROVINCE FROM 2000 TO 2014

K. LIANG, L.C. SUI and Y.Q. GUO

School of Geology Engineering and Geomatics, Chang'an University,
YanTa Road (No.126), Xi'an, Shaanxi, China, 710054

Keywords: NET PRIMARY PRODUCTION, CASA MODEL, NPP TRENDS, SPATIO-TEMPORAL PATTERNS.

INTRODUCTION

Net primary production (NPP) refers to the amount of dry organic matter produced by plants per unit time and per unit area, which is a key link in the biogeochemical cycle. NPP is an important index of ecosystem function (Melillo, 1993; Running, 2004; Crabtree, 2009) and a key element in the carbon cycle (Crabtree, 2009; Piao, 2011), reflecting the integrated effects of climate change and human activities on terrestrial vegetation. Research into ecosystem NPP, especially on a regional scale, has attracted much scholarly attention and much progress has been made in recent years (Cramer, 1999; Del, 2008). However, at present the spatial pattern of NPP change and the direction of change with time remains an understudied topic.

This study use the CASA model to accurately reflect the spatial and temporal variability in the NPP of Shaanxi province based on the GIMMS AVHRR NDVI data (8 km spatial resolution) for 2000-2014 and monthly meteorological data(monthly precipitation, monthly mean temperature and monthly solar radiation). The NPP value from 2000 to 2014 was used by linear trend estimation method to do some statistical analyses and calculate the rate of NPP change. This study is of great significance in ascertaining the health of vegetation ecosystem in Shaanxi province, and, by extension, the condition of the territorial ecological security protection. The results could provide a scientific basis for sustainable utilization and ecological reconstruction of this area, and related policy-making activities.

METHODS

(1) The CASA model. The CASA model (Potter, 1993) was adopted to calculate NPP in this article. The NPP estimation theory of the CASA model is determined by two variables of the absorbed photo synthetically active radiation (APAR) and light utilization efficiency (ε).

$$\mathrm{NPP}(x,t) = \mathrm{APAR}(x,t) * \varepsilon(x,t) \qquad (1)$$

where NPP is the amount of dry organic matter on the grid cell x in time t; APAR is the fraction of photo synthetically active radiation intercepted by green vegetation on grid cell x in time t; and ε is the light utilization efficiency on the grid cell x in time t.

To allow for the effects of temperature and water stress on ε, we calculate it as:

$$\varepsilon(x, t) = \varepsilon_{max} * T(x, t) * W(x, t) \qquad (2)$$

where ε_{max} is the maximum possible efficiency; T account for effects of temperature stress on grid cell x in time t and W account for effects of water stress on grid cell x in time t.

The parameter calculation method the CASA model uses refers to Piao (2006), Gao (2007), Potter (1993) and Potter (2004), with the monthly maximum possible efficiency of Shaanxi province grassland ε_{max} set as 0.542 $gC \cdot MJ^{-1}$,evergreen coniferous forest ε_{max} set as 0.389 $gC \cdot MJ^{-1}$, evergreen broad-leaved forest ε_{max} set as 0.985 $gC \cdot MJ^{-1}$, shrub ε_{max} set as 0.429 $gC \cdot MJ^{-1}$, river basin ε_{max} set as 0.542 $gC \cdot MJ^{-1}$, swamp ε_{max} set as 0.542 $gC \cdot MJ^{-1}$ and farmland ε_{max} set as 0.542 $gC \cdot MJ^{-1}$, based on Zhou (2008).

(2) The NPP calculation. The NPP calculation was carried out as follows: (a) for the NDVI data, we converted the half month MVC data from the GIMMS AVHRR NDVI 2001-1014 Shaanxi province dataset to GRID data files, and extracted monthly maximum NDVI data using ENVI to reduce the cloud

impact. We then adopted the method of Sellers (1996) to calculate the monthly FPAR (fraction of PAR absorted by the green vegetation canopy); for meteorological data, we used the spatial interpolation method for monthly meteorological data(monthly precipitation, monthly mean temperature and monthly solar radiation) to obtain grid maps of meteorlogical elements using ANUSOLIN; we set the coordinate system of all spatial data as WGS84 and set the spatial resolution of all spatial data resampling as 1km. (b) The CASA model program is compiled using MTLAB language with Arcgis 10.1 to simulate the monthly NPP of the Shaanxi province. (c) Using the ArcGIS Spatial Analyst module, we quantitatively analyzed the patterns and spatio-temporal characteristics of NPP in the Shaanxi province.

(3) Spatial distribution of terrestrial NPP in Shaanxi Province.

According to statistics, annual total NPP in Shaanxi province changed in the range of 1451-2067 $gC\cdot m^{-2}\cdot a^{-1}$, the mean value of annual NPP is 1880.6 $gC\cdot m^{-2}\cdot a^{-1}$, the maximum value was observed in 2010 (Figure 1), and the minimum value was observed in 2001. Overall, the annual NPP value got a slow increase in the past few years, the linear slope of the trend line was 23.61. The significance level of trend equation is 0.65.

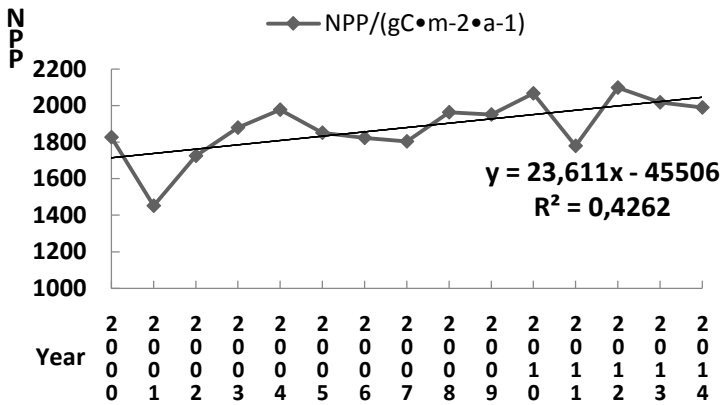

Figure 1. The trend of annual NPP in Shaanxi Province.

As is shown in the Figure 2, NPP average value had a total decreasing trend from south to north influenced by latitude and longitude, climates, topography factors. The biggest increase of NPP located in the capital of Shaanxi province, which reflected that XI'AN had a good balance in ecosystem. The lowest growth in value located in the city with the abundant coal production, such as TONGCHUAN, YANAN, YULIN. The NPP had a large increase in southern Shaanxi province, where there has the QINLING Mountains.

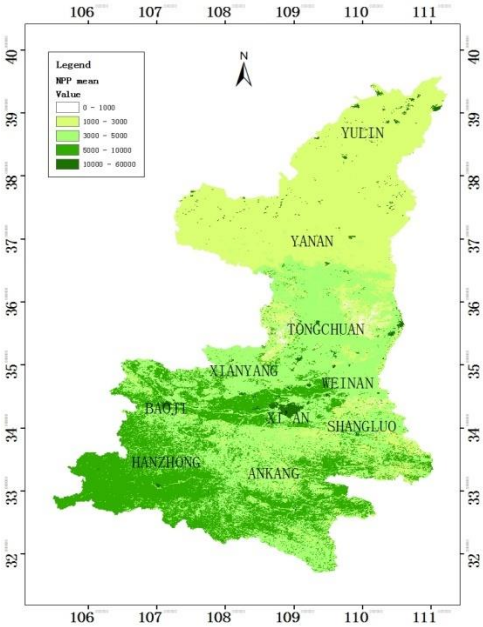

Figure 2. The spatial pattern of average NPP from 2000 to 2014.

If we respectively treat 0<NPP<3000, 3000<NPP<10000, 1000<NPP<65535 as Lower NPP, Medium NPP and High NPP (Table 1), then we can got the proportion of what they accounted for the total area of Shaanxi province. And the proportion is 39.1%, 69.5% and 1.3%, NPP>1000 ($gC \cdot m^{-2} \cdot a^{-1}$) accounted for 98%.

Table 1. The area ratio of different NPP mean value levels from 2000 to 2014, Shaanxi Province

Level	Interval	Area ratio(%)
Lower NPP	0<NPP<1000	0.7
	1000<NPP<3000	38.4
Medium NPP	3000<NPP<5000	43.6
	5000<NPP<10000	15.9
High NPP	10000<NPP<65535	1.3

(4) Annual terrestrial mean NPP variability. It is shown in Figure 3 that in the year 2014, northern Shaanxi had a huge increase; the difference value of NPP is greater than 0, and less than 0 in southern Shaanxi, which contrast to the year 2000. The area of increasing place were more than decreasing place, however, what is very worrying is the worse condition of natural ecosystem. Besides, the rate of NPP trends (Figure 4) in the past 15 years shown a more accurate variation than Figure 3. It weaken the influence of the extremely climate factors.

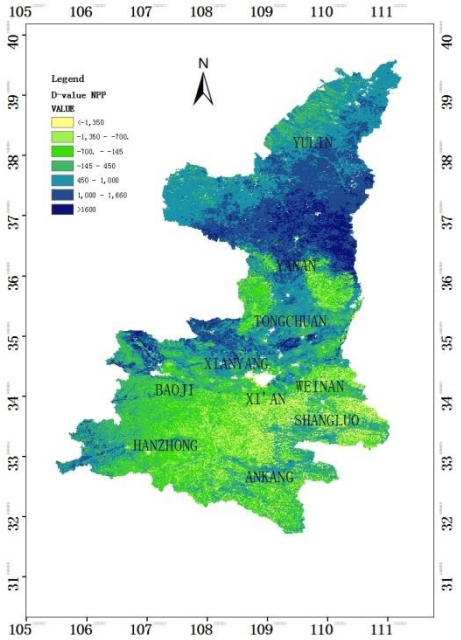

Figure 3. Difference of NPP over 15 years.

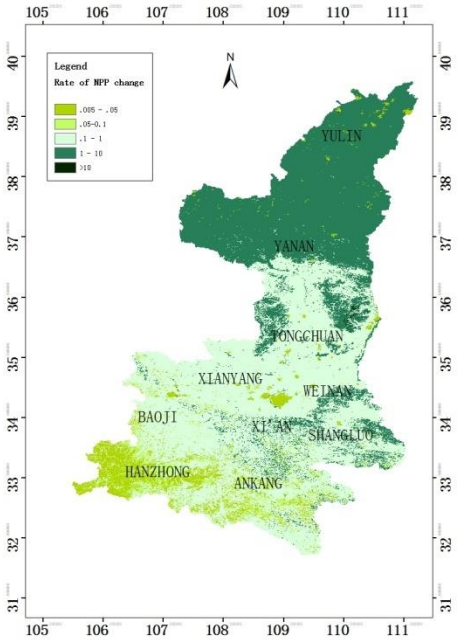

Figure 4. Rate of NPP changes in 15 years

CONCLUSIONS

In this study, we used CASA model with monthly mean values of temperature, precipitation, solar radiation and GIMMS AVHRR NDVI data simulation results, we analyzed the spatial distribution, interannual variations, and changing trend of Shaanxi Province's terrestrial carbon fluxes. We made dynamic simulations from 2000 to 2014 and an increasing trend was superimposed on the large interannual variation. Nevertheless, the model estimates of NPP had to be validated with data from field measurements. We will evaluate and validate the model estimates as the data become available.

ACKNOWLEDGEMENTS

The authors would like to thank the China Meteorological Data Sharing Service System for the monthly mean values of temperature, precipitation, solar radiation and Environmental and Ecological Science Data Centre for West China, National Natural Science Foundation of China (http://westdc.westgis.ac.cn) for the GIMMS AVHRR NDVI data. The authors were supported financially by the National Natural Science Foundation of China (No.41372330).

REFERENCES

Crabtree R, Potter C, Mullen R, *et al* (2009). A modelling and spatial-temporal analysis framework for monitoring environment change using NPP as an ecosystem indicator, *J. Remote Sensing of Envionment* **113**, 7.

Cramer W, Kicklighter D W, Bondeau A, *et al* (1999). Comparing global models of terrestrial net primary productivity (NPP): Overview and key results, *J. Global Change Biology* **5**, S1.

Del Grosso S, Parton W, Stohlgren T, *et al* (2008). Global potential net primary production predicted from vegetation class, precipitation, and temperature, *J. Ecology* **89**, 8.

Gao Q Z, Wan Y F, Li Y E, *et al* (2007a). Grassland net primary productivity and its spatio temporal distribution in Northern Tibet: A study with CASA model, *J. Chinese Journal of Applied Ecology* **18**,11.

Melillo J M, Mcguire A D, Kicklighter D W, *et al* (1993). Global climate change and terrestrial net primary production, *J. Nature* **363**, 6426.

Piao S, Ciais P, Lomas M, *et al* (2011). Contribution of climate change and rising CO2 to terrestrial carbon balance in East Asia: A multi-model analysis, *J. Global and Planetary Change* **75**.

Piao S, Fang J, He J (2006). Variations in vegetation net primary production in the Qinghai-Xizang Plateau, China, from 1982 to 1999, *J. Climate Change* **74**,1.
Potter C (2004). Predicting climate change effects on vegetation, soil thermal dynamics, and carbon cycling in ecosystems of interior Alaska, *J. Ecological Modelling* **175**,1.
Piao C S, Randerson J T, Field C B, *et al* (1993). Terrestrial ecosystem production: A process model based on global satellite and surface data, *J. Global Biogeochemical Cycles* **7**, 4.
Running S W, Nemani R R, Heinsch F A, *et al* (2004). A continuous satellite-derived measure of global terrestrial primary production, *J. Bioscience* **65**, 6.
Zhou C P, Ouyang H, Wang Q X, et al (2008). Estimation of net primary production in Tibetan Plateau, *J. Acta Geographica Sinica* **59**, 1.

QUANTIFYING SNOW ALBEDO RADIATIVE FORCING AND ITS FEEDBACK USING SATELLITE OBSERVATIONS

XIAO LIN[1, 2, 3], CHE TAO[1, 3]

[1]. Key Laboratory of Remote Sensing of Gansu Province, Cold and Arid Regions Environmental and Engineering Research Institute, Chinese Academy of Sciences, Lanzhou 730000, China

[2]. University of Chinese Academy of Sciences, Beijing 200049, China

[3]. Heihe Remote Sensing Experimental Research Station, Cold and Arid Regions Environmental and Engineering Research Institute, Chinese Academy of Sciences, Lanzhou 730000, China

Keywords: RADIATIVE FORCING, CLIMATE FEEDBACK, SNOW ALBEDO, REMOTE SENSING

INTRODUCTION

The globally averaged surface temperature has increased by 0.85 °C over the period 1880 to 2012 (IPCC, 2013), while higher latitudes seems to exhibit more warming than tropics (Screen, 2010, Serreze, 2006). This is apparently true in the North Hemisphere (Crook, 2014) and polar egions (e.g., the polar ampilication) (Clark, 1999). The leading cause of the amplified warming is invoked by snow and ice albedo feedback (Kay, 2011). Basically, processes in the climate system that can either amplify or dampen the climate response to an external perturbation are referred to as climate feedbacks (IPCC, 2013). In this case, in a warmer climate, snow and ice retreat, the exposing land become less reflective, thus absorbing more solar radiation, warming the Earth further, finally, the globally averaged surface temperature was amplified by the snow and ice retreat, indicating a positive feedback.

DATA

Remote sensing data (MOD10C1 and MYD10C1 of MODIS), meteorological reanalysis data (Snow albedo, albedo, 2m air temperature data of ECMWF), radiative kernel data (surface albedo radiative kernel under clear sky of CAM 3) in quantifying snow albedo radiative forcing and its feedback using radiative kernel method on global scale.

All data were uniformed to a spatial resolution of 0.25°×0.25°, radiative kernel data were kept temporal resolution of monthly while all other data were uniformed to daily scale from 2002~2011.

METHODS

Multi-source data were used in purpose of achieving an observation based result at a finer data resolution. In addition, surface albedo feedback is as well estimated and a simple comparison was made with model result.

Snow albedo feedback was quantified as the change in the net downward TOA shortwave radiative flux per temperature change caused by changes in surface albedo as:

$$\lambda = -\frac{\Delta G}{\Delta T} \tag{1}$$

where λ is the feedback parameter with unit of W m^{-2} $^{o}C^{-1}$, T is global mean air surface temperature in ^{o}C. That's to say, the key procedure is the quantifying of radiative forcing, which was calculated in the following equation:

$$G_S(t,R) = \frac{1}{A(R)} \int_R S_x(t,r) \frac{\partial \alpha}{\partial S_x}(t,r) \frac{\partial H}{\partial \alpha}(t,r) dA(r) \tag{2}$$

This method is followed by Flanner et al. (2011), where G_S is the radiative forcing of snow albeodo with unit of W m^{-2}, which is a function of time t and study area R, R has a total area of A and cellsize r, S_x is the fraction of snow cover (SCF) while $\frac{\partial \alpha}{\partial S_x}(t, r)$ represents the albedo contrast between snow cover regions and snow free area, $\frac{\partial H}{\partial \alpha}(t, r)$is the radiative change against the coincident change of albedo change. Also, we assume that $\frac{\partial H}{\partial \alpha}$ and α, $\frac{\partial \alpha}{\partial S_x}$and S_x are independent with each other.

CONCLUSION

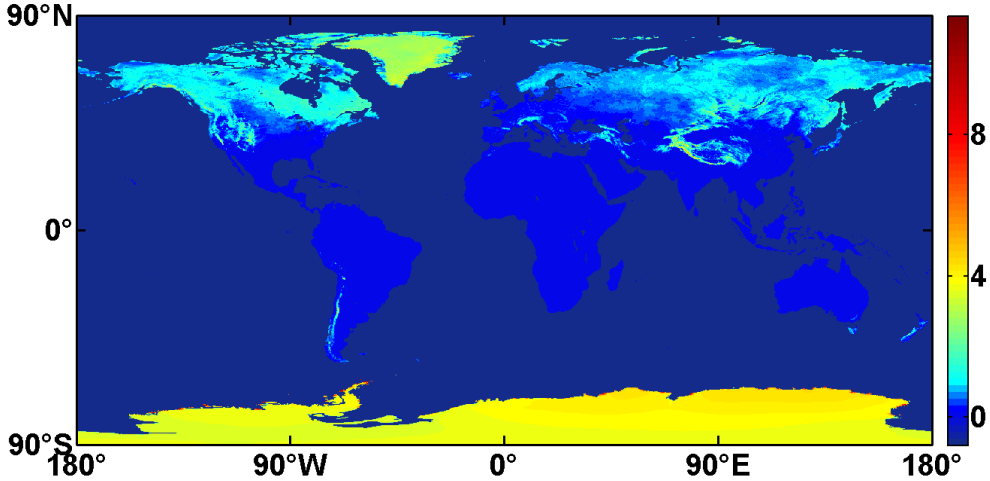

Fig. 1 Global annual mean snow albedo radiative forcing between 2002~2011(W m^{-2})

The figure above shows the global annual mean snow albedo radiative forcing between 2002~2011, Specifically, apart from the Antarctic, mid to high latitude of the North Hemisphere has the strongest snow albedo radiative forcing between 0.5~1.5 W m^{-2}, among which Greenland and Tibeten plateau exhibit stronger radiative forcing that reaches 3~5 W m^{-2}, while Antarctica has a stronger radiative forcing about 4~6 W m^{-2}. The strongest radiative forcing exists at the edge of the Antarctica, where experiences strong accumulation and depletion of snow every year.

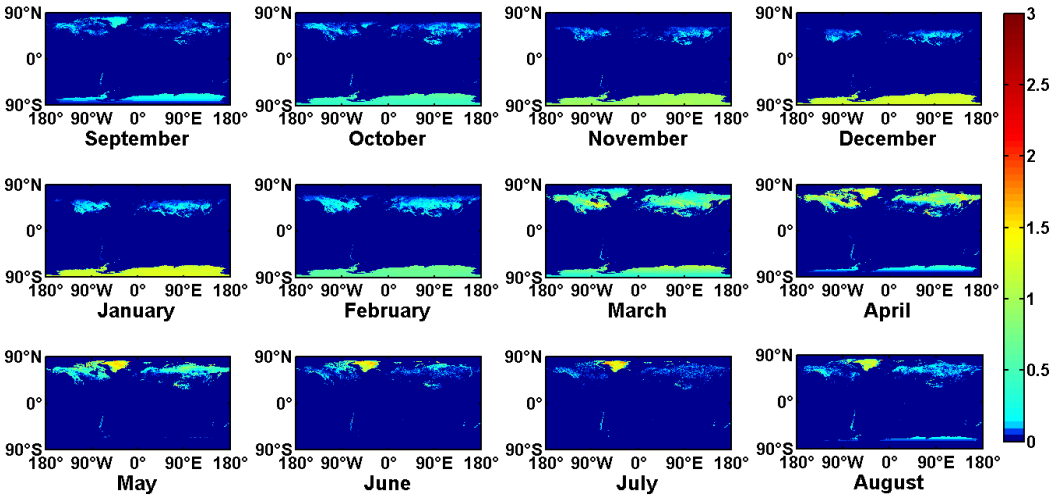

Fig. 2 Global mean monthly snow albedo radiative forcing between 2002~2011(W m^{-2})

Monthly snow albedo radiative forcing between 2002~2011 was shown in Fig. 2, the monthly anomaly is also deeply affected by solar motion. For specific, from Sep. to Dec., when sun moves from the equator to the tropic of Capricorn, the North Hemisphere absorbs decreasing solar radiation, areas

inside of the Arctic Circle gradually into polar night, when snow albedo radiative forcing of the North Hemisphere decreases. On the other hand, the South Hemisphere absorbs more solar radiation, melts more snow at the same time. As a result, there is also a decrease in snow albedo radiative forcing, except in Antarctica. Because of the "stable" snow cover, snow albedo radiative forcing in Antarctica increases as a result of the increasing absorption of solar radiation.

Based on snow albedo radiative forcing result and global annual mean surface air temperature, we used least-squares linear trend to calculate the feedback based on equation (2), the result is 0.17 W m^{-2} $^{o}C^{-1}$.

Since it's difficult to validate the result of snow albedo feedback, we testified it through a proxy indicator: the surface albedo feedback.

Firstly, we made a coarse estimation of surface albedo feedback based on snow albedo feedback. Flanner et.al (2011) used to percentage the respective contribution of snow and ice albedo feedback to surface albedo feedback in the North Hemisphere, showing that in low, central and high albedo contrast scenarios, snow albedo feedback account for 38%, 46% and 49% of the total surface albedo feedback. Within this, we made a coarse conversion that surface albedo feedback is between 0.35 W m^{-2} $^{o}C^{-1}$ ~0.45 W m^{-2} $^{o}C^{-1}$ upon our calculation. Then, we compared the result with other snow albedo feedback results.

Table 1 climate feedbacks estimated for the CMIP5 AOGCMs

Model	Surface albedo feedback (W m^{-2} $^{o}C^{-1}$)
BNU–ESM	0.4
CanESM2	0.3
CCSM4	0.4
HadGEM2–ES	0.3
INM–CM4	0.3
IPSL–CM5A–LR	0.2
MIROC5	0.3
MPI–ESM–LR	0.3
MRI–CGCM3	0.3
Global mean	0.3
90% uncertainty	0.1

Table 1 was extracted from IPCC AR5 (2013), which displays the climate feedback parameter estimated for the CMIP5 AOGCMs, as a result, the global mean Surface albedo feedback from models is 0.3±0.1 W m^{-2} $^{o}C^{-1}$. In the meanwhile, calculation with observation data, take the representative Flanner's calculation as an example, surface albedo feedback of the North Hemisphere is between 0.3~1.1 W m^{-2} $^{o}C^{-1}$, which is different from model work. In IPCC AR5, it also mentioned to the differences between model work and observation calculation. Noticing that one possible explanation is the CMIP5 models underestimate the strength of the feedback as did the CMIP3 models based upon the systematic errors in simulated sea ice coverage decline relative to observed rates, which to some extent proves our result to be reliable and a probable underestimate in model simulation.

ACKNOWLEDGEMENTS

This work was supported by the Chinese National Natural Science Foundation (41271356).

REFERENCES

Clark P U, Alley R B, Pollard D. Northern Hemisphere ice-sheet influences on global climate change [J]. Science, 1999, 286(5442): 1104-1111.

Climate change 2013-the physical science basis: Working group I contribution to the fifth assessment report of the IPCC[M]. Cambridge University Press, 2013.

Crook J A, Forster P M. Comparison of surface albedo feedback in climate models and observations [J]. Geophysical Research Letters, 2014, 41(5): 1717-1723.

Flanner M G, Shell K M, Barlage M, et al. Radiative forcing and albedo feedback from the Northern Hemisphere cryosphere between 1979 and 2008[J]. Nature Geoscience, 2011, 4(3): 151-155.

Kay J E, Holl M M, Alexra J. Inter-annual to multi-decadal Arctic sea ice extent trends in a warming world[J]. Geophysical Research Letters, 2011, 38(15):98-106.

Screen J A, Ian S. The Central Role of Diminishing Sea Ice in Recent Arctic Temperature Amplification[J]. Nature, 2010, 464(7293):1334-7.

Serreze M C, Francis J A. The Arctic Amplification Debate [J]. Climatic Change, 2006, 76(76):241-264.
Crook J A, Forster P M. Comparison of surface albedo feedback in climate models and observations [J]. Geophysical Research Letters, 2014, 41(5): 1717-1723.

A PRELIMINARY STUDY OF IMPROVING GLOBAL LEAF AREA INDEX (LAI) ESTIMATION BASED ON DATA ASSIMILATION RESEARCH TESTBED AND THE COMMUNITY LAND MODEL VERSION 4

X. L. LING [1,2], C. B. FU [1], Z. L. YANG [2], and W. D. GUO [1]

[1] Institute for Climate and Global Change Research, School of Atmospheric Sciences, Nanjing University, Nanjing 210093, People's Republic of China.

[2] Department of Geological Sciences, John A. and Katherine G. Jackson School of Geosciences, University of Texas at Austin, Austin, Texas, USA.

Keywords: DATA ASSIMILATION, COMMUNITY LAND MODEL, LEAF AREA INDEX, CARBON AND NITROGEN CYCLE

INTRODUCTION

The leaf area index (LAI) influences the exchanges of momentum, carbon, energy, and water between the terrestrial biosphere and the atmosphere. As such, it is a key variable in regulating the global carbon, energy, and water cycles. In-situ observation can provide accurate LAI data, while it is not easy for widely world use. Modern land surface models have included prognostic carbon and nitrogen components to simulate the LAI (for example, Thornton and Zimmermann, 2007), but these LAI simulations show biases in both amplitude and phase. Land data assimilation, combining observation and simulation together by mathematical variation method or filter method, can provide the most accurate variable estimation, and achieve spatial and temporal extension. Satellite-derived data could provide continuous temporal and spatial LAI product, which is the data basis for land data assimilation.

METHODS

The land data assimilation system is the Community Land Model version 4 (CLM4.0) with the prognostic carbon–nitrogen (CN) option (hence CLM4CN), which is linked with the Data Assimilation Research Testbed (DART) developed by the National Centre for Atmospheric Research (NCAR). 80 atmospheric forcing data are achieved by running DART and the Community Atmosphere Model (DART/CAM). Random 40-member atmospheric forcing is used to drive the CLM4CN with or without LAI data assimilation. In our LAI data assimilation, the Global Land Surface Satellite LAI data (GLASS LAI) LAI is assimilated into the CLM4CN at a frequency of every 8 days, and the total leaf area index, (leaf carbon and leaf nitrogen) are adjusted at each time step.

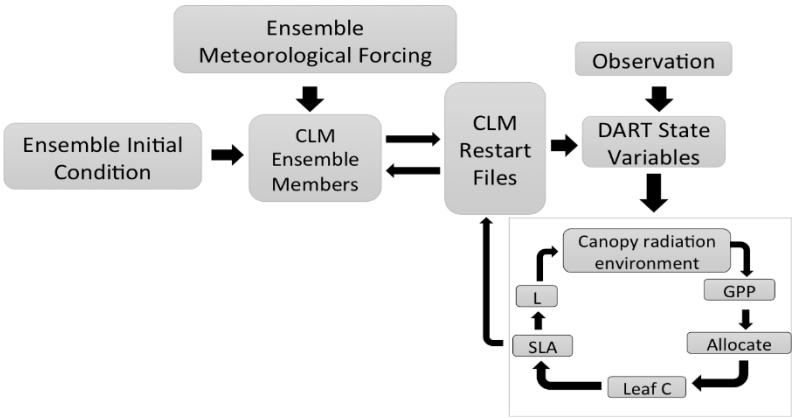

Figure 1. The procedure of LAI assimilation using coupled DART and CLM4CN (DART/CLM4CN).

The procedure of LAI assimilation using DART/CLM4CN is illustrated in Figure 1. Different ensemble meteorological atmospheric forcing are used to drive the CLM Ensemble members with ensemble initial conditions, and generate ensemble CLM restart files. If there is an observation, DART will absorb it by mathematical filter method, and get an updated value as the analysed results. After finishing this step of assimilation, DART will send analysed value back to the CLM rest files as the initial data, and move on to the next time step.

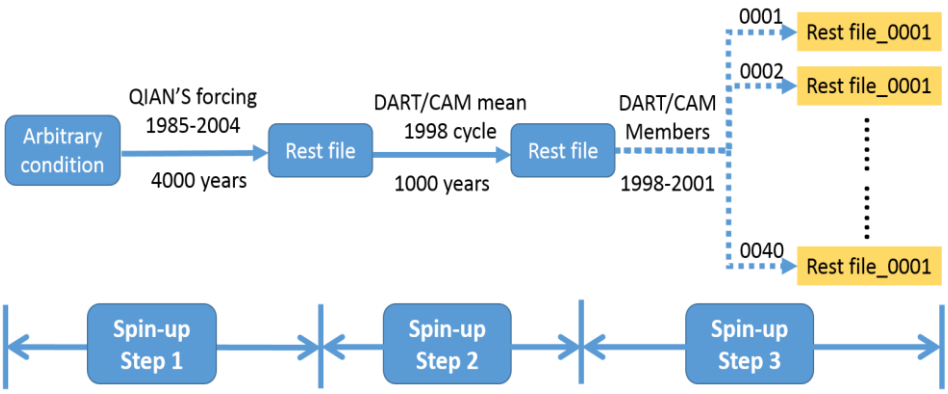

Figure 2. Spin-up process for ensemble initial condition.

To achieve ensemble initial conditions, 3 stage of spin-up process were conducted to make all pools in carbon and nitrogen model reach their steady state. First of all, single Qian's forcing (Qian et al., 2006) was used to drive the model for 4000 years (Shi et al., 2013). Next, the ensemble mean of 40 atmospheric forcing members for the year of 1998 was used to driving the single CLM4CN for 1000 years. And for the last stage, 40 ensemble atmospheric forcing members were used to drive the ensemble CLM4CN members for 40 plus 4 years from 1998 to 2001, and we can achieve 40 ensemble initial conditions.

In order to find out the best assimilation method, three experiments are designed as shown in Table 1. In the CTL experiment, no assimilation is conducted, while in the NO-CN and C-N experiments, GLASS LAI is assimilated, exclude and include carbon and nitrogen control especially. Furthermore, 4 different assimilation algorithms include Ensemble Kalman Filter (EnKF, Evensen, 1994), Ensemble Adjust Kalman Filter (EAKF, Anderson, 2001), Kalman Filter (KF, Kalman, 1960), and Particle Filter (PF) is discussed.
Based on the assimilated LAI, the ability for simulating the land surface variables and land-atmosphere exchange variables is estimated.

Experiment	Assimilated variables	Updated variables	Assimilation algorithm
CTL	-	-	-
NO-CN	GLASS LAI	LAI	EAKF
C-N	GLASS LAI	LAI, Leaf C, Leaf N	EAKF, EnKF, KF, PF

Table 1. Experiment design for LAI assimilation using DART/CLM4CN

CONCLUSIONS

The spatial distribution of global LAI in July 2002 for (a) observation, (b) simulation, (c) assimilation without C-N constrain, and (d) assimilation with C-N constrain is shown in Figure 2. Moderate Resolution Imaging Spectroradiometer LAI (MODIS LAI) is used for estimation. The results show that the C-N experiment performed the best for all experiment designed, and the assimilation results are better in low latitude regions than higher latitude regions. In detail, the CLM4-CN simulated LAI systematically overestimats the global LAI, especially in low latitude. If there was no C-N control during assimilation,

the analysed LAI is almost the same as simulation. While if updating both LAI and leaf carbon and leaf nitrogen, the analysed LAI can be corrected, especially in low latitude regions.

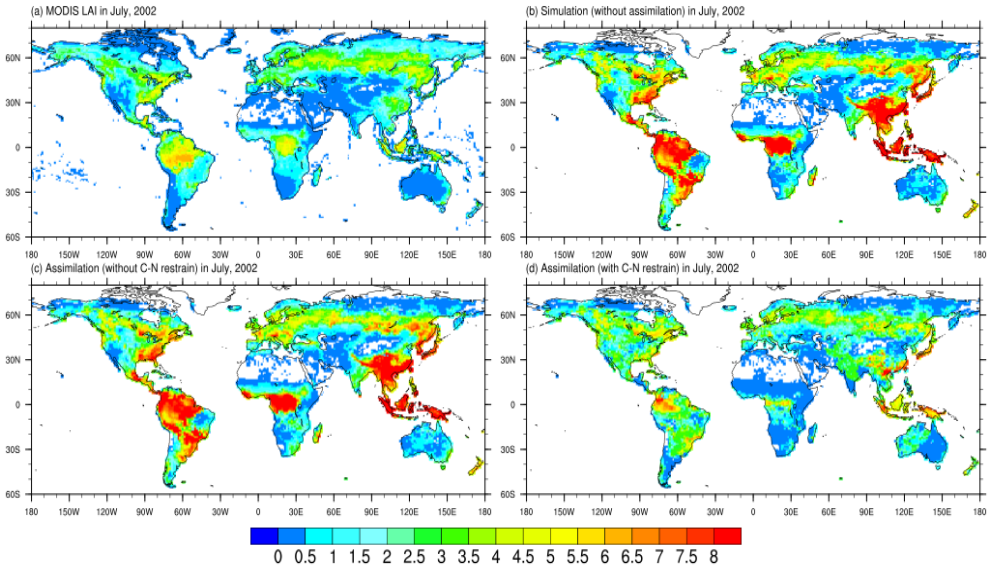

Figure 3. The spatial distribution of global LAI in July 2002 for (a) observation, (b) simulation, (c) assimilation without C-N constrain, and (d) assimilation with C-N constrain.

The assimilation ability for different mathematical algorithm is showed in Figure 4. The results showed that, when the LAI value and its amplitude are small, the analysed LAI is more relied in modelling, which situation is obvious in mid and high latitude in northern hemisphere. In contract, if the amplitude is large for LAI data, and the bias of modelling and observation is large, the analysed LAI always relies in observation. The results show that the Ensemble Adjust Kalman Filter as well as including carbon-nitrogen control is the best choice.

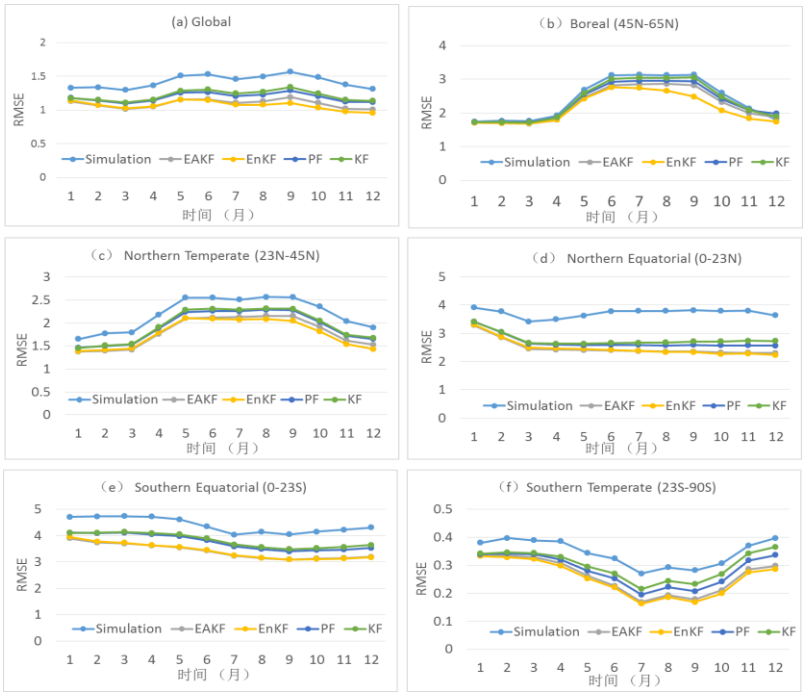

Figure 4. Time series of RMSE for assimilated LAI and observation for different sub-regions in 2002: (a) global, (b) boreal, (c) northern temperate, (d) northern equatorial, (e) southern equatorial, and (f) southern temperate.

Based on the assimilated LAI and potential LAI data, the difference for land surface variables, and land-atmosphere exchange variables between assimilation and simulation are also analysed, as to see if assimilation can improve the simulation ability. The results show that land surface temperature at 2-meter high increase with the decrease of global LAI, especially in the west of Eurasia with the value of 1.6 K, the Amazon region and the centre of Africa take second place, with the difference of 1.1 K and 1.0 K especially. As seen in Figure 5, simulation strongly underestimates the 2-metre air temperature in the centre of Amazon, the northern and centre of Arica, and most regions in Eurasia; while overestimates 2-metre air temperature in the centre of North America, the east and southeast of Eurasia, and most regions of Austria. After improving the global LAI, the most obviously improved regions locate in the Amazon regions, the centre of Africa, the east and northeast of Asia, the southeast of North America, and the west of Eurasia. Furthermore, the region with largest LAI variations is not the region with largest variations for the other variables, which is associated with the land surface vegetation cover type.

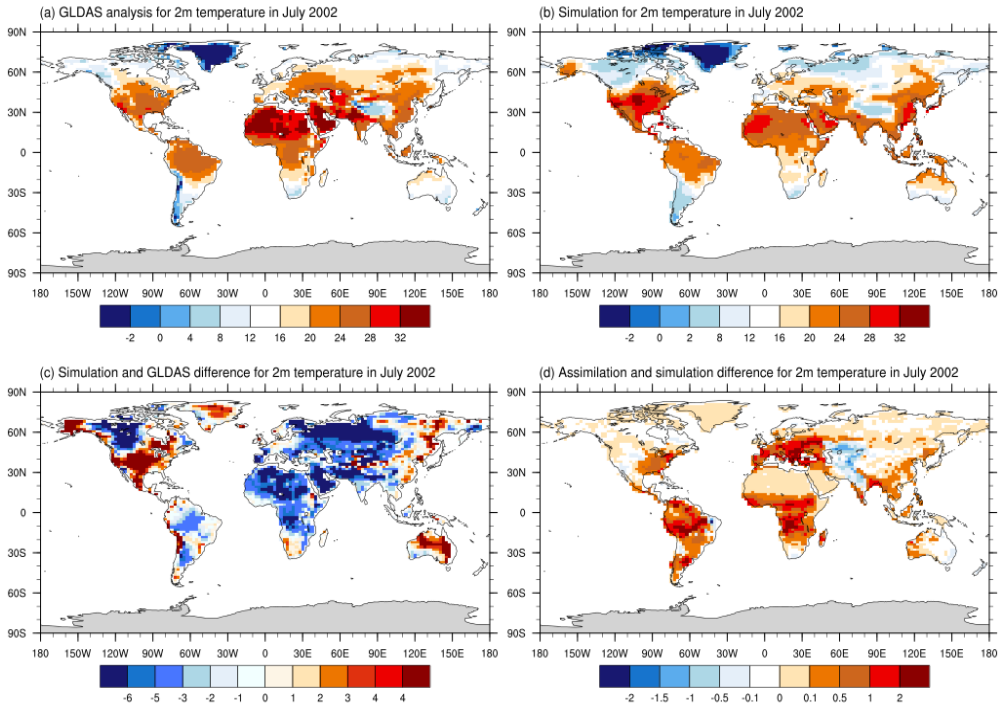

Figure 5. 2-meter air temperature distribution in July 2002, for (a) observation, (b) simulation (CTL experiment), (c) difference between simulation and observation, and (d) difference between assimilation and simulation.

ACKNOWLEDGEMENTS

This study is jointly supported by the Jiangsu Collaborative Innovation Center for Climate Change and the Joint International Research Laboratory of Atmospheric and Earth System Sciences (JirLATEST). Many thanks to Doctor L. Zhao and Y. F. Zhang for all technical support on running DART and CLM4CN.

REFERENCES

Anderson, J. L., T. Hoar, K. Raeder, H. Liu, N. Collins, R. Torn, and A. Arellano (2009). The data assimilation research testbed: A community facility, *Bull. Am. Meteorol. Soc.*, **90(9)**, 1283-1296.

Anderson, J. L. (2001). An ensemble adjustment Kalman filter for data assimilation, *Mon Wea Rev*, **129**, 2884-2903.

Evensen, G. (1994). Sequential data assimilation with a nonlinear quasi-geostrophic model using monte-carlo methods to forecast error statistics. *Journal of Geophysical Research-Oceans*, **99(C5),** 10143-10162.

Kalman, R E. (1960). A new approach to linear filtering and prediction problems. *Transactions of the ASME – Journal of Basic Engineering*, **82(D)**, 35-45.

Qian, T., A. Dai, K.E. Trenberth, and, K.W. Oleson (2006). Simulation of global land surface conditions from 1948 to 2004: Part I: Forcing data and evaluations. *J. Hydrometeor.*, **7**, 953-975.

Shi, M. J., Z. L. Yang, D. M. Lawrence, R. E. Dickinson, and Z. M. Subin (2013). Spin-up processes in the Community Land Model version 4 with explicit carbon and nitrogen components. *Ecological Modelling*, **263**, 308-325.

Thornton, P. E. and N. E. Zimmermann (2007). An improved canopy integration scheme for a land surface model with prognostic canopy structure. *Journal of Climate*, **20**, 3902-3923.

Xiao, Z. Q., S. L. Liang, J. D. Wang, P. Chen, X. J. Yin, L. Q. Zhang, and J. L. Song (2014). Use of General Regression Neural Networks for Generating the GLASS Leaf Area Index Product From Time-Series MODIS Surface Reflectance, *IEEE TRANSACTIONS ON GEOSCIENCE AND REMOTE SENSING*, **52(1)**, 209-223

TREE WATER RELATIONS DURING WINTER

A. LINTUNEN[1], T. PALJAKKA[1], L. LINDFORS[1,2] and T. HÖLTTÄ[1]

[1]Department of Forest Sciences, University of Helsinki, Post Office Box 27, FI-00014, Helsinki, Finland

[2]Laboratory of Plant Growth and Development, Department of Biological Sciences, University of Osaka, 1-1 Yamadaoka, Suita, Osaka Prefecture 565-0871, Japan

Keywords: CELL DAMAGE, EXTRACELLULAR FREEZING, ICE NUCLEATION TEMPERATURE, WINTER EMBOLISM

INTRODUCTION

Boreal trees experience frequent freeze–thaw cycles annually. Water in tree xylem and other apoplastic (i.e. outside the cells) spaces inevitably freezes when temperatures drop a few degrees below zero. Freezing of apoplastic sap causes two kinds of consequences for trees. First, gases dissolved in liquid water form bubbles during freezing, and these bubbles are a risk of expanding during thawing and blocking the water transport conduits by air (Sperry and Sullivan, 1992). This is called freeze-thaw embolism. The other important aspect of freezing stress experienced by trees is frost induced cellular damage. Cellular damage can be caused either by membrane rupture through symplastic (i.e. inside the living cells) ice crystal formation, or through extreme cell dehydration and plasmolysis caused by low water potential created by apoplastic ice (Ristic and Ashworth, 1993).

In this paper, we will study tree water relations during winter from four different viewpoints:
i) apoplastic freezing temperature, and how it is determined in trees
ii) dynamics between apoplastic freezing and leaf gas-exchange in evergreen conifers
iii) fate of gases during the apoplastic freezing process - are they all trapped inside the ice
iv) cell damage, and how it can be measured

METHODS

To measure apoplastic freezing temperature of different tree species and tree parts (i.e. stems, branches, roots), we collected 70 samples during March and April from woody species in Southern Finland near Helsinki. The samples were cooled in a weather chamber (Weiss Umwelttechnik WK112340/40) and the apoplastic freezing temperature was detected as freezing exotherm by monitoring apoplastic temperature of the samples. After the freezing experiment, 100-µm-thick cuts were prepared from the samples, and the size of the largest conduits within each sample was measured. See in more detail from Lintunen et al., 2013.

To measure the dynamics of leaf gas-exchange during apoplastic freezing process, we conducted a freeze–thaw cycle in a weather chamber for eight 4-years-old *Pinus sylvestris* seedlings. Each experiment consisted of an overnight stabilization period, freezing to -8˚C, thawing, and 14-h recovery period. The experiments were done in April during spring recovery of photosynthetic capacity. We measured ambient, xylem temperatures, xylem and phloem diameter change, leaf gas-exchange and chlorophyll fluorescence. See in more detail from Lindfors et al., 2015.

Escape of gases during the apoplastic freezing process was measured in a laboratory conditions with three winter-acclimated *Pinus sylvestris* saplings and three *Picea abies* saplings. CO_2 efflux was measured from the stem with gas exchange cuvette and infrared gas analyser during freezing experiment down to -10˚C in

a weather chamber. CO_2 efflux was also measured in field from a mature *Pinus sylvestris* tree in SMEAR II station, Finland, during years 2006 to 2009. See in more detail from Lintunen et al., 2014.

Cell damage during an apoplastic freezing process as an indicator of winter tolerance was measured from seven broadleaved tree species that had been planted as urban trees in Helsinki, Finland. Cell damage in -25˚C was measured both during winter and during spring recovery with electrolyte leakage method (Flint et al., 1967). Together with electrolyte leakage, we measured irreversible diameter variations of the sample branches to see if the varying degree of electrolyte leakage shows up as irreversible frost-induced dimensional changes of the branches, as the membrane rupture would disable cell swelling upon thawing to its pre-freezing dimensions. See in more detail from Lintunen et al., 2015.

RESULTS AND DISCUSSION

We found that the apoplastic freezing temperature of water in the xylem increases with increasing conduit size regardless of the species or tree part (Fig. 1). Conduit size determines the size of the largest particles that are able to penetrate through the pit pores and catalyse ice nucleation; different sized organic and inorganic nuclei are commonly found in plants (Wisniewski et al., 2002). Apoplastic freezing temperature in xylem conduits determines the frozen time period and the number of freeze-thaw cycles a tree experience during winter.

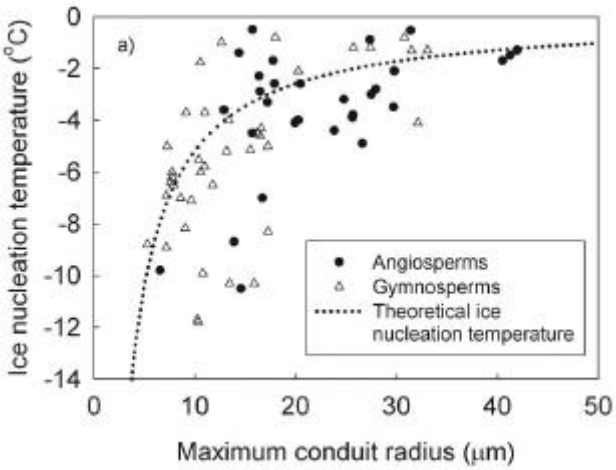

Figure 1. Measurements (N 5 70) of ice nucleation temperature of water in trees and maximum conduit radius. The narrowest conduits were found in conifers and the widest in deciduous species. Curve for the theoretical relationship is drawn. (From Lintunen et al. 2013).

Photosynthetic rate declines quickly following apoplastic freezing in xylem and needles, almost parallel to a rapid shrinking of xylem diameter (Fig. 2). The very distinct dynamics of photosynthetic rate and stomatal conductance reveals that the decreased photosynthetic rate reflects impaired dark reaction rather than stomatal closure.

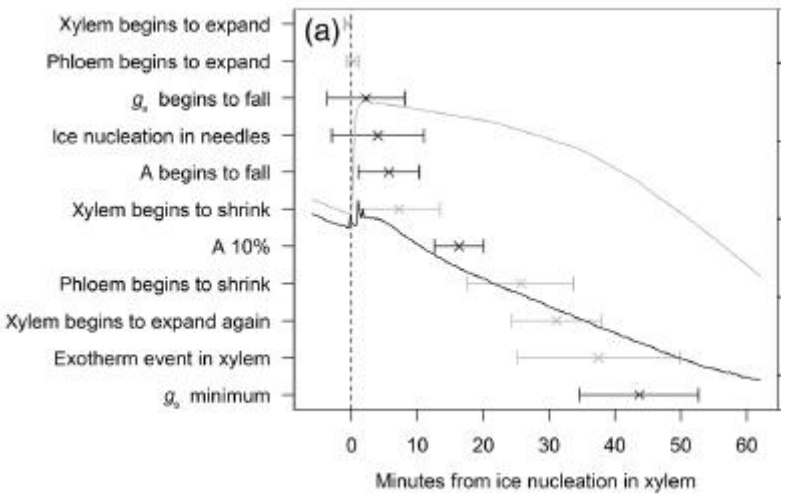

Figure 2. Dynamics of phenomena related to stem (grey solid lines and grey horizontal bars) and to needles (black solid lines and black horizontal bars) following apoplastic freezing in xylem. The zero on the x-axis and the vertical dashed line refer to the moment of ice nucleation in xylem. Cross marks refer to the average timing (±SD) of the phenomena that are explained on the side y-axis. (From Lindfors et al., 2015)

We showed empirically both in the laboratory and in the field (Table 1)

that an important aspect of freeze-thaw embolism has been overlooked: all gases dissolved in liquid water upon freezing are not trapped inside the ice in the stem as previously assumed, but even 50% is extracted through the bark. The efficiency of gas extraction from the xylem upon freezing could be an important factor affecting the risk of embolism upon thawing.

Table 1. Average size of the freezing-related CO_2 burst connected to freezing measured in the laboratory and in the field (data from Lintunen et al. 2014)

Species	Type	No of repetitions	Mean stem diam, cm	Mean CO_2 burst µmol m^{-2}	SE µmol m-2
Pinus sylvestris	Lab	3	0.8	636	105
Picea abies	Lab	3	0.8	524	202
Pinus sylvestris	Field	24	6.9	5276	816

Cell damage is higher during spring recovery phase than during winter. This was shown with two different methods: electrolyte leakage and irreversible diameter shrinkage (Fig. 4). Irreversible shrinkage of branch diameter due to freezing stress seems to be a good and non-destructive method to indicate winter tolerance in trees.

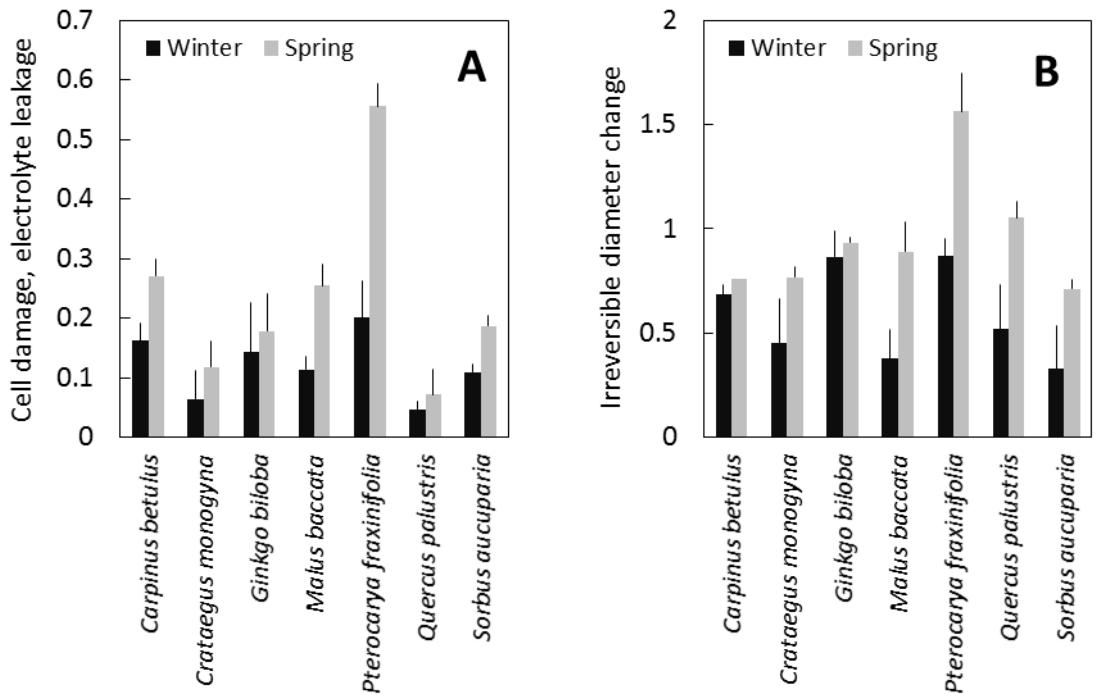

Figure 4. Index of cell damage (A) and irreversible diameter shrinkage (B) at −25 °C is shown for winter and early spring for each species with standard error (data from Lintunen et al. 2015). The irreversible diameter shrinkage is calculated as shrinkage to branch diameter percentage, and it is square root transformed.

CONCLUSIONS

Trees in boreal forest experience tens of freeze-thaw cycles annually. Apoplastic freezing prevents photosynthesis, and causes stress for trees by freeze-thaw embolism and by cellular damage. The number of freeze-thaw cycles is especially high during spring time when the temperature is low, but sun is

warming up the trees during middays. Low apoplastic freezing temperature decreases frost-damage due to decreased number of freeze-thaw cycles, and makes it possible for an evergreen tree to photosynthesize on sunny days even when the ambient temperature is below zero.

ACKNOWLEDGEMENTS

This work was supported by the Academy of Finland grant no. 272041.

REFERENCES

Lindfors, L., Hölttä, T., Lintunen, A., Porcar-Castell, A., Nikinmaa, E., and E. Juurola. (2015) Dynamics of leaf gas exchange, chlorophyll fluorescence and stem diameter changes during freezing and thawing of Scots pine seedlings. Tree Physiology, doi: 10.1093/treephys/TPV095

Lintunen, A., Hölttä, T. and M. Kulmala (2013) Anatomical regulation of ice nucleation and cavitation helps trees to survive freezing and drought stress. Scientific Reports 3: 2031

Lintunen, A., Lindfors, L., Kolari, P., Juurola, E., Nikinmaa, E. and T. Hölttä (2014) Bursts of CO_2 released during freezing offer a new perspective on avoidance of winter embolism in trees. Annals of Botany 114: 1711-1718.

Lintunen, A., Paljakka, T., Riikonen, A., Lindén, L., Lindfors, L., Nikinmaa, E. and T. Hölttä (2015) Irreversible diameter change of branches correlates with other methods for estimating frost tolerance of living cells in freeze- thaw experiment: a case study with seven urban tree species in Helsinki. Annals of Forest Science 72: 1089-1098.

Ristic, Z. and E.N. Ashworth (1993) Ultrastructural evidence that intracellular ice formation and possibly cavitation are the sources of freezing injury of supercooling wood tissue of *Cornus florida* L. Plant Physiol 103:753–761.

Sperry, J.S. and J.E.M. Sullivan (1992) Xylem embolism in response to freeze–thaw cycles and water stress in ring-porous, diffuse-porous and conifer species. Plant Physiology 100: 605–613.

Wisniewski, M., Fuller, M., Glenn, D. M., Gusta, L., Duman, J. and M. Griffith (2002) Extrinsic ice nucleation in plants: What are the factors involved and can they be manipulated? In Plant Cold Hardiness: (Eds. Li, P. H. & Palva, E. T.) Gene Regulation and Genetic Engineering 211–222 (Kluwer Academic).

EFFICIENT REMOTE SENSING DATA STORAGE AND MANAGEMENT BASED ON PARALLEL FILE SYSTEM AND NOSQL DATABASE

J. LIU[1, 5], Y. XUE[1, 2] and J. GARCKE[3, 4]

[1]Key Laboratory of Digital Earth Science, Institute of Remote Sensing and Digital Earth, Chinese Academy of Sciences, Beijing 100094, China

[2]Faculty of Life Sciences and Computing, London Metropolitan University, 166-220 Holloway Road, London N7 8DB, UK

[3]Fraunhofer Institute for Algorithms and Scientific Computing SCAI, 53754, Sankt Augustin, Germany

[4]Institute for Numerical Simulation, University of Bonn, 53115, Bonn, Germany

[5]University of Chinese Academy of Sciences, Beijing 100049, China

Keywords: Remote sensing, Aerosol optical depth, Parallel file system, NoSQL.

INTRODUCTION

The development of sensor technologies have enabled remote sensing data with higher spatial and higher spectral resolutions. Together with the requirements of global detection and monitoring for environment and long term time series data analysis, the remote sensing data are undergoing an explosive growth (Ma et al. 2014). The remote sensing data are recognized as ‘‘Big Data’’ in some certain sense (Huadong Guo 2014). To turn the massive remote sensing data into remote sensing information, great efforts have been made towards the incorporation of HPC (high performance computing) techniques in remote sensing domain (Lee et al. 2011; Liu et al. 2015). However, the efficient storage and management of the diversity, high dimensionality, high resolution, large spatial coverage, time series and unstructured remote sensing data is fundamental to the remote sensing processing and analysis.

In this paper, we exploit the efficient remote sensing data storage and management solutions based on parallel file system and NoSQL (Not only Structured Query Language) database for time series retrieval AOD (Aerosol Optical Depth) dataset.

METHODS

To store and manage massive remote sensing data, the current solution pattern for practical remote sensing data centers can be divided into mainly three categories (Lu et al. 2011), i.e. the file system based solution, the database solution, the mixture of file system and database. The mixture pattern mostly manages the metadata of remote sensing image data in commercial relational database, and stores the remote sensing image data as files in the cantered or distributed file system, which largely reduces the data amount storing and managing in database and allows efficient access.

Parallel file systems and NoSQL databases are considered as the mainstream techniques to address the big data storing and managing (Ma et al. 2014). In this paper we studied the solution combining the BeeGFS with the MongoDB, the system framework is shown in Figure 1. BeeGFS was developed at the Fraunhofer Institute for industrial mathematics in 2007 released as “FhGFS” to as a fixible, scalable and easy to use product, and labelled as BeeGFS in 2014, and already been popularly used in small, medium and large HPC systems (http://www.beegfs.com/content/). MongoDB is an open source NoSQL database with high scalable, high reliable and high performance. MongoDB can realize most query functions similar with traditional relational database. Besides, it is collection-oriented storage and can support complex unfixed data structure (Chodorow 2010). As shown in Figure 1, the client module of BeeGFS

was deployed on application nodes, the MongoDB server was launched on specific MongoDB database node, while the computing nodes runs the MongoDB client side.

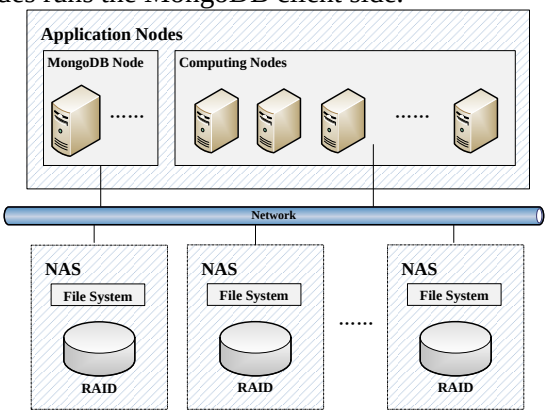

Figure 1. The architecture for remote sensing data storage and management.

For remote sensing data organization towards time series quantitative retrieval datasets, we classified the remote sensing data into three categories, i.e. the original data such as the MODIS (Moderate Resolution Imaging Spectroradiometer) Level 2 HDF (Hierarchical Data Format) data, the temporary data which can be used or shared with later processing or other application procedures, and the retrieved dataset like AOD (Aerosol Optical Depth). The initial hierarchy of the data file organization in the parallel file system is shown in Figure 2. Under the three major categories, the remote sensing data are organized according to the sensor type, data type, spatial resolution, record date and image files. The hierarchy can be extended on demand. Under the tree model of the file system, the leaf node represents the image file and each file can be identified through its global directory path.

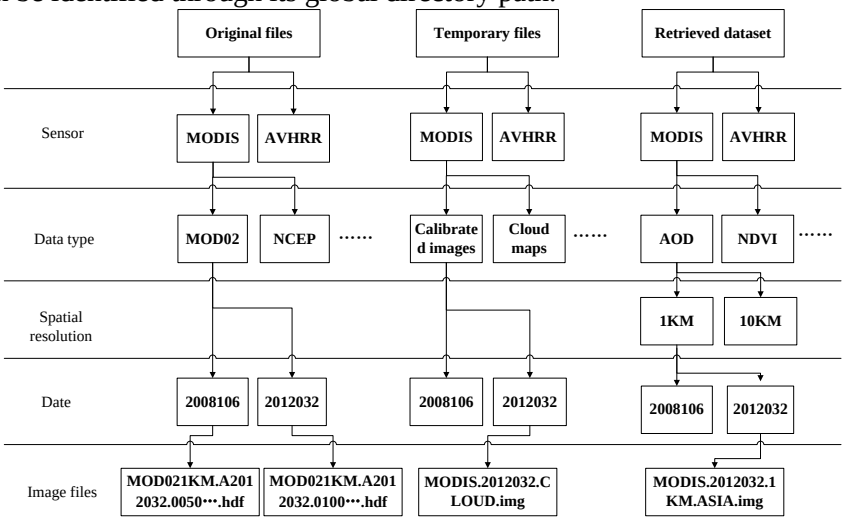

Figure 2. The initial hierarchy of the data file organization in the parallel file system.

For the metadata stored in MongoDB, we take the retrieval of AOD dataset from MODIS satellite data using the SRAP (Synergetic Retrieval of Aerosol Properties) - MODIS algorithm as a study case. **Error! Reference source not found.** shows the analogy of basic concept between NoSQL database and relational database. Three databases are created respectively for original files, temporary files and retrieved datasets.

Table 4. The analogy of basic concept between NoSQL database and relational database.

NoSQL database	Relational database
Collection	Table
Key	Column
Value	Value
Document/Object	Records/Rows

As a database can contain multiple collections, the collections correspond to the applications. For instance, the collection labelled as “AOD_SRAP_MODIS” has been created for three databases for the AOD retrieval using SRAP-MODIS application and all metadata of related remote sensing data are inserted to the collections of three databases. One collection contains metadata information with diversity structure in common. **Error! Reference source not found.** shows an example of metadata stored in MongoDB in BSON (Binary JSON) format. MongoDB enables unfixed modes for documents stored in collections of databases as shown in **Error! Reference source not found.**, which reduces the complexity for designing the tables and avoids huge overhead for instance, of join operations across multiple tables when large data emerge.

Table 5. An example of metadata in MongoDB.

	MOD03	NCEP

Metadata in BSON	{
	file_name:"MOD03.A2012032.0225.006.2012285162432.hdf ",
	file_path:"/home/jliu/……/MOD03.A2012032.0225.006.2012285162432.hdf ",
	time_resolution: "1_day ",
	time: "2012032",
	type: "MOD03",
	latitude_min: "48.95527648925781",
	latitude_max: "71.81368255615234",
	longitude_min: "112.05449676513672",
	longitude_max "166.38233947753906"
	}
		{
		file_name:" N201203200_O3_TOMSOMI_24h.hdf ",
		file_path:"/home/jliu/……/ N201203200_O3_TOMSOMI_24h.hdf ",
		time_resolution: "1_day ",
		time: "2012032",
		type: "Ozone"
		}

Having designed the organization of data files in the parallel file system and metadata in MongoDB, a remote sensing data storage and management system prototype was constructed. The prototype was implemented with MongoDB C++ API, and Figure 3 shows the modules of system prototype, which supports the storage, indexing, update and time-space query.

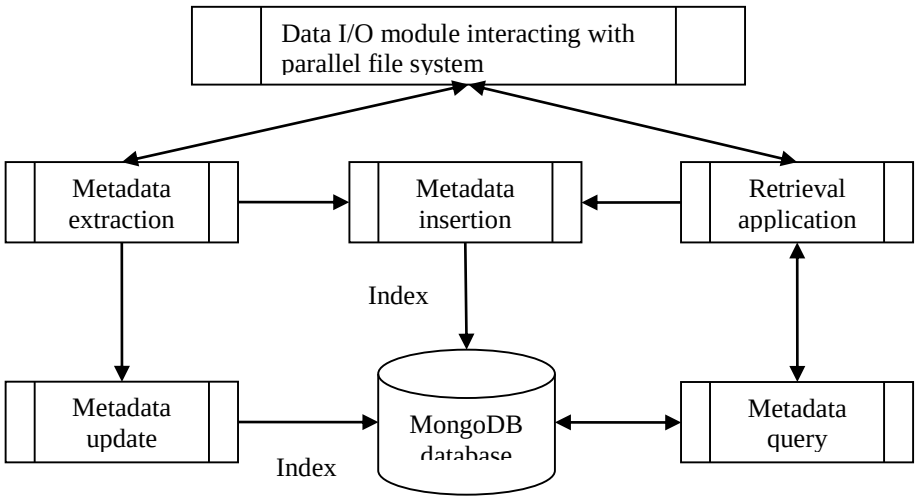

Figure 3. Modules of data storage and management system prototype.

CONCLUSIONS

The increasing amount of remote sensing data and complexity of these multi-source diversity data has pose great challenges to efficient transformation into information and knowledge. Ahead of processing,

analysing, efficient storage and management of remote sensing data need to be addressed. This paper puts forward a solution combined the parallel file system BeeGFS and NoSQL database MongoDB and implement a system prototype supporting the storage, indexing, information update and time-space query with a AOD retrieval application. The proposed solution takes advantages of high I/O performance, high scalability, reliability and easy-to-use of BeeGFS, as well as the flexibility, scalability and high performance for “Big” data case. The mixture solution provides a promising tool for the quantitative remote sensing retrieval application with huge amount time-series large spatial coverage data.

ACKNOWLEDGEMENTS

This work was supported by the joint doctoral promotion program between Fraunhofer and Chinese Academy of Sciences, and we would thank the Fraunhofer SCAI algorithm and scientific computing institute for the cluster used in this paper.

REFERENCES

Chodorow, Kristina. 2010. "MongoDB: The Definitive Guide." *Oreilly Vlg Gmbh & Co*.

Huadong Guo, Lizhe Wang, Fang Chen, Dong Liang. 2014. "Scientific big data and Digital Earth." *Chinese Journal* no. 59 (35):5066-5073.

Lee, C. A., S. D. Gasster, A. Plaza, Chein I Chang, and Bormin Huang. 2011. "Recent Developments in High Performance Computing for Remote Sensing: A Review." *IEEE Journal of Selected Topics in Applied Earth Observations & Remote Sensing* no. 4 (3):508-527.

Liu, Jia, D. Feld, Yong Xue, and J. Garcke. 2015. "Multicore Processors and Graphics Processing Unit Accelerators for Parallel Retrieval of Aerosol Optical Depth From Satellite Data: Implementation, Performance, and Energy Efficiency." *IEEE Journal of Selected Topics in Applied Earth Observations & Remote Sensing* no. 8 (5):1-12.

Lu, Xuefeng, Chengqi Cheng, Jianya Gong, and Li Guan. 2011. "Massive remote sensing data storage and management techniques." *Chinese Science: Technical Sciences* (12):1561-1573.

Ma, Yan, Haiping Wu, Lizhe Wang, Bormin Huang, Rajiv Ranjan, Albert Zomaya, and Wei Jie. 2014. "Remote sensing big data computing: Challenges and opportunities." *Future Generation Computer Systems* no. 51:47-60.

A STUDY OF CHARACTERISTICS OF WATER CLOUDS OVER HYYTIÄLÄ BASED ON CLOUDSAT/CALIPSO DATA

Y. LIU[1, 2], O. KRÜGER[3], H. GUO[1], J. ZHANG[1], M. KULMALA[3], T. PETÄJÄ[3,4]

[1]Institute of Remote Sensing and Digital Earth, Chinese Academy of Sciences, Beijing, China

[2]University of Chinese Academy of Sciences, Beijing, China

[3]Department of Physics, P.O. Box 64, 00014 University of Helsinki, Helsinki, Finland

[4]Joint International Research Laboratory of Atmospheric and Earth System Sciences & School of Atmospheric Sciences, Nanjing University, China.

Keywords: CLOUD MACROPHYSICS, MICROPHYSICS, PRECIPITATION, CLOUDSAT, CALIPSO

INTRODUCTION

Clouds and cloud systems play several crucial roles in the energy cycle of our planet (Hartmann et al., 1992; Webb et al., 2006). They control the global energy budget through their influences on the distribution of radiative heating within the atmosphere and at the surface. For example, even small changes in cloud albedo can significantly alter the radiative transfer processes. Apart from the radiative effects, clouds also have influences on the water cycle of the Earth (Stephens, 2002). The impact of clouds on earth energy mainly lies on their macrophysical and microphysical characteristics (Sassen and Wang, 2011). Thus, exploring the general macrophysics and microphysics of clouds is of prime importance to improve our understanding on cloud processes.

Resorting to a large amount of observations of clouds is best bet for us to explore cloud systems globally. By virtue of its large coverage areas, high spatial and temporal resolution, satellite-borne instruments have become a promising observational tool in providing global cloud optical and microphysical properties. Besides the impact of aerosols on cloud properties in source regions of biogenic aerosols is of high interest. However, very few researches have focused on the clouds characteristics over such areas and in particular over the boreal forest system of Northern Europe. Considering Hyytiälä area as a typical area of biogenic emissions, systematic satellite assessment of warm water clouds is desperately needed for judging the potential impact of aerosols on clouds.

The paper is organized as follows: Section 2 describes the datasets used and presents the main analyses conducted. Analyses results are presented in section 3. The overall conclusions including future activities are drawn in section 4.

METHODS

In this work, the data products collected from the CloudSat during 2010 are 2B-GEOPROF, 2B-CWC-RVOD, 2B-TAU and ECMWF-AUX. Specifically, the 2B-GEOPROF product identifies the cloud vertical structure of radar reflectivity and cloud mask (Marchand et al., 2008); 2B-CWC-RVOD product (Wood, 2008) provides information about the cloud liquid water path (LWP); and 2B-TAU product (Polonsky et al., 2008) provides information about column optical depth and cloud effective radius of the whole cloud layer. In addition, altitude and temperature profiles were obtained from the European Centre for Medium-Range Weather Forecasts Auxiliary (ECMWF-AUX) dataset matched to the CloudSat radar footprint. We analysed data for the full year 2010, however, during winter only a limited amount of data was available.

This study uses data with cloud effective radius less than 35 um and cloud optical depth greater than 1. Only single-layer and warm (liquid-phase) clouds were selected for analysis. The single-layer requirement was identified according to the method of Haynes and Stephens (2007). The latter (liquid -phase) requirement was identified by the CloudSat cloud mask criterion and an echo-top temperature warmer than 273K. The cloud LWP was used to serve as an indirect indicator for the life stages of warm clouds in attempt to study the temporal varies in warm clouds information (Petty, 2006; L'Ecuyer et al., 2009; Chen et al., 2011). We formed the overall averages of different parameters as a function of LWP values in five LWP groups including 0.0-0.5, 0.5-1.0, 1.0-1.5, 1.5-2.0, and 2.0-2.5 kg m-2, respectively.

RESULTS

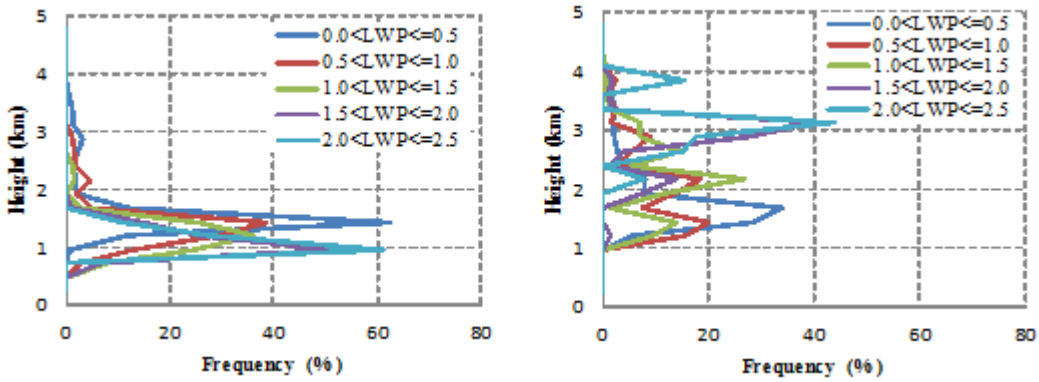

Fig.1. Probability distribution functions (PDFs) of (left) cloud base heights and (right) cloud top heights for single-layer warm clouds over Hyytiälä area for 2010 (data for January, February and December are not available). Color solid lines stand for the various liquid water path (LWP) with an interval of 0.5 kg m^{-2}.

Figure 1 shows the probability distribution function (PDFs) of cloud base height and cloud top height under different liquid water path categories in Hyytiälä area. In general the distribution of cloud base height is highly frequent in the range from 0.5 to 2 km, while the distribution of cloud top height results between 1 to 4 km. This phenomenon is reasonable. What's more, the distribution of cloud base height shows low frequency below the height of 1 km, which may indicate that sensitivities of CPR are reduced in the lowest 1 km near the surface (Li et al., 2013). Further it can be seen that for increase of liquid water path, the maximum frequency of occurrence of cloud top height steadily increases from 1.5 to 3.0 km in Hyytiälä area. It can be explained that the cloud geometrical thickness increases with developing cloud system. In addition, cloud base height decreases with the increase of liquid water path. Overall the relationship between liquid water path and cloud top height indicates that the clouds growth in the vertical is related to larger cloud liquid water path when more drizzle is produced.

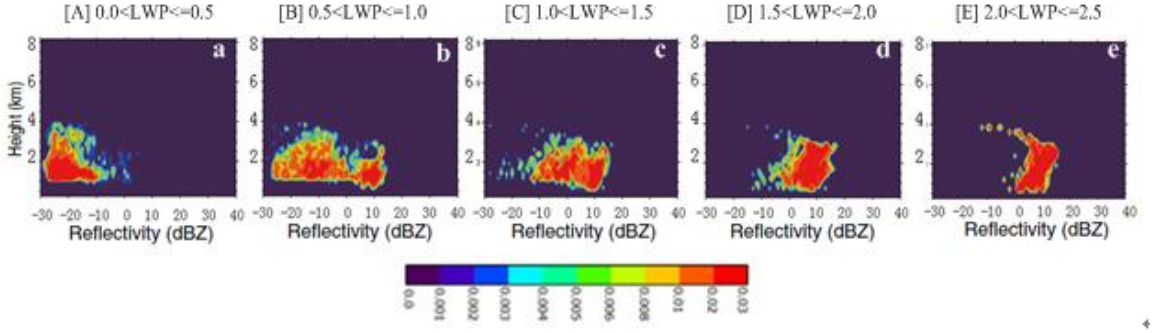

Fig.2. Contoured frequency by latitude diagrams (CFADs) of radar reflectivity for all cloudy profiles classified according to LWP with an interval of 0.5 kg m^{-2} over Hyytiälä area for 2010 (data for January, February and December are not available). The bin size is 1 dBZ in the horizontal and 0.24 km in the vertical.

Figure 2 shows the CFADs of radar reflectivity for all single layer warm cloudy profiles. According to Suzuki et al. (2011), the definition of precipitation categories is as follows: (i) non-precipitating (Z_e < -15 dBZ), (ii) drizzle (-15 < Z_e< 0 dBZ), and (iii) precipitating (0 dBZ < Z_e). As shown in Figure 2, the highest occurrence frequency of radar reflectivity is highly centralized in the region with radar reflectivity smaller than -15 dBZ throughout the entire cloud layers when LWP is in the range from 0 to 0.5 kg m^{-2}. It suggests that the clouds in initial stage are primarily composed of small droplets. The feature of downward particle growth above 1.5 km should be attributed to the evaporation process resulted from entrainment. On the contrary, the reflectivity below 1.5 km get increased gradually with an increase of height, probably because of the condensation process which is driven by stronger updrafts until embryos of drizzle formed from the small cloud droplets. Furthermore, low-level clouds have a wide range of reflectivity values, illustrating the particle size of cloud droplets start to develop and evolve slowly to drizzle mode. The highest occurrence frequency of radar reflectivity in the range from -15 dBZ to 0 dBZ becomes pronounced when LWP is up to 0.5-1.0 kg m^{-2}, indicating that the clouds include the drizzle mode. As shown in Figure 1c, the value of radar reflectivity continues to increase with decreasing height and finally reaches 10 dBZ in the height of 0.5 km. This feature manifests that clouds gradually transfer from drizzle mode to rain mode and the raindrops start to develop. In figures 2d and 2e, the occurrence frequency of radar reflectivity becomes more obvious in the range from 0 to 15 dBZ, and even reaches 15 dBZ finally, revealing that the rain is severe when LWP is greater than 1.5 kg m^{-2}. On the whole, these features discussed above show a broad droplet spectrum including the processes of cloud droplets growth and transition to rain clouds associated with the increase of LWP.

CONCLUSIONS

The general macrophysical and microphysical characteristics of single-layer warm clouds over Hyytiälä area were examined using standard CloudSat/CALIPSO products during 2010. In order to better understand the transition processes over target areas, the LWP is used as an indicator for the life stages of clouds in this study. It is interesting to find that cloud base heights have a narrow mode between 1 and 1.5km, while the distribution of cloud top heights occurrence frequency shift from lower altitude to higher altitude as LWP increases in the Hyytiälä area. It reveals geometrical thickness of clouds increases following the evolution of warm clouds. The reflectivity profiles exhibit the vertical-structure of cloud particles which are possibly connected to microphysical processes for increasing cloud LWP. For illustrating the growth processes from cloud droplets to drizzle and precipitation associated with clouds, the CFADs of radar reflectivity and their change with an increase of LWP are explored.

In summary, the study will greatly help to understand the macrophysics and transitional processes and relationships among cloud droplets, drizzle and precipitation in warm clouds over Hyytiälä. This knowledge is needed when judging the effects of biogenic aerosols originating from the boreal forest

system on cloud albedo and precipitation. The changing cloud properties in turn are an important factor for the radiation processes over Hyytiälä. Therefore it is expected that the work will contribute significantly to our analysis of bio-geophysical feedback based on in-situ measurements and satellite data.

ACKNOWLEDGEMENTS

We thank CloudSat Data Processing Center at CIRA/Colorado State University for providing the CloudSat data products used in our work.
Academy of Finland Center of Excellence on Atmospheric Sciences and Nordic Center of Excellence in e-Science (E-STICC).

REFERENCES

Chen, R., Z. Li, R. J. Kuligowski, R. Ferraro and F. Weng (2011). A study of warm rain detection using A-Train satellite data, Geophys. Res. Lett., 38, L04804, doi:10.1029/2010GL046217.

Hartmann, D.L., M.E. Ockert-Bell and M.L. Michelsen (1992). The effect of cloud type on Earth's energy balance: Global analysis, J. Clim. 5, 1281-1304.

Haynes J.M. and G.L. Stephens (2007). Tropical oceanic cloudiness and incidence of precipitation: early results from CloudSat. Geophys Res Lett, 34: L09811, doi:10.1029/2007GL029335.

L'Ecuyer, T. S., W. Berg, J. Haynes, M. Lebsock and T. Takemura (2009). Global observations of aerosol impacts on precipitation occurrence in warm maritime clouds, J. Geophys. Res., 114, D09211, doi:10.1029/2008JD011273.

Marchand, R., G. G. Mace, T. Ackerman and G. Stephens (2008). Hydrometeor detection using CloudSat-An earth-orbiting 94-GHz cloud radar, J. Atmos. Oceanic Technol., 25, 519–533.

Petty, G. W. (2006). A First Course in Atmospheric Radiation, 2nd ed., pp. 452, Sundog Pub, Wisconsin.

Polonsky, I., et al. (2008), CloudSat Project: Level 2 Cloud Optical Depth Product Process Description and Interface Control Document, pp. 21, Colo. State Univ., Fort Collins.

Sassen, K., Z. Wang (2011). The clouds of the middle troposphere: composition, radiative impact, and global distribution. Surveys in Geophysics, 33:677-691, doi:10.1007//s10712-011-9163-x.

Stephens G.L., D.G. Vane, R.J. Boain, G.G. Mace, K. Sassen, Z. Wang, et al (2002). The CloudSat mission and the A-Train. Bull Am Meteorol Soc. 83 (12),1771-1790.

Suzuki, K., G. Stephens, S.C. Van de Heever, T.Y. Nakajima (2011). Diagnosis of the warm rain process in cloud-resolving models using joint CloudSat and MODIS observations. J. Atmos. Sci. 68, 2655-2670, doi:10.1175/JAS-D-10-05026.1.

Webb, M., C.A. Senior, D.M.H. Sexton, W.J. Ingram, et al (2006). On the contribution of local feedback mechanisms to the range of climate sensitivity in two GCM ensembles. Clim. Dyn. 27(1), 17-38.

Wood, N. (2008). CloudSat Project: Level 2B Radar-Visible Optical Depth CloudWater Content (2B-CWC-RVOD) Process Description Document, pp. 26, Colo. State Univ., Fort Collins.

EFFECTS OF THE SOIL FREEZE−THAW PROCESS ON THE REGIONAL CLIMATE OF THE TIBET PLATEAU

SIQIONG LUO, BOLI CHEN, SHIHUA LÜ, YU ZHANG, DI MA

Key Laboratory of Land Surface Process and Climate Change in Cold and Arid Regions, Cold and Arid Regions Environmental and Engineering Research Institute, Chinese Academy of Sciences, Lanzhou 730000, China

Keywords: TIBET PLATEAU · SOIL FREEZE−THAW PROCESS · REGIONAL CLIMATE EFFECT ·CLM3.5 · REGCM4

ABSTRACT: Single-point and regional simulation experiments on the Tibet Plateau, both with and without consideration of the soil freeze−thaw process, were set up with CLM3.5 and RegCM4 models. Comparison of the simulated soil temperature and moisture, surface energy flux, and upper−lower atmospheric circulation showed that the regional climate can be influenced by the freeze−thaw process of soil. The results indicate that the freeze−thaw process is a buffer to the seasonal changes in soil and near-surface temperatures and strengthens the energy exchange between the soil and the atmosphere. During the freeze (thaw) process, releasing (absorbing) of phase change energy retards the cooling (heating) effect of air temperature on soil. The soil freeze−thaw process increases (decreases) the surface heat source of the plateau in winter (summer), which increases (decreases) the near-surface temperature in winter (summer). Promoted by atmospheric circulation, the soil freeze−thaw process influences climate at the high and low altitudes of the plateau; this may also contribute to the maintenance of the South Asia High. In the early stages of permafrost degradation, the regional climate effects of freezing and thawing may accelerate the degradation of permafrost.

ONSET OF NEW PARTICLE FORMATION WITHIN A RISING MIXED BOUNDARY LAYER: ZEPPELIN FLIGHTS OVER HYYTIÄLÄ

H. E. MANNINEN[1], J. LAMPILAHTI[1], S. MIRME[2], T. NIEMINEN[1,3], M. EHN[1,4], I. PULLINEN[4], K. LEINO[1], S. SCHOBESBERGER[1], J. KANGASLUOMA[1], T. YLI-JUUTI[1,3], R. TILLMANN[4], R. KRECJI[1,5], R. VÄÄNÄNEN[1], A. WAHNER[4], D. R. WORSNOP[1], F. ROHRER[4], T. PETÄJÄ[1], T. F. MENTEL[4] and M. KULMALA[1]

[1]Department of Physics, University of Helsinki, Finland.

[2]Institute of Physics, University of Tartu, Estonia.

[3](now at) Department of Applied Physics, University of Eastern Finland, Kuopio, Finland.

[4]Institute for Energy and Climate Research, Forschungszentrum Jülich, Germany.

[5]Department of Environmental Science and Analytical Chemistry & Bolin Centre for Climate Research, Stockholm University, Sweden.

Keywords: ATMOSPHERIC PARTICLES, NUCLEATION AND GROWTH, PBL, BOREAL FOREST.

INTRODUCTION

At this moment, the mechanisms of secondary particle formation and the vapours participating in this process are not truly understood. Especially, in which part of the atmosphere the new particle formation takes place and which are the triggering chemical compounds, is still an open question. Until now, there exists only a few atmospheric dataset measured in lower troposphere over the Northern boreal forests. Our aim is to supplement the on-ground measurements with airborne measurements to cover the cryosphere-aerosol-cloud-climate interactions within the planetary boundary layer (PBL). The PBL is chemically and physically the most dynamic part of the atmosphere as it has high loading of aerosol particles and their gaseous precursors. Within PEGASOS project (European FP7-project), we measured the chemical and physical processes within the PBL to detect directly the very first steps of particle formation in the atmosphere. These measurements of the vertical and the horizontal extension of secondary particle formation were performed using an instrumented airship, Zeppelin (Manninen et al., in preparation). In addition to an instrumented airship, we had Cessna aircraft measurements (Schobesberger et al., 2013), and ground based in-situ measurements (Petäjä et al., in preparation). Using Zeppelin, we focused on the time of the development of the PBL (altitudes up to 1 km) from sunrise until noon to measure vertical profiles of aerosol particles and chemical compounds. This is also the time when new particle formation typically occurs at ground level.

METHODS

On spring 2013, Zeppelin was measuring nucleation occurring in the boreal forest area, Southern Finland, especially over Hyytiälä field site. SMEAR-II (Station for Measuring Forest Ecosystem–Atmosphere Relations II) station located in Hyytiälä, Southern Finland (61°51´N, 24°17´E, 181 m a.s.l.). The station is equipped with extensive facilities to continuously and comprehensively measure forest-ecosystem–atmosphere interactions (Hari and Kulmala, 2005). Hyytiälä is a rural background site with low local particle matter emissions.

We aimed on measuring the vertical and the horizontal extension for particle formation events which are known to be regional, large scale phenomena at ground level. This because we can follow the homogenously growing nucleation mode particles starting from the early morning all the way until late afternoon (Kulmala et al., 2013). The vertical profile measurements with Zeppelin represent the particle and gas concentrations in the lower parts of the atmosphere: the residual layer, the nocturnal boundary layer, and the PBL. At the same time, the ground based measurements records present conditions in the surface layer. Horizontal, almost Lagrangian, experiments are possible as the airship drifts with the air mass. The key instruments to measure the onset of NPF were an Atmospheric Pressure interface Time-Of-Flight mass spectrometer (APi-TOF), a Particle Size Magnifier (PSM), and a Neutral cluster and Air Ion Spectrometer (NAIS). These instruments are able to measure particles at the size range ~1-2 nm where the onset of atmospheric nucleation and cluster activation takes place. The PSM and NAIS can be used to resolve directly the nucleation rate and growth rate, which are the dominant factors in determining how much cloud condensation nuclei can be produced via new particle formation. The instruments are described in more detailed in Kulmala et al. (2013) and reference therein.

We developed a supporting new particle formation forecast tool for airborne studies (Nieminen et al., 2015). Flight measurements are technically more demanding and require a greater detail of planning than field studies at the ground level. The high cost of flight hours and limited time available during a single research flight for the measurements demanded an analysis tool that would forecast whether or not there is a good chance for a NPF event. We developed a generalized methodology to derive particle formation event probability that was used to optimise flying hours. Based on the existing knowledge we derived a method for estimating the nucleation probability that utilizes forecast air mass trajectories, weather forecasts and air quality model predictions. With the forecast tool we were able to predict the occurrence of particle formation events for the next day with more than 90% success rate (Nieminen et al, 2015). This forecast tool is used during all flight campaigns.

RESULTS

The high time resolution of the instruments allowed us to observe the starting time, location and altitude of the new particle formation. The results suggest that the new particle formation begins simultaneously inside the mixed and the surface layer but does not take place in the residual layer (Manninen et al., in preparation). A case study from Hyytiälä, measured on May 8, 2013 shows that the regional particle formation begins simultaneously and evolved uniformly inside the mixed layer. When the zeppelin measures in the residual layer we see very little small ions (~0–11 cm^{-3}) and there is no apparent increase in their concentration. We estimate that the new particle formation began 8:40-8:46 at the ground site and 8:36–8:58 at the zeppelin, few hours after sunrise during the vertical growth of the mixed layer. Greater uncertainty in the zeppelin measurement time estimate is due to the zeppelin visiting the residual layer and not being able to measure inside the mixed layer.

After the onset of particle formation the small ion concentration is ~80-140 cm^{-3}. Similarly H_2SO_4 is homogeneous as a function of altitude inside the mixed boundary layer. Additionally, the total particle concentration in the size range of 2.5–3.0 nm within the boundary layer was observed homogenously distributed with respect to altitude. In general, higher total particle concentrations were measured on the ground at SMEAR-II station than higher within the developed boundary layer.

Interestingly, we observed both a regional and a “local” component of the NPF event. The regional NPF occurred over a large area, as expected, and was homogeneous at least inside the mixed layer covered by the measurement site. More interestingly, the “local” component of the NPF manifested as a long, narrow and concentrated plume of particles that moved horizontally across the measurement site as the local wind direction changed. The growth rate of the regional and “local” NPF event particles was approximately the same (~2 nm/h), whereas the concentration was with a factor 7 higher within the “local” plume.

These measurements are part of the PEGASOS project, an European collaboration project, which aims to quantify the magnitude of regional to global feedbacks between the atmospheric chemistry and physics, and thus quantify the changing climate. The Zeppelin flights are observing radicals, trace gases, and aerosols inside the lower troposphere over Europe in several locations during 2012-2013 (http://pegasos.iceht.forth.gr/). The main nucleation (particle formation focused) campaigns were performed in Po Valley, Northern Italy (Summer 2012), and Hyytiälä, Southern Finland (Spring 2013).

CONCLUSIONS

The high time resolution of the instruments allowed us to observe the starting time, location and altitude of the new particle formation. The onset of NPF was usually observed on-board Zeppelin when it was measuring inside the rising mixed layer which is connected to the surface layer by effective vertical mixing. The newly formed, subsequently growing, particles were observed to be homogeneously distributed inside the mixed layer.

ACKNOWLEDGEMENTS

This research has been funded by the ERC-Advanced "ATMNUCLE" grant no. 227463), the Academy of Finland (Center of Excellence project no. 272041), the Eurostars Programme under contract no. E!6911 and the European Commission under the Framework Programme 7 (FP7-ENV-2010-265148). The Zeppelin is accompanied by an international team of scientists and technicians. They are all warmly acknowledged.

REFERENCES

Hari, P. and Kulmala, M.: Station for measuring ecosystem–atmosphere relations (SMEAR II), *Boreal Environ. Res.*, 10, 315–322, 2005.

Kulmala, M., Kontkanen, J., Junninen, H., Lehtipalo, K., Manninen, H.E., Nieminen, T., Petäjä, T., Sipilä, M., Schobesberger, S., Rantala, P., Franchin, A., Jokinen, T., Järvinen, E., Äijälä, M., Kangasluoma, J., Hakala, J., Aalto, P.P., Paasonen, P., Mikkilä, J., Vanhanen, J., Aalto, J., Hakola, H., Makkonen, U., Ruuskanen, T.M., Mauldin III, R.L., Duplissy, J., Vehkamäki, H., Bäck, J., Kortelainen, A., Riipinen, I., Kurtén, T., Johnston, M.V., Smith, J.N., Ehn, M., Mentel, T.F., Lehtinen, K.E.J., Laaksonen, A., Kerminen, V.-M. and Worsnop, D.R.: Direct observations of atmospheric nucleation, *Science* 339, 943-946, doi:10.1126/science.1227385, 2013.

Nieminen, T., Yli-Juuti, T., Manninen H. E., Petäjä, T., Kerminen, V.-M., and Kulmala, M.: Technical Note: New particle formation event forecasts during PEGASOS-Zeppelin Northern mission 2013 in Hyytiälä, Finland. Atmos. Chem. Phys., 15, 12385-12396, doi:10.5194/acp-15-12385-2015, 2015.

Schobesberger, S.et al.: Airborne measurements over the boreal forest of southern Finland during new particle formation events in 2009 and 2010. Boreal Env. Res. 18: 145–163, 2013.

ENVIRONMENTAL AND CLIMATIC CHANGES IN THE NORTHERN HEMISPHERE AND INTERNATIONAL ECOLOGICAL CO-OPERATION

G.G. MATISHOV[1]

[1]Southern Scientific Centre of the Russian Academy of Sciences,
Rostov-on-Don, 344006, Russia.

Keywords: CLIMATE, NORTHERN HEMISPHERE, ECOLOGY, ECOSYSTEM.

INTRODUCTION

The climate of the Earth changes continuously. The character of climate evolution is partially determined by natural causes, such as variations of the parameters of the earth's orbit, variability of the components of meteorological regime and the long-term changes which characterize the climate fluctuations. Of certain impact is anthropogenic activity.

The marine ecosystems of the Northern Hemisphere are geologically relatively young and are in the process of constant development in conformity with the global climate variability and anthropogenic impact. To understand climate and paleoclimate it is important to be aware of the development of the global climatic zones. Under the influence of the global climatic fluctuations, the outlines, sizes, and the conditions of tropical and bipolar belts changed. During the warming period the latitude gradients of temperatures decreased and the width of tropical belt increased, while during the cooling period the reverse situation was observed. There was the belt of oceanic periglacial outside the continental glaciations. Turbidity currents and streams, which originated from the melting of glacial shields of Scandinavia, Iceland, Greenland, Canada, spread over the continental slope forming a dense network to the abyssal plains. Huge Scandinavian glacier started to melt 14 thousand years ago. Part of the thawing water runoff entered the Caspian Sea and the Azov-Black Sea basin by the Volga, Don, and Dnieper. The Late Holocene had a complex rhythmical pattern of natural processes and covered both the periods of cooling and warming. It is in particular typical of the last millennium within which the Little Ice Age and Medieval Climate Optimum (AD 950-1250) may be determined in different regions of the Northern Hemisphere.

METHODS

A series of paleontological methods is applied to reconstruct the climate of different chrono-sections of the Pleistocene and Holocene. The Sea of Azov being a large estuarine water body is a good example for the studies of paleoclimate. The Sea of Azov started to form as an independent sea basin in the beginning of the Holocene and ancient Azov and New Azov layers may be determined. By the current moment vast research material and data have been accumulated by the institutes of the Russian Academy of Sciences, which allow studying specific geomorphologic features and stratigraphy of the New Azov sediments in detail, determining the mean sedimentation rate of the New Azov deposits, determining the main regularities of spore and diatom algae distribution. Sea deposits accumulated within the Sea of Azov contain information both about the changes of physical-geographical conditions in the coastal areas and the entire South of the East European Plain. Studying paleo-soils is important for the restoration of fertility of the contemporary steppe black soil areas. As a result, we may say that the general trend towards aridification of climate covering the entire South of the East European Plain was not continuous in the Sub-Boreal and Sub-Atlantic periods of the Holocene. At least three periods with much more humid conditions have been determined in the spore-pollen spectra of sea deposits, with each lasting for several centuries: in the Late Sub-Boreal, in the Middle Sub-Atlantic, and during the Little Ice Age.

The most significant increase of the heat and moisture availability/content over the entire space of non-tropic Eurasia took place during the optimum of the last inter-glacial period. The temperature of January significantly increased in the northern areas of the continent with deviations being 12-10˚C. The value of deviations gradually decreased in western and southern directions, though temperature values remained higher than the current ones by 1-2˚C on the territories of Kazakhstan, the Northern Caspian and Azov-Black Sea Regions. In July the area of the highest temperature increase (by 8-6˚C) shifted to North-East of Europe. At the same time, the annual amount of precipitations increased by 100 mm (up to 300 mm in the West) in the southern regions (the Azov-Black Sea and Central Asia) while along the polar basin coasts it reached 200 mm.

Overall, it should be noted that during the warming period a certain heat availability increase was observed on the territories of the moderate and high latitudes of Eurasia (though at different levels). The redistribution of precipitation amount followed a different pattern. The value of precipitation increased in the direction of lower latitudes, thus contributing to biotic processes in the arid landscape systems typical of the latitudes. It seems probable that the formation of such landscapes in the past favoured, for example, the operation and functioning of and along the Great Silk Route/Road.

The key factor to determine the current status of marine ecosystem conditions, for example, is the quantitative output from spatial and temporal time-series of indicators of change. To cope with the issue a five module array of indicators linking natural science to social science metrics has been applied to assess changing conditions in Large Marine Ecosystems (LMEs): (i) productivity, (ii) fish and fisheries, (iii) pollution and ecosystem health, (iv) socioeconomics, and (v) governance (Sherman 2014b). The modules are customized for each LME through the application of a transboundary diagnostic analysis (TDA) and the development of a strategic action plan (SAP) prepared by the nations sharing LME goods and services.

CONCLUSIONS

A specific analysis of possibilities of applying the similar patterns of global climate changes in the past when planning the economic development between eastern and western regions of Eurasia under the conditions of current and future global climate changes should be carried out.

The interaction of the organism and environment is an integrated complex of interrelations and the progress in the environmental studies nowadays may be achieved only on condition that there is a synthesis of various research directions and efforts of scientists from different countries.

REFERENCES

Matishov, G.G. (1987). *The World Ocean and Glaciation of the Earth,* (Mysl', Moscow, USSR) (in Russian).

Velichko, A.A. (Ed.) (1993). *Development of Landscapes and Climate of Northern Eurasia: Late Pleistocene – Holocene, Vol. I* (Nauka, Moscow, Russia) (in Russian).

Sherman, K., M. Sissenwine, V. Christensen, A. M. Duda, G. Hempel, C. Ibe, S. Levin, D. Lluch-Belda, G. Matishov, J. McGlade, M. O'Toole, S. Seitzinger, H. R. Skjoldal, Q. Tang, J. Thulin, V. Vandeweerd and K. Zwanenburg (2005). A global movement toward an ecosystem approach to marine resources management. *Marine Ecology Progress Series, 300* (Theme Section: Politics and socio-economics of ecosystem-based management of marine resources): 275-279.

Sherman, K. (2014b). Toward ecosystem-based management (EBM) of the world's large marine ecosystems during climate change. *Environmental Development,* 11: 43-66.

ANALYSIS OF LONG-TERM CARBON STOCKS IN PERMAFROST-DOMINATED FOREST ECOSYSTEMS OF NORTH-EAST RUSSIA

T.C. MAXIMOV, A.V. KONONOV, A.P. MAKSIMOV, R.E. PETROV, M.P. TERETENTYEVA

Institute for Biological Problems of Cryolithozone, SB RAS

Institute for Natural Sciences, North Eastern Federal University

This report presents the results of long-term monitoring studies (2000-2015) on flux tower measurements in permafrost forest ecosystems (moderate and high productivities) using eddy-covariance and IRGA approaches in North-East Russia under conditions of global warming.

The basic components of ecosystem gas exchange were studied: photosynthesis and respiration of plants, respiration of ecosystems and NEE depending on hydrological and temperature regimes of the growing season.

Biogeochemical, physiological, and biochemical features of the main components of the carbon cycle of forest ecosystems were assessed, as well as an estimation of the components of carbon dioxide exchange of ecosystems was done, and the effect of exogenous and endogenous environmental factors on the carbon cycle was investigated.

The multiyear results showed that one hectare of permafrost forests with Larix cajanderi in the North-East of Russia in the process of photosynthesis sequestrated up to 1.5±0.2 t C ha^{-1} $season^{-1}$ in extremely dry years and up to 4.0±0.2 t C ha^{-1} $season^{-1}$ in wet years, which is 2.5 times more than in dry seasons.

The main factor affecting the rate of soil respiration in permafrost forests of the North-East of Russia is rather soil temperature than precipitation. Precipitation causes short peaks of CO2 emission by soil and almost does not affect the seasonal balance of soil carbon flux. So, in dry years, up to 3.5±0.1 t C ha^{-1} $year^{-1}$ is released on average, and in wet years, the intensity of soil CO_2 emission increases 1.2-1.7 times, reaching 5.2±0.2 t C ha^{-1} $year^{-1}$.

Interannual variation of Net Ecosystems Exchange in the permafrost zone is 1.7 to 2.4 t C ha^{-1} $year^{-1}$, which results in the upper limit of annual deposit capacity of 450-617 M t C $year^{-1}$, with the total area of these forests in Russia being 257.1 M ha.

The larch forests of Siberia accumulate annually 0.4 to 1.0 G t C $year^{-1}$. Net Biome Productivity of Siberian larch forests are estimated in the range of 0.26-0.86 G t C year-1depending on hydro-thermal conditions of the growing season.

CLUSTER EVENTS IN A BOREAL FOREST: COMPARING NIGHT-TIME WITH DAY-TIME ION CLUSTERS FROM 2003–2013

S. B. MAZON[1], J. KONTKANEN[1], H. E. MANNINEN[1], T. NIEMINEN[1], V.-M. KERMINEN[1], M. KULMALA[1]

[1]Department of Physics, University of Helsinki, Finland.

Keywords: NIGHTTIME EVENTS, NEW PARTICLE FORMATION, ATMOSPHERIC IONS, AEROSOLS.

INTRODUCTION

New particle formation (NPF) events are commonly observed and studied during daylight hours when photochemical oxidation takes place. However, nucleation mode particles have been observed intermittently during the night-time in various locations around the world (eg. Suni *et al.* 2008 for Tumbarumba, Australia; Kalivits *et al.* 2012 for Finokalia, Crete; Junninen *et al.* 2008 and Lehtipalo *et al.* 2011 for Hyytiälä, Finland; Kecorius *et al.* 2015 for Beijing, China). This study presents 11 years (2003–2013) of ion data from SMEAR II station, Hyytiälä, Finland, where a third (30–34%) of the days presented a nocturnal sub-3 nm event in both positive and negative polarities. Furthermore, 2–3 nm negative ion events (or *cluster events*, CE) were identified during night-time (18:00–24:00) and compared to 2–3 nm ion concentrations during daytime NPF events in order to investigate if stable clusters can form and grow (Kulmala *et al.* 2014) past the constant ion pool during night-time.

METHODS AND CONCLUSIONS

An 11 year (2003–2013) time series of ion data from SMEAR II station, Hyytiälä, Finland, was analysed for sub-3 nm nocturnal events. Positive and negative ion data was obtained from the Balancing Scanning Mobility Analyser (BSMA; Tammet 2014) with a size range from ~0.8–8 nm (mobility range of 3.2–0.032 $cm^2 V^{-1} s^{-1}$). Data were visually analysed using 48-h number size concentration surface plots, with midnight between Day 1 and Day 2 as the centre of the plot, in parallel with positive and negative 0.9–3 nm ion diurnal concentrations. A nocturnal ion event was classified as such based on an increase in ion concentration and a visual 'bump' (in a higher size channel) on the surface plot.

A third of the data presented an event during the median time window of 19:00–04:00 hrs in both polarities (negative ions: n = 1324 d, positive ions: n = 1172 d). To investigate nocturnal clustering outside the constant small ion pool (<2 nm), we identified nocturnal events solely from the increase in negative ion concentration (≥70 cm–3) from the 2–3 nm ion band (hereafter 'cluster events', CE). The median CE 2–3 nm ion concentrations rose from a background ~10 cm–3 to an event peak of ~100 cm–3 between 19:00–20:30 local time (Fig. 1). A similar analysis of 2–3 nm ion concentrations was applied to daytime hours (08:00–12:00) during ongoing NPF events. Similar median 2–3 nm ion concentrations were found during NPF events (39 cm^{-3}) and CE (31 cm^{-3}), clearly higher than during non-event days and nights (~1.9 and 2.6 cm^{-3}, respectively). While the cluster ion pool (0.9–1.5 nm) median concentrations were similar in day and night events and non-events, CE showed enhanced small ion concentrations (1.5–2 nm; median 235 cm^{-3}) compared to NPF days (96 cm^{-3}) and day- and night-time non-events (~20 cm^{-3}). This indicates a substantial enhancement of small ions is occurring during CE nights, which can surpass those during NPF events. However, in terms of possible growth, concentrations of ~2.4–7 nm ions were substantially lower during CE (median: <10 cm^{-3}), compared to NPF events (median: 52 cm^{-3}), indicating ions >3 nm in size are not effectively produced in the night-time. Additionally, most CE nights (90%) occurred following an NPF or an undefined day, with only 10% occurring after a daytime non-event. This study (Mazon *et al.* 2016) suggests an enhancement of small ion clusters is a common occurrence in nighttime (18:00–24:00) Hyytiälä, with ion concentration levels similar to those during daytime NPF, but which fail to grow into larger sizes.

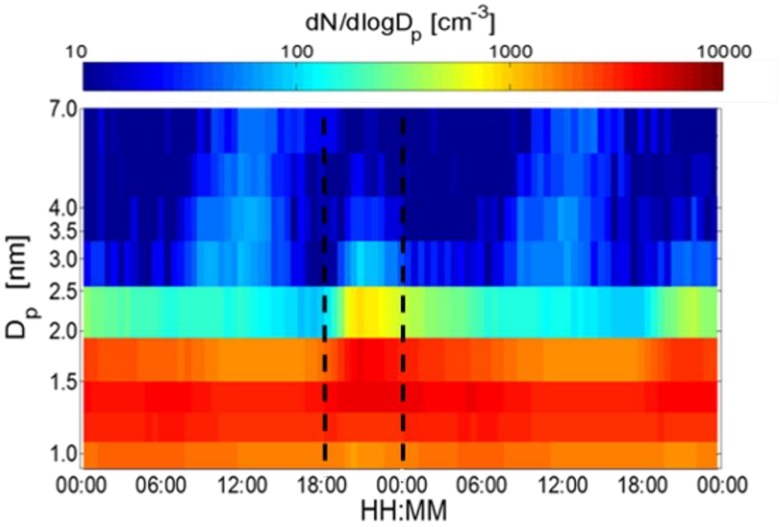

Figure 1. An 48-h average (n = 166 d) BSMA number concentration surface plot for nocturnal cluster events (CE) classified as such from 2–3 nm negative ion concentrations. The CE can be seen between 18:00–24:00 hrs of the first day. The presence of NPF events is evident in both days around noon.

ACKNOWLEDGEMENTS

This project has received funding from the European Union's Horizon 2020 research and innovation programme under grant agreement No 654109 (ACTRIS-2), and the European Union Seventh Framework Programme (FP7/2007-2013) under grant agreement n° 262254 (ACTRIS). We also thank the Academy of Finland Center of Excellence program, the Cryosphere-Atmosphere Interactions in a Changing Arctic Climate (CRAICC), and the European Research Council Project (ATMNUCLE).

REFERENCES

Junninen, H., Hulkkonen M., Riipinen I., Nieminen T., Hirsikko A., Suni T., Boy M., Lee S.-H., Vana M., Tammet H., Kerminen V.-M. and Kulmala M. (2008). Observations on nocturnal growth of atmospheric clusters, *Tellus* **60B**, 365–371.

Kalivitis, N. Stavroulas I., Bougiatioti A., Kouvarakis G., Gagné S., Manninen H. E., Kulmala M. and Mihalopoulos N. (2012). Night-time enhanced atmospheric ion concentrations in the marine boundary layer, *Atmos. Chem. Phys* **12**, 3627–3638.

Kecorius S., Zhang S., Wang Z., Gröss J., Ma N., Wu Z., Ran L., Hu M., Wang P., Ulevicius V. and Wiedensohler A. (2015). Nocturnal aerosol particle formation in the North China Plain. *Lithuanian J. Phys.*, **55**(1), 44–53.

Kulmala M, T. Petäjä, M. Ehn, J. Thornton, M. Sipilä, D.R. Worsnop and V.-M. Kerminen (2014). Chemistry of Atmospheric Nucleation*:* On the Recent Advances on Precursor Characterization and Atmospheric Cluster Composition in Connection with Atmospheric New Particle Formation, *Annu. Rev. Phys. Chem.* **65**, 21–37.

Mazon, S. B., J. Kontkanen, H. E. Manninen, T. Nieminen, V.-M. Kerminen and M. Kulmala (2016). Cluster events in a boreal forest: comparing night-time with day-time ion clusters in 2003–2013, *Boreal Environ. Res*., Spec Issue (in review).

Lehtipalo, K., Sipilä M., Junninen H., Ehn M., Berndt T., Kajos M. K., Worsnop D. R., Petäjä T. and Kulmala M. (2011) Observations of nano-CN in the nocturnal boreal forest. *Aerosol Sci Technol* **45**, 499–509.

Suni, T. M. Kulmala, A. Hirsikko, T. Bergman, L. Laakso, P. P. Aalto, R. Leuning, H. Cleugh, S. Zegelin, D. Hughes, E. van Gorsel, M. Kitchen, M. Vana, U. Horrak, S. Mirme, A. Mirme, S. Sevanto, J. Twining and C. Tadros (2008). Formation and characteristics of ions and charged aerosol particles in a native Australian Eucalypt forest, *Atmos Chem Phys* **8**, 129–139, doi:10.5194/acp-8-129-2008.

Tammet, H. (2006) Continuous scanning of the mobility and size distribution of charged clusters and nanometer particles in atmospheric air and the Balanced Scanning Mobility Analyzer BSMA . *Atmos Res* **82**, 523–535.

LIGHT ABSORBING PARTICLES AND DENSITY OF MELTING SURFACE SNOW

O. MEINANDER[1], A. VIRKKULA[1,2], A. KONTU[3], J. SVENSSON[1], H.-R. HANNULA[1], DAGSSON-WALDHAUSEROVA[4,5,6,7], P., AROLA[8], A., BACKMAN, L. [1], MANNINEN[1], T., DE LEEUW G. [1, 2] and M. LEPPÄRANTA[2]

[1]Finnish Meteorological Institute, Research and Development, Helsinki, Finland.

[2]Department of Physics, University of Helsinki, Finland.

[3]Arctic Research Center, Finnish Meteorological Institute, Sodankylä, Finland

[4] Agricultural University of Iceland, Faculty of Environmental Sciences, Hvanneyri, Iceland

[5] University of Iceland, Institute of Earth Sciences, Reykjavik, Iceland

[6] Czech University of Life Sciences Prague, Faculty of Environmental Sciences, Prague, Czech Republic

[7]University of Iceland, Faculty of Physical Sciences, Reykjavik, Iceland

[8]Finnish Meteorological Institute, Kuopio, Finland.

Keywords: BLACK CARBON, SOOT, SNOW DENSITY, SWE, SNOW MELT.

INTRODUCTION

Light absorbing particles deposited in snow can reduce albedo and increase snow melt (Bond et al. 2013). When the snow melt starts, the impurities can be washed down through the snow with melt water, or remain in the snow. For example, Black Carbon (BC) is less likely to be washed down through the snow with melt water (Doherty et al. 2013). We have investigated the relationship of snow impurities and surface snow density in case of Arctic seasonally melting snow. Referring to Meinander et al. (2014), no relationship is expected to be found for cold non-melting surface snow. Only the water retention capacity of melting dirty snow is expected to be diminished due to impurities, and a lower snow density follows.

METHODS

We have measured the density and the BC (Fig. 1) in the surface snow samples of Sodankylä (67°,25'N,26°35'E), Finland, beyond the Arctic Circle. BC was analyzed using the filter-based thermal-optical method, described in Forsström et al. (2009).

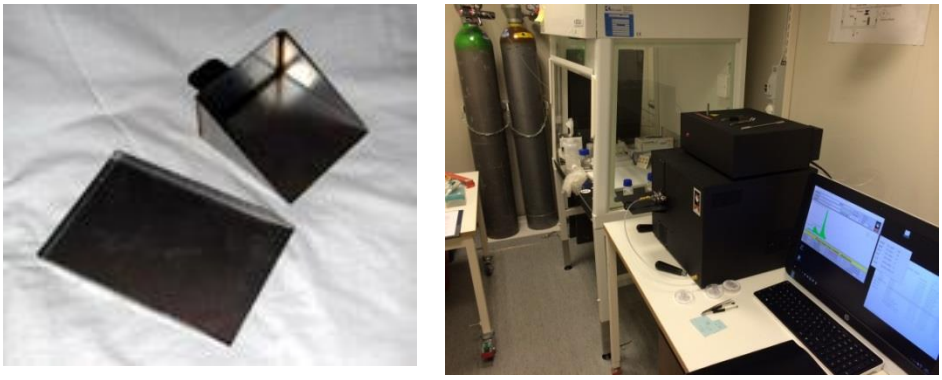

Figure 1. The Snow density cutter and the Sunset OC/EC Laboratory analyser.

We have gathered all our field and experimental data from Sodankylä during 2009-2013 (Table 1, Figures 2 and 3, and Fig. 2 of Meinander et al. (2014)). Thereafter, we have made additional laboratory experiments that confirm that the water holding capacity does indeed decrease when light absorbing impurities are artificially added in the snow. More recently, we have gained new Sodankylä field data for spring 2014, which also show some indication for a possible relationship of snow density and BC in this very small but independent field data set (Figure 3). The new BC data are collected and reported as [μg/cm^2] to have data that can be better utilized for transport modelling purposes.

BC (ppb)	Melting snow density (kg/m^3)
0-20	392
21-40	-
41-60	392,420, 428
61-80	368, 420
81-100	368, 420, 428
101-120	360, 368
121-140	360, 420, 428
141-160	-
161-180	-
181-200	380, 416
201-400	364, 392
401-600	360
601-800	368

Table 1. The experimental measurement data on Sodankylä melting surface snow density and BC.

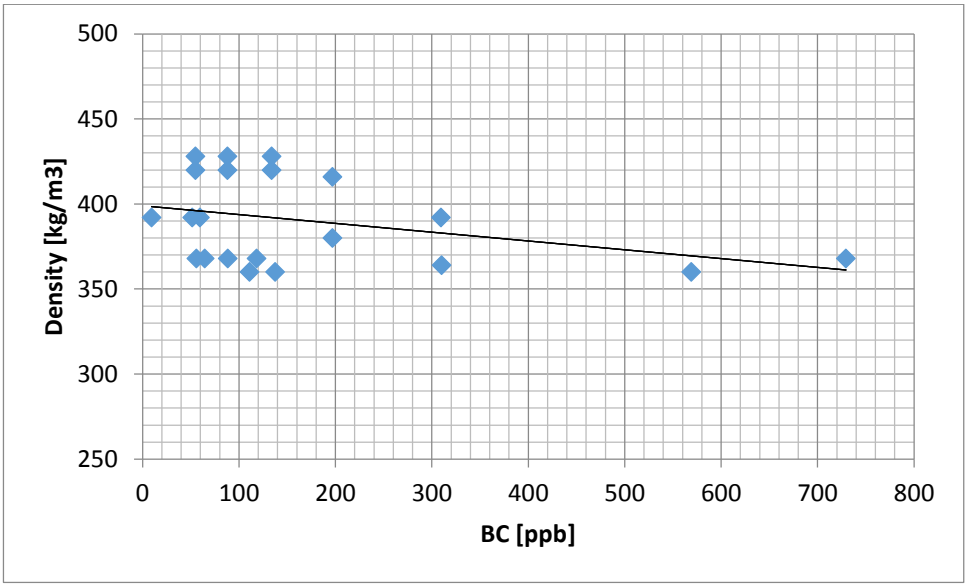

Figure 2. The BC [ppb] and density [kg/m^3] observations for melting surface snow in Sodankylä in 2009-2013.

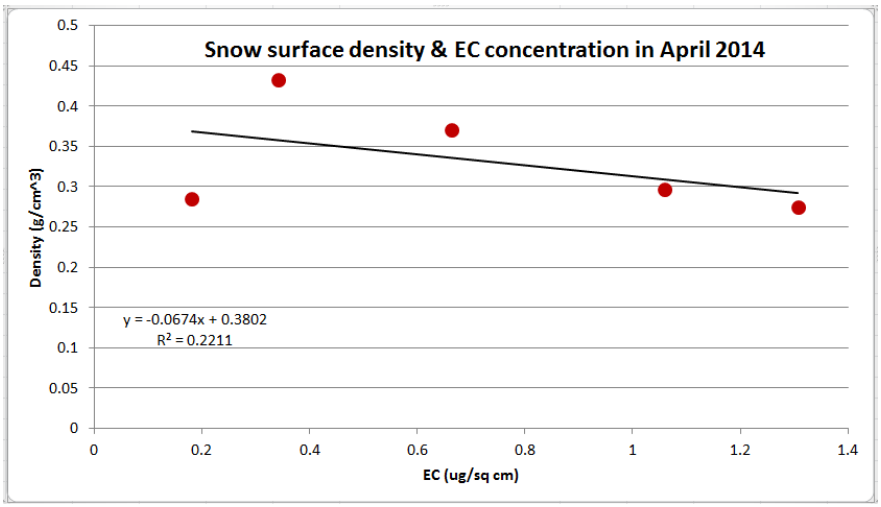

Figure 3. The BC [µg/cm^2] and density [g/cm^3] for melting surface snow of Sodankylä in April 2014.

CONCLUSIONS

More data from Sodankylä and elsewhere are needed to confirm further the observed relationship and to investigate if other parameters are essential to explain and understand the relationship of snow density and BC, in case of melting surface snow. Three possible reasons for the decreased snow density were suggested in Meinander et al. (2014). The importance of decreased density comes also as snow density multiplied by snow depth equals the important climate model parameter of snow water equivalent (SWE).

ACKNOWLEDGEMENTS

This work was supported by the Nordic Center of Excellence (NCoE) “Cryosphere-atmosphere interactions in a changing Arctic climate“ (CRAICC) Finnish Academy of Sciences Excellence project 272041, and the Academy of Finland project 254195 “Arctic Absorbing Aerosols and Albedo of Snow (A4)”.

REFERENCES

Bond, T. C., Doherty, S. J., Fahey, D. W., Forster, P. M., Berntsen, T., DeAngelo, B. J., Flanner, M. G., Ghan, S., Kärcher, B., Koch, D., Kinne, S., Kondo, Y., Quinn, P. K., Sarofim, M. C., Schultz, M. G., Schulz, M., Venkataraman, C., Zhang, H., Zhang, S., Bellouin, N., Guttikunda, S. K., Hopke, P. K., Jacobson, M. Z., Kaiser, J. W., Klimont, Z., Lohmann, U., Schwarz, J. P., Shindell, D., Storelvmo, T., Warren, S. G. and Zender, C. S.: Bounding the role of black carbon in the climate system: A scientific assessment, J. Geophys. Res.-Atmos., 118, 5380–5552, doi:10.1002/jgrd.50171, 2013.

Doherty, S. J., Warren, S. G., Grenfell, T. C., Clarke, A. D., and Brandt, R. E.: Light-absorbing impurities in Arctic snow, Atmos. Chem. Phys., 10, 11647–11680, doi: 10.5194/acp-10-11647-2010, 2010.

Forsström, S., Ström, J., Pedersen C. A., Isaksson, E., and Gerland, S.: Elemental carbon distribution in Svalbard snow, J. Geophys.Res., 114, D19112, doi:10.1029/2008JD011480, 2009.

Meinander, O., Kontu, A., Virkkula, A., Arola, A., Backman, L., Dagsson-Waldhauserová, P., Järvinen, O., Manninen, T., Svensson, J., de Leeuw, G., and Leppäranta, M.: Brief communication: Light-absorbing impurities can reduce the density of melting snow, The Cryosphere, 8, 991-995, doi:10.5194/tc-8-991-2014, 2014.

DOES INCREASING TEMPERATURE INCREASE CARBONACEOUS AEROSOL DIRECT RADIATIVE EFFECT?

T. MIELONEN[1], A. HIENOLA[2], H. KOKKOLA[1], T. KÜHN[1,3], J. MERIKANTO[2], H. KORHONEN[2], A. AROLA[1], P. KOLMONEN[2], L. SOGACHEVA[2], S. ROMAKKANIEMI[1] and G.F.R DE LEEUW[2]

[1] Finnish Meteorological Institute, Kuopio, Finland.

[2]Finnish Meteorological Institute, Helsinki, Finland.

[3]University of Eastern Finland, Applied Physics, Kuopio, Finland.

Keywords: REMOTE SENSING, CLIMATE MODELLING, AEROSOL, LAND SURFACE TEMPERATURE.

INTRODUCTION

Aerosols are an important regulator of the Earth's climate. They scatter and absorb incoming solar radiation and thus cool the climate by reducing the amount of energy reaching the atmospheric layers and the surface below (direct effect) (e.g. Charlson et al., 1992). A certain subset of the particles can also act as initial formation sites for cloud droplets and thereby modify the microphysics, dynamics, radiative properties and lifetime of clouds (indirect effects) (Albrecht, 1989; Twomey, 1991; Stevens and Feingold, 2009). The magnitude of aerosol radiative effects remains the single largest uncertainty in current estimates of anthropogenic radiative forcing (IPCC, 2013).

One of the key quantities needed for accurate estimates of anthropogenic radiative forcing is an accurate estimate of the radiative effects from natural unperturbed aerosol. The dominant source of natural aerosols over Earth's vast forested regions are biogenic volatile organic compounds (BVOC) which, following oxidation in the atmosphere, can condense onto aerosol particles to form secondary organic aerosol (SOA) and significantly modify the particles' properties. In accordance with the expected positive temperature dependence of BVOC emissions (Penuelas and Staudt, 2010; Duncan et al., 2009), several previous studies have shown that some aerosol properties, such as mass concentration and ability to act as cloud condensation nuclei (CCN), also correlate positively with temperature at many forested sites (e.g. Tunved et al., 2006; Leaitch et al., 2011; Paasonen et al., 2013). There is conflicting evidence as to whether the aerosol direct effects have a temperature dependence due to increased BVOC emissions.

The main objective of this study is to investigate the causes of the observed effect of increasing temperatures on the aerosol direct radiative effect, and to provide a quantitative estimate of this effect and of the resulting negative feedback in a warming climate. More specifically, we will investigate the causes of the positive correlation between aerosol optical depth (AOD) and land surface temperature (LST) over boreal forests where biogenic emissions are a significant source of atmospheric particles. In addition to BVOCs, SOA formed in clouds and biomass burning emissions could also explain the temperature dependence of aerosol direct radiative effect.

METHODS

The study is done using a combination of satellite data and climate modelling. Key remote sensing data used are the aerosol optical depth and land surface temperature products available from the ESA Aerosol-CCI and GlobTemperature projects, together with ancillary data, such as column concentrations of carbon monoxide (CO), nitrogen dioxide (NO_2) and water vapour, and aerosol profiles and soil moisture. For the

modelling work we are using the aerosol-chemistry climate model ECHAM-HAMMOZ, which describes all known relevant atmospheric aerosol processes.
The core data sets for this study are provided by the Advanced Along Track Scanning Radiometer (AATSR) that flew on the ESA polar orbiting Environmental Satellite ENVISAT (2002-2012). We are using AATSR AOD data available from the ESA Aerosol CCI project and AATSR LST data from ESA's GlobTemperature project. More specifically, we are using daily Level 3 AOD data with spatial resolution of 1x1 degrees from the full mission (2002-2012). The Level 3 data with spatial resolution of 1x1 degrees was chosen because it is close to the spatial resolution of climate models.

AOD retrieved from satellite radiance data contains contributions from all aerosol types present in the atmospheric column. To discriminate the natural contributions to the AOD from other contributions (such as aerosol particles emitted by forest fires or pollution transported from elsewhere), we are using ancillary data. Since we focus on remote areas of Eurasia, we need to rely on satellite data since ground-based information is very sparse. Here we are using the daily Level 3 CO column concentration data retrieved from NASA's Atmospheric Infrared Sounder (AIRS) instrument for the years 2002-2012. CO is used as a proxy for biomass burning aerosols available from satellite-based measurements. In addition, we are using Level 3 total column water vapour measurements from the same instrument. The water vapour burden is used in the evaluation of model output and in our analysis of the satellite based AOD-LST relationship. In addition, we are using the following NASA products to support our analysis: NO_2 from the Ozone Monitoring Instrument (OMI) and aerosol profiles from the Cloud-Aerosol Lidar with Orthogonal Polarization (CALIOP). NO_2 is used to identify aerosols that are mixed with anthropogenic pollution. Daily Level 3 OMI NO2 data are available from 2005 onwards. The Level 3 aerosol profiles from CALIOP are monthly data with 2×5 degree spatial resolution, which are available from 2006 onward. The CALIOP profiles are used in the evaluation of the vertical distribution of aerosols in the climate model. Furthermore, we are using data from ESA's Soil Moisture-CCI. The homogenized and merged soil moisture product provides daily surface soil moisture with a global coverage and a spatial resolution of 0.25°. Soil moisture information is used in the evaluation of model output and in our analysis of the satellite based AOD-LST relationship.

ECHAM-HAMMOZ is an aerosol-chemistry climate model which model describes all known relevant atmospheric aerosol processes: emissions, removal, aerosol microphysics, chemistry, radiative effects, and aerosol-cloud interactions. It includes the main atmospheric aerosol compounds: sulfate, organic carbon, sea salt, black carbon and mineral dust. Moreover, ECHAM-HAMMOZ includes the interactive biogenic emission model MEGAN, which determines emissions of terpenes and isoprenes as a function of temperature, available solar radiation, soil moisture, and carbon dioxide concentrations. For biomass burning emissions, the Global Fire Emissions Database (GFED) is used. In this study, we simulate the years 2002-2012 which are covered by satellite observations. Simulations are nudged using ECMWF reanalysis data to ensure compatibility between the model and the observed atmospheric conditions.

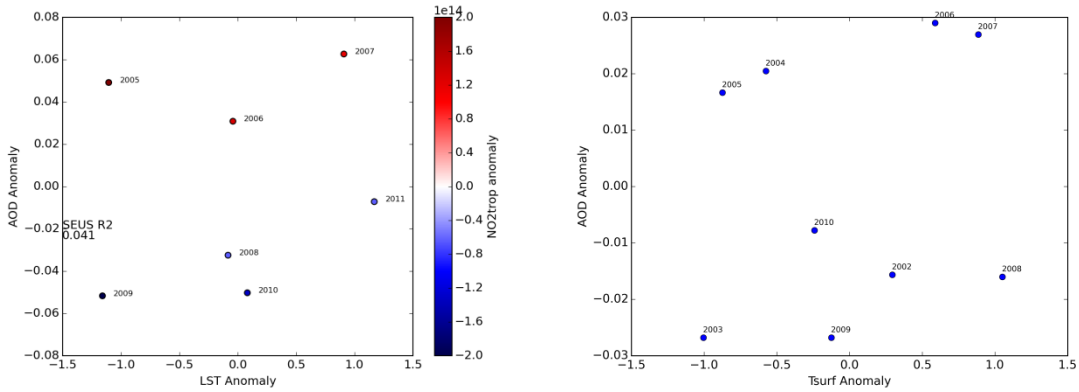

Figure 1. Interannual anomalies in summertime regional mean temperature vs. aerosol optical depth over southeastern US for 2003-2011 a) based on AATSR retrievals b) ECHAM-HAMMOZ simulations. The color scale in the left column represents the tropospheric NO_2 anomalies.

CONCLUSIONS

Goldstein et al. (2009) detected an exponential dependence between the temperature and AOD in southeastern US, and hypothesized it to arise from enhanced natural BVOC emissions on warmer days. As a first step in our work, we wanted to check if we are able to detect a similar feature with the AATSR data sets and with the climate model. For the period from 2000 to 2005, AATSR data showed similar AOD-temperature dependency as reported by Goldstein et al. (2009). On the other hand, for the whole dataset from 2000 to 2010, there is no clear dependency between AOD and LST. This is illustrated in Figure 1, in which panel a) shows the AOD anomaly as a function of LST anomaly, and panel b) shows the modelled AOD anomaly as a function of surface temperature. However, another factor that showed significant correlation was NO_2, which can be considered a proxy for anthropogenic pollution. From Figure 1 a), it can be seen that the highest AOD anomalies correspond to the highest tropospheric NO_2 anomalies. This indicates that the dominant factor affecting AOD anomalies comes from anthropogenic emissions. When the data was normalized with the NO_2 anomaly, there remained a correlation between AOD and LST which can be caused by BVOC's

ACKNOWLEDGEMENTS

This research has received funding from the Academy of Finland Centre of Excellence (grant no. 272041) and the Living Planet Fellowship (ESA).

REFERENCES

Albrecht, B.A. (1989). Aerosols, Cloud Microphysics, and Fractional Cloudiness. Science 245 (4923): 1227–30.

Charlson et al., 1992 Charlson, R. J., Schwartz, S. E., Hales, J. M., et al. (1992). Climate forcing by anthropogenic aerosols. Science 255, 423–430.

Goldstein, A.H., C.D. Koven, C.L. Heald, I. Fung (2013). Biogenic Carbon and Anthropogenic Pollutants Combine to Form a Cooling Haze over the Southeastern US, Proceedings of the National Academy of Sciences, 106, 8835-8840.

International Panel on Climate Change (2013). Climate Change 2013: The Physical Science Basis. Contribution of Working Group I to the Fifth Assessment Report of the Intergovernmental Panel on Climate Change, edited by: Stocker, T. F., Qin, D., Plattner, G.-K., Tignor, M., Allen, S. K., Boschung, J., Nauels, A., Xia, Y., Bex, V., and Midgley, P. M., Cambridge University Press, Cambridge, United Kingdom and New York, NY, USA, 1535 pp., 2013.

Leaitch, W. R. et al., 2011, Temperature response of the submicron organic aerosol from temperate forests, Atmos Env., 45, 6696-6704.

Paasonen, P., Asmi, A., Petäjä, T., Kajos, M. K., Aijala, M., Junninen, H., Holst, T., Abbatt, J. P. D., Arneth, A., Birmili, W., van der Gon, H. D., Hamed, A., Hoffer, A., Laakso, L., Laaksonen, A., Leaitch, W. R., Plass-Duelmer, C., Pryor, S. C., Raisanen, P., Swietlicki, E., Wiedensohler, A., Worsnop, D. R., Penuelas, J. and Staudt, M., 2010, BVOCs and global change, Trends in Plant Sci., 15, 133-144.

Stevens, B., and G. Feingold (2009). Untangling aerosol effects on clouds and precipitation in a buffered system. Nature, 461, doi:10.1038/nature08281

Tunved, P., Hansson, H. C., Kerminen, V-M., Strom, J., Dal Maso, M., Lihavainen, H., Viisanen, Y., Aalto, P. P., and Komppula, M., Kulmala, M. (2006). High natural aerosol loading over boreal forests. Science, 312(5771), 261-263. 10.1126/science.1123052.

Twomey, S. (1991). Aerosols, clouds, and radiation. Atmos. Environ., 25, 2435–2442.

REMOTE-SENSING INDICATORS OF URBAN EFFECTS IN THE ARCTIC: FOCUS ON NORTHERN WEST SIBERIA

V. V. MILES [1] & I. A. EZAU [1]

[1]Nansen Environmental and Remote Sensing Center, N-5006, Norway, Bergen /Bjerknes Centre for Climate Research, N-5007 Bergen, Norway
E-mail: victoria.miles@nersc.no

Urbanization in the Arctic and sub-Arctic is an increasingly important anthropogenic influence on climate, and has significantly affected terrestrial ecosystems. The most evident effects associated with urbanization are the transformation of natural ecosystems, as well as the urban heat island effect (UHIE), when urban and suburban areas are warmer then rural areas. To test the urbanization effect in the Arctic we focus on northern West Siberia, where we compare the effect of recent urbanization as well as the effect of the climate change on the vegetation across several northern bioclimatic zones. Twenty-eight urban areas, some with more than 100,000 inhabitants, were selected. We use a combination of remote-sensing indicators and investigate how changes in population growth and urban development affect the ecosystems in and surrounding urban areas. Normalized Difference Vegetation Index (NDVI) values derived from Moderate Resolution Imaging Spectroradiometer (MODIS) NDVI products are used to evaluate the state and dynamics of vegetation. Land Surface Temperature (LST) derived from MODIS LST products are used to evaluate the extent of the UHIE on these changes. We assess relationships between NDVI and LST and develop a strategy for their combined application.

ICE FOR NATURAL GAS STORAGE

N.S. MOLOKITINA[1], A.O. DRACHUK[1,2], L.S. PODENKO[1]

[1]Institute of Earth Cryosphere, SB RAS, Malygin str. 86, Tyumen, Russia.

[2]Institute of Physics and Technology , Tyumen State University, 15 a Perekopskaya st., Tyumen, Russia.

.

Keywords: GAS HYDRATE, ICE, HYDROPHOBIC FUMED SILICA NANOPARTICLES.

INTRODUCTION

The development and practical application of alternative hydrate technologies of transportation and storage of natural gas in the form of hydrates in Cold regions is actively studied at present (*Gautier et al., 2009, Rehder et al., 2012, Falenty et al., 2014*). However, technological problems can be retired by a slow rate of a hydrate formation and ice to hydrate conversion (*Ribeiro and Lage, 2008*).

One of common methods for resolution this problem for example the use of dispersed ice to prepare the gas hydrates can be achieved in the laboratory. In this case the hydrate formation rate and the storage capacity can be significantly enhanced by increase of an ice-gas phase contact area (*Fukumoto et al., 2001*).

In existing models it is proposed that the growth of methane hydrates from ice occurred in two steps (*Staykova et al., 2003; Kuhs et al., 2006; Falenty et al., 2011*). In first step, film-like hydrates were quickly formed from ice on the surface of ice. Subsequently, in second step which was defined by gas diffusion through the film to unreacted ice the hydrate formation rate decreased due to those films. The reduction of ice particle size can be decreased the diffusion step of the hydrate formation, and hence it can be increased the hydrate formation rate and the storage capacity (*Staykova et al., 2003; Kuhs et al., 2006; Falenty et al., 2011; Rivera and Janda, 2012*).

Sintering presses of ice particles led to the reduction of ice dispersity (*Blackford, 2007*), and hence the hydrate formation rate and the storage capacity decreased. Recently it was shown that dispersed ice which was stable to the sintering of ice particles could be prepared by a rapid grinding frozen water with an adding of hydrophobic fumed silica nanoparticles (*patent RF No2473850*). However it was not carried out the hydrate formation from the dispersed ice stabilized by hydrophobic nanoparticles prepared by rapid grinding frozen water with the adding of hydrophobic nanoparticles earlier.

METHODS

In this paper, the results of measurements on the formation rate of natural gas hydrates from ice stabilized by hydrophobic nanoparticles and that was prepared by the grinding frozen water with hydrophobic nanopowder were reported.

It was used distilled water and a hydrophobic fumed silica powder Aerosil® R202 (Evonik Industries AG, Germany) with a specific surface area of 100 $m^2 \cdot g^{-1}$ (by BET), a bulk density of about 60 $g \cdot l^{-1}$, and a carbon content of 3.5–5.0 wt%.

Influence of a content of the stabilized agent and a size of ice particles on the formation rate of natural gas hydrates from dispersed ice stabilized by Aerosil was studied. For this purpose kinetic curves of gas hydrate formation which was obtained from dispersed ice system with varying degrees of dispersity were plotted. Dispersed ice was prepared by grinding frozen distilled water with the adding of Aerosil content of either 5 or 10 wt %.

According to these studies it was investigated that the hydrate formation rate and amount of hydrates which was formed from ice particles increased if it had been added Aerosil at the grinding of ice. The initial rate of natural gas hydrate formation which was obtained in dispersed ice system prepared with

Aerosil was more than 4 times than in ordinary ground ice. The conversion rate from ice to hydrate was higher by 15 % more for ice that was prepared with Aerosil than for ordinary ground ice.

Also it was shown that the increase the dispersity of ice ground with the adding of hydrophobic nanoparticles led to the increase amount of hydrates which were being formed from ice particles. The conversion rate from ice to natural gas hydrates was higher by 20 % more for a sample with the average size of ice particles of about 75 μm than in the sample with the average size of ice particles of about 170 μm.

CONCLUSIONS

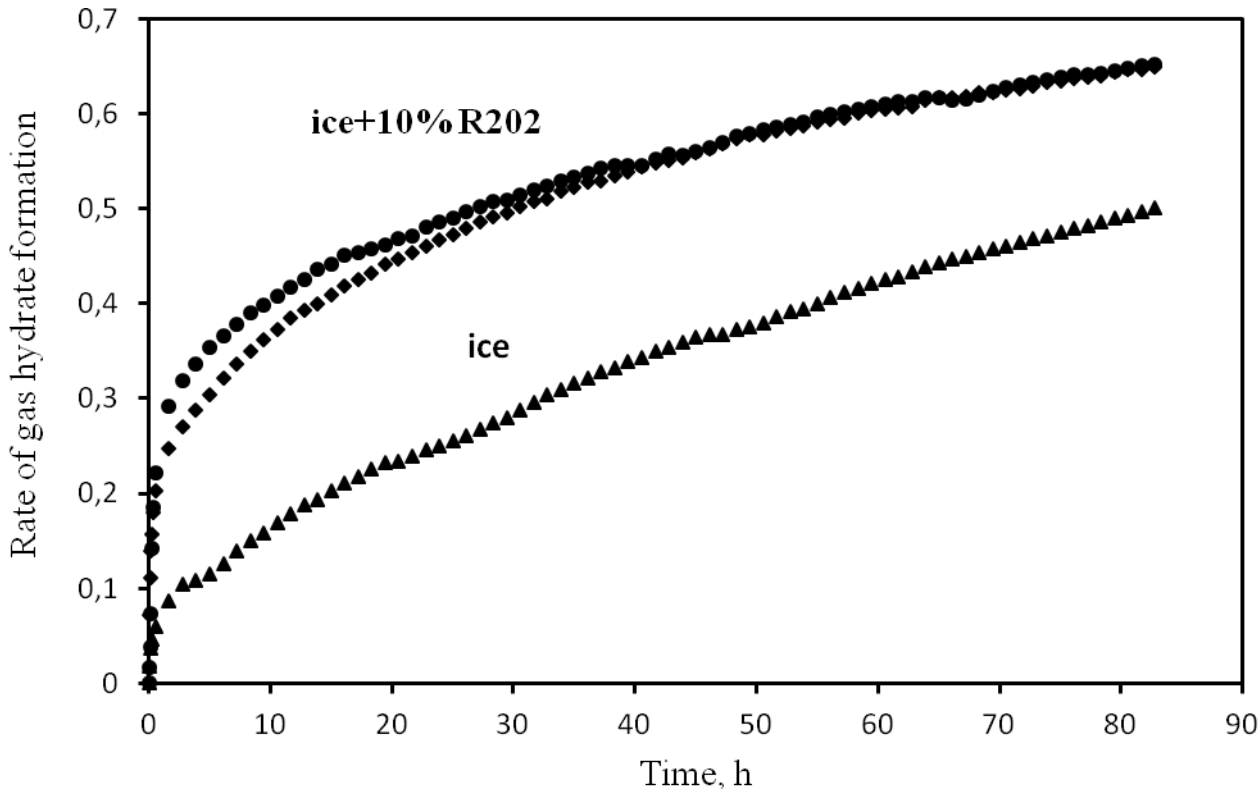

Figure 1. Kinetic curves of gas hydrate formation.

ACKNOWLEDGEMENTS

This work was supported in part by Scientific Research Foundation's State Academies of Sciences Program for 2013–2017 (priority field VIII.77.2.); by the Russian Foundation for Basic Research, project no. 16-38-00279 mol_a; and by RF Presidential Grant no. NSh-3929.2014.5; Basic Research Programs of the RAS (program no. 8, and program the Arctic); the Siberian branch of the RAS (interdisciplinary project no. 144).

REFERENCES

Blackford, Jane R. (2007). Sintering and microstructure of ice: a review // JOURNAL OF PHYSICS D-APPLIED PHYSICS 40, R355.

Falenty, A., Genov, G., Hansen, T. C., Kuhs, W. F., Salamatin, A. N. (2011). JOURNAL OF PHYSICAL CHEMISTRY C115, 4022.

Falenty, A., Kuhs, W.F., Glockzin, M., Rehder, G. (2014). “Self-preservation” of CH 4 hydrates for gas transport technology: Pressure − temperature dependence and ice microstructures // Energy & Fuels 28, 6275.

Fukumoto, K., Tobe, J., Ohmura, R., Mori, Y. H. (2001) Hydrate formation using water spraying in a hydrophobic gas: a preliminary study // AICHE JOURNAL 47, 1899.

Gautier, D. L., Bird, K. J., Charpentier, R. R. et al. (2009). Assessment of Undiscovered Oil and Gas in the Arctic // SCIENCE 324, 1175.

Kuhs, W. F., Staykova, D. K., Salamatin, A. N. (2006). Formation of Methane Hydrate from Polydisperse Ice Powders // JOURNAL OF PHYSICAL CHEMISTRY B 110, 13283.

Rehder, G., Eckl, R., Elfgen, M. et al. (2012). Methane hydrate pellet transport using the self-preservation effect: A techno-economic analysis // Energies 5, 2499.

Ribeiro, C. P., Lage, P. L. C. (2008). Modelling of hydrate formation kinetics: State-of-the-art and future directions // CHEMICAL ENGINEERING SCIENCE 63, 2007.

Rivera, J. J., Janda, K. C. (2012). Ice Particle Size and Temperature Dependence of the Kinetics of Propane Clathrate Hydrate Formation // JOURNAL OF PHYSICAL CHEMISTRY C 116, 19062.

Staykova D. K., Kuhs, W. F., Salamatin, A. N., Hansen T. J. (2003). Formation of porous Gas Hydrates from Ice Powders: Diffraction Experiments and Multistage Model // JOURNAL OF PHYSICAL CHEMISTRY B 107, 10299.

Melnikov, V.P., Podenko, L.S., Nesterov, A.N. et al. (2013). Method of ice dispersion. Patent RF No2473850, F25C 5/02, B02C 19/00. Earth Cryosphere Institute, SB, RAS. №2011125973/13. Claims priority 23.06.2011.

DECOMPOSING PROCESSES REGULATE BVOC EMISSIONS FROM BOREAL SOIL DURING FALL

M. MÄKI[1], J. HEINONSALO[2], H. HELLÉN[3] and J. BÄCK[1]

[1]Dept. of Forest Sciences, P.O. Box 27, FI-00014 University of Helsinki, Finland.

[2]Dept. of Food and Environmental Sciences, P.O. Box 66, FI-00014 University of Helsinki, Finland.

[3]Finnish Meteorological Institute, P.O. BOX 503, FI-00101 Helsinki, Finland.

Keywords: MICROBIAL ACITIVITY, ISOPRENOIDS, MYCORRHIZAL FUNGI, BOREAL SOIL

INTRODUCTION

BVOC production processes have not been determined and quantified in boreal soil, although they cover few percent to tens of percent of the ecosystem flux and soil is a significant source during fall when photosynthetic activity of trees and ground vegetation is low (Aaltonen *et al.*, 2011, 2013). This study was focused on soil isoprenoid emissions, lipophilic sub-group of volatile organic compounds (VOCs), including hemiterpenes, monoterpenes and sesquiterpenes. The main sources have suggested to be degrading litter (Aaltonen *et al.*, 2011; Faiola *et al.*, 2014) and tree roots, especially damaged ones (Aaltonen *et al.*, 2011, 2013; Hayward *et al.*, 2001). Decomposing microbes produce energy for microbial metabolism by degrading organic and nitrogen rich compounds and microbial activity is the known BVOC source (Insam and Seewald, 2010). Temperature regulates these processes (Asensio *et al.*, 2007) through enzyme activity (Guenther *et al.*, 1993) and monoterpenes are released from storage structures when temperature dependent vapor pressure will change (Schurgers *et al.*, 2009). Temperature dependent BVOC production means that climate change can have a broad impact on soil processes since BVOCs control them in a complex way. BVOCs can inhibit enzyme activity, nitrification and mineralization activity (Smolander *et al.*, 2012; Adamczyk *et al.*, 2015) which means that nitrogen availability can change in boreal forest where soil is typically nutrient poor and enzymes accelerate soil processes. Soil can be a sink of isoprenoids (Insam and Seewald, 2010) when microbes use isoprenoids as a carbon source and BVOCs can also stimulate or inhibit the growth of soil fungal species (Mackie and Wheatley, 1999). Microbial BVOC production depends on microbial community structure (Bäck *et al.*, 2010), microbial biomass (Wieder *et al.*, 2013), oxygen and nutrient availability, the physiological state of microbes (Insam and Seewald, 2010) and substrate quality (Stotzky and Schenk, 1976). Freezing-thawing events can also increase isoprenoid emissions by contributing organic matter degradation (Aaltonen *et al.*, 2013). The aim of this study was to determine and quantify soil isoprenoid sources and to demonstrate how temperature regulates isoprenoid flux.

METHODS

Measurements were executed in a southern boreal forest at the SMEAR II (Station for Measuring Forest Ecosystem-Atmosphere Relations) station (61°51'N, 24°17'E, 180 m above sea level) (Hari and Kulmala, 2005). Forest is a 55-yr old Scots pine stand (*Pinus sylvestris*). *Sorbus aucubaria*, *Betula pendula* and *Picea abies* are growing in below-canopy. Soil above a bedrock is Haplic Podzol and soil depth is about 0.5-0.7 m above bedrock. The ground vegetation is formed by shrubs like *Vaccinium vitis-idaea* and *Vaccinium myrtillus*, mosses like *Pleurozium schreberi*, *Dicranum polysetum*, *Dicranum scorparium*, and *Hylocomium splendens* and grasses like *Deschampsia flexuosa* and *Melampyrum sylvaticum*. Vegetation cover of different species on experimental plots were determined in July 2015. Measurements were conducted on three different experimental sites (North, West and South) around the station.

The experimental sites have been established in 2012. Each site includes 20 experimental plots with the different belowground and aboveground treatments which were used to regulate carbon flow from trees and ground vegetation to soil microbes through roots and mycorrhizal fungi. The experimental plots were trenched by digging around a square volume (0.9 x 0.9 m) of soil and cutting roots between experimental plot and surrounding ground. Soil C input by tree root allocation was controlled by comparing untouched soil (no mesh, Con, 24 plots) to experimental plot where decomposing microbes were present but ingrowth of tree roots and soil fungi was inhibited by placing isolating mesh around the soil volume (mesh size 1 µm, code Tr1µm, 18 plots) or to the treatment where access of microbes and mycorrhizal fungi was allowed but the ingrowth of tree roots was inhibited (mesh size 50µm: Tr50µm, 18 plots). The isolating mesh allowed water and nutrients exchange. Ground vegetation allocates part of photosynthetically produced C into the soil and the effect of ground vegetation was monitored with different vegetation covers. Ground vegetation was growing normally (Normal, 24 plots) or vegetation was removed by cutting (Cut, 18 plots). Soil temperature sensors were placed in soil surface layer (depth 0-5 cm) and data was logged every fourth hour from May to October in 2012–2015. 15–18 plots were measured during one week and it took two weeks to measure whole experimental set-up (30–36 plots). We measured on 11 different weeks and the experimental set-up was measured 5–6 times. First period was 15th – 24th of April (14 measurements, some plots were not measured), second 30th of April – 10th of May (35), third 21th of May – 24th of June (35), fourth 21th of July to 21th of August (34), fifth 31th of August – 9th of October (39) and the last one 19th – 23th of October (18).

Hemiterpene, monoterpene and sesquiterpene concentrations in the chamber headspace were measured with two dynamic (steady-state flow-through) glass chambers placed on permanent soil collars (diameter 0.0217 m). Different compounds from incoming and outgoing air were sampled for 1.5 – 2 hours by using sampling flow (0.1 l min^{-1}) into two Tenax TA-Carboback-B adsorbent tubes. Filtered (active carbon trap and MnO2-coated copper net) ambient air was continuously pumped into the chamber and chamber air volume was flushed for 0.5 hour before sampling to stabilize the system. The measured compounds were hemiterpenes (isoprene and 2-methyl butenol), monoterpenes (α-pinene, camphene, β-pinene, myrcene, Δ3-carene, p-cymene, limonene, terpinolene, 1.8-cineol and linalool) and sesquiterpenes (longicyclene, iso-longifolene, β-caryophyllene, aromadendrene and α-humulene). Tenax TA-Carboback-B adsorbent tubes were kept in cold (5 ºC) and analyzed next week from sampling in laboratory, by a thermodesorption instrument (Perkin Elmer TurboMatrix 650, Waltham, USA) connected to a gas-chromatograph (Perkin-Elmer Clarus 600, Waltham, USA) and a mass selective detector (Perkin-Elmer Clarus 600&, Waltham, USA). The emission rates (µg m^{-2} h^{-1}) of the different compounds were calculated from a concentration difference between incoming and outgoing air for soil area (coved with chamber, 0.042 m^2) and time using flow rates.

Monoterpene fluxes from different treatments were not normally distributed when distributions were tested using Kolmogorov-Smirnov and Shapiro-Wilkin tests. For this reason, non-parametric Kruskal-Wallis test at the significance level of <0.05 was used to determine if distributions of the different treatments were statistically different (Figure 2a.).

CONCLUSIONS

The highest monoterpene emissions (9-149 µg m^{-2} h^{-1}) were measured from non-trenched forest soil in October (Figure 1.) and this strong seasonality was confirmed by earlier study in 2010 (Aaltonen *et al.*, 2011). The timing of high fall emissions probably depends on temperature which determines annual litterfall. Degrading litter from roots, shoots and leaves have been discovered to be a major source of isoprenoids (Aaltonen *et al.*, 2011; Hellén *et al.*, 2006; Faiola *et al.*, 2014). In this study, decomposing microbes (Tr1µmCut) were discovered to produce highest flux during fall when vegetation was removed and flux was significantly higher than flux from non-trenched soil (ConNormal, p value 0.027, Figure 2a.). Decomposing microbes produced as much isoprenoids as soil were ingrowth of mycorrhizal fungi and decomposing microbes was allowed. Decomposing microbes are known to be an important contributor to soil BVOC production (Isodorov and Idanova, 2002).

Sesquiterpene flux was found to be dependent on temperature (Figure 2b.) and the most common sesquiterpenes emitted in our study were β-caryophyllene and aromadendrene. β-caryophyllene is the most common sesquiterpene emitted by Scots pine (Bäck *et al.*, 2012) which indicates fine roots and needle litter to be an important sesquiterpene source. Decomposers (*Ophiostoma abietinum*) have also been reported to emit sesquiterpenes (Bäck *et al.*, 2010).

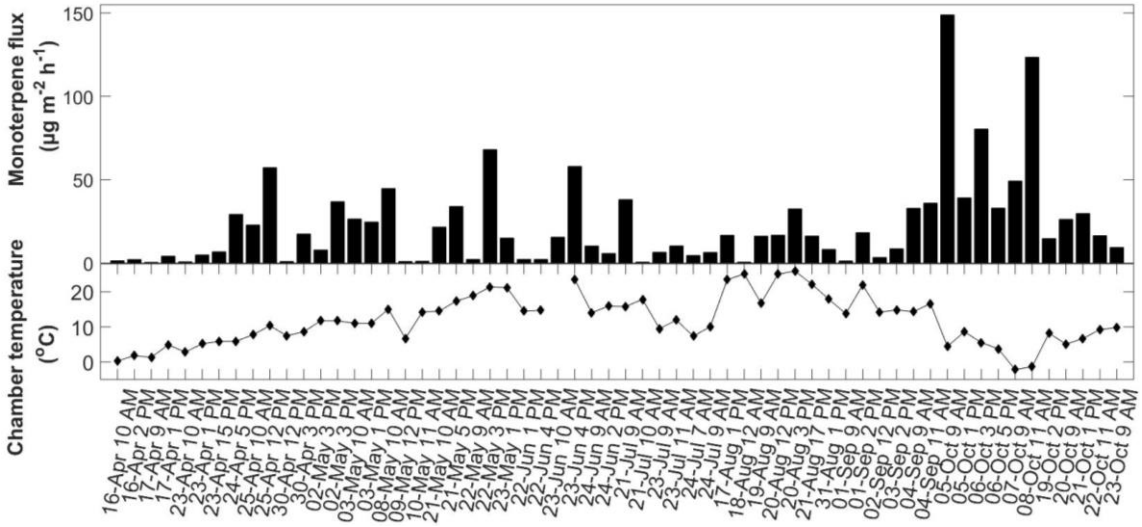

Figure 1. Monoterpene flux (µg m^{-2} h^{-1}) and chamber temperature (°C) of singel measurements from 16th of April to 23th of October in 2015 from non-trenched forest soil.

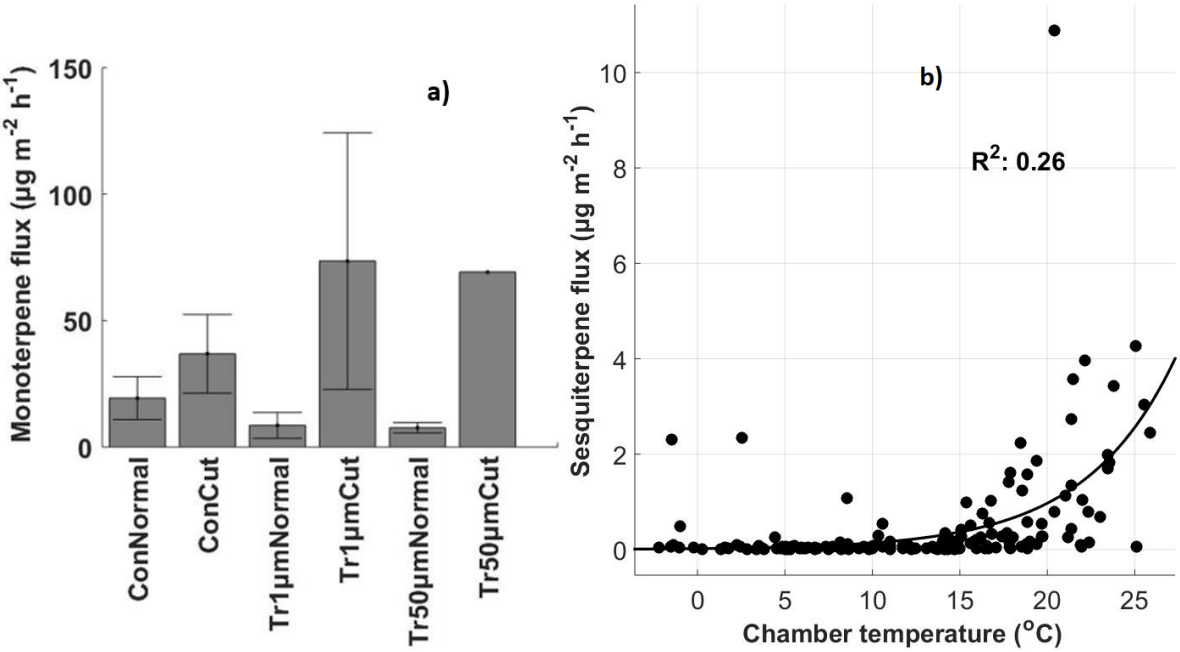

Figure 2. Mean and standard deviation of monoterpene fluxes (µg m^{-2} h^{-1}) from different trenching treatments between 19th of October and 23th of October 2015 (a). Temperature dependence of sesquiterpene flux (µg m^{-2} h^{-1}) from all the trenching treatments from 16th of April to 23th of October in 2015 (b).

When studying the different monoterpene sources separately, temperature was discover to be the most important parameter explaining the flux from mycorrhizal fungi and decomposing microbes (Figure 3a. and 3b.), although it has been said that single environmental parameter cannot be used to explain the flux (Aaltonen *et al.*, 2013). Monoterpene flux was found to correlate negatively with chamber (R^2 = 0.82) and

soil temperature (R^2 = 0.70) and negative correlation can be explain by litterfall which is a major carbon and nitrogen source into soil and this resource flow accelerates decomposing processes when extracellular enzymes of microbes and mycorrhizal fungi degrade organic compounds.

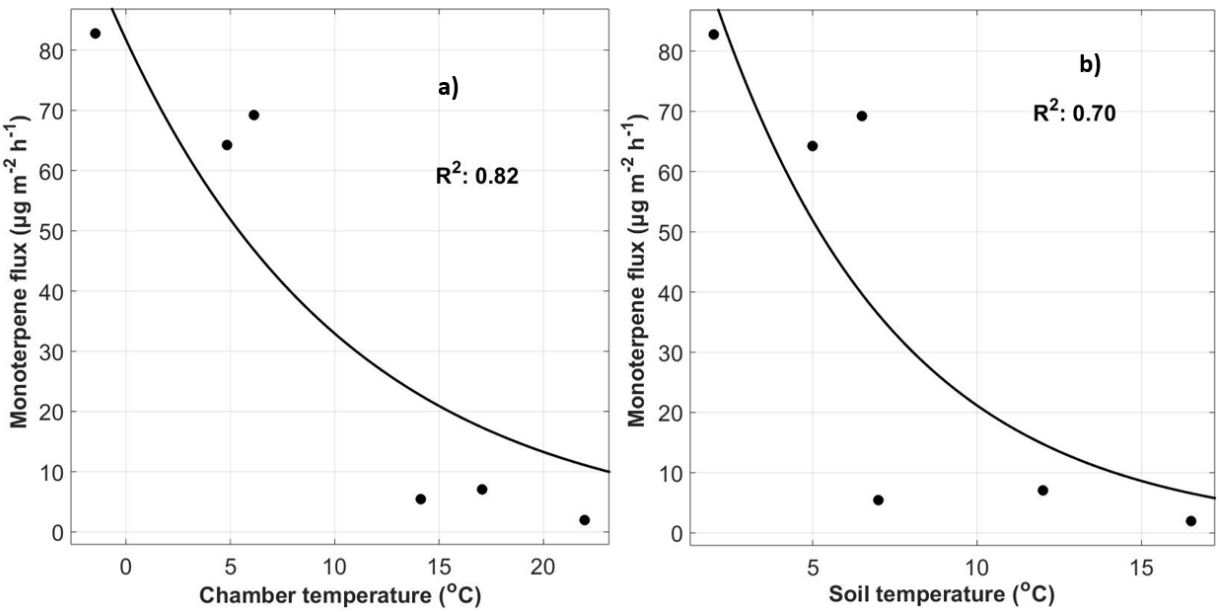

Figure 3. Temperature dependence of monoterpene flux (µg m^{-2} h^{-1}) from the treatment Tr50µmCut where ingowth of decomposing microbes and mycorrhizal fungi was allowed (a = chamber temperature and b = soil temperature) from 16th of April to 23th of October in 2015.

Our data indicates that the importance of different monoterpene sources varies during the growing season and this data will be used to discover how carbon and nitrogen competition between decomposing microbes and mycorrhizal fungi and carbon allocation from tree roots into soil accelerates BVOC flux from boreal soil.

ACKNOWLEDGEMENTS

This work was supported by Academy of Finland Center of Excellence (grant no. 272041) and by a grant from the Jenny and Antti Wihuri Foundation.

REFERENCES

Aaltonen, H., Pumpanen, J., Pihlatie, M., Hakola, H., Hellén, H., Kulmala, L., Vesala, T., and Bäck, J. (2011). Boreal pine forest floor biogenic volatile organic compound emissions peak in early summer and autumn, Agr. Forest Meteorol., 151, 682–691, 2011.

Aaltonen, H., Aalto, J., Kolari, P., Pihlatie, M., Pumpanen, J., Kulmala, M., Nikinmaa, E., Vesala, T. & Bäck, J. (2013). Continuous VOC flux measurements on boreal forest floor. *Plant and soil*, *369*(1-2), 241-256.

Adamczyk, S., Adamczyk, B., Kitunen, V., & Smolander, A. (2015). Monoterpenes and higher terpenes may inhibit enzyme activities in boreal forest soil. *Soil Biology and Biochemistry*, *87*, 59-66.

Asensio, D., Peñuelas, J., Filella, I., & Llusià, J. (2007). On-line screening of soil VOCs exchange responses to moisture, temperature and root presence. *Plant and Soil*, *291*(1-2), 249-261.

Bäck, J., Aaltonen, H., Hellén, H., Kajos, M. K., Patokoski, J., Taipale, R., Pumpanen, J., & Heinonsalo, J. (2010). Variable emissions of microbial volatile organic compounds (MVOCs) from root-associated fungi isolated from Scots pine. *Atmospheric Environment*, *44*(30), 3651-3659.

Bäck, J., Aalto, J., Henriksson, M., Hakola, H., He, Q., & Boy, M. (2012). Chemodiversity of a Scots pine stand and implications for terpene air concentrations. *Biogeosciences*, *9*(2), 689-702.

Faiola, C. L., VanderSchelden, G. S., Wen, M., Elloy, F. C., Cobos, D. R.,Watts, R. J., Jobson, B. T., and VanReken, T. M. (2014): SOA Formation Potential of Emissions from Soil and Leaf Litter, Environ. Sci. Technol., 48, 938–946.

Guenther, A. B., Zimmerman, P. R., Harley, P. C., Monson, R. K., & Fall, R. (1993). Isoprene and monoterpene emission rate variability: model evaluations and sensitivity analyses. *Journal of Geophysical Research: Atmospheres (1984–2012)*, *98*(D7), 12609-12617.

Hari, P. & Kulmala, M. 2005. Station for Measuring Ecosystem–Atmosphere Relations (SMEAR II). Boreal Environment Research 10: 315–322.

Hayward, S., Muncey, R. J., James, A. E., Halsall, C. J., & Hewitt, C. N. (2001). Monoterpene emissions from soil in a Sitka spruce forest. *Atmospheric Environment*, *35*(24), 4081-4087.

Hellén, H., Hakola, H., Pystynen, K. H., Rinne, J., & Haapanala, S. (2006). C 2-C 10 hydrocarbon emissions from a boreal wetland and forest floor. *Biogeosciences*, *3*(2), 167–174.

Insam, H., & Seewald, M. S. (2010). Volatile organic compounds (VOCs) in soils. *Biology and fertility of soils*, *46*(3), 199-213.

IPCC AR5 (2013), Climate change 2013: The physical science basis, in Contribution of Working Group I (WGI) to the Fifth Assessment Report (AR5) of the Intergovernmental Panel on Climate Change (IPCC). [Available at http://www.ipcc.ch/report/ar5/wg1/.]

Isidorov, V., & Jdanova, M. (2002). Volatile organic compounds from leaves litter. *Chemosphere*, *48*(9), 975-979.

Mackie, A. E., & Wheatley, R. E. (1999). Effects and incidence of volatile organic compound interactions between soil bacterial and fungal isolates. *Soil Biology and Biochemistry*, *31*(3), 375–385.

Schurgers, G., Arneth, A., Holzinger, R., & Goldstein, A. H. (2009). Process-based modelling of biogenic monoterpene emissions combining production and release from storage. *Atmospheric chemistry and physics*, *9*(10), 3409-3423.

Smolander, A., Kanerva, S., Adamczyk, B., & Kitunen, V. (2012). Nitrogen transformations in boreal forest soils—does composition of plant secondary compounds give any explanations?. *Plant and Soil*, *350*(1-2), 1-26.

Stotzky, G., Schenck, S., & Papavizas, G. C. (1976). Volatile organic compounds and microorganisms. *CRC critical reviews in microbiology*, *4*(4), 333-382.

Wieder, W. R., Bonan, G. B., & Allison, S. D. (2013). Global soil carbon projections are improved by modelling microbial processes. *Nature Climate Change*, *3*(10), 909–912.

COMBINING AIRBORNE AND LIDAR MEASUREMENTS FOR ATTRIBUTION OF AEROSOL LAYERS

A.NIKANDROVA[1], R. VÄÄNÄNEN[1], K.ATLASKINA[1], V-M. KERMINEN[1],M. KULMALA[1], T. PETÄJÄ[1], M. KOMPPULA[2] and E. O'CONNOR[3]

[1]University of Helsinki, Department of Physics
P.O. Box 64, FIN-00014, Finland.

[2]Finnish Meteorological Institute, Kuopio, Finland

[3]Finnish Meteorological Institute, Helsinki, Finland

Keywords: LIDAR, AEROSOL, AIRBORNE.

INTRODUCTION

Atmospheric aerosols remain one of the largest sources of uncertainty in climate predictions (IPCC, 2013). Understanding the vertical distribution of aerosols and their optical properties is important for determining the aerosol direct and indirect radiative forcing (Haywood and Ramaswamy, 1998). Lidar measurements are able to show the evolution of aerosol layers with high resolution in space and time (Wandinger et al, 2011). More detailed information about particles sizes and concentration, but with lower spatial resolution, can be obtained by in-situ airborne measurements. Therefore, the main objective of this study was to combine airborne and lidar measurements in order to understand the temporal, vertical and spatial variability of aerosol properties in the lower troposphere.

METHODS AND DATA

A High Spectral Resolution Lidar (HSRL) was deployed in Hyytiälä from March to September 2014 as a part of the US DoE ARM (Atmospheric Radiation Measurement) mobile facility during the BAECC (Biogenic Aerosols – Effects on Cloud and Climate) Campaign. HSRL measures aerosol backscatter and depolarization with 1 second resolution at 532 nm. Airborne campaigns took place in April and September 2014 during the operational time of HSRL. The flight tracks were above Hyytiälä at altitudes below 4 km and at quite low speeds (<200 km/h), which allowed measurements with good temporal and spatial resolution. A Cessna FR172F aircraft was modified to carry instruments, including a Scanning Mobility Particle Sizer (SMPS), Optical Particle Sizer (OPS) and a CO2/H2O analyser (LI-COR LI-840). The SMPS has a temporal resolution of 2 min and it measures particle sizes from 0.1 to 0.23 µm, while the OPS has a 10 s resolution and measures particle sizes from 0.3 to 9 µm. A schematic measurement set-up can be seen in Fig. 1.

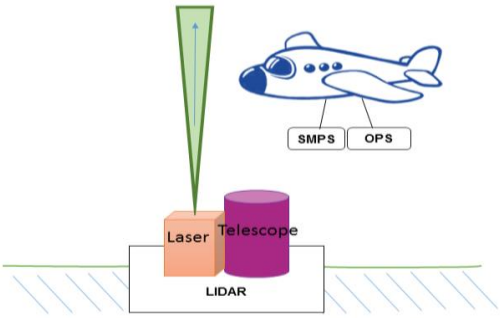

Figure 1. Schematic figure of the measurement setup: high spectral resolution lidar operating continuously in Hyytiälä, with the Cessna airplane, carrying SMPS and OPS, making ascents and descents in the vicinity, within 30 km.

RESULTS AND CONCLUSIONS

April 10 2014 was one of the case study days. It was a clear sky day with air masses coming from the north. A new particle formation event was detected using ground-based measurements at the SMEAR station in Hyytiälä. Cessna measurements were performed from 10 to 13 UTC. Figure 2 shows the HSRL backscatter cross section during this time period, and a number of layers can be seen: the lowest layer corresponds to a well-mixed boundary layer that reaches from the surface up to 1200 m, then there is a middle layer at 1200-2000 m, followed by an upper layer that stretches from 2000 m to 2600 m. The profiles of the LI-COR relative humidity (RH) measurements made on board the aircraft support the identification of these layers. The highest RH values of 60% were detected at the top of the boundary layer, while a dry layer from 1200 to 2000 m had the lowest values (5-10%). At 2000 m, the RH started to grow, reaching 15% and then staying constant at the upper layer. A radiosonde was launched during the time Cessna when was flying and its relative humidity profile is shown in blue on the figure 2. This profile was very similar to that obtained from Cessna, confirming the recognised layers.

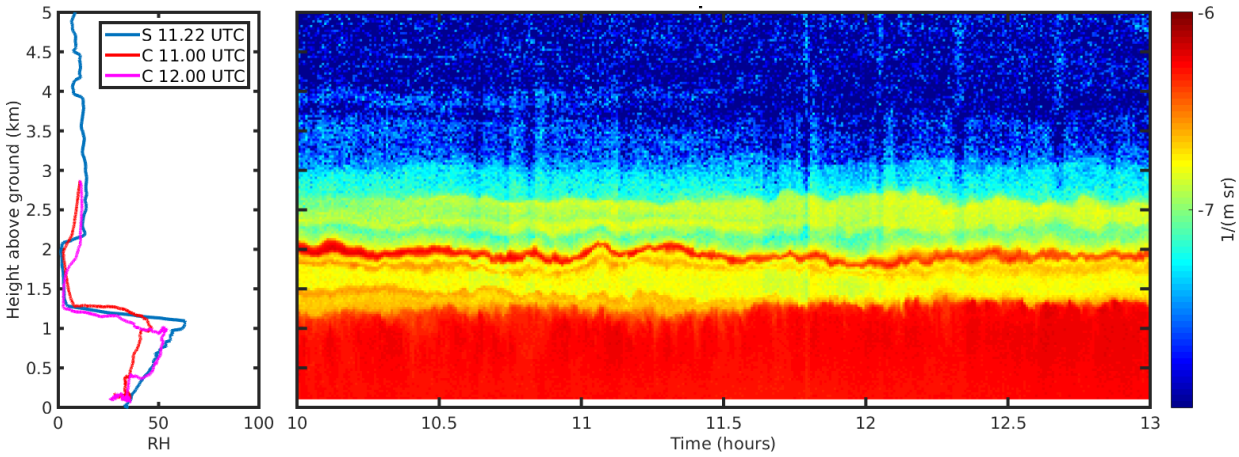

Figure 2. To the right, HSRL backscatter cross section at 10-13 UTC on April 10th 2014 measured at the same time as Cessna was flying. The left panel shows the relative humidity profiles averaged for the Cessna ascent (red) and descend (pink) as well as RH profile from a radiosonde (blue) that was launched at 11:22. Well-mixed boundary layer reaches from the surface up to 1200 m, followed by a dry layer between 1200 and 2000 m, and finally a more humid upper layer between 2200 and 2600 m.

Figure 3 shows the mean and standard deviation of the aerosol size distributions measured by the SMPS and the OPS at the detected layers. Since aerosol particles were dried before entering the SMPS, the growth factor (GF) for SMPS data was calculated according to Laakso et al. (2009) to account for the growth due to the relative humidity. From the three layers in the Figure 3, the boundary layer had the highest particle concentration in all the size ranges, especially in the Aitken mode. The high concentration in small sizes

was caused by a nucleation event that took place earlier that morning. The middle layer was dominated by accumulation mode particles between 0.1 and 0.6 µm. The lidar usually detects aerosols starting from 0.1 µm, so stronger scattering was seen for this layer in Figure 2 as compared with upper layer. The upper layer had fewer particles in this size range, yet more particles in the Aitken mode (10-40 nm). This layer had probably been in contact with the surface air some time ago where the small particles were formed but were not able to grow since then. For the large particles, the OPS measured the highest concentrations again in the boundary layer. Compared with the middle layer, the upper layer had more particles at sized larger than 800 nm. The difference in the RH between the layers is not enough to explain the particle growth in the moister layer, and thus, it is likely that these layers had different origins. The HYSPLIT (Hybrid Single Particle Lagrangian Integrated Trajectory Model, http://ready.arl.noaa.gov/HYSPLIT.php) backward trajectories confirmed that the layers did indeed originate from different locations. Figure 3 shows the potential for remotely-sensed elevated aerosol layer attribution through a combination of the backscatter and humidity properties, together with a trajectory analysis.

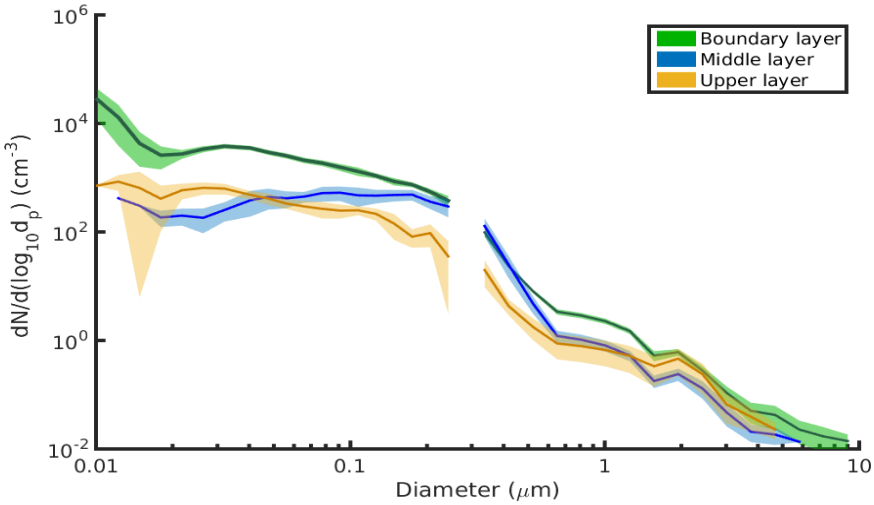

Figure 3. Mean and standard deviation of aerosol size distributions measured by airborne SMPS and OPS for the layers seen by the lidar in Fig.2.

Vertical backscatter profiles were calculated from the size distribution obtained by the SMPS and OPS by using Mie scattering approximations for 532 nm, assuming spherical water droplets. Figure 4 shows similarities between the calculated profile and the one averaged from the HSRL for the same time. The profiles show good agreement in layering, with few deviations probably due to the scattering assumption used (aerosol particles have different scattering properties to water droplets, especially if dry). The molecular scattering was not taken into account in the calculations, so the calculated backscatter profile was always smaller than that measured by the HSRL.

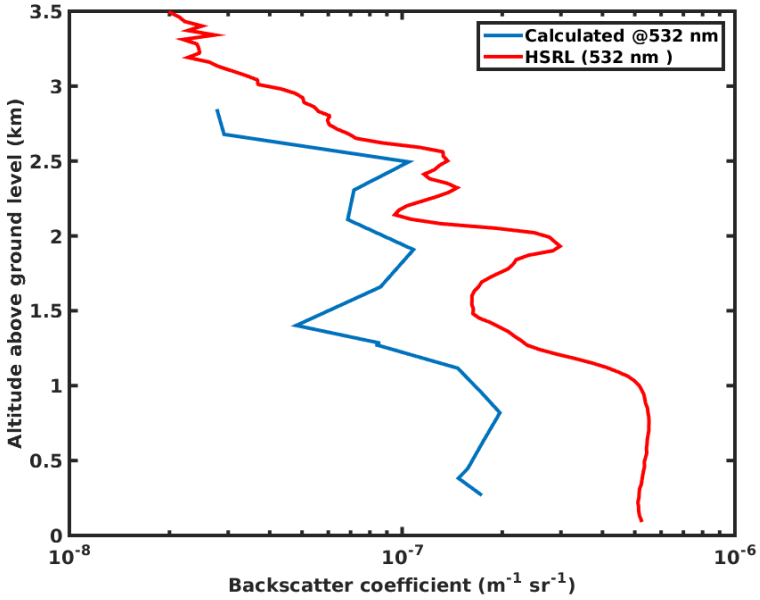

Figure 4. Vertical profiles of particle backscatter coefficient for 10 April between 11:00 and 11.30. The red profile was directly measured by the HSRL and blue one was calculated with the Mie approximation from the size distribution measured by Cessna for a wavelength of 532 nm.

ACKNOWLEDGEMENTS

This work was supported by the Academy of Finland Centre of Excellence program (project no 272041). We also acknowledge the use of HSRL data in collaboration with the U.S. Department of Energy as part of the Atmospheric Radiation Measurement (ARM) Climate Research Facility during BAECC (AMF campaign in Hyytiälä, Finland).

REFERENCES

Haywood, J. M and Ramaswamy, V. (1998). Global sensitivity study of the direct radiative forcing due to antropogenic sulfate and black carbon. *J. Geophys. Res.* **103**, 6043 - 6058

IPCC: The Physical Science Basis, Contribution of Working group I to the Fifth Assessment Report of the Intergovernmental Panel on Climate Change (2013), edited by: Stocker, T.F., Qin, D., Plattner, G.-K. and others, Cambridge University Press, Cambridge, United Kingdom and New York, NY, USA.

Laakso, L., Petäjä, T., Lehtinen, K., Kulmala, M., Paatero, J., Horrak, U., Tammet, H., Juotsensaari, J. (2004). Ion production rate in a boreal forest based on ion, particle and radiation measurement. *Atmos. Chem. Phys.*, **4**, 1933-1943

Wandinger, U., Muller, D, Bockmann, C., Althausen, D., Matthias, V., Bosenberg, J., Stohl., A, Ansmann., A. (2002). Optical and microphysical chracterization pf biomass-burning and industrial pollution aerosol from multiwavelenght lidar and aircraft measurements. *J. Geophys. Res.* **107**, 8125

FEEDBACK OF AEROSOL POLLUTION TO ATMOSPHERIC CHEMISTRY IN EASTERN CHINA

W. NIE[1,2], A.J. DING[1,2], Z. XU[1,2], X. HUANG[1,2], X.G. CHI[1,2], Y.N. XIE[1,2], V.-M. KERMINEN[3], T. PETAJA[3], A. VIRKKULA[3], M. KULMALA[3], X. Q. YANG[1,2], J. N. SUN[1,2],and C. B. FU[1,2]

[1]Institute for Climate and Global Change Research & School of Atmospheric Sciences, Nanjing University, Nanjing, 210023, China
[2]Collaborative Innovation Center of Climate Change, Nanjing, Jiangsu Province, China
[3]Division of Atmospheric Sciences, Department of Physics, University of Helsinki, Helsinki, Finland

Keywords: FEEDBACK, DUST, NITROUS ACID, SULFATE

INTRODUCTION

"New" issues have been arisen in atmospheric science accompanied with strong aerosol pollution recently in eastern China. For example, a feedback loop between aerosol pollution and boundary layer has been proved occurring towards to a more stable boundary layer and strong aerosol pollution (Ding et al., 2013a; Tuukka et al., 2016). For the atmospheric chemistry, it also has the potential to induce some "new" processes by the largely enhanced surface area and mixed plumed of nature particles (e.g. dust and biomass burning particles) and anthropogenic emissions. In this work, the focuses are on these possible "new" chemical processes related to atmospheric oxidation capacity and secondary aerosol formation.

METHODS

A long term and comprehensive measurement was conducted from 2011 at the SORPES "flagship" central site in Xianlin of Nanjing (Ding et al., 2013b). It is a regional background site, located on the top of a hill (118°57'10" E, 32°07'14", 40 m a.s.l.) in the Xianlin campus of Nanjing University and about 20 km east of the suburban Nanjing city. A suite of trace gases, aerosols, and meteorological quantities were measured, including O_3, NO_x, SO_2, HONO, particle chemical compositions (water soluble ions, OC and EC), size distribution, and optical properties. Besides the long term measurement at SORPES site, some intensive campaigns were also made focusing on some special processes, e.g. a campaign during the spring in 2009 at the top of Mt. Heng with the target on Asian dust.

CONCLUSIONS

Several "new" chemical processes have been observed towards relating to the secondary aerosol formation or atmospheric oxidation capacity. First, dust particles have been supposed to induce heterogeneous photochemical processes, which in turn promote the formation of HONO and new particles (Nie et al., 2012; Nie et al., 2014). These processes can be largely enhanced once the dust particles are "polluted" by anthropogenic pollutions. These results provide evidences on the role of aerosol-related photochemistry, which would enhance the atmospheric oxidation capacity. Figure 1 shows the proposed 3-step heterogeneous photochemical processes involving Asian dusts during long-range transport in the atmosphere.

Secondly, biomass burning particles were proved to enhance the conversion rate of NO_2 to HONO, which is one of the major sources of OH (Nie et al., 2015). Higher particle loadings, larger specific surface areas and higher NO_2 conversion efficiency of biomass burning particles (Figure 2) are supposed to be the major reasons. In addition, once the biomass burning particles mixed with anthropogenic pollutions, the HONO production potentials from the conversion of NO_2 to HONO was further significantly enhanced. Given that biomass burning particles are easily mixed with anthropogenic pollution in eastern China, their influences on the HONO budget, radical pool, and thus the formation of secondary aerosols are expected to be important (Nie et al., 2015).

Thirdly, NO_2 was recently found to be a possibly important oxidant to convert SO_2 to sulphate under the condition of mineral dust and biomass burning plumes (Xie et al., 2015; He et al., 2014). Especially during the biomass burning induced haze events (Xie et al., 2015), the oxidation processes by NO_2 became critical when the formation of other oxidants were suppressed. More interestingly, one of the "by-products" of the reaction of SO_2 and NO_2 is HONO, which can further enhance the atmospheric oxidation capacity. All these results suggest some new or neglected

chemical processes can be induced or promoted during the environment of heavy aerosol pollution in eastern China, which may feedback to the secondary aerosol formation.

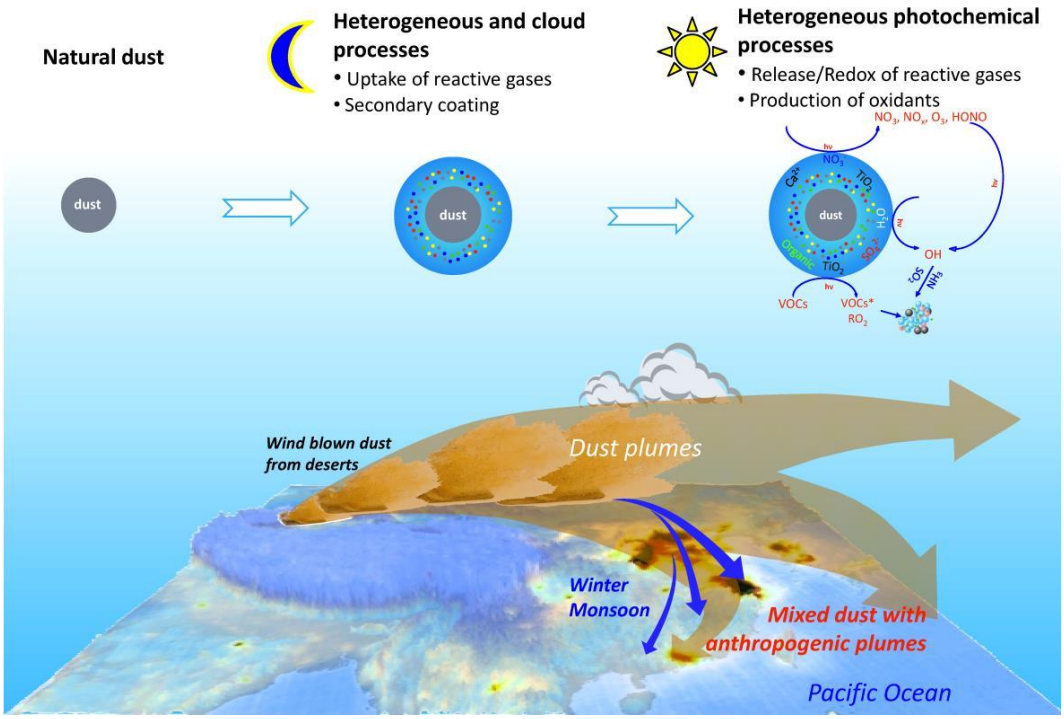

Figure 1 Schematic description of the heterogeneous photochemical processes involving Asian dusts during long-range transport in the atmosphere. Copyright 2014 Nature. (Figure 4 in Nie et al., 2014)

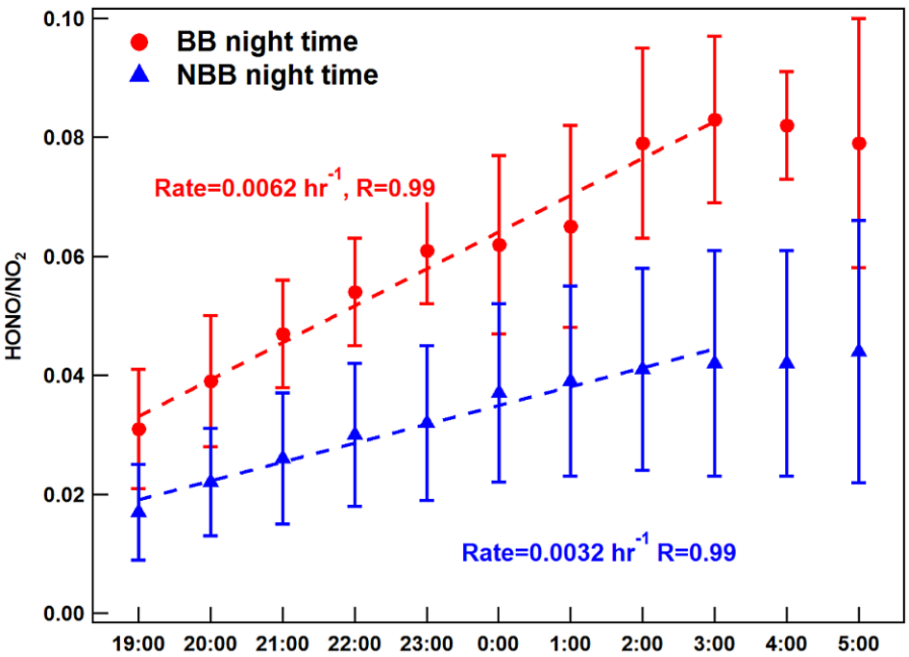

Figure 2 Ratios of HONO to NO_2 for nighttime samples of biomass burning (BB) and non-biomass burning plumes (NBB). The change rates were calculated from 19:00 to 03:00. Error bars are the standard deviations. (Figure 6 in Nie et al., 2015)

ACKNOWLEDGEMENTS

This work was funded by National Natural Science Foundation of China (D0512/41305123 and D0510/41275129), the MOST 973 Program (2010CB428500), and the Jiangsu Provincial Science Fund for Distinguished Young Scholars (No. BK20140021).

REFERENCES

Ding, A. J., Fu, C. B., Yang, X. Q., Sun, J. N., Petäjä, T., Kerminen, V. M., Wang, T., Xie, Y., Herrmann, E., Zheng, L. F., Nie, W., Liu, Q., Wei, X. L., and Kulmala, M. (2013a). Intense atmospheric pollution modifies weather: a case of mixed biomass burning with fossil fuel combustion pollution in eastern China, *Atmos. Chem. Phys.*, **13**, 10545.

Ding, A. J., Fu, C. B., Yang, X. Q., Sun, J. N., Zheng, L. F., Xie, Y. N., Herrmann, E., Nie, W., Petäjä, T., Kerminen, V. M., and Kulmala, M. (2013b). Ozone and fine particle in the western Yangtze River Delta: an overview of 1 yr data at the SORPES station, *Atmos. Chem. Phys.*, **13**, 5813.

He, H., Wang, Y., Ma, Q., Ma, J., Chu, B., Ji, D., Tang, G., Liu, C., Zhang, H., and Hao, J. (2014). Mineral dust and NOx promote the conversion of SO_2 to sulfate in heavy pollution days, *Sci. Rep.*, **4**, 4172.

Nie, W., Ding, A., Wang, T., Kerminen, V.-M., George, C., Xue, L., Wang, W., Zhang, Q., Petaja, T., Qi, X., Gao, X., Wang, X., Yang, X., Fu, C., and Kulmala, M. (2014). Polluted dust promotes new particle formation and growth, *Sci. Rep.*, 4, 6634.

Petäjä, T., Järvi, L., Kerminen, V. M., Ding, A. J., Sun, J. N., Nie, W., Kujansuu, J., Virkkula, A., Yang, X., Fu, C. B., Zilitinkevich, S., and Kulmala, M. (2016), Enhanced air pollution via aerosol-boundary layer feedback in China, , *Sci. Rep.*, **6**, 18998.

Xie, Y., Ding, A., Nie, W., Mao, H., Qi, X., Huang, X., Xu, Z., Kerminen, V.-M., Petäjä, T., Chi, X., Virkkula, A., Boy, M., Xue, L., Guo, J., Sun, J., Yang, X., Kulmala, M., and Fu, C. (2015), Enhanced sulfate formation by nitrogen dioxide: Implications from in situ observations at the SORPES station, *J. Geophys. Res.-Atmos.*, **120**, 12679.

DYNAMICS OF CARBON, NITROGEN AND OTHER CLIMATE RELEVANT TRACE GASES MEASURED AT SMEAR ESTONIA

S.M. NOE[1], A. KRASNOVA[1], D. KRASNOV[1], Ü. NIINEMETS[1], K. JÕGISTE[2], U. HÕRRAK[3], M. VANA[3], S. MIRME[3], K. KOMSAARE[3] and A. KANGUR[2]

[1]Institute of Agricultural and Environmental Sciences, Estonian University of Life Sciences, Kreutzwaldi 1, Tartu, Estonia.

[2]Institute of Forestry and Rural Development, Estonian University of Life Sciences, Kreutzwaldi 1, Tartu, Estonia.

[3]Institute of Physics, University of Tartu, Ülikooli 18, Tartu, Estonia.

Keywords: CARBON AND NITROGEN, BIOGEOCHEMICAL CYCLES, DYNAMICS, SMEAR ESTONIA.

INTRODUCTION

Since 2012, the Estonian Station for Measuring Ecosystem-Atmosphere Relations (Hari and Kulmala 2005) SMEAR Estonia was build and became stepwise operational (Noe *et al.* 2016b). Measurements of CO_2, H_2O, CH_4, O_3, NOx, and SO_2 are conducted continuously since 2013 (Niinemets *et al.* 2013; Noe *et al.* 2016a). Starting 2015, measurements of soil respiration, tree growth, aerosols and air ions are completing the trace gas measurements. On the 130 m tall mast are meteorological instruments to assess the 3 dimensional turbulent air movement, solar radiation, air temperature, pressure and relative humidity placed on all together six heights. Via a piping system, ambient sample air is drawn to the main cottage where gas analysers are placed and aerosol and air ion measurements are conducted at a separate cottage. Additionally two 30 m high towers for direct access to the trees and aerosol fluxes are currently available.

METHODS

Here we present some results from the first years of continuous ecosystem-atmosphere measurements obtained above a hemiboreal mixed forest canopy at the SMEAR Estonia (Noe *et al.* 2016b)site. In detail, we present seasonal characteristics of CO_2 fluxes measured above the canopy, seasonal and diurnal dynamics of ozone and some episodic examples of ozone, NOx, and SO_2 together with the horizontal wind speed.

Carbon fluxes were measured applying the Eddy covariance technique at 30 m height. A 3D sonic anemometer (uSonic-3 Class A, Metek GmbH, Germany) and an infrared gas analyser (LI7200, LiCor Inc., USA) are combined to measure turbulent wind, CO_2 and H_2O mixing ratios. The data have been processed using the EddyUH (University of Helsinki, Helsinki, Finland) package. Half hourly averaged fluxes of CO2 where binned into monthly chunks and median values have been calculated for each month (Fig. 1).

Ambient mixing ratios of O_3, NOx and SO_2 were drawn from 30 m height to the main cottage and analysed by trace gas analysers (models i49, i43-TL, i42-TLE, all Thermo Fischer Scientific Inc., USA) and stored each 10 s to a computer. Half hourly median values were calculated. Applying this database, we calculated monthly binned median values to estimate the seasonal variation in O_3 ambient mixing ratios and the diurnal dynamics (Fig. 2).

To assess dependencies between O_3, NOx and SO_2 we used two one-day examples, one in February and one in May 2015. For these periods, we calculate normalised mixing ratios to allow a temporal better location of possible correlations between these gases due to atmospheric chemistry, transport and biogenic processes. A linear model was set up to describe the dependence between theses gases. All visualisations, calculations, statistics and data processing were done using Wolfram Mathematica (version 10.3.1, Wolfram Research Inc., USA).

CONCLUSIONS

The carbon fluxes have been measured since several years at the SMEAR Estonia (Noe *et al.* 2011, 2016b) station but became continuous recently. That allows assessing the hemiboreal mixed forests activity in greater detail and enables to compare it to other boreal and temperate sites. Figure 1 shows that during the seasons 2014 and 2015 the uptake of carbon by the ecosystem grows from March/April on until June. From July to September carbon uptake shrinks and from October to February, the ecosystems activity is low and carbon is emitted back to the atmosphere.

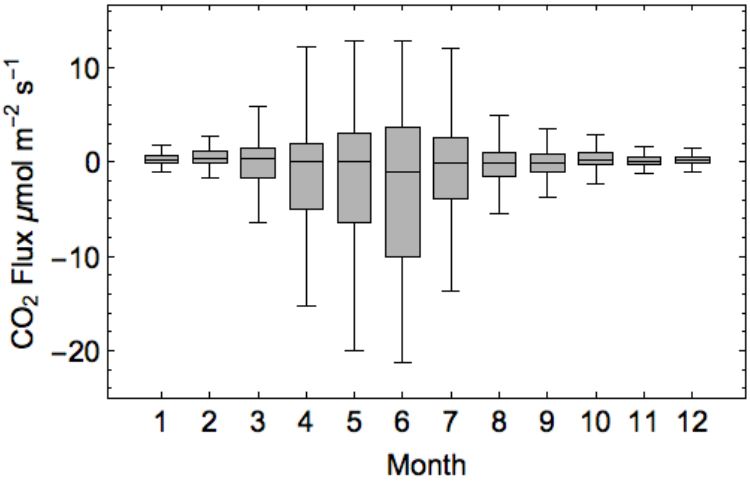

Figure 1. Monthly median CO_2 fluxes measured at 30 m above the forest canopy at SMEAR Estonia.

Atmospheric ozone followed a seasonal pattern with highest ambient mixing ratios in spring and lowest in autumn (Fig. 2). Even though highest ozone levels occurred during spring, their daily variation is during that period still moderate and covers about 10 ppb. During late autumn at the minimal the diurnal variation was about 5 ppb. Highest diurnal variation occurred in summer where a difference of 25 ppb from the morning low to the afternoon high levels was measured. Because ozone plays an important role in the formation of atmospheric aerosols from biogenic vapours (Kulmala *et al.* 2013; Ehn *et al.* 2014) and is modulated by other atmospheric pollutants like NOx and sulphuric compounds that are transported between the atmosphere and biosphere in biogeochemical cycles we investigated possible correlations between these gases (Fig. 3 and 4).

NOx and SO_2 are originated to large extent from anthropogenic sources (fossil fuel burning, transport, heating) and may be transported from distant places to the measurement site (Riuttanen *et al.* 2013; Noe *et al.* 2016a). On 28th February 2015, we found a rather strong depletion of ambient ozone mixing ratios, a dropt of almost 8 ppb that was in line with a strong rise in NOx (Fig. 3A and 3B). At 16:00, wind turned from southwest to east (Fig. 3C) and a steep increase of NOx (about 6 ppb) and SO_2 (0.7 ppb) were recorded. In the same time O_3 and NOx had a strong negative correlation (Pearson's correlation coefficient) r = -0.94 while for SO_2 we found r = -0.69. At 17th May 2015, O3 had only a weak negative correlation according to NOx (r = -0.58) and a weaker positive for SO_2 (r = 0.31). That suggests that pollution levels may have a substantial impact on local air quality and the aerosol formation potentials.

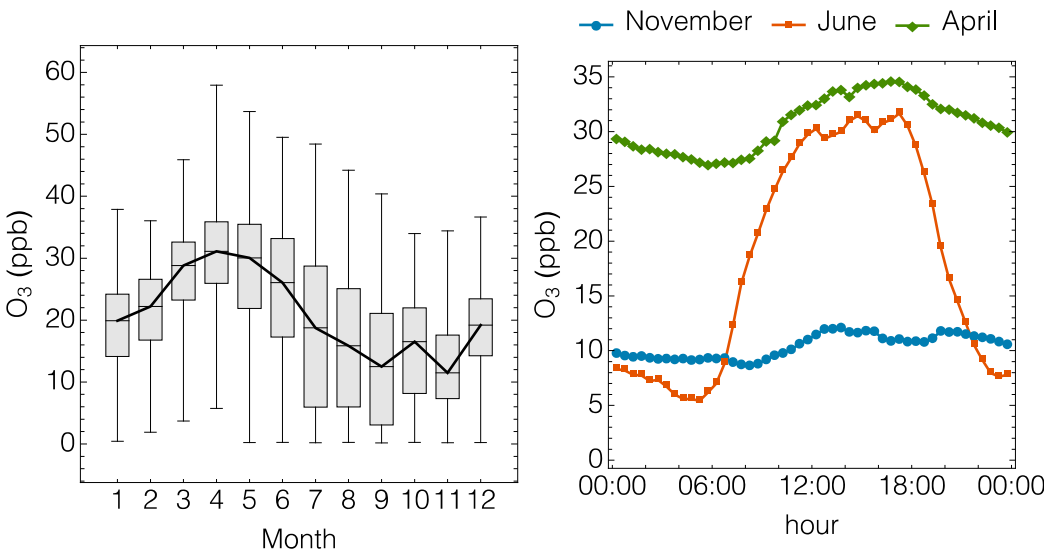

Figure 2. Seasonal variation of ambient O_3 mixing ratios (monthly medians, left panel) and diurnal variation of O_3 in different seasons (Spring, Summer, and late autumn, right panel).

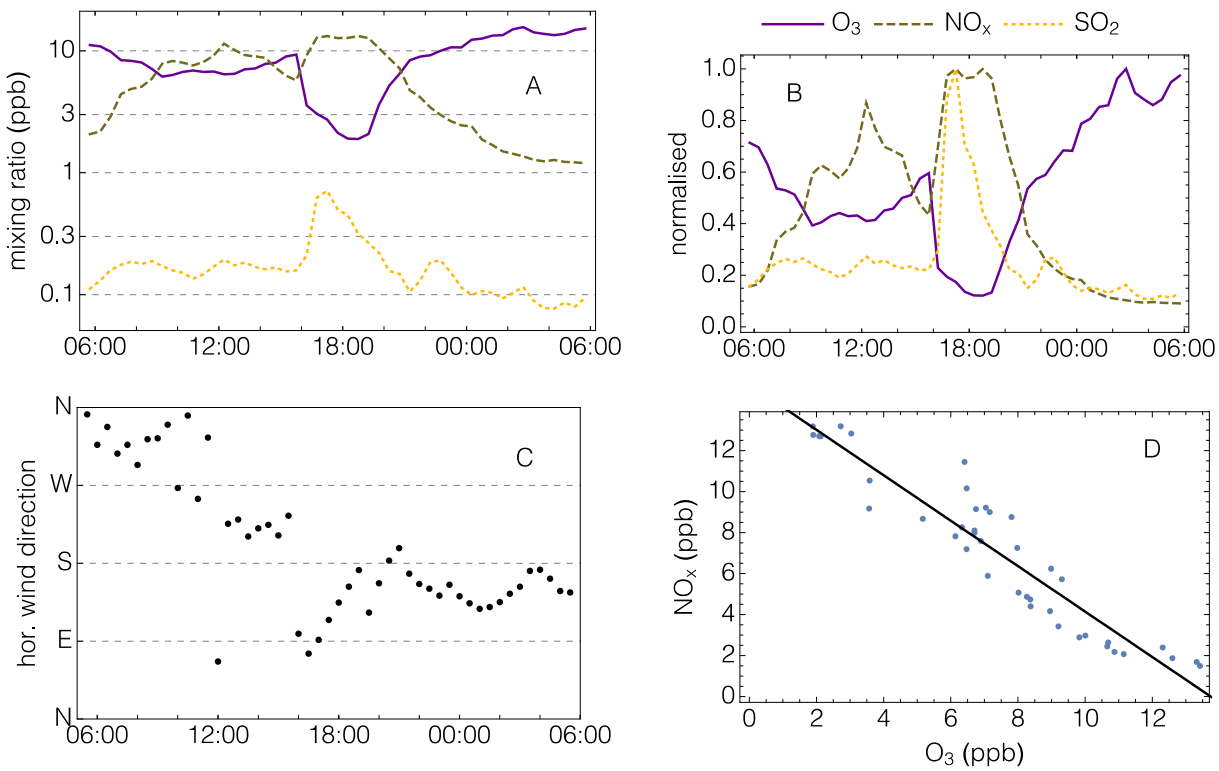

Figure 3. Ambient mixing ratios of O_3, NOx, and SO_2 measured at the 28th February 2015. Panel (A) shows the diurnal dynamic on a logarithmic scale. (B) shows the normalised ambient mixing ratios. (C) gives the horizontal wind speed and (D) the linear relationship between O_3 and NOx fitted to a linear model (y = mx + b).

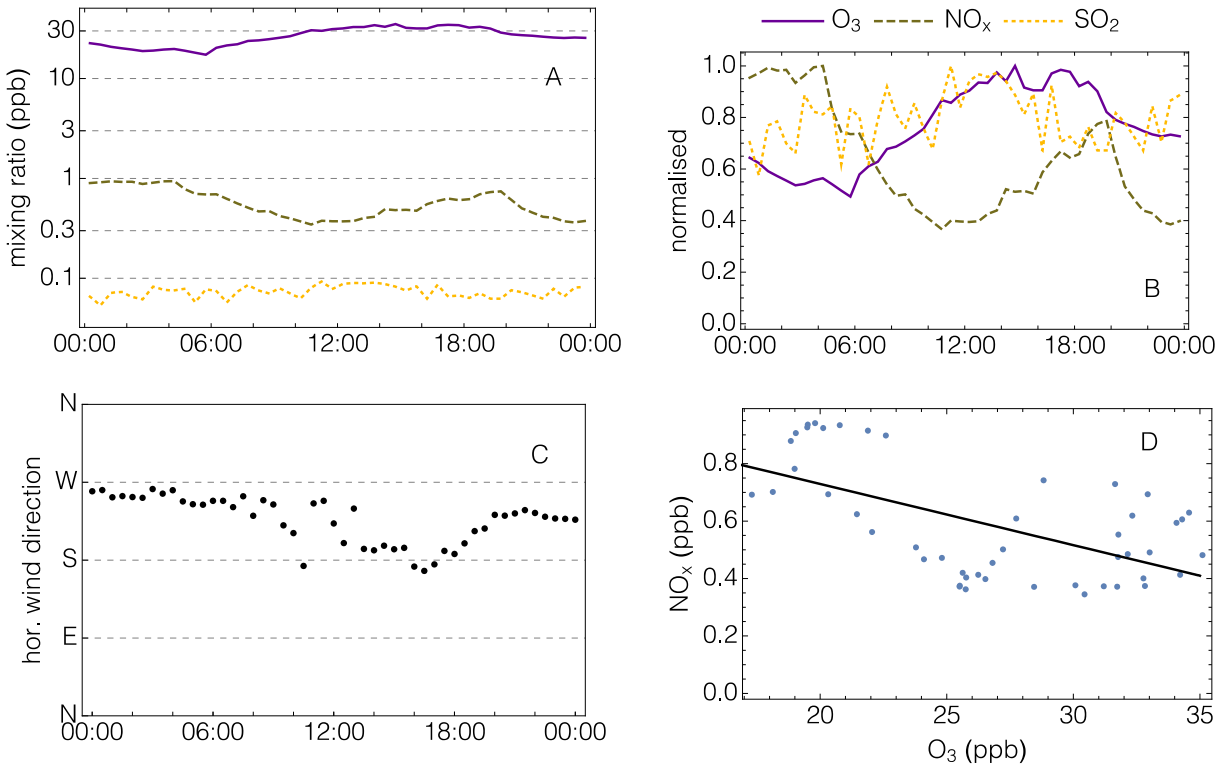

Figure 4. Ambient mixing ratios of O_3, NOx, and SO_2 measured at the 17th May 2015. As above (A) shows the diurnal dynamic on a logarithmic scale. (B) the normalised ambient mixing ratios, (C) the horizontal wind speed and (D) the linear relationship between O_3 and NOx fitted to a linear model (y = mx + b).

ACKNOWLEDGEMENTS

The authors received financial supported by the Estonian Ministry of Science and Education (institutional grants IUT-8-3 and IUT-20-52 and IUT-20-11), the European Commission through European Regional Fund (the "Centre of Excellence in Environmental Adaptation", the "Environmental Conservation and Environmental Technology R&D Programme" project BioAtmos (3.2.0802.11-0043), the "Internationalization of Science Programme" project INSMEARIN (10.1-6/13/1028), the "Estonian Research Infrastructures Roadmap" project Estonian Environmental Observatory (3.2.0304.11-0395)), and the European Research Council (advanced grant 322603, SIP-VOL+).

REFERENCES

Ehn M., Thornton J.A., Kleist E., Sipila M., Junninen H., Pullinen I., Springer M., Rubach F., Tillmann R., Lee B., Lopez-Hilfiker F., Andres S., Acir I.-H., Rissanen M., Jokinen T., Schobesberger S., Kangasluoma J., Kontkanen J., Nieminen T., Kurten T., Nielsen L.B., Jorgensen S., Kjaergaard H.G., Canagaratna M., Maso M.D., Berndt T., Petaja T., Wahner A., Kerminen V.-M., Kulmala M., Worsnop D.R., Wildt J. & Mentel T.F. 2014. A large source of low-volatility secondary organic aerosol. *Nature* 506: 476–479.

Hari P. & Kulmala M. 2005. Station for Measuring Ecosystem–Atmosphere Relations (SMEAR II). *Boreal Env. Res.* 10: 315–322.

Kulmala M., Kontkanen J., Junninen H., Lehtipalo K., Manninen H.E., Nieminen T., Petäjä T., Sipilä M., Schobesberger S., Rantala P., Franchin A., Jokinen T., Järvinen E., Äijälä M., Kangasluoma J., Hakala J., Aalto P.P., Paasonen P., Mikkilä J., Vanhanen J., Aalto J., Hakola H., Makkonen U., Ruuskanen T., Mauldin R.L., Duplissy J., Vehkamäki H., Bäck J., Kortelainen A., Riipinen I., Kurtén T., Johnston M. V, Smith J.N., Ehn M., Mentel T.F., Lehtinen K.E.J., Laaksonen A., Kerminen V.-M. & Worsnop D.R. 2013. Direct observations of atmospheric aerosol nucleation. *Science* 339: 943–946.

Niinemets Ü., Ciccioli P., Noe S.M. & Reichstein M. 2013. Scaling BVOC Emissions from Leaf to Canopy and Landscape: How Different Are Predictions Based on Contrasting Emission Algorithms? In: Niinemets Ü. & Monson R.K. (eds.), *Biology, Controls and Models of Tree Volatile Organic Compound Emissions*, Springer

Netherlands, Dordrecht, pp. 357–390.
Noe S.M., Kimmel V., Hüve K., Copolovici L., Portillo-Estrada M., Püttsepp Ü., Jõgiste K., Niinemets Ü., Hörtnagl L. & Wohlfahrt G. 2011. Ecosystem-scale biosphere–atmosphere interactions of a hemiboreal mixed forest stand at Järvselja, Estonia. *Forest Ecology and Management* 262: 71–81.
Noe S.M., Krasnov D., Krasnova A., Cordey H.P.E. & Niinemets Ü. 2016a. Seasonal variation and characterisation of reactive trace gas mixing ratios over a hemiboreal mixed forest site in Estonia. *Boreal Env. Res.* 21: in press.
Noe S.M., Niinemets Ü., Krasnova A., Krasnov D., Motallebi A., Kängsepp V., Jõgiste K., Hõrrak U., Komsaare K., Mirme S., Vana M., Tammet H., Bäck J., Vesala T., Kulmala M., Petäjä T. & Kangur A. 2016b. SMEAR Estonia: Perspectives of a large-scale forest ecosystem – atmosphere research infrastructure. *Forestry studies* 62: in press.
Riuttanen L., Hulkkonen M., Dal Maso M., Junninen H. & Kulmala M. 2013. Trajectory analysis of atmospheric transport of fine particles, SO2, NOx and O3 to the SMEAR II station in Finland in 1996--2008. *Atmos. Chem. Phys.* 13: 2153–2164.

INTEGRATED AQUATIC STUDIES BASED A CONTINUOUSLY OPERATED MEASURING PLATFORM: POSSIBILITIES AND CHALLENGES

A. OJALA[1,3], I. MAMMARELLA[2], J. BÄCK[3], J. PUMPANEN[3,4], M. RANTAKARI[5], H. MIETTINEN[5], J. HEISKANEN[2], E. PELTOMAA[5], K.-M. ERKKILÄ[2], M. PROVENZALE[2], P. HARI[3], T. VESALA[2] and M. KULMALA[2]

[1]Department of Environmental Sciences, University of Helsinki, Niemenkatu 73, Lahti, Finland

[2]Department of Physics, University of Helsinki, P. O. Box 64, Helsinki, Finland

[3]Department of Forest Sciences, University of Helsinki, P. O. Box 27, Helsinki, Finland

[4]Department of Environmental and Biological Sciences, University of Eastern Finland, P. O. Box 1627, Kuopio, Finland

[5]Department of Environmental Sciences, University of Helsinki, P. O. Box 65, Helsinki, Finland

Keywords: BIOGEOCHEMICAL CYCLES, CARBON MONITORING, CLIMATE CHANGE, LAKE-ATMOSPHERE INTERACTIONS

INTRODUCTION

Freshwater ecosystems are an intrinsic component of Northern landscape, especially in areas which were covered by ice sheet during the last Weichselian glaciation. Thus, there are more than a million lakes in the European territory alone and three out of four lakes are in Norway, Sweden, Finland and North West Russia where on average 5-10 % of the surface area is covered by lakes; there are also regions where the lake percentage is 20-30 %. Besides earlier glaciation, presence of permafrost and peatlands increases the abundance of lakes and thus positively affects the number of lakes e.g. in Siberia (Smith *et al.*, 2007). In addition to recreation and fishery, the important ecosystem services provided by these numerous lakes include climate change mitigation, sediment and nutrient retention and processing as well as hydrological regulation. Climate change mitigation is through hydrological buffering and carbon sequestration; inland waters are known to sequester significant amounts of carbon produced in the surrounding terrestrial ecosystems thus possibly reducing the impact of climate change. For instance in northern Europe the areal carbon stocks in lake sediments are larger than in forest soil or woody biomass (Kortelainen *et al.*, 2004). Through biogeochemical processing organic carbon – produced in lake ecosystems themselves or laterally transported from the surrounding catchment areas – is mineralized to methane (CH_4) and carbon dioxide (CO_2). This carbon mineralization renders the lake ecosystems supersaturated with CH_4 as well as CO_2 finally resulting in atmospheric fluxes (Cole *et al.*, 1994).

Despite the obvious importance of northern lacustrine ecosystems, there has been limited activities in long-term integrative research, where lakes would be studied as fully and truly open systems instead of considering them as isolated entities of their own. In reality all lakes are in constant and close contact with the atmosphere as well as the surrounding terrestrial ecosystems, i.e. lakes are a nexus of lateral and vertical fluxes of energy and material. To improve the state of affairs we need well-established, high-quality research infrastructures with continuous measurements encompassing all major components of lacustrine ecosystems. With continuous measurements we also salute lakes as highly dynamic systems which are impossible to comprehend only on the basis of discrete, even sporadic grab sampling.

Here we present a lake platform to measure continuously fluxes and concentrations of elements of biogeochemical importance in aquatic environment using state-of-the art measuring techniques. The aim is to study a boreal lacustrine ecosystem as a part of the land-atmosphere continuum (peatland-forest-

streams-lake-atmosphere) in the context of climate change, i.e. to truly integrate the aquatic research with terrestrial and atmospheric studies. The methodologies are adopted and adapted from atmospheric physics and forest sciences to enhance synergy and ensure smooth integration of results. Besides element (e.g. carbon) cycling we also study lacustrine fluxes of energy and momentum as well as the lake as a source of volatile organic compounds (VOCs) with potential importance in atmospheric aerosol formation.

METHODS

The research is being carried out in southern Finland in Lake Kuivajärvi (61°50' N, 24°17' E) in close vicinity of the Helsinki University Forestry Field Station and the SMEAR II station for measuring ecosystem-atmosphere relations, established in 1995 (Hari and Kulmala, 2005). The site also belongs to the pan-European ICOS (Integrated Carbon Observation System) measuring network. The Lake-SMEAR platform in the middle of the lake was launched in 2009. The lake is a typical boreal humic lake with high concentration of organic carbon of terrestrial origin and thus dark water colour (Heiskanen *et al.,* 2014). Length of the lake is 2.6 km and maximum depth ca. 13 m. The oblong lake with a strong channeling effect for wind has a surface area 0.62 km^2. The size of the catchment area is 940 ha and it consists of drained peatlands and managed coniferous forests. The core of the platform instrumentation is the eddy covariance (EC) apparatus for atmospheric measurements of turbulent fluxes of momentum, heat, CO_2 and H_2O. Besides continuous CO_2 flux measurements with EC, we have also had long a long measuring campaign of CH_4 flux measurements with EC. Water temperature is continuously measured with Pt-100 sensors installed from the surface to the bottom; this thermistor chain reveals thermal stratification of the lake in detail. The short and long wave radiation is measured with a CNR-1 net radiometer, mounted at 1 m above the water surface. The ambient relative humidity (RH) and air temperature are measured with a Rotronic MP106A-sensor. For the continuous measurements of water column concentrations of CO_2 at the depths of 0.2 m, 0.5 m, 1.0 m and 3.0 m, we use a closed measuring loop consisting of gas-impermeable tubing, a CO_2 analyzer (CARBOCAP® MP343) and semipermeable silicone rubber tubing for gas collection. The LI-193 Spherical Quantum Sensor is used for measuring the photosynthetically active radiation (PAR) in the water at 0.2 m depth. By combining the water column CO_2 data with irradiance measurements we can estimate photosynthetic carbon uptake by aquatic phytoplankton as well as mineralization of organic carbon back to CO_2 (Hari *et al.,* 2008). For more information about the platform, see Heiskanen *et al.* (2014) and Mammarella *et al.* (2015)

Besides the continuous measurements, we have discrete samplings for background data on water chemistry as well as biological components. We also sample gas concentrations (CO_2, CH_4, N_2O) throughout the water column. For investigations of lateral processes, we have sampled also the streams and rivers flowing into and out from the lake. In addition, intensive campaigns with specific aims and international collaborators are regularly conducted (e.g. Faust *et al.,* 2015). A simplified platform concept has also been taken to other lacustrine and riverine locations (Huotari et *al.,* 2013).

RESULTS

The platform has already produced data series on gas fluxes and lake physics and vastly increased our perspective on dynamics and functioning of lacustrine ecosystems, e.g. how prone they are for physical disturbances driven by weather events and how those disturbances are then reflected in the system. (Heiskanen *et al.,* 2014; Mammarella *et al.,* 2015). Information about lake physics (e.g. heat fluxes) is then used in conjunction with data on biogeochemistry and biology thus opening up new avenues to scientific findings and more holistic understanding of ecosystem functioning. For instance, we have been able to extend the studies of lake-atmosphere gas transfer from purely wind based inspection to include heat fluxes as well (Heiskanen *et al.,* 2014). We have also shown that in lake ecosystems VOCs are not released in the daytime, but at night, possibly as a result of convective heat flux which helps to release compounds produced by water column microbes during daytime stratification. The multidisciplinary collaboration has already resulted also in some surprising results, since we have made the first observation of airborne organic and inorganic arsenic cations, detected in real time not only within the boreal forest, but also over the lake (Faust *et al.,* 2015). The river and stream studies around the lake have so far

revealed the importance of lateral transport processes in carbon cycling and fluxes of this boreal lake; in this respect the hot spots can be found in the riparian zone, i.e. in the interface between the terrestrial and lacustrine ecosystem, while the hot moments are in spring when snow melting results in rapid but intensive flooding periods. We have also shown that despite great challenges it is possible to use an EC measuring platform also in a large river (Huotari *et al*, 2013).

CONCLUSIONS

The measuring platform has proven to be a scientifically sound approach in lacustrine climate change studies. So far it has appeared most advantageous in vertical flux studies, especially in the lake-atmosphere interphase where - in contrast to traditional discrete point sampling - the approach greatly improves temporal resolution of observations, i.e. instead of daily, weekly or even monthly sampling the platform now collects data continuously. In terms of spatial coverage it also represents an improvement since the data are representative of a larger footprint area whose size and location can be estimated on the basis of modelling. However, the platform only measures the open pelagic part in the deepest basin of the lake and thus the e.g. metabolically active shallow vegetated shore line areas are still ignored. More observations are also needed e.g. from water column physics around the measuring platform, hence the need to employ several thermistor chains instead of one. Further improvements are also needed in water column measurements, including biology (e.g. enzymes involved in photosynthesis and production of VOCs) and in measurements in the sediment-water interphase which is crucial for CO_2 and CH_4 studies as well as biogeochemical research in general. With close co-operation with modellers we will in future also be able to more closely link the lake studies with terrestrial studies and fully assess the pros and cons of the approach in the catchment scale.

ACKNOWLEDGEMENTS

This work was supported by EU projects InGOS and GHG-LAKE (project no. 612642), Nordic Centre of Excellence DEFROST, and National Centre of Excellence (272041), ICOS (271878), ICOS-FINLAND(281255), ICOS-ERIC (281250), CarLAC (281196), PACE (139291) and project 256082 (Flux measurements of greenhouse gases for agricultural, lake and wetland ecosystems and process modeling of wetland methane production) funded by Academy of Finland. We are also grateful for the starting grant granted by University of Helsinki to establish the platform (project VESIHIISI).

REFERENCES

Cole, J. J., Caraco, N. F., Kling, G. W. & Kratz, T. K. (1994). *Carbon dioxide supersaturation in the surface water of lakes.* Science **265**, 1568-1570. DOI: 10.1126/science.265.5178.1568.

Faust, J. A., Junninen, H., Ehn, M., Chen, X., Ruusuvuori, K., Kieloaho, A.-J., Jokinen, T., Worsnop, D. R., Kulmala, M. and Petäjä, T. (2015). Real-time detection of arsenic carions from ambient air in boreal forest and lake environments. doi: 10.1021/acs.est.lett.5b00308.

Hari, P. and Kulmala, M. (2005). Station for measuring ecosystem-atmosphere relations (SMEAR II). *Boreal Environment Res.* **10**, 315-322.

Hari, P., Pumpanen, J., Huotari, J., Kolari, P., Grace. J., Vesala, T. & Ojala, A. (2008). High-frequency measurements of productivity of planktonic algae using rugged nondispersive infrared carbon dioxide probes. *Limnol. Oceanogr.: Methods* **6**, 347-354.

Heiskanen, J. J., Mammarella, I., Haapanala, S., Pumpanen, J., Vesala, T., MacIntyre, E. and Ojala, A. (2014). Effects of cooling and internal wave motions on gas transfer coefficients in a boreal lake. *Tellus B* **66**, 22827, httpx//dx.doi.org/10.3402/tellusb.66.22827.

Huotari, J., Haapanala, S., Pumpanen, J., Vesala, T. and Ojala, A. (2013). Efficient gas exchange between a boreal river and the atmosphere. *Geophys. Res. Lett*. **40**, 1-4, doi: 10.1002/2013GL057705, 2013.

Kortelainen, P., Pajunen, H., Rantakari, M. and Saarnisto, M. (2004). A large carbon pool and small sink in boreal Holocene lake sediments. *Global Change Biol.* **10**, 1648-1653. DOI: 10.1111/j.1365-2486.2004.00848.x.

Mammarella, I., Nordbo, A., Rannik, U., Haapanala, S., Levula, J., Laakso, H., Ojala, A., Peltola, O., Heiskanen, J., Pumpanen, J. and Vesala, T. (2015). Carbon dioxide and energy fluxes over a small boreal lake in southern Finland. *J. Geophys. Res. Biogeosci.* **120**, 1296-1314, doi: 10.1002/2014JG002873.

Smith, L. C., Sheng, Y. and MacDonald, G. M. (2007). A first pan-Arctic assessment of the influence of glaciation, permafrost, topography and peatlands on Northern hemisphere lake distribution. *Permafrost and Periglac. Process*. **18**, 201-208. DOI: 10.1002/ppp.581.

ANTHROPOGENIC PARTICLE NUMBER EMISSIONS AND THEIR SIZE DISTRIBUTIONS IN NORTHERN AND EASTERN EURASIA

P. PAASONEN[1,2,3], K. KUPIAINEN[2,3], Z. KLIMONT[2], A. VISSCHEDIJK[4], H. DENIER VAN DER GON[4], and M. AMANN[2]

[1]Division of Atmospheric Sciences, Department of Physics, University of Helsinki, PL 64, 00014 University of Helsinki, Finland.

[2]International Institute for Applied Systems Analysis (IIASA), Schlossplatz 1, A-2361 Laxenburg, Austria.

[3]Finnish Environment Institute (SYKE), PL 140, 00251 Helsinki, Finland.

[4]Department of Climate, Air and Sustainability, TNO, Princetonlaan 6, 3584 CB Utrecht, the Netherlands

Keywords: PARTICLE NUMBER EMISSIONS, NUMBER SIZE DISTRIBUTION, EMISSION SCENARIO MODEL, AEROSOL-CLOUD INTERACTIONS.

INTRODUCTION

The health and climate effects of aerosol particles are strongly affected by the size and number of particles. Ultrafine particles (UFP), with diameters d_P below 100 nm, can enter through lungs into human cardiovascular system and cause adverse health effects which differ from those of larger particles (WHO, 2013). On the other hand, particles with diameters d_P close to or over 100 nm can be activated as cloud droplets, thus cooling the climate (Stocker *et al.*, 2013). During the last years we have implemented particle number emission factors with size distributions to the global emission scenario model GAINS (Greenhouse gas and Air pollution Interactions and Synergies). Where the previous stage of this project provided the current and future emission estimate for Europe (Paasonen *et al.*, 2013), the update to GAINS Global allows the improvement of the modelling of global climate as well as regional air quality with better description of particle number emissions. However, significant uncertainties remain in emissions from several key sources outside Western countries, due to the shortness of literature on the emissions factors from these sources. In this presentation the anthropogenic particle number emission estimates for 2010-2030 in Europe, Russia and China are presented under the current legislation –scenario, and the main sources of uncertainties are pointed out.

METHODS

The GAINS (Greenhouse gas – Air pollutant Interactions and Synergies) model (Amann *et al.*, 2011) is an integrated assessment model, which brings together information on the sources and impacts of air pollutant and greenhouse gas emissions and their interactions. GAINS combines data on economic development with the structure, control potential and costs of emission sources. The political scenarios in GAINS allow for researchers and modellers to study the future global emissions and their spatial distribution and for decision makers to compare the costs and outcomes of regulations and investments on new technologies. GAINS describes the inter-relations between the effects and emissions of various pollutants (SO_2, NO_x, PM, NMVOC, NH_3, CO_2, CH_4, N_2O, F-gases) that contribute to these effects. GAINS assesses more than 1000 measures to control the emissions to the atmosphere for each of its 168 regions (mainly countries, out of which some divided in regions, e.g. China consisting of 32 regions and Russia into European and Asian parts). However, the emissions are also gridded down to 0.5°×0.5° resolution, which facilitates the modelling of the resulting concentrations and their effects .In its optimization

mode, GAINS identifies the least-cost balance of emission control measures across pollutants, economic sectors and countries that meet user-specified air quality and climate targets.
The annual emissions E in a country (or region) i are calculated as

$$E_i = \sum_{jkm} E_{ijkm} = \sum_{jkm} A_{ijkm} X_{ijkm} \mathrm{EF}_{ijkm},$$

where the indices and symbols refer to

j	Source sector (e.g. domestic single house heating boilers)
k	Fuel (e.g. firewood, coal)
m	Abatement technology (e.g. pellet boilers, boilers with electrostatic precipitator)
A	Volume of annual activity (typically annual energy consumption in sector j with fuel k)
X	Share of abatement technology of the activity m (so that $\sum_m X_m = 1$)
EF	Emission factors for each sector-fuel-technology –combination (emissions per activity unit)

Lately we have introduced aerosol particle number emission factors (PNEF) with corresponding particle (number) size distributions (PSD) to GAINS (Paasonen *et al.*, 2013). For road transport PNEFs and PSDs are based on the latest version of TRANSPHORM database (Vouitsis *et al.*, 2013), for the global analysis extended with separate PNEFs and PSDs for varying fuel sulphur contents. For other sources, emission factors are obtained from the literature and from a previous emission inventory by TNO (Denier van der Gon *et al.*, 2009; Kulmala *et al.*, 2011). The implemented emission factors and size distributions represent the emissions of both primary and secondary particles after cooling and initial dilution to the surrounding air. Particle size distributions in size range 3-1000 nm are described with 8 size bins, facilitating their application in modelling purposes.

RESULTS

Particle number emissions are dominated by ultrafine particle (UFP, d_P <100 nm) emissions, which form close to 80 % of the global emissions (see lower panel of Fig. 1).

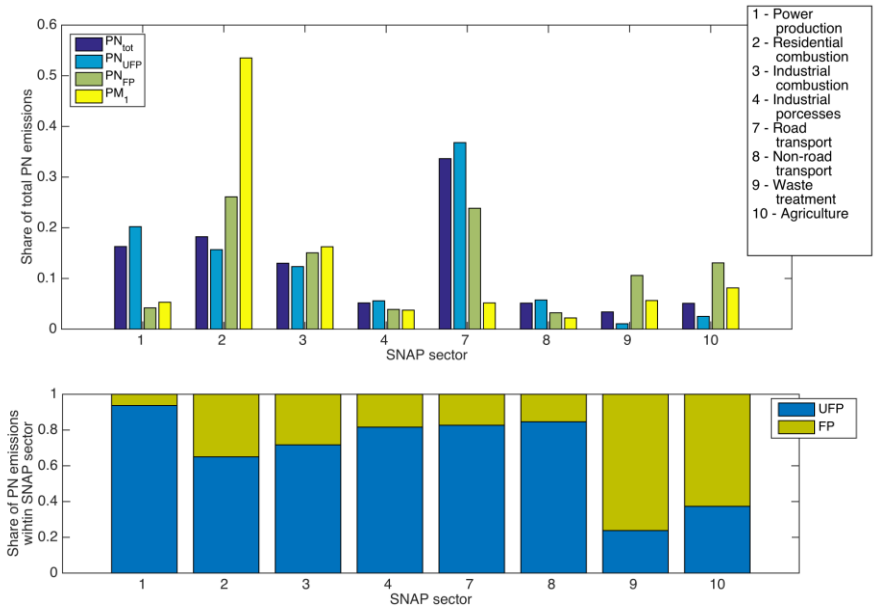

Figure 1. Upper panel: global shares of different source sectors in aerosol number emissions of all (PN_{tot}), ultrafine (PN_{UFP}) and fine (PN_{FP}) particles and aerosol mass emissions of particles with diameters below 1 µm (PM_1) on 2010. Lower panel: shares of ultrafine and fine particles in PN emissions for each sector.

The upper panel of Fig. 1 shows, for year 2010, the shares of different sources in global continental total particle number emissions (PN_{tot}), in number emissions of ultrafine particles (UFP) and fine particles (FP, here d_P >100 nm), as well as in mass emissions of particles with $d_P <$ 1000 nm ($d_P <$ 1 µm, PM_1). The main number source of UFP is road transport, representing 40 % of the total UFP emissions and thus being the largest contributor to total aerosol particle number emissions. Also power production contributes to the UFP emissions with 20 % share, mainly due to emissions from coke production, and residential combustion has a shaere of 17 %. The shares of residential combustion and road transport in FP number emissions are quite similar, roughly 30 % each, whereas the PM_1 mass emissions are clearly dominated by residential combustion (> 50 %). These differences indicate the need for assessing the size segregated number emissions of aerosols in addition to mass emissions.

The annual PN emissions and their estimated future trend in each source sector in Europe, Russia and China, are depicted in Figure 2. The future trend is based on the Current Legislation (CLE) baseline scenario created in the ECLIPSE project, specifically version 5 of this scenario (ETP_CLE_v5, Klimont et al., 2016; Stohl et al., 2015). In 2010, the emissions in Europe were clearly dominated by road transportation. In China, the estimated major sources were coke production (the dominant source in China under power production), residential coal combustion and industrial combustion, and in Russia the emissions from power production, industrial processes, road transport and other transport (the last including emissions from gas pipeline compressors) were roughly equal.

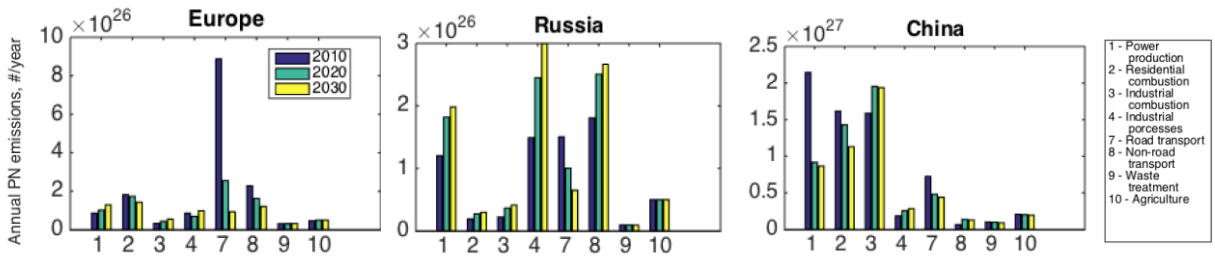

Figure 2. Contributions of different source sectors to particle number emissions in Northern and Eastern Eurasia, from 2010 to 2030. Note the differences in y-axis scles.

The actions determined in current legislation are foreseen to decrease the emissions efficiently in Europe and in China. In Europe this decrease is caused by the drastic decrease foreseen in traffic emissions due to improving emission abatement technologies, which, even though targeted for particulate mass emissions, have a strong impact on number emissions. In China, the decreases in emissions are driven by decreases in coke production and residential coal combustion emissions, both partly related to the increase in the electricity network replacing the coal fired cooking stoves. On the contrary, in Russia, the increases in activities in industrial processes, power production sector and combustion in gas pipeline compressors cause increase in total emissions.

The uncertainties in the emissions from different sources and regions are very different. In Western countries, where the main PN source is road traffic and the ultralow sulphur content is the standard in diesel fuel, the overall uncertainty levels can be considered relatively low. Also the residential wood combustion emissions, another important PN source in Western countries, are relatively well described, as the PNEFs are based on large number of articles on different types of stoves, boilers and fireplaces. On the contrary, the PN emissions in China and Russia are dominated with sources for which PNEFs are much less representative. E.g. the PNEFs and PSDs for coke production and residential coal combustion, both being among the main UFP sources especially in China, are both based on only one research article each (Weitcamp et al., 2005; Bond et al., 2002, respectively). Furthermore, for various combustion sources, the nucleation mode particles (d_P < 30 nm) formed immediately after emissions to atmosphere, are often not well represented in the literature. This shortcoming causes presumably underestimations for emissions

from combustion sources excluding road transport, for which the effect of fuel sulphur content (increasing the nucleation mode emissions) is taken into account.
In addition to the uncertainties in PNEFs, the total uncertainties have a significant contribution from the imperfect determination of the activity levels. The overall uncertainties, with an emphasis on the Northern and Eastern Eurasia, and possible ways to decrease them will be discussed in the presentation.

CONCLUSIONS

Estimation of global anthropogenic particle number emissions, including the information on their size distribution, was performed with the GAINS-Global model. The first results show that currently the dominating source in terms of particle numbers is road transport, covering close to 40 % of global emissions. However, in China and Russia also coke production, residential and industrial combustion, as well as industrial processes and gas pipeline compressors are estimated to have a significant contribution to particle number emissions. The emissions are estimated to decrease towards 2030's due to improving emission abatement techniques in Europe and China, whereas in Russia the total emissions are predicted to increase due to steep increase in activity levels, which overrules the technical improvements. The presented results are subject to significant uncertainties, mainly due to scarcity of published information on the particle number emission factors and size distributions in several source sectors, especially in terms of nucleation mode particles with diameters below 30 nm. However, introducing the particle number emissions to GAINS model provides new information on the changes in anthropogenic PN emissions required in modelling the future climate and air quality, as well as helps building the basis for possible future limitations on particle number emissions. The comparison of the GAINS emissions to previous global emission estimates and the comparisons between the modelled PN concentrations and atmospheric observations in Northern and Eastern Eurasia are presented in an abstract submitted to the 2nd PEEX Science Conference by Xausa et al. (2016).

ACKNOWLEDGEMENTS

This work was funded by the Academy of Finland Centre of Excellence (grants no. 1118615 and 272041) and European Commission 7th Framework projects ECLIPSE (Project no. 282688), PEGASOS (265148) and 'Assessment of hemispheric air pollution on EU air policy' (contract no. 07.0307/2011/605671/SER/C3). We thank Leonidas Ntziachristos and Ilias Vouitsis at Aristotle University of Thessaloniki (Greece) for help and assistance in applying the emission factors for road transport sector and professor Qiang Zhang from Tsinghua University (Beijing, China) for the spatial distribution of Chinese power plants for 2000, 2005, and 2010.

REFERENCES

Amann, M. et al. (2011). Cost-effective control of air quality and greenhouse gases in Europe: modeling and policy applications. EMS 26, 1489–1501.

Bond, T. C. et al. (2002). Primary particle emissions from residential coal burning: Optical properties and size distributions, J. Geophys. Res., 107(D21), 8347.

Denier van der Gon, H. et al. (2009). Size-resolved Pan European Anthropogenic Particle Number Inventory, EUCAARI Deliverable 141.

Klimont, Z., et al. (2016). Global anthropogenic emissions of particulate matter. *In preparation*.

Kulmala, M. et al. (2011). General overview: European Integrated project on Aerosol Cloud Climate and Air Quality interactions (EUCAARI) - integrating aerosol research from nano to global scales. Atmos. Chem. Phys. **11**, 13061–13143.

Paasonen , P. et al. (2013), Aerosol particle number emissions and size distributions: Implementation in the GAINS model and initial results. IIASA Interim Report, IR-13-020.

Stocker, T. F., et al. (2013), Technical Summary. In: Climate Change 2013: *The Physical Science Basis. Contribution of Working Group I to the Fifth Assess- ment Report of the Intergovernmental Panel on Climate Change*. Cambridge Univ. Press, Cambridge, UK and New York, NY, USA.

Stohl, A., et al (2015). Evaluating the climate and air quality impacts of short-lived pollutants, Atmos. Chem. Phys., 15, 10529-10566, doi:10.5194/acp-15-10529-2015.
Vouitsis, I., Ntziachristos, L., Han, Z. (2013). Methodology for the quantification of road transport PM emissions, using emission factors or profiles. TRANSPHORM Deliverable D1.1.2.
Weitkamp, E. A., et al. (2005), Fine particle emission profile for a large coke production facility based on highly time-resolved fence line measurements. Atm. Environ., 39, 36, 6719-6733.
WHO (2013). Review of evidence on health aspects of air pollution – REVIHAAP [WWW Document]. URL http://www.euro.who.int/__data/assets/pdf_file/0020/182432/e96762-final.pdf (accessed 3.27.13).
Xausa, F. et al. (2016). Implementation of a new size-segregated aerosol number emissions module in global climate modelling. Abstract to the 2nd Pan-Eurasian Experiment (PEEX) Science Conference.

SOIL CO_2 EFFLUX RATES AFTER WILDFIRES IN CENTRAL SIBERIAN ECOSYSTEMS

A.V. PANOV[1], G.K. ZRAZHEVSKAYA[1], M.A. KORETS[1], A.V. BRYUKHANOV[1], N.V. SIDENKO[1], A.V. TIMOKHINA[1], M. HEIMANN[2]

[1]V.N. Sukachev Institute of Forest SB RAS, Krasnoyarsk, Russia

[2]Max Planck Institute for Biogeochemistry, Jena, Germany

Keywords: WILDFIRE, SIBERIAN FORESTS, SOIL RESPIRATION.

INTRODUCTION

Fire is a main disturbance factor in boreal forest ecosystems, which is very important to the ecology of these sensitive forests and plays a central role in carbon cycling. The rapid influence of fire on carbon cycle occurs through the emission of carbon into the atmosphere during biomass burning (Andreae, Merlet, 2001). Besides this direct influence fire initiates succession and thus regulates patterns of C accumulation through net primary production and also influences the soil thermal and moisture regime, which, in turn, affect patterns of soil respiration (Richter *et al*., 2000, O'Neill *et al*., 2002). Since 2006 the Zotino Tall Tower Observatory (ZOTTO; www.zottoproject.org) a research platform for large-scale climatic observations is operational in Central Siberia (60°48'N, 89°21'E). The data of high-frequency trace gas measurements at the tall tower are used in atmospheric inversion studies to infer the distribution of C sinks and sources over central part of Northern Eurasia (Lavrič *et al*., 2011, Heimann *et al*., 2014). We present our estimates of carbon release to the atmosphere through soil respiration in boreal forest ecosystems of Central Siberia after large-scale wildfires that occured in 2012 in the tall tower footprint area.

METHODS

Burned landscapes in the tall tower footprint area were estimated based on Landsat ETM 5,8 satellite images. For selected burned areas a magnitude of ecological change caused by fires ("burn severity") was measured and mapped with a Normalized Burn Ratio index (*dNBR*) (Cocke, Fulé, Crouse, 2005) and further calibrated by a complementary field based Composite Burn Index (*CBI*) (Key, Benson, 2006). Additionally, values of combustion efficiency (*CE*) (Andreae, Merlet, 2001) for studied areas were calculated based on the time series of CO/CO_2 mixing ratios measured at 300 m a.g.l. in fire plumes at ZOTTO while air transport from specific wildfires upwind of the measurement site was traced based on ensembles of 24-hrs backward trajectories from ARL NOAA HYSPLIT model (Draxler, Rolph, 2003). Active fire spots were detected from Terra/Aqua MODIS satellite data. Field investigations were performed on study plots established after fire in the dominant ecosystems of Central Siberia (lichen pine, moss pine, mixed forest, dark forest and peat bog) where estimations of woody C pools and their mapping were made with a laser-based field instrumentation system. Soil respiration rates were measured within the plots using a dynamic closed chamber method by a portable LI-6400 system.

CONCLUSIONS

Within all studied ecosystems soil efflux rates 3 yrs after fire demonstrated 15 - 25% lower values compared to the pre-fire conditions (fig.1a). The highest values within ecosystems after fire have been found out in wet and less disturbed dark coniferous and mixed forests (up to 3,8 $\mu molC/m^2/s$). In these ecosystems fires occured mostly in a smoldering phase (*CE* = 0,92 - 0,93) and a field calibrated *dNBR* didn't exceed 25 – 30%. Such fires could cause only a surface mineralization that resulted in soil fertilization after fire and a spread vegetation cover was found within the plots. A linear regression

analysis (fig.1b) has shown a strong correlation (r^2=0.91 – 0.98) of soil efflux rates and soil temperature (10 cm depth), which confirms the essential input of autotrophic respiration into a total C flux.

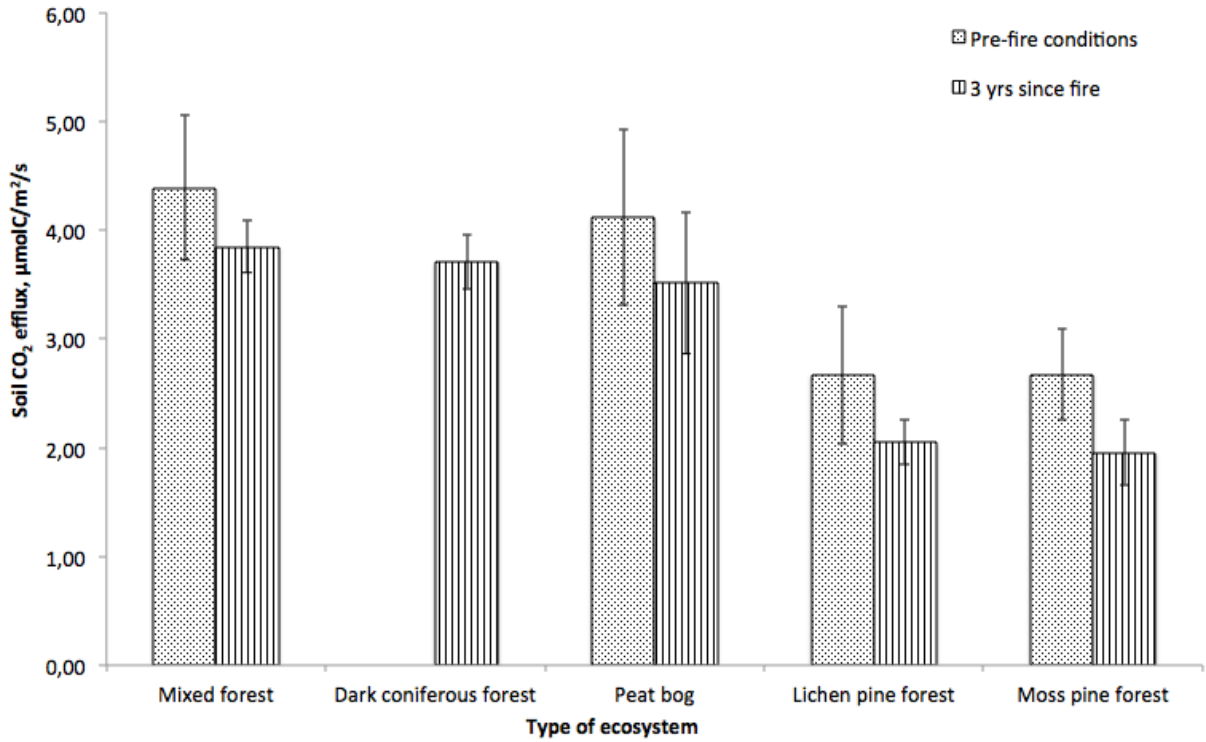

a)

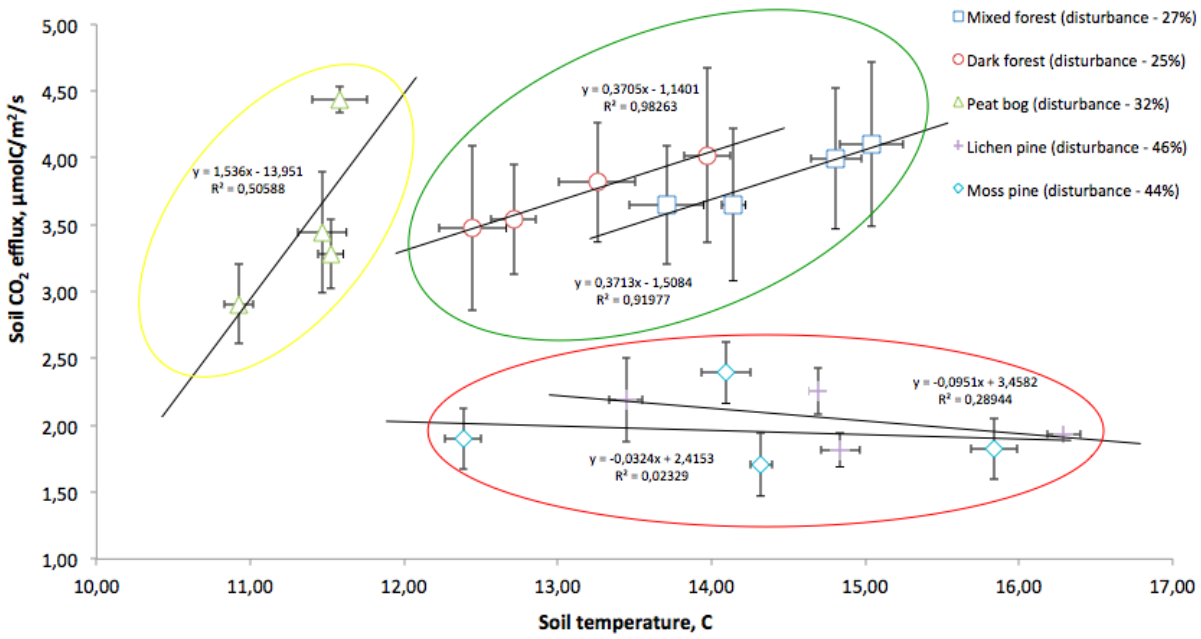

b)

Figure 1. Soil CO_2 efflux rates prior and after wildfires (a), and a linear regression analysis of soil CO_2 efflux rates and soil temperature (10 cm depth) (b).

In turn the lowest values (2,5 μmolC/m^2/s) were typical within the dry pine stands with the highest *dNBR* (≈ 45%), where *CE* could reach up to 0,99 demonstrating a prevailing flame phase of fire. Within these plots we found out >80% of dead trees and highly damaged vegetation cover with patches of exposed mineral soil. Decomposition processes in C cycling of such ecosystems are believed to be prevailing. Linear regressions analysis of efflux rates and soil temperature didn't demonstrate any correlation (r^2=0.02), which also suggests a primarily heterotrophic origin of C flux.

ACKNOWLEDGEMENTS

This work was supported by the Max Planck Society (Germany), project of RSF # 14-24-00113 and RFBR grant # 15-45-04423.

REFERENCES

Andreae, M.O. and Merlet, P (2001). Emission of trace gases and aerosols from biomass burning. *Global Biogeochem. Cycles*. **15**. P. 955-966.

Cocke, A.E., Fulé, P.Z., Crouse, J.E (2005). Comparison of burn severity assessments using Differenced Normalized Burn Ratio and ground data. *International Journal of Wildland Fire*. **14**. P. 189–198.

Draxler, R., Rolph, G (2003). HYSPLIT (HYbrid Single-Particle Lagrangian Integrated Trajectory) Model access via NOAA ARL READY. NOAA Air Resources Laboratory [Website]. - http://ready.arl.noaa.gov/HYSPLIT.php.

Heimann, M., Schulze, E.-D., Winderlich, J. *et al.* (2014). The Zotino Tall Tower Observatory (ZOTTO): Quantifying Large Biogeochemical Changes in Central Siberia. *Nova Acta Leopoldina*. **399**. P. 51–64.

Key, C.H., Benson, N.C (2006). Landscape assessment (LA) sampling and analysis methods // *USDA Forest Service Gen. Tech. Rep*. 55 p.

Lavrič, J., Heimann, M., Gerbig, C. *et al.* (2011). A look up at the Zotino Tall Tower Observatory. *Meteorol. Techn. Intern*. **Sept.** P. 6–10.

O'Neill, K. P., Kasischke, E. S., and Richter, D. D (2002). Seasonal and decadal patterns of soil carbon uptake and emission along an age-sequence of burned black spruce stands in interior Alaska. *J. Geophys. Res*., **107**.

Richter, D., Kasischke, E. S., and O'Neill, K. P (2000). *Postfire stimulation of microbial decomposition in black spruce (Picea mariana L.) forest soils: A hypothesis, in Fire, Climate Change, and Carbon Cycling in the North American Boreal Forest*. (Springer-Verlag, New York). pp. 197-213.

VARIATIONAL MODELING TECHNOLOGY WITH DATA ASSIMILATION FOR ENVIRONMENTAL PREDICTION AND RISK ASSESSMENT

V.V. PENENKO[1,2], A.V. PENENKO[1,2], and E.A. TSVETOVA[1]

[1]Institute of Computational Mathematics and Mathematical Geophysics,
Novosibirsk, 630090, Russia,

[2] Novosibirsk National State University

Keywords: COUPLED ATMOSPHERIC HYDRODYNAMICS AND CHEMISTRY, DIRECT AND INVERSE PROBLEMS, VARIATIONAL DATA ASSIMILATION, ENVIRONMENTAL RISK.

INTRODUCTION

In the frames of PEEX Modelling Platform, we develop a set of mathematical tools for construction of integrated models for solution of interconnected problems of atmospheric environment and climate (Bocquet , 2015) . The central point is a variational approach for solving direct and inverse problems of atmospheric hydrodynamics and chemistry. Variational principles with weak constraints (Penenko, 2009) provide handy tools for these purposes. They allow us to consist and effectively use the complicated mathematical models of the studied processes together with different types of data available from various monitoring systems including information in the form of images. Traditional methods to inverse the operators of observations have a limited capacity even for modern computer systems. After such inversion of the results of remote observations, it is necessary to present them in terms of the state functions of four-dimensional dynamics of the atmosphere, and then to associate them with some models of transport and transformation of relevant substances. Unlike this approach, variational principles make it possible to organize the system simulation from the problem statement to obtaining the results as well as to ensure the operational assimilation of incoming information in the system.

MODELS OF PROCESSES

For our purposes, we use a set of mathematical models to solve the joint problems of hydrodynamics and chemistry of the atmosphere. The structure of these models can be represented in the operator form:

$$L(\boldsymbol{\varphi},\mathbf{Y},\mathbf{r}) \equiv \frac{\partial \boldsymbol{\varphi}}{\partial t} + G(\boldsymbol{\varphi},\mathbf{Y}) - \mathbf{f} - \mathbf{r} = 0\,, \quad \boldsymbol{\varphi}(\mathbf{x},t) \in Q(D_t)\,, \tag{1}$$

$$\boldsymbol{\varphi}^0 = \boldsymbol{\varphi}_a^0 + \boldsymbol{\xi} \quad , \quad \mathbf{Y} = \mathbf{Y}_a + \boldsymbol{\zeta}\,, \tag{2}$$

where $Q(D_t) \in L_2(D_t)$ is a real space of state vector-functions $\boldsymbol{\varphi}(\mathbf{x},t) = \left\{\varphi_i(\mathbf{x},t), i = \overline{1,n}\right\}$; $G(\boldsymbol{\varphi},\mathbf{Y})$ is non-linear differential operator; $\mathbf{f}$ is a source function; $\mathbf{Y}$ is a vector of model parameters changing within a range of admissible values $R(D_t)$, $\boldsymbol{\varphi}^0$ is an initial state, $\boldsymbol{\varphi}_a^0, \mathbf{Y}_a$ are their *apiori* estimates; $D_t = D \times [0,\bar{t}\,]$, D is a domain of the space coordinates, $t \in [0,\bar{t}\,]$ is a time interval. The domain D can be the global one on the spherical Earth or a limited part of the global system. Functions $\mathbf{r},\boldsymbol{\xi},\boldsymbol{\zeta}$ in (1) - (2) describe the uncertainties and errors of the corresponding objects.

In the combined models of the dynamics and chemistry, the state functions have a block structure with elements of three types. The variables of the hydrodynamic block are the velocity vector, temperature, density, pressure. The categories of moisture in the hydrological cycle of the atmosphere are water vapor, cloud water, rain, water in the liquid phase, and water in the solid phase (ice, snow). There is a set of

substances in gaseous and aerosol states. Each object in the system (1)-(2) (except constants) depends on spatial coordinates and time.

MODELS OF OBSERVATIONS

The measurement data of the real behavior of the investigated processes are the key elements of all forecasting techniques. We build the simulation system so that we can use all the available information from various observing systems: contact (in situ) and remote ones. Formally, description of the models for satellite observations, lidar and microwave monitoring systems has the same structure. It seems appropriate to use the available observations from unmanned aircrafts and data sensing from sun photometers of the AERONET system.

Satellite observation tools measure emitted or reflected radiation from the Earth's surface, atmosphere or hydrosphere objects. The results of measurements with modern methods and tools of remote sensing are represented as repeated periodically multispectral and hyperspectral images. After pre-processing of sensing data, these images are available in digital form. Typically, each basic element (pixel) of such an image contains a locally averaged data in the dimensions of the following types: spatial coordinates, time, wavelength or frequency of radiation, etc. Characteristics of the dynamics and composition of the atmosphere and water bodies in the images contain the results of the integrated spectral signal along the directions of the trajectories sensing. Sequence of images shows the spatial-temporal dynamics of the processes. The contact observation (in situ) gives the information that clearly ties the specific elements of space and the time intervals. Their use in conjunction with data from remote observations improves the accuracy of the representation of the totality of information.

Consider some ways to incorporate observational data into the modeling system using variational principles. To exploit them in the framework of variational organization of the computing technology together with the process models, we formulate the model of observations, which expresses the functional relationship between the measurement results and their images computed through the state functions of models (1)-(2).

We denote a set of measurement data $\boldsymbol{\Psi}_k \in \boldsymbol{\Psi}(D_t^k, \omega_\nu)$ on $D_t^k \subset D_t$ and define the set of observational models $H_k(\boldsymbol{\varphi})$ for the formation of images of measured values in terms of the state functions of the processes models (1) - (2):

$$\boldsymbol{\Psi}_k = H_k(\boldsymbol{\varphi}) + \boldsymbol{\eta}_k \,. \tag{3}$$

Function $\boldsymbol{\eta}_k$ in (3) describes the uncertainty of representation and errors of models and observations. Observation values are defined on the set of subdomains $D_{tk}^m \in D_t^m \subset D_t$ and on the set of spectral bands of measuring systems, which we denote by ω_ν. Models of observations carry out the operations to convert the data, calculated on the results of the simulated state functions $\boldsymbol{\varphi} \in Q(D_t)$ of the process models (1)-(2), to the objects $\boldsymbol{\psi} = \{\boldsymbol{\psi}_k\}$ from "the space of observations" Ψ. In turn, the adjoint operators $\left[\partial H_k(\boldsymbol{\varphi}) / \partial \boldsymbol{\varphi}\right]^T$ move information from the space of observations Ψ to the space of the state functions $Q(D_t)$.

Some typical examples of such models of observations are the models of remote sensing the atmospheric temperature and gas and aerosol composition from satellite (Showengerdt, 2007), lidar sensing of the atmosphere(Zuev et al,1986) and others.

FUNCTIONALS FOR ASSESSING THE QUALITY OF THE OBSERVATION MODELS AND DATA ASSIMILATION

For the purposes of data assimilation and inverse problem solution, we introduce a quality function that expresses the total measure of the residuals between measured and calculated values from the model of the characteristics of the studied processes

$$\Phi_0(\boldsymbol{\varphi}) = \sum_{k=1}^{K} \frac{1}{2} \int_{D_t} \left(W_{1k} \boldsymbol{\eta}_k, \boldsymbol{\eta}_{k,} \right) \chi_k(\mathbf{x}, t) dDdt \equiv \left(W_1 \boldsymbol{\eta}, \boldsymbol{\eta} \right)_{D_t^m} . \tag{4}$$

Vector $\boldsymbol{\eta}_k = \boldsymbol{\psi}_k - H_k(\boldsymbol{\varphi})$ determines the discrepancy between the measured values of the characteristics of the process and images of these characteristics, calculated using appropriate models of observations; the symbol (,) defines the energy inner product in L_2 - space; W_{1k} are block-diagonal weight matrices for the formation of scalar products in the space of the measured characteristics $\Psi(D_t^m, \omega_\nu)$, χ_k are weighting functions whose supports represent the spatio-temporal localization of the systems and the results of observations. The summation in (4) is carried out for all types of observations, and integration is fulfilled over the whole domain D_t for all types of observations. The structure of the matrices W_{1k} depends on the specifics of the measurement data of the corresponding types.

VARIATIONAL PRINCIPLE WITH WEAK CONSTRAINTS

To combine the entire set of heterogeneous elements in the system of "model of processes & data and model of observations", we define a variational principle with weak constraints for the assessment of the extended functional (Penenko, 2009):

$$\begin{aligned} \Phi(\boldsymbol{\varphi}, \mathbf{Y}, \mathbf{r}, \boldsymbol{\xi}, \boldsymbol{\varphi}^*) \equiv & \int_{D_t} \left(\frac{\partial \boldsymbol{\varphi}}{\partial t} + G(\boldsymbol{\varphi}, \mathbf{Y}) - \mathbf{f} - \mathbf{r}, \boldsymbol{\varphi}^* \right) dDdt + \\ & 0,5\alpha_1 (W_1 \boldsymbol{\eta}, \boldsymbol{\eta})_{D_{t,\nu}}^m + 0,5\alpha_2 (W_1 \mathbf{r}, \mathbf{r}) + \alpha_2 (W_1 \boldsymbol{\xi}, \boldsymbol{\xi}). \end{aligned} \tag{5}$$

Here, the first term on the right is the functional of integral identity for the process models. Its structure is determined based on the balance equation of the total energy of the system (1) - (2); adjoint functions $\boldsymbol{\varphi}^* \in Q^*(D_t) \in L_2(D_t)$ are of the same structure as $\boldsymbol{\varphi} \in Q(D_t)$. They are the distributed Lagrange multipliers that we introduce into the system to account for the process models as constraints on the class of state functions $\boldsymbol{\varphi}$ to estimate the functional (4) and to solve the assimilation problem for data included in models of observations (3). The following three functionals in (5) express the total measure of uncertainty in the model-observation system; $\alpha_k > 0$, W_k are the weighting factors and matrices.

To solve the problems, we build the consistent discrete analogs of the functionals (4) and (5). To this goal, we use the method of decomposition and splitting techniques as well as the adjoint integrating factor method (Penenko et al, 2014). Finally, to solve the problem of variational data assimilation, we get four systems of equations:

$$\partial \Phi^h / \partial \boldsymbol{\varphi}^* = 0; \;\; \partial \Phi^h / \partial \boldsymbol{\varphi} = 0; \;\; \partial \Phi^h / \partial \mathbf{r} = 0; \;\; \partial \Phi^h / \partial \boldsymbol{\xi} = 0 . \tag{6}$$

The first two of them are the systems of the main and adjoint problems. The following two systems of equations serve for finding uncertainties. Equations (6) express the stationary conditions of functional (5) with respect to variations of its vector arguments $\boldsymbol{\varphi}^*, \boldsymbol{\varphi}, \mathbf{r}, \boldsymbol{\xi}$. When using methods of splitting and decomposition, the system (6) are solved by direct non-iterative algorithms (Penenko et al, 2015b) at each time step $t_{j-1} \le t \le t_j$. After their solution we form a sensitivity relations of the functional (5) to variations $\delta \mathbf{Y}$ and $\delta \mathbf{f}$ of vectors $\mathbf{Y}$ and $\mathbf{f}$:

$$\delta \Phi^h = \left(\frac{\partial \Phi^h}{\partial \mathbf{Y}}, \delta \mathbf{Y} \right) + \left(\frac{\partial \Phi^h}{\partial \mathbf{f}}, \delta \mathbf{f} \right). \tag{7}$$

These relationships provide a definition of sensitivity functions required for quantitative analysis of process models in the space of parameters and sources of impacts. The equations of feedback for the solution of inverse problems we form on their basis. Uncertainty function $\mathbf{r}$ gives information on the degree of accuracy of the process models in relation to the information set used in (7) for assimilation. Derivatives of the functionals (4) and (5) for constructing the systems (6) and the relations (7) are determined in the Gateaux sense. The set of algorithms (6) and (7) is consistent by construction.

The main objects of the study are the regions of Siberia and the Arctic (Fig.1). In the report, we present some results of applying the developed models and algorithms.

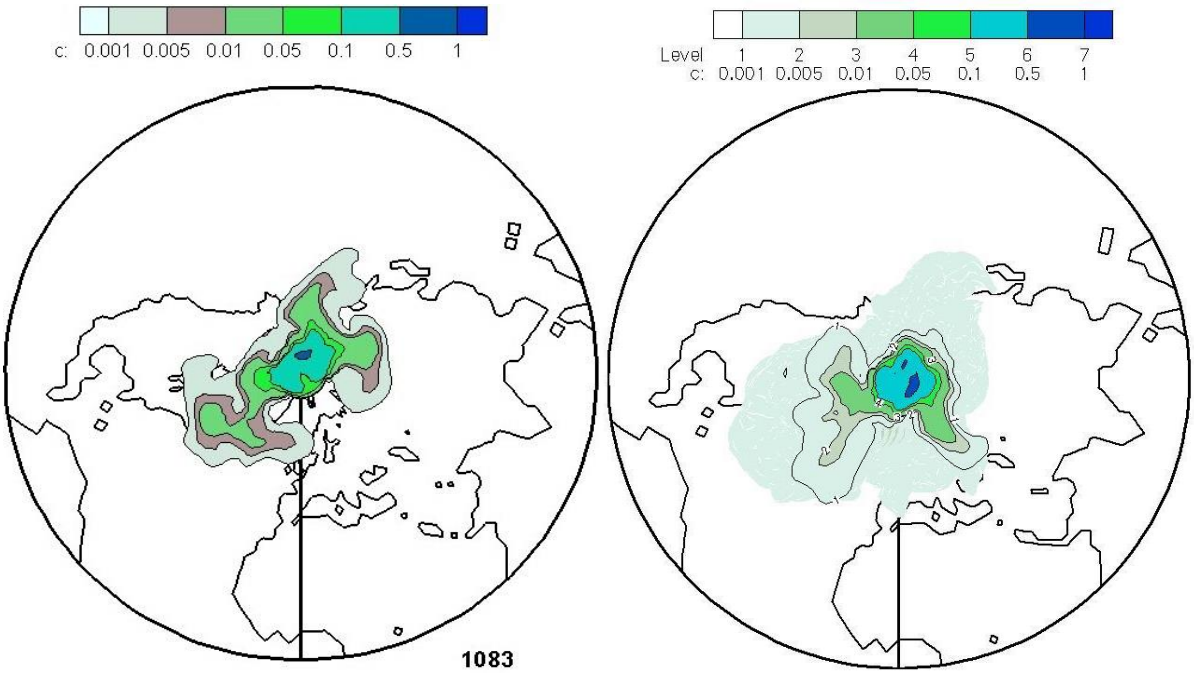

(a) (b)

Fig.1 : Risk function ($\frac{\partial \Phi^h}{\partial \mathbf{f}}$) for Arctic as receptor of pollutants (a) and integrated sensitivity function for a typical February (b)

DIRECT ALGORITHM FOR SEQUENTIAL DATA ASSIMILATION

For the development of numerical algorithms, we use the splitting methods (Marchuk, 1982). Furthermore we apply the additive properties of the functionals and present the basic objects in (5) in the form:

$$\frac{\partial \boldsymbol{\varphi}}{\partial t} = \sum_{\alpha=1}^{q}\left(\gamma_\alpha \frac{\partial \boldsymbol{\varphi}}{\partial t}\right); \ \sum_{\alpha=1}^{q}\gamma_\alpha = 1; \ G(\boldsymbol{\varphi}, \mathbf{Y}) = \sum_{\alpha=1}^{q}\Lambda_\alpha \boldsymbol{\varphi}; \ \mathbf{f} = \sum_{\alpha=1}^{q}\mathbf{f}_\alpha; \ \mathbf{r} = \sum_{\alpha=1}^{q}\mathbf{r}_\alpha \ . \qquad (8)$$

Here q is the number of splitting stages, γ_α are the positive weights. In this case, it becomes possible to use the idea of an additive representation (Samarskii and Vabishevich, 2001) to construct numerical approximations. To obtain discrete approximations in D_t, let us introduce its decomposition into a set of finite volumes D_t^h and corresponding analogues of functional spaces: $L_2(D_t^h), Q^h(D_t^h), Q^{*h}(D_t^h), R^h(D_t^h)$.

The methods of decomposition and splitting are widely used for optimization. The idea behind these methods is that the algorithm for solving large problem is reduced to solution of a set of simpler tasks, approximating, in a sense, the original one. Here we consider the application of the methods to the

problems of variational data assimilation. We describe the structure of the computational algorithm for implementation of 4D variational data assimilation problem. First of all, we carry out the decomposition of the overall problem in the domain D_t in time on the set of consistently solved problems in subdomains:

$$D_t^h = \bigcup_{j=1}^{J} D_{tj}^h; \quad D_{tj}^h = D^h \times [t_{j-1}, t_j], \quad \Phi^h(\boldsymbol{\varphi}, \boldsymbol{\varphi}^*, \mathbf{Y}, \mathbf{r}, \boldsymbol{\psi}) = \sum_{j=1}^{J} \sum_{\alpha=1}^{q} \Phi_{j\alpha}^h, \tag{9}$$

where $\Phi_{j\alpha}^h$ is a part of the total functional (5) , related to the time interval $[t_{j-1}, t_j]$ and the splitting stage α; q is the total number of stages.

Let $\left\{\boldsymbol{\psi}_k^j\right\} \in \Psi(D_t^m)$ $(k = \overline{1,K}, K \geq 1)$ be a set of data coming into the modeling system within the interval $\left[t_{j-1}, t_j\right]$ from different monitoring systems; index k is conditional number of monitoring system. Based on these assumptions, we consider a version of the algorithm for sequential data assimilation with discrete windows of assimilation $[t_{j-1}, t_j]$. As noted above, for the discretization of functionals and models, the additively-averaged splitting schemes are used. They permit the parallel organization of calculations at the splitting stages. We have consistently defined the solution on D_t^h and on the main grid in time $\omega_t^h \equiv \{t_j, \quad j = \overline{0,J}\}$. For the implementation of the decomposition and splitting scheme within time intervals, we form a subsidiary subgrid structure with four-dimensional phase spaces $\left\{\boldsymbol{\varphi}_\alpha^j, \boldsymbol{\varphi}_\alpha^{*j}, \mathbf{r}_\alpha^j, \alpha = \overline{1,q}\right\} \in \bigcup_{\alpha=1}^{q} Q_\alpha^h(D_t^h) \subset Q^h(D_t^h)$, having a parallel organization for the components $\Phi_{j\alpha}^h$ in (9) for the splitting parameter α. The transition from the basic structure of the solution $\left\{\boldsymbol{\varphi}^j\right\}$ to subgrid $\left\{\boldsymbol{\varphi}_\alpha^j\right\}$ is implemented at $t = t_{j-1}$, and the return from subgrid structure to the basic one is carried out at $t = t_j$. A detailed description of the algorithm can be found in (Penenko A and Penenko V., 2014, Penenko et al, 2015a,b). Some calculations using a version of the direct algorithms are described in (Penenko A and Penenko V., 2014), where we make the assimilation of data within the splitting scheme on the stage of convection-diffusion. The main algorithmic unit is of the universal character. It operates directly with observational data and therefore it can be "implanted" in different modeling techniques with various sets of data.

CONCLUSION

In conclusion, we formulate the main goals and objectives of our research concerning the prospects of the PEEX modeling platform. They are:

- development of models of atmospheric dynamics with consideration of chemical and biogenic processes of transfer and transformation of gas and aerosol impurities in the atmosphere;
- creation of effective numerical methods of variational data assimilation of the ground-based and space observations;
- design of algorithms for solving inverse problems on identification of sources of impact and environmental risk assessments;
- assessment of changes in air quality and transboundary exchanges.

ACKNOWLEDGEMENTS

This work was partially supported by the Presidium of RAS under Program No I.33P and by the RFBR grant 14-01-00125 .

REFERENCES

Bocquet M., H. Elbern, H. Eskes, et.al (2015)Data assimilation in atmospheric chemistry models: current status and future prospects for coupled chemistry meteorology models *Atmos. Chem. Phys*., 15, 5325–5358.

Marchuk, G.I. (1982). *Methods of numerical mathematics*, (Springer-Verlag, New York)

Penenko, V. V. (2009). Variational methods of data assimilation and inverse problems for studying the atmosphere, ocean, and environment, *Numerical Analysis and Applications*, **2,** No 4, 341.

Penenko, A.V. and V.V. Penenko (2014), Direct data assimilation method for convection-diffusion models based on splitting scheme. *Computational technologies*, **19** Issue 4, 69 (In Russian).

Penenko, V.V., E.A. Tsvetova, A.V. Penenko (2014) Variational approach and Euler's integrating factors for environmental studies, *Computers and Mathematics with Applications*, **67**, Issue 12, 2240.

Penenko, V. V. , E. A. Tsvetova, and A. V. Penenko (2015a) Development of variational approach for Direct and Inverse problems of atmospheric hydrothermal dynamics and chemistry, *Izvestiya, Atmospheric and Oceanic Physics, Vol. 51, No. 3, pp. 311–319.*

Penenko, V.V. , Tsvetova, E.A., Penenko, A.V. (2015b) Methods based on the joint use of models and observational data in the framework of variational approach to forecasting weather and atmospheric composition quality *Russian meteorology and hydrology*, V. 40,Issue: 6, Pages: 365-373.

Samarskii, A.A., Vabischevich, P.N., (2001). *Additive Schemes for the Problems of Mathematical Physics*, Moscow, Nauka

Showengerdt ,R. A., (2007). *Remote Sensing. Models and Methods for Image Processing*, Elsevier, Amsterdam

Zuev, V. Ye.. Kaul, , B. V, Samokhvalov, I. V., Kirkov, K. I. , Tsanev V. I (1986). *Lazernoe zondirovanie industrialnykh aerozoley*, Novosibirsk , Nauka (In Russian) .

ASSESSMENT OF ANTHROPOGENIC CONTAMINATION IN GEOCRYOLOGICAL AREAS OF THE ARCTIC ZONE OF WESTERN SIBERIA

S. A. PETROV[1], N. L. MAMAEVA[1,2], D. A. KHRUPA[1], V. A. MALCHEVSKIY[1]

[1]- The Tyumen Scientific Center of the Siberian Branch of the Russian Academy of Sciences, Tyumen.
[2]- Tyumen State Oil-Gas University, Tyumen.

Keywords: ANTHROPOGENIC POLLUTION, WESTERN SIBERIA, ECOSYSTEM, ARCTIC

INTRODUCTION

The Russian Arctic – the territory which is characterized by severe climatic conditions of accommodation of the population and at the same time at all severity of an image, the Arctic possesses the most fragile and unique ecosystem on our planet (Mamayeva, Kvashnina, Petrov, 2011; Mamaeva, Petrov, 2013). Russia is included into the three of global leader in production of hydrocarbons. in addition, more than 90% of all gas and about 10% of oil are extracted in the Russian sector of the Arctic. Development of the Arctic gas and oil resources, from prospecting prior to initial operation of greenfields, it is a source of the increased ecological danger (Mamaeva, Petrov, 2015). According to the specialists' research the oil and gas industry by danger of environmental impact rank third among present-day production. Flagship products of branch (oil, gas, hydrocarbon condensate, sulfur etc.) pose immediate danger to flora and fauna, human health (Dorozhukova, Yanin, 2002; Zotova, Dedyusova, 2012).

Territory of the Yamalo-Nenets Autonomous Okrug (YNAO), which provides more than 54% of overall production of primary energy resources of the country, has high resource potential and is the main oil and gas base of the Russian Arctic. In this regard studying of the ecological aspects of management of natural resources, resulting from human impact on environment of the Russian sector of the Arctic is important today.

METHODS

Ourself considered anthropogenic pollution of the effluents and atmosphere air in the Purovsky area of Yamalo-Nenets Autonomous Okrug (YNAO). Here more than 120 raw hydrocarbon deposits are opened and also 45% of gases, 80% of oil and gas well condensate from all extent of production of the YNAO are obtained. The settlement of Samburg and the city Tarko-Sal are chosen as supporting points of studying of ecological aspects of environmental management. They, according to geocryological subdivision into districts, refer to the Northern zone Harasavey-Novourengoysky subband of Ustpurovsko-Tazovsky area and the Central zone to the Igarko-Numtinsky subband of Purovsky area respectively (Geocryology of the USSR. Western Siberia / Under the editorship of E.D. Yershov, 1989). The characteristic of the effluents and emissions in atmospheric air geocryologic areas is presented in table 1.

Enucleate that effluents discharge in surface-water bodies in Purovsky geocryologic area as compared to Ustpurovsko-Tazovsky geocryologic area is more on the following polluting substances: Iron (1,57±0,17 tons and 0,37±0,11 tons respectively at $p<0,001$), chlorides (0,02 ± 0,004 thous. tons and 0,01 ± 0,002 thous. tons respectively at $p<0,05$), ammonium nitrogen (10,89 ± 1,66 tons and 1,01 ± 0,17 tons respectively at $p <0,001$).

Except quality of surface-water bodies pollution of atmospheric air in these geocryologic areas is considered. It has been established that emissions of the polluting substances in the atmosphere is also more in Purovsky geocryologic area. Therefore we carried out calculation of dispersion of the polluting substances to the atmosphere according to the unified program of calculation of pollution of atmosphere

«Eco the center». On the map in scale made from the satellite Ustpurovsko-Tazovsky and Purovsky geocryologic areas are designated. Comparison of the maximum ground level concentration of the polluting substances in the atmosphere with short-term exposure limit was carried out.

№	Substance identification	Ustpurovsko-Tazovskaya	Purovskaya
1.	Effluents		
1.1.	Synthetic surface active substance, tons	0,04 ± 0,01	0,07 ± 0,02
1.2.	Phosphorus the general, tons	0,25 ± 0,05	0,37 ± 0,09
1.3.	Iron,tons	0,37 ± 0,11	1,57 ± 0,17**
1.4.	Sulfates, thous. tons	0,01 ± 0,001	0,02 ± 0,01
1.5.	Chlorides, thous. tons	0,01 ± 0,002	0,02 ± 0,004*
1.6.	Fmmonium nitrogen, tons	1,01 ± 0,17	10,89 ± 1,66**
2.	Emissions in atmospheric air		
2.1.	In total from them, tons:	8609,35 ± 1574,71	395978,10 ± 34298,67**
2.1.1.	Strong substances	104,88 ± 15,14	14210,65 ± 676,63**
2.1.2.	Gaseous and liquid, in total from them:	8504,53 ± 1576,76	381767,50 ±31927,93**
2.1.2.1.	Sulphur dioxide	82,71 ± 11,54	929,47 ± 39,84**
2.1.2.2.	Carbonic oxide	4023,41 ± 693,40	215444,20 ±24814,86**
2.1.2.3.	Nitrogen oxide	1334,06 ± 235,74	23789,00 ± 1161,49**
2.1.2.4.	Hydrocarbon(without VOC)	2972,47 ± 692,52	136530,20 ±14237,04**
2.1.2.5.	Volatile organic component (VOC)	124,45 ± 43,55	5292,12 ± 732,57**

Table 1. The characteristic of the effluents and emissions in atmospheric air in geocryologic areas of the Purovsky YNAO (*- statistical significance, significance of differences (* - p<0,05, ** - p<0,001).

In calculations of dispersion of ground level concentration of the polluting substances in atmospheric air took into account climatic conditions, condition of the air basin, parameters of air-gas mix taking into account features of technological processes (fig. 1).

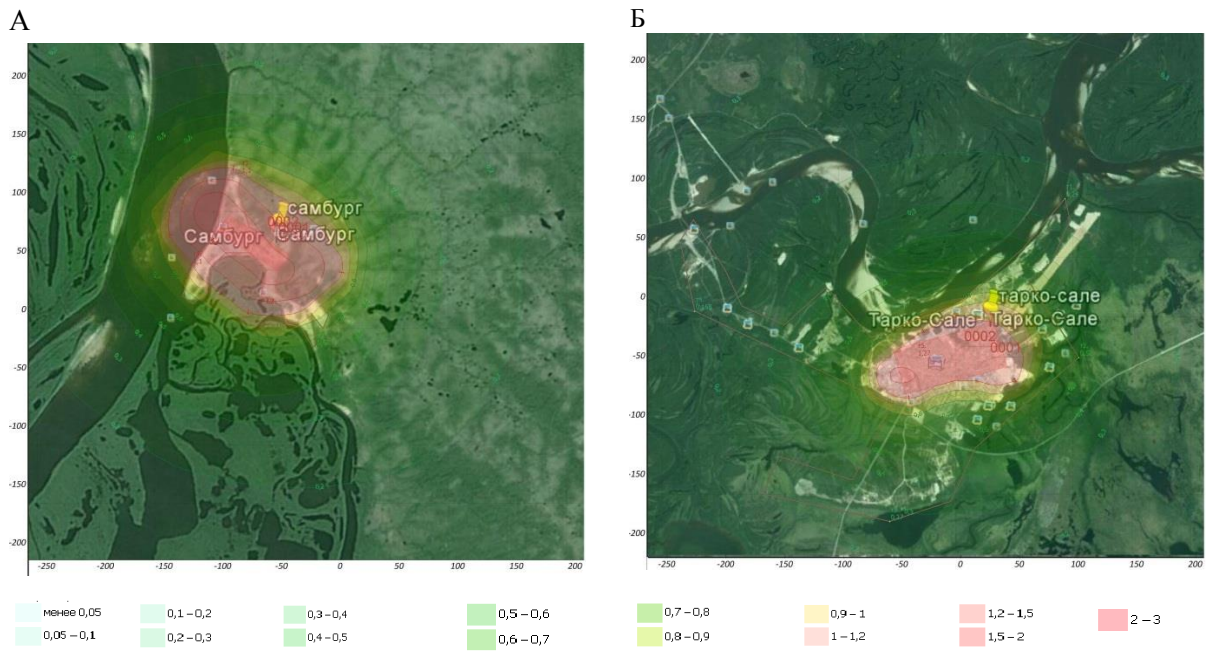

Figure 1. Ustpurovsko-Tazovskaya's schematic map (A) and Purovska (B) of geocryologic areas, with isolines of settlement concentration on all considered polluting substances and groups of the summation expressed in short-term exposure limit. (Scale 1:2500).

Excess of short-term exposure limit in the atmosphere of strong substances (smuts) by 1, 5 times, carbon oxide by 1, 2 times was established in Purovsky geocryologic area. Excess of short-term exposure limit of nitrogen dioxide (by1.2 times) was revealed in Purovskaya and in Ustpurovsko-Tazovsky(by 3 times) geocryologic areas. Have effect of an incomplete summation: nitrogen dioxide ,sulfur dioxide. Their excess in Ustpurovsko-Tazovsky geocryologic area made 2,7 short-term exposure limit, in Purovskoy - 1,08 short-term exposure limit. The majorant on all considered polluting substances and groups of summation in Ustpurovsko-Tazovsky geocryologic area made 3 short-term exposure limit, , in Purovskoy - 1,5 short-term exposure limit.

Research of influence of the polluting substances on a condition of immune system of the tundra Nenets living in the settlement of Samburg and in Tarko-Sal was conducted. Indigenous small-numbered peoples of the North are the most sensitive to various to anthropogenous factors (Mamaeva, Petrov, 2013). It has been found that microscopic firm particles (soot) possess resorptive action and lead to development general toxical, gonadotoxic , embryotoxic, mutafacient, cancerogenic and other effects (Mamaeva, Petrov, 2013).

Important source of pollution of the atmosphere is carbon oxide. It is formed when burning fuel, in car exhaust, in a tobacco smoke. Excess of short-term exposure limit on carbon oxide by 1,2 times in Purovsky geocryologic area was revealed. It is known that it can cause greenhouse effect ((Mamaeva, Petrov, 2013; Mamayeva, Kvashnina, 2011).

Highest profile in pollution of atmospheric air is played by compounds of nitrogen oxides. Taking into account transformation of harmful substances in the atmosphere recalculation of this type of pollution on components – NO2 and NO for all types of technological processes and vehicles was carried out. In Ustpurovsko-Tazovsky geocryologic area excess on dioxide of nitrogen was made by 3 short-term exposure, in Purovskaya – 1,2 short-term exposure. The group of summation of dioxide of nitrogen and dioxide of sulfur was considered. It has been established that his group of the polluting substances excess of short-term

exposure limit by 2,7 times in Ustpurovsko-Tazovsky geocryologic area and in Purovskaya – in 1,08 time. At interaction of nitrogen oxides and sulfurs with water can be formed nitric (HNO3) and sulfuric (H2SO4) of acid. Source of pollution of atmospheric air compounds of nitrogen oxides are firing, wilderness fire, the industrial enterprises, meteorological factor (Mamayeva, Petrov, 2015; Mamayeva, Kvashnina, Petrov). Biogeochemical processes in water and terrestrial ecosystems lead to exhaustion of living resources (birds, animals, fishes, wild harvest and others). In the eventual result changes to traditional sociocultural way of indigenous ethnic groups of the North (Dorozhukova, Yanin, 2002; Mamaeva, Petrov, 2013). Ecological backlash sharply affects on a state of health and wellbeing of the population living here.

CONCLUSIONS

Ensuring balance between anthropogenic activities and preservation of the environment has to become the key pillar of development of the Arctic. It can be reached the following methods:

1. Providing system of monitoring of a state of environment in the Arctic zone.
2. Development and application of new equipment, emerging technology and materials adapted for climatic conditions of the Arctic, development and application of new equipment, emerging technology and materials adapted for climatic conditions of the Arctic, the minimizing volumes of emissions of the polluting substances in water and atmospheric of ecosystems.
3. Solution to a question of the international cooperation in development of programs of sociocultural adaptation of indigenous minority of the North of the North to technogenic development of the Arctic areas.

ACKNOWLEDGEMENTS

Work is performed with assistance of a grant of the Russian Fundamental Research Fund 15-55-71004.

REFERENCES

Geocryology of the USSR. Western Siberia / Under the editorship of E.D. Yershov (1989).

Dorozhukova S. L., Yanin E.P. (2002) Environmental problems of oil and gas extraction territories (on the example of the Tyumen region). *Scientific and technical aspects of environmental protection.* **6,** 57-95.

Zotova L.I., Dedyusova S.Yu. (2012) Assessment of crisis ecological situations in the developed regions of a cryolithic zone of the Tyumen North. *Tenth International conference on permafrostology (TICOP): Resources and risks of regions with permafrost in the changing world Volume 3: Articles in Russian.(*Tyumen, Russia), 193-198.

Mamayeva N. L., Petrov S. A. (2015) Environmental problems of the Arctic zone of the Russian Federation. *News of higher education institutions. Oil and gas*. **5**, 148-152.

Mamayeva N. L., Kvashnina S. I., Petrov S. A. (2011) Influence of ecological and climatic factors on a cryolithic zone of Western Siberia. *News of higher education institutions. Oil and gas*. **4**, 119-122.

Mamayeva N. L., Kvashnina S. I. (2011) Environmental problems in oil and gas branch in the Tyumen North. *News of higher education institutions. Oil and gas*. **5**, 123-125.

Mamaeva N.L., Petrov S.A. (2013) The influence of geo-ecological characteristics on the body condition of the indigenous Yamal population. *Tyumen state university herald*. **6**, 122 - 127.

BIOGENIC AEROSOLS – EFFECTS ON CLOUDS AND CLIMATE (BAECC) STUDY AS AN EXAMPLE FOR SCIENTIFIC INTEGRATION

T. PETÄJÄ[1], D. MOISSEEV[1], E. O'CONNOR[2,3], V. SINCLAIR[1], A. MANNINEN[1], H.K. LAPPALAINEN[1], V-M. KERMINEN[1] AND M. KULMALA[1]

[1]Department of Physics, University of Helsinki Finland

[2]Finnish Meteorological Institute, Helsinki, Finland

[3]University of Reading, UK

Keywords: COMPREHENSIVE ATMOSPHERIC OBSERVATIONS, AEROSOL PARTICLES.

Atmospheric aerosol particles impact human health in urban environments, whilst on regional and global scales they can affect climate patterns, the hydrological cycle, and the intensity of radiation that reaches the Earth's surface. In spite of recent advances in the understanding of aerosol formation processes and the links between aerosol dynamics and biosphere-atmosphere-climate interactions, great challenges remain in the analysis of related processes on a global scale. Boreal forests, situated in a circumpolar belt in the Northern latitudes throughout the United States, Canada, Russia and Scandinavia, are, of all biomes, among the most active areas of atmospheric aerosol formation. The formation of aerosol particles and their growth to cloud condensation nuclei sizes in these areas are associated with biogenic volatile organic emissions (BVOC) from vegetation and soil (Kulmala et al. 2004, Paramonov et al. 2013, Paasonen et al. 2013).

One of the world's most comprehensive observation sites in a boreal forest environment, measuring atmospheric aerosols, biogenic emissions and an extensive suite of relevant atmosphere-biosphere parameters, is SMEAR-II (Station for Measuring Forest Ecosystem-Atmosphere Relations, Hari and Kulmala, 2005) in Hyytiälä, Finland. The station has been monitoring biosphere-atmosphere interactions continuously since 1996, and is operated by the University of Helsinki, Division of Atmospheric Sciences, together with the university's Forest Science Department. The U.S. Department of Energy's Atmospheric Radiation Measurement (ARM) Program operated its ARM Mobile Facility 2 (AMF2) in Hyytiälä next to SMEAR-II during an intensive measurement campaign called "The Biogenic Aerosols - Effects on Clouds and Climate (BAECC) experiment". The campaign started in February 2014 and ended in September 2014. (Petäjä, 2013, Petäjä et al. 2016).

The BAECC experiment provided a bridge from an 18-year long SMEAR-II observation record (at the time of the campaign) to the impact of biogenic aerosol on clouds, precipitation and climate. Simultaneous observations of precursor vapor emission, aerosol, cloud, and precipitation microstructure enable such an analysis. The work has enabled us to connect the burst-like emissions of biogenic VOCs (Aalto et al. 2015) being indicative of the onset of photosynthesis of the biosphere to the aerosol processes (Petäjä et al. 2016). Within BAECC we also explored the microphysical processes in connection with (Kneifel et al. 2015, Kalesse et al. 2016). Furthermore, the BAECC initiated development of measurement capacity in Hyytiälä (Manninen et al. 2015) as well as provided a framework to compare satellite observations against the ground based measurements (Sporre et al. 2015). This is a crucial step in expanding the in-situ ground based observations to a larger spatial scales.

In the next steps, the comprehensive active remote sensing during the BAECC will give new insights into the importance of elevated aerosol layers to columnar optical closure (Zieger et al. 2015) and the BAECC dataset is well positioned in perspective with the long time series available from Hyytiälä, and utilized in modeling efforts ranging from process models to global climate models in the future.

ACKNOWLEDGEMENTS

This work was partly supported by the Office of Science (BER), U.S. Department of Energy via BAECC (Petäjä), BAECC-SNEX (Moisseev), European Commission via projects ACTRIS, ACTRIS-TNA, ACTRIS2, BACCHUS, PEGASOS and Academy of Finland Centre of Excellence in Atmospheric Sciences. The BAECC SNEX was also supported by NASA Global Precipitation Measurement (GPM) Mission ground validation program. The deployment of AMF2 to Hyytiälä was enabled and supported by ARM. Argonne National Laboratory's work was supported by the U.S. Department of Energy, Assistant Secretary for Environmental Management, Office of Science and Technology, under contract DE-AC02-06CH11357. The authors gratefully acknowledge the support of AMF2 and SMEAR-II for their support in initiating the BAECC campaign, its implementation, operation and data analysis.

REFERENCES

Aalto, J., Porcar-Castell, A., Atherton, J., Kolari, P., Pohja, T., Hari, P., Petäjä, T. and Bäck, J. (2015) Onset of photosynthesis in spring speeds up monoterpene synthesis and leads to emission bursts, Plant, Cell & Environ. 38, 2299-2312.

Hari, P. and Kulmala, M. (2005). Station for Measuring Ecosystem – Atmosphere Relations (SMEAR II), Boreal Environ. Res. 10, 315-322.

Kalesse, H., Szyrmer, W., Kneifel, S., Kollias, P. and Luke, E. (2016). Fingerprints of a riming event on cloud radar Doppler spectra: observations and modeling, Atmos. Chem. Phys. 16, 2997-3012.

Kneifel , S , von Lerber , A , Tiira , J , Moisseev , D , Kollias , P and Leinonen , J. (2015). Observed relations between snowfall microphysics and triple-frequency radar measurements, J. Geophys. Res. 120 , 6034-6055. Doi: 10.1002/2015JD023156.

Kulmala, M., Vehkamäki, H., Petäjä, T., Dal Maso, M., Lauri, A., Kerminen, V.-M., Birmili, W. and McMurry, P.H. (2004). Formation and growth rates of ultrafine atmospheric particles: a review of observations. J. Aerosol Sci. 35, 143-176.

Manninen, A.J., Vakkari, V., O'Connor, E.J. and Petäjä, T. (2015). A generalized background correction algorithm for a HALO Doppler lidar and its application to data from Finland, Atmos. Meas. Technol. 8, 11139-11170.

Paasonen, P., Asmi, A., Petäjä, T., Kajos, M.K., Äijälä, M., Junninen, H., Holst, T., Abbatt, J.P.D., Arneth, A., Birmili, W., Denier van den Gon, H., Hamed, A., Hoffer, A., Laaksonen, A., Laakso, L., Leaitch, R., Plass-Dülmer, C., Pryor, S.C., Räisänen, P., Swietlicki, E., Wiedensohler, A., Worsnop, D.R., Kerminen, V.-M. and Kulmala, M. (2013). Warming-induced increase in aerosol number concentration likely to moderate climate change, Nature Geosci., 6, 438-442

Paramonov, M., Aalto, P.P., Asmi, A., Prisle, N., Kerminen, V.-M., Kulmala, M. and Petäjä, T. (2013). The analysis of size-segregated cloud condensation nuclei counter (CCNC) data and its implications for cloud droplet activation, Atmos. Chem. Phys. 13, 10285-10301.

Petäjä, T. (2013). Science Plan Biogenic Aerosols – Effects on Clouds and Climate (BAECC), US Department of Energy, Office of Science, DOE/SC-ARM-13-024.

Petäjä, T., O'Connor, E.J., Moisseev, D., Sinclair, V.A., Manninen, A.J., Väänänen, R., von Lerber, A., Thornton, J.A., Nicoll, K., Petersen, W., Chandrasekar, V., Smith, J.N., Winkler, P.M., Krüger, O., Hakola, H., Timonen, H., Brus, D., Laurila, T., Asmi, E., Riekkola, M.-L., Mona, L., Massoli, P., Engelmann, R., Komppula, M., Wang, J., Kuang, C., Bäck, J., Virtanen, A., Levula, J., Ritsche, M. and Hickmon, N. (2015) BAECC, A field campaign to elucidate the impact of Biogenic Aerosols on Clouds and Climate, Bull. Am. Met. Soc. (in press), doi: 10.1175/BAMS-D-14-00199.1.

Sporre, M.K., O'Connor, E.J., Håkansson, N., Thoss, A., Swietlicki, E. and Petäjä, T. (2015). Comparison of MODIS and VIIRS cloud properties with ARM ground-based observations over Finland, Atmos. Meas. Technol. Discuss. doi:10.5194/amt-2016-26.

Zieger, P., Aalto, P.P., Aaltonen, V., Äijälä, M., Backman, J., Hong, J., Komppula, M., Krejci, R., Laborde, M., de Leeuw, G., Pfüller, A., Rosati, B., Tesche, M., Tunved, P., Väänänen, R. and Petäjä, T. (2015) Low hygroscopic scattering enhancement of boreal aerosol and the implications for a columnar optical closure study, Atmos. Chem. Phys. 15, 7247–7267.

CONTEMPORARY TENDENCIES IN PRIMARY PRODUCTION DYNAMICS IN THE ARCTIC OCEAN UNDER CONDITIONS OF GLOBAL WARMING

D. V. POZDNYAKOV[1,2], and L. H. PETTERSSON[2]

[1] Scientific Foundation ”Nansen International Environmental and Remote Sensing Centre, St. Petersburg, 7, 14th Line. V.I.199034, Russian Federation

[2] Nansen Environmental and Remote Sensing Centre, Bergen, Thormølhensgate 47, N-5006,

Keywords: ARCTIC OCEAN, PHYTOPLANKTON, PRIMARY PRODUCTION, UNDER-ICE BLOOMS

INTRODUCTION

The ongoing and projected climate change in the Arctic is accompanied by a host of consequences of both physical and biological nature. In turn, variations in the primary production (PP) rate in the Arctic affect the carbon cycle in the atmosphere–ocean system and ultimately lead, through feedback mechanisms, to climate change at the global scale. Under warmer conditions, the amount of carbon sequestered by the Arctic Ocean can be expected to increase. Thus, an adequate estimation of this increase is a task of significant importance.

The size of the Arctic Ocean and the phytoplankton spatial and temporal variability means that to observe the phytoplankton dynamics, remote sensing is necessitated. To accomplish this goal, an appropriate PP model/retrieval algorithm needs to be either developed or selected from the suggested so far for the oceanic tracts at high latitudes. A selection of a most adequate model is possible through a rigorous comparison of PP retrievals with gridded *in situ* determinations of PP performed (*i*) on the day of satellite overflight, and (*ii*) within the swath imaged by the spaceborne sensor. Conditionally, such determinations could be called matchups. Thus, a wide statistical database of matchups is mandatory. Besides, to cover the longest possible time period of observations, the data on phytoplankton chlorophyll (*chl*) concentration from at least a couple of sensors are to be used, and such data should be strictly compatible/harmonious. Apart from *chl*, PP models need as input parameters some auxiliary data (e.g. sea surface temperature (SST), photosyntheticaly active radiation (PAR)). Data on ice edge location, and cloudiness are also indispensible. To meet these challenges, both satellite and *in situ data* should be judiciously selected and processed to minimize the factors capable of compromising the results obtained. Below, all these issues are covered. In quantifying PP special procedures were developed to overcome such impediments as cloud masking and determination of phytoplankton concentration within (*i*) overcast areas, and (*ii*) areas of massive growth of coccolithophore algae, as well as (*iii*) in the shelf zone prone to a significant influence of land and river runoff.

In addition to spaceborne assessments of PP in ice-free areas and the respective temporal variation tendencies, we discuss the deficiency of such data because of neglect of under-ice PP production, which, according to findings reported in the literature, might account for a significant part of the total PP in the Arctic.

DATA SOURCES AND METHODS

Shipborne data. The compiled *gridded* shipborne database covers the time period of 1958–2005 and incorporates gridded PP determinations (ca 9000) the area lying north of 65°N beyond the Polar Circle. When selecting the *in situ* data eligible for algorithm *validation*, the major criteria were the closeness of the chlorophyll maximum to the water surface, the shortest possible time difference between the *in situ* measurement and the ocean colour sensor overflight, and the location of the sampling station within a 16 km radius area around the pixel for which the comparison was performed.

As mentioned above, in addition to the PP at surface *in situ* data, data on PP profiles were collected as well as a wealth of contemporaneous *in situ* data on *chl*, SST, cloudiness level, incident PAR; PAR diffuse attenuation coefficient, K_d; euphotic depth; remote-sensing reflectance above the water surface (R_{rs}); mixed layer depth (MLD); and water temperature and salinity profile, etc.

The collected *in situ* data cover not only the pelagic areas (such as the north Atlantic ice-free surface, the Russian Sector of the Central Arctic, and the Canadian Basin) but also the peripheral seas: Greenland, Barents, White, Pechora, Kara, Laptev, Chukchi, and Beaufort.

Spaceborne data. The following most recently reprocessed SeaWiFS and MODIS-Aqua monthly binned ocean colour gridded data set was used: the OceanColor MEASURES Project data (Reprocessing R20010). The latter (further referred to as MEASURES data) are obtained with the GSM retrieval algorithm and a special procedure of partial removal of cloudiness (http://adsabs.harvard.edu/abs/2008AGUFMIN51B1156M). The collected set of data (1998-2010) is level 3 monthly averaged retrieval results at a spatial resolution of 4 km. SeaWiFS and MODIS-Aqua data (Level 3) were processed with the Levenberg–Marquardt technique–based BOREALI algorithm (Korosov et al. 2009) for processing ocean colour data from (*a*) the Arctic *shelf* zone encompassing the Arctic seas and (*b*) *Emiliania huxleyi* bloom areas (Petrenko et al., 2013). Sea-surface temperature, ice-free surface, and cloudiness data were obtained from SSM/I sequential sensors, the longest time series is on sea ice (32 years). The time series (24 years, until 2009) on SST is from sequential sensors, the Advanced Very High Resolution Radiometer (AVHRR), and partly (8 years) from MODIS. The data from the sequential sensors posted on the sites are harmonized by respective agencies with due account of the specific radiometric parameters inherent in each successive sensor. To avoid the optical interference arising at cloud edges (for references, see Robinson, 2004), and hence the ensuing inaccuracies in our quantitative determinations, we excluded a two-pixel-wide water strip bordering the cloud-edge projection on the water surface in all assessments of *chl* concentrations and eventually the values of PP.

The entire area of the Arctic Ocean can be partitioned into pelagic and shelf zones based on morphometric and geomorphologic parameters such as bed slope and its gradient. Since pelagic and shelf zones are known to differ essentially in terms of water optical properties, the algorithms for the retrieval of *chl* should be specialized for both types of area.

PP retrieval algorithm. As a PP retrieval algorithm, after a rigorous comparison with in situ data, we selected the Behrenfeld and Falkowski parameterization, which is a vertically generalized/depth-integrated production model (VGPM). $(PP)_{eu}$ in the entire euphotic zone (Behrenfeld and Falkowski, 1997). This model requires as input variables *chl* at the depth nearest to the surface, incident PAR irradiance, $E_o(\lambda)$, and SST. Importantly, the above relationship holds for SST ranging from –1°C to +29°C.

chl retrieval algorithms.

For the <u>shelf zone</u>, which is prone to a significant influence of land and river run-off, coastal waters, and hence is optical impacted by *chl*, suspended minerals (*sm*) and the coloured fraction of dissolved organic matter (*dom*), the BOREALI algorithm was exploited as the NASA standard algorithms are untenable for such conditions. The same algorithm (but in a modified form) was applied to processing *E. huxleyi* bloom areas in pelagic areas.

For the ice-free <u>pelagic region</u> of the Arctic Ocean, we employed The Garver–Siegel–Maritorena semi-analytical (SA) ocean colour algorithm (GSM algorithm) that retrieves simultaneously the phytoplankton *chl* concentration, the absorption coefficient for dissolved and detrital materials [$a_{cdm}(443)$], and the particulate backscatter coefficient [$b_{bp}(443)$] (Maritorena et al., 2002).

SST retrieval algorithm. The NASA algorithm four-term expression was employed (http://yyy.rsmas.miami. edu/groups/rrsl/pathfinder/Algorithm/algo_index.html#algo-pathsst and <u>http://modis.gsfc.nasa.gov/data/atbd/atbd_mod25</u>).

<u>Cloudiness effect reduction.</u> The complete description of this innovative approach is detailed in Peterenko et al. (2013).

<u>Compatibility of SeaWiFS and MODIS data</u>. There were hitches in SeaWiFS operation in July and September in 2008, and September in both 2009 and 2010. To fill the gaps, we used MODIS-Aqua data for the above months. Our analysis has shown for 2002–2010 that for about 90% of the pixels compared, the ratio between $chl_{SEAWIFS}$ and chl_{MODIS} is 0.81, i.e. $chl_{SEAWIFS} = 0.81 chl_{MODIS}$ (RMSD = 0.11). We also checked this result employing normalized water leaving radiance (*nLw*)-based analysis, and found no bias.

RESULTS AND DISCUSSION

Pelagic ice-free zone. Table 1 illustrates the revealed trend in annual PP: starting from 1998, annual PP in the ice-free pelagic zone of the Arctic has been increasing at a rate of 1.1% per year, so that according to our estimations, PP in this zone increased by 14.5% over 13 years. The absolute values of PP varied during this period within the interval extending from ~380 Tg C until ~510 Tg C. The mean PP per unit area in this zone over the vegetation period between 1998 and 2010 is assessed at 89 mg C m^{-2} day^{-1}. The same Table illustrates the estimated respective trends in the variables that are believed to be consequential for the established PP dynamics.

Through comparing the retrieved data on phytoplankton productivity, pp (in mg C m^{-2} day^{-1}) with the respective gridded *in situ* data, the mean square deviation for satellite pp data was quantified and considered as the error of pp retrievals, δpp. Further, PP (Tg C day^{-1}) was calculated for each pixel: $(PP)_{pixel} = (pp)_{pixel}\ \sigma$, where $(pp)_{pixel}$ is the phytoplankton productivity per pixel (in m^2), and σ is the pixel surface (in m). The PP retrieval error was calculated as $\delta(PP)_{pixel} = \delta pp\ \sigma$. The value of PP for the pelagic zone is a result of summation of all $(PP)_{pixel} = \Sigma\ PP_{pixel}$. The resultant error for the pelagic zone was quantified analogously: $\delta\ (PP) = \Sigma\delta\ (PP)_{pixel}$.

A similar procedure was exploited for determining PP and δ(PP) within the shelf zone and the entire Arctic Basin. The respective values of δ(PP) were then used to plot the error bars.

As a result, the PP error proved to be 24%, 26%, and 25% for the pelagic, shelf zones, and the entire Arctic, respectively.

Variable	Trend (%)	Statistical significance
PP	+14.5	98
Ice-free area	+18	99
chl	+17	99
PAR	-2	93
SST	+22	99

Table 1. Pelagic zone of the ice-free Arctic Basin: 13- year trends in the dynamics of annual PP, ice cover, *chl*, PAR, and SST. Time period: 1998–2010.

*Ice-free shelf zone***.** Table 2 illustrates the revealed trend in, PP: starting from 1998, PP in the ice-free shelf zone of the Arctic has been increasing at a rate of~1.3% per year. So, according to our estimations, PP in this zone increased by 17.4% over 13 years. The absolute values of PP varied during this period within the interval extending from ~360 until ~500 Tg C $year^{-1}$. The mean daily PP per unit area in this zone over the vegetation period between 1998 and 2010 is assessed at 93 mg C m^{-2} day^{-1}. Table 1 also shows the estimated respective trends in the variables that are believed to be consequential for the established PP dynamics.

We found that the maximum daily PP per unit area in the ice-free shelf zone occurs in May. Its mean value for this month over 1998–2010 is about 105 g C m^{-2} day^{-1}. PP has been increasing to eventually reach in 2010 a value of ~113 g C m^{-2} day^{-1} against ~104 g C m^{-2} day^{-1} in 1998, which implies a trend of 8.1% per 13 years.

Comparing the PP dynamics in pelagic and shelf zones, at the early stages of the vegetation period, the monthly production in the pelagic zone nearly equals that in the shelf zone. But further on, the PP maximum shifts from May (registered for the shelf zone) to June for the pelagic zone. This is a quite expected result as SST (highly determining the phytoplankton productivity) in the shelf zone increases faster than it does in the deep, initially colder, pelagic waters. However, in July, PP in both zones becomes closely comparable. During the period August–October, the water in the shelf zone remains warmer than it is in the pelagic zone, thus determining a less steep decrease in PP compared to the pelagic waters.

For the pelagic zone, the $(PP)_{max}$ mean value over 1998–2010 for June is about 130 gC m^{-2} day^{-1}. In the case of the shelf zone, the respective value is less than 110 g C $m^{-2}day^{-1}$.

Variable	Trend (%)	Statistical significance
PP	+17.4	98
Ice-free area	+58	99
chl	+13	99
PAR	-1	93
SST	+19	99

Table2. Shelf zone of the ice-free Arctic Basin: 13-year trends in the dynamics of annual PP, ice cover, *chl*, PAR, and SST. Time period: 1998–2010.

*Entire ice-free Arctic Basin***.** Summation of our estimations of PP in the ice-free pelagic and shelf zone showed that in absolute values, PP varied within the range from 770 Tg C year^{-1} to 1980 Tg C year^{-1}. Over 13 years, PP has been increasing at a rate of 15.9% or about 1.2% per year (statistical significance = 99%). Over the vegetation period, the mean PP production per unit area in the entire ice-free Arctic Basin between 1998 and 2010 is assessed at 91 mg C m^{-2} day^{-1}.

Interannual variations and linear trends in PP over the sectors encompassing the Arctic seas.
The revealed temporal variations in annual PP for the Arctic sectors (conditionally named after the respective seas they incorporate) exhibit significant individual features (Table 3), which is reflected in the respective values of trends. As Table 3 illustrates, the greatest share in the total annual PP over the ice-free Arctic Basin belongs to two sectors, viz. the Barents and Greenland sectors (~35% and 30%, respectively). The least productive marine environments in the Arctic are the East Siberian and Chukchi sectors.
In summary, the annual PP of the Arctic seas either equaled or, more often, prevailed over the annual PP in the pelagic zone, with the exception of 2005 and 2007.
Data in Table 3 allows to numerically compare the quantified PP data for each sector. Here the differences for most seas are significant. The causal reasons of this dissimilitude is discussed below in the final section.

Arctic sector	Trend (%)	
	Over 1998-2010	Per year
Kara Sea	22.4	1.7
Laptev Sea	54.	4.2
Greenlan Sea	-13.6	-1
East Siberian Sea	112.7	8.6
Chukchi Sea	57.2	4.4
Beaufort Sea	14.7	1.1
Barents Sea	19.7	1.4
Baffin Sea	9.9	0.8

Table 3. Trends in annual PP for the eight individual Arctic sectors conditionally named after the respective seas.

Assessment of the phytoplankton productivity trend in the ice-free arctic basin prior to 1998.
According to the *in situ* data we collected, the annual phytoplankton productivity in the Arctic has been growing at a rate of 0.69%, 0.67%, and 0.71% during, respectively, the 1959–2005, 1959–1997, and 1998–2005 time intervals. The *annual* rate of productivity determined from space is assessed at 0.86%. The difference between the *in situ* and spaceborne assessments of productivity for the period 1998 –2005 resides in the fact that the prevailing body of *in situ* measurements was restricted to the shelf zone.

Our estimations indicate that monthly mean PP per unit area has a tendency to increase: in the pelagic zone, during the last 13 years the respective trend for the month of maximum PP $m^{-}2$ day^{-1} (occurring in June) constituted 10.9%. A similar situation is found for the shelf zone: the month of maximum PP per m^2 (occurring in May); the trend constituted 8.1%. These results are consistent with our finding of a steady growth of *chl* in both zones over the period 1998–2010 (Tables 1 and 2). Obviously, the inferred enhancement of three important factors, viz. *chl*, the ice-free area, and the ice-free period duration (according to Arrigo and van Djiken, 2011), sea ice retreated a total of 28 days earlier in 2009 than in 1998), largely explains the observed trends in PP in the Arctic.

Our assessments have shown that the highest increase in PP over the studied 13 years has occurred in the eight sectors that remained until 1998 the least productive ones: the trend constituted over 112% and 57%, respectively, for the East Siberian and Chukchi sectors. In the sectors with a higher trophic status (Kara, Barents, Greenland, Beaufort, and Baffin sectors), the trend did not exceed 20%. In terms of PP, the Laptev sector is in the middle between productive and oligotrophic Arctic sectors; however, its PP trend proved to be as high as ~55%.

Located over a shallow and broad shelf plateau, this sea is a recipient of a high influx of river water, sediments, and nutrients during summer, and long-lasting sea-ice cover from October to May. The ongoing climatic changes have brought about a significant reduction in ice cover and an appreciable increase in open water period (Arrigo and van Dijken, 2008). This is accompanied by a steadily increasing precipitation over the catchment of explicitly as well as the Lena River (Peterson et al. 2002). It could be conjectured that a combined action of the above factors brought about the above very steep increase in PP. At the same time, the Kara Sea seems to be subjected to very similar external forcing; however, the trend is far weaker. This implies the necessity of a more detailed and quantitative analysis of the driving mechanisms that resulted in the ~50% trend in PP in the Laptev Sea/sector between 1998 and 2010.

The trend of ~19.7% in PP in the Barents sector is certainly due to the appreciable increase in the ice-free area and duration of the ice-free period. However, the nutrient' balance dynamics might also be a controlling factor as the freshwater-driven enhancement of stratification comes to prevail over the nutrient supply from deep waters (Hansen et al. 2003). The mechanisms of the decrease of PP across the Greenland Sea sector (as we have mentioned above, which was also observed by Arrigo and van Dijken (2011)) over the time period 1998–2010 are not evident, and need a specifically focused study.

The deficiency of the results presented above reside in neglect of PP in the ice and in the water column beneath it. Meanwhile, there are *in situ* measurements indicating that the contribution of PP of this origin might be significant. Thus, Gosselin et al. (1997) accomplished sampling of ice and water column phytoplankton concentrations and PP along a route extending from Fram Strait to Bering Strait (in the latitudinal belt 70°N - 90°N), and found that PP in ice (as compared to that in the water column) contributed up to 57 % in some areas, although in the majority of the performed stations it varied within 2-5%. Arigo et al., 2012. reported from their ICECAPE 2011 expedition in the Chukchi Sea that along two 250-km transects extending from open water far into the ice pack depth-integrated phytoplankton biomass beneath the ice (0.5-1.8 m thick) was about fourfold greater than in open water. This massive under- ice bloom extended for over 100 km into the ice pack. Regardless of the fact that the under-ice light climate was less favorable than that for ice-free areas, it proved to be sufficient to support the phytoplankton bloom, which grew twice as fast as low light as their ocean counterparts. This is a direct indication of (*i*) a remarkable ability of sub-ice microalgae to accommodate themselves to low-light conditions, and (*ii*) that this effect must be expected along the entire ice-edge across the Arctic. Both findings explicitly point to the necessity of taking into account in-ice and sub-ice PP contributions to the Arctic total PP.

ACKNOWLEDGMENTS

This research was performed under the FP7 Programme (grant 'MONARCH-A FP7- SPA.2009.1.1.02'). We express our gratitude to persons and institutions that provided us with *in situ* data (as specified in Petrenko et al., 2013).

REFERENCES

Arigo et al. (2012). Massive Phytoplankton Blooms under Arctic Sea Ice. *Science* **336**, 1408.

Arrigo, K., and van Dijken, G.(2008). Changes in Arctic Ocean Primary Production from 1998–2008.http://www.arcticnet.ulaval.ca/pdf/talks2008/arrigoKevin.pdf

Arrigo, K., and van Dijken, G. (2011). Secular Trends in Arctic Ocean Net Primary Production. *J. Geophysical Research* **116** (C09011), 1–15.

Behrenfeld, M., and Falkowski, P. (1997). Photosynthetic Rates Derived from Satellite-Based Chlorophyll Concentration. *Limnology and Oceanography* **42**(1), 1–20.

Gosselin, M., Levasseur, M., Wheeeler, P., Horner, R., and Booth, B. (1997). New measurements of phytoplankton and ice production in the Arctic Ocean. Deep-Sea Research II **44**(8), 1623-1644.

Korosov, A. Pozdnyakov, D., Folkestad, A., Pettersson, H., Sorensen, K., and Shuchman, R. (2009). Semi-Empirical Algorithm for the Retrieval of Ecology-Relevant Water Constituents in Various Aquatic Environments. *Algorithms* **2**, 470–497.

Maritorena, S., Siegel, D., and Peterson, A,. 2002. Optimization of a Semi-Analytical Ocean Colour Model for Global-Scale Applications. *Applied Optics* **41**(15), 2705–2714.

Petrenko, D., Pozdnyakov, D., Johannessen, J., Counillion, F.,and Sychov, V., 2013. Satellite derived primary production in the Arctic Ocean. International Journal of Remote Sensing, 34(11), pp. 3903-3937.

Robinson, I. S. 2004. Measuring the Oceans from Space: The Principles and Methods of Satellite Oceanography. Springer Praxis Books/Geophysical Sciences, Chichester, pp. 194-246.

DRIVERS OF TERRESTRIAL CARBON RELEASE TO RIVERS: CENTRAL SIBERIAN PLATEAU CASE STUDY

A.S. PROKUSHKIN[1], I.V. TOKAREVA[1], M.A. KORETS[1], R. AMON[2], O.S. POKROVSKY[3]

[1]V.N. Sukachev Institute of Forest SB RAS, 660036, Krasnoyarsk, Russia

[2]Department of Marine Sciences, Texas A&M University at Galveston, Galveston, USA.

[3]GET-CNRS, 14 avenue Edouard Belin, 31400 Toulouse, France;

Keywords: CENTRAL SIBERIAN PLATEAU, RIVERS, DISSOLVED ORGANIC AND INORGANIC CARBON

INTRODUCTION

Siberian watersheds underlain by permafrost play an important role in global element cycling and are vulnerable to air temperature rise and permafrost degradation (Frey and Smith 2005; Tarnocai et al. 2009; Kharuk et al. 2011; Pan et al. 2011; Dolman et al. 2012). Changes in land–atmosphere exchange of C in forests and tundra of Central and Eastern Siberia and hydrological trends in these regions linked to climate warming have been recognized as general ecological concerns in recent decades (Peterson et al. 2002; McGuire et al. 2009; Dolman et al. 2012). The vulnerability of the large soil organic carbon pool in permafrost-controlled ecosystems (Tarnocai et al., 2009) to increasing temperatures (Grosse et al., 2011) is a key questions in numerous studies conducted in Northern circumpolar regions, including the basins of the largest Siberian rivers (Frey and Smith 2005; Raymond et al. 2007; Holmes et al. 2012). However, the controls of carbon transfer from terrestrial to aquatic systems and its allocation in inland waters (Raymond et al. 2007; Prokushkin et al. 2008, 2011; Amon et al. 2012; Holmes et al. 2012) still receive considerably less attention.

We examined variations in concentrations, fluxes and partitioning of C species in rivers and streams, which drain watersheds differing in extent of permafrost, air temperature, vegetation types, and fire history. Knowledge of how the contemporary environmental factors influence the carbon cycle in the catchments within the gradient of sub-Arctic rivers from the south to the north (space-for-time substitution) provide important insights into biogeochemical consequences of permafrost degradation under the global warming scenario.

Another major factor driving biogeochemical processes in boreal forest ecosystems is wildfires. Fire can transform subarctic forest landscapes, leading to changes in organic matter and nutrient loading to receiving streams and rivers. The influence of fire-driven variability on nutrient retention and transport is poorly understood within the permafrost terrains. To understand fire effects on the hydrochemical characteristics of the streams draining the continuous permafrost terrains of Central Siberian Plateau, we selected the chronosequence of basins which had been severely disturbed by fire (>80% of basin area) in time range from 1 to 110 years ago. The major research tasks were: (1) to specify the changes in sources and composition of solutes released from watersheds in response to permafrost degradation and fire-caused disturbance, (2) to identify the major basin parameters affecting a solute release, and (3) to analyze the role of post-fire forest succession in stream biogeochemistry dynamics.

STUDY AREA AND METHODS

Study area

Central Siberian Plateau is the vast upland area in the central part of northern Asia. Covering an area of roughly 1.5 million sq km, the plateau lies on the Siberian Platform at an average elevation of 500–700 m a.s.l. Central Siberian Plateau includes a vast trap province covered by a 248-Ma-old flood basalt complex of an area of 340 000 km^2. Despite some textural differences between different formations (i.e.,

Nidymskaya, Kochechumskaya, Yambukanskaya formations), Siberian basalts are very homogeneous in chemical and mineralogical compositions and are represented by tholeiites typical for all trap formations of the world (Pokrovsky et al., 2005).

The region of interest belongs to the central and southern part of the basaltic province and includes parts of the Nizhnyaya Tunguska (including its 6 tributaries) and Podkamennaya Tunguska River basins. Total watershed area of selected rivers is about 500 000 km^2 or roughly one third of Central Siberian Plateau. Permafrost extends throughout the study area from continuous permafrost in the north to its isolated patches in southern part of the basins of Nizhnyaya Tunguska and Podkamennya Tunguska Rivers (Fig.1) (Brown et al. 1998). The mean annual air temperatures vary between the basins from -10.9 to -6.3°C (2001-2013, grid data 0.5°x0.5°, British Atmospheric Data Centre).

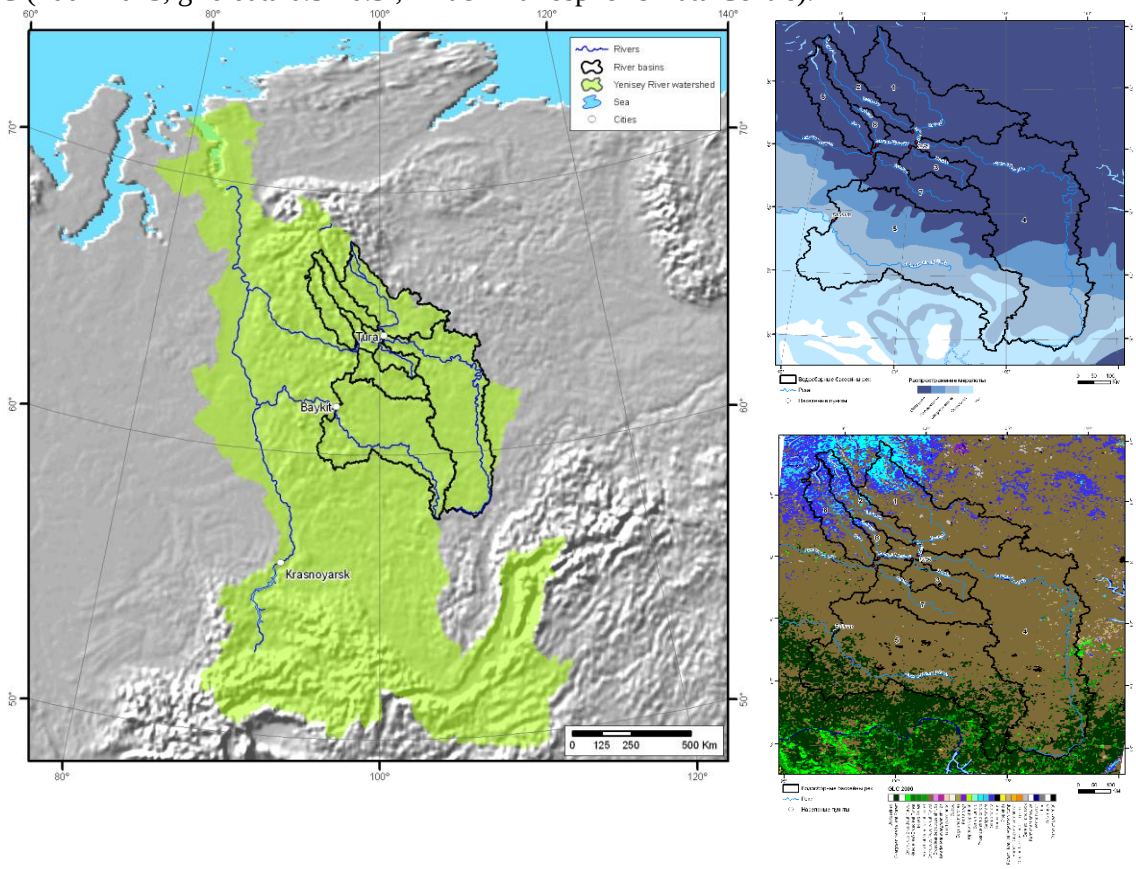

Fig. 1. The locations of eight rivers of Central Siberian Plateau within the Yenisei River basin. Inserts are permafrost types and distribution of vegetation classes within the basins of the major rivers of Central Siberian Plateau: 1 – Kochechum, 2 – Tembenchi, 3 – Nidym, 4 – N Tunguska, 5 – P Tunguska, 6 – Vivi, 7 – Taimura and 8 – Yambukan.

To analyze biogeochemical parameters of rivers and streams, we regularly collected water and river suspended matter (RSM) samples from eight rivers of Central Siberian Plateau and 17 small streams of the Nizhnyaya Tunguska River basin. River water were sampled at a monthly interval under ice conditions (October-April), twice a week at snowmelt freshet (from mid May to beginning of June) and on a weekly basis in summer and autumn (mid June-September). Water samples were collected from just beneath the water surface and at the middle currents of the rivers. Samples were immediately filtered (pre-weighed 0.22 μm, Millipore) and stored in a refrigerator prior to analyses. We analyzed $\delta^{18}O$ and δD, dissolved organic carbon (DOC), dissolved inorganic carbon (DIC) total dissolved nitrogen (TN); nitrate nitrogen, nitrite nitrogen, ammonium nitrogen, phosphorus; main anions and cations, spectral and fluorescent properties of dissolved organic matter.

RESULTS AND DISCUSSION

Seasonal and inter-annual dynamics of C species concentrations in rivers and streams of Central Siberia Plateau. During the entire period of observations (2005-15), concentrations of dissolved and particulate C species (DOC, DIC and POC) in river and stream waters were characterized by high inter-seasonal variations depending on flow regimes. The differences in the discharge of the rivers might reach an order of magnitude between highest and lowest values among seasons (freshet *vs*. winter low flow) (Fig. 2).

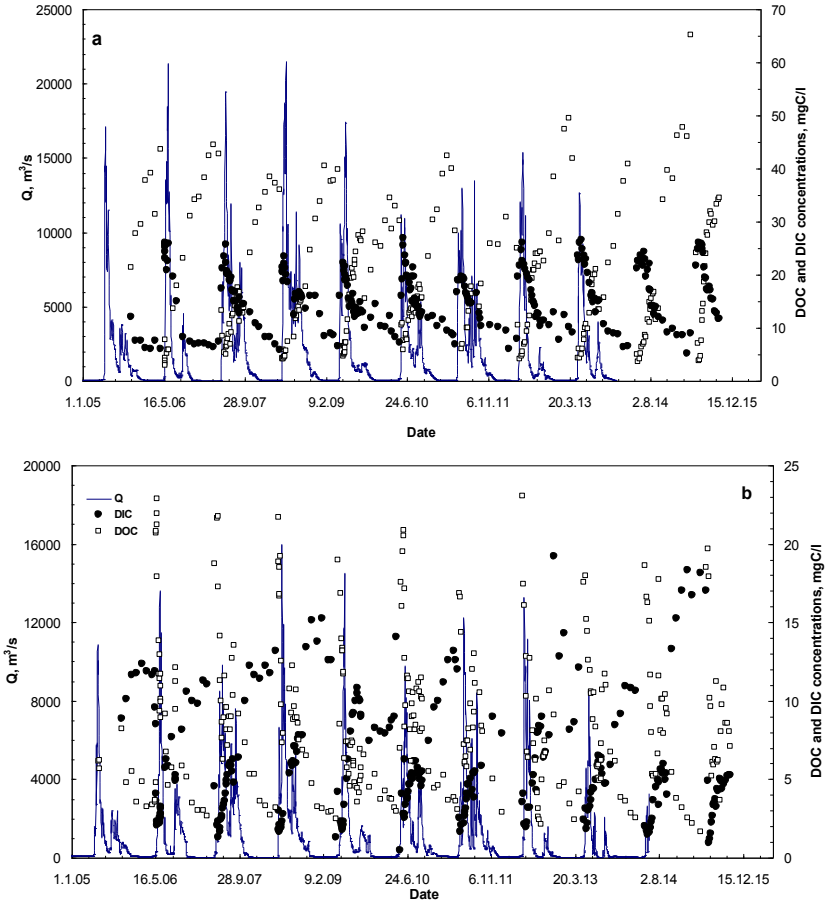

Fig. 2. The 2005-2015 dynamics of river discharge and DOC and DIC concentrations in Nizhnyaya Tunguska (a) and Kochechum (b) Rivers.

On the other hand, northernmost rivers demonstrated preceding maximum of DOC concentrations relatively to the peak of discharges. Such pattern occurred most likely due to the lower stocks of water-mobilized OC in alpine headwater portions of northern basins and thus dilution of "low elevations" DOC-rich waters in rivers. Particularly, all northern tributaries demonstrated 1.5-2.0-fold lower DOC values as compared to the streams sampled near Tura and draining forested terrains. Concentrations of POC were also the highest (up to 1.2 mgC l^{-1}) in freshet period, despite the lowest C_{org} content (<3%) in RSM released in this season.

During the summer-autumn season, DOC concentrations were gradually decreasing with flushes, as discharges increased after rain events. SUVA, a measure of aromaticity of DOC, and HMW DOC (>1 kDa) were also decreasing during frost-free period. Minimum DOC concentrations and SUVA were observed in winter lowflow in April, and the lowest HMW DOC appeared at summer base flow (July). As opposed to DOC, dissolved inorganic C demonstrated the lowest concentrations during spring being steadily increasing from summer to winter. Summer-autumn stormflows resulted in short-term drops of DIC concentrations in river waters.

Annual total dissolved carbon export from basins of Central Siberia Plateau (3-10 gC/m^2/a) is among the largest reported for the greatest rivers of Northern hemisphere (e.g. McGuire et al., 2009,

Dolman et al., 2012) and is largely controlled by annual runoff. So the terrigenic C export increases with increasing annual water yield in rivers at the rate of 0.015 to 0.029 gC/m^2/mm. Southern rivers demonstrate larger export values per unit runoff, suggesting larger stocks of mobilizeable C in their basins. In geographic context, both DIC and DOC concentrations showed an increasing trend from the northern to southern part of Central Siberian Plateau and correlated positively with MAAT (r=0.89, p=0.045) and forested area (r=0.86, p=0.07), whereas there was weak negative relationship with continuous permafrost distribution (r=-0.66, p=0.22). These findings suggest two likely limitations for river export of terrigenous C across Central Siberia: (1) low productivity of ecosystems with respect to potentially mobilizable organic C and, slow weathering rates with concomitant small formation of bicarbonate limit the pools of organic and inorganic C that can be mobilized for transport in rivers (source-limited), and (2) mobilization of available pools of C is constrained by low precipitation reflected in low runoff in the severe continental climate of interior Siberia (transport-limited). Thus, the growth of C release might be projected for the basins of Siberia as precipitation and ecosystem productivity would increase with warming on these watersheds.

Long-term-dynamics of hydrochemical composition of streams after fire disturbance. To analyze the fire effect on hydrochemical composition of streams in continuous permafrost region we have obtained the long-term dynamics (2005-15) of the mean seasonal (May-September) concentrations of major cations, anions, DIC and DOC for 17 streams of the Nizhnyaya Tunguska River basin with respect to the post-fire succession (Fig. 3). DOC concentrations showed a drastic drop immediately after a fire. DOC concentrations recovery rates based on seasonal mean values calculated against “control” 110 year old basin demonstrated linear growth of DOC concentrations (ca. 0.12 mgC/l/a) with time after a fire up to 55 years. The maximum post-fire active layer thickness (ALT) and maximum concentrations of the major cations reached 15-20 years after fire, however, they lagged 5-10 years as compared with DIC behavior (max: 10-12 years following fire). We may, thus, presume that the main source of DIC in analyzed streams was microbiological processes of organic soil matter mineralization reaching its maximum sooner than ALT peak. A further decrease in DIC concentration in the streams might be attributed to exhausting of labile pool of organic carbon.

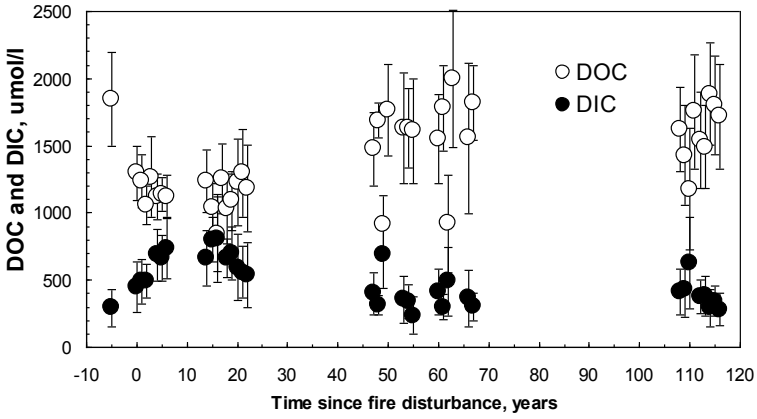

Fig. 3. Dynamics of mean seasonal (May-September) concentrations of DOC and DIC in the streams of Nizhnyaya Tunguska River basin after fire disturbance.

CONCLUSIONS

The amounts of terrigenic carbon exported from watersheds of Central Siberian Plateau are among the largest reported for subarctic terrains of Northern hemisphere. Nevertheless, our studies revealed several factors limiting contemporary riverine export of terrigenous C from permafrost-affected landscapes of Central Siberia.

There are limitations of C release from Northern alpine zones implied by low productivity of ecosystems with respect to low amounts of potentially mobilizable organic C in ecosystems and slow weathering rates with concomitant small formation of bicarbonate, which both limit the pools of organic and inorganic C that can be mobilized for transport in rivers. Periodic wildfires exert further controls to riverine C release decreasing the amounts of labile OC through the combustion and lower solubility of

remained OM, but accelerating its mineralization in soils to CO_2 and DIC. In this context fires have opposite effects for DOC and DIC behavior in rivers, which resultant for total C export from fire-affected basins remains poorly quantified. Not least important limitation of terrigenic C species release from Central Siberian watersheds is the constrain by low precipitation and, respectively, low mobilization of C in terrestrial ecosystems under severe continental climate of interior Siberia.

The growth of C release from Central Siberian watersheds is projected as precipitation and ecosystem productivity would increase with warming on these watersheds. On the other hand increasing temperatures might amplify occurrence and severity of fires. Such complex interactions and responses of terrestrial ecosystems to global climate change require further analysis of biogeochemical processes involved in C release to aquatic systems. Particularly there is an urgent need for biogeochemical and ecohydrological modeling of processes of production and hydrological transport of C in rivers and its further release to the Arctic Ocean.

ACKNOWLEDGEMENTS

This work is supported by Russian Science Foundation grant #14-24-00113.

REFERENCES

Amon R.M.W., Rinehart A.J., Duan S., Louchouarn P., Prokushkin A., Guggenberger G., Bauch D., Stedmon C., Raymond P.A., Holmes R.M., McClelland J.W., Peterson B.J., Walker S.A., Zhulidov A.V. Dissolved organic matter sources in large Arctic rivers // Geochimica et Cosmochimica Acta, 2012, № 94, 217–237.

Brown J, Ferrians O J Jr, Heginbottom J A and Melnikov E S 1998 revised February 2001 Circum-arctic map of permafrost and ground ice conditions Boulder, CO: National Snow and Ice Data Center/World Data Center for Glaciology. Digital media

Dolman A.J., Shvidenko A., Schepaschenko D., Ciais P., Tchebakova N., Chen T., van der Mole1 M.K, Belelli Marchesini L., Maximov T.C., Maksyutov S., Schulze E.-D. An estimate of the terrestrial carbon budget of Russia using inventory-based, eddy covariance and inversion methods // Biogeosciences. 2012. № 9. C. 5323–5340.

Frey K.E., Smith, L.C. Amplified carbon release from vast West Siberian peatlands by 2100 // Geophys. Res. Letters. 2005. № 32. L09401. doi:10.1029/2004GL022025.

Grosse G., Harden J., Turetsky M., McGuire A.D., Camill P., Tarnocai C., Frolking S., Schuur E.A.G., Jorgenson T., Marchenko S., Romanovsky V., Wickland K.P., French N., Waldrop M., Bourgeau C.L., Striegl R.G. Vulnerability of high latitude soil organic carbon in North America to disturbance // Journal Of Geophysical Research, VOL. 116, G00K06, doi:10.1029/2010JG001507, 2011

Holmes R.M., McClelland J.W., Peterson B.J., Tank S.E., Bulygina E., Eglinton T.I., Gordeev V.V., Gurtovaya T.Y., Raymond P.A., Repeta D.J., Staples R., Strieg R.G., Zhulidov A.V. Zimov S.A. Seasonal and annual fluxes of nutrients and organic matter from large rivers to the Arctic Ocean and surrounding seas // Estuaries and Coasts. 2012. № 35. P. 369–382.

Kharuk V.I., Ranson K.J., Dvinskaya M.L., Im S.T. Wildfires in northern Siberian larch dominated communities // Environ. Res. Lett. 2011. № 6. 045208. doi:10.1088/1748-9326/6/4/045208.

McGuire A.D., Anderson L.A. Sensitivity of the carbon cycle in the Arctic to climate change // Ecol. Monographs. 2009. № 79(4). P. 523-555.

Pan Y., Birdsey R.A., Fang J., Houghton R., Kauppi P.E., Kurz W.A., Phillips O.L., Shvidenko A., Lewis S.L., Canadell J.G., Ciais P., Jackson J.B., Pacala S., McGuire A.D., Piao S., Rautiainen A., Sitch S., Hayes, D. A large and persistent carbon sink in the world's forests // Science. 2011. № 333. P. 988–993.

Peterson BJ, Holmes RM, McClelland JW, Vorosmarty CJ, Lammers RB, Shiklomanov AI, Shiklomanov IA, Rahmstorf S Increasing river discharge to the Arctic Ocean // Science, 2002, 298, 2171–2173.

Pokrovsky O.S., Schott J., Kudryavtzev D.I. and Dupré B. Basalt weathering in Central Siberia under permafrost conditions // Geochim Cosmochim Acta, 2005, 69, 5659–5680.

Prokushkin A. S., Tokareva I.V., Prokushkin S.G., Abaimov A.P., Guggenberger GFluxes of Dissolved Organic Matter in Larch Forests in the Cryolithozone of Central Siberia // Rus. J. Ecol., 2008, 39(3), 151–159.

Prokushkin A.S., Pokrovsky O.S., Shirokova L.S., Korets M.A., Viers J., Prokushkin S.G., Amon R., Guggenberger G., McDowell W.H. Sources and flux pattern of dissolved carbon in rivers of the Yenisey basin draining the Central Siberian Plateau // Environmental Research Letters, 2011, 6. doi:10.1088/1748-9326/6/4/045212.

Raymond P.A., McClelland J.W., Holmes R.M., Zhulidov A.V., Mull K., Peterson B.J., Striegl R.G., Aiken G.R., Gurtovaya T.Y. Flux and age of dissolved organic carbon exported to the Arctic Ocean: A carbon isotopic study of the five largest arctic rivers // Global Biogeochem. Cycles. 2007. № 21. GB4011, doi:10.1029/2007GB002934.

Tarnocai C., Canadell J.G., Schuur E.A.G., Kuhry P., Mazhitova G., Zimov S. Soil organic carbon pools in the northern circumpolar permafrost region // Global Biogeochem. Cycles. 2009. № 23, GB2023, doi:10.1029/2008GB003327

SATELLITE-BASED SNOW WATER EQUIVALENT ESTIMATION AND CLIMATOLOGY ANALYSIS OVER CENTER ASIA AND XINJIANG PROVINCE, CHINA

YUBAO QIU[1], HUADONG GUO[1]

[1] *Institute of Remote Sensing and Digital Earth, China*
(No.9 Dengzhuang South Road, Haidian District, Beijing 100094, China, qiuyb@radi.ac.cn)

Keywords: Snow Water Equivalent, Remote Sensing, Center Asia, Xinjiang Province, Snow Climatology

(The abstract is relevant to the seasonal snow water distribution and decades' snow climatology at the Central Asia, and Xinjiang, China, which is one of the important water income over there.)

Abstract:
The Central Asia, and adjacent areas, such as, Russia, western China, and its southern neighboring countries are highly continental climate, within the central region of Eurasia continent, its water resource are mainly from the precipitation and supplies from mountain glacier melting. Snow precipitation is an important water resource that balances the water redistribution through the atmosphere transportation. Through the snow depth observations, the snow precipitation accumulation can be estimated statistically by the *in situ* and remote sensing. Geographically, the seasonal snow water at winter covers most of the northern Center Asia, especially, Kazakhstan, and the Xinjiang Province, China. Over the last decades, global warming and its combined temperature and water vapor changing came into being a large influence to the snow water distribution.

Aiming to the understanding on the Snow Water Equivalent (SWE) distribution and its climatology in the last decades, we conduct a research on the estimation of Snow Water Equivalent (SWE) from satellite-based passive microwave observations, with the support and validation from the sparsely distributed *in situ* snow measurements over the Center Asia, and Xinjiang, China. An empirical algorithm was developed with monthly coefficients which considered the changing snow attributions in the winter time, the algorithm prototype is,

Snow Depth (cm) = (monthly changed coefficient) * (Tb_{17}-Tb_{37}) + Interception

The *in situ* measurement in Xinjiang province was employed to validate the algorithm monthly, the validation result showed that it achieved a 37.21% Mean Relative Error (MRE), about 40% validation sites achieve 20% MRE, when compared with the traditional algorithm (Chang'92, and NASA operational algorithm), the new updated algorithm has an improvement there.

The long time series of satellite observations are used for a climatology analysis, there are the Advanced Microwave Scanning Radiometer - Earth Observing System (AMSR-E) sensor on NASA's Aqua satellite (2002~2011) and Microwave Radiometer Imager (MWRI) on Fengyun-3 satellite (2011~now), which tells the snow water available spatially in a broad area on a high time resolution.

The winter SWE reveals an obvious seasonal trend of SWE time series distribution. The SWE increased from November through December, and reach the peak value at February, then it begins the spring melting season from March. Most of the snow cover pixels concentrate at two SWE value scopes, one is below 40mm and another is between 80 to 120mm. The lower SWE places are mainly on the Center Asia lowland plain area, and the margin area of desert of Tarim basin, while the relative higher SWE distribute over the Northern Kazakhstan and Mountain areas, it shows a clear spatial variable distribution from south to north.

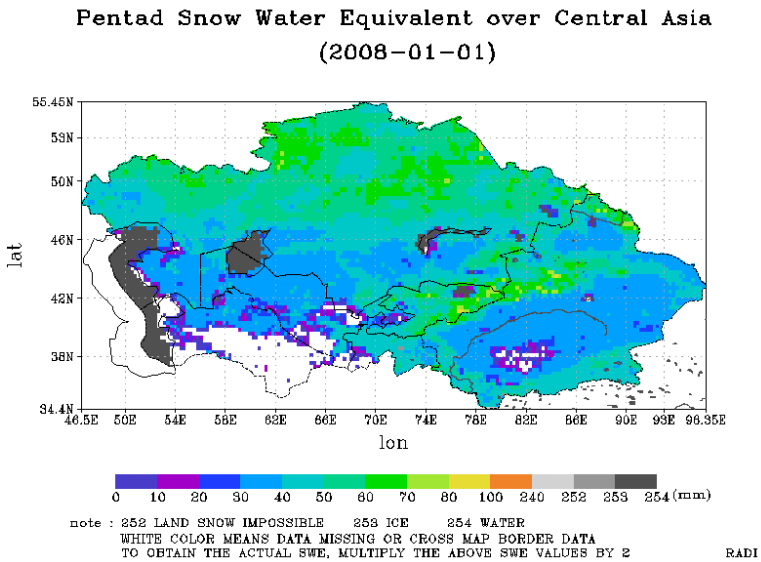

Fig 1. An example of the Pentad SWE (5days) product at Center Asia and Xinjiang Province, China

From the validation and analysis, the retrieved SWE products shows it's feasibility over Center Asia and Xinjiang, China. A further analysis is undergoing from multi and consecutive satellite measurements.

This work is supported by the Chinese National Programs for Science and Technology Development (grand no. 2012BAH27B05) and National Natural Science Funds Fund (41371351).

EFFECTS OF LAND SURFACE HETEROGENEITIES ON CONVECTIVE BOUNDARY LAYERS
WHAT DID WE LEARN FROM LARGE-EDDY SIMULATIONS SO FAR?

S. RAASCH,

Institute of Meteorology and Climatology, Leibniz Universität Hannover,
Germany.

Keywords: SURFACE HETEROGENEITIES, CONVECTIVE BOUNDARY LAYER, LARGE-EDDY SIMULATION.

INTRODUCTION

Differences in land use represent inhomogeneities of the land surface, which range from meso-scale down to the micro scale. Typically, variations of land use on such scales are not resolved in operational weather forecast models, and it is still an open question, if and how these heterogeneities affect the turbulence and vertical transport within the atmospheric boundary layer (ABL), especially under convective conditions with horizontally varying sensible and latent surface heat-flux. As a general effect, the differential heating may create so-called thermal secondary circulations (SC), which can extend up to the top of the convective boundary layer (CBL) and which even may effect the entrainment of warm air from the capping inversion.
Since more than 20 years, large eddy simulations are used to study such heterogeneity effects. In the beginning, the focus was on idealized one-dimensional (stripe) or two-dimensional (chessboard) patterns of prescribed surface sensible heat-flux. Simulations used relatively coarse grid spacings of 50-100 m. Research was later extended to more complex real world heterogeneity patterns, and very high resolutions down to 5-10 m were used e.g. to examine entrainment processes. While most of the studies in the past assumed variations in surface fluxes solely due to the (static) features of the specific land use type (e.g. forest, crops, lakes, etc.), recent research starts to focus on dynamic heterogeneities caused by cloud shadows. Further emphasis is now given on questions like how surface heterogeneities affect turbulence measurements or if, in turn, heterogeneity effects can be detected from such measurements. This paper provides some of the major results of LES of surface heterogeneity effects based on studies performed by the LES working group of the Institute of Meteorology and Climatology at Leibniz Universität Hannover during the last 15 years. The **PA**rallelized **L**ES **M**odel PALM (Raasch and Schröter, 2001; Maronga *et al.*, 2015) has been used for all simulations presented here.

STUDIES FOR IDEALIZED HETEROGENEITIES

One of the early findings from studies for idealized one- and two-dimensional sensible heat-flux heterogeneities was that significant SCs that extend up to the top of the CBL only develop when the wavelength/scale λ of heterogeneities is increased to z_i, the CBL height, or larger. Effects of smaller heterogeneities are limited to the lower parts of the boundary layer. Mean profiles of first and second order moments are hardly affected by the heterogeneities, except the entrainment heat-flux, which appears to increase for $\lambda \sim z_i$. While in general moderate background winds of 5 ms^{-1} eliminate all impacts of surface inhomogeneities, SCs still appear for higher wind speeds depending on the wind direction relative to the orientation of the heterogeneities, e.g. for wind directions along the stripes, or along the diagonals of the chessboard pattern (Raasch and Harbusch, 2001). Letzel and Raasch (2003) have shown that one dimensional stripes with $\lambda >> z_i$ can create temporal oscillations in the SC strength which are slowly damped in time. Due to the oscillation, instantaneous vertical profiles of the turbulent heat-flux can significantly deviate from the linear shape which appears under homogeneous conditions.

In a recent high spatial resolution study Sühring *et al.* (2014) found for one-dimensional stripes a complex dependence of the entrainment rate on the heterogeneity-parameters. Compared to the homogeneously-heated mixed layer, a decreased entrainment was observed for small heat-flux amplitudes, and an increased entrainment for large amplitudes. For large heat-flux amplitudes the largest entrainment was observed for patch sizes in the order of z_i, while for significantly smaller or larger patch sizes entrainment was similar as in the homogeneous case. Interestingly, the entrainment rate does not depend on the local position, i.e. it has the same strength over both the strong and less heated patch (Fig. 1).

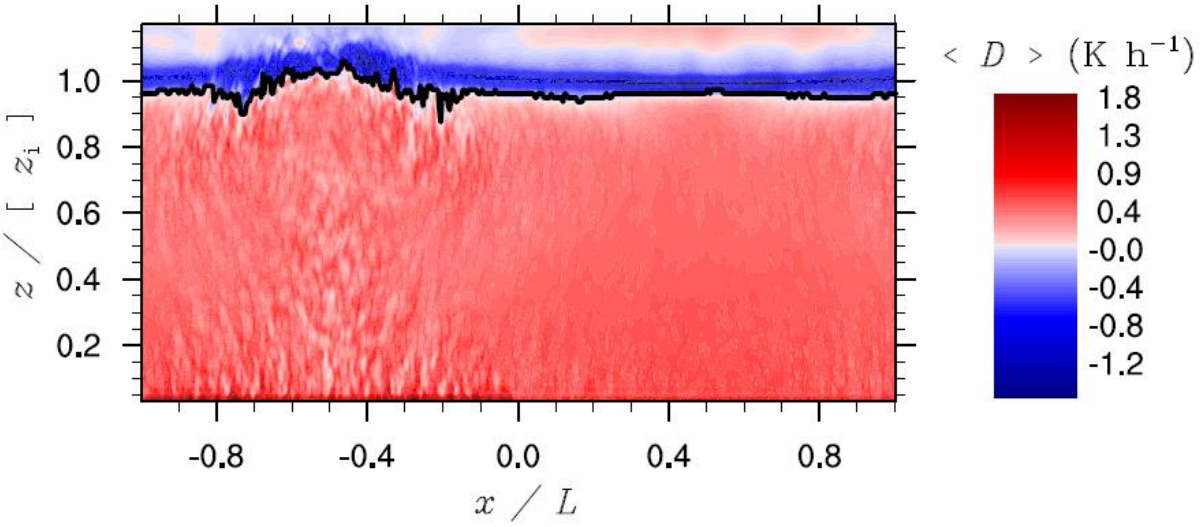

Figure 1. Instantaneous vertical cross-section of the cooling/heating rate D averaged along y for a simulation with a one-dimensional heterogeneity of wavelength L = 3200 m and a mean surface heat-flux of 0.1 K ms^{-1} (from Sühring *et al.*, 2014). The stronger heated patch is located on the left hand side (x<0). Obviously, the cooling of the inversion layer by entrainment does not depend on the location along x.

LES coupled with a Lagrangian stochastic particle model has also been used to calculate footprints for virtual measurement sensors under conditions of idealized heterogeneities (Steinfeld *et al.*, 2008). Comparisons of LES-derived footprints with those calculated by conventional analytical Lagrangian backward footprint models with simple parameterizations of flow conditions show that the analytical models mostly perform well and fail only in areas where the flow patterns are dominated by pronounced SCs (Markkanen *et al.*, 2010).

STUDIES FOR COMPLEX HETEROGENEITY PATTERNS

Only a few LES studies have been performed for real heterogeneities so far, which is mainly a consequence of limited available and suitable observation data. One exception is the LITFASS-2003 experiment which has been carried out in a 20x20 km^2 area south east of Berlin, Germany (Mengelkamp *et al.*, 2006). Maronga and Raasch (2013) investigated the impact of observed surface heterogeneities on the CBL during this experiment. LES, driven by observed near-surface sensible and latent heat-fluxes, were performed for the diurnal cycle and compare well with observations. The SC patterns vary between local and roll-like structures, depending on the background wind conditions (see Fig. 2). For higher background wind speeds, the flow feels an effective surface heat-flux pattern that derives from the original pattern by streamwise averaging. This effective pattern generates a roll-like SC with roll axes along the mean boundary-layer wind direction. Mainly the upstream surface conditions control the SC pattern, where the fetch increases with increasing background wind speed. The study already showed that sufficient time averaging and ensemble averaging is required to separate the heterogeneity-induced signals from the raw LES turbulence data, which might be an important reason why experiments over heterogeneous terrain in the past did not give any clear evidence of heterogeneity-induced effects.

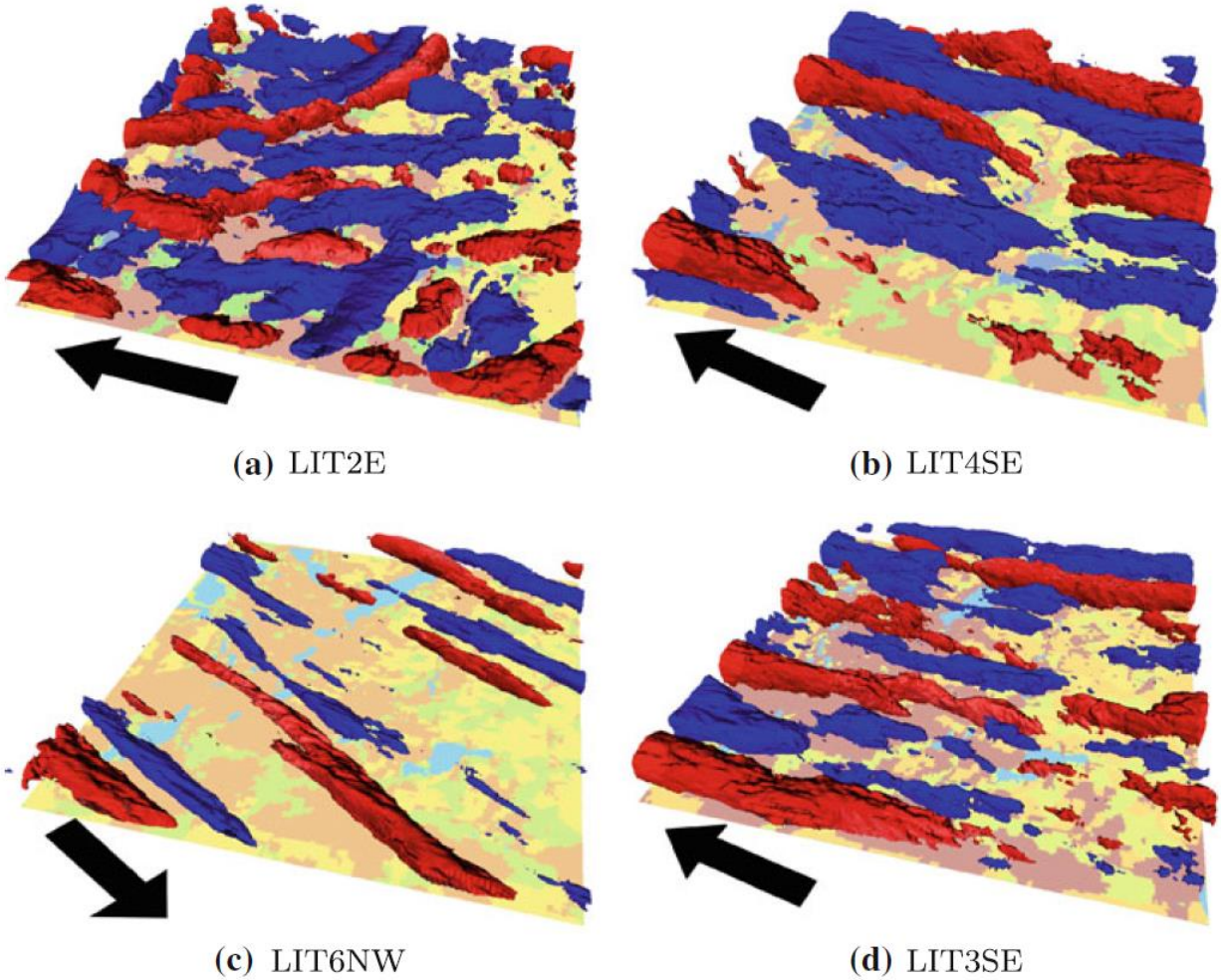

Figure 2. Secondary circulations over the LITFASS area (20 km × 20 km), determined from the LITFASS simulations at 1300 UTC (a–d). Subfigure captions give the magnitude and direction of the background wind, e.g. LIT2E means a background wind with 2 ms^{-1} from east. The figure shows isosurfaces of the heterogeneity-induced vertical velocity. The red isosurface refers to w = 0.3m s^{-1} (updrafts), the blue one to w = −0.3m s^{-1} (downdrafts). The bottom surface displays the prescribed kinematic heat-flux with low values in blue and high values in red color (from Maronga and Raasch, 2013).

This problem has been further studied by Sühring and Raasch (2013), who performed virtual flight measurements in an ensemble of up to 20 LITFASS-LES simulations, where each ensemble run started with different perturbations of the initial wind field. The resulting ensemble-averaged heat-fluxes indicated a clear dependence on the underlying surface up to the top of the CBL (also proving that there is no blending height in such convective cases). However, a large scatter between the flux measurements in different ensemble runs was observed, which was the result of insufficient sampling of the largest turbulent eddies. The random and systematic errors based on the integral length scale did not indicate such a large scatter. For the given flight leg lengths (up to 15 km based on the actual flights performed during the measurement campaign), at least 10-15 statistically independent flight measurements were necessary to give a significant estimate of heterogeneity-induced signals in the CBL. This clearly demonstrates that such kind of short single leg flights are not suitable for capturing heterogeneity-induced turbulent heat-flux patterns in the CBL.

In another LES study based on the LITFASS experiment, Maronga *et al.* (2014) were able to show that Monin-Obukhov theory relationships (MOST) and local free convection scaling, which are used for calculating surface sensible heat-fluxes from the structure parameter for temperature C_T^2, work fairly well

in the surface layer above heterogeneous surfaces. This demonstrated that the scintillometer technique, which calculates fluxes from structure functions of the refractive index, can be applied in heterogeneous terrain. However, it was found that the structure parameter for humidity C_q^2 does not follow MOST, which is ascribed to entrainment of dry air at the top of the boundary layer. Therefore, latent heat-fluxes may be difficult to determine from scintillometer measurements.

Gryschka *et al.* (2008) showed that cloud street patterns typically observed during cold air outbreaks are usually triggered by upstream sea-ice surface heterogeneities, and not by flow internal instability mechanisms (inflection point instability), as it was believed for decades of years. The mechanism which creates roll-like circulations is probably the same as found for the LITFASS simulations of pure land surface heterogeneities. In a follow-up paper, Gryschka *et al.* (2014) demonstrated that the SCs (rolls) can substantially contribute to the vertical turbulent transport (which has also been found by many other studies before), but that the magnitude of the total fluxes were not affected by them, so that the roll-specific transport has not to be regarded in turbulence parameterizations of larger-scale models.

DYNAMIC HETEROGENEITIES - THE EFFECTS OF CLOUD SHADOWS

While most of the studies in the past assumed variations in surface fluxes solely due to the (static) features of the specific land use type (e.g. forest, crops, lakes, etc.), recent research starts to focus on dynamic heterogeneities caused by clouds. The shadows of shallow cumulus clouds (shallow Cu) affect the CBL in several ways. One important effect is the reduction of solar irradiation at the land surface due to surface shading by clouds, which blocks further warming of the land surface, resulting in a decreased near-surface heat-flux in the shaded areas. This way, a field of shallow Cu produces a heterogeneous heat-flux pattern at the land surface, which varies dynamically within the lifetime of the cloud. With patch sizes of the heterogeneity equal to or larger than z_i, the heat-flux pattern has the potential to generate (dynamic) SCs, which extend throughout the entire boundary-layer depth. Hence the SCs caused by (stationary, static) heterogeneities of the surface itself might be modified under the presence of clouds. There also might be complex interactions between the clouds and their shadows which additionally depend on the solar zenith angle ϑ.

Gronemeier *et al.* (2015) have studied for the first time how dynamic SC caused by shallow Cu interact with static SC and how they affect the cloud field characteristics. They found that over a homogeneous surface and for zero background wind, shadows trigger dynamic SC with different strengths, depending on ϑ. It is found that large ϑ favour the development of dynamic SC. Over a heterogeneous surface with a simple striped pattern of near-surface heat-flux distribution H, the strength of static SC is effectively reduced at small ϑ. At large ϑ the effect on the SC depends on the orientation of the stripes of H to the shadow-casting direction of the clouds. The influence of shadows is only small if they are cast perpendicular to the striped heterogeneity. If the stripes and the shadow-casting direction are parallel, the static SC is reduced in strength also for large ϑ. However, in this case a dynamic SC develops as well. Shadow effects on the cloud field characteristics also vary with ϑ. The results show that small ϑ favour the development of small clouds with a reduced lifetime while a large ϑ promotes the development of larger clouds with an extended lifetime compared to non-shading clouds. Fig. 3 shows, as an example, how the cloud field (represented by the liquid water path) above a striped static heterogeneity orientated parallel to the shadow-casting direction varies with ϑ.

In general, the study showed that dynamic SC induced by cloud shadows can be of the same strength as static SC. Therefore, when considering cloud shadow effects over heterogeneous surface, static SC are distinctly changed. In such case not only ϑ but also the orientation of the heterogeneity in relation to the shadow-casting direction is important. This means that the majority of previous studies focusing on static SC should be treated with care as their results might be valid for cloud-free situations only.

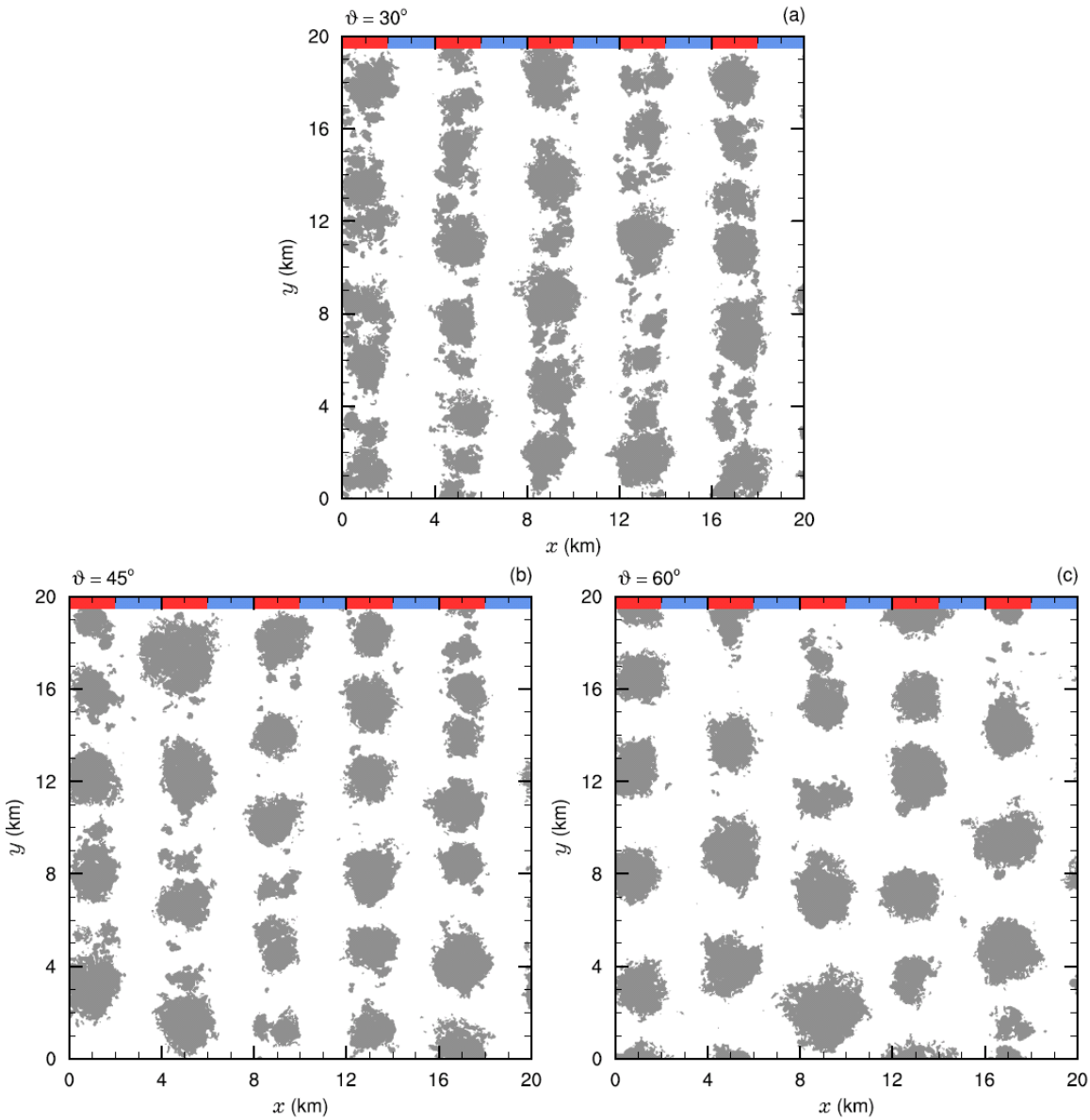

Figure 3. Liquid water path lwp for simulations with striped heterogeneity orientated parallel to the shadow-casting direction and (a) $\vartheta = 30°$, (b) $\vartheta = 45°$, and (c) $\vartheta = 60°$ after 4.5 hours simulation time. The grey colour represents areas with lwp > 0 m. The striped pattern of the static surface heterogeneous heat-flux is indicated by red and blue bars (hot and cold stripes, respectively) at the top (from Gronemeier *et al.*, 2016).

OUTLOOK

The impact of background wind on cloud shadow effects may be of interest for future analysis. Another step towards reality would be to consider the diurnal cycle of both the zenith angle ϑ and the azimuth angle. This approach may limit shadow effects observed for small ϑ due to the short period of time during a day where those angles are present, but still a clear influence on boundary-layer dynamics is expected. After many years of idealized setups, LES studies of surface heterogeneity are becoming able to better reproduce real world conditions now.

ACKNOWLEDGEMENTS

During the last 15 years, this work was supported by the German Research Foundation (DFG) under grants RA 617/2, RA 617/16, RA 617/20, RA 617/21, RA 617/24, by the Niedersächsiche Technische Hochschule (NTH) under grant BU 2.2.3, and by the German Ministry of Science and Education (BMBF) under grant 01LD0103.
All simulations were performed on massively parallel computers at The North-German Supercomputing Alliance (HLRN) in Hannover and Berlin, Germany.

REFERENCES

Gronemeier, T., F. Kanani-Sühring, and S. Raasch (2015): The formation of secondary circulations: Can non-stationary surface heterogeneities induced by cloud shadows compete with stationary heterogeneities induced by surface features?, *Boundary-Layer Meteorol.*, under revision.

Gryschka, M., C. Drüe, D. Etling and S. Raasch (2008): On the influence of sea-ice inhomogeneities onto roll convection in cold-air outbreaks, *Geophys. Res. Lett.*, **35**, L23804, DOI: 10.1029/2008GL035845.

Gryschka, M., J. Fricke and S. Raasch (2014): On the Impact of Forced Roll Convection on Vertical Turbulent Transport in Cold-air Outbreaks, *J. Geophys. Res.*, **119**, 12,513, DOI: 10.1002/2014JD022160.

Letzel, M.O. and S. Raasch (2003): Large-eddy simulation of thermally induced oscillations in the convective boundary layer, *J. Atmos. Sci.*, **60**, 2328,DOI: 10.1175/1520-0469(2003)060<2328:LESOTI>2.0.CO;2.

Markkanen, T., G. Steinfeld, N. Kljun, S. Raasch and T. Foken (2009): Comparison of conventional Lagrangian stochastic footprint models against LES driven footprint estimates, *Atmos. Chem. Phys.*, **9**, 5575.

Maronga, B. and S. Raasch (2013): Large-Eddy Simulations of Surface Heterogeneity Effects on the Convective Boundary Layer During the LITFASS-2003 Experiment, *Boundary-Layer Meteorol.*, **148**, 309, DOI: 10.1007/s10546-012-9748-z.

Maronga, B., O. K. Hartogensis, S. Raasch and F. Beyrich (2014): The effect of surface heterogeneity on the structure parameters of temperature and humidity - An LES case study for the LITFASS-2003 experiment, *Boundary-Layer Meteorol.*, **153**, 441, DOI: 10.1007/s10546-014-9955-x.

Maronga, B., Gryschka, M., Heinze, R., Hoffmann, F., Kanani-Sühring, F., Keck, M., Ketelsen, K., Letzel, M. O., Sühring, M., and S. Raasch (2015): The Parallelized Large-Eddy Simulation Model (PALM) version 4.0 for Atmospheric and Oceanic Flows: Model Formulation, Recent Developments, and Future Perspectives, *Geosci. Model Dev.* **8**, 2515, DOI: 10.5194/gmd-8-2515-2015.

Mengelkamp, H.-T., F. Beyrich, G. Heinemann, F. Ament, J. Bange, F. Berger, J. Bösenberg, T. Foken, B. Hennemuth, C. Heret, S. Huneke, K.-P. Johnsen, M. Kerschgens, W. Kohsiek, J.-P. Leps, C. Liebethal, H. Lohse, M. Mauder, W. Meijninger, S. Raasch, C. Simmer, T. Spieß, A. Tittebrand, J. Uhlenbrock and P. Zittel (2006): Evaporation over a heterogeneous land surface: The EVA-GRIPS project, *Bull. Amer. Meteor., Soc.*, **87**, 775.

Raasch, S. and G. Harbusch (2001): An analysis of secondary circulations and their effects caused by small-scale surface inhomogeneities using large-eddy simulation, *Boundary-Layer Meteorol.*, **101**, 31, DOI: 10.1023/A:1019297504109.

Raasch, S. and M. Schröter (2001): PALM - A large-eddy simulation model performing on massively parallel computers, *Meteorol. Z.* **10**, 363, DOI: 10.1127/0941-2948/2001/0010-0363.

Sühring, M., B. Maronga, F. Herbort and S. Raasch (2014): On the effect of surface heat-flux heterogeneities on the mixed-layer top entrainment., *Boundary-Layer Meteorol.*, **151**, 531, DOI: 10.1007/s10546-014-9913-7.

Steinfeld, G., S. Raasch and T. Markkanen (2008): Footprints in homogeneously and heterogeneously driven boundary layers derived from a Lagrangian stochastic particle model embedded into large-eddy simulation, *Boundary-Layer Meteorol.*, **129**, 225.

TOTAL COLUMN OF CARBON MONOXIDE AND METHANE OVER EURASIA: LONG-TERM TRENDS, SEASONAL AND WEEKLY VARIATIONS ANALYSIS BASED ON GROUND-BASED AND SATELLITE SPECTROSCOPIC OBSERVATIONS

V. S. RAKITIN[1], G. WANG[2], P. WANG[2], A.V. DZHOLA[1], A.N. SAFRONOV[1], E. I. GRECHKO[1], A.V. SHILKIN[3]

[1] A.M. Obukhov Institute of Atmospheric Physics, Russian Academy of Sciences, Moscow, Russian Federation

[2] Institute of Atmospheric Physics, Chinese Academy of Sciences, Beijing, People Republic of China

[3] NPO "Typhoon", Roshydromet, Obninsk, Russian Federation

Keywords: REMOTE SENSING, COLUMN, ATMOSPHERIC POLLUTION, CO AND CH_4 TRENDS

ABSTRACT

Analysis of the CO total column (TC) long-term spectroscopic measurements in Moscow and Beijing for period from 1992 to 2015 years is presented. Similar data of CO and CH_4 columns over Zvenigorod Scientific Station (ZSS) in 1970-2015 years are analyzed. Obtained trends has compared with similar estimates produced by use of satellite data (AIRSv6, 2003-2015).

Also CO TC weekly cycles obtained from ground-based and orbital measurements for all three sites are discussed.

INSTRUMENTATION

Ground-based observation of CO, CH_4 and H_2O total content (TC) were produced by absorption spectroscopy method with using identical grating spectrometers of medium resolution (0,2 cm^{-1}) with solar-tracking system, Dianov-Klokov at all. 1989, Golitsyn at all, 2015). Long-term data sets are available from 1970 (regular for Zvenigorod, Moscow province and for Moscow) and from 1992 (episodically, i.e. autumn months for Beijing).

Satellite data (product AIRSv6, L3, i.e. diurnal averaged for 1°x1° CO and CH_4 TCs, ascending only for 2003-2015) were used to investigate space -temporal distributions of this species and their long-term trends (Aumann at all, 2003, Worden at all, 2013).

RESULTS

Typical levels of anthropogenic CO and aerosols pollution of atmosphere in Beijing is 2–5 times stronger in comparison with Moscow ones (Golitsyn at all, 2015).

Long-term trends and annual variations of CO TC over Moscow and Beijing obtained by ground-based measurements for autumn season (1998-2014, Oct-Nov) are presented on Fig.1.

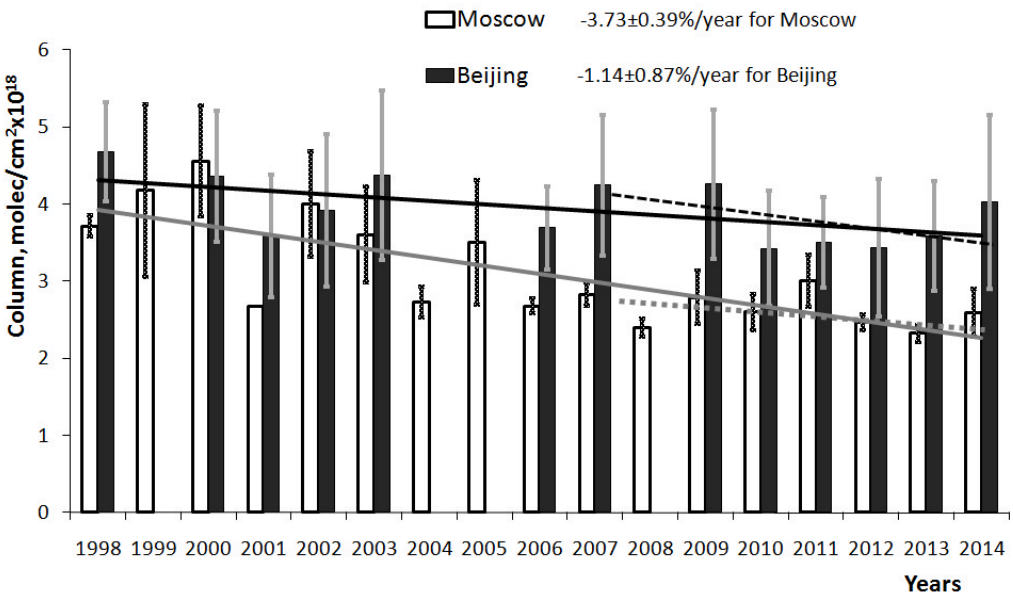

Figure 1. CO TC trends over Moscow and Beijing in accord of ground-based spectroscopic IAP RAS and IAP CAS observations. Autumn season (October-November of 1998-2014).

Background CO EC measured in Zvenigorod (Moscow province) decresed during this time-period; however in summer and autumn months of 2007-2015 CO TC trend over Zvenigorod changed it sign. In this seasons of 2007-2015 rate of CO TC increase was 0,2-0,4%/year depending on season. Spatial distribution of CO TC trends obtained for different seasons of 2007-2015 according to AIRSv6 data is in agreement with our ground-based data (significant decrease in South-East Asia and stabilization or slight increase over North of Europe and Asia in summer and autumn seasons), see please Fig.2.

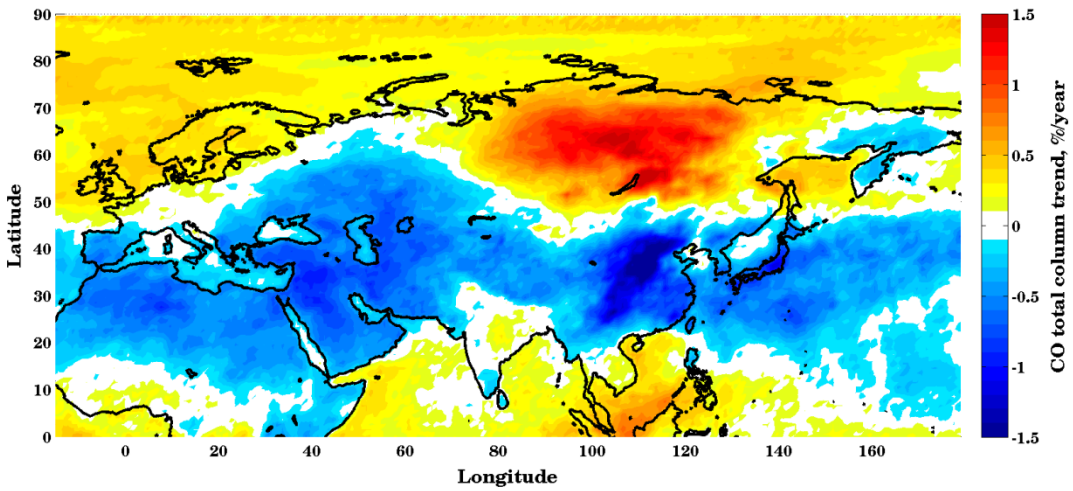

Figure 2. CO TC trends over Eurasia for summer (June-August) season of 2007-2015 years according AIRSv6 diurnal data. Strong increase over Siberia dui to emissions from forest fires in 2012-2015 years.

Also should be noted the positive trends (0,6%/year) in CO TC obtained in autumn season for Peterhof, 2007-2014 (data of Saint-Petersburg University, Makarova at al., 2011, P. Wang at al, 2016).
Rate of CH_4 TC increase in Moscow region is 0.5% per year for 1972-2015 (Fig.3).

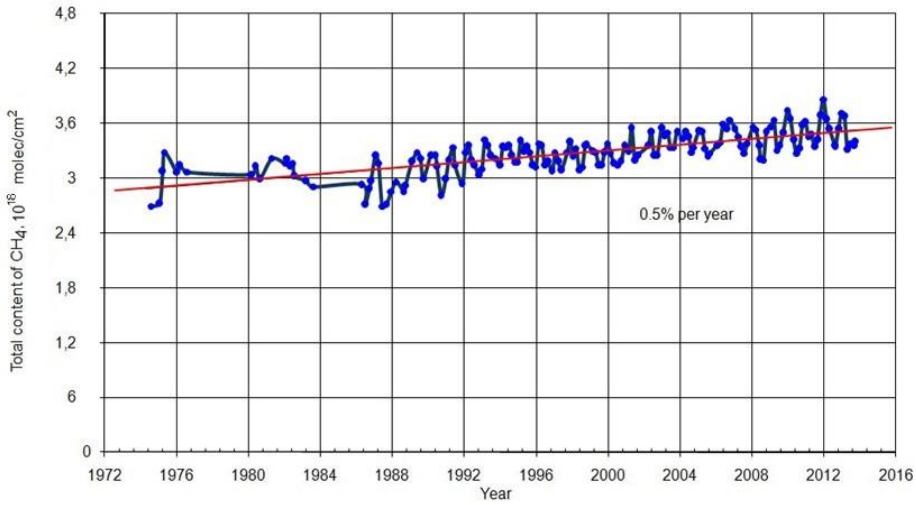

Figure 3. Two-monthly averaged CH_4 TC over Zvenigorod (Moscow province in 1972-2014 years.

After 2007 the means of CH_4 TC positive trend have increased over most of south-latitude and middle-latitude Eurasian regions, in accordance with AIRSv6 (Fig.4 a,b).

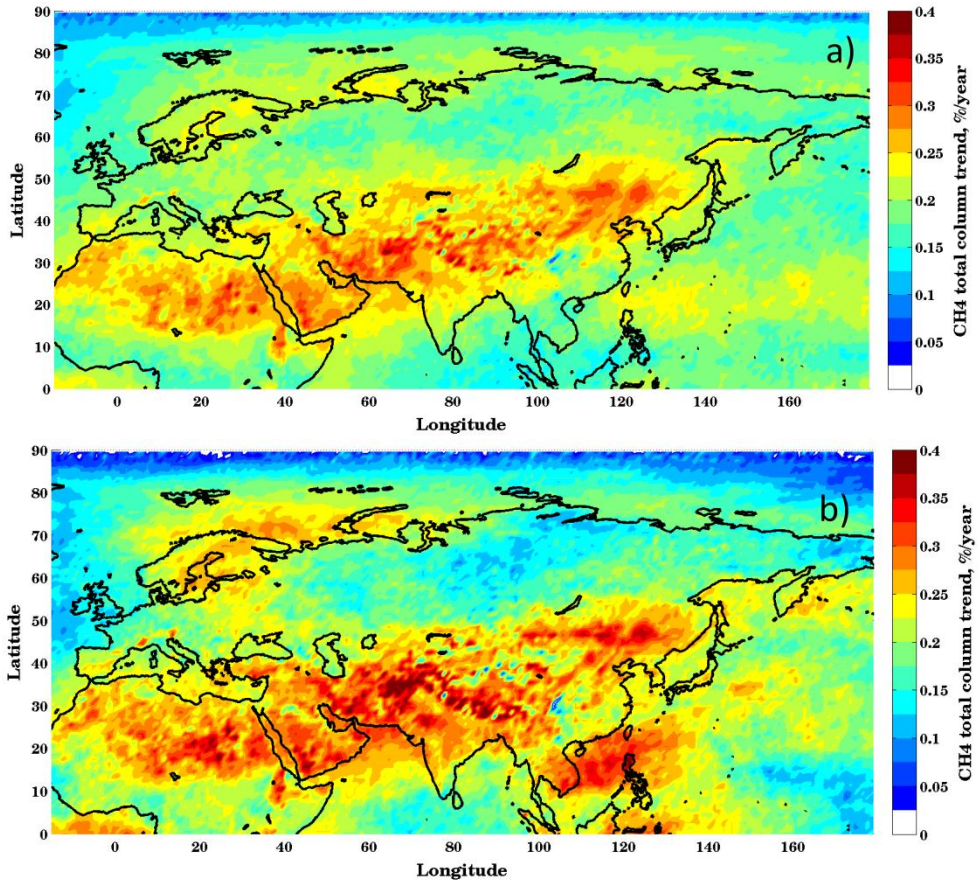

Figure 4. AIRSv6 CH_4 TC trends over Eurasia: a) – autumn (Sep-Nov) for 2003-2015 years; b) – the same for 2007-2015 years.

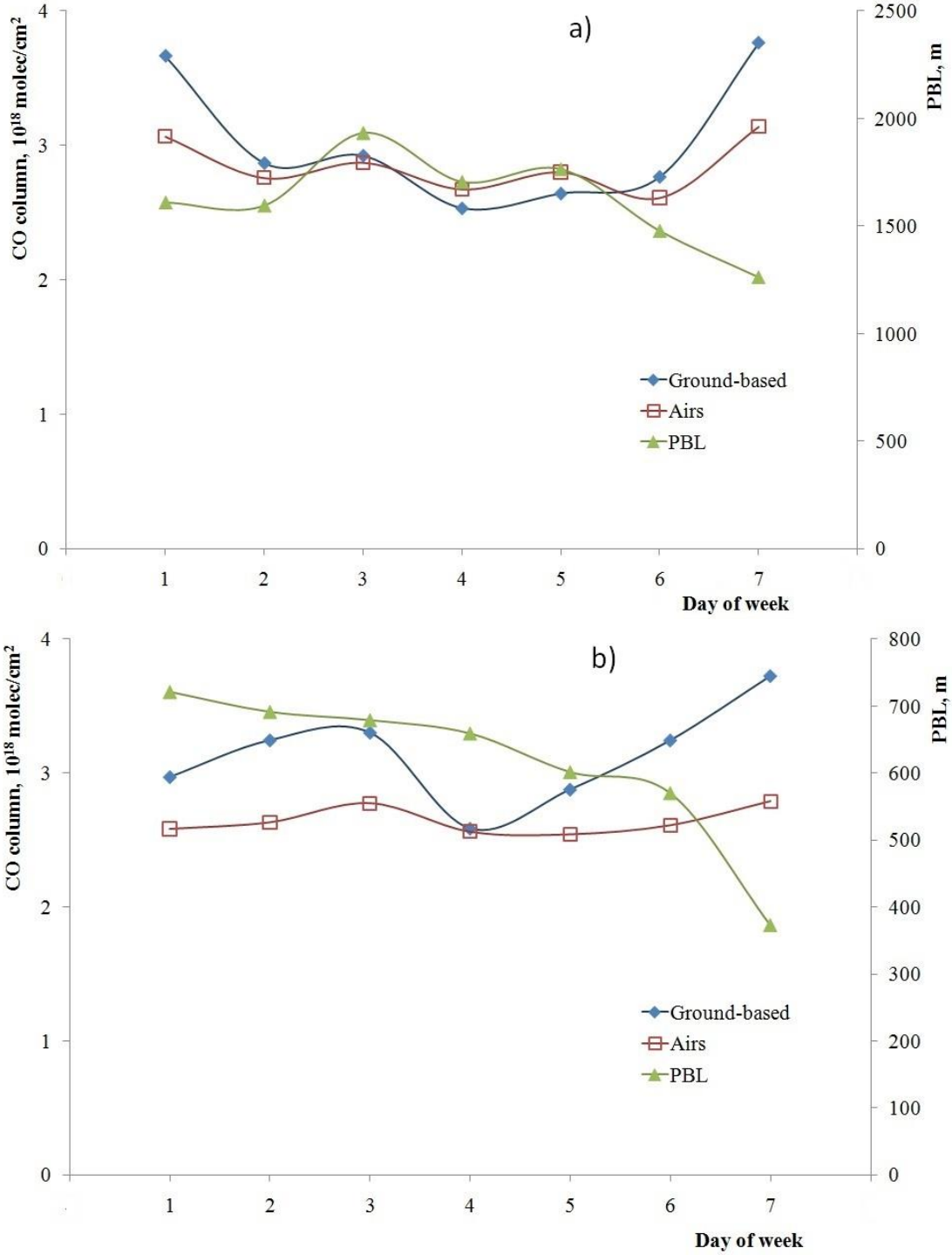

Figure 5. Weekly cycles of CO TC (ground-based and AIRSv6 measurements for 2010-2014) and height of PBL during measurements. All data are presented for sunny days, when ground-based CO TC observations have produced; time of observation and PBL-calculations is local 10:30-13:30: a) April-June; b) December-February

ACKNOWLEDGEMENTS

This work was supported by the Russian Scientific Foundation under grant №14-47-00049 and partially by the Russian Foundation for Basic Research (grant № 16-05-00287).

REFERENCES

Dianov-Klokov, V. I., Yurganov L. N., Grechko E. I. at al. Spectroscopic measurements of atmospheric carbon monoxide and methane. 1: Latitudinal distribution // J.Atmos.Chem., 1989. V8. №2. p. 139–151

Aumann, H. H., Chahine, M. T., Gautier, C., Goldberg, M., Kalnay, E., McMillin, L., Revercomb, H., Rosenkranz, P. W., Smith, W. L., Staelin, D., Strow, L., and Susskind, J.: AIRS/AMSU/HSB on the Aqua Mission: Design, Science Objectives, Data Products and Processing Systems // IEEE T. Geosci. Remote, 41, 253–264, 2003.

H. M. Worden, M. N. Deeter, C. Frankenberg at al. Decadal record of satellite carbon monoxide observations // Atmos. Chem. Phys., 13, 837–850, 2013 doi:10.5194/acp-13-837-2013

G.S. Golitsyn, E.I. Grechko, Genchi Wang, Wang Busan, A.V. Dzhola, A.S. Emilenko, V.M. Kopeikin,V.S. Rakitin, A.N. Safronov, E.V. Fokeeva Pollution research in Moscow and Beijing carbon monoxide and aerosol // Izvestiya , Atmospheric and Oceanic Physics, 2015, V.51 №1, P.1-12

M. V. Makarova, A. V. Poberovskii, S. I. Osipov. Time Variations of the Total CO Content in the Atmosphere near St. Petersburg // Izvestiya , Atmospheric and Oceanic Physics, 2011. Vol. 47, № 6. P. 739-746

Pucai Wang, N. F. Elansky, Yu. M. Timofeev, Gengchen Wang, G. S. Golitsyn, M. V. Makarova, V. S. Rakitin, Yu. Stabkin, A. I. Skorokhod, E. I. Grechko, E.V. Fokeeva, A. N. Safronov A study of the long-term trends of CO total column for urban and background regions using ground-based and satellite spectroscopic measurements // Advances in Atmospheric Science J., 2016, in print

INTERCOMPARISON OF SURFACE HEAT TRANSFER IN THE ARCTIC FOR MULTIPLE REANALYSES, SATELLITE DATA AND FIELD OBSERVATIONS

I.A. REPINA[1,2], M.I. VARENTSOV[1,3], A.A. ANIFEROV[1], A.Yu. ARTAMONOV[1], A.Yu. MAZILKINA[1]

[1]A.M. Obukhov Institute of Atmospheric Physics RAS, Moscow, Russia

[2]Space Research Institute RAS, Moscow, Russia

[3]Lomonosov Moscow State University, Department of Geography, Moscow, Russia

Keywords: HEAT FLUXES, ARCTIC OCEAN, REANALYSES, SATELLITE DATA.

INTRODUCTION

The Arctic climate has changed substantially over the recent decades, more than anywhere else on Earth (IPCC, 2014). Arctic warming has been more than twice as large as the global average (Serreze *et al*., 2009; Richter-Menge and Jeffries, 2011). The impacts are pan-Arctic and manifold, including changes in sea-ice thickness and extent, permafrost, vegetation and ecosystems. These changes, in turn, affect life and nature in both the Arctic and possibly at lower latitudes (e.g., Murray *et al*., 2010). Unfortunately, the processes responsible for this enhanced temperature increase, sometimes referred to as Arctic amplification, as well as associated feedback mechanisms and Arctic climate sensitivity are poorly understood (ACIA, 2005; Tjernström *et al*., 2012).

The decline in sea ice has enhanced the Arctic temperature amplification in reanalyses (Serreze *et al*. 2009; Screen and Simmonds 2010). Although limitations have been found in these data sources at high latitudes (Bromwich et al. 2007), the International Arctic Buoy Programme (IABP) has been providing reasonably good surface pressure data for the sea-ice-covered Arctic region since 1979, contributing to real-time operational forecasting. However, a decrease in the number of Arctic drifting buoys, associated with the recent abrupt decreases in sea ice, has affected the accuracy of the atmospheric reanalysis products (Inoue *et al.* 2009).

As the performance of the model used in the sea ice simulation in the Intergovernmental Panel on Climate Change (IPCC) for its Fourth Assessment Report (AR4) is an important factor for reproducing the surface air temperature over the Arctic Ocean (Liu *et al.* 2008), reanalyses data have similar problems, at least potentially. Because marginal ice zones are characterized by more complex air-ice-sea interactions, the treatment of the sea ice concentration is a potential source of uncertainty in reanalyses, particularly for surface heat budgets. Accurate turbulent air–sea fluxes (i.e. momentum, latent heat, and sensible heat) are of great interest in regard to a wide variety of air–sea interaction issues. The main sources of such fluxes over the global ocean are numerical weather prediction models, voluntary observing ships, and remotely sensed data. If the heat fluxes over the fractional ice-covered area are calculated implicitly using an ice-concentration cut-off threshold (e.g., 55%, Serreze *et al.* 2009), they are underestimated (overestimated) in a higher (lower) ice-covered area, resulting in misleading surface air temperatures. This study evaluated surface heat fluxes from reanalyses (ERAInterim, NCEP/NCAR, ASR) in the Arctic Ocean during summer and fall. Several types of surface conditions are compared: very new ice cover during a period of low temperature, ice-free conditions, ice with leads and melt ponds, pack ice and marginal ice zone. Meteorological and micrometeorological observations were used to validate the temperature profiles and surface heat fluxes in the major reanalyses.

METHODS

We use data from Nansen and Amundsen Basins Observation system (NABOS) project to evaluate the performance of reanalyses in the Arctic Ocean. The NABOS field experiment was carried out in the central part of the Arctic basin and in the eastern Arctic seas during summer and fall period of 2004-2009, 2013 and 2015. (Polyakov *et al.*, 2011)

Sonic anemometer data were synchronized with those of gas analyzer to compute eddy covariance fluxes of sensible and latent heat and momentum (Burba, 2012). When the ship was moving the turbulent equipment was installed on the bow using a 10 m mast (height of measurements was 15 m) to optimally reduce the dynamical and thermal ship body effects. Signals from turbulence sensors and motion sensors were sent to a PC based data acquisition system. The system samples all data at 10 Hz and after filtering out high frequency noises and low frequency trends, ship motion correction was applied to the wind velocity data. For the temperature signal, it is well calibrated and sound virtual temperature effects can be reduced later. Eddy covariance fluxes were obtained by involving spectral corrections (Moncrie *et al.*, 2004), compensation for density fluctuations (Webb *et al.*, 1980), sonic temperature correction for humidity (Van Dijk *et al*., 2004), time lag compensation, double rotation for tilt correction, block averaging, and statistical tests (Vickers and Mahrt, 1997). The running averaging interval was chosen equal to 20 min with 10-min time step.

We selected three atmospheric reanalysis datasets: the European Centre for Medium-Range Weather Forecasts (ECMWF) Interim reanalysis (ERA-Interim) (Simmons et al. 2007), the National Centers for Environmental Prediction - National Center for Atmospheric Research reanalysis data sets (NCEP/NCAR) (Kalnay et al. 1996) and the Arctic System Reanalysis (ASR): a regional reanalysis, forced by ERA-Interim at the lateral boundaries and incorporating model physics adapted to Arctic conditions, developed to serve as a state of-the-art, high-resolution synthesis tool for assessing Arctic climate variability and monitoring Arctic climate change (Bromwich *et al*., 2010).. The time resolution of these reanalyses is 6 hours. We also use satellite heat budget reanalyze the Objectively Analysed Air–Sea Fluxes (OAFLUX) (Yu, *et al*, 2004).

RESULTS

The onboard measurements of turbulent characteristics were carried out on all routes of the vessel. Based on these data the fluxes of sensible and latent heat, momentum and surface roughness parameter were calculated. Unstable and neutral stratifications were typically observed during the measurements. When the ship was moving through the ice, the air temperature was close to the ice surface temperature. If the ice cover was absent, exposing sea water, an intensive energy exchange was observed. The positive heat fluxes (from the ocean to the atmosphere) were observed above leads and small clearing zone, but neutral fluxes were measured above the perennial ice.

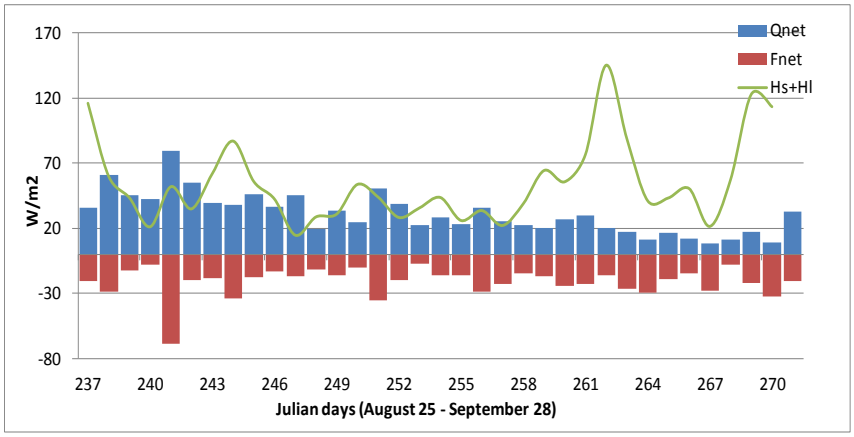

Figure 1. The average total heat balance of the period of observation. Lnet – longwave radiation balance; Qnet – shortwave radiation balance; H, HL – turbulence latent and sensible heat fluxes.

Figure 1 shows the total heat balance for the entire observation period in summer-fall period 2015. As it should be in the summer, the radiation balance is the main contributor to the common heat balance by incoming solar radiation. The exception is the marginal ice zones, leads and the transitional period between autumn and winter period, when incoming solar radiation is practically absent. In these cases, the turbulent balance is the main contributor to the total heat flux from the ocean to the atmosphere. Therefore, if there is open water and new ice in the fall-winter period, the turbulent energy exchange begins to play a key role in the total energy balance, while over fields of perennial and annual ice its value is negligible.

Figures 2, 3 show the intercomparison of different atmospheric and surface parameters with reanalisys data. The measurements were carried out in fall of 2008 and in summer of 2013. The ASR was changed to COSMO model calculation at 2013.

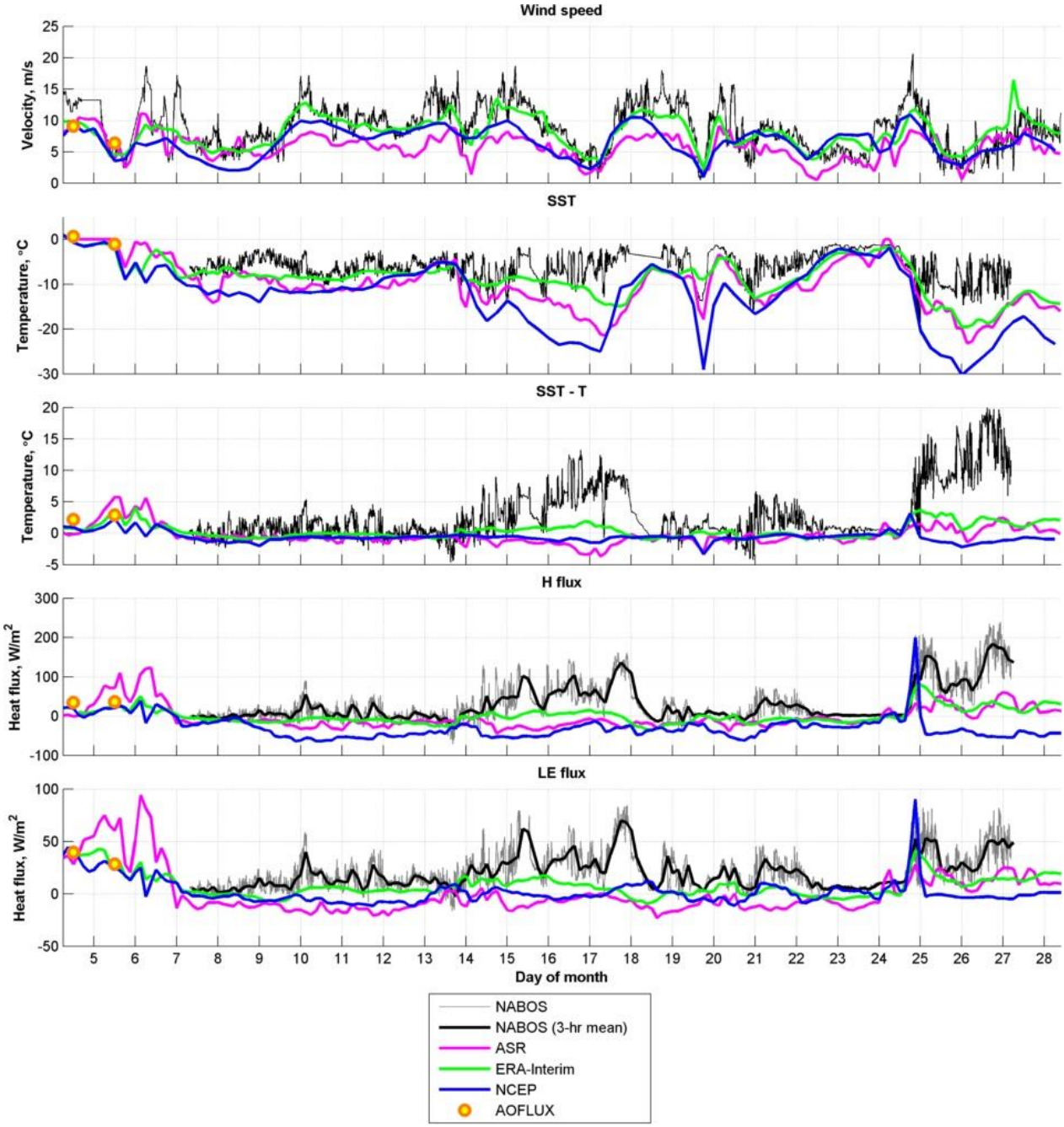

Figure 2. The intercomparison of measurement data and reanalysis in Arctic Ocean for October 2008.

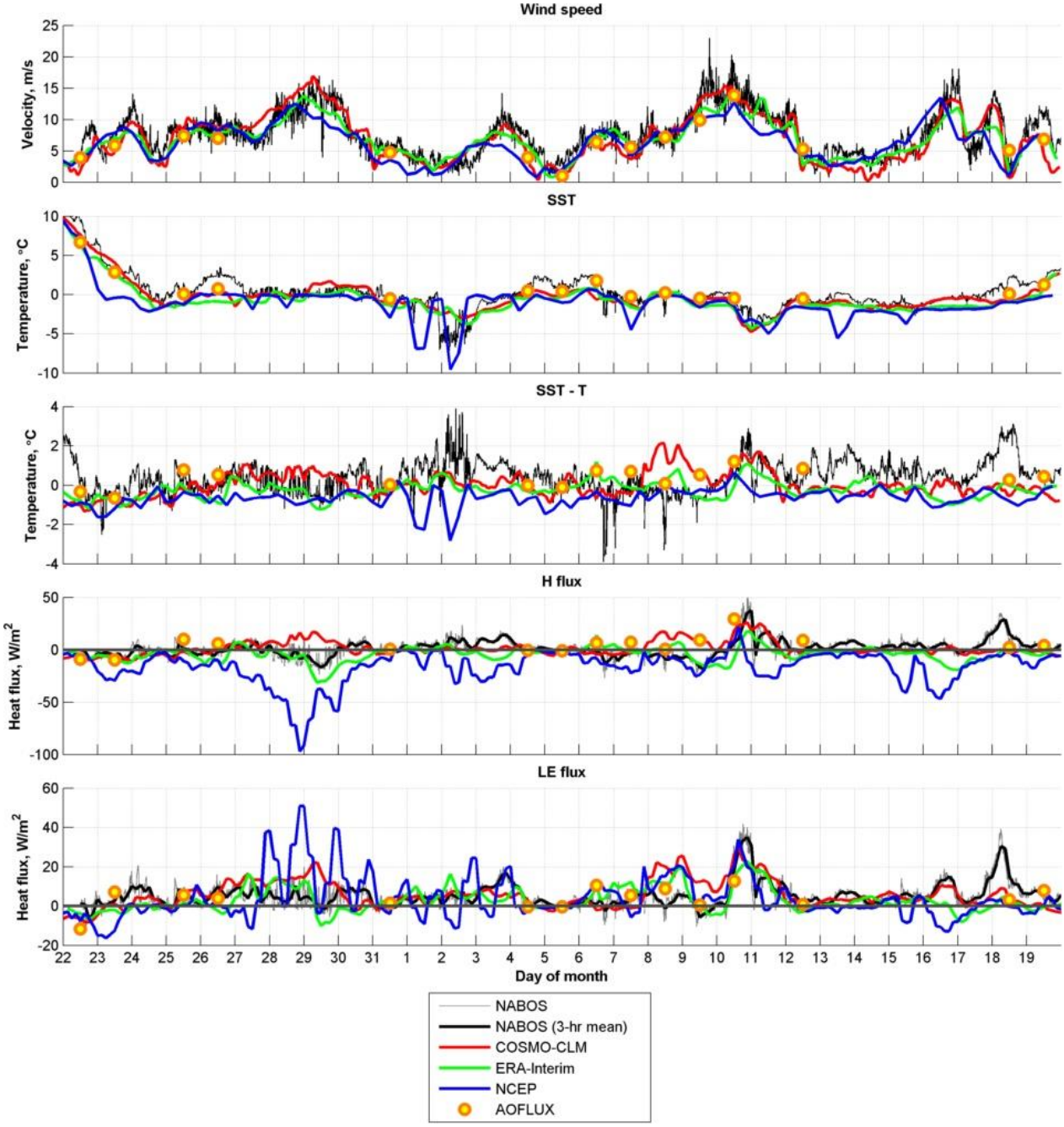

Figure 2. The intercomparison of measurement data and reanalysis in Arctic Ocean for August-September 2013.

Basic meteorological variables from all reanalyses – i.e., 2m temperature (T_2m), and scalar wind speed (Us) – show reasonable agreement with observations. This means that they generally follow the observed temporal variability. The main contribution to the difference between the data and the reanalysis makes the surface temperature. The largest differences are observed in fall time. At that time, measurements were carried out in the area of consolidated ice cover. The vessel normally takes the route with light ice conditions. Therefore, contribution of turbulence fluxes is substantial. In all compared cases the difference between calculated and measured heat fluxes are large enough, especially in the areas of leads and in the marginal ice zones.

For open water validation of the satellite data is performed through a comprehensive comparison with daily, *in situ* values of LHF and SHF. The satellite-derived daily LHF has bias, RMS, and correlation of 5

W m^{-2}, 27 W m^{-2}, and 0.89, respectively. For SHF, the statistical parameters are –2 W m^{-2}, 10 W m^{-2}, and 0.94, respectively. The main departures are found at marginal ice zone, where satellite latent and sensible heat fluxes are generally larger.

CONCLUSION

The results from in situ observations indicate that leads, polynyas, and puddled surfaces can play a significant role in the balance of the Arctic energy budget and climate change, through the turbulent fluxes from the ice free area plus ice mixed regions of the Arctic Ocean.
A computation of sensible heat flux at the surface is formulated on the basis of spatial variations of the surface temperature estimated from satellite data. Based on the comparison of field experiments data, satellite-derived data and reanalysis the causes of underestimation of the values of turbulent heat fluxes in the Arctic modern reanalysis are investigated. Obtained differences are related to the temperature and structural inhomogeneity of the surface and the development of space-organized convection fields. Reanalyses data are sometimes used to calculate the surface heat budgets over polynyas and to estimate ice production in polar/sub-polar oceans. In particular, the near-surface air temperature and wind fields, which are difficult to observe using satellites or with in-situ measurements are key parameters for estimating turbulent heat fluxes. If the sea-ice concentration and SST in reanalyses are not treated appropriately, careful attention is needed when using the resultant air temperature for such calculations.

ACKNOWLEDGEMENTS

This work was supported by the Russian Scientific Foundation under grant 14-37-00053.

REFERENCES

ACIA (2005): *Impact of a warming Arctic: Arctic Climate Impact Assessment*, Cambridge University Press, 989–1020, 2005.

Bromwich, D.H., R.L. Fogt, K.I. Hodges, and J.E. Walsh (2007). A tropospheric assessment of the ERA-40, NCEP, and JRA-25 global reanalyses in the polar regions, *J. Geophys. Res.* **112**, D10111, doi:10.1029/2006JD007859.

Bromwich D.H., Y.-H. Kuo, M.C. Serreze, J.E .Walsh, L.-S. Bai, M. Barlage, K.M. Hines, and A. Slater (2010). Arctic System Reanalysis: Call for Community Involvement, *EOS* **91**, 13–20.

Burba, G. (2013). Eddy Covariance Method for Scientific, Industrial, Agricultural and Regulatory Applications: a Field Book on Measuring Ecosystem Gas Exchange and Areal Emission Rates. LI-COR Biosciences, Lincoln, USA, 331 pp.

Inoue, J., T. Enomoto, T. Miyoshi, and S. Yamane (2009). Impact of observations from Arctic drifting buoys on the reanalysis of surface felds, *Geophys. Res. Lett.* **36,** L08501, doi:10.1029/2009GL037380.

IPCC (2014). Climate Change 2014: Synthesis Report. Contribution of Working Groups I, II and III to the Fifth Assessment Report of the Intergovernmental Panel on Climate Change [Core Writing Team, R.K. Pachauri and L.A. Meyer (eds.)]. IPCC, Geneva, Switzerland, 151 pp.

Kalnay, E., and co-authors (1996). The NCEP/NCAR 40-year reanalysis project, *Bull. Amer. Meteor. Soc*. **77**, 437−471.

Liu, J., Z. Zhang, Y. Hu, L. Chen, Y. Dai, and X. Ren (2008). Assessment of surface air temperature over the Arctic Ocean in reanalysis and IPCC AR4 model simulations with IABP/POLES observations. J. Geophys. Res., 113, D10105, doi: 10.1029/2007JD009380.

Moncrieff J.B., R. Clement, J. Finnigan, and T. Meyers (2004) Averaging detrending and filtering of eddy covariance time series, X. Lee, W.J. Massman, B.E. Law (Eds.), Handbook of Micrometeorology: A Guide for Surface Flux Measurements, Kluwer Academic, Dordrecht , pp. 7–31.

Murray, M. S., Anderson, L., Cherkashov, G., Cuyler, C., Forbes, B., Gascard, J. C., Haas, C., Schlosser, P., Shaver, G., Shimada, K., Tjernstrцm, M., Walsh, J., Wandell, J., and Zhao, Z. (2010).

International Study of Arctic Change: Science Plan, (ISAC International Program Office, Stockholm).

Polyakov, I.V., V.A. Alexeev, I.M. Ashik, S. Bacon, A. Beszczynska-Möller, E.C. Carmack, Dmitrenko I.A., Fortier L., Gascard J.-C., Hansen E., Hölemann J., Ivanov V.V., Kikuchi T., Kirillov S., Lenn Y.-D., McLaughlin F.A., Piechura J., Repina I., Timokhov L.A., Walczowski W. and R. Woodgate (2011). Fate of early 2000s arctic warm water pulse, *Bulletin of the American Meteorological Society*. **92,** 5, 561-566, doi: 10.1175/2010BAMS2921.1.

Richter-Menge, J. and M. Jeffries (2011) The Arctic, in: State of the Climate 2010, *B. Am. Meteorol. Soc*. **92**, S143–S160.

Screen, J.A., and I. Simmonds (2010). The central role of diminishing sea ice in recent Arctic temperature amplification, *Nature* **464,** 7293, 1334-1337.

Serreze, M.C., A.P. Barrett, J.C. Stroeve, D.N. Kindig, and M.M. Holand (2009). The emergence of surface-based Arctic amplification, *The Cryosphere* **3**, 11–19, doi:10.5194/tc-3-11-2009.

Simmons, A., C. Uppala, D. Dee, and S. Kobayashi (2007). ERA-Interim: New ECMWF reanalysis products from 1989 onwards, *ECMWF Newsletter* **110**, 25−35.

Tjernstrom, M., C.E. Birch, I.M. Brooks, M.D. Shupe, Persson, P. O. G., Sedlar, J., Mauritsen, T., Leck, C., Paatero, J., Szczodrak, M., and C.R. Wheeler (2012). Meteorological conditions in the central Arctic summer during the Arctic Summer Cloud Ocean Study (ASCOS), *Atmos. Chem. Phys*. **12**, 6863–6889, doi:10.5194/acp-12-6863-2012.

Van Dijk, A., A.F. Moene, and H.A.R. de Bruin (2004). The Principles of Surface Flux Physics: Theory, Practice and Description of the ECPack Library. Meteorology and Air Quality Group, Wageningen University, Wageningen, The Netherlands, p. 99.

Vickers, D., and L. Mahrt (1997). Quality control and flux sampling problems for tower and aircraft data, *J. Atmos. Ocean. Technol.* **14** , 512–526.

Webb, E.K., G.I., Pearman, and R. Leuning (1980). Correction of flux measurements for density effects due to heat and water vapour transfer, *Q. J. R. Met. Soc.* **106**, 85–100.

Yu, L., R.A. Weller, and B. Sun. (2004). Improving Latent and Sensible Heat Flux Estimates for the Atlantic Ocean (1988–1999) by a Synthesis Approach, *Journal of Climate* **17**: 373–393.

PASSIVE MICROWAVE REMOTE SENSING OF LAKE FREEZE-THAW OVER EURASIA

RUAN YONGJIAN[12], QIU YUBAO[1], YU XIAOQI[1]

[1] Laboratory of Digital Earth Science, Institute of remote sensing and digital earth, Chinese Academy of Sciences, Beijing 100094, China.

[2] School of architectural and surveying and mapping engineering, Jiangxi University of Science and Technology, Jiangxi, Ganzhou, 341000, China.

Keywords: EURASIA, LAKE ICE, FREEZING AND THAWING MONITORING, MICROWAVE REMOTE SENSING, CLIMATE CHANGE

INTRODUCTION

Abstract: Lake ice is an important component of the hydrosphere and cryosphere, especially over high-latitudes regions of Eurasia, the long-term changes of freezing and thawing time can directly reflect the changes of climate and lake itself. Using long time series of passive microwave Brightness Temperature data from AMSR-E(Advanced Microwave Scanning Radiometer for EOS) and FY3 MWRI(FengYun-3B/ Microwave Radiation Imagery), the freezing and thawing parameters of the lakes from 2002 to 2015 were estimated employing the denoising low-pass method Savitzky-Golay filter, embed in the TIMESAT. The method was validated with the MODIS (Moderate Resolution Imaging Spectroradiometer) data which it shows that the accuracy is within 2 days. The ice duration shows that the four test lakes are mostly in a shrinking trend about 4-10 days for the last 14 years, while the SillingCo has an explicit increasing on the freezing ice duration.

Lake ice is an important component of hydrosphere and cryosphere, and it is a good insulator reflecting the vast majority of solar irradiated on the lake surface, avoid the lakes warning up too quickly, thereby inhibiting algae bloom and the release of Lake carbon dioxide and methane(Duguay, 2003; Dunham, 2012).

There are large number distribution of lakes in high latitude and high altitude area of the Eurasian, and only for Qinghai Tibet Plateau, there are thousands of lakes distribution (Yao, 2015), because the lake is a heat source, its lake ice phenology is directly related to the heat absorption and radiation of lakes, therefore, lake ice plays an important role in the climate change of the surrounding area. At present, the lake freeze-thaw studies in boreal lakes of Eurasia mainly focus on the individual lakes using the in-situ measurement (e.g the Plateau only Qinghai Lake is monitored onsite), while few research focus on the remote sensing of thaw and freezing like Qinghai Lake, NamCo Lake with the help of passive microwave remote sensing (Che, 2009;Ke, 2013) . There is a need to understand the whole scenery of lake ice phenology over Eurasia. In this paper, we using the microwave radiometer measurement from onboard AMSR-E and FY3-MWRI sensor to extract the freeze-thaw parameters of different lakes across the Eurasia of Northern region, whose radius are larger than 0.25km. The aim is to study the whole lake physical changes, and provide basic data for large scale lake ice model.

METHODS

2.1 Passive microwave data

The AMSR-(2002 to 2011)E and MWRI(2010 to now) microwave radiometer can provide the high quality of longtime series and high time resolution of earth observation data, which make it possible for long time series remote sensing monitoring the freeze-thaw of lakes. The data used in this paper is AMSR-E (multi frequency, dual polarization) L2A data and FY3B MWRI Level 2 data.

2.2 One-dimensional signal freeze-thaw point extraction

The Brightness Temperature noises make it difficult to confirm the lake freeze-thaw accurate date, while the Savitzky-Golay filter is a special kind of low-pass filter in Software TIMESAT algorithm to remove the noise. If in a time series data of arrays (ti, yi), i=1, 2...according to f(t) to fit the model function(Jönsson, 2004), the equation can be expressed as follows (1):

$$f(t) = c_1\varphi_1(t) + c_2\varphi_2(t) + \ldots + c_M\varphi_M(t) \qquad (1)$$

When the 6π/N. The first basis function determines the base level whereas the pairs of sine and cosine functions correspond to, respectively, one and two annual lake ice change.

The biggest feature of adaptive Savitzky- Golay filter is when filtering noise, can ensure the signal shape at the same time, and constant width traversing searching through after removing the outliers and and replace each data value y_i, i = 1...N by a linear combination of nearby values in a window, as follows (2):

$$\sum_{i=-n}^{n} c_j y_i + j \qquad (2)$$

A large number of experiments found that when a cycle of freezing time amplitude threshold is generally 0.4 ~ 0.6 and ablation for 0.9~1.

RESULT AND ANALYSIS

The previous research experience and studies show that, the temperature of transition season relationship between the freezing and thawing period of lake can be predicted. The freezing and thawing days will change about 4~7day with 1°C change (Palecki, 1986). In this paper, using the above method to denoise and extracting the freezing and thawing extreme point of lake.

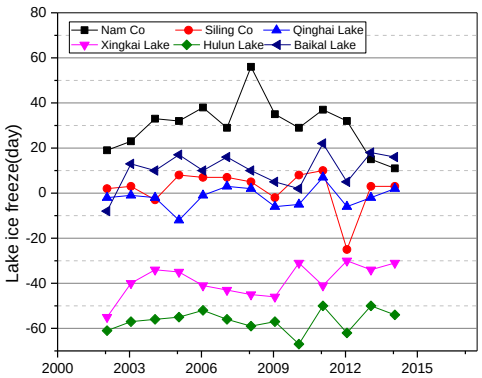

Fig.1 the onset time series of lake ice over Eurasia

Regarding the onset of lake ice, Fig 1 shows that the SilingCo Lake, Xingkai Lake and Hulun Lake experienced a trend of earlier freezing date in near 14 years (Fig. 1), while the NamCo has a delay before 2008, but after that time, it experienced a sharp advance in the ice onset. The Qinghai Lake and Baikal Lake has a stable ice onset date. A clear break up were observed over the test lakes (4 lakes at this time) except the SilingCo Lake, which has an obvious delay from 2002 to 2015 (see Fig 2).

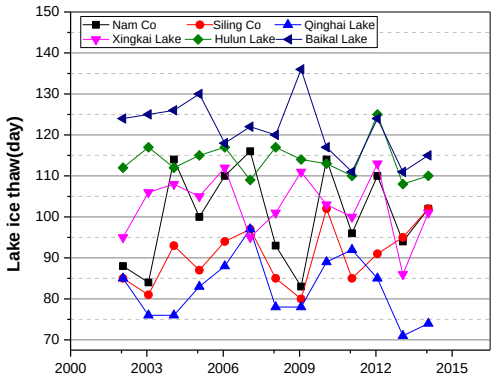

Fig. 2 the break-up time series of lake ice over Eurasia

These induced that the ice duration of the four test lakes are mostly in a shrinking trend about 4-10 days for the last 14 years, while the SillingCo has an explicit increasing on the freezing ice duration.

The lake ice duration of Baikal Lake, Qinghai Lake, Xingkai Lake and Hulun Lake indicate their decreasing trend, while the SillingCo and NamCo (side by side) have the same overall trend, but the NamCo explore a unstable status.

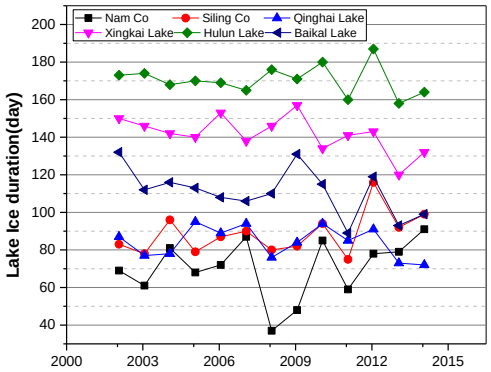

Fig.3 the ice duration of lakes over Eurasia

More analysis of the variation of the small and medium-sized lakes in the Eurasia continent is in further progress.

ACKNOWLEDGEMENTS

This work is supported in part by National Natural Science Foundation of China (Grant No. 41371351 and 41120114001) and Chinese Special Fund for Meteorology-Scientific Research in the Public (GYHY201206040).

REFERENCES

Benson B J, Magnuson J J, Jensen O P, et al. Extreme events, trends, and variability in Northern Hemisphere lake-ice phenology(1855-2005).Climatic Change, 2012, 112:299-323.

Che Tao, Li Xin, Jin Rui.Monitoring the frozen duration of Qinghai Lake using satellite passive microwave remote sensing low frequency data. Chinese Science Bulletin, 2009, 54: 2294-2299.

Duguay, C. R., Flato, G. M., Jeffries, M. O., Menard, P.,Morris, K., and Rouse, W. R.: Ice-cover variability on shallow lakes at high latitudes: model simulations and observations, Hydrol. Process.,17, 3465–3483, 2003.

Jönsson, P. and Eklundh, L. TIMESAT - a program for analysing time-series of satellite sensor data. Computers and Geosciences, , 2004,30, 833-845.

Jönsson, A.M., Eklundh, L., Hellström, M., Bärring, L. and Jönsson, P. Annual changesin MODIS vegetation indices of Swedish coniferous forests in relation to snow dynamics and tree phenology, Remote Sensing of Environment, , 2010,114, 2719-2730

Ke Chang-Qing, Tao Anqi, Jin Xin. Variability in the ice phenology of Nam Co Lake in central Tibet from scanning multichannel microwave radiometer and special sensor microwave/imager: 1978-2013. Journal of Applied Remote Sensing, 2013, 7 (1), 073477, doi: 10.1117/1.JRS.7.073477

Palecki M A, Barry R G. Freeze-up and break-up of lakes as an index of temperature changes during the transition seasons: A case study for Finland. Journal of Applied Meteorology and Climatology, 1986, 25: 893-902.

YAO Xiaojun, LI Long, ZHAO Jun, et al. Spatial-temporal variations of lake ice in the Hoh Xil region from 2000 to 2011.Acta Geographica Sinica,2015,70(7):1114-1124.DOI:10.11821/dlxb201507008

MULTIDISCLIPINARY AIR QUALITY CAPACITY BUILDING

T.M. RUUSKANEN[1,2], P. SIHVONEN[1,3], L. RIUTTANEN[1], A. LAURI[1] and M. KULMALA[1]

[1]Division of Atmospheric Sciences, Department of Physics, University of Helsinki, PL64, Finland.

[2]Nature and Environment group, Palmenia Centre for Continuing Education, University of Helsinki, PL53, Finland.

[3]Heinola upper secondary school, Rajakatu 29, 18100 Heinola, Finland.

Keywords: TRAINING, MULTI-DISCIPLINARY, PEDAGOGY, ATMOSPHERE.

GRAND CHALLENGES

The world is constantly changing and we are facing big challenges. Air quality is one of the Grand Challenges that EU and other authorities have listed. WHOs (2014) current estimate is that outdoor air pollution causes 3.7 million premature deaths in the world, more than a quarter of them in China.

CAPACITY BUILDING

Effective solutions rise from comprehensive understanding. The academic experts need to keep their knowledge and skills up to date and to widen their knowledge with horizontal learning of the adjunct fields of science related. Successful operation of a SMEAR type measurement station requires continuous updating of knowledge and skills and consistent planned capacity building. Atmospheric research involves several fields of science such as chemistry, physics, meteorology and earth system sciences, deepening and widening expertise is required. Horizontal learning principle has been shown to be a good example of collaborative problem solving and participatory action research (Hennessy and Murphy, 1999). The shift from discipline-tied fundamental education towards multidisciplinarity is imperative for a successful career in climate and global change science (Nordic Climate Change Research, 2009).

The first Air Quality Education in a Changing World workshop focused on invited participants were invited to discuss the status of academic atmospheric science education and share their views on the societies needs on air quality knowledge transfer using from the academia to public and private sector. Hosted by Nanjing University and jointly arranged with the University of Helsinki in April, 2015. Keynote presentations from Tsinghua, Peking, Fudan and Sun Yat-Sen University, Chinese Research Academy of Environment Sciences, Institute of Remote Sensing and Digital Earth (RADI) CAS, Shanghai Environmental Monitoring Center discussed: What knowledge needs to be transferred and what are the skills that each target group needs? The comprehensive atmosphere earth system measurements: What kind of observation infrastructures best improve the air quality in China? Effective knowledge transfer and innovative thinking methods: What kind of knowledge transfer is needed for sustainable air quality solutions?

Table 1. Key contents of air quality education for primary target groups.

To whom?	**What?**
Policy makers	Air quality policy making, air quality effects on economy, green GDP
Future policy makers	Math, physics, chemistry in an interdisciplinary view
Industry: engineers, plant managers	Green technology
General public	Health, Exposure, Effects of government policies
University students	Research oriented education
People working with AQ related issues: forecasters, health professionals	Updating knowledge, methods and skills, Holistic big picture, Sharing existing expertise
Media	Air quality and health issues, social and economy impacts of air quality
Environmental protection bureau	Data processing and analysis, Operational modelling, regional modelling

DESIGN RESEARCH

The air quality capacity building frameworks built around learners and specialists of atmospheric science as well as education and their interaction can be supported by design research (Edelson, 2002). The design research focuses not only on study of the students and their learning, but also the process of designing and making new education material as well as on the suitability of different education methods.

Solution oriented thinking, need for updating skills as well as knowledge of rapidly changing air quality situation were on the top list of the capacity building list of the first Air Quality Education in a Changing World workshop participants. Reliable, research based education that has a holistic view on the whole big picture of causes and effects of processed affecting air quality would support making of long lasting solutions. Also basic understanding of the processes behind atmospheric processes is needed for building a foundation for evaluating new information. Learning lasts a lifetime, the university professors pointed out that even deepen their knowledge and widen their skills along their career and even when they give a course to the students. Learning of skills, such as maintenance of monitoring system, operation of emission models or effective data-analysis, can be supported by use of the tools and methods in training and enhance the transfer use of them to the daily work.

ACKNOWLEDGEMENTS

This work was supported by the University of Helsinki, Rectors strategic funding and the Finnish Centre of Excellence, Academy of Finland grant no. 272041. The Atmospheric education research team wishes to thank Dr. Kirsi Kettula, prof. Jari Lavonen and researchers contributing to education material development for constructive discussion and feedback.

REFERENCES

Edelson, D. C. (2002). Design research: What we learn when we engage in design. Journal of the Learning Sciences, 11(1), 105-121

Hennessy, S. and Murphy, P. (1999). The Potential for Collaborative Problem Solving in Design and Technology, International Journal of Technology and Design Education 9(1), 1–36.

Nordic Climate Change Research, 2009: NordForsk Policy Briefs 2009-8. Mandag Morgen, 2009

World Health Organization WHO. (2014). Burden of disease from Ambient Air Pollution for 2012, Summary of results. [Ref. 23.5.2014]. www.who.int/phe/health_topics/outdoorair/databases/AAP_BoD_results_March2014.pdf?ua=1

ARCTIC AEROSOLS AND PARTICLE FORMATION IN NORTHERN GREENLAND

N. SARNELA[1], H. JUNNINEN[1], L. AHONEN[1], T. JOKINEN[1], J. MIKKILÄ[1], O. PERÄKYLÄ[1], D. WIMMER[1], T. PETÄJÄ[1], H. SKOV[2,3], M. KULMALA[1] AND M. SIPILÄ[1]

[1] University of Helsinki, Department of Physics, P.O. Box 64, 00014 University of Helsinki, Finland.

[2] Department of Environmental Science, Aarhus University, Roskilde, Denmark.

[3]University of Southern Denmark, Institute of Chemical Engineering and Biotechnology and Environmental Technology, Odense, Denmark.

Keywords: ATMOSPHERIC AEROSOLS, ARCTIC RESEARCH, MASS SPECTROMETRY.

INTRODUCTION

The Arctic environment is known to be especially sensitive to global warming and clouds are in the key role of radiative balance of the Arctic environment. Globally, the net radiative effect of clouds is cooling due to their ability to reflect solar radiation back to space. As a contrary of other parts of the world, in the Arctic environment, clouds often have warming effect because the longwave radiation gets caught in between the bright ice or snow-covered surfaces and the clouds (Garret *et al.,* 2002) and the solar radiation is scarce during the most of the year. Cloud properties and their formation is connected to the aerosol population and their ability to act as cloud condensation nuclei.

New particle formation is a process where molecular clusters form from atmospheric vapours by condensation and/or chemical reactions. Later the clusters can grow into larger particle sizes and act as cloud condensation nuclei. New measurement techniques have enabled studying even the first steps of new particle formation. In previous studies sulphuric acid (Sipilä *et al.,* 2010) and oxidized organic compounds (Ehn *et al.,* 2014) have been seen to be responsible of new particle formation. Until recent years the composition of newly formed particles has not been studied in the Arctic. Since there is little if any vegetation in the Polar Regions the organics are not likely to play a significant role in particle formation. Instead there has been observed iodine during new particle formation events (Allan *et al.,* 2015).

The spring time in the Arctic has several interesting features. During the spring, the solar radiation increases fast, in less than two months from total darkness into midnight sun, enabling several air chemistry processes to start. One of these processes is ozone depletion event which has been detected in the Arctic atmosphere after the sun rise (Barrie *et al.,* 1988; Simpson *et al.,* 2007). During these events the ozone concentration decreases from ~40 ppbv almost to 0 ppbv due to photochemical degradation. These events have been connected mainly to bromine oxides but also to other halogen oxides (Barrie *et al.,* 1988; Simpson *et al.,* 2007). Another characteristic phenomenon during the Arctic spring is so called Arctic haze, which means increased particle concentration in the troposphere due to pollution transportation into the Polar Regions (Quinn *et al.,* 2007). The otherwise pristine Arctic atmosphere is strongly influenced by anthropogenic emissions and seasonal atmospheric transport and it has clearly higher concentrations of atmospheric aerosols during spring time. In the cold Arctic winter the stratification of the atmospheric surface boundary layer is stable, and the precipitation is low. Due to those reasons the lifetime of aerosols is significantly longer (from 3 to 7 weeks) during the cold time of the year, compared to summer when the lifetime is from 3 to 7 days (Sirois and Barrie, 1999).

We conducted a measurement campaign in the Arctic having three major objectives: 1) getting more insight into new particle formation and nucleation processes in the Arctic, 2) trying to characterize Arctic

haze and 3) indentificating and characterizing the changes in atmospheric chemistry from dark to sunlight period.

MEASUREMENT CAMPAIGN AND INSTRUMENTATION

We conducted an intensive measurement campaign called Nordic Center of Excellence "Cryosphere atmospheric Interaction in a Changing Climate (CRAICC)" in Villum research station in Northern Greenland (81º 36'N 16º39'W, Fig. 1). The Villum research station is on the small peninsula Prinsesse Ingeborg Halvø in the vicinity of Station Nord military camp and a new, in 2015 deployed, Atmospheric Observatory is located about 2 km from the Station Nord. The campaign started in mid-February 2015 and was going on until the end of August 2015.

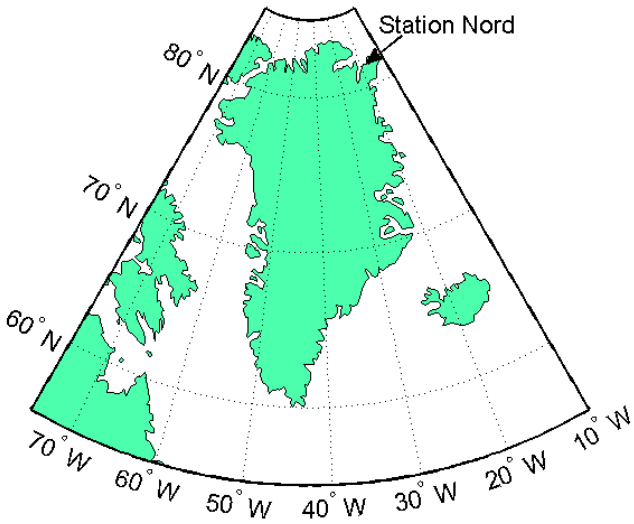

Figure 1. The location of Station Nord where also Villum research station is situated

The Villum research station has continuous measurements of meteorological parameters and ozone concentration. Also gaseous elemental mercury, black carbon and filter pack measurements have been conducted there during the last ten years. Particle size distribution of 10 – 900 nm has been measured with Scanning Mobility Particle Sizer (SMPS, Wang and Flagan, 1990) since 2010. During the CRAICC measurement campaign we used several mass spectrometers, particle spectrometers and particle counters in addition of the continuous measurements to study vapour and particle concentrations and the new particle formation on the site.

We had nitrate-CI-APi-TOF (Chemical Ionization Atmospheric Pressure interface Time-Of-Flight mass spectrometer, Jokinen *et al.*, 2012) to measure extremely low volatility vapours such as sulphuric acid and molecular clusters. We used acetate-CI-APi-TOF (Bertram *et al.*, 2011) to measure low volatility vapours such as formic acid. Ambient ions were measured with APi-TOF (Junninen *et al*., 2010). Particle concentrations of 0.8 – 40 nm particles were measured with Air Ion Spectrometer (AIS, Mirme and Mirme, 2013), sub-3 nm particles were measured with Particle Size Magnifier (PSM, Vanhanen *et al.*, 2010) and the particle composition was measured with an Aerosol Mass Spectrometer (Canagaratna *et al.*, 2007).

PRELIMINARY RESULTS

The measurement campaign was successful and we got data from the whole over six month period. We observed several ozone depletion events between March and May. During ozone depletion events we also observed increased concentrations of chlorine oxides. Generally the aerosol particle concentrations were

low during the measurement campaign, but occasionally we observed elevated particle concentrations and some particle growth events. Also sub-3 nm particle concentrations were observed during these events. The measured vapour concentrations varied between spring and summer time. We detected high concentrations of iodic acid in late spring (April – May) when the solar radiation was more intense. During the summer time the snow started to melt and the iodic acid concentrations decreased. According to the preliminary analysis, it seems that the composition of particles was different during the spring and summer time. It appears that iodine oxides are important in the spring time particle formation. We observed iodine oxide clusters that are similar that have been seen during particle events in coastal site in Ireland (Sipilä *et al.*, 2016, *under review*). These results support the results of Allan et al. who detected iodine in Arctic aerosols larger than 30 nm but this is the first time that iodine oxide has been seen in molecular clusters in the Arctic. When the snow started to melt the role of iodine oxides in the particle formation seemed to decrease and the role of sulphuric acid increased. The data analysis is still in progress and we are going to further examine these results.

ACKNOWLEDGEMENTS

We want to thank personnel in the Villum research station and Station Nord for their invaluable help during the measurement campaign. We thank the tofTools team for providing tools for mass spectrometry data analysis. The Nordic Center of Excellence "Cryosphere atmospheric Interaction in a Changing Climate (CRAICC)" and Academy of Finland Center of Excellence (272041) are acknowledged for funding the research.

REFERENCES

Allan, J. D., Williams, P. I., Najera, J., Whitehead, J. D., Flynn, M. J., Taylor, J. W., Liu, D., Darbyshire, E., Carpenter, L. J., Chance, R., Andrews, S. J., Hackenberg, S. C., and McFiggans, G. (2015) Iodine observed in new particle formation events in the Arctic atmosphere during ACCACIA, *Atmos. Chem. Phys.*, **15**, 5599.

Barrie, L.A., Bottenheim, J. W., Schnell, R. C., Crutzen, P. J. and Rasmussen R. A. (1988) An Ozone destruction and photochemical reactions at polar sunrise in the lower Arctic atmosphere, *Nature*, **334**, 138.

Bertram, T. H., Kimmel, J. R., Crisp, T. A., Ryder, O. S., Yatavelli, R. L. N., Thornton, J. A., Cubison, M. J., Gonin, M., and Worsnop, D. R. (2011) A field-deployable, chemical ionization time-of-flight mass spectrometer, *Atmos. Meas. Tech.*, **4**, 1471.

Canagaratna, M. R., Jayne, J. T., Jimenez, J. L., Allan, J. D., Alfarra, M. R., Zhang, Q., Onasch, T. B., Drewnick, F., Coe, H., Middlebrook, A., Delia, A., Williams, L. R., Trimborn, A. M., Northway, M. J., DeCarlo, P. F., Kolb, C. E., Davidovits, P., and Worsnop, D. R. (2007) Chemical and microphysical characterization of ambient aerosols with the aerodyne aerosol mass spectrometer, *Mass Spectrometry Reviews*, **26**, 185.

Ehn, M., Thornton, J. A., Kleist, E., Sipila, M., Junninen, H., Pullinen, I., Springer, M., Rubach, F., Tillmann, R., Lee, B., Lopez-Hilfiker, F., Andres, S., Acir, I-H., Rissanen, M. P., Jokinen, T., Schobesberger, S., Kangasluoma, J., Kontkanen, J., Nieminen, T., Kurten, T., Nielsen, L. B., Jorgensen, S., Kjaergaard, H. G., Canagaratna, M., Dal Maso, M., Berndt, T., Petaja, T., Wahner, A., Kerminen, V-M., Kulmala, M., Worsnop, D. R., Wildt, J. and Mentel, T. F. (2014) A large source of low-volatility secondary organic aerosol, *Nature*, **506**, 476.

Garret, T. J., Radke, L. F. and Hobbs, P. V. (2002) Aerosol effect on cloud emissivity and surface longwave heating on the Arctic, *J. Atmos. Sci*, **59**, 769.

Jokinen, T., Sipilä, M., Junninen, H., Ehn, M., Lönn, G., Hakala, J., Petäjä, T., Mauldin III, R. L., Kulmala, M., and Worsnop, D. R. (2012) Atmospheric sulphuric acid and neutral cluster measurements using CI-APi-TOF, *Atmos. Chem. Phys.*, **12**, 4117.

Junninen, H., Ehn, M., Petäjä, T., Luosujärvi, L., Kotiaho, T., Kostiainen, R., Rohner, U., Gonin, M., Fuhrer, K., Kulmala, M., and Worsnop, D. R. (2010) A high-resolution mass spectrometer to measure atmospheric ion composition, *Atmos. Meas. Tech.*, **3**, 1039.

Mirme, S. and Mirme, A. (2013) The mathematical principles and design of the NAIS – a spectrometer for the measurement of cluster ion and nanometer aerosol size distributions, *Atmos. Meas. Tech*., **6**, 1061.

Quinn, P. K., Shaw, G., Andrews, E., Dutton, E. G., Ruoho-Airola, T. and Gong, S.L. (2007) Arctic haze: current trends and knowledge gaps, *Tellus*, **59B**, 99.

Simpson, W. R., von Glasow, R., Riedel, K., Anderson, P., Ariya, P., Bottenheim, J., Burrows, J., Carpenter, L. J., Frieß, U., Goodsite, M. E., Heard, D., Hutterli, M., Jacobi, H.-W., Kaleschke, L., Neff, B., Plane, J., Platt, U., Richter, A., Roscoe, H., Sander, R., Shepson, P., Sodeau, J., Steffen, A., Wagner, T., and Wolff, E (2007) Halogens and their role in polar boundary-layer ozone depletion, *Atmos. Chem. Phys*., **7**, 4375.

Sipilä, M., Berndt, T., Petäjä, T., Brus, D., Vanhanen, J., Stratmann, F., Patokoski, J., Mauldin III, R.L., Hyvärinen, A.-P., Lihavainen H. and Kulmala, M. (2010) The Role of Sulfuric Acid in Atmospheric Nucleation, *Science*, **327**, 1243.

Sipilä, M., Sarnela, N., Jokinen, T., Henschel, H., Junninen, H., Kontkanen, J., Richters, S., Kangasluoma, J., Franchin, A., Peräkylä, O., Rissanen, M. P., Ehn, M., Vehkamäki, H., Kurten, T., Berndt, T., Petäjä, T., Worsnop, D.R., Ceburnis, D., Kerminen, V.-M., Kulmala, M. and O'Dowd, C. (2016) Molecular scale evidence of new particle formation via sequential addition of 2 HIO_3, and subsequent restructuring to I_2O_5, *Manuscript submitted for publication.*

Sirois, A. and Barrie, L. A. (1999) Arctic lower tropospheric trends and composition at Alert, Canada: 1980-1995, *J. Geophys. Res.*, **104**, 11599.

Vanhanen, J., Mikkilä, J., Lehtipalo, K., Sipilä, M., Manninen, H. E., Siivola, E., Petäjä, T. and Kulmala, M. (2010) Particle size magnifier for nano-CN detection, *Aerosol Sci. Technol*., **45**, 533.

Wang, S. C. and Flagan, R. C. (1990) Scanning Electrical Mobility Spectrometer, Aerosol Sci. Technol., 13, 230.

NEW SNOW DEPTH DISTRIBUTION OVER ARCTIC SEA ICE FROM HISTORICAL DATA

E.V.SHALINA[1], S.SANDVEN[2]

[1]Nansen International Environmental and Remote Sensing Centre, St. Petersburg, Russia.

[2]Nansen Environmental and Remote Sensing Center, NERSC, Bergen, Norway.

Keywords: SEA ICE, SNOW DEPTH, ARCTIC, REMOTE SENSING.

INTRODUCTION

Most of the Arctic sea ice is covered with the snow almost all the year round. Snow cover plays an important role in the sea ice transformations. In winter the snow ensures high sea ice surface albedo of about 0.9 associated with low energy absorption . On the other hand, snow insulates the sea ice from the influence of cold air and reduces the rate of ice growth. After snow begins to melt in spring producing melt ponds, reduction of the surface albedo and higher energy absorption results in a more rapid ice melt. Thus knowledge of snow depth is important for description of thermodynamical processes.

Information on snow depth is also very important for sea ice thickness retrieval from satellite and airborne lidar and radar altimeter measurements and their subsequent conversion to ice thickness (Laxon *et al*., 2013; Kwok *et al*., 2009; Kern *et al*., 2015). Sea ice thickness is one of the key indicators of climate variability and change. It is an important parameter that moderates the heat exchange between the ocean and the atmosphere, it also has an influence on the extent of sea ice deformation and sea ice circulation in the Arctic Ocean. Sea ice thickness is required for evaluating changes in sea ice volume that reflect changes in the heat budget of the Arctic. Figure 1 shows the parameters involved in sea ice thickness retrieval using measured sea ice freeboard: snow depth + ice freeboard (or ice+snow freeboard). Snow loading (snow depth + density) on sea ice is required for retrievals of sea ice thickness.

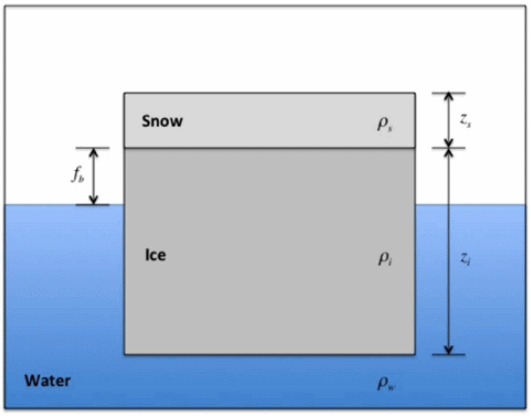

Figure 1. Parameters involved in sea ice thickness retrieval from airborne and space borne altimeters.

There are few in situ observations of characteristics of snow covering the Arctic sea ice. A well-known and widely used Warren climatology [Warren *et al*., 1999, hereinafter WC] provides distribution of the snow depth and density on the basis of the analysis of the Soviet North Pole (NP) drifting stations data collected in 1937 and 1954-1991. That climatology offers monthly data that represent the means over the whole period of observations. The NP program comprised of drifting stations that generally were set up on multiyear ice floes, usually not more than two stations being established in the Arctic in any given year. During the NP program measurements have been provided on the same ice field throughout the lifetime of the chosen floe. Naturally, the applicability of WC is limited to the region where multiyear ice exists.

In this study we analyze snow data from airborne Soviet expeditions Sever collected in the Arctic in 1959-1986. The main advantage of Sever observations is that airborne expeditions provided thorough examination of the ice and snow characteristics of the Arctic marginal seas (see Fig. 2b). The main goal of this study is to produce a reliable map of snow depth over the Arctic sea ice in the end of winter season with the focus on the marginal sea ice. We integrated new data with NP data in the central Arctic. This new climatology could be used as a proxy in ice thickness retrievals from satellite altimeter measurements and as an input in sea ice models.

DATA

The landings of the high-latitude airborne expeditions Sever generally took place from mid March into early May, when there was enough light to operate, but before summer melt made safe landings impossible. As to the ice types where the landings took place, they were quite diverse. Variety of ice types where Sever ice and snow measurements have been conducted is the main difference between high latitude information collected by NP and Sever expeditions.

Data from Sever expeditions are accumulated in the NSIDC G02140 dataset, nsidc.org/data/g02140. The dataset contains sea ice and snow measurements of 23 parameters, including ice thickness and snow depth on the runway and surrounding area; ridge, hummock, and sastrugi dimensions, their areal coverage and snow depth; and snow density. Not all parameters were measured at every landing. In this study we have processed and analysed only snow data collected in March, April and May because most of the data have been collected during that months. The number of landing sites where snow measurements were conducted in those months is 2331.

Distribution of monthly mean positions of NP drifting stations in 1954-1991 for the March, April and May and landing sites of Sever expeditions where snow measurements were conducted in 1959 -1986 in the same months are shown in Figure 2. It demonstrates that drifting station observations cover mainly the central part of the Arctic while airborne expeditions provide data over larger areas with thorough examination of the ice and snow characteristics of the marginal seas.

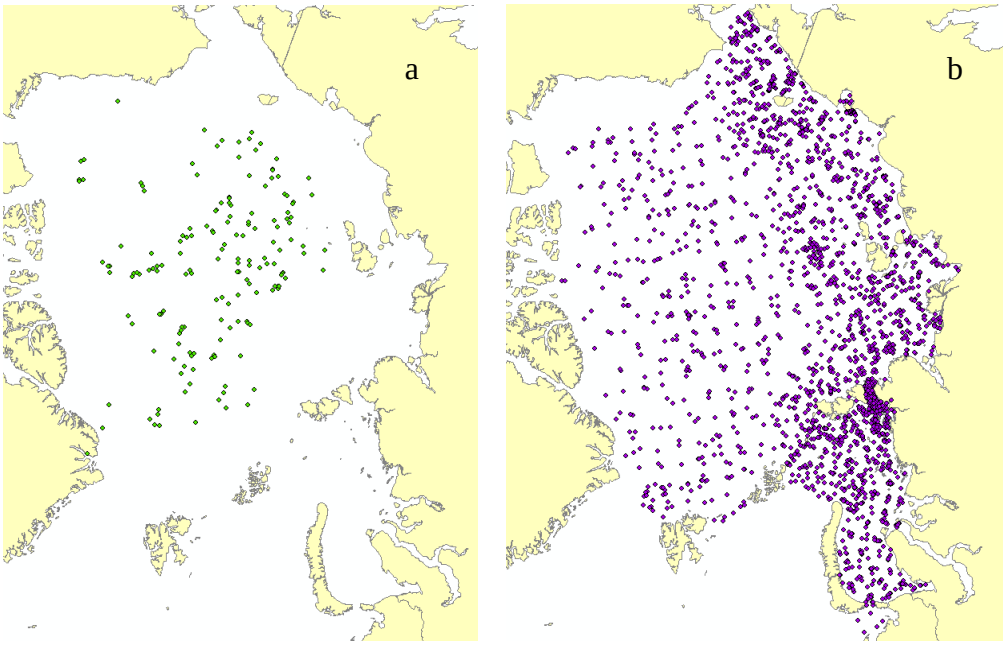

Figure 1. Monthly mean positions of NP drifting stations in 1954-1991 (a) and Sever expeditions landings where snow measurements were conducted in 1959-1986 (b). Only observations in March, April and May are shown.

RESULTS

Snow depth varies significantly within the Arctic region. It varies in time (both seasonally and interannualy) and space (over large distances and even within a single floe). As to the factors that determine snow depth, on one hand, it is ice age and intensity of precipitation. The older the ice, the more time snow has to accumulate and the deeper it gets, depending on the intensity of precipitation. On the other hand, wind and ice roughness also have their share in determining snow depth. Rough ice traps snow blown by the wind more efficiently than smooth ice. Another manifestation of snow depth deviation caused by wind is sastrugi, irregular ridges and grooves of snow formed on the ice surface by the action of the wind. Snow depth variations caused by wind (sastrugi and increased snow depth near the ice ridges and hummocks) can be called local variations. Snow depth variations at a larger scale are synoptic in origin (Sturm *et al*., 2006) or caused by different age of ice where snow cover has been built up.

Spatial changes of snow depth over large distances are analyzed here using Sever expeditions observations made on the level ice around the landing point. In the data set this parameter is described as snow depth on prevailing landing area ice. Data are shown in Figure 3a.

Sever snow data have been merged with NP snow measurements in order to develop a map of snow depth on the sea ice for the most part of the Arctic Ocean (Fig. 3b). Since representative snow data from Sever expeditions are available for March, April and May, the NP data have been selected accordingly, and the result snow map is valid for the same months, i.e. it characterize the average snow cover developed on the sea ice by the end of winter. The time period when measurements have been taken is 1959-1988 for Sever data and 1954-1991for NP data. The geographical distribution is calculated using a least-squares regression fit. We found that a third-order polynomial is best to interpolate available snow observations. The main difference between our developed snow depth distribution shown in Figure 3b and WC is that the new one describes thoroughly snow depth over sea ice in the marginal seas.

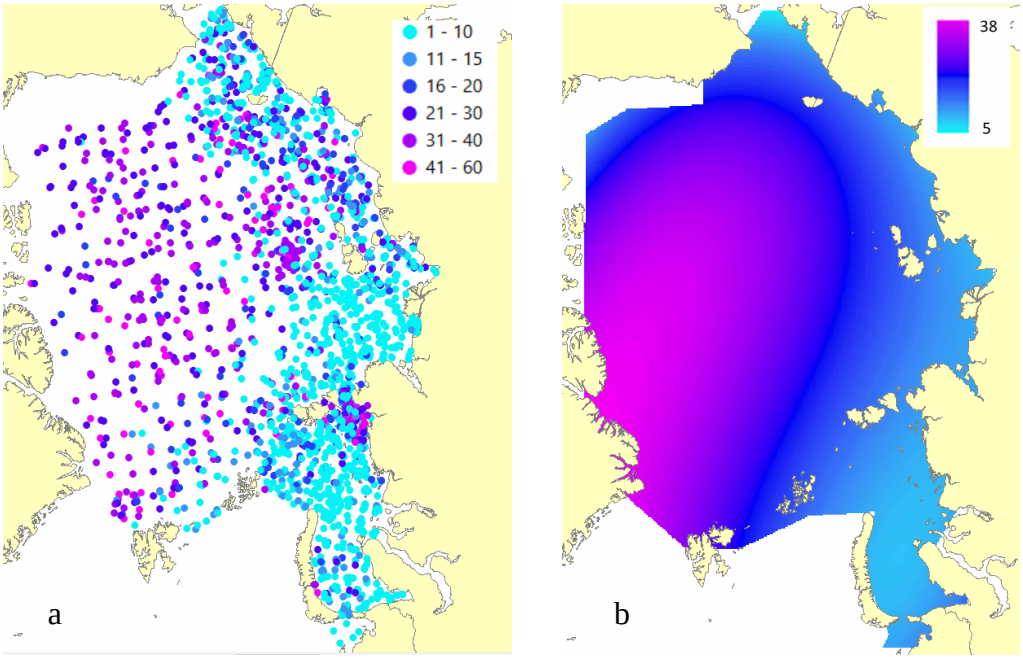

Figure 3. Spatial distribution of measured snow depth on the sea ice from Sever expeditions made in March, April and May, 1959-1988 (a) and snow depth gridded data based on both NP and Sever expeditions observations, average for March, April and May (b).

Relatively high values (and highest in the Russian marginal seas) of the snow depth in the East-Siberian Sea are explained by presence there quite a large portion of multiyear ice in the period under consideration. The snow depth on the ice in that sea (averaged from all observations) changed from 15 cm (near the coast) to 20 cm and more in its northern part. Why snow depth in the Chukchi Sea is that high is less clear. It may be caused by the fact that multiyear ice has been moved here by the Beaufort Gyre and

drifted through this sea into the Pacific Ocean. The range of average snow depth values on the prevailing landing area ice observed by Sever expeditions in that sea is 12 – 18 cm. The lowest snow depth has been observed in the Kara Sea where old ice is seldom encountered. In the central part of that sea the average snow depth changed from 6 – 9 cm and was higher in the areas covered by relatively stable ice massifs and fast ice. The multiyear ice in the Laptev Sea is found more often than in the Kara Sea, its concentrations being defined by wind direction and ocean currents. Consequently, snow depth on the ice was higher in the areas that could be covered by old ice and was in the same range as in the Kara Sea in other parts of the Laptev Sea.

CONCLUSIONS

A new distribution of snow depth on the sea ice has been developed that match the Arctic state previous to the present warming period. Since that time the Arctic has changed dramatically (Kwok *et al*., 2009; SWIPA, 2011; IPCC, 2013; Serreze and Barry, 2011) however the diversity of ice types where Sever expeditions carried out measurements allows to draw dependence between snow depth and ice type and to estimate snow depth in new conditions.

ACKNOWLEDGEMENTS

This work was supported by the ESA-CCI Sea-Ice-ECV project.

REFERENCES

IPCC (2013) Climate Change 2013: The Physical Science Basis. Contribution of Working Group I to the Fifth Assessment Report of the Intergovernmental Panel on Climate Change [Stocker, T.F., D. Qin, G.-K. Plattner, M. Tignor, S.K. Allen, J. Boschung, A. Nauels, Y. Xia, V. Bex and P.M. Midgley (eds.)]. - Cambridge University Press, Cambridge, United Kingdom and New York, NY, USA. - 1535 p.

Kern, S., Khvorostovsky, K., Skourup, H., Rinne, E., Parsakhoo, Z. S., Djepa, V., Wadhams, P., and Sandven, S. (2015). The impact of snow depth, snow density and ice density on sea ice thickness retrieval from satellite radar altimetry: results from the ESA-CCI Sea Ice ECV Project Round Robin Exercise, *The Cryosphere*, 9, 37-52, doi:10.5194/tc-9-37-2015.

Kwok, R., Cunningham, G. F., Wensnahan, M., Rigor, I., Zwally, H. J., and Yi, D. (2009). Thinning and volume loss of the Arctic Ocean sea ice cover: 2003–2008, *J. Geophys. Res*., 114, C07005, doi:10.1029/2009JC005312.

Laxon, S. W., Giles, K. A., Ridout, A. L., Wingham, D. J., Willatt, R., Cullen, R., Kwok, R., Schweiger, A., Zhang, J., Haas, C., Hendricks, S., Krishfield, R., Kurtz, N., Farrell, S. L., and Davidson, M. (2013). CryoSat-2 estimates of Arctic sea ice thickness and volume, *Geophys. Res. Lett*., 40, 1–6.

Serreze, M.C. and Barry, R.G. (2011) Processes and impacts of Arctic amplification: A research synthesis. *Global and Planetary Change*. V. 77, P.85-96.

Sturm, M., J. Maslanik, D. Perovich, J. Stroeve, J. Richter-Menge, T. Markus, J. Holmgren, J. Heinrichs, and K. Tape. (2006). Snow Depth and Ice Thickness Measurements from the Beaufort and Chukchi Seas Collected During the AMSR-Ice03 Campaign. *IEEE Transactions on Geoscience and Remote Sensing - Part 1*, 44(11): 3009-3020, doi:10.1109/TGRS.2006.878236.

SWIPA (2011) Arctic Monitoring and Assessment Programme, Snow, Water, Ice, Permafrost in the Arctic (SWIPA). *Climate Change and the Cryosphere - Arctic Monitoring and Assessment Programme (AMAP*), Oslo, Norway. - 538 p.

Warren, S. G., Rigor, I. G., Untersteiner, N., Radionov, V. F., Bryazgin, N. N., Aleksandrov, Y. I., and Colony, R. (1999). Snow depth on Arctic sea ice, *J. Climate*, 12, 1814–1829.

ATTRIBUTION OF CLIMATE IMPACTS TO ORGANIZATIONS: GAS AND OIL OPERATION IN THE ARCTIC

A. SHCHERBININ[1,2], R. MAKKONEN[1], P. PAASONEN[1] and S. JUHOLA[2]

[1] Department of Physics, University of Helsinki, Helsinki, Finland.

[2] Department of Environmental Sciences, University of Helsinki, Helsinki, Finland.

Keywords: ORGANIZATIONS, EMISSIONS, MODELING, ARCTIC, GAS AND OIL.

INTRODUCTION

There is an increasing interest in the Arctic, both in terms of the impacts of climate change on it, as well as the emerging opportunities arising from these developments. The Arctic areas face a number of stresses, related to erosion of biodiversity (Barber et al., 2014; Arctic Biodiversity Assessment, 2013; and climate change (Post et al., 2009, IPCC 2013). The 5th Assessment Report (AR5) of the Intergovernmental Panel on Climate Change (IPCC) estimated that the Arctic region is warming faster than the global average, between 2.2±1.7 °C and 8.3±1.9 °C by the end of this century depending on the concentration of greenhouse gases (GHGs) in the atmosphere (IPCC 2013).

These rising temperatures and melting sea ice increase the likelihood of new sources of hydrocarbons, minerals, fishing grounds, hydropower, and perhaps even fresh water for resource extraction (see e.g. Avango, 2013; Smith, 2010). These developments affect the Arctic regions directly by increasing the risk of pollution and land use conflicts due to accelerating resource extraction (Rusten et al. 2014). These scenarios of the increase in the extraction of hydrocarbon resources are likely to increase the emissions from the Arctic in the future (Roiger et al. 2015).

The response of Arctic climate to anthropogenic emissions is highly sensitive to the source location. For instance, Sand et al (2013) showed that the local climate forcing due to black carbon (BC) is twice as sensitive (per unit mass emitted) for the Arctic emissions compared to mid-latitude emissions. The Arctic surface temperature response from Arctic BC emissions was close to five-fold as compared to mid-latitude sources. Thus, it is expected that any large-scale future anthropogenic activities in the Arctic will have significant climate impact via modification of radiative fluxes and effects on cryosphere. In light of the expected changes and high sensitivity of Arctic climate to anthropogenic impacts and overall importance of the Arctic in global environment, studying future anthropogenic activities and their climate effects in the Arctic appears to be timely and crucial.

As noted in Roiger et al. (2015), local emission sources are rather sparse in the Arctic, due to overall absence of major anthropogenic activities. However, there are several regions with exceptionally intensive anthropogenic emissions from industrial sources: in particular, sulphur emissions from Kola peninsula smelting complex, although currently decreasing due to economic downfall (Kyrö et al 2014), and BC emissions from flaring activities on the cites of oil and gas extraction in northern Russia (Stohl et al. 2013), which have a potential to grow significantly with increasing development of gas and oil extraction cites as well as extension of human activities to other areas in the Arctic.

We concentrate our efforts to build a robust framework that would address research needs for these emerging topics connected to climate science especially in the Arctic area. Our method combines the use of organizational studies techniques, emission models and climate simulations.

METHODS

The proposed methodological approach includes following blocks:

1) *Organizational study.* Most of the anthropogenic GHG emissions result from the activities of industrial organizations, market or governmental (Hede, 2014). Naturally, looking at the

performance of organizations and their projected activity levels one can solve the first part of the society-climate feedback equation.

2) *Industrial processes and emissions.* Each organization undertakes particular physical operations that contribute both to the primary activity of that organization and impacts the environment. With the use of emissions models like GAINS it is possible to distinguish these operations with regards to particular operations and estimate the resulting emissions.

3) *Scenarios.* In order to assess the future activity of organizations we create scenarios that represent minimum and maximum of the projected activity level and resulting emissions. In these scenarios it is very important to connect the amount of resulting emissions not only to the activity level, but to the mitigation efforts as well. Thus, it enables policy application of the research results.

4) *Geographic plotting.* The final step of the proposed approach is to integrate the scenarios to existing baseline emissions scenarios and implement it in the climate model (ECHAM5.5-HAM2, for instance). One technical obstacle in implementation phase might arise as the scales of the scenarios and gridded data are not compatible. First, GAINS uses rather big areas to divide the globe onto regions – that might prevent us from a direct use of economic statistics in creating scenarios as the latter is usually tied to a specific administrative region. Second, gridded emissions are usually not tied to economic or administrative regions that are used to reference economic and industrial indicators. To overcome this obstacle we propose a use of GIS tools to integrate the scenario integration and feedback verification.

5) *Climate effects.* Finally, we model resulting adjusted emissions scenarios in such a manner that allows us to see climate effects of particular operations of particular organizations resulting from particular decisions (for instance, to reduce the atmospheric emissions). Essentially, the attribution of climate effects to particular organization for illustrative purposes requires us to focus on Short lived Climate Forces, pollutants that have immediate effect on a local climate.

CASE STUDY AND FUTURE APPLICATIONS

One of a few regions with high anthropogenic activities emissions is Yamalo-Nenetskiy Autonomous Okrug (YNAO), northern region of Russian Federation where over 60% (as of 2010) of all Russian natural gas is being produced and 99% of all Arctic gas for that matter. In this paper we present a case study of major changes YNAO will undergo in the near future according to the Program of Complex Development of the Yamal Peninsula and the Adjacent Waters developed by the administration of the YNAO together with Gazprom OJSC (Gazprom 2015) and specifically associated emissions and expected climate responses to these changes. For instance, according to the plans of Gazprom (major socio-economic actor and source of BC emission in the region) it is expected that current levels for gas and oil extraction will double by 2030, through implementation of Yamal-megaproject - a development programme of new gas and oil production sites on Yamal peninsula (Gazprom 2015). An area which has been before relatively pristine and free from larger anthropogenic emission sources (Stohl et al. 2013).
Furthermore, we focus on estimating possible impacts on the environment and the socio-economic situation of the local population that implementation of this project might cause. In order to do this, we produce a geographic profile of the region, including the structure of local economy and identification of key organisations involved in the development of the region to provide context for the study; further, we analyse the program of development of Yamal peninsula and implementation of Yamal megaproject by 2030; next, we estimate the future atmospheric emissions associated with this project using GAINS model (IIASA, 2015) and simulate pollutant transport and resulting climate effects of this contribution via aerosol-climate model ECHAM5.5-HAM2.
Beyond the described case study we give an overview of major developments in the Arctic region: centres of possible future activities and existing infrastructure.

CONCLUSIONS

With regards to the case study, our conclusions show that, according to the project documentation new production centres will be introduced in Yamal peninsula and are supposed to be fully functional in 2030. Planned annual production levels at these sites are comparable to the overall production in YNAO for gas, oil and gas condensate in 2010 and make 360 billion cubic meters (bcm) of natural gas, 10 million tonnes (mt) of crude oil and 8 million tonnes of gas condensate respectively. These activity levels can result in substantial increase in associated anthropogenic emissions, more specifically, introduce sources of BC emissions to Yamal peninsula for up to 12 kt annually, using consensus estimates from GAINS model. Such significant increase in BC emissions in polar region leads to substantial changes in radioactive forcing and sea ice extent. Finally, we conclude that full implementation of policies related to utilization of associated petroleum gas and decreasing flaring activities, can result in substantial decrease in BC emissions in YNAO which can eliminate immediate negative climate effects related to gas and oil development on Yamal peninsula.

Finally, we conclude that the proposed methodological framework can be used in future climate research, especially the one related to the Arctic region. Attribution of climate effects to organizations contributes positively both to physical and social aspects of climate science: enhancing the prediction capabilities of climate scenarios and illustrating direct effects of particular policies on the immediate environment of the organizations.

REFERENCES

Avango, Dag, Annika E. Nilsson, and Peder Roberts. "Assessing Arctic futures: voices, resources and governance." *The Polar Journal* 3.2 (2013): 431-446.

Barber, D. G., et al. "Frost flowers on young Arctic sea ice: The climatic, chemical, and microbial significance of an emerging ice type." *Journal of Geophysical Research: Atmospheres* 119.20 (2014): 11-593.

Cofala J. et al. (2007). Scenarios of global anthropogenic emissions of air pollutants and methane until 2030 *Atmos. Environ.* **41** 8486–99

Federal Media Portal (2014). Oil and Gas of Yamal (Neft I Gas Yamala), available at: http://www.allrussia.tv/yanao/economics/ (last access: 4 December 2014).

Federal State Statistic Service of Russia (2014). Regional Gross Domestic Product for YNAO, available at:http://cbsd.gks.ru/ (last access: 4 December 2014).

Gazprom (2014) Yamal Megaproject, available at: http://www.gazprom.com/about/production/projects/mega-yamal/ (last access: 4 December 2014).

Heede, Richard. "Tracing anthropogenic carbon dioxide and methane emissions to fossil fuel and cement producers, 1854–2010." *Climatic Change* 122.1-2 (2014): 229-241.

Intergovernmental Panel on Climate Change. *Climate Change 2013: The physical science basis: Working group I contribution to the fifth assessment report of the Intergovernmental Panel on Climate Change*. Cambridge University Press, 2014.

Kutepova, E.A. et al. (2011). Associated Gas Utilization in Russia: Issues and Prospects, *Annual Report KPMG Moscow* **3**.

Kyrö, Ella-Maria, et al. "Long-term aerosol and trace gas measurements in Eastern Lapland, Finland: the impact of Kola air pollution to new particle formation and potential CCN." *EGU General Assembly Conference Abstracts*. Vol. 16. 2014.

Luhmann, N. (2012). *Theory of Society Volume 1-2*. (Stanford University Press, Stanford, USA).

Macknick, J. (2011). Energy and CO2 emission data uncertainties *J. Carbon Management* 2(2), 189–205

OGP (2011). Environmental performance in EP industry – 2010 data, *International Association of Oil and Gas Producers* **466**.

Post, Eric, et al. "Ecological dynamics across the Arctic associated with recent climate change." *Science* 325.5946 (2009): 1355-1358.

Roiger, Anke, et al. "Quantifying emerging local anthropogenic emissions in the Arctic region: the ACCESS aircraft campaign experiment." *bulletin of the american meteorological Society* 96.3 (2015): 441-460.

Rusten, M., et al. "Arctic Risk Picture-Management of Safety and Environmental Risk." *Offshore Mediterranean Conference and Exhibition*. Offshore Mediterranean Conference, 2015.

Sand, M. et al. (2013) Arctic surface temperature change to emissions of black carbon within Arctic or midlatitudes. *J. of Geophysical Research: Atmospheres* 118(14), 7788–7798.

Stier et al. (2005): The aerosol-climate model ECHAM5-HAM, *Atmos. Chem. Phys.* **5**, 1125-1156

Stohl, A. et al. Black carbon in the Arctic: the underestimated role of gas flaring and residential combustion emissions, *Atmos. Chem. Phys*. **13**, 8833-8855.

PARTICLE CLIMATOLOGY IN CENTRAL EAST CHINA RETRIEVED FROM MEASUREMENTS IN PLANETARY BOUNDARY LAYER AND IN FREE TROPOSPHERE AT A 1500-M-HIGH MOUNTAINTOP SITE

X.J. SHEN[1], J.Y. SUN[1,2*], X.Y. ZHANG[1], N. KIVEKÄS[3], Y.M. ZHANG[1], T.T. WANG[1,4], X.C. ZHANG[5], Y. YANG[1], D.Z. WANG[6], Y. ZHAO[6], D.H. QIN[2]

[1]Key Laboratory of Atmospheric Chemistry of CMA, Institute of Atmospheric Composition, Chinese Academy of Meteorological Sciences, Beijing, China.

[2]State Key Laboratory of Cryospheric Sciences, Cold and Arid Region Environmental and Engineering Research Institute, Chinese Academy of Sciences, Lanzhou, China.

[3]Finnish Meteorological Institute, P.O. Box 503, 00101 Helsinki, Finland.

[4]Heilongjiang Province Meteorological Bureau, Harbin, China.

[5] CMA Meteorological Observation Centre, Beijing, China.

[6] Taishan National Basic Meteorological Observation Station, Tai'an, China.

Keywords: PARTICLE NUMBER SIZE DISTRIBUTION, NEW PARTICLE FORMATION EVENT, PLANETARY BOUNDARY LAYER, FREE TROPOSPHERE.

INTRODUCTION

Particles with diameters ranging from 0.1 µm to 1 µm are highly effective at scattering solar radiation via the direct aerosol effect (Haywood and Boucher, 2000). Particles larger than about 0.1 µm may also act as cloud condensation nuclei (CCN) and contribute to indirect radiative effects (Köhler, 1937; Twomey, 1977). These effects are thought to result in a negative global mean radiative forcing by aerosol particles (IPCC, 2013). However, large uncertainties still remain due to the absence of adequate information about spatio–temporal variability of global aerosol concentration, aerosol physico–chemical properties, and aerosol–cloud interaction (IPCC, 2013). Particle number size distribution (PNSD) displays a large variability with the particle diameter ranging from a few nanometers to tens of micrometers, depending on different emission sources and atmospheric processes. The number concentration of particles also varies from less than 100 particles per cubic centimeter in remote areas to several tens of thousands in polluted urban areas (Kulmala *et al.*, 2004).

All particle populations measured in ambient conditions are affected by particle sources of varying geographical extent, and the particles are typically well mixed throughout the turbulent planetary boundary layer (PBL), making it difficult to separate between different particle sources. A high-altitude mountain station is located above PBL for at least some part of the time, allowing a view of the particle population on larger geographical scale. The location of the site in free troposphere (FT) air allows the evaluation of transport from further away and exchanges with the planetary boundary layer (Gao *et al.*, 2005). Compared to other methods of studying FT air, the advantage of mountaintop observatories is that they provide the opportunity to conduct long-term measurements in the FT.

METHODS

The measurements were made at Taishan National Basic Meteorological Observation Station located at the summit of Mt. Tai (36.25°N, 117.10°E, 1534 m asl.), and lasted from July 2010 to February 2012. Mt. Tai is located in the middle of Shandong Province and surrounded by Jiangsu, Anhui, Hebei and Henan

provinces (Fig. 1). Hebei, Henan and Shandong belong to the largest provinces with many cities exceeding 5 million in population. The terrain around Mt. Tai consists of lower hills and mountains with peak heights < 1000 m asl. to the west of Mt. Tai and densely populated lowland areas to other directions.

Aerosols were sampled through a PM_{10} impactor and a $PM_{2.5}$ cyclone in sequence. The relative humidity of the sample air was maintained below 30% with an automatic regenerating adsorption aerosol dryer in the inlet line. PNSD was measured using a scanning mobility particle sizer (SMPS, TSI Inc., USA) system a twin differential mobility particle sizer (TDMPS, TROPOS, Germany).

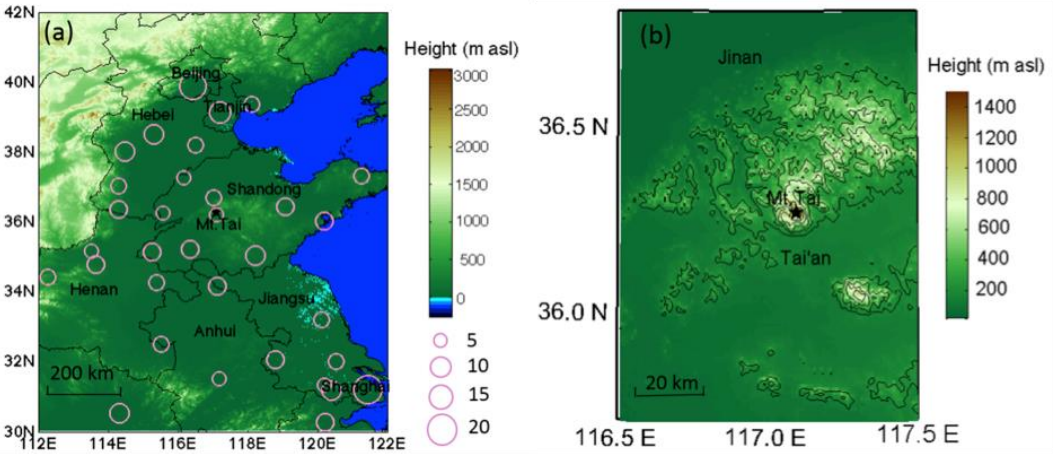

Fig. 1. (a) The map of North China Plain and central east China showing the location of Mt. Tai and the major cities with population larger than 5 million. The circles indicate the population in unit of million inhabitants. (b) The topography of the area surrounding Mt. Tai within 60 km distance.

CONCLUSIONS

Aerosol particle number size distribution (PNSD) in the size range of 3 nm–2.5 µm was continuously measured at Mt. Tai, a mountaintop station in central east China from July 2010 to March 2012. The mean number concentration of submicron particles, reduced to 1013 hPa, was 11800 cm^{-3}. The typical particle number concentrations at Mt. Tai were significantly higher than that at other high elevation sites around the world.

New particle formation (NPF) events were observed on 32% of the days, most frequently in spring. The mean particle formation rate (J_3) of 4.0 cm^{-3} s^{-1} and growth rate (GR) of 6.1 nm h^{-1}. It was found that the formation rate and condensation sink could be even an order of magnitude higher than most studies at the other high elevation stations. The newly formed particle modes were observed grow into the size where they can act as potential cloud condensation nuclei within a day. This could be very important for aerosol-cloud interactions, especially at the sites with high RH. During NPF days, Number concentration of nucleation and Aitken mode was much higher than those during non-NPF days, indicating significant contribution of NPF event to particle number concentrations in those size ranges. However, accumulation mode particle number concentration was found to be higher during non-NPF days.

Based on the diurnal cycles of absolute humidity as well as of normalized accumulation mode particle number concentrations, time periods 12:00–17:00 and 23:00–07:00 local time were selected to represent PBL and FT conditions (Fig. 2), respectively. This selection was supported by the meteorological sounding data. The mean particle number concentrations of Aitken and accumulation mode in PBL conditions were about twice of those in FT conditions, but nucleation mode number concentration was more than 10 times higher in PBL than in FT. This does not mean that NPF is limited to PBL, but rather that NPF is limited to daytime and the newly formed particles grow fast enough to grow out from nucleation mode before 23:00 local time.

The particle number concentrations also exhibited pronounced seasonal variations in both PBL and FT air (table 1), being highest in summer and lowest in winter during non-NPF event days. This could be linked to seasonality of air mass transport pathways, emission sources and PBL evolution. The particle number and mass concentrations were about 30–200% and 25–50% higher, respectively, in PBL than those in FT, depending on the season and NPF events.

The high particle number and mass concentrations observed at Mt. Tai were found to be systematical. The high number concentration of Aitken and accumulation mode also in FT conditions revealed that this is a large scale regional phenomenon, and that the diurnal cycle in PBL height can pump large amounts of particles into free troposphere, especially in low moving air masses in the summer. This indicates that any actions to improve air quality at CEC must be taken at regional level, and that the effects and their climate implications observed at Mt. Tai can be extrapolated to larger areas in CEC. The observations at Mt. Tai can provide the opportunity to conduct long-term measurements in the FT, as well as PBL in central east China, which are important for evaluating the effect of aerosols on climate and for validating the performance of atmospheric chemical transport models.

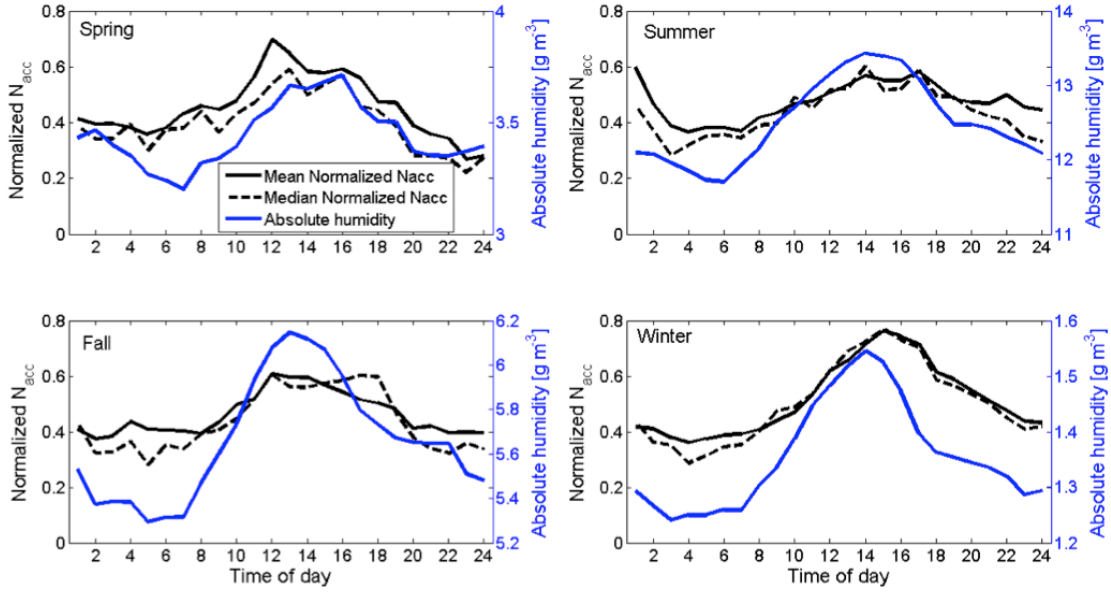

Fig. 2. The seasonal mean diurnal pattern of absolute humidity and mean and median normalized particle number concentrations of accumulation mode on days without NPF events (a–d).

Table 1. Seasonal mean and standard deviation of particle number concentration and mass concentration of $PM_{2.5}$ in PBL and FT conditions during non-NPF days and NPF days, respectively.

	Number concentration (cm^{-3})		Mass concentration (μg m^{-3})	
	PBL	FT	PBL	FT
Non-NPF days				
Spring	8400 ± 5500	6100 ± 3800	40 ± 22	32 ± 22
Summer	9800 ± 3900	7500 ± 3000	65 ± 38	53 ± 35
Fall	8300 ± 7300	5600 ± 4100	43 ± 24	28 ± 21
Winter	8100 ± 4300	5400 ± 3200	37 ± 20	25 ± 19
NPF days				
Spring	20400 ± 11800	6700 ± 4500	43 ± 28	29 ± 20
Summer	16300 ± 7400	5300 ± 3500	48 ± 25	32 ± 24
Fall	16700 ± 8700	5500 ± 3800	35 ± 19	26 ± 16
Winter	10900 ± 4800	4700 ± 2500	28 ± 15	24 ± 23

ACKNOWLEDGEMENTS

This work was supported by National Basic Research Program of China (2011CB403401), the National Natural Science Foundation of China (41175113, 41405132) and CAMS Basis Research Project (2013Z007, 2013Y004), Special Fund for Meteorological Research in the Public Interest (GYHY-200906038, GYHY201206037), and Finnish Center of Excellence 272041 (Centre of Excellence in Atmospheric Science - From Molecular and Biological processes to The Global Climate). This work is also partially supported by the CMA Innovation Team for Haze-fog Observation and Forecasts. The authors would like to thank Prof. Tareq Hussein for providing the program for PNSD modal fitting and Dr. Jianpin Guo for providing meteorological sounding data. We would also like to thank the Mt. Tai observational station staff for the help of operating and maintaining the instruments.

REFERENCES

Gao, J., Wang, T., Ding, A.J. and Liu, C.B. (2005). Observational Study of Ozone and Carbon Monoxide at the Summit of Mount Tai (1534 m a.s.l.) in Central-eastern China. *Atoms. Envrion.* **39**, 4779–4791.

Haywood, J. and Boucher, O. (2000). Estimates of the Direct and Indirect Radiative Forcing due to Tropospheric Aerosols: A Review. *Rev. Geophysical* **38**, 513–543.

IPCC, Climate Change 2013 (2013). *The Physical Science Basis. Contribution of Working Group I to the Fifth Assessment Report of the IPCC.* (Cambridge University Press, London, U.K.).

Kulmala, M., Vehkamäki, H., Petäjä,T., Dal Maso, M., Lauri, A., Kerminen, V.M., Birmili, W. and McMurry, P.H. (2004). Formation and Growth Rates of Ultrafine Atmospheric Particles: A Review of Observations. *J. Aerosol Sci.* **35**, 143–176.

Köhler, H. (1936). The Nucleus in and the Growth of Hygroscopic Droplets. *Trans. Faraday Soc.* **32**, 1152–1161.

Twomey, S. (1977). The Influence of Pollution on the Short Wave Albedo of Clouds. *J. Atmos. Sci.* **34**, 1149–1152.

SIMULATED IMPACTS OF DIFFERENT VEGETATION LANDCOVER DATASETS ON THE HIGH-LATITUDE LAND SURFACE CLIMATE

X.L. SHI[1], L. YU[2], S.P. NIE[1], Y.W. ZHANG[1], and W.Y ZHOU[1]

[1]Division of Climate System Modeling, National Climate Center, China Meteorological Administration, No. 46, Zhongguancun Nandajie, Haidian District, Beijing, P. R. China.

[2]Ministry of Education Key Laboratory for Earth System Modeling, Center for Earth System Science, Tsinghua University, Beijing, 100084.

Keywords: LAND COVER DATA, LAND SURFACE MODEL, NUMERICAL SIMULATION, TEMPERATURE.

INTRODUCTION

Land cover (LC) information has significant impacts on climate models. LC type and fraction, as well as some LC-dependent parameters, control the land surface biogeophysics and biogeochemistry processes, as well as weather and climate through land-atmosphere coupling processes (Lawrence and Chase, 2010). Among various LC types in the model, vegetation has the most intensive and extensive impacts on the model results (Shi *et al*., 2016). But large differences exist in various LC remote sensing datasets because of the differences of original data, remote sensing inversion, time periods, and so on.

Vegetations at high-latitude areas play particular roles in the land and climate systems according to numerous observation and model simulations. In this paper, three newly-produced remote sensing vegetation LC datasets of the year 2000 are compared and applied in the land surface and atmosphere component models of Beijing Climate Center Climate System Model (BCC_CSM, Wu *et al*., 2014) to investigate the impacts on land surface climate. The vegetation is classified into 15 types according to the plant function type (PFT) as in NCAR/CLM3 (Oleson *et al.*, 2004).

METHODS

The new vegetation LC datasets include FROM-GLC (Gong *et al*., Yu *et al*., 2013), GlobeLand30 (Chen *et al*., 2013) and CG-LTDR (Liu *et al*., 2014) for the year 2000. Because of vegetation classification differences, the three remote sensing datasets were, respectively, processed in LC types and spatial resolutions to meet the requests of BCC model.

Numerical simulations of BCC land surface (BCC_AVIM) and climate (BCC_AGCM) were conducted and compared. The control runs with original vegetation LC datasets (noted as CTL) from MODIS, the experiments with three new datasets were made under the same configurations as CTL, besides the vegetation cover information of PFTs and the fractions within model grids.

CONCLUSIONS

The vegetation LC datasets had consistent spatial distribution features but with different fractions within the model grid (around 110km), especially for the tree, grass and crop types. The simulations with these datasets also show general similar climate states as observed temperature and rainfall. The differences between revised LC datasets and CTL experiments were analyzed to present impacts of vegetation on land surface climate. Results show that applications of the new vegetation LC datasets in BCC_CSM component models were somewhat effective in decreasing the biases of the high-latitude areas, but just as agreed to other studies, none of the vegetation LC datasets had the best performances for all variables.

ACKNOWLEDGEMENTS

This work was supported by the welfare project (No. 201506023, 201106014-3), and 863 projects "Research on global land cover remote sensing mapping and key technologies".

REFERENCES

Chen, J., J. Chen, X. Cao, et al. (2015). Global Land Cover Mapping at 30m Resolution: a POK-based Operational Approach，*ISPRS Journal of Photogrammetry and Remote Sensing* , 103: 7-27.

Gong, P. , J. Wang, L. Yu, et al. (2013). Finer resolution observation and monitoring of global land cover: first mapping results with Landsat TM and ETM+ data. *Int J Remote Sens* **34**, 2607-2654.

Lawrence, P.J. and T.N. Chase (2010). Investigating the climate impacts of global land cover change in the community climate system model. *Int. J. Climatol.* **30**, 2066-2087.

Liao A P, Chen L J, Jun Chen, et al., 2014. High-resolution remote sensing mapping of global land water. Science China: Earth Sciences, 57: 2305–2316, doi: 10.1007/s11430-014-4918-0.

Oleson, K.W., Y.J. Dai, G.B. Bonan, et al. (2004). *Technical Description of the Community Land Model (CLM)*, (NCAR Technical . Note - 461 + STR, 173pp).

Shi, X.L., S.P. Nie, W.M. Ju, et al. (2016). Climate Impacts of the GLobeLand30 Land Cover Dataset on the Beijing Climate Center Climate Model Simulations. *SCIENCE CHINA: Earth Sciences,* accepted (in Chinese).

Wu, T.W., L.C. Song, W.P. Li, et al. (2014). An overview of BCC climate system model development and application for climate change studies. *J. Meteorol. Res.* **28**, 35-56.

Yu, L., J. Wang, P. Gong (2013). Improving 30 meter global land cover map FROM-GLC with time series MODIS and auxiliary datasets: a segmentation based approach. *Int J Remote Sens* **34**, 5851-5867.

RELATIONSHIP BETWEEN INTER-ANNUAL WILDFIRE DENSITY AND ET/PET RATIO IN SOUTH CHINA

Z. SHIRAZI[1], and F. CHEN[2]

Key Laboratory of Digital Earth Science,
Institute of Remote Sensing and Digital Earth,
Chinese Academy of Sciences, Beijing 10094, China

Keywords: WILDFIRE, FIRE HAZARD, TIME SERIES, CLIMATE

INTRODUCTION

An extreme fire event in certain cases is comparable to other major natural hazards in term of its adverse affects on economy, human health and safety. Wild fires have tendency to destroy large fields of land and make them uncultivable effecting agriculture and hence economy of the region. Fires have local (degradation of vegetation, loss of biodiversity, property and life) and global (human health and atmospheric pollution and green house gasses) effects. Wildfire even influences the regional climate by changing the energy budget. They have affected forest in many countries including in the tropics. They are currently covering 3% of world vegetated land surface(Flannigan et al. 2000; Bravo de Guenni 2005; Anderson & Bausch 2006; Herawati & Santoso 2011; Doerr & Santin 2013). Forests are a valuable and declining resource in China and high risk of forest loss is expected in eastern China (Zhong et al. 2003; Scholze et al. 2006). Statistically the numbers of fires and burn areas fluctuate largely and are mostly influenced with atmospheric conditions. Southern China has large numbers of fires whereas, burn area in the north east and Inner Mongolia is large. The fire risk period in North East and Inner Mongolia are in spring and autumn from March to June and September to November respectively. Meanwhile, in South and Southwest of China there is a long fire risk period from November to end of April (Zhong et al. 2003; Ai-feng 2011; Chen et al. 2014). Fire conditions are a consequence of variations in environmental parameters that lead to drying of vegetation and results in a fire incident if an ignition event occurs. Therefore, identifying the effects of different environmental parameters and their variation can help explain fire activity. The focus of this study is to identify common underlying environmental factors that contribute to onset of wild fires in China. These environmental factors can help in predicting fire activity on a large scale and provide hints towards mitigation of the fire problem. Due to long fire risk period and high number of fires, South China was decided to be the focus of this study.

METHODS

Ai-feng (2011) found that temperature is positively correlated with fire in most of China however, Abatzoglou & Kolden (2013) suggested that parameters such as potential evapotranspiration, that link atmospheric drivers with fire activity, will explain fire activity better in a region. Many studies have use potential evapotranspiration and other derivatives ((Lafon & Quiring 2012; Lin et al. 2014; Swenson & Wahr 2006; Cooke et al. 2007) . This study focused on the relationship between ET/pET ratio (evapotranspiration/ potential evapotranspiration) and fire density in the South China region during the winter dry season. A grid base correlation analysis was carried out using time series remote sensing data products between fire and a ratio between evapotranspiration and potential evapotranspiration to help isolate their spatial relationships and to identify if this parameter has influence on the fire activity over the entire South China region.

CONCLUSIONS

The results show a negative correlation between fire density and ET/pET ratio. Water available to terrestrial system is not unlimited and is controlled by PPt. ET is the output of water back to the atmospheric component due to various environmental aspects (wind, humidity, temperature, etc.). These environmental conditions are represented by the pET. So the pET represents the demand of water by the atmosphere. ET is always less or equal to pET. Difference between ET and pET will increase if the terrestrial system is deficient of water and the ET/pET ratio will decrease and will be indicative of dry conditions (McConnell et al. 2008; Fu et al. 2008; Shukla & Mintz 1982; Arnell et al. 1995; Fu et al. 2013). PPt under dry conditions can increase the ET by increasing the available water (Gao 2010), however temporarily if the amount of PPt is low, it might not be able to change the conditions due to high pET.

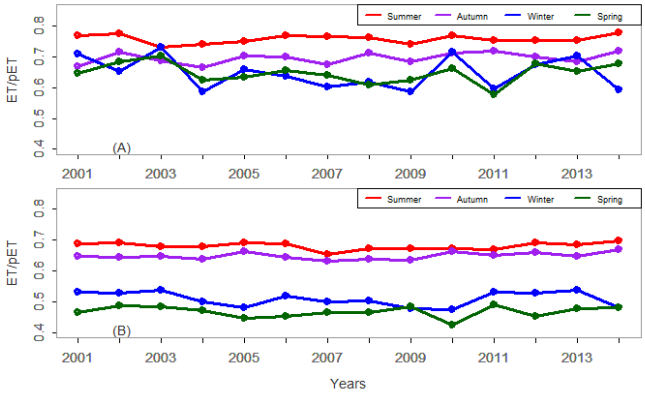

Figure1. Seasonal trends of ET/ pET ratio in the South East (A) South West (B)

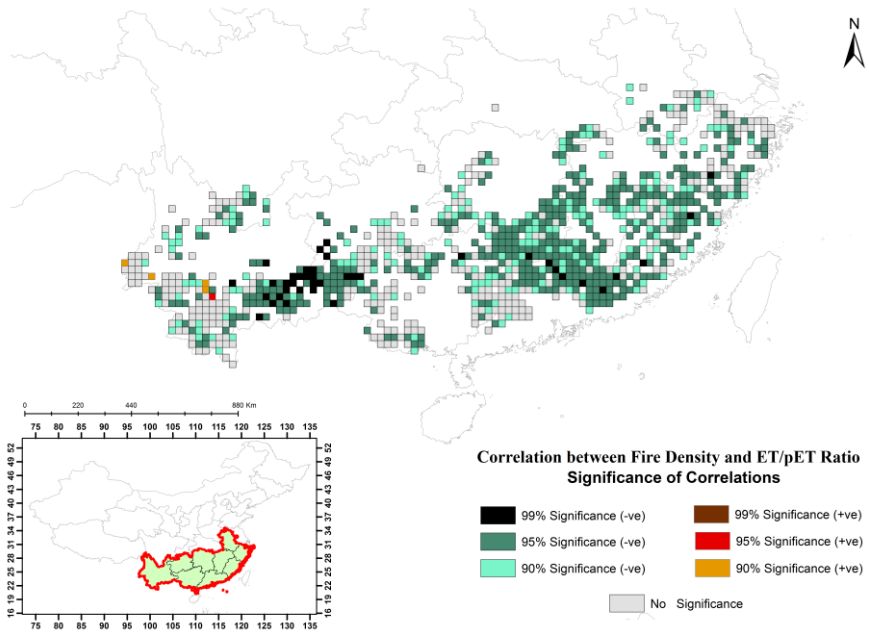

Figure2. Correlation between fire densities in the South China with ratio between ET/pET.

Various studies have discussed the trends of ET and pET in China over varying time scales (Gao et al. 2007; Fan & Thomas 2013; Yao et al. 2014), however their respective relationship seem to have lacked attention. Our results suggest that the relative relationship of ET and pET or trends of ET/pET, can likely explain the fire activity in the South China region.

Both pET and ET are controlled by multiple parameters, such as sunshine duration, wind speed, relative humidity, maximum and minimum air temperature, etc. and are defined by their complex interaction and variations in their role of importance both spatially, seasonally and temporally (Gao et al. 2007; Fan & Thomas 2013). These parameters are in turn influenced by variations in large scale atmospheric systems, and might eventually determine the severity of the fire season in the South China region. Therefore these results suggest link of wildfires in the South China to large scale climatic systems

ACKNOWLEDGEMENTS

This work was funded by Chinese Academy of Sciences- World Academy of Sciences (CAS-TWAS) President's Fellowship Program for developing countries

REFERENCES

Abatzoglou, J.T. & Kolden, C. a., 2013. Relationships between climate and macroscale area burned in the western United States. *International Journal of Wildland Fire*, 22(7), pp.1003–1020.

Ai-feng, L.U., 2011. Study on the relationship among forest fire, temperature and precipitation and its spatial-temporal variability in China. *Agricultural Science & Technology-Hunan*, 12(9), pp.1396–1400.

Anderson, J. & Bausch, C., 2006. *Climate change and natural disasters : Scientific evidence of a possible relation between recent natural disasters and climate change*, Available at: Institute for European environmental policy.

Arnell, N. et al., 1995. *Climate Change 1995: The IPCC Second Assessment Report Hydrology and Freshwater Ecology Chapter 10*, Available at: https://www.ipcc-wg2.gov/publications/SAR/SAR_FrontMatter.pdf [Accessed October 22, 2015].

Bravo de Guenni, L., 2005. Chapter 16: Regulation of Natural Hazards : Floods and Fires. *Ecosystems and Human Well-bing: Current State and Trends*, pp.441–453.

Chen, F. et al., 2014. The Influence of Precipitation and Consecutive Dry Days on Burned Areas in Yunnan Province, Southwestern China. *Advances in Meteorology*, 2014, pp.1–11. Available at: http://www.hindawi.com/journals/amete/2014/748923/.

Cooke, W. et al., 2007. Integrating Climatic and Fuels Information into National Fire Risk Decision Support Tools. *USDA Forest Service Proceedings RMRSP46CD*, pp.555–569. Available at: http://www.gri.msstate.edu/publications/docs/2007/03/6207Cooke_et_al_FireRisk_DSS.pdf.

Doerr, S. & Santin, C., 2013. *Wildfire: A Burning Issue for Insurers?*, Lloyd's. Available at: https://www.lloyds.com/~/media/lloyds/reports/emerging risk reports/wildfire final.pdf.

Fan, Z.-X. & Thomas, A., 2013. Spatiotemporal variability of reference evapotranspiration and its contributing climatic factors in Yunnan Province, SW China, 1961–2004. *Climatic Change*, 116(2), pp.309–325. Available at: http://link.springer.com/10.1007/s10584-012-0479-4.

Flannigan, M.D., Stocks, B.J. & Wotton, B.M., 2000. Climate change and forest fires. *Science of The Total Environment*, 262(3), pp.221–229. Available at: http://www.sciencedirect.com/science/article/pii/S0048969700005246\nC:\Users\Kellen_Nelson\zotero_datafiles\storage\R8R2RSKR\S0048969700005246.html.

Fu, C. et al., 2008. *Regional Climate Studies of China* C. Fu et al., eds., Available at: http://books.google.com/books?hl=en&lr=&id=SEO_RyNDJ0gC&oi=fnd&pg=PA1&dq=Regional+Climate+Studies+of+China&ots=HZ0Ol0pE1I&sig=1bvzkVCyYAAEwB8HMfdjdFeOjyg.

Fu, G. et al., 2013. Temporal variation of extreme rainfall events in China, 1961–2009. *Journal of Hydrology*, 487, pp.48–59. Available at: http://linkinghub.elsevier.com/retrieve/pii/S0022169413001339.

Gao, G., 2010. *Changes of Evapotranspiration and Water Cycle in China during the Past Decades*. University of Gothenburg. Available at: http://hdl.handle.net/2077/21737.

Gao, G. et al., 2007. Trend of estimated actual evapotranspiration over China during 1960–2002. *Journal of Geophysical Research*, 112(D11), p.D11120. Available at: http://doi.wiley.com/10.1029/2006JD008010.

Herawati, H. & Santoso, H., 2011. Tropical forest susceptibility to and risk of fire under changing climate: A review of fire nature, policy and institutions in Indonesia. *Forest Policy and Economics*, 13(4), pp.227–233. Available

at: http://www.sciencedirect.com/science/article/pii/S1389934111000189.
Lafon, C.W. & Quiring, S.M., 2012. Relationships of Fire and Precipitation Regimes in Temperate Forests of the Eastern United States. *Earth Interactions*, 16(11), pp.1–15. Available at: http://journals.ametsoc.org/doi/abs/10.1175/2012EI000442.1.
Lin, H.-W. et al., 2014. Management and climate contributions to satellite-derived active fire trends in the contiguous United States. *Journal of Geophysical Research: Biogeosciences*, 119(4), pp.645–660. Available at: http://www.pubmedcentral.nih.gov/articlerender.fcgi?artid=4508926&tool=pmcentrez&rendertype=abstract [Accessed October 15, 2015].
McConnell, D. (University of A. et al., 2008. *The Good Earth: Introduction to Earth Science* 1st ed. M. J. Kemp & L. Recker, eds., McGraw hill. Available at: http://www.ncbi.nlm.nih.gov/pubmed/15003161.
Scholze, M. et al., 2006. A climate-change risk analysis for world ecosystems. *Proceedings of the National Academy of Sciences of the United States of America*, 103(35), pp.13116–13120.
Shukla, J. & Mintz, Y., 1982. Influence of Land-Surface Evapotranspiration on the Earth's Climate. *Science*, 215(4539), pp.1498–1501. Available at: http://www.jstor.org/stable/1688150.
Swenson, S. & Wahr, J., 2006. Estimating Large-Scale Precipitation Minus Evapotranspiration from GRACE Satellite Gravity Measurements. *Journal of Hydrometeorology*, 7(2), pp.252–270.
Yao, Y. et al., 2014. Spatial and Decadal Variations in Potential Evapotranspiration of China Based on Reanalysis Datasets during 1982–2010. *Atmosphere*, 5, pp.737–754. Available at: http://www.mdpi.com/2073-4433/5/4/737/.
Zhong, M. et al., 2003. Statistical analysis on current status of China forest fire safety. *Fire Safety Journal*, 38(3), pp.257–269.

REACTIVE GASES OVER CENTRAL SIBERIA: OBSERVATIONS AND BALANCE

A.I. SKOROKHOD[1], I.B. BELIKOV[1], K.B.MOISEENKO[1], N.V.PANKRATOVA[1], Y.A.SHTABKIN[1] and M.HEIMANN[2]

[1]A.M.Obukhov Institute of Atmospheric Physics RAS, Department of Atmospheric Chemistry, Moscow, Russia

[2]Max Planck Institute for Biogeochemistry, Jena, Germany

Keywords: ATMOSPHERIC CHEMISTRY, OZONE, REACTIVE GASES, EMISSIONS, OBSERVATIONS, BALANCE, ZOTTO

INTRODUCTION

Direct observations of atmospheric air composition are very important for comprehensive studies of atmospheric chemical processes in Northern Eurasia both on regional and continental scales. Particularly, such observations allow for discriminating long term atmospheric trends driven by changes in regional climate and ecosystems as well as increasing anthropogenic burdens. Atmospheric air composition (including greenhouse gases and aerosols) trends and variability are still insufficiently known for most of the nearly uninhabited areas of Northern Eurasia. The lack of knowledge on key factors affecting the regional balance of chemically active compounds limits the accuracy of both global and regional models currently used to simulate climatological and ecosystem changes in this highly important region.
This gap is partially filled by observations at the Zotino Tall Tower Observatory (ZOTTO) located in Central Siberia (60N, 90E). The observatory has been launched in 2006 and is governed by an international scientific consortium. Since that time, ZOTTO observations play an important role as they provide unique information about concentrations of greenhouse and reactive trace gases, as well as aerosols (Heimann *et al*., 2014). In this work background trace gases (such as O_3, NO, NO_2, CO) concentrations and their variability are considered based on the results of continuous (March 2007 – June 2015) measurements at the ZOTTO station. Particularly, it is shown that these data can be used to validate model assessments of reactive gases transport and balance.

METHODS

This work uses results of direct observations of O_3, NO, NO_2 at ZOTTO in 2007-2015 performed by the A.M.Obukhov Institute of Atmospheric Physics RAS. For O_3 a Dasibi1008 instrument with a measurement interval between 0 and 1000 ppbv and nominal accuracy of 1 ppbv was used. The instrument was calibrated against the ozone generator GP-024 and Russian national standard SPR No. 038. Nitrogen oxide- and nitrogen dioxide-mixing ratios were measured by TE-42C-TL two-channel chemiluminescent gas analyzers. The method is based on the luminescence radiation from the chemical reaction between NO and O_3. To measure NO_2, a catalytic converter reducing NO_2 to NO was used. The measurement range is 0.05-400 ppbv with a general error of 1%. All equipment is located in the underground laboratory at the base of the Tall Tower. The air sampling inlet is installed at height 6 m above the ground.
For O_3 balance calculations the GEOS-Chem model (http://acmg.seas.harvard.edu/geos/, version 10-01) was used. This is a numerical Eulerian global chemical transport model of atmospheric composition, which takes into account all basic natural and anthropogenic sources and sinks of chemically active gases and aerosols. The meteorological fields and data on the underlying surface with time resolutions of 3 h (two-dimensional fields) and 6 h (three-dimensional fields) are taken from the GEOS-GMAO global data assimilation system (http://gmao.gsfc.nasa.gov/GEOS/) and projected onto a computational grid (4°x5° or 2.0°x2.5°) of the model. The model assimilates the following basic emission databases: EDGAR4.2 for anthropogenic, MEGAN2.1 for biogenic and GFED3 for natural fires emissions (Shtabkin *et al*., 2016).

To calculate the regional balance of ozone 3 main regions (including Western Europe, European Russia, and Siberia where ZOTTO is located) were defined in the Northern Eurasian domain (Figure 1).

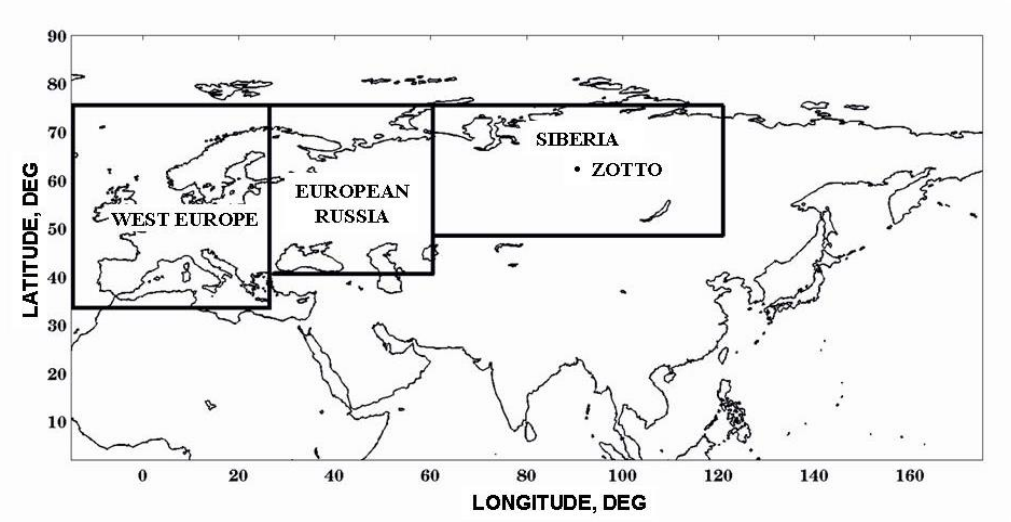

Figure 1. Macro-regions used to calculate the average annual and seasonal ozone balance for 2007 - 2012 by the GEOS-Chem model.

CONCLUSIONS

The ZOTTO observatory is located in a remote site that is suggested to be unpolluted. Therefore, the variability of trace gases is likely to be determined by natural atmospheric processes. Nevertheless analyses of CO and aerosol observations at ZOTTO indicated that only about 30% of time the air there is pristine (Chi *et al.*, 2013). Ozone is influenced by pollution indirectly through photochemical reactions, which are weak at that latitude but there is a good correlation with air transport direction and ozone level (Engvall-Stjernberg *et al.*, 2012). It is known that the main ozone precursors NOx are transported to ZOTTO from industrial regions of Southern Siberia (Vivchar *et al.*, 2009). The impact of natural fires is irregular but it yields stronger plumes compared to Siberian cities (Vasileva *et al*., 2011). During severe biomass burning episodes such as during summer 2012 ozone concentration can increase nearly up to 80 ppbv (Table 1). The mean annual concentration of ozone is around 25 ppbv, while NOx is normally far below 1 ppbv.

Concentration, ppbv	[O_3]	[NO]	[NO_2]	[NOx]
Maximum*	79.3	8.359	7.250	10.090
Mean	25.6	0.080	0.619	0.686
Median	23.8	0.035	0.443	0.483
Lower 25%	18.2	0.029	0.263	0.292
Upper 25%	31.2	0.055	0.782	0.856
Standard deviation	10.2	0.219	0.611	0.690

*- minimum for all these gases is below detection limit and can be considered as “0”

Table 1. Climatology of observations of O3, NO and NO2 at ZOTTO in 2007-2015 (based on 1h averages)

Ozone surface concentration at ZOTTO has an evident seasonal course (Figure 2). The pronounced peak is observed in spring and is caused by intense stratosphere-troposphere exchange and activation of meridional transport associated with the destruction of the circumpolar vortex. This effect may be

amplified by influence of long-range transport from southern and western directions as well (Skorokhod *et al.*, 2015). Spring peak is quite stable and does not vary appreciably from year to year. In April average ozone concentration is close to 40 ppbv, and 90 percentile is within 52 ppbv. As it was found from analyses of TROICA train-based observations across Northern Eurasia such ozone seasonal variations are typical for unpolluted continental regions of Russia (Pankratova *et al.*, 2011).

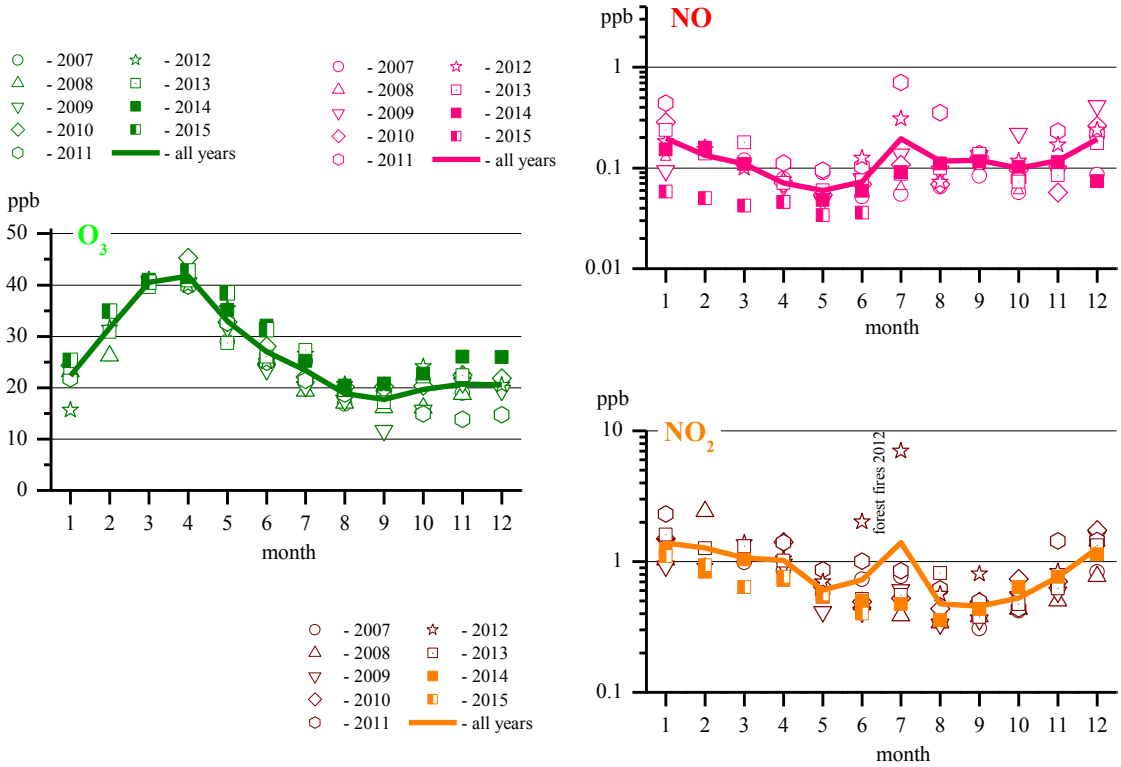

Figure. 2. Annual course by monthly averaged concentrations of O_3, NO and NO_2

Numerical simulation of ground ozone (Figure 3) and its precursors (CO, NOx) by global transport and chemical model GEOS-Chem with a fairly low resolution reproduces measured at ZOTTO concentrations pretty well (Shtabkin *et al.*, 2016), indicating the uniformity of the atmospheric photochemical systems in the boreal Eurasian zone. Significant perturbations are induced by wildfires both in the Asian and European parts of Russia, whose contribution in general prevails over long-range and regional transport from anthropogenic sources (Vivchar *et al.*, 2010).

The standard output of the GEOS-chem model was used to calculate various inputs to the regional ozone balance at both seasonal and annual scales, averaged for the period 2007 – 2012 (Table 2). To compare the ozone balance under different conditions calculations were made for the 3 regions of Northern Eurasia shown in Fig. 1. One can see considerably lower chemical activity in Siberia compared to the European territory of Russia and Western Europe and evident seasonal course for chemical production/loss and total ozone burden. Unlike the chemical generation and the sinks of ozone, its burden in Siberia does not vary significantly throughout the year. This feature is probably caused by compensating vertical and horizontal advection, however these constituents of the ozone balance should be clarified during further model runs.

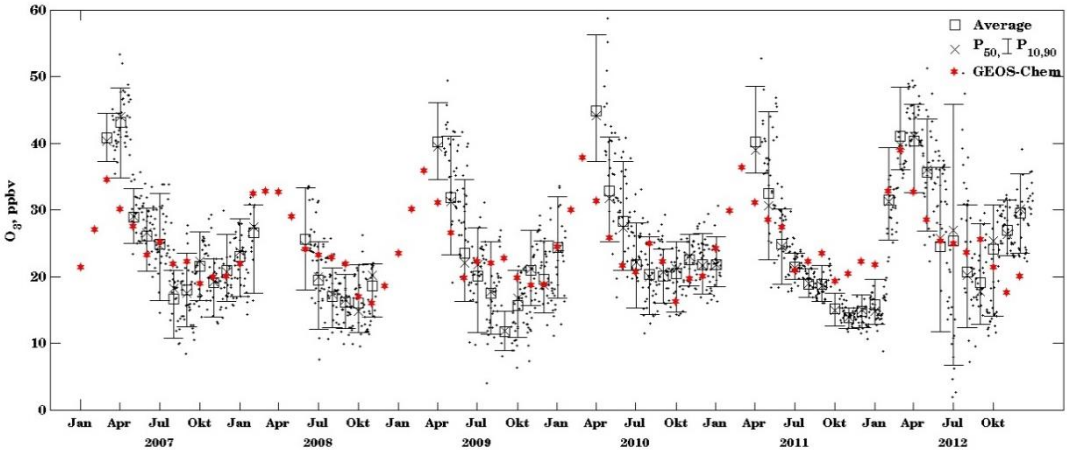

Figure 3. Comparison of surface O_3 concentrations observed at ZOTTO in 2007-2012 with those (1 month time resolution) calculated by GEOS-Chem model.

Region	Chemical production (Tg O_3 /year)	Chemical loss (Tg O_3/year)	Burden (Tg O_3)
Western Europe			
Annual	69.96	31.35	2.42
European Russia (ETR)			
Annual	46.80	17.95	1.52
Siberia			
Spring	5.99	2.12	1.65
Summer	18.45	11.91	1.64
Autumn	3.94	1.62	1.41
Winter	0.44	0.46	1.51
Annual	28.82	11.91	1.55

Table 2. Mean ozone balance in 2007-2012 in the atmospheric boundary layer calculated for Siberia and Europe by GEOS-Chem model (standard emissions).

ACKNOWLEDGEMENTS

This work was supported by the Russian Scientific Fund under grant 14-47-00049and by the Russian Academy of Sciences (Program #0150-2015-0053).

REFERENCES

Chi X. *et al* (2013) Long-term measurements of aerosol and carbon monoxide at the ZOTTO tall tower to characterize polluted and pristine air in the Siberian taiga, *Atmos. Chem. Phys*., **13**, 12271.

Engvall -Stjernberg A.-C. et al. (2012) Low concentrations of near-surface ozone in Siberia. *Tellus B*, **64**, 11607.

Heimann M. et al. (2014) The Zotino Tall Tower Observatory (ZOTTO): Quantifying Large Scale Biogeochemical Changes in Central Siberia. *Nova Acta Leopoldina*, **117**, 51.

Pankratova N.V. *et al* (2011) Ozone and nitric oxides in the surface air over Northern Eurasia according to observational data obtained in TROICA experiments. *Izv. Atm. and Ocean. Phys*. **47 (**3), 313.

Shtabkin Yu.A. *et al* (2016) Sources of and variations in tropospheric CO in Central Siberia: numerical experiments and observations at the Zotino Tall Tower Observatory. *Izv. Atm. and Ocean. Phys*. **52** (1), 45.

Skorokhod A.I. et al. (2015) Direct observations of reactive atmospheric gases at ZOTTO station in the middle of Siberia as a base for large-scale modeling of atmospheric chemistry over Northern Eurasia. *Geophysical Research Abstracts*, **17**, EGU2015-4531-1.

Vivchar A. V. *et a*l (2009) Identifying anthropogenic sources of nitrogen oxide emissions from calculations of Lagrangian trajectories and the observational data from a tall tower in Siberia during the spring–summer period of 2007, *Izv. Atm. and Ocean. Phys*. **45** (3), 302.

Vivchar, A.V. *et al* (2010) Estimates of carbon monoxide emissions from natural fires in Northern Eurasia as applied to the problems of regional air transport and climate, *Izv. Atm. and Ocean. Phys*. **46** (3), 281.

Vasileva A.V. *et a*l (2011) Assessment of the regional atmospheric impact of wildfire emissions based on CO observations at the ZOTTO tall tower station in central Siberia. *J. Geophys. Res*. **116,** D07301.

FIRST YEAR OF RESEARCH ACTIVITIES AT VILLUM RESEARCH STATION, STATION NORD, NORTH GREENLAND

H. SKOV[1,2], R. BOSSI[1,2], A. MASSLING[1,2], J.K. NOJGAARD[1,2], I.E. NIELSEN[1,2], K. VORKAMP[1,2], U. GOSEWINKEL[1,2], R. LANGE[1,2], MARIA BECH POULSEN[1,2], J.H. CHRISTENSEN[1,2], K.M. HANSEN[1,2], M. BILDE[1,3], AND M. GLASIUS[1,3], TINA ŠANTL-TEMKIV[1,4,5,6], KAI FINSTER[1,5], S. PILGAARD[1,5] AND L.L. SØRENSEN[1,5]

[1]Arctic Research Center, Aarhus University,

[2]Department of Environmental Science;
Frederiksborgvej 399, 4000 Roskilde, Denmark

[3]Department of Chemistry; Aarhus University,

[4]Stellar Astrophysics Centre, Department of Physics and Astronomy, Aarhus University

[5]Department of Bioscience, Aarhus University

[6]Department of Ergonomics and Aerosol Technology, Faculty of Engineering, Lund University, Department of Bioscience; Aarhus University.

Keywords: ARCTIC HAZE, LONG RANGE TRANSPORT, ATMOSPHERIC POLLUTION, PARTICLES.

INTRODUCTION

The main source of atmospheric pollution at Villum Research Station, Station Nord (VRS) is long range transport from sources in Eurasia (1, 2). The station has been operated since 1990 (previously called Station Nord) with a break between 2003 and 2007 (both years included). In 2013 a major grant of 9.3 mill € given by the Villum Foundation made it possible to build a new modern research Station in the High Arctic with all the facilities to host research groups from all natural science disciplines. The Station includes 6 laboratories; a "dirty" laboratory, a chemical laboratory, a microbiological laboratory and a cleaner laboratory (though not following a certified standard) and finally a house dedicated to atmospheric measurements. This house is equipped with two atmospheric monitoring laboratories and it is located 2 km from the central station complex in order to minimize local contamination. The station is located in the uppermost north-eastern corner of Greenland at 81° 36'5.26" N, 16° 39'43.31" W, 24 m ASL. The time zone is UTC -4. Polar sunset is 16th October and polar sunrise is 25th February. It is located at a small peninsula called Princess Ingeborg's Peninsula. The location is where the winter transport from Eurasia via Siberia first hit land again after being transported up over the North Pole.
There is a strong seasonal variation in the concentration of anthropogenic pollution in high Arctic. During summer there is a minimum of long range transport of air pollutants because VRS is located north of the polar front. A maximum in pollutants concentration has been observed during late winter and spring, as the polar front is located at more southern latitudes, thus opening for emission sources at mid-latitudes. This leads to a distinctive seasonal pattern with maximum concentration in late winter and spring and minimum during summer of e.g. sulphate and sulphur dioxide (1, 2). VRS is furthermore located at one of the places on Earth where the largest temperature increase is expected to occur (3). The aim of the station is to investigate the causes and consequences of a still warmer climate in High Arctic and how they affect the biosphere, atmosphere, geosphere, cryosphere and marine environment.
The first campaign year at VRS was in 2015. More than 70 scientists visited VRS and there were more than 1500 overnights at the Station. The visitors carried out a wide spectrum of research projects, see

(www.villumresearchstation.dk or http://www.asp-net.org/content/2015-station-nord-campaign#overlay-context=node/7).

METHODS

The base for the campaigns at VRS is the presence of long time series of selected pollutants (Metadata can be seen on www.villumresearchstation.dk), where the data are available for the users of the station (open source politic). As an example the time series for sulphate and sulphur dioxide is shown in Figure 1.

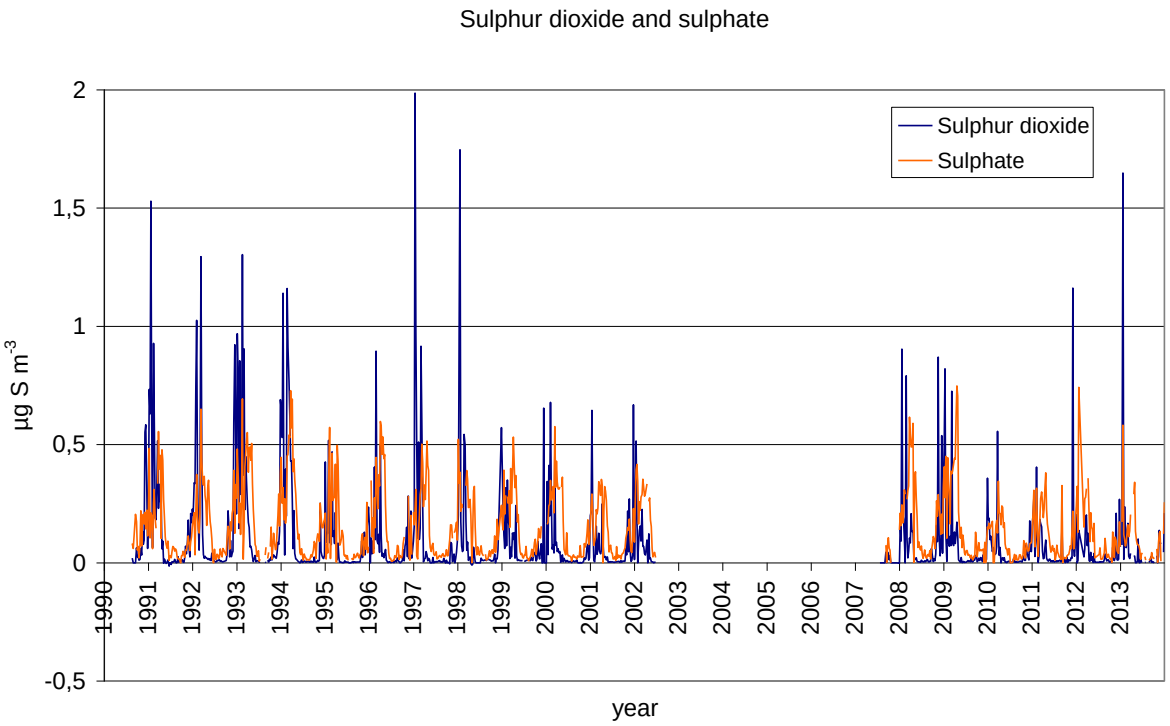

Figure 1 Time series of sulphur dioxide and sulphate concentrations at Villum Research Station, Station Nord in North Greenland.

The data have already been used to make new parameterisations of sulphur chemistry in the Danish hemispheric Model (DEHM) (1, 2, 4) but also to be a base for process oriented field campaigns (5-9) so the scientist will know the characteristics of the period where they carry out their study.

CONCLUSIONS

The atmospheric measurements were almost all carried out at the new air monitoring house, see Figure 2

Figure 2. Picture of the new air monitoring house at Villum Research Station, Station Nord located 2 km outside the central complex of Station Nord.

In the presentation some of the main atmospheric findings will be presented from the 2015 campaign with focus on black carbon and particles.

ACKNOWLEDGEMENTS

This work was financially supported by the Danish Environmental Protection Agency with means from the MIKA/DANCEA funds for Environmental Support to the Arctic Region, which is part of the Danish contribution to “Arctic Monitoring and Assessment Program” (AMAP), to the Danish research project “Short lived Climate Forcers” (SLCF) and Climate Forcers in the High Arctic. The findings and conclusions presented here do not necessarily reflect the views of the Agency. This work was also supported by the Nordic Centre of Excellence (NCoE) Cryosphere-Atmosphere Interactions in a Changing Arctic Climate (CRAICC). The Villum Foundation is acknowledged for funding the construction of Villum Research Station, Station Nord. The authors are also grateful to the staff at Station Nord for their excellent and unwavering support and the technicians Bjarne Jensen, Christel Christoffersen and Keld Mortensen for outstanding technical support.

REFERENCES

1. Heidam NZ, Christensen J, Wåhlin P, Skov H. Arctic atmospheric contaminants in NE Greenland: levels, variations, origins, transport, transformations and trends 1990-2001. Science of the Total Environment. 2004;331(1-3):5-28.
2. Nguyen QT, Skov H, Sørensen L-L, Jensen B, Grubbe A, G.Massling A, et al. Source apportionment of particulate matter at Station Nord, North East Greenland. Atmospheric Chemistry and Physics. 2013;13:35–49.
3. Stendel M, Christensen JH, Petersen D. Arctic climate and climate change with a focus on Greenland. In: Meltofte H, Christensen TR, Elberling B, Forchhammer MC, Rasch M, editors. Advances in Ecological Research, Vol 40: High-Arctic Ecosystem Dynamics in a Changing Climate. Advances in Ecological Research. 40. San Diego: Elsevier Academic Press Inc; 2008. p. 13-43.
4. Christensen JH. The Danish Eulerian hemispheric model - A three-dimensional air pollution model used for the Arctic. Atmospheric Environment. 1997;31(24):4169-91.
5. Fenger M, Sørensen LL, Kristensen K, B. J, J.K. N, Massling A, et al. Sources of Anions in Aerosols in Northeast Greenland during Late Winter. To be submitted to ACP. 2011.
6. Nguyen QT, Kristensen TB, Hansen AMK, Skov H, Bossi R, Massling A, et al. Characterization of humic-like substances in Arctic aerosols. Journal of Geophysical Research-Atmospheres. 2014;119(8):5011-27.

7. Massling A, Nielsen IE, Kristensen D, Christensen JH, Sorensen LL, Jensen B, et al. Atmospheric black carbon and sulfate concentrations in Northeast Greenland. Atmospheric Chemistry and Physics. 2015;15(16):9681-92.
8. Bossi R, Skov H. Three years (2008-2010) measurements of atmospheric concentrations of organochlorine pesticides (OCPs) at Station Nord, North East Greenland. Environmental Science: Processes and Impact. 2013;DOI: 10.1039/C3EM00304C.
9. Vorkamp K, Bossi R, Riget FF, Skov H, Sonne C, Dietz R. Novel brominated flame retardants and dechlorane plus in Greenland air and biota. Environmental Pollution. 2015;196:284-91.

RUSSIA'S CLIMATE POLICIES AND LOCAL REALITY

Y. SKRYZHEVSKA[a], V-P. TYNKKYNEN[b] and S. LEPPÄNEN[c]

[a] Department of Geography, Miami University of Ohio, Oxford, OH, USA;

[b] Department of Social Research & Aleksanteri Institute, University of Helsinki, P.O. Box 42, FI-00014 University of Helsinki, Finland;

[c] Center for Markets in Transition, Aalto University School of Business, P.O. Box 21230, FI-00076 AALTO, Finland

In their latest report, the IPCC acknowledges the importance of local governments in conducting climate change (CC) adaptation measures. However, the role of local governments has not been widely discussed in the CC policy literature. In this paper, we attempt to bridge this gap by utilizing the unique interview data from 14 Russian localities, the results of which revealed three key findings. First, the federal government of Russia recognizes the problem of CC, but due to budget constraints local authorities cannot implement adaptation actions in their regional planning. Second, only 2 of the 14 surveyed regions have a CC adaptation plan, while a few others incorporate some adaptation measures in their socio-economic development plans. Third, regions with notable agricultural, forestry and fishing sectors have experienced a more significant impact from CC on their economies, and most of the interviewed regional authorities perceived these effects as negative.

NUMERICAL MODELLING OF LAKE-ATMOSPHERE CONTINUUM IN FORESTED LANDSCAPES

V.M. STEPANENKO[1], A.V. GLAZUNOV[2], I.A. REPINA[3,4], and V.N. LYKOSOV[2,1]

[1]Lomonosov Moscow State University, Russia.

[2]Institute of Numerical Mathematics, Russian Academy of Sciences, Moscow, Russia.

[3]A.M.Obukhov Institute of Atmospheric Physics, Russian Academy of Sciences, Moscow, Russia

[4]Space Research Institute, Russian Academy of Sciences, Moscow, Russia

Keywords: LAKES, FOREST, ABL, GREENHOUSE GASES, NUMERICAL MODELLING.

INTRODUCTION

Lakes cover significant part of land surface in many regions, especially in high latitudes: in Canada, Finland, Karelia, Western Siberia, North-Eastern Siberia, etc. In the course of last decade, for adequate simulation of energy, moisture and momentum exchange between atmosphere and hydrologically heterogeneous land surface, lake models have been introduced into many Numerical Weather Prediction systems and Earth system models (ESMs) (Mironov et al. 2010; Dutra et al. 2010; Subin et al. 2012). This caused significant regional impacts on simulated weather and climate. Simultaneously, it was important to identify differences in the performance of lake model formulations involved. LakeMIP project, launched for this purpose, resulted in conclusion that the surface temperature is the lake's characteristic, fairly well reproduced by most of 1D lake models in contrasting climates, regardless the complexity of vertical diffusion scheme used (Stepanenko et al. 2013; Stepanenko et al. 2014; Thiery et al. 2014).

Meanwhile, a broad empirical evidence has been collected, arguing that inland freshwaters are a globally important component of carbon cycle due to emitting methane and carbon dioxide (Tranvik et al. 2009; Bastviken et al. 2011). Moreover, a positive feedback can be expected between global warming and greenhouse gases (GHGs) emissions from lakes, at least through lakes' temperature. Evidently, pure empirical data analysis is very limited in its capability to quantify contributions of a variety of physical and biogeochemical processes to lakes' GHG fluxes, and climate-lake feedbacks. A need for process-based lake biogeochemical models resulted in emergence of first models (Stepanenko et al. 2011; Tan et al. 2015; Tan and Zhuang 2015) of this kind, potentially capable to represent biogeochemical ties between lakes and climate system, if included in ESMs. However, a number of problems arise, considering the lake-atmosphere coupling that are partially addressed in this paper. These problems can be divided into two groups: in-lake processes and the energy and gas transfer in the atmospheric boundary layer above (Figure 1). In inhomogeneous landscapes (*e.g.*, lakes surrounded by forest), the latter problem becomes even more intricate.

In-lake processes can be generally distinguished as biotic and abiotic. Biotic processes include methane production by *Archaea*, methane oxidation, photosynthesis, biochemical and sedimentary oxygen demand. The key abiotic factors are water temperature and turbulence characteristics. The temperature of sediments is crucial, as methane production is exponentially dependent on temperature. In this connection, it is important that 1D lake models may predict bottom temperature with errors of several degrees (Stepanenko et al. 2013). This is primarily caused by inaccuracies of turbulence closure used in a lake model. Note, that imperfect turbulence closure in a water object would lead to erroneous methane and CO_2 transport from the bottom (where they are produced) to the atmosphere. Extremely stable stratification in metalimnion of

lakes in summer, with Ri >> 0.25, poses a question of possibility for gas transfer either by weak turbulence (Zilitinkevich et al. 2012) or by breaking of internal waves (MacIntyre et al. 2009). Vertical mixing in a lake is very sensitive to momentum flux from the atmosphere. For small lakes, the surface wave field is non-saturated in respect to wind, and a fraction of momentum flux from above is consumed by wave development (Lin et al. 2002) that reduces shear-production of turbulence in a lake and the mixed-layer deepening (Stepanenko et al. 2014). In turn, less turbulence in the surface mixed layer decreases the gas exchange at the air-water interface, as for CH_4 and CO_2 this exchange is controlled at the liquid side (Donelan and Wanninkhof 2002). The situations complicates, when the water body is enclosed by bluff topography, such as forest, that violates conditions of applicability of Monin-Obukhov similarity theory (MOST). On the other hand, such heterogeneous landscape limits usefulness a widespread direct eddy covariance (EC) method for measuring turbulent fluxes, as a significant portion of footprint may fall outside a lake. As a consequence, heat balance of a lake does not close (Nordbo et al. 2011). Moreover, the footprint calculation itself becomes less tractable with standard footprint models.

In this paper, we elucidate the problems stated above with the results of our recent research, and draw perspectives for future studies.

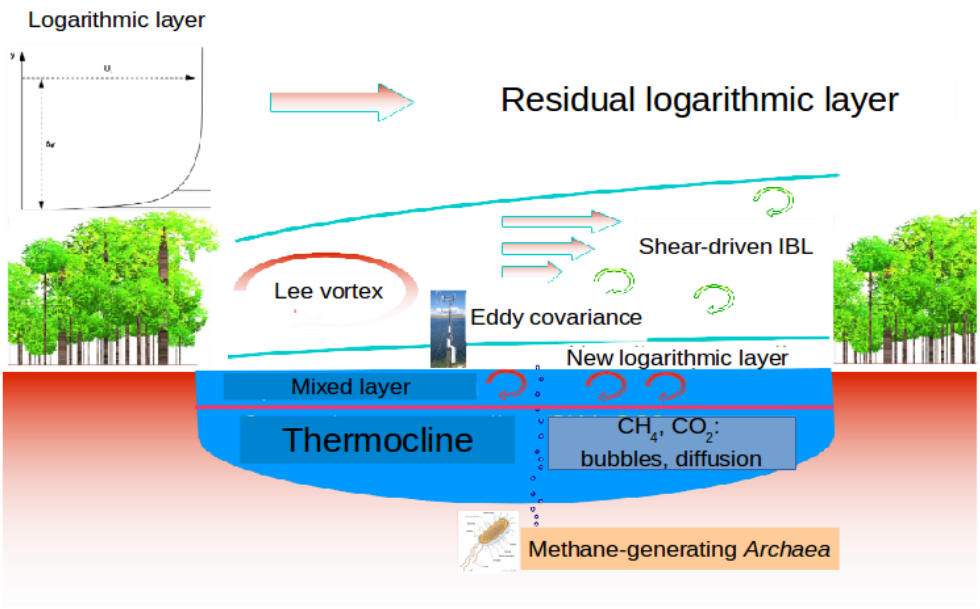

Figure 1. Schematic for key processes regulating dynamic, thermodynamic and biogeochemical interaction between the atmosphere and lake in a forested landscape

LARGE EDDY SIMULATION OF ATMOSPHERIC BOUNDARY LAYER ABOVE A LAKE

We performed a large eddy simulation (LES) study of atmospheric boundary layer (ABL) developing over a lake, surrounded by a forest (Glazunov and Stepanenko 2015). The LES model was that of Institute of Numerical Mathematics, Russian Academy of Sciences (Glazunov et al. 2010; Glazunov 2014). The forest was represented as a set of parallelepipeds, explicitly resolved on the model's grid. A special experimental setup ensured a flow entering the domain to possess statistics of stationary ABL above forest. The lake was of elliptical shape with semiaxes of 200 m and 60 m, the “tree” heights varied in different experiments from 8 to 16 m, and the finest regular mesh resolution was 0.5 m. The temperature difference between the lake surface and the atmosphere was set to 5 K or -5 K. Calculations were performed on “Lomonosov” supercomputer of Lomonosov Moscow State University (Sadovnichy et al. 2013).

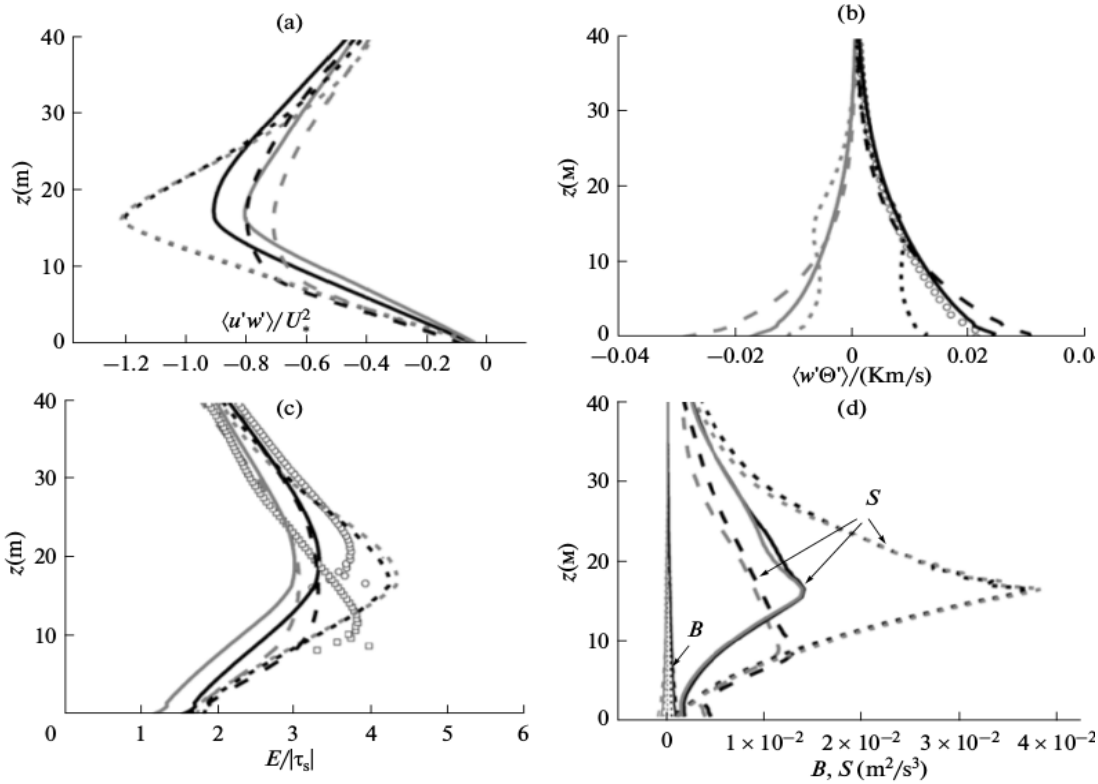

Figure 2. (adopted from (Glazunov and Stepanenko 2015)). Profiles of lake-area-averaged turbulence characteristics. (a) Vertical turbulent momentum flux normalized to the squared friction velocity, (b) turbulent flux of potential temperature, (c) turbulent kinetic energy (TKE), and (d) shear generation *S* and buoyancy generation *B* of TKE. Wind blows along the lake, the tree height is 16 m (solid line); wind blows along the lake, the height is 8 m (dashed line); and wind blows across the lake, the height is 16 m (dotted line). Grey curves denote stable stratification. Black curves mark unstable stratification. Circles in (b) show heat flux in the run with a coarse grid. Squares and circles in (c) show TKE in the windstream.

The three important conclusions may be inferred from these results. First, the flow and its turbulent statistics are very inhomogeneous in horizontal. Second, the constant-flux layer is very shallow, so that at typical height of measurements above water (1.5 – 2 m), momentum flux differs twice from that at the surface. And third, the absolute value of fluxes appears to be insensitive to stratification, because shear production of turbulent kinetic energy dominates over that by buoyancy. Thus, MOST fails to represent vertical fluxes in such case.

MEASUREMENTS OF TURBULENCE INHOMOGENEITY OVER A LAKE

Motivated by LES experiments we conducted a field experiment aiming to get the features of real turbulent flow over a lake, surrounded by canopy. We installed EC measurements in 6 points on a small lake of *ca.* 100 m length bounded by forest and located nearby the White Sea Biological Station of Moscow State University (Figure 3, left): three of them were 2D wind sensors and three were 3D ones. At the central point, two 3D sonic anemometers were mounted at different heights. The measurements were continuously run for 5 days. Results of these observations corroborate the following LES-derived conclusions (Figure 3, right): (i) the ABL is horizontally inhomogeneous in terms of both first moments (wind speed, not shown) and second moments (TKE, not shown, and vertical fluxes); (ii) the constant-flux layer does not exist (or is very thin) over a lake. Evidently, the significant vertical variability of fluxes is at least partially caused by horizontal advection in heterogeneous landscape. Moreover, our measurements suggest that the heat flux may change sign either in horizontal or in vertical.

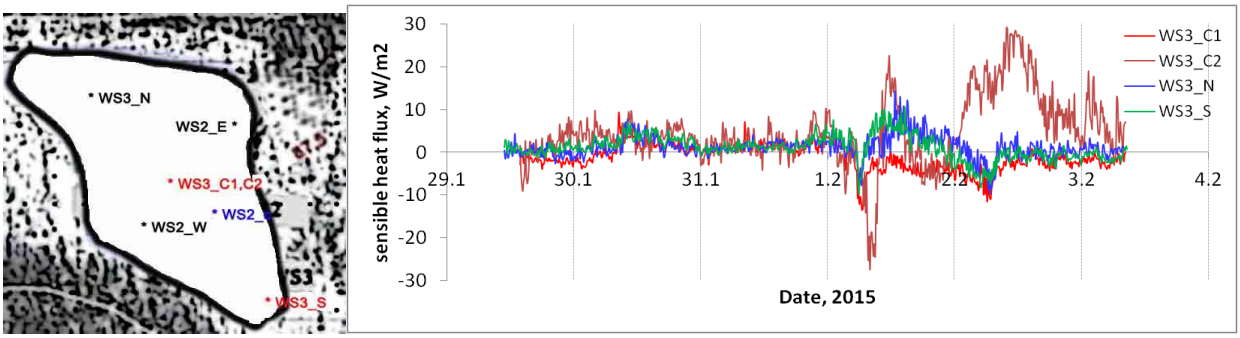

Figure 3. Eddy covariance measurements over Verkhnee Lake, Kindo peninsula, White Sea coast. *Left*: locations of sonic anemometers: WS2_* labels mark 2D sensors, WS3_* – 3D anemometers, "WS3_C1,C2" denotes central point with two levels of measurements. *Right*: sensible heat flux at different points and heights, from 29.01.2015 to 03.02.2015.

MODELLING THE THERMAL REGIME AND GREENHOUSE GASES IN LAKES

From a lake modelling perspective, calculation of surface heat and momentum fluxes has not been identified as a significant problem in lake temperature simulation. These models have been used *inter alia* for small lakes surrounded by forest with surface flux scheme based on MOST, and were successful in capturing seasonal cycle of lake's temperature (Stepanenko et al. 2014; Manrique-Suñén et al. 2013; Heiskanen et al. 2015) and GHGs dynamics (Stepanenko et al. 2016). However, for small Valkea-Kotinen Lake (Finland) which served as a prototype for LES simulations described above, in some lake models surface drag coefficient was tuned or the scheme for split up of momentum flux was applied (Stepanenko et al. 2014). This was done to avoid unrealistic mixed-layer deepening. Nonetheless, no need was identified for correcting MOST sensible or latent heat flux schemes to get realistic seasonal temperature course.

CONCLUSIONS

Thus, we arrive to a seeming contradiction between LES simulation of ABL, EC measurements and laboratory results (Markfort et al. 2014) at one side, all arguing for drastic violation of MOST over lakes in forested landscapes, and, on the other side, a practice of 1D lake modelling, that is successful in representing thermal regime on seasonal and synoptic time scales, using MOST-based schemes. To explain this contradiction, one can expect that errors of MOST schemes of different signs may compensate on large time scales, or that the errors of surface flux schemes in a *coupled* system should reduce. Indeed, if the exchange coefficient for heat is under- or overestimated, the surface temperature in a lake model should adjust in a way to reduce flux error. If we consider the corresponding adjustment of the air temperature, it may add one more "degree of freedom" to a system for compensating the flux error.

ACKNOWLEDGEMENTS

The authors are grateful to Russian Foundation of Basic Research for partial financial support of this study (grants 15-35-20958, 14-05-91752, 14-05-00510, 14-05-00038, 14-05-91754).

REFERENCES

Bastviken, D. et al., 2011. Freshwater Methane Emissions Offset the Continental Carbon Sink. *Science*, 331(6013), p.50. Available at: http://www.sciencemag.org/content/331/6013/50.abstract.

Donelan, M.A. and Wanninkhof, R., 2002. Gas Transfer at Water Surface --Concepts and Issues. In *Gas Transfer at Water Surfaces*. American Geophysical Union, pp. 1–10.

Dutra, E. et al., 2010. An offline study of the impact of lakes on the performance of the ECMWF surface scheme. *Boreal Environment Research*, 15, pp.100–112.

Glazunov, A. V., 2014. Numerical simulation of stably stratified turbulent flows over flat and urban surfaces. *Izvestiya, Atmospheric and Oceanic Physics*, 50(3), pp.236–245. Available at: http://link.springer.com/10.1134/S0001433814030037 .

Glazunov, A.V., Dymnikov, V.P. and Lykossov, V.N., 2010. Mathematical modeling of spatial spectra of atmospheric turbulence. *Russian Journal of Numerical Analysis and Mathematical Modelling*, 25(5), pp.431–451.

Glazunov, A.V. and Stepanenko, V.M., 2015. Large Eddy Simulation of Stratified Turbulent Flows over Heterogeneous Natural Landscapes. *Izvestiya, Atmospheric and Oceanic Physics*, 51(4), pp.351–361. Available at: http://link.springer.com/article/10.1134/S0001433815040027.

Heiskanen, J. J., I. Mammarella, A. Ojala, V. Stepanenko, K.-M. Erkkilä, H. Miettinen, H. Sandström, W. Eugster, M. Leppäranta, H. Järvinen, T. Vesala, and A. Nordbo (2015), Effects of water clarity on lake stratification and lake-atmosphere heat exchange. J. Geophys. Res. Atmos., 120, 7412–7428. doi: 10.1002/2014JD022938.

Lin, W. et al., 2002. Drag Coefficients with Fetch-Limited Wind Waves*. *Journal of Physical Oceanography*, 32(11), pp.3058–3074. Available at: http://dx.doi.org/10.1175/1520-0485(2002)032<3058:DCWFLW>2.0.CO.

MacIntyre, S. et al., 2009. Turbulent mixing induced by nonlinear internal waves in Mono Lake, California. *Limnology and Oceanography*, 54(6), pp.2255–2272. Available at: http://aslo.org:8081/lo/toc/vol_54/issue_6/2255.pdf.

Manrique-Suñén, A. et al., 2013. Representing Land Surface Heterogeneity: Offline Analysis of the Tiling Method. *Journal of Hydrometeorology*, 14(3), pp.850–867. Available at: http://dx.doi.org/10.1175/JHM-D-12-0108.1.

Markfort, C.D., Porté-Agel, F. and Stefan, H.G., 2014. Canopy-wake dynamics and wind sheltering effects on Earth surface fluxes. *Environmental Fluid Mechanics*, 14(3), pp.663–697. Available at: http://dx.doi.org/10.1007/s10652-013-9313-4.

Mironov, D. et al., 2010. Implementation of the lake parameterisation scheme FLake into the numerical weather prediction model COSMO. *Boreal Environment Research*, 15(2), pp.218–230.

Nordbo, A., S. Launiainen, I. Mammarella, M. Leppäranta, J. Huotari, A. Ojala, and T. Vesala (2011), Long-term energy flux measurements and energy balance over a small boreal lake using eddy covariance technique, J. Geophys. Res., 116, D02119, doi:10.1029/2010JD014542.

Sadovnichy, V. et al., 2013. ”Lomonosov”: Supercomputing at Moscow State University. In *Contemporary High Per formance Computing: From Petascale Toward Exascale*. pp. 283–307.

Stepanenko, V. et al., 2014. Simulation of surface energy fluxes and stratification of a small boreal lake by a set of one-dimensional models. *Tellus, Series A: Dynamic Meteorology and Oceanography*, 66(1).

Stepanenko, V.M. et al., 2013. A one-dimensional model intercomparison study of thermal regime of a shallow, turbid midlatitude lake. *Geoscientific Model Development*, 6(4), pp.1337–1352. Available at: http://www.geosci-model-dev.net/6/1337/2013/gmd-6-1337-2013.html.

Stepanenko, V.M. et al., 2011. Numerical modeling of methane emissions from lakes in the permafrost zone. *Izvestiya, Atmospheric and Oceanic Physics*, 47(2), pp.252–264. Available at: http://link.springer.com/10.1134/S0001433811020113.

Stepanenko, V.M. et al., 2016. A model for temperature, methane, carbon dioxide and oxygen dynamics in lakes. Submitted to *Geoscientific Model Development*.

Subin, Z.M. et al., 2012. Boreal lakes moderate seasonal and diurnal temperature variation and perturb atmospheric circulation: analyses in the Community Earth System Model 1 (CESM1). *Tellus A*, 64. Available at: http://www.tellusa.net/index.php/tellusa/article/view/15639/xml.

Tan, Z. and Zhuang, Q., 2015. Arctic lakes are continuous methane sources to the atmosphere under warming conditions. *Environmental Research Letters*, 10(5), p.054016. Available at: http://stacks.iop.org/1748-9326/10/i=5/a=054016.

Tan, Z., Q. Zhuang, and K. W. Anthony (2015), Modeling methane emissions from arctic lakes: Model development and site-level study, J. Adv. Model. Earth Syst., 7, 459–483, doi:10.1002/2014MS000344.

Thiery, W. et al., 2014. LakeMIP Kivu: evaluating the representation of a large, deep tropical lake by a set of one-dimensional lake models. *Tellus, Series A: Dynamic Meteorology and Oceanography*, 66.

Tranvik, L.J. et al., 2009. Lakes and reservoirs as regulators of carbon cycling and climate. *Limnol. Oceanogr.*, 54(6), pp.2298–2314.

Zilitinkevich, S.S. et al., 2012. A Hierarchy of Energy- and Flux-Budget (EFB) Turbulence Closure Models for Stably-Stratified Geophysical Flows. *Boundary-Layer Meteorology*, 146(3), pp.341–373. Available at: http://link.springer.com/10.1007/s10546-012-9768-8.

THE PROJECT "LAKE ONEGO AND ITS WATERSHED: GEOLOGICAL HISTORY, ANTHROPOGENIC TRANSFORMATION AND CURRENT STATE", PRELIMINARY RESULTS

D.A. SUBETTO, N.A. BELKINA, N.M. KALINKINA, G.S. BORODULINA, A.I. SIDOROVA, A.U.TARASOV, M.S. POTAKHIN, M.B.ZOBKOV, N.N. FILATOV, M.S. BOGDANOVA, V.N. BAKLAGIN, A.V. LITVINENKO, T.S SHELEKHOVA, U.U. FOMINA AND N.B.LAVROVA

Northern Water Problems Institute Karelian Research Center RAS
Russia

Keywords: PALEOGEOLIMNOLOGY, WATER RESOURCES, HYDROGEOLOGY, GEOECOLOGY, HYDROBIOLOGY.

INTRODUCTION

Lake Onego is the second largest lake in Europe. The fundamental scientific problem the project is aimed, integrates the research of the historical development of Onego Lake, the dynamics of catchment area development and the current state of the lake. The project is being developed for study of the patterns and changing of Lake Onego ecosystem under influence of anthropogenic and climatic factors. The multipurpose use of lake and water consumption should have a scientific basis. The project include paleogeographic, archaeological, geochemical investigations of catchment area and paleolimnological, geoecological, hydrobiological researches of Onego Lake.

METHODS

The history and evolution of Lake Onego since deglaciation and in the present time are revealed as a result of paleogeographic investigations, based on the study of sediment cores. More exact dating of bottom sediments are obtained. Detailed paleogeographic reconstruction of lake and its watershed development are performed. Paleogeographic maps for individual time periods are formed, the main hydrological characteristics of the lake at different stages of its development are calculated using ArcGis and Surfer. The history of human habitation on the shores of Onego Lake are identified on the base of radiocarbon dating of calcinated bones from archaeological sites located on the different highest hypsometric positions. Chemical analyses of water and sediments and biological parameters were performed in accordance with the guiding documents of the Ministry of natural resources and ecology of the Russian Federation (Manual..., 2009).

RESULTS

Search the earliest archaeological sites in the south-east coast was continued. Radiocarbon dating of calcinated bones from archaeological sites of the northern shore of Onego Lake located on the highest hypsometric positions provided evidences of human habitation on the shores of Onego Lake during the Late Preboreal and at the turn of Preboreal / Boreal periods (Tarasov, 2014, 2015).
Technology of construction paleoreconstructions and calculation of basic morphometric characteristics of the lake using ArcGis and Surfer and have been developed and applied in practice. Reconstructions of the main stages in the development of Lake Onego in the the late-glacial period been met. Basic morphometric characteristics of Lake Onego in the present condition and its mirror for a number of historical periods have been identified (http://onegolake.ru; http://www.arcgis.com/apps/MapJournal index.html?appid=47d76ba2004e463d96eba1d8a1825fe1).

Database of sediments of the Onego Lake and small lakes located within its basin has been extended. Paleoecological and paleoclimatic reconstruction of the lake Sjirgozero were made on the basis of spore-pollen and diatom analyses of bottom sediments.
Estimates of average annual and seasonal isotopic composition of precipitation based deposition patterns in time were clarified. Average compositions of precipitation of the cold period of the year, reaching for the spring runoff were calculated. The main spring replenishment of groundwater was estimated. The amount of evaporation during the warm period of the year and the dynamics of changes in the isotopic composition of the water due to the occurrence of this process under natural conditions were evaluated. The equations of change in isotopic composition of residual water upon evaporation at different temperature conditions were obtained. The dependence of the angular coefficient of the equations from average daily air temperature was set. The average isotopic composition of river runoff on the results of the weekly (daily during high) observations r. Neglinka was evaluated. The chronological graphs of the isotopic composition of river water that reflects the power structure of the watercourse were obtained. Monitoring the isotopic composition of waters of the Petrozavodsk Bay of Onego lake and its tributaries allowed us to assess the intensity of its seasonal water exchange (Borodulina, 2015). Groundwater with anomalously light isotopic composition were revealed that allowed us to estimate paleotemperature conditions in the area of nutrition.
Characterization of the structure of the water balance of Lake Onego, a characteristic of modern economic use of water bodies of catchment of (water, wastewater) and their retrospective analysis are given on the basis of GIS-technologies. Map-scheme of distribution of water loads for the catchment area is built.The features of transformation of hydrological regime, water balance elements and the level of the lake under influence of climate changes were assessed. Calculations of changes in the hydrological regime of the lake are made. Forecasts for 10-30 years under different scenarios of regional climate change are obtained. On the basis of model experiments forecasts lake ecosystem change under different scenarios of nutrient loading are given. The level of permissible anthropogenic load on the main pollutants and biogenic elements are determined. Recommendations on minimization of risks of emergence of emergency situations of ecological character that may lead to pollution of lakes and damage was developed.
According the data obtained in 2015 the most toxic sediments were found in Kondopozskaya Bay, Petrozavodskaya Bay, Unizkaya Bay, in the Central Part of Lake Onego. The supernatant liquid which was obtained in the bioassay of Kondopozskaya Bay sediments was characterized by the lowest pH values. It determines by influence on the Bay of pulp and paper mill wastewater. Overall, the bioassay results of 2015 agree well with the data on 2014. Based on the analysis of data for the years 1989-2014 the decrease in the total number of macrobenthos organisms 4 times was found. This decline coincided with the fall of 1.76 times the anthropogenic load on the bay. Thus, it was found that at the present time the oligotrophization of Lake Onego occurs. It is shown that the main phases of primary production cycle in the pelagic zone of Lake Onego depend on cyclical geographic environmental factors (temperature and incident solar radiation). The seasonal primary production maximum is formed by non-diatom phytoplankton chlorophyll. The development of non-diatom phytoplankton is limited to low concentrations of phosphorus in the water. The criteria of primary production stability in Lake Onego are proposed. Analysis of the phytoplankton community data in Lake Onego in the period 1964-2011 showed that the phytoplankton abundance and biomass in 1990s were on average 1.5 times higher than in the 2000s. The next period (2005-2011) is characterized by the weakening of anthropogenic impact on the Lake. Reducing of the anthropogenic eutrophication of the lake in recent years has led to an decrease in phytoplankton productivity and trends in the transition to oligotrophic stage (Kalinkina, etc 2015; Sidorova, 2015). The generalization of bacterial communities data for Lake Onego during 40 years period is done. It is shown that in the area of Kondopozskaya Bay, polluted by pulp-and-paper wastewaters, the maximum degree of quantitative indicators variability is observed. It is connected with the dynamics of anthropogenic load on the Bay. In the 2000s compared to the 1990s the destruction of organic matter increased, 3-fold rise of bacteria biosynthetic activity was determined. In the central part of Lake Onego the noticeable quantitative changes of bacterioplankton was identified too. In the 1980s the grown of the saprophytic bacteria was found there. Since the beginning of the 90s, after entering of the biological treatment of municipal wastewater in the industrial center of Petrozavodsk, and currently there is decline in bacterial numbers.

Analysis of changes in the chemical parameters of the surface layer of sediments of Lake Onego as a result of anthropogenic impact was performed. The change in the distribution of quantitative and qualitative composition of organic matter, nutrients, iron and manganese in the surface layer of sediments is an indicator of production processes in lake. Revealed that the distribution of sediment physical characteristics and content elements of the mineral part of sediments are indicators of land management and operation of mining enterprises in the catchment of Lake Onego. Analysis of the data showed that the dynamics of changes in concentrations of phosphorus in sediments of Lake Onego for the past 40 years corresponds to the nature of changes in the external phosphorus load and is determined by the processes of eutrophication of the lake. The decrease in the concentration of phosphorus in sediments in the last decade indicates a stabilization of the ecosystem of lake Onego after a period of intensive eutrophication in the late eighties. A new integrated approach to the calculation of the internal nutrient load, based on the evaluation of the layer thickness of sediments involved in the active exchange of matter with the water column was developed and applied in practice. Assessing internal phosphorus load in Lake Onego revealed its decrease compared to the beginning of the century. It is shown that the accumulation and retention of phosphorus by iron compounds in the sediments is a geochemical mechanism hindering the development processes of eutrophication (Belkina, 2015).
Website of "Lake Onego" was developed (http://onegolake.ru).
The monograph "The Largest lake-reservoir North-West of European Russia: current state and changes of ecosystems under climatic and anthropogenic influences" was published.

ACKNOWLEDGEMENTS

The study has been financially supported by the Russian Science Foundation (#14-17-00766).

REFERENCES

Anastasiya Sidorova. Distribution and population characteristics of Baikalian invader Gmelinoides fasciatus (Crustacea: Amphipoda) in lake Onego. 4th European Large Lakes Symposium. Ecosystem Services and Management in a Changing World. August 24-28, 2015, Joensuu, Finland. P. 30-31.

Borodulina G.S. Investigation of hydrology of catchment area of small river in Karelia (Russia) by high-resolution record of δ2H and δ18O in precipitations and river water, including experimental evaluation of evaporation. Book of extended synopses. International Symposium on Isotope Hydrology: Revisiting Foundations and Exploring Frontiers. Poster session 3. Vienna (2015 г.)

Kalinkina N.M., Sidorova A.I., Galibina N.A., Nikerova K.M. The toxicity of Lake Onego sediments in connection with the natural and anthropogenic factors influence // Environment. Technology. Resources. Proceedings of the 10th International Scientific and Practical Conference. June 18-20, 2015. Volume 2. Rezekne: Rezeknes Augstskola, 2015. P. 124-127.

Manual on chemical analysis of surface waters. Part1/under.ed. Baeva L.V.. - Rostov-on–Don. NOK-2009. -1044p.

Natalia Belkina The chemical composition of sediments as indicator of changes in the ecosystem of Lake Onega under the influence of anthropogenic factors / Keynote presentations of 4th European Large Lakes Symposium August 24-28, 2015, Joensuu. P.14.

Tarasov A. Spatial separation between manufacturing and consumption of stone axes as an evidence of craft specialization in prehistoric Russian Karelia // Estonian Journal of Archaeology, 2015. №19(2), pp. 83-109.

Tarasov A., Choroshun T., Zobkov M. Geoarchaeology of Onega Lake: Current state of research and prospections for future work // Paleolimnology of Northern Eurasia. Proceedings of the international conference. Petrozavodsk, 21-25 September 2104. Petrozavodsk, 2014. P. 109.

The Largest lake-reservoir North-West of European Russia: current state and changes of ecosystems under climatic and anthropogenic influences. Petrozavodsk, KRC press. 2015. 375 p.

ADAPTOGENESIS OF OAT (AVENA SATIVA L.) TO OIL POLLUTION OF SOIL

A.M. SUBBOTIN, M.V. NARUSCHKO, A.S. BAZHIN, S.A. PETROV, L.F. KALENOVA

Tyumen Scientific Center SB RAS, 625026, 86,Malygina str., Tyumen, Russia

Keywords: adaptogenesis, Avena sativa L., oil pollution of soil

INTRODUCTION

Is actively conducted searching for ways and methods to increase the adaptive properties of plants in the conditions of soil pollution by hydrocarbons. This is due to anthropogenic impact on phytobiocenosis in the development and exploitation of oil and gas complex. Oil contamination of the environment in varying degrees leads to oppression, degradation, and sometimes complete loss of vegetation (Petukhova, 2008). One way of solving this problem is the use of biological fertilizers and phyto-stimulants on the basis of micro-organisms. Over the past decade, based on bacteria of the genus Bacillus derived a number of drugs that increase the productivity of plants (Fitosporin-M, Bactofit, Gamair, Integral, and other) and can increase their adaptive properties. Is actual a searching of the natural activators of the biological potential of plants based on strains of bacteria isolated from permafrost. Microorganisms from the permafrost preserve their viability for a long time at low temperatures and slow metabolism, adapted to the adverse environmental factors, have high adaptability to soil and climatic conditions of Western Siberia. Their impacts on the eco phenotypic parameters of modern organisms are virtually unexplored. On this issue, there are only the first studies (Brouchkov, Melnikov, Sukhovei et al., 2011; Enoktaeva, Kalenova, Subbotin, 2014). Purpose of work - estimate the effect of some strains of bacteria of the genus Bacillus, isolated from the permafrost on the morphological and physiological indicators of Avena sativa L. in oil contamination of the soil conditions.

METHODS

An experimental study was conducted in 2013 on the seeds of Avena sativa L. We used strains of microorganisms of the genus Bacillus, selected by us from the IMF Western and Eastern Siberia and the identifying of sequencing method 16S RNA: B1M -Bacillus sp., B1T - Bacillus megaterium, B2CH - Bacillus pumilus. Initial 16S RNA resulting sequence was compared with the GenBank database, using BLAST database (Altschul et al., 1997). Editing sequences was performed using BioEdit (Saitou, 1987; Tamura, 2007). For the experiment, the density of the suspension of bacterial cultures was adjusted to the working concentration $1x10^7$ microbial cells / ml (m.c./ml). The resulting suspension was carried presowing grains Avena sativa L .. The plants were grown for 20 days. To simulate the oil-contaminated soil sample used oil GOST 5185-2002. Oil in an amount of 2, 5, 10 grams were added, respectively, in 98, 95, 90 grams of pure sand and mixed thoroughly. Treated seed of oat were seeded on previously contaminated with oil products (in the required concentration) soil. In each embodiment of the experiment planted 100 seeds. In control embodiments seeds sown on a clean, not contaminated soil - control-1 (K-1); in the control-2 (K-2) - the seeds were sown on the oil-contaminated soil without seed treatment a bacteria suspension. The seeds are germinated at + 22 ° C and natural photoperiod duration. The germination of the seedlings was evaluated by 5, 10, 15, 20 days. On the 20 days study, we measured morphometric parameters. Measured: the number of roots, the maximum length of the root, coleoptile and stem sprout length, the number of leaves, length and width the first leaf, the area of the lamina, the sprout mass and root mass. (Daniel, Gustavo, 1991). Assess the content of photosynthetic pigments: chlorophyll a (chl. *a*), b (chl. *b*) and carotenoids (*k*). The content of chlorophyll *a*, *b* and carotenoids were determined by spectrophotometry. Statistical processing of the data was performed using the program «SPSS ver. 11.5.for Windows ».

Evaluation of germination Avena sativa L. has shown that the oil pollution of soil (C-2) there is a significant inhibition of germination. Processing of seeds bacterial suspension in two variants of the experiment did not lead to an increase in germination. In the treatment of seed a bacteria suspension of strain B1M, germination on oil-contaminated soil was 2-4 times higher than in the Control-2. At 2% of oil contamination of the substrate found to, the reducing of almost all the studied parameters compared to C-1. Compared with the Control-2 was an increase in the length of the sprout (strain B1T); length of the first leaf (all tested strains), width and area the first leaf (strain B1T); number (all the test strains), and the mass of roots (B1T strains and B2CH). At 5% of oil contamination substrate observed increase in the mass of roots in seedling Avena sativa L., processed B1M and B2CH strains, as compared to Control-1. Regarding Control-2 are observed increase of the number of roots (B1M and B1T strains) and the mass of roots (B1M and B2CH strains). Morphometry of oat plants at a 10% contamination of the soil was revealed an increase number and masses of seedlings, processing B1M strain, as compared to Control-1. Regarding Control-2 there is an increase in length sprouts (strains B1M and B2CH), coleoptile length, length and area the first leaf (strain B1M). Was observed the increase in the length and number of roots (B1M and B2CH strains), increase in the mass of roots (B1M and B2CH strains) and the mass sprouts (strain B1M). Absorption of light quanta in the visible spectrum (400-700 nm), which have sufficient energy for photosynthesis, have the organic compounds - pigments.

Analysis of the content of pigments of photosynthesis in Avena sativa L. at 2% of the soil pollution model (Table 1) showed an increase in the basic chlorophyll *a* (strains B1M and B2CH) and auxiliary chlorophyll *b* (B1T strain) on the Control-2.

Variants of the experiment	Percentage of contamination	Chlorophyll *a*	Chlorophyll *b*	*k*
Control -1	Without oil	62,04	47,44	41,40
Control - 2	2%	57,33	30,46	37,48
	5%	62,59	32,09	41,74
	10%	34,93	17,44	34,71
B1M	2%	42,38	22,13	37,46
	5%	41,78	20,65	38,73
	10%	27,59	17,31	31,43
B1T	2%	30,40	29,03	36,96
	5%	39,29	17,45	33,63
	10%	22,56	16,37	23,45
B2CH	2%	45,44	22,87	35,29
	5%	38,07	17,88	33,00
	10%	22,25	17,30	37,85

Table 1. Contents of photosynthetic pigments (mg / 100 g) in seedlings Avena sativa L.

This shows less inhibition of the photosynthetic system of seedlings. At 5% of oil pollution there is an increase in chlorophyll content and in all variants of the experiment compared to the control-2. An increasing carotenoids content in the experimental variant treated B1M strain,that indicating a greater ability strain B1M to neutralize the damaging effect of hydrocarbons. At contamination of the substrate 10% of oil, an increase in the content of chlorophyll *a* and *b* in seedlings Avena sativa L., treated the strain B1M, compared to the control -2. Increased content of carotinoids in the embodiment, the treated B1T strain, compared with the two controls. Thus, for preplant treatment of seeds Avena sativa L. strains of bacteria have the increase of basic chlorophyll a. This indicates an increase activity of the photosynthetic system, particularly at the 5% level of soil contamination. We observe the increasing the content level of carotenoids, which indicates the activation of protective antioxidant systems of plants and ability to neutralize the damaging effect of hydrocarbons. During the study found that the most promising as a further development of the phyto-stimulants are strains B1M and B2CH and strain B1T. Seed germination of oat treated by strain B1M (2% and 10% of soil contamination), significantly higher than the Control-2

(P <0.05). Morphometric analysis the data obtained showed that oat seedlings under the influence of strain B1M significantly (P <0.05) increase the following parameters: the length of the sprout, the mass sprout and weight of roots for soil pollution 10% and the number of root at 5% contamination. The action of the strain B1T significantly (P <0.05) increased sprout length, root mass, the width of the first leaf when soil is polluted by 2%. In the embodiment with the strain B2CH increased (P <0.05) length of the first leaf, root length and weight of roots at 2% contamination; root length, number of roots and root mass at pollution of 10%. A study of the photosynthetic system found that at high soil pollution oil (10%), oat seedlings suffer the smallest stress during processing strains B1M, B1T, B2CH compared to the Control-2.

Thus, some strains of bacteria isolated from the IMF, has a positive effect on growth and development of oat seedlings under conditions of oil pollution.

REFERENCES

Petukhova G.A. (2008) *Mechanisms of resistance to oil pollution protection* (Tyumen: Tyumen State University Publishing).

Sidorenko O.D., Voyno L.I. (1999) The use of microorganisms of the rhizosphere as a promising bacterial drug for cropping. *Bulletin of TSU*, **4(1),** 87-91.

Brouchkov A. V., Melnikov V. P., Sukhovei Yu. G. et al. (2011) Relict Microorganisms of Cryolithozone as Possible Objects of Gerontology. *Advances in Gerontology*. **1(1)**, 39–44.

Subbotin A.M., Gnatchenko L.N., Petukhova G.A. (2011) A study of physiological parameters of the culture of ciliates Paramecium caudatum under the influence of bacterial culture filtrate genus Acinetobacter. *Bulletin of the Orenburg State University*, **12**, 149-150.

Subbotin A.M., Kalenova L.F., Bazhin A.S. (2012) The influence of some strains of bacteria isolated from permafrost on the immune and physiological parameters of mice. *Bulletin of the Ural Medical Academia*. **4**, 164

Kalenova L.F., Novikova M.A., Subbotin A.M., Bazhin A.S. (2015) Effekts of Temperature on Biologikal Activity of Permafrost Microorganisms. *Bulletin of Exsperimental Biology and Medicine*. **185(6)**, 772-775.

Kalenova L.F., Novikova M.A., Subbotin A.M. (2015) Effects of permafrost microorganisms on skin wound reparation. *Bulletin of Experimental Biology and Medicine*. **158(4)**, 478-482.

Enoktaeva O.V., Kalenova L.F., Subbotin A.M. (2014) Effect metabolites Bacillus sp. from permafrost on the survival of fish embryos. *Bulletin of the Tyumen State University*. **12.**

FUTURE EARTH: CO-DESIGNING GLOBAL CHANGE RESEARCH TO RESPOND TO GRAND SOCIETAL CHALLENGES

T. SUNI and I. KOSKINEN

Future Earth Finland, National Committee for Global Change Research, Division of Atmospheric Sciences, Department of Physics, University of Helsinki, Helsinki, Finland

European Alliance of Global Change Research Committees, Division of Atmospheric Sciences, Department of Physics, University of Helsinki, Helsinki, Finland

Keywords: GLOBAL SUSTAINABILITY, FUTURE EARTH, STAKEHOLDER ENGAGEMENT, GLOBAL CHANGE

INTRODUCTION

In 2014, a new national boundary organisation for the global change research programme Future Earth, "Future Earth Finland" (FEF), was established in Finland (www.futureearthfinland.fi). A number of similar Future Earth boundary organisations are now being formed around the world but, having rapidly created close collaboration with key stakeholders (ministries, environment-utilising enterprises, NGOs, funders, private sector, and cities & municipalities), Future Earth Finland is pioneering the difficult work of bringing scientists and end-users of scientific results together to *co-design* and *co-produce* information relevant to societal decision-making and sustainable development. Future Earth Finland is also the leader of the European Alliance of global change research committees, a European network of 24 national committees advancing global change research and Future Earth objectives in their countries (www.ea-globalchange.org). One of the aims of the European Alliance is to support its member countries to extend their current national committee activities towards significant societal influence; another is to act as a platform for scientific discussion on European scientific priorities and to facilitate the introduction of these priorities in EU scientific strategy and funding. Future Earth Finland and the European Alliance have a joint secretariat at the Division of Atmospheric Sciences in the University of Helsinki.

SCIENCE IN SUPPORT OF SOCIETY

Social scientists have studied the relationship between science and society for almost a century. In order to maintain scientific objectivity and credibility and to inhibit the influence of politics in science, first studies emphasised separating science from society (Bush 1945). However, over the latest decades, it has become clear that the requirement to separate science from society is not realistic. Values and politics inevitably influence science through investments in research infrastructures and funding. Scientists themselves are part of the society with their own values and goals.

Because of the separation of science from society, most decisions are made without sufficient use of scientific information available (Lemos et al. 2012, Kirchhoff et al. 2013) This finding has led to analyses of factors that influence the usability and applicability of scientific results. Among the main factors are 1) the amount and quality of the interaction between the producers and users of science; and 2) the applicability of scientific knowledge for the users' needs (De la Vega-Leinert *et al.* 2008, Van den Hove 2007, Lemos & Morehouse 2005). Factors that advance the utilisation of scientific knowledge include co-designing and co-producing research (Fig. 1). This requires long-term and trust-building relationships between producers and users of scientific knowledge. One good way of maintaining such relationships is via "boundary organisations" that act as brokers or mediators between science and society with credibility in the eyes of both (Kirchhoff et al. 2013).

Creating interaction processes between the producers and users of scientific results leads to knowledge that responds directly to the needs of the users; that the users consider more credible; and that the users trust enough to actually utilise. An interactive relationship also helps the users understand the nature of the science process and the value of scientific knowledge in the generation of knowledge. This diminishes barriers for utilising scientific results, such as notions of scientific knowledge being too uncertain, inaccurate, or unreliable as basis for decision-making.

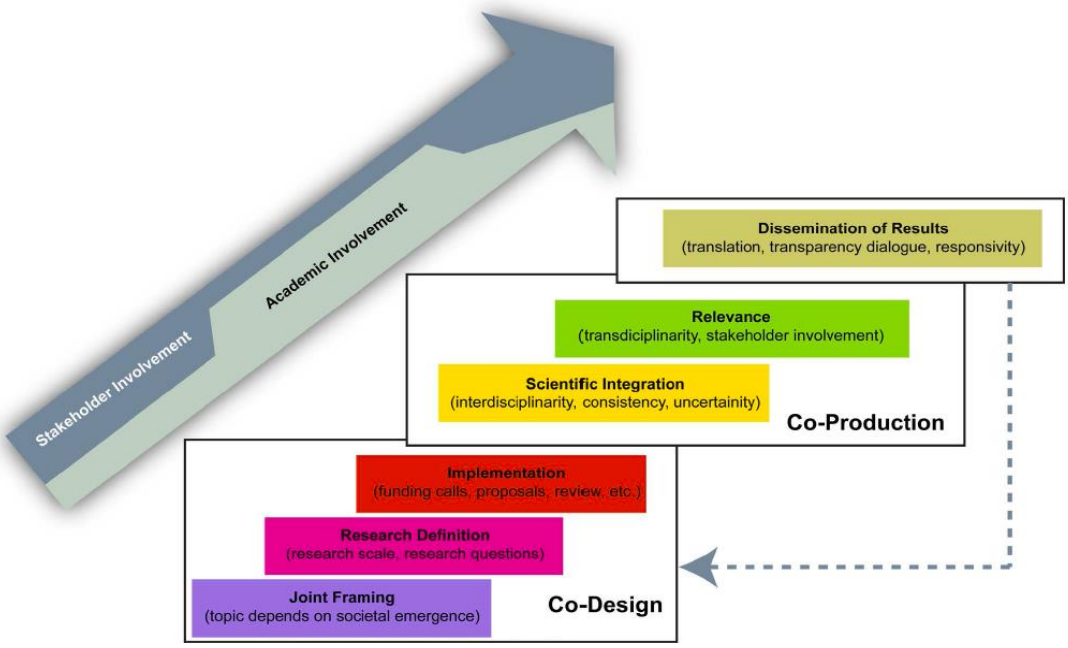

Figure 1. A schematic of co-design between producers and users during the entire lifetime of a scientific research project. “Stakeholders” are defined here as groups that influence the production of the scientific results or are influenced by the scientific results. Future Earth (2013).

FUTURE EARTH: KNOWLEDGE TO SUPPORT TRANSFORMATION TOWARDS SUSTAINABILITY

Under the lead of the International Council for Science (ICSU), the International Social Science Council (ISSC), three United Nations divisions (UNU, UNEP, UNESCO), and the Belmont forum, a new institutional framework, "Future Earth", is forming to support global environmental research activities that would reflect the multiple challenges of using the Earth’s resources in a sustainable way (Future Earth 2013). While the infrastructure of the emerging “Future Earth” organisation is still forming, the basic principles have been laid down: firstly, to facilitate a closer interaction between the environmental and socioeconomic sciences in approaching the eight focal challenges outlined in the Future Earth Strategic Research Agenda (Future Earth SRA 2014, Table 1), and secondly, to advance the *co-design* and *co-production* of knowledge as a collaboration of scientists and those who need scientific results (end-users, stakeholders) (Fig. 1). The objective of FEF and the European Alliance will be to contribute to this process and participate in the formulation of Future Earth structure and research themes while implementing the objectives in Europe and beyond. Future Earth work is carried out by the Science and Engagement committees, the globally distributed secretariat, the international core projects (integrative science) and the national committees such as Future Earth Finland (local engagement, policy relevance, and co-design with stakeholders) (Fig. 2).

FUTURE EARTH FINLAND

Sustainability problems are in many senses global, but the solutions are mostly local and depend significantly on local conditions such as local economic and political systems and cultures, the state of well-being, local environmental conditions, demographic issues, and the severity and nature of local environmental problems. As Future Earth aims not only at advancing understanding of global change and sustainability issues via the work of the international core projects but also at contributing to solutions (Future Earth 2013), it will require understanding of these local factors and an access to local decision-makers and stakeholders that are instrumental in implementing the solutions and adapting them to local needs. However, this can only be achieved through national *boundary organisations* (Kirchhoff et al. 2013) aiming to act as mediators between scientists and the various end-users of the scientific results: decision-makers on all levels, funders, NGOs, media, citizens, and the private sector.

FEF acts as just such a boundary organisation at the Centre of Excellence. Its management committee consists, in equal numbers, of environmental scientists, social scientists, and stakeholders (ministry, city, and private sectors). During its short lifetime, FEF has created an efficient network of researchers and stakeholders and become a trusted mediator and facilitator of their interaction. FEF works through a novel concept of "A living lab network of global change research" that operates on three levels: 1) increasing understanding of global change as a phenomenon; 2) bringing scientists and stakeholders together to increase understanding of one another's needs and aims, including practical consortium-building for strategic funding calls; and 3) hands-on co-design by means of pilot projects on global change –related issues such as bioeconomy, circulation economy, and regional social equality. As an example of the Living lab activities, FEF organised a Future Earth Townhall meeting in May 2015 where researchers and stakeholders discussed national priorities related to Future Earth key focal challenges (Table 1). FEF is also conducting a small research project on the usability of global change research. The research includes interview material with 8 national and international boundary organisations, and the results will be submitted as an opinion piece in an international journal in early 2016. Finally, FEF participates as an interaction partner in several funding applications for the Strategic Research Council and the Nessling foundation.

Table 1. Key focal challenges in the Future Earth Strategic Research Agenda 2014.

1. Deliver water, energy, and food for all, and manage the synergies and trade-offs among them, by understanding how these interactions are shaped by environmental, economic, social and political changes.
2. Decarbonise socio-economic systems to stabilise the climate by promoting the technological, economic, social, political and behavioural changes enabling transformations, while building knowledge about the impacts of climate change and adaptation responses for people and ecosystems.
3. Safeguard the terrestrial, freshwater and marine natural assets underpinning human well-being by understanding relationships between biodiversity, ecosystem functioning and services, and developing effective valuation and governance approaches.
4. Build healthy, resilient and productive cities by identifying and shaping innovations that combine better urban environments and lives with declining resource footprints, and provide efficient services and infrastructures that are robust to disasters.
5. Promote sustainable rural futures to feed rising and more affluent populations amidst changes in biodiversity, resources and climate by analysing alternative land uses, food systems and ecosystem options, and identifying institutional and governance needs.
6. Improve human health by elucidating, and finding responses to, the complex interactions amongst environmental change, pollution, pathogens, disease vectors, ecosystem services, and people's livelihoods, nutrition and well-being.
7. Encourage sustainable consumption and production patterns that are equitable by understanding the social and environmental impacts of consumption of all resources, opportunities for decoupling resource use from growth in well-being, and options for sustainable development pathways and related changes in human behaviour.
8. Increase social resilience to future threats by building adaptive governance systems, developing early warning of global and connected thresholds and risks, and testing effective, accountable and transparent institutions that promote transformations to sustainability.

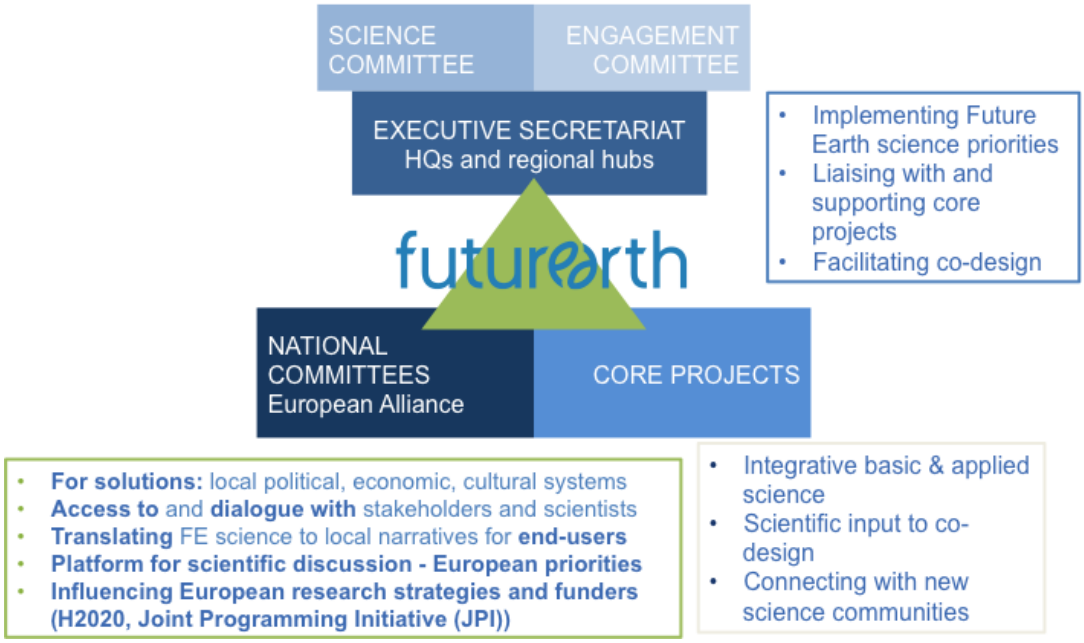

Figure 2. The structure of Future Earth and the equally important roles of the international core projects (integrative science) and of the national boundary organisations (national committees) such as Future Earth Finland (local engagement, policy relevance, and co-design with stakeholders) and their regional networks such as the European Alliance.

EUROPEAN ALLIANCE

The aim of the European Alliance is to build an active network of national committees that implement the co-design objective of Future Earth at the national and regional level. National committees provide understanding about local factors by acting as a link between the science community and the local decision-makers and stakeholders who are instrumental in implementing the solutions and adapting them to local needs. National committees vary from one national contact point to individual global environmental change program committees and to fully integrated Future Earth committees.

The main objectives of the European Alliance are

- to engage the European global change committees in the work of Future Earth and support its members to develop their activities towards societal relevance and dialogue with local stakeholders and policy-makers
- to work together with core projects to form operative networks of local and regional stakeholders, policy-makers, and scientists working on specific projects
- to merge European scientists and stakeholders communities to jointly determine European research priorities and interests and to introduce them into the on-going discussion on research strategy on the European level.

In 2014-2015, the Alliance took the lead in developing Future Earth activities in Europe. It facilitates a dialogue among European funders of global change research and Future Earth, is leading a COST Action proposal for Future Earth networking in Europe, and hosted a regional workshop for Future Earth in Europe in Innsbruck on 5-6 November where it brought together, for the first time, the different operators in Future Earth: core projects, national committees, secretariats, and Science and Engagement committees and a number of European stakeholders to discuss European strategy and needs. The work will continue in the next workshop on 22-23 November 2016 in Stockholm, Sweden. In addition, the Alliance forms part of a European Future Earth Task Force for Co-design Training and Strategy and brings together the data harmonisation efforts of Future Earth, ESFRI research infrastructures, and the key global change initiative,

the Pan-Eurasian Experiment (PEEX), acting as a collaboration platform for these in the Future Earth Data and Information Task force.

CONCLUSIONS

FEF and the European Alliance can provide PEEX an unparalleled view and channels to some of the largest international global change –related research programmes, funding instruments, and research infrastructure efforts. In the current and future research funding and research policy landscape, research is expected to more and more meet the demands of society. This requires new kind of understanding of the science-policy interface and new ways to communicate scientific findings to the wider society. FEF and the European Alliance help PEEX to stay in the forefront in the on-going paradigm shift where the grand challenges are to be solved in collaboration between top science and science-society interaction.

ACKNOWLEDGEMENTS

This work is supported by the Maj and Tor Nessling foundation and the Council of Finnish Academies.

REFERENCES

Bush V. 1945. Science the Endless Frontier. Washington, DC: US Gov. Print. Off. Washington, DC: US Gov. Print. Off.

De la Vega-Leinert, A., Schröter, D., Leemans, R., Fritsch, U. and Pluimers, J. A stakeholder dialogue on European vulnerability, Regional Environmental Change, 8, 109–124 (2008)

Future Earth Initial Design Report of the Transition Team 2013. Paris: International Council for Science (ICSU), p. 50–52.

Future Earth Strategic Research Agenda 2014. Paris: International Council for Science (ICSU).

Kirchhoff C, Lemos M, and Dessai S 2013. Actionable Knowledge for Environmental Decision Making: Broadening the Usability of Climate Science, Annu. Rev. Environ. Resour. 2013. 38:393–414

Lemos MC, Kirchhoff CJ, Ramparasad V. 2012. Narrowing the climate information usability gap. Nat. Clim. Change 2:789–94

Lemos, M. C. and Morehouse, B. The Co-Production of Science and Policy in Integrated Climate Assessments, Global Environmental Change, 15, 57–68 (2005).

Van den Hove, S. A rationale for science-policy interfaces, Futures, 39, 807–826 (2007)

LIGHT-ABSORBING IMPURITIES IN SURFACE SNOW FROM SODANKYLÄ, SUBARCTIC FINLAND 2009-2015

J. SVENSSON[1], O. MEINANDER[1], A. KONTU[2], H.-R. HANNULA[2], A. VIRKKULA[1], E. ASMI[1], H. LIHAVAINEN[1]

[1]Finnish Meteorological Institute, Research and Development, Helsinki, Finland.

[2]Arctic Research Center, Finnish Meteorological Institute, Sodankylä, Finland.

Keywords: SNOW ALBEDO, LIGHT-ABSORBING IMPURITIES, ARCTIC.

INTRODUCTION

Snow albedo is a physical parameter that has a key role in the radiative balance in the Northern Hemisphere and the Arctic, especially during the winter and spring. Albedo is mainly affected by the snow grain size, solar zenith angle, and the presence of light-absorbing impurities (LAI). The most effective LAI in reducing snow albedo is black carbon (BC), which has been shown to affect Arctic snow cover (Flanner *et al.*, 2007). Once BC is deposited on snow, the albedo decreases and the absorption of solar radiation by the snow increases, thus leading to warming of the snow and an earlier onset of snow melt. In this work, we present a unique dataset of BC from surface snow in Arctic Finland, covering the years 2009-2015.

METHODS

Snow samples were collected at the same location within the Finnish Meteorological Institute's Arctic observatory in Sodankylä, Finland on a weekly basis during the months with snow. A surface layer of roughly 5 cm was collected which thereafter was melted and filtered using the methods of Forsström *et al.* (2009). The filter substrate was analysed for elemental carbon (EC), which was used as a proxy of BC, using a thermal-optical carbon analyser (Sunset instruments).

CONCLUSIONS

The seasonal trend in BC of the surface snow is show in figure 1. The BC has been observed to stick to the snow surface and accumulate during snow melt, which also has been observed elsewhere (e.g. Doherty *et al.*, 2013). The data further suggests that the EC concentrations in the surface snow in Sodankylä are decreasing for the measuring period (table 1).

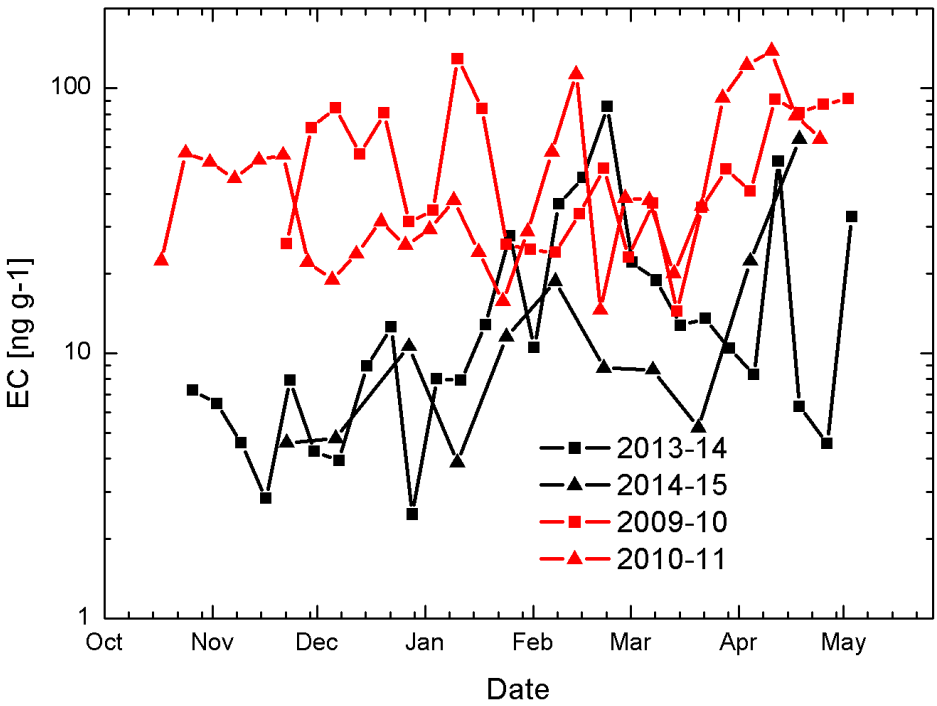

Figure 1. Seasonal trend in EC in the surface snow observed in 2013-14, 2014-15 (black lines), and 2009-10, 2010-11 (red lines).

Year	Jan average EC concentrations	Apr average EC concentrations
2010	72 (±40)	60 (±25)
2011	29 (±6)	94 (±40)
2012	28 (±13)	50 (±73)
2013	11 (±9)	40 (±31)
2014	9 (±4)	18 (±20)
2015	7 (±5)	31 (±30)

Table 1. Monthly (January and April) average EC concentrations from each sampling year.

ACKNOWLEDGEMENTS

This work was supported by the Academy of Finland project 254195 “Arctic Absorbing Aerosols and Albedo of Snow (A4),” and the Nordic research and innovation initiative Cryosphere-Atmosphere Interactions in a Changing Arctic Climate (CRAICC).

REFERENCES

Doherty, S. J., Grenfell, T. C., Forsström, S., Hegg, D. L., Brandt, R. E., and Warren, S. G (2013). Observed vertical redistribution of black carbon and other insoluble light-absorbing particles in melting snow. *J. Geophys. Res.*, **118**, doi:10.1002/jgrd.50235.

Flanner, M. G., Zender, C. S., Randerson, J. T., and Rasch, P. J (2007). Present-day climate forcing and response from black carbon in snow, *J. Geophys. Res.*, **112**, doi:10.1029/2006JD008003.

Forsström, S., Ström, J., Pedersen, C. A., Isaksson, E., and Gerland, S (2009). Elemental carbon distribution in Svalbard snow, *J. Geophys. Res.*, **114**, doi:10.1029/2008JD011480.

AERODYNAMIC PARAMETERS ESTIMATION FOR A HIGH-RISE REGION OF SHANGHAI

Y.Q. TANG[1], J.G. TAN[1], C.S.B. GRIMMOND[2], Y.Y. CHANG[1] and X.Y. AO[1]

[1]Shanghai Institute of Meteorological Science, Shanghai Meteorological Service, Shanghai, 166 Puxi Road, China.

[2]Department of Meteorology, University of Reading, Earley Gate, PO Box 243, Reading, RG6 6BB, United Kingdom.

Keywords: AERODYNAMIC PARAMETERS, URBAN, AERODYNAMIC METHODS, MORPHOMETRIC METHODS.

INTRODUCTION

Aerodynamic parameters play an important role in parameterizations of land-atmosphere interactions in numerical models. Methods to determine the aerodynamic roughness length for momentum (z_0) and zero-plane displacement length (z_d) can be grouped into those that require atmospheric observations (Grimmond *et al*. 1998) and morphometric methods based on the spatial arrangement of surface roughness elements (Grimmond *et al*. 1999; Kanda *et al*. 2013).

The need for the aerodynamic parameters comes about from the use of the logarithmic law to describe the wind profile. For neutral conditions, this is:

$$U_z = (u_*/k)* \ln [(z-z_d) / z_0]$$

where U_z is mean wind speed at a height (z), u_* is the friction velocity and k is the Von Karman constant. The two logarithmic wind profile approaches, Su and Es methods (Grimmond *et al*.1998), can reduce the effects of multiple source areas inherent in to multiple level observations. The Es method also has the advantage of being able to determine u_* with sonic measurement directly. Both the two methods require a value of z_d which could be determined by temperature variance method (TVM, Rotach 1994) using sonic data, or morphometric methods using roughness element characteristics.

Using observations in the real world and wind tunnel a wide range of methods have been developed to express this behaviour in response to changes in characteristics of the spatial arrangement of the surface roughness elements, e.g. Ra (Raupach 1994), Ma (Macdonald *et al*. 1998) and Ka (Kanda *et al*. 2013) method. This needs to take into account porous, bluff, arrangement, density or consistency of the building heights.

The objective of this study is to assess the size of aerodynamic parameters for an area of Shanghai using a variety of methods based on both observations and morphometric characteristics. This type of high rise zone has been little studied because of the challenges of undertaking measurements in this type of area and because until recently the often relatively small spatial extent of such areas within cities making finding sufficient fetch difficult.

METHODS

The study site located at Xujiahui (XJH, 31.19 °N, 121.43 °E), is a densely built-up commercial and residential area similar to large parts of central Shanghai. A fast response sensor and a slow response anemometer are mounted on a 25 m tower installed on the roof of the 55 m high building which locates in Shanghai Meteorological Service.

Aerodynamic methods have been used with observations from multiple cup-anemometer observations, single cup-anemometers, sonic anemometers, and lidars. The temperature variance method (TVM, Rotach 1994) is used in estimation of zero plane displacement height (z_d), Su and Es methods (Grimmond *et al*., 1998)are used in Roughness length calculation, for both EC (Eddy covariance system) and single cup-anemometer data are available in study site.

Morphometric methods analyse the properties of surface roughness elements (buildings and vegetation) in any direction, independent of meteorological observations. Three morphometric methods are used here: Ra (Raupach, 1994), Ma (Macdonald *et al*., 1998) and Ka (Kanda *et al*., 2013). Grimmond *et al*. (1999) found the first two methods performing well over a range of cities whereas the more recent Kanda et al. (2013) modified the Ma method for tall building areas, which is very applicable in the Shanghai context.

CONCLUSIONS

In terms of the values calculated, the Three morphometric methods, Ra, Ka and Ma show similar variations (the correlation coefficient (R^2) values between Ka and Ma, Ra and Ma, Ka and Ra are 0.90, 0.85, 0.87 for z_d respectively, and 0.75, 0.48, 0.57 for z_0 respectively); and the two anemometric methods, Es and Su exhibit similar performance (R^2 value 0.91 for z_0) through all approaches have some differences. The distribution of z_d by TVM method might fit the building density and arrangement better.

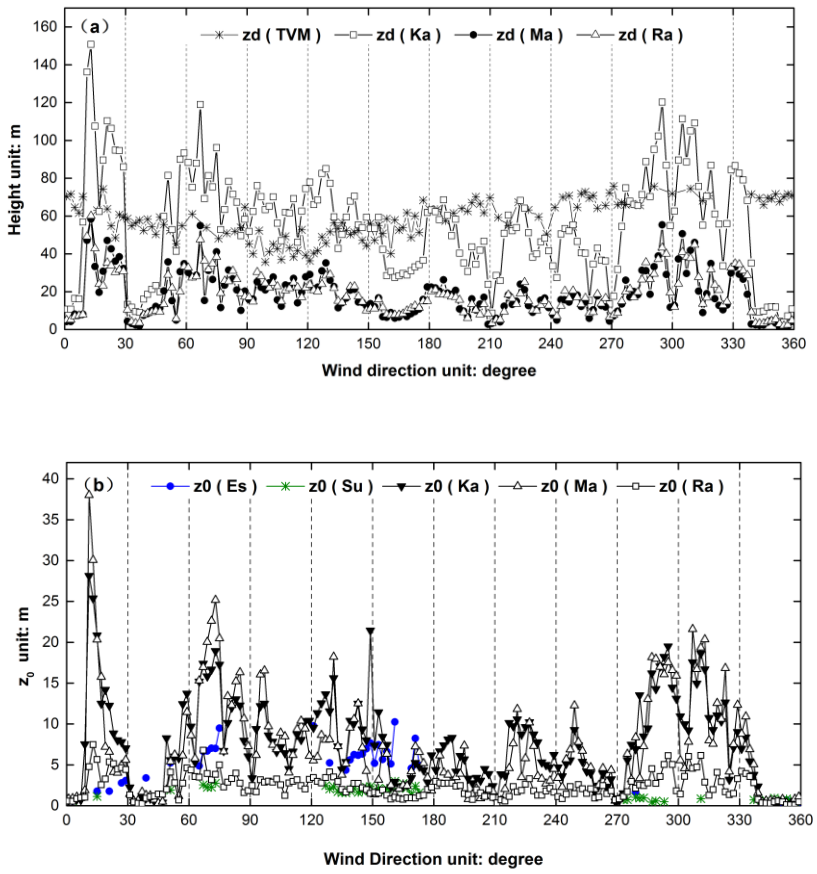

Figure 1. (a) Zero-plane displacement lengths(z_d) calculated by TVM, Ka, Ma and Ra method, (b) aerodynamic roughness lengths(z_0) calculated by Es, Su, Ka, Ma and Ra method.

The values of z_d determined by the TVM method are proportional to parameter C1 (Figure 2. a), inversely proportional to the parameter C3 (Figure 2. b) and affected by wind speed. The zd values increase by 9.1% on average with a 28.6% increment in C1; and decrease by 14.7% on average with a 10.5% increment in

C3. The z_d values calculated by Ka method with regressed constants Group 1 were larger by 11.96% - 28.34% than those using Group 2, and R^2=1.00 (Figure 2. c).

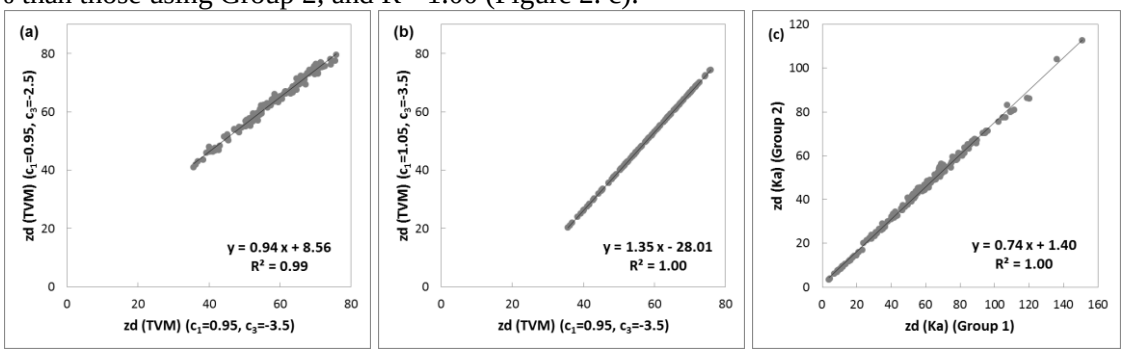

Figure 2. Linear relation of zero-plane displacement length between different parameters set (a) (b) by TVM and (c) by Ka in Xujiahui Site.

The z_d values by TVM method decrease as wind speed increases (Figure 3. a), z_0 values by both Es and Su method did not show big differences between different wind speed range selections (Figure 3. b and c). The z_0 values calculated by Es method and Su method are inversely proportional to z_d (Figure 4.).

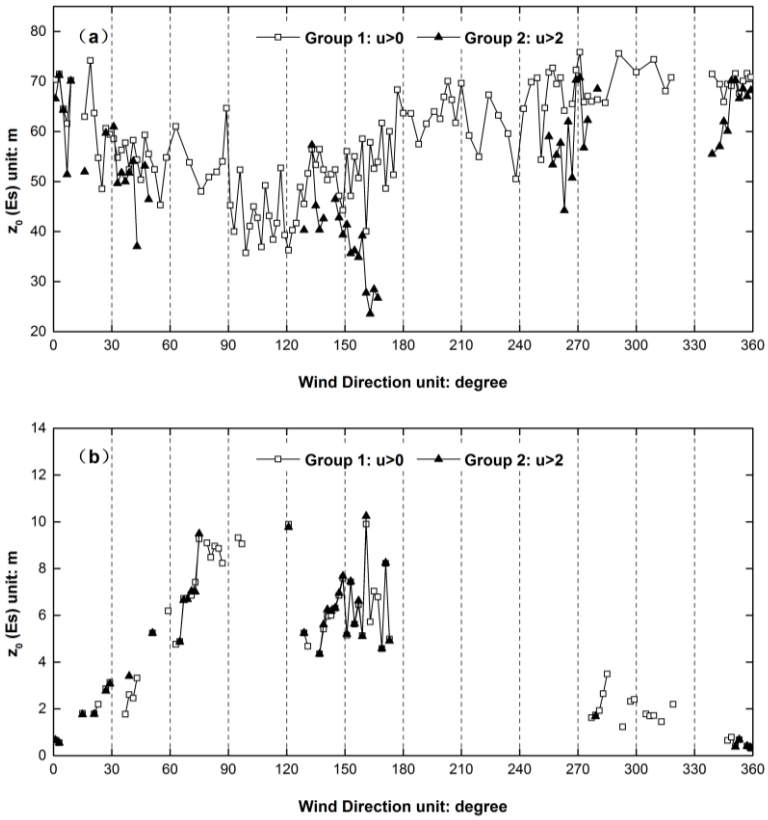

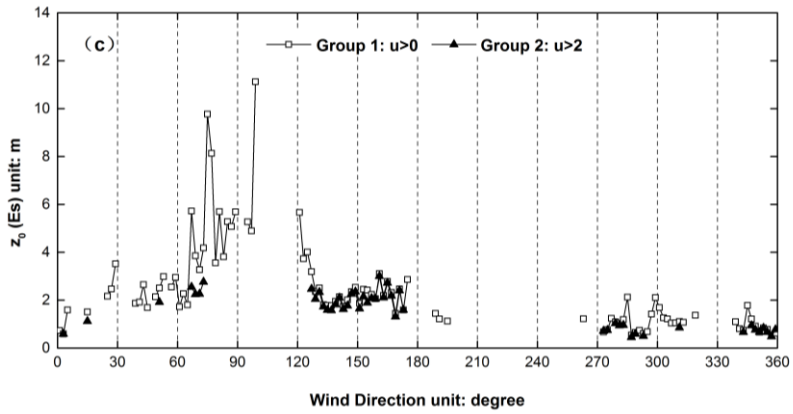

Figure 3. Comparison of wind speed (m/s) sensitivity analysis for (a) TVM method, (b) Es method and (c) Su method.

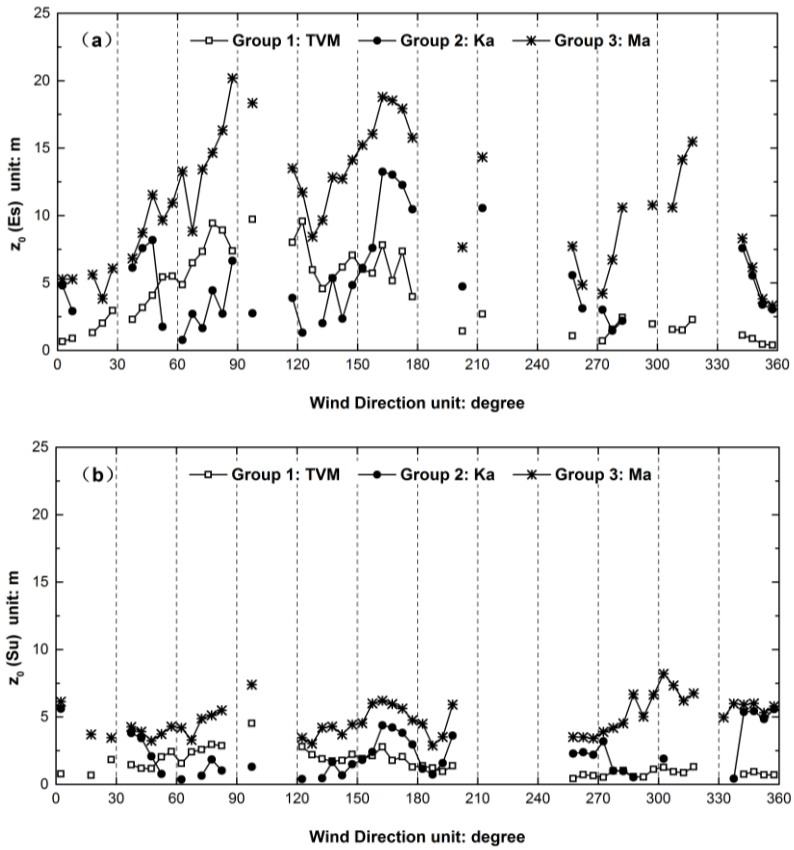

Figure 4. Comparison of z_d value sensitivity analyses for (a) Es and (b) Su methods.

ACKNOWLEDGEMENTS

Special thanks are due to Ping Hu and Jun Sun for observation sites information collections, Ziwei Xu and Tingting Shi for their help in sonic data quality controls. This material is based upon work supported by The Natural Science Foundation of China (Grant No.41275021), China Special Fund for Meteorological Research in the Public Interest (Grant No. GYHY201306010), and the Research program of Shanghai Meteorological Service (Grant No.YJ201404, QM201411).

REFERENCES

Beljaars A.C.M., P. Schotanus, F.T.M. Nieuwstadt (1983). Surface layer similarity under nonuniform fetch conditions. *J Appl Meteor* **22**, 1800-1810.

Grimmond C.S.B., T.S. King, M. Roth, *et al*. (1998). Aerodynamic roughness of urban areas derived from wind observations. *Boundary-Layer Meteor* **89**, 1- 24.

Grimmond C.S.B., T.R. Oke (1999). Aerodynamic properties of urban derived from analysis of surface form. *J Appl Meteor* **38**, 1262-1292.

Grimmond C.S.B., J.A. Salmond, T. R. Oke, *et al*. (2004). Flux and turbulence measurements at a densely built-up site in Marseille: Heat, mass (water and carbon dioxide), and momentum. *J Geophys Res Atmos* **109**, D24101.

Kanda M., A. Inagaki, T. Miyamoto, *et al*. (2013). A new aerodynamic parametrization for real urban surfaces. *Boundary-Layer Meteor* **148**, 357-377.

Macdonald R.W., R.F. Griffiths, D.J. Hall (1998). An improved method for the estimation of surface roughness of obstacle arrays. *Atmos Environ* **32**, 1857–1864.

Millward-Hopkins J.T., A.S. Tomlin, L. Ma, *et al*. (2013). Aerodynamic parameters of a UK city derived from morphological data. *Boundary-layer meteor* **146** (3), 447-468.

Raupach M.R. (1994). Simplified expressions for vegetation roughness length and zero-plane displacement as functions of canopy height and area index. *Boundary-Layer Meteor* **71**, 211-216.

Rotach M.W. (1994). Determination of the zero plane displacement in an urban environment. *Boundary-Layer Meteor* **67**, 187-193.

THE COMPLICATE OBSERVATIONS AND MULTI-PARAMETER LAND INFORMATION CONSTRUCTIONS ON ALLIED TELEMETRY EXPERIMEN (COMPLICATE)

X. TIAN[1], Z.Y. LI[1], E.X. CHEN[1], Q.W. LIU[1], and M. YAN[1]

[1]Institute of Forest Resource Information Techniques, Chinese Academy of Forestry, Beijing, 100091, Republic of China.

Keywords: COMPLEX LAND SURFACE; REMOTE SENSING INFORMATION; DYNAMIC ANALYSIS AND MODELING; SCALE EXTENSION; FOREST VERTICAL PARAMETERS; SOIL AND VEGETATION PARAMETERS.

INTRODUCTION

The term "Complex Land Surface" refers to land-surface systems with complicated landscapes and processes resulting from coexistent landscapes or rugged terrain within an observation footprint. Complex land surfaces are national condition of China and characterized by variations in topography, soil, climate, vegetation and their structural (horizontal and vertical) compositions, including complex terrains, fragmented landscapes, various land types, and diverse land properties (Young and Wang, 2001). Dynamic analysis and modeling, as well as observations of Earth systems, are the basic tools required for understanding complex land surfaces. As a part of Earth's observation systems, remote sensing represents ensemble information regarding the radiation characteristics of the pixel or footprint. Dynamic analysis and the modeling of remote sensing information are key for transubstantiating instant observations of remote sensing into space-time continuum information of land surface parameters (Li *et al.*, 2012; Li and Strahler, 1988). Estimations of land surface parameters using remote sensing models have led to numerous achievements. However, due to heterogeneity of mixed pixels, mechanisms of radiative transfer and scattering for complex land surfaces are still not well-known and more investigations are required (Chen *et al.*, 2006; Verhoef and Bach, 2007). Recognition of the scale extension of remote sensing information is also a problem (Garrigues *et al.*, 2006; Katzfuss and Cressie, 2011). Therefore, to achieve better accuracy for the complex land surface parameters, such as the forest vertical distribution of canopy biophysical and biochemical parameters, the hydro-thermal parameters of soil and vegetation, the methodology required for dynamic analysis and modeling of remote sensing information must be further developed (Thomas *et al.*, 2011; Shi *et al.*, 2012; Hakala *et al.*, 2012; Ni *et al.*, 2013; Mladenova *et al.*, 2014).

In the context of dynamic analysis and the modeling of remote sensing information, the basic theory of quantitative remote sensing is facing new chances and challenges. Launched by the National Basic Research Program (the 973 Program) of China in 2013, the research program entitled with "Dynamic analysis and modeling of remote sensing information for complex land surface" (hereafter referred to as the 973 Remote Sensing Program for CLS) was designed to meet national strategic demands for improving dynamic analysis and the modeling of remote sensing information using developments in Earth observation techniques. Under the condition of a "complex land surface", the 973 Remote Sensing Program for CLS focuses on the following: 1) the modeling of the radiative transfer of active and passive (visible, thermal infrared, and microwave) remote sensing; 2) dynamic analysis and modeling of the spatial-temporal scale transfer for multi-scale and long time-series remote sensing information; 3) the development of a synergistic inversion theory for key land surface parameters using multi-mode remote sensing; 4) establishing a new methodology system for dynamic analysis and the modeling of forest vertical structure information; 5) obtaining three-dimensional information of biophysical and biochemical parameters; and 6) obtaining the hydro-thermal parameters of soil using multi-dimensional remote sensing information.

In order to strengthen the theory and the method for dynamic analysis and the modeling of remote sensing information, and to achieve the scientific objectives of the 973 Remote Sensing Program for CLS, the Complicate Observations and Multi-Parameter Land Information Constructions on Allied Telemetry

Experiment (COMPLICATE) was conceived. The COMPLICATE is divided into two campaigns, one campaign that was designed for continuous and elaborate experiments performed at remote sensing test sites and the other designed for simultaneous satellite-borne, airborne, and ground-based experiments conducted on complex land surfaces. Using soil and vegetation as a research entity, COMPLICATE strengthens the established observing infrastructures by performing continuous and elaborate experiments and conducting new and simultaneous space-borne, airborne, and ground-based campaigns over typical complex land surfaces in order to improve dynamic analyses and the modeling of remotely sensed information. Information on the program's background, its scientific issues and objectives, completed and ongoing campaign measurements, and the current status of COMPLICATE are introduced here.

SCIENTIFIC ISSUES AND OBJECTIVES

Here, by COMPLICATE, three major scientific issues of quantitative remote sensing are addressed. The first issue is the characterization of spatial heterogeneity and radiative transfer, as well as the scattering mechanisms of remote sensing on complex land surfaces. The second issue addressed is the mechanism of spatial and temporal scale extensions for remote sensing information on complex land surfaces. Due to multi-scale heterogeneity, land surface complexity inherently incurs uncertainties for pixel information extractions. The final issue is determining the synergic inversion mechanisms of soil and vegetation parameters using multi-mode remote sensing on complex land surfaces.

The overall objective of COMPLICATE is to pioneer observing techniques to, as follows: 1) obtain dynamic information regarding soil and vegetation of complex land surfaces, 2) develop innovative measuring systems (i.e., new instruments and sensors and alterable full waveform observing platforms, as well as experimental schemes) on multiple scales, and 3) fulfill the multidisciplinary desires of precise dynamic information for remote sensing.

METHODS

EXPERIMENTAL PLATFORMS AND SITES

Since the launch of the 973 Remote Sensing Program for CLS, COMPLICATE has been utilized by two categories of experimental campaigns. The first campaign focuses on the time-series and delicate observations of radiative and scattering components, as well as the parameters of soil and vegetation on complex land surfaces. Such experiments are mainly based on existing and ongoing developments of observation infrastructures established within the remote sensing test sites of Huailai and Baoding in Hebei province, China. The campaign placed an emphasis on the controllability and quantitative interpretations of experimental objectives, as well as measured the accuracy of the instrument using deliberate experimental schemes. Based on the long-term observations of dynamic information for soil and vegetation, the dataset is expected to lead to the development and validation of models.

The other task of COMPLICATE was to conduct comprehensive satellite, airborne, and ground-based observations in order to extract and validate information for the dynamic modeling of soil and vegetation parameters using multi-parameter remote sensing data. During the campaigns, various missions including microwaves within the X and P bands, hyperspectral system, charge-coupled device (CCD), LiDAR and digital camera were located onboard the aircraft or unmanned aerial vehicle (UAV). Multi-source satellite remote sensing data were acquired and several continuous and intensive observations were conducted. Experiments were conducted within several typical complex land surfaces in China, including the Greater Khingan (GK) in Inner Mongolia, the Pu'er (PE) in Yunnan Province, and the Heihe River Basin (HRB) in Gansu Province.

ETHICS STATEMENT

The COMPLICATE did not involve any endangered or protected species. All experiments were conducted at Huailai, Baoding, GK, PE and HRB sites. The Huailai and Baoding sites are managed by the State Key Laboratory of Remote Sensing Science in the Institute of Remote Sensing and Digital Earth of Chinese

Academy of Sciences, and the State Key Laboratory of Remote Sensing Science in Research Center for Remote Sensing and GIS and School of Geography of Beijing Normal University, respectively. The permits of the ground measurements in GK, PE and HRB sites were issued by the Forestry Bureau of Greater Khingan of Inner Mengolia, the State Forestry Administration of P.R. China, and the Cold and Arid Regions Environmental and Engineering Research Institute of Chinese Academy of Sciences, respectively. The permits of the airborne flights in GK and PE sites were issued by the local departments of air force of P.R. China. The individual in this manuscript has given written informed consent (as outlined in PLOS consent form) to publish these case details.

EXPERIMENTS AND OBSEVATIONS

COMPLICATE concerns observations for the dynamic analysis and modeling of remotely sensed information on the typical complex land surfaces of China. Complexity is constructed by natural heterogeneity (GK, PE, and HRB) or artificial inhomogeneity (at the Huailai and Baoding sites). COMPLICATE is divided into three types of experiments, including the airborne remote sensing experiment (ARSE), the radiative transfer mechanism experiment (RTME), and the integrated experiment (IE). In particular, the IE consists of the scale extension experiment (SEE) and the synergistic inversion experiment (SIE).

The ARSE enhances the observability of remote sensing on complex land surfaces by acquiring multi-parameter remote sensing data. The experiment complements data support and links ground or near-surface based measurements to satellite remote sensing observations. The RTME stresses radiative and scattering mechanisms and the dynamic modeling of remote sensing information. The SEE is concentrated on the spatial and temporal scale extension of remote sensing information. The SIE focuses on forest vertical structure information (physical, biophysical, and biochemical) and hydro-thermal parameters for soil and vegetation. In other words, the RTME provides the basic dataset as well as derivative radiative and scattering transfer models for the scale extension methods developed from the SEE, both that improve the applicability of synergistic inversion models calibrated and validated by the SIE.

THE AIRBORNE REMOTE SENSING EXPERIMENT (ARSE)

Airborne SAR missions were flown over the GK site with coverage of more than 5,619 km2 during September of 2013. The airborne SAR system, namely CASMSAR, was integrated using a SAR data acquisition system, a SAR mapping workstation, and a SAR data preprocessing and distribution system. The system is the first airborne SAR mapping system in China and was developed by the Chinese Academy of Surveying and Mapping (CASM) in collaboration with several research institutes in China (Zhang *et al.*, 2012).

Two airborne LiDAR experiments have been conducted since the summer of 2012. The first, with an onboard LiDAR (Leica ALS60, Leica Geosystem AG, Heerbrugg, Switzerland) and CCD-Leica RCD105, Leica Geosystem AG, Heerbrugg, Switzerland) (Table 2) was conducted over the GK site, covering KEY (~130 km2) and KEG (~230 km2), from August to September of 2012. Following 153 flight lines and employed on the Yun-5 aircraft, the LiDAR+CCD mission acquired cloud point data with an average density of 8.0 points/m2 and a 0.2 m resolution for CCD data. LiDAR and CCD missions provided information for modeling forest and crop structural and biogeophysical parameters (forest density, vegetation height, canopy width and shape, canopy coverage, LAI, LAD, clumping index, etc.), and terrain factors (altitude, slope, aspect, roughness, etc.). With a very high resolution (0.5 m) and with accurate observations within key experimental areas, in the context of complex land surfaces, LiDAR+CCD missions will help advance remote sensing models for the following: 1) radiative transfer and scattering simulations; 2) scale transformations; 3) synergistic inversions of forest structural, biophysical, and biochemical information; and 4) soil and vegetation parameters.

THE RADIATIVE TRANSFER MECHANISM EXPERIMENT (RTME)

The RTME aims to develop, calibrate, and validate new radiative transfer models in both the optical and microwave regions for mixed land covers such as crop-forests or corn-wheat. Therefore, the RTME focuses on observations of the radiation distribution (including the energy balance), the bidirectional reflectance distribution function (BRDF), the albedo, the reflectance, the brightness temperature, radiation fluxes (latent and sensible heat), and other related parameters (meteorological parameters, soil moisture, LAI, vegetation height, biomass and coverage, canopy height, fraction of absorbed photosynthetically active radiation (FAPAR), etc.). Based on the ongoing upgrade of infrastructures located at the Huailai site, the system integrates current ground-based remote sensing facilities and techniques in order to develop innovative methods for synergizing ground-based remote sensing observations and measurements of relevant parameters.

INTEGRATED EXPERIMENT (IE)

The IE consisted of the SEE, and the SIE. The IE aims to improve the applicability of multi-source remote sensing within integrated scaling extensions and the synergistic inversions of forest vertical structure information and hydro-thermal parameters for soil and vegetation under conditions of complex land surfaces.

THE SCALE EXTENSION EXPERIMENT (SEE)

The SEE was composed of spatial and temporal scale extension experiments (SSEE and TSEE, respectively). The SSEE was mainly performed over KEG during 2013. We designed multi-scale comprehensive observations for vegetation structural parameters in order to calibrate and validate the spatial scale transformation models. Specifically, the SSEE provided calibration and validation data for the development of general conceptual scaling models, the development of parameterized physical scaling models, and an analysis of the optimal scale for analyzing scaling effects and scaling calibrations for indirect ground measurements on real vegetation structural parameters, as well as for the development and validation of scale transformation models for retrieving vegetation structural parameters.

THE SYNERGISTIC INVERSION EXPERIMENT (SIE)

Synergistic inversions require the vegetation, biophysical, and biochemical parameters. The following experiements were conducted in 2013: (1) The experiments of forest vertical structure were essentially concerned with parametes at the tree component, the individual tree and the forest plot.
Five forest inventories were conducted: two at KEY, two at KEG, and one at PE. Five sizes were measured for the forests: 10×10 m2 (43 plots at the PE site and 80 plots at the KEY site), 30×30 m2 (59 plots at the KEG site), 45×45 m2 (18 plots at the KEG, with each containing nine 15×15 m2 sub-plots), and forest cycloidal sample with a diameter of 10 to 15 m (39 plots at the PE site). Specifically, at the KEY site, 80 plots comprised a forest sampling stripe with a 10 m width and an 800 m length, whereas the forests were relatively homogeneous with one tree species, *Betula platyphylla Suk*. (2) The experiments for the vertical distribution of canopy biophysical and biochemical parameters consist of multi-angle observations by active and passive optical instruments on multilayer canopy biophysical and biochemical parameters. (3) The experiments of the hydro-thermal parameters of soil and vegetation were emphasized using in-situ, hydro-thermal measurements of soil and vegetation through the implementation of elaborative and controlled measurements (including the surface freeze/thaw status), the LST, the vegetation canopy temperature, and the vegetation water content.

SATELLITE DATA ACQUISITION

To fulfill the scientific objectives of the 973 Remote Sensing Program for CLS, the collection of satellite data was also an important part of COMPLICATE. Multi-sensor data was collected, including multi-spectral, hyperspectral optical data, LiDAR data, and active and passive microwave data (Table 6). Data

were obtained without charge under the framework of the data sharing program and international cooperation, or by commercial purchase. Commercial data were almost always obtained during periods of airborne campaigns and corresponding ground measurements with the exception of SPOT-6, which was obtained at the conclusion of the experiment due to extremely cloudy conditions.

CONCLUSIONS

COMPLICATE has a five year (2013 to 2017) design of experimental progressions that accompanies implementations of the 973 Remote Sensing Program for CLS. The program seeks to improve the observability, understanding, and applicability of remotely sensed dynamic modeling information for complex land surfaces. Since the launch of the program, COMPLICATE has strengthened established observing infrastructures in order to perform continuous and elaborate experiments and has also conducted new and simultaneous airborne, space-borne, and ground-based campaigns over complex land surfaces. By performing comprehensive, multiscale, continuous and elaborate experiments, COMPLICATE has collected a multiscale but spatiotemporally consistent data set for the dynamic analysis and modeling of remotely sensed information for retrieving soil-vegetation parameters under the condition of complex land surface. The 973 Remote Sensing Program for CLS addresses scientific issues that have hindered the applicability of quantitative remote sensing modeling for a long period of time. The overall background, scientific issues and objectives, the status of completed and ongoing campaign measurements, and the current status of COMPLICATE have been addressed here.

As compared with previous remote sensing campaigns, COMPLICATE seeks to understand complex land surfaces using complete information integration. Based on the data set from COMPLICATE, dynamic analyses and calibrations and validations of models have been conducted.

The remaining experimental plan is currently undergoing discussions and improvements, and we have much confidences that a fruitful outcome for quantitative remote sensing studies, focusing on dynamic analyses and the modeling of remote sensing for complex land surfaces, will be achieved and led by implementing COMPLICATE.

ACKNOWLEDGEMENTS

We thank the participants of COMPLICATE, including scientists, engineers, pilots and students. We thank expert and consultant committee members of the 973 Remote Sensing Program for CLS for sagacious comments and their advice on experimental design, implementation, and orientation.

REFERENCES

Alexander, F.R. and J.O. Nathan (1986). *An Introduction to Ultrasonic Nebulisation,* (Cambridge University Press, Cambridge, U.K.).

Chapman, D.H. (1975). Optical scattering from combustion aerosols, *J. Aerosol Science* **36**, 3456.

Finn, P., G.N. Diver and K.T. Wake (1998). Aerosol measurements in Iceland, in Proc. 13th Int. Conf. on Marine Aerosols, Reykjavik (Wiley, New York), 631.

Young, S.S. and C.Y.Wang (2001). Land-cover change analysis of China using global-scale Pathfinder AVHRR Land cover (PAL) data, 1982-92, Int J. Remote Sens 22, 1457−1477.

Li, X., R. Jin, X.D. Pan, T.J. Zhang and J.W. Guo (2012). Changes in the near-surface soil freeze-thaw cycle on the Qinghai-Tibetan Plateau, *Int J. Appl Earth Obs Geoinf* **17**, 33−42.

Li, X.W. and A.H. Strahler (1988). Modeling the gap probability of a discontinuous vegetation canopy, *IEEE Trans Geosci Remote Sens* **26**, 161−170.

Chen, Y., A. Hall and K.N. Liou (2006). Application of three-dimensional solar radiative transfer to mountains, *J. Geophys Res Atmos* 111: D21111. doi: 0.1029/2006JD007163.

Verhoef, W. and H. Bach (2007). Coupled soil-leaf-canopy and atmosphere radiative transfer modeling to simulate hyperspectral multi-angular surface reflectance and TOA radiance data, *Remote Sens Environ* **109**, 166−182.

Garrigues S., D. Allard, F. Baret and M. Weiss (2006). Influence of landscape spatial heterogeneity on the non-linear estimation of leaf area index from moderate spatial resolution remote sensing data, *Remote Sens Environ* **105**, 286−298.

Katzfuss, M. and N. Cressie (2011). Spatio-temporal smoothing and EM estimation for massive remote sensing data sets, *J Time Ser Anal* **32**, 430−446.

Thomas, V., T. Noland, P. Treitz and J.H. Mccaughey (2011). Leaf area and clumping indices for a boreal mixed-wood forest: lidar, hyperspectral, and Landsat models, *Int J Remote Sens* **32**, 8271−8297.

Shi J.C., Y. Du, J.Y. Du, L.M. Jiang, L.N. Chai, K.B. Mao, P. Xu, W.J. Ni, C.Xiong, Q. Liu, C.Z. Liu, P. Guo, /q. Cui, Y.Q., Li, J.Chen, A.Q. Wang, H.J. Luo and Y.H. Wang (2012). Progresses on microwave remote sensing of land surface parameters. *Sci. China Earth Sci* **55**, 1052−1078.

Hakala, T., J. Suomalainen, S. Kaasalainen and Y. Chen (2012). Full waveform hyperspectral LiDAR for terrestrial laser scanning, *Opt Express* **20**, 7119−7127.

Ni, W.J., G.Q. Sun, Z.Y. Zhang, Z.F. Guo and Y.T. He (2013). Co-registration of two DEMs: impacts on forest height estimation from SRTM and NED at mountainous areas, *IEEE Trans Geosci Remote Sens* **11**, 273−277.

Mladenova, I.E., T.J. Jackson, E. Njoku, R. Bindish, S. Chan, M.H. Cosh, T.R.H. Holmes, R.A.M. de Jeu, L. Jones, J. Kimball, S. Paloscia and E. Santi (2014). Remote monitoring of soil moisture using passive microwave-based techniques - Theoretical basis and overview of selected algorithms for AMSR-E, *Remote Sens Environ* **144**, 197−213.

Zhang, J.X., Z. Zhao, G.M. Huang and Z. Lu(2012). CASMSAR: An Integrated Airborne SAR Mapping System, *Photogramm Eng Remote Sensing* **78**, 1110−1114.

THE ISOTOPIC COMPOSITION OF ATMOSPHERIC CO_2 AND CH_4 OVER CENTRAL SIBERIA

A.TIMOKHINA[1], A. PROKUSHKIN[1], Y.V. LAVRIC[2], M. HEIMANN[2]

[1]V.N. Sukachev Institute of Forest, SB RAS, 660036, Krasnoyarsk, Russia.

[2]Max-Planck-Institute for Biogeochemistry, 07701, Jena, Germany.

Keywords: STABLE ISOTOPIC RATIO OF CO_2 AND CH_4, ZOTTO, SIBERIA

INTRODUCTION

The boreal and arctic zones of Siberia housing the large amounts of carbon stored in the living biomass of forests and wetlands, as well as in soils and specifically permafrost, play a crucial role in earth's global carbon cycle (Dolman *et al.*, 2012). Changes in carbon dioxide (CO_2) and methane (CH_4) emissions from Siberian ecosystems under climate change might have a substantial impact on the temporal variations of the atmospheric CO_2 and CH_4 on global scale. The long-term studies of greenhouse gases (GHG) concentrations in his region are important instruments to analyze the response of these systems to climate change. In parallel to GHG observations, the measurements of their stable isotopic composition can provide a powerful tool for distinguishing contribution of individual GHG sources to their atmospheric variations, since each source has its own isotopic signature (Umezawa *et al.*, 2012a). Several short-term aircraft observations of CO_2, CH_4 and these stable isotope ratios with frequency of about one or two times a month were conducted over West and Central Siberia in late 1990's (Lloyd *et al.*, 2002; Sugawara *et al.*, 1996) and, more recently only over gas field region of Surgut (Yamada *et al.*, 2005; Umezawa *et al.*, 2012b). These observations revealed that there are two major sources of CO_2 and CH_4 over west Siberia including the biogenic (wetlands and forest effluxes) and anthropogenic emissions, and their inputs are different throughout a year. The aim of this study is to distinguish the contributions of different types of these sources in the temporal variability of atmospheric CO_2 and CH_4 concentrations over Central Siberia based on isotopic composition of these greenhouses gases obtained for ZOTTO footprint area (Zotino Tall Tower Observatory) during 2008 – 2013 (2010 – 2013 for stable isotope composition of CH_4).

METHODS

The ZOTTO is located in Central Siberia at 60°N, 90°E, about 20 km west of the Yenisei River (114 m a.s.l.). A comprehensive forest inventory conducted within a radius of 100 km around the Zotino has shown that west part of ZOTTO footprint includes light taiga dominated by *Pinus sylvestris* and wetlands, and the dark taiga forest dominated by *Pinus sibirica*, *Abies sibirica*, *Picea obovata* to the east (Klimchenko *et al.*, 2011). Podzols are the predominant soil type. The nearest villages (Zotino, Vorogovo, Krivlyak, Sandakches and others) are no closer than 25 km from ZOTTO. Their total population does not exceed 3000, and there are no industrial facilities. The closest large city of Krasnoyarsk, population of about one million, is situated about 700 km to the south of the station. Due to low population density and remoteness from industrial centers, direct anthropogenic impact on the study region is insignificant. The continuous CO_2 and CH_4 measurement is performed by the EnviroSense 3000i analyzer (Picarro Inc., USA, CFADS-17) based on the Wavelength Scanned Cavity Ring-Down Spectroscopy (WSCRDS) technique from six height up to 301 m a.g.l. (Winderlich *et al.*, 2010). In parallel to continuous measurements of GHG the flask sampling program has been initiated to get insights to isotopic composition of GHG. One-liter glass flasks are routinely taken weekly or bi-weekly in triplicate at 301 m a.g.l.. The flasks were filled for 15 minutes with the rate of 2 l/minute under the pressure of about 900 hPa. The coming air was dried while passing through the system consisting of two refrigerators. The air was cooled to 6 C in the first refrigerator and to –92 C in the second one. The excessive moisture settled

on glass balls, which had been preliminarily installed in the chiller trap. The piping system was blown through for 40 minutes with the rate of 2 l/minute before each air sampling. After that, they transported to MPI-BGC (Jena, Germany) for laboratory analyses of the CO_2 and CH_4 concentrations, the stable isotope ratio of $\delta^{13}C$-CO_2, $\delta^{18}O$-CO_2, $\delta\ ^{13}C$-CH_4 and δD-CH_4 by using the Gas-Chromatography-Isotope Ratio Mass Spectrometry (GC-IRMS) technique.
We present the continuous measurements of CO_2 and CH_4 only from 301 m a.g.l. where were selected only daytime value between 1300 and 1700 (local standard time, which is UTC+7) and then averaged these data. This minimizes the impact of incomplete vertical mixing during night. Finally, we used a digital filtering technique developed by Thorning *et al*. (1989) to obtain trimmed daily averages and extract a seasonal cycle from the time series of the CO_2, CH_4 concentrations and the stable isotope ratio of $\delta^{13}C$-CO_2, $\delta^{18}O$-CO_2, $\delta\ ^{13}C$-CH_4 and δD-CH_4.

RESULTS

In a seasonal cycle, the magnitudes of $\delta^{13}C$-CO_2 and $\delta^{18}O$-CO_2 from best fit curves are -1.4±0.1 ‰ (-7.6 to -9.0 ‰) and -2.2±0.2 ‰ (-0.1 to -2.3), respectively (figure 1). The seasonal pattern of $\delta^{13}C$-CO_2 opposes the CO_2 concentrations, with a gradual enrichment in heavy isotope occurring during May – July, reflecting its discrimination in photosynthesis (Farquhar *et al.*, 1993), and further depletion in August – September as photosynthetic activity decreases comparatively to ecosystem respiration. Relationship between the CO_2 concentrations and respective $\delta^{13}C$-CO_2 (Keeling plot) points to an isotopic source signature for growing season (May – September) of -27.3±1.4 ‰ and of -30.4±2.5‰ for winter (January – March). Obviously, CO_2 is isotopically lighter in wintertime due to its anthropogenic emission. The CO_2 which added to the atmosphere from fossil fuel facilities is depleted in heaver carbon isotope (has more negative values), since $\delta^{13}C$-CO_2 of diesel and gasoline of Russian origin range from -28 to -32‰, and $\delta^{13}C$-CO_2 emission of natural gas combustion from West Siberia gas field region are of -30 to -68 ‰ (Nemchenko *et al.*, 1999; Goncharov *et al.*, 2009; Masalaite *et al.*, 2012). During the vegetation period, atmospheric $\delta^{13}C$-CO_2 mainly corresponds to $\delta^{13}C$-CO_2 into plant biomass varying from -28 to -26‰. The behavior of $\delta^{18}O$-CO_2 is influenced by both high photosynthetic rate in June (enrichment of atmospheric CO_2 by $\delta^{18}O$-CO_2 as consequence of CO_2 equilibrium with isotopically heavier leaf water) and respiratory activity of forest floor in the June – October period (depletion of respired CO_2 by $\delta^{18}O$-CO_2 because of the use of isotopically lighter soil water by microorganisms) (Lloyd *et al.*, 2002).
There is large temporal variation of $^{13}\delta C$-CH_4 (-50.0 to -46.1 ‰) with a clear minimum in the late summer (August) that corresponds to CH_4 concentration maximum and reflects biogenic sources of methane in the surrounding peat bogs (figure 2). The δD-CH_4 varies from -77.4 to -110.2 ‰ and shows no seasonal cycle with many irregular spikes during a year. Keeling plot analysis between the CH_4 concentration and isotopic composition revealed that isotopic signature of source in the winter (December – February) is -61.3±2.2 ‰ and -247.5±17.7 ‰ for $\delta^{13}C$-CH_4 and δD-CH_4 respectively. For growing season (June – September) the corresponding values for $\delta^{13}C$-CH_4 and δD-CH_4 are -76.4±2.6 ‰ and -342.2±14.8 ‰. Many studies have revealed that stable isotopic ratios of CH_4 from different sources widely vary (Umezawa *et al.*, 2012a; Umezawa *et al.*, 2012b). Since, the values of $\delta^{13}C$-CH_4 and δD-CH_4 emitted from the wetlands ranging from -40 to -80 ‰ and -400 to -300‰, respectively (Whiticar and Schaefer, 2007). For CH_4 emission mostly from natural gas of West Siberia gas field region, the values of $\delta^{13}C$-CH_4 and δD-CH_4 vary from -38 to -68 ‰ and -205 to -258 ‰, respectively (Nemchenko *et al.*, 1999; Goncharov *et al.*, 2009). The strong depletion of methane in heavy isotopes throughout a year is the indication of continuous CH_4 emissions from biogenic sources.

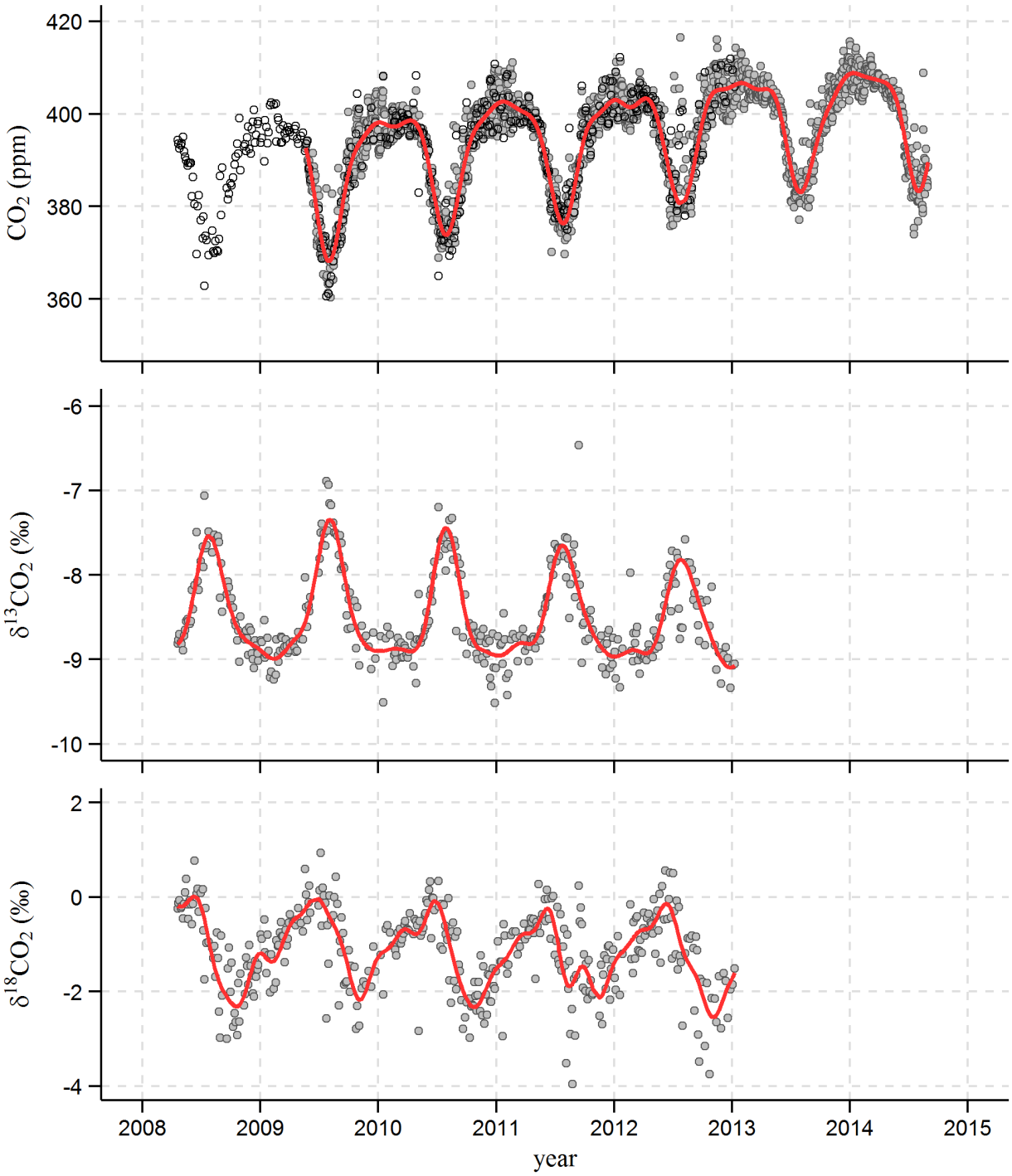

Figure 1. Temporal variations of CO_2 concentrations obtained by continuous measurements (WSCRS, white circles) and periodic sampling in glass flasks (GC-IRMS, grey circles), $\delta^{13}C$-CO_2 and $\delta^{18}O$-CO_2 at 301 m a.g.l. at ZOTTO during 2008 – 2014. The best fit curves obtained by Thorning *et al.* (1898) are also shown in red lines.

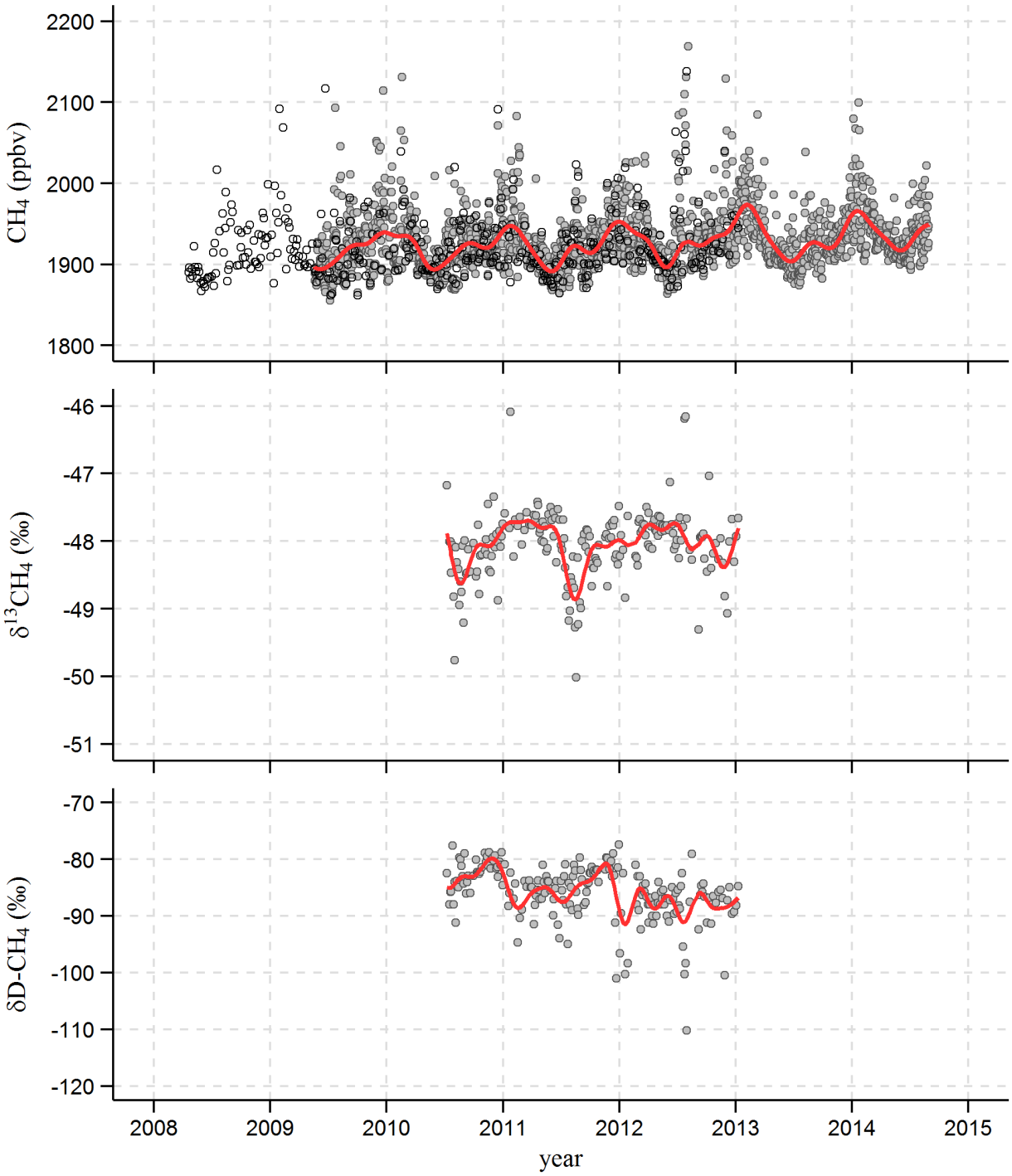

Figure 2. Temporal variations of CH_4 concentrations obtained by continuous measurements (WSCRDS, white circles) and periodic sampling in glass flasks (GC-IRMS, grey circles), $\delta^{13}C$-CH_4 and δD-CH_4 at 301 m a.g.l. at ZOTTO during 2008 – 2014. The best fit curves obtained by Thorning *et al.* (1898) are also shown in red lines.

ACKNOWLEDGEMENTS

The study has been supported by cooperation agreement between SIF SB RAS and MPI-BGC and RSF grant (14-24-00113).

REFERENCES

Dolman A.J., A. Shvidenko, D. Schepaschenko, P. Ciais, N. Tchebakova, T. Chen, M. K. van der Molen, L. Belelli Marchesini, T. C. Maximov, S. Maksyutov, and E.-D. Schulze (2012). An estimate of the terrestrial carbon budget of Russia using inventory-based, eddy covariance and inversion methods, *Biogeosciences*, **9**, 5323–5340.

Umezawa T., T. Machida, K. Ishijima, H. Matsueda, Y. Sawa, P. K. Patra, S. Aoki, and T. Nakazawa (2012a). Carbon and hydrogen isotopic ratios of atmospheric methane in the upper troposphere over the Western Pacific, *Atmos. Chem. Phys.*, **12**, 8095–8113.

Lloyd J., R.L. Langenfelds, R.J. Francey, M. Gloor, N.M. Tchebakova, D. Zolotuokhine, W.A. Brand, R.A. Werner, A. Jordan, C.A. Allison, V. Zrazhewske, O. Shibistova, E.-D. Schulze (2002). A trace-gas climatology above Zotino, central Siberia, *Tellas*, **54B(5),** 749–767.

Sugawara, S., T. Nakazawa, G. Inoue, T. Machida, H. Mukai, N. K. Vinnichenko, and V. U. Khattatov (1996), Aircraft measurements of the stable carbon isotopic ratio of atmospheric methane over Siberia, *Global Biogeochem. Cycles*, **10(2)**, 223–231.

Yamada, K., N. Yoshida, F. Nakagawa, and G. Inoue (2005), Source evaluation of atmospheric methane over western Siberia using double stable isotopic signatures, *Org. Geochem.*, **36**, 717–726.

Umezawa T., M. Toshinobu, S. Aoki, and Nakazawa T. (2012b). Contributions of natural and anthropogenic sources to atmospheric methane variations over western Siberia estimated from its carbon and hydrogen isotopes, *Global Biogeochem. Cycles*, **26(4)**, GB4009

Klimchenko A.V., S.V. Verkhovets, O.A. Slinkina, and N.N. Koshurnikova (2011). Reserves of heavy slash in the middle-taiga ecosystems along Yenisei Siberia, *Geography and natural resources*, **2**, 91-97. In Russian.

Winderlich J., H. Chen, C. Gerbig, T. Seifert, O. Kolle, J.V. Lavric, C. Kaiser, A. Hofer, and M. Heimann (2010). Continuous low-maintenance CO_2/CH_4/H_2O measurement at the Zotino Tall Tower Observatory (ZOTTO) in Central Siberia, *Atmos. Meas. Tech.*, **3**. 1113-1128.

Thoning K.W., P.P. Tans, and W.D. Komhyr (1989). Atmospheric carbon dioxide at Nauna Loa Observatory 2. Analysis of the NOAA GMCC Data, 1974-1985, *Journal of Geophysical Research*, **94(D6)**, 8549-8565.

Farquhar G.D., J. Lloyd, J.A. Taylor (1993). Vegetation effects on the isotope composition of oxygen in atmospheric CO_2. *Nature*, **363**, 439-442

Nemchenko N.N., A.S. Rovenskaya, M. Shoell (1999). The origin of natural gases in the huge gas field of northern West Siberia, *Oil and Gas geology*, **1-2**, 45-56. In Russian.

Goncharov I.V., N.V. Oblasov, V.V. Samoylenko, V.A. Krinin (2009). Origin of hydrocarbon gases in Vankor oilfield area, in Proc. 7th Int. Conf. “Chemistry of oil and gas”, Tomsk, 191-194. In Russian.

Masalaite A., A. Garbaras, and V. Remeikis (2012). Stable isotopes in environmental investigations, *Lithuanian Journal of Physics*, **52(3)**, 261-268.

Whiticar M. and H. Schaefer (2007). Constraining past global tropospheric methane budgets with carbon and hydrogen isotope ratios in ice, *Phil. Trans. R. Soc. A*, **365**, 1793–1828.

METHANE FLUXES ON SIBERIAN PERMAFROST TUNDRA: UNRAVELLING INDIVIDUAL LAND COVER TYPES FROM EDDY COVARIANCE DATA

J.-P. TUOVINEN[1], M. AURELA[1], T. VIRTANEN[2], J. HATAKKA[1], M. LINKOSALMI[1], V. IVAKHOV[3], A. MAKSHTAS[4] and T. LAURILA[1]

[1]Finnish Meteorological Institute, Atmospheric Composition Research, P.O. Box 503, FI-00101 Helsinki, Finland.

[2]Department of Environmental Sciences, University of Helsinki, Finland.

[3]Voeikov Main Geophysical Observatory, St Petersburg, Russia.

[4]Arctic and Antarctic Research Institute, St Petersburg, Russia.

Keywords: ARCTIC TUNDRA, METHANE FLUXES, FLUX FOOTPRINT, HETEROGENEOUS SURFACE, EDDY COVARIANCE.

INTRODUCTION

Biosphere-atmosphere exchange of greenhouse gases (GHGs) is commonly measured with the micrometeorological eddy covariance (EC) technique (Aubinet *et al.*, 2012). In contrast to chamber-based flux measurements that can be focused on small-scale patches of individual plant communities, the EC method provides data on an ecosystem scale, i.e. for an area ranging from hectares to square kilometres. This spatial integration inherent in the EC data is a strong asset if the objective is to assess the physiology and GHG exchange of a relatively homogeneous ecosystem. Heterogeneous surfaces, however, may entail issues on the interpretation of spatial representativeness, as the contribution of different surface cover types varies depending on the footprint of measurement, i.e. wind direction and atmospheric mixing.

As part of the International Arctic Systems for Observing the Atmosphere (IASOA) activities (Uttal *et al.*, 2015), exchange fluxes of the main GHGs, i.e. carbon dioxide (CO_2) and methane (CH_4), are measured on permafrost tundra at Tiksi in northern Siberia (Aurela *et al.*, 2015); the main aims are to quantify the balances of these gases and understand the biological and environmental controls involved. The surface area covered by the footprint of these EC measurements is a prime example of a heterogeneous source/sink distribution, as it consists of a mosaic of different vegetation and other land cover types following a hydrological gradient from a drier upland area to a wetter valley.

The objective of this work is to examine possibilities for deriving land cover specific information from EC flux measurements, which inevitably aggregate different surface characteristics. Flux estimates that distinguish systematic differences in the source/sink strength within the study area are especially required for regional upscaling of the measured GHG fluxes and for unbiased gap filling of the flux time series. Here we present a first approach, in which we formulate a simple linear inversion problem based on flux footprint modelling.

METHODS

The flux measurement station at Tiksi (71º35.665’N, 128º53.273’E, 7 m a.s.l.) is situated on the shore of the Laptev Sea, close to the Lena river estuary. The permafrost in the area is continuous, and the typical depth of the active layer in August is 30–50 cm. The mean annual temperature and precipitation are –12.7 ºC and 323 mm, respectively (Aurela *et al.*, 2015).

Continuous EC measurements of CO_2 and energy fluxes were started in July 2010, and in June 2011 the system was extended to cover the CH_4 fluxes as well (Aurela *et al.*, 2015). The EC instrumentation consists of a USA-1 (METEK) sonic anemo/thermometer, an LI-7000 (Li-Cor) CO_2/H_2O analyzer and an RMT-200 (Los Gatos Research) CH_4 analyzer. The 10-Hz EC data were processed according to standard procedures and averaged over 30-min periods. Supporting measurements include air temperature and humidity, different radiation components, soil temperature and humidity, water table depth and soil heat flux. Precipitation and snow depth are measured at the nearby Tiksi Hydrometeorological Observatory.

Quickbird and WorldView2 satellite images are available for the Tiksi region from 15 July 2005 and 11 August 2012. Making use of the local vegetation and soil surveys (Linkosalmi *et al.*, 2015), these images were processed to produce maps of land cover class (LCC) and leaf area index (LAI) using superivised classification and nonlinear regression, respectively. The maps have a 2-m resolution and cover an area of 5 km × 5 km surrounding the EC mast. The LCC map represents the dominant surface type within each pixel. Eight LCCs were defined: (1) bog, (2) dry fen, (3) wet fen, (4) lichen tundra, (5) shrub tundra, (6) tussock tundra, (7) bare soil and (8) water. Further classes can be added by separating these LCCs into low and high subclasses depending on terrain elevation.

We calculated the flux footprints for each 30-min flux averaging period by using the analytical footprint model developed by Kormann and Meixner (2001). The EC measurements provide the necessary input data for this model (mean wind speed and direction, friction velocity, Obukhov length and the variance of lateral wind speed). A footprint field represents the relative contribution of each LCC pixel to the flux measurement, from which the total contribution of each LCC can be summed. In addition, weighted LAI values were calculated from the LCC-specific LAI estimates and footprint distributions.

Assuming that the CH_4 flux does not vary among the pixels with the same LCC, the measured flux was expressed as a weighted arithmetic mean of the LCC-specific fluxes, where these fluxes are unknown and the weights are obtained from the footprint calculations. Assuming further that the LCC-specific fluxes remain constant during a fixed period (or, alternatively, within a data set screened for a limited temperature range), we obtained a set of linear algebraic equations that can be solved for the LCC-specific fluxes. In practice, this linear system is overdetermined, in which case we sought for the least-square solution through QR factorization of the weight matrix.

The flux data were first screened by removing periods of weak turbulence and instrument failure. The model outlined above was fitted to a random sample of 50% of the data and validated against the remaining half. For producing cross-validation statistics, a Monte Carlo procedure was introduced by repeating the random calibration-validation partitioning of the data for 10,000 times. For the preliminary results presented here, the LCCs listed above were aggregated into four groups: (1) lowland wet fen, (2) other wet fen and tussock tundra, (3) non-vegetated surface and (4) other surfaces.

RESULTS

Figure 1 presents an example of the results calculated with the simple model described above. The observations shown in Figure 1 correspond to a random sample of quality-controlled EC flux data collected in July–August 2014 (500 observations). The model was calibrated by fitting the unknown LCC-specific CH_4 fluxes to these data. The predicted ecosystem-scale CH_4 fluxes shown in Figure 1 were calculated with the LCC-specific fluxes that were determined from the validation data from the same period (500 independent observations).

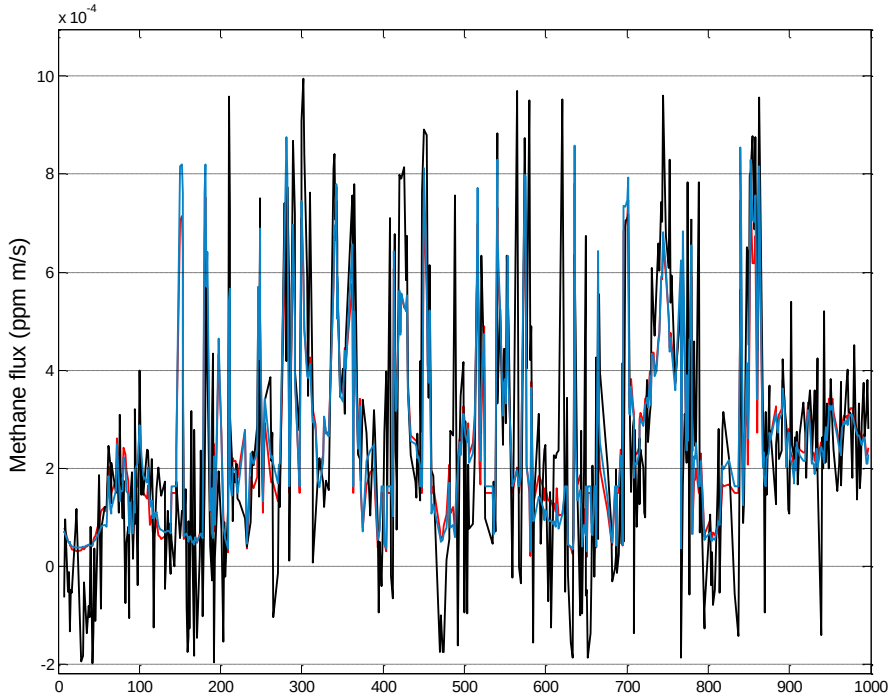

Figure 1. An example of model performance: observed (black), fitted (red) and predicted (blue) CH_4 fluxes at Tiksi in July–August 2014. The plot is based on a random sample from a screened data set and thus does not depict a continuous time series.

Table 1 presents statistics of the model performance as a mean of 10,000 random calibration–validation partitionings of the data. These results indicate that the agreement between observations and model predictions calculated for the data not used in the calibration step is very similar to that obtained for the optimized calibration fit.

Table 1. Model performance statistics.

	Calibration	Validation
Correlation	0.720	0.717
RMSE[a]	0.120	0.121

[a]Root Mean Square Error, μg m^{-2} s^{-1}

The LCC-based CH_4 fluxes resulting from the repeated model calibration are presented in Table 2. As expected, the pixels that were both classified as wet fen and located in a wetter part of the area (Group 1) were estimated as the highest emitters. The second group consisting of other wet fen and tussock tundra acted as a moderate source of CH_4, while the non-vegetated surfaces appear as a weak sink.

Table 2. Estimates of methane fluxes for LCC-based groups.

Group	Flux (mean ± standard deviation, μg m^{-2} s^{-1})
1	1.06 ± 0.06
2	0.22 ± 0.03
3	–0.08 ± 0.03
4	0.01 ± 0.02

(1) lowland wet fen, (2) other wet fen and tussock tundra, (3) non-vegetated, (4) other

ACKNOWLEDGEMENTS

This work was supported by the Academy of Finland (Greenhouse gas, aerosol and albedo variations in the changing Arctic, project no. 269095; Carbon balance under changing processes of Arctic and subarctic cryosphere, project no. 285630), the European Commission (Changing permafrost in the Arctic and its global effects in the 21st century, PAGE21) and the Nordic Council of Ministers (DEFROST, a Nordic Centre of Excellence within NordForsk).

REFERENCES

Aubinet, M., T. Vesala and D. Papale, eds. (2012). *Eddy Covariance – A Practical Guide to Measurement and Data Analysis*, Springer, Dordrecht, 438 pp.

Aurela, M., T. Laurila, J.-P. Tuovinen, J. Hatakka, M. Linkosalmi, T. Virtanen, J. Mikola, E. Asmi, V. Ivakhov, V. Kondratyev, T. Uttal and A. Makshtas (2015) CH_4 and CO_2 exchange on permafrost tundra in Tiksi, Siberia, in Proceedings of the 1st Pan-Eurasian Experiment (PEEX) Conference and the 5th PEEX Meeting, *Report Series in Aerosol Science* **163**, 61–62.

Kormann, R. and F.Z. Meixner (2001) An analytical footprint model for non-neutral stratification. *Boundary-Layer Meteorology* **99**, 207–224.

Linkosalmi, M., M. Aurela, T. Virtanen, J. Nyman, J. Mikola, E. Vähä, V. Ivakhov, V. Kondratyev, A. Makshtas and T. Laurila (2015) Measuring plant and soil characteristics to produce land cover classification and explain carbon fluxes in Arctic tundra, in Proceedings of the 1st Pan-Eurasian Experiment (PEEX) Conference and the 5th PEEX Meeting, *Report Series in Aerosol Science* **163**, 244–245.

Uttal, T., S. Starkweather, J.R. Drummond, T. Vihma, A.P. Makshtas, L.S. Darby, J.F. Burkhart, C.J. Cox, L.N. Schmeisser, T. Haiden, M. Maturilli, M.D. Shupe, G. de Boer, A. Saha, A.A. Grachev, S.M. Crepinsek, L. Bruhwiler, B. Goodison, B. McArthur, V.P. Walden, E.J. Dlugokencky, P.O.G. Persson, G. Lesins, T. Laurila, J.A. Ogren, R. Stone, C.N. Long, S. Sharma, A. Massling, D.D. Turner, D.M. Stanitski, E. Asmi, M. Aurela, H. Skov, K. Eleftheriadis, A. Virkkula, A. Platt, E.J. Førland, Y. Iijima, I.E. Nielsen, M.H. Bergin, L. Candlish, N.S. Zimov, S.A. Zimov, N.T. O'Neill, P.F. Fogal, R. Kivi, E.A. Konopleva-Akish, J. Verlinde, V.Y. Kustov, B. Vasel, V.M. Ivakhov, Y. Viisanen and J.M. Intrieri (2015) International Arctic Systems for Observing the Atmosphere (IASOA): An International Polar Year Legacy Consortium. *Bulletin of the American Meteorological Society*, doi:10.1175/BAMS-D-14-00145.1, in press.

MONITORING AND ASSESSMENT OF REGIONAL AIR QUALITY IN CHINA USING SPACE OBSERVATIONS (MARCO POLO)

R. VAN DER A [A,] *, B. MIJLING [A], J. DING [A], D. BALIS [B], J. STAVRAKOU [C], A. MAHURA [D], K.KOURTIDIS [E], G. DE LEEUW [F], J. BAI [G], B. MARTÍNEZ [H], V. AMIRIDIS [I], P. XIE [J], R. TIMMERMANS [K], L. ZENG [L], Q. ZHANG [M], N. VELDEMAN [N], Y. XUE [O]

[a] Royal Netherlands Meteorological Institute (KNMI), De Bilt, Netherlands - avander@knmi.nl

[b] Aristotle University of Thessaloniki (AUTH), Greece

[c] Belgian Institute for Space Aeronomy (BIRA-IASB), Belgium

[d] Danish Meteorological Institute (DMI), Denmark

[e] Democritus University of Thrace (DUTH), Greece

[f] Finnish Meteorological Institute(FMI), Finland

[g] Institute of Atmosphere Physics (IAP), China

[h] IsardSAT, Spain

[i] National Observatory Athens (NOA), Greece

[j] Hefei Institute of Physical Sciences, China

[k] Netherlands Organization for Applied Scientific Research (TNO), Netherlands

[l] Peking University, China

[m] Tsinghua University, China

[n] Flemish Institute for Technological Research (VITO), Belgium

[o] London Metropolitan University, UK

Keywords: EMISSION ESTIMATES, SATELLITE, AIR QUALITY, TRACE GASES

ABSTRACT

In this paper we will present the EU-project 'MarcoPolo'. The main objective of MarcoPolo is to improve air quality monitoring, modelling and forecasting over China using satellite data and by combining Chinese and European expertise. Due to the strong economic growth in the China in the past decade, air pollution has become a serious issue in many parts of the country. For this reason up-to-date regional air pollution information and means of emission control for the main pollutants are becoming more and more important. Within a previous EU-project, 'Air Quality Monitoring and Forecasting in China' (AMFIC), it was concluded that modelling of air quality are hampered by the rapidly changing emission data due to economic growth in China. In addition, air quality policies could not directly be related to changes in emissions. Therefore, within the MarcoPolo project, the focus will be placed on emission estimates from space, together with chemical transport models, and the refinement of these emission estimates by spatial downscaling and by source sector apportionment. A wide range of satellite data will be used from various

* Corresponding author. This is useful to know for communication with the appropriate person in cases with more than one author.

satellite instruments to derive emission estimates for NO_x, SO_2, PM and biogenic sources. By combining these emission data with known information from the ground, a new emission database for MarcoPolo will be constructed. The improved emission inventory will be input to the regional and local air quality models.

VARIATIONS OF AEROSOL OPTICAL PROPERTIES DURING A POLLUTED WINTER PERIOD IN NANJING, CHINA

A.VIRKKULA[1,2,3], X. CHI[1], A. DING[1], Y. SHEN[1], W. NIE[1], X. QI[1], L. ZHENG[1], T. PETAJA[3], M. KULMALA[3]

[1]Institute for Climate and Global Change and School of Atmospheric Sciences, Nanjing University, China

[2]Finnish Meteorological Institute, FI-00560, Helsinki, Finland

[3]Department of Physics, University of Helsinki, FI-00014, Helsinki, Finland

Keywords: ABSORPTION, SCATTERING, WAVELENGTH DEPENDENCY, BROWN CARBON

INTRODUCTION

The direct climatic effects of aerosols are due to scattering and absorption of light. In short, light scattering by aerosols cools the atmosphere and absorption heats it. These processes can even affect the stability of polluted boundary layer, which in turn affects the boundary layer height and consequently particle concentration in it (Petäjä et al., 2016). Both light scattering and absorption depend on the size and chemical composition of particles as well as the wavelength of radiation. Therefore wavelength-dependent measurements of aerosol optical properties yield information on the aerosol sources and size distributions. For instance, light absorbing carbonaceous aerosol consists mainly of black carbon (BC) but also of some organics, usually called brown carbon (BrC). They have different spectral absorption: BrC absorbs UV radiation more efficiently than BC.

Spectral aerosol optical properties were measured in Nanjing, China, in September 2013 – January 2015. The measurements were conducted at the SORPES station (118°57' E, 32°07' N, 40 m above mean sea level) in the Xianlin campus of Nanjing University. The station can be considered as an urban background station with little influence of local emissions (Ding et al., 2013a, b). The data used in the present work were discussed earlier by Virkkula et al. (2015). It was shortly mentioned there that several-day long pollution episodes with high scattering and absorption coefficients were observed in winters of 2013 and 2014. They were not analyzed in detail because the goal of the paper was to gain understanding on the interpretation of an aethalometer data processing algorithm. In the present work variations of spectral absorption and scattering during pollution episodes observed in December 2013 are analyzed.

METHODS

Total scattering coefficients (σ_{sp}) and backscattering coefficients (σ_{bsp}) at λ = 450 nm, 525 nm, and 635 nm were measured with an ECOTECH Aurora 3000 nephelometer. A 7-wavelength aethalometer (AE-31) was used for measuring light absorption at λ = 370 nm, 470 nm, 520 nm, 590 nm, 660 nm, 880 nm, and 990 nm. The aethalometer reports Black Carbon (BC) concentrations but from these data absorption coefficients were calculated according to both Arnott *et al*. (2005) and Collaud Coen *et al*. (2010) algorithms.

Light scattering by particles depends on the wavelength roughly as $\sigma_{sp} \propto \lambda^{-\alpha sp}$ where α_{sp} is the Ångström exponent of scattering. It is often used as a qualitative indicator of the dominant particle size, with large values (> 2) indicating the dominance of small particles, and small values (< 1) the dominance of large particles. The α_{sp} presented in the subsequent analyses was calculated over the nephelometer wavelength range 450 – 635 nm by fitting the data line to the line $\ln(\sigma_{sp},\lambda) = -\alpha_{sp} \ln(\lambda) + C$. The backscatter fractions ($b = \sigma_{bsp}/\sigma_{sp}$) were calculated as the ratio of the backscattering coefficient and the truncation-corrected

total scattering coefficients at the nephelometer wavelengths. The backscatter ratio is a measure related to the angular distribution of light scattered by aerosol particles. From b it is possible to estimate the average upscatter fraction β and aerosol asymmetry parameter that are key properties controlling the aerosol direct radiative forcing. b is also related to particle size: for small particles it is larger than for big particles. Also absorption depends on the wavelength roughly as $\sigma_{ap} \propto \lambda^{-\alpha ap}$ where α_{ap} is the Ångström exponent of absorption. The wavelength dependency of absorption yields information on the absorbing material. For pure BC particles σ_{ap} is approximately inversely proportional to λ, in other words the Ångström exponent of absorption $\alpha_{ap} \approx 1$ but for aerosol containing also light-absorbing organics α_{ap} is higher, especially due to absorption of ultraviolet (UV) light (e.g., Kirchstetter *et al*., 2004; Lewis *et al*., 2008). Often light absorbing aerosol emissions from traffic are BC with $\alpha_{ap} \approx 1$. In the literature α_{ap} has been used for estimating the contibution of traffic and wood burning emissions to observed light absorbing aerosols (e.g., Sandradewi *et al*., 2008) even though this method contains serious uncertainties (e.g., Harrison *et al*., 2013). Here α_{ap} was calculated both over the full wavelength range of the aethalometer with the same approach as α_{sp} , i.e. by fitting the data to $\ln(\sigma_{ap},\lambda) = - \alpha_{ap} \ln(\lambda) + C$, and for individual wavelength pairs from $\alpha_{ap}= - \ln(\sigma_{ap}(\lambda_1)/\sigma_{ap}(\lambda_2))/ \ln(\lambda_1/\lambda_2)$. Below the α_{ap} calculated from absorption measured at the UV wavelength λ = 370 and at visible blue light at λ = 470 nm is presented.

The absorption coefficients at the Aethalometer wavelengths were interpolated logarithmically to the nephelometer wavelengths to calculate the single-scattering albedo ($\omega_0 = \sigma_{sp}/(\sigma_{sp}+\sigma_{ap})$). It is a measure of the darkness of aerosols. At low ω_0 values aerosols heat the atmosphere and at high values cool it, depending also on b, and other parameters (e.g., Haywood and Shine, 1995). ω_0 is approximately 0.3 for pure BC particles (e.g., Mikhailov *et al*., 2006) and 1 for purely scattering aerosol, for example ammonium sulfate. It also varies as a function of wavelength but below ω_0 only at λ = 520 nm is discussed.

RESULTS

Scattering and absorption coefficients were very high during December 2013: the average (± standard deviation) $\sigma_{sp} \approx 820 \pm 575$ Mm^{-1} at λ = 525 nm and $\sigma_{ap} \approx 50 \pm 25$ Mm^{-1} at λ = 520 nm. The 95th percentiles were $\sigma_{sp} \approx 2030$ Mm^{-1} at λ = 525 nm and $\sigma_{ap} \approx 96$ Mm^{-1} at λ = 520 nm. The time series plot (Fig. 1) shows that the most intense pollution episode lasted from 4 to 9 December during which σ_{sp} remained > 1000 Mm^{-1} most of the time. The single-scattering albedo, ω_0 was clearly higher during the pollution episode than before and after it. An interesting feature of the episode is that the Ångström exponent of scattering, α_{sp} decreased during this period from about 1.4 to about 0.5 and the backscatter fraction decrased to about 0.1. Similar process took place also during the second highest pollutíon episode 24 – 26/12 when σ_{sp} increased and α_{sp} and b decreased almost steadily until the sharp end of the episode.

There was a very clear diurnal cycle of both σ_{sp} and σ_{sp} during most of the month, even during the highly polluted periods. Most of the maximum scattering and absorption coefficients were reached at night which suggests they were due to lower boundary layer at night and therefore less volume for mixing which leads to higher concentrations within the mixing layer. There were very clear diurnal cycles of ω_0 and α_{ap} (Fig 1, middle panel). Most nights ω_0 was lower than during the following day which suggests that at daytime some scattering material condensed on the BC particles that were present there already during the night. Very often also the maximum α_{ap} was reached at night suggesting a strong contribution of BrC. This type of diurnal cycle did not take place every day, however. For instance, when the strong pollution episode started on 4 December ω_0 increased from the previous daytime value of about 0.9 to 0.95 at night (period 1 in Fig. 1). That transition was also associated with a strong growth of α_{ap}.

The period 2 denoted in Fig 1 is different from period 1 in that both scattering and absorption decreased from night to day but also ω_0 decreased suggesting that there was a change in the air mass origins. The shift was also associated with strong variations in the α_{ap} but the peak was again reached at night or early morning suggesting this may have something to do with solar radiation. During period 3 there was first a strong decrease of particles: σ_{sp} decreased by almost an order of magnitude, σ_{sp} somewhat less resulting in

the decrease of ω_0 from > 0.95 to about 0.90. The following night there was a very sharp increase in σ_{ap} and decrease of ω_0. Since α_{ap} also decreased to close to 1 the increase in absorption can be interpreted to be mainly due to BC and not BrC.

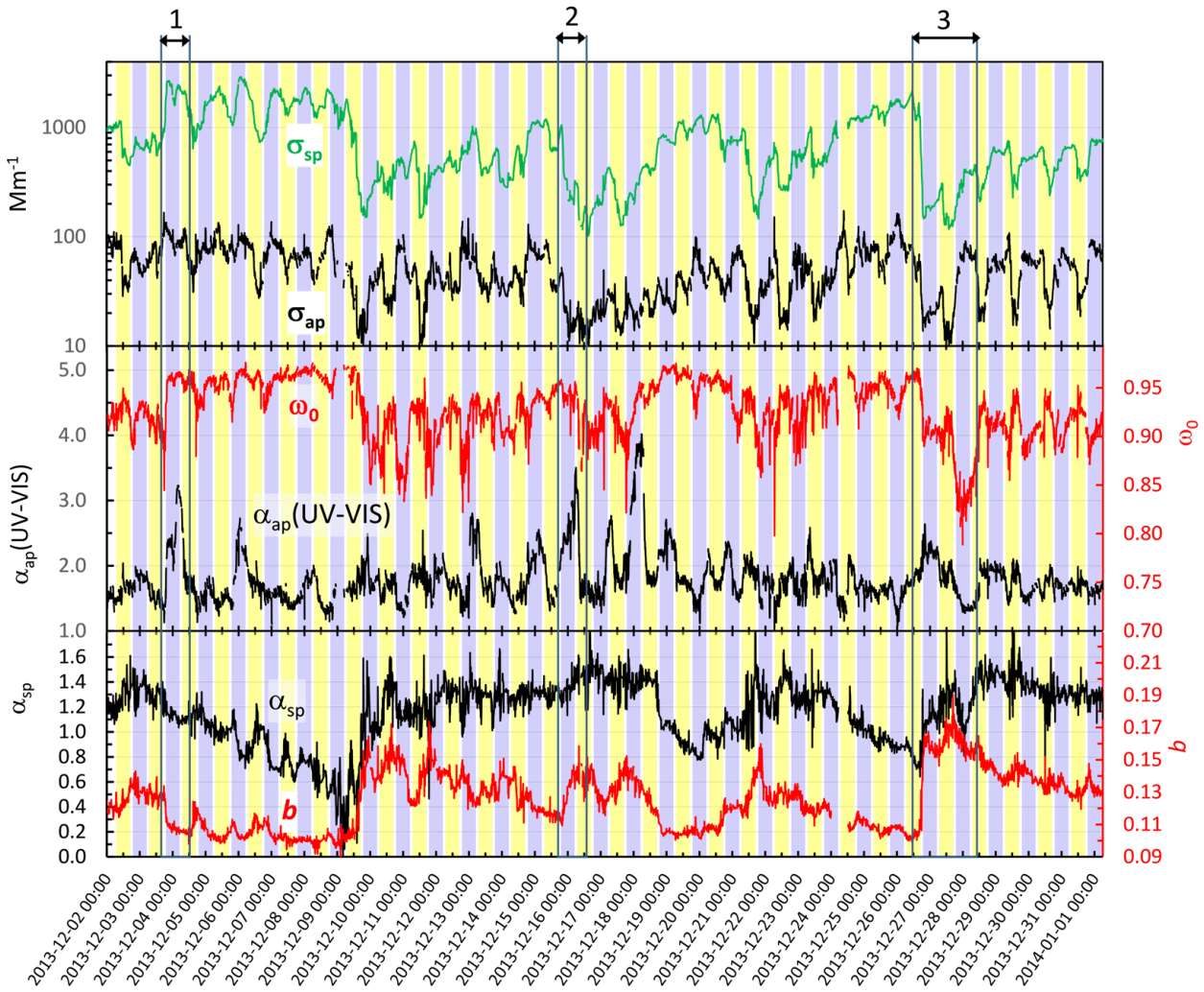

Figure 1. Selected 5-minute-averaged aerosol optical propeties observed at SORPES in December 2013. Upper panel: scattering coefficient (σ_{sp}) at λ = 525 from about 1.4 to and absorption coefficient (σ_{ap}) at λ = 520; middle panel: single scattering albedo (ω_0) at λ = 520 and Ångström exponent of absorption (α_{ap}(UV-VIS)) calculated between the ultravíolet and visible wavelengths λ = 370 and 470 nm; lower panel: Ångström exponent of scattering (α_{sp}) calculated over the visible wavelengths λ = 450 – 635 nm, and backscatter fraction at λ = 525 nm. Indication of the time of the day: the grey stripes are centered at midnight, the yelow stripes at noon of each day. The numbers 1 – 3 above the panels denote selected periods discussed in the text.

CONCLUSIONS

The single-scattering albedo, ω_0 was clearly higher during the heavy pollution episodes than outside the episodes suggesting the aerosol consisted primarily of light-scattering secondary compounds, probably sulfates. The α_{sp} and b decreased during intense pollution episodes, which shows that the particle sizes grew during them. When the episodes ended both α_{sp} and b increased clearly suggesting that the particles in the cleaner air were smaller than during the pollution episode. The wavelength-dependent absorption measurements indicated that α_{ap} increased in some cases very clearly, suggesting the role of BrC is significant. In the future the data will be used for assessing the contribution of traffic and other emissions

to light absorbing aerosol according to published algorithms. The diurnal cycle of ω_0 suggests that the light absorbing aerosol, mainly BC, gets coated by condensation of some light-scattering material formed by photochemical rections during daytime. This will be studied in the near future by taking also the aerosol chemical composition measured at the station (Xie *et al*., 2015) into account.

ACKNOWLEDGEMENTS

The research was supported by the Jiangsu Provincial Natural Science Fund (No.BK20 140 021), National Science Foundation of China (D051/41275129) and 5 Academy of Finland's Centre of Excellence program (Centre of Excellence in Atmospheric Science – From Molecular and Biological processes to the Global Climate, project no. 272041).

REFERENCES

Arnott, W. P., Hamasha, K., Moosmuller, H., Sheridan, P. J., and Ogren, J. A. (2005). Towards aerosol light-absorption measurements with a 7-wavelength aethalometer: evaluation with a photoacoustic instrument and 3-wavelength nephelometer, *Aerosol Sci. Tech*., **39**, 17–29.

Collaud Coen, M., Weingartner, E., Apituley, A., Ceburnis, D., Fierz-Schmidhauser, R., Flentje, H., Henzing, J. S., Jennings, S. G., Moerman, M., Petzold, A., Schmid, O., and Baltensperger, U. (2010). Minimizing light absorption measurement artifacts of the Aethalometer: evaluation of five correction algorithms, *Atmos. Meas. Tech*., **3**, 457–474.

Ding, A. J., Fu, C. B., Yang, X. Q., Sun, J. N., Zheng, L. F., Xie, Y. N., Herrmann, E., Nie, W., Petäjä, T., Kerminen, V. M., and Kulmala, M.: Ozone and fine particle in the western Yangtze River Delta: an overview of 1 yr data at the SORPES station, *Atmos. Chem. Phys.*, 13, 5813-5830, 10.5194/acp-13-5813-2013, 2013a.

Ding, A. J., Fu, C. B., Yang, X. Q., Sun, J. N., Petäjä, T., Kerminen, V. M., Wang, T., Xie, Y., Herrmann, E., Zheng, L. F., Nie, W., Liu, Q., Wei, X. L., and Kulmala, M.: Intense atmospheric pollution modifies weather: a case of mixed biomass burning with fossil fuel combustion pollution in eastern China, *Atmos. Chem. Phys.*, 13, 10545-10554, 10.5194/acp-13-10545-2013, 2013b.

Haywood, J. M., and Shine, K. P.: The effect of anthropogenic sulfate and soot aerosol on the clear sky planetary radiation budget, *Geophys. Res. Lett*., 22(5), 603–606, 1995.

Harrison, R.M., Beddows, D.C.S., Jones, A.M., Calvo, A., Alves, C., Pio, C. (2013) An evaluation of some issues regarding the use of aethalometers to measure wood smoke concentrations. *Atmos.Environ*. 80, 540 – 548.

Kirchstetter, T. W., Novakov, T., and Hobbs, P. V.: Evidence that the spectral dependence of light absorption by aerosols is affected by organic carbon, *J. Geophys. Res*., 109, D21208, doi:10.1029/2004JD004999, 2004.

Lewis, K., Arnott, W.P., Moosmüller, H., and Wold, C. E.: Strong spectral variation of biomass smoke light absorption and single scattering albedo observed with a novel dual-wavelength photoacoustic instrument, *J. Geophys. Res.*, 113, D16203, doi:10.1029/2007JD009699, 2008.

Mikhailov, E., Vlasenko, S., Podgorny, I., Ramanathan, V., and Corrigan, C.: Optical properties of soot-water drop agglomerates: An experimental study, *J. Geophys. Res*., 111, 1–16, 2006.

Petäjä, T., Järvi, L., Kerminen, V.-M., Ding, A. J., Sun, J. N., Nie, W., Kujansuu, J. , Virkkula, A., Yang, X., Fu, C.B., Zilitinkevich, S., and Kulmala, M. (2016). Enhanced air pollution via aerosol-boundary layer feedback in China. *Scientific Reports, 6*, 18998. http://doi.org/10.1038/srep18998

Sandradewi, J., Prevot, A.H., Szidat, S., Perron, N., Rami Alfarra, M., Lanz, V., Weingartner, E., Baltensperger, U. (2008) Using aerosol light absorption measurements for the quantitative determination of wood burning and traffic emission contributions to particulate matter. *Environ.Sci.Technol.* 42, 3316 – 3323.

Virkkula, A., Chi, X., Ding, A., Shen, Y., Nie, W., Qi, X., Zheng, L., Huang, X., Xie, Y., Wang, J., Petäjä, T., and Kulmala, M. (2015). On the interpretation of the loading correction of the aethalometer, *Atmos. Meas. Tech.*, **8**, 4415-4427, doi:10.5194/amt-8-4415-2015.

Xie, Y, Ding, A., Nie, W., Mao, H., Qi, X., Huang, X., Xu, Z., Kerminen, V.-M., Petäjä, T., Chi, X., Virkkula, A., Boy, M. , Xue, L., Guo, J., Sun, J., Yang, X., Kulmala, M., and Fu, C.: Enhanced sulfate formation by nitrogen dioxide: Implications from in-situ observations at the SORPES Station, *J. Geophys. Res.*, 120, doi:10.1002/2015JD023607, 2015

ON THE INTERPRETATION OF THE LOADING CORRECTION OF THE AETHALOMETER

A. VIRKKULA[1,2,3,4], X. CHI[1,2], A. DING[1,2], Y. SHEN[1,2], W. NIE[1,2,3], X. QI[1,2], L. ZHENG[1,2], X. HUANG[1,2], Y. XIE[1,2], J. WANG[1,2], T. PETÄJÄ[3], M. KULMALA[3]

[1]Institute for Climate and Global Change and School of Atmospheric Sciences, Nanjing University, China

[2] Collaborative Innovation Center for Climate Change, Jiangsu Province, China

[3]Department of Physics, University of Helsinki, FI-00014, Helsinki, Finland

[4]Finnish Meteorological Institute, Research and Development, FI-00560, Helsinki, Finland

Keywords: AETHALOMETER, ABSORPTION COEFFICIENT, CORRECTION ALGORITHM, LOADING EFFECT

INTRODUCTION

Aerosols affect climate directly by scattering and absorbing solar radiation. For the assessment of the direct radiative forcing it is crucial that both light scattering and absorption are measured accurately. Globally, probably the most widely used aerosols absorption measurement method is the aethalometer, produced by Magee Scientific. It converts the reduction of light transmittance directly into black carbon (BC) mass concentrations, which are further used for calculating the light absorption coefficient (σ_{ap}). However, the calculation is not straightforward since light transmittance is not reduced only by the light-absorbing aerosols but also by scattering aerosols and by interactions between the filter fibers and accumulated aerosols. Algorithms have been developed to take these effects into account (e.g., Weingartner et al. 2003; Arnott et al., 2005; Schmid et al., 2006; Virkkula et al., 2007; Collaud Coen et al., 2010). The algorithm presented by Virkkula et al (2007) corrects the BC mass concentration for the loading effect by multiplying the uncorrected concentrations with the function $f = 1 + kATN$ where k is the so-called compensation parameter and ATN is the attenuation reported by the aethalometer. It has been observed in many studies that the value of k varies in time and place, so far no attempts for explaining this site-related and seasonal varaiation of the values of k have been published. The goal of the present work is to study whether the backscatter fraction ($b = \sigma_{bsp}/\sigma_{sp}$) and single-scattering albedo ($\omega_0 = \sigma_{sp}/(\sigma_{sp}+\sigma_{ap})$) could be the factors explaining the k variations in past and new aethalometer measurements.

MEASUREMENTS AND METHOD

The measurements were conducted at the SORPES station (118°57' E, 32°07' N, 40 m above mean sea level) in the Xianlin campus of Nanjing University. The station can be considered as an urban background station with little influence of local emissions (Ding et al., 2013a, b). Total scattering coefficients (σsp) and backscattering coefficients (σbsp) at λ = 450 nm, 525 nm, and 635 nm were measured with an ECOTECH Aurora 3000 nephelometer. The scattering and backscattering coefficients are presented at STP conditions. The raw total scattering coefficients were corrected for truncation errors following the formulas presented by Müller et al. (2011). To be used in the aethalometer data processing the truncation-corrected σ_{sp} at the nephelometer wavelengths were interpolated and extrapolated to the aethalometer wavelengths.

A 7-wavelength aethalometer (AE-31) was used for measuring light absorption at λ = 370 nm, 470 nm, 520 nm, 590 nm, 660 nm, 880 nm, and 950 nm. The aethalometer reports BC mass concentrations were first used to calculate the uncorrected attenuation coefficients, here $\sigma 0$, by multiplying the original non-corrected BC mass concentration given by the aethalometer with the wavelength-dependent BC mass

attenuation coefficient used by the instrument's software. To calculate the absorption coefficients (σ_{ap}) several algorithms have been presented which in principle can be expressed in the form of

$$\sigma_{ap} = \frac{f\sigma_0 - s\sigma_{sp}}{C_{ref}},$$

where f is a loading correction function, s is a fraction of light scattering coefficient σ_{sp} that causes reduction of light transmittance and would be interpreted as absorption (= apparent absorption) if not taken into account, and Cref the multiple scattering correction factor.

In the present work absorption coefficients were calculated according to both Arnott et al. (2005) and Collaud Coen et al. (2010) algorithms with the respective mean Cref values of 4.12 and 4.26 obtained for the Cabauw station by Collaud Coen et al. (2010). The differences of the absorption coefficients calculated from these two algorithms were small and all the conclusions to be presented below were the same. Therefore, even though both algorithms were used, most of the absorption coefficients presented in figures below were calculated with the formula by Collaud Coen et al. (2010). The hypothesis here is that all particles sampled on the filter prior to the spot change affect the k factor. Therefore all scattering and absorption coefficients, single scattering albedos and backscatter fractions were averaged for each aethalometer filter spot sampling period. No conventional hourly averages are presented.

CONCLUSIONS

Aerosol optical properties were measured with a 7-wavelength aethalometer and a 3-wavelength nephelometer at the suburban site SORPES in Nanjing, China, in September 2013 – January 2015. The most important result obtained from the analysis of the data is that quantities calculated from two independent methods, i.e., backscatter fraction measured with the nephelometer and the compensation parameter k, calculated from the aethalometer data with the Virkkula et al. (2007) algorithm were correlated (Figure 1). For example, at λ = 660 nm the daily-averaged compensation parameter k ≈ 0.0017 ± 0.0002 and 0.0042 ± 0.0013 when backscatter fraction at λ = 635 nm was in the ranges of 0.100 ± 0.005 and 0.160 ± 0.005, respectively.

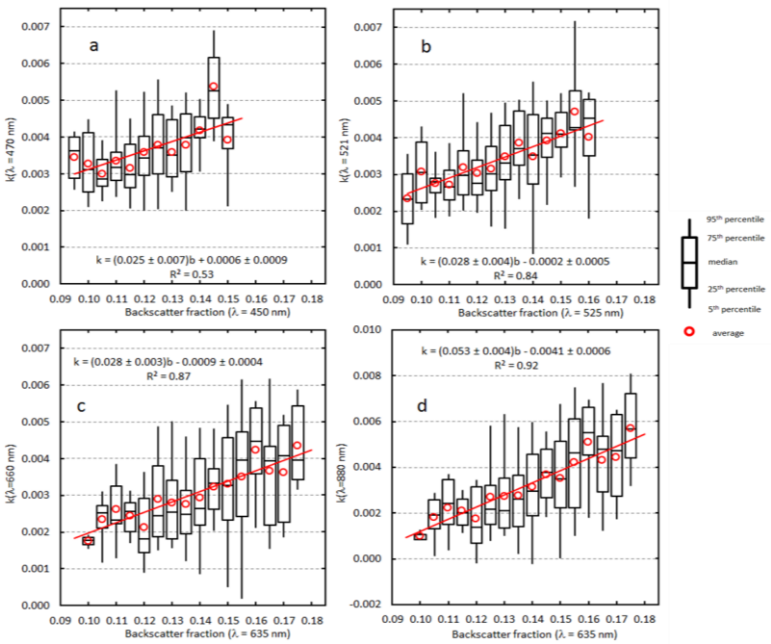

Figure 1. Daily-averaged compensation parameters of blue (λ = 470 nm), green (λ= 520 nm), red (λ= 660 nm), and near-infrared (λ = 880 nm) light classified into 0.005-wide bins of backscatter fraction at the nearest nephelometer

wavelengths (λ = 450, 525, and 635 nm).

Also the wavelength dependency of the compensation parameter depended on the backscatter fraction. : when b(λ = 525 nm) was less than approximately 0.13 the compensation parameter decreased with wavelength and at larger b it increased with wavelength (Figure 2). This dependency has not been considered in any of the algorithms that are currently used for processing aethalometer data.

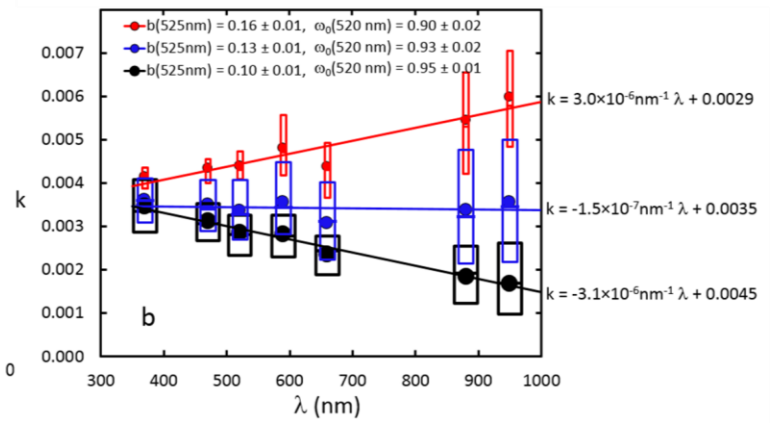

Figure 2. Wavelength dependency of the k factor in the whole data after classification into three bins of green backscatter fraction. In the box plots present the 25th to 75th percentiles, the middle lines the medians and the circles the averages in each bin. Linear regression fittings to the average k in each wavelength and backscatter bin.

The compensation parameter also depended on single-scattering albedo ω_0 so that k decreased with increasing ω_0. For the green light (λ = 521 nm) in the ω_0 range 0.870 ± 0.005 the average (± standard deviation) k ≈ 0.0047 ± 0.006 and in the ω_0 range 0.960 ± 0.005 k ≈ 0.0028 ± 0.0007. This difference was larger for the near-infrared light (λ = 880 nm): in the ω_0 range 860 ± 0.005 k ≈ 0.0055 ± 0.0023 and in the ω_0 range 0.960 ± 0.005 k ≈ 0.0019 ± 0.0011 (Figure 3).

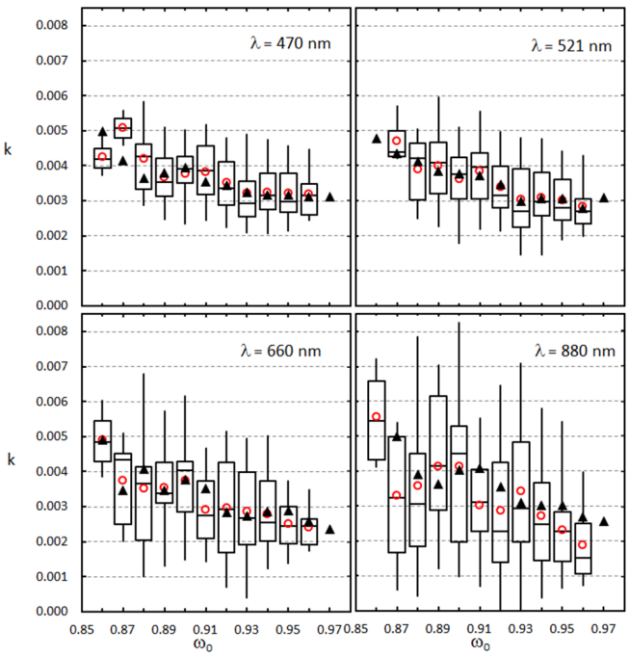

Figure 3. Daily-averaged compensation parameters of blue (λ= 470 nm), green (λ= 520 nm), red (λ = 660 nm), and near-infrared (λ= 880 nm) light classified into 0.01-wide bins of singlescattering albedo (ω_0) at the same wavelengths. The box plots present the 5th, 25th, 50th, 75th, and 95th percentiles and the circles the averages in each bin. Most ω_0 bins are based on σap calculated with the Collaud Coen et al. (2010) algorithm, the black triangles are the averages of compensation parameters classified into ω_0 bins with the

σap calculated by using the Arnott et al. (2005) algorithm

The interpretation of the above results is complicated by the fact that b and ω_0 were not independent: the particles with the lowest single-scattering albedo had the highest backscatter fractions. In spite of the uncertainties, the most important conclusion is that the backscatter fraction of the aerosol has a very clear effect on the aethalometer data and it should be taken into account. To quantify this in terms of σ_{ap} or BC mass concentrations, assume that b = 0.16 and that ATN = 80, a typical value for the red wavelength prior to filter spot change. The above average k for the red wavelength yield for the whole compensation function f = 1+kATN ≈ 1.34. This means that without the compensation the BC mass concentration or the absorption coefficient may be even tens of percent too low.

The underlying reasons for the effect of the backscatter fraction are the variations in the enhanced scattering due to variations in the asymmetry parameter and variations in the penetration depth of the particles into the filter, which depend on their size. This observation is important especially in China where anthropogenic pollution is often mixed with desert dust: backscatter fraction is large for small particles and small for large particles such as soil dust.

ACKNOWLEDGEMENTS

The research was supported by the Jiangsu Provincial Natural Science Fund (No.BK20140021), National Science Foundation of China (D0510/41275129) and Academy of Finland's Centre of Excellence program (Centre of Excellence in Atmospheric Science – From Molecular and Biological processes to The Global Climate, project no. 272041) .

REFERENCES

Arnott, W. P., Hamasha, K., Moosmuller, H., Sheridan, P. J., and Ogren, J. A.: Towards aerosol light-absorption measurements with a 7-wavelength aethalometer: evaluation with a photoacoustic instrument and 3-wavelength nephelometer, Aerosol Sci. Tech., 39, 17–29, doi:10.1080/027868290901972, 2005.

Collaud Coen, M., Weingartner, E., Apituley, A., Ceburnis, D., Fierz-Schmidhauser, R., Flentje, H., Henzing, J. S., Jennings, S. G., Moerman, M., Petzold, A., Schmid, O., and Baltensperger, U.: Minimizing light absorption measurement artifacts of the aethalometer: evaluation of five correction algorithms, Atmos. Meas. Tech., 3, 457–474, doi:10.5194/amt-3-457- 2010, 2010.

Ding, A. J., Fu, C. B., Yang, X. Q., Sun, J. N., Zheng, L. F., Xie, Y. N., Herrmann, E., Nie, W., Petäjä, T., Kerminen, V. M., and Kulmala, M.: Ozone and fine particle in the western Yangtze River Delta: an overview of 1 yr data at the SORPES station, Atmos. Chem. Phys., 13, 5813-5830, 10.5194/acp-13-5813-2013, 2013a.

Ding, A. J., Fu, C. B., Yang, X. Q., Sun, J. N., Petäjä, T., Kerminen, V. M., Wang, T., Xie, Y., Herrmann, E., Zheng, L. F., Nie, W., Liu, Q., Wei, X. L., and Kulmala, M.: Intense atmospheric pollution modifies weather: a case of mixed biomass burning with fossil fuel combustion pollution in eastern China, Atmos. Chem. Phys., 13, 10545-10554, 10.5194/acp-13-10545-2013, 2013b.

Müller, T., Laborde, M., Kassell, G., and Wiedensohler, A.: Design and performance of a three-wavelength LED-based total scatter and backscatter integrating nephelometer, Atmos. Meas. Tech., 4, 1291–1303, doi:10.5194/amt-4-1291-2011, 2011.

Müller, T., Virkkula, A., and Ogren, J.: Constrained two-stream algorithm for calculating aerosol light absorption coefficient from the Particle Soot Absorption Photometer, Atmos. Meas. Tech., 7, 4049-4070, 2014, DOI: 10.5194/amt-7-4049-2014, 2014.

Schmid, O., Artaxo, P., Arnott,W. P., Chand, D., Gatti, L. V., Frank, G. P., Hoffer, A., Schnaiter, M., and Andreae, M. O.: Spectral light absorption by ambient aerosols influenced by biomass burning in the Amazon Basin. I: Comparison and field calibration of absorption measurement techniques, Atmos. Chem. Phys., 6, 3443–3462, 2006.

Virkkula, A., Mäkelä, T., Yli-Tuomi, T., Hirsikko, A., Koponen, I. K., Hämeri, K., and Hillamo, R.: A simple procedure for correcting loading effects of aethalometer data. J. Air & Waste Management Association, 57, 1214–1222, DOI:10.3155/1047-3289.57.10.1214, 2007.

Weingartner, E., Saathoff, H., Schnaiter, M., Streit, N., Bitnar, B., and Baltensperger, U.: Absorption of light by soot particles: determination of the absorption coefficient by means of aethalometers, J. Aerosol Sci., 34, 1445–1463, 2003.

SOME RESULTS OF SPACE MONITORING OF VEGETATION COVER OF KAZAKHSTAN ARID AND SEMI-ARID ZONES BY LONG TERM SERIES OF VEGETATION INDEXES

I.S. VITKOVSKAYA[1], M.ZH. BATYRBAYEVA[1] and L.F. SPIVAK[2]

[1]The National Centre of Space Researches and Technologies of the Republic of Kazakhstan,

[2]International University of Nature, Society and Man "Dubna", Russia

Keywords: REMOTE SENSING, LONG TERM SERIES OF VEGETATION INDEX, TENDENCY, DROUGHT

INTRODUCTION

Most of the territory of the Republic of Kazakhstan, located in the arid and semi-arid zones, is vulnerable to the observed climate changes. The last decade for the territory of Kazakhstan is characterized by intensification of climate continentalization with increasing the frequency of droughts, their intensity and geographical coverage. According (III - VI National Notification of the Republic of Kazakhstan to the United Nations Framework Convention on Climate Change. Astana, 2013) the expected climate change in the near decade will reduce the moisture availability for agricultural crops, enhance of aridity, shift of the zones with sufficient humidification towards northern latitudes and decrease in grain yields.

Increased frequency of unfavorable and extreme weather conditions are characteristic on the territory of Kazakhstan in the last decade. Droughts of varying intensity and duration occur almost every year. It leads to a sharp decline in grain yields, violations of the functioning of the pastures.

The system of vegetation monitoring in Kazakhstan is based on traditional methods using the data of ground meteorological network and remote sensing data. Network of meteorological stations is still rare and conducted measurements are interpolated for large territories. Satellite observing system does not have these disadvantages, enabling regular monitoring of ground surface in different parts of the spectrum and for large areas, often located in sparsely populated, inaccessible places. In addition, the accumulated long time series of satellite data allow us to evaluate not only the current state of the vegetation, but their changes in different periods.

At present time detection of vegetation changes in the Republic of Kazakhstan, the estimation of the scale of these changes, the ability to forecast of further development have practical significance and require special attention.

METHODS

Long-term series of differential and integral vegetation indices calculated from satellite data of low and medium resolution for the growing season (April - September) of 2000-2015 were used for monitoring of state of Kazakhstan arid and semi-arid areas' natural and cultural vegetation.

Differential vegetation indexes NDVI (Rose *et al*., 1973), VCI (Kogan, 1990), calculated as 10-day composites allow to define the state of the vegetation and its changes during the growing season.

Integrated vegetation indexes (Spivak *et al*., 2012), are effectively used for the analysis of long-term changes in productivity of vegetation. Index IVI characterizes the amount of green biomass accumulated during the vegetation season and is calculated by summing the NDVI- composites in each pixel. Index IVCI (Integral Vegetation Conditions Index) is used for the analysis of inter seasonal variations of the effect of weather conditions influence on the state of vegetation.

Values of VCI, IVCI less than 30% are a good indicator of drought because a decrease of yield is noted equal or more 20% in this case (Kogan, 1990).

CONCLUSIONS

A clearly trend of reducing the values of the integral index of vegetation for vegetation cover of Kazakhstan territory was revealed in the period of 2000-2015. This trend is accompanied by year's variations related to the weather conditions. The center of gravity of aridity enhance falls on the second part of the study period. Since 2004, practically every second year is dry for the territory of the Republic or it's parts. Amplitudes of the deviations of the values of indices from trend line, caused by weather conditions year are increasing. At the same time, the spatial-temporal characteristics of drought - the duration and territorial coverage – are increasing.

Vegetation conditions indexes are the main in the detection and monitoring of droughts. In practice of remote sensing the value of IVCI equal to 0.3 is a threshold in the detection of dry conditions. The map of appearance of low values of the integral index of vegetation conditions IVCI (less than 0.3) was formed on the territory of Kazakhstan. It is actually a map of the frequency of droughts.

Analysis of distributions of integral indices for Kazakhstan territory as a whole and for individual regions and districts, in the period 2000-2015 showed significant trend of decreasing values of IVCI, that characterizes the increase of stress impact of weather conditions in the last decade.

Values of the coefficients in the equations of IVCI linear trends allow to evaluate the degree of degradation of vegetative cover on any territory. Similar calculations have allowed zoning the territory of the Republic. It is noted a greater degree of vegetation degradation in the south-western regions of Kazakhstan.

Obtained results characterize the increase of the frequency of droughts, their intensity and spatial coverage. Similar calculations can be made for different scaled objects (oblast, district, a group of fields) to determine the extent of the dryness of season by the help of satellite information.

Zoning of the Republic territory was done on the basis of digital maps of normalized IVI index for period 2000-2015. Five zones of different vegetative productivity were detected. Since 2003, the area of zones with low vegetation productivity, typical for deserts and semi-deserts, increases due to their move to the north. It is noted the deterioration of state of vegetation for almost all central part of Kazakhstan during the analyzed period.

As analysis of the location and size of selected zones with different vegetation productivity showed that in years with favorable weather conditions there is a significant increase in areas with high vegetation productivity and consequently reduction of areas with low productivity. On the other hand, there is a spatial expansion of areas with low productivity and moving it in the steppe zone, in the more northern part of the republic, in those years when the vegetation is affected by adverse weather conditions.

Trends have been identified: for areas with high vegetation productivity is negative; for areas with low productivity positive; perennial values of the area of the middle zone, which corresponding to steppe zone, fluctuated around a constant value in the presence of annual variations. The combination of the boundaries of the middle zone for all observation years shows an interesting pattern: it moves in south direct to the 46^0 - 49^0 N for all wet years, and to the north direct to $47^0$30'- 54^0 N for the all dry years.

In world practice of remote sensing the value of IVCI equaled to 0.3 is the threshold for the detection of dry conditions. The analysis of components of range (0-0.3) of IVCI index for territory of Kazakhstan shows: 1) values of IVCI (0 - (0.1)) are a major contributor; 2) long-term changes for the area of a sites with low values of IVCI have a positive trend to increase since 2002; 3) more stringent condition (IVCI<0,1) becomes significant for the entire territory of the republic practically since 2006, due to an increase in the frequency of dry years in the second half of the observation period 2000-2015.

The developed methodology can be used to assess the current state of the vegetation cover and determining of the trend of changes in the state of vegetation due to climatic factors by long-term remote sensing data for different levels of spatial differentiation in Kazakhstan.

ACKNOWLEDGEMENTS

This work was supported by The National Centre of Space Researches and Technologies of the Republic of Kazakhstan under grant “Investigation of spatio-temporal variations in drought conditions by state of vegetation cover in Kazakhstan on the basis of remote sensing of the Earth from space”.

REFERENCES

III - VI National notification of the Republic of Kazakhstan to the United Nations Framework Convention on Climate Change (2013), (Astana), 274.

Rouse, J.W., R.H. Haas, J.A. Schell and D.W. Deering (1973). Monitoring vegetation systems in the great plains with ERTS, in Proc. Third ERTS Symposium, (NASA SP-351), **1,** 309-317.

Kogan, F. (1990). Remote sensing of weather impacts on vegetation in non-homogeneous areas, *Int.Journal of Remote Sens.*, **11**, 1405-1419.

Spivak, L., I. Vitkovskaya, M. Batyrbayeva, A. Terekhov (2012). The experience of land cover change detection by satellite data, *Front. Earth Sci*., (Higher Education Press and Springer-Verlag, Berlin Heidelberg.), **6**, 2, 140–146.

REALTIVE VORTICITY AS A DYNAMIC FACTOR OF THE ARCTIC SEA ICE VARIABILITY

V.A. VOLKOV[1], A.V. MUSHTA[1,2] and A.YU. YUROVA[1]

[1] Nansen International Environmental and Remote Sensing Centre, St. Petersburg, 14th Line 7, Vasilievsky Island, Russian Federation.

[2] Institute of Earth Sciences, Saint-Petersburg State University, St. Petersburg, Universitetskaya nab., 7-9, Russian Federation

Keywords: ARCTIC, SEA ICE, ICE DRIFT, VORTICITY

INTRODUCTION

In the last decades the Arctic sea ice area was reduced to the record low values but high interannual variability was observed. Fluctuations of ice cover are not simply reflecting the change in the global radiative balance of the Earth due to greenhouse gas emission but are strongly influenced by atmospheric circulation, which determines the dynamics of air masses between the northern and middle latitudes. It is due to development of anticyclonic field over most of the Arctic basin, the lack of strong advection of warm air masses from midlatitude zone, the predominance of eastern air flows and minimal cloud cover that the most favourable conditions for increasing of the sea ice cover in the Arctic basin were formed. While this mode is lacking from circulation pattern or is infrequent such conditions favours ice decline. The variability of atmospheric pressure and wind fields over the ocean also leads to the formation of different types of surface water and ice circulation - with developed or weak Anticyclonic circulation or Transpolar drift. The variability of the ice drift under the influence of the global atmospheric circulation plays an important role in the formation of the conditions that defines the changing of multi-year ice area and the average thickness of the ice in the Arctic Ocean.

METHODS

The joint analysis of the variability of drift field and changes in atmospheric circulation types was carried out within the framework of the manual classification of large-scale atmospheric processes in the Arctic by Vangengeim-Girs-Dydina (Dydina, 1982; Przybylak, 2000). According to this classification major typical groups of synoptic situations in the Arctic are few (A, B, V, G, D and K according to position and intensity of low and high pressure centers) and all the period of instrumental observation can be spited accordingly into 6 groups that sub-sample each of those 6 types from the whole sample for the winter period (archive exists back to1939). We hypothesize here that the synoptic situation is reflected in the specific features of the vorticity fields, both in the atmosphere (wind vectors) and the ocean (sea-ice drift vectors). We therefore calculated the relative vorticity in the ECMWF atmospheric reanalysis ERA-Interim data wind vectors (gridded at 0.75 degrees for the period 1979-now) and sea ice drift fields both for entire Polar winters 1979-2012 and subdivide into 6 groups distinguished in Vangengeim-Girs-Dydina classification. Angular momentum transfer was also calculated to investigate the coupling between the atmosphere and ice fields motion. Satellite-derived Polar Pathfinder sea-ice drift vectors (gridded at 25km), a merged product of drift vectors from SMMR (1978–1987), SSM/I (1987–2006) and AVHRR (1981–2012) images (http:// nsidc.org/data/nsidc-0116.html) were provided by the US National Snow and Ice Data Center (NSIDC). Drift velocities were obtained by a maximum cross-correlation method, using daily composites of brightness temperature fields from the vertical and horizontal polarization of both the 37GHz (SMMR and SSM/I) and the 85.5GHz channels (SSM/I), as well as signals of the visible and

thermal channels of AVHHR data, to calculate displacement vectors for special patterns, which have high correlation between sequential days (e.g. Ninnis et al, 1986).

CONCLUSIONS

We found that relative vorticity is a good indicator of the circulation type and circulation type can serve as a predictor of ice conditions in the Arctic. It was shown that if the atmospheric circulation type B (it is characterized by the development of high pressure system over most of the Arctic basin and the lack of strong advection of warm air masses from middlatitudes) is predominant it contributes significantly to the creation of conditions for ice buildup, and, in opposite, decline in frequency of B type signalizes for ice decline. Vorticity combined, for example, with intensity of the zonal and meridian flow and being formalized as indices (e.g. Walsh et al, 1996; Philipp et at, 2014) could also potentially form a basis for automation of Vangengeim-Girs-Dydina classification that is manual by now.

ACKNOWLEDGEMENTS

This work was supported by the subsidence from The Ministry of Education and Science of the Russian Federation № 14.618.21.0005.

REFERENCES

Dydina, L.A. (1982). Specific Features of Synoptic Processes Development in the Arctic Area and their Utilisation in Medium-term Forecasts, Gidrometeoizdat, Leningrad, p. 224 (in Russian).

Ninnis, R.M., W.J. Emery and M.J. Collins (1986). Automated extraction of pack ice motion from advanced very high resolution radiometer imagery. J. Geophys. Res., 91(C9), 10,725–10,734.

Philipp, A., Beck, C., Huth, R., & Jacobeit, J. (2014). Development and comparison of circulation type classifications using the COST 733 dataset and software. International Journal of Climatology.

Przybylak, R. (2000). Diurnal temperature range in the Arctic and its relation to hemispheric and Arctic circulation patterns. International journal of climatology, 20(3), 231-253.

Walsh, J. E., Chapman, W. L., & Shy, T. L. (1996). Recent decrease of sea level pressure in the central Arctic. Journal of Climate, 9(2), 480-486.

DYNAMICS OF ARIDITY IN PREDBAIKALIE AT PRESENT CLIMATE CHANGES

N.N.VOROPAY[1,2], E.V.MAKSYUTOVA[1]

[1]V.B.Sochava Institute of Geography SB RAS, Irkutsk, Russia.

[2]Institute of Monitoring of Climatic and Ecological Systems SB RAS, Tomsk, Russia.

Keywords: CLIMATE CHANGE, AIR TEMPERATURE, PRECIPITATION, ARIDITY, PREDBAIKALIE, SELYANINOV HYDROTHERMAL COEFFICIENT, PED' INDEX, LANDSCAPES.

The problem of climate change has been attracting the attention of researchers and is one of the most important science questions today. Air temperature is one of the main climate parameters; so characteristics of its yearly variation, trend and interannual variability have been fully studied. Present-day data show that global surface air temperature in the 20th century has increased by 0.6 ºC.

For Predbaikalie, comparable to other regions of south-East Siberia, we have the most complete data base including information on hydroclimatic parameters from the beginning of instrumental observations till 2012. Since 1960 within most of Predbaikalie the air temperature has been increasing, while observed total precipitation and shortwave solar radiation has been decreasing. Distribution of changes intensity of the climatic elements is different.

It should be mentioned that, the study of variations of single climatic elements furthered the study of the integral characteristics of the territory, which were different humidity or aridity indices, being in most cases combinations of air temperature and precipitation values. In Russia well-known Selyaninov hydrothermal coefficient is often used.

$$HTC = \frac{\sum R}{0.1\sum T}$$

- ∑R – sum of precipitation (mm) for vegetation season;
- ∑T - average daily temperature accumulated mean above 10 ºC for the period above 10 ºC.

We determined arid conditions in steppe and forest-steppe landscapes within the territory of the South-East Siberia for the period of active vegetation from June to August. The applied limits were: 0.8 – drought, 0.4 –severe drought.

Drought frequency was calculated for certain months and for the active vegetation period. June is a critical month for droughts; during cyclonical activity periods in July and August sufficient or extreme moistening is usually registered. Averaged HTC values for the vegetation period do not reflect actual extreme events revealed for single months. Then, the drought territory in different years was evaluated. There the maximum drought area occurs in June.

Forecasting, of a single meteorological characteristic and complex indices such as HTC, is one of the main tasks in climatology. Its reliability is determined by the sufficient information base, which includes long-term data of instrumental observations from meteorological stations. However, data from the majority of Predbaikalie stations were registered only from 1940`s. Only the Irkutsk station had more information on air temperature and precipitation since the late 19th century. In this respect, we were confronted with a problem of possible reconstruction of meteoparameter series by means of a regression model.

To reconstruct HTC it is possible to use linear regression equations as significant correlation coefficients equal to 0.25-0.96 (significance ≤ 0.05). Application results were obtained only for those stations, where linear correlation

coefficients-with Irkutsk station are higher than 0.90 (Ust'-Ordynskiy and Khomutovo in September). In other cases, low correlation coefficients result in smoothing-out of reconstructed time series. It leads to the decrease of amplitude variations and loss of critical values for separate years. Those values characterize the drought condition, and in particular severe drought, if the correlation coefficient is less than 0.80, we can state only general variation regularities in the reconstructed series, which would indicate only duration of these existing cycles, but not drought occurrence frequency.

As a result of long-term variability of environmental factors, both natural and anthropogenic, the structural and functional characteristics of landscapes are changing, and under extreme conditions they completely can be transformed.

To study droughts in different landscapes index S_i, suggested by D.A. Ped', is the most appropriate. One drought or excessive moistening of a particular region in a definite season is characterized not by the air temperature and precipitation values, but by their anomalies compared to climatic norms:

$$S = \frac{\Delta T}{\sigma_T} - \frac{\Delta R}{\sigma_R}$$

where $\Delta T, \Delta R$ are anomalies (deviations from the norm) of monthly air temperatures and precipitation, σ_T, σ_R - mean-square deviations. The following conditions are used for determinations of extreme events:

For droughts $\Delta T>0$ *and* $\frac{\Delta T}{\sigma_T}>0$, $\Delta R<0$ *and* $\frac{\Delta R}{\sigma_R}<0$, *then* $Si>0$

For excessive moistening $\Delta T<0$ *and* $\frac{\Delta T}{\sigma_T}<0$, $\Delta R>0$ *and* $\frac{\Delta R}{\sigma_R}>0$, *then* $Si<0$

We estimate the intensity of drought: weak $1.0 < S_i < 2.0$; medium $2.0 \le S_i < 3.0$; severe $S_i \ge 3.0$. We estimate the intensity of excessive moistening: low $-2.0 < S_i < -1.0$; medium $-3.0 < S_i \le -2.0$; high $S_i \le -3.0$.

Analysis results of index S_i distribution are comparable to the results of Selyaninov coefficients; there is a high correlation between indices.

Index S_i was calculated for 36 weather stations from Predbaikalie. We studied long-term variations of air temperature and precipitation for 1940-2006 (from May to September). Studied weather stations are located in different physiogeographic conditions: at plain and plateau landscapes (Middle and South Taiga, Steppe and Forest zone) and mountain landscapes (Taiga, Tundra, Bald and Nival areas).

Annual amplitude of index varies from 5.5 to 9.8. The maximum values are observed in the Forest-Steppe zone in May and June (3.4-4.2) in the South Taiga - in May, July, August (3.9-4.7), in the Middle Taiga zone - in June (4.0) and in August (4.2-4.8). Stations located in the Taiga, Tundra, Bald and Nival landscapes have maximal values in May and August (3.6-5.6). Minimum indexes observed at the Steppe and Forest zones in July and September (-4.1 ÷ -6.0), at the South Taiga in July (-3.5 ÷ -5.7), at Middle Taiga in May (-4.8 ÷ -6.7) and September (-5.0), at mountain stations in July-September (-4.0 ÷ -5.7).

According to obtained data there were periods when Predbaikalie was embraced by drought. It was from 1990 to 2008. Year 2002 was extra dry. This year during the vegetation months the numbers of droughts were more than 60%. In 2007 the whole study area was embraced by drought from July to September. Where were years of continuous dry periods from 2 to 5 months (1979, 1986, 1993, 2002, 2003, 2005, and 2007). Moisture excessive periods were mostly recorded at the beginning of the studied period.

Tendencies of changes in S_i index were calculated for the 60-year period (1940-2000). Trend values in most cases are statistically insignificant. In the Steppe and Forest-Steppe stations droughts frequency

increases in May. In the Taiga zone droughts increased in the active vegetation season (from June to August). In September, both positive and negative trends are observed. Positive trends (up to 0.4 per 10 years) are the maximum by modulus.

The beginning of instrumental observation period for most stations Predbaikalie occurs only at 40s of XX century. We calculate the index for the long-term weather station Irkutsk since 1882. Significant trends were found in May. However, the amplitude of interannual fluctuations increases in recent decades. In different months this increase occurs due to the prevalence of extreme deviations of either positive or negative sign. For example, the positive extremes prevail in June, negative - in July, August and September. Thus, we can talk about a redistribution of dry and wet periods within the vegetation season. The number of weak atmospheric droughts has increased in all months of the growing season. The number of periods with weak excessive moisture is decreases. The medium intensity of phenomens have complicated structure of changing.

Droughts increases in all months, wet periods decrease in May and June, and increases from July to September. The extreme droughts increases in the first half of the summer and wet periods increases in August and September.

CONCLUSION

The statistically significant trend of aridity increasing in the territory Predbaikalie observed only in May.

Redistribution of dry and excessive moisture periods during the growing season was found for 1940-2000 compared with 1882-1939. The number of weak and medium atmospheric droughts during the months of the growing season has increased. There has been an increase in the frequency of strong drought in the first half of the summer and a decrease in August and September.

The relations of heat and moisture in the Predbaikalie for long-term period of instrumental observations experience periodic fluctuations in the absence of significant trends. Thus, the boundaries of natural areas over the past 100 years did not undergo significant changes.

THE CHARACTERISTICS OF VERTICAL DISTRIBUTION AND REGIONAL TRANSPORT OF $PM_{2.5}$ WITHIN THE LOWER TROPOSPHERE DURING HIGH POLLUTION EPISODE WINTER OF 2015 IN SHANGHAI, CHINA BASED ON TETHERED BALLOON

DONGFANG WANG[1,2], QINGYAN FU[2,*], AIJUN DING[4], GUANGLI XIU[3], ZHI NING[5], JUNTAO HUO[2], YUSEN DUAN[2], XIN YANG[1,*], XIAOHAO WANG [2], YONG YANG [2], KUN ZHANG[3]

[1]Shanghai Key Laboratory of Atmospheric Particle Pollution and Prevention, Department of Environmental Science and Engineering, Fudan University, Shanghai 200433, China

[2]Shanghai Environmental Monitoring Center, Shanghai 200235, China

[3] School of Resources and Environmental Engineering, East China University of Science and Technology, Shanghai 200237, China

[4]Institute for Climate and Global Change Research & School of Atmospheric Sciences, Nanjing University, Nanjing, 210093, China

[5] School of Energy and Environment, City University of Hong Kong, Tat Chee Avenue, Kowloon, Hong Kong Special Administrative Region

Keywords**:** $PM_{2.5}$; VERTICAL PROFILE; REGIONAL TRANSPORT; TETHERED BALLOON; SHANGHAI; YRD

ABSTRACT

A tethered balloon-based field campaign was launched for the vertical observation of air pollutants within the lower troposphere of 1000m in Shanghai， one megacity of China during the heavy pollution season in 2015. A custom-designed big load 200kg observation platform relying on tethered balloon and ground-based devices were synchronously deployed for the measurement of multiple air pollutants and meteorological parameters. The high pollution episode was captured to reveal the characteristics of vertical distribution and regional transport of $PM_{2.5}$ in Yangtze River Delta (YRD) on Dec. 14. The observed shallow boundary layer less than 400m in early morning and night caused the high concentration of $PM_{2.5}$ on the lower troposphere around the ground due to the nocturnal inversion, which ascended to more than 800m during the daytime. Wind profiles showed that the dominant wind direction was northwesterly from ground level to the top of boundary layer. Vertical profiles of $PM_{2.5}$ and relevant gaseous pollutants revealed that $PM_{2.5}$ concentration generally kept at a constant level from ground to the top of boundary layer but decreased from 200~300μg/m^3 to lower than 10μg/m^3 when the height exceeded the boundary layer. However, a thin layer of high concentration $PM_{2.5}$ emerged above the top of boundary layer in the early morning, suggesting the regional transport existed at high altitude. The vertical distribution of SO_2 was similar to the profile of $PM_{2.5}$, while the high concentration of SO_2 at about 800m in the afternoon suggested the significant transport of primary pollution. With the support of Lagrange pollutant dispersion model, the source regions of transported $PM_{2.5}$ at different altitudes were identified in farther northwestern regions around Shanghai. The results indicated that the pollutants above the boundary layer came from long-distance transport, while the pollutants within the boundary layer came from short-distance transport. The pollutants from long-distance can be transported to ground by vertical convection. A further analysis suggested that the axis between Nanjing and Shanghai was an important transport pathway and the emissions from Suzhou-Wuxi-Changzhou cities in the Yangtze River Delta (YRD) contributed the pollution to Shanghai during this high pollution episode.

This study provided a further insight of vertical distribution and regional transport of $PM_{2.5}$ and relevant pollutants over the YRD, which can supply implications to the government for the joint control and management of $PM_{2.5}$ pollution in YRD.

Correspondence to: Qingyan Fu (qingyanf@semc.gov.cn); Xin Yang (yangxin@fudan.edu.cn)

PERFORMANCE EVALUATION OF LINE SOURCE DISPERSION MODELS FOR SHORT-TERM ESTIMATION AT ROAD INTERSECTION

D. WANG[1], Z. WANG[1] and Z.R. PENG[1,2]

[1] Center for ITS and UAV Applications Research, State Key Laboratory of Ocean Engineering, School of Naval Architecture, Ocean & Civil Engineering, Shanghai Jiao Tong University, Shanghai 200240, China

[2] Department of Urban and Regional Planning, University of Florida, Gainesville, FL 32611-5706, USA

Keywords: FINE PARTICULATE MATTER, LINE SOURCE DISPERSION MODEL, URBAN AIR QUALITY, SHORT-TERM ESTIMATION

INTRODUCTION

In urban area, human suffers from health effects of ambient air pollution. Fine particulate matter ($PM_{2.5}$), carbon monoxide (CO) and other air pollutants has been widely concerned around the world. $PM_{2.5}$ has been shown to be related to lung cancer and other serious health effects (Cohen et al., 2005). Road intersections are more contaminated due to large variations in traffic, such as traffic flow (free, interrupted, or congested), vehicular state (idle, acceleration, deceleration, cruise, etc.), vehicle type (cars, buses, trucks, etc.) (He et al., 2009; Soulhac et al., 2009; Gokhale, 2011; Mazzeo and Venegas, 2012). Hence, the effective estimation is thus critical for relieving the health risk in such a microenvironment.

Some approaches have already been used to estimate air pollutants levels at intersections. For example, computational fluid dynamics (CFD) models are used to simulate the dispersion of air pollutants at intersections but the modeling results of them are less validated compared to the real field measurements (Chu et al., 2005); line source dispersion models, such as M-GFLSM, CAL3QHC, and CALINE4 have also been applied for the estimation of pollutants concentrations at intersections with the acceptable results in previous studies while these models just demonstrate their feasibility of forecasting air pollutants at longer time scales such as daily and hourly (Gokhale and Raokhande, 2008; Kho et al., 2014). Due to the complex traffic conditions and variable meteorology, air pollutants dispersions could be more complex around intersections in comparison with other traffic environments (Tiwary et al., 2011). Moreover, the concentrations of air pollutants at road intersections have been proved to vary in minutes due to the influence of traffic signals (Zito et al., 2008; He et al., 2012), which inevitably increases the complexity of pollutants predictions. Although serious adverse health consequences of short-term exposures to high level of air pollutants have been identified (Kumar et al., 2013), few studies have focused on the fine-scale (e.g., minute-scales) evaluation of air pollutants. Hence, it is necessary to test whether the present models are suitable for the fine-scale estimation, so that correspondent application can help to evaluate the health risk of short-term exposure.

This paper attempts to estimate the performances of two popular air quality models (i.e., CAL3QHC and CALINE4) used to predict air pollutants levels at 5-min scale) at a suburban intersection in Shanghai at three time periods (i.e., morning and afternoon peak hours, and midday) as well as distinguishing wind speeds. Two typical traffic-related air pollutants (i.e., PM2.5 and CO) were selected here. PM2.5 is not only an immediate product of traffic emissions but also a secondary product by physical and chemical reactions (Health Effects Institute, 2010). Conversely, CO is a stable gaseous pollutant and mainly contributed by engine combustions, its structure could hardly be changed in the outdoor environments (Zito et al., 2008). These two pollutants with different nature can be used to further examine the sensitivity of the two models to different pollutants.

METHODS

In this study, an intersection located in the suburb of Shanghai was selected for data collection. This signalized intersection consists of Dongchuan Road and Cangyuan Road perpendicular to each other (Figure 1). Shanghai Jiao Tong University (SJTU) sits northeast to the intersection, while residences are in other directions. There is always congestion at this intersection at peak hours. Dongchuan Road is a four-lane road, and the traffic flow is mainly composed of cars, buses and trucks. Cangyuan Road is a two-lane road, and its traffic flow includes trucks, and also cars and buses. Due to the openness around the intersection, there is hardly a canyon effect of air pollutant dispersion. The road geometry is shown in Figure 1, together with locations of the sampling. The azimuth bearing of Cangyuan Road is 20 degrees to the north and the bearing of Dongchuan Road is 110 degrees to the north.

The whole field campaign lasted for four days in spring 2013, and daily measurement was split into peak (morning (7:00~9:00), evening (16:00~18:00)) and off-peak (midday (11:00~14:00)) periods. Experiments simultaneously referred to roadside and setback monitoring. Roadside monitoring was moveable on four corners of the intersection, from Site 1a to Site 1d in turn during every sampling period of a day, whereas as a background reference site the setback (Site 2 in Figure 1) sat on SJTU campus with about 300m northeast to the intersection.

Figure 1. Field measurement site.

All the data were collected at a time scale of one minute. The 1-min average concentrations of $PM_{2.5}$ and CO were measured using portable devices (TSI Sidepak AM 510 Personal Aerosol Monitor for $PM_{2.5}$ and Langan Model T15n CO Measurer for CO). These devices were set up 1.7m above the ground, since this height is close to breathing zone of adult pedestrians. The Davis Vantage VUE Weather Station sat on SJTU campus (Site 2 in Figure 1), and it was mounted 2.5m above the ground to measure meteorological parameters, such as temperature, wind direction and wind speed. $PM_{2.5}$ and CO concentrations are presented in Figure 2a and 2b, respectively. Figure 2c shows the wind rose.

Traffic data were collected by using video cameras. All the vehicles were sorted into four types: light-duty diesel vehicles (LDDV), heavy-duty diesel vehicles (HDDV), light-duty gasoline vehicles (LDGV) and heavy-duty diesel vehicles (HDGV). The traffic volume of each vehicle type from each direction was counted, which will be used in the model application part. The total volumes of each vehicle type are shown in Figure 2d. As Figure 2d shows, the traffic flow is mainly composed by LDGV.

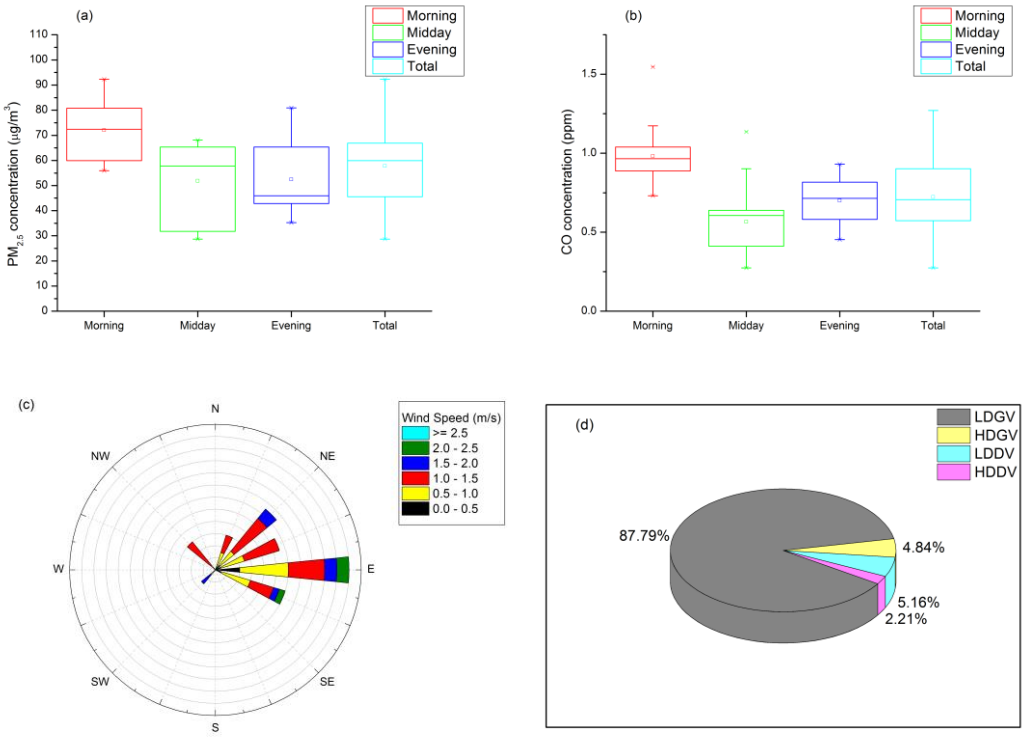

FIGURE 2 Data description. (a)$PM_{2.5}$ concentration (b) CO concentration (c) Wind rose (d) Volume type.

In order to estimate the performances of CAL3QHC and CALINE4 used to predict air pollutants levels at 5-min scale, these two models were applied at the road intersection. As Figure 3 shows, there are eight links in CAL3QHC model Link A, Link B, Link C and Link D are represented for Dongchuan Road. Link A and Link B constitute one direction of Dongchuan Road, while Link C and Link D constitute another direction. Link A and Link C account for the approach part of Dongchuan Road, while Link B and D account for the departure part. Link E to H are represented for Cangyuan Road, and the meanings are similar with Link A to D. Link A, Link C and Link E, Link G are set as queue link, while the other links are set as free flow link. The total length of Link A and Link B is 2km, and the total length of Link E and F is also 2km. The positions of Site 1a to 1d (receptors) are as Figure 3 shows.

In CAL3QHC model application case, we used 5-min average traffic and meteorological data to estimate short-term concentrations in five minutes. For this purpose, 5-min average meteorological data (such as temperature, wind speed and wind direction) were used as meteorological inputs. And traffic volumes on each link for inputting were converted from traffic volumes of each link in five minutes, for inputs of traffic volumes need one-hour average data.

$$V_{input} = V_{5\min} \times 12 \qquad (1)$$

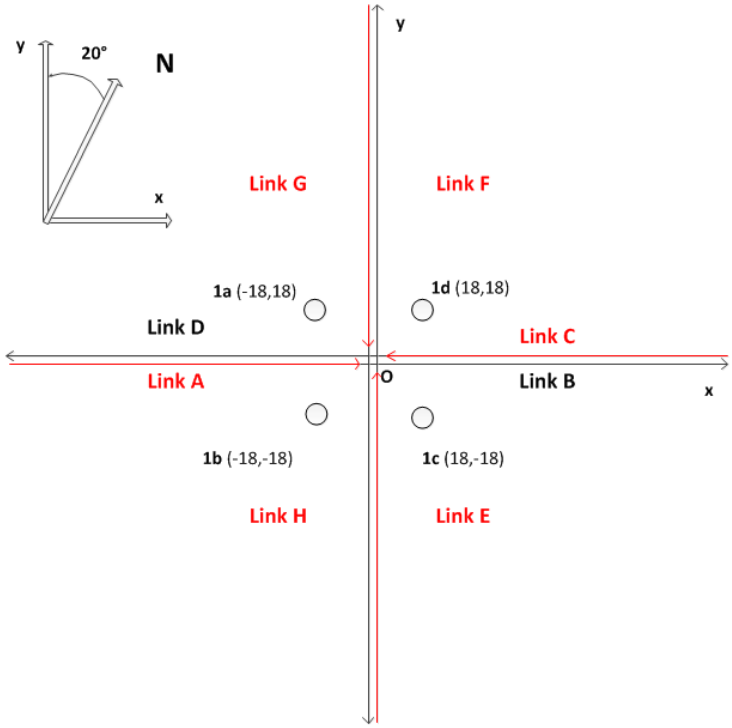

FIGURE 3 Line geometry system for CAL3QHC.

The setting of link geometry for CALINE4 was the same as for CAL3QHC, the only difference was that all the links in CALINE4 is free flow link, for there was not a queue link setting in CALINE4. Meteorological data were 5-min average data, and traffic volume inputs were calculated by Eq. (1). The wind direction is assumed to be almost the same in 5 minutes. Thus, the input value of wind direction standard deviation is settled to be 5 degrees (the minimum acceptable value for CALINE4).

To evaluate the performance of CAL3QHC and CALINE4 involving modeling ability and precision, various statistical indexes were presented. The absolute bias (AB) is used to evaluate the bias between predicted and observed values, while fractional bias (FB) is a dimensionless number to evaluate the bias. FB varies between -2 and +2, and 0 means that there is no bias. Root mean square error (RMSE) emphasizes the variation of the model estimation, and normalized mean square error (NMSE) is a normalized form of RMSE ranged between 0 and 1. Index of agreement (*d*) is intended to be a descriptive measure, which can be applied in order to make cross-comparisons between models. Instead of the correlation coefficient (r) or the coefficient of determination (r^2), the value of *d* is not a correlation measure, but a measure to describe how error free the model prediction is. It ranges from 0 to 1, and the value of 1 represents a perfect agreement of the predicted and observed values, while 0 indicates a complete disagreement. There statistical criteria are defined by Eqs. (2)-(6):

$$\mathrm{AB} = \bar{P} - \bar{O} \tag{2}$$

$$\mathrm{FB} = \frac{(\bar{P} - \bar{O})}{(\bar{P} + \bar{O})/2} \tag{3}$$

$$\mathrm{RMSE} = \sqrt{\frac{\sum_{i=1}^{n} (P_i - O_i)^2}{n}} \tag{4}$$

$$\mathrm{NMSE} = \frac{\overline{(P_i - O_i)^2}}{\bar{P} \cdot \bar{O}} \tag{5}$$

$$d = 1 - \frac{\sum_{i=1}^{n}(P_i - O_i)^2}{\sum_{i=1}^{n}[|P_i - \bar{O}| + |O_i - \bar{O}|]^2} \quad (6)$$

CONCLUSIONS

Table 1 Performance measures of CAL3QHC and CALINE4

Parameters	$PM_{2.5}$ (μg/m^3)		CO (ppm)	
	CAL3QHC	CALINE4	CAL3QHC	CALINE4
Absolute bias (AB)	-2.50	-0.74	**0.03**	0.48
Fractional bias (FB)	-0.04	**-0.01**	0.04	0.50
Root mean square error (RMSE)	4.67	4.77	**0.50**	1.08
Normalized mean square error (NMSE)	**0.01**	**0.01**	0.45	1.33
Index of agreement (*d*)	**0.98**	**0.98**	0.51	0.25

Table 1 shows the performance measures for total data. The results show that in this case, CAL3QHC has lower RMSE and NMSE than CALINE4 for CO concentration estimation, and CAL3QHC also has lower AB and FB. The *d* value of CAL3QHC also shows better performance than the *d* value of CALINE4 result. For $PM_{2.5}$ concentration estimation, both CAL3QHC and CALINE4 have low RMSE and NMSE, and the *d* value is pretty good as well. In contrast with CO concentration estimation, CALINE4 has lower AB and FB than CAL3QHC for $PM_{2.5}$ concentration estimation.

To evaluate the performances of models using at 5-min scale, the results were compared with Gokhale's study in India (Gokhale and Raokhande, 2008). PM_{10} and $PM_{2.5}$ concentrations were predicted at day scale by three different models, include CAL3QHC in that study. The NMSE, FB and IA of $PM_{2.5}$ results were 0.5, -0.3, and 0.5 respectively. Compared with Table 1, the performance of CAL3QHC at 5-min scale is not worse than the day-scale results, while CALINE4 does not perform well for CO. CAL3QHC uses traffic signal parameters in estimation, while CALINE4 does not; That may interpret why CAL3QHC generally perform better than CALINE4.

This study presents a successful try of short-term estimation at intersection by using line source dispersion models. However, monitoring campaign in varied areas and seasons are required for further study.

ACKNOWLEDGEMENTS

The authors wish to acknowledge the support from the State Key Laboratory of Ocean Engineering of China (GKZD010059). We also would like to thank Yusen Duan and Huxiong Cui from Shanghai Environmental Monitoring Center for their assistance in the instrumental calibration. Finally, we are grateful to Yelun Liu, Jingjing Chang, Daozheng Zhang from the Center for ITS and UAV Applications Research at Shanghai Jiao Tong University for their hard work in data collection and processing.

REFERENCES

Benson, P. E. (1992). A review of the development and application of the caline3 and 4 models. Atmospheric Environment Part B Urban Atmosphere, 26(3), 379-390.

Cohen, A. J., Anderson, H. R., Ostro, B., Pandey, K. D., Krzyzanowski, M., Künzli, N., Gutschmidt, K., Pope, A., Romieu, I., Samet, J. M. and Smith, K. (2005). The global burden of disease due to outdoor air pollution.. Journal of Toxicology & Environmental Health Part A, 68(13-14), 1301-1307.

Chu, A. K. M., Kwok, R. C. W., & Yu, K. N. (2005). Study of pollution dispersion in urban areas using computational fluid dynamics (CFD) and geographic information system (GIS). Environmental Modelling & Software, 20(3), 273–277.

Gokhale, S., and Raokhande, N. (2008). Performance evaluation of air quality models for predicting pm10 and pm2.5 concentrations at urban traffic intersection during winter period.. Science of the Total Environment, 394(1), 9–24.

Gokhale, S. (2011). Traffic flow pattern and meteorology at two distinct urban junctions with impacts on air quality. Atmospheric Environment, 45(10), 1830-1840.

He, H. D., Lu, W. Z., & Xue, Y. (2009). Prediction of pm10 concentrations at urban traffic intersections using semi-empirical box modelling with instantaneous velocity and acceleration. Atmospheric Environment, 43(40), 6336–6342.

He, H. D., & Lu, W. Z. (2012). Urban aerosol particulates on Hong Kong roadsides: size distribution and concentration levels with time. Stochastic Environmental Research & Risk Assessment, 26(2), 177-187.

Health Effects Institute. (2010). Traffic-related air pollution: a critical review of the literature on emissions, exposure, and health effects. Environment, 131, 409-444.

Huang, K., Zhuang, G., Lin, Y., Fu, J. S., Wang, Q., & Liu, T., et al. (2011). Typical types and formation mechanisms of haze in an eastern asia megacity, Shanghai. Atmospheric Chemistry & Physics, 12(1), 105-124.

Ishaque, M. M., & Noland, R. B. (2008). Simulated pedestrian travel and exposure to vehicle emissions. Transportation Research Part D Transport & Environment, 13(1), 27–46.

Kho, F. W. L., & Law, P. L. (2014). A predictive study: carbon monoxide emission modeling at a signalized intersection. Journal of Engineering Science & Technology.

Kumar, A., & Goyal, P. (2013). Forecasting of air quality index in delhi using neural network based on principal component analysis. Pure & Applied Geophysics, 170(4), 711-722.

Mazzeo, N. A., & Venegas, L. E. (2012). Hourly NOx concentrations and wind direction in the vicinity of a street intersection. International Journal of Environment & Pollution, 48(1/2/3/4), 96-104.

Soulhac, L., Garbero, V., Salizzoni, P., Mejean, P., & Perkins, R. J. (2009). Flow and dispersion in street intersections. Atmospheric Environment, 43(18), 2981-2996.

Tiwary, A., Robins, A., Namdeo, A., & Bell, M. (2011). Air flow and concentration fields at urban road intersections for improved understanding of personal exposure. Environment International, 37(5), 1005-18.

Zito, P., Chen, H., & Bell, M. C. (2008). Predicting real-time roadside CO and NO2 concentrations using neural networks. Intelligent Transportation Systems IEEE Transactions on, 9(3), 514-522.

TWO-YEAR COMPARISON OF METHANE FLUX MEASUREMENTS USING STATIC CHAMBER AND EDDY COVARIANCE TECHNIQUES ON AN ALPINE WETLAND ON THE QINGHAI-TIBETAN PLATEAU

K. WANG, X.H. ZHENG, Z.S. YAO, H. ZHANG, L. MA and L. LI

Institute of Atmospheric Physics, Chinese Academy of Sciences,
Huayanli 3, Chaoyang, Beijing 100029, China.

Keywords: METHANE, WETLAND, CHAMBER, EDDY COVARIANCE.

INTRODUCTION

The Qinghai-Tibetan Plateau (QTP) has a vast area of alpine wetlands with nearly 50,000 km^2 (Zhao *et al.*, 2010). These wetlands have stored a great amount of organic carbon in the soil due to low decomposition rate under cold environment over the past thousands of years. The QTP wetlands are potential great sources of CH_4 since they are currently experiencing rapid climate change and massive human activities. It is of great importance to investigate the dynamics and the budget of CH_4 of the QTP wetlands.

The static chamber and eddy covariance (EC) are the most commonly used techniques for measuring CH_4 emissions from natural ecosystems. The static chamber is very popular basically due to its simplicity in use and principle, however, is criticized for discontinuous series of measurements over a limited area. Moreover, the chambers may bias the emission estimates due to modification in the micro-environment inside the enclosed space. The EC measurement of CH_4 flux becomes available during the last decade due to development in commercial fast-response gas analysers based on laser absorption spectroscopy (e.g. RMT200 from Los Gatos Research and LI-7700 from LI-COR). The EC technique provides integrated continuous measurements over a large area, which enables us to reveal the diurnal pattern of CH_4 emissions. However, sometimes the application of EC may be limited due to the high expense of instruments, the non-ideal field conditions (the assumptions of EC theory should be fulfilled) and the requirements in daily instrumental maintenance and continuous power supply.

Obviously it is necessary to carry out comparison measurements between static chamber and eddy covariance. It gives us a chance to investigate the sources of the differences between the CH_4 fluxes measured by the two methods, further to evaluate the applicability of methods. However, so far, we found only one comparison study that using both methods on a heterogeneous QTP wetland (Yu *et al.*, 2013). This study was only conducted for several weeks during growing season, thus may not be sufficient to address the issues mentioned above. In this study we carried out nearly two-year measurements of the CH_4 fluxes from a grazed wetland on the QTP with both EC and static chamber techniques. Our aims are to (1) compare the CH_4 fluxes measured by the two methods; (2) quantify the CH_4 flux uncertainties produced by static chamber and EC measurements; (3) estimate the annual budget of the CH_4 emissions of a QTP wetland.

METHODS

The wetland is located in Zoige County, Sichuan Province of China (102º43′29.94″ E, 34º02′06.82″ N, 3300 m a.s.l.). The mean annual air temperature of this area was 3.0 ºC, and the mean annual precipitation was 479 mm, of which more than 80% occurs between May and September. There is an average slope of 4º from the southwest to the northeast of the experimental area. Similar to many other wetlands on Tibetan-Qinghai Plateau, this wetland is classified as peatland, with micro-topography that characterized by a great many dry hummocks that stands higher due to seasonal freezing and thawing. The water table

could vary between –100 cm and 5 cm relative to the flat surfaces throughout the year. The plant community of the wetland is dominated by *Carex parva Nees* and *Kobresia humilis*, as well as several other species like *Potentilla ansrina* and *Deschampsia littoralis*. The wetland is jointly managed by 32 local households. Normally they graze sheep, yak, horse and dairy cattle on the wetland in winter (from October to December) and summer (June and July). The average grazing intensity is approximately 2.7 sheep units ha^{-1} yr^{-1}.

The EC mast was set up in the centre area of the wetland (Figure 1 and Figure 2). The measuring system consisted of a three-dimensional sonic anemometer (Wind MasterPro, Gill Instruments, UK), an LI-7700 open-path infrared methane analyser (LI-COR Biosciences, USA) and a data logger (LI-7550, LI-COR Biosciences, USA) that stored the 10 Hz raw data. The anemometer and LI-7700 were mounted at an average height of 2.2 m above ground. The measurement was started on November 27, 2013 and ended on October 30, 2015. CH_4 fluxes were computed with the EddyPro 5.0 software (LI-COR) at averaging interval of 30 min. Owing to the malfunction of the sonic anemometer, unfortunately, the flux data from July to December of 2014 was missing. The post-processing of the raw flux data, including quality control and gap filling, was done following the method proposed by Schrier-Uijl *et al.* (2010).

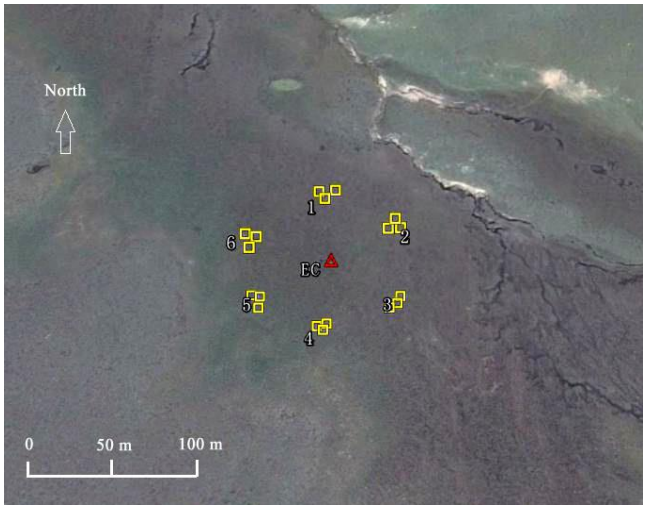

Figure 1. The Google earth image of the wetland on October 14, 2015. The red triangle and yellow empty boxes represent the position of the eddy covariance (EC) tower and the chamber base collars, respectively.

Figure 2. The eddy covariance (EC) measuring system on the wetland.

The static chamber measurements were conducted 1–2 times every week form November 26, 2013 to October 28, 2015. Eighteen stainless steel base collars (50 cm × 50 cm) were permanently installed 40–50

m away from the EC mast. They were divided into six groups, which were located in different direction sectors around the EC mast (Figure 1). The three base collars of each group were installed on the hummock (H), puddle (P) and the flat area (F) between hummock and puddle, respectively. Five gas samples were collected manually from the enclosed opaque chamber (50 cm × 50 cm × 40 cm) that covered on each base collar during the period of 8:00–10:00 of local time. The gas samples were soon analysed with a gas chromatogram (7890A, Agilent Technologies, USA), and the CH_4 concentration data was used to calculate the CH_4 fluxes with non-linear model (Wang *et al.*, 2013). The proportion of the area of the three different surfaces (H, P and F) were roughly estimated by field survey at three 10 m × 10 m plots around the EC tower, which were used to calculate the weighted chamber fluxes. The annual cumulative CH_4 flux was estimated by applying linear interpolation on the daily fluxes.

CONCLUSIONS

The major uncertainty in the half-hourly EC fluxes was random and was estimated to be 60% on average. It is mainly caused by the one-point sampling uncertainty (Kroon *et al.*, 2009). However, the flux uncertainty over longer time spans will become much smaller due to increasing independent realizations. As a result, the annual uncertainty in the EC measurements was estimated to be less than 5%.

There were several systematic uncertainties in the chamber measurements. First, the spatial variability of CH_4 emission of this study was more than 90%. We found such significant variation was closely related to water table, which would produce large uncertainty when up-scaling chamber measurements to landscape scale. Second, the non-linear flux model was not desirable when the number of valid gas concentration was less than five, thus the linear model results have to be accepted (Wang *et al.*, 2013), and therefore lead to underestimated fluxes. In this study this term of uncertainty was estimated to be 20%. Third, the daily CH_4 emission based on manual chamber measurements was prone to systematic bias due to the diurnal variation of CH_4 fluxes. We carried out the gas sampling between 8:00–10:00 to minimize this effect, however, uncertainty still remained.

The annual CH_4 emission from chamber measurements was 3.21 g C m^{-2} in 2014 and 1.63 g C m^{-2} in 2015. Due to the long-term data loss of EC measurements in 2014, we only estimated the annual emission of 2015 to 2.38 g C m^{-2}. This result was nearly 46% greater than that of the chamber measurements. We also compared the hourly CH_4 fluxes, showing that EC fluxes were 70% larger than chamber fluxes. According to the uncertainty analysis, the difference in the emission estimates was most likely caused by the heterogeneous source strengths of CH_4 of the wetland. In this study results produced by the static chamber and EC techniques could be comparable if the spatial uncertainty is taking into account.

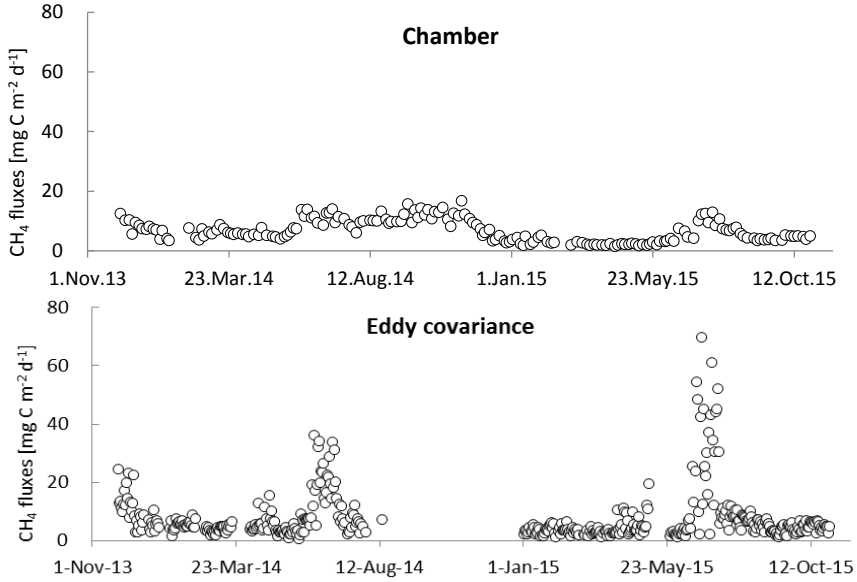

Figure 3. Daily methane fluxes measured by chamber (upper) and eddy covariance (lower) techniques.

ACKNOWLEDGEMENTS

This work was supported by the National Program on Key Basic Research Project (Grant No. 2014CB417106) and the "Strategic Priority Research Program - Climate Change: Carbon Budget and Relevant Issues" of the Chinese Academy of Sciences (Grant No. XDA01020304).

REFERENCES

Kroon, P.S., A. Hensen, H.J.J. Jonker, H.G. Ouwersloot, A.T. Vermeulen, and F.C. Bosveld (2009). Uncertainties in eddy covariance flux measurements assessed from CH_4 and N_2O observations. *Agric. For. Meteorol.*, doi:10.1016/j.agrformet.2009. 08.008.

Schrier-Uijl, A.P., P.S. Kroon, A. Hensen, P.A. Leffelaar, F. Berendse, E.M. Veenendaal (2010). Comparison of chamber and eddy covariance-based CO_2 and CH_4 emission estimates in a heterogeneous grass ecosystem on peat. *Agr. Forest Meteorol.* 150, 825–831.

Wang, K., X. Zheng, M. Pihlatie, T. Vesala, C. Liu, S. Haapanala, I. Mammarella, Ü. Rannik, and H. Liu (2013). Comparison between static chamber and tunable diode laser-based eddy covariance techniques for measuring nitrous oxide fluxes from a cotton field, *Agr. Forest Meteorol.* 171–172, 9–19.

Yu, L., H. Wang, G. Wang, W. Song, Y. Huang, S. Li, N. Liang, Y. Tang, and J.S. He (2013). A comparison of methane emissionmeasurements using eddy covariance and manual and automated chamber-based techniques in Tibetan Plateau alpine wetland, Environ. Pollut. 181, 81–90.

Zhao, L., J. Li, S. Xu, H. Zhou, Y. Li, S. Gu, and X. Zhao (2010). Seasonal variations in carbon dioxide exchange in an alpine wetland meadow on the Qinghai-Tibetan Plateau, *Biogeosciences* 7(4), 1207–1221.

INVERSION OF VEGETATION COMPONENTS BASED ON THE SPECTRAL MIXTURE ANALYSIS USING HYPERION DATA

MINGCHANG WANG, XUEFENG NIU, SHENGBO CHEN, FENGYAN WANG, GUODONG YANG

College of Geo-exploration Science and Technology, Jilin University, Changchun 130026, China.

Keywords: BIDIRECTIONAL REFLECTANCE MODEL; HYPERSPECTRAL; SPECTRAL MIXTURE ANALYSIS (SMA);CANOPY ALBEDOS; VEGETATION COMPONENTS.

INTRODUCTION

The problem of spectral mixture is always the focus and difficulties of image classification and quantitative remote sensing. Due to the spatial resolution limitation of sensors and the complex diversity of land surface, a single pixel is rarely composed of a single uniform material, and the problem of spectral mixture generally exists in remotely sensed images. Based on the mixture spectra of different components in instantaneous field of view (Johnson *et al*.,1983), spectral mixture analysis (SMA ; Adams et al., 1986; Keshava et al., 2002), an important analysis tool for vegetation remote sensing, was successfully applied to the quantitative remote sensing inversion (Elmore *et al*., 2000). Global change of spatial-temporal pattern of vegetation was very crucial in vegetation remote sensing (Myneni *et al*.,1997). High temporal resolution remote sensing provided us a key data source to monitor the annual change of phenology and vegetation cover (Funk *et al*., 2006). Moreover, SMA was successfully used to analyze the components of surface materials on the moon and Mars(Bell *et al*.,2002) and monitor the change of urban environment (Phinn *et al*.,2002), turbidity value of waterbody (Yamagata *et al*., 2001) and land degradation(Haboudane *et al*.,2002). SMA was a more powerful analysis method than the traditional vegetation index as a result of its complete vegetation spectral characteristics (Riano *et al*., 2002). SMA was used to simulate biophysical parameters of boreal forests and vegetations in Southern California to determine the changes of vegetation coverage, land coverage and vegetation seasonal variations (Roberts *et al*., 2003) . A kernel-driven BRDF model applied to the classification of hyperspectral images showed its competitive power (Fauvel *et al*.,2012). The spectral unmixing effects between linear spectral mixture analysis and constraint linear spectral mixture analysis were compared (Wang *et al*.,2009) Generally, there are five kinds of SMA models: linear model, probabilistic model, geometric optical model, random geometric model, and fuzzy analysis model, among which linear model is most popular and is commonly used.

Reflectance measured by remote sensor not only depends on the characteristics and structures of object surface, but also rests with intensity and position of light source and sensor position, so it is inconvenience to the research work. However, the oriented hemispherical reflectance (albedo) can solve the problem caused by observation direction. Therefore, in the study, on the basis of atmospheric correction and geometric calibration, the albedos of pixels will be calculated based on BRDF model of vegetation canopies. On the other hand, the end-member spectra of vegetation will be measured by Analytica Spectra Devices (ASD) spectrometer in the field, and the corresponding albedos will be calculated. Then the vegetation components will be inversed using SMA model. Moreover, the field sampling data will be used to validate the accuracy of the inversion of vegetation components.

METHODS

Radiative transfer model of vegetation canopies is the basis for the quantitative inversion of vegetation parameters, also an important premise for studying and simulating the plant growth pattern and process. The radiative transfer characteristics of vegetation canopies mainly depend on three factors: direction of light source, canopy structure and optical characteristic within the canopies. Based on the photon radiative theory of vegetation canopies, the canopy structure determines the photonic transmission and reflection, and the optical characteristic of blade determines whether a photon is absorbed or scattered. Radiative transfer model of vegetation canopies and linear SMA model can be used to calculate vegetation albedos, which are better than vegetation reflectance in linear SMA model and can be used to inverse the vegetation components in the study area.

Study area and Data preprocessing

The study area, located in Huma county of Heilongjiang province, is a high vegetation-covered area, where vegetation coverage is more than ninety-five percent and vegetation grow well, including a great species of feral herbaceous and woody plants, such as White birch, Lespedeza, Mongolian oak and Cotton grass. The outcrops are mainly late Proterozoic, Paleozoic, Mesozoic and Cenozoic strata, and East-West and North-South trending structures grow well. The soil coverage is 0.2 to 3 meters, depending on the terrain and underlying lithology, and the soil stratification is distinct. Hyperion Imaging Spectrometer, a new generation of hyperspectral sensor, is loaded on earth observation satellite platform EO-1, sun synchronous orbit satellite, launched on Nov. 21, 2000 by NASA. The orbit altitude is 615km, orbit inclination is 98.7°.Within the territory of China , its imaging time is about 10:00 a.m. (GMT). Data for the study, located in the red frame, shown in figure 1, was acquired on Sept. 28, 2011.

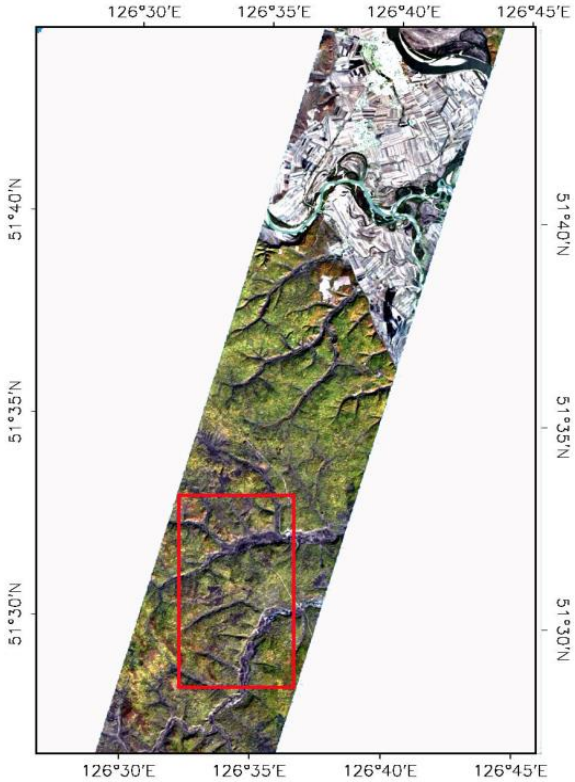

Figure 1. Hyperion data for the study area

A series of operations in Hyperion data preprocessing should include removal of zeroed bands and strongest water vapor bands, fixing of bad pixels, removal of dark vertical strips, Hyperion smile reduction, atmospheric correction and geometric correction . Of all the 242 bands, 44 zeroed bands, 2 repeated bands and 17 strongest water vapour bands were removed, so 179 bands left were ready for further analysis, in which 3 strongest water vapour bands were reserved. The accuracy of spectral information is the premise for the recognition of vegetation types using hyperspectral data. The detailed procedure was described as follows. Firstly, using the parameters of radiometric calibration provided by Hyperion data, image digital number (DN) were converted to the apparent radiances of the altimetric sensors illuminated by the sun. Secondly, using FLASH module in ENVI software, aerosol model or atmospheric correction model was selected for the atmospheric and radiometric correction according to the actual situations of geological, geographic and atmospheric environments.

Hyperspectral measuring

To meet the imaging time of satellite data, the hyperspectral measurements were carried out in the field in September, 2011. Analytical Spectral Devices (ASD) Inc., FieldSpec Pro 3 Hi-res (350-2500nm), was

mounted to a revolving platform to detect the spectra of the target materials. The FieldSpec Pro 3 Hi-Res is ideally suited for mineralogy research, as well as other applications that require high spectral resolution in the Short Wave Infrared regions. It offers the added benefit of 3nm resolution in the 350-1000nm range, 8.5nm in the 1000-1800nm range, and 6.5nm in the 1800-2500nm range. The measuring time was from 10:00 to 15:00 under the conditions of cloudless sky. Before the spectral measurement, the whiteboard calibration was needed. For a point to be measured, we calculated its mean value based on the fifteen times of resampling. For the dominant species such as mongolian oak, birch and lespedeza, the spectra of blade reflectance were directly measured. For the cotton grass, one kind of herb plant, we measured its canopy spectrum, as shown in figure 2. According to the spectral characteristics measured in situ, we chose some particular reflectance indices with wavelength of 559 nm, 691 nm, 993 nm, 1245 nm and 2234 nm.

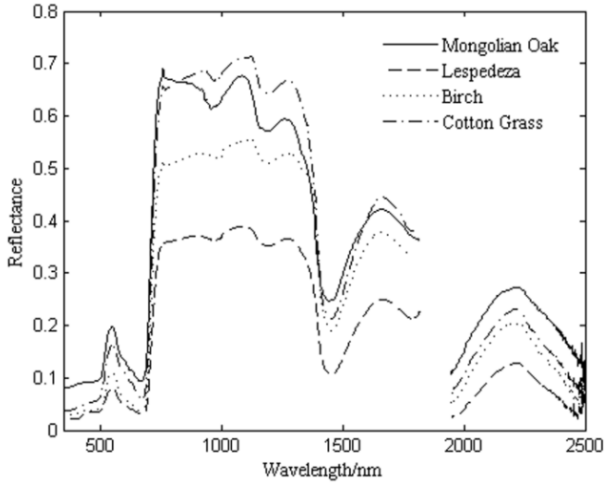

Figure 2.Vegetation spectral curves in the study area

Albedo model of satellite remote sensing data

According to bidirectional reflectance model of vegetation canopies (Verstraete *et al*.,1990; Bernardpinty *et al*.,1990; Woessner and Hapke,1987), and with respect to the reflectance of a perfectly reflecting Lambertian surface under the same conditions of illumination and observation, the bidirectional reflectance of a canopy ρ can be expressed as,

$$\rho(\theta_1,\phi_1;\theta_2,\phi_2) = \frac{\omega}{4\pi}\frac{\kappa_1}{\kappa_1\mu_2+\kappa_2\mu_1}\cdot[P_\upsilon(g)P(g)+H(\mu_1/\kappa_1)H(\mu_2/\kappa_2)-1] \quad (1)$$

$$\mu_1 = \cos\theta_1 \quad (2)$$

$$\mu_2 = \cos\theta_2 \quad (3)$$

$$\cos g = \cos\theta_1\cos\theta_2 + \sin\theta_1\sin\theta_2\cos(\phi_1-\phi_2) \quad (2)$$

$$H(x) = \frac{1+x}{1+(1-\omega)^{1/2}x} \quad (3)$$

Where, θ_1, and Φ_2 is the illumination zenith angle and solar azimuth angle, θ_2, and Φ_2 is the observation zenith angle and observation azimuth angle, g is the phase angle between the incident and the outgoing directions, ω is the average single-scattering albedo of the particles, $P(g)$ is the average phase function of the scatterer, $Pv(g)$ is hot spot effect, k_1 is average cosine of angle between leaf normal and illum*ination* direction, k_2 is average cosine of angle between leaf normal and observation direction, and $H(\mu_1/k_1)H(\mu_2/k_2)$ is the approximate function to account for multiple scattering.

$P_v(g)$ is the function that accounts for the joint transmission of the incident and outgoing radiation, which can be expressed as,

$$P_{\upsilon}(g)=\left\{\frac{\Lambda}{2}\frac{\kappa_1\mu_2+\kappa_2\mu_1}{\mu_1\mu_2}(\frac{\pi}{a})^{1/2}\exp(\frac{b^2}{a})\cdot[erf(\sqrt{a}\frac{2r}{G}-erf(\frac{b}{\sqrt{a}}))]\right.$$
$$\left.+\exp(\frac{4}{3\pi}\frac{2r}{G}\frac{\kappa_2\Lambda}{\mu_2})[\exp(-\frac{\kappa_1\mu_2+\kappa_2\mu_1}{\mu_1\mu_2})\Lambda\frac{2r}{G})-\exp(\frac{\kappa_1\mu_2+\kappa_2\mu_1}{\mu_1\mu_2}\Lambda h)]\right\} \quad (6)$$

$$G=[\tan^2\theta_1+\tan^2\theta_2-2\tan\theta_1\tan\theta_2\cos(\phi_1-\phi_2)]^{1/2} \quad (7)$$

$$a=(1-\frac{4}{3\pi})\frac{G\kappa_2\Lambda}{2r\mu_2} \quad (8)$$

$$b=\frac{\kappa_1\Lambda}{2\mu_1} \quad (9)$$

Where, r is the radius of the horizontal sun fleck, Λ is leaf area density of the canopy.

$$P(g)=\frac{(1-\Theta^2)}{(1+\Theta^2-2\Theta\cos\Omega)^{3/2}} \quad (10)$$

Where, the scattering angle Ω equalsπminus g, and Θ is the asymmetric factor ranging from -1 (backward scattering) to + 1 (forward scattering).

$$\kappa_i(\mu_i)=\psi_1+\psi_2\mu_i \quad (11)$$

$$\psi_1=0.5-0.6333\chi_l-0.33\chi_l^{\ 2} \quad (12)$$

$$\psi_2=0.877(1-2\psi_1) \quad (13)$$

Where, i equals 1 or 2, the two directions of illumination and observation.

$$\chi_l=\pm\int_0^{\pi/2}|1-g_L(\theta_l)|\sin(\theta_l)d\theta_l \quad (14)$$

Where, θ_l is the leaf zenith angle, $g_L(\theta_l)$ is the leaf angle distribution.

$$V_p(g)=4(1-\frac{4}{3\pi})\frac{G}{2r\Lambda}\frac{\mu_2}{\kappa_2} \quad (15)$$

In order to convenient for inversion purposes, it is feasible to simplify the expression $P_v(g)$. If the phase angle g is more than 20°, then the backward scattering effect will be reduced, so it can be ignored. If the particles are far more than the wavelength of the incident light and close to the random distribution, and the first-order surface scattering can be regarded as isotropous, then $P(g)$ equals 1 and the hotspot effect is ignored, so the simplified model can be expressed as,

$$\rho(\mu_1,\mu_2)=\frac{\omega}{4\pi}\frac{\kappa_1}{\kappa_1\mu_2+\kappa_2\mu_1}\cdot[H(\mu_1/\kappa_1)H(\mu_2/\kappa_2)] \quad (16)$$

The reflectance measured in the field, different from the reflectance observed by the satellite, is the ratio with whiteboard, and the albedos of mixture vegetations and end-member vegetations acquired by the sensor can be calculated according to the expression listed above respectively.

Albedo model of ground ASD spectrometer

The albedo from ground measurement is the ratio of whiteboard, which is different from that of satellite observation, and the function is expressed as follow:

$$\rho_C=\frac{\omega}{4\pi}\frac{1}{\mu_0+\mu}\left\{\left[1+B(g)\right]P(g)+[H(\mu_1/\kappa_1)H(\mu_2/\kappa_2)]-1\right\} \quad (17)$$

When the backscattering effect is ignored and the phase function is simplified as $P(g)=1$, equation (17) can be expressed as follow:

$$\rho_C=\frac{\omega}{4}\frac{1}{\mu_0+\mu}[H(\mu_1/\kappa_1)H(\mu_2/\kappa_2)] \quad (18)$$

SMA model

Mixed pixel signals are generally modeled using either linear mixture model (LMM) or nonlinear mixture model (NLMM). A mixture model converts the image's DN to numerical fractions of a few end-members. End-members are spectra of proxies for materials on the ground. Processing dominate spectral signatures of mixed pixels is still an unresolved matter. As a rule of thumb, linear mixing is associated to mixtures for which the pixel components appear in spatially segregated patterns. If, however, the components are in intimate association, light typically interacts with more than one component owing to its multiply scattering, and the mixing systematics are highly nonlinear (Keshava & Mustard, 2002).The underlying physical assumption of LMM is that each incident photon interacts with a single pixel component only. A mixed pixel signal (*r*) can as such be described as a linear combination of pure spectral signatures of its constituent components, weighted by their sub-pixel fractional cover (Adams et al., 1986):

$$r = M_f + \varepsilon \tag{19}$$

Where, *M* is a matrix in which each column corresponds to the spectral signal of a specific end-member, f is a column vector $[f1, \ldots, fm]^T$ denoting the cover fractions occupied by each of the m end-members in the pixel, ε is the portion of the spectrum that cannot be modeled using these end-members(Ben Somers et al.,2011).

CONCLUSIONS

In this study, we inversed vegetation components based on bidirectional reflectance model of vegetation canopies and spectral mixture analysis using Hyperion data, and validated the accuracy of the results through field sampling. Inversion results of vegetation components was shown in figure 3.The results showed it was feasible to inverse vegetation components based on linear mixture model of spectral albedos of vegetation canopies. Because of the spectral differences within the same end-member, the end-members measured in the field were limited, and comparatively difficult to select. Moreover, purity and quantity of end-members affected the unmixing of mixture pixel model largely. Although the end-members measured in the field could be determined accurately, the noises caused by various factors (atmospheric, radiant, and topographic effects) resulted in inconsistency with image pixel spectra, undoubtedly affecting the accuracy of inversion of vegetation components.

Lack of considering the effect of adjacent pixels is a comparative weakness for the traditional linear spectral unmixing based on reflectivity. However, the linear mixture model based on spectral albedo will preferably reduce the mutual interference of reflectance spectrum.

Albedo of vegetation mixed spectra is decomposed (unmixed) into two parts: pure pixel which represents the commixture spectral characteristics and decomposition coefficients on behalf of concentration information. Then the corresponding components abundance can be estimated. What’s more, the rationality of spectral unmixing method based on albedo would be proved.

Based on the field ecological quadrate investigation, the inversion results are identical with the field survey. Nevertheless, there are still many uncertain factors while retrieving the vegetation components based on spectral unmixing model. For the high vegetation-covered study area, the effect of soil reflectance will be ignored, inevitably, the spectral unmixing will be influenced to some extent.

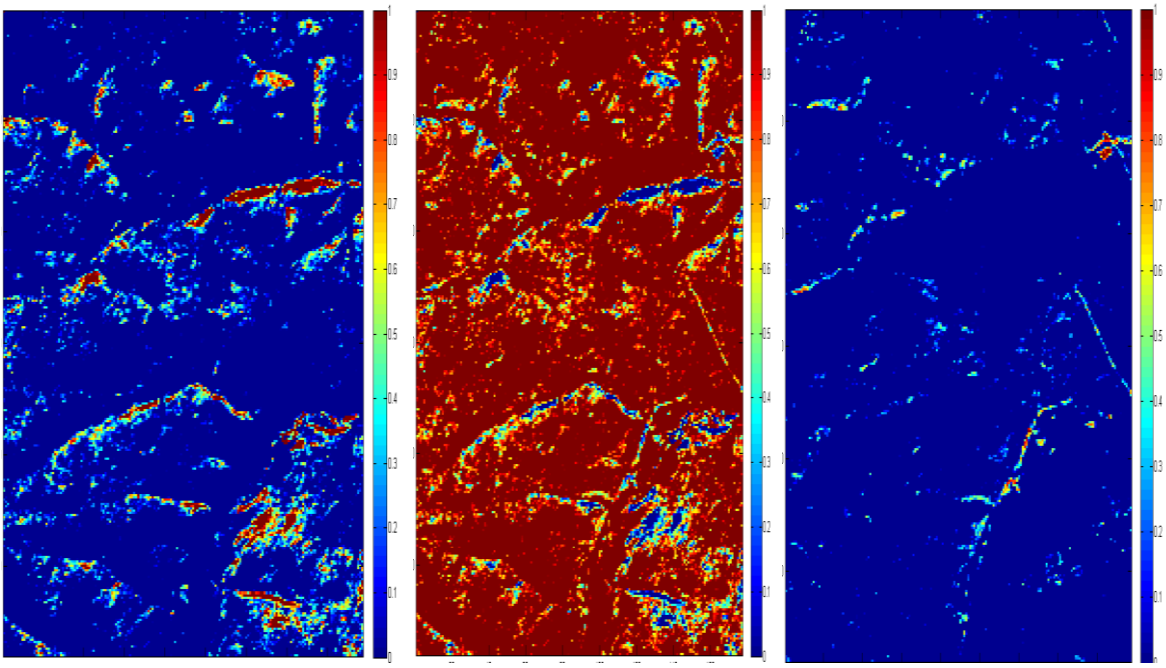

A B C

Figure3. Inversion of vegetation components (A: Lespedeza, B: Birch, C: Cotton grass)

ACKNOWLEDGEMENTS

This study was supported by the National Natural Science Foundation of China (No.40971187), the Funded By Open Research Fund Program of Key Laboratory of Digital Mapping and Land Information Application Engineering, National Administration of Surveying, Mapping and Geoinformation (No.GCWD201402), Laboratory of Regional Development and Environmental Response(2015(B)003).

REFERENCES

Adams, J. B., Smith, M. O., & Johnson, P. E. (1986),Spectral mixture modeling -A new analysis of rock and soil types at the Viking Lander-1 site.*Journal of Geophysical Research, Solid Earth and Planets* 91: 8098−8112.

Ben Somers, Gregory P. Asner, Laurent Tits, Pol Coppin.(2011), Endmember variability in Spectral Mixture Analysis: A review.*Remote Sensing of Environment* 115(7):1603–1616.

Bell, J. F., Farrand, W. H., Johnson, J. R.,et al. (2002), Low abundance materials at the Mars Pathfinder landing site: An investigation using spectral mixture analysis and related techniques. *Icarus* 158:56-71.

Elmore, A. J., Mustard, J. F., Manning, S. J., et al. (2000), Quantifying vegetation change in semiarid environments: Precision and accuracy of spectral mixture analysis and the normalized difference vegetation index. *Remote Sensing of Environment* 73:87-102.

Fauvel M, Chanussot J, Benediktsson J A.(2012), A spatial–spectral kernel-based approach for the classification of remote-sensing images.*Pattern Recognition* 45: 381–392.

Funk, C. C., Brown, M. E. (2006),Intra-seasonal NDVI change projections in semi-arid Africa. *Remote Sensing of Environment* 01:249−256.

Johnson, P. E., Smith, M. O., Taylor-George, et al. (1983), A semiempirical method for analysis of the reflectance spectra of binary mineral mixtures. *Journal of Geophysical Research* 88:3557–3561.

Haboudane, D., Bonn, F., Royer, A., et al.(2002),Land degradation and erosion risk mapping by fusion of spectrally-based information and digital geomorphometric attributes. *International Journal of Remote Sensing* 23:3795–3820.

Keshava, N., & Mustard, J. F.(2002), Spectral unmixing. *IEEE Signal Processing* 9:44−57.

Myneni, R. B., Keeling, C. D., Tucker, C. J.,et al.(1997),Increased plant growth in the northern high latitudes from 1981 to 1991. *Nature* 386:698−702.

Pinty B, Verstraete M M, Dickinson R E. (1990),A Physical Model of the Bidirectional Reflectance of Vegetation Canopies 2. *Inversion and Validation. Journal of Geophysical Research*, 95:11767-11,775.

Riano, D., Chuvieco, E., Ustin, S., et al. (2002), Assessment of vegetation regeneration after fire through multitemporal analysis of AVIRIS images in the Santa Monica Mountains. *Remote Sensing of Environment* 79: 60-71.

Roberts, D. A., Dennison, P. E., Gardner, M., et al.(2003),Evaluation of the potential of Hyperion for fire danger assessment by comparison to the airborne visible infrared imaging spectrometer. *IEEE Transactions on Geoscience and Remote Sensing* (in press).

Phinn, S., Stanford, M., Scarth, P., et al. (2002),Monitoring the composition of urban environments based on the vegetation –impervious surface_soil (VIS) model by subpixel analysis techniques.*International Journal of Remote Sensing* 23: 4131–4153.

S.,Yamagata, Y., Nakamura, F., Kaneko, M. (2001), Development of WTI and turbidity estimation model using SMA—application to Kushiro Mire, eastern Hokkaido, *Japan. Remote Sensing of Environment* 77: 1–9.

Verstraete, M. M., B. Pinty, R. E. Dickinson. (1990), A physical model of the bidirectional reflectance of vegetation canopies, 1:Theory.*Geophys. Res., this issue*, 95:11755-11765.

Wang Q.J., Lin Q.Z., Li M. X, et al. (2009), Comparison of two spectral mixture analysis models.*Spectroscopy and Spectral Analysis* 29(10):2602-2605.

Woessner, P., B. Hapke.(1987), Polarization of light scattered by clover. *Remote Sens. Environ.*, 21:243-261.

Zhang H., Yao Z. Y., Quan H., et al.(1999),New idea on the botano-geochemical exploration in Daxinganling forest covered area. *Journal of Precious Metallic Geology*, 8(1):38-40.

EMISSIONS OF NITRATED PHENOLS IN FINE PARTICLES FROM BIOMASS BURNING

X.F. WANG, R.R. GU, L.W. WANG, L.K. XUE, W.X. XU, Y.T. ZHANG, B. CHEN, W.J. LI and W.X. WANG

Environment Research Institute, Shandong University, Jinan, 250100, China

Keywords: NITRATED PHENOLS, BIOMASS BURNING, EMISSION, RATIO, FACTOR.

Nitrated phenols are toxic and do harm to human health and ecosystem. As one of the major components of brown carbon, the particulate nitrated phenols in atmosphere also have impact on the Earth's radiative forcing and regional climate. Previous filed studies in various locations have indicated the importance of biomass burning acting as a major source of atmospheric nitrated phenols. However, up to now, little is known on the emission characteristics and emission factors. In the present study, biomass burning experiments were conducted in laboratory for five common biomass fuels in North China including wheat straw, corn stalk, corncob, dead wood and fallen leaves. The biomass fuels were burned in a stove under three conditions, *i.e.*, with flames (flaming), with small flames (weakly flaming) and without any flame (smoldering). The biomass burning smoke went through a tunnel for cooling and was collected on quartz filter by $PM_{2.5}$ sampler in a chamber. The filter samples were then extracted with methanol and the sample solutions were concentrated to a very small volume. Ten nitrated phenols including nitrophenols, nitroguaiacols, nitrocatechols and nitrosalicylic acids were identified and quantified using the HPLC tandem MS method. The emission ratios of nitrated phenols to $PM_{2.5}$ varied from hundreds to one thousand μg mg^{-1} for flaming fires and were several to dozens μg mg^{-1} for smoldering fires. The most abundant species were nitrocatechols which accounted for ~90% under flaming condition. Other nitrated phenolic compounds were in very low content in fine particles, possibly because they mainly existed in gas phase instead of particulate phase due to the relatively high volatility. The mass ratios of nitrated phenols to organic matters in biomass burning smoke were close to or even smaller than that in the ambient air, indicating the vital importance of secondary formation to the ambient particulate nitrated phenols. In flaming fires, the emission factors of nitrated phenols were estimated to be 2.0 – 15.1 mg kg^{-1} for the five biomass fuels. This study presents the emission profiles of fine particulate nitrated phenols from burning of common biomass fuels and provides basic data from related modeling studies.

SPATIO-TEMPORAL ANALYSIS OF GREENLAND SNOWMELT USING MICROWAVE RADIOMETIER DATA (1988-2014)

XINGDONG WANG [1,2] , CHENG WANG [1] and XIAOHUAN XI [1]

[1]Institute of Remote Sensing and Digital Earth, Chinese Academy of sciences, No.9, Dengzhuang South Road, Haidian District, Beijing, 100094, China

[2]College of Information Science and Engineering, Henan University of Technology, Zhengzhou, Henan, No.100, Lianhua Road, Gaoxin District, Zhengzhou, Henan, 450001, China

Keywords: SMOWMELT SPATIO-TEMPORAL VARIETY DETECTION, MICROWAVE RADIOMETER, IMPROVED WAVELET TRANSFORM, GREENLAND

INTRODUCTION

Global climate and environmental change is a hot issue, and Greenland is the key region of global climate and environment change, and the Greenland ice and snow change is one of the most important factors affecting the global climate and environment change (Oza, 2015). The polar regions have the role of the 'amplifier' for the global climate and environment change, and both historical and modern observations show that the magnitude of the polar climate and environmental change is two times higher than the middle and low latitude regions, which is more easy to monitor the subtle change. The observations and simulation results show that the interannual variations of the range and surface characteristics of Greenland ice and snow (mainly reflectance) have significant effects on the global water vapor circulation, global heat balance and climate change, such as temperature and precipitation distribution (Torinesi *et al*., 2003; Picard and Fily, 2006). The interaction of the Greenland ice sheets and adjacent geospheres has a huge impact on the global climate and environment. The melt of the Greenland ice sheet will cause the change of the surface humidity, and then cause the collapse of the ice shelves and the movement of the ice (Xiong *et al*., 2014). By means of remote sensing, the snowmelt changes of the Greenland is effectively detected, and it has a great promotion effect on the global climate and environment change.

Long time series of large-scale microwave radiometers SMM/I and SMMR data have carried out a large number of ice-sheet freeze-thaw detection methods and change research, and achieved good results in Greenland and other regions (Abdaati and Steffen, 2001; Dupont *et al*., 2012; Tedesco *et al*., 2009; Mernild *et al*., 2011; Fettweis *et al*., 2007; Fettweis *et al*., 2006; Dupont *et al*., 2012; Mote, 2007; Takala *et al*., 2009). In this study, we obtained the 27-year average melt onset date, end date, duration as well as annual variation of the melt areas and the variation of the melt pixels with the seasons based on the improved wavelet transform method (Liang *et al*., 2014). Based on this, the Greenland snowmelt spatio-temporal change characteristics are obtained. The Greenland snowmelt spatio-temporal mechanism is analyzed combining with the observation of the Greenland surface.

METHODS

Microwave radiometer passively receives the temperature radiation of the ground objects (Fretwell *et al*., 2013) , and the microwave radiometric brightness temperature is very sensitive to the variation of the liquid water content in the snow, with the melt onset and end date, the bright temperature will have the dramatic changes. The paper mainly uses the SSM/I microwave radiometer data from January 13, 1988 to December 31, 2014, which is derived from the NSIDC (National Snow and Ice Data Center). The selected data channel is the 19 GHz horizontal polarization channel of the sensor SSM/I with F11, F13 and F17 platforms, and their ranks and data accuracy are the same, and stored in the same format. The difference is that SSM/I for 27 years and the sensors are equipped with F11, F13 and F17 different platforms. Therefore, it is necessary to study the different platform data are normalized to the same platform.

The overlap dates of the different kinds of data are from April 29 to December 3 in 1991, and from December 30 to May 3 in 1995, and from September 30 to January 1 in 2009. Using these overlap data can do the regression treatment by formula (1) calibrated to F8 platform.

$$T_1 = a * T_2 + b \quad (1)$$

Where, T_1 is the brightness temperature data of 19GHz band of the F8 platform, and T_2 is the brightness temperature data for platform F11, F13 and F17 corresponding to the bright temperature data, respectively, and a and b are the regression parameters as shown in Table 1.

Data transformation	Slope	Intercept	Correlation coefficient
Transform SSM/I F11 and F13 19H into SSM/I F8 19H	1.008	-1.17	R>0.99
Transform SSM/I F17 into SSM/I F8 19H	1.0286	-3.0094	R>0.99

Table 1 Regression parameter from different sensors and platform data

After all the data is normalized, use the improved wavelet-transform snowmelt detection algorithm to deal with the microwave radiometer data to extract 27-year snowmelt information.

Snowmelt detection algorithm based on wavelet transform

The basic principle of the freeze-thaw detection algorithm based on wavelet transform is (Liu *et al*., 2005; Liang *et al*., 2013): the edges of dramatic changes of the long time series brightness temperature data reflects the ice-sheet melt or freeze-up onset date (Joshi *et al*., 2001), and the melt onset date of each year is the first sharp rising edge of the brightness temperature for the curve of the time axis, and melt end date of each year is the last sharp falling edge of the brightness temperature for the curve of the time axis, and melt duration is the sum of each melt duration in a year. The method can detect whether each pixel is experienced freezing and thawing and freeze-thaw date.

The main disadvantages of the double Gauss model fitting the classification threshold of the dry and wet snow are as follows: (1)The distribution model of the dramatic changes and slow changes points is not satisfied with the double Gauss model. (2) For the Levenberg - Marquardt fitting algorithm, the initial value of the input is different, and the result is different, and the results are related to the input of the initial value. (3) The process of the algorithm is complicated.

Because of the above problems of the double Gauss model fitting the classification threshold of the dry and wet snow, the generalized Gauss model (automatic threshold method) is introduced to divide the dry and wet snow (Semmens *et al*., 2013). Its advantages are as follows: (1) Less manual input is needed. (2) The classification result is the only one.

Automatic threshold segmentation based on generalized Gaussian model

In the selected sample areas, the optimal classification threshold of dry snow and wet snow is obtained by the generalized Gauss model. The shape factor of the method is introduced, which can handle more curves with different shapes, and it has great progress compared with the double Gauss model. The principle of the model is as follows:

Let $h(X_l)(X_l = 0,1,\cdots,\mathrm{L}-1)$ is the histogram of the image, and L represents the gray level of the image. If the image is binarized, the histogram of $h(X_l)$ can be seen as the mixed probability density function of the dry snow and the wet snow in the images. In order to obtain the classification optimal threshold T^* of the dry snow and the wet snow, the image is binarized, and the KI criterion of the generalized Gaussian model is introduced:

$$J(T)=\sum_{X_l=0}^{T}h(X_l)[b_1(T)|X_l-m_1(T)|]^{\beta_1(T)}+\sum_{X_l=T+1}^{L-1}h(X_l)[b_2(T)|X_l-m_2(T)|]^{\beta_2(T)}+ \quad (2)$$
$$H(\Omega,T)-[P_1(T)\ln a_1(T)+P_2(T)\ln a_2(T)]$$

Where:

$$\begin{cases} P_1(T)=\sum_{X_l=0}^{T}h(X_l),\quad m_1(T)=\frac{1}{P_1(T)}\sum_{X_l=0}^{T}X_l h(X_l) \\ P_2(T)=1-P_1(T), m_2(T)=\frac{1}{P_2(T)}\sum_{X_l=T+1}^{L-1}X_l h(X_l) \\ \sigma_1^2(T)=\frac{1}{P_1(T)}\sum_{X_l=0}^{T}[X_l-m_1(T)]^2 h(X_l) \\ \sigma_2^2(T)=\frac{1}{P_2(T)}\sum_{X_l=T+1}^{L-1}[X_l-m_2(T)]^2 h(X_l) \end{cases}$$

$P_1(T)$ and $P_2(T)$ are the priori probability for the dry snow and the wet snow, respectively. $m_1(T)$ and $m_2(T)$ are the average value for the dry snow and the wet snow, respectively. $\sigma_1^2(T)$ and $\sigma_2^2(T)$ are the variance for the dry snow and the wet snow, respectively. $H(\Omega,T)$ is the entropy of $\Omega=\{\omega_1,\omega_1\}$. β_i is the shape parameter of $p(X_l\mid\omega_i)=a_i e^{-[b_i|X_i-m_i]^{\beta_i}}$ $(i=1,2)$. a_i and b_i are the positive constant. The calculated steps of a_i, b_i and β_i are detailed in the literature presented by Sharifi and Leongarcia in 1995. In order to get the optimal automatic partitioning threshold T^*, the smallest error probability optimization is done by formula (2), namely:

$$T^*=\arg\min_{T=0,1,\ldots,L-1} J(T) \quad (3)$$

T value is the optimal threshold T^* of the dry snow and the wet snow when formula (3) takes the minimum value.

Snowmelt detection algorithm based on improved wavelet transform

The biggest difference between the improved method and the original method is to determine the optimal classification threshold of dry snow and wet snow by using the double Gauss model, and the improved method is to use the generalized Gauss model to determine the optimal classification threshold for dry snow and wet snow.

By the multi-scale wavelet decomposition and the measured temperature data for long time series of microwave radiometer brightness temperature data, the temporal resolution is one day, the ice-sheet freeze-thaw detection accuracy based on the improved wavelet transform method is plus and minus one day.

CONCLUSIONS

It can been seen from the Greenland 27-year snowmelt spatio-temporal variety characteristics by using microwave radiometers SSM/I data (1988-2014) for Greenland snowmelt monitoring based on improved wavelet transform. The melt spatial distribution shows that the majority of melt areas are located on the edge of Greenland ice shelves. The temporal distribution of melt areas shows that the Greenland snowmelt varies with years with some rule. The melt areas are 1, 941, 875 square kilometres in 2012, and its areas are the largest. The melt areas are 916, 875 square kilometres in 1992, and its areas are the smallest. In addition, the Greenland snowmelt varies with the seasons. It is particularly acute in summer, and its melt peak is in June, July and August.

ACKNOWLEDGEMENTS

This work was supported by National Natural Science Foundation of China (General Program, No. No.41076129), Supported by Foundation of He'nan Educational Committee(No. 14A420003) and Funded by Jiangxi Province Key Lab for Digital Land(No. DLLJ201405).

REFERENCES

Abdaati, W. and K. Steffen (2001). Greenland ice sheet melt extent: 1979-1999, *Journal of Geophysical Research* **106** (D24), 33983-33989.

Dupont, F., A. Royer, A. Langlois, *et al.* (2012). Monitoring the melt season length of the Barnes Ice Cap over the 1979-2010 period using active and passive microwave remote sensing data, *Hydrological Processes* **26** (17), 2643-2652.

Fettweis, X., H. F. Lefebre and J. P. van Ypersele (2006). The 1988-2003 Greenland ice sheet melt extent using passive microwave satellite data and a regional climate model, *Climate Dynamics* **27** (5), 531-541.

Fettweis, X., J. P. van Ypersele, H. Gallée, *et al.* (2007). The 1979-2005 Greenland ice sheet melt extent from passive microwave data using an improved version of the melt retrieval XPGR algorithm, *Geophysical Research Letters* **34** (5), L05502 (DOI: 10.1029/2006GL028787).

Fretwell, P., H. D. Pritchard, D. G. Vaughan, *et al*. (2013). Bedmap2: improved ice bed, surface and thickness datasets for Antarctica, *Cryosphere* **7** (1), 375-393.

Joshi, M., C. J. Merry, K. C. Jezek and J. F. Bolzan (2001). An edge detection technique to estimate melt extent on the Greenland ice sheet using passive microwave data. Geophysical, *Geophysical Research Letters* **28** (18), 3497-3500.

Liang, L., H. D. Guo, X. W. Li and X. Cheng (2013). Automated ice-sheet snowmelt detection using microwave radiometer measurements, *Polar Research* **32**, UNSP 19746 (DOI: 10.3402/polar.v32i0.19746).

Liu, H. X., L. Wang and K. C. Jezek (2005). Wavelet-transform based edge detection approach to derivation of snowmelt onset, end and duration from satellite passive microwave measurements, *International Journal of Remote Sensing* **26** (21), 4639-4660.

Mote, T. L. (2007). Greenland surface melt trends 1973-2007: Evidence of a large increase in 2007, *Geophysical Research Letters* **34** (22), L22507 (DOI: 10.1029/2007GL031976).

Oza, S. R. (2015). Spatial-temporal patterns of surface melting observed over Antarctic ice shelves using scatterometer data, *Antarctic Science* **27** (4), 403-410.

Picard, G. and Fily, M. (2006). Surface melting observations in Antarctica by microwave radiometers: Correcting 26-year time series from changes in acquisition hours, *Remote Sensing of Environment*, **104** (3), 325-336.

Semmens, K. A., J. Ramage, A. Bartsch and G. E. Liston (2013). Early snowmelt events: detection, distribution, and significance in a major sub-arctic watershed, *Environmental Research Letters* **8** (1), 014020 (DOI: 10.1088/1748-9326/8/1/014020).

Sharifi, K. and A. Leongarcia (1995). Estimation of shape parameter for generalized Gaussian distributions in subband decomposition of video, *IEEE Transaction on Circuit and Systems for Video Technology* **5** (1), 52-56.

Takala, M., J. Pulliainen, S. J. Metsamaki and J. T. Koskinen (2009). Detection of Snowmelt Using Spaceborne Microwave Radiometer Data in Eurasia From 1979 to 2007, *IEEE Transactions on Geoscience and Remote Sensing* **47** (9), 2996-3007.

Tedesco, M., M. Brodzik, R. Armstrong, M. Savoie and J. Ramage (2009). Pan arctic terrestrial snowmelt trends (1979-2008) from spaceborne passive microwave data and correlation with the Arctic Oscillation, *Remote Sensing of Environment* **36**, L21402 (DOI: 10.1029/2009GL039672).

Torinesi O., M. Fily and C. Genthon (2003). Variability and trends of the summer melt period of Antarctic ice margins since 1980 from microwave sensors, *Journal of Climate* **16** (7), 1047−1060.

Xiong, Z. Q., X. D. Wang, X. W. Li and L. Liang (2014). Antarctic Ice-sheet freeze-thaw detection based on improved physical model, *Chinese Journal of Electronics* **23** (1), 209-212.

VARIABILITY IN ESTUARINE SALINITY AND INUNDATION WITH CHANGING CLIMATE

Y. WANG and R.M. CASTELAO

The Georgia coast (Northeast America) is characterized by complex estuarine systems that contain inter-connected channels and are associated with high-diversity of biological resources. Increases in freshwater withdrawal from rivers to support upstream urbanization, changes in the frequency of drought occurrence, and sea level rise can potentially lead to changes in estuarine salinity and inundation frequency. A high-resolution hydrodynamical model is used to describe salinity and inundation variability in the estuary in order to understand the coastal response to climate change. Numerical simulations show that different levels of sea level rise can lead to substantial changes in salinity and inundation. As sea level rises and the majority of creeks and intertidal areas become inundated, freshwater from the Altamaha River flowing toward the ocean is partially blocked and diverted toward the adjacent marsh areas, leading to reduced salinity in those regions. Near the river mouth and at Sapelo Sound farther north, salinity is predicted to increase significantly.

DIRECT MEASUREMENT OF REACTIVE UPTAKE OF N2O5 AND YIELD OF CLNO2 ON AMBIENT AEROSOLS IN NORTH CHINA PLAIN

Z. WANG[1], Y. THAM[1], T. WANG[1]*, W. WANG[1], X. WANG[2], N. MA[3], K. LU[4], Y. ZHANG[4], A. WIEDENSOHLER[3], W. WANG[2]

[1]Department of Civil and Environmental Engineering, The Hong Kong Polytechnic University, Hong Kong, China

[2]Environment Research Institute, Shandong University, Jinan, Shandong, China

[3]Department Experimental Aerosol & Cloud Microphysics, Leibniz Institute for Tropospheric Research (TROPOS), Leipzig, Germany

[4]College of Environmental Sciences and Engineering, Peking University, Beijing, China

Keywords: HETEROGENEOUS UPTAKE, N_2O_5, CIMS, NORTH CHINA.

ABSTRACT

Dinitrogen pentoxide (N2O5) is a reactive intermediate in atmospheric oxidation of nitrogen oxides (NOx), which plays important roles in atmospheric chemistry, photochemical smog and haze pollution. Recent studies have indicated significant knowledge gaps in the uptake of N2O5 on particle surfaces and subsequent production of nitryl chloride (ClNO2), as well as the important impacts on aerosol formation and the next-day photochemistry. In June/July 2014, an intensive field study on N2O5 and ClNO2 was carry out at a rural site in North China Plain (NCP), by using a chemical ionization mass spectrometry system (CIMS). A simplified aerosol flow reactor coupled to CIMS was employed to in-situ measure the reactive uptake coefficient of N2O5 (γN2O5) and yield of ClNO2 (ϕClNO2) on ambient aerosols. Fast uptake of N2O5 and subsequent production of ClNO2 was observed, and the measured γN2O5 ranged from 0.04 to 0.20, with an average of 0.12, and ϕClNO2 ranged from 0.14 to 0.94, with an average of 0.51. The determined γN2O5 in this study is much higher than the values derived from lab studies and field data in other places, while the observed ϕClNO2 was comparable to previous studies. A lumped value of γϕ was determined in order to reduce the uncertainties of γ raised from short reaction time and high reactor surface. The average of γϕ for all cases was 0.054, which can be considered as the lower limit of γN2O5 by assuming unit ClNO2 yield. The observed fast uptake of N2O5 was consistent with the high ambient ClNO2 concentration (> 2 ppbv) and aerosol nitrate formation measured in this inland region. This fast heterogeneous process may be unique and universal in the high aerosol loading condition in North China Plain, underlining the need to better parameterize the heterogeneous processes on ambient aerosols at different locations and conditions.

ACKNOWLEDGEMENTS

This work was supported by the National Natural Science Foundation of China (41275123) and Hong Kong RGC Collaborative Research Fund (C5022-14G).

*Correspondence to: T. Wang, E-mail: cetwang@polyu.edu.hk

ONLINE MEASUREMENTS OF FLUORESCENT AEROSOL PARTICLES AT A POLLUTED REGIONAL SITE IN THE NORTH CHINA PLAIN: INSIGHTS INTO THE POTENTIAL IMPACT OF BURNING ACTIVITIES

ZHIBIN WANG[1], XIAWEI YU[1,3], SIMONAS KECORIUS[2], ZHOUQING XIE[3], GAVIN MCMEEKING[4], CHRISTOPHER PÖHLKER[1], MINGHUI, ZHANG[1], ALFRED WIEDENSOHLER[2], UWE KUHN[1], YAFANG CHENG[1], ULRICH PÖSCHL[1], HANG SU[1]

[1]Multiphase Chemistry and Biogeochemistry Departments, Max Planck Institute for Chemistry, Mainz 55128, Germany

[2]Leibniz-Institute for Tropospheric Research, Leipzig 04318, Germany

[3]School of Earth and Space Sciences, University of Science and Technology of China, Hefei 230026, China

[4]Droplet Measurement Technologies, Boulder 80301, USA

Keywords: BIOAEROSOLS, WIBS, FLUORESCENT AEROSOL PARTICLES, ANTHROPOGENIC BURNING ACTIVITY.

Bioaerosols are the main subset of super-micron particles, and significantly influence the evolution of cloud and precipitation, as well as the public health. Currently, the detection of ambient biological materials in real-time is mainly based on the presence of fluorophores in the particles. Two single particle fluorescence devices, ultraviolet aerodynamic particle sizer (UV-APS; TSI Inc., St. Paul, MN, USA) and wideband integrated bioaerosol spectrometer (WIBS; DMT Inc., Boulder, CO, USA), have been widely used. In this study, we present the WIBS measurement results to characterize the fluorescent aerosol particles (FAP) at a polluted regional site (Xianghe, 39.80 °N, 116.96 °E) in the North China Plain. We observed approximately 1~2 orders of magnitude higher number concentration of FAP as compared with those of previous studies in clean environments (Huffman et al., 2010;Gabey et al., 2011;Gabey et al., 2013;Toprak and Schnaiter, 2013;Healy et al., 2014), as shown in Fig.1. We found the good agreement between the FAP number fraction in coarse mode particles (> 1 μm) and BC mass fraction in fine particles (< 1 μm), possibly indicating a majority of the observed FAP is to a certain extent related to the anthropogenic burning activities nearby. This interference and uncertainty should be especially noticed when performing fluorescence measurements in the polluted area, where the certain non-biological compounds (such as SOA, PAH and soot) may significantly lead to a positive fluorescence measurement artifacts and an overestimation of actual fluorescent biological aerosol particles. We also proposed several approaches to distinguish biological aerosol particles based on the fluorescence spectral and intensities, which aims to reduce the potential misattribution and provide extra dimensions in the differentiation and identification of fluorescent aerosol particle.

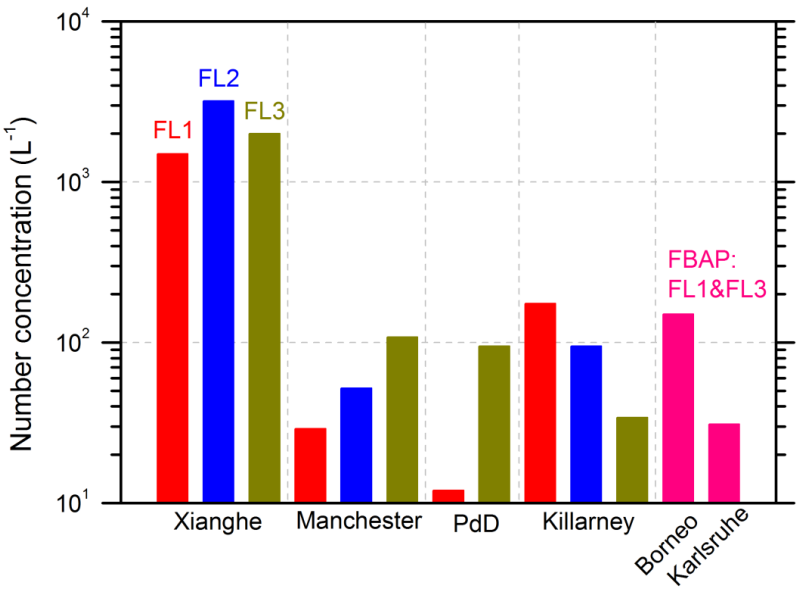

Figure 1. Comparisons of Xianghe data with other previous studies: Manchester, UK (Gabey et al., 2011), Puy de Dôme (PdD), France (Gabey et al., 2013), Killarney, Ireland (Healy et al., 2014), Borneo, Malaysia (Gabey et al., 2010) and Karlsruhe, Germany (Toprak and Schnaiter, 2013). The fluorescent particles in FL1, FL2 and FL3 channels are indicated by red, blue and yellow, respectively. FBAP (pink) refers to particles fluorescent both in FL1 and FL3 channels.

ACKNOWLEDGEMENTS

This study was supported by the Max Planck Society and the Sino German Science center (No. GZ663). We gratefully acknowledge Pucai Wang for local accommodation support.

REFERENCES

Gabey, A. M., Gallagher, M. W., Whitehead, J., Dorsey, J. R., Kaye, P. H., and Stanley, W. R.: Measurements and comparison of primary biological aerosol above and below a tropical forest canopy using a dual channel fluorescence spectrometer, Atmos Chem Phys, 10, 4453-4466, 10.5194/acp-10-4453-2010, 2010.

Gabey, A. M., Stanley, W. R., Gallagher, M. W., and Kaye, P. H.: The fluorescence properties of aerosol larger than 0.8 µm in urban and tropical rainforest locations, Atmos Chem Phys, 11, 5491-5504, 10.5194/acp-11-5491-2011, 2011.

Gabey, A. M., Vaitilingom, M., Freney, E., Boulon, J., Sellegri, K., Gallagher, M. W., Crawford, I. P., Robinson, N. H., Stanley, W. R., and Kaye, P. H.: Observations of fluorescent and biological aerosol at a high-altitude site in central France, Atmos Chem Phys, 13, 7415-7428, 10.5194/acp-13-7415-2013, 2013.

Healy, D. A., Huffman, J. A., O'Connor, D. J., Pöhlker, C., Pöschl, U., and Sodeau, J. R.: Ambient measurements of biological aerosol particles near Killarney, Ireland: a comparison between real-time fluorescence and microscopy techniques, Atmos Chem Phys, 14, 8055-8069, 10.5194/acp-14-8055-2014, 2014.

Huffman, J. A., Treutlein, B., and Pöschl, U.: Fluorescent biological aerosol particle concentrations and size distributions measured with an Ultraviolet Aerodynamic Particle Sizer (UV-APS) in Central Europe, Atmos Chem Phys, 10, 3215-3233, 10.5194/acp-10-3215-2010, 2010.

Toprak, E., and Schnaiter, M.: Fluorescent biological aerosol particles measured with the Waveband Integrated Bioaerosol Sensor WIBS-4: laboratory tests combined with a one year field study, Atmos Chem Phys, 13, 225-243, 10.5194/acp-13-225-2013, 2013.

THE BREEZE INDUCED MODIFICATION OF THE LOCAL CIRCULAION IN A COASTAL MOUNTAINOUS VALLEY – A CASE STUDY FOR BERGEN, NORWAY.

T. WOLF[1], I. ESAU[1] AND J. REUDER[2]

[1]Nansen Environmental and Remote Sensing Center and Bjerknes Centre for Climate Research, Bergen, Norway

[2]Geophysical Institute, University of Bergen and Bjerknes Centre for Climate Research, Bergen, Norway

Keywords: LARGE EDDY SIMULATION, BREEZE CIRCULATION, URBAN AIR POLLUTION, VALLEY CIRCULATION.

INTRODUCTION

We will present our high resolution Large Eddy Simulations (LES) of the topography and breeze induced circulation in a coastal city located in an elongated valley under stably stratified conditions. For the study we used the realistic relief of central Bergen, Norway. We will put forward an interaction between the large-scale circulation, the topography and a local land-breeze on the dispersion of pollutants inside the valley.

For megacities and industrial areas air pollution is a common hazard for the health of the local populations [e.g. *Zhang et al.*, 2012]. Bergen on the other hand has overall low emissions with no major industry and only a population of around 300 000 inhabitants. Despite that, the city has during wintertime repeatedly been suffering from high air pollution exceeding governmental thresholds. Such air pollution episodes have given the city unfortunate national and international media attention as during the last air pollution episode early January 2016 http://www.theguardian.com/cities/2016/jan/19/log-fires-traffic-fumes-cause-bergen-air-pollution. These episodes are connected to persistent winter-time temperature inversions inside the Bergen valley that lead to an accumulation of the local emissions – a phenomenon also known as cold air pools. Such cold air pools are often the reason for adverse air quality in mountainous terrain [e.g. *Schicker and Seibert*, 2009a; *Lareau et al.*, 2013]. In Bergen the vertical temperature stratification of persistent cold air pools does not necessarily need to be sustained by warm air advection above the valley like e.g. in the Western U.S. [*Reeves and Stensrud*, 2009]. Instead, they can essentially be seen as nocturnal cold air pools that last for several days because of the high latitude and the correspondingly short winter days. In addition, the already complex dynamic phenomenon of stably stratified flows in a mountainous area is further complicated by the city's proximity to the Bergen fjord – a large sea inlet that holds a comparatively high temperature.

In previous studies we published our analyses of the existence and properties of the temperature inversions in Bergen [*Wolf et al.*, 2014] and the large-scale circulation during air pollution events [*Wolf and Esau*, 2014; *Wolf et al.*, 2015]. We found that usually temperature inversions are connected to weak South-Easterly winds and low temperatures as predicted from ERA-Interim. It should here be kept in mind that the Bergen valley is only 1 km wide at the base and therefore not resolved in the ERA-Interim reanalysis [*Dee et al.*, 2011], meaning that this data should be a good representation of the larger-scale circulation above the Bergen valley. Previously, we assumed that a shading effect and a successive detachment of the air at the valley floor from the free atmospheric circulation as it is typically the case for cold air pools might favour the persistent temperature inversions inside the valley. Preliminary simulations with a large Eddy Simulation model however suggested that the temperature contrast of the warm fjord and the cold land might have a significant effect on the circulation at the valley floor. In this study we will present a more detailed analysis of exactly this effect.

METHODS

For the LES simulations we used the Parallelized Large Eddy Simulation Model (PALM) [*Maronga et al.*, 2015]. The model is based on the non-hydrostatic, filtered, incompressible Navier–Stokes equations in Boussinesq approximated form. The governing equations are solved on a Cartesian grid. Topography is represented by, bottom-surface mounted obstacles occupying full grid-cells. For the production of the topographic input at a 10 m resolution we used measurements from laser scanning data provided by the Bergen municipality. The data were processed in ArcMap and Matlab. Turbulence closure is parameterized using a modified 1.5-order SGS closure [*Deardorff*, 1980; *Saiki et al.*, 2000].

Case name	Wind scenario	T_{fjord} [K]
Case 0*	sc 1	/
Case 1	sc 1	270.65
Case 2	sc 1	273.15
Case 3	sc 1	275.65
Case 4	sc 1	278.15
Case 5	sc 2	273.15
Case 6	sc 2	275.65
Case 7	sc 2	278.15
Case 8	sc 2	280.65

Table 1: PALM simulations.
* Simulation with Neumann BC and 0 K*m/s shf over entire domain

For all simulations we used a 10 m horizontal and vertical resolution. Since Bergen is located inside a valley that is again surrounded by multiple valleys we used periodic boundary conditions (BC) in the x- and y-directions. In order to guarantee a smooth flow through the domain we used a linear interpolation to the opposite side of the domain. For all other BC we used the default options in Palm, except for the bottom BC for the potential temperature. Here we modified the PALM model code in order to be able to use mixed BC. Over land the long-wave (LW) radiative cooling usually leads to a negative kinematic turbulence surface sensible heat flux (SHF). We therefore prescribed a constant SHF of -0.025 K·m/s. The water surfaces in the valley as a first approximation can be seen to have a constant temperature. The surface temperatures that we assumed for the Bergen fjord for each run are specified in Table 1. Over all other water bodies we used 273.15 K as surface temperature, corresponding to the assumption of a thin layer of ice on the water.

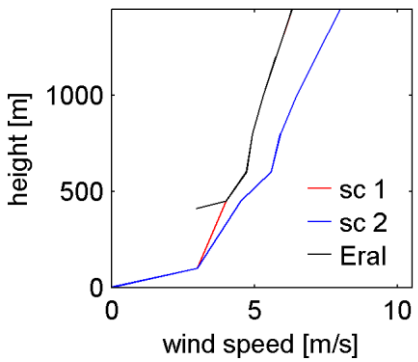

Fig. 1: Geostrophic wind profile scenarios used for the PALM simulations. The black lines show the mean ERA-Interim (EraI) wind profile over the Bergen valley for all high pollution cases (they start only at 410 m due to the low horizontal resolution of ERA-Interim). Above 450 m the red and black line are overlapping.

Our aim was to assess the conditions during typical high pollution events. As initial conditions we therefore used a constant gradient of 0.0055 K/m for the vertical potential temperature. For the geostrophic winds we used two different scenarios (Fig.1). The baseline scenario assumes the vertical wind-speed profile of the mean over all days with at least one hourly measurement at the high traffic reference station of more than 200 µg/m^3 nitrogen dioxide. The mean wind-direction changed only little

with height and we therefore kept it constant at 110°. Because of the low resolution of ERA-Interim the surface is assumed to be at 410 m. Above 450 m we therefore used the actual ERA-Interim wind-speed profile. The wind-speed at 410 m we assumed for a height of 100 m and used linear velocity changes between the surface and 100 m height, and 100 m and 450 m height. For the other scenario we used 1.5 times the wind speed gradients of the baseline scenario above 100 m.

In order to analyse the dispersion conditions in the valley we additionally emitted a passive tracer with a constant flux per grid-point from every grid-point over land with topographic height below 70 m.

RESULTS

The simulations done for this study are sensitivity studies and not expected to resolve all flow features. However, some flow features should be highlighted here in comparison to conveniently available measurements. Fig. 2 shows the 15 min mean wind field from case 2 after 12 h simulation time for the model level centred at a height of 55 m and the SHF. The fjord temperature of 2.5° C in case 2 should be reasonable for high pollution events after an extended cold spell due to a cooling of the water surface from the warm bulk water temperature (assumed to be warmer than 5° C) over time. The fjord surface can cool down without causing significant mixing of the water because of the stratification induced from a fresh-water surface layer from run-off during rainy periods. The model level at 55 m is the closest level to the height of an elevated AMS in the middle of the Bergen valley.

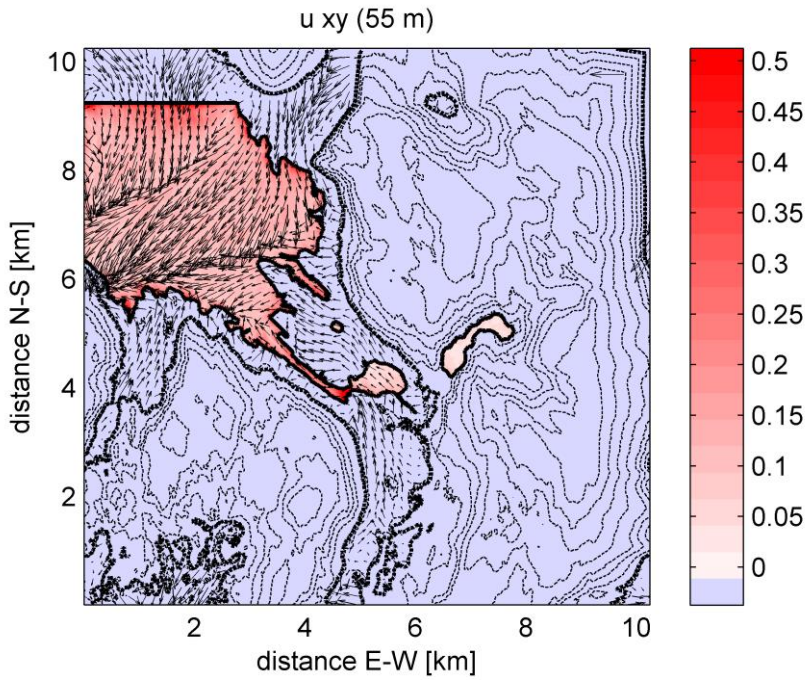

Fig. 2: The 55 m wind-field from case 2 together with the SHF in [K*m/s] for the end of the 12 h simulation time. The 55 m topographic line is indicated by the thick black dashed line. The thin dashed lines indicate topography at 50, 100, 150, 200, 300, 400, 500 and 600 m. The water-land interface is shown by the thick solid line.

The temperature difference between the land and the sea causes flow convergence over the fjord as visible in minima of the SHF and convergence of the wind-vectors. This results in a mean down-valley flow in the interior of the valley – the breeze induced circulation. Case 0 as a reference test does not show such a down-valley flow. With decreasing height, the South-Easterly geostrophic winds are rotated to North-Easterly winds that then are channelled inside the valley to an up-valley flow. While of course dynamically a neutrally stratified flow is different from a flow under stable stratification, this up-valley flow still exists in the upper part of the valley. Dependent on the geostrophic wind-speed scenario, closer to the valley floor this topography induced up-valley flow is balanced more or less by the down-valley

flow for fjord surface temperatures between 0º C and 2.5º C, respectively. For warmer fjord surface temperatures the flow close to the valley floor is directed down the valley. During temperature inversions in the Bergen valley the wind-direction at the AMS is almost exclusively down the valley meaning it is likely that the fjord-land surface temperature difference is most of the time sufficiently high in order to overcome any up-valley flows higher up in the valley.

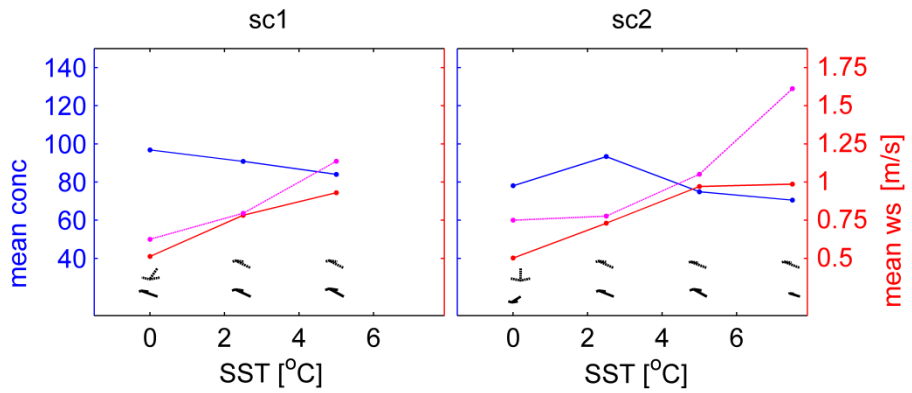

Fig. 3: Mean passive tracer concentration (blue) and wind-speed at 55 m (pink, dashed) and 10 m above the surface (red, full) for the city centre. The black arrows show the mean wind-speeds at 55 m (top row) and 10 m (bottom row). The city centre is the part of the city located closest to the Bergen fjord in Fig. 2, beyond the large water body in the middle of the valley at approximately 5 and 4 km in the E-W and N-S direction, respectively.

This has large implications for the dispersion conditions inside the valley as shown in Fig. 3. For the higher wind-speed scenario 2 a clear transition from a mean down- to a mean up-valley flow is visible. The transition simultaneously corresponds to a maximum in the passive tracer concentration for the lowest down-valley wind-speeds where stagnation is the strongest. This is partially also connected to the setup of the tracer emission. During up-valley winds the clean air over the fjord is transported into the city quickly leading to much lower tracer concentrations. Considering the real emission patter in Bergen, ships that are lying in the harbour might have a significant impact on the air quality within the city dependent on the balance between the topography and the breeze induced circulation. This is especially relevant since the convergence front over the fjord is moving further into or out of the valley, depending on the exact combination of the assumed fjord surface temperature and the wind-speed scenario.

It should however be kept in mind that the simulations done here are not completely realistic. The simulated inversion heights in the middle of the valley were between 85 and 145 m. Inversions measured with an angular scanning microwave radiometer in the middle of the valley were most of the time between 70 and 270 m high meaning that the inversion height in our simulations is likely underestimated. This might be connected to a missing treatment of LW radiative transfer in the air or a too small domain – a recent measurement effort during a high pollution event showed the inversion height in the Southern part of the Bergen valley to be even slightly higher than where the usual measurements are done. The Southern part of the valley might therefore serve as a cold air reservoir. In future simulations, the effect of this will be assessed. However, the circulation at the valley floor and up to a height of approximately 100 m should be the most relevant feature for the dispersion of air pollutants inside the city. Since the simulated inversions mostly are deeper than this threshold it might be reasonable to assume that the circulation below is represented reasonably well.

CONCLUSIONS

We have conducted high resolution LES simulations in order to assess the breeze induced circulation in an urbanized coastal valley. We have found indications for a balancing between the large-scale circulation that is modified by the local topographic features and a land-breeze circulation forced by a positive sea-land temperature contrast. This might have large implications on the distribution of pollutants in the valley with respect to the question of the impact of ships on the local air pollution. The results should also be

relevant to other coastal harbour cities at high latitudes. The Bergen harbour authority is highly interested in our work and we are currently beginning a new research project on the exact effect of the emissions from ships on the air quality inside the city centre funded by the Bergen harbour authority.

ACKNOWLEDGEMENTS

This study was supported by the Ph.D. studentship funding from the GC Rieber Foundation, the FinKlima project of the Regional research foundation for Western Norway and the REGSCEN internal project of the Bjerknes Centre for Climate Research. The GIS-based input data for the construction of the computational domain have been provided by the Bergen municipality.

REFERENCES

Deardorff, J. W. (1980), Stratocumulus-capped mixed layers derived from a three-dimensional model, *Boundary-Layer Meteorol.*, *18*(4), 495–527, doi:10.1007/BF00119502.

Dee, D. P. et al. (2011), The ERA-Interim reanalysis: configuration and performance of the data assimilation system, *Q. J. R. Meteorol. Soc.*, *137*(656), 553–597, doi:10.1002/qj.828.

Lareau, N. P., E. Crosman, C. D. Whiteman, J. D. Horel, S. W. Hoch, W. O. J. Brown, and T. W. Horst (2013), The Persistent Cold-Air Pool Study, *Bull. Am. Meteorol. Soc.*, *94*(1), 51–63, doi:10.1175/BAMS-D-11-00255.1.

Maronga, B., M. Gryschka, R. Heinze, F. Hoffmann, F. Kanani-Sühring, M. Keck, K. Ketelsen, M. O. Letzel, M. Sühring, and S. Raasch (2015), The Parallelized Large-Eddy Simulation Model (PALM) version 4.0 for atmospheric and oceanic flows: model formulation, recent developments, and future perspectives, *Geosci. Model Dev.*, *8*(8), 2515–2551, doi:10.5194/gmd-8-2515-2015.

Reeves, H. D., and D. J. Stensrud (2009), Synoptic-Scale Flow and Valley Cold Pool Evolution in the Western United States, *Weather Forecast.*, *24*(6), 1625–1643, doi:10.1175/2009WAF2222234.1.

Saiki, E. M., C. Moeng, and P. P. Sullivan (2000), Large-eddy simulation of the stably stratified planetary boundary layer, , (October 1999), 1–30.

Schicker, I., and P. Seibert (2009), Simulation of the meteorological conditions during a winter smog episode in the Inn Valley, *Meteorol. Atmos. Phys.*, *103*(1-4), 211–222, doi:10.1007/s00703-008-0346-z.

Wolf, T., and I. Esau (2014), A proxy for air quality hazards under present and future climate conditions in Bergen, Norway, *Urban Clim.*, *10*, 801–814, doi:10.1016/j.uclim.2014.10.006.

Wolf, T., I. Esau, and J. Reuder (2014), Analysis of the vertical temperature structure in the Bergen valley, Norway, and its connection to pollution episodes, *J. Geophys. Res. Atmos.*, *119*(18), 10,645–10,662, doi:10.1002/2014JD022085.

Wolf, T., I. Esau, and Reuder J (2015), The Large-Scale Circulation during Air Quality Hazards in Bergen, Norway, in *Report Series in Aerosol Science: Proceedings of the 1st Pan-Eurasian Experiment (PEEX) Conference and the 5th PEEX Meeting*, vol. 163, edited by M. Kulmala, S. Zilitinkevich, H. K. Lappalainen, E.-M. Kyrö, and J. Kontkanen, pp. 471 – 476, Helsinki, Finland.

Zhang, J. P. et al. (2012), The impact of circulation patterns on regional transport pathways and air quality over Beijing and its surroundings, *Atmos. Chem. Phys.*, *12*(11), 5031–5053, doi:10.5194/acp-12-5031-2012.

CLOUD DETECTION BASED ON TEXTURE FEATURE AND SUPPORT VECTOR MACHINE

WU TINGTING[1], HAN LING[1] AND LIU QING[1]

[1]Chang'an University, Xian 710064,China.

Keywords: Landsat satellite image, cloud detection, texture feature, support vector machine.

INTRODUCTION

With the rapid development of satellite remote sensing technology, it has been widely used in the environment, agriculture, meteorology and other fields .But satellite images are often affected by cloud cover, resulting in the satellite images cannot be directly applied and analyzed,if we set aside the image it will increase the cost of satellite photographs, and for some regions with more rain, it's hard to find photograph area completely free of cloud.Therefore,we should first detect the cloud.The test data in this paper is Landsat multispectral satellite images, Landsat satellite is a United States land satellite system. Since 1972, launched its first satellite, Landsat-1, to the current Landsat-7.Landsat-7 data:7 spectral bands and a panchromatic band.

METHODS

This paper selects 1056 Landsat satellite multispectral images,these images covering every province in China and be classified according to different seasons and different types of cloud.First of all,to stretch the image,different remote sensing images have different normalized range, in order to make different images have analogy and experimental results have reference value,we test a large number of sample data and finally the DN value of the cloud image in the test data is normalized from 0 to 950 range.And then band math,this paper according to the different characteristics such as absorption and reflectance in different band , choose reflection and absorption sensitive bands to extract cloud.In order to enhance the sensitivity of cloud, weaken the effect of terrain shadow and radiated interference, prominent features of the reflected radiation characteristics.Then, based on the image texture features GLCM to extract cloud, application GLCM different texture measures to extract texture features, select the texture to help cloud detection and band combination with the original image, Then supervised classification, in order to extract the cloud.However some smaller together cloud texture is more complex, using texture features extraction can cause miscarriage, there are some terrain covered in thick snow, using this method will be miscarriage of justice into the cloud.For the misjudged image taken support vector machine (SVM) classifier which kernel function is radial basis function (RBF) to distinguish, First, through edge segmentation algorithm to separate cloud and ground objects and determine the best threshold, then select the appropriate kernel,kernel functions can be used to solve the problem of low dimension space vector set hard to be divided.Radial basis kernel function, whether it is low dimensional, high dimensional, small sample, large sample, radial basis function (RBF) are applicable, with a wide domain of convergence, is an ideal classification function, Using this method to extract cloud.

CONCLUSIONS

The method can solve the problem that the highlight area is mistaken for the cloud caused by the traditional CART decision tree classification method . The method can be adapted to different regions in China.This paper tests 1056 images, accuracy is 96.8%, the accuracy of the cloud detection has been significantly improved.

ACKNOWLEDGEMENTS

This work was supported by the Fundamental Research Funds for the Central Universities（310826161009）.

REFERENCES

Haralick, R.M. (1973). Textural Features for Image Classification, *J.IEEE Trans Syst Man Cybern* **3**, 610.

Welch, R.M. and Sengupta,S.K.and Chen,D.W. (1988). Cloud Field Classification Based Upon High Spatial Resolution Textural Features ,Part I, Gray Level Cooccurrence Matrix Approach, *J. Geophys Res* **93**,12663.

Welch, R.M. and Sengupta,S.K.and Goroch,A.K. (1992).Polar Cloud and Surface Classification Using AVHRR Imagery: An Intercomparis on of Methods, *J. Appl Meteoro* **31**,405.

CAO Qiong and ZHENG Hong and LI Xingshan(2007).A Method for Detecting Cloud in Satellite Remote Sensing Image Based on Texture, *J.Acta Aeronautica Et Astronautica Sinica* **28**, 661.

YANG Qingqing and WANG Kelin and CHEN Hongsong and TIAN Richang(2009).Band math combined with PCA method of fusion research,*J.Science of Surveying and Mapping* **5**, 34.

HE Quanjun and CAO Jing and HUANG Jiang and WU Zhijun(2006).Based on multi-spectrum synthesis of MODIS data cloud detection research,*J.Remote Sensing For Land and Resources* **3,**69.

SUN Lei and CAO Xiaoguang(2014). Feature extraction based on combined textural features from panchromatic cloud and snow region,*J.Electronic Design Engineering* **2**,22.

CHEN Bo and ZHANG Youjing and CHEN Liang(2007).RS Image classification based on SVM method with texture ,*J. Engineering of Surveying and Mapping* **16**, 5.

ZHANG Qian and YANG Yaoquan(2012). Based on the research of kernel function of support vector machine, *J. Electric Power Science and Engineering* **28**, 5.

OBSERVED NON-UNIFORM WARMING ON THE QINGHAI-TIBETAN AND MONGOLIAN PLATEAU FROM 1961 TO 2013

TONGHUA WU, REN LI, TIANYE WANG and LIN ZHAO

Cryosphere Research Station on the Qinghai-Tibet Plateau, State Key Laboratory of Cryospheric Sciences, Cold and Arid Regions Environmental and Engineering Research Institute, Chinese Academy of Sciences, 320 Donggang West Road, Lanzhou, China

Keywords: CLIMATIC WARMING; QINGHAI-TIBET PLATEAU; MONGOLIAN PLATEAU; GROUND THERMAL REGIME

Abstract: The majority of the QTP and the MP are underlain by permafrost and seasonally frozen ground. We have examined trends in air temperature and freezing/thawing index for the Qinghai-Tibetan Plateau (QTP) and the Mongolian Plateau (MP) during the last 51 years. The non-parametric statistical analysis results reveal a clear picture of climatic warming in both regions. Generally, the magnitudes of warming trend on the QTP and MP are similar for annual air temperature and freezing/thawing index. While the characteristics of seasonal warming are different in those two regions. The warming of QTP is mainly due to winter warming, which is consistent with the conclusions previous studies drawn. While the warming of MP is primarily caused by autumn warming, characterized by a slightly winter cooling trend during the last two decades. The different features of seasonal warming on both plateaus would be expected to result in diverse impacts on the ground thermal regime.

INTRODUCTION

IPCC (2007) suggest the global mean surface temperature has increased by 0.74 °C ±0.18 °C when estimated by a linear trend during the past 100 years. The most significant and strongest warming occurred in the last 40 yr. The striking warming trend on the Qinghai-Tibet Plateau (QTP) and the Mongolia Plateau (MP) has been documented in recent years. Liu and Chen (2000) found that the linear rates of temperature increase during 1955-1996 amounted to 0.16 °C/decade for the annual average and 0.32 °C/decade for the winter average respectively, which were greater than those for the Northern Hemisphere as a whole. You et al (2010) revealed that the mean annual air temperature on the QTP has risen significantly with an annual trend of 0.25 °C/decade, which based on the analysis of trends in the monthly and seasonal mean temperature over the QTP and its various subregions during the period of 1961-2004. Guo et al (2012) identified that the air temperature on the QTP had undergone a significant warming during the period from 1961 to 2007 with an average warming rate of 0.28 °C/decade for the 71 meteorological stations over the plateau. There is some evidence that the QTP is an amplifier of global warming (Kang et al 2010) and the rate of warming in the QTP Three Rivers Source Region amounts to 0.32 °C/decade between 1960 and 2009 (Liang et al 2012). Lan et al (2013) described the prevailing warming trend over the northern Tibetan Plateau during 1957-2009 using observations from 81 meteorological stations. As for one of the largest land-locked countries in the world with an average elevation of 1580 m a.s.l., Mongolia has also been subjected to a marked warming in recent decades. Dagvadorj et al (2009) reported the mean annual air temperature in Mongolia had increased by 1.66 °C from 1940 to 2001, which the increasing winter temperature was predominant compared with that in other three seasons. Recent observation records from 48 meteorological stations of Mongolia also suggest that the mean annual air temperature has increased by 2.14 °C during the last 70 years (Dagvadorj et al., 2009). However, there were still relatively few published literatures introducing the characteristics of climatic changes on the whole MP. In addition, it is of great significance to compare the characteristics of regional climate changes on the QTP and the MP.

The air freezing/thawing index can be used to predict permafrost distribution, the seasonal ground frozen depth, and to estimate the active layer thickness in permafrost regions (Frauenfeld et al 2007).

Long-term variability of air freezing and thawing index is also an important indicator of climate change. Previous studies indicated that long-term freezing/thawing index climatology could strongly resemble the cold/warm season temperature in cold regions (Frauenfeld et al 2007). For the permafrost regions, air temperature and thawing index was proved to be significantly related to dynamics of the active layer (Frauenfeld et al 2011). As for the seasonally frozen ground regions, the ground freezing depth is strongly influenced by mean annual air temperature and freezing index. The long-term trends of air temperature and freezing/thawing index could be assessed to provide insight into understanding the potential influence of climate changes to permafrost and seasonally frozen ground.

In this study, we analyzed long-term trends in the mean annual and seasonal air temperature and the air freezing/thawing index on the QTP and the MP from 1961 to 2011. Our objective was to analyze different spatiotemporal warming patterns occurred in those regions, which were the largest permafrost regions in Central Asia. At the same time the potential impacts of climatic warming associated with the changes in frozen ground will be discussed. This study will be expected to contribute to understand the driving forces of frozen ground dynamics and their environmental significance.

DATA AND METHODS

The monthly air temperature data used in this study were originated from the China Meteorological Administration, the Institute of Meteorology and Hydrology of Mongolia, and Monthly Climatic Dataset for the World provided by National Climatic Data Center, United States (The monthly air temperature data for Mongolia over the period of 2007-2012). The mean annual air temperature was obtained by averaging the monthly temperature over a 12-month annual period. On the QTP, 76 meteorological stations which have continuous monthly records of air temperature were used. As for the MP, 24 meteorological stations with continuous records of monthly air temperature were used. The locations of meteorological stations were shown in Figure 1. The data quality control and homogeneity testing has been undertaken with rudimentary logic checks and reliable homogeneous reference series establishment described by Li et al (2009). The overall quality of all those dataset is fairly good, with 76% of stations whose temperature time series having no missing data on the QTP and the integrity of temperature times series at each station being over 95%. As for the MP stations, the integrity of temperature times series at each station is over 98%. The few missing data were substituted by the average between the data of the previous and the following month. When this standard was not possible to satisfy, the recorded values in neighboring stations with high correlation (r greater than 0.90 over 95% confidence level) were used to fill the air temperature time series.

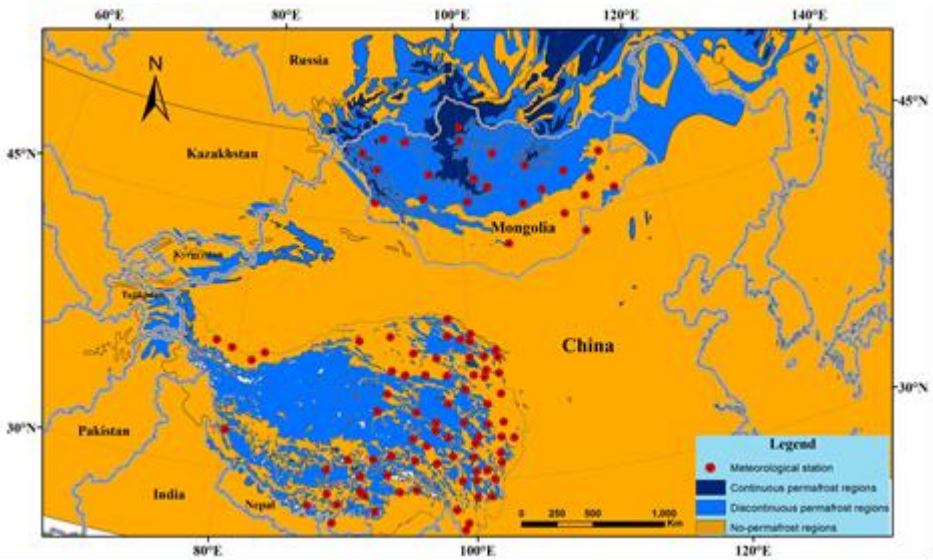

Figure 1 The locations of meteorological stations and permafrost distribution over the QTP and the MP

The seasonal mean air temperatures were calculated by averaging the monthly values. Seasons were defined as follows: spring spanning March, April and May, summer including June, July and August, autumn spanning September, October and November, winter including December, January and February.

The common record period for all data sources is 51 years spanning January 1961 to June 2012. The air freezing/thawing index is defined as the cumulative number of degree-days below/above 0 °C for air temperature during a given time period. There are a lot of studies to introduce the freezing and thawing indices of air temperature (Frauenfeld et al 2007, Frauenfeld and Zhang 2011, Vasil'ev et al 2012). The widely applied air freezing/thawing index during the past decades was described by Frauenfeld et al. (2007). The accuracy of using monthly temperature data in the calculation of the approximate freezing/thawing index was discussed in previous literature (Frauenfeld et al., 2007, Wu et al 2011).

Trend analysis was conducted using the Mann-Kendall test with Sen's estimator of slope (Mann 1945, Sen 1968, Kendall 1975). This non-parametric method is robust and particularly useful for trend detection in climatic change studies since it is not affected by the distribution of the time-series data and is not sensitive to outliers. The serial auto-correlation in the data time-series was corrected for the Mann-Kendall test using the method suggested by Yue and Wang (2004). The monotonic trends were determined using the 5% and 1% significance level.

RESULTS AND DISCUSSION

3.1 Spatiotemporal change of mean annual air temperature

The trends of mean annual and seasonal air temperatures and their magnitude (in °C/decade) over the QTP and MP were obtained by the Mann-Kendall test and the Sen's slope estimator. All of the stations over the QTP were characterized by a significant increase in mean annual air temperature at the 99% confidence levels, except Maduo station at the 95% confidence level. Figure 2a shows that positive trend has clearly prevailed over the QTP in the study period. The warming period from 1961 to the middle of 1990s was characterized by a smooth increase in mean annual air temperature. It seems that the warming has been accelerated since the middle of 1990s (Figure 2a). The trend of regional annual temperature time series over the QTP amounts to 0.33 °C/decade at the 99% confidence level. The magnitude of warming ranged between 0.13 °C/decade at Deqin station and 0.57 °C/decade at Zaduo station. The spatial pattern of trends for mean annual air temperature over the QTP was shown in Figure 3. The stations with great magnitude of warming were located in the northern and northeastern of QTP, where underlain by seasonally frozen ground at those stations.

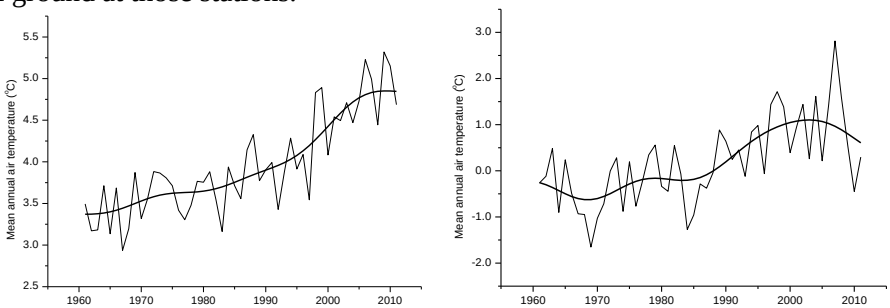

a QTP b MP

Figure 2 Regional annual temperature time series on the QTP (a) and the MP (b). The bold line shows the 9-year moving average

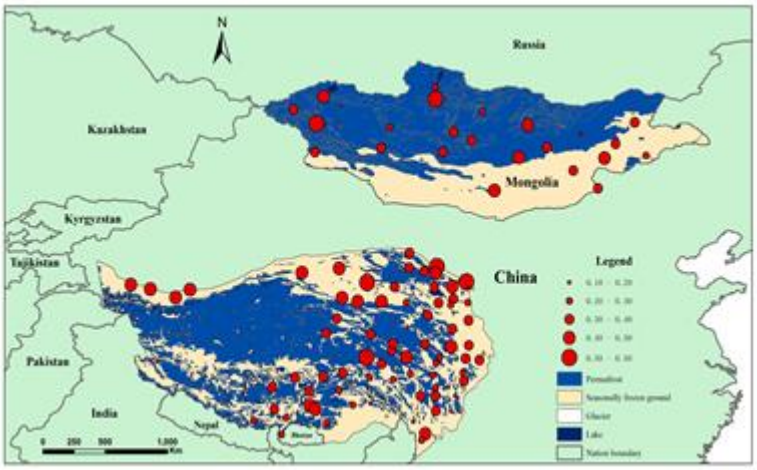

Figure 3 Permafros distribution on the QTP and MP. Spatial patterns of trends for mean annual air temperatures on the QTP and MP over the period 1961-2011. The size of the solid dot is proportional to the magnitude of the trends

On the MP, the trends of mean annual air temperature at about 92% of stations (22 stations) showed significant increase at the 99% confidence level, except that there is insignificant warming trend occurring at Uliastai and Undurkhaan station. Figure 2b shows the regional annual temperature time series on the MP. It is evident that the warming period during 1961-2005 was characterized by a smooth increase in mean annual air temperature, followed by a cooling trend in recent years. Generally over the past 51 years, annual temperature on the MP has risen at a rate of 0.37 °C/decade at the 99% confidence level, which is slightly higher than that on the QTP. The increasing trends of mean annual air temperature in Mongolia ranged between 0.12 °C/decade at Undurkhaan station and 0.58 °C/decade at Baruunturuun station. No coherent trends were seen at all stations, while three stations who located in permafrost regions (Baruunturuun, Khovd, and Muren station) showed significant warming trends at a rate greater than 0.50 °C/decade.

3.2 Spatiotemporal change of seasonal air temperature

For the QTP as a whole, the greatest seasonal warming is found in winter (0.45 °C/decade), and the increasing trends for spring, summer and autumn air temperature are 0.25 °C/decade, 0.29 °C/decade and 0.36 °C/decade, respectively. The seasonal warming trends are all statistically significantly at the 99% confidence level over the QTP.The regional seasonal temperature time series on the QTP. The synchronous warming in the four seasons was revealed. Therefore warming of the QTP during the last 5 decades is mostly due to warming in winter. And for the MP as a whole, the greatest increase in seasonal air temperature is found in autumn (0.44 °C/decade). The increasing trends for spring, summer and winter air temperature are 0.34 °C/decade, 0.35 °C/decade and 0.32 °C/decade respectively. Similarly, the seasonal warming trends are all statistically significantly at the 99% confidence level on the MP. The warming on the MP is mostly due to warming in autumn in recent decades. The regional seasonal temperature time series on the MP. It is clear that there was accelerating warming in summer since the beginning of the 1990s and a shift of warming trend to cooling occurred in winter on the MP during the last two decades, which agrees well with the viewpoint that a large-scale cooling trends across northern Eurasia occurring during the same period (Cohen et al 2012).

Figure 4 shows the spatial distribution pattern of the trends in seasonal air temperature for 76 meteorological stations over the QTP and 24 stations on the MP. The relatively homogeneous warming trends were discovered at most of stations in autumn and winter on the QTP. While over the MP the warming in summer and autumn is relatively conspicuous and homogeneous.

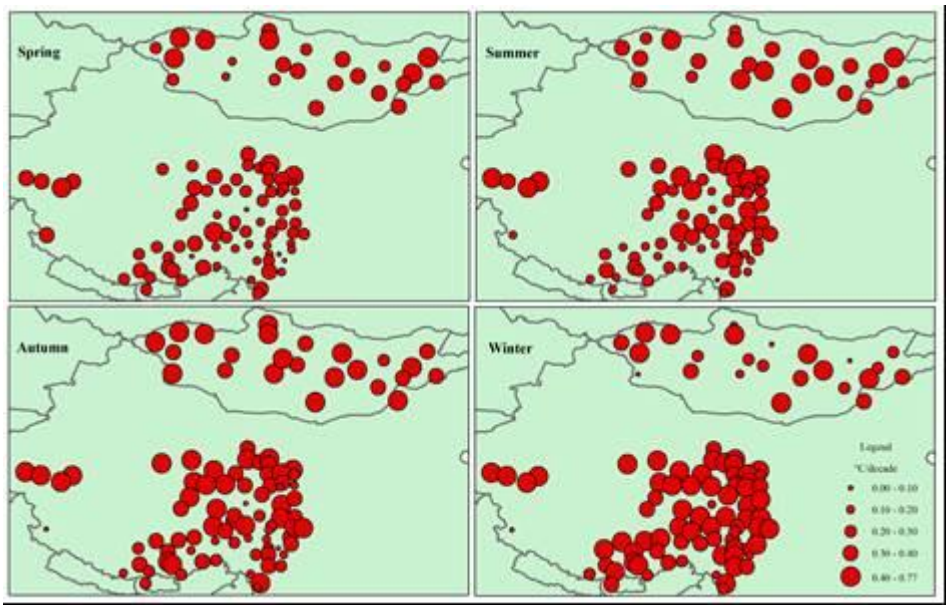

Figure 4 Spatial patterns of trends for seasonal air temperatures on the QTP and MP over the period 1961-2011. The size of the solid dot is proportional to the magnitude of the trends

3.3 Spatiotemporal change in air freezing/thawing index

The regionally averaged time series of air freezing and thawing index on the QTP both indicate very remarkable interannual variability corresponding to above-mentioned annual and seasonal warming characteristics. Over the QTP, the freezing index has decreased significantly during the past 51 years at a rate of 56.7 °C-days/decade at the 99% confidence level, and the thawing index has experienced a statistically significant increase of 68.2 °C-days/decade at the 99% confidence level. The trends of both freezing and thawing index implied a continuous warming over the QTP during the past 51 years. For the regionally averaged time series of air freezing and thawing index on the MP, the tendencies of freezing and thawing index showed similar characteristics as those on the QTP. Generally, the freezing index has exhibited a significant decrease of 57.5 °C-days/decade since 1961 over the MP (at the 99% confidence level), which was less than that of Arctic freezing index changes from 1966/1967 through 2001 (85.6 oC-days/decade) (Frauenfeld et al 2007). Interestingly, it is evident that there is a slight increase for freezing index since the middle of 1990s, which might due to cooling trend in winter during the last decade on the MP. It is consistent with the large-scale cooling trends occurring across northern Eurasia during the last two decades reported by Cohen et al (2012). The variability in regionally averaged time series of thawing index over the MP. A statistically significant tendency was found over the period 1961-2011 with a rate of 68.3 °C-days/decade (at the 99% confidence level), corresponding to the occurring pronounced summer warming on this plateau.

The spatial patterns of trends for freezing/thawing index changes could provide important implication about climate changes and their impacts on ground thermal regime. Figure 5 shows the trends of freezing and thawing index for the study regions during the period 1961-2011. It is clear that there are large regions of statistically significant decreases in the freezing index on the QTP and MP, consistent to general cold-season warming in these regions. On the QTP, the freezing index at seven stations equals to 0 or changes into 0 °C-days from 1961 to 2011. The freezing index at 97% of stations (67 stations) has showed a statistically significant decrease during 1961-2011, among them 90% of stations (62 stations) at the 99% confidence level. And the decreasing trends in freezing index at 36 out of 69 stations were more than 60.0 °C-days/decade. While over the MP, the freezing indices at 75% of stations over the MP have significantly decreased during the past 51 years. The decreasing trends in freezing index at 11 out of 24 stations were more than 60.0 °C-days/decade. The only positive trend of freezing index at the Undurkhaan station is not statistically significant. For the trends of thawing index, the significant increasing trends were found in the northern and eastern QTP (Figure 5), which could greatly impact the active layer thickness in the permafrost regions. The trends of thawing index at all stations on the MP are statistically significantly at the 99% confidence level. The trend values vary between 33.2 °C-days/decade and 90.3 °C-days/decade

over the MP. The thawing index has changed relatively homogeneously at all stations in the whole MP (Figure 5).

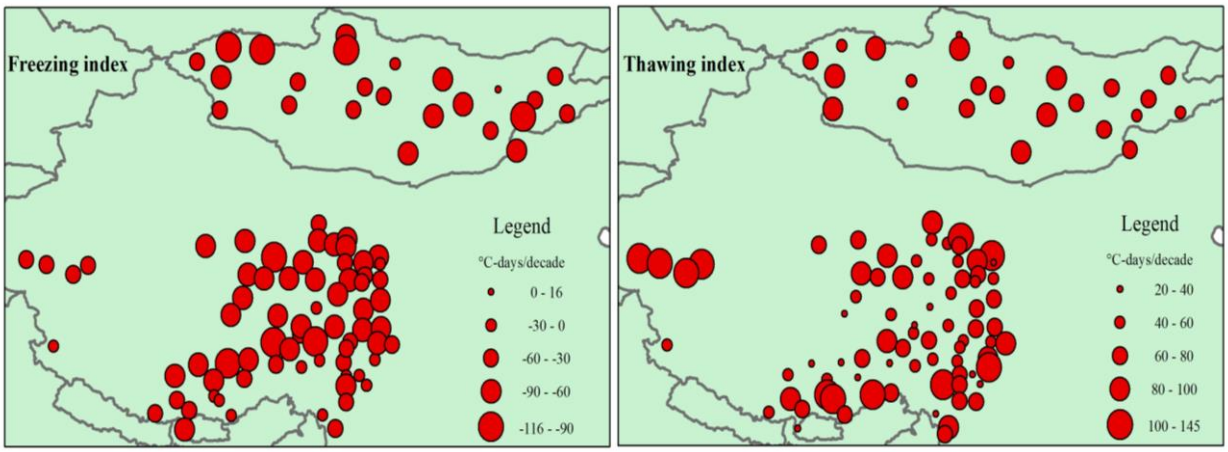

Figure 5 Spatial patterns of trends for air freezing and thawing indices on the QTP and MP over the period 1961-2011. The size of the solid dot is proportional to the magnitude of the trends

CONCLUSIONS

This study represents an examination of the trends in air temperature and freezing/thawing index on the QTP and the MP during 1961-2011. The spatial distribution of warming trends in both regions is also revealed. The results show that annual and seasonal warming trends in those two regions were prevailing. Finally the possible impacts of extensive warming on the ground thermal regime are discussed. Based on analyses of the long-term records for a 51-year period, some main conclusions have been obtained:

1. The mean annual air temperature shows a similar increasing trend both on the QTP and on the MP. The annual air temperature has significantly increased 0.33 °C/decade for the QTP while 0.37 °C/decade for the MP over the period 1961-2011.
2. The trends of spring, summer, autumn, and winter air temperature on the QTP are 0.25 °C/decade, 0.29 °C/decade, 0.36 °C/decade, and 0.45 °C/decade, respectively. While the trends on the MP being 0.34 °C/decade, 0.35 °C/decade, 0.44 °C/decade, and 0.32 °C/decade, respectively. That is to say, the warming of QTP is mostly due to winter warming while the warming of MP primarily due to autumn warming. Furthermore, a cooling trend in winter is found during the last two decades on the MP.
3. During the recent 5 decades, on the QTP the freezing index has significantly decreased at a rate of 56.7 °C/decade, and the thawing index has experienced a statistically significant increase of 68.2 °C/decade. As for the MP the freezing index has also significantly decreased by 57.5 °C/decade and the thawing index has exhibited significant increase of 68.3 °C/decade.

ACKNOWLEDGEMENTS

The study conducted in this paper is financially supported by National Major Scientific Project of China “Cryospheric Change and Impacts Research” (2013CBA01803), the National Natural Sciences Foundation of China (Grant Nos. 41271086 and 41271081), and the Hundred Talents Program of the Chinese Academy of Sciences (Grant No. 51Y251571).

REFERENCES

Cohen J L, Furtado J C, Barlow M A, Alexeev V A, and Cherry J E 2012 Arctic warming, increasing snow cover and widespread boreal winter cooling Environ. Res. Lett. 7 014007

Dagvadorj D, Natsagdorj L, Dorjpurev J, and Namkhainyam B 2009 Mongolia Assessment Report on Climate Change Published by Ministry of Environment, Nature and Tourism, Mongolia, Ulaanbaatar, Mongolia.

Frauenfeld O W, Zhang T, and McCreight J L 2007 Northern hemisphere freezing/thawing index variations over the twentieth century Int. J. Climatol. 27 47-63
Frauenfeld O W and Zhang T 2011 An observational 71-year history of seasonally frozen ground changes in the Eurasian high latitudes Environ. Res. Lett. 6 044024
Guo D and Wang H 2012 The significant climate warming in the northern Tibetan Plateau and its possible causes Int. J. Climatol. 32 1775-1781
Kang S, Xu Y, You Q, Fl¨ugel W A, Pepin N and Yao T 2010 Review of climate and cryospheric change in the Tibetan Plateau Environ. Res. Lett. 5 015101
IPCC 2007 Observations: surface and atmospheric climate change Climate Change 2007: The Physical Science Basis. Contribution of Working Group I to the 4th Assessment Report of the Intergovernmental Panel on Climate Change ed S Solomon, D Qin, M Manning, Z Chen, M Marquis, K B Averyt, M Tignor and H L Miller (Cambridge: Cambridge University Press)
Lan C, Zhang Y, Wang Q, Zhang L, Zhou B, Hao Z, and Su F 2013 Climate change on the Northern Tibetan Plateau during 1957-2009: spatial patterns and possible mechanisms J. Climate 26 85-109
Li Q, Zhang H, Chen J, Li W, Liu X, and Jones P 2009 A mainland China homogenized historical temperature dataset of 1951-2004 Bulletin of the American Meteorological Society 90 1062-1065
Liang L, Li L, Liu C, and Lan C 2012 Climate change in the Tibetan Plateau Three Rivers Source Region: 1960-2009 Int. J. Climatol. Doi:10.1002/joc.3642
Liu X and Chen B 2000 Climatic warming in the Tibetan Plateau during recent decades International Journal of Climatology 20 1729-1742
Mann H B 1945 Nonparametric tests against trend Econometrics 13 245-259
You Q, Kang S, Pepin N, Flügel W A, and Sanchez-Lorenzo A 2010 Climate warming and associated changes in atmospheric circulation in the eastern and central Tibetan Plateau from a homogenized dataset Glob. Planet. Change 72 11–24
Yue S and Wang C 2004 The Mann-Kendall test modified by effective sample size to detect trend in serially correlated hydrological series Water Resources Management 18 201-218
Vasil'ev I S, Vasil'ev A I, and Torgovkin Y I 2012 Air freezing and thawing indices in Yakutia and their mapping Russian Meteorology and Hydrology 37 170-176
Wu T, Wang Q, Zhao L, Batkhishig O, and Watanabe M. 2011 Observed trends in surface freezing/thawing index over the period 1987-2005 in Mongolia Cold Regions Science and Technology 69 105-111

IMPLEMENTATION OF A NEW SIZE-SEGREGATED AEROSOL NUMBER EMISSIONS MODULE IN GLOBAL CLIMATE MODELING

F. XAUSA[1], P. PAASONEN[1], R. MAKKONEN[1], V-M. KERMINEN[1]

[1]Division of Atmospheric Sciences, Department of Physics, University of Helsinki, Finland

Keywords: AEROSOL, NUMBER SIZE DISTRIBUTION, GAINS, GLOBAL CLIMATE, ECHAM

INTRODUCTION

The aerosol-climate model ECHAM-HAM (Stier et al., 2005) is an important tool that is nowadays used to generate climate change projections. However, the input anthropogenic aerosol emissions that are currently taken from the Aerosol Comparison emission inventory (AeroCom) are determined by mass and converted into modal size number distribution by the ECHAM-HAM according to emission sources. New size-segregated aerosol number emissions from 3 to 1000 nanometers in diameter for anthropogenic sources have been recently developed (Paasonen et al., 2013a) in the Greenhouse Gas and Air pollution Interactions and Synergies (GAINS) model (Amann et al., 2011). This study investigated the feasibility of implementing the GAINS global emissions in modeling through a simulation-based comparison with AeroCom emissions using the ECHAM-HAM model. This analysis included a focus on the boreal and arctic areas over Europe, Russia and China to spot important differences between the two datasets in the Pan-Eurasian-Experiment (PEEX) regions(Kulmala et al., 2015) through a climate modeling point of view (Paasonen et al., 2013b).

METHODS

The new global emissions from GAINS model were extracted and implemented in the ECHAM-HAM model to update its current version of emission sectors. Once the new emission modules were implemented, a preliminary evaluation of the GAINS and AeroCom inventories differences was performed. Figure 1 shows the ratio of the total anthropogenic emissions of GAINS over AeroCom on a logarithmic scale. GAINS emissions were pre-processed to have the same chemical composition shares as AeroCom, however the size distribution of aitken and accumulation modes was kept as in GAINS. Finally, the data was converted into an ECHAM-HAM readable format and ready for input.

The simulations were carried out with baseline 2000 AeroCom and 2010 global GAINS emissions, and initialized with a 3-months spin off time window, followed by a 1-year actual simulation for analysis. Meteorological data of 2009 (spin off) and 2010 were used in both simulations. The ECHAM-HAM was set up with a 192x96 (~200Km) grid resolution (T42) and 31 hybrid-sigma layers. At the completion of the simulations, an analysis of particle number size distribution and concentration including a temporal assessment was performed, including model versus observation data taken from several measurement stations around the globe. The vertical mean of the lowest three layers was used to to reduce model noise when generating global geo-gridded plots. The lowest layer was used for model versus ground observation analysis. Two different instruments for particles below and above 300 nanometers were used to collect the observation data in Tomsk: the Diffusional Aerosol Spectroscope (DAS), and Grimm Aerosol Technik GmbH & Co. Germany (GRIMM). The Differential Mobility Particle Sizer (DMPS) was used in Nanjing.

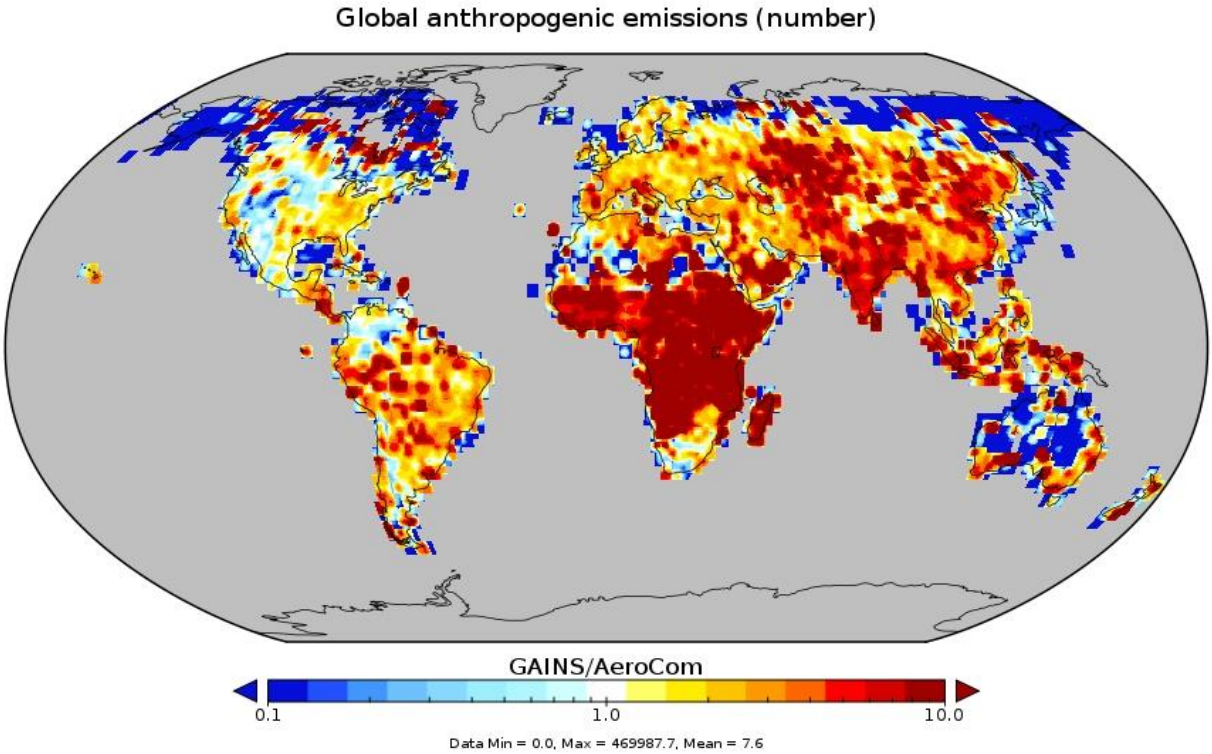

Figure 1. GAINS over AeroCom anthropogenic emissions ratio.

CONCLUSIONS

The analysis of particle size distribution revealed that GAINS implementation produced a higher estimation of particles number in accumulation mode when compared to most of the measurement stations, leading the model to estimate the number of particles above 0.1 micrometer in diameter closer than AeroCom. This difference was consistent with the higher emissions of GAINS anthropogenic emissions in accumulation mode. Overall, the ECHAM was able to get closer to observation in terms of such bigger particles with GAINS. However, the model showed higher limitations in estimation of aitken and nucleation modes compared to observation data. Figure 2 illustrates the modelled lognormal size distribution versus available observation data at three measurement stations in the PEEX regions, two stations in Tomsk(56.5°N, 85.1°E), Russia, and Nanjing(32.12°N, 118.95°E), China. Both GAINS and AeroCom size distributions were estimated by the sum of all the seven modes that are computed in the ECHAM simulation which include soluble and insoluble shares(Vignati et al., 2004).

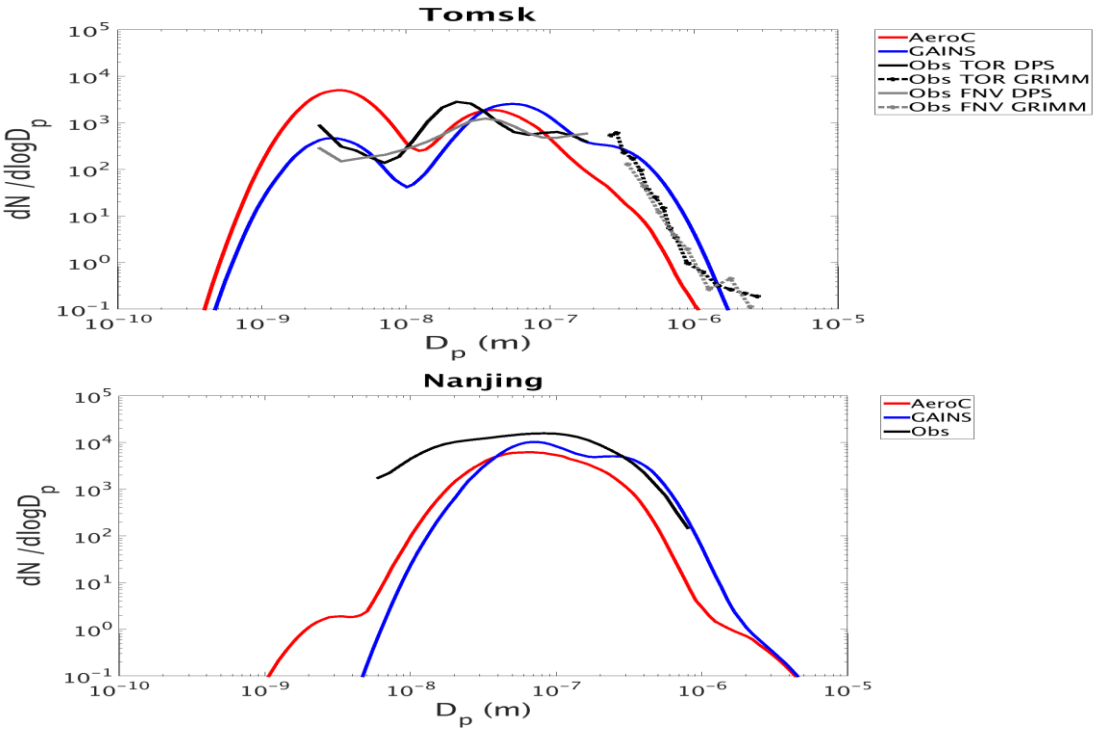

Figure 2. Lognormal distribution of model (red and blue) versus observation (black and grey) in Tomsk and Nanjing.

Figure 3 shows the analysis of Cloud Condensation Nuclei (CCN) at 0.2% supersaturation on global scale which played a key role in identifying the contribution of GAINS to the radiative forcing over the PEEX regions. GAINS produced a relatively higher change in CCN in the boreal and arctic regions, especially during colder season with GAINS/AeroCom CCN ratios reaching above 10 in January in eastern Siberia and northern China.

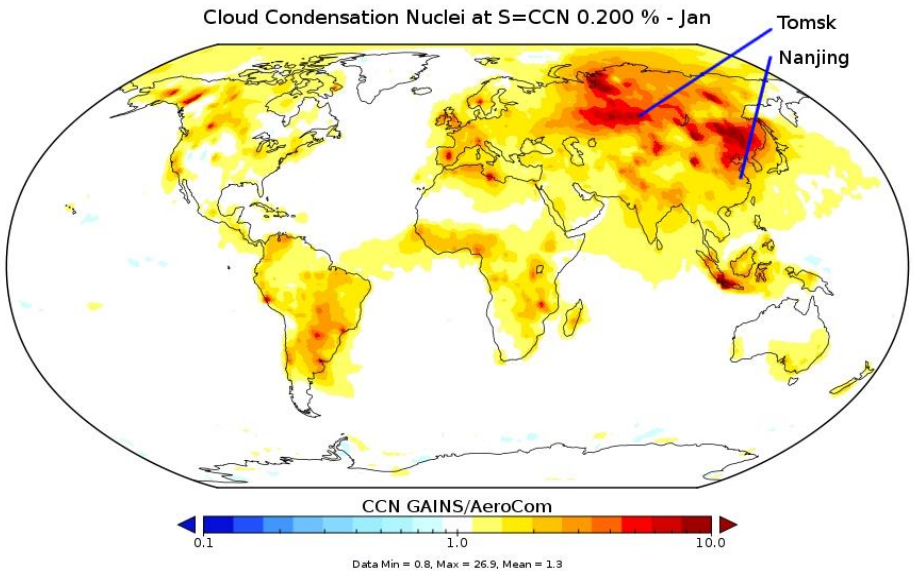

Figure 3. Ratio of GAINS over AeroCom CCN at 0.2% saturation.

The ECHAM simulations with updated GAINS emissions for anthropogenic activities produced particle concentrations leading towards the improvement of the model estimations at most measurement sites, especially when comparing accumulation and coarse mode concentrations. Furthermore, the overall

experiment revealed significant changes over the PEEX regions in terms of particle concentration and possible effects on radiative forcing. Overall, the GAINS proved to be able to compete with previously used input datasets in global climate modeling.

ACKNOWLEDGEMENT

This work is financially supported by Tor and Maj Nessling foundation grant N° 201600369 and Physics department of University of Helsinki.

REFERENCES

Amann, M., Bertok, I., Borken-Kleefeld, J., Cofala, J., Heyes, C., Höglund-Isaksson, L., Klimont, Z., Nguyen, B., Posch, M., Rafaj, P., Sandler, R., Schöpp, W., Wagner, F., Winiwarter, W. 2011: Cost-effective control of air quality and greenhouse gases in Europe: modeling and policy applications. Environmental modeling and Software, in press, doi: 10.1016/j.envsoft.2011.07.012.

Kulmala, M., Lappalainen, H. K., Petäjä, T., Kurten, T., Kerminen, V.-M., Viisanen, Y., Hari, P., Sorvari, S., Bäck, J., Bondur, V., Kasimov, N., Kotlyakov, V., Matvienko, G., Baklanov, A., Guo, H. D., Ding, A., Hansson, H.-C., and Zilitinkevich, S. 2015: Introduction: The Pan-Eurasian Experiment (PEEX) – multidisciplinary, multiscale and multicomponent research and capacity-building initiative, Atmos. Chem. Phys., 15, 13085-13096, doi:10.5194/acp-15-13085-2015.

Paasonen, P., Visshedjik, A., Kupiainen, K., Klimont, Z., Denier Van der Gon, H., Kulmala, M. 2013a: Aerosol Particle Number Emissions and Size Distributions: Implementation in the GAINS Model and Initial Results. IIASA Interim Report IR-13-020. International Institute for Applied Systems Analysis, Laxenburg, Austria.

Paasonen, P., Asmi, A., Petaja, T., Kajos, M. K., Aijala, M., Junninen, H., Holst, T., Abbatt, J. P. D., Arneth, A., Birmili, W., van der Gon, H. D., Hamed, A., Hoffer, A., Laakso, L., Laaksonen, A., Leaitch, W. R., Plass-Duelmer, C., Pryor, S. C., Raisanen, P., Swietlicki, E., Wiedensohler, A., Worsnop, D. R., Kerminen, V-M., Kulmala, M. 2013b: Warming-induced increase in aerosol number concentration likely to moderate climate change, Nature Geoscience. 6, 6, 438-442.

Stier, P., Feichter, J., Kinne, S., Kloster, S., Vignati, E., Wilson, J., Ganzeveld, L., Tegen, I., Werner, M., Balkanski, Y., Schulz, M., Boucher, O., Minikin, A., and Petzold, A. 2005: The aerosol-climate model ECHAM5-HAM, Atmos. Chem. Phys., 5, 1125-1156, doi:10.5194/acp-5-1125-2005.

Vignati, E., J. Wilson, and P. Stier. 2004: M7: An efficient size-resolved aerosol microphysics module for large-scale aerosol transport models, J. Geophys. Res., 109, D22202, doi:10.1029/2003JD004485.

IMAGE FUSION OF AATSR AOD PRODUCTS BASED ON THE MAXIMUM LIKELIHOOD ESTIMATE METHOD

YANQING XIE[1], YONG XUE[2,3], CHENG FAN[2], YAHUI CHE[2], AND JIE GUANG[2]

[1]College of Geoscience and Surveying Engineering, China University of Mining and Technology, D11 Xueyuan Road, Beijing 100083, China

[2]Key Laboratory of Digital Earth Sciences, Institute of Remote Sensing and Digital Earth, Chinese Academy of Sciences, No. 9 Dengzhuangnan Road, Beijing 100094, China

[3]Faculty of Life Sciences and Computing, London Metropolitan University, 166e220 Holloway Road, London N78 DB, UK

Keywords: AOD, IMAGE FUSION, MAXIMUM LIKELIHOOD METHOD.

INTRODUCTION

The traditional station measurement of aerosol optical depth (AOD) is currently widely employed. But this traditional approach has limitations with respect to wide-range coverage and spatial continuity. Comparing with traditional station observation, satellite remote sensing provides a possibility to high frequency monitor continuously spatial coverage of AOD (Xue et al., 2014). Based on these advantages, satellite measurements are widely applied to the monitoring of aerosol AOD in recent decades. However, the values of the AOD provided by different satellites show spatial and temporal differences due to the instrument characteristics and aerosol retrieval algorithms used for each instrument (Xu et al., 2015). This greatly limits its application in the direction of climate change and quantitative remote sensing. Through fusion of image from different remote sensors and methods, we can improve the image spatial coverage of valid values and accuracy, and further improve its application range (Xu et al., 2015).

METHODS

In this paper, we use the maximum likelihood method to determine the weights of various images involved in fusion to produce an Asian regional AOD data set in 2008 based on three AOD products: ADV, ORAC and SU that obtained from the Advanced Along-Track Scanning Radiometer (AATSR) according to the error size of each pixel. First of all, we compare the values of various products with the ground observation values obtained from the Aerosol Robotic Network (AERONET) and the China Aerosol Remote Sensing Network (CARSNET) to determine the error size of the pixels of the various products. Then, we study and determine the relationship between the values of the remote sensing observations and the value and surface albedo, so as to determine the error size of the observation value in the absence of the ground sensing station. Finally, we determine the weight of the fusion according to the root mean square error of the different products (Xu et al., 2015).

CONCLUSIONS

After comparing the original data and the fused data with the CARSNET observations, we find that the absolute error of the fused image is smaller than any of the original data. Meanwhile, the proportion of the fused AOD image with valid value is greatly large than any of the original products. Thus, the fusion increases the spatial coverage.

ACKNOWLEDGEMENTS

The data that we use in uncertainty analysis and validation come from AERONET and CARSNET sites, we thank their staff for establishing and maintaining these stations very much.

REFERENCES

1. H. Xu, J. Guang, Y. Xue, Gerrit de Leeuw, Y. H. Che, Jianping Guo, X.W. He, T.K. Wang, 2015, A Consistent Aerosol Optical Depth (AOD) Dataset over Mainland China by Integration of Several AOD Products. *Atmospheric Environmen*t. Volume **114**, August 2015, Pages 48–56.
2. Yong Xue, Xingwei He, Hui Xu, Jie Guang, Jianping Guo, and Linlu Mei, 2014, CHINA COLLECTION 2.0: The Aerosol Optical Depth Dataset from the Synergetic Retrieval of Aerosol Properties Algorithm. *Atmospheric Environment*, Volume 95, October 2014, Pages 45–58.

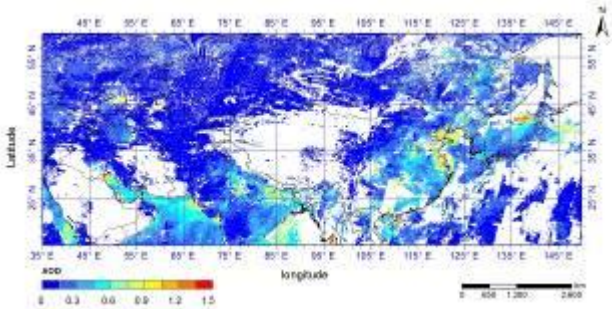

Fig. 1. The AOD spatial distribution of the original AATSR-ADV AOD data over the study area in May 2008

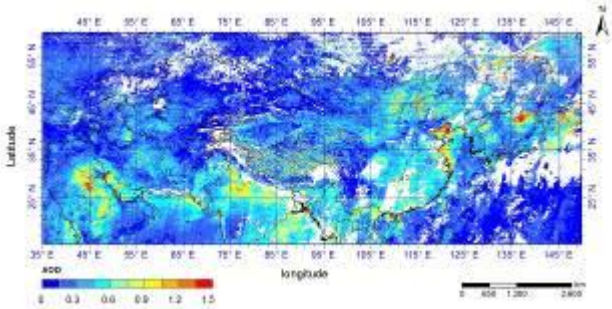

Fig. 2. The AOD spatial distribution of the original AATSR-ORAC AOD data over the study area in May 2008

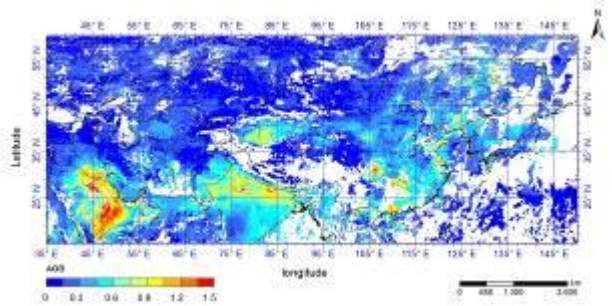

Fig. 3. The AOD spatial distribution of the original AATSR-SU AOD data over the study area in May 2008

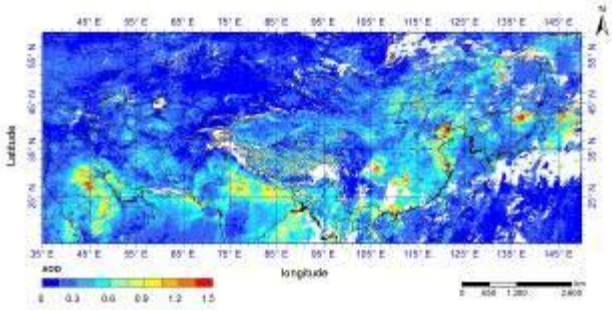

Fig. 4. The AOD spatial distribution of the fused AOD over the study area in May 2008

ATMOSPHERIC HULIS-CARBON IN $PM_{2.5}$ AND PM_1 IN SHANGHAI: IMPLICATION FOR HAZE POLLUTION

G. Xiu[1*], M. Zhao[1], T. Qiao[1], J. Yu[2]

[1] State Environmental Protection Key Lab of Environmental Risk Assessment and control on Chemical Processes. School of Resources & Environmental Engineering, East China University of Science and Technology, Shanghai 200237, P.R.China;

[2] Department of Chemistry, Hong Kong University of Science and Technology, Clear Water Bay, Kowloon, Hong Kong, China

Keywords: HULIS CARBON, $PM_{2.5}$, PM_1, SHANGHAI, HAZE POLLUTION

INTRODUCTION

Humic-like substances (Hulis) are a class of organic compounds extracted in atmospheric aerosol particles, which comprised of polycyclic ring structures with hydrocarbon side chains and hydroxyl, carboxyl and carbonyl groups (Graber and Rudich, 2006). Hulis is an important composition of particulate matter (PM) not only because Hulis carbon (Hulis-C) accounting for around half or more of WSOC in previous studies (Krivacsy et al., 2008; Kuang et al., 2015; Zhao et al., 2015a), but also because Hulis-C is suggested to play important roles in atmosphere by affecting hygroscopic growth (Gysel et al., 2004). It therefore is necessary to investigate the source, temporal and spatial variation of Hulis-carbon for haze pollution. Additionally, Hulis is recognized to be important representative of brown carbon (BrC) and they have potential contribution to the light-absorbing organic matter in the atmosphere (Hoffer et al., 2006).

Shanghai, with over 2.3 million populations, is the core city of the Yangtze River Delta Region (YRDR) and significantly disturbed by haze pollution due to elevated PM and ozone concentration Haze pollution is compounded by coal burning, vehicle exhaust emission and burning biomass combustion. Thus the concentration and contribution of Hulis in Shanghai are of great significance. But few studies have reported some relevant information. In order to attain a better understanding of the characteristics and sources of Hulis, we conducted a one-year field in urban Shanghai in the study. We focused on the influence of major sources on Hulis during different processes.

METHODS

The sampling site is on the roof top of a building in East China University of Science and Technology (ECUST) (N31°8'43", E121°25'31"), around 15 m above ground, which is located in the south western part of Shanghai and surrounded by a residential area with few major anthropogenic industrial sources. A five-channel Spiral Ambient Speciation Sampler (SASS, Metone Instrument Inc., OR, USA) was used to collect PM2.5 samples from 00:00 to 24:00 LT at a flow of 6.7 L/min.

Chemical species analyzed in the PM2.5 samples included carbonaceous components (OC, EC, WSOC and Hulis-C), water-soluble inorganic ions (SO42-, NO3-, NH4+, Na+ and K+), elements (Al and Fe) and three sugar compounds (levoglucosan, mannosan, and galactosan). Hulis in the aqueous extract of each filter was isolated by SPE (HLB), and 84%–90% of Hulis-C in SPE was eluted by 1.5 ml of 2% methanol–ammonia solution. The solution was dried using nitrogen and 10 ml ultrapure water was added. A TOC analyzer was used to analyze Hulis-C.

CONCLUSIONS

The peak of Hulis-C concentration occurred in December and the Hulis-C concentrations were relatively lower in summer (from June to August). The monthly variation trend of Hulis-C was roughly similar to that of the levoglucosan. Levoglucosan had a large seasonal contrast due to enhanced biomass burning emissions during some specific periods, as can be seen from the higher average concentrations in winter and autumn (Zhang et al., 2012). In PM2.5, the hydrophilic (non-hydrophobic) part of WSOC was dominant from February to Mary and Hulis-C/WSOC ratios only ranged from ~30% to ~40%.

Components/Species	Annual (Mean±SD)	Components/Species	Annual (Mean±SD)
$PM_{2.5}$ (μg/m^3)	53.22±45.90	Levoglucosan (ng/m^3)	94.16±131.84
OC (μg/m^3)	9.88±9.17	Sodium ion (Na+) (μg/m^3)	0.86±1.16
SOC (μg/m^3)	5.01±5.05	Aluminum (Al) (ng/m^3)	245.97±163.90
WSOC (μg/m^3)	5.45±4.51	Iron (Fe) (ng/m^3)	400.39±247.56
Hulis-C (μg/m^3)	2.61±2.58	OC/PM2.5 (%)	18.88±5.36
SIA (μg/m^3)	28.34±25.35	SIA/PM2.5 (%)	52.51±19.25
Sulfate (μg/m^3)	10.12±8.05	WSOC/OC	60.48±20.06
Nitrate (μg/m^3)	9.33±12.09	Hulis-C/WSOC	48.22±18.66
Ammonium (μg/m^3)	9.20±6.43		

Hulis comprises a significant fraction of WSOC and influences the water uptake properties of aerosols (Lin et al., 2010b). In this study, Hulis-C in PM_1 rose from 1.44 μg/m^{3}on normal days to 2.21 μg/m^3 on mild haze days, 4.32 μg/m^3 on slight haze days and 7.38 μg/m^3 moderate haze days, respectively. Corresponding values in $PM_{1\text{-}2.5}$ were 0.24 μg/m^3, 1.32 μg/m^3, 4.17 μg/m^3 and 10.37 μg/m^3.

For WSOC of PM1, higher correlation between WSOC and POC was observed by comparison with that of SOC, indicating that primary sources might dominate. While for $PM_{1\text{-}2.5}$, the different results were obtained. Hulis-Carbon had good correlation with POC and SOC both for PM1 and for $PM_{1\text{-}2.5}$.

Correlations	**PMs**	**POC**	**SOC**
WSOC	**PM_1**	**0.719**	**0.574**
	$PM_{1\text{-}2.5}$	**0.421**	**0.625**
Hulis-C	**PM_1**	**0.593**	**0.610**
	$PM_{1\text{-}2.5}$	**0.601**	**0.657**

. While for Hulis-Carbon, The conrrelation

In the study, it was demonstrated that biomass burning and secondary aerosol processes were major sources of Hulis-C. But the contributions of biomass burning in late autumn and winter were distinctly higher than those in summer. Meanwhile, the higher nitrate concentrations and NO3-/SO42- mass ratios were found in winter and late autumn. And Hulis-C showed the strong correlations with NO3-/SO42- and NOR, which indicated that Hulis-C formation processes might relate to nitrate formation. Therefore, in late autumn and winter, the contributions of biomass burning and secondary aerosol reactions accompanied with nitrate formation on Hulis-C were considerable. In summer, the positive correlation between the sum of O3 and NO2 and Hulis-C was found. The photochemical reactions occurred frequently, thereby contributing to Hulis-C formation.

ACKNOWLEDGEMENTS

This work was supported financially by Ph.D. Programs Foundation of Ministry of Education of China (No.20120074140001) and NSFC (21277044).

REFERENCES

Graber, E.R., Rudich, Y., 2006. Atmospheric HULIS: How humic-like are they? A comprehensive and critical review. Atmospheric Chemistry and Physics 6, 729-753.

Gysel, M., Weingartner, E., Nyeki, S., Paulsen, D., Baltensperger, U., Galambos, I., Kiss, G., 2004. Hygroscopic properties of water-soluble matter and humic-like organics in atmospheric fine aerosol. Atmospheric Chemistry and Physics 4, 35-50.

Hoffer, A., Gelencser, A., Guyon, P., Kiss, G., Schmid, O., Frank, G.P., Artaxo, P., Andreae, M.O., 2006. Optical properties of humic-like substances (HULIS) in biomass-burning aerosols. Atmospheric Chemistry and Physics 6, 3563-3570.

Lin, P., Huang, X.F., He, L.Y., Yu, J.Z., 2010b. Abundance and size distribution of HULIS in ambient aerosols at a rural site in South China. Journal of Aerosol Science 41, 74-87.

Krivacsy, Z., Kiss, G., Ceburnis, D., Jennings, G., Maenhaut, W., Salma, I., Shooter, D., 2008. Study of water-soluble atmospheric humic matter in urban and marine environments. Atmospheric Research 87, 1-12.

Kuang, B.Y., Lin, P., Huang, X.H.H., Yu, J.Z., 2015. Sources of humic-like substances in the Pearl River Delta, China: positive matrix factorization analysis of $PM_{2.5}$ major components and source markers. Atmospheric Chemistry and Physics 15, 1995-2008.

Zhang, R., Jing, J., Tao, J., Hsu, S.C., Wang, G., Cao, J., Lee, C.S.L., Zhu, L., Chen, Z., Zhao, Y., Shen, Z., 2014. Chemical characterization and source apportionment of $PM_{2.5}$ in Beijing: seasonal perspective (vol 13, pg 7053, 2013). Atmospheric Chemistry and Physics 14, 175-175.

Zhao, M.F., Huang, Z.S., Qiao, T., Zhang, Y.K., Xiu, G.L., Yu, J.Z., 2015. Chemical characterization, the transport pathways and potential sources of $PM_{2.5}$ in Shanghai: Seasonal variations. Atmospheric Research 158, 66-78.

*: corresponding author: Prof. Guangli Xiu, xiugl@ecust.edu.cn ,tel: 86-21-64251927.
School of Resources and Environmental Engineering, Shanghai, China.

INVESTIGATION OF MACKENZIE RIVER DISCHARGE AND NDVI RELATIONSHIP

WEIXIN XU[1], DAQING YANG[2], YANPING LI[3], RUIXIANG XIAO[1]

[1] Qinghai Institute of Meteorological Sciences, Xining, China
[2] Notional Hydrology Research Centre, Saskatoon, Canada
[3] Global Institute for Water Security and School of Environment and Sustainability, University of Saskatchewan, Saskatoon, Canada

Abstract

This study, based on the analyses of long-term discharge and NDVI data, revealed a strong seasonal consistency between NDVI and discharge over the Mackenzie River Basin in Canada. The flow-NDVI association is particularly strong in the early growing season (the 9th to 11th bi-weeks). During this period, discharge rapidly rises and reaches the peak, while NDVI increases around the 9th bi-week and reaches the maximum at the 14th bi-week. In the mid and late summer, both discharge and NDVI decline gradually. Correlation analyses identify two sensitive periods while NDVI significantly responds to discharge variations, i.e. the 9th - 12th bi-week and 14th - 17th bi-weeks, respectively. In the first period, the biweekly NDVI highly correlates to the 9th biweekly discharge, indicating that spring flow has a strong influence on vegetation growth in the early growing season. Spatially, almost all the basin shows a high correlation, except Mackenzie and Rocky Mountains and the region near the eastern edge of the basin. For the 2nd period of 14th - 17th bi-weeks, the NDVI relates closely to discharge with lags of 0-5 bi-weeks. Trends analyses suggest river discharge increased during 1982 to 2006 in most seasons except summer. The NDVI trends during the growing season during the 9th to 18th bi-weeks clearly correspond to discharge changes. Examination of extreme flow years and corresponding NDVI conditions over the basin also reveal that lower runoff year was associated with a lower basin NDVI with an earlier maximum, while the higher flow year was linked with a higher NDVI and a longer growing season.

NITROUS ACID IN A POLLUTED SUBTROPICAL ATMOSPHERE: SEASONAL VARIABILITY, DIRECT VEHICLE EMISSIONS AND HETEROGENEOUS PRODUCTION

ZHENG XU[1,2,4*], TAO WANG[1,2,], JUEQI WU[2], LIKUN XUE[2], PETER K. K. LOUIE[3], CONNIE W. Y. LUK[3],WEI NIE[4], AIJUN DING[4]

[1]Environment Research Institute, Shandong University, Ji'nan, Shandong 250100, PR China

[2]Department of Civil and Environmental Engineering, The Hong Kong Polytechnic University, Hong Kong, PR China

[3]Environmental Protection Department, Government of the Hong Kong Special Administrative Region, Hong Kong, PR China

* Now at [4]Institute for Climate and Global Change Research & School of Atmospheric Sciences, Nanjing University, Nanjing, 210023, China

Keywords : NITROUS ACID; SEASONAL VARIATION; VEHICLE EMISSION; HETEROGENEOUS REACTION

INTRODUCTION

Nitrous acid (HONO) has received considerable attention in the past few decades due to its important role in the HOx cycle (Kleffmann et al., 2005). HONO sources in the atmosphere can be classified into two categories: direct emissions and chemical formation. Direct emissions includes the release of HONO from fossil fuel combustion (Kurtenbach et al., 2001) and the microbial activities of soil (Su et al., 2011; Su et al., 2008b). Among chemical formation, heterogeneous processes are commonly accepted as the least understood pathway to the production of HONO. For example, nitrogen dioxide (NO_2) can be converted to HONO on the ground (Harrison at al., 1998), wet surfaces (Finlayson-Pitts et al., 2003), soot particles (Ammann et al., 1998;), and organic substrates (Ammann et al., 2005). These processes have been considered the primary contributor to nocturnal HONO formation, but they cannot sustain the frequently observed elevated daytime HONO concentration levels

During 2011-2012, HONO and its related parameters were measured at a suburban coastal site in the southern part of the PRD during four select months (one month in each season) to research the HONO seasonal and diurnal variations, deduces the emission factors and heterogeneous conversion

METHODS

The filed measurement was conducted at the suburban site in Tung Chung, which is a newly developed residential area in the northern part of Lantau Island, about 3 km away from Hong Kong International Airport. During the filed campaign, HONO was measured by a commercial long path absorption photometer instrument (QUMA, Model LOPAP-03).Additional, other related parameter including common meteorological parameters, NO, NOx, CO, O_3, particle size distribution, and JNO_2 was also measured(Xu et al., 2015).

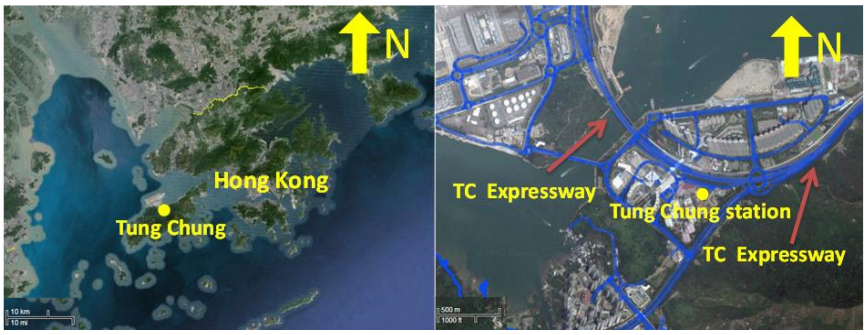

Figure 1 Google Map showing the location of Tung Chung Station, roads (in blue lines), and the surrounding regions.

CONCLUSIONS

A four-month field measurement of HONO was conducted at a suburban site (Tung Chung) in Hong Kong, which is the first study ofthe seasonal variation of HONO in the PRD region. The average concentrations of HONO in the spring, summer, autumn and winter were 0.36, 0.66, 0.93 and 0.91 ppb, respectively. The corresponding HONO/NOx ratios were 0.020, 0.027, 0.026 and 0.021.
The HONO concentration at night was significantly influenced by vehicle emissions. The derived emission ratio (HONO/NOx) was in the range of 0.39-1.6%. The strong correlation between the HONO/NOx and freshly emitted BC indicated the rapid formation of NO_2 on the BC emitted from the vehicles. An empirical method was derived to estimate the contribution of vehicle emissions of HONO.

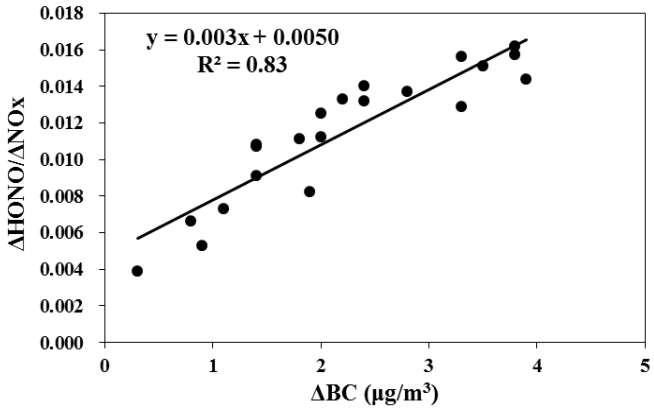

Figure 2 Correlation between $\Delta HONO/\Delta NO_x$ and freshly emitted BC in the 21 fresh plumes

High daytime HONO concentrations (over 1 ppbV) were frequently observed, which cannot be explained by gas-phase reaction (NO+OH). Correlation analysis suggests that a heterogeneous reaction of NO_2 on aerosol appears to be a significant source of daytime HONO at the site, especially in the summer polluted atmosphere when the aerosol loading is high.

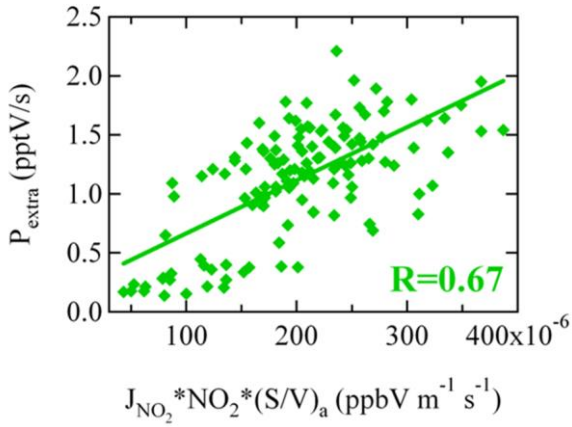

Figure 3 Correlations between P_m and proxies of photo-enhanced aerosol source in the summer case

ACKNOWLEDGEMENTS

This work was supported by the Hong Kong Environment and Conservation Fund (Project No. 7/2009), the Hong Kong Environmental Protection Department and the Hong Kong Polytechnic University Project of Strategic Significance.

REFERENCES

Ammann, M., Kalberer, M., Jost, D., Tobler, L., Rössler, E., Piguet, D., Gäggeler, H., Baltensperger, U., 1998. Heterogeneous production of nitrous acid on soot in polluted air masses. Nature 395, 157-160.

Ammann, M., Rössler, E., Strekowski, R., and George, C.: Nitrogen dioxide multiphase chemistry: Uptake kinetics on aqueous solutions containing phenolic compounds, Phys. Chem. Chem. Phys., 7, 2513–2518, 2005.

Finlayson-Pitts, B.J., Wingen, L.M., Sumner, A.L., Syomin, D., Ramazan, K.A., 2003. The heterogeneous hydrolysis of NO2 in laboratory systems and in outdoor and indoor atmospheres: An integrated mechanism. Physical Chemistry Chemical Physics 5, 223-242.

Harrison, R., Collins, G., 1998. Measurements of Reaction Coefficients of NO2 and HONO on Aerosol Particles. Journal of Atmospheric Chemistry 30, 397-406.

Kleffmann, J., Gavriloaiei, T., Hofzumahaus, A., Holland, F., Koppmann, R., Rupp, L., Schlosser, E., Siese, M., Wahner, A., 2005. Daytime formation of nitrous acid: A major source of OH radicals in a forest. Geophysical Research Letters 32, L05818.

Kurtenbach, R., Becker, K.H., Gomes, J.A.G., Kleffmann, J., Lörzer, J.C., Spittler, M., Wiesen, P., Ackermann, R., Geyer, A., Platt, U., 2001. Investigations of emissions and heterogeneous formation of HONO in a road traffic tunnel. Atmospheric Environment 35, 3385-3394.

Su, H., Cheng, Y.F., Oswald, R., Behrendt, T., Trebs, I., Meixner, F.X., Andreae, M.O., Cheng, P., Zhang, Y., Poschl, U., 2011. Soil Nitrite as a Source of Atmospheric HONO and OH Radicals. Science 333, 1616-1618.

Su, H., Cheng, Y.F., Shao, M., Gao, D.F., Yu, Z.Y., Zeng, L.M., Slanina, J., Zhang, Y.H., Wiedensohler, A., 2008b. Nitrous acid (HONO) and its daytime sources at a rural site during the 2004 PRIDE-PRD experiment in China. Journal of Geophysical Research 113, D14312.

Xu, Z., Wang, T., Wu, J., Xue, L., Chan, J., Zha, Q., et al., 2015. Nitrous acid (HONO) in a polluted subtropical atmosphere: seasonal variability, direct vehicle emissions and heterogeneous production at ground surface. Atmos. Environ. 106, 100–109.

PARTICULATE NITRATE AND SULFATE AT URBAN AND MOUNTAIN SITES IN THE NORTH CHINA PLAIN: DECADAL CHANGE FROM 2005-2015 AND FORMATION MECHANISMS

L.K. XUE[1], L. WEN[1], L.X. YANG[1], X.F. WANG[1], Y.T. ZHANG[1], T. WANG[2] and W.X. WANG[1]

[1] Environment Research Institute, Shandong University, Ji'nan, Shandong, China.

[2] Department of Civil and Environmental Engineering, Hong Kong Polytechnic University, Hong Kong, China.

Keywords: NIRTATE, SULFATE, MULTI-PHASE CHEMICAL MODEL, NORTH CHINA PLAIN

INTRODUCTION

Sulfate and nitrate are principal components of fine particulates and play important roles in atmospheric chemistry and air pollution. Haze induced by elevated levels of $PM_{2.5}$ has been of increasing concern in China in recent years. North China Plain (NCP) is the most industrialized region in northern China and suffers from severe haze problem. In the past decade, dramatic changes in anthropogenic emissions of sulfur dioxide (SO_2) and nitrogen oxides (NO_X) have occurred in China, which would have led to changes in the abundances of sulfate and nitrate aerosols in the ambient air. Quantifying the trend/changes in sulfate and nitrate particulates and elucidating their formation mechanisms are critical for evaluating the existing control measures and formulating future strategies to mitigate the haze pollution in China.

METHODS

A series of intensive field measurements were conducted at two sites in the last decade. The measurement sites are located in the downtown Ji'nan, the capital city of Shandong province, and the mountain-top of Mt. Tai – the highest mountain in the NCP region. A multi-phase chemical box model based on the RACM/CAPRAM was deployed to understand the formation mechanisms of nitrate and sulfate aerosols.

CONCLUSIONS

High levels of nitrate and sulfate were observed at both sites despite different temporal variations. Significant increases in the nitrate concentrations, nitrate/$PM_{2.5}$ and nitrate/sulfate ratios are found in both Ji'nan (2005-2015) and Mt. Tai (2007-2014), indicating the worsening situation of reginal nitrate pollution. The major formation pathways of sulfate and nitrate are illustrated. The daytime nitrate formation is mainly controlled by the availability of NO_2 and to a lesser extent NH_3, and the nighttime formation is primarily limited by NO_2 and O_3. NH_3 tends to prompt the nitrate formation at daytime but play a negative role in the nighttime. The complicated coupling effects of SO_2/NO_2, O_3, NH_3 and water content on the sulfate/nitrate formation are also elucidated.

ACKNOWLEDGEMENTS

This work was supported by the National Natural Science Foundation of China (NSFC, 41275123) and Shandong University.

REFERENCES

L. Wen, L. K. Xue, L. X. Yang, X. F. Wang, Y. H. Zhu, T. S. Chen, T. Wang, and W. X. Wang. Summertime particulate nitrate pollution in the North China Plain: increasing trend and formation mechanisms, in preparation for a journal paper (and abstract also submitted to the EGU conference 2016).

POSITIVE MATRIX FACTORIZATION ON CI-APi-TOF SPECTRA – TOWARD THE UNDERSTANDING OF FORMATION MECHANISMS OF HIGHLY OXIDIZED MULTIFUNCTIONAL COMPOUNDS IN A BOREAL FOREST ENVIRONMENT

C. YAN[1], W. NIE[1,2], M. ÄIJÄLÄ[1], S. HÄME[1], M. P. RISSANEN[1], T. JOKINEN[1], H. JUNNINEN[1], M. SIPILÄ[1], M. KULMALA[1], D. WORSNOP[1,3], M. EHN[1]

[1]Department of Physics, University of Helsinki, Helsinki, Finland

[2]Nanjing University, Nanjing, China

[3]Aerodyne Research Inc. Billerica, Massachusetts 01821, USA

Keywords: HOMs, PMF, CI-APi-TOF.

INTRODUCTION

Atmospheric particles exert an important impact on climate forcing. One important source of these particles is the nucleation and subsequent growth of the new aerosol particles, which potentially has a large contribution to cloud condensation nuclei (CCN) in global scale (Merikanto et al., 2009).

In the past decade, organic vapors are an important secondary source of atmospheric particles, through the condensation of their oxidation products on pre-existing particles aerosols (Jimenez et al. 2009, Hallquist et al. 2009). These products are usually highly oxidized multifunctional compounds (HOMs) formed via multi-step oxidation process. More recent studies have shown that some extremely low volatile oxidation products can contribute to the initial growth of newly formed particles (Riipinen et al. 2012, Ehn et al. 2014, Tröstl et al, 2016), and even participate in the nucleation (Riccobono et al 2014, Kirkby et al. 2016).

Accurate prediction of the climate impact of these HOMs requires quantitative understanding of the HOM formation. Several studies have suggested that the formation of HOMs includes several auto-oxidation processes followed by a termination reaction, and the molar yield in NO_x-free conditions is about a few percent depending on the species of VOC and oxidant (Ehn et al. 2014, Jokinen et al 2014, Rissanen et al 2014).

However, ambient HOM formation is more complicated due to the complexity of the real atmosphere. For example, the presence of nitrogen oxides (NO, NO_2) and nitrate radical (NO_3) can influence the HOM formation pathway, resulting in different products and yields. Here we present the first application of Positive Matrix Factorization (PMF) on HOMs detected with nitrate ion (NO_3^-) based chemical ionization – atmospheric pressure interface – mass spectrometer (CI-APi-TOF) in a boreal forest environment. The PMF successfully deconvolves the bulk HOM spectrum into several factors, each of which can be assigned to a specific formation pathway, thus improves our understanding of HOM formation from different sources. The results also inspire the future PMF application on similar data sets, which is important to understand the HOM formation in other environment.

METHODS

In this study, the measurement data was obtained from SMEAR II located in Hyytiälä, Southern Finland in spring 2012. The station is surrounded by boreal conifer forest and is described as a rural continental background measurement site (e.g. in Manninen et al., 2010). There are also occasionally polluted air masses reaching the site causing high aerosol loadings and high concentrations of gas-phase pollutants. Ambient meteorological conditions as well as concentrations of several trace gases are continuously monitored at the

station. Besides, a quadruple Proton Transfer Reaction mass spectrometer (PTR-MS) was deployed year-round to measure the volatile organic compounds (VOCs) from both under and above the canopy (Rantala et al., 2014). These co-located measurements are important in verifying the PMF solutions.

The estimation of measurement uncertainty (error matrix) is critical in PMF and since there was no previous research on applying PMF to CI-APi-TOF data, we derived the equation of error matrix for this new data set based on laboratory experiments, which showed good agreement with the equation used in aerosol mass spectrometer (AMS). The free parameters in the equation seem to be independent of temperature, instrument tuning, and detected chemical species.

The PMF solutions are firstly evaluated based on the mathematical diagnostics, including the Q value, Q distribution, and the fraction of explained variation by the model. Further verification of PMF results relies on the interpretability, which needs many considerations including: 1) a direct comparison of the retrieved factors to reported reference mass spectra; 2) key molecules as the fingerprint of a specific source; 3) The temporal correlation between the factors and related trace gases; 4) the repetitive temporal or diurnal variation patterns that indicate specific human activities or meteorological patterns; and 5) information regarding to air masses such as wind direction analysis or air mass trajectories.

CONCLUSIONS

PMF solution with 6 factors gives the most reasonable (interpretable) results. The profiles of each factor are shown in Figure 1. In general, 3 factors are considered as major contributors to daytime HOM formation, 2 factors are dominating the nighttime HOM formation, as well as one factor being identified as a representative of transported pollution.

The two nighttime factors are assigned to oxidation of monoterpene initiated by Ozone and nitrate radical, respectively. The factor of "O_3 + monoterpene" is verified by comparing the factor profile to the reference mass spectrum reported by Ehn et al. (2014). The uncentered correlation coefficient (Ulbrich et al. 2009) is 0.93. For the factor of "NO_3 + monoterpene", More than 80% of dimers are nitrogen-containing compounds, which is considered as its unique fingerprint. The nitrogen atom(s) inherited from the parent peroxy radicals (RO_2) indicates that at least one RO_2 radical is from the NO_3-initiated oxidation of monoterpene.

The three daytime factors are all NO_x related. The factor of "NO + NO_3/O_3 + monoterpene" appears in early morning concurrently with the increase of NO. The major peaks in this factor are identified as $C_{10}H_{15}NO_{9,11}$ and $C_{10}H_{16}N_2O_{9,11}$, which are produced by "O_3 + monoterpene + NO" and "NO_3 + monoterpene + NO", respectively. The "Daytime nitrates – type I" and "Daytime nitrates – type II" factors have diurnal patterns similar to global radiation, indicating that some photochemical processes are involved in both of them. The major peaks in "Daytime nitrates – type I" are mostly 10-carbon compounds, while the "Daytime nitrates – type II" is dominating by some lighter HOMs, e.g. 7-carbon compounds.

Apart from the above-mentioned factors that are considered as local factors, the gray factor in figure 1 is interpreted as "transport" factor. The only prominent peak in this factor is identified as nitrophenol, a commonly used tracer for biomass burning.

Figure 2 shows the overall contributions of each factor during the sampling period. In general, the contributions of daytime factors, nighttime factors, and transport factor are 51 %, 28%, and 21%, respectively. NO_x (and NO_3) is involved in most of the factors, indicating its significant impact on HOM formation.

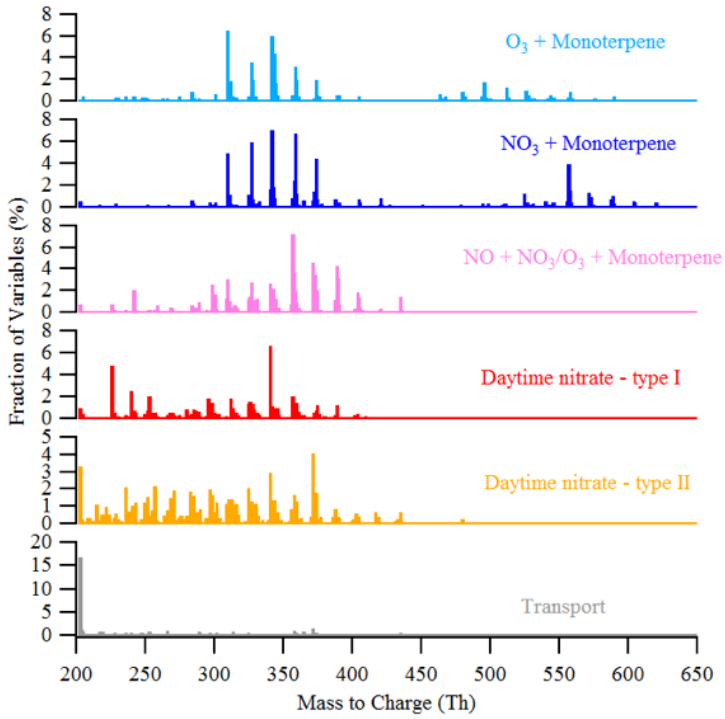

Figure 1. Profiles of 6-factor PMF solution. The x-axis denotes the mass-to-charge of each variable, and y-axis is the fraction of variables in each factor.

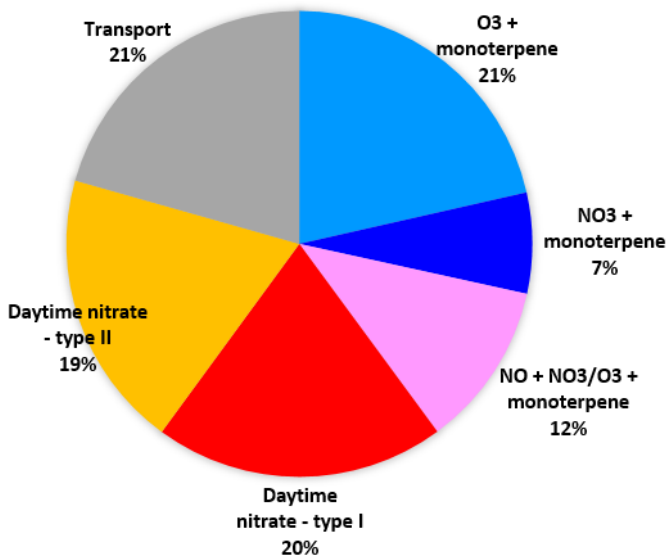

Figure 2. The contributions of each factor to total detected HOMs

ACKNOWLEDGEMENTS

This study was supported by Academy of Finland Centre of Excellence programs (project no. 272041 and 1118615).

REFERENCES

Ehn, M., et al. (2014). A large source of low-volatility secondary organic aerosol. *Nature* **506**: 476-479.

Hallquist, M., et al. (2009). The formation, properties and impact of secondary organic aerosol:current and emerging issues. *Atmospheric Chemistry and Physics* **9**(14): 5155-5236.

Jimenez, J., et al. (2009). Evolution of organic aerosols in the atmosphere. *Science* **326**:1525-1529.

Jokinen, T., et al. (2014). Rapid Autoxidation Forms Highly Oxidized RO2 Radicals in the Atmosphere. *Angewandte Chemie International Edition* **53**(52): 14596-14600.

Kirkby, J., et al. (2016). Ion-induced nucleation of pure biogenic particles. Submitted to *Nature.*

Manninen, H., et al. (2010). EUCAARI ion spectrometer measurements at 12 European sites–analysis of new particle formation events. *Atmospheric Chemistry and Physics* **10**(16): 7907-7927.

Merikanto, J., et al. (2009). Impact of nucleation on global CCN. *Atmospheric Chemistry and Physics* **9**(21): 8601-8616.

Rantala, P., et al (2014). Continuous flux measurements of VOCs using PTR-MS—reliability and feasibility of disjunct-eddy-covariance, surface-layer-gradient, and surface-layer-profile methods. *Boreal Environment Research* **19**: 87-107.

Riccobono, F., et al. (2014). Oxidation products of biogenic emissions contribute to nucleation of atmospheric particles. *Science* **344**(6185): 717-721.

Riipinen, I., et al. (2012). The contribution of organics to atmospheric nanoparticle growth. *Nature Geoscience* **5**(7): 453-458.

Rissanen, M. P., et al. (2014). The Formation of Highly Oxidized Multifunctional Products in the Ozonolysis of Cyclohexene. *Journal of the American Chemical Society* **136**(44): 15596-15606.

Tröstl, J., et al. (2016). Low-volatility organic compounds are key to initial particle growth in the atmosphere. Submitted to *Nature*.

Ulbrich, I. M., et al. (2009). Interpretation of organic components from Positive Matrix Factorization of aerosol mass spectrometric data. *Atmospheric Chemistry and Physics* **9**(9): 2891-2918.

SIMULATION OF FOREST CARBON FLUX BY MODEL INCORPORATION AND ASSIMILATION

M. YAN[1], Z.Y. LI[1], L. ZHANG[2], X. TIAN[1], E.X. CHEN[1]

[1] Institute of Forest Resource Information Techniques, Chinese Academy of Forestry, Beijing, 100091, Republic of China.

[2] Institute of Remote Sensing and Digital Earth, Chinese Academy of Sciences, Beijing, 100094, Republic of China.

Keywords: CARBON FLUX, MOD_17, BIOME-BGC, ENKF.

INTRODUCTION

Acting as substantial CO_2 sinks, forest ecosystems have been the focus of many scientific issues. However, carbon fluxes are dynamic in forests and are impacted by various impacts: climatic variations, natural disturbances, and human activities (Richardson *et al*., 2007; Schimel *et al*., 2001). Consequently, quantifying forest carbon fluxes and their variations is of fundamental importance. Two main methods have been undertaken in the past: observation and simulation. Eddy covariance (EC) can observe CO_2 exchange between vegetation and environment directly and accurately, but it is expensive and hard to extend regional scale. Meanwhile, various models have been developed for the simulating and forecasting the carbon fluxes for site and regional scales.

Remote sensing-based models provide a regular GPP estimate of Earth's terrestrial surface at a 1 km resolution (Heinsch et al., 2003; Running et al., 1999). Relying on the applicability and explicability of remote sensing data, the MODIS MOD_17 GPP (MOD_17) model cannot explain the intrinsic characteristics of ecological processes (e.g., photosynthesis, respiration, transpiration, allocation, etc.). Biome-BGC is a widely used process-based model for explicit simulations of vegetation photosynthesis, respiration, carbon, nitrogen, and hydrological cycles (Running and Hunt, 1993). But the model needs abundant input data and accurate calibrations for each biome type (Chiesi *et al*., 2012). Also it is inevitable to errors occur during the simulation because of the uncertainties from the model, input data and parameters.

So the integration of the optimized MOD_17 and Biome-BGC models was investigated for the calibration of the complicated Biome-BGC model and make full use of their advantages. The integration scheme was first conducted in the forest site in this study, and then it will be extended to regional scale.

As we know, data assimilation has been proved to be a reliable way to integrate observations from multiple sources and models for the correction of errors during the simulation. It has been used in many studies. Demarty *et al*. (2007) assimilated MODIS LAI products within the Dynamic Global Vegetation Model using Ensemble Kalman Filter (EnKF), and concluded that the assimilation had a significant positive impact on the simulation of carbon fluxes. Wang *et al*. (2009) designed a soil water content data assimilation scheme in the Lund-Jena Dynamic Global Vegetation Model (LPJ-DGVM), and improved the performances of carbon and water fluxes. Moreover, the performances of carbon and water fluxes obtained from Biome-BGC were improved by Zhang *et al*. (2015) using the assimilation of observed and MODIS LAI in the model.

In this work, two years (2003-2004) carbon fluxes of the forest site in Changbai Mountains were first simulated using Biome-BGC with the input meteorological data, forest site information and default eco-physiological parameters. Then the model was calibrated using the reproduced GPPs obtained from the optimized MOD_17 model. In order to correct the errors during the simulation, time series Global LAnd Surface Satellite (GLASS) LAI products were assimilated in Biome-BGC model and the model tracks were timely corrected. Finally, daily GPPs were validated against EC measurements at Changbai Mountains forest site.

METHODS

MOD_17 is a widely used remote sensing-based model, and is based on the radiation conversion efficiency concept of LUE (Monteith, 1972) and is driven by maximum LUE (LUE_{max}), a scalar of the 8-day vapor-pressed deficit (VPD), a scalar of the 8-day minimum air temperature (T_{min}), and absorbed photosynthetically active radiation (APAR, MJ day^{-1}). It can descript vegetation activities accurately over regional or global scales. However, minor uncertainties still exist in the biome specific parameter and input data. So it is necessary to optimize the model using refined biome specific parameter (maximum light use efficiency, LUEmax), meteorological data (8-day minimum temperature, VPD and PAR), and fPAR from the GLASS products.

Biome-BGC is a process-based model and is driven by meteorological data (i.e. daily maximum temperature, minimum temperature, precipitation, VPD, shortwave radiation and day length), site information (e.g. latitude, elevation, and slope), soil texture and 44 eco-physiological parameters. It relies on abundant ground information and parameters, so it is difficult to calibrate this model to adapt the local environmental conditions and characterize the forest processes over various biome types.

The integration of the optimized MOD_17 and Biome-BGC was deployed to take full advantage of the space-continuity of remote sensing data and time-continuity characteristics of forest processes. Then the eco-physiological parameters were calibrated by fitting the 8-day GPPs of 10 forest plots obtained from the optimized MOD_17 to those from Biome-BGC. When the best agreement occurred, the corresponding parameters of Biome-BGC were determined. It is necessary to mention that a sensitivity analysis using Extended Fourier Amplitude Sensitivity Test (EFAST) was performed prior to the calibration in order to determine the critical parameters affecting the model behaviors.

EnKF is one of the most popular sequential data assimilation algorithms for non-linear model operators. It is based on Monte Carlo or ensemble generations to solve the time evolution of the probability density of the model state. The basic analysis steps include initialization of the ensemble, forecasting, Kalman gain matrix and analyzing (Evensen, 1994).

In Biome-BGC, LAI is calculated as follows:

$$LAI = C_{leaf} \cdot SLA \quad (1)$$

where C_{leaf} (kg m^{-2} C) is the carbon state variable and SLA is the special leaf area (m^2 kg^{-1} C).

$$C_{leaf \cdot t} = C_{leaf \cdot t-1} + \Delta C_{leaf \cdot t} \quad (2)$$

The current $C_{leaf \cdot t}$ is summed by the carbon content of previous day ($C_{leaf \cdot t-1}$) and the change of the leaf carbon content ($\Delta C_{leaf \cdot t}$). $\Delta C_{leaf \cdot t}$ means the circulation and transformation of the carbon, and the accuracy of the $C_{leaf \cdot t}$ directly related to the rate of photosynthesis in Biome-BGC. During the assimilation, the observations (time series LAI during 2003 and 2004) were converted into the C_{leaf} through the linear equation.

CONCLUSIONS

Using refined meteorological data and calibrated LUE_{max} using EC measurements, as well as the GLASS *f*PAR products, the optimization of the MOD_17 model was performed. The results (Figure 1) demonstrated that the simulated GPPs (with R^2 = 0.88, RMSE = 12.254 gC/m^2/8d) improved substantially compared to the original MODIS GPPs (with R^2 = 0.62, RMSE = 22.562 gC/m^2/8d), especially during the growing seasons. So the reproduced 8-day GPPs were used for subsequent calibration of the Biome-BGC model.

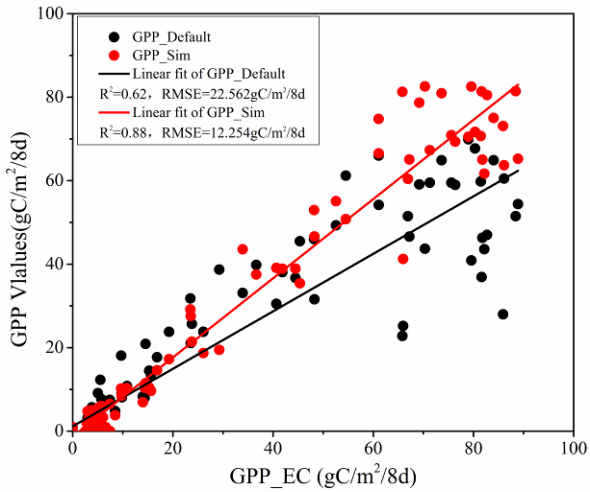

Figure 1. Validations of 8-day GPP simulated from the original and optimized MOD_17.

The simulations of forest GPP through the default, calibrated and assimilated Biome-BGC were provided in Figure 2. As expected, the results obtained from the original Biome-BGC were unsatisfactory compared with the EC measurements (Figure 3(a), R^2=0.72, RMSE=2.419 gC/m^2/d), especially in growing seasons of 2003 and 2004. The calibrated Biome-BGC using the optimized MOD_17 performed much better (Figure 3(b), R^2=0.87, RMSE=1.583 gC/m^2/d). Noticeably, the outliers during the summer of 2003 and 2004 were corrected, which was mainly impacted by the maximum stomatal conductance and fraction of leaf nitrogen in Rubisco (Chiesi *et al*., 2007).

Two years (2003 and 2004) LAI products were assimilated into Biome-BGC using EnKF with the ensemble window of 8 days. Figure 4 indicated that there existed significant difference between GLASS LAI and that simulated from Biome-BGC, especially in non-growing seasons. Generally, the simulated LAI after assimilation fitted well with GLASS LAI, except for a few fluctuations in winter. Also the performances of GPP obtained from the assimilated model agreed well with EC measurements (Figure 3 (c), R^2=0.92, RMSE=1.261 gC/m^2/d).

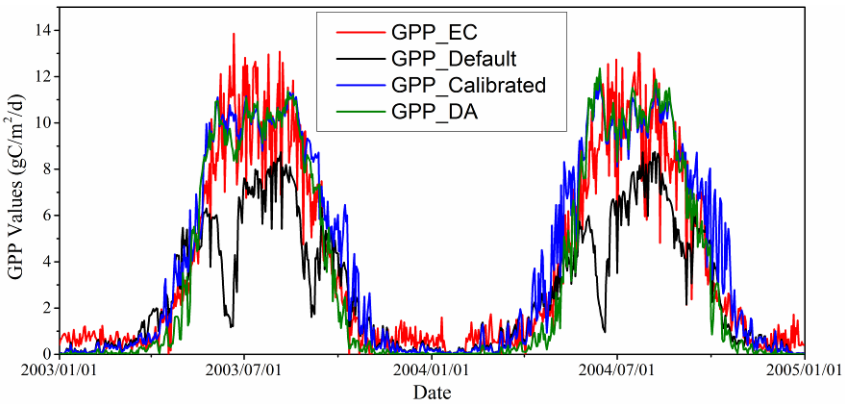

Figure 2. Comparisons of GPP performances obtained from the default, calibrated and assimilated Biome-BGC during 2003 and 2004. GPP_EC, EC measurements; GPP_Default, GPPs obtained from the Biome-BGC with the default parameters; GPP_Calibrated, GPPs obtained from the calibrated Biome-BGC using the optimized MOD_17 model; GPP_DA, GPPs obtained from the assimilated Biome-BGC.

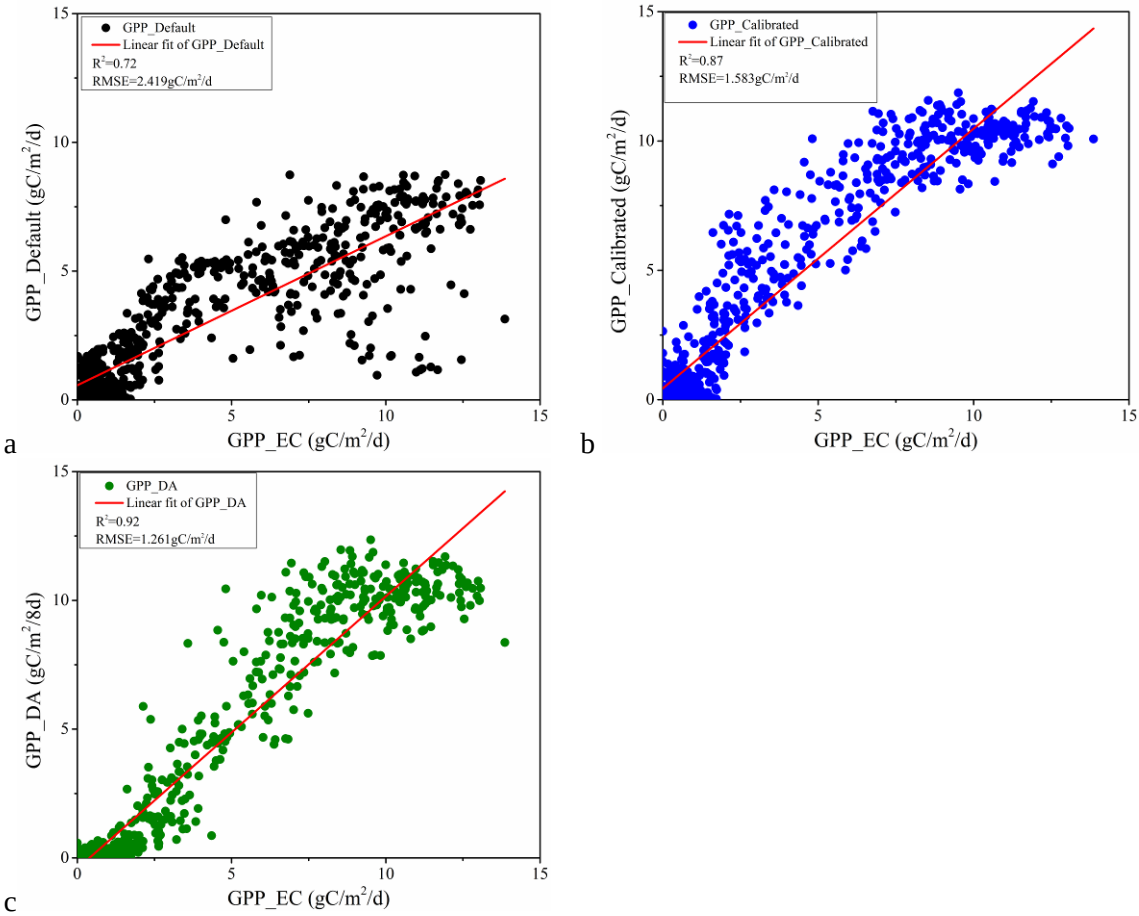

Figure 3. Validations of daily GPP simulated from the original (a), calibrated (b) and assimilated Biome-BGC (c).

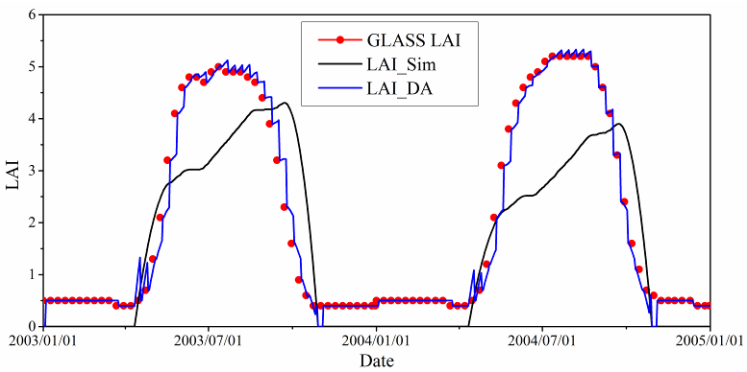

Figure 4. Comparisons of GLASS LAI, model simulated LAI and assimilated LAI during 2003 and 2004.

ACKNOWLEDGEMENTS

This study is supported by National 973 Program (2013CB733404) and Demonstration system of high resolution remote sensing applications in forestry (21-Y30B05-9001-13/15). We thank the data support for meteorological data, flux data and GLASS products.

REFERENCES

Chiesi, M.F., G. Chirici, P. Corona, P. Duce, R. Salvati, D. Spano, F.P. Vaccari and F. Maselli (2012). Use of BIOME-BGC to simulate water and carbon fluxes within Mediterranean macchia, *iForest* **5**, 38.

Chiesi, M.F., F. Maselli, M. Moriondo, L. Fibbi, M. Bindi and S.W. Running (2007). Application of BIOME-BGC to simulate Mediterranean forest processes, *Ecol. Model.* **206**,179–190.

Demarty, J., F. Chevallier, A.D. Friend, N. Viovy, S. Piao and P. Ciais (2007). Assimilation of global MODIS leaf area index retrievals within a terrestrial biosphere model, *Geophys. Res. Lett.* **34**, doi:10.1029/2007GL030014.

Evensen, G. (1994). Sequential data assimilation with a non-linear quasi-geostrophic model using Monte Carlo methods to forecast error statistics, *J. Geophys. Res.* **99**, 10143-10162.

Heinsch, F.A., M. Reeves, P. Votava, S. Kang, C. Milesi, M. Zhao, J. Glassy, W.M. Jolly, R. Loehman and C. F. Bowker (2003). GPP and NPP (MOD17A2/A3) Products NASA MODIS Land Algorithm, *MOD17 User's Guide*, 1-57.

Monteith, J. (1972). Solar radiation and productivity in tropical ecosystems, *Journal of applied ecology*, **9**, 747-766.

Richardson, A.D., D.Y. Hollinger, J.D. Aber, S.V. Ollinger and B.H. Braswell (2007). Environmental variation is directly responsible for short-but not long-term variation in forest-atmosphere carbon exchange, *Global Change Biol*. **13**, 788-803.

Running, S.W. and E.R. Hunt (1993). *Scaling physiological processes: Leaf to globe*, (Academic Press, San Diego, U.S.A.).

Running, S.W., R. Nemani, J.M. Glassy and P.E. Thornton (1999). MODIS daily photosynthesis (PSN) and annual net primary production (NPP) product (MOD17) Algorithm Theoretical Basis Document. University of Montana, SCF At-Launch Algorithm ATBD Documents (available online at: www. ntsg. umt. edu/modis/ATBD/ATBD_MOD17_v21. pdf).

Schimel, D.S., J.I. House, K.A. Hibbard, P. Bousquet, P. Ciais, P. Peylin, B.H. Braswell, M.J. Apps, D. Baker and A. Bondeau (2001). Recent patterns and mechanisms of carbon exchange by terrestrial ecosystems, *Nature* **414**, 169-172.

Wang, X.X., M.G. Ma, X.J. Han and Y. Song (2009). Assimilation of soil moisture in LPJ-DGVM, in Proc. of SPIE, Conf. on Remote Sens. for Agriculture, Ecosystems and Hydrology XI as Part of the 16th Int. Symposium on Remote Sens., Berlin (SPIE, Germany), 747220-747220.

Zhang, T.L., R. Sun, C.H. Peng, G.Y. Zhou, C.L. Wang, Q. A. Zhu and Y. Z. Yang (2015). Integrating a model with remote sensing observations by a data assimilation approach to improve the model simulation accuracy of carbon flux and evapotranspiration at two flux sites, *Science China Earth Sciences*, 1-12.

ANALYSIS AND EVALUATION OF SOIL EROSION IN SOUTHERN RED SOIL EROSION AREA: A CASE IN GANZHOU

YANG Liu[1] , LI Hengkai[1]

[1] Faculty of Architectural and Surveying Engineering, Jiangxi University of Science and Technology, Ganzhou 341000, Jiangxi, China.

Keywords: soil erosion, RUSLE equation, HJ-CCD, red soil hilly region.

INTRODUCTION

Under various outside forces, soil erosion is the process that soil material is stripped, transport, deposition. It is the most widespread natural process in Earth's surface, and it also contributes to land degradation in the world's largest environmental problem (Oldeman L R, 1994). Which represented by the remote sensing space science development, has provided strong technical support for soil erosion, especially combines with the revised universal soil equation (RUSLE). Which make soil erosion dynamic in real-time, quantitative, used widely (Demirci A et al., 2012; Sun W et al., 2013). Hilly red soil of the South is one of the most serious soil erosion in China. (CHENG D et al., 2010) In order to better carry out comprehensive management of soil erosion in the area, based on the studies in Ganzhou city, guided by the SL657-2014 standard, combined HJ-CCD images and RULSE model, this paper undertook the soil erosion remote sensing assessment and analysis of spatial-temporal evolution of soil erosion in this area. It would provide technical and scientific basis to monitor and control of water and soil erosion in this region.

METHODS

Soil types in Ganzhou dominated by acid soil, it is poor corrosion resistance and very susceptible to water erosion. The data used in this study include remote sensing image data, rainfall data, topographic data, soil data, land-use data and so on. Remote sensing image data was HJ-CCD image data with the spatial resolution of 30m of China Resource Satellite Application Center. Firstly, environment satellite CCD data were preprocessed to obtain two Ganzhou remote-sensing images in 2008 and 2013. Each image consists of two view CCD images. Then the DEM data mosaicked and clipped by Ganzhou boundary vector data, finally Ganzhou DEM data would be obtained.

Based on the regional situation, the revised universal soil loss equation (RUSLE), the model is defined as shown in the formula (Li Hengkai et al., 2013): A=K×L×S×P×R×C. where A is the computed annual soil loss per unit area(Mg ha-1 year-1); R is the rainfall-runoff erosivity factor (MJ mm ha^{-1} h^{-1} $year^{-1}$); K is the soil erodibility factor (Mg h MJ-1 mm-1); S is slope steepness factor (angle); L is slope length factor (m); C is the cover and management factor (dimensionless); P is the support practice factor (dimensionless). This model is the key to determining the index value of each factor of equations. Using the available experimental data, combining ENVI and ArcGIS software, respectively, we could calculate the value of each factor in the formula. And we unified each factor to GRID layers in the WGS84 coordinate system, unified all factors ultimately grid for 30m×30m, multiplied all factors with RUSLE model, South Jiangxi rank data and layers of soil erosion intensity were obtained. To determine RUSLE model each factor's value with below methods.

Rainfall-runoff erosivity factor: calculation of rainfall erosivity models usually have monthly rainfall erosion force model and daily rainfall erosion force model in the South area with abundant rainfall, last model performs more stable and higher accuracy. Zhang Wenbo(2002) calculated rainfall-runoff erosivity with formula (1).

$$R_i = \alpha \sum_{j=1}^{m} (D_j)^{\beta} \tag{1}$$

Where R_i is i-th half-month erosion, D_j is j-th daily rainfall (D_j ge 12 mm,otherwise it is 0), m is the days of half a month of erosive rainfall, α、β are parameters, calculated with formula (2) and (3). And year rainfall-runoff erosivity calculated with formula (4).

$$\alpha = 21.586\beta^{-7.1891} \tag{2}$$

$$\beta = 0.8363 + 18.177/P_{d12} + 24.455/P_{y12} \tag{3}$$

$$R = \alpha\sum_{i=1}^{24} Ri \tag{4}$$

Where P_{d12} is the average daily rainfall that daily rainfall is more than 12mm, P_{y12} is the average year rainfall that daily rainfall is more than 12mm. This study obtained year rainfall-runoff erosivity based on 2008 and 2013 daily rainfall data meteorological stations of 18 counties in South Jiangxi. R value of counties connected correspondingly with counties in ArcMap, generated R distribution grid map.

Soil erodibility factor: Sharpley A N and Williams J R(1990) think K value are just related to sand grain, silt, clay and organic matter. K value is calculated with formula (5).

$$K = \{0.2 + 0.3\exp[-0.0256SA(1 - SI/100)]\} * [\frac{SI}{CL + SI}]^{0.3} * [1.0 - \frac{0.25c}{c + \exp(3.72 - 2.95c)}] * [1.0 - \frac{0.7SA_1}{SA_1 + \exp(-5.51 + 22.9SA_1)}] \tag{5}$$

Where SA is mass fraction of sand grain, SI is mass fraction of silt, CL is mass fraction of clay, C is mass fraction of organic matter, and SA_1=1-SA. By using factor turn raster method, the 4 soil index factor converted to grid values, the last distribution grid map of K values are obtained by raster calculator.

Slope steepness factor and Slope length factor: Improved algorithm to calculate slope length factor l values for each slope in the study area. L value calculate with formula (6).

$$L = (\text{Flow Accumulation} * \text{Cell Size}/22.13)^m \tag{6}$$

Where flow accumulation stands the pixel's accumulated area which water flows uphill, cell size is pixel' side length, m stands slope length exponent, m calculated as formula (7):

$$m = \begin{cases} 0.5 & \beta \geq 5\% \\ 0.4 & 3\% \leq \beta < 5\% \\ 0.3 & 1\% \leq \beta < 3\% \\ 0.2 & \beta < 1\% \end{cases} \tag{7}$$

Where β stands pixel gradient. And slope steepness factor calculated with formula (8).

$$S = \begin{cases} 10.8\sin\theta + 0.03 & \theta < 5^\circ \\ 16.8\sin\theta - 0.5 & 5^\circ \leq \theta < 10^\circ \\ 21.91\sin\theta - 0.96 & \theta \geq 10^\circ \end{cases} \tag{8}$$

Where S stands slope steepness factor, θ is slope. Finally, L factor times S factors obtained LS factor.

Cover and management factor: C value calculated with formula (9).

$$C = \begin{cases} 1 & V_f = 0 \\ 0.6508 - 0.3436\lg V_f & 0 < V_f \leq 78.3\% \\ 0 & V_f > 78.3\% \end{cases} \tag{9}$$

Where V_f stands vegetation coverage. When vegetation cover is greater than 78.3%, there will be no soil erosion, so C value is close to 0. When the vegetation coverage rate is 0, the more soil erosion, C value is closer to 1. And V_f was calculated by formula (10).

$$V_f = (NDVI - NDVI_{soil}) / (NDVI_{Veg} - NDVI_{Soil}) \tag{10}$$

Where *NDVI* is the normalized difference vegetation index, $NDVI_{soil}$ is the *NDVI* value of bare soil or vegetation-free areas, and $NDVI_{Veg}$ is the *NDVI* values of complete vegetation.

Support practice factor: p values are between 0~1, 0 represents that the area of soil erosion does not occur, and 1 represents that any area of water conservation measures have been taken. Land use information can fully reflect the message of water conservation measures. This study based on research results of Renard K G et al., (1997) and considering the actual situation in South Jiangxi, P values can be sure as table 1.

Tab1 The p value of different land use types in the study area

Land Use Type	Cultivated Land	Construction Land	Jungle Land	Water Region	Sparse Woodland	Bare Land	Grass Land
P Value	0.2	0.3	1	0	0.7	0	1

Remote sensing images were supervised classification with ENVI, and categories were shown in Tab 1. Then different land use types would be given corresponding value in Tab 1 with ArcGIS software, lastly, distribution grid map of P value would be obtained.

CONCLUSIONS

Based on the above calculation methods and processes, combined with RUSLE equation and ArcGIS raster calculator, spatial distribution map of soil erosion in research areas in 2008 and 2013 years could be obtained. According to China's water and soil conservation in Xingguo County, Jiangxi province, in the Bulletin of soil and water conservation stations data in 2013 year, we validated the calculation results of soil erosion. Taking Xingguo County soil and water conservation stations in gold runoff the 2nd and 5th district as two testing site, which residential location is 115 ° 13 ' 45 'E and 26 ° 16 ' 45 'N, erosion observed were 1423.60t/km2 and 3230.10T/km2 respectively. By 2013 this corresponds to a value is validated, this volume of soil erosion 1234.70 t/km2, 2603.30 t/km2. So it indicated the RUSLE calculation model of soil erosion in high accuracy, and the model has a certain credibility.

ACKNOWLEDGEMENTS

This work was supported by National Natural Science Fund (41261093), Jiangxi provincial science and technology topics (GJJ14416), Jiangxi province social sciences planning issues (14YJ20).

REFERENCES

Oldeman L R. The global extent of soil degradation[J]. Soil resilience and sustainable land use, 1994, (9) : 19-36.

Demirci A, Karaburun A. Estimation of soil erosion using RUSLE in a GIS framework: a case study in the Buyukcekmece Lake watershed, northwest Turkey [J]. Environmental Earth Sciences, 2012, 66(3):903-913.

Sun W, Shao Q, Liu J. Soil erosion and its response to the changes of precipitation and vegetation cover on the Loess Plateau [J]. Journal of Geographical Sciences, 2013, 23(6): 1091-1106.

CHENG D, LIAO C, ZHANG P, et al. Discussion on Comprehensive Management Techniques System of Water and Soil Losses in Hilly Red Soil Region in South of China[J]. Journal of Yangtze River Scientific Research Institute, 2010, 11: 023. (In Chinese)

LI H,WU L,LI F. Optimal fractal band selection on HJ-1 CCD image for land use classification[J]. Journal of Remote Sensing, 2013, 17(6):1752-1586.(In Chinese)

Zhang W B, Xie Y, Liu B Y. Rainfall erosivity estimation using daily rainfall amounts[J]. Scientia Geographica Sinica, 2002, 22(6): 705-711.(In Chinese)

Sharpley A N, Williams J R. EPIC-erosion/productivity impact calculator: 1. Model documentation[J]. Technical Bulletin-United States Department of Agriculture, 1990, 3-9.

McCool D K.Revised slope length factor for the universal soil loss equation[J].Transactions of the Am Soc of Agric Engrs,1989,32(5):1570~1576.

Renard K G, Foster R, Weesies G, McCool D K, Yoder D C. Predicting rainfall erosion by water: a guide to conservation planning with the Revised Universal Soil Loss Equation (RUSLE).USDA Agriculture Handbook, 1997, 703: 1-367.

THREE EPOCHS OF DATA ON GLACIER CHANGES ON THE TIBETAN PLATEAU DERIVED FROM LANDSAT IMAGERY, FROM THE 1970S TO 2013

QINGHUA YE[1], JIBIAO ZONG[1], LIDE TIAN[1], J. GRAHAM COGLEY[2], CHUNQIAO SONG[3], WANQIN GUO [4]

[1] Key Laboratory of Tibetan Environment Changes and Land Surface Processes, Institute of Tibetan Plateau Research, Chinese Academy of Sciences (CAS), Beijing 100101, China

[2] Department of Geography, Trent University, Peterborough, Ontario, CANADA K9L 0G2

[3] Department of Geography, University of California, Los Angeles, 1255 Bunche Hall, Los Angeles, CA 90095, United States

[4] Cold and Arid Regions Environmental and Engineering Research Institute, Chinese Academy of Sciences, Lanzhou, China

Keywords: GLACIER AREA CHANGES; TIBETAN PLATEAU; INTERIOR DRAINAGE BASINS; EXTERNAL DRAINAGE BASINS; GLACIER DATA.

Glacier area on the Tibetan Plateau (TP hereafter) and its change were studied in different drainage basins based on time series of Landsat satellite images since the 1970s. High-resolution optical images of good quality, with minimal cloud and snow cover, were selected. There were 263 images from Landsat MSS in the 1970s, 150 images from Landsat7 ETM+ in 1999-2002, and 148 images from the Operational Land Imager (OLI) of Landsat 8 in 2013–2014. All satellite data were mosaicked to represent three periods, i.e. M1970s, M2000s, and M2013/2014. The most frequent year in each period was adopted as the mosaic image date: i.e. 1976, 2001 and 2013. However the uncertainty of each of these dates was allowed for. Glacier outlines were digitized manually on the three mosaics**,** with reference to the SRTM Digital Elevation Model v4.1 and Google Earth imagery. Only debris-free ice was delineated and analysed in this study. Glacier area mapping uncertainty was evaluated at three study sites where previous measurements over matching periods were available: Mt. Qomolangma (Everest), Mt. Naimona'Nyi, Mt. Geladandong. The largest difference between the data sets was within ~±7%.

Glacier shrinkage on the TP was substantial but spatially variable between the 1970s and 2013. In the 1970s, glaciers covered 1.7% of the TP study area as a whole. Glacier area on the TP has decreased from 44,366 ± 2827 km^2 in the 1970s to 42,210 ± 1621 km^2 in 2001 (area change was -2,156 km^2), and further decreased to 41,137 ± 1616 km^2 in 2013 (area change was -1,073 km^2). Glacier shrinkage rate was more marked in marginal (external) drainage basins of the south-east TP than in the interior drainage basins of the north-west TP, from the maximum of -0.43% a^{-1} (at -1.60% a^{-1} during 1994-2013) in the Mekong River catchment down to the minimum rate of -0.12% a^{-1} in the Tarim interior drainage from 1976 to 2013.

ESTIMATING METHANE UPTAKE FROM GLOBAL FOREST AND GRASSLAND BY A STATISTICAL MODEL

LIJUN YU[1,*], YAOHUANG[2,*], WEN ZHANG[1], WENJUAN SUN[2], TINGTING LI[1]

[1] LAPC, Institute of Atmospheric Physics, Chinese Academy of Sciences, Beijing 100029, China.

[2] State Key Laboratory of Vegetation and Environmental Change, Institute of Botany, Chinese Academy of Sciences, Beijing 100093, China.

Methane (CH_4) is one of the most potent greenhouse gases, and forest and grassland are the major biological sinks of CH_4. Here we used an empirical model to evaluate the spatiotemporal changes of soil CH_4 sinks during 1981 to 2010. We estimated that the mean sinks of global forest and grassland soil were 10.97 and 4.50 Tg CH_4 yr^{-1}, respectively. Both for forest and grassland, CH_4 oxidation rate enhanced from north to south, and dry tropical climate zone was the largest CH_4 sink. From 1981 to 2010, forest CH_4 sink increased significantly ($P<0.05$) by the rate of 6.77 Gg CH_4 yr^{-1}. Moreover, grassland CH_4 sinks also increased very significantly ($P<0.01$) by the rate of 6.27 Gg CH_4 yr^{-1}. The largest increasing rate was in Polar/Boreal grassland by 5.74 Gg CH_4 yr^{-1} ($P<0.01$), while CH_4 uptakes decreased by 0.36 Gg CH_4 yr^{-1} ($P<0.01$) in warm dry temperate. Under the background of global warming, soil methane sink of forest and grassland is likely to be enhanced in future.

CLOUD REMOVING METHOD FOR DAILY SNOW MAPPING OVER CENTRAL ASIA AND XINJIANG, CHINA

XIAOQI YU[1,2], YUBAO QIU[1], HUADONG GUO[1], LIJUAN CHEN[1, 3]

[1] Institute of Remote Sensing and Digital Earth, Laboratory of Digital Earth Science, Dengzhuang South Road, Haidian District, Beijing, China, 100094, qiuyb@radi.ac.cn

[2] College of Geographical Information System, Liaoning Technical University, Fuxin, China

[3] College of Geographical Science, Fujian Normal University, Fuzhou, China

Keywords: CENTRAL ASIA, CLOUD REMOVING, MODIS, SNOW MAPPING.

INTRODUCTION

Central Asia and Xinjiang, China are conjunct areas, located in the hinterland of the Eurasian continent, where the snowfall is an important water resource supplement form. In this paper, based on the daily snow product from Moderate Resolution Imaging Spectroradiometer (MODIS A1), a cloud removing method was developed by considering the regional snow distribution characteristics with latitude and altitude dependence respectively. In the end, the daily cloud free products was compared with the same period of eight days MODIS standard product, revealing that the cloud free snow products are reasonable, while could provide higher temporal resolution, and more details over Center Asia and Xinjiang Province.

DATA AND CHARACTERISTIC ANALYSIS

The V005 version of Terra MODIS and Aqua MODIS daily snow classification products MOD10A1 and MYD10A1 were download by NSIDC website. Digital elevation model DEM (Elevation Model) is selected by the USGSEROS data center where responsible for data archiving and reporting SRTM_DEM elevation data to the public.

Currently there are many cloud algorithms, Andreas Juergen Dietz et al[1] by previous methods, carrying out the study on the applicability of the different algorithms, including: MODIS daily combination, adjacent temporal deduction, near four pixel method, near eight pixel method, elevation filtering, long time series method in order to deal with the cloud. In this paper, based on the near eight pixels to analyze characteristics. However after the near eight pixels algorithm analysis, there is still cloudy, so we try to improve the snowline method.

In Central Asia, 88.5% of the region at an altitude of 1000 meters below, 8.8% area is located between an altitude of 1000 m to 3500 m, 2.5% area is located between an altitude of 3500 m to 5000 m, and only 0.1% area higher than 5000 m above sea level[2]. The article will divide the elevation into three segments, respectively, less than 0,0-2000meters, and 2000-8429meter. And through vertical zoning,we get the rules of mountain snow line changes by 8 days maximum snow synthetic products,further analysis the characteristics of snow line with altitude dependence.

According to eight days maximum snow cover products in Central Asia and China's Xinjiang region, when statistical longitude is 45 to 96 degrees and there are most land pixel value below snow pixels, statistics the latitude of variation range of snow pixel values,every 8 days to get a snowline of latitude, the latitude snowline range is approximately 30 to 58 degree,and then analysis the characteristics of latitude snowline of plain area.

METHOD

According to the snowline changes of latitude and elevation mentioned above, we draw a feasible scheme as figure 1 shows.

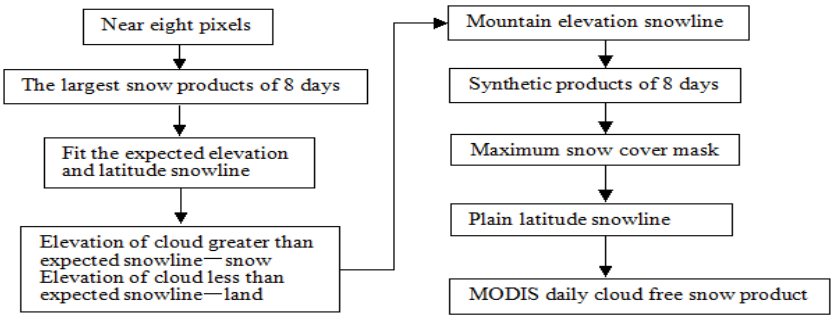

Fig.1 Cloud removal algorithm flow chart

COMPARATIVE ANALYSIS AND VERIFICATION

On the basis of near eight pixels and mountain snowline method, 8 days maximum snow products are synthesized,after comparison founding that there are differences in part of the mountain area. The existence of different due to part of the mountain is processed with snowline , and make the cloud cover ratio decreased.The overall effect is better when using snowline algorithm to remove cloud in Central Asia and Xinjiang,China region.

There are following verification index of snow products, including the total accuracy of snow classification image P(%), reflects the image recognition accuracy of snow and snow free pixels,snow identification accuracy R (%) can only reflects the recognition accuracy of snow pixels, Accuracy is the correct classification accuracy of pixels, but when there are large snow free areas in the image,the statistics will bring the errors.F score is perhaps the most useful, is the balance of precision and recall. In binary snow products, TP said there is snow pixel both in reference data and the data to be verified; TN said that no snow in two kinds of products; FP said that there is no snow in reference data but the validation data has;FN said there is no snow in validation data but the reference data has.

In Fractional snow cover products, including the root mean square error (RMSE), deviation (Bias) and correlation coefficient, etc.FSCext and FSCref represent the reference data and the data to be evaluated.

	Binary snow extent products	Fractional snow extent products
Statistical Parameters	$Precision=\frac{TP}{TP+FP}$	$RMSE=\sqrt{\frac{1}{N_{ui}}\sum_{j=0}^{y}\sum_{i=0}^{x}(FSC_{EXT}(i,j)-FSC_{REF}(i,j))^2}$
	$Recall=\frac{TP}{TP+FN}$	$BIAS=\frac{1}{N_{ui}}\sum_{j=0}^{y}\sum_{i=0}^{x}(FSC_{EXT}(i,j)-FSC_{REF}(i,j))$
	$Accuracy=\frac{TP+TN}{TP+TN+FP+FN}$	$N_{equ}=\sum_{j=0}^{y}\sum_{i=0}^{x}\frac{FSC(i,j)}{100}$
	$f=2*\frac{Precision*Recall}{Precision+Recall}=\frac{2TP}{2TP+FP+FN}$	$CorrCoef=\frac{\sum_{j=0}^{y}\sum_{i=0}^{x}(FSC_{EXT}(i,j)-\overline{FSC_{EXT}})(FSC_{REF}(i,j)-\overline{FSC_{REF}})}{\sqrt{\sum_{j=0}^{y}\sum_{i=0}^{x}(FSC_{EXT}(i,j)-\overline{FSC_{EXT}})^2\sum_{j=0}^{y}\sum_{i=0}^{x}(FSC_{REF}(i,j)-\overline{FSC_{REF}})^2}}$

Table 1. Statistical parameters in binary and fractional snow extent products

When using these metrics, it should be noted that the idea of using aggregated high-resolution snow data (either binary or fractional) to‘simulate’ coarse resolution FSC includes a certain limitation. This means

that particularly at low snow fractions but also at higher snow fractions, FSC aggregated from high-resolution FSC is persistently higher than direct coarse resolution FSC . This is a typical way of using high resolution data for validations; however the issue of different scales in FSC retrievals is present regardless of the retrieval method applied.

ACKNOWLEDGEMENTS

This work is supported in part by National Natural Science Foundation of China (Grant No. 41371351 and 41120114001) and Chinese Special Fund for Meteorology-Scientific Research in the Public (GYHY201206040).

REFERENCES

[1] Andreas Juergen Dietz, Claudia Kuenzer, Ursula Gessner & Stefan Dech.Remote sensing of snow –a review of available methods. International Journal of Remote Sensing,2012, 33(13):4094-4134.

[2]Andreas Juergen Dietz, Claudia Kuenzer, Christopher Conrad. Snow-cover variability in central Asia between 2000 and 2011 derived from improved MODIS daily snow-cover products. International Journal of Remote Sensing,2013, 34(11):3879-3902.

ASSESSMENT AND HYDROLOGIC APPLICATIONS OF THE LATEST SATELLITE-GAUGE PRECIPITATION ESTIMATES OVER THE HUAIHE RIVER BASIN

HUILING YUAN[a, b, *] and RUOCHEN SUN[a]

[a] School of Atmospheric Sciences and Key Laboratory of Mesoscale Severe Weather/Ministry of Education, Nanjing University, Nanjing, China

[b] Jiangsu Collaborative Innovation Center for Climate Change, China

Keywords: QUANTITATIVE PRECIPITATION ESTIMATE (QPE); SATELLITE-GAUGE; GAUGE ADJUSTMENT; TRMM; CMORPH; HYDROLOGIC SIMULATION

INTRODUCTION

To date, a number of newly developed satellite-gauge quantitative precipitation estimates (QPE) QPEs have not been evaluated thoroughly, especially their hydrologic applicability at the basin scale. Recently, at China Meteorological Administration (CMA), an operational daily satellite-gauge product with 0.25° resolution (CMORPH CMA; Yu et al., 2015) has been produced, which combines the raw CMORPH QPE data with daily precipitation observations from about 2400 gauges in China. It is of interest to verify whether fine resolution satellite-gauge QPEs may serve as a better alternative to conventional gauge observations to monitor rainfall over river basins in the heterogeneous Chinese continent. In this study, four satellite-gauge QPEs on a 0.25°× 0.25° grid, including TRMM 3B42V7, CMORPH CRT, CMORPH BLD and newly developed CMORPH CMA are evaluated over the Huaihe River basin in China during 2003-2012 in comparison with the China Gauge-based Daily Precipitation Analysis (CGDPA; Shen and Xiong, 2015). The hydrologic capability of fine satellite-gauge QPEs and their impact on streamflow simulations at the basin scale have been investigated, through the input forcing for the distributed Variable Infiltration Capacity (VIC, Liang et al., 1994, 1996) model.

METHODS

A set of verification metrics were used to quantitatively analyze the overall performance of the four satellite-gauge QPEs, in both precipitation products and resulting streamflow simulations, including systematic bias (Bias), bias adjusted root-mean square error (aRMSE), Pearson correlation coefficient (CC) and relative error (RE), equitable threat score (ETS), Frequency Bias, probability of detection (POD) and false alarm ratio (FAR), and Nash-Sutcliffe Coefficient of Efficiency (NSCE).

The VIC distributed hydrologic model was used to simulate the rainfall–runoff process in this study. The CGDPA and four satellite-gauge QPEs are used to drive the VIC with three vertical soil layers over the Huaihe River basin, and hydrologic simulations using different forcing QPEs are compared. Six important parameters related to soil properties and base flow (such as the exponent of variable infiltration capacity curve, the maximum velocity of base flow, the second and the third soil-layer thicknesses, etc.) were calibrated.

CONCLUSIONS

Gauge adjustment procedures in the production of satellite-gauge QPEs greatly affect their quality of precipitation estimation. For streamflow modeling, the errors of QPEs are also propagated into hydrologic simulations, since hydrological processes in distributed hydrologic models are sensitive to the total precipitation amount as well as rainfall intensity distributions.

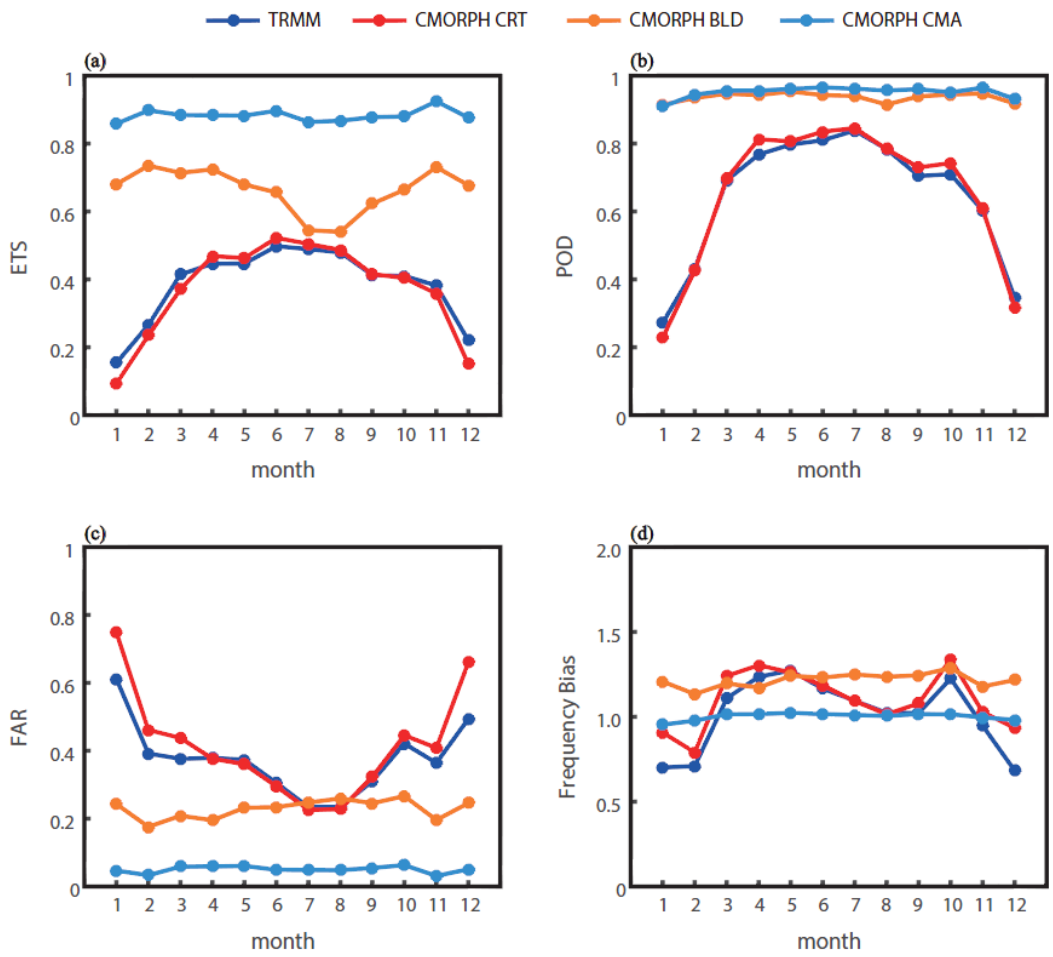

Figure 1. (a) ETS, (b) POD, (c) FAR and (d) Frequency Bias of different daily satellite-gauge QPEs against CGDPA at the thresholds of 1 mm/day, 10 mm/day, 25 mm/day, 50 mm/day during 2003-2012

ACKNOWLEDGEMENTS

This work is supported by the National Basic Research Program of China (973 Program) (2013CB430106), the R&D Special Fund for Public Welfare Industry (meteorology) (GYHY201206005), the National Natural Science Foundation of China (41175087), and High Performance Computing Center of Nanjing University.

REFERENCES

Yu, J., Shen, Y., Pan, Y., Xiong, A., 2015. Comarative assessment between the daily merged precipitation dataset over China and the world's popular counterparts (in Chinese). Acta. Meteorol. Sin. 73, 394-410.

Sun, R., H. Yuan*, X. Liu, and X. Jiang, 2015: Evaluation of the latest satellite-gauge precipitation products and their hydrologic applications over the Huaihe River basin. Submitted to Journal of Hydrology (second-round review).

ACCURACY OF RIVER NETWORK EXTRACTED FROM DIFFERENT DEM DATASET AND THE RELATIONSHIP WITH TERRAIN UNDULATION

BAI YUN[1], ZHANG JIAHUA[1]

[1] Institution of Remote Sensing and Digital Earth, CAS.

Keywords: DAZHANGXI RIVER BASIN, DEM, RIVER NETWORK, TERRAIN UNDULATION

INTRODUCTION

River network is important data for hydrology research. Except for field investigation, river network could be obtained by vectorization from RS images and extraction from DEM. For large area, obtaining river network from DEM data is the most convenient and quickest way. But in this way, uncertainties are also introduced to the result, which is primarily from the Terrain condition and accuracy of DEM itself. Current paper compares two usually used DEM dataset at the river basin of Dazhangxi a tributary of Minjiang River in South China. We also analyze the relationship between terrain undulation and accuracy of river net extracted from different DEM datasets. Current research aim to detect the factors that affect the river extraction, providing information for the utilize of DEM in hydrology science.

METHODS

Work flow chart is shown in Figure 4.

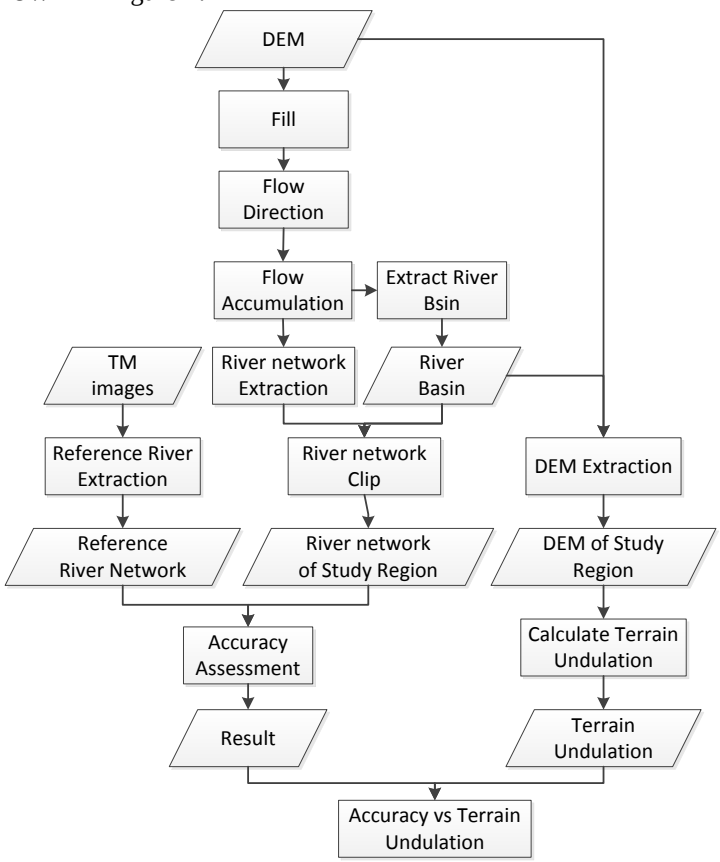

Figure 4 Work flow chart

Terrain undulation could be explained as the difference of between maximum and minimum elevation value within a limited region. It is an important factor for classification of landform types. As shown in Figure 5, in the DEM dataset a region is formed of 25 cells, the terrain undulation of this region is calculated by Eq.(4).

$$r = \max(c_i) - \min(c_j); i, j = 1, 2..25 \text{ -} \quad \textbf{(4)}$$

c1	c2	c3	c4	c5
c6	c7	c8	c9	c10
c11	c12	c13	c14	c15
c16	c17	c18	c19	c20
c21	c22	c23	c24	c25

Figure 5 Martrix for Calculation of Terrain Undulation

We use D8 algorism to calculate calculate the river network from DEM, and reference river network if vectoring from TM images. Accuracy assessment calculated from Eq.(5), result of which is defined in current paper as off-set length.

$$E = \frac{\sum A_i}{\sum L_{si}} \text{ -} \quad \textbf{(5)}$$

Where (Figure 6) E represent for the accuracy (off-set length), the less, the better; A_i is the area of the polygon formed by extracted river and reference river; and L_{si} is the length of the reference river that form A_i .

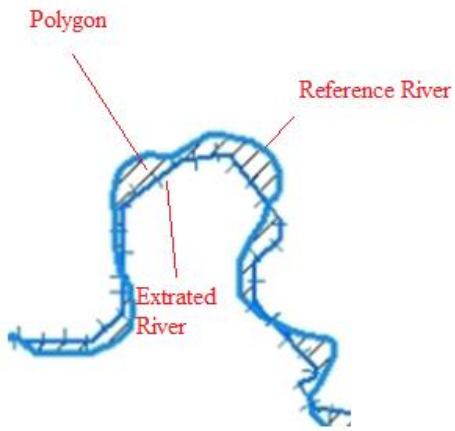

Figure 6 Intersection of River Net

CONCLUSIONS

Using 50m as the interval to classify the terrain undulation of study region. And off-set length within each elevation class is calculated by Eq.(5). For the terrain undulation of each classification, the middle value is used for corresponding classes. By analysing the off-set length vs reclassified terrain undulation, we find the terrain undulation has significantly affected the accuracy of extracted river network. The

accuracy linearly increases with the increase of terrain undulation (Figure 7). And Figure 7 also shows that when terrain undulation is less than 800m, ASGTM dataset work better than SRTM dataset.

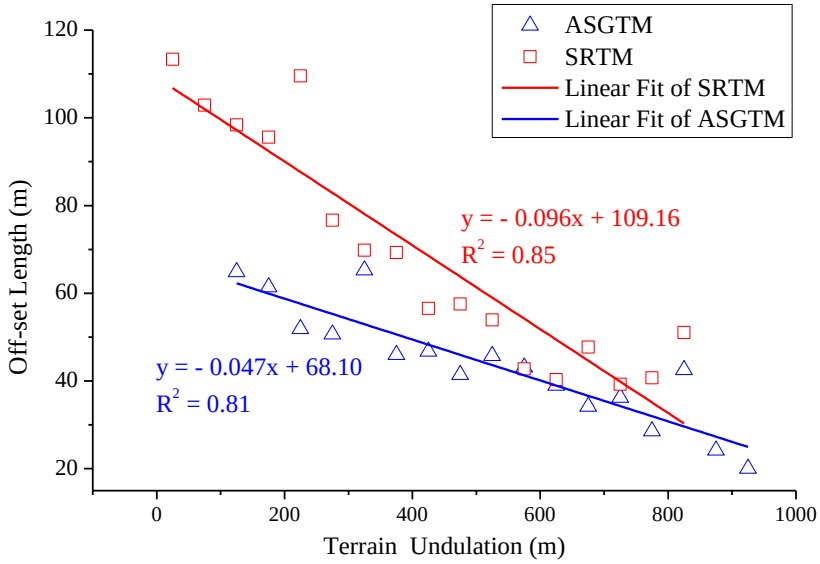

Figure 7 Off-set length of extracted river network vs terrain undulation

REFERENCES

Lingling, Cao, & Qiuwen, Zhang. (2007). Digital river network extraction and application based on SRTM. *Yangtze River, 38*(08), 150-152 (In Chinese).

O'Callaghan, John F., & Mark, David M. (1984). The extraction of drainage networks from digital elevation data. *Computer Vision, Graphics, and Image Processing, 28*(3), 323-344. doi: http://dx.doi.org/10.1016/S0734-189X(84)80011-0

Wei, Zhang, & Ainong, Li. (2012). Study on the opitmal scale for calculating the relief amplitude in china based on dem. *Geography and geo-information science, 28*(04), 8-12 (In Chinese with English Abstract).

Wei, ZHANG, Xin, YANG, Guo-an, TANG, Shi-jie, ZHU, & Cai-li, LI. (2012). DEM-based flow direction algorithms study of stream extraction and watershed delineation in the low relief areas. *Science of Surveying and Mapping, 37*(02), 94-96 (In Chinese with English Abstract).

Xingli, Jia, Jinliang, Xu, Hongzhi, Yang, & Liping, Zhao. (2012). Calculation of broken index of surface based on GIS. *Journal of Chong Qing University, 35*(11), 126-130 (In Chinese with English Abstract).

Yuan, LIU, Mai-chun, ZHOU, Zhi-jing, CHEN, & Shaowen, Li. (2012). Comparison of Drainage Network Extraction from Different DEM Data Sources: A Case Study of Hanjiang River Basin. *SCIENTIA GEOGRAPHICA SINICA, 23*(09), 1112-1118 (In Chinese with English Abstract).

Yuheng, LIU, & Honggen, XU. (2012). Comparisons of water systems extracted f rom DEM with two dif ferent processing methods. *RESOURCES SURVEY & ENVIRONMENT, 33*(03), 206-210 (In Chinese with English Abstract).

BOREAL ECOSYSTEM BIOGECHEMISTRY SIFTED THROUGH THE CATCHMENT-RESOLVING ANALYSIS

A. YU. YUROVA[1] J. TANG[2], B. TUPEK[3]

[1] Nansen International Environmental and Remote Sensing Centre, St. Petersburg, 14th Line 7, Vasilievsky Island, Russian Federation.

[2] Department of Biology, University of Copenhagen, Ole Maaløes Vej 5, DK-2200 Copenhagen, Denmark

[3] The Finnish Forest Research Institute, Luke, PO Box 18 (Jokiniemenkuja 1), FI-01301 Vantaa, Finland

Keywords: CATENA, ECOSYSTEM MODEL, DISTRIBUTED HYDROLOGY, DOC

INTRODUCTION

Network of eddy-flux towers has been established worldwide to quantify the net exchange of carbon between the ecosystems and the atmosphere. However, unlike with the weather station network it was really quantified what density of the station network is sufficient to provide information within permitted uncertainty range. Here we hypotheses that considering catenary and permafrost related variability of carbon exchange that is mostly neglected in the analysis can provide completely different picture than the data from the eddy-flux towers alone (e.g. Yurova and Lankreijer, 2007; Siewert et al, 2015). Specific aims of the study were: 1) to develop a process-based model of soil water and temperature regime (including the presence of permafrost) and carbon exchange for a hillslope with a usage of LANDSAT satellite data on NPP (Net Primary Production) and soil organic matter dynamic model supplemented with parameterization of the dissolved organic carbon (DOC) lateral transport and export; 2) to analyse the results of field studies of soil carbon exchange for different positions on a hillslope performed for a number of test sites across boreal forest and tundra (Russia, Sweden, Finland); 3) to analyse found spatial features of net ecosystem exchange (NEE) and link them to the weather conditions with the developed model and see additional information acquired compare to that of the eddy-flux tower alone.

METHODS

The distributed hydrological model was prepared that enables simulations of soil temperature and water content for different soil layers, the thawing depth and freezing depth, evapotranspiraion and runoff on the 2.5D grid (laterally distributed and having limited number of soil layers, Tang et al, 2014). In the current model version the 30x30 m griddcells are coupled laterally trough horizontal water exchange in saturated and unsaturated zones. Based on climatic mean hydrological variables the gridcells were classified in xeric, mesic, moist and and riparian zones for the test hillslopes in Northern Sweden – Abisko ans Krycklan and in Finland (Tupek et al., 2008). The DOC lateral transport and export to the stream was also calculated for Abisko site (Tang et al., work in progress). Bayesian approach was used for the initialization of the soil pools based on multi-layer field observations of the soil carbon content made in Swedish, Finnish and Russian sites.

Few indices that quantify leaf area index (LAI) based on LANDSAT satellite imagery were validated based on 2D representation of the LIDAR imagery (newly developed approach) and the manual measurements. It was found that RSR (reduced simple ratio) explained as much as 65% of the spatial variability in LAI for the studied plots as compared to 50% obtained using more widely used NDVI (Normalized Difference Vegetation Index). It was therefore used as a proxy for LAI, and NPP was calculated using FPAR and light use efficiency approach. ROMUL model was used to simulate soil organic matter dynamics and above and belowground turnover rates prescribed.

Annual carbon exchange was studied for the classified sub-sample of gridcells separately, then aggregated to a hillslope unit and compared with eddy-flux tower data.

CONCLUSIONS

It was found that the Northern boreal forest (Krycklan, Sweden) has rather predictable pattern of the hillslope soil carbon accumulation with the maximum at the forest-stream transition and minimum (20% of the maximum) near the water divide, while intermediate positions have around 50% of the maximum carbon storage. Most of carbon is accumulated in the organic horizons with proportion being the highest (92%) in the riparian zone. No definite link between the position on the slope and the carbon storage was found for the tundra soils on the permafrost (Russia). It is the combination of the deepening of the permafrost thawing depth and the excessive soil moisture that lead to the high accumulation of soil carbon – primarily in organic horizons.

The model showed good correspondence between the simulated and observed soil carbon pools for the boreal forest when the Bayesian method of soil pool initialization was used and historical information about the last disturbance incorporated. The results for the tundra ecotones are more modest, but the model is currently under development.

The sensitivity of NPP and NEE of the xeric mesic and wet sites to weather variations (precipitation and temperature) is very site-specific and may even have opposite sign for different site classes. It is the mesic sites where the temporal variability of the water table position is high that can demonstrate the switches between the carbon sink and source regime, but xeric and wet sites are also sensitive to weather variations (Tupek et al, 2015). The aggregated response of the distributed hillslope carbon balance can show carbon sink when eddy-flux tower is showing carbon source.

ACKNOWLEDGEMENTS

This work was supported by the grant from Russian Foundation for Basic Research № 15-05-01368.

REFERENCES

Siewert, M. B., Hanisch, J., Weiss, N., Kuhry, P., Maximov, T. C., & Hugelius, G. (2015). Comparing carbon storage of Siberian tundra and taiga permafrost ecosystems at very high spatial resolution. *Journal of Geophysical Research: Biogeosciences*,*120*(10), 1973-1994.

Tang, J., Pilesjö, P., Miller, P. A., Persson, A., Yang, Z., Hanna, E., & Callaghan, T. V. (2014). Incorporating topographic indices into dynamic ecosystem modelling using LPJ-GUESS. *Ecohydrology*,*7*(4), 1147-1162.

Tupek, B., Minkkinen, K., Kolari, P., Starr, M., Chan, T., Alm, J., & Nikinmaa, E. (2008). Forest floor versus ecosystem CO2 exchange along boreal ecotone between upland forest and lowland mire. Tellus B, 60(2), 153-166.

Tupek, B., Minkkinen, K., Vesala, T., & Nikinmaa, E. (2015, April). Sensitivity of the boreal forest-mire ecotone CO2, CH4, and N2O global warming potential to rainy and dry weather. In *EGU General Assembly Conference Abstracts* (Vol. 17, p. 4170).

Yurova A., Lankreijer H. (2007). Carbon storage in the organic layers of boreal forest soils under various moisture conditions: a model study for Northern Sweden sites. Ecological Modelling, 204, 475-484

MICROLANDSCAPE STRUCTURE OF SOUTH TUNDRA LANDSCAPES BASED ON A FIELD SURVEY

E.A. ZAROV[1], L.L. GOLUBYATNIKOV [2] and E.D. LAPSHINA[1]

[1]UNESCO chair "Environmental dynamics and global climate change", Yugra state university, Khanty-Mansiysk, KhMAO-Yugra, Russian Federation.

[2] Laboratory of mathematical ecology, A.M. Obukhov Institute of Atmospheric Physics of Russian Academy of Sciences, Moscow, Russian Federation.

Keywords: microlandscapes, south tundra, ecosystem description.

INTRODUCTION

West Siberian tundra zone occupied 311 279 km^2. It is 11 % of the West Siberia area [Gvozdetskii, 1968]. South tundra takes around 6 % of this area. And there is 29 % of this territory covered by wetlands [Romanova, 1985] usually locating on watersheds. Also continues permafrost is characteristic for whole this zone [Tarnocai et al., 2009]. So the projected climate changes could lead to the degradation of permafrost and tundra wetlands carbon involvement in biogeochemical processes.
There is insufficient data about the structure and properties of the West Siberian tundra zone landscapes data for reliable forecasts the impact of climate change on global processes due to its inaccessibility. Also the actively developing oil and gas infrastructure influences increasing pressure on vulnerable northern landscapes. It makes scientifically important to investigate this area to define more information about its structure and functioning.
It has been chosen a key area in south tundra to describe a microlandscape structure of the subdivided landscapes.

METHODS

The study area is located in the south tundra (67.43457 N, 78.6146 E), around 35 km south-east from Tazovskiy, on the Pur-Taz watershed (right Lukyiaha-river terrace). In previous years it had been carried out the general landscape structure of the key area on a base of satellite images and filed survey [Zarov, 2015]. The research area was subdivided for 9 dominant and typical landscapes (Table 1).

№	Class
1	Water
2	Hasyrey* (1st type)
3	Hasyrey* (2nd type)
4	Yernik**
5	Dry- lichen land
6	Polygon-patterned wetland
7	Wet-sedge
8	Thaw (1st type)
9	Thaw (2nd type)

Table 1. Subdivided landscapes
* - pour out lake by thermokarst processes
** - dwarf shrubs thicket

All landscapes were subdivided for the microlandscapes forming its structure based on the field survey. The main criterias were the vegetation cover and location in relief. It has been subdivided 20 unique microlandscaes. For each it was measured pH, EC, t, depth of permafrost and water table, and described the vegetation and microrelief.

Class Polygon-patterned wetland

Microlandscape 1 – shrubby polygon in polygon-patterned wetland
It is the small (8*8 m) polygon covered by *Ericaceae* shrubs – *Ledum palustre* (till 45 %), lichens (40 %). The permafrost depth is 29.5 cm, no liquid water.
Microlandscape 2 – lichen polygon in polygon-patterned wetland
This microlandscape is similar to the previous one but more abundantly covered by lichens (till 90 %) and sometimes has larger area (14*14 m). *Ericaceae* shrubs are also presented – *Ledum palustre* (30 %). The permafrost depth is 26.7 cm, no liquid water.
Microlandscape 3 – thaw on the polygon edge
This area presents the process of polygons thermodegradation. The surface is a bit lower surrounded area covered by *Sph.fuscum* (100 %) and *Ericaceae* shrubs – *Andromeda polifolia*, *Ledum palustre* (50 %). Sometimes there are the small rolls occurs, reflected the high degradated polygons. The permafrost depth is 31.4 cm, water table on 15.7 cm. Water has acidic pH= 3.407 and EC=52.33 µSm.
Microlandscape 4 – the crack between the polygons.
These are the cracks (1.2-3.0 m width) between the polygons originated by thermokarst processes. The wetland water (pH=3.876 and EC=32.667 µSm) flows through it. Area covered by *Sph.balticum* (100 %), sedges and *Eriophorum Russiolum* take 35 %. The permafrost depth is 38.0 cm, water table on 2.7 cm.
Microlandscape 5 – the lakes in the polygons centre
There is a water filled depression caused by a local thermokarst processes. Usually it has 11*11 m size, surrounded by small rolls. Water has pH=4.248, EC=23.000 µSm. The permafrost locates on 46.1 cm.
For the entire class soils are presented by peat and organic litter.

Class Thaw (1nd type)
Microlandscape 6 – thaw covered by shrubs
This is a transition wet zone between polygon-patterned wetland and zone of recharge (microlandscape 8) covered by mosses (*Sph.obtusum*, *Sph.riparium*) for 100 %, sedges and *Eriophorum Russiolum* (till 85 %) and *B.nana* (till 5 %). The permafrost depth is 28.0 cm, water table on 14.0 cm, pH=4.136, EC=36.667 µSm.
Microlandscape 7 – thaw covered by bushes
This is the similar to previous zone but more abundantly covered by shrubs and bushes (*B.nana*, willow) till 50 %, sedges take till 80 %, mosses (*Sph.obtusum*) make a continuous carpet. The permafrost depth is 26.1 cm, water table on 20.2 cm, pH=4.465, EC=31.330 µSm
For the entire class soils are presented by peat and organic litter.

Class Thaw (2nd type)

Microlandscape 8 – thaw with flowing water
This is a wet zone conjugated polygonal wetlands. Area covered by sphagnum mosses (100 %) - *Sph.lenense*. *Carex* and *Eriohporum russiolium* takes 45-80 %. The permafrost depth is 40.8 cm, water table on 6.3 cm. Water has pH=4.052, EC=19.375 µSm
For the entire class soils are presented by peat and organic litter.

Class Wet-sedge
Microlandscape 9 – sedge with mosses
It is a flat area covered by sphagnum (*Sph.obtusum*) for 100 %. Sedges (*C.limosa*) take 50 % of all area, sometime (around 5 %) water is open. The permafrost depth is 39.4 cm, water table on 9.3 cm. Water has

less acidic pH=4.385 and the smallest EC=15.75 µSm. There is beginning of palsa forming occur place to place.
Microlandscape 10 – sedge with mosses and shrubs
Area for 100 % is covered by mosses (*Sph.obtusum, Warnstorfia exannulata, Scapania paludicola*). *Ericaceae* shrubs presented by *Andromeda polifolia, Ledum palustre* and *Chamaedaphne calyculata* and cover 70 % of a bit (till 10 cm) elevated area. The permafrost depth is 38.33 cm, water table on 6.3 cm. Water has pH=4.561, EC=20.000 µSm.
Microlandscape 11 – sedge with open water
It is the most water abundant zone with sedge and cotton-grass cover till 40-70 %. The rest is occupied by water with pH=4.602 and EC=8 µSm. The permafrost depth gets the maximum for the investigated area 51.00 cm.
For the entire class soils are presented by peat and organic litter.

Class Yernik
Microlandscape 12 – shrubs on the small slopes
This is a zone of good drainage covered by shrubs (till 60 cm height) - the dominants are *B.nana* (75 %) and willow (15 %), and hypnum mosses and lichens. Permafrost is located on 35 cm and there is no liquid ground water.
Microlandscape 13 – shrubs on the steep slopes
This is a zone of high vegetation abundance. The surface is covered by *Sph.girgensohnii, Anlacomnim palustris, Hejlocom spelud, Pleurozium schreberi, Palytrichum strictum*. The shrubs have 1.5-2.0 m height and presented dominantly by B.nana. Permafrost is located on 35.3 cm and there is no ground water.
For the entire class soils are presented by organo-mineral material and organic litter.

Class Dry- lichen land
Microlandscape 14 – typical dry-lichen lands
This subclass is located on the top of small mineral hills, thereby water doesn't stay here for a long. It forms the characteristic lichen-covered (*Cladonia stillaris, Cl.rangifer, Abectoria ochlia, Cetraria cucullata*) areas. *B.nana, Ledum palustre* and willow take 10-20 %. Permafrost stays lower 50 cm.
Microlandscape 15 – dry-lichen lands with shrubs
This is a flat part on mineral soils with ever-present thixotropy. Lichens cover 100 % of tussocky area. Tussocks occupy around 45 % and covered by *Ericaceae* shrubs. Permafrost is presented on 35 cm.
Microlandscape 16 – shrubs on the steep slopes
This is the most water saturated mineral soil area on the border with lakes and hollows. All area is densely populated by 30-30 cm height tussocks (till 75 %) with sedges and cotton-grasses. Place in-between is occupied by sphagnum (*Sph.fuscum, Polytricum strictum*) and lichens (*Cladonia stelarris, Cladonia Rangeferina, Cetraria Cƨlculata*). Permafrost is presented on 26 cm.
For the microlandscapes 14-15 soils are presented by mineral material and for microlandscape 16 – by organo-mineral material.

Class Hasyrey (1st type)
Microlandscape 17 – Hasyrey (1st type)
This class had not been subdivided for microlandscapes. On its area is presented *B.nana* (20-60 %) and willow (10 %), mosses and lichens (*Pleurosium schreberi, Hylocomium splendens, Aulacomnium palustre, Polytrichum commune*) till 100 %. Permafrost is presented on 25.7 cm.
Soils are presented by organo-mineral material.

Class Hasyrey (2st type)
Microlandscape 18 – Hasyrey (1st type)
This class also had not been subdivided on microlandscapes. Surface is covered by *Sph.balticum* for 100 %, Eriophorum russiolium takes till 50 %. The permafrost depth is 35.8 cm, water table on 7.58 cm. Water has pH=4.001, EC=29.667 µSm.
Soils are presented by peat.

Class Water.
This class had been subdivided for 2 microlandscapes – deep water (***Microlandscape 19***) and shallow water (***Microlandscape 20***) for the reason of different interaction with atmosphere.

CONCLUSIONS

It has been carried out a field survey of the key area located in West Siberia south tundra. In previous studies we subdivided 9 landscape classes on a base of satellite images. This investigation let to subdivide those classes on the microlandscapes basing on the criterias vegetation cover and location in relief.
This studying help us to better understand the structure and functioning of tundra ecosystems in future and to predict the potential respond to the climate changes.

ACKNOWLEDGEMENTS

This work was supported by the Russian foundation for basic research under grant 14-05-00193.

REFERENCES

Gvozdetskii N.A. (1968). Fiziko-geograficheskoe raionirovanie SSSR. Harakteristike regionalnih edinits. [Physico-geographical zoning of USSR. Characteristic of the regional units], Moscow, MSU publishing house, 575 p.

Romanova E.A., R.T. Bybina, E.F. Golitsyna, G.M. Ivanova, L.I. Usova, and L.G. Trushnikova (1977). Tipologicheskaya karta bolot Zapadno-Sibirskoi ravniny [Typological map of wetlands of West Siberian Lowland], GUGK, Leningrad, Scale 1:2,500,000.

Tarnocai C., Canadell J. G., Schuur E. A. G., Kuhry P., Mazhitova G., and Zimov S. (2009). Soil organic carbon pools in the northern circumpolar permafrost region, *Global biogeochemical cycles*, **23**, GB2023.

Zarov E.A. (2015). The south tundra landscape structure map based on remote sensing data and field survey, *Proceedings of the 1st Pan-Eurasian Experiment (PEEX) Conference and the 5th PEEX Meeting*, 488-492 pp.

ABOUT POSSIBILITY TO STUDY MESO - AND MICROSCALE INTERACTIONS WITHIN THE SYSTEM “CLIMATE-TERRESTRIAL ECOSYSTEMS” IN THE FRAMEWORK OF THE PAN-EURASIAN EXPERIMENT PEEX

YU.A. KURBATOVA, I.M. KURGANOVA, N.A. ZAYTSEVA

The Eurasia region embraces various natural--climatic zones from Arctic tundra to semi-deserts, so it is an excellent natural model to study the atmosphere-biosphere interactions under conditions of both the present-day and changing climate. Functioning of the fundamental biosphere chain "plants – soils – the atmosphere" and its mutual compensating properties can be estimated through a system of data on the interconnected black carbon fluxes and reservoirs. The interactions do mainly run within the atmospheric boundary layer that is poorly presented by standard meteorological observations. We propose to organize a Project aimed at carrying out a series of special observations of the boundary layer state which are to be performed on a network of sites located in different landscape zones. The project will make possible to obtain new data on the state of the boundary layer. Obviously, these stations should be equipped by similar or comparable instruments to measure meteorological quantities and at the same time to estimate fluxes of heat, moisture and carbon in the layer from the ground surface to levels up to 50-100 m. The observations should be made according to the coordinated and agreed program. The countries invited to perform such project are Russia, Finland, and Estonia. Others are welcomed. A possible network of stations, the necessary equipment and the program are discussed in the report.

О ВОЗМОЖНОСТИ ИЗУЧЕНИЯ МЕЗО- И МИКРОМАСШТАБНЫХ ВЗАИМОДЕЙСТВИЙ В СИСТЕМЕ “КЛИМАТ-НАЗЕМНЫЕ ЭКОСИСТЕМЫ” В РАМКАХ ПАН-ЕВРАЗИЙСКОГО ЭКСПЕРИМЕНТА PEEX

Н.А. ЗАЙЦЕВА, Ю.А. КУРБАТОВА, И.М. КУРГАНОВА:

Регион Евразии охватывает разные природно--климатические зоны от арктической тундры до полупустынь, благодаря чему он представляет собой отличную природную модель для изучения атмосферно-биосферного взаимодействия как в условиях современного, так и меняющегося климата. Функционирование основополагающей биосферной цепочки «растения – почва – атмосфера» и ее скомпенсированность могут быть оценены через систему взаимосвязанных между собой потоков и резервуаров углерода. Это взаимодействие активно осуществляется в пограничном слое атмосферы, который слабо освещается стандартными метеорологическими наблюдениями. Для получения новых данных о состоянии пограничного слоя предлагается организовать сеть специальных наблюдательных площадок, оснащенных однотипной аппаратурой для измерения метеорологических величин и одновременно для оценки потоков тепла, влаги и углерода в слое от поверхности земли до уровней порядка 50-100 м.

SATELLITE BASED DROUGHT AND VEGETATION CHANGES OVER SEMI-ARID AREAS

ZHANG ANZHI[1] and JIA GENSUO[1]

RCE-TEA, Institute of Atmospheric Physics, Chinese Academy of Sciences, Beijing, China

Keywords: SATELLITE, MIDI, DROUGHT, NDVI

Drought is one of the most common and costliest natural disasters, and has adversely affected water resources, agricultural production, and welfare of people especially in semi-arid regions, where precipitation limitation is already at high risk. Furthermore, semi-arid vegetation productivity is mainly constrained by precipitation, and further limited by temperature in middle latitudes. Reliable monitoring of drought and its impact on vegetation at regional scale is essential and lacking. Moreover, it is also an important scientific issue of climate change and regional responses. To date, studies have been mainly based on investigating drought and its impact using meteorological data and ground observations, but the usage of satellite data is still limited. This study focused on monitoring regional drought and its connection with vegetation using multi-sensor satellite based Microwave Integrated Drought Index (MIDI) and vegetation indicators over semi-arid ecosystem. The MIDI can consistently and continuously monitor drought cross space and time in all weather conditions. Spatial-temporal comparisons among MIDI, climate variables (precipitation and temperature), drought indices and vegetation indices (Normalized Difference Vegetation Index, NDVI) over different semi-arid areas were carried out. In general, the spatial patterns of drought and vegetation trend were heterogeneous, while drought intensified accompanied by higher temperature and lower precipitation. The vegetation (NDVI) showed similar trend and variation as MIDI with lagged responses. Our results is valuable for investigating the impact of drought on vegetation especially over semi-arid ecosystems, and providing us operational tool for drought and its impacts detection based on satellite remote sensing .

ASSESSING THE CARBON AND WATER FLUXES IN GLOBAL RANGELANDS

L. ZHANG[1, 2*], J.F. XIAO[3], Y. ZHENG[1] and Y. ZHOU[1]

[1]Key Laboratory of Digital Earth Science, Institute of Remote Sensing and Digital Earth, Chinese Academy of Sciences, Beijing 100094, China

[2]Hainan Key Laboratory of Earth Observation, Hainan 572029, China.

[3]Earth Systems Research Center, Institute for the Study of Earth, Oceans, and Space, University of New Hampshire, Durham, NH 03824, USA.

Keywords: GLOBAL RANGELANDS, UPSCALING, CARBON FLUXES, ET, GIMMS NDVI3g.

INTRODUCTION

Terrestrial carbon-water flux is one of the main components of global climate change and regional sustainable development. Intensive studies on carbon and water fluxes in forest ecosystems have been undertaken globally. As one of the most widespread and diverse vegetation ecosystems in terrestrial land, rangelands have a large potential for carbon sequestration, and potentially slow down the increasing rate in the global greenhouse gas and temperature (White *et al.*, 2000). Moreover, climate changes and human activities have strong impact on carbon and water cycles in global rangelands. However, there are few studies focused on the comprehensive investigations of carbon and water fluxes in rangeland ecosystems, although some studies are limited to in situ and regional observations. Therefore, it is difficult to assess the impacts of climate changes and human activities on carbon and water budgets in rangelands at global scale without a profound understanding of the carbon-water flux changes. The upscaling method developed recently provides a new approach to the estimation of carbon and water fluxes. Using this method, this research developed a FluxScale model for estimating carbon and water fluxes by scaling up fluxes from site observations to the global coverage. This study further analyzed the spatio-temporal characteristics of the carbon and water budgets in the global rangelands and their dynamical variations under the changing climate patterns. This study demonstrates a comprehensive study in carbon and water fluxes over global rangelands.

METHODS

This study developed a data-driven upscaling method (FluxScale) (Zhang *et al.*, 2014) to estimate carbon and water fluxes in global rangelands using a boosting-like regression-tree ensemble technique. By integrating the 15-year flux tower data, 30-year new-generation GIMMS NDVI3g (Pinzon and Tucker, 2014), climate data, land cover data, the research used the FluxScale model to estimate the 30-year carbon and water fluxes and map the net ecosystem productivity (NEP), gross primary productivity (GPP), evapotranspiration (ET) for the global rangelands. The accuracy of the FluxScale model is high with r values of 0.91, 0.88, and 0.77 for GPP, ET, and NEP, respectively. The estimated GPP and ET agreed well with the MODIS data products, showing the similar magnitudes and spatial patterns between the two data sets. The FluxScale model is simple and has relatively high accuracy and robustness comparing to other methods. The technique is also easy to be adopted by other applications of flux estimations.

CONCLUSIONS

This research quantified the carbon and water fluxes in global rangelands (Figure 1) and examined the spatio-temporal patterns and their responses to climate changes. During 1982-2011, the global rangelands have a net carbon uptake of 49.70 g C/m^2/yr. The global rangeland estimates are 809.83 g C/m^2/yr (30.32

Pg C/yr) for GPP, 493.69 mm/yr (18484.36 km^3/yr) for ET, 1.60 g C/kg H_2O for WUE, respectively. In general, the global rangeland ecosystems play a role of carbon sink; the NEP increases slowly, and GPP and ET increase significantly over the 30 years, which means that the global rangeland ecosystem has the potential to be a carbon sink. The increasing trend of water use efficiency (WUE) is mainly affected by the temperate ecosystems of the South Hemisphere. This research summarizes the spatio-temporal patterns of the fluxes and their climatic drivers in six typical rangeland regions, emphasizing the spatial-temporal variations of the fluxes among different regions. Australia Rangeland is a weak carbon source. Mongolia and China Rangelands are week carbon sinks and the Great Plains and Central Asia are weak carbon sources.

This study helps understand the influence of global climate change on carbon and water cycles and processes in rangeland ecosystems, and provides scientific support for the efforts that improve production capacity and increase the carbon sequestration capacity in the rangelands.

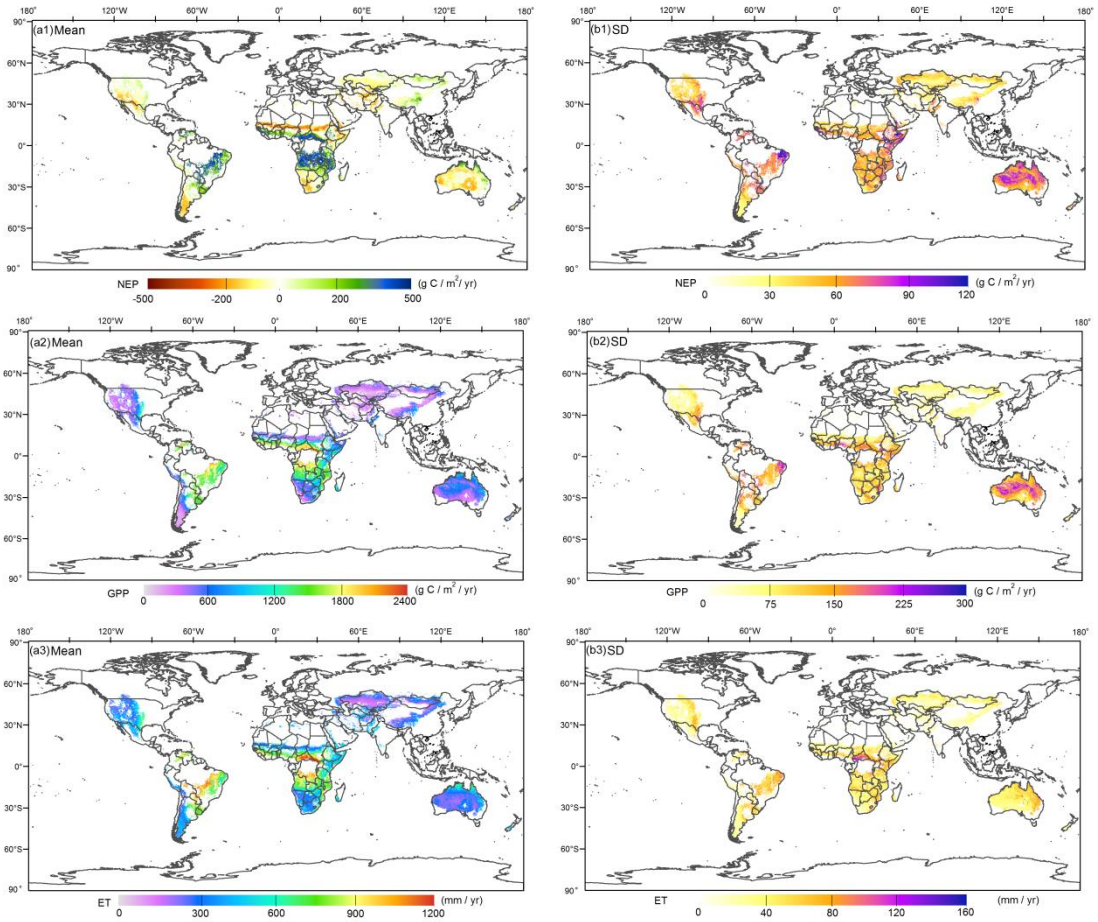

Figure 1. (a) Annual mean and (b) standard deviation (SD) of NEP, GPP, ET for global rangelands (1982-2011) (Positive sign for NEP denotes carbon uptake, and negative sign denotes carbon release).

ACKNOWLEDGEMENTS

The study was supported by the International Cooperation and Exchanges NSFC (Grant No. 41120114001).

REFERENCES

Pinzon, J. and C. Tucker (2014). A Non-Stationary 1981–2012 AVHRR NDVI3g Time Series. *Remote Sensing* 6 (8): 6929-6960.

White, R., S. Murray, and M. Rohweder (2000). Grassland ecosystems. *Pilot analysis of global ecosystems.* World Resources Institute, Washington DC.

Zhang, L., H. Guo, G. Jia, B. Wylie, T. Gilmanov, D. Howard, L. Ji, J. Xiao, J. Li, W. Yuan, T. Zhao, S. Chen, G. Zhou and T. Kato (2014). Net ecosystem productivity of temperate grasslands in northern China: An upscaling study. *Agricultural and Forest Meteorology* 184: 71-81.

ANALYSIS ON CORRELATION BETWEEN NPP OF DIFFERENT VEGETATION TYPE AND AIR TEMPERATURE, PRECIPIATION LAI AND NDVI IN EAST ASIAN MONSOON REGION—A CASE IN HEBEI PROVINCE

Sha ZHANG[1], Jinguo YUAN[2] and Jiahua ZHANG[1]

[1]Institute of Remote Sensing and Digital Earth, Chinese Academy of Sciences,
No.9 Dengzhuang South Road, Haidian District, Beijing, 100094, China.

[2] College of Resource and Environmental Sciences,Hebei Normal University,
No.20 East Road of 2nd Ring South, Shijiazhuang, 050024, China

Keywords: NET PRIMARY PRODUCTIVITY (NPP), CLIMATE FACTORS, LAI, NDVI.

INTRODUCTION

Inter-annual variability and decadal variations of the East Asian monsoon are large. The spatial and temporal variability of terrestrial ecosystems in East Asia showed significant response to the East Asian monsoon climate(Jiang Chao *et al.*, 2013; Fu Congbin *et al.*,2002). China, which is located in the East Asian monsoon region, is extremely sensitive to global climate change(Zhao Dongsheng *et al.*,2011). The inter-annual variabilities of monsoon's forward or backward and its abnormal intensity have great influence on climate change , especially in easten China, which is in control of East Asian monsoon.

Vegetation plays an important role in global cycle of matter and energy, and it can absorb CO_2, mitigate the concentration rise of greenhouse gas, adjust the balance of global carbon cycle, and keep global climate stable(Piao Shilong *et al*., 2001).

Hebei Province, which is located in eastern China, belongs to the East Asian monsoon region and has main vegetation types. So, we choose Hebei as the study area. This paper used meteorological station data and MODIS data including LAI, NDVI and land cover type data to make analysis on the correlation between NPP of different vegetation types and air temperature, precipitation, LAI and NDVI under the background of East Asian monsoon climate. It is of typically representative significance for research on vegetation response to climate change in East Asian monsoon region. It also can provide evidence for us to choose better parameters when we built biological models and to make improvement for models.

METHODS

To get the distribution of air temperature and precipitation from meteorological station data, we need to interpolate the station data. First, we calculated the original ten-days' data to get yearly data. Second, according to the principle of even distribution , we randomly selected 97 stations to interpolate by 25 methods(Table 1) and the other 45 stations to verify. Third, we chose the better method using the formula followed to verify the interpolation values. The method with smallest RMSE was chosen as the best method. At last, IDW with power 2.5 and Kriging with exponential semivariogram model were selected as the better interpolation methods for air temperature and precipitation respectively.

$$\mathrm{RMSE} = \sqrt{\frac{1}{n-1}\sum_{i=1}^{n}(Z_{a,i} - Z_{e,i})^2} \tag{1}$$

where, n is the number of stations for verifying, $Z_{a,i}$ is the real value of the verifying station and $Z_{e,i}$ is the evaluated value of the same station. Then, we used the selected interpolation methods to do interpolation with all 142 stations to get the space distribution of annual air temperature and precipitation. Finally, we calculated the correlation coefficients between NPP and the two climate factors respectively.

Main interpolation methods	Parameters setting
Inverse Distance Weighing(IDW)	Power: 0.5, 1, 1.5, 2, 2.5 and 3 respectively
Kriging	Kriging method: ordinary Semivariogram model: spherical, circular, exponential, gaussian and linear respectively
Spline	Spline type: regularized and tension respectively
Trend	Type of regression: linear Polynomial order: from 1 to 12, step length was 1.

Table 1. Interpolations and parameters setting .

For MODIS LAI with time scale of 8 days and MODIS NDVI 16 days, we also calculated them to get yearly data first, and then calculated the correlation coefficients between NPP and LAI and NDVI respectively.

When we got the space distribution of correlation coefficients between NPP and the different factors , we employed the tool of zonal statistics to obtain the correlation coefficients between different vegetation types' NPP and these factors.

CONCLUSIONS

The zonal statistics results using both MODIS vegetation types map and 1:1,000,000 vegetation types map from Chinese Academy of Sciences showed that during 2000-2012, annual NPP of cropland was higher than other vegetation types(Figure 1 and Figure 2).

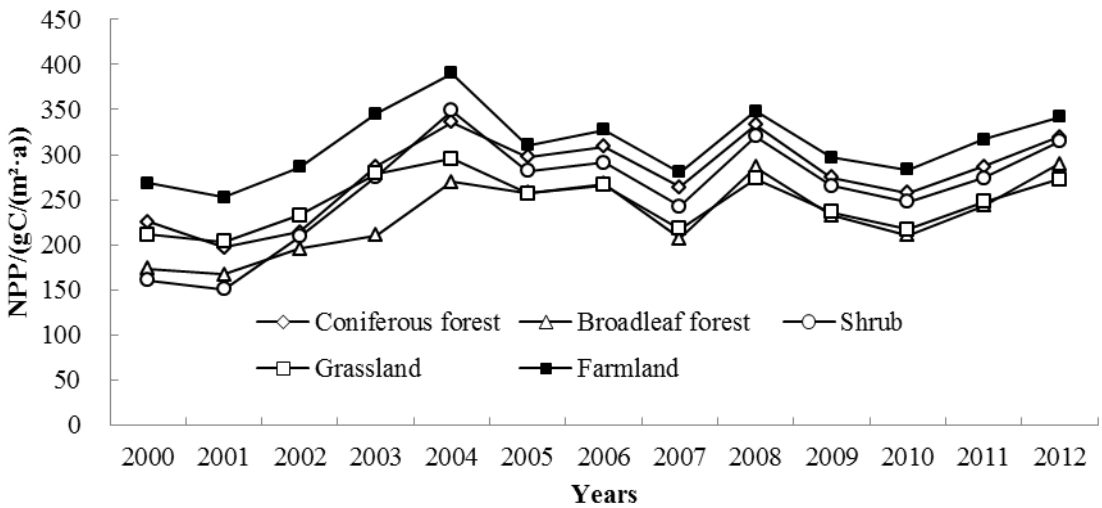

Figure 1. NPP of different vegetation types from MODIS vegetation type map

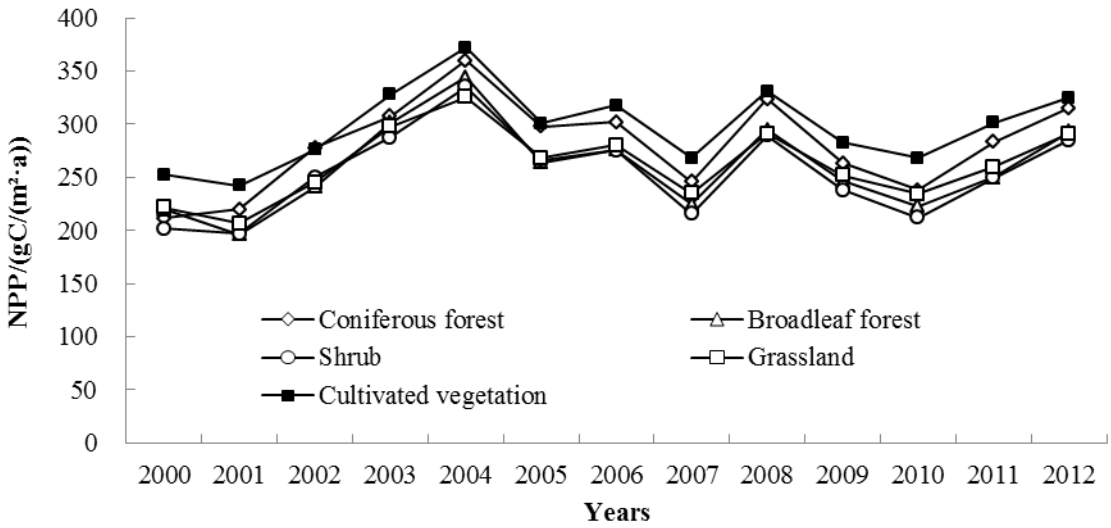

Figure 2. NPP of different vegetation types from 1:1,000,000 vegetation type map

Correlation coefficients between annual NPP of different vegetation types and each factors are shown in Table 2. The conclusions are as follows: (1) different vegetation types have different correlation coefficients with a same factor; (2) results from two kinds of vegetation types maps showed that the highest correlation with LAI and NDVI was grassland NPP, then farmland or cultivated vegetation, the lowest was unsure; (3) under the background of East Asian monsoon climate , the higher correlation with air temperature and precipitation was NPP of coniferous forest or broadleaf forest, not farmland or cultivated vegetation.

		A	B	C	D	E
NPP_air temperature_R	Mean1	**-0.2484**	-0.2214	-0.2006	-0.2142	-0.0574
	Mean2	-0.0486	**-0.2177**	-0.2030	-0.2140	-0.0814
NPP_air temperature_R^2	Mean1	**0.1038**	0.0797	0.0755	0.0755	0.0593
	Mean2	0.0577	0.0707	0.0659	**0.0808**	0.0647
NPP_precipitation_R	Mean1	**0.4102**	0.1285	0.1500	0.2642	0.3378
	Mean2	0.0046	**0.3842**	0.1174	0.3513	0.2918
NPP_ precipitation _R^2	Mean1	**0.2563**	0.1004	0.1269	0.1645	0.1860
	Mean2	0.0657	**0.2588**	0.1150	0.2046	0.1547
NPP_LAI_R	Mean1	0.2823	0.1505	0.1315	**0.5249**	0.3229
	Mean2	0.2086	0.3565	0.2789	**0.5528**	0.3642
NPP_ LAI _R^2	Mean1	0.1818	0.1551	0.1514	**0.3904**	0.1918
	Mean2	0.1787	0.2431	0.2196	**0.3997**	0.2409
NPP_NDVI_R	Mean1	0.3489	0.2830	0.2919	**0.5764**	0.4221
	Mean2	0.3378	0.4785	0.3921	**0.5914**	0.4483
NPP_NDVI _R^2	Mean1	0.2071	0.1729	0.1725	**0.4046**	0.2450
	Mean2	0.2096	0.3099	0.2424	**0.4136**	0.2768

Table 2 Correlation coefficients between NPP of different vegetation types and each factors

Note : A: Coniferous forest; B: Broadleaf forest; C: Shrub; D: Grassland; E: Farmland or cultivated vegetation . mean 1 is result from MODIS vegetation types map and mean 2 from 1:1,000,000 vegetation types map. Farmland is one type of MODIS vegetation types, and cultivated vegetation is one of 1:1,000,000 vegetation types map.

ACKNOWLEDGEMENTS

The authors are grateful for free data including 1:1,000,000 vegetation types map provided by "Environmental & Ecological Science Data Center for West China, National Natural Science Foundation of China"(http://westdc.westgis.ac.cn), meteorological station data provided by Institute of Meteorological Science of Hebei Province and MODIS products which are obtained through the online Data Pool at the NASA LP DAAC, USGS/ EROS Center, Sioux Falls, South Dakota.

REFERENCES

Fu Congbin, Wen Gang, Xie Li, et al (2002). The Diagnosis and Simulation Studies on Climate and Ecosytem Interactions in East Asia Monsoon Region[J]. *Journal of Nanjing University(Natural Sciences)*, 38(3):281-294.

Jiang Chao, Xu Yongfu, Ji Jinjun(2013). Response of the summer terrestrial carbon cycle in the East Asian monsoon region to East Asian monsoon[J]. *Climatic and Environmental Research(in Chinese)*, 18(3):329-341.

Piao Shilong, Fang jingyun, Guo Qinghua(2001). Application of CASA model to the estimation of Chinese terrestrial net primary productivity[J]. *Acta Phytoecologica Sinica*, 25(5):603-608.

Zhao Dongsheng, Wu Shaohong, Yin Yunhe (2011) .Variation trends of natural vegetation net primary productivity in China under climate change scenario[J]. *Chinese Journal of Applied Ecology*, 22(4) : 897 －904.

A CATCHMENT MODEL COUPLLING THE CYCLING PROCESSES OF WATER, CARBON AND NITROGEN: ATTEMPTS OF ESTABLISHMENT AND VALIDATION

XUNHUA ZHENG[1], WEI ZHANG[1], YONG LI[2], BO ZHU[3], CHUNYAN LIU[1]

[1] State Key Laboratory of Atmospheric Boundary Layer Physics and Atmospheric Chemistry, Institute of Atmospheric Physics, Chinese Academy of Sciences, Beijing 100029, P. R. China

[2] Key Laboratory of Agro-ecological Processes in Subtropical Regions, Institute of Subtropical Agriculture, Chinese Academy of Sciences, Hunan 410125, PR China

[3] Key Laboratory of Mountain Environment Evolvement and Regulation, Institute of Mountain Hazards and Environment, Chinese Academy of Sciences, Chengdu, 610041, P. R. China

Keywords: DNDC, CNMM, WATER, CARBON AND NITROGEN CYCLING.

INTRODUCTION

Nitrogen (N) is an essential component of ecosystems and a key controller for ecological conditions and functioning in the atmosphere, biosphere, hydrosphere and pedosphere (Breuer et al., 2008). Intensive modern agriculture with high application rates of nitrogenous fertilizer and low efficiency of its use result in the excessive N remained in the soil and extraordinary change in nitrogen cycle, which produces a series of environmental problems at the catchment, regional or even global scales (Deng et al., 2011). Therefore, the understanding of the N cycle has shifted from how to promote food production to a realization of sustainablility of the intensive agricultural systems which not only sustain the food production in a highly efficient manner, but also lowest possible environmental hazards (Galloway et al., 2008).

Effective quantifying the N losses from the terrestrial ecosystems is essential for establishing sustainable ecosystems. Many field experiments have been conducted to investigate the N losses at different spatial scales (e.g., Deng et al., 2011; Wolf et al., 2010). However, field experiments generally have focused on specific N pathways, which indicates that field experiments alone are difficult to quantify all of the N losses through various pathways. In addition, the heterogeneity of N activity in the soil implies that extrapolation of the field measurements to catchment or over extended time periods is an enduring challenge. Process-based models have been developed to overcome this limitation. Considering the N losses jointly controlled by water flow and N transformations in soils, to date, few models focus on both hydrological and biogeochemical processes, which hinders the estimation of the total N losses from catchment. Recent studies show that the accuracy for the simulation of non-point source pollution of streams can be improved through the coupling of more detailed N transformation models within distributed hydrological models (Ferrant et al., 2011). Breuer et al. (2008) reviewed the widely used hydro-biogeochemical catchment models and implied that the coupling of a hydrology and a biogeochemistry model seems to be an efficient approach in intensive agricultural context to quantify the total N losses from catchment.

Therefore, in this study, a new hydro-biogeochemical catchment model with more detailed N cycling was established and applied to simulate the total N losses from catchment. The model approach adopted for the present work was to couple the biogeochemical processes of DNDC into the hydrological framework of CNMM. The objectives of this study are threefold: (i) to describe the scientific processes of coupled biogeochemical parts; (ii) to validate the CNMM-DNDC based on field observations from a agro-forest catchment; (iii) to identify the key N loss element of the catchment.

METHODS

The decomposition, nitrification, denitrification and fermentation modules of DNDC were incorporated into the hydrological framework of CNMM (Catchment Nutrient Management Model) base on the VS2010 programing platform. The integrated decomposition and fermentation processes were simulated with first-order kinetic function. Nitrification and denitrification were computed using first-order and Michaelis-Menten kinetics and the Pirt functions based on the "anaerobic balloon" model. The coupling model which was named as CNMM-DNDC can simulate not only the crop growth, carbon and nitrogen cycling and related gas emissions, but also horizontal and vertical movements of water, carbon and nitrogen at catchment.

The coupling model was validated against the abundant and reliable observation datasets (daily soil temperature and moisture, crop yields, CH_4 and N_2O emissions, surface runoff and subsurface drainage flows, nitrate loading from typical agricultural sites and drainage flows, nitrate loading from the catchment outlet) from a small agro-forest catchment in Southwest China, with the spatial and temporal resolution of 15 m × 15 m and three-hour, respectively, so as to evaluate the model performance in simulating water, carbon and nitrogen cycling.

CONCLUSIONS

The results showed that CNMM-DNDC could well simulate the energy balance, hydrology, plant growth and carbon and nitrogen cycling of different land uses at catchment. The simulation results of 2008 indicated that 1) ammonia volatilization and nitrate loading were the major nitrogen loss ways for the entire catchment; 2) croplands were considered as principle sources of various carbon and nitrogen losses; 3) precipitation and applied fertilizer amount were the key controller of nitrate loading. The coupling model showed the potential for comprehensive regulation of carbon and nitrogen cycling.

ACKNOWLEDGEMENTS

This study was jointly supported by the Ministry of Science and Technology (2012CB417106) and the National Natural Science Foundation of China (41321064, 41375152).

REFERENCES

Breuer, L., VachÉ, K.B., Julich, S., Frede, H.-G. (2008). Current concepts in nitrogen dynamics for mesoscale catchments, *Hydrological Sciences Journal* **53**, 1059-1074.

Deng, J., Zhou, Z., Zhu, B., Zheng, X., Li, C., Wang, X., Jian, Z. (2011). Modeling nitrogen loading in a small watershed in southwest China using a DNDC model with hydrological enhancements, *Biogeosciences* **8**, 2999-3009.

Ferrant, S., Oehler, F., Durand, P., Ruiz, L., Salmon-Monviola, J., Justes, E., Dugast, P., Probst, A., Probst, J.-L., Sanchez-Perez, J.-M. (2011). Understanding nitrogen transfer dynamics in a small agricultural catchment: Comparison of a distributed (TNT2) and a semi distributed (SWAT) modeling approaches, *Journal of Hydrology* **406**, 1-15.

Galloway, J.N., Townsend, A.R., Erisman, J.W., Bekunda, M., Cai, Z., Freney, J.R., Martinelli, L.A., Seitzinger, S.P., Sutton, M.A. (2008). Transformation of the nitrogen cycle: recent trends, questions, and potential solutions, *Science* **320**, 889-892.

Wolf, B., Zheng, X., Bruggemann, N., Chen, W., Dannenmann, M., Han, X., Sutton, M.A., Wu, H., Yao, Z., Butterbach-Bahl, K. (2010). Grazing-induced reduction of natural nitrous oxide release from continental steppe, *Nature* **464**, 881-884.

SPATIONTEMPORAL VARIABILITY IN SNOW PHENOLIGY OVER EURASIAN CONTINENT DURING 1966-2012

X. ZHONG[1], T. ZHANG[2], K. WANG[3], L. ZHENG[4], H. WANG[2]

[1]Cold and Arid Regions Environmental and Engineering Research Institute, Chinese Academy of Sciences, China

[2]MOE Key Laboratory of Western China's Environmental Systems, College of Earth and Environmental Sciences, Lanzhou University, China

[3]University of Colorado, Boulder, USA

[4]Chinese Antarctic Center of Surveying and Mapping, Wuhan University, China

Keywords: SNOW COVER PHENOLOGY, IN SITU MEASUREMENTS, EURASIAN CONTINENT, SPATIOTEMPORAL VARIABILITY.

INTRODUCTION

Snow cover is a key part of the cryosphere, which is a critical component of the global climate system. Changes in snow cover serve as indicators of climate change because of its interactions and feedbacks with surface energy fluxes, moisture fluxes, hydrological processes, and atmospheric and oceanic circulation (Brown and Goodison 1996; Armstrong and Brown 2008).Snow cover timing and duration are two main characteristics of snow cover. Snow extent is strongly influenced by the two factors. There is a critical effect of snow cover duration (SCD) on the surface energy budget, and it also directly affects the surface albedo (Bulygina et al., 2009). The dates of onset and termination of snow cover are primary controls on ecosystem carbon exchange in many seasonally snow-covered areas (IGOS, 2007) and it is a predictor of atmospheric carbon accumulation (Callaghan and Hohansson, 2011). Due to the high sensitivity of snow to climate change, the changes of snow cover timing and duration are occurring. The tendencies of changes in snow phenology are influenced by more recent changes in the weather pattern and climate (Bulygina et al., 2009).

Each winter, the average maximum terrestrial snow extent covers nearly 50 million km^2, or 50% of the Northern Hemisphere land surface (Robinson et al., 1993; IGOS, 2007). A large fraction of the Eurasian continent is covered by snow during winter seasons, and some areas are covered by snow for more than half a year. There are long-term and large-scale snow cover measurements and observations across the Eurasian continent. These measurements provide valuable data and information for snow cover studies and snow cover change detection. Therefore, Eurasia is a significant region for investigating the varieties of timing and SCD.

Although satellite data augment scarcity of snow cover data from ground stations at high altitude, the accuracy of these data is affected by clouds, underlying surface conditions, and inversion algorithms. In contrast, ground-based measurements can provide more accurate and longer time-series information, which are key to investigations of the climatology and variability of snow phenology.

In most studies of snow cover timing and duration over Eurasia, the study areas mainly focus on Siberia, northern Eurasia, China, and the Tibetan Plateau. However, there is no integrated snow dataset covering the whole Eurasian continent, and no studies of snow cover timing and duration on a regional basis in Eurasia. The objective of this study is to investigate the climatology and variability of snow phenology over the Eurasian continent from 1966 to 2012.

METHODS

There are many different methods to compute snow cover timing and duration (Bulygina et al, 2009). According to the daily snow depth, the day with snow depth equals to or greater than 1 cm is defined as a snow cover day, which can be used to calculate the date of onset and end of snow cover, snow cover duration and the number of snow cover days in our research. To minimize the random and systematic errors, we implemented quality control of snow data according to the quality assessment criteria assigned by NSIDC: snow data from stations with <20 years of measurements during 1971-2000 were excluded, and the data exceeding two standard deviations compared with the long-term annual average value were also omitted. Therefore, we used data from 1103 unique stations to analyze the climatology and variation of snow cover timing and duration over the Eurasian continent.

We defined the period from 1 July of a current year to 30 June of the following year as a snow year. Because the procedures for taking snow observations changed in the past across the former USSR, there were some inhomogeneities in the snow depth data. However, there has been no change in the observation procedure since 1965 (Bulygina et al. 2009). Therefore, we used snow data during the snow years from 1966 to 2012 in this study.

Wavelet analysis was used in our research to analyze the long-term variations of snow phenology. Wavelet analysis is a method to solve the problem of recovering a true signal from indirect of noisy data (Graps, 1995). When we analyze a data set using wavelets, the filter we used is an averaging filter. If the values are too small or too big, they might be omitted. However, the main features of the dataset are not significantly affected. The wavelet coefficients which result from filtering are used in an inverse wavelet transformation to reconstruct the data set. The new data set are represented as the smoothed lines of wavelet analysis in figures.

CONCLUSIONS

Our results showed that both of the earliest snow accumulated and latest date of termination of snow cover occurred in the coast of Arctic. The longest period of SCD and ND was more than 270 days and the shortest period less than 10 days (Fig.1). The distributions of FD, LD, SCD and ND generally represented the latitudinal zonality over the Eurasian Continent (Fig.2).

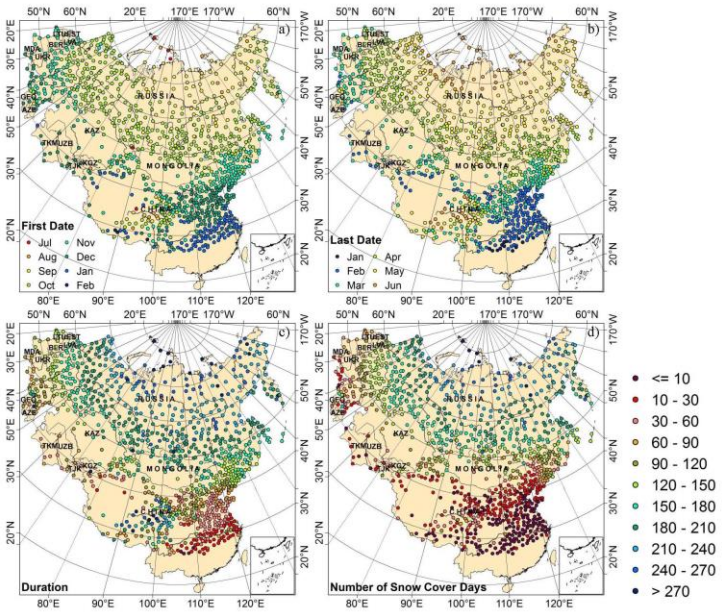

Figure 1. Long-term annual means of FD (a), LD (b), SCD (c) and ND (d) from 1966 through 2012 across the Eurasian continent.

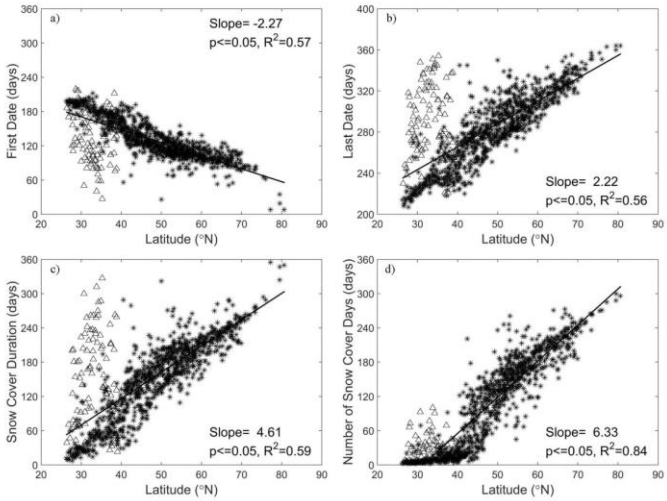

Figure 2. FD (a), LD (b), SCD (c) and ND (d) changes with latitude for all stations. Asterisks show the mean of each station across the Eurasian continent except Tibetan Plateau during 1966-2012; triangles represent the mean of each station in Tibetan Plateau; the thick line is a linear regression trend.

There were statistically significant long-term variations in FD, LD and SCD during the period from 1966 through 2012 over the Eurasian Continent. The long-term trend of FD represented a later change, and the rate was about 1.2 day per decade. LD presented an advanced trend with the rate of -1.2 day per decade. The later FD and earlier LD trends resulted in the shrinking of SCD (about 2.7 day per decade) (Fig.3).

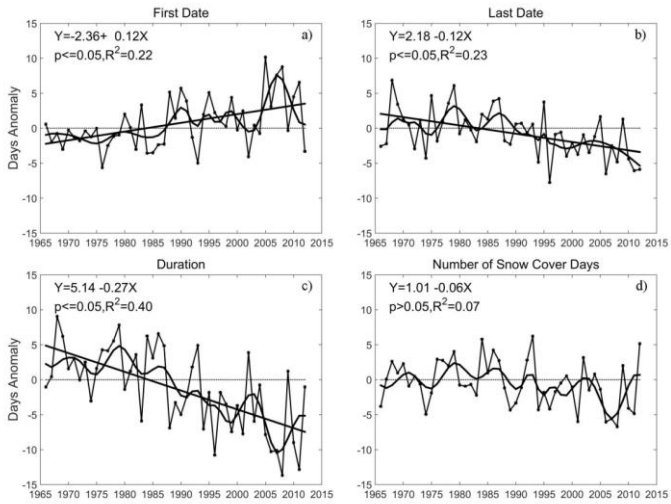

Figure 3. Composite of inter-annual variation of FD (a), LD (b), SCD (c) and ND (d) from 1966 through 2012 with respect to the 1971-2000 mean across the Eurasian continent. The line with dots is the anomalies of FD, LD, SCD and ND; the thick curve represents the smoothed curve using wavelet analysis; the thick line presents a linear regression trend.

Compared with precipitation, the correlation between ND and air temperature was more significant. ND lengthened with the air temperature decreased (Fig.4). Our results showed that the delay in FD was mainly caused by the autumn warming; the earlier date of the termination of snow cover was closely related to the increasing air temperature during the snow melt months; the changes in SCD were mainly controlled by the changes of air temperature in autumn and spring. In addition to the air temperature in spring and autumn, the shortened ND was affected by the rising temperature during the entire cold season (Fig.5).

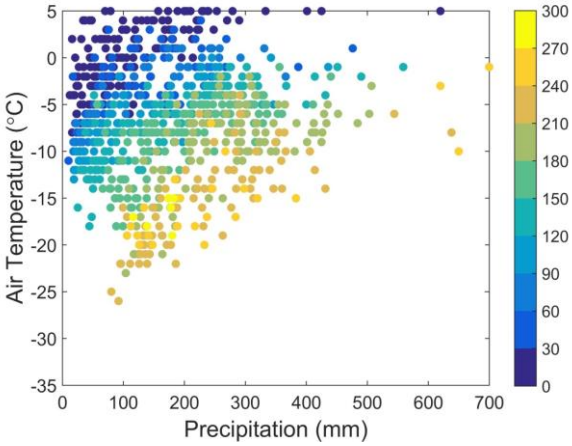

Figure 4. Long-term means of ND, air temperature and precipitation for 1031 stations from November through March during 1966-2012 over the Eurasian Continent. The different colors represent ND of each station.

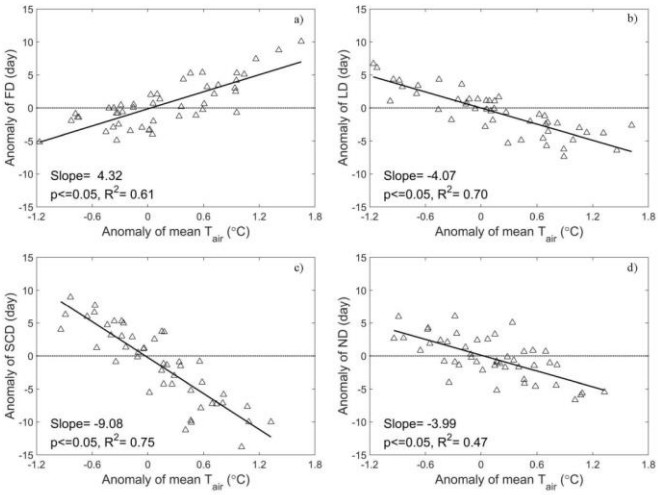

Figure 5. Relationship between anomalies of autumn mean air temperature (September through November) and FD (a), anomalies of spring mean air temperature (March through May) and LD (b), anomalies of annual mean air temperature (July of the current year to June of the following year) and SCD (c), anomalies of annual mean air temperature and ND (d) from 1966 through 2012 across the Eurasian Continent. Triangles represent the anomaly of each station; the thick line is a linear regression trend.

ACKNOWLEDGEMENTS

This work was supported by the National Key Scientific Research Program of China (2013CBA01802) and the Project for Incubation of Specialists in Glaciology and Geocryology of the National Natural Science Foundation of China (J1210003/ J0109)

REFERENCES

Armstrong, R. L. and R. Brown (2008). *Introduction, Snow and climate: Physical processes, surface energy exchange and modeling*, (Cambridge University Press, Cambridge, U.K.).

Brown, R. D. and B. E. Goodison (1996). Interannual variability in reconstructed Canadian snow cover, 1915-1992, *J. Climate* **9**, 1299-1318.

Bulygina O. N., V. N. Razuvaev, and N. N. Korshunova (2009). Changes in snow cover over Northern Eurasia in the last few decades, *Environ. Res. Lett.* **4,** 045026. doi:10.1088/1748-9326/4/4/045026.

Callaghan, T.V. and M. Hohansson (2011). Chapter 4, Changing snow cover and its impacts, In *Snow, Water, Ice and Permafrost in the Arctic (SWIPA): Climate Change and the Cryosphere.* Oslo: Arctic Monitoring and Assessment Programme (AMAP), 58pp.

Graps, A. (1995). An introduction to wavelets, *IEEE Computational Science & Engineering* **2 (2)**, 50-61.

IGOS (2007). Integrated Global Observing Strategy Cryosphere Themem Report - For the monitoring of our environment from space and from earth, WMO/TD-No.1405, World Meteorological Organization, Geneva, 100 pp.

Robinson, D. A., K. F. Dewey, and R. R. Heim (1993). Global snow cover monitoring: An update, *B. Am Meteorol. Soc.* **74,** 1689-1696.

SIMULATING OZONE DRY DEPOSITION AT A BOREAL FOREST WITH A MULTI-LAYER CANOPY DEPOSITION MODEL

P. ZHOU[1], L. GANZEVELD[2], Ü
. RANNIK[1], L. ZHOU[1, *], R. GIERENS[1], D. TAIPALE[3, 4], I. MAMMARELLA[1] and M. BOY[1]

[1]Department of Physics, University of Helsinki, P.O. Box 64, FI-00014, Helsinki, Finland.

[2]The Meteorology and Air Quality Department, Wagningen UR, P.O. Box 16, 6700AA, Wagningen, Netherlands.
[3]Department of Forest Sciences, University of Helsinki, P.O. Box 27, FI-00014, Helsinki, Finland.

[4]Department of Plant Physiology, Estonian University of Life Sciences, Kreutzwaldi 1, EE-51014, Estonia.
[*]now at U.S. Environmental Protection Agency, Research Triangle Park, NC, USA.

Keywords: MULTI-LAYER MODEL, TROPOSPHERIC OZONE, DRY DEPOSITION, CANOPY WETNESS.

INTRODUCTION

In boreal forest, the uptake mechanisms of O3 are determined by the turbulence intensity above and within the canopy, the diffusive transfer in the quasi-laminar boundary layer above the leave surface, the biological properties of the plants, surface wetness condition, and soil type (Ganzeveld and Lelieveld, 1995). Among them the effect of canopy wetness on O3 deposition has got a lot of discussions in previous studies. For boreal forest, a number of works revealed an enhancement of the O3 uptake under dew or high humidity conditions. For example, Altimir et al. (2006) found that the gathered moisture on the surface when the relative humidity (RH) being over 60 - 70% enhanced the non-stomatal O3 uptake in a Scots pine forest. At the same site as in Altimir et al. (2006), Rannik et al. (2012) revealed a strong sensitivity of the nighttime O3 uptake to RH.

These removal processes all together thus have determined the contribution of O3 fluxes of forest ground surface and understory vegetation, the vertical distribution of O3 concentration as well as the non-stomatal uptake fraction, which were considered as three crucial challenges to understand the relationship between eddy-covariance measurements and O3 plant uptake (Launiainen et al., 2013). Therefore in order to predict and analyse the impacts of different factors on O3 uptake, as well as the vertical distribution of O3 deposition flux inside the canopy at boreal forests, we implemented in this study a multi-layer process-based O3 dry deposition model into the 1-D chemical transport model SOSAA (a model to Simulate the concentrations of Organic vapours, Sulphuric Acid and Aerosols) (Boy et al., 2011; Zhou et al., 2014). This deposition model is based on the dry deposition representation of the Multi-Layer Canopy CHemistry Exchange Model (MLC-CHEM), which was originally described in Ganzeveld and Lelieveld (1995) and has been already applied in several model systems (e.g., Ganzeveld et al., 2010).

The long-term continuous measurements and intermittent campaigns at SMEAR II have provided a vast amount of datasets, which are highly appropriate for validating the newly implemented model. Within the datasets we selected a featured month with hot and dry conditions in the first two weeks, possibly representing a future climate at this site (Williams et al., ACP, 2011), followed by two cooler weeks.

This study is a starting point of considering gas dry deposition processes in SOSAA, further analysis of BVOCs deposition issues will be done on the basis of this study in the follow-up research.

METHODS

In this newly implemented multi-layer dry deposition model the O3 flux as a function of dry deposition processes is calculated at each layer as

$$F=[O_3]*V_d$$

where F is the O3 deposition flux (ppbv m s^{-1}), [O3] is the O3 concentration (ppbv), Vd is the deposition velocity (m s−1). Vd can be computed with the resistance analogy method as

$$V_d=\frac{LAI}{r_{veg}}+\frac{\delta}{r_{soil}+r_{ac}}$$

where LAI is the all-sided leaf area index for each layer, δ is 0 for overstory layers and 1 for the bottom layer which includes ground vegetation and soil surface. rveg is the leaf surface resistance (s m^{-1} , the same below for resistances), rsoil is the soil resistance and rac is the turbulence resistance depending on the transportation from lowest vegetation to the soil surface. The canopy wetness fraction fwet is a function of RH

$$f_{wet}=\left\{\begin{matrix} 1 & 0.9\leq RH \\ \frac{RH-0.7}{0.2} & 0.7\leq RH<0.9 \\ 0 & RH<0.7 \end{matrix}\right\}$$

The further detailed description is shown in Fig. 1.

CONCLUSIONS

In this study the newly implemented O3 dry deposition module has been applied to simulate the time period from Aug 1st to Aug 31st, 2010 (day of year 213 to 243) at the boreal forest measurement site SMEAR II (the Station to Measure Ecosystem Atmosphere Relation II) in Finland.

In this study, the model has been evaluated by comparing measured and modelled O3 fluxes and concentration profiles, which showed a good agreement. We found that nearly all the O3 uptake occurs below 0.8 hc inside the canopy (Fig. 2). During daytime, both stomatal uptake and wet skin uptake play a significant role in total O3 uptake for high humidity conditions. While under low humidity conditions only stomatal uptake exists besides the soil deposition. During nighttime, stomatal uptake is not zero, but is much smaller compared to the wet skin uptake under high humidity conditions. For low humidity conditions at night, the intensities of stomatal uptake and wet skin uptake are similar and both of them are smaller compared to the soil deposition. Therefore, the canopy wetness plays a more crucial role at nighttime, especially under high humidity conditions.

The modelled contribution of understory deposition below 4.2 m during daytime (~40%) are comparable with that (35%-45%) in Launiainen et al. (2013), but it is much higher at nighttime (about 50% - 70%) than the result (25% - 30%) in the same paper. This discrepancy at nighttime is likely due to the overestimation of soil uptake.

ACKNOWLEDGEMENTS

This work was supported by Maj ja Tor Nesslingin funding, CRAICC (Cryosphere-atmosphere interactions in a changing Arctic climate), eSTICC (eScience tools for investigating Climate Change in

Northern High Latitudes), FCoE (The Centre of Excellence in Atmospheric Science - From Molecular and Biological processes to The Global Climate). The authors also wish to acknowledge CSC - IT Center for Science, Finland, for computational resources.

REFERENCES

Altimir, N., P. Kolari, J.-P. Tuovinen, et al. (2006). Foliage surface ozone deposition: a role for surface moisture?, *Biogeosciences*, **3**, 209-228.

Boy, M., A. Sogachev, J. Lauros, et al. (2011). SOSA - a new model to simulate the concentrations of organic vapours and sulphuric acid inside the ABL - Part 1: Model description and initial evaluation, *Atmospheric Chemistry and Physics*, 11, 43-51.

Ganzeveld, L. and J. Lelieveld (1995). Dry deposition parameterization in a chemistry general circulation model and its influence on the distribution of reactive trace gases, *J. Geophys. Res.*, **100(D10)**, 20999 - 21012.

Ganzeveld, L., L. Bouwman, E. Stehfest, et al. (2010). Impact of future land use and land cover changes on atmospheric chemistry-climate interactions, *J. Geophys. Res.*, **115**, D23301.

Launiainen S., G. G. Katul, T. Grönholm et al. (2013). Partitioning ozone fluxes between canopy and forest floor by measurements and a multi-layer model, *Agricultural and Forest Meteorology*, **173**, 85–99.

Rannik, Ü., N. Altimir, I. Mammarella, et al. (2012). Ozone deposition into a boreal forest over a decade of observations: evaluating deposition partitioning and driving variables, *Atmos. Chem. Phys.*, **12**, 12165-12182.

Williams, J., J. Crowley, H. Fischer, et al. (2011). The summertime Boreal forest field measurement intensive (HUMPPA-COPEC-2010): an overview of meteorological and chemical influences, *Atmos. Chem. Phys.*, **11**, 10599-10618.

Zhou L., T. Nieminen, D. Mogensen, et al. (2014). SOSAA – A new model to simulate the concentrations of organic vapours, sulphuric acid and aerosols inside the ABL – Part 2: Aerosol dynamics and one case study at a boreal forest site, *Boreal Environment Research*, **19 (suppl. B)**, 237-256.

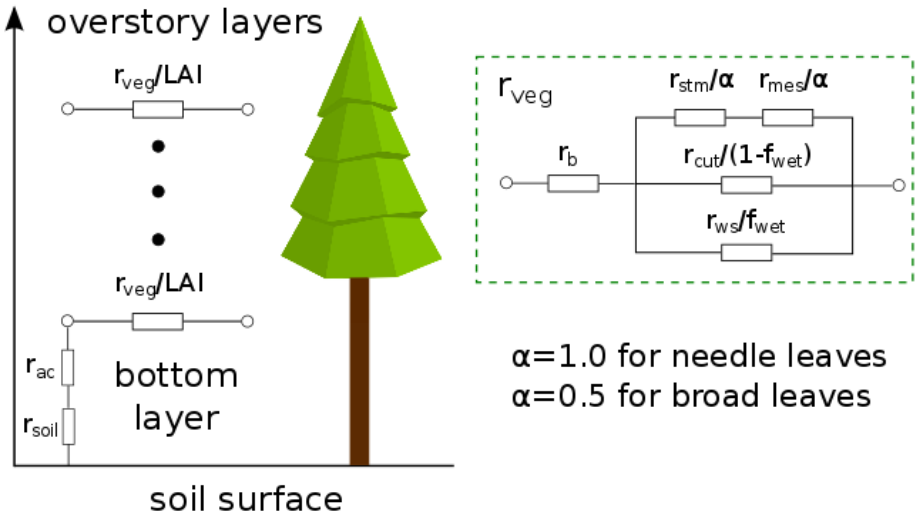

Figure 1: Diagram of resistance analogy method used in the O3 dry deposition model. The overstory layers and the bottom layer are considered separately. The bottom layer includes the understory vegetation and soil surface. rac is the turbulence resistance depending on the transportation from lowest vegetation to the soil surface. rsoil is the soil resistance, rveg represents the resistance to vegetation leaves, which is plotted on the right-hand side in details. Here rb is the quasi-laminar boundary layer resistance above the leaf surface, rstm is stomatal resistance and rmes is the mesophyll resistance. rcut means cuticular resistance, rws is the resistance to wet skin. fwet is the wet skin fraction. α is a correction factor reflecting the leaf shape, which is 1.0 for needle leaves and 0.5 for broad leaves. All the variables are defined for each layer. Note that here LAI is the all-sided leaf area for each layer.

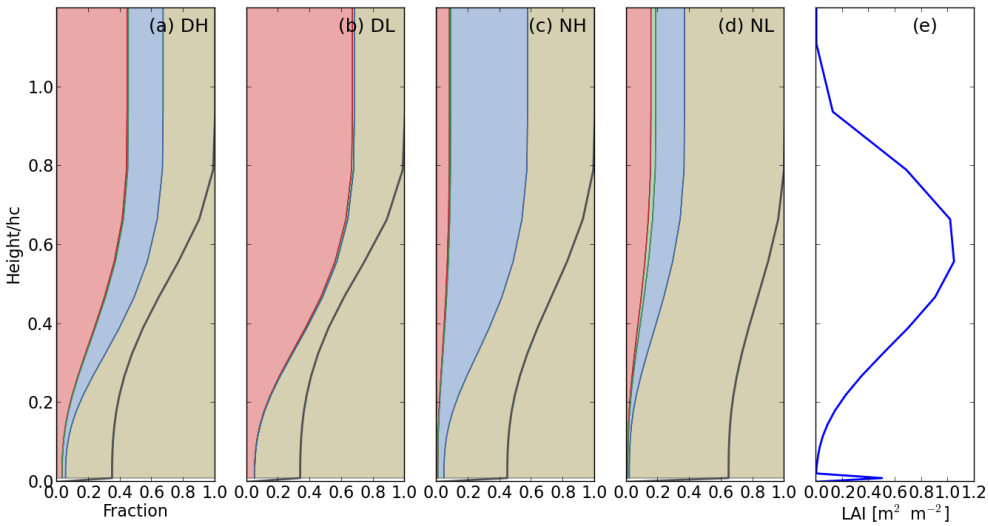

Figure 2: Simulated vertical profiles of cumulative O3 deposition flux normalized by O3 flux at the canopy top (solid black line) for four conditions DH (a), DL (b), NH (c) and NL (d). D and H represent daytime and nighttime, H and L represent high and low humidity, respectively. Shaded areas are the contribution fractions for different deposition pathways, including stomatal uptake (red), cuticular uptake (green), wet skin uptake (blue) and soil uptake (pale brown). The all-sided LAI profile for each layer is also plotted (e). Height is normalised by canopy height hc.

COGNITIVE CHAOS: TURBULENCE AND PLANETARY BOUNDARY LAYERS IN EARTH SYSTEMS

S.S. ZILITINKEVICH[1-5]

[1]Finnish Meteorological Institute, Helsinki, Finland

[2]Division of Atmospheric Sciences, University of Helsinki, Finland

[3]Department of Radio Physics, University of Nizhniy Novgorod, Russia

[4]Faculty of Geography, Moscow University, Russia

[5]Institute of Geography, Russian Academy of Sciences, Russia

Turbulence is ever present in fluid geospheres and performs vitally important services to Earth-system:

- linking the atmosphere, hydrosphere, lithosphere, biosphere and cryosphere into a unified system via strongly turbulent planetary boundary layers (PBLs);
- transporting the energy, matter and momentum in the vertical across the atmosphere and hydrosphere.

Moreover, geophysical turbulence comprises a *cognitive chaos* that owns the property of self-control preventing the dangers of collapse in very stable stratification and irresistible domination in turbulent convection. It is due to this property that chaos and order in the atmosphere and hydrosphere are kept in the shares optimal for functioning the biosphere and the Earth system as a whole.

It is widely believed that in very stable stratifications, at Richardson numbers (Ri) exceeding the critical value $Ri_c \sim 0.25$, turbulence inevitably decays and the flow becomes laminar. This is so, indeed, in the low-Reynolds-number (Re) flows, e.g. in laboratory experiments. However, very high Re flows typical of the atmosphere and ocean beyond PBLs are turbulent in spite of the strongly supercritical stratifications ($10 < Ri < 10^2$). Until recently, this paradox remained unsolved.

The Energy- and Flux-Budget (EFB) turbulence closure theory (Zilitinkevich et al., 2007, 2008, 2009, 2013) has exposed that paradoxical self-preservation of supercritically stably stratified turbulence is due to the feedback involving the following mechanisms overlooked in traditional theory:

- conversion of turbulent kinetic energy unto turbulent potential energy,
- self-control of the negative, down-gradient turbulent heat transfer through efficient generation of the counteracting, positive, counter-gradient heat transfer by turbulent potential energy.

It is due to this feedback that geophysical turbulence is maintained up to strongly supercritical stratifications. In so doing, the familiar "strong-mixing turbulence" regime typical of boundary-layers and characterised by the practically constant turbulent Prandtl number, $Pr_T \sim 1$, at $Ri > Ri_c$ gives way to the newly recognised wave-like turbulence regime, wherein Pr_T sharply increases with increasing Ri.

It is precisely the wave-like turbulence that dominates the free atmosphere and ocean. Modellers have long been aware that beyond PBLs the turbulent heat/mass transfer is much weaker than the momentum transfer. The EFB theory gives physical explanation and quantification to this rule and provides realistic method for modelling geophysical turbulence up to very stable stratifications.

Convective motions driven by the potential energy of unstable stratification develop over warm surfaces and very efficiently transfer the heat, matter and momentum in the vertical, thus moderating heat waves and preventing extreme air pollution. Conventional theories treated convective mixing as usual turbulence characterised by the forward energy cascade from larger to smaller eddies. This approach contradicts modern experimental evidence. Observations of turbulent convection in nature, large-eddy simulation (LES) and direct numerical simulation (DNS) have revealed ever present large-scale self-

organised cells or rolls reminding long-lived secondary circulations in lab experiments rather than usual short-lived, breaking turbulent eddies. Convective cells are known in viscous convection since Benard (1900) and Rayleigh (1916); but rolls, originated from the large-scale turbulent instability (Elperin et al, 2002, 2005) have no analogy in viscous convection.

According to modern views, self-organised motions originate from convective turbulence through the inverse transfer of kinetic energy – from smaller to larger plums. This mechanism is overlooked in the familiar heat/mass transfer law: $Nu = 0.14\ Ra^{1/3}$, the Monin-Obukhov similarity theory and other classical theories. Self-organisation of convective turbulence limits the share of chaos in the core of convective layers and therewith involves the near-surface convective winds, which generate mechanical turbulence and enhance the near-surface heat/mass transfer up to two orders of magnitude (Zilitinkevich et al., 2006).

REFERENCES

Zilitinkevich, S.S., 1973: Shear convection. *Boundary-Layer Meteorol*., **3**, 416-423.

Zilitinkevich S.S., Hunt J.C.R., Grachev A.A., Esau I.N., Lalas D.P., Akylas E., Tombrou M., Fairall C.W., Fernando H.J.S., Baklanov A., Joffre S.M., 2006: The influence of large convective eddies on the surface layer turbulence. *Quart. J. Roy. Met. Soc*. **132**, 1423-1456.

Zilitinkevich S., Esau I., Baklanov A., 2007: Further comments on the equilibrium height of neutral and stable planetary boundary layers. *Quart. J. Roy. Met. Soc.* **133**, 265-271.

Zilitinkevich S., Elperin T., Kleeorin N., Rogachevskii I., Esau I., Mauritsen T., Miles M.W., 2008: Turbulence energetics in stably stratified geophysical flows: strong and weak mixing regimes. *Quart. J. Roy. Met. Soc*. **134**, 793-799.

Zilitinkevich S.S., Elperin T., Kleeorin N., Rogachevskii I., Esau I.N., 2013: A hierarchy of energy- and flux-budget (EFB) turbulence closure models for stably stratified geophysical flows. *Boundary-Layer Meteorol.* **146**, 341-373

Zilitinkevich S., Kulmala M., Esau I., Baklanov A., 2015: Megacities – refining models to personal environment. *WMO Bulletin* **64** (1), 20-22.